

ZOOLOGICAL SCIENCE

An International Journal

VOLUME 5

1988

published by

The Zoological Society of Japan

CONTENTS

VOLUME 5

REVIEWS

- de Pomerai, D. I.: The transdifferentiation of neural retina into lens *in vitro* 1
- Tsuneki, K.: The neurohypophysis of cyclostomes as a primitive hypothalamic center of vertebrates 21
- Meusy, J.-J. and G. G. Payen: Female reproduction in malacostracan Crustacea 217
- Nishioka, R. S., K. M. Kelley and H. A. Bern: Control of prolactin and growth hormone secretion in teleost fishes 267
- Gause, G. G.: Taxon-specific crystallins 727
- Kuroda, H., S. Obata, K. Takemoto, M. Ishiguro and H. Sato: The mechanism and physiological function of electrical changes during fertilization of sea urchin gametes 733
- De Santis, R. and M. R. Pinto: The pathway of sperm-egg interaction in ascidians: biology and chemistry 919
- Urano, A.: Neuroendocrine control of anuran anterior preoptic neurons and initiation of mating behavior 925
- Gremigni, V.: Planarian regeneration: An overview of some cellular mechanisms ... 1153
- Mohri, H. and N. Hosoya: Two decades since the naming of tubulin — The multi-facets of tubulin — 1165
- Special Issue on Advances
in Cell Division Research*
- Sakai, H.: General introduction to the special issue on Advances in Cell Division Research 505
- Dan, K.: Mechanism of equal cleavage of sea urchin egg: transposition from astral mechanism to constricting mechanism 507
- Mazia, D.: Mitotic poles in artificial parthenogenesis: a letter to Katsuma Dan ... 519
- Inoué, S.: The living spindle 529
- Nakano, Y. and Y. Hiramoto: Measurement of spindle birefringence by the optical integration method 539
- Hamaguchi, Y.: *In vivo* cytochemistry in cell division 545
- Yoneda, M.: Computed profiles of compressed sea-urchin eggs with elastic membranes 553
- Yamao, W. and T. Miki-Noumura: Effect of hexyleneglycol on meiotic division of starfish oocytes 563
- Longo, F., W. H. Clark, Jr. and G. W. Hirsch: Gamete interactions and sperm incorporation in the nemertean, *Cerebratulus lacteus* ... 573
- Schattem, H., C. Howard, G. Coffe, C. Simerly and G. Schattem: Centrosomes, centrioles and post-translationally modified microtubules during fertilization 585
- Palazzo, R. E., J. B. Brawley and L. I. Rebhun: Spontaneous aster formation in cytoplasmic extracts from eggs of the surfclam 603
- Ohta, K., M. Toriyama, S. Endo and H. Sakai: Mitotic apparatus-associated 51-kD protein in mitosis 613
- Sato, H. and J. Bryan: The thermodynamics of molecular association in the mitotic spindle with or without heavy water (D₂O) 623
- Harris, P. J.: Metaphase to anaphase transition of sea urchin eggs examined in caffeine-induced monasters 639
- Kojima, M. K.: Marked elongation of the anaphase spindle by treatments with local anesthetics in sea urchin eggs 645
- Sluder, G.: Control mechanisms of mitosis: The role of spindle microtubules in the timing of mitotic events 653
- Sawada, T.: The mechanism of ooplasmic segregation in the ascidian egg 667
- Kawamura, K.: The contraction wave in the cortex of dividing neuroblasts of the grasshopper 677
- Sawai, T.: Participation of the subcortical and interior cytoplasm in cleavage division of newt eggs 685
- Ohnuma, M. and I. Mabuchi: Partial purifica-

tion and characterization of a factor which dissociates 45K protein-actin complex from sea urchin egg.....	691
Bonder, E. M., D. J. Fishkind, J. H. Henson, N. M. Cotran and D. A. Begg: Actin in cytokinesis: Formation of the contractile apparatus	699
Schroeder, T. E. and J. J. Otto: Immunofluorescent analysis of actin and myosin in isolated contractile rings of sea urchin eggs	713

ORIGINAL PAPERS

Physiology

Azuma, K.: Hypersensitivity after offset of adapting light in vertebrate photoreceptors	33
Takei, Y., J. Okubo and K. Yamaguchi: Effects of cellular dehydration on drinking and plasma angiotensin II level in the eel, <i>Anguilla japonica</i>	43
Ozaki, M.: A possible sugar receptor protein found in the labellum of the blowfly, <i>Phormia regina</i>	281
Okano, Y., E. David, K. Honda and S. Inoué: Auditory evoked potentials dynamically related to sleep-waking states in unrestrained rats	291
Tazaki, K.: The anatomy and physiology of the stomatogastric nervous system of <i>Squilla</i> . II. The cardiac system	299
Obika, M.: Ultrastructure and physiological response of leucophores of the medaka <i>Oryzias latipes</i>	311
Lindström, M., H. Nilson and V. B. Meyer-Rochow: Recovery from light-induced sensitivity loss in the eye of the crustacean <i>Mysis relicta</i> in relation to temperature: a study of ERG-determined V/log I relationships and morphology at 4°C and 14°C	743
Naitoh, T., K. Takeuchi and I. Takabatake: Mode of melanosome migration in teleostean melanophores	759
Yasuyama, K., T. Kimura and T. Yamaguchi: Musculature and innervation of the internal reproductive organs in the male cricket, with special reference to the projection of unpaired median neurons of the terminal abdominal ganglion	767
Khin Maung Saing: Functional innervation of the intrinsic thumb muscles of the fruit bat <i>Pteropus medius</i>	781
Inoda, T., H. Ohtake and M. Morisawa: Activation of respiration and initiation of motility in rainbow trout spermatozoa ...	939
Hidaka, T. and S. Yukiya: Excitatory and inhibitory junction potentials recorded from the red muscle of marine teleost, puffer fish	947
Negishi, S.: The involvement of microtubules in the light response of medaka melanophores	951
Grundström, N., H. Sundgren, J.-O. G. Karlsson, and H. Elwing: A simple and efficient method for photometric estimation of the state of pigment aggregation in fish melanophores	959
Endo, Y.: Non-synaptic release of transmitter-containing vesicles from the enteric neurons of the rat small intestine	965
Nishi, T., M. Kobayashi, M. Isomura, H. Ishida and Y. Shigenaka: Direct evidence for axopodial fusion preceding cell-to-cell contact in a heliozoan <i>Echinospaerium</i> (COMMUNICATION)	179
Srivastav, A. K. and L. Rani: Phosphocalic response to vitamin D ₃ treatment in freshwater snake, <i>Natrix piscator</i> (COMMUNICATION)	893

Cell Biology

Zama, N. and H. Katow: A method of quantitative analysis of cell migration using a computerized time-lapse videomicroscopy	53
Iwasaki, S. K. Miyata and K. Kobayashi: Fine structure of the filiform papillar epithelium from the tongue of the frog, <i>Rana nigromaculata</i>	61
Suganuma, Y. and H. Yamamoto: Conjugation in Tetrahymena: Its relation to concanavalin A receptor distribution on the cell surface	323
Iwasaki, S. and K. Kobayashi: Fine structure of the dorsal tongue surface in the Japanese toad, <i>Bufo japonicus</i> (Anura, Bufonidae)	331
Okamoto, M.: Fine structure of the iris mus-	

- cle in the Japanese common newt, *Cynops pyrrhogaster*, with special reference to innervation..... 337
- Fujishima, M. and K. Hoshide: Light and electron microscopic observations of *Holospira obtusa*: A macronucleus-specific bacterium of the ciliate *Paramecium caudatum* . 791
- Ishida, H., Y. Shigenaka and M. Imada: Fibrillar system and possible control mechanism for the cycle of contraction and elongation of *Spirostomum ambiguum* 973
- Ebitani, N. and T. Kubo: An established marine fish cell line with high plating efficiency (COMMUNICATION) 183

Genetics

- Saitoh, M. and Y. Obara: Meiotic studies of interracial hybrids from the wild population of the large Japanese field mouse, *Apodemus speciosus speciosus* 815
- Nakamura, T.: Female heterogametic sex-determination in *Xenopus laevis* as reconfirmed by repeated diploid gynogenesis (COMMUNICATION) 187
- Narusé, K., A. Shimada and A. Shima: Gene-centromere mapping for 5 visible mutant loci in multiple recessive tester stock of the medaka (*Oryzias latipes*) (COMMUNICATION)..... 489
- Shimada, A., A. Shima and N. Egami: Establishment of multiple recessive tester stock in the fish *Oryzias latipes* (COMMUNICATION) 897
- Ota, H., T. Hikida, M. Matsui and M. Hasegawa: Karyotype of a scincid lizard, *Carlia fusca*, from Guam, the Mariana Islands (COMMUNICATION) 901

Immunology

- Nagata, S.: T cell-specific antigen in *Xenopus* identified with a mouse monoclonal antibody: Biochemical characterization and species distribution 77
- Nagata, S.: T cell-specific XTLA-1 antigens from *Xenopus laevis* tadpole and froglet are not identical (COMMUNICATION)..... 493

Biochemistry

- Suzuki, T., R. Muramatsu, T. Kisamori and T. Furukohri: Myoglobin of the shark *Galeus nipponensis*: Identification of the exceptional amino acid replacement at the distal (E7) position and autoxidation of its oxyform . 69
- Tsuneoka, M., K. Maruyama and K. Ohashi: *In vitro* dimerization of I-protein, an A-I junctional component of skeletal muscle myofibrils 347
- Kawamura, S. and M. Murakami: Light-induced Michaelis constant increase is rapid and inherent in cGMP phosphodiesterase in frog rod outer segments..... 801
- Hung, F. and Y. Shaoyi: Isolation and identification of crucian (*Carassius auratus* L.) hemoglobin and its subunits..... 809

Developmental Biology

- Fujisawa, H. and S. Amemiya: Temperaturedependence in reaggregation of cells dissociated from sea urchin embryos with different seasonal growth 85
- Mitsunaga, K., Y. Fujino and I. Yasumasu: Probable participation of mitochondrial Ca^{2+} transport in calcification of spicules and morphogenesis in sea urchin embryos.... 93
- Numakunai, T., Z. Hoshino and S. Kajiwara: Spawning of three intraspecific groups of the ascidian, *Halocynthia roretzi* (Drasche), in the wild, and fertilization among them ... 103
- Tahara, U.: Normal stages of development in the lamprey, *Lampetra reissneri* (Dybowski) 109
- Tsunemoto, M., O. Numata, T. Sugai and Y. Watanabe: Analysis of oral replacement by scanning electron microscopy and immunofluorescence microscopy in *Tetrahymena thermophila* during conjugation 119
- Iwamatsu, T., T. Ohta, E. Oshima and N. Sakai: Oogenesis in the medaka *Oryzias latipes* — stages of oocyte development .. 353
- Tsuchiyama-Omura, S., B. Sakaguchi, K. Koga and D. F. Poulson: Morphological features of embryogenesis in *Drosophila melanogaster* infected with a male-killing spiroplasma 375
- Suematsu, N., H. Takeda and T. Mizuno: Glandular epithelium induced from urinary

bladder epithelium of the adult rat does not show full prostatic cytodifferentiation 385

Uchiyama, H. and T. Mizuno: Sexual dimorphism in the genital tubercle of the duck: Studies on the normal development and histogenesis 823

Yamamoto, M., M. Ishine and M. Yoshida: Gonadal maturation independent of photic conditions in laboratory-reared sea urchins, *Pseudocentrorus depressus* and *Hemicentrotus pulcherrimus* 979

Yamamoto, M.: Normal embryonic stages of the pygmy cuttlefish, *Idiosepius pygmaeus paradoxus* Ortmann 989

Mizuno, T., H. Takeda, N. Suematsu, N. Hirou-naka and I. Lasnitzki: Absence of androgen receptors in the prostatic glandular epithelium derived from testicular feminization mutant (*Tfm*) mice 999

Yasumasu, S., I. Iuchi and K. Yamagami: Medaka hatching enzyme consists of two kinds of proteases which act cooperatively (COMMUNICATION) 191

Sivasubramanian, P.: Interspecific trans-plantation of developing tissues and their subsequent differentiation in flies (COM-MUNICATION) 497

Reproductive Biology

Awaji, M. and I. Hanyu: Effects of water temperature and photoperiod on the begin-ning of spawning season in the orange-red type medaka 1059

Kosaka, T., M. Obata, T. R. Saito and K. W. Takahashi: Effects of adult male cohabita-tion on precocious puberty in early weaning female guinea pigs (COMMUNICATION) 1137

Endocrinology

Engström, W., E. Dafgård and S. Falkmer: Comparative effects *in vitro* of *Myxine*, *Squalus*, avian and mammalian insuins on DNA-synthesis in 3T3 mouse fibroblasts . 133

Ueda, H., T. Kosaka and K. W. Takahashi: Effects of long-term progesterone treatment on synchronized ovulation in guinea pigs 139

Endo, K., T. Masaki and K. Kumagai:

Neuroendocrine regulation of the develop-ment of seasonal morphs in the Asian comma butterfly, *Polygonia c-aureum* L.: Difference in activity of summer-morph-producing hor-mone from brain-extracts of the long-day and short-day pupae 145

Hyodo, S., M. Fujiwara, S. Kozono, M. Sato and A. Urano: Development of an *in situ* hybridization method for neurohypophysial hormone mRNAs using synthetic oligonuc-leotide probes 397

Seki, T., S. Kikuyama and M. Suzuki: Effect of hypothalamic extract on the prolactin release from the bullfrog pituitary gland with special reference to thyrotropin-releasing hormone (TRH) 407

Hirohama, T., H. Uemura, S. Nakamura and T. Aoto: Atrial natriuretic peptide (ANP)-immunoreactivity and ultrastructures of car-diocytes in fish 833

Tanaka, S., H. Iwasawa and K. Wakabayashi: Plasma levels of androgens in growing frogs of *Rana nigromaculata* 1007

Oota, Y. and I. Koshimizu: Vascular supply of hypophysis in the turtle, *Geoclemys reevesii* 1013

Yamashita, T., K. Kawamoto, and S. Kawashi-ma: Fetal and postnatal development of arginine vasopressin-immunoreactive neurons in the mouse 1019

Hyodo, S., M. Fujiwara, M. Sato and A. Ura-no: Molecular and immuno-histochemical study on expressions of vasopressin and oxytocin genes following sodium loading 1033

Nishida, M., J. Kawada, H. Ishizuka and S. Katsura: Goitrogenic action of manganese on female mouse thyroid through three generations 1043

Masaki, T., K. Endo and K. Kumagai: Neuroendocrine regulation of the develop-ment of seasonal morphs in the Asian comma butterfly, *Polygonia c-aureum* L.: Is the factor producing summer morphs (SMPH) identical to the small prothoracicotropic hor-mone (4K-PTTH)? 1051

Srivastav, A. K. and S. P. Srivastav: Corpus-cles of Stannius of *Clarias batrachus* in response to 1,25 dihydroxyvitamin D₃ admi-

- nistration (COMMUNICATION)..... 197
- Fujimori, M., Y. Sasayama and C. Oguro: Translocation of ^{45}Ca from the endolymphatic sacs to the bone in *Rana nigromaculata* (COMMUNICATION)..... 201
- Endo, Y. and T. Endo: S-100 protein-like immunoreactive cells in the brain-midgut endocrine system of the insect *Periplaneta americana* (COMMUNICATION)..... 905
- Kobayashi, Y. and S. Kawashima: Changes of acetylcholinesterase activity in rat supraoptic nucleus cell bodies during water deprivation (COMMUNICATION) 911

Morphology

- Fujikara, K., S. Kurabuchi, M. Tabuchi and S. Inoue: Morphology and distribution of the skin glands in *Xenopus laevis* and their response to experimental stimulations.... 415
- Tsuneki, K. and M. Oujji: Absence of blood vessels in the brain of six species of primitive salamanders..... 847
- Chiba, A. and Y. Honma: Fine structure of agranular cells in the gummy shark (*Mustelus manazo*) Adenohypophysis..... 1065
- Amasaki, H., M. Daigo and N. Meguro: Morphological observations of the large intestine in the common vole, *Microtus arvalis* Pallas (COMMUNICATION) 205

Behavior Biology

- Pandey, S. C. and S. D. Pandey: Sexual maturation in female wild mice: Combined effect of adults' urinary chemosignals and minimum time of exposure to stimulus substances for bringing the effects..... 153
- Verrell, P. A.: Sexual interference in the alpine newt, *Triturus alpestris* (Amphibia, Urodela, Salamandridae) 159
- Ooka-Souda, S., H. Kabasawa and S. Kinoshita: Circadian rhythms in locomotor activity of the hagfish, *Eptatretus burgeri*. II. The effect of brain ablation..... 431
- Ooka-Souda, S. and H. Kabasawa: Circadian rhythms in locomotor activity of the hagfish, *Eptatretus burgeri*. III. Hypothalamus: a locus of the circadian pacemaker?..... 437
- Weldon, P. J.: Feeding responses of Pacific

- snappers (genus *Lutjanus*) to the yellowbelly sea snake (*Pelamis platurus*)..... 443
- Daumae, M. and T. Kimura: Factors regulating urination patterns in male and female mice (*Mus musculus*)..... 855
- Ebino, K. Y., K. Yoshinaga, T. R. Saito and K. W. Takahashi: Coprophagy as an innate behavior in the mouse 863
- Kohda, Y. and M. Watanabe: Preference of striped backgrounds by striped fishes (COMMUNICATION)..... 501
- Saito, T. R., K. kamata, M. Nakamura and M. Inaba: Maternal behavior in virgin female rats following removal of the vomeronasal organ (COMMUNICATION)..... 1141

Ecology

- Hanzawa, N., N. Taniguchi and K. Numachi: Geographical differentiation in populations of Japanese dace *Tribolodon hakonensis* deduced from allozymic variation 449
- Konishi, K. and R. Quintana: The larval stages of three pagurid crabs (Crustacea: Anomura: Paguridae) from Hokkaido, Japan 463
- Ohgushi, R., S. Yamane and S. F. Sakagami: Ecological distribution and habitat-linked density of colonies of stenogastrine wasps in tropical S. E. Asia 869
- Takahashi, H. and H. Iwasawa: Interpopulation variations in clutch size and egg size in the Japanese salamander, *Hynobius nigrescens* 1073
- Meserve, L. A. and M. A. R. Gonzalez: Thyroid status and ambient temperature as influences on weaning in young mice..... 1083
- Matsumoto, T.: Colony composition of the wood-feeding cockroach, *Panesthia australis* Brunner (Blattaria, Blaberidae, Panesthiinae) in Australia (COMMUNICATION) 1145
- Egami, N., O. Terao and Y. Iwao: The life span of wild populations of the fish *Oryzias latipes* under natural conditions (COMMUNICATION)..... 1149
- Asada, N.: Invasion of *Drosophila albomicans* to the mainland of Japan (COMMUNICATION)..... 915

Taxonomy

- Nakasone, Y.: Land hermit crabs from the Ryukyus, Japan, with a description of a new species from the Philippines (Crustacea, Decapoda, Coenobitidae) 165
- Sawada, I. and A. L. Molan: Two new hymenolepidid cestodes, *Vampirolepis molani* sp. n. and *V. iraqensis* sp. n., from Iraqi bats 483
- Kristensen, R. M. and Y. Shirayama: *Pliciloricus hadalis* (Pliciloricidae), a new loriferan species collected from the Izu-Ogasawara Trench, Western Pacific 875
- Uchikawa, K., K. Nakata and F. S. Lukoschus: Mites of the genus *Myobia* (Trombidiformes, Myobiidae) parasitic on *Apodemus* mice in Korea and Japan, with reference to their immature stages 883
- Hirayama, A.: A ghost shrimp with four-articulate fifth pereopods (Crustacea: Caprellidea: Phtisicidae) from northwest Australia 1089
- Xia, Z. W. and M. J. Toda: The *Drosophila immigrans* species-group of the subgenus *Drosophila* (Diptera: Drosophilidae) in Yunnan, China 1095
- Nakasone, Y.: Larval stages of *Coenobita purpureus* Stimpson and *C. cavipes* Stimpson reared in the laboratory and survival rates and growth factors of three land hermit crab larvae (Crustacea: Anomura) 1105
- Hayashi, T. and M. Matsui: Biochemical differentiation in Japanese newts, genus *Cynops* (Salamandridae) 1121

Others

- Proceedings of the 59th Annual Meeting of the Zoological Society of Japan 1189
- Book reviews 1340
- Announcements 1342
- Author index 1345
- Instructions to Authors 209
- Erratum 212

Vol. 5 No. 1

February 1988

QL
2864
1H

ZOOLOGICAL SCIENCE

An International Journal

PHYSIOLOGY
CELL and MOLECULAR BIOLOGY
GENETICS
IMMUNOLOGY
BIOCHEMISTRY
DEVELOPMENTAL BIOLOGY
REPRODUCTIVE BIOLOGY
ENDOCRINOLOGY
BEHAVIOR BIOLOGY
ENVIRONMENTAL BIOLOGY
ECOLOGY and TAXONOMY

published by **Zoological Society of Japan**

distributed by **Business Center for Academic Societies Japan**
VSP, Zeist, The Netherlands

ISSN 0289-0003

ZOOLOGICAL SCIENCE

The Official Journal of the Zoological Society of Japan

Editor-in-Chief:

Hideshi Kobayashi (Tokyo)

Managing Editor:

Seiichiro Kawashima (Hiroshima)

Assistant Editors:

Takeo Machida (Hiroshima)

Sumio Takahashi (Hiroshima)

Kazuyoshi Tsutsui (Hiroshima)

The Zoological Society of Japan:

Toshin-building, Hongo 2-27-2, Bunkyo-ku,
Tokyo 113, Japan. Tel. (03) 814-5675

Officers:

President: Nobuo Egami (Tsukuba)

Secretary: Hideo Namiki (Tokyo)

Treasurer: Tadakazu Ohoka (Tokyo)

Librarian: Shun-Ichi Uéno (Tokyo)

Editorial Board:

Howard A. Bern (Berkeley)

Walter Bock (New York)

Aubrey Gorbman (Seattle)

Horst Grunz (Essen)

Robert B. Hill (Kingston)

Yukio Hiramoto (Chiba)

Susumu Ishii (Tokyo)

Yukiaki Kuroda (Mishima)

Koscak Maruyama (Chiba)

Roger Milkman (Iowa City)

Hiromichi Morita (Fukuoka)

Kazuo Moriwaki (Mishima)

Tokindo S. Okada (Okazaki)

Andreas Oksche (Giessen)

Hidemi Sato (Nagoya)

Hiroshi Watanabe (Shimoda)

Mayumi Yamada (Sapporo)

Ryuzo Yanagimachi (Honolulu)

ZOOLOGICAL SCIENCE is devoted to publication of original articles, reviews and communications in the broad field of Zoology. The journal was founded in 1984 as a result of unification of Zoological Magazine (1888-1983) and *Annotationes Zoologicae Japonenses* (1897-1983), the former official journals of the Zoological Society of Japan. ZOOLOGICAL SCIENCE appears bimonthly. An annual volume consists of six numbers more than 1000 pages including an issue containing abstracts of papers presented at the annual meeting of the Zoological Society of Japan.

MANUSCRIPTS OFFERED FOR CONSIDERATION AND CORRESPONDENCE CONCERNING EDITORIAL MATTERS should be sent to:

Dr. Seiichiro KAWASHIMA, Managing Editor, Zoological Science, Zoological Institute, Faculty of Science, Hiroshima University, 1-1-89 Higashisenda-machi, Naka-ku, Hiroshima 730, Japan, in accordance with the instructions to authors which appear in the first issue of each volume. Copies of instructions to authors will be sent upon request.

SUBSCRIPTIONS. ZOOLOGICAL SCIENCE is distributed free of charge to the members, both domestic and foreign, of the Zoological Society of Japan. To non-member subscribers within Japan, it is distributed by Business Center for Academic Societies Japan, 6-16-3 Hongo, Bunkyo-ku, Tokyo 113. Subscriptions outside Japan should be ordered from the sole agent, VSP, Utrechtseweg 62, 3704 HE Zeist (postal address: P. O. Box 346, 3700 AH Zeist), The Netherlands. Subscription rates will be provided on request to these agents. New subscriptions and renewals begin with the first issue of the current volume.

All rights reserved. No part of this publication may be reproduced or stored in a retrieval system in any form or by any means, without permission in writing from the copyright holder.

© Copyright 1988, The Zoological Society of Japan

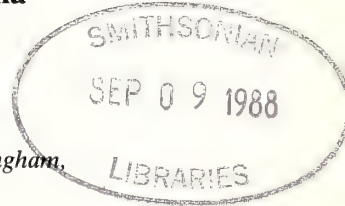
[Publication of Zoological Science has been supported in part by a Grant-in-Aid for
Scientific Publication from the Ministry of Education, Science and Culture, Japan.]

REVIEW

The Transdifferentiation of Neural Retina into Lens *in vitro*

DAVID I. DE POMERAI

Department of Zoology, University of Nottingham, Nottingham,
NG7 2RD, United Kingdom



I. INTRODUCTION; PRECEDENTS

During long-term monolayer culture, chick embryo neuroretinal (NR) cells lose most of their differentiated characteristics and convert extensively into both melanised pigment cells [1] and crystallin-containing lens-fibre-like cells (lentoids; [2]). These changes are best described by the term 'transdifferentiation' [3,4], because the NR cells giving rise to these foreign phenotypes remain incompletely characterised. But clearly no retinal cell would ever give rise to lens or pigmented progeny during the course of normal development *in situ*. The confusingly similar terms 'metaplasia' and 'cell-type conversion' are best reserved for those systems where the initial cell type is both fully differentiated and postmitotic.

The best example fulfilling these criteria is Wolffian lens regeneration from dorsal iris following lentectomy in adult newts (reviewed in [5]). Lens removal, coupled with a stimulating influence emanating from the neural retina (possibly a growth factor; [6]), causes the marginal cells of the iris to re-enter mitosis and become depigmented. Those dorsal iris cells which divide fastest (cell cycle time < 48 hr) later convert into crystallin-expressing lens cells, whereas those which divide more slowly (cell cycle time > 72 hr) later withdraw from mitosis, become repigmented and so revert to an iris phenotype. This decision is not irrevocable, however, since serial lentectomy (i.e. removing an earlier lens regenerate) will cause some dorsal iris

cells to convert into lens even though they had previously decided not to do so [7]. Yamada and McDevitt [8] suggest that those cells which convert into lens must pass through a critical number (> six) of cell divisions within the 20-day proliferative period following lentectomy, whereas cells passing through fewer than four mitoses (including ventral iris cells) would instead redifferentiate as pigment cells. Increased synthesis of extracellular matrix components is associated with the depigmentation/proliferation and repigmentation phases of this process *in vivo*, but not with lens formation [9]. Cultures prepared from dispersed iris cells can also give rise to lens tissue *in vitro*, but this process neither requires NR influence, nor is it restricted only to dorsal iris (cells from ventral iris are equally lentoidogenic in culture; [10]). This relaxation may arise because iris cells of either type can pass through an unrestricted number of mitoses *in vitro*, although they do so on average more slowly than during lens regeneration *in vivo*.

Similarities between chick NR transdifferentiation and Wolffian lens regeneration from newt iris include both the endpoint attained (lens-fibre-like cells) and the neural (optic cup) origin of both starting tissues. Differences include the embryonic nature and heterogeneity of cell types in the NR system, in contrast to adult iris tissue composed of postmitotic and fully differentiated melanocytes. An intermediate case is provided by the transdifferentiation of chick embryo tapetal cells into lens *in vitro*, where the initial tapetum consists solely of melanin-containing pigmented epithelial (PE) cells. As shown by Eguchi and Okada [11] using

clonal culture techniques, a single pigmented cell can give rise to crystallin-containing lentoids among its progeny, demonstrating a definitive switch of cell type *in vitro*.

Lower vertebrates show extensive powers of regeneration, and transdifferentiations between adult cell types have been demonstrated e.g. in *Hydra* [12] and in various marine medusae [13,14]. However, the differentiated states of most vertebrate cell types seem much more stable, and few instances of transdifferentiation have been described outside the eye system [15]. Neural crest cells give rise to a very diverse range of cell types *in vivo*, but this may reflect cellular heterogeneity in the neural crest population with respect to differentiation potential [16]. Rat pancreatic cells can apparently convert into hepatocytes *in vivo* as a consequence of drug treatment or copper depletion/repletion [17], and different types of amphibian chromophore can interconvert to some extent *in vitro* [18]; however, these changes occur between cell types sharing a common embryonic ancestry. The interconvertibility of embryonic NR and tapetal phenotypes is another example in this category, since both tissues derive from the optic cup. But this will not suffice to explain the ability of optic cup tissues (neural) to convert into lens (normally induced from head ectoderm) *in vivo* or *in vitro*. Such an ability is also shared by cultured cells from chick embryo pineal [19], a neural structure homologous to the median eye of lower vertebrates. At least in certain reptiles (e.g. *Anolis*; [20]) this median eye includes a cellular lens of neural derivation, containing authentic lens crystallins.

II. TISSUE-SPECIFIC FUNCTIONS

a. Retinal markers

The chick retina comprises a single glial cell-type, the radially arranged Müller fibres, plus several different neuronal cell types arranged in layers (*viz.*, photoreceptor, horizontal, bipolar, amacrine and ganglion cells). These latter express a wide variety of differentiated functions, including several neurotransmitter-synthesising enzymes (e.g. choline acetyltransferase, CAT; glutamic

acid decarboxylase, GAD) and corresponding receptor/uptake systems [21–24]. Most retinal neurones (apart from photoreceptors) express tetanus toxin receptors on their surfaces, and like other electrically excitable cells they can be stained by Merocyanin 540. Although many of these neuronal markers are expressed transiently in monolayer cultures of NR cells, both the markers and the neuronal cells themselves are lost in a characteristic sequence during the first few weeks *in vitro* [24].

The differentiated characteristics of NR glial (Müller) cells include the enzymes glutamine synthetase (GS) and carbonic anhydrase II (CA). Retinal GS activity is induced by glucocorticoid hormones (e.g. cortisol), first appearing at about the 16th day during embryonic development; immunologically detectable GS is confined to the Müller cells and absent from neurones. Retinal explants or aggregate cultures of dissociated NR cells can be induced to express GS precociously by treatment with cortisol from about the 7th day onwards, but hormonal induction of GS is negligible in dispersed monolayer cultures of such cells [25]. This implies a requirement for histotypic contacts between retinal neurones and glia in order for GS to be expressed in the latter, such contacts being disrupted in sparse monolayer cultures but retained in explants and restored in aggregates. In dense monolayer cultures of NR cells, cortisol treatment induces transient GS activity [26]; immunocytochemical staining shows this GS expression to be limited to those glial cells in intimate contact with neurones [27]. By contrast, CA is found in many neuronal cell types as well as in glia during early retinal development, but later disappears from the former and becomes glial-specific, after which CA expression increases only within the Müller cells [28]. Recent studies with cloned GS and CA DNA probes show that the respective patterns of GS and CA activity closely parallel the expression of their corresponding mRNAs [29].

b. Lens markers

Terminally differentiated lens fibres lose their nuclei and most cell organelles, their cytoplasm becoming filled with very high levels of crystallins.

Lens cells also express specific membrane proteins, including the MP26 species characteristic of gap junctions in the lens [30]. The crystallins are characteristic structural polypeptides which together comprise the vast bulk of soluble lens protein; they are present only at trace levels in non-lens tissues [31]. Crystallins fall into four main classes, designated α , β , γ and δ , of which the first two are found throughout the vertebrates. δ Crystallin is confined to birds and reptiles, where it largely or wholly replaces the γ class prominent in fish, amphibia and mammals [32, 33]. In chick embryo lens there are two δ crystallin polypeptides of Mr 48 and 50 kd [34], at least six β crystallins ranging from 21 to 35 kd, and two main α species of 19 and 20 kd [35]. DNA sequences corresponding to most of these chick crystallins have now been cloned [36–41], and DNA sequences published for the αA and two δ crystallin genes [42–45].

The chick αA crystallin gene contains two introns and encodes an unexpectedly long (~1600 nt) mRNA with an extensive 3'-terminal untranslated region. The αA promoter includes both TATATATA and CAAT boxes, located respectively at -26 to -31 and -67 to -70 bp relative to the cap site [42]. DNA sequences responsible for lens-specific expression of this gene have been identified by fusing αA 5'-promoter fragments onto the structural gene encoding chick δ crystallin, and then microinjecting the chimaeric genes into mouse lens cells in culture. Since mice have no endogenous δ gene, expression of the constructs can be monitored by immunocytochemistry. This analysis reveals an important sequence element located between -242 and -189, which can function when reversed in orientation or even (to some extent) when moved 1.7 kbp downstream from the cap site; this element may thus fulfil an enhancer-like function [46]. Expression from the αA promoter seems to be wholly restricted to lens, with no detectable expression in non-lens cells [42].

The chicken genome contains two closely related δ crystallin genes designated $\delta 1$ and $\delta 2$, which are linked 4.2 kbp apart in the same orientation, 5'- $\delta 1$ -spacer- $\delta 2$ -3'. Both genes are highly complex and are split at homologous positions by 16 introns each. Three exons (7, 12 and

15) are identical between $\delta 1$ and $\delta 2$, while most of the rest (apart from exons 1 and 2) show >70% sequence identity; even the introns (apart from B, E and I) contain extensive sequence homologies [44, 45]. The $\delta 1$ mRNA sequence includes two possible translation initiation codons (AUG) located 19 amino acids apart in the predicted protein sequence; these would yield two δ polypeptides of Mr 50,750 and 48,900, respectively [44]. Selective use of these alternative initiation codons may explain how changes in ionic balance can modify the relative synthetic rates of the 48 and 50 kd δ polypeptides [47]. This derivation of both polypeptides from $\delta 1$ now appears much more likely than one species arising from $\delta 1$ and the other from $\delta 2$. Hybridisation experiments using intron-specific probes suggest that in lens the $\delta 1$ gene is at least 100-fold more active transcriptionally than $\delta 2$ [42, 45]. Notably, the 5'-promoter region of the $\delta 1$ gene contains a CAAT box (-67 to -70) and two consensus core enhancer sequences (at -308 and +350), whereas the $\delta 2$ gene lacks these features [48]. TAAAA boxes are found 5' to the $\delta 1$ (-24 to -28) and $\delta 2$ (-26 to -30) genes, and both promoters support similar levels of transcription by an *in vitro* cell-free system [42]. However, when the $\delta 1$ and $\delta 2$ promoter regions (approx. 350 bp) are fused to bacterial chloramphenicol acetyltransferase (bChAT) genes and introduced into chick lens cells, the $\delta 1$ promoter supports significantly (~5-fold) higher bChAT expression than does the $\delta 2$ promoter [48].

Microinjection of a complete $\delta 1$ gene sequence (plus 5'-flanking regions) into mouse cells of various types demonstrates that δ expression is mainly lens-specific, i.e. much higher in lens than in non-lens cells such as fibroblasts [49]. Promoter deletion experiments indicate that high-level expression of the $\delta 1$ gene in mouse lens cells requires only the promoter region from -80 to +35, whereas the 20-fold lower level of expression in fibroblasts requires an extra 12 bp of 5'-flanking sequence (from position -92; [50, 51]). Transient expression assays on $\delta 1$ genes introduced into a wide variety of mouse cell types, show that high-level δ expression is possible only in lens and embryonic epidermal cells, whereas other cell

types permit only low-level expression (even in brain or retinal glia, or in tapetal cells; [51]). The $\delta 1$ promoter region includes a GC-rich inverted repeat bracketing the CAAT box between -78 and -59; if various GC-rich DNA fragments are coinjected along with the $\delta 1$ gene into mouse lens cells, then δ expression is greatly reduced, suggesting that these GC-rich sequences may compete for the ubiquitous transcription factor Sp1 [52]. Consensus sequences for the TGGCA-binding factor are also found in the $\delta 1$ promoter (-60 to -48). Finally, brief mention should be made of recent studies of δ expression in transgenic mice [53] and fish [54] carrying introduced $\delta 1$ genes (neither mice nor fish have δ genes of their own). In the transgenic fish (medaka), low levels of δ expression are found in many tissues and there is no restriction to lens, perhaps because the DNA signals for lens-specific expression of the chick $\delta 1$ gene have diverged too far from those used by the fish's own crystallin genes [54]. By contrast, in transgenic mice the introduced $\delta 1$ gene is expressed chiefly in lens tissue, albeit at lower levels than in transient $\delta 1$ expression assays using mouse lens cells. However, δ expression is also unexpectedly detectable in certain pyramidal neurones of the anterior piriform cortex [53].

III. FOUNDER CELLS AND EXTRALENTICULAR CRYSTALLINS

Although a single melanised tapetal cell can give rise to lens cells among its clonal progeny [11], a similar analysis of NR transdifferentiation gives less clear-cut results. Clonal cultures of 8 day NR produce three types of colony, respectively containing lentoids, or pigment cells, or neither [55]; but no single cell generates both lens and pigmented progeny in the same colony. In clonal cultures of 3.5 day NR cells, however, some colonies eventually develop lentoids, some pigment cells, some neither and some *both* [56]. Moreover, at earlier stages most colonies contain both neuron-like and epitheloid cells, presumably derived from a single neuroepithelial precursor. Thus many of these early NR cells appear to be multipotent, since up to four distinct phenotypes can emerge amongst their progeny, two of which

are foreign to NR.

In mass cultures of later (6 to 10 day) NR, two major categories of cell emerge after a few days *in vitro* [2]. These are: (i) flattened epitheloid (E) cells adhering to the substrate (presumably Müller glia or their precursors); and (ii) rounded neuron-like (N) cells, which often form clusters interconnected by neurite processes, and which attach preferentially to the underlying E cells (unless using highly adhesive substrates such as polylysine; [23, 57]). The lentoids which appear after 4-5 weeks in these cultures are likely to be derived from E cell progenitors, since N cells are mostly lost before this stage [2]. Several lines of evidence confirm this; thus lentoid appearance is promoted in E-cell cultures prepared by the selective elimination of N cells, using either mild dissociation [57] or the neurotoxin chionoform-ferric chelate [58]. In a reaggregate culture system (see section IV below) which speeds up transdifferentiation, CA-expressing retinogial cells from 13 or 16 day NR convert directly into crystallin- and MP26-expressing lentoid cells [30, 59]. Moreover, pre-treatment of the NR tissue with the gliotoxin α -aminoadipic acid greatly reduces lentoid formation [30]. In a similar reaggregate culture system, retinal N cells pre-labelled using tetanus toxin do not subsequently express δ crystallin, as shown by double immunofluorescent staining; thus few if any lens cells are derived directly from N cells [60]. With NR material from much earlier (3.5 day) embryos, however, there is some evidence for N cells converting into lentoids. This has come both from time-lapse photography and from chimaeric cultures combining quail N cells with chick E cells or *vice versa*; in either combination, both quail and chick δ crystallins are expressed in late cultures, suggesting that some cells in the N fractions (all of which can be stained with Merocyanin 540) do go on to form lens [61].

Related questions are raised by the presence of crystallin transcripts (and proteins; [31]) in a variety of embryonic non-lens tissues. Broadly these fall into three categories:

(i) Tissues such as early chick embryonic heart and liver which show no potential for transdifferentiation, nor for enhanced crystallin expression *in vitro*. Nevertheless, a small proportion of

cell clusters in such tissues contain nucleus-confined δ transcripts detectable by *in situ* hybridisation, whereas neighbouring cells contain none [62, 63].

(ii) Tissues where a low level of δ expression *in vivo* becomes enhanced during *in vitro* culture, but lentoids never develop and other crystallin types (e.g. α) are not expressed. This category includes 6 day chick embryo brain [64] and 3.5 day embryo limb bud cells [65]. Some 30% of cells in 3.5 day adenohypophysis contain δ protein, but in this case δ expression decreases during *in vitro* culture, and also during later development *in vivo* [66, 67].

(iii) Tissues which are able to transdifferentiate when cultured *in vitro*, forming lentoids which express high levels of several crystallin types. This group includes not only chick embryonic NR and tapetum (see above) but also 3.5 day embryo brain [68] and 8 day quail embryo pineal [19]. The three neural tissues (NR, brain, pineal) can also transdifferentiate into pigment cells, while cultured explants of early embryonic tapetum can convert into neuroretinal derivatives [69].

Several studies have monitored crystallin transcripts in non-lens tissues, initially by solution hybridisation with cDNAs prepared from abundant lens mRNAs [70]. The levels of such transcripts in chick NR tissue drop 10-fold between 3.5 and 8 days of embryonic development, and become almost undetectable by hatching [71]. This trend apparently correlates with the declining ability of NR from older embryos to transdifferentiate into lens [72]. More recent studies using a cloned δ probe confirm the decline of δ transcript levels in later embryonic NR tissue [73], and also detect δ transcripts in other non-lens tissues such as 3.5 day embryo brain and limb bud. Most of these extralenticular δ transcripts are larger than the 2 kb δ messenger [63] and presumably represent nuclear precursors, although δ mRNA-sized transcripts predominate in the case of 3.5 day NR [73]. *In situ* hybridisation shows that most extralenticular δ transcripts are indeed confined to the nuclei of certain cell groups [62], though cytoplasmic hybridisation is also detectable in 3.5 day NR [74].

Although it is tempting to link extralenticular

(ectopic) δ transcription with transdifferentiation potential, this relationship does not hold good in all cases ((i) and (ii) above). Could ectopic δ expression merely reflect a general leakiness of transcriptional control for this gene (cf. low expression of δ 1 genes introduced into mouse fibroblasts, reviewed earlier)? But this would predict a uniformly low level of δ expression in all nuclei, rather than the clustering of strongly positive cells surrounded by a majority of nonexpressing cells, as revealed by *in situ* hybridisation [62]. Nevertheless, the proportion of δ -expressing cells is much greater in those tissues capable of transdifferentiation (e.g. \sim 15% in 3.5 day NR) than in those unable to do so (e.g. 0.1% in 3.5 day heart; [63]). Transcripts of α A crystallin are barely detectable in both NR and tapetum from 8 day embryos, whereas δ RNAs are far more abundant in NR, and transcripts encoding the 25 kd β crystallin are undetectable in either tissue [41, 63, 75].

An antiserum directed against the α -crystallin fraction from chick lens stains only Müller glia and their precursors in sections of chick NR tissue [76]; however, it remains unclear whether this antiserum recognises (i) α crystallin itself, or (ii) a related polypeptide, or (iii) an unrelated protein copurifying with lens α crystallin and also present in glia. It is worth noting that lens epithelial cells contain glial fibrillary acidic protein, previously thought to be confined to neural-derived cells [77]. A recent report [78] shows that 8–9 day chick embryo NR contains a subclass of glial-like cells immunostaining positively for δ crystallin. These δ -positive cells form a loose meshwork at the retinal/optic nerve boundary (Fig. 1); they are of glial morphology, and some at least express glial markers such as CA and GS (although GS remains undetectable in most NR glial cells until much later). It remains to determine (i) the level and function of δ crystallin in these cells, and (ii) whether they also express other lens markers (e.g. α A crystallin or MP26). Plausibly, these δ -positive glia might represent the elusive founder cells which act as lens precursors in transdifferentiating NR cultures. If so, the transformation of cell phenotype involved in this system may be less fundamental than was previously supposed.

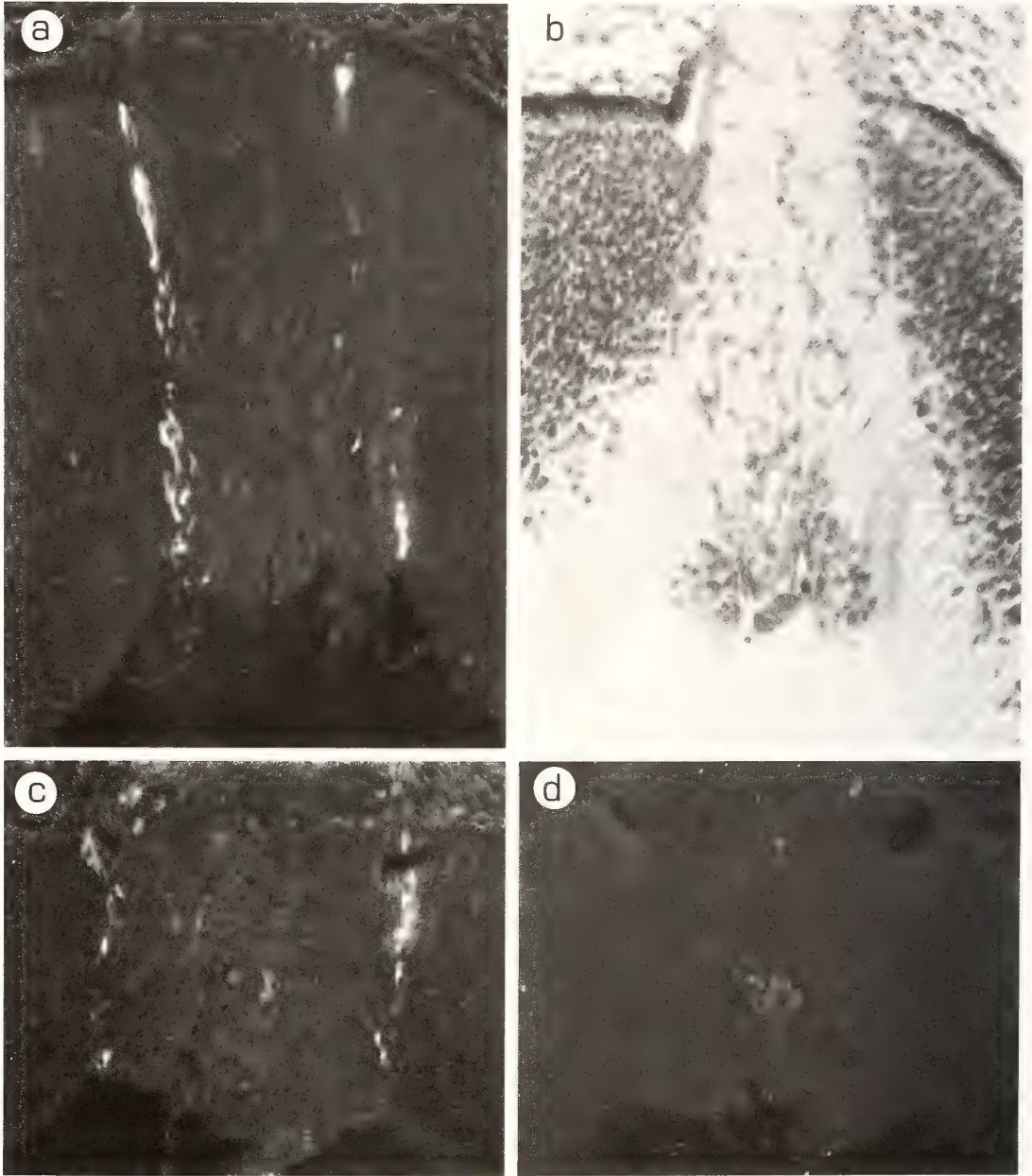


FIG. 1. Boundary cells immunostaining positively for δ crystallin in sections of 9 day embryonic neural retina. Panels a and b show adjacent sections stained with anti- δ -crystallin (followed by an FITC-linked second antibody), and with haematoxylin/eosin respectively. Panels c and d show sections from a different preparation stained with anti- δ -crystallin before (c) and after (d) the adsorption of the antiserum with a lens lysate. Experimental details are given in reference 78. Photographs kindly supplied by Dr. P. Linsler. Magnification $\times 375$.

But could a small population of such founder cells directly give rise to all the lentoidal tissue pro-

duced under optimal conditions *in vitro* (sections IV and V), even assuming a significant advantage

over other E cells in terms of survival and/or proliferation? One intriguing possibility, based on the model of Pritchard [79], is that δ -positive glia might act as "leader cells" *in vitro*, encouraging their neighbours (initially δ -negative) to join them in the process of conversion into lens. Overall, there seem to be significant overlaps between the gene sets active in lens and those actually or potentially expressed in NR glial cells [76, 78].

IV. CELL-SURFACE CHANGES ASSOCIATED WITH TRANSDIFFERENTIATION

As noted in section IIa, histotypic contacts between retinal neurones and Müller cells are prerequisite for the latter to respond to cortisol by expressing GS mRNA and protein [25, 28, 29]. Disruption of such contacts, for instance by culturing NR cells as dispersed monolayers, results in a loss of GS inducibility associated with a rapid depletion of intracellular cortisol receptors [80]. Both features are retained in aggregate cultures prepared from freshly dissociated NR cells, and notably some aspects of retinal tissue organisation are restored under such conditions. Such aggregate cultures of NR cells also fail to transdifferentiate into lens even after 28 days *in vitro* [81]. Nor is any transdifferentiation observed when dissociated NR cells are maintained for 4 days in monolayer culture, then redissociated and cultured as reagggregates for a further 24 days [81]. However, if the monolayer phase of culture is extended to 8–10 days prior to reaggregation, then lentoids form within the reagggregates much more rapidly and extensively than in parallel cultures maintained as monolayers throughout [59, 81]. This is true not only for 8–9 day NR, but also for 13 and even 16 day NR, where glial cells are postmitotic [59]. As discussed in the previous section, the lentoidal tissue formed in this reaggregate system derives from NR glial cells (sensitive to α -aminoadipic acid; [30]) but not from tetanus-toxin-binding neurones [60].

These studies suggest a radical change in the state of cell determination among NR glial cells between the 4th and 10th days of monolayer culture; furthermore, this 'transdetermination' can

occur even if mitosis is inhibited by using serum-free medium during this period [81]. The levels of δ crystallin mRNA in 30-day reaggregate NR cultures (i.e. 10 days as monolayers, then a further 20 days as reagggregates) reach 27% of those in newly hatched chick lens; this compares with 0.7% in 30-day monolayer cultures (where most lentoid formation occurs after 30 days) and less than 0.02% in 30-day aggregate cultures of the same NR cells [82]. δ Crystallin mRNA is just detectable (at <0.01% of the level in lens) after 10 days of monolayer culture, suggesting that transdetermination may coincide with the first onset of δ transcription in some NR cells.

However, δ crystallin may not be the most informative marker as regards this transdetermination event. Studies by Moscona and co-workers [30] show that the lens membrane protein MP26 is absent from fresh retina or newly dissociated NR cells; however, it becomes immunologically detectable in a few scattered cells after only 3 days of monolayer culture, and is expressed by most of the glial-like cells after 5 to 7 days. In lens, the MP26 protein is associated with gap junctions, although these are not found in the lentoids formed in reaggregate NR cultures [83]. α A crystallin transcripts are also detectable after only 7 days in monolayer NR cultures [41].

One important feature of this system is a dramatic change in the affinities of different retinal cell types for each other. Aggregates of freshly dissociated NR cells display an interspersion of glial (Müller) cells among retinal neurones of various types, reflecting a preferential affinity between glial and neuronal cells which is mediated in part by the cell-surface protein R cognin (expressed by all retinal cell types; [84]). In monolayer culture, however, the NR glial cells (but not neurones) rapidly lose both R cognin and their affinity for retinal neurones [83]. As a result, when such monolayer cultures are dissociated and reagggregated after 8 to 10 days *in vitro*, the modified glial cells adhere preferentially to each other, forming CA-positive cores which rapidly develop into crystallin-positive lentoids. Retinal neurones are excluded from cores, instead forming peripheral shells which do not participate in lentoidogenesis [30, 59, 83]. The loss of both R

cognin and affinity for neurones can be delayed for several days in monolayer cultures of NR cells by treatment with retinoic acid [85]. Lentoidogenesis, even in so-called 'monolayer' NR cultures, is frequently associated with multilayering of the E cells, and can be promoted by artificially folding the cell sheet [86]; this effect may also operate via increased contacts between modified glial cells.

Other important cell-surface phenomena include those mediated by the extracellular matrix (ECM), whose role is particularly clear in the tapetal transdifferentiation system. Growing tapetal cells on a collagen rather than plastic substrate blocks the appearance of lens cells but reinforces melanisation [87]. Moreover, treatment of tapetal cells with hyaluronidase promotes their transdifferentiation into lens (see next section; [88,89]), an effect which is presumably due to the degradation of ECM components. This situation recalls the enhanced synthesis of ECM associated with iris cell proliferation and repigmentation, but *not* with lens conversion, following lentectomy in adult newts [9]. Recent studies in our laboratory suggest that the ECM is also profoundly modified during lentoidogenesis in monolayer NR cultures, and is affected by medium hexose levels (Flor-Henry and de Pomerai, in preparation).

V. MEDIUM INFLUENCES ON TRANSDIFFERENTIATION

Several early studies noted the differential effects on NR transdifferentiation of various medium formulations [86, 90], and of specific supplements such as bicarbonate (which promotes pigment cell formation; [91]) or insulin (which promotes both growth and lentoidogenesis; [92]). A combination of horse serum and high glucose, used to promote neuronal survival and differentiation in many neural culture systems, exerts a similar influence on chick NR cells *in vitro*, but also strongly inhibits transdifferentiation into lens [57]. This was used to assay the state of cell determination in NR cultures, by transferring them from standard into nonpermissive medium or *vice versa* at various times, then later assaying the amount of δ crystallin produced [93]. Subsequently, this approach was refined by combining

minimum essential medium (MEM) with both horse and foetal calf sera; this allows extensive transdifferentiation at the normal glucose concentration (6 mM; FH), but blocks lentoid formation when supplemented with glucose to 18 mM final (FHG; [94]). NR cultures changed from nonpermissive FHG into permissive FH medium can only transdifferentiate into lens if transferred on or before 21 days *in vitro*, but fail to do so if transferred later than 24 days. Conversely, cultures changed from FH into FHG medium are blocked (no δ production) if transferred prior to the 15th day *in vitro*, but are able to transdifferentiate extensively if transferred on the 18th day or later.

These experiments argue against the possibility of cell selection, whereby a subpopulation of lens precursor cells would overgrow the other cell types present under FH conditions, but would be eliminated or selectively disadvantaged under FHG conditions. Rather, determinative events appear to act between the 15th and 21st days of culture, such that NR cells become committed either to follow a lens differentiation pathway, or else not to do so [94]. The only external variable here is the concentration of glucose, although this could have multiple effects on the heterogeneous NR cell population in culture. In fact, all parameters of glucose metabolism studied (including glucose uptake, utilisation of the pentose shunt, lactate production and glycogen accumulation) are strongly stimulated in FHG as compared to FH cultures [95]. However, when inhibitors or antagonists of these metabolic processes are added as continuous supplements to FHG cultures, the effects vary markedly. At one extreme, iodoacetate inhibits lactate production but scarcely stimulates transdifferentiation [96]; at the other, ouabain both reduces glucose uptake and promotes lentoid formation almost to FH levels. Transdifferentiation is also enhanced by forskolin (an activator of adenylyl cyclase) or dibutyryl cAMP, both of which reduce glycogen accumulation in FHG cultures via cAMP-stimulated glycogenolysis. The intermediate levels of glycogen and δ crystallin in such cultures, relative to those in FH and FHG controls, suggest an inverse relationship between the two markers [95].

Because glycogen is a differentiated feature of retinal Müller cells, its accumulation *in vitro* might preclude E cells from later converting into lens. Enhanced glial differentiation leading to reduced transdifferentiation may also underlie the marked inhibition of lentoidogenesis observed in cortisol-supplemented dense NR cultures, which transiently express GS activity [26]. However, the known involvement of retinal neurones in this latter process (section IIa) poses the question of whether neuronal influences might similarly affect glycogen production and so mediate in the glucose block on transdifferentiation. *In situ* histochemistry shows that both glycogen and its main synthetic enzyme are localised in NR glial cells underlying clusters of neurones [95], reminiscent of the situation with cortisol induction of GS in dense monolayer cultures [27]. Moreover, neurones survive better under FHG conditions and show prolonged expression of CAT as compared with FH controls [94]. An inhibitory effect of retinal neurones on transdifferentiation can also be demonstrated by recombining N and E cell fractions together; low N:E ratios allow extensive lentoid development, whereas high N:E ratios block this process [97]. Recent studies of glucose effects on transdifferentiation in neurone-stripped E-cell cultures suggest that the glucose block may be mediated partly via enhanced neuronal survival/differentiation, and partly by direct effects of high glucose on the E cells (Tobal *et al.*, in preparation).

Reducing the level of glucose in MEM below 6 mM results in poor survival of NR cells. But if glucose-free MEM is supplemented with 6 mM fructose, then δ crystallin production is strongly stimulated (by ~4-fold) and lentoids appear earlier than in 6 mM glucose control cultures (Flor-Henry and de Pomerai, in preparation). We are currently studying how these changes in hexose regime affect the extent and type of ECM production.

A second effective means for inhibiting NR transdifferentiation into lens involves the use of medium 199 in place of MEM [98]. Medium transfer experiments show that cultures maintained for 20 or even 30 days in 199 can still transdifferentiate extensively about 10 days after transfer into MEM, i.e. such cultures never be-

come committed *not* to form lens (in contrast to the high glucose block). The reasons for this contrast will be discussed in the next section. We have tentatively identified the inhibitory agent in 199 as acetate, since supplementation of MEM with acetate significantly reduces NR conversion into lentoids (Flor-Henry, unpublished).

Another issue to be addressed briefly in this section concerns the influence of serum factors on NR transdifferentiation into lens. de Pomerai and Gali [99] found that different types of serum exert a much greater influence on this process than do different batches of the same serum type. Specifically, adult serum (from chicken, horse or even newborn calf) supports little if any crystallin accumulation, whereas foetal calf serum (FCS) or embryo extract (bovine or chick) allows extensive lentoid formation. The active agents in embryonic/foetal sera appear to be of low molecular weight, able to diffuse out through a dialysis membrane. Thus, the dialysis medium (MEM plus low-MW serum components) supports transdifferentiation, whereas the dialysed serum (macromolecular fraction, plus MEM) does not. The active low-MW fraction is partially sensitive to both heat and immobilised trypsin treatments [100], suggesting that it could include small polypeptides such as growth factors. By contrast, adult sera appear to contain macromolecular components which inhibit transdifferentiation [99].

In the parallel tapetal system, modifications of the medium conditions can be used to obtain three types of culture, *viz.*, (i) dedifferentiated tapetal cells, none of which express melanin or crystallin proteins; (ii) repigmented tapetal cells, all of which are fully melanised; and (iii) transdifferentiated lentoidal cells expressing abundant crystallins [88, 89]. The key variables include phenylthiourea (which inhibits melanin production) and hyaluronidase (presumably acting on ECM components), whose presence together in the medium favours (i) and (iii), but whose absence favours (ii). High culture densities also promote (iii), ascorbic acid is helpful both for (ii) and (iii), while dialysed FCS is used throughout. The availability of pure cell populations in each of these three states should greatly facilitate future molecular studies [75].

VI. CRYSTALLIN REGULATION DURING TRANSDIFFERENTIATION

During the later stages of NR or PE transdifferentiation, the levels of putative crystallin mRNAs (hybridising to abundant lens cDNAs) increase by at least two orders of magnitude above the traces detectable earlier [101–103]; *in vitro* translation confirms that the most abundant translatable mRNAs in late NR cultures are those encoding crystallins. A longstanding question in developmental biology asks whether a given phenotype can only be attained by way of an invariant and coordinated programme of gene expression. If such were the case for lens, then crystallin genes should be activated as a battery and expressed in the same order during transdifferentiation as during normal lens development. The data on extralenticular crystallin expression cited earlier (section III) cannot easily be reconciled with this simplistic view. For instance, increasing levels of δ expression in 6 day embryonic brain cultures do not entrain any detectable expression of other crystallins such as α [64]. Evidence from earlier immunological studies also suggests that the various crystallin classes must be regulated independ-

ently, e.g. during lentoid formation in NR as compared to lens epithelium cultures *in vitro* [104]. Recent investigations by Clayton and co-workers [63] fully confirm this view, using three specific DNA probes to monitor the levels of δ , αA and $\beta 25$ crystallin mRNAs during normal lens development and during transdifferentiation of both NR and tapetal (PE) cultures. These findings are summarised in Table 1.

Whereas δ is the first crystallin detectable in the 2 day embryonic lens rudiment, in both NR and PE transdifferentiation systems αA crystallin mRNA is expressed many days before the appearance of δ mRNA. δ Transcripts are easily detectable in fresh NR tissue (day 0), but apparently disappear during the early stages of culture. Detectable δ mRNA does not reappear until about 20 days in NR cultures and thereafter increases steeply; in PE cultures this sharp rise in δ mRNA occurs even later. Fresh NR and PE tissues contain only faint traces of αA transcripts. However, in NR cultures significant levels of αA mRNA (plus a prominent precursor) are already expressed after 7 days *in vitro*, rising by 21 days to a moderate level which does not further increase up to 42 days. A similar but slightly later trend is

TABLE 1. Crystallin mRNA levels during lens development *in vivo* and during lentoidal transdifferentiation from NR or PE *in vitro*

Stage	Normal lens development			NR cultures <i>in vitro</i>			PE cultures <i>in vitro</i>			Time in culture
	αA^1	$\beta 25^2$	δ^2	αA^1	$\beta 25$	δ^3	αA^1	$\beta 25$	δ^4	
2 day embryo	—	—	++	(+)	—	+	(+)	—	(+)	0 (fresh tissue)
8 day embryo	+	(+)	+++	+	—	—	—	—	—	7 days
15 day embryo	+	+	++++	(+)	—	—	—	+	—	14 days
Hatching (21 days)	++	++	+++	+	+	(+)	++	+	—	21 days
1 month posthatch	+++	+++	++	++	+	++	++	+	(+)	28 days
1 year posthatch	+++	+++	—	++	+	+++	++	+	+	35 days
				++	+	++++	++	+	+	35 days
				++	+	++++	++	+++	+++	42 days
				ND	ND	ND	++	+++	ND	49 days

Relative levels of these three mRNAs are expressed very approximately as follows: ND, not done; —, undetectable; (+), trace; +, low level; ++, moderate level; +++, high level; +++++, very high level. Unless otherwise indicated, these estimates were derived (subjectively) from Northern blots in reference 63. Additional sources include: ¹, reference 41; ², reference 127; ³, reference 105; and ⁴, reference 75.

Note that absolute mRNA levels cannot be compared accurately between the three probes used, nor between tissues. The relative mRNA levels in lens are at least an order or magnitude higher than those attained in NR or PE cultures, hence the numbers of +'s are not comparable across the 3 sets of data.

apparent for αA mRNA in PE cultures. The contrast in $\beta 25$ mRNA levels is much more striking; this mRNA is expressed only at low levels in later NR cultures, but shows a curious two-phase accumulation profile in PE cultures, being present at fairly low levels between 14 and 35 days, then rising to high levels at 42 and 49 days. The data just cited imply independent transcriptional regulation for these three crystallin genes [63]; they are not coordinately expressed. Only the steep rise in δ mRNA levels in late NR and PE cultures correlates temporally with the appearance of lentoids, whereas other lens 'markers' (e.g. αA transcripts or MP26; see section IV) may appear long before the overt emergence of lens-fibre-like cells.

In situ hybridisation studies confirm that δ transcripts are undetectable during the first to third weeks of NR culture [74, 105]. After about 20 days, a few clusters of cell nuclei are found to be expressing δ transcripts, but no hybridisation is apparent over the cytoplasm. Nuclear RNAs extracted from NR cultures at this stage contain only a 4 kb δ precursor but no fully processed (2 kb) δ mRNA [105]. This nuclear restriction phase persists until about 25 days, but by 30 days δ hybridisation is abundant over both nuclei and cytoplasm in many areas of the culture, though groups of strongly hybridising nuclei can still be observed in non-lentoidal regions [105]. These and other indications suggest that NR cells become able to synthesise δ transcripts at high levels a few days before they acquire the capacity to process these transcripts (to the 2kb δ mRNA) or to export δ messengers from the nuclei [74, 105].

Non-permissive high glucose (FHG) cultures show very little hybridisation with a δ probe at late (35–40 day) stages, suggesting that δ transcripts are either not synthesised at all (a transcriptional block) or else are rapidly degraded within the nuclei [105]. By contrast, in late 199 cultures δ transcripts can be detected in Northern blots of total cellular but not cytoplasmic RNAs. *In situ* hybridisation confirms that many nuclei in such cultures contain δ transcripts, but these are either not exported to, or else are rapidly degraded in, the cytoplasm. Both δ precursors and the predominant 2 kb δ mRNA are present in late 199

nuclei; thus medium 199 must act on δ mRNA export or stabilisation, but not on δ transcript synthesis or processing [105]. This affords a simple explanation for the observation that transferring late 199 cultures into MEM medium always results in transdifferentiation about 10 days later [98].

In the tapetal transdifferentiation system, δ precursors (but not mRNA) are readily detectable in fully dedifferentiated cultures, but disappear rapidly from repigmenting cultures, and are only present at trace levels in fresh tapetum. By contrast, dense lentoidal cultures of these cells express the 2kb δ mRNA and corresponding protein at very high levels [75].

If crystallin genes are regulated differently during lentoidal transdifferentiation *in vitro* as compared to lens development *in vivo*, one can ask whether there are any correlative differences in the DNA or chromatin of the crystallin gene regions. DNA methylation patterns in the δ locus (as revealed by digestion with methylation-sensitive or -insensitive isoschizomer restriction enzymes) do not correlate with the levels of δ expression in a range of chick tissue types [106]. Nor does the pattern of δ gene methylation change detectably during NR transdifferentiation, despite a 100–1000 fold increase in δ expression [107]. Nevertheless, there is evidence that the δ locus does become hypomethylated in postmitotic lens fibres *in vivo*, an event which occurs after the onset of high δ expression [108, 109]. Although gene expression bears no direct relationship to DNA hypomethylation [110], there is a clearer link with the pattern of DNase I-hypersensitive sites (HSS) in the 5' regions near active genes. In the chick vitellogenin gene system, one specific HSS appears only when expression is induced hormonally [111]. Alternative sets of HSS are associated with (i) low-level constitutive expression of the chick lysozyme gene in macrophages, and (ii) high-level hormone-induced expression of the same gene in oviduct [112]. We have initiated studies along these lines, using a form of direct end-labelling to look for DNase I-generated sub-bands among the major restriction fragments of the δ locus [113]. As shown in Figure 2, our data indicate several HSS in the 5' region of the $\delta 1$ gene, only one of which (at -1000) shows the same location in both lens and

transdifferentiated NR cultures. Another HSS lying close to the transcription initiation site differs only slightly in location between the two tissues. However, the two sites at -2000 and -3750 in lens are apparently replaced by a single site at -1500 in transdifferentiated NR cultures [113]. Another relevant finding from this study suggests a radical change in the chromatin conformation of the δ locus during NR culture, from largely DNase-I-resistant (nucleosomal chromatin) in fresh tissue and early 10 day cultures, to largely DNase-I-sensitive (smooth-fibre chromatin) in later 25 and 35 day cultures [113]. This conformational change in the δ locus seems to occur within most cells, and may prepare the way for the widespread appearance of δ transcripts in many nuclei between 20 and 30 days.

The gene transfer approach has recently been used in attempts to assay the potential for crystallin expression in cultured cells undergoing transdifferentiation. One interesting observation is that mouse retinal glial cells (which do not themselves transdifferentiate into lens *in vitro*) express transfected δ genes only at low levels in early cultures, but at much higher levels in late cultures, suggesting that the latter have moved at least some way towards transdifferentiation [114]. A more detailed experimental study used chick α , chick δ or viral promoters respectively linked to bChAT reporter genes [115], the fusion constructs being introduced into chick NR cells cultured under lentoidogenic (low N:E ratio) or non-lentoidogenic (high N:E ratio) conditions. The levels of bChAT expression from the viral promoter are high in early cultures of both types, but decline to low levels by 10 days. By contrast, bChAT expression from the α or δ promoters is low initially, but rises steeply between 10 and 20 days only in the lentoidogenic cultures (expression remains low in the blocked cultures). These results suggest that onset of expression for the introduced fusion genes somewhat precedes the onset of high-level transcription from the endogenous crystallin genes (particularly in the case of δ). In these experiments the α construct is expressed much more efficiently than the δ construct after 20 days *in vitro* (cf. 21-day values in Table 1); it would be interesting to determine whether the

reverse would be true after 35 or 40 days of culture. Possible relationships between the onset of expression for such fusion genes and the determinative phenomena discussed earlier (sections IV and V) deserve careful investigation.

VII. LINKS WITH OTHER SYSTEMS

Although there are few well-documented instances where differentiated vertebrate cells give rise to new phenotypes (see section I), there are at least two processes which can alter the pattern of gene expression in such cells either transiently or permanently. These are (i) the induction of a stress response by heat shock or other environmental insults [116], and (ii) oncogenesis associated with the activation of endogenous proto-oncogenes [117]. In this context, it is noteworthy that α crystallins share limited sequence homologies with small heat shock proteins [118], and some β/γ crystallins with certain oncogenes [119]. The only such instance reported for δ crystallin, however, is an intriguing antigenic relationship

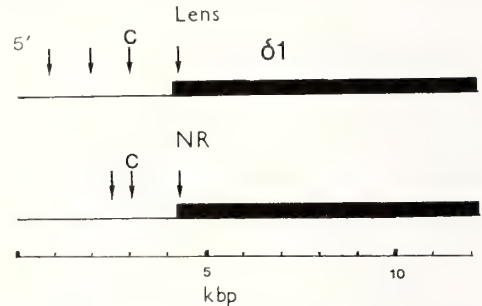


Fig. 2. Approximate locations of DNase-I-hypersensitive sites in the 5'-flanking region of the $\delta 1$ gene in lens (upper panel) and in late transdifferentiated cultures of NR cells (lower panel). Nuclei from such material were treated with extremely low levels of DNase I and then digested completely with Bam HI, Hind III or Eco RI restriction endonucleases. The presence of DNase-I-generated sub-bands was noted upon Southern blotting the DNA fragments and probing with a full-length $\delta 1$ cDNA clone, p δ CR17 [39]. The DNase-I-hypersensitive sites indicated by arrowheads show the simplest derivation of the observed sub-bands from restriction fragments of known size [113].

The site marked C is shared both by lens and late NR cultures, and that which lies just within the $\delta 1$ gene may also be shared.

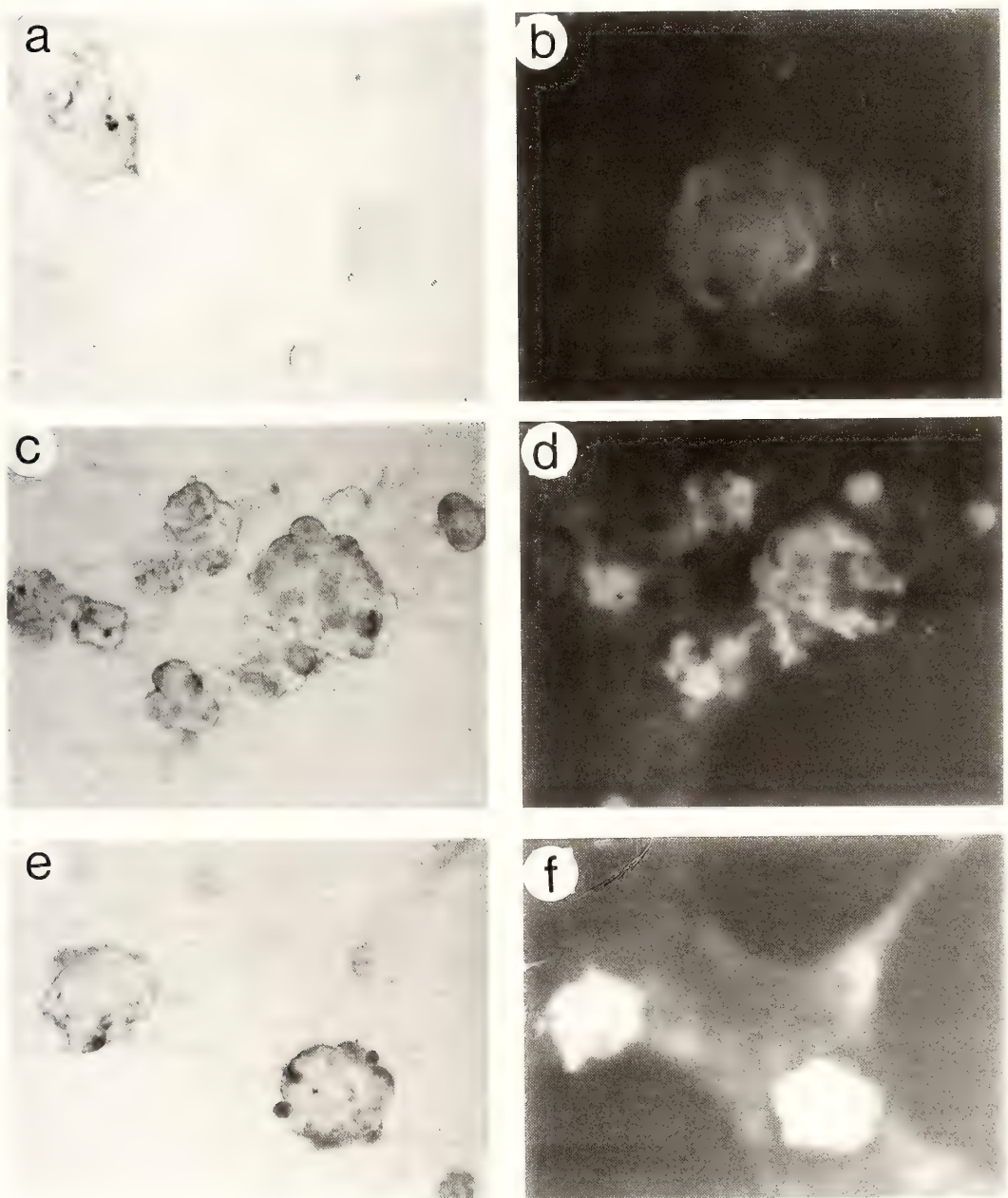


FIG. 3. Co-localisation of pp60^{c-src} and δ crystallin in NR-derived lentoids. NR cultures were stained with rabbit anti-pp60^{v-src} followed by PAP, and then with rat anti- δ -crystallin followed by rhodamine-linked anti-rat IgG. Panels a and b show negative controls in which preimmune rabbit serum replaced the anti-pp60^{v-src} (panel a), and where the rat anti- δ treatment was omitted (panel b). Panels c and e show PAP staining for pp60^{c-src} in lentoids, while panels d and f show rhodamine immunofluorescence for δ crystallin in the same fields. Magnification $\times 200$. Full details are given in reference 137. Note that (unlike δ) pp60^{c-src} is not uniformly present throughout lentoids.

with feather keratin [120].

a. Stress response

In most cell types from bacteria to man, exposure to a temperature increase of $\sim 5^{\circ}\text{C}$ above ambient, or to various toxic agents (arsenite, Cd^{++} , aminoacid analogues), results in a suspension or diminution of the normal protein synthetic pattern and in the rapid induction of a small number of characteristic heat shock proteins (HSPs). The major HSPs are of approximate Mr 70 kd, 85–90 kd, and one or more in the 22–28 kd range. The induction of these HSPs is regulated transcriptionally, but they themselves exert generalised post-transcriptional effects on the expression of normal cellular proteins, and rescue a heat-shock-induced block on pre-mRNA splicing ([121]; note that most HSP genes are intron-free). Even if cells are maintained continuously at the higher temperature, the heat shock response eventually fades out, with HSP expression diminishing and the normal pattern of protein synthesis being resumed. This results from complex autoregulatory interactions among the HSPs [122].

Carr and de Pomerai [123] investigated whether a stress response (e.g. to adverse conditions experienced during culture) might play any role in NR transdifferentiation. Under standard (FH) permissive conditions, transient exposure of NR cultures to heat shock does not result in precocious crystallin expression, although both 70 and 85 kd HSPs are readily induced. A 24 kd HSP, induced by sodium arsenite (but not by heat) in NR cells and by heat in lens, comigrates with one of the β crystallins on SDS gels, but proves to be immunologically related [124, 125]. However, NR cells cultured in medium 199 display an intriguing response to heat shock. In the first place, 199 cultures maintained continuously at 43°C (heat shock temperature) readily transdifferentiate into lentoids and express high levels of δ crystallin, in sharp contrast to the block on both apparent at 37°C [126]. Secondly, δ crystallin synthesis can be induced by transferring late 199 cultures from 37°C to 43°C , although the kinetics of this induction are much slower (several days) than those for the HSPs (a few hours). Further experiments suggest (i) that actinomycin does not block increased δ

synthesis if added after the commencement of the heat shock response, and (ii) that agents such as sodium arsenite can elicit a similar response in late 199 cultures kept throughout at 37°C . Thus HSP induction somehow relieves a block on the export or stabilisation of δ mRNAs which normally operates in late 199 cultures at 37°C [105]. An effect via pre-mRNA splicing seems much less likely, since the bulk of δ transcripts confined to late 199 nuclei are already in the 2 kb δ mRNA size-class.

It is curious that δ synthesis should be stimulated at all following heat shock (a response expected only from authentic HSPs). In fact, this is also true in chick embryo lenses, where δ synthesis increases by some 20% during HSP induction [124]. During post-hatching stages of chick lens development, when δ protein synthesis is low although δ mRNA remains present [127], heat shock treatment of lens epithelial explants induces a very marked (2–5 fold) stimulation of δ synthesis [126]. It will be interesting to determine whether these heat shock responses also involve the export and/or stabilisation of δ mRNAs that were previously confined to the nuclei. There is also the intriguing possibility that stress might transiently exert similar effects when culturing cells which show ectopic δ transcript expression *in vivo*.

b. Oncogene expression

Cellular proto-oncogene products function at various levels in the transduction of signals across the cell membrane and in the control of cell proliferation [128]. In the latter context, transcription of the *c-myc* proto-oncogene has been demonstrated both in dedifferentiated tapetal cultures and in prelentoidal NR cultures, but not in crystallin-expressing lentoidal cultures from either source [125, 129]. The correlation between multilayering of the NR cell sheet (loss of contact inhibition?) and lentoidogenesis may suggest another tenuous link with cancer cells.

The proto-oncogene *c-src* encodes a membrane-associated tyrosine kinase (pp60^{c-src}) homologous to the transforming protein of Rous Sarcoma Virus (pp60^{v-src}). Whereas the latter induces rapid cell proliferation and transformation, the former does

not, even when grossly overexpressed by NR cells infected with an RSV variant carrying the *c-src* gene in place of *v-src* [130]. The normal function of the *c-src* gene may be linked with differentiation rather than proliferation, since high levels of pp60^{c-src} are expressed during the differentiation of postmitotic neurones in chick NR [131] and cerebellum [132], as well as during smooth muscle development [133] and early neural tube induction [134] in the chick embryo.

Maximal expression of pp60^{c-src} protein and its kinase activity occurs in chick NR tissue at around the 13th day of embryonic development [131, 135]; this appears to be regulated transcriptionally, since *c-src* mRNA levels also peak at this time [136, 137]. During the early stages of NR culture, pp60^{c-src} is expressed at moderate levels in neuronal cells, as shown by *in situ* immunocytochemistry. However pp60^{c-src} kinase activity increases sharply in late lentoidogenic (FH) cultures but falls in blocked FHG or 199 cultures [137]. Immunocytochemical staining confirms that most of the pp60^{c-src} protein in late FH cultures is confined to lentoidal structures (Fig. 3). In lens, pp60^{c-src} kinase activity increases during embryonic development, and is maximal in the lens epithelial fraction of newly hatched chick lens [137]. These data suggest an elevated level of pp60^{c-src} expression during the onset of lens fibre differentiation, but a lower level in established lens fibres (both *in vivo* and in transdifferentiated NR cultures). Notably, lens fibre cells are highly elongated (as are smooth muscle and neuronal cells), and it may be that pp60^{c-src} mediates in the cytoskeletal and/or cell surface reorganisation required during cell elongation. We are currently using a *c-src*-carrying RSV variant (kindly supplied by Dr. R. Jove) to determine whether high levels of pp60^{c-src} expression might enhance NR transdifferentiation into lens. If so, this would draw another sharp contrast between the *c-src* and *v-src* gene products. RSV infection of chick lens cells [138] or quail NR cells [139] blocks lens fibre differentiation and crystallin expression. This block depends on the *v-src* function, since it can be relieved by shifting to a non-permissive temperature in the case of RSV mutants encoding a temperature-sensitive *v-src* product. With ts-RSV transformed quail NR cells,

such a shift results in appearance of δ plus α crystallin mRNAs and α protein within 48 hours, whereas δ protein and lentoids only appear after a further 5 days. By contrast, quail NR cells transformed with a different retrovirus (Mill Hill 2) permanently express both α and δ crystallins and also contain stem cells for lentoid production [139].

VIII. CONCLUDING REMARKS

The preceding pages of this review have tried to summarise current knowledge of NR transdifferentiation into lens (and closely related systems). Sections III to VII have dealt with the main events in approximately chronological order. In this final section, I wish to pose some of the many questions which remain open.

In the first place, it is apparent that the end result of NR transdifferentiation, namely a close approximation to a lens-fibre phenotype, is arrived at as the culmination of a complex sequence of events which initially bear little relationship to lens formation *in vivo*. There can be no question of simply switching on some master programme for lens development. How such diverse routes converge on a common endpoint remains a fascinating question.

Further investigations are needed to elucidate the nature of the NR founder cells which give rise to lentoids *in vitro*. Are they restricted to progeny of the δ -positive 'boundary' cells identified *in vivo* [78], or could such cells influence their neighbours in culture to join them in lentoidogenesis [79]? This may become amenable to analysis if the δ -positive cells can be identified and tagged in early NR cultures. The significance of ectopic δ expression is another problem requiring attention. What is the pattern of δ gene regulation in the expressing cells, and is there a distinction of kind or only of degree between the levels of δ transcription observed in those tissues able to transdifferentiate into lens and in those unable to do so? How easy is it for retinal glial cells to switch on a subset of lens markers (e.g. δ and α A crystallins, MP26), even under conditions which do not lead on to lentoid formation?

Clarification is needed as to whether the deter-

minative events revealed by reaggregation experiments (effective between 4 and 10 days) are different in kind from those implied by medium transfers (occurring between 15 and 21 days). The former may coincide temporally with MP26 and α A expression, while the latter correlate more closely with the onset of δ expression, or at least with the widespread conformational change of δ -locus chromatin from DNase I-resistance to sensitivity. However, it may be less confusing to think of determination in this system as progressive rather than multistep, since the timing of any commitment to form lens may be largely a function of the stabilising or destabilising effects of later culture conditions. Thus increased glial cell contacts in reaggregates are evidently conducive to lentoid formation, whereas high glucose levels favour more normal glial differentiation through a stimulation of glycogen production. Either way, a single discrete determination decision appears unlikely. The control of crystallin gene expression during NR transdifferentiation raises several further questions. It is generally assumed (though not yet proven) that the rate of δ gene transcription must increase greatly when δ transcripts begin to accumulate within the nuclei. RNA processing, export and stabilisation controls would subsequently amplify this primary transcriptional event [74, 105]. If this model is approximately correct, then what factors are responsible for activating δ transcription? Positively acting transcription factors would be expected to interact with the 5'-flanking regions of the δ 1 gene, a feature which would prove amenable to foot-printing analysis. The locations of protein-binding and DNase-I-hypersensitive sites in the δ gene region will need to be compared in detail between lens tissue and transdifferentiated cultures. Preliminary work along these lines suggests partially overlapping sets of DNase-I-hypersensitive sites (Fig. 2). Conceivably, the common site(s) might correlate with high-level δ expression (a feature of both lens and NR lentoids), while the differences might reflect the fact that (some) NR cells originally expressed only low levels of δ [78]. Could transdifferentiation involve some kind of 'overshoot' in the expression of such lens markers, since low levels seem to be tolerated in several non-lens tissues,

but high levels are appropriate only to lens?

The link between heat shock and post-transcriptional events (δ mRNA export and/or stabilisation) in late 199 cultures poses the following question; do HSPs bind directly to intranuclear δ mRNAs and move with them out into the cytoplasm? (It is known that HSPs do move from nucleus to cytoplasm during recovery from heat shock; [140]). The generality of such post-transcriptional controls over crystallin expression also remains to be clarified, both in lens and non-lens tissues.

Finally, the role of *c-src* expression in developing lens fibres requires more detailed exploration. Is pp60^{c-src} also expressed in lentoids derived *in vitro* from tapetum? Can *c-src*-substituted RSV stimulate lentoid development under appropriate NR culture conditions? Why indeed does *c-src* expression affect NR cells so differently from *v-src* expression [130, 137]? Some elucidation may be forthcoming from studies of quail NR cells transformed with ts-RSV or Mill Hill 2 viruses, which should provide homogeneous cell populations after a few subcultures. These will afford a unique opportunity to follow the time course of molecular events during transdifferentiation in a largely synchronous system [139].

ACKNOWLEDGEMENTS

The author is grateful to his associates (Mr. M. McLaughlin, Mr. M. Flor-Henry, Dr. K. Tobal and Dr. K. C. Perry) for permission to quote unpublished findings, and for many stimulating discussions in this field. The Cancer Research Campaign and SERC are thanked for financial support. Particular thanks are due to Dr. P. Linsler for the photographs in Fig. 1, to Mrs. R. M. Clayton for permission to use her data in Table 1, and to Mrs. E. O. Wigginton and Ms. J. Barton for typing the manuscript.

REFERENCES

- 1 Itoh, Y., Okada, T. S., Ide, H. and Eguchi, G. (1975) *Dev. Growth Differ.*, **17**: 39-50.
- 2 Okada, T. S., Itoh, T., Watanabe, K. and Eguchi, G. (1975) *Dev. Biol.*, **45**: 318-329.
- 3 Okada, T. S. (1980) *Curr. Topics Dev. Biol.*, **16**: 349-390.
- 4 Okada, T. (1983) *Cell Differ.*, **13**: 177-183.

- 5 Yamada, T. (1977) Control Mechanisms in Cell-type Conversions in Newt Lens Regeneration. (Monogr. Dev. Biol., ed. by A. Wolsky, Vol. 13), S. Karger, Basel.
- 6 Cuny, R., Jeanny, J.-C. and Courtois, Y. (1986) *Differentiation*, **32**: 221-229.
- 7 Borst, D. E., Di Rienzo, S. M. and McDevitt, D. S. (1981) *J. Cell Biol.*, **91** (supplement): 28a.
- 8 Yamada, T. and McDevitt, D. S. (1984) *Differentiation*, **27**: 1-12.
- 9 Kulyk, W. M. and Zalik, S. E. (1982) *Differentiation*, **23**: 29-35.
- 10 Eguchi, G., Abe, S. and Watanabe, K. (1974) *Proc. Natl. Acad. Sci. U.S.A.*, **71**: 5052-5056.
- 11 Eguchi, G. and Okada, T. S. (1973) *Proc. Natl. Acad. Sci. U.S.A.*, **70**: 1495-1499.
- 12 Bode, H., Dunne, J., Heinfeld, S., Huang, L., Javios, L., Koizumi, O., Westerfield, J. and Yaross, M. (1986) *Curr. Topics Dev. Biol.*, **20**: 257-280.
- 13 Schmid, V. and Adler, H. (1984) *Cell*, **38**: 801-809.
- 14 Schmid, V. and Adler, H. (1986) *Curr. Topics Dev. Biol.*, **20**: 117-135.
- 15 Okada, T. S. (1986) *Dev. Growth Differ.*, **28**: 213-221.
- 16 Weston, J. A. (1986) *Curr. Topics Dev. Biol.*, **20**: 195-210.
- 17 Rao, M. S., Scarpelli, D. G. and Reddy, J. K. (1986) *Curr. Topics Dev. Biol.*, **20**: 63-78.
- 18 Ide, H. (1986) *Curr. Topics Dev. Biol.*, **20**: 79-87.
- 19 Watanabe, K., Aoyama, H., Tamamaki, N., Yasujima, M., Nojyo, Y., Ueda, Y. and Okada, T. S. (1985) *Cell Differ.*, **16**: 251-257.
- 20 McDevitt, D. S. (1972) *Science*, **175**: 763-764.
- 21 Crisanti-Combes, P., Pessac, B. and Calothy, G. (1978) *Dev. Biol.*, **65**: 228-232.
- 22 Guerinot, F. and Pessac, B. (1979) *Brain Res.*, **162**: 179-183.
- 23 de Pomerai, D. I. and Carr, A. (1982) *Exp. Eye Res.*, **34**: 553-563.
- 24 de Pomerai, D. I., Kotecha, B., Flor-Henry, M., Fullick, C., Young, A. and Gali, M. A. H. (1983) *J. Embryol. Exp. Morphol.*, **77**: 201-220.
- 25 Linser, P. J. and Moscona, A. A. (1979) *Proc. Natl. Acad. Sci. U.S.A.*, **76**: 6476-6480.
- 26 de Pomerai, D. I., Carr, A., Soranson, J. and Gali, M. A. H. (1982) *Differentiation*, **22**: 6-11.
- 27 Linser, P. J. and Moscona, A. A. (1983) *Dev. Biol.*, **96**: 529-534.
- 28 Linser, P. J. and Moscona, A. A. (1981) *Proc. Natl. Acad. Sci. U.S.A.*, **78**: 7190-7194.
- 29 Vardimon, L., Fox, L. E. and Moscona, A. A. (1986) *Proc. Natl. Acad. Sci. U.S.A.*, **83**: 9060-9064.
- 30 Moscona, A. A., Brown, M., Degenstein, L., Fox, L. and Soh, B. M. (1983) *Proc. Natl. Acad. Sci. U.S.A.*, **80**: 7239-7243.
- 31 Clayton, R. M., Campbell, J. C. and Truman, D. E. S. (1968) *Exp. Eye Res.*, **7**: 11-29.
- 32 Clayton, R. M. (1974) In "The Eye", vol. 5. Ed. by H. Davson and L. T. Graham, Jr., Academic Press, New York & London, pp. 399-494.
- 33 Piatigorsky, J. (1984) *Cell*, **38**: 620-621.
- 34 Reszelbach, R., Shinohara, T. and Piatigorsky, J. (1977) *Exp. Eye Res.*, **25**: 583-593.
- 35 Thomson, I., Wilkinson, C. E., Burns, A. T. H., Truman, D. E. S. and Clayton, R. M. (1978) *Exp. Eye Res.*, **26**: 351-362.
- 36 Bhat, S. P. and Piatigorsky, J. (1979) *Proc. Natl. Acad. Sci. U.S.A.*, **76**: 3299-3303.
- 37 Bower, D. J., Errington, L. H., Wainwright, N. R., Sime, C., Morris, S. and Clayton, R. M. (1981) *Biochem. J.*, **201**: 339-344.
- 38 Hejtmancik, J. F. and Piatigorsky, J. (1983) *J. Biol. Chem.*, **258**: 3382-3387.
- 39 Nickerson, J. M. and Piatigorsky, J. (1984) *Proc. Natl. Acad. Sci. U.S.A.*, **81**: 2611-2615.
- 40 Yasuda, K., Nakajima, N., Isobe, T., Okada, T. S. and Shimura, Y. (1984) *EMBO J.*, **3**: 1397-1402.
- 41 Errington, L. H., Bower, J., Cuthbert, J. and Clayton, R. M. (1985) *Biol. Cell*, **54**: 101-108.
- 42 Yasuda, K. and Okada, T. S. (1986) *Oxford Surv. Eukaryotic Genes*, **3**: 183-209.
- 43 Ohno, M., Sakamoto, H., Yasuda, K., Okada, T. S. and Shimura, Y. (1985) *Nucleic Acids Res.*, **13**: 1593-1606.
- 44 Nickerson, J. M., Wawrousek, E. F., Hawkins, J. W., Wakil, A. S., Wistow, G. J., Thomas, G., Norman, B. L. and Piatigorsky, J. (1985) *J. Biol. Chem.*, **260**: 9100-9105.
- 45 Nickerson, J. M., Wawrousek, E. F., Borrás, T., Hawkins, J. W., Norman, B. L., Filpula, D. R., Nagle, J. W., Ally, A. H. and Piatigorsky, J. (1986) *J. Biol. Chem.*, **261**: 552-557.
- 46 Okazaki, K., Yasuda, K., Kondoh, H. and Okada, T. S. (1985) *EMBO J.*, **4**: 2589-2595.
- 47 Shinohara, T. and Piatigorsky, J. (1977) *Nature (Lond.)*, **270**: 406-411.
- 48 Borrás, T., Nickerson, J. M., Chepelinsky, A. B. and Piatigorsky, J. (1985) *EMBO J.*, **4**: 445-452.
- 49 Kondoh, H., Yasuda, K. and Okada, T. S. (1983) *Nature (Lond.)*, **301**: 440-442.
- 50 Hayashi, S., Kondoh, H., Yasuda, K., Soma, G., Ikawa, Y. and Okada, T. S. (1985) *EMBO J.*, **4**: 2201-2207.
- 51 Kondoh, H., Hayashi, S., Takahashi, T. and Okada, T. S. (1986) *Cell Differ.*, **19**: 151-160.
- 52 Hayashi, S. and Kondoh, H. (1986) *Mol. Cell Biol.*, **6**: 4130-4132.

- 53 Kondoh, H., Katoh, K., Takahashi, Y., Fujisawa, H., Yokoyama, M., Kimura, S., Saito, M., Nomura, T., Hiramoto, Y. and Okada, T. S. (1987) *Dev. Biol.*, **120**: 177-185.
- 54 Ozato, K., Kondoh, H., Inohara, H., Iwamatsu, T., Wakamatsu, Y. and Okada, T. S. (1986) *Cell Differ.*, **19**: 237-344.
- 55 Okada, T. S. (1977) *Dev. Growth Differ.*, **19**: 47-55.
- 56 Okada, T. S., Yasuda, K., Araki, M. and Eguchi, G. (1979) *Dev. Biol.*, **68**: 600-617.
- 57 de Pomerai, D. I. and Gali, M. A. H. (1981) *J. Embryol. Exp. Morphol.*, **62**: 291-308.
- 58 Shinde, S. L. and Eguchi, G. (1982) In "Problems of Normal and Genetically Abnormal Retinas". Ed. by R. M. Clayton, J. Haywood, H. W. Reading and A. Wright, Academic Press, London & New York, pp. 37-48.
- 59 Moscona, A. A. and Degenstein, L. (1980) *Cell Differ.*, **10**: 36-41.
- 60 de Pomerai, D. I., Takagi, S., Kondoh, H. and Okada, T. S. (1984) *Dev. Growth Differ.*, **26**: 111-119.
- 61 Kondoh, H., Takagi, S., Nomura, K. and Okada, T. S. (1983) *Roux' Arch. Dev. Biol.*, **192**: 256-261.
- 62 Jeanny, J.-C., Bower, D. J., Errington, L. H., Morris, S. and Clayton, R. M. (1985) *Dev. Biol.*, **112**: 94-99.
- 63 Clayton, R. M., Jeanny, J.-C., Bower, D. J. and Errington, L. H. (1986) *Curr. Topics Dev. Biol.*, **20**: 137-151.
- 64 Takagi, S. (1986) *Roux' Arch. Dev. Biol.*, **195**: 15-21.
- 65 Kodama, R. and Eguchi, G. (1982) *Dev. Biol.*, **91**: 221-226.
- 66 Barabanov, V. M. (1977) *Dokl. Akad. Nauk. SSSR*, **224**: 195-198.
- 67 Ueda, Y. and Okada, T. S. (1986) *Cell Differ.*, **19**: 179-185.
- 68 Nomura, K. (1982) *Differentiation*, **22**: 179-184.
- 69 Tsunematsu, Y. and Coulombre, A. J. (1981) *Dev. Growth Differ.*, **23**: 297-311.
- 70 Jackson, J. F., Clayton, R. M., Williamson, R., Thomson, I., Truman, D. E. S. and de Pomerai, D. I. (1978) *Dev. Biol.*, **65**: 383-395.
- 71 Clayton, R. M., Thomson, I. and de Pomerai, D. I. (1979) *Nature (Lond)*, **282**: 628-629.
- 72 de Pomerai, D. I. and Clayton, R. M. (1978) *J. Embryol. Exp. Morphol.*, **47**: 179-193.
- 73 Agata, K., Yasuda, K. and Okada, T. S. (1983) *Dev. Biol.*, **100**: 222-226.
- 74 Bower, D. J., Errington, L. H., Pollock, B. J., Morris, S. and Clayton, R. M. (1983) *EMBO J.*, **2**: 333-338.
- 75 Eguchi, G. (1986) *Curr. Topics Dev. Biol.*, **20**: 21-37.
- 76 Moscona, A. A., Fox, L., Smith, J. and Degenstein, L. (1985) *Proc. Natl. Acad. Sci. U.S.A.*, **82**: 5570-5573.
- 77 Hatfield, J. S., Skoff, R. P., Maisel, H. and Eng, L. (1984) *J. Cell Biol.*, **98**: 1895-1898.
- 78 Linsler, P. J. and Irvin, C. K. (1987) *Dev. Biol.*, **121**: 499-509.
- 79 Pritchard, D. J. (1986) *Foundations of Developmental Genetics*. Taylor Francis, London.
- 80 Saad, A. D., Soh, B. M. and Moscona, A. A. (1981) *Biochem. Biophys. Res. Comm.*, **98**: 701-708.
- 81 Okada, T. S., Nomura, K. and Yasuda, K. (1983) *Cell Differ.*, **12**: 85-92.
- 82 Yasuda, K., Okuyama, K. and Okada, T. S. (1983) *Cell Differ.*, **12**: 177-183.
- 83 Ophir, I., Moscona, A. A., Loya, N. and Ben-Shaul, Y. (1985) *Cell Differ.*, **17**: 149-157.
- 84 Ophir, I., Moscona, A. A. and Ben-Shaul, Y. (1983) *Cell Differ.*, **13**: 133-141.
- 85 Degenstein, L. and Moscona, A. A. (1986) *Exp. Eye Res.*, **43**: 93-102.
- 86 Clayton, R. M., de Pomerai, D. I. and Pritchard, D. J. (1977) *Dev. Growth Differ.*, **19**: 319-328.
- 87 Yasuda, K. (1979) *Dev. Biol.*, **68**: 618-623.
- 88 Itoh, Y. and Eguchi, G. (1986) *Cell Differ.*, **18**: 173-182.
- 89 Itoh, Y. and Eguchi, G. (1986) *Dev. Biol.*, **115**: 353-362.
- 90 Agata, K., Kondoh, H., Takagi, S., Nomura, K. and Okada, T. S. (1980) *Dev. Growth Differ.*, **22**: 571-577.
- 91 Pritchard, D. J., Clayton, R. M. and de Pomerai, D. I. (1978) *J. Embryol. Exp. Morphol.*, **48**: 1-21.
- 92 de Pomerai, D. I. and Clayton, R. M. (1980) *Dev. Growth Differ.*, **22**: 49-60.
- 93 de Pomerai, D. I. and Gali, M. A. H. (1981) *Dev. Growth Differ.*, **23**: 229-236.
- 94 de Pomerai, D. I. and Gali, M. A. H. (1982) *Dev. Biol.*, **93**: 534-538.
- 95 Karim, S. A. M., Flor-Henry, M. and de Pomerai, D. I. (1987) *Cell Differ.*, **22**: 29-46.
- 96 Karim, S. A. M. (1987) Ph.D. Thesis, University of Nottingham.
- 97 Takagi, S., Kondoh, H., Nomura, K. and Okada, T. S. (1983) *J. Embryol. Exp. Morphol.*, **73**: 97-109.
- 98 Gali, M. A. H. and de Pomerai, D. I. (1984) *Differentiation*, **25**: 238-246.
- 99 de Pomerai, D. I. and Gali, M. A. H. (1982) *Dev. Growth Differ.*, **24**: 233-243.
- 100 Gali, M. A. H. (1983) Ph. D. Thesis, University of Nottingham.
- 101 Thomson, I., Wilkinson, C. E., Jackson, J. E., de

- Pomerai, D. I., Clayton, R. M., Truman, D. E. S. and Williamson, R. (1978) *Dev. Biol.*, **65**: 372-382.
- 102 Thomson, I., de Pomerai, D. I., Jackson, J. F. and Clayton, R. M. (1979) *Exp. Cell Res.*, **122**: 73-81.
- 103 Thomson, I., Yasuda, K., de Pomerai, D. I., Clayton, R. M. and Okada, T. S. (1981) *Exp. Cell Res.*, **135**: 445-449.
- 104 de Pomerai, D. I., Pritchard, D. J. and Clayton, R. M. (1977) *Dev. Biol.*, **60**: 416-427.
- 105 Carr, A. and de Pomerai, D. I. (1985) *Dev. Biol.*, **111**: 119-128.
- 106 Bower, D. J., Errington, L. H., Cooper, D. N., Morris, S. and Clayton, R. M. (1983) *Nucleic Acids Res.*, **11**: 2513-2521.
- 107 Errington, L. H., Cooper, D. N. and Clayton, R. M. (1983) *Differentiation*, **24**: 33-38.
- 108 Grainger, R. M., Hazard-Leonards, R. M., Samaha, F., Hougan, L. M., Leek, M. R. and Thomsen, G. H. (1983) *Nature (Lond.)*, **306**: 88-91.
- 109 Sullivan, C. H. and Grainger, R. M. (1986) *Proc. Natl Acad. Sci. U.S.A.*, **83**: 329-333.
- 110 Bird, A. P. (1986) *Nature (Lond.)*, **321**: 209-213.
- 111 Burch, J. B. E. and Weintraub, H. (1983) *Cell*, **33**: 65-76.
- 112 Fritton, H. P., Igo-Kemenes, T., Nowock, J., Strech-Jurk, U., Theisen, M. and Sippel, A. E. (1984) *Nature (Lond.)*, **311**: 163-166.
- 113 McLaughlin, M. (1987) Ph. D. Thesis, University of Nottingham.
- 114 Kondoh, H. and Okada, T. S. (1986) *Curr. Topics Dev. Biol.*, **20**: 153-164.
- 115 Kondoh, H., Ueda, Y., Hayashi, S., Okazaki, K., Yasuda, K. and Okada, T. S. (1987) *Cell Differ.*, **20**: 203-207.
- 116 Schlessinger, M. J., Ashburner, M. and Tissieres, A. (1982) *Heat Shock: from Bacteria to Man*. Cold Spring Harbour Press.
- 117 Bishop, J. M. (1983) *Ann. Rev. Biochem.*, **52**: 301-354.
- 118 Ingolia, T. D. and Craig, E. A. (1982) *Proc. Natl. Acad. Sci. U.S.A.*, **79**: 2360-2364.
- 119 Crabbe, M. J. (1985) *Biosci. Rep.*, **5**: 167-174.
- 120 Kodama, R. and Eguchi, G. (1983) *Dev. Growth Differ.*, **25**: 261-270.
- 121 Yost, H. J. and Lindquist, S. (1986) *Cell*, **45**: 185-193.
- 122 Di Domenico, B. J., Bugaisky, G. E. and Lindquist, S. (1982) *Cell*, **31**: 593-603.
- 123 Carr, A. and de Pomerai, D. I. (1985) *Dev. Growth Differ.*, **27**: 435-445.
- 124 Collier, N. C. and Schlessinger, M. J. (1986) *Exp. Eye Res.*, **43**: 103-118.
- 125 Carr, A. (1985) Ph.D. Thesis, University of Nottingham.
- 126 de Pomerai, D. I. and Carr, A. (1987) *Dev. Growth Differ.*, **29**: 37-46.
- 127 Hejtmancik, J. F., Beebe, D. C., Ostrer, H. and Piatigorsky, J. (1985) *Dev. Biol.*, **109**: 72-81.
- 128 Heldin, C. H. and Westermark, B. (1984) *Cell*, **37**: 9-20.
- 129 Eguchi, G., Agata, K., Itoh, Y. H. and Itoh, Y. (1985) *Cell Differ.*, **16** (supplement): 127S.
- 130 Iba, H., Jove, R. and Hanafusa, H. (1985) *Mol. Cell. Biol.*, **5**: 2856-2859.
- 131 Sorge, L. K., Levy, B. T. and Maness, P. F. (1984) *Cell*, **36**: 249-257.
- 132 Fults, D. W., Towle, A. C., Lauder, J. M. and Maness, P.F. (1985) *Mol. Cell. Biol.*, **5**: 27-32.
- 133 Barnekow, A. and Bauer, H. (1984) *Biochim. Biophys. Acta*, **727**: 94-102.
- 134 Maness, P. F., Sorge, L. K. and Fults, D. W. (1986) *Dev. Biol.*, **117**: 83-89.
- 135 Cotton, P. C. and Brugge, J. S. (1983) *Mol. Cell. Biol.*, **3**: 1157-1162.
- 136 Vardimon, L., Fox, L. E. and Moscona, A. A. (1986) *Mol. Cell. Biol.*, **6**: 4109-4111.
- 137 Ellis, D. K., Carr, A. and de Pomerai, D. I. (1987) *Development*, **101**: 847-856.
- 138 Jones, R. E., de Feo, D. and Piatigorsky, J. (1981) *Vision Res.*, **21**: 5-9.
- 139 Simonneau, L., Crisanti, P., Lorinet, A. M., Alliot, F., Courtois, Y., Calothy, G. and Pessac, B. (1986) *Mol. Cell. Biol.*, **6**: 3704-3710.
- 140 Velazquez, J. M. and Lindquist, S. (1984) *Cell*, **36**: 655-662.

REVIEW

The Neurohypophysis of Cyclostomes as a Primitive Hypothalamic Center of VertebratesKAZUHIKO TSUNEKI¹*Department of Biology, Shimane University, Matsue,
Shimane 690, Japan*

INTRODUCTION

The function of the adenohipophysis of gnathostome vertebrates is regulated by the hypothalamus usually by means of releasing or inhibiting neurosecretory hormones (regulating hormones) liberated to portal vessels which irrigate the adenohipophysis. The activities of the pars intermedia of gnathostomes and of the pars distalis of teleost fishes also are regulated commonly by direct innervation of secretory cells. The region of the hypothalamus where regulating hormones are released to portal vessels (in non-teleostean gnathostomes) or delivered directly to the pars distalis (in teleosts) is called the median eminence [1]. Therefore, the median eminence is considered as a device where external and internal environmental information integrated in the hypothalamus is transferred to the central endocrine organ (adenohipophysis) in the form of neurosecretory regulating hormones. This information transfer system constitutes the most fundamental neuroendocrine integration circuit of gnathostome vertebrates and enables them to adapt appropriately to changing environments.

A related question of some interest is how such an information transfer system evolved in the ancestral vertebrates. Among living vertebrates, agnathan cyclostomes (hagfishes and lampreys) are the closest relatives to the ancestor of vertebrates

and therefore the hypothalamo-hypophysial region of these animals has been investigated by comparative endocrinologists who anticipated that the hypothalamo-hypophysial system of cyclostomes might represent the most primitive condition of the central neuroendocrine circuit of vertebrates. The present article reviews recent advances made in the study of the hypothalamo-hypophysial system in cyclostomes, with special attention focused on the median eminence as the essential component of this system. In recent years, Gorbman [2, 3] also has reviewed the characteristics of the cyclostome hypothalamo-hypophysial system. Various problems related to this topic have been reviewed by Gorbman [4] (on reproduction), Nozaki [5] (on immunocytochemistry in brain and pituitary), and Chiba and Honma [6] (on the brain ventricular system).

CHARACTERISTICS OF CYCLOSTOME NEUROHYPOPHYSIS*Hagfish*

The diencephalic region of the hagfish is shown in Figure 1. The hypothalamo-hypophysial system is also illustrated diagrammatically in Figure 2. The neurohypophysis is a flattened sac connected to the hypothalamus by a short neurohypophysial stalk. The lumen of the sac reaches the hypothalamic third ventricle. In the neurohypophysis, three regions may be distinguished topologically. The anterior dorsal wall is a region rostral to the stalk. The posterior dorsal wall is a region caudal to the

Received June 1, 1987

¹ Present address: Department of Biology, College of General Education, Osaka University, Toyonaka, Osaka 560, Japan.

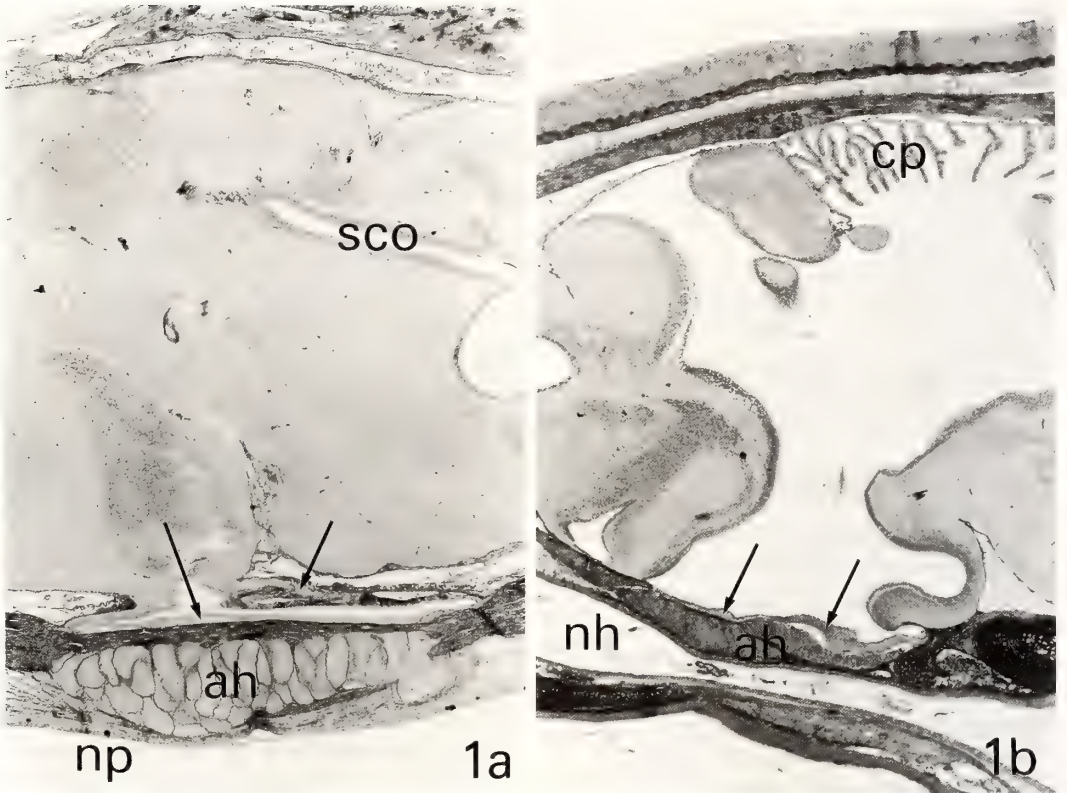


FIG. 1. a. Sagittal section of the diencephalon of the hagfish, *Eptatretus burgeri*. Arrows indicate the neurohypophysial sac. The adenohypophysis (ah) is embedded in connective tissue. The left side is rostral. np, nasopharyngeal duct; sco, subcommissural organ. $\times 33$. b. Sagittal section of the diencephalon of the brook lamprey, *Lampetra reissneri*. Arrows indicate the neurohypophysis. In contrast to the hagfish, the ventricle is spacious. The left side is rostral. ah, adenohypophysis; cp, mesencephalic choroid plexus; nh, nasohypophysial duct. $\times 43$.

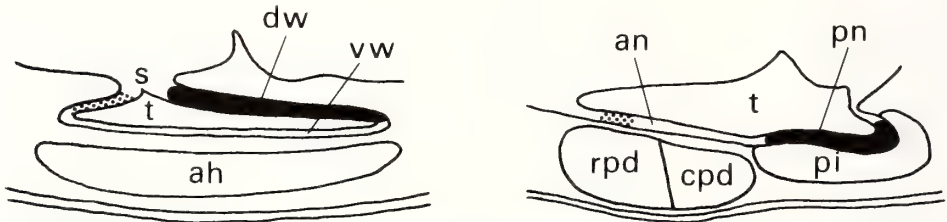


FIG. 2. Diagrammatic illustration of the pituitary region of the hagfish (left) and the lamprey (right). Black area is stained densely with paraldehyde fuchsin and dotted area is stained moderately with paraldehyde fuchsin. ah, adenohypophysis; an, anterior neurohypophysis; cpd, caudal pars distalis; dw, dorsal wall of the neurohypophysis; pi, pars intermedia; pn, posterior neurohypophysis (pars nervosa); rpd, rostral pars distalis; s, stalk; t, third ventricle; vw, ventral wall of the neurohypophysis.

stalk. The ventral wall constitutes the ventral region of the neurohypophysial sac. The wall of these three regions is rather thin and is composed of an ependymal layer and a subependymal nerve

fiber layer. The fiber layer of the posterior dorsal wall is densely stained by classical neurosecretory stains such as Gomori's paraldehyde fuchsin. The fiber layer of the anterior dorsal wall is moderately

stained with paraldehyde fuchsin and that of the ventral wall is not stained or only weakly and sporadically stained with paraldehyde fuchsin. Blood vessels are richly distributed around the dorsal surface of the posterior dorsal wall. The adenohypophysis is a flat disk composed of cell nests. It is located just under the neurohypophysis, being separated from it by a rather thick layer of connective tissue (about 50 to 60 μm in thickness in the Western Pacific hagfish, *Eptatretus burgeri*). The adenohypophysis does not differentiate a pars intermedia and most of its cells are chromophobic in traditional light microscopical stainings.

The hagfish hypothalamo-hypophysial system does not appear to have a median eminence-like structure at first glance. Nevertheless, some authors have sought to identify a possible hagfish median eminence. Thus, Olsson [7] in his light microscopical study tentatively identified the median eminence in the vascularized brain floor just rostral to the neurohypophysial stalk in the Atlantic hagfish, *Myxine glutinosa*. In the Eastern Pacific hagfish, *Eptatretus stouti*, Gorbman *et al.* [8] studied hypothalamo-hypophysial vascularization with an ink-injection method and found a prehypophysial vascular network (in the chiasmatic region) which is drained by a portal system to the caudodorsal wall of the neurohypophysis. The significance of this peculiar portal system was unknown. There appeared to be only a few vertical blood vessels connecting the ventral wall of the neurohypophysis with the adenohypophysis [8]. Later, in the same species, Nishioka and Bern [9] studied fine structure of the vascularized chiasmatic region and considered this area as a possible median eminence, although they could not detect neurosecretory axon terminals. Under these circumstances, it is fair to say that the median eminence of *M. glutinosa* or of *E. stouti* could not be sufficiently characterized to be identified with certainty.

In 1972, Kobayashi and Uemura [10] studied the ultrastructure of the neurohypophysial sac of *E. burgeri* and revealed many axon terminals containing secretory granules in the ventral wall of the neurohypophysial sac. They also found about 20 vertical blood vessels connecting the ventral wall

of the neurohypophysis with the adenohypophysis. The number of vertical blood vessels issuing from the ventral wall of the neurohypophysial sac appeared to be slightly higher in *E. burgeri* (a shallow-water inhabitant) than in *E. stouti* (a deep-water inhabitant). According to Kobayashi and Uemura [10], the axon terminals in the ventral wall of the neurohypophysis of *E. burgeri* could be classified into three types by the size of their granules (about 65, 80, and 110 nm in diameter). In the dorsal wall, axon terminals containing much larger granules were frequent. In gnathostomes, it was well known that the median eminence possesses axon terminals with granules predominantly smaller than 100 nm (probably containing regulating hormones and/or monoamines) and the neural lobe (pars nervosa) possesses axon terminals with granules predominantly much larger than 100 nm (probably containing neural lobe hormones such as arginine vasotocin). Encouraged by those findings, Kobayashi and Uemura [10] concluded that the ventral wall of the neurohypophysis of the hagfish is a structure comparable to the median eminence of gnathostomes and the dorsal wall represents the neural lobe. In *E. stouti*, Henderson [11] also revealed neurosecretory axon terminals in the ventral wall of the neurohypophysial sac. Following these electron microscopical works, it was histochemically demonstrated in *E. burgeri* that the fiber layer of the ventral wall contains acetylcholinesterase but that of the caudodorsal wall does not [12]. This histochemical study shows at least the difference in the neurotransmission mechanism between the ventral wall and the dorsal wall. Afterwards, with the aid of a computer, Tsuneki *et al.* [13] classified the secretory granules found in the ventral and dorsal walls of the neurohypophysis of *E. burgeri* and substantiated the theory of Kobayashi and Uemura [10] (Fig. 3).

The problem of whether the ventral wall of the hagfish neurohypophysis should be designated the median eminence depends on the definition of median eminence. If we adhere to the definition of the median eminence as a structure where portal vessels to the adenohypophysis originate, then the ventral wall of the hagfish neurohypophysis cannot be considered as the median eminence because of the absence of a typical portal system directed to

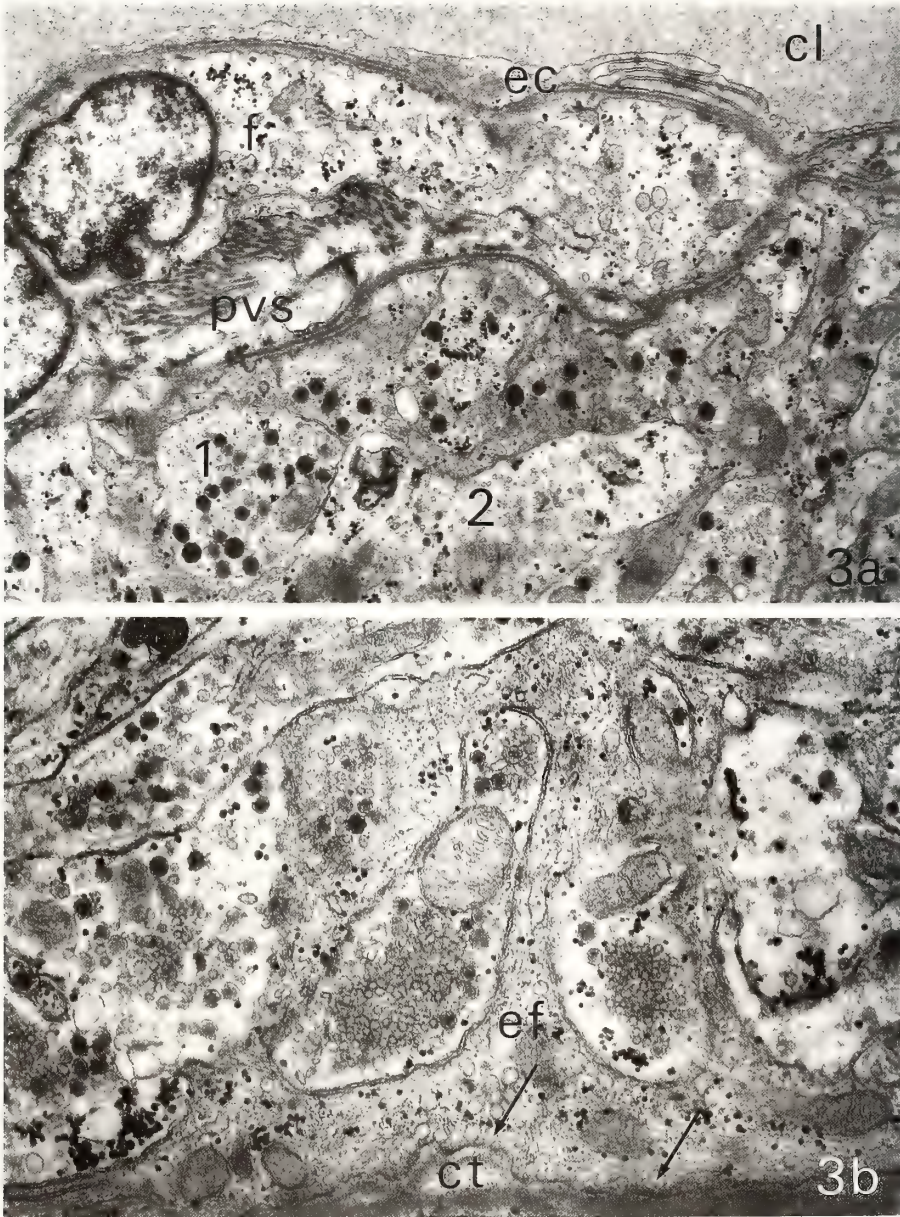


FIG. 3. a. Outer layer of the dorsal wall of neurohypophysis of the hagfish, *Eptatretus burgeri*. 1, type 1 axon containing granules from 140 to 200 nm in diameter; 2, type 2 axon containing granules from 80 to 95 nm; cl, capillary lumen; ec, endothelial cell; f, fibroblast-like cell; pvs, perivascular space. $\times 12,900$. b. Outer layer of the ventral wall of the neurohypophysis of the hagfish, *Eptatretus burgeri*. Neurosecretory axon terminals contain granules of about 85 to 110 nm in diameter. These terminals do not directly contact the underlying connective tissue (ct), but are interposed by ependymal end feet (ef). Arrows indicate small vacuoles in the ependymal end feet. $\times 24,000$.

the adenohypophysis. However, if the median eminence is considered as the region where neurosecretory axons other than those leaving for

the neural lobe terminate in the vicinity of the pars distalis, then the ventral wall of the hagfish neurohypophysis should be termed the median

eminence. In any event, there is no doubt that the ventral wall of the hagfish neurohypophysis represents a primitive median eminence-like structure, at least on anatomical grounds. If we do not consider the ventral wall of the neurohypophysial sac as the median eminence-equivalent region, then we cannot explain the existence of neurosecretory axon terminals in this region.

These morphological findings on the hagfish hypothalamo-hypophysial system prompted functional studies. Since the adenohipophysis is separated from the ventral wall of the neurohypophysis by a rather thick and poorly vascularized connective tissue, the problem arises of how the contents of the granules in the axon terminals in the ventral wall are delivered to the adenohipophysis. The most probable mechanism is by diffusion. Blood vessels located between the neurohypophysis and adenohipophysis may be involved in material transfer only to a limited extent because of their extremely small number compared to the median eminence of gnathostomes. The problem of diffusion in the hagfish was experimentally investigated by Kobayashi and his colleagues. In 1975, Nozaki *et al.* [14] found that intraventricularly injected peroxidase reaches the adenohipophysis through ependymal cells of the ventral wall of the neurohypophysis and the connective tissue layer. More recently, Tsukahara *et al.* [15] demonstrated that intraventricularly injected trypan blue reaches the connective tissue layer and ferric ions even penetrate into the adenohipophysial cells within ten minutes after injection. These studies clearly show that at least some substances can reach the adenohipophysis through diffusion across the connective tissue layer between the neurohypophysis and the adenohipophysis.

In *M. glutinosa*, European authors also have studied the relation between the neurohypophysis and the adenohipophysis. Fernholm [16] revealed a contact between the ventral wall of the neurohypophysis and the adenohipophysial tissue in 6.5% of the animals he examined. This anatomical relation is reminiscent of the close apposition between the neural lobe and the pars intermedia in lampreys and many gnathostomes. Schultz and Adam [17] and Schultz *et al.* [18] reported the occurrence of a few nerve terminals in the dorso-

lateral part of the adenohipophysis. Therefore, direct information transfer through innervation may also operate in some individuals but this system apparently plays a minor role if any. Lametschwandtner [19] studied the vascularization in the hypothalamo-hypophysial region with a corrosion cast method and confirmed the earlier ink-injection study by Gorbman *et al.* [8] that showed the absence of a typical portal system in *E. stouti*.

Recent immunohistochemical studies on the hagfish hypothalamo-hypophysial region have resulted in some odd findings. Although immunohistochemical studies of the distribution of arginine vasotocin yielded the same results as classical Gomori's staining [20, 21], the attempts to find immunoreactive LHRH, TRH, substance P, endorphin, α -MSH, and ACTH in tissue sections all failed to give positive results in the species so far studied [20–24]. With an immunological method, LHRH was detected in small amounts in extracts of the whole brain of the South African hagfish, *Eptatretus hexatrema* [27], but not in *E. stouti* [28]. Immunoreactive somatostatin does not exist in the neurohypophysis in *E. burgeri* and *E. stouti*, although it is demonstrable in the brain [20, 21]. Synthetic TRH had no effect on thyroidal activities either *in vivo* [25] or *in vitro* [26]. Peculiarly enough, there are no reports of the distribution of monoamine fluorescence in the hagfish neurohypophysis, although monoamine oxidase was histochemically detected in the ventral as well as the dorsal wall of the neurohypophysis [12]. Therefore, ultrastructurally demonstrable secretory granules in the axon terminals in the ventral wall are totally unknown as to their contents except for a few large granules (about 160 to 200 nm in diameter) probably containing arginine vasotocin. However, it is hardly conceivable that there are granules without any biologically active substances. They may contain substances which do not cross-react with the antisera currently used or are simply insufficient in amount to be detected immunocytochemically.

Gorbman [29, 30] reexamined the old Dean-Conel's preparation of embryos of *E. stouti* and demonstrated that the hagfish adenohipophysis is not of ectodermal origin, but instead it is peculiarly

of endodermal origin. However, no one could argue that the structure concerned is not the adenohipophysis (but see [31]). Although a FMRF-amide-like substance is the only substance so far successfully revealed immunocytochemically in the hagfish adenohipophysis [24], the adenohipophysis contains many secretory cells with electron-dense granules although the number of granules per cell is apparently small. In *M. glutinosa*, either two [32] or five [33] types of secretory cells have been demonstrated. In *E. burgeri*, three types of secretory cells are found [34, 35]. Bioassay experiments revealed ACTH-like and TSH-like activities in extracts of the pituitary of *E. stouti* [36, 37]. Hypophysectomy did not cause a significant change in thyroidal activity [38, 39], but it slightly interfered with the normal development of the gonad, especially in *E. burgeri* [40]. Therefore, the hagfish possesses a definite adenohipophysis, although it is apparently poorly differentiated both histologically and functionally.

Lamprey

The neurohipophysis of the lamprey forms the ventral floor of the third ventricle (Figs. 1 and 2). The posterior part of the neurohipophysis is densely stained with paraldehyde fuchsin except for ependymal cells. The ventral surface is covered with a capillary plexus and a pars intermedia. This portion of the neurohipophysis is frequently called the complete neurohipophysis, but actually it is a part of the neurohipophysis and corresponds to the neural lobe both topologically and in the paraldehyde fuchsin-stainability of nerve fibers which release their contents into the general circulation. The anterior part of the floor of the third ventricle also consists of an ependymal layer and a nerve fiber layer. This part of the neurohipophysis is usually called the infundibulum. It is separated from the underlying pars distalis by a layer of connective tissue which has a thickness of only about 2 to 8 μm in the non-parasitic brook lamprey, *Lampetra (Lethenteron) reissneri*. The rostral region of the anterior part of the neurohipophysis is moderately stained with paraldehyde fuchsin. Although the anterior part of the neurohipophysis is not vascularized [41], this region was compared to the median eminence of

gnathostomes topologically [10, 42]. This assertion is rather natural, because the relation between the neurohipophysis and the adenohipophysis in lampreys is anatomically similar to that in chondrosteans and holosteans in which the anterior part of the neurohipophysis forms an unequivocal median eminence [43]. The adenohipophysis of lampreys is composed of three regions; the rostral pars distalis, caudal (proximal) pars distalis, and pars intermedia. In contrast to the hagfish, there are many chromophilic cells, especially in the rostral pars distalis and pars intermedia.

The ultrastructure of the anterior part of the neurohipophysis (anterior neurohipophysis) was first studied in *Lampetra (Entosphenus) tridentata* [44]. This region contains many neurosecretory axon terminals. The predominant types of granules in the axons are 65 to 100, 95 to 140, and 140 to 220 nm in diameter, respectively. The axon terminals with the smaller granules are more frequently encountered than in the posterior neurohipophysis (neural lobe) where the predominant type of granules is about 160 to 200 nm in diameter. The axon terminals in the rostral region of the anterior neurohipophysis frequently abut on the basal lamina of connective tissue, while those in the caudal part of the anterior neurohipophysis mostly end on the intervening ependymal end feet. In the parasitic river lamprey, *Lampetra (Lethenteron) japonica*, neurosecretory axon terminals occasionally abut directly on the basal lamina of connective tissue even in the caudal part of the anterior neurohipophysis (unpublished). In the ventral wall of the neurohipophysis of the hagfish, ependymal end feet usually intervene between neurosecretory axon terminals and the basal lamina of connective tissue. (See Oota *et al.* [45] for the significance of ependymal intervention in release of neurosecretory materials.) In *Lampetra (Lampetra) fluviatilis*, Belenky *et al.* [46] also studied the ultrastructure of the anterior neurohipophysis (the "proximal neurosecretory contact region" in their terminology) and obtained essentially the same results as in *L. tridentata*. These ultrastructural characteristics of the lamprey anterior neurohipophysis may offer support for the earlier suggestion that this region might be the lamprey median eminence (Fig. 4). The surface

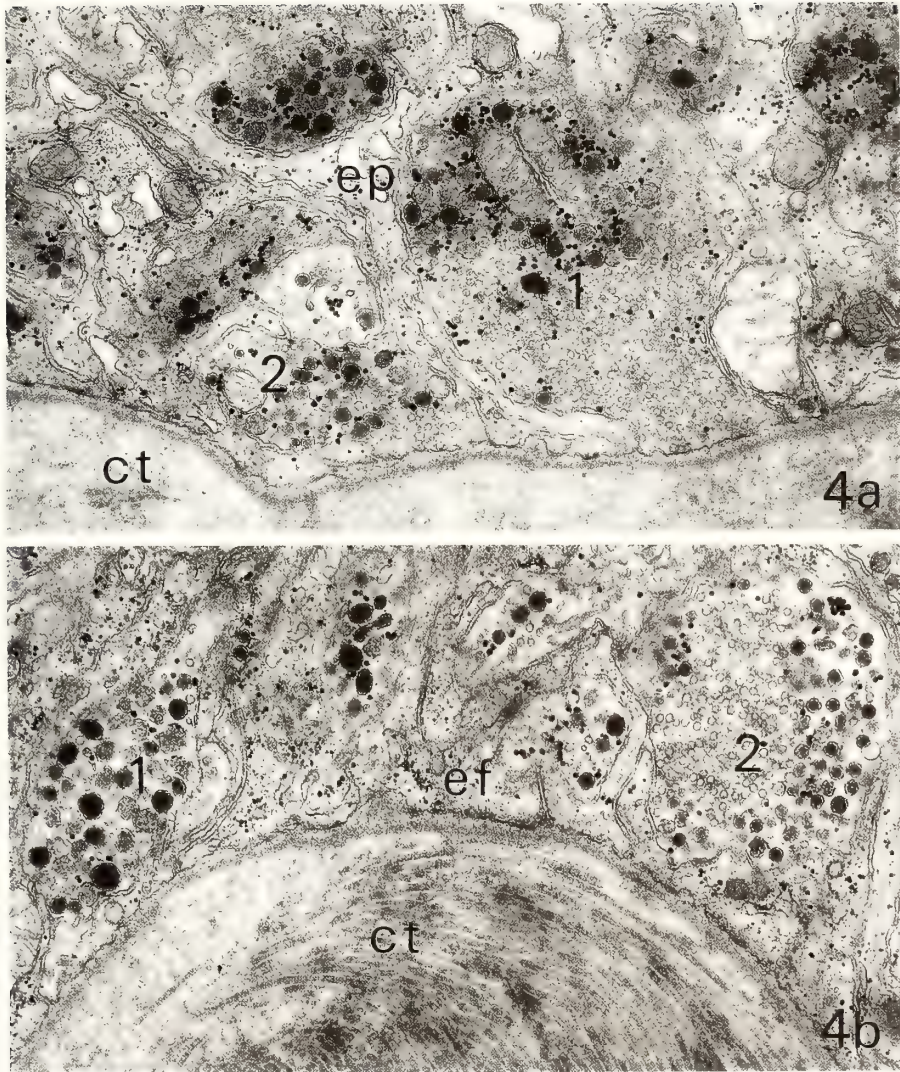


FIG. 4. a. Outer layer of the rostral part of the anterior neurohypophysis of the river lamprey, *Lampetra japonica*. Axon terminal 1 contains granules from 120 to 150 nm and axon terminal 2 contains granules from 110 to 130 nm in addition to numerous synaptic vesicles. These axon terminals directly abut on the basal lamina of connective tissue (ct). ep, ependymal process. $\times 20,300$. b. Outer layer of the caudal part of the anterior neurohypophysis of the lamprey, *Lampetra japonica*. Axon terminal 1 contains granules from 130 to 170 nm and axon terminal 2 contains granules from 85 to 110 nm. In the area shown, only ependymal end feet (ef) abut on the basal lamina of connective tissue (ct). $\times 20,300$.

fine structure of ependymal cells of the anterior neurohypophysis of the lamprey also differs from that of the neural lobe in the degree of ciliation [47]. The substances contained in the granules in the axon terminals of the anterior neurohypophysis may reach the adenohypophysis by diffusion through the thin connective tissue sheet, because

virtually no blood vessels exist between the anterior neurohypophysis and the pars distalis. Ultrastructural studies also did not reveal nerve fibers in the pars distalis [44] or the pars intermedia in *L. tridentata* and *L. fluviatilis* [48, 49]. In *L. japonica*, bundles of nerve fibers are found close to the pars intermedia, under the capillary plexus, but their

destination is not clear (unpublished). They are apparently rare and may play a minor role, if any, in the regulation of pars intermedia activity.

In lampreys, immunohistochemical distributions of biologically active substances in the hypothalamo-hypophysial region have been rather extensively studied. The neural lobe contains immunoreactive LHRH (in *L. japonica* and *L. tridentata*), met-enkephalin (in *L. tridentata*), growth hormone (in *Petromyzon marinus*), prolactin (in *P. marinus*), as well as arginine vasotocin (in *L. fluviatilis*) [22, 23, 50-52]. The rostral part of the anterior neurohypophysis contains immunoreactive arginine vasotocin (in *L. fluviatilis*), LHRH (in *L. japonica* and *P. marinus*), enkephalin (in *Lampetra (Lethenteron) lamottenii*), and substance P (in *P. marinus*) [23, 50, 53, 54]. The caudal part of the anterior neurohypophysis contains immunoreactive arginine vasotocin (in *L. fluviatilis*), LHRH (in *L. japonica* and *P. marinus*), and enkephalin (in *L. lamottenii*) [23, 50, 54]. The LHRH system is only faintly stained immunohistochemically in the ammocoetes larvae of *Lampetra (Lampetra) richardsoni* [55]. TRH and LHRH were also detected immunologically in the lamprey brain [28, 56]. However, the amino acid sequence of lamprey LHRH appears to be different from that of mammalian LHRH [28]. Monoamine fluorescence occurs in the anterior neurohypophysis as well as in the neural lobe [57, 58]. Although the intensity of fluorescence is stronger in the neural lobe, the histochemical activity of monoamine oxidase is stronger in the anterior neurohypophysis than in the neural lobe [59]. The presence of monoamines in the anterior neurohypophysis was further confirmed by autoradiographical study with ³H-dopamine [58]. Therefore, the median eminence-equivalent anterior neurohypophysis of lampreys is an active secretory organ at least in adults, as determined not only ultrastructurally but also immunohistochemically and by routine histochemistry.

Somatostatin is not detected in the neurohypophysis, but in *P. marinus* somatostatin-immunoreactive neurons are abundant in the ventral hypothalamus and they are liquor-contacting neurons [52]. (See [6] and papers cited therein for liquor-contacting neurons in lampreys.)

Based on this immunocytochemical observation, Wright [52] suggested the possibility that somatostatin is released into the third ventricle, is absorbed by ependymal cells, and reaches the pars distalis by diffusion through connective tissue. The differential distribution of secretory cells in the dorso-ventral direction in the rostral pars distalis in lampreys further supports the possibility of diffusion of hypothalamic substances [44]. Experimental studies on the hypothalamic regulation of adeno-hypophysial activity are scarce. Although the apparently normal functioning of heterotopically implanted pituitary in *L. fluviatilis* [60] appears discouraging, the effectiveness of exogenously administered LHRH in accelerating ovulation in *P. marinus* [61] may be encouraging for future research.

The highly secretory nature of the lamprey adeno-hypophysis is beyond doubt. Ultrastructurally, it contains several types of secretory cells with abundant granules [61-63]. Some cell types also possess abundant secretory granules even in larvae [63, 64]. Hypophysectomy experiments also revealed that the adeno-hypophysis is involved in the induction of secondary sex characters, spawning, color change, metamorphosis, and so on (reviewed in [60, 65], see also [66]). Immunocytochemical identification of secretory cell types is currently being actively pursued in *P. marinus* by Wright [52, 67, 68]. This topic is beyond the scope of this review and here it may be sufficient to note that there are TSH-like cells in the rostral pars distalis and LH-like, GH-like, and prolactin-like cells in the caudal pars distalis of the upstream migrants. Nozaki [5] summarized their studies on the immunocytochemical distribution of proopiomelanocortin-related peptides such as enkephalin, ACTH, and MSH in the lamprey adeno-hypophysis as well as other substances. According to him, there is some difference between *L. tridentata* and *P. marinus* and the interpretation of results are complicated although there are stainable cells. Proopiomelanocortin-related peptides also occur in the adeno-hypophysis of *L. lamottenii* [54]. In *Lampetra (Okkelbergia) aepyptera* and *L. fluviatilis*, bioassay experiments demonstrated ACTH-like activity in extracts of the lamprey adeno-hypophysis [69, 70].

These observations taken together suggest that the lamprey hypothalamo-hypophysial system is highly active compared to that of the hagfish and rather resembles that of gnathostomes. However, it must be emphasized that the lamprey anterior neurohypophysis (median eminence-equivalent region) is not supplied with portal vessels or any other kind of significant blood vessels.

EVOLUTIONARY PERSPECTIVES

As reviewed in the previous section, the median eminence-equivalent structure has been revealed ultrastructurally both in the hagfish and lamprey. In lampreys, immunohistochemical studies also demonstrated the presence of hypothalamic regulating hormones in this region. The adenohypophysis of both hagfish and lamprey is a secretory organ at least ultrastructurally. In lampreys, the adenohypophysis appears to be active also functionally. Therefore, the neurohypophysis-adenohypophysis relation seen in cyclostomes is fundamentally similar to that seen in gnathostomes. The most significant difference is the absence of portal circulation in cyclostomes. The virtually avascular or at most only sporadically vascularized median eminence-like organ of cyclostomes may represent the most ancient type of vertebrate median eminence and the neurosecretory regulating hormones might reach the adenohypophysis by diffusion at the stage before the development of portal vessels and direct innervation. It is unlikely that the condition in cyclostomes was brought about by degeneration from the stage where the neurohypophysis and adenohypophysis were intimately linked anatomically. Lampreys are fundamentally anadromous animals and reproduce only once at the end of their life cycle. Hagfishes are purely marine animals and they reproduce more than once in their life cycle. In spite of these basic differences in life strategy, the fundamental relation between the neurohypophysis and adenohypophysis is the same, that is, the common absence of typical portal vessels, in lampreys and hagfishes. Therefore, this condition is better interpreted as primitive rather than degenerate. Immunohistochemical failure in detecting biologically active substances in the hagfish

hypothalamo-hypophysial region is usually explained by degenerative condition of these animals living in the deep sea under constant temperature and continuous darkness. However, it is zoological nonsense to claim that the hagfish is more degenerate than protochordates (see below). The basic hagfish should be sought in shallow water species such as *E. burgeri*. *M. glutinosa* is apparently degenerate compared to *E. burgeri*. *E. burgeri* is a strictly seasonal breeder [71-73] and shows a distinct nocturnal activity rhythm [74, 75]. They are highly voracious and active animals, and do not look degenerate although they are certainly specialized to some extent in their burrowing habit. The apparent poor development of the hagfish hypothalamo-hypophysial system may be explained not by degeneration, but by primitiveness associated with some specialization.

It is a current popular belief that the lamprey and hagfish are very different animals with totally different lineages and the difference in the hypothalamo-hypophysial system is taken as one piece of evidence supporting this interpretation (see [76] for references). In a variety of animal taxa, the primitive group frequently shows greater morphological diversity than the advanced group, but such diversity should not be necessarily taken as the evidence of di- or polyphyletic origin of the primitive group. The old concept that the cyclostomes constitute a monophyletic group should be reexamined [77], although the virtually avascular median eminence apparently represents sympleosiomorphy.

Finally, it may be asked how the hypothalamo-hypophysial relations in vertebrates originated. Two possibilities may exist; first, the hypothalamo-hypophysial system evolved as an entirety, and second, the pituitary independently developed and later it was incorporated under hypothalamic influence. As far as the embryologically intimate relation between the hypothalamus and the pituitary is concerned, the first possibility seems to be more likely. The embryological relation between these two organs may be more profound than usually considered, because the hypothalamo-hypophysial unit actually appears as a real unit from the neuroectodermal ventral neural ridge in the chick [78]. The development of the unsepara-

ble hypothalamo-hypophysial system as a central information transfer system might be one of the factors that endowed the original vertebrates with the great possibility for future development and more elaborate refinement of this system might have opened the way for the original gnathostomes to vast prosperity. However, it is unknown how the relation between the central nervous system and the central endocrine organ developed during the transition from the invertebrate level of body organization to the vertebrate level of organization. A possible clue might be sought in extant protochordates, but the evidence is equivocal.

In amphioxus, the epithelial cells of Hatschek's pit, a possible homologue of the vertebrate adenohypophysis, possess secretory granules [79]. Hatschek's pit also is claimed to contain immunoreactive LH [80]. It originates from the preoral pit of larvae, although the real germinal origin of Hatschek's pit itself is unclear. In adults, Hatschek's pit is located below the notochord on the right side in the oral vestibule and is rather remote from the brain vesicle although the ventral area of the brain vesicle contains neurosecretory axon terminals [81]. A detailed study of the vascular system around the brain vesicle and Hatschek's pit is not available, but the small size of amphioxus might make diffusion workable in transporting material as well as the involvement of blood vessels. Nerve fibers may occur in Hatschek's pit but the terminals have not been conclusively demonstrated [79, 82].

In ascidians, both the neural gland and the cerebral ganglion appear to develop from the neural tube of larvae during metamorphosis [83]. Therefore, they are probably ectodermal in origin and develop together as the hypothalamo-hypophysial unit of the chick. In adults, the neural gland directly abuts on the cerebral ganglion either dorsally or ventrally. In ascidians, the circulatory system is of the open type and diffusion across sparse connective tissue may be important in transporting materials. Recent immunocytochemical studies have demonstrated various biologically active substances, including LHRH and somatostatin, in the cerebral ganglion of ascidians [84, 85]. Pestarino reported in a series of papers [86-88] that the neural gland of *Styela plicata*

contains immunoreactive ACTH, MSH, prolactin, and so on. Therefore, the cerebral ganglion-neural gland complex of ascidians appears to be more developed immunocytochemically than the hypothalamo-hypophysial system of the hagfish. However, the presence of various biologically active substances in the ascidian neural gland is somewhat puzzling, because the cells of the neural gland do not contain secretory granules at the ultrastructural level at least in *Ciona intestinalis* [89].

These studies in protochordates are intriguing in themselves, but do not necessarily solve the problem of the origin of the hypothalamo-hypophysial system of vertebrates. Neither ascidians nor amphioxus (Acrania) possess a head. The head supplied with several sensory organs and a complex central nervous system is a prerequisite for the emergence of active animals such as vertebrates. The development of the hypothalamo-hypophysial system as a central information transfer system must have waited for the development of a complex head during the transition from invertebrates to vertebrates.

ACKNOWLEDGMENT

I would like to express my sincere thanks to Prof. H. Kobayashi for his reading of the manuscript. My works cited in this review indeed were carried out under his guidance. I would like to thank also Dr. S. R. Vigna for reading the manuscript and Prof. M. Ouji for his continuous advice and encouragement.

REFERENCES

- 1 Kobayashi, H., Matsui, T. and Ishii, S. (1970) *Int. Rev. Cytol.*, **29**: 281-381.
- 2 Gorbman, A. (1980) *Can. J. Fish. Aquat. Sci.*, **37**: 1680-1686.
- 3 Gorbman, A. (1980) In "Hormones, Adaptation and Evolution". Ed. by S. Ishii, T. Hirano and M. Wada, Japan Sci. Soc. Press, Tokyo, pp. 81-92.
- 4 Gorbman, A. (1983) In "Fish Physiology, IX-A". Ed. by W. S. Hoar, D. J. Randall and E. M. Donaldson, Academic Press, Orlando, pp. 1-29.
- 5 Nozaki, M. (1985) In "Evolutionary Biology of Primitive Fishes". Ed. by R. E. Foreman, A. Gorbman, J. M. Dodd and R. Olsson, Plenum Press, New York, pp. 433-454.
- 6 Chiba, A. and Honma, Y. (1986) In "Indo-Pacific

- Fish Biology". Ed. by T. Uyeno, R. Arai, T. Taniuchi and K. Matsuura, Ichthyol. Soc. of Japan, Tokyo, pp. 76-85.
- 7 Olsson, R. (1959) *Z. Zellforsch.*, **51**: 97-107.
 - 8 Gorbman, A., Kobayashi, H. and Uemura, H. (1963) *Gen. Comp. Endocrinol.*, **3**: 505-514.
 - 9 Nishioka, R. S. and Bern, H. A. (1966) *Gen. Comp. Endocrinol.*, **7**: 457-462.
 - 10 Kobayashi, H. and Uemura, H. (1972) *Gen. Comp. Endocrinol.*, Suppl. 3: 114-124.
 - 11 Henderson, N. E. (1972) *Acta Zool. (Stockh.)*, **53**: 243-266.
 - 12 Tsuneki, K., Urano, A. and Kobayashi, H. (1974) *Gen. Comp. Endocrinol.*, **24**: 249-256.
 - 13 Tsuneki, K., Adachi, T., Ishii, S. and Oota, Y. (1976) *Cell Tissue Res.*, **166**: 145-157.
 - 14 Nozaki, M., Fernholm, B. and Kobayashi, H. (1975) *Acta Zool. (Stockh.)*, **56**: 265-269.
 - 15 Tsukahara, T., Gorbman, A. and Kobayashi, H. (1986) *Gen. Comp. Endocrinol.*, **61**: 348-354.
 - 16 Fernholm, B. (1972) *Gen. Comp. Endocrinol.*, Suppl. 3: 1-10.
 - 17 Schultz, H. J. and Adam, H. (1975) *Norw. J. Zool.*, **23**: 297-306.
 - 18 Schultz, H. J., Patzner, R. A. and Adam, H. (1979) *Cell Tissue Res.*, **204**: 67-75.
 - 19 Lametschwandner, A. (1982) *Mikroskopie (Wien)*, **39**: 35-42.
 - 20 Nozaki, M. and Gorbman, A. (1983) *Cell Tissue Res.*, **229**: 541-550.
 - 21 Tsukahara, T., Shioda, S., Nakai, Y. and Kobayashi, H. (1983) *Zool. Mag. (Tokyo)*, **92**: 386-392.
 - 22 Crim, J. W., Urano, A. and Gorbman, A. (1979) *Gen. Comp. Endocrinol.*, **37**: 294-305.
 - 23 Nozaki, M. and Kobayashi, H. (1979) *Arch. Histol. Jpn.*, **42**: 201-219.
 - 24 Jirikowski, G., Erhart, G., Grimmelikhuijzen, C. J. P., Triepel, J. and Patzner, R. A. (1984) *Cell Tissue Res.*, **237**: 363-366.
 - 25 Tsuneki, K. and Fernholm, B. (1975) *Acta Zool. (Stockh.)*, **56**: 61-65.
 - 26 Dickhoff, W. W., Crim, J. W. and Gorbman, A. (1978) *Gen. Comp. Endocrinol.*, **35**: 96-98.
 - 27 King, J. A. and Millar, R. P. (1980) *Endocrinology*, **106**: 707-717.
 - 28 Sherwood, N. M. and Sower, S. A. (1985) *Neuropeptides*, **6**: 205-214.
 - 29 Gorbman, A. (1983) *Am. Zool.*, **23**: 639-654.
 - 30 Gorbman, A. and Tamarin, A. (1985) In "Evolutionary Biology of Primitive Fishes". Ed. by R. E. Foreman, A. Gorbman, J. M. Dodd and R. Olsson, Plenum Press, New York, pp. 165-185.
 - 31 Dodd, J. M. and Dodd, M. H. I. (1985) In "Evolutionary Biology of Primitive Fishes". Ed. by R. E. Foreman, A. Gorbman, J. M. Dodd and R. Olsson, Plenum Press, New York, pp. 295-319.
 - 32 Fernholm, B. (1972) *Z. Zellforsch.*, **132**: 451-472.
 - 33 Patzner, R. A., Erhart, G. and Adam, H. (1982) *Cell Tissue Res.*, **223**: 583-592.
 - 34 Oota, Y. (1974) *Rep. Fac. Sci., Shizuoka Univ.*, **9**: 67-78.
 - 35 Tsuneki, K. (1976) *Acta Zool. (Stockh.)*, **57**: 137-146.
 - 36 Buckingham, J. C., Leach, J. H., Plisetskaya, E., Sower, S. A. and Gorbman, A. (1985) *Gen. Comp. Endocrinol.*, **57**: 434-437.
 - 37 Dickhoff, W. W. and Gorbman, A. (1977) *Gen. Comp. Endocrinol.*, **31**: 75-79.
 - 38 Henderson, N. E. (1976) *Can. J. Zool.*, **54**: 180-184.
 - 39 Matty, A. J., Tsuneki, K., Dickhoff, W. W. and Gorbman, A. (1976) *Gen. Comp. Endocrinol.*, **30**: 500-516.
 - 40 Patzner, R. A. and Ichikawa, T. (1977) *Zool. Anz. (Jena)*, **199**: 371-380.
 - 41 Gorbman, A. (1965) *Arch. Anat. Microsc. Morphol. Exp.*, **54**: 163-194.
 - 42 Rühle, H.-J. and Sterba, G. (1966) *Z. Zellforsch.*, **70**: 136-168.
 - 43 Hansen, G. N. (1971) *Kong. Dans. Vidensk. Selsk. Biol. Skr.*, **18**: 1-64.
 - 44 Tsuneki, K. and Gorbman, A. (1975) *Gen. Comp. Endocrinol.*, **25**: 487-508.
 - 45 Oota, Y., Kobayashi, H., Nishioka, R. S. and Bern, H. A. (1974) *Neuroendocrinology*, **16**: 127-136.
 - 46 Belenky, M. A., Konstantinova, M. S. and Polenov, A. L. (1979) *Cell Tissue Res.*, **204**: 319-331.
 - 47 Shioda, S., Honma, Y., Yoshie, S. and Hosoya, Y. (1977) *Arch. Histol. Jpn.*, **40**: 41-49.
 - 48 Tsuneki, K. and Gorbman, A. (1975) *Cell Tissue Res.*, **157**: 165-184.
 - 49 Polenov, A. L., Belenky, M. A. and Konstantinova, M. S. (1974) *Cell Tissue Res.*, **150**: 505-519.
 - 50 Goossens, N., Dierickx, K. and Vandesande, F. (1977) *Cell Tissue Res.*, **177**: 317-323.
 - 51 Nozaki, M. and Gorbman, A. (1984) *Gen. Comp. Endocrinol.*, **53**: 335-352.
 - 52 Wright, G. M. (1986) *Cell Tissue Res.*, **246**: 23-31.
 - 53 Nozaki, M. and Gorbman, A. (1986) *Gen. Comp. Endocrinol.*, **62**: 217-229.
 - 54 Dores, R. M., Finger, T. E. and Gold, M. R. (1984) *Cell Tissue Res.*, **235**: 107-115.
 - 55 Crim, J. W., Urano, A. and Gorbman, A. (1979) *Gen. Comp. Endocrinol.*, **38**: 290-299.
 - 56 Jackson, I. M. D. and Reichlin, S. (1974) *Endocrinology*, **95**: 854-862.
 - 57 Tsuneki, K., Kobayashi, H., Yanagisawa, M. and Bando, T. (1975) *Cell Tissue Res.*, **161**: 25-32.
 - 58 Belenky, M. A., Chetverukhin, V. K. and Polenov,

- A. L. (1979) *Cell Tissue Res.*, **204**: 333-342.
- 59 Tsuneki, K. (1974) *Cell Tissue Res.*, **154**: 17-27.
- 60 Larsen, L. O. and Rothwell, B. (1972) In "The Biology of Lampreys, 2". Ed. by M. W. Hardisty and I. C. Potter, Academic Press, London, pp. 1-67.
- 61 Sower, S. A., Dickhoff, W. W., Gorbman, A., Rivier, J. E. and Vale, W. W. (1983) *Can. J. Zool.*, **61**: 2653-2659.
- 62 Båge, G. and Fernholm, B. (1975) *Acta Zool. (Stockh.)*, **56**: 95-118.
- 63 Percy, R., Leatherland, J. F. and Beamish, F. W. H. (1975) *Cell Tissue Res.*, **157**: 141-164.
- 64 Wright, G. M. (1983) *J. Morphol.*, **176**: 325-339.
- 65 Hardisty, M. W. and Baker, B. I. (1982) In "The Biology of Lampreys, 4B". Ed. by M. W. Hardisty and I. C. Potter, Academic Press, London, pp. 1-115.
- 66 Joss, J. M. P. (1985) *Gen. Comp. Endocrinol.*, **60**: 58-62.
- 67 Wright, G. M. (1983) *Cell Tissue Res.*, **230**: 225-228.
- 68 Wright, G. M. (1984) *Gen. Comp. Endocrinol.*, **55**: 269-274.
- 69 Eastman, J. T. and Portanova, R. (1982) *Gen. Comp. Endocrinol.*, **47**: 346-350.
- 70 Baker, B. I. and Buckingham, J. C. (1983) *Gen. Comp. Endocrinol.*, **52**: 283-290.
- 71 Kobayashi, H., Ichikawa, T., Suzuki, H. and Sekimoto, M. (1972) *Jpn. J. Ichthyol.*, **19**: 191-194.
- 72 Patzner, R. A. (1978) *Acta Zool. (Stockh.)*, **59**: 57-61.
- 73 Tsuneki, K., Ouji, M. and Saito, H. (1983) *Jpn. J. Ichthyol.*, **29**: 429-440.
- 74 Fernholm, B. (1974) *Mar. Biol.*, **27**: 351-356.
- 75 Ooka-Souda, S., Kabasawa, H. and Kinoshita, S. (1985) *Zool. Sci.*, **2**: 749-754.
- 76 Hardisty, M. W. (1982) In "The Biology of Lampreys, 4B". Ed. by M. W. Hardisty and I. C. Potter, Academic Press, London, pp. 165-259.
- 77 Yalden, D. W. (1985) *Zool. J. Linn. Soc.*, **84**: 291-300.
- 78 Takor, T. T. and Pearse, A. G. E. (1975) *J. Embryol. Exp. Morphol.*, **34**: 311-325.
- 79 Tjoa, L. T. and Welsch, U. (1974) *Cell Tissue Res.*, **153**: 175-187.
- 80 Zhiyi, Z., Yitao, Z. and Dayuan, C. (1982) *Kexue Tongbao*, **27**: 1233-1234.
- 81 Obermüller-Wilén, H. (1979) *Acta Zool. (Stockh.)*, **60**: 187-196.
- 82 Welsch, L. T. and Welsch, U. (1978) *Zool. Jb. Anat.*, **100**: 564-578.
- 83 Elwyn, A. (1937) *Bull. Neurol. Inst. N. Y.*, **6**: 163-177.
- 84 Georges, D. and Dubois, M. P. (1980) *C. R. Acad. Sci. Paris*, **D290**: 29-31.
- 85 Fritsch, H. A. R., Van Noorden, S. and Pearse, A. G. E. (1982) *Cell Tissue Res.*, **223**: 369-402.
- 86 Pestarino, M. (1984) *Gen. Comp. Endocrinol.*, **54**: 444-449.
- 87 Pestarino, M. (1985) *Cell Tissue Res.*, **240**: 497-500.
- 88 Pestarino, M. (1985) *Gen. Comp. Endocrinol.*, **60**: 293-297.
- 89 Lane, N. J. (1971) *Z. Zellforsch.*, **120**: 80-93.

Hypersensitivity after Offset of Adapting Light in Vertebrate Photoreceptors

KATSU AZUMA

Department of Biology, Osaka Medical College, Sawaragicho 2-41, Takatsuki, Osaka 569, Japan

ABSTRACT—Bullfrog and albino rat retinas were superfused with physiological solutions containing chemicals in order to suppress slow component (slow PIII) of distal PIII. Twenty μM of $[\text{Ba}^{2+}]$ in the superfusate suppressed the slow PIII of frog, but concentration of higher than 500 μM was required to suppress that of rat. A gliotoxin, L- α amino adipate (L- α AA), abolished the b-waves of both frog and rat and the slow PIII of frog. However, the gliotoxin did not suppress the slow PIII of rat. Measurements of the fast PIII isolated by these chemicals and of the light-induced decrease of $[\text{K}^+]_o$ were carried out in frog retina with Ag/AgCl electrodes and K^+ -selective microelectrodes, respectively. At 0.09 mM $[\text{Ca}^{2+}]_o$ (low Ca) or in the presence of 50 μM IBMX (phosphodiesterase inhibitor), the amplitude of fast PIII in the early dark after the offset of adaptation light was larger than that in the initial dark (called hypersensitivity). The hypersensitivity observed at low Ca was suppressed by reducing $[\text{Na}^+]_o$.

The low Ca or IBMX induced a remarkable overshoot of $[\text{K}^+]_o$ at the offset of the adaptation light. A decrease of $[\text{K}^+]_o$ induced by a light flash was remarkable in the dark after the offset of the adaptation light at low Ca or in the presence of IBMX. The hypersensitivity of rat photoreceptors was investigated by measuring distal PIII or fast PIII isolated by a capacity-coupled method. It was confirmed that low Ca or IBMX could induce the hypersensitivity of photoreceptors of rat.

INTRODUCTION

It has been generally accepted that visual sensitivity decreases in light (light adaptation) and subsequently recovers in the dark (dark adaptation) in photoreceptors of both invertebrates and vertebrates. Several authors, however, have reported an unusual adaptive property of invertebrate photoreceptors, i. e., an enhancement of sensitivity after the offset of adapting light. This phenomenon has been named facilitation [1, 2]. On the other hand, no similar phenomenon has been found at normal condition in vertebrates. However, when an isolated frog retina was superfused with low Ca solution, the photoreceptors exhibited an increase of sensitivity in the dark after the offset of adaptation light. This phenomenon has been called "hypersensitivity" by Azuma and Azuma [3]. On the basis of experiments using

stimuli and adapting lights of different wavelengths, Azuma and Azuma [3, 4] have suggested that the hypersensitivity is mainly due to red rods. A phenomenon like hypersensitivity was briefly reported in an isolated skate retina [5] and confirmed in a frog retina [6]. Furthermore we found that IBMX could induce hypersensitivity even in normal $[\text{Ca}^{2+}]_o$ [4]. As these inhibitors have been reported to change the response properties of photoreceptors [7], studies on hypersensitivity may give useful information about visual excitation and adaptation.

In the previous experiments [3, 4], we measured the transretinal potential of the frog by the following methods and assumed it as a receptor potential. The distal PIII was separated by an aspartate treatment from frog ERG [8, 9], led off by means of extracellular Ag/AgCl electrodes and capacity-coupled with 0.3-1 sec time constant in order to eliminate the slow PIII which originated in Müller cells [10, 11]. Recently it has been reported that the slow PIII is suppressed in the

presence of Ba^{2+} [12, 13]. The suppression of slow PIII by Ba^{2+} is due to its blocking effect on the $g_K(K^+$ -conductance) of Müller cells [13]. On the other hand, several authors have reported of the gliotoxic effects of L- α amino adipate (L- α AA). When the reagent was applied to the isolated retina of skate [14] or, was intravitreally injected to the eyes of frog [15], chicken [15, 16] and rat [17], the loss of ERG (b-waves) with the extensive damage of Müller cell structures was observed. Therefore, in this study, we tried to eliminate the slow PIII of frogs and of albino rats by the treatments of Ba^{2+} and L- α AA instead of capacity-coupled method [3, 4], and reexamined the phenomenon of hypersensitivity.

In this paper, we have also examined the effects of $[Na^+]_o$ on the hypersensitivity, and measured $[K^+]_o$ in the interstitial space of frog retina as the first step to elucidate ionic mechanism of hypersensitivity. Furthermore, we have used albino rat retinas whose photoreceptors are mainly rods. It is interesting whether hypersensitivity is observed or not in mammalian retina. All the present results support our hypothesis that hypersensitivity is caused by the increase of Na^+ -gradient across rod photoreceptor membrane [3].

MATERIALS AND METHODS

Measurements of transretinal potentials of frog and rat

Adult bullfrogs (*Rana catesbeiana*) and albino rats (100–150 g) were dark adapted overnight. The frogs were pithed and the rats were anesthetized with diethylether. The eye balls of these animals were enucleated under dim red light. In order to measure transretinal photoreceptor potential, retinas were isolated from the eye balls. The isolated retina was spread on a piece of nylon mesh and inserted into a superfusion chamber (a gift from Prof. W. Sickel of Cologne Univ.). Transretinal photoresponses were led off by means of Ag/AgCl electrodes embedded in the chamber and amplified by a FET instrumentation amplifier (Teledyne Philbrick 4253).

Measurements of $[K^+]_o$ of frog retina

In order to measure the interstitial $[K^+]_o$ of the frog isolated retina, it was fixed receptor-side up in a small chamber that had a transparent bottom. This chamber was set on the stage of an inverted microscope. The interstitial $[K^+]_o$ was measured by K^+ -selective double-barrelled microelectrodes and a differential electrometer (WPI FD-223). The microelectrode was prepared following the method described by Fujimoto and Kubota [18]. One barrel was an ion-selective electrode and contained a K^+ -selective liquid exchanger (WPI, IE-190) in the tip, and the remainder of this barrel was filled with 1 M KCl. The other barrel was a reference electrode filled with 1 M LiCl. The K^+ -selective microelectrode was advanced toward the receptor surface of the retina from above by using a hydraulic microdrive, until the electrode tip touched the surface. The electrode then was advanced in a few μm steps, and its tip was positioned at the depth where the amplitude of the light-evoked decrease in $[K^+]_o$ was maximal. Immediately after an experiment, the K^+ -selective microelectrode was calibrated using solutions having various $[K^+]$ and a fixed background of 110 mM $[Na^+]$. Using the calibration data and the log-linear, least-squared error regression analysis [19], parameters (A and S) of the following equation were obtained: $V_{K^+} = A \cdot \log_{10}([K^+]_o + [Na^+]_o/S) + V_o$, where V_{K^+} is the differential potential between the two barrels (K^+ -selective barrel positive), A is the logarithmic slope and S is the selectivity coefficient for K^+ over Na^+ , and V_o is a constant. The value of A was 55–58 mV/decade, and S was about 50. V_{K^+} referenced to an Ag/AgCl electrode was displayed on an oscilloscope (Sony/Tektronix Corp. 5103N) and recorded permanently on a pen recorder (TOA Electronics LTD., FBR-252A) through a transient memory (Kawasaki Electronica Co., Ltd., HR-1200).

Solutions of superfusion (superfusates)

The superfusate of frog retina (pH 7.6) contained 80 mM NaCl, 2.5 mM KCl, 25 mM $NaHCO_3$, 1.2 mM $MgCl_2$, 25 mM glucose, 3 mM HEPES and an appropriate concentration of

CaCl_2 . The superfusate of rat retina was almost the same as that of the frog retina, except for the concentration of NaCl (110 mM) and KCl (5 mM). A low $[\text{Na}^+]$ superfusate was prepared by the equimolar substitution of choline-chloride instead of NaCl . In order to suppress slow PIII, L - α AA or BaCl_2 with Na-aspartate was used. The superfusate was run off at the rate of 1 ml/min. The temperature of the superfusate was maintained at $21 \pm 1^\circ\text{C}$ for frogs and at $25 \pm 1^\circ\text{C}$ for rats.

The procedures of stimulations of retinas were previously described in detail [3]. The unattenuated intensity of the stimulus light (500 nm) was $6.3 \times 10^{-7} \text{ W/cm}^2$.

RESULTS

Suppression of slow PIII by chemicals

Figure 1 shows the effects of $[\text{Ba}^{2+}]_o$ on frog distal PIII. The superposed photoresponses drawn in (a) were recorded after 10 min of superfusion

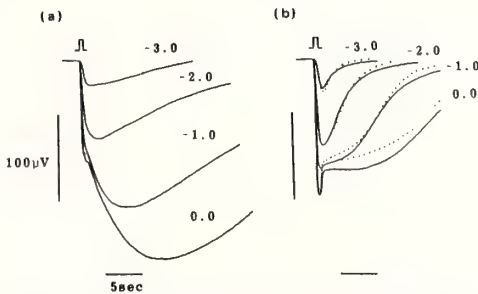


FIG. 1. The effect of $[\text{Ba}^{2+}]_o$ on frog distal PIII. The superposed responses, drawn in (a), were elicited by 0.5 sec-stimuli at four different intensities with 2 min-interval after 10 min of the superfusion with the physiological solution containing 5 mM Na-aspartate. After recording these, the superfusate was changed to the one that contained 5 mM Na-aspartate plus $10 \mu\text{M Ba}^{2+}$. The responses drawn by the continuous line in (b), were obtained by the same stimuli as in the case of (a) after 10 min of the superfusion. The responses drawn by dotted lines indicate those obtained after 10 min of further superfusion with the solution that contained 5 mM Na-aspartate plus $20 \mu\text{M Ba}^{2+}$. The numeral on each response indicates the stimulus intensity expressed by the negative logarithm of the (neutral density) filter. The downward deflection means that ganglion side of the retina becomes negative with respect to the receptor side.

with the physiological solution containing 5 mM Na-aspartate. Each response contained a remarkably slow component (slow PIII). After recording these responses, the superfusate of the retina was switched to the one that contained 5 mM Na-aspartate plus $10 \mu\text{M Ba}^{2+}$. As shown in (b), the superfusion of 10 min with the Ba^{2+} solution suppressed slow PIII component (continuous lines) and the further superfusion of 10 min with the one that contained 5 mM Na-aspartate plus $20 \mu\text{M Ba}^{2+}$ was more effective (dotted line). Thus $[\text{Ba}^{2+}]_o$ higher than $20 \mu\text{M}$ could suppress the slow PIII of the frog distal PIII. On the other hand, the slow PIII of rat was barely suppressed by Ba^{2+} of concentration higher than $500 \mu\text{M}$ (data not shown).

Figure 2 shows the effect of L - α AA on frog distal PIII. These superposed responses were elicited by the same stimuli as in Figure 1 after 10 min (a) and 120 min (b) of the superfusion with the physiological solution containing 10 mM L - α AA instead of 5 mM Na-aspartate. The recovery phase of each response elicited by an identical stimulus was more rapid in (b) than in (a). Thus 10 mM L - α AA abolished frog b-wave within 10 min, and completed the suppression of the slow PIII within 120 min. However, concentration higher than 10 mM L - α AA solution hardly helped to shorten the superfusion time necessary for suppression of the slow PIII. L - α AA at 2 mM abolished frog b-wave, but not the slow PIII. In the case of rat retina, L - α AA at 10 mM could also suppress b-wave, but not

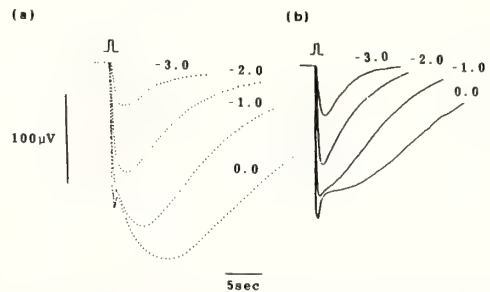


FIG. 2. The effect of L - α AA on frog distal PIII. The superposed responses were obtained by the same stimuli as in Fig. 1 at 10 min (a) and at 120 min (b) after the superfusion with the physiological solution containing 10 mM L - α AA. The downward deflection of responses and the numeral on each response mean the same as in Fig. 1.

slow PIII. The isomer, D- α AA, suppressed neither the b-wave nor the slow PIII of both the animals.

Hereafter, the residual fast component of the distal PIII of frog after treatment with the chemicals will be called fast PIII which is assumed to be the response of receptor origin.

Hypersensitivity by measuring chemicals-isolated fast PIII in frog photoreceptors

Figure 3 shows the effects of $[Ca^{2+}]_o$ and light

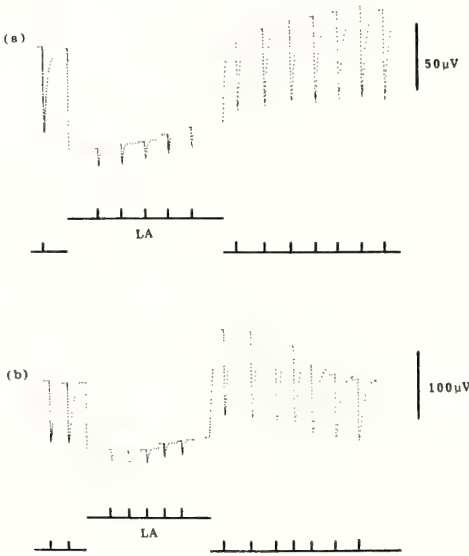


FIG. 3. The effects of $[Ca^{2+}]_o$ and light adaptation on the amplitude of L- α AA-isolated fast PIII. The records in (a) were obtained after 120 min of the superfusion with the physiological solution containing 10 mM L- α AA and 0.9 mM Ca^{2+} (control solution). After recording, the superfusate was changed to the one that contained 10 mM L- α AA and 0.09 mM Ca^{2+} . The records in (b) were obtained after 10 min of superfusion with the low Ca solution. The isolated frog retina was stimulated by the light flash (-3 log units, 0.5 sec) before, during and after the light adaptation. The horizontal lines labeled LA indicate a 5 min light adaptation (white light, 8×10^{-5} lux). The fast PIII responses during and after the adaptation were recorded at 30 sec, 1, 2, 3 and 4 min after the onset of the adaptation light and at 10, 30 sec, 1, 2, 4, 6 and 8 min after the offset of the light, respectively. The bottom traces in (a) and (b) are flash light monitors. The time base is discontinuous. The downward deflection of responses means the same as in Fig. 1.

adaptation on the fast PIII isolated by L- α AA. At 0.9 mM $[Ca^{2+}]_o$, as shown in (a), the amplitude of fast PIII response at 10 sec-dark after the offset of adaptation light was smaller than that in the initial dark, and the amplitude of the response recovered after 8 min of the offset. As shown in (b), reducing $[Ca^{2+}]_o$ from 0.9 mM to 0.09 mM led to an increase (about 1.3 times) in the amplitude of fast PIII elicited by the same stimulus light. The amplitude at 10 sec-dark after the offset of adaptation light was 1.4 times larger than that in the initial dark, and then the amplitude of response recovered after 8 min of the offset (called hypersensitivity). The offset of the adaptation light caused a large upward deflection of transretinal d.c. potential (hereafter called off-response). The amplitude of the off-response was 1.3 times larger than that of the initial downward deflection (hereafter called on-response) induced by the onset of the adaptation light.

In this paper, we defined the gain of fast PIII as the ratio of the amplitude of fast PIII at 10 sec-dark after the offset of adapting light to that in the initial dark. Also we termed the ratio of off-response to on-response as the off-/on-response. Figure 4 shows the correlation between

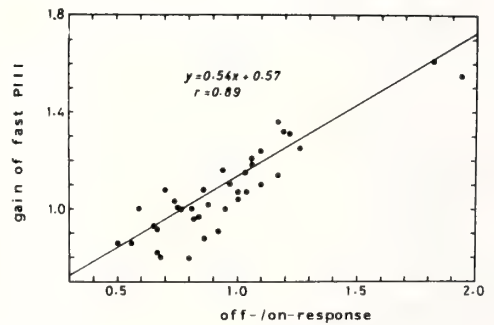


FIG. 4. The correlation between the gain of fast PIII and the magnitude of off-response. The isolated retina was superfused with the physiological solution containing 20 μ M Ba^{2+} , 5 mM Na-aspartate and various Ca^{2+} concentrations. The superfused retina was stimulated by the flash light before and after the light adaptation. The duration of adaptation light was varied from 5 min to 20 min. The straight line was drawn following to the first order equation (shown in the figure) obtained by the regression analysis. The intensities of stimulus and adaptation lights were the same as in Fig. 3.

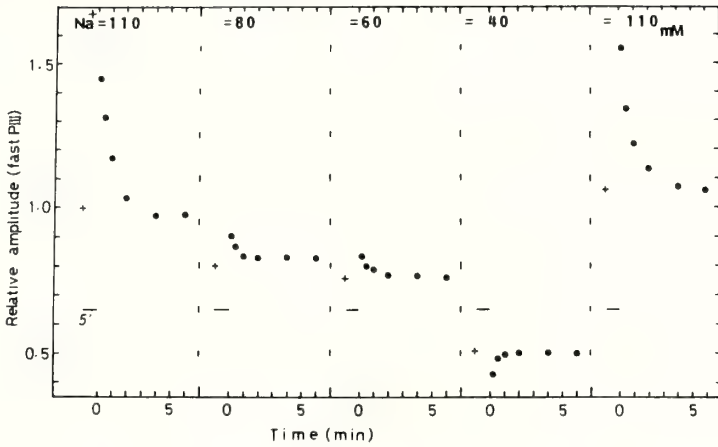


FIG. 5. The effect of $[Na^+]_o$ on hypersensitivity. The isolated retina was superfused with the solutions containing $20 \mu M Ba^+$, $5 mM Na$ -aspartate, $0.09 mM Ca^{2+}$ and various Na^+ concentrations. The superfused retina was stimulated by the flash light before and after the light adaptation. In reducing $[Na^+]_o$, the equivalent to reduced $[Na^+]$ was replaced by choline. The symbol + at each $[Na^+]_o$ indicates an amplitude of fast PIII response evoked by the stimulus in the dark before the onset of the adaptation light. The amplitude of fast PIII at each $[Na^+]_o$ was normalized by that in the dark measured originally at $110 mM [Na^+]_o$. The data were obtained from the same retina. The conditions of stimulus and adaptation lights were the same as in Fig. 3.

the gain of fast PIII and the off/on-response. This result was obtained from several retinas superfused with the solution containing various Ca^{2+} concentrations. The correlation coefficient between them was about 0.9, which was obtained by a linear, least-squared error regression analysis. It can be said that the hypersensitivity (the gain of fast PIII > 1) occurs in the case of off/on-response larger than 0.8.

Figure 5 shows the effect of $[Na^+]_o$ on the hypersensitivity. The hypersensitivity was remarkable at low $[Ca^{2+}]_o$ solution containing $110 mM [Na^+]$ (normal concentration), where the gain of fast PIII was about 1.5. Hypersensitivity was less remarkable at 80 or $60 mM [Na^+]_o$ and could not be observed any more at $40 mM [Na^+]_o$. The recovery of $[Na^+]_o$ to normal concentration induced again a remarkable hypersensitivity (the gain of fast PIII = 1.5). The off/on-response also decreased with reducing $[Na^+]_o$ (data not shown).

Figure 6 illustrates the effect of $[Ca^{2+}]_o$ on the gain of fast PIII at various $[Na^+]_o$. In normal $[Na^+]_o$, lowering $[Ca^{2+}]_o$ from $0.9 mM$ to $0.6 mM$ induced hypersensitivity (the gain of fast PIII > 1), but in $80 mM [Na^+]_o$, lowering $[Ca^{2+}]_o$ to $0.4 mM$

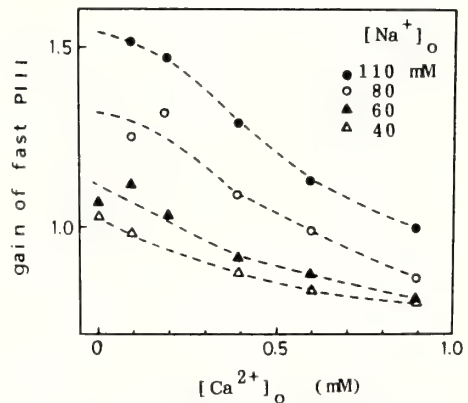


FIG. 6. $[Ca^{2+}]_o$ -dependence of hypersensitivity at four different Na^+ concentrations. Each value obtained from the retina superfused with the solutions containing the various concentrations of Na^+ and of Ca^{2+} was normalized by the one obtained from the same retina superfused with the control solution ($110 mM Na^+$ and $0.9 mM Ca^{2+}$). The conditions of stimulus and adaptation lights were the same as in Fig. 3.

was required in order to induce hypersensitivity. In $40 mM [Na^+]_o$, hypersensitivity scarcely occurred even at $0.01 mM [Ca^{2+}]_o$ (the gain of fast

PIII=1). Thus, the hypersensitivity induced by low Ca was markedly inhibited by reducing $[Na^+]_o$. On the other hand, the change of $[K^+]_o$ little influenced the hypersensitivity (data not shown).

Hypersensitivity of rat photoreceptors

Figure 7 shows the effect of $[Ca^{2+}]_o$ on rat distal PIII responses before and after light adaptation. At 1 mM $[Ca^{2+}]_o$, the distal PIII response at 10 sec-dark after the offset of the light was smaller than that in the initial dark, and then the ampli-

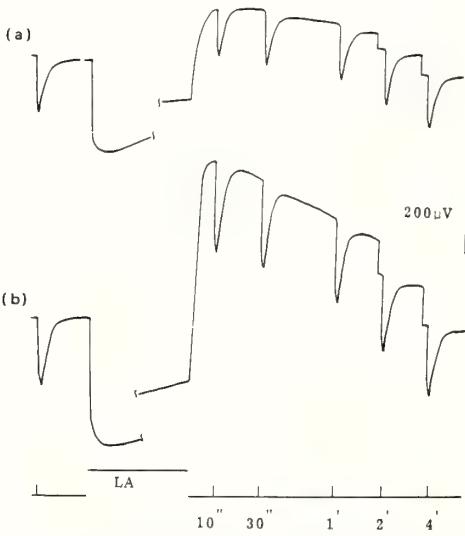


FIG. 7. The effects of $[Ca^{2+}]_o$ and adapting light on the distal PIII of albino rat. The d.c. record in (a) was obtained after 10 min of the superfusion with the physiological solution containing 10 mM Na-aspartate and 1 mM Ca^{2+} . After the recording, the superfusate was changed to the one that contained 10 mM Na-aspartate and 0.1 mM Ca^{2+} . The record in (b) was obtained after 10 min of the superfusion with the low Ca solution. The downward deflection means the same as in the case of Fig. 1. The bottom traces in (a) and (b) are flash light monitors. Horizontal bars labeled LA indicate 5 min-light adaptation (white light, 2×10^{-3} lux). PIII responses elicited by the flash light (-1.5 log units, 0.5 sec) were recorded at 2 min before the onset of adaptation light and at appropriate periods after the offset of the adaptation light (indicated beneath each flash light monitor). The time base is discontinuous. The d.c. recordings were obtained from the same retina (each response includes slow PIII component).

tude of the response recovered within several minutes(a). Reducing $[Ca^{2+}]_o$ from 1 mM to 0.1 mM led to the increase (about 1.2 times) in the amplitude of distal PIII response. In addition, the amplitude at 10 sec-dark after the offset of the light was 1.5 times larger than that in the initial dark, and the off-response was 1.8 times larger than on-response(b). Though data were not shown, the hypersensitivity of rat photoreceptors was induced by IBMX as already reported in the frog retina [4].

Figure 8 shows the stimulus-response curves for the fast PIII of the rat in 0.1 mM, 1 mM and 2 mM $[Ca^{2+}]_o$. In the case, the fast PIII was measured by the capacity-coupled method as described in the previous paper [3], because the slow PIII of rat retina could scarcely be suppressed by chemicals already described. The smooth curves in the figure were obtained from calculations based on the following equation:

$$V = V_{\max} I^n / (I^n + I_s^n) - (1) \quad (\text{Naka and Rushton [20])}$$

where V is the response amplitude related to a stimulus intensity (I), V_{\max} is the saturated response amplitude and I_s is the half saturation

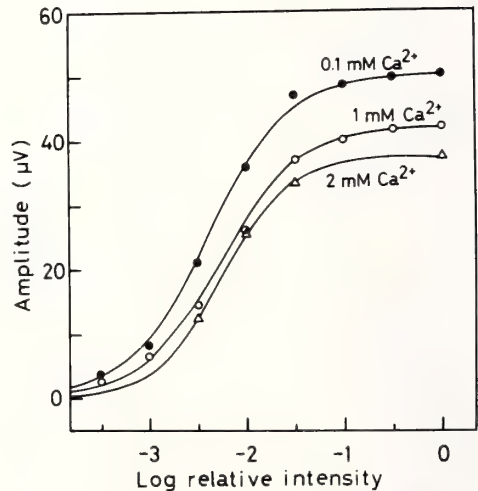


FIG. 8. The effects of $[Ca^{2+}]_o$ on the stimulus-response curves of rat fast PIII. The isolated retina was superfused with the physiological solution containing 10 mM Na-aspartate and various Ca^{2+} concentrations. Fast PIII component was elicited by 0.5 sec-stimuli of various intensities. The measurements were carried out consecutively with the same retina.

constant. The constants, I_s and n , were determined by using the log-linear, least-squared error method to fit each set of data points. The values of $I_s(n)$ obtained were -2.3 (1.3), -2.3 (1.0) and -2.4 (1.0) for 2 mM, 1 mM and 0.1 mM $[Ca^{2+}]_o$, respectively. Reducing $[Ca^{2+}]_o$ from 2 mM to 0.1 mM caused the increase (1.3 times) of V_{max} .

Figure 9 shows stimulus-response curves at 0.1 mM $[Ca^{2+}]_o$ in the dark (curve 1), in the light at 20 sec (curve 2) and 8 min (curve 3) after the onset of adaptation light for 10 min, and at 10 sec-dark after the offset of the light (curve 4). The smooth curve in each condition was obtained from calculations based on the equation 1. The values of $I_s(n)$ were -2.5 (1.1), -2.3 (1.7), -2.2 (1.5) and -2.6 (1.1) for curves 1, 2, 3 and 4, respectively. As indicated by the change from curve 1 to curve 2, the light adaptation decreased V_{max} by half. During the light adaptation, I_s decreased slightly, and V_{max} increased about 1.5-fold (from curve 2 to

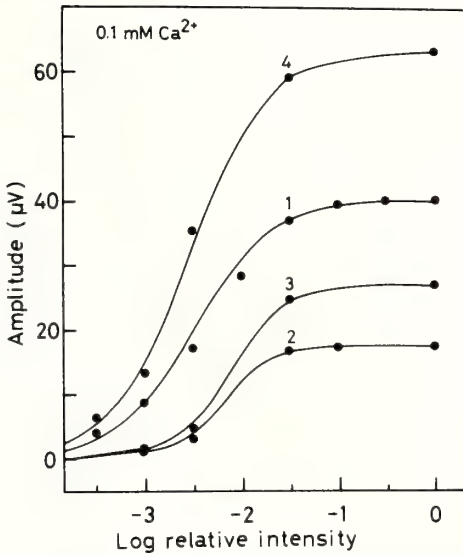


FIG. 9. The effect of adapting light on the stimulus-response curve of rat fast PIII at 0.1 mM $[Ca^{2+}]_o$. Curve 1 was obtained from the measurement in the dark. Curves 2 and 3 were obtained from the measurements after 20 sec and 8 min of the onset of adaptation light, respectively. Curve 4 was obtained from the measurement at 10 sec-dark after the offset of the light. These experiments were carried out by 0.5 sec-stimuli of various intensities and constant adapting light (2×10^{-3} lux) from the same retina.

3). I_s at 10 sec-dark after the offset of the light was slightly smaller than that at the initial dark condition, but V_{max} increased markedly by about 1.5 times (from curve 1 to 4).

Measurements of $[K^+]_o$ in the frog retina

Figure 10(a) shows the light-induced changes of $[K^+]_o$ at normal $[Ca^{2+}]_o$. The onset of adaptation light induced the downward deflection of V_{K^+} which was corresponding to the decrease of $[K^+]_o$ in the interstitial space of the frog retina. The decrease reflects the reduction of K^+ -efflux through rod membranes by the adaptation light [19]. In the dark after offset of the adaptation light, $[K^+]_o$ tended to recover to the initial dark

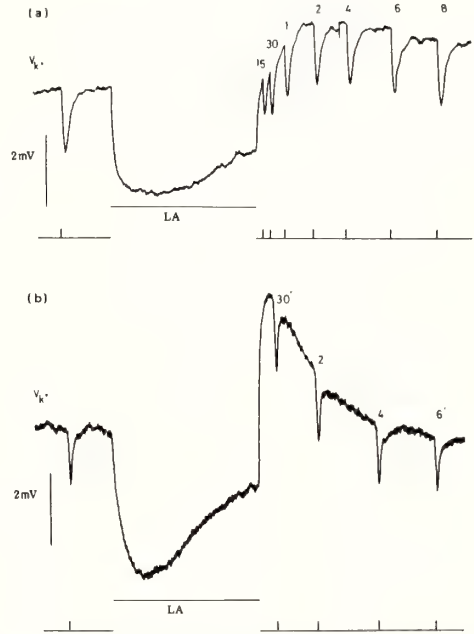


FIG. 10. Light-induced changes of $[K^+]_o$ in the isolated retina at two different $[Ca^{2+}]_o$. (a) 0.9 mM $[Ca^{2+}]_o$. (b) 0.09 mM $[Ca^{2+}]_o$. The isolated retina was superfused with the solution containing 20 μ M Ba^{2+} with 5 mM aspartate and 0.9 mM Ca^{2+} or 0.09 mM Ca^{2+} . Horizontal bars labeled LA indicate 5 min-light adaptation. K^+ -responses elicited by 1 sec-stimuli were recorded at 2 min before the onset of the adaptation light and at appropriate periods after the offset of the light (indicated above each response). The bottom traces in (a) and (b) are flash light monitors. The intensities of stimulus and adaptation lights were the same as in Fig. 3.

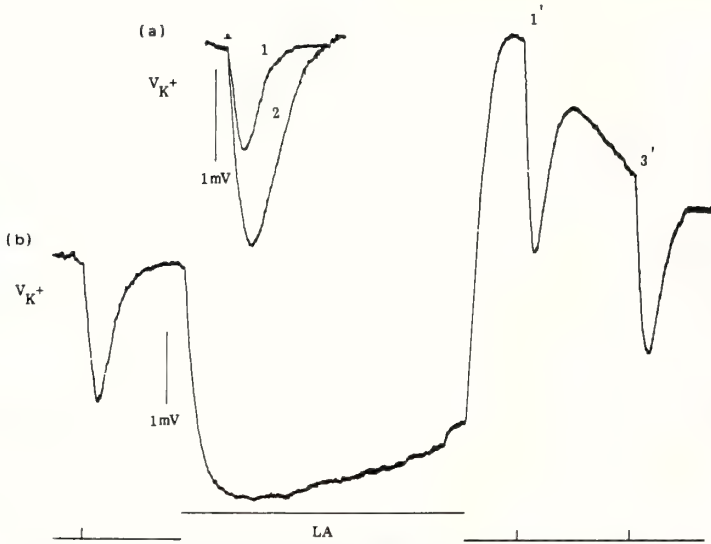


FIG. 11. The effect of IBMX on light-induced change of $[K^+]_o$ in the isolated retina. In (a) K^+ -response in the superfusate with $50 \mu M$ IBMX (curve 2) is compared with that in the normal superfusate (curve 1). Record in (b) was obtained from the retina superfused with the IBMX contained solution. In part (b), horizontal bars labeled LA indicate 5 min-light adaptation. K^+ -responses elicited by the flash light were recorded at 2 min before the onset on the adaptation light and at appropriate periods after the offset of the light (indicated above each response). The bottom trace is the flash light monitor. The conditions of stimulus and adaptation lights were the same as in Fig. 10.

level, which indicated the recovery of K^+ -efflux. The figure also shows that the decrease of $[K^+]_o$ evoked by a light flash (hereafter termed K^+ -response) is influenced by light adaptation. At normal $[Ca^{2+}]_o$, K^+ -response became markedly smaller during light adaptation (data not shown), and recovered gradually in the dark after the offset of the adaptation light. Figure 10(b) shows the effect of the adaptation light on K^+ -response at low Ca (0.09 mM). K^+ -response became smaller during the illumination (data not shown), but the K^+ -response at 30 sec-dark after the offset of the light was larger than that in the initial dark, and then K^+ -response recovered within 6 min. The figure also shows that the level of $[K^+]_o$ remarkably overshoots the initial dark level after the offset of the adaptation light.

In the previous paper [4], we reported that IBMX induced hypersensitivity of frog photoreceptors even at normal $[Ca^{2+}]_o$. We tested whether IBMX caused the transient increase of K^+ -response after the offset of adaptation light.

As shown in Figure 11(a), the amplitude of K^+ -response was enlarged, and its time course was elongated by the addition of $50 \mu M$ IBMX. The similar effects of the reagent on fast PIII were observed (data not shown). Figure 11(b) shows the effect of adapting light on K^+ -response at normal $[Ca^{2+}]_o$ in the presence of $50 \mu M$ IBMX. The amplitude of K^+ -response at 30 sec-dark after the offset of the adaptation light was about 1.4 times larger than that in the initial dark, and the overshoot of $[K^+]_o$ was also remarkable.

DISCUSSION

In this experiment, L- α AA abolished the b-wave of frog ERG rapidly, and the slow PIII of it slowly, but D- α AA did not. This suggests that the L- α AA is an agonist of the amino acids (aspartate and glutamate) which can suppress the b-wave. The suppression effect of the L- α AA on slow PIII which originates in Müller cell [10, 11] is consistent with other authors' result [15] showing that the

α AA can cause the severe destruction of frog Müller cell. As discussed by Casper and Reif-Lehler [16], the difference in the effects between L- and D- α AA may be a result of the differences in conformation and receptor interactions.

On the other hand, neither of the two isomers of α AA was effective on the slow PIII of albino rat (see results). This seems to contradict with other authors' result [17] showing that intravitreal injection of the DL- α AA to the rat causes morphological changes indicating the destruction of the Müller cells. The discrepancy may be due to the differences between isolated retina (this experiment) and living eye (other authors), or because α AA can not destroy the membrane itself of the Müller cells.

Ba^{2+} suppressed the slow PIII of frog at concentration higher than 20 μ M, which was consistent with Matsuura's result [13], and barely suppressed the slow PIII of the rat at concentration higher than 500 μ M. As Ba^{2+} is considered to be a blocker of the g_K of Müller cell [12, 13], it can be said that Ba^{2+} is more accessible to the K^+ -channel of frog Müller cell than to that of rat Müller cell.

In this report, the hypersensitivity was observed in measuring chemicals-isolated fast PIII of frog. The hypersensitivity was also observed in rat retinas at low Ca or in the presence of IBMX, as in frog retinas. These findings corroborate the conclusion described previously [3] that the hypersensitivity is a phenomenon in rod photoreceptor itself. A similar phenomenon was reported in skate retina [5]. Therefore it can be said that the hypersensitivity is popular in the vertebrate photoreceptor.

In measuring $[K^+]_o$ of frog retina under the conditions causing the hypersensitivity, K^+ -response increased markedly in the dark after the offset of adaptation light, where the large overshoot in $[K^+]_o$ was observed at the offset (see results). This is consistent with Oakley's result [21]. The overshoot indicates the rapid increase of K^+ -efflux, and the increase of K^+ -response is corresponding to the reinforcement in suppression of K^+ -efflux by flash light. As suggested by Oakley and Steinberg [22], the change of K^+ -efflux is caused by that of Na^+ -influx through rod

membrane. Therefore it can be said that the large overshoot in $[K^+]_o$ indicates the transient increase in Na^+ -dark current.

It was confirmed that IBMX induced hypersensitivity of the photoreceptors of both frogs and rats. The reagent induced a similar effect on $[K^+]_o$ change as that of low Ca (see results). As already shown, reducing $[Na^+]_o$ suppressed the hypersensitivity, and the alternation of $[K^+]_o$ was less effective. From these results, we consider the cause of hypersensitivity as follows. The hypothesis is composed of three assumptions. 1) The g_{Na} of rod photoreceptors in the dark increases under such condition as low Ca or the existence of IBMX [23], which intensifies Na^+ -influx and K^+ -efflux and then leads to the increase of $[Na^+]_i$ and the decrease of $[K^+]_i$. 2) Light adaptation causes the decrease in g_{Na} , which reduces both Na^+ -influx and K^+ -efflux, and then leads to the decrease of $[Na^+]_i$ and the increase of $[K^+]_i$, i.e., the increase of Nernstian potentials of the two ions across rod membranes. This is because Na^+ - K^+ -pump works even during the light adaptation. 3) In the dark following the light adaptation, the recovery of g_{Na} to the initial dark level is faster than that of the Nernstian potentials which increases during light adaptation. If these assumptions are reasonable, the following events will be expected. The large Na^+ -dark current is observed immediately after the offset of the adaptation light, and the increase of fast PIII amplitude (hypersensitivity) occurs in the early dark after the offset. The first and second assumptions are supported by the data of X-ray microanalysis [24]. The data have shown that reducing $[Ca^{2+}]_o$ from 1.8 mM to 0.18 mM induces the increase of $[Na^+]_i$ and the decrease of $[K^+]_i$ in rod photoreceptors, and that light adaptation causes a highly significant reduction of $[Na^+]_i$ and an increase of $[K^+]_i$.

Lowering $[Na^+]_o$ may give the rod photoreceptors the following effects. The lowering induces the decrease of Na^+ -dark current [23] resulting in the decrease of Na^+ -influx. The difference of Na^+ -influx between dark and light adaptations under such condition is markedly less than that under normal $[Na^+]_o$ condition. Therefore, low $[Na^+]_o$ condition can not induce the increases of Nernstian potentials of Na^+ and K^+ during light

adaptation. This may be a reason why the lowering in $[Na^+]_o$ suppresses the hypersensitivity. As the change of $[Na^+]_o$ gives the effect on the activity of Na^+-Ca^{2+} exchange pump [23], it was not excluded that the pump is not related to the hypersensitivity.

ACKNOWLEDGMENT

I wish to thank Professors N. Iwasaki and M. Fujimoto for continuous encouragement and technical advice. I am indebted to Dr. M. Azuma, with whom I worked in the early phases of this project, for technical assistance and helpful discussions.

REFERENCES

- Hanani, M. and Hillman, P. (1976) Adaptation and facilitation in the barnacle photoreceptor. *J. Gen. Physiol.*, **67**: 235–249.
- Ventura, D. F. and Puglia, N. M. (1977) Sensitivity facilitation in the insect eye. A parametric study of light adapting conditions. *J. Comp. Physiol.*, **14**: 35–49.
- Azuma, M. and Azuma, K. (1979) The increase in sensitivity following light illumination in frog photoreceptors. *Vision Res.*, **19**: 1171–1175.
- Azuma, M. and Azuma, K. (1982) The action of phosphodiesterase inhibitors on the hypersensitivity of frog photoreceptor. *Vision Res.*, **22**: 151–155.
- Dowling, J. E. and Ripps, H. (1972) Adaptation in skate photoreceptors. *J. Gen. Physiol.*, **60**: 698–719.
- Hanawa, I., Ando, H. and Takahashi, K. (1981) Enhancement of visual response after illumination in the isolated frog retina. *Exp. Eye Res.*, **32**: 719–727.
- Brown, J. E. and Waloga, G. (1981) Effect of cyclic nucleotide and calcium ions on Bufo rods. In "Molecular Mechanism of Photoreceptor Transduction". Ed. by W. Miller, Academic Press, New York, pp. 369–380.
- Furukawa, T. and Hanawa, I. (1955) Effects of some common cations on electroretinogram of the toad. *Jpn. J. Physiol.*, **5**: 289–300.
- Murakami, M. and Kaneko, A. (1966) Differentiation of PIII subcomponents in cold-blooded vertebrate retinas. *Vision Res.*, **6**: 627–636.
- Witkovsky, P., Dudek, F. E. and Ripps, H. (1975) Slow PIII component of the carp retina. *J. Gen. Physiol.*, **65**: 119–134.
- Fujimoto, M. and Tomita, T. (1979) Reconstruction of the slow PIII from the rod potential. *Invest. Ophthalmol. Visual Sci.*, **18**: 1090–1093.
- Bolnick, D. A., Walter, A. E. and Sillman, A. J. (1979) Barium suppress slow PIII in perfused bullfrog retina. *Vision Res.*, **19**: 117–119.
- Matsuura, T. (1984) Effects of barium on separately recorded fast and slow PIII responses in bullfrog retina. *Experientia*, **40**: 817–819.
- Szamer, R. B., Ripps, H. and Chappell, R. L. (1981) Changes in ERG-wave and Müller cell structure induced by alpha-aminoadipic acid. *Neurosci. Lett.*, **21**: 307–312.
- Bonaventure, N., Roussel, G. and Wioland, N. (1981) Effects of D, L- α -amino adipic acid on Müller cells in frog and chicken retinae in vivo: relation to ERG b-wave, ganglion cell discharge and tectal evoked potentials. *Neurosci. Lett.*, **27**: 81–87.
- Casper, D. S. and Reif-Lehrer, L. (1983) Effects of alpha-aminoadipate isomers on the morphology of the isolated chick embryo retina. *Invest. Ophthalmol. Vis. Sci.*, **24**: 1480–1488.
- Pedersen, O. and Karlsen, R. L. (1979) Destruction of Müller cells in the adult rat by intravitreal injection of DL- α -aminoadipic acid: an electron microscopic study. *Exp. Eye Res.*, **28**: 569–575.
- Fujimoto, M. and Kubota, T. (1976) Physicochemical properties of a liquid ion exchanged micro-electrode and its application to biological fluids. *Jpn. J. Physiol.*, **26**: 631–650.
- Oakley, B., II (1983) Effects of maintained illumination upon $[K^+]_o$ in the subretinal space of the isolated retina of the toad. *Vision Res.*, **23**: 1325–1337.
- Naka, K. I. and Rushton, W. A. H. (1966) S-potentials from colour units in the retina of fish (Cyprinidae). *J. Physiol.*, **185**: 536–555.
- Oakley, B., II (1984) Effects of low $[Ca^{2+}]_o$ upon $[K^+]_o$ during and after maintained illumination of the isolated retina of the toad. *Vision Res.*, **24**: 815–819.
- Oakley, B., II and Steinberg, R. H. (1982) Effects of maintained illumination upon $[K^+]_o$ in the subretinal space of the frog retina. *Vision Res.*, **22**: 767–773.
- Hodgkin, A. L., McNaughton, P. A., Nunn, B. J. and Yaw, K. W. (1984) Effect of ions on retinal rods from *Bufo marinus*. *J. Physiol.*, **35**: 649–680.
- Somlyo, A. P. and Walz, B. (1985) Elemental distribution in *Rana pipiens* retinal rods: Quantitative electron probe analysis. *J. Physiol.*, **358**: 185–195.

Effects of Cellular Dehydration on Drinking and Plasma Angiotensin II Level in the Eel, *Anguilla japonica*

YOSHIO TAKEI, JUNKO OKUBO and KEN'ICHI YAMAGUCHI¹

Department of Physiology, Kitasato University School of Medicine, Sagamihara, Kanagawa 228, and ¹Department of Physiology, Niigata University School of Medicine, Niigata, Niigata 951, Japan

ABSTRACT—An intra-arterial injection of 0.5 ml of 7% NaCl, 14% NaCl, 65% sucrose, or 61% sucrose in 0.9% NaCl into the dorsal aorta of freshwater (FW) eels, which theoretically causes cellular dehydration by 2.8% (7% NaCl and sucrose solutions) or 5.7% (14% NaCl), consistently inhibited drinking for 1 hr after injection, compared with controls injected with 0.9% NaCl. Drinking was not stimulated by any of the injections for up to 5 hr. Plasma angiotensin II (AII) level increased consistently 15 min after any of the injections, and the increase became smaller after 4 hr. Plasma Na level increased for 4 hr after the injection of hypertonic saline, whereas a decrease was observed after the injection of hypertonic sucrose. Drinking was also inhibited after injection of 0.5 ml of 7% NaCl into eels adapted to 1/3 seawater (SW), which is isosmotic to plasma, or into those exposed to 1/3 SW or SW for 1.5 hr. Plasma AII level increased in all the experimental groups after 15 min, but the increase was significant only in 1/3 SW-adapted eels. Plasma Na level increased for 4 hr after injection of 7% NaCl in 1/3 SW-exposed and SW-exposed eels, but the increase was no more significant after 4 hr in 1/3 SW-adapted eels. Collectively, drinking was decreased and plasma AII was increased by the stimuli to cellular dehydration in the eel. These results are the converse of those obtained for mammals and birds, in which administration of a hypertonic solution of NaCl induces drinking and reduces plasma AII level.

INTRODUCTION

It is generally accepted that intravascular administration of hypertonic solution of solutes which are impermeable to the cell membrane and, thus, causes cellular dehydration, induces drinking in mammals [1], birds [2, 3] and reptiles [4], while intravascular administration of hypertonic NaCl inhibits renin release in mammals [5] and birds [6]. Thus, administration of hypertonic NaCl is dipsogenic in mammals and birds, even though the levels of angiotensin II (AII), another potent dipsogen [1], are suppressed by such treatment. In fishes, Hirano [7] reported that the rate of drinking is increased in freshwater (FW) eels by a slow infusion of hypertonic NaCl solution. However, our preliminary data suggest that injection of

hypertonic NaCl failed to stimulate drinking in FW eels [8]. Thus, the effect of hypertonic solutions on drinking in fishes remains to be established. Furthermore, it is unknown how increased plasma osmolality, or cellular dehydration, influences plasma AII levels in the eel. AII has been shown to stimulate drinking in the eel [9] and other fishes [10-13].

The present study was undertaken to examine further the effect of cellular dehydration on drinking and plasma AII level in the eel. As stimuli to cellular dehydration, we made a single injection of hypertonic NaCl and sucrose instead of infusion, to avoid dilution of the osmotic load during the infusion by water influx across the gill. We used not only FW eels but those adapted or exposed to 1/3 seawater (SW) or full-strength SW as experimental animals, since the influx of water across the gill after the osmotic load might be smaller in these eels than in FW eels. However,

SW-adapted eels were removed from the experiment because we preliminarily found that Na ions loaded were excreted immediately after injection of hypertonic NaCl into these eels.

MATERIALS AND METHODS

Animals

Cultured Japanese eels, *Anguilla japonica*, were purchased from a local dealer. They were kept in groups of 20 in 1-ton, FW tanks for more than 1 week before use. Some eels were transferred to a 0.5-ton, 1/3-SW tank, and acclimated for more than 2 weeks before use (1/3 SW-adapted eels). Water in the tank was continuously filtered, aerated and thermoregulated at $18 \pm 0.5^\circ\text{C}$. Eels were not fed after purchase, and weighed 197 ± 1 g (mean \pm SEM, $n=102$) at the time of experiments.

Surgical procedures

After the eels were anesthetized with 0.1% tricaine methanesulfonate (Sigma), a vinyl tube (o.d.: 2.0 mm) was inserted into the esophagus, and 2 polyethylene tubes (o.d.: 0.8 mm) were inserted into the dorsal and the ventral aorta, respectively. The blood stream through these aortae was not occluded by the cannulation as described previously [14]. The eels that bled more than approximately 0.05 ml were excluded from the experiment. After the surgery, the eels were transferred to a plastic trough through which aerated and thermoregulated (18°C) water was circulated. In this condition, the cannulated eels usually survived more than 2 weeks. The circulating water through the trough could be changed from FW to 1/3 SW or SW by turning a 3-way stop cock. The catheter placed in the esophagus was connected to a drop counter for continuous measurement of drinking rate [7]. The drunk water that dropped from the esophageal catheter was not reintroduced into the stomach. The catheters in the aortae were connected to syringes filled with saline containing Ca heparin (10 U/ml). Eels were allowed to recover for more than 18 hr post-operatively.

Experimental protocol

Four different groups of eels were used in this experiment, eels adapted to FW, those adapted to 1/3 SW, those exposed to 1/3 SW for 1.5 hr and those exposed to SW for 1.5 hr. The FW eels were injected with 0.5 ml of one of the solutions of 0.9% NaCl, 7% NaCl, 14% NaCl, 65% sucrose, and 61% sucrose in 0.9% NaCl into the dorsal aorta in 1 min, whereas 0.5 ml of blood was withdrawn simultaneously from the ventral aorta at the same rate as the injection. The blood was collected into a chilled syringe which contained 12.5 μl each of 125 mM disodium EDTA, 25 mM o-phenanthroline and 0.2% neomycin sulfate (Wako Chemicals, Tokyo), and used for radioimmunoassay of AII. The sucrose solutions were approximately isosmotic to 7% NaCl (ca. 2.5 Osm). The 1/3 SW-adapted eels, 1/3 SW-exposed eels and SW-exposed eels were injected with 0.5 ml of either 0.9% or 7% NaCl, and 0.5 ml of blood was also withdrawn simultaneously as described for FW eels. The injection-withdrawal procedure was repeated 15 min and 4 hr after the initial procedure, but the injection at these times consisted of 2% dextran (molecular weight : 60,000–90,000, Wako Chemicals, Tokyo) in 0.9% NaCl. Dextran was added to maintain colloidal osmotic pressure. Before each procedure, 50 μl of blood were collected into capillary tubes for measurements of the hematocrit and concentrations of Na and K ions in plasma.

Water intake was measured every 5 min after injection by means of the number of drops that emerged from the esophageal catheter (0.03 ml/drop). The measurement was continued for up to 5 hr because in another poikilothermal animal, the iguana, drinking response to cellular dehydration occurred much more slowly than in the homeothermal mammals and birds [4]. For radioimmunoassay of AII, 0.5 ml of blood withdrawn at time 0, 15 min and 4 hr was centrifuged at $2,500 \times g$ at 2°C for 15 min. Immunoreactive AII was extracted from plasma with acetone and petroleum ether, and the concentration was determined as reported previously [15]. The antibody used in this assay exhibited 100% cross-reactivity with natural eel Asn¹-Val⁵ AII [16, 17], and the

dilution curve of the assayable AII, extracted from pooled eel plasma, was superimposable on the standard curve of authentic Asp¹-Ile⁵ AII. The concentrations of Na and K ions in plasma were determined with an atomic absorption spectrophotometer (Hitachi 180-80) after 1/2,000 and 1/100 dilutions, respectively. Double distilled water collected into the capillary tube and diluted as above was used as a blank for spectrophotometry. All determinations were made in duplicate.

Analysis of data

Variation of data is a common problem when we attempt to quantify some parameter accompanying behavior, because the behavior is so vulnerable to environmental influences. In fact, the water intake of the eel measured in the present experiments was also variable, and it seems that the variation masks the actual change in water intake after injection. Thus, the change in water intake in each eel during the periods from 1 to 5 hr after injection of the hypertonic solution was classified into an increase, no change, or a decrease compared with the intake during the same time period before injection, and statistically compared with that of controls injected with 0.9% NaCl by the nonparametric Fisher's

exact probability test. Actual water intakes before and after injections were also given in the text. The changes in plasma AII, Na and K levels and the hematocrit after injection of hypertonic solutions were expressed as ratios to the values before injection (zero-time value) to make the actual changes clearer. The zero-time values were also given in the text. By doing this, it is also possible to compare the degree of the changes among these parameters after injection. The changes in plasma AII, Na and K levels and hematocrit after injection of the hypertonic solution were compared with those of controls by the nonparametric van der Waerden test [18]. Data that fell outside the range of other data of the same group was excluded by means of the Smirnov-Grubbs test. Significance was determined at $P < 0.05$. All results are expressed as means \pm SEM.

RESULTS

Drinking rate

Thirty one of 79 eels did not drink at all in FW, and the mean water intake of FW eels was 0.04 ± 0.01 ml/5 min/eel ($n=79$). However, FW eels started drinking copiously upon exposure to

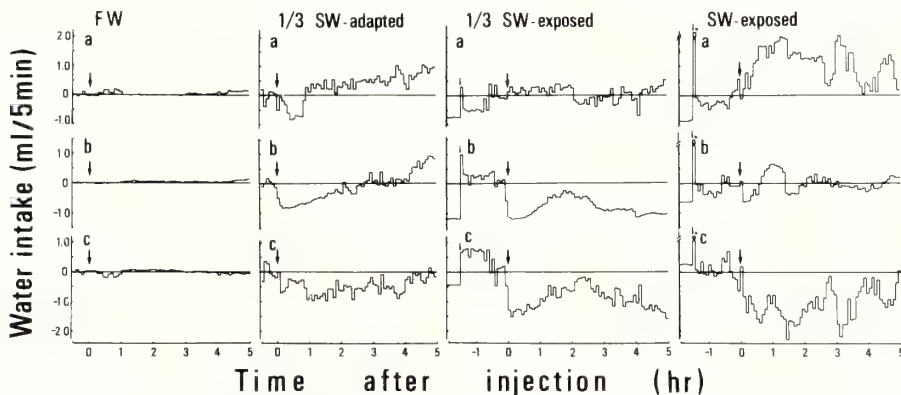


FIG. 1. Changes in water intake after injection of 0.5 ml of (a) 0.9% NaCl, and (b) 7% NaCl in FW eels (a, $n=12$; b, $n=9$), 1/3 SW-adapted eels (a, $n=14$; b, $n=9$), 1/3 SW-exposed eels (a, $n=9$; b, $n=8$), and SW-exposed eels (a, $n=4$; b, $n=5$). The change in water intake after injection of 7% NaCl was also expressed in terms of the difference from the mean intake of controls injected with 0.9% NaCl (b-a) to make the effect of 7% NaCl clearer (c). Each 5-min intake after injection was subtracted by the 5-min intake calculated from the 30-min intake before injection. Due to the great variation of water intake among individuals, standard error of the mean was not given. The actual water intakes are given in Table 2. Smaller arrows indicate the time of exposure to 1/3 SW or SW, and larger arrows indicate the time of injection. *5-min water intakes were 2.84 ml (a), 4.07 ml (b), and 1.23 ml (c).

1/3 SW (1.58 ± 0.25 ml/initial 5 min/eel; latency = 46 ± 1 sec, $n=17$) or SW (4.27 ± 0.55 ml/initial 5 min/eel; latency = 50 ± 15 sec, $n=9$) (Fig. 1). This initial drinking was followed by a decreased rate of drinking for 1–2 hr. Thus, the eels exposed to 1/3 SW or SW for 1.5 hr were drinking at the rate of 0.85 ± 0.11 ml/5 min/eel ($n=17$) and 0.84 ± 0.09 ml/5 min/eel ($n=9$), respectively. Following this temporary decrease in drinking rate, the rate increased again to higher and constant levels of approximately 3 ml/5 min/eel and 1 ml/5 min/eel, respectively, in SW-exposed and 1/3 SW-exposed eels (Fig. 1). Thus, 1/3 SW-adapted eels were drinking at a constant rate of 1.35 ± 0.08 ml/5 min/eel ($n=23$) at the time of injection.

Change in drinking rate after osmotic stimuli

Although the drinking rate of FW eels before injection of hypertonic solutions was variable (Table 1), it was apparent that the drinking rate was slightly inhibited for 1–2 hr after injection of hypertonic solutions, as compared with a slight increase in drinking rate in controls injected with 0.9% NaCl. The decrease in drinking rate was statistically significant for 1 hr after injection of any of the hypertonic solutions compared with the change in controls (Table 1). The decrease continued up to 4 hr after injection of 14% NaCl, and up to 5 hr after injection of 61% sucrose in saline.

The eels were slightly hyperactive for a few minutes after injection of hypertonic solutions, but it was apparent that the behavior thereafter was quite normal.

Injection of 0.9% NaCl had little effect on drinking in FW, 1/3 SW-exposed and SW-exposed eels, but it inhibited drinking for 1 hr after injection in 1/3 SW-adapted eels (Fig. 1a). The drinking rate appears to have increased in SW-exposed eels after injection of 0.9% NaCl, but this is a natural increase which should have occurred without injection as mentioned above. On the other hand, injection of 7% NaCl clearly inhibited drinking in 1/3 SW-adapted and 1/3 SW-exposed eels, and inhibited the natural increase in SW-exposed eels (Fig. 1b). Therefore, when the change in drinking rate after injection of 7% NaCl was corrected by subtraction with the change after injection of 0.9% NaCl, the inhibition of drinking became more evident in all groups of eels (Fig. 1c, Table 2). The degree and duration of the inhibition were greater in 1/3 SW-adapted, 1/3 SW-exposed, and SW-exposed eels than in FW eels, probably due to the greater rate of drinking before injection. Statistical analyses revealed that the inhibition was significant for 1 hr in FW eels, for 2–5 hr in 1/3 SW-adapted eels, for 1–5 hr in 1/3 SW-exposed eels, and for 1–3 hr in SW-exposed eels (Table 2).

TABLE 1. Changes in water intake after injection of 0.9% NaCl, 7% NaCl, 14% NaCl, 65% sucrose, and 61% sucrose in 0.9% NaCl in FW eels

Injection	Number of eels	Water intake during each time period after injection (ml)					
		-1-0 hr	0-1 hr	0-2 hr	0-3 hr	0-4 hr	0-5 hr
0.9% NaCl	11	0.63 ± 0.53	0.91 ± 0.59 (10 0 1)	1.43 ± 0.69 (9 0 2)	1.97 ± 0.87 (9 0 2)	2.90 ± 1.07 (9 0 2)	4.44 ± 1.67 (9 0 2)
7% NaCl	9	0.22 ± 0.15	0.09 ± 0.06 (4 1 4)*	0.82 ± 0.49 (6 1 2)	1.34 ± 0.69 (6 1 2)	1.74 ± 0.76 (6 1 2)	2.38 ± 0.86 (6 1 2)
14% NaCl	12	0.26 ± 0.16	0.16 ± 0.07 (2 8 2)*	0.29 ± 0.17 (3 7 2)*	0.50 ± 0.24 (4 6 2)*	0.80 ± 0.33 (4 6 2)*	1.99 ± 0.83 (5 6 1)
65% sucrose	10	0.09 ± 0.08	0.08 ± 0.05 (3 4 3)*	0.74 ± 0.38 (6 3 1)	1.59 ± 0.67 (7 3 0)	2.31 ± 0.96 (7 3 0)	3.66 ± 1.52 (7 3 0)
61% sucrose in saline	11	0.81 ± 0.31	0.11 ± 0.05 (0 4 7)*	0.24 ± 0.11 (0 4 7)*	0.93 ± 0.45 (1 3 7)*	1.73 ± 0.86 (3 3 5)*	3.09 ± 1.58 (2 3 6)*

Since the drinking rate of each animal was so variable, the change in water intake of each animal during the time periods of 1–5 hr after injection was classified into an increase (+), no change (0), or a decrease (–) compared with the intake during the corresponding time period before injection, and analyzed by the nonparametric statistics. In parentheses are numbers of eels that showed different drinking responses (+, 0, –). * $P < 0.05$ compared with the change in controls injected with 0.9% NaCl. Values are means \pm SEM.

TABLE 2. Changes in water intake after injection of 7% NaCl in FW eels, 1/3 SW-adapted eels, 1/3 SW-exposed eels and SW-exposed eels

Group of eels	Number of eels	Corrected water intake of each time period after injection of 7% NaCl (ml)				
		0-1 hr	0-2 hr	0-3 hr	0-4 hr	0-5 hr
FW	9	-0.81±0.06 (0 0 9)*	-0.59±0.49 (2 0 7)	-0.61±0.69 (3 0 6)	-1.14±0.76 (4 0 5)	-2.06±0.86 (3 0 6)
1/3 SW adapted	9	-5.04±2.82 (4 0 5)	-13.76±4.39 (0 0 9)*	-19.95±4.99 (0 0 9)*	-26.59±6.56 (1 0 8)*	-28.31±8.47 (0 0 9)*
1/3 SW exposed	8	-6.03±1.49 (0 0 8)*	-10.26±1.79 (0 0 8)*	-9.88±2.31 (0 0 8)*	-12.52±3.23 (0 0 8)*	-17.58±4.41 (0 0 8)*
SW exposed	5	-12.90±2.18 (0 0 5)*	-31.10±5.26 (0 0 5)*	-41.72±10.00 (0 0 5)*	-56.08±16.67 (1 0 4)	-64.18±20.41 (1 0 4)

The water intake after injection of 7% NaCl was corrected by subtraction with the mean intake of controls injected with 0.9% NaCl. For reference, see Fig. 1c. Due to the variation of individual water intake, changes in water intake during the time periods of 1-5 hr after injection were classified into an increase (+), no change (0), or a decrease (-) compared with the intake during the corresponding time period before injection, and analyzed by the nonparametric statistics. In parentheses are numbers of eels that showed different drinking responses (+, 0, -). *P<0.05 compared with the intake before injection. Values are means±SEM.

TABLE 3. Levels of angiotensin II, Na and K ions in plasma, and hematocrit in FW eels, 1/3 SW-adapted eels, 1/3 SW-exposed eels and SW-exposed eels before injection of hypertonic solutions

Eels	Angiotensin II (pg/ml plasma)	Na (mM)	K (mM)	Hematocrit (%)
FW	109.7±12.9 (47)	140.9±2.8 (32)	2.69±0.13 (32)	28.2±1.0 (52)
1/3 SW-adapted	101.8±24.1 (20)	155.7±3.4* (23)	2.50±0.19 (22)	20.3±1.5* (22)
1/3 SW-exposed	135.9±32.7 (15)	132.8±2.8* (19)	2.60±0.12 (19)	24.0±2.1* (18)
SW-exposed	182.4±31.8* (7)	137.0±6.6 (9)	2.12±0.15* (9)	25.9±2.6 (9)

These values correspond to the zero-time values in Figs. 2 and 3. Numbers of animals are in parentheses. *P<0.05 compared with the corresponding value for FW eels. Values are means±SEM.

Plasma AII, Na, and K levels and hematocrit

The levels of AII, Na and K ions in plasma, and the hematocrit of FW eels, 1/3 SW-adapted eels, 1/3 SW-exposed eels and SW-exposed eels before injection of hypertonic solutions are shown in Table 3. These values are the means of zero-time values in Figures 2 and 3. It was found that plasma AII level tended to be higher in 1/3 SW and SW-exposed eels than in FW eels, but the difference was significant only in SW-exposed eels.

Plasma Na level was significantly higher in 1/3 SW-adapted eels than in FW eels, but it was lower in 1/3 SW-exposed eels.

Changes in plasma AII, Na and K levels and hematocrit after osmotic stimuli

Plasma AII level invariably increased 15 min after injection of any of the hypertonic solutions in FW eels compared with controls injected with 0.9% NaCl (Fig. 2). The increase became smaller after 4 hr, but it was still significant in eels injected

with 14% NaCl or 65% sucrose. Plasma Na level increased for 4 hr after injection of hypertonic solutions of NaCl, while the level decreased for 4 hr after injection of hypertonic solutions of sucrose. The changes in plasma K level were not consistent after injection of hypertonic solutions (Fig. 2). Hematocrit invariably decreased after injection of hypertonic solutions, and the degree of the decrease at 15 min was greater after injection of sucrose solutions than after injection of NaCl solutions. In controls injected with 0.9% NaCl, plasma AII, Na and K levels did not change but the hematocrit decreased after injection.

Plasma AII level increased in 1/3 SW-adapted eels 15 min after injection of 7% NaCl as observed

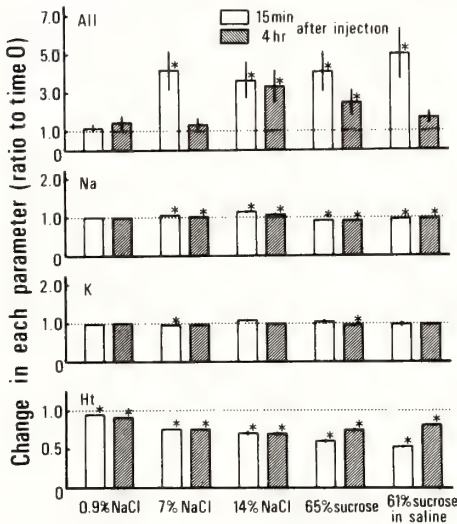


FIG. 2. Changes in plasma angiotensin II (AII), Na and K levels and hematocrit (Ht) 15 min (plain columns) and 4 hr (shaded columns) after injection of 0.5 ml of 0.9% NaCl (AII, $n=12$; Na, $n=6$; K, $n=6$; Ht, $n=12$), 7% NaCl (AII, $n=7$; Na, $n=8$; K, $n=8$; Ht, $n=8$), 14% NaCl (AII, $n=9$; Na, $n=12$; K, $n=12$; Ht, $n=10$), 65% sucrose (AII, $n=10$; Na, $n=3$; K, $n=3$; Ht, $n=11$) and 61% sucrose in 0.9% NaCl (AII, $n=9$; Na, $n=3$; K, $n=3$; Ht, $n=11$) in FW eels. Each change is expressed in terms of a ratio to the value before injection (zero-time value). The zero-time values of AII, Na, K and Ht in FW eels are shown in Table 3. * $P < 0.05$ compared with any changes in the corresponding controls injected with 0.9% NaCl. Values are means \pm SEM.

in FW eels, while the increase was not significant for 4 hr after injection in 1/3 SW and SW-exposed eels (Fig. 3). Plasma Na level increased in all groups of eels for 4 hr after injection of 7% NaCl, except in 1/3 SW-adapted eels after 4 hr. Plasma K level and hematocrit invariably decreased 15 min after injection of 7% NaCl, but the levels were restored to normal after 4 hr except in SW-exposed eels (Fig. 3). In controls injected with 0.9% NaCl, plasma AII, Na and K levels did not change in 1/3 SW-adapted eels, 1/3 SW-exposed eels and SW-exposed eels except for the AII level 4 hr after injection in SW-exposed eels (ratio to zero-time value, 1.54 ± 0.24 , $n=3$). The hematocrit consist-

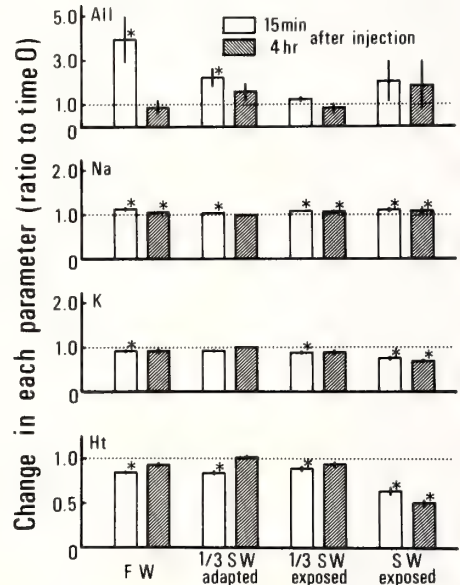


FIG. 3. Changes in plasma angiotensin II (AII), Na and K levels and hematocrit (Ht) 15 min (plain columns) and 4 hr (shaded columns) after injection of 0.5 ml of 7% NaCl in FW eels (AII, $n=7$; Na, $n=8$; K, $n=8$; Ht, $n=8$), 1/3 SW-adapted eels (AII, $n=12$; Na, $n=9$; K, $n=9$; Ht, $n=9$), 1/3 SW-exposed eels (AII, $n=8$; Na, $n=9$; K, $n=9$; Ht, $n=9$), and SW-exposed eels (AII, $n=4$; Na, $n=5$; K, $n=5$; Ht, $n=5$). Each change is expressed in terms of a ratio to the value before injection (zero-time value), and corrected by subtraction with the mean change of controls injected with 0.9% NaCl. The zero-time values of AII, Na, K and Ht in each group of eels are described in Table 3. * $P < 0.05$ compared with the zero-time value. Values are means \pm SEM.

ently decreased after injection of 0.9% NaCl as observed in FW eels: 0.86 ± 0.04 and 0.80 ± 0.02 (15 min and 4 hr after injection, $n=13$) in 1/3 SW-adapted eels, 0.88 ± 0.03 and 0.81 ± 0.02 ($n=9$) in 1/3 SW-exposed eels, and 0.90 ± 0.04 and 0.88 ± 0.05 ($n=4$) in SW-exposed eels.

DISCUSSION

Intravascular administration of hypertonic solutions of NaCl or sucrose, which theoretically causes cellular dehydration by 1.60% in rats, 2.15% in dogs and 1.23% in humans, induces copious drinking [1]. The administration of hypertonic NaCl is also dipsogenic in birds (pigeons, [2]; quail, [3]) and a reptile (iguana, [4]). Assuming that total body water is 65% of body weight in birds [19] and 74% in reptiles [20], the minimal cellular dehydration for elicitation of drinking appears to be 1.03% in pigeons, 0.73% in quail, and less than 2% in iguanas, when the value is calculated by the equation given by Fitzsimons [1]. Thus, the administration of hypertonic NaCl, which causes cellular dehydration by as much as 2%, is potentially dipsogenic in all classes of truly terrestrial vertebrates. In the present experiment, however, an intra-arterial injection of 0.5 ml of 7% NaCl, 65% sucrose or 61% sucrose in saline into FW eels, which theoretically causes cellular dehydration by 2.81%, failed to induce drinking for 5 hr after injection, and actually inhibited drinking for 1 hr. The injection of 14% NaCl was not dipsogenic, either, in FW eels. Thus, the drinking response to stimuli to cellular dehydration appears to differ in the eel from the responses in terrestrial animals.

When the changes in drinking rate, plasma Na and AII levels in FW eels after hypertonic saline are compared closely with those of quail, the weak dipsogenicity of cellular dehydration in the eel becomes more evident. In the quail, injection of 0.5 ml of 7% NaCl injected in the same protocol as employed in this study induced immediate copious drinking although plasma AII level decreased to less than half [21]. Plasma Na level returned to the control level within 15 min after injection in the quail, but, as illustrated in Figure 2, plasma Na level was still higher than the control level even

after 4 hr in FW eels. This is probably due to the poor ability of FW fishes to excrete excess salts [20]. Thus, stimuli to cellular dehydration continued for more than 4 hr after injection of the hypertonic solution in FW eels. Further, plasma AII level increased after the injection in the eel. Even with these favorable conditions for elicitation of drinking, eels did not increase drinking rate for 4 hr after injection of hypertonic solutions.

It is possible that the injection of hypertonic solutions into FW eels increased the osmotic influx of water across the gill, and the resultant expansion of blood volume inhibited drinking. However, the expansion of blood volume after the same degree of osmotic load was shown to be smaller in the eel than in the quail [22], while drinking was induced in the quail [21] and inhibited in the eel as in the present study. Furthermore, in eels adapted or exposed to 1/3 SW or SW, the expansion of blood volume might be smaller after injection of 7% NaCl than in FW eels, but drinking was also inhibited after injection of 7% NaCl into these eels. Thus, it is possible that the eels are more sensitive to the inhibition of drinking by expansion of blood volume, and/or that the osmotic mechanism for stimulation of drinking is less developed in the eel than in terrestrial vertebrates.

It is rather unexpected that plasma Na concentration was smaller in esophagus-cannulated eels after exposure to 1/3 SW and SW for 1.5 hr (Table 3). This result indicates that these eels did not suffer from cellular dehydration when injections were made 1.5 hr after the exposure. We also obtained preliminary data that when FW eels with esophageal fistula were exposed to SW, plasma Na levels decreased for 1–2 hr, then increased gradually, whereas if drunk SW was reintroduced into the esophagus by a pulse injector synchronized with a drop counter, plasma Na concentration increased within 15 min after exposure to SW (unpublished observations). However, the increase continued thereafter linearly until death in the former eels, while the latter eels could adjust the plasma Na to the physiological level and could survive thereafter. It is without doubt that esophageal-cannulated eels in FW or isosmotic 1/3 SW did not suffer from cellular dehydration.

Hirano [7] observed that a slow infusion of

hypertonic NaCl into FW eels induced drinking in some FW eels. This result appears to be inconsistent with the present result. One possible interpretation of this discrepancy could be the difference in the route of administration. We did not adopt infusion because eels are aquatic species and, thus, the hypertonic solution given might be diluted by an influx of environmental water across the gill during the slow infusion. Another possibility arises from the experimental procedures. We withdrew 0.5 ml of blood simultaneously with the injection for radioimmunoassay of AII. We chose these procedures in order to follow the changes in drinking rate, plasma AII, Na and K levels at the same time in a single animal. We found that these procedures themselves did not cause significant changes in plasma AII, Na and K levels as exemplified by the changes in controls injected with 0.9% NaCl, but the drinking rate appears to be more vulnerable to the influence of these procedures (Fig. 1). However, it should be emphasized that the inhibition of drinking was invariably observed in FW, 1/3 SW-adapted, 1/3 SW-exposed and SW-exposed eels after injection of hypertonic solutions compared with controls injected with isotonic saline according to the same protocol.

It is generally accepted that, in mammals, the macula densa responds to increased levels of Na or Cl ions in the tubular urine by inhibiting renin release from the juxtaglomerular cells. Thus, the administration of hypertonic solution of NaCl results in a decrease of plasma AII level [5]. The inhibitory role of the macula densa in renin release appears to be active in birds also, because an increased load of NaCl decreased plasma renin activity in anesthetized chickens [23], and decreased plasma AII level in the conscious quail [21]. In the present study, however, injection of 7% and 14% NaCl elevated plasma AII levels in FW eels and 1/3 SW-adapted eels. Since the primary factor that determines plasma AII level appears to be plasma renin activity [5], it is assumable that renin release was not inhibited, but rather stimulated by injection of the hypertonic NaCl solutions in the eel. Consistent with this assumption is a report that the macula densa does not exist in fishes [6]. It appears that an increase in

plasma osmolality itself is stimulatory for renin release, because hypertonic sucrose consistently increased plasma AII levels in the eel as shown in the present study (Fig. 2), and increased plasma osmolality by dextran or human serum albumin, but not by NaCl, increased renin release in anesthetized dogs [24]. Thus, it appears that the injection of hypertonic NaCl solution increased renin release in the eel due to the absence of the macula densa. The present results seem to support the role of the macula densa in the control of renin release from the phylogenetic point of view. A direct measurement of renin release is being undertaken in the eel to substantiate this assumption.

On the other hand, injection of 7% NaCl failed to cause significant increases in plasma AII level in 1/3 SW and SW-exposed eels. This result could be due to a depletion of stored renin in the juxtaglomerular cells after exposure to 1/3 SW or SW, since it has been shown that plasma AII level increases after exposure to SW [8], as confirmed by the result of SW-exposed eels in the present study (Table 3). Responses of renin to external osmolality have also been reported in the eel; plasma renin activity was increased by the transfer of eels from FW to SW [25], and decreased by the transfer from SW to dilute media [26, 27].

In summary, the present study showed that the drinking rate was rather inhibited, and plasma AII level was increased after an intra-arterial injection of hypertonic solutions of NaCl and sucrose in the eel. These results are in contrast to those obtained in terrestrial animals that drinking is induced by intravascular administration of hypertonic solutions in mammals, birds and reptiles, and plasma AII level is decreased by intravascular administration of hypertonic NaCl solutions in mammals and birds.

ACKNOWLEDGMENTS

The authors express their appreciation to Dr. Tetsuya Hirano, Ocean Research Institute, University of Tokyo, for his valuable advice and critical reading of this manuscript. This investigation was supported in part by a Grant-in-Aid (574307) from the Ministry of Education, Japan.

REFERENCES

- 1 Fitzsimons, J. T. (1979) The Physiology of Thirst and Sodium Appetite, Cambridge Univ. Press, Cambridge, pp.32-94, p. 149 and pp. 158-165.
- 2 Kaufman, S. and Peters, G. (1980) Regulatory drinking in the pigeon *Columba livia*. *Am. J. Physiol.*, **239**: R219-R225.
- 3 Kobayashi, H. and Takei, Y. (1982) Mechanisms for induction of drinking with special reference to angiotensin II. *Comp. Biochem. Physiol.*, **71A**: 485-494.
- 4 Fitzsimons, J. T. and Kaufman, S. (1977) Cellular and extracellular dehydration, and angiotensin as stimuli to drinking in the common iguana *Iguana iguana*. *J. Physiol.* (London), **265**: 443-463.
- 5 Keeton, T. K. and Campbell, W. B. (1981) The pharmacologic alteration of renin release. *Pharmacol. Rev.*, **32**: 81-227.
- 6 Sokabe, H. and Ogawa, M. (1974) Comparative studies of the juxtaglomerular apparatus. *Int. Rev. Cytol.*, **37**: 271-327.
- 7 Hirano, T. (1974) Some factors regulating water intake in the eel, *Anguilla japonica*. *J. Exp. Biol.*, **61**: 737-747.
- 8 Takei, Y., Uemura, H. and Kobayashi, H. (1985) Angiotensin and hydromineral balance: With special reference to induction of drinking behavior. In "Current Trends in Comparative Endocrinology". Ed. by B. Lofts and W. N. Holmes. Hong Kong Univ. Press, Hong Kong, pp. 933-936.
- 9 Takei, Y., Kobayashi, H. and Hirano, T. (1979) Angiotensin and water intake in the Japanese eel, *Anguilla japonica*. *Gen. Comp. Endocrinol.*, **38**: 466-475.
- 10 Beasley, D., Shier, D. N., Malvin, R. L. and Smith, G. (1986) Angiotensin-stimulated drinking in marine fish. *Am. J. Physiol.*, **250**: R1034-R1038.
- 11 Carrick, S. and Balment, R. J. (1982) The renin-angiotensin system and drinking in the euryhaline flounder, *Platichthys flesus*. *Gen. Comp. Endocrinol.*, **51**: 423-433.
- 12 Kobayashi, H., Uemura, H., Takei, Y., Itazu, N., Ozawa, M. and Ichinohe, K. (1985) Drinking induced by angiotensin II in fishes. *Gen. Comp. Endocrinol.*, **49**: 295-306.
- 13 Malvin, R. L., Schiff, D. and Eiger, S. (1980) Angiotensin and drinking rates in the euryhaline killifish. *Am. J. Physiol.*, **239**: R31-R34.
- 14 Hirano, T. and Hasegawa, S. (1983) Effects of angiotensins and other vasoactive substances on drinking in the eel, *Anguilla japonica*. *Zool. Sci.*, **1**: 106-113.
- 15 Yamaguchi, K. (1981) Effects of water deprivation on immunoreactive angiotensin II levels in plasma, cerebroventricular perfusate and hypothalamus of the rat. *Acta Endocrinol.*, **97**: 137-144.
- 16 Hasegawa, Y., Nakajima, T. and Sokabe, H. (1983) Chemical structure of angiotensin formed with kidney renin in the Japanese eel, *Anguilla japonica*. *Biomed. Res.*, **4**: 417-420.
- 17 Khosla, M. C., Nishimura, H., Hasegawa, Y. and Bumpus, F. M. (1985) Identification and synthesis of [1-Asparagine, 5-Valine, 9-Glycine] angiotensin I produced from plasma of American eel *Anguilla rostrata*. *Gen. Comp. Endocrinol.*, **57**: 223-233.
- 18 Conover, W. J. (1980) Practical Nonparametric Statistics, John Wiley & Sons, New York, 2nd ed.
- 19 Skadhauge, E. (1981) Osmoregulation in Birds, Springer Verlag, Berlin, Heidelberg and New York, p. 4.
- 20 Bentley, P. J. (1971) Endocrine and Osmoregulation, Springer Verlag, Berlin, Heidelberg and New York, p. 6 and pp. 218-226.
- 21 Takei, Y., Okawara, Y. and Kobayashi, H. (1988) Control of drinking in birds. In "Progress in Avian Osmoregulation". Ed. by M. R. Hughes and A. C. Chadwick. Leeds Philosophical and Literary Society Ltd., Leeds (in press).
- 22 Takei, Y. and Hatakeyama, I. (1987) Changes in blood volume after hemorrhage and injection of hypertonic saline in the conscious quail, *Coturnix coturnix japonica*. *Zool. Sci.*, **4**: 803-811.
- 23 Nishimura, H. and Bailey, J. R. (1982) Intrarenal renin-angiotensin system in primitive vertebrates. *Kidney Int.*, **22**: S185-S192.
- 24 Hall, J. E. and Guyton, A. C. (1976) Changes in renal hemodynamics and renin release caused by increased plasma oncotic pressure. *Am. J. Physiol.*, **231**: 1550-1556.
- 25 Sokabe, H., Oide, H., Ogawa, M. and Utida, S. (1973) Plasma renin activity in Japanese eels (*Anguilla japonica*) adapted to seawater or in dehydration. *Gen. Comp. Endocrinol.*, **21**: 160-167.
- 26 Henderson, I. W., Jotinsankasa, V., Mosely, W. and Oguri, M. (1976) Endocrine and environmental influences upon plasma cortisol concentrations and plasma renin activity of the eel, *Anguilla anguilla* L. *J. Endocrinol.*, **70**: 81-95.
- 27 Nishimura, H., Sawyer, W. H. and Nigrelli, R. F. (1976) Renin, cortisol and plasma volume in marine teleost fishes adapted to dilute media. *J. Endocrinol.*, **70**: 47-59.

A Method of Quantitative Analysis of Cell Migration Using a Computerized Time-lapse Videomicroscopy

NOBUO ZAMA and HIDEKI KATOW¹

Laboratory of Computer Science and ¹Laboratory of Biology, Rikkyo University,
Nishi-Ikebukuro, Tokyo 171, Japan

ABSTRACT—A quantitative analysis of the cell migration *in vitro* has been realized by examining a distance of the migration performed by the cells, and the results are represented by a format called the “cell migration pattern”. We have composed a system which is capable to calculate the cell migration patterns, and to carry on such statistical tests as the parametrics as well as the non-parametrics to compare and evaluate the significant differences among the cell migration patterns. The system consists of an inverted phase contrast microscope, a video camera which is connected with the microscope, a monitor TV, a time-lapse video cassette recorder, a position analyzer, and a micro-computer. This system can trace 7 cells at a time and calculate above migration criterion. The system was applied to analyze the migratory behavior of the primary mesenchyme cells of the sea urchin blastulae in different culture conditions as a model case. Its desired functions were fully demonstrated in the present study.

INTRODUCTION

The cell migration is one of the elemental processes in the morphogenesis of the multicellular animals, and the importance of the extracellular matrix as a substratum for the migration has long been recognized (e. g. [1-3]). However, despite the recent increasing demand that the morphogenetic movements, particularly the cell migration, should be analyzed quantitatively [4, 5], it has not been fulfilled mainly because of technical difficulties. In order to obtain proper data for the quantitative analysis one has to incubate the cells in various culture conditions, to record and compare their behavior, and finally to examine whether there are any significant differences among them using appropriate statistical tests. One of the difficulties associated with the analysis, moreover, was that there have been few methods to organize raw data. In order to deal with these difficulties, it has been proposed that the cell migration is quantified by 1) examining a distance

of the migration performed by the cells, 2) organizing these data into a proper format, such as the “cell migration pattern” [4, 5], and by 3) comparing the patterns statistically. However, those whole procedures required truly time-consuming laborious works to complete. Development of a new method, therefore, has been awaited to adequately and promptly handle those processes.

Recently, the technology of computer graphics has been remarkably developed with the improvements of a computer performance along with the progress of the computer application techniques. Since this technology enables us to send the images to a computer as input data and process them in desirable manner for the researchers, we have composed a new system which processes the images of moving cells, and automatically calculates the results in a short period. The system is capable to handle up to 7 cells simultaneously.

The present system was applied to analyze the migration of the primary mesenchyme cells of the sea urchin, *Pseudocentrotus depressus*, in two different culture conditions as a model case. These culture conditions resulted in visually similar cell migration patterns [6] so that proper statistical

Accepted July 6, 1987

Received May 15, 1987

¹ To whom requests of reprints should be addressed.

treatments were required.

The present system has succeeded to evaluate the present model case, and to demonstrate the desired functions.

MATERIALS

The eggs of the sea urchin, *Pseudocentrotus depressus*, were collected by intracoelomic injection of 0.5M KCl, and raised in an artificial sea water, Jamarin U (Jamarin Laboratory, Osaka) until the mesenchyme blastula stage at 20°C. The primary mesenchyme cells were separated from the mesenchyme blastulae with the method presented previously [4, 5]. The cells were incubated in the artificial sea water containing 40 µg/ml of horse plasma fibronectin, which was kindly provided by Dr. M. Hayashi, Ochanomizu Women's University, Tokyo. This culture condition was designated as an experiment group 1. Aliquots of cells were incubated in a culture medium which was composed of the same amount of fibronectin and 40 µg/ml of a synthetic peptide, Arg-Gly-Asp-Ser, which is known to inhibit the fibronectin dependent cell migration with proper concentration [7] (Experiment group 6). The experiment numbers were retained to be the same as that of the previous study [6] in this paper in order to keep the integrity of the data with that study. The synthetic peptide has been kindly provided by Dr. K. M. Yamada, National Institutes of Health, U. S. A. The effect of the synthetic peptide on fibronectin dependent cell migration has been studied previously in the sea urchin primary mesenchyme cells [6]. Those experiment groups were chosen as model case in this study since it has been known from the previous studies that they possess visually similar cell migration patterns (Fig. 6), so that the statistical examinations were strongly required to evaluate any significant differences between them. The outcome of the examinations, therefore, was to provide whether there was any effect of the synthetic peptide on the fibronectin dependent primary mesenchyme cell migration *in vitro*.

In order to apply the technology of the computer graphics, an inverted phase contrast microscope with Nomarski optics (Nikon, Tokyo) was con-

nected with a video camera (WV-1500, National, Tokyo), a monitor TV (WV-5400, National, Tokyo), a time-lapse video cassette recorder (VHS type, AG-6010, National, Tokyo), a position analyzer (VPA-1100, Nippon Jimu Koki Co. Ltd., Tokyo), and with a microcomputer (CZ-802C, Sharp Co., Osaka) (Figs. 1 and 2). Although the system was capable to handle as many cells as the researchers desire at a time, regarding human errors that were predicted to happen more frequently correlated with the increasing number of cells to be handled at a time during a process to pick up the initial data, the number of cells to be



FIG. 1. The composition of the cell migration analysis system. Images from a microscope are recorded with a time-lapse video cassette recorder (2) through a video TV camera (1) and displayed in a monitor TV (3). The images are also sent to a microcomputer (6) through a position analyzer (4). The images are superimposed in the computer CRT with the coordinates of the cells collected through a light pen (5).

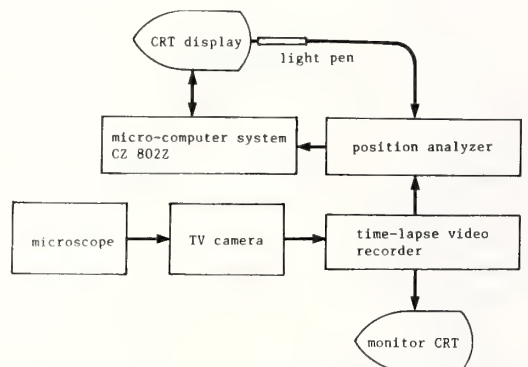


FIG. 2. A chart indicating flows of informations with arrows in the system.

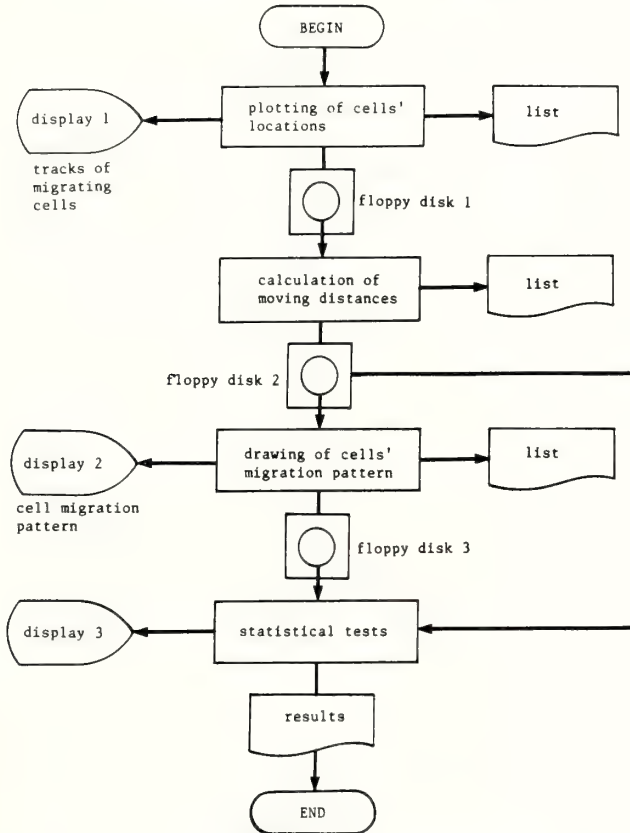


FIG. 3. A summary of the information flow.

handled at a time was set to be at most 7. After tracing the tracts of the cells in the computer display, cathode ray tube (CRT), the system prints out the results of the moving distances and tracts of individual cells, and stores these data in the floppy disks. Then the computer calculates the cell migration patterns from the stored data, and carries on statistic tests. The tests include a χ^2 -test and an F-test as the parametric tests, and two non-parametric tests, a Kolmogorov-Smirnov test and a Mann-Whitney test (Fig. 3).

METHODS AND RESULTS

General explanation of the system

The migration of the cells was recorded using the monochrome video camera by the time-lapse video cassette recorder through the inverted phase

contrast microscope which was installed with Nomarski optics. The recorded images of the migrating cells were played back chronologically, and the static images were obtained by manually ceasing the running of the video tapes at every 5 min of recorded time, which was indicated in the video display by a time-generator installed in the time-lapse video cassette recorder (Fig. 4a). Each location of the cells was detected on the static image displayed in the microcomputer CRT through the position analyzer by pointing the cells with a light pen one by one (Fig. 2). The light pen was installed in the position analyzer which had change-over switches and push buttons.

The position analyzer also was able to carry on two operating modes, an axis-setting mode and a measurement-mode, which can be changed from a mode to another with the change-over switch. Prior to operating the analyzer, one has to initiate

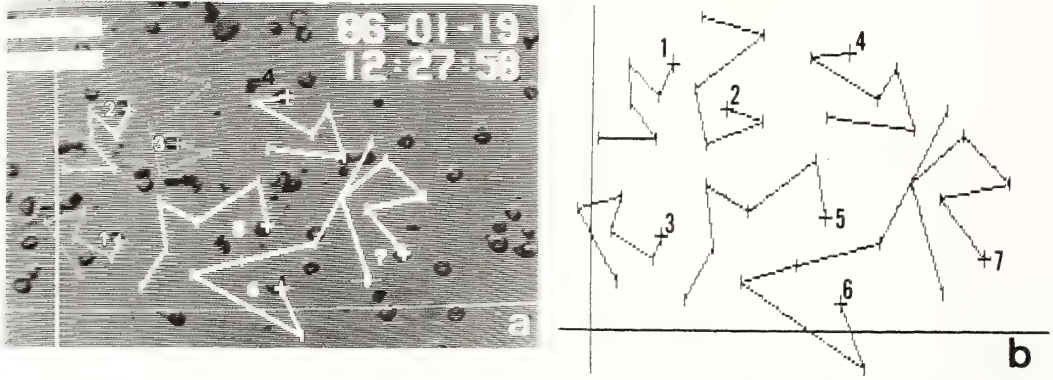


FIG. 4. (a) The superimposed images of the cells and their migration tracts shown with bars. The initial locations of the cells were indicated with crosses by the numbers. By reading the time displayed at the upper right corner of the CRT, the video tape was chronologically ceased to run manually to collect the new locations of the cells. (b) The cell migration tracts were extracted from the superimposed images in the CRT, and were printed out for further analysis.

the procedure by setting the switch to the axis-setting mode and then point a place in monitored image with the light pen in order to set up the axis of the coordinate which was programmed to display with a cross in the computer CRT as well as in the monitor TV.

After changing the mode to the measurement, a process of data input was started to repeat the pointing of original locations of each cell displayed in the computer CRT with the light pen (A data input process) (Fig. 4). The values of the coordinates of each location of the cells were sent to the microcomputer. The processing CZ-802C microcomputer superimposes any images coming from the external device, such as the video cassette recorder in this system, to the images already displayed in the computer CRT (Fig. 4a). The images of tracts of the migrating cells were extracted from the superimposed images in the computer CRT to the computer and were printed out after the completion of the data input process (Fig. 4b).

The input raw data were stored in floppy disks and then used for calculation by the computer according to the program that will be mentioned elsewhere in this paper (Fig. 3). The calculated data including the statistically treated ones were finally printed out on the paper. Five-inch floppy disks were used to store the values of coordinates of the cells as well as the results of the process, and

3.5-inch floppy disks were used to store the program written with Hu-BASIC [8]. They were necessary for processing the data and the system to control the microcomputer [9].

Operating process

The processing program for the microcomputer was designated in accordance with the following operating process. In this system every experiment was assigned numerically with an experiment group number (Group number) first, and as an experimental condition was identical with the others the group number of the experiment was defined to be the same as those. The numbers after the experiment group number in printouts showed that of trials in one experiment group (Experiment number) (Fig. 5).

The computation was initiated according to the following steps.

- 1) To put the computer system on action, and load necessary computer program to the computer.
- 2) To switch on the video cassette recorder, and make the computer superimpose the picture of the recorded images of the cells in the computer CRT.
- 3) To locate original positions of the cells. As one makes a picking-up program run, the computer asks one the origin of the coordinate on the head of the first picture frame of the video display.

A	B	C	D	E	F	G
1	1	1	43.859701	2.8662313	1.6747438	10.77033
1	1	2	11.242641	.70266304	.56438997	5
1	1	3	45.29032	2.8306575	2.5037077	15.264337
1	1	4	10.828427	.6767767	.56041984	4.2426407
1	1	5	30.083405	1.8802128	1.3273264	5.8309319
1	1	6	15.242641	.95266304	.67934708	2.236068
1	1	7	67.28308	4.2051925	3.5019643	12.041595
1	1	8	22.394353	1.4121396	.80654566	3.6055313
1	1	9	30.028532	1.8767832	1.0592243	4.1231056
1	1	10	22.906114	1.4316321	1.1199926	2.236068
1	1	11	8.8284271	.5517767	.67232029	3.1622777
1	1	12	32.719362	2.0449601	1.3546211	7.2501099
1	1	13	32.397817	2.0248636	1.0737949	3
1	1	14	20.307136	1.269196	.48506808	3.1622777
1	1	15	9.5625	.49607837	2.236068	
1	1	16	39.492056	2.4682535	1.8449271	10
1	1	17	25.217478	1.3760923	.71689478	6
1	1	18	49.379369	3.0862106	2.1698789	6.7082039
1	1	19	13.828427	.8642767	.58592642	5
1	1	20	8.5	.5	4.2426407	
1	1	21	42.004057	2.6252535	1.3282911	10
1	1	22	98.621634	6.1638521	5.9715942	5.3851648
1	1	23	37.575963	2.3484977	1.8157804	3
1	1	24	32.14433	2.0090206	1.6028051	11.313700
1	1	25	22.41811	1.4011319	1.1139828	4.4721359
1	2	1	24.021912	1.2643112	.65524001	3.6055313
1	2	2	74.485114	3.9202692	2.0500534	9.2195444
1	2	3	24.307136	1.2793229	.74204446	7.0710678

Fig. 5. Print out of the initially treated data sent to "floppy disk 2" from "floppy disk 1". A; group numbers. B; experiment numbers. C; point numbers which are put onto every cells examined. In this case 25 cells were examined. D; actual total migration distances, which are the sum of total length of bars drawn between every points traced according to a cell's migration tract. E; average migration distances performed by a cell during 100 min of examination period in this case. F; S. D. of the average migration distance. G; short cut distance between the original locations and the last one.

The coordinate was set to be $x, y=30, 150$ in this system (Fig. 4). The number of cells one can pick up from the frame at a time was anywhere up to 7 as has been stated before in this paper. The program was made so that one can input the coordinate values of the cells to computer as one taps a key of the input-keyboard after pointing the cells with the light pen, and the input was confirmed with the display of a cross on each point (the cell) in the computer CRT (Fig. 4). The crosses retained at the original locations of the cells through the process until completion of the data transfer to the secondary floppy disks for restoration for further data processing (Fig. 3). In a secondary picture frame of the video display, 5 min of computer CRT display-time after the first picture frame, one points the cell's new locations following the numbers displayed near the crosses represented the original locations of each cell, and tapping the key at each time after pointing the new

locations of the cells with the light pen, which was confirmed by a bar drawn between the original point and the new one (Fig. 4). This procedure was repeated through the last picture frame which was set initially by researchers as an observation period. For instance, if one is to collect the locations of the cells every 5 min for 100 min of the observation period, the number of the picture frames will be 21 including the first one, a time zero. The process is needed to be repeated according to the number of cells to be examined, such as 5 times when one handles 35 cells in total and 7 cells at a time.

During the procedure the computer displayed the tract of each cell with the bars of different colors according to the cells (Fig. 4a). The total number of cells examined and that of input procedure were confirmed by the computer momentarily on the CRT display at the end of each process. The data picking-up program was terminated by tapping a key of the keyboard.

The coordinate values of the cells obtained by the above procedure were stored in 5-inch floppy disks (Floppy disk 1).

4) Calculation. The data in the "Floppy disk 1" were the starting point of the following procedures. The first step of the procedures was "calculation of moving distance" as was labeled accordingly in a block of Figure 3 chart. This step consisted of the following two substeps.

a) To calculate the migration distances of the cells from the coordinates of them at each moment.

b) To put all the data of different disks together into one disk (Floppy disk 2) in order to organize the data as the same experiment group (Fig. 5).

The second step signed "drawing of cell migration pattern" in a block of Figure 3 chart was started from the floppy disk 2. This step consisted of the following two substeps.

a) To draw a histogram of the moving distances of the cells in an experiment.

b) To convert the histogram to the cell migration pattern.

The floppy disk 3 stored all the histograms and the cell migration patterns carried on in a series of experiments (Fig. 6).

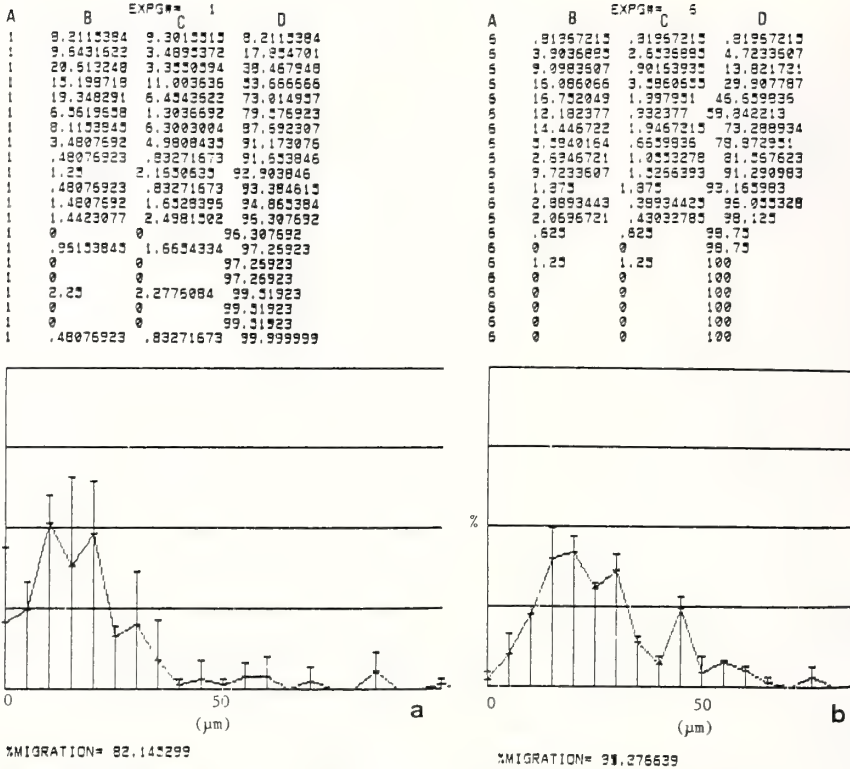


Fig. 6. The cell migration patterns of experiment group 1(a) and 6(b). In both (a) and (b) the top numeral columns indicate and experiment group number (A), a proportion of the cells clarified in a group indicated with percent (B), S. D. of the B(C), and an integral from the first cell group indicated with percent (D). The bottom graphs indicate the cell migration patterns with S. D. s, which are shown with vertical bars. The very bottom of the graphs indicates the percent migration values.

```

EXPERIMENT GROUP NUMBER      1
TOTAL NUMBER OF CELLS        114
MEAN                          23.718702
UNBIASED VARIANCE             356.10723

EXPERIMENT GROUP NUMBER      6
TOTAL NUMBER OF CELLS        140
MEAN                          29.745062
UNBIASED VARIANCE             225.69918

VARIANCES ARE DIFFERENT

FF= 1.39
FO= 1.5777959

MEANS ARE DIFFERENT
    
```

Fig. 7. The print out of the parametric test results. FF and FO indicate the results of F-test. The conclusion of the F-test is indicated with terse statement.

5) Statistical treatments. For the parametric tests, the following procedures were pursued (Fig. 7).

- a) To test the equality of the variances by an F-test.
- b) If the two variances are equal, after estimation of the population variance a t-test was applied to examine the equality of the means.
- c) If the two variances are unequal, a Welch test was applied to examine the equality of the means.

In case of the primary mesenchyme cells, however, it was regarded to be inadequate to evaluate above data solely based on the parametric statistics which premise a standardized cell migration behavior [10, 11] due to rather poorly understood migratory behavior of the cells. Under the

consideration, in addition to above two parametric tests further two non-parametric tests, a Kolmogorov-Smirnov test and a Mann-Whitney test were adopted as well (Fig. 8). Therefore, one can examine the equality of variances of two results and that of the means [10, 11].

The statistical tests were applied to both the data in the "Floppy disk 2" and "Floppy disk 3", and were particularly useful to clarify any potential and significant differences among the cell migration

patterns. One of these statistical treatments was available by tapping a key of the keyboard. The results with 5% error were displayed instantaneously in computer CRT and printed out upon researcher's request (Figs. 7 and 8).

In the present model case the experiment groups 1 and 6 were significantly different with each other despite the visually similar cell migration patterns and rather close percent migration values (Fig. 6). Therefore, it was concluded that the synthetic peptide Arg-Gly-Asp-Ser interfered the fibronectin dependent migration of the primary mesenchyme cells in this concentration *in vitro*.

DISCUSSION

Two methods have been reported to input the image informations into the computer in order to process the informations for particular analysis. A method is to convert whole picture frame of images to the digital informations, and then input them to the computer (the digitization method) [8, 9, 12]. The other is to pick up only necessary informations from each image displayed with appropriate extracting devices (the direct extracting method) [12].

Applying the former method, one carries on a great variety of processes, since the whole informations on the images can be referred. The amount of informations to be processed by this method, however, becomes enormous and therefore costly hardwares are required to be deployed. Moreover, the input data obtained often contain unnecessary informations as well. The latter method which was adopted in the present research was shown to be rather simple. The performance of the system was indicated to be sufficient for the present research aims.

For the statistical tests, the non-parametric tests were used to examine the equality of the medians of two different kind of distributions, and the parametric tests were used to examine the variances and the means of the data. The medians, however, were not always adequate to adopt as a sole statistical criterion, because, if small portion of an experiment group which involves extremely large migration distances in a parameter, the median does not represent proper feature of the

```

MANN-WHITNEY TEST
R1= 9329.264  R2= 11770.736
U0= 3279.2639
SIG= 406.0124
Z0= 4.2381368
MANN-WHITNEY TEST(5% SINGLE-SIDE)
          DIFFERENCE IS SIGNIFICANT

KOLMOGOROV SMIRNOV TEST
Z(1)
0
.03
7.3919663E-02
.1313134
.24646227
.23758879
.26355122
.20734711
.14403373
.12300126
.10086223
1.6128625E-02
2.1863177E-03
-1.1899433E-02
-1.8173077E-02
-2.4423077E-02
-1.4807692E-02
-2.7307692E-02
-2.7307692E-02
-4.807692E-03
0
MAX= .26355122
KAI= 13.891849
KOLMOGOROV-SMIRNOV TEST(5%-SINGLE)
          DIFFERENCE IS SIGNIFICANT

```

FIG. 8. The print out of two non-parametric tests, a Mann-Whitney test and a Kolmogorov-Smirnov test. In Mann-Whitney test R1, R2 indicate orders in experiment group 1 and 6, respectively. Conclusion of the calculation with 5% error was printed out after listing intermediate calculations (U0, SIG, Z0) with terse statement. In Kolmogorov-Smirnov test intermediate calculations were displayed after Z(1), and MAX is smaller than KAI, which means difference of experiment group 1 and 6 is approved as is indicated with the last terse statement as a conclusion.

parameter. In this case seeking the mean of the data which is calculated based on the parametric tests is to be more accurate [9].

In the model case the statistically proved inter-ruptive effect of the synthetic peptide onto fibronectin dependent primary mesenchyme cell migration has been supported by further observations performed in higher concentrations of the synthetic peptide [6]. Therefore, an adequacy of the present system's function was fully proved.

The present computer program will be available from our laboratories upon researchers requests.

ACKNOWLEDGMENT

This research has been supported in part by a Grant-in-Aid for Scientific Research from the Ministry of Education, Science and Culture, Japan to H. K. (Nos. 61540535 and 61304009).

REFERENCES

- 1 Hynes, R. O. (1981) Fibronectin and its relation on cellular structure and behavior. In "Cell Biology of Extracellular Matrix". Ed. by E. D. Hay, Plenum Press, New York, pp. 295-334.
- 2 Katow, H. (1987) Sea urchin primary mesenchyme cells. In "Developmental Systems and Cell Behavior". Ed. by H. Katow and H. Mizoguchi, Baifukan, Tokyo, pp. 3-33. (In Japanese)
- 3 Solursh, M. (1985) Migration of sea urchin mesenchyme cells. In "Developmental Biology: A Comprehensive Synthesis". Vol. 2. Ed. by L. W. Browder, Plenum Press, New York, pp. 391-432.
- 4 Katow, H. and Hayashi, M. (1985) Role of fibronectin in primary mesenchyme cell migration in the sea urchin. *J. Cell Biol.*, **101**: 1487-1491.
- 5 Katow, H. (1986) Behavior of sea urchin primary mesenchyme cells in artificial matrices. *Exp. Cell Res.*, **162**: 401-410.
- 6 Katow, H. (1987) Inhibition of cell surface binding of fibronectin and fibronectin-promoted cell migration by synthetic peptides in sea urchin primary mesenchyme cells *in vitro*. *Dev. Growth Differ.*, **29**: 573-589.
- 7 Yamada, K. M., Akiyama, S. K., Hasegawa, E., Humphries, M. J., Kennedy, D. W., Nagata, K., Urushihara, H., Olden, K. and Chen, W.-T. (1985) Recent advances in research on fibronectin and other cell attachment proteins. *J. Cell. Biochem.*, **28**: 79-97.
- 8 Manual of Hu-BASIC (1984) Sharp Co. Ltd., Osaka. (In Japanese)
- 9 Manual of microcomputer CZ-802C (1984) Sharp Co. Ltd., Osaka. (In Japanese)
- 10 Kendall, M. G. and Stuart, A. (1973) The Advanced Theory of Statistics. Vol. 2, 4th ed., Charles Griffin, London.
- 11 Gibbons, J. D. (1985) Nonparametric Statistical Inference. 2nd ed., M. Dekker, New York.
- 12 Foley, J. and Van Dam, A. (1982) Fundamentals of Interactive Computer Graphics. Addison-Wesley Reading, Massachusetts.

Fine Structure of Filiform Papillar Epithelium from the Tongue of the Frog, *Rana nigromaculata*

SHIN-ICHI IWASAKI, KEN MIYATA and KAN KOBAYASHI

*Department of Anatomy, School of Dentistry at Niigata,
The Nippon Dental University, Niigata 951, Japan*

ABSTRACT—Light and transmission electron microscopies were used to investigate the ultrastructure of filiform papillar epithelium from the tongue of the frog, *Rana nigromaculata*. A large part of the epithelium was composed of cells which contained many small, electron-dense granules. Ciliary cells and mucous cells were situated among these cells. Plasma cells and cells which contained many fat droplets were rarely seen within the epithelium. The possible functional roles of these epithelial cells were discussed.

INTRODUCTION

Physiologists frequently use frog tongues in their studies [1-3] because of the many taste organs or sensory discs on the fungiform papillae which are distributed among the filiform papillae on the dorsal surface. Electron microscopic studies of the structure of the sensory papillae include those of Graziadei [4], Graziadei and DeHan [5], and Düring and Andres [6], all of whom have reported that almost the entire surface of each sensory disc is covered with microvilli. However, more recent studies [7-9] have revealed that most of the surface of the sensory discs is covered with a honeycomb structure which can be seen after removal of the layer of superficial mucus. However, reports describing the features of the lingual epithelium apart from the sensory papillae are quite few in number [7-9]. In particular, the histological structures in the lingual epithelium of the frog have been practically ignored. In the present study, light and transmission electron microscopies were used to investigate the ultrastructure of the tongue of the frog, *Rana nigromaculata*.

Scanning electron microscopic observations have revealed significant differences in the dorsal surface of the tongue between frogs [7-9] and

mammals [10-12]. These differences appear to be related to differences in the function of the tongue. The present study was also designed to clarify the cellular features of the mucosal epithelium, and a brief discussion of its possible functional roles is included.

MATERIALS AND METHODS

Tongues from five male and five female adult frogs, *Rana nigromaculata*, were used in the present study. These frogs were collected in the area around the city of Niigata in June and July of 1984. The animals were perfused from the heart with Karnovsky fixative which contained glutaraldehyde and paraformaldehyde [13], under MS-222 anesthesia. The tongue was then removed and refixed in the same fixative. After rinsing in 0.1M cacodylate buffer, the samples were post-fixed in phosphate-buffered 1% osmium tetroxide solution [14] at 4°C for 1.5 hr. Postfixation was followed by dehydration, embedding in Epon-Araldite, ultrathin sectioning and double staining with uranyl acetate and lead citrate. The specimens were then observed under a transmission electron microscope (Hitachi H-500). Thick sections from the blocks embedded in Epon-Araldite were stained with 0.2% toluidine blue in 2.5% Na₂CO₃. Micrographs of the sections, taken with an Olympus BH-2 light microscope, were compared with the transmission electron micrographs.

RESULTS

When sections of lingual tissue embedded in Epon-Araldite were examined by light microscopy (Fig. 1), the dorsal mucosa of the tongue was seen to be composed of filiform and fungiform papillae. The filiform papillae were somewhat smaller than the fungiform papillae; however, their number was larger than that of fungiform papillae. The epithelium of the upper part of the filiform papillae was thicker than that of the basal part. Translucent cells which were filled with mucus occupied about 40% (by volume) of the epithelium. A high proportion of mucous cells was seen particularly in the upper area of the filiform papillae. The connective tissue of the lamina propria and the smooth muscle penetrated deeply into the center of each papilla. Relatively large numbers of the glandular structures were distributed within the lamina propria.

By transmission electron microscopy (Figs. 2-8), there were predominantly three types of epithelial cells observed in the mucosal epithelium of the tongue dorsum. One type of epithelial cell contained electron-dense, oval or round granules; another type of cell was the mucous cell; and the third type was the ciliated cell. Cells containing electron-dense granules occupied over 50% (by

volume) of the epithelium, and were situated over the entire area of the filiform papillar epithelium. Mucous cells occupied about 40% (by volume) of the filiform papillar epithelium. However, the volume of each mucous cells was several times larger than that of cells which contained electron-dense granules. Therefore, the actual number of mucous cells was much lower. These cells were located mainly on the upper part of the filiform papillae. Ciliated cells occupied about 5% (by volume) of the filiform papillar epithelium. These cells were scattered over the entire epithelium. The basal lamina was intercalated between the epithelium and the lamina propria throughout the mucosa of the filiform papillae.

Some of the cells with electron-dense granules, located in the upper area of the filiform papillar epithelium, contained these granules only in the region just beneath the free surface of the cells (Fig. 2). In other cells, these granules were distributed throughout the cytoplasmic area (Fig. 3). In both types of cells, the nucleus was located in the basal or central area of the cells (Figs. 2 and 3). Some cells contained not only many electron-dense, oval or round granules but also a few electron-lucent granules (Fig. 2). Rough-surfaced endoplasmic reticulum was well-developed in the cytoplasm of some granular cells (Figs. 2 and 3).

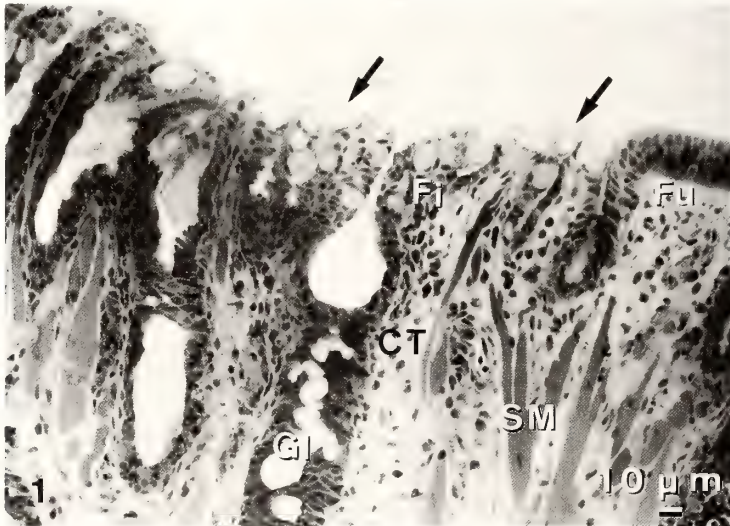


FIG. 1. Light micrograph of the lingual dorsal epithelium in Epon-Araldite-embedded tissue from a frog, *Rana nigromaculata*. Fi: filiform papilla, Fu: fungiform papilla, CT: connective tissue, SM: smooth muscle, Gl: glandular structure, arrows: mucous cells.

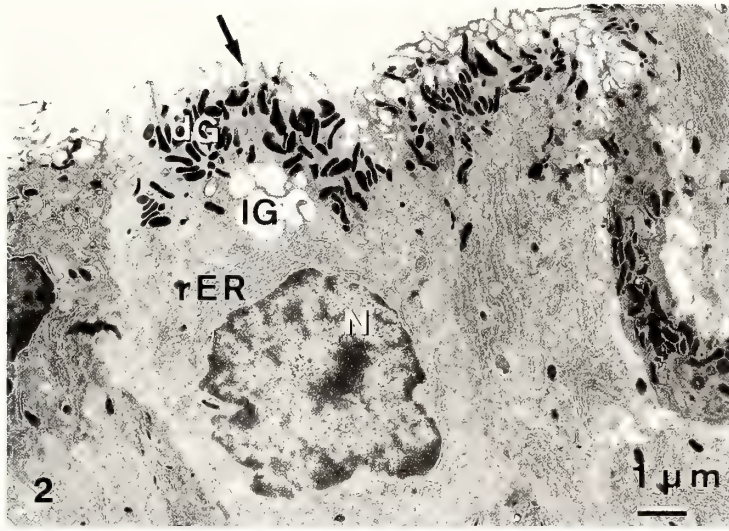
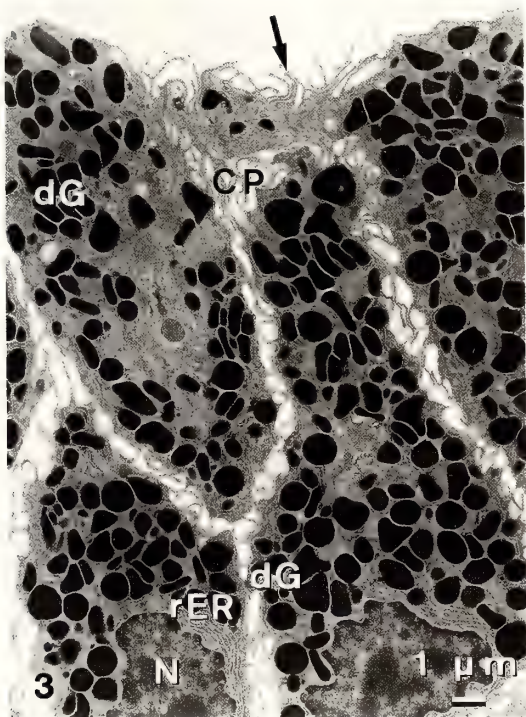


FIG. 2. Transmission electron micrograph of the epithelial cells in the upper part of a lingual filiform papilla from a frog, *Rana nigromaculata*. N: nucleus, rER: rough-surfaced endoplasmic reticulum, dG: electron-dense granules, IG: electron-lucent granules, arrow: micro-ridges.



Cells in which the cytoplasm was filled with mucous granules were frequently observed among the epithelial cells which contained electron-dense granules (Fig. 4).

In the basal part of the filiform papillae, the thickness of the epithelium was somewhat reduced. Cells which contained many electron-dense, small granules also contained a few electron-lucent granules. These cells mainly occupied the basal region of the epithelium. In this area, cells in which the cytoplasm was filled with mucus were rarely observed (Fig. 5).

In both the upper and basal regions of the filiform papillae, microridges, which have been formerly demonstrated by scanning electron microscope [9], were widely found on the free surface of the granular cells (Figs. 2-4, arrows). The cell surface which faced adjacent cells had abundant cellular processes (Figs. 3-5).

FIG. 3. Transmission electron micrograph of cells which contain a large number of electron-dense granules in the epithelium on the upper part of a lingual filiform papilla. N: nucleus, rER: rough-surfaced endoplasmic reticulum, dG: electron-dense granules, CP: cellular processes, arrow: micro-ridges.

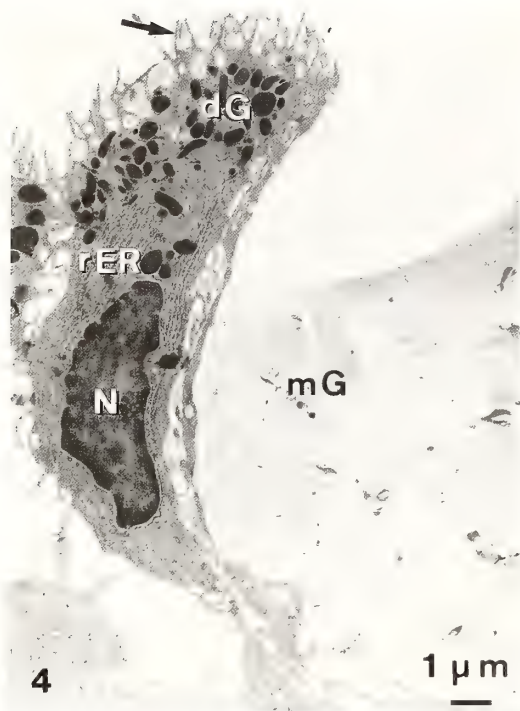


FIG. 4. Electron-dense granular cells and a mucous cell in the upper part of a filiform papilla. N: nucleus, rER: rough-surfaced endoplasmic reticulum, dG: electron-dense granules, mG: mucous granules, arrow: microridges.

Ciliated cells were scattered among these granular cells in both the upper and basal regions of the filiform papillar epithelium. The ciliated cells had cilia and microvilli, also previously revealed by scanning electron microscopy [9], on their free surfaces. Just beneath the free surface of these cells, basal bodies (Figs. 6 and 7, BB) and electron-dense vesicles (Fig. 7, arrow) can be recognized. Many lysosomes, mitochondria, rough-surfaced endoplasmic reticulum and free ribosomes were distributed throughout cytoplasm (Figs. 6 and 7).

In the basal region of the epithelium, the basal lamina was located between the epithelium and the lamina propria (Fig. 8, arrow). In the basal region of the cytoplasm of granular cells, there were a few electron-dense granules and the rough-surfaced endoplasmic reticulum was well-developed (Fig. 8). In the basal portion of the cytoplasm of ciliated cells, mitochondria and glycogen granules were abundant (Fig. 8).

Plasma cells (Fig. 9) and cells which contained many fat droplets (Fig. 10) could also be found in the epithelium, although they were very few in number.

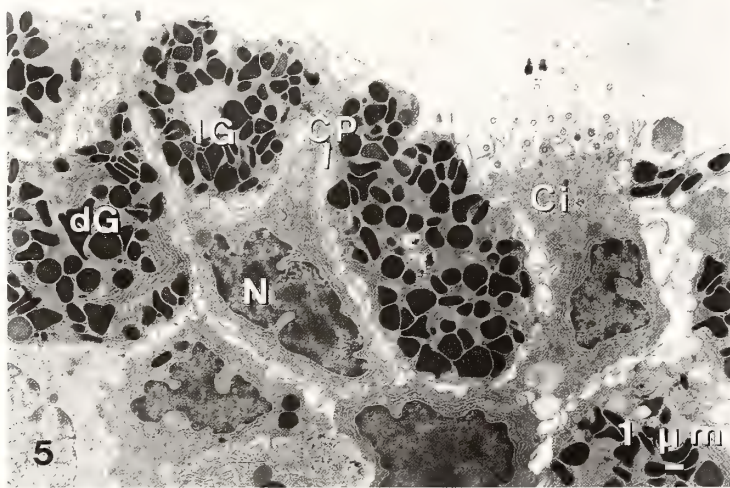


FIG. 5. The epithelium of the basal part of a filiform papilla. N: nucleus, dG: electron-dense granules, lG: electron-lucent granules, Ci: ciliated cell, CP: cellular processes.

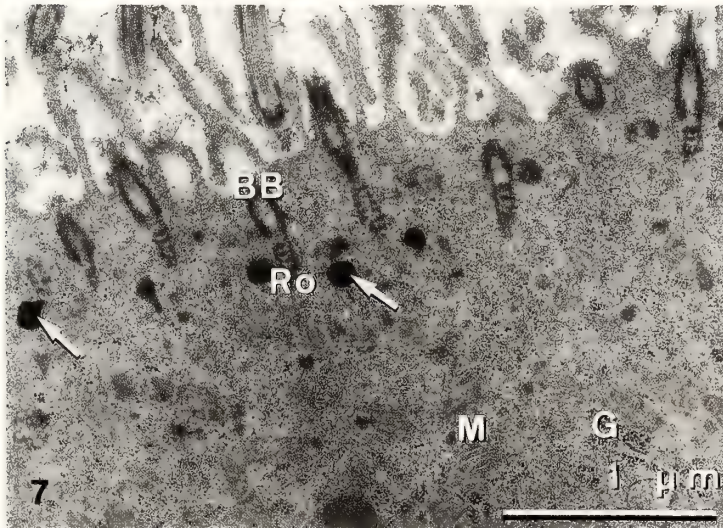
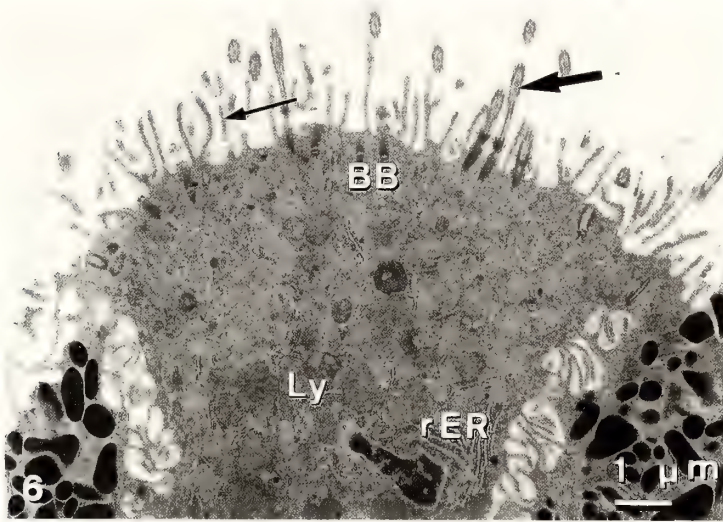


FIG. 6. A ciliated cell in the filiform papillar epithelium. rER: rough-surfaced endoplasmic reticulum, BB: basal bodies, Ly: lysosomes, CP: cellular processes, thick arrow: cilia, thin arrow: microvilli.

FIG. 7. Higher magnification of the free-surface side of a ciliated cell. BB: basal bodies, Ro: ciliary rootlet, M: mitochondrion, G: glycogen granules, arrows: electron-dense vesicles.

DISCUSSION

Anuran tongues play an important functional role in the uptake of food, in the sense of taste [1-3], and in the secretion of mucus [9, 10]. In mammals, tongues function mainly as the organ used for uptake of food and for the sense of taste [4], and are not so important for secretion of mucus. Salivary glands are the main mammalian

organs which serve this function. Furthermore, in a few species of reptiles [15, 16], mucous glands are located in a restricted area of the tongue, and the taste organs are located on various areas of the oral mucosa [16, 17]. Thus, it seems that there may be variations in the function and structure of the tongue based on the evolution of animals. The present study indicates that mucous cells occupy about 40% (by volume) of the filiform papillar

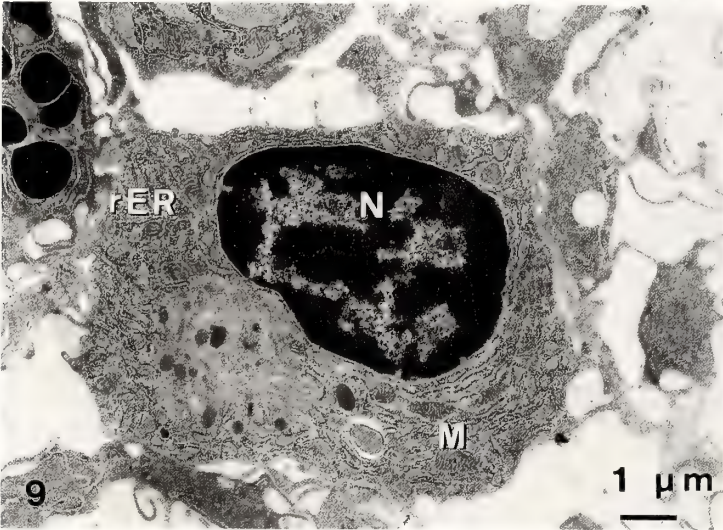
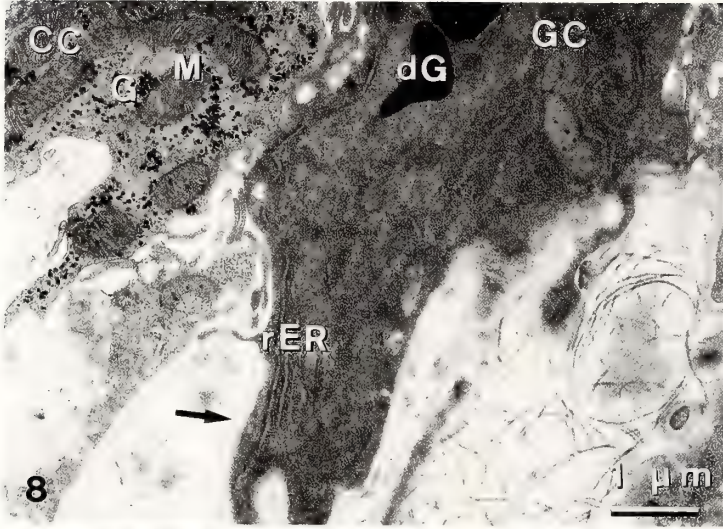


FIG. 8. Basal region of a granular cell (GC) and a ciliated cell (CC) in the mucosal epithelium of a filiform papilla. rER: rough-surfaced endoplasmic reticulum, dG: electron-dense granules, M: mitochondria, G: glycogen granules, arrow: basal lamina.

FIG. 9. A plasma cell located within the epithelium of a filiform papilla. N: nucleus, rER: rough-surfaced endoplasmic reticulum, M: mitochondria.

epithelium of the frog. Furthermore, the glandular structures, which are analogous to the lingual glands of mammals, were observed under light microscope in the lamina propria beneath the filiform papillae. These results demonstrate that the lingual dorsal mucosa of the frog is the main organ for the secretion of mucus.

The present study also indicates that a large part of the epithelium of the filiform papillae consists of

cells which contain many electron-dense, oval or round granules. The functional role of these granules is not obvious, but there are three possibilities. One is that these granules may be immature forms of mucous granules; another is that they may be serous granules. Yet still other possibility is that they may be organelles which are analogous to the Paneth cell granules of the gastrointestinal tract [18]. The results of the

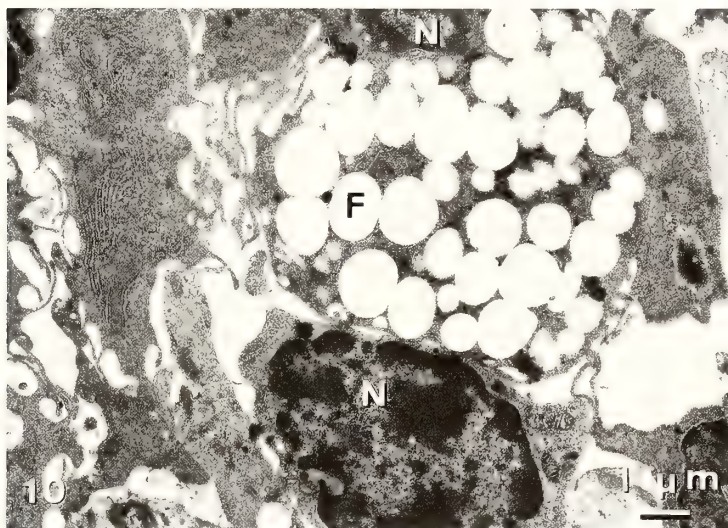


FIG. 10. A cell with many fat droplets within the epithelium of a filiform papilla. N: nucleus, F: fat droplets.

present study show that some of the lingual epithelial cells contain both electron-dense and electron-lucent granules. However, there was no evidence that there were any transitional stages between electron-dense granules and mucous granules. Thus, we are inclined to suggest that the electron-dense granules are a different type of granule from the mucous granule. The fine structure and electron-density of these granules seem to be similar to those of serous granules observed in the salivary glands of mammals [19–21]. However, the exact function of these granules remains to be elucidated. The small electron-lucent granules found between electron-dense, oval or round granules may be secretory versions of electron-dense granules.

Mature mucous cells, in which almost all the cytoplasm is filled with mucous granules, are similar to the goblet cells found in the gastrointestinal tract and trachea of mammals [22, 23].

Ciliated cells were observed to contain many lysosomes. This indicates that these ciliated cells may be involved in phagocytosis, as are similar cells in the human trachea [24, 25]. Thus, the lingual epithelium may have some functional role in addition to its role in the sense of taste.

In mammals, a greater part of the lingual dorsal epithelium is stratified squamous epithelium, and

various degrees of keratinization of the epithelium have been observed in different areas of the tongue [26–28]. In frogs, on the other hand, keratinization was not recognized at all in the lingual epithelium, and the epithelium was composed of various kinds of cells, i.e., electron-dense granular cells, ciliated cells, and cells of connective tissue origin. These differences may be partially based on the undifferentiated state of the frog's tongue as opposed to that of the mammalian tongue. It is possible that the lingual dorsal epithelium of the frog contains cells which are similar to those located in the mucosal epithelium of the gastrointestinal tract and/or the trachea of mammals. This hypothesis will be examined in more species of anurans in the future.

In our previous studies using scanning electron microscopy [8, 9], we clearly showed that micro-ridges are widely distributed on the cell surface of the filiform papillar epithelium. The present study indicates that the granular cells have both micro-ridges on the free surfaces of cells, and cellular processes on the other surfaces which face the adjacent cells. Thus, the micro-ridges may be the result of an altered pattern of arrangement of these cellular processes. The cellular processes seem to function as connecting structure between adjacent cells [29]. As suggested by Sperry and Wassersug

[30], microridges or cellular processes on the free surface probably facilitate the spreading and holding of mucus.

REFERENCES

- 1 Taglietti, V., Maffini, S. and Casella, C. (1971) The recovery cycle of gustatory fibres during chemical stimulation of the tongue. *Arch. Sci. Biol.*, **55**: 155–164.
- 2 Sato, T and Beidler, L. M. (1975) Membrane resistance change of the frog taste cells in response to water and NaCl. *J. Gen. Physiol.*, **66**: 735–763.
- 3 Akaike, N., Noma, A. and Sato, M. (1976) Electrical responses of frog taste cells to chemical stimuli. *J. Physiol.*, **254**: 87–107.
- 4 Graziadei, P. P. C. (1969) The ultrastructure of vertebrate taste buds. In "Olfaction and Taste". Ed. by C. Pfaffmann, Rockefeller Univ. Press, New York, pp. 315–330.
- 5 Graziadei, P. P. C. and DeHan, R. S. (1971) The ultrastructure of frogs' taste organs. *Acta Anat.*, **80**: 563–603.
- 6 Düring, M. v. and Andres, K. H. (1976) The ultrastructure of taste and touch receptors of the frog's taste organ. *Cell Tissue Res.*, **165**: 185–198.
- 7 Jeager, C. B. and Hillman, D. E. (1976) Morphology of gustatory organs. In "Frog Neurobiology". Ed. by R. Linal and W. Precht, Springer-Verlag, Berlin, pp. 588–606.
- 8 Iwasaki, S. and Sakata, K. (1985) Fine structure of the lingual dorsal surface of the bullfrog. *Okajimas Folia Anat. Jpn.*, **61**: 437–450.
- 9 Iwasaki, S., Miyata, K. and Kobayashi, K. (1986) Studies on the fine structure of the lingual dorsal surface in the frog, *Rana nigromaculata*. *Zool. Sci.*, **3**: 265–272.
- 10 Švejda, J. and Škach, M. (1971) Die Zunge der Ratte im Raster-Elektronenmikroskop (Stereo-scan). *Z. mikrosk.-anat. Forsch.*, **84**: 101–116.
- 11 Steffik, D. E., Singh, B. B., Mckinney, R. V. Jr. and Boshell, J. L. (1983) Correlated TEM, SEM, and histological observations of filiform papillae of the cow tongue. *Acta Anat.*, **117**: 21–30.
- 12 Iwasaki, S., Miyata, K. and Kobayashi, K. (1987) Comparative studies of the dorsal surface of the tongue in three mammalian species by scanning electron microscopy. *Acta Anat.*, **128**: 140–146.
- 13 Karnovsky, M. J. (1965) A formaldehyde-glutaraldehyde fixative of high osmolality for use in electron microscopy. *J. Cell. Biol.*, **27**: 137A–138A.
- 14 Millonig, G. (1961) Advantages of a phosphate buffer for OsO₄ solutions in fixation. *J. Appl. Physics*, **32**: 1637.
- 15 Iwasaki, S. and Miyata, K. (1985) Scanning electron microscopy of the lingual dorsal surface of the Japanese lizard, *Takydromus tachydromoides*. *Okajimas Folia Anat. Jpn.*, **62**: 15–26.
- 16 Schwenk, K. (1986) Morphology of the tongue in the tuatara, *Sphenodon punctatus* (Reptilia: Lepidosauria), with comments on function and phylogeny. *J. Morphol.*, **188**: 129–156.
- 17 Iwasaki, S., Miyata, K. and Kobayashi, K. (1985) Fine structure of the oral epithelial cell surface in the Japanese lizard, *Takydromus tachydromoides*. *Jpn. J. Oral Biol.*, **27**: 956–964.
- 18 Cheng, H. (1974) Origin, differentiation and renewal of the four main epithelial cell types in the mouse small intestine. IV. Paneth cells. *Am. J. Anat.*, **141**: 521–536.
- 19 Hand, A. R. (1971) Morphology and cytochemistry of the Golgi apparatus of rat salivary gland acinar cells. *Am. J. Anat.*, **130**: 141–158.
- 20 Riva, A. and Riva-Testa, F. (1973) Fine structure of acinar cells of human parotid gland. *Anat. Rec.*, **176**: 149–166.
- 21 Ichikawa, M. and Ichikawa, A. (1977) Light and electron microscopic histochemistry of the serous secretory granules in the salivary glandular cells of the Mongolian gerbil (*Mongolian meridianus*) and rhesus monkey (*Macaca irus*). *Anat. Rec.*, **189**: 125–140.
- 22 Cheng, H. (1974) Origin, differentiation and renewal of the four main epithelial cell types in the mouse small intestine. II. Mucous cells. *Am. J. Anat.*, **141**: 481–502.
- 23 Dalen, H. (1983) An ultrastructural study of tracheal epithelium of the guinea-pig with special reference to the ciliary structure. *J. Anat.*, **136**: 47–67.
- 24 Krstić, R. V. (1984) Illustrated Encyclopedia of Human Histology. Springer-Verlag, Berlin, pp. 424–425.
- 25 Fawcett, D. W. (1986) A Textbook of Histology, 11th ed. W. B. Saunders Co., Philadelphia, pp. 16–19.
- 26 Cane, A. K. and Spearman, R. I. C. (1969) The keratinized epithelium of the house-mouse (*Mus musculus*) tongue: its structure and histochemistry. *Arch Oral Biol.*, **14**: 829–841.
- 27 Farbman, A. I. (1970) The dual pattern of keratinization in filiform papillae on rat tongue. *J. Anat.*, **106**: 233–242.
- 28 Iwasaki, S. and Miyata, K. (1985) Light and transmission electron microscopic studies on the lingual dorsal epithelium of the musk shrew, *Suncus murinus*. *Okajimas Folia Anat. Jpn.*, **62**: 67–88.
- 29 Krstić, R. V. (1979) Ultrastructure of the Mammalian Cell. Springer-Verlag, Berlin, pp. 238–239.
- 30 Sperry, D. G. and Wassersug, R. J. (1976) A proposed function for microridges on epithelial cells. *Anat. Rec.*, **185**: 253–258.

Myoglobin of the Shark *Galeus nipponensis*: Identification of the Exceptional Amino Acid Replacement at the Distal(E7) Position and Autoxidation of Its Oxy-form

TOMOHIKO SUZUKI, REIKO MURAMATSU, TOMOMI KISAMORI
and TAKAHIRO FURUKOHRU

*Department of Biology, Faculty of Science, Kochi University,
Kochi 780, Japan*

ABSTRACT—Myoglobin was isolated from red muscle of the shark *Galeus nipponensis* and its spectral properties were examined. The spectrum of *Galeus* oxymyoglobin (MbO₂) was similar to those of mammalian myoglobins, while that of metmyoglobin was rather different.

The partial amino acid sequence around E-helix region of *Galeus* myoglobin was determined with the aid of sequence homology. The distal (E7) histidine, which is widely conserved in mammalian hemoglobins and myoglobins, was replaced by glutamine in the globin of *Galeus*. The autoxidation rate of *Galeus* MbO₂ was examined in 0.1 M buffer at 25°C over pH ranges of 4.5–10.5. *Galeus* MbO₂ was extremely unstable between pH 6 and 10.5, and the pH dependence of autoxidation was much smaller than that of mammalian MbO₂. This property may be partly due to the absence of a distal (E7) histidine in *Galeus* myoglobin.

INTRODUCTION

The distal (E7) histidine is one of the most important residues and is widely conserved in vertebrate hemoglobins and myoglobins. This residue is capable of forming a hydrogen bond to the bound dioxygen and stabilizing it [1], as well as of protecting the FeO₂ bonding from easy access of solvent just like a gate to the heme pocket[2].

In vertebrate myoglobins so far sequenced, only five myoglobins have the exceptional amino acid replacement at position E7. Two are from Asian and African elephants, and the remaining three are from the sharks belonging to Triakididae; *Mustelus antarcticus* [3], *Galeorhinus australis* [4] and *Galeorhinus japonicus* [5]. In all cases, the distal (E7) histidine is replaced by glutamine. Therefore comparison of these myoglobins with usual myoglobins would provide some new information on the role of the distal (E7) residue in a myoglobin molecule.

In this paper, we report the isolation procedure, spectral characteristics, pH dependence for autoxidation and partial amino acid sequence of myoglobin from the shark *Galeus nipponensis* (Scyliorhinidae). *Galeus* myoglobin has been shown to have the distal (E7) glutamine in place of histidine, and to have the unique properties for spectrum and autoxidation.

MATERIALS AND METHODS

Materials

Sephadex G75 was a product of Pharmacia. DEAE-cellulose was purchased from Whatman (DE32, microgranular form). TPCK-treated trypsin and chymotrypsin were purchased from Worthington. The reagents for sequence determination were of Sequanal grade from Nakarai Chemicals Ltd.

Myoglobin preparation

Native oxymyoglobin (MbO₂) and metmyoglo-

bin (metMb) from *Galeus nipponensis* were isolated directly from red muscle according to our previous method [5, 6]. All procedures were carried out at low temperature (0–4°C) as far as possible. The water extract was fractionated with ammonium sulfate between 60 and 95% saturation at pH 8.0. The crude myoglobin solution was passed through a Sephadex G75 column equilibrated with 5 mM Tris-HCl buffer (pH 8.7) to separate myoglobin from hemoglobin. The myoglobin fraction was then applied to a DEAE-cellulose column (2×15 cm) equilibrated with 5 mM Tris-HCl buffer (pH 8.7), and eluted with a linear gradient of 15 mM (250 ml) to 100 mM (250 ml) Tris-HCl buffer (pH 8.5), to separate MbO₂ completely from metMb. The myoglobins thus obtained were dialyzed against 5 mM Tris-HCl buffer (pH 8.5), and were kept at low temperature (0–4°C) until use. The myoglobin concentration was determined spectrophotometrically after conversion to cyanometmyoglobin, using extinction coefficient of 11.3 mM⁻¹cm⁻¹ at 540 nm [7]. Absorption spectrum was recorded in a Hitachi 220A spectrophotometer.

Partial amino acid sequence determination

The major MbO₂ was selected for sequence determination. The methods of removal of heme, carboxymethylation of free cysteine and enzymatic digestion were the same as previously described [8, 9].

The whole protein was digested with trypsin for 5 hr at 37°C. The tryptic peptides were purified by high-performance liquid chromatography (HPLC) (Hitachi 655) with a linear gradient of acetonitrile in 10 mM ammonium acetate as solvent at room temperature. The column (2.6×150 mm) was packed with Lichrosorb RP8 (Merck). The whole protein was also digested with chymotrypsin for 5 hr at 37°C. The chymotryptic peptides were first fractionated by HPLC (RP8), and each fraction (2 ml each) was purified further by HPLC (Cosmosil 5C₁₈-P, 4.6×150 mm, Nakarai Chemicals Ltd.) with a linear gradient of acetonitrile in 0.1% trifluoroacetic acid (TFA).

Peptides were routinely hydrolyzed with TFA/HCl (1/2, v/v) containing 0.02% phenol at 170°C for 30 min in evacuated sealed tubes. Amino acid

analysis was performed in a Hitachi 835–50 amino acid analyzer.

The amino acid sequence was determined by the manual Edman method with modification [8]. Phenylthiohydantoin amino acid derivatives were identified by HPLC packed with Cosmosil 5PTH column (4.6×250 mm, Nakarai Chemicals Ltd.) with isocratic elution.

Autoxidation rate measurements

The measurements were carried out in 0.1 M buffer over pH range of 4.5–10.5 at 25°C according to our standard method [10–12]. A 2 ml of solution containing 0.2 M appropriate buffer was placed in a test tube and incubated in a water bath at 25±0.1°C for 15 min. The reaction was started by adding 2 ml of fresh MbO₂ solution (60 μM) which had been incubated in water bath at 25±0.1°C for 5 min, and the reaction mixture was quickly transferred to the quartz cell thermostated at 25±0.1°C. The changes in absorption spectrum from 450 to 650 nm were recorded at measured intervals of time in a Hitachi 100–50 or Hitachi 220A spectrophotometer. The buffers used were acetate, 4-morpholinoethanesulfonic acid, phosphate, Tris-HCl, cyclohexylaminoethanesulfonic acid and cyclohexylaminopropanesulfonic acid.

RESULTS

Myoglobin preparation and spectral properties

We could isolate the native MbO₂ and metMb directly from red muscle of *Galeus nipponensis*, according to the same method as used in other shark myoglobins [5, 6]. From 50 g of red muscle, about 20 mg of myoglobin (7 mg in oxy-form and 13 mg in met-form) was obtained. The spectroscopic properties of the isolated MbO₂ and metMb are compared in Tables 1 and 2, respectively, with those from other sources. The spectrum of *Galeus* MbO₂ was similar to those of mammalian MbO₂s, while that of metMb was rather different.

Partial amino acid sequence determination

Figure 1 shows the HPLC pattern of the tryptic peptides of *Galeus* myoglobin. From the comparison with the sequences of related shark myoglo-

TABLE 1. Absorption maxima, extinction coefficients and characteristic extinction ratios of oxymyoglobins at pH 8.0

Source	Reference	Absorption maximum (nm) (extinction coefficient ($\text{mM}^{-1}\text{cm}^{-1}$))				alpha/beta	gamma/UV
		alpha	beta	gamma	UV		
Sperm whale	10	581 (15.4)	543 (14.3)	418 (129)	280 (36.6)	1.08	3.52
Bovine	17	581 (15.5)	544 (14.5)	418 (134)	280 (36.4)	1.07	3.68
<i>Heterodontus</i>	12	578 (15.2)	542 (14.9)	418 (132)	278 (35.4)	1.02	3.73
<i>Aplysia</i> *	13	578 (13.8)	543 (13.4)	418 (120)	278 (33.6)	1.03	3.57
<i>Dolabella</i> *	11	578 (13.4)	543 (13.1)	418 (117)	274 (31.9)	1.02	3.67
<i>Galeorhinus</i> *	5	579 (15.7)	543 (14.8)	418 (127)	278 (41.3)	1.06	3.08
<i>Galeus</i> *	This work	577 (15.6)	542 (14.7)	417 (124)	280 (42.6)	1.06	2.92

* These myoglobins are lacking the distal (E7) histidine.

TABLE 2. Absorption maxima, extinction coefficients and characteristic extinction ratio of acid metmyoglobin

Sources	Reference	Absorption maximum (nm) (extinction coefficient ($\text{mM}^{-1}\text{cm}^{-1}$))			gamma/CT
		CT ^{alpha}	CT	gamma	
Sperm whale	18	635 (3.55)	505 (9.47)	409.5 (157)	16.6
Horse	19	630 (4.2)	505 (10.2)	408 (160)	15.7
<i>Heterodontus</i>	12	630 (4.1)	500 (9.49)	407 (162)	17.1
<i>Aplysia</i> *	19	640 (3.8)	505 (13.1)	400 (99)	7.6
<i>Dolabella</i> *	12	640 (3.3)	506 (11.9)	402 (97.5)	8.2
<i>Galeorhinus</i> *	12	640 (3.1)	505 (12.2)	398 (105)	8.6
<i>Galeus</i> *	This work	637 (3.2)	504 (12.7)	393 (104)	8.2

* These proteins are lacking the distal (E7) histidine.

bins, two peptides (T1 and 2) containing E-helix region were isolated. The chymotryptic peptides of *Galeus* myoglobin were first fractionated into 21 fractions, and from the 6th and 8th fractions two peptides (C1 and 2) were purified by rechromatography (Fig. 2). Amino acid compositions of the peptides are shown in Table 3.

Amino acid sequence of the peptide was determined by manual Edman degradation as shown in Figure 3. The continuity between the peptides T1 and T2 is supported by the peptide C1. The lysine residue at position 73 was determined from the amino acid composition of peptide T2. We could determine the sequence of 28 residues around the

TABLE 3. Amino acid compositions of tryptic and chymotryptic peptides containing the E-helix region

A.A.	T1	T2	C1	C2
Asp	3.0 (3)	3.2 (3)	1.0 (1)	2.0 (2)
Thr				
Ser	0.9 (1)			
Glu	1.1 (1)	1.1 (1)	1.1 (1)	
Gly		1.0 (1)		1.2 (1)
Ala	2.0 (2)	3.0 (3)	2.0 (2)	1.1 (1)
Cys				
Val		2.1 (3)*	1.4 (2)*	0.6 (1)*
Met				
Ile	1.0 (1)	0.6 (1)*		0.6 (1)*
Leu	2.0 (2)	2.1 (2)	1.0 (1)	1.2 (1)
Tyr				
Phe				
Lys	2.0 (2)	2.0 (2)	1.0 (1)	1.1 (1)
His				
Arg				
Pro				
Trp				
Total	12	16	8	8
Sequence	46-57	58-73	57-64	65-72
Yield (%)	50.2	47.6	41.4	5.8

The values in parentheses are the number of residues determined by sequencing

* Due to Val-Val and/or Ile-Val bonds

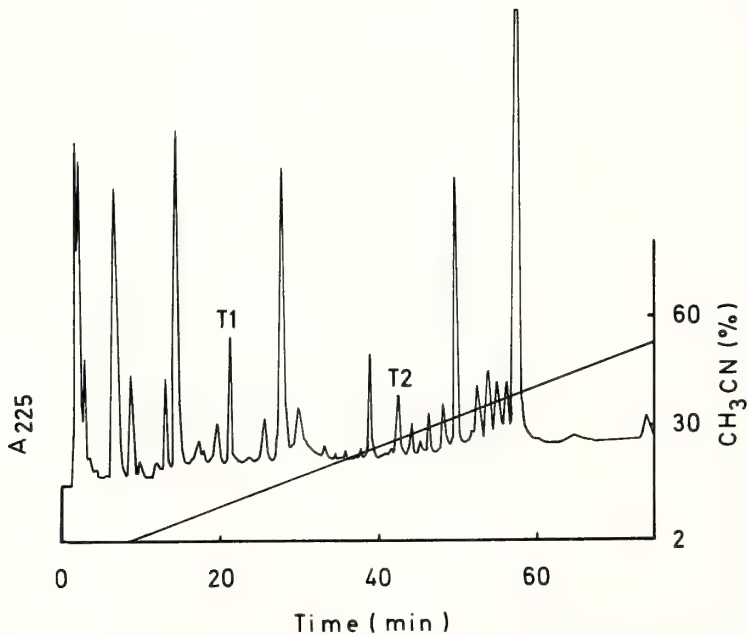


Fig. 1. HPLC pattern of the tryptic peptides of *Galeus* myoglobin. The column was packed with Lichrosorb RP8 and equilibrated with 10 mM ammonium acetate containing 2% acetonitrile.

bin without the distal histidine. Therefore, *Galeus* myoglobin with the value of 8.2 seemed to lack the distal (E7) histidine. This was confirmed by the

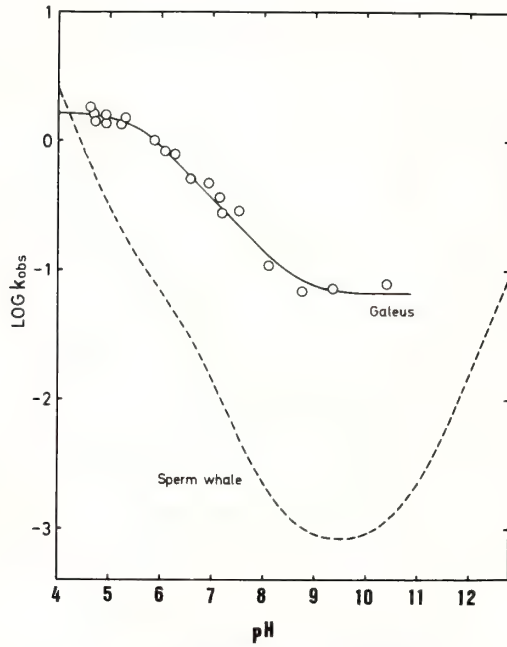


FIG. 4. The $\log(k_{\text{obs}})$ versus pH profile for the autoxidation of *Galeus* MbO₂ in 0.1 M buffer at 25°C, with that of sperm whale MbO₂ [10] for comparison. Myoglobin concentration, 30 μ M.

partial amino acid sequence determination around E-helix region.

The partial amino acid sequence of *Galeus* myoglobin is aligned with those of the myoglobins from the sharks *Heterodontus portusjacksoni* (Heterodontidae) [15], *Heterodontus japonicus* [12], *Mustelus antarcticus* (Triakidae) [3], *Galeorhinus australis* (Triakidae) [4], and *Galeorhinus japonicus* [5] as shown in Figure 5. Table 4 shows the number of amino acid differences in Figure 5. In a limited sequence of 28 residues in *Galeus* myoglobin, 7 (25%), 9 (32%) and 15–16 (54–57%) are different from those in the corresponding positions in *Galeorhinus*, *Mustelus* and *Heterodontus* myoglobins, respectively. In the six globins, 9 residues appear to be invariant. The phylogeny of these globin chains from Table 4 seems to be in good agreement with that from classical taxonomy.

In contrast to the "primitive" sharks, *Heterodontus portusjacksoni* and *H. japonicus*, the distal (E7) histidine of *Galeus* myoglobin is replaced by glutamine as in the cases of other "modern" sharks, *Galeorhinus* and *Mustelus*, as shown in Figure 5. On the other hand, the distal (E11) valine at position 63, which also affects on the oxygenation properties of mammalian hemoglobin and myoglobin, is conserved in all the shark

	46	50	55	60	65	70	73																					
<i>Galeus nipponensis</i>	Ser	Ile	Ala	Gln	Leu	Lys	Asp	Asn	Ala	Asp	Leu	Lys	Ala	Gln	Ala	Asp	Val	Val	Leu	Asn	Ala	Leu	Gly	Asn	Ile	Val	Lys	Lys
<i>Galeorhinus australis</i>	Ser	Leu	Gly	Glu	Leu	Lys	Asp	Thr	Ala	Asp	Ile	Lys	Ala	Gln	Ala	Asp	Thr	Val	Leu	Lys	Ala	Leu	Gly	Asn	Ile	Val	Lys	Lys
<i>Galeorhinus japonicus</i>	Ser	Leu	Gly	Glu	Leu	Lys	Asp	Thr	Ala	Asp	Ile	Lys	Ala	Gln	Ala	Asp	Thr	Val	Leu	Arg	Ala	Leu	Gly	Asn	Ile	Val	Lys	Lys
<i>Mustelus antarcticus</i>	Ser	Leu	Gly	Glu	Leu	Gly	Asp	Thr	Ala	Ala	Ile	Lys	Ala	Gln	Ala	Asp	Thr	Val	Leu	Ser	Ala	Leu	Gly	Asn	Ile	Val	Lys	Lys
<i>Heterodontus portusjacksoni</i>	Pro	Val	Gln	Gln	Leu	Gly	Asn	Asn	Glu	Asp	Leu	Arg	Lys	His	Gly	Val	Thr	Val	Leu	Arg	Ala	Leu	Gly	Asn	Ile	Leu	Lys	Gln
<i>Heterodontus japonicus</i>	Pro	Val	Glu	Gln	Leu	Gly	Asn	Asn	Glu	Asp	Leu	Arg	Lys	His	Gly	Val	Thr	Val	Leu	Arg	Ala	Leu	Gly	Asn	Ile	Leu	Lys	Gln
	D										E																	

FIG. 5. Comparison of amino acid sequences (positions 46 to 73) of shark myoglobins. The distal (E7) residues are boxed. Asterisks indicate the invariable residue in the six globins. The helical segments (D and E) of "myoglobin fold" are also shown.

TABLE 4. Sequence homologies (number of different residues) in positions 46 to 73 between shark myoglobins

	<i>Galeus n.</i>	<i>Galeorhinus a.</i>	<i>Galeorhinus j.</i>	<i>Mustelus a.</i>	<i>Heterodontus p.</i>
<i>Galeorhinus a.</i>	7				
<i>Galeorhinus j.</i>	7	1			
<i>Mustelus a.</i>	9	3	3		
<i>Heterodontus p.</i>	15	17	16	17	
<i>Heterodontus j.</i>	16	16	15	16	1

myoglobins.

Recently it was shown that *Aplysia* [13] and *Dolabella* [11] MbO₂s, which lack the distal (E7) histidine, are extremely unstable and that the pH dependence of the stability is quite different from that of sperm whale MbO₂. This unusual stability was attributed to the absence of a distal (E7) histidine [11, 13]. However it should be noted that there are many amino acid differences, other than the distal residue, between molluscan and mammalian myoglobins, with only 20–25% of the residues identical. Therefore it seems to be of great interest to examine the stability of *Galeus* MbO₂, which is more related to mammalian globins and lacks the distal (E7) histidine, for further elucidation of the role of distal (E7) residue. Judging from the partial amino acid sequence shown in Figure 5, the sequence homology between *Galeus* and sperm whale myoglobins is about 50%.

The pH dependence for autoxidation of *Galeus* MbO₂ is shown in Figure 4. *Galeus* MbO₂ was extremely unstable between pH 6 and 10.5, and the pH dependence was quite different from that of sperm whale MbO₂. For example, *Galeus* MbO₂ is autoxidized 2.2, 25 and 88 times faster at pHs 4.5, 7.0 and 9.2, respectively. The most striking feature is the fact that unlike sperm whale MbO₂ the autoxidation rate of *Galeus* MbO₂ is not enhanced with increase in the concentration of hydrogen ion under pH 6.

We reported previously the unique stability properties of MbO₂s from the sharks *Proscyllium* and *Galeorhinus* [6, 12]. Their pH dependences for autoxidation are very similar to that of *Galeus* myoglobin, and this fact implies that there is some structural analogy among the three shark myoglobins. As shown in Figure 5, *Galeus* and *Galeorhinus* myoglobins are lacking the distal (E7) histidine; the sequence of *Proscyllium* myoglobin is not known yet. On the other hand, since there are only 50% homologies in the sequences between the sharks and sperm whale myoglobins, it is difficult to attribute the difference in the pH dependence of autoxidation to a particular residue. However the distal (E7) residue ought to be of primary importance, because the E7-histidine is the only residue capable of interacting directly

with bound dioxygen and stabilizing it [1]. Therefore, our comparative studies on autoxidation of shark MbO₂s without the distal (E7) histidine strongly support the idea that the distal (E7) histidine participates in the autoxidation reaction as a catalytic residue facilitating the movement of a catalytic proton [16]. If a myoglobin lacks the distal (E7) histidine, the autoxidation rate will not be accelerated under acidic pHs such as seen in Figure 4.

Finally, it is interesting to note that all the vertebrate myoglobins with the exceptional replacement at position E7 have glutamine at this position in place of histidine. From physiological and evolutionary points of view, this must be discussed in near future.

ACKNOWLEDGMENTS

We thank Drs. O. Okamura and Y. Machida for identification and supply of the shark *Galeus nipponensis*. This paper is dedicated to Professor Shun-Ichi Umezawa in honor of his retirement from Kochi University.

REFERENCES

- 1 Phillips, S. E. V. and Schoenborn, B. P. (1981) Neutron diffraction reveals oxygen-histidine hydrogen bond in oxymyoglobin. *Nature*, **292**: 81–82.
- 2 Tucker, P. W., Phillips, S. E. V., Perutz, M. F., Houtchens, R. and Caughey, W. S. (1978) Structure of hemoglobins Zurich [His E7 (63) beta→Arg] and Sidney [Val E11 (67) beta→Ala] and the role of the distal residues in ligand bending. *Proc. Natl. Acad. Sci. USA*, **75**: 1076–1080.
- 3 Fisher, W. K., Koureas, D. D. and Thompson, E. O. P. (1980) Myoglobins of cartilaginous fishes. II. Isolation and amino acid sequence of myoglobin of the shark *Mustelus antarcticus*. *Aust. J. Biol. Sci.*, **33**: 153–167.
- 4 Fisher, W. K., Koureas, D. D. and Thompson, E. O. P. (1981) Myoglobins of cartilaginous fishes. III. Amino acid sequence of myoglobin of the shark *Galeorhinus australis*. *Aust. J. Biol. Sci.*, **34**: 5–10.
- 5 Suzuki, T., Suzuki, T.-N. and Yata, T. (1985) Shark myoglobins. II. Isolation, characterization and amino acid sequence of myoglobin from *Galeorhinus japonicus*. *Aust. J. Biol. Sci.*, **38**: 347–354.
- 6 Suzuki, T. and Kisamori, T. (1984) Shark myoglobins-I. Isolation and characterization of myoglobins from the sharks, *Squalus japonicus* and *Proscyllium habereri*. *Comp. Biochem. Physiol.*, **78B**: 163–166.

- 7 Drabkin, D. L. (1950) The distribution of the chromoproteins, hemoglobin, myoglobin, and cytochrome *c*, in the tissues of different species, and the relationship of the total content of each chromoprotein to body mass. *J. Biol. Chem.*, **182**: 313–333.
- 8 Suzuki, T., Furukohri, T. and Gotoh, T. (1985) Subunit structure of extracellular hemoglobin from the polychaete *Tylorrhynchus heterochaetus* and amino acid sequence of the constituent polypeptide chain (IIC). *J. Biol. Chem.*, **260**: 3145–3154.
- 9 Suzuki, T. and Gotoh, T. (1986) The complete amino acid sequence of giant multisubunit hemoglobin from the polychaete *Tylorrhynchus heterochaetus*. *J. Biol. Chem.*, **261**: 9257–9267.
- 10 Suzuki, T. and Shikama, K. (1983) Stability properties of sperm whale oxymyoglobin. *Arch. Biochem. Biophys.*, **224**: 695–699.
- 11 Suzuki, T. (1986) Amino acid sequence of myoglobin from the mollusc *Dolabella auricularia*. *J. Biol. Chem.*, **261**: 3692–3699.
- 12 Suzuki, T. (1987) Autoxidation of oxymyoglobin with the distal (E7) glutamine. *Biochem. Biophys. Acta*, **914**: 170–176.
- 13 Shikama, K. and Katagiri, T. (1984) *Aplysia* oxymyoglobin with an unusual stability property. *J. Mol. Biol.*, **174**: 697–704.
- 14 Wang, C. M. and Briniger, W. S. (1979) A correlation of the visible and Soret spectra of dioxygen- and carbon monoxide-heme complexes and five-coordinate heme complexes with the spectra of oxy-, carboxy-, and deoxyhemoglobins. *Biochemistry*, **18**: 4960–4977.
- 15 Fisher, W. K. and Thompson, E. O. P. (1979) Myoglobin of the shark *Heterodontus portusjacksoni*; isolation and amino acid sequence. *Aust. J. Biol. Sci.*, **32**: 277–294.
- 16 Sugawara, Y. and Shikama, K. (1980) Autoxidation of native oxymyoglobin. Thermodynamic analysis of the pH profile. *Eur. J. Biochem.*, **110**: 241–246.
- 17 Gotoh, T. and Shikama, K. (1976) Autoxidation of native oxymyoglobin from bovine heart muscle. *Arch. Biochem. Biophys.*, **163**: 476–481.
- 18 Hanania, G. I. H., Yeghiayan, A. and Cameron, B. F. (1966) Absorption spectra of sperm-whale ferri-rimyoglobin. *Biochem. J.*, **98**: 189–192.
- 19 Rossi-Fanelli, A. and Antonini, E. (1957) A new type of myoglobin isolated and crystallized from the muscles of *Aplysia*. *Biochimica*, **22**: 335–342.

T Cell-Specific Antigen in *Xenopus* Identified with a Mouse Monoclonal Antibody: Biochemical Characterization and Species Distribution

SABURO NAGATA

*Tokyo Metropolitan Institute of Gerontology, Sakaecho 35-2,
Itabashiku, Tokyo 173, Japan*

ABSTRACT—A mouse monoclonal antibody (mAb) produced against *Xenopus laevis* thymocytes, named XT-1, recognizes a thymus-dependent (T) cell-specific antigen, provisionally designated XTLA-1. For biochemical characterization of the XTLA-1 antigen, the lysates of surface-radioiodinated thymocytes and splenocytes were immunoprecipitated with the XT-1 mAb, and analysed by SDS-polyacrylamide gel electrophoresis (SDS-PAGE) and two-dimensional electrophoresis. The results indicate that the XT-1 mAb precipitates peptides with N-linked and other glycans, reduced form of that have an apparent molecular weight of approximately 120 KD and isoelectric point of pH 5.3-6.1. The species distribution study employing immunofluorescence showed that the XTLA-1 antigen was expressed on T cells from *X. laevis*, *X. borealis* and LG15 (*X. laevis* × *X. gilli* hybrid clone), but not on those from a frog (*Rana nigromaculata*), toad (*Bufo japonicus*), newt (*Cynopus pyrrhogaster*), teleost fish (*Oryzias latipes*), chicken, mouse and man. The XTLA-1 antigen may provide a useful marker of *Xenopus* T cells.

INTRODUCTION

The immunobiology of the anuran amphibia, *Xenopus*, has recently been extensively studied and demonstrated that the immune system of this frog is remarkably like that of the man and experimental mammals. Thus, *Xenopus*, a widely used experimental animal in the developmental biology, may provide an alternative experimental model to the mouse in the study of developmental aspects of the immune system. Especially, studies with embryonic transplantation chimeras were informative to understand the process of early stem cell migration into the thymus and emigration of thymus-dependent (T) cells from the thymus [1-4]. Informations on the differentiation of functionally distinct lymphocyte subpopulations are, however, relatively poor mainly because of the lack of reagents that enable the identification of lymphocyte subpopulations. Therefore, we have tried to produce reagents that can identify cell

surface markers on *Xenopus* T cells and their subsets.

In a series of previous papers [5-7], we described a specific cell surface markers on *X. laevis* T cells that can be identified by a mouse monoclonal antibody (mAb), XT-1. The studies on the tissue distribution [5], ontogeny, effect of early-larval thymectomy [6] and some functional aspects [7] of cells that have antigens recognized by this mAb suggest that the antigen may provide a marker for the cells in T lineage. The present paper describes the basic molecular nature and species distribution of this antigen, designated XTLA-1.

MATERIALS AND METHODS

Animals

Xenopus laevis used in the present study were major histocompatibility complex (MHC) homozygous, partially inbred J and K strain animals established in Dr. Katagiri's laboratory of Hokkaido University [8, 9]. *X. borealis* were

kindly provided by Dr. Tochinaï of Hokkaido University and isogenic LG15 clone frogs (interspecies hybrids between *X. laevis* and *X. gilli*), originally established in Dr. Du Pasquier's laboratory at the Basel Institute for Immunology [10], were from Dr. Cohen of the University of Rochester. The thymectomy on day 5 postfertilization was performed by the method of Tochinaï [8]. Japanese newts *Cynopus pyrrhogaster*, frogs *Rana nigromaculata*, toads *Bufo japonicus*, newly-hatched chickens, Japanese medaka (Teleost fish) and mice (C57BL/6, C3H and DBA strains) were purchased from commercial dealers.

Antibody

The mouse hybridoma producing XT-1 mAb was produced against J thymocytes as described previously [5]. The immunoglobulin G (IgG) fraction enriched for XT-1 mAb was isolated from the hybridoma ascites by an affinity chromatography on the column of protein A Sepharose CL-4B beads (Pharmacia).

Radioiodination of cells

Thymocyte and spleen cell suspensions in amphibian phosphate buffered saline (APBS; 100 mM NaCl, 10 mM sodium phosphate buffer, pH 7.2) were prepared from animals at least 5 months after the completion of metamorphosis. Splenocyte preparations were enriched for lymphocytes by depleting erythrocytes with sedimentation at $1\times g$. The cell suspensions containing 5×10^7 viable cells in 500 μ l APBS were added with 50 μ l of 25 U/ml lactoperoxidase solution (Calbiochem), 50 μ l of 5 U/ml glucose oxidase (Sigma), 1 mCi of carrier-free 125 I (Amersham) and 50 μ l of 0.2 M glucose, and incubated at room temperature for 15 min with gentle agitation. The cells were washed with APBS containing 0.1% NaN_3 , and then incubated for 30 min on ice in 1 ml lysis buffer (0.5% Nonidet P-40, 10 mM Tris-HCl, pH 7.2, 150 mM NaCl and 1 mM phenylmethylsulfonyl fluoride). The lysates were cleared by centrifugation at $8000\times g$ for 10 min.

Immunoprecipitation and gel electrophoresis

For immunoprecipitation, 100 μ l lysates in the Eppendorf tubes were precleared by incubation

for 1 hr on ice with 20 μ g normal mouse IgG and then for 30 min with 25 μ l packed protein A-Sepharose CL-4B beads. The precleared samples were immunoprecipitated with 20 μ g mAb for 6–16 hr on ice, followed by protein A-Sepharose CL-4B beads. For one-dimensional SDS-polyacrylamide gel electrophoresis (SDS-PAGE), the samples were extracted by boiling the beads for 5 min in Laemmli's SDS sample buffer and electrophoresed on 7% polyacrylamide gel with a discontinuous buffer system [11]. Two-dimensional electrophoresis for isoelectric point and molecular size was performed according to the method of O'Farrell *et al.* [12], and two-dimensional nonreducing and reducing SDS-PAGE according to the method of Allison *et al.* [13]. The electrophoresed gels were fixed with 10% methanol-10% acetic acid, dried on filter paper, and autoradiographed on Kodak 5R X-ray film with Cronex enhancer screen (Dupont) at -70°C .

Glycosidase digestion

Digestions of immunoprecipitates with endo- β -N-acetylglucosaminidase F (endo F), which removes N-linked glycans, were performed as described previously [14]. Briefly, immunoprecipitates on 20 μ l packed protein A beads were eluted by boiling for 5 min in 30 μ l of 100 mM Tris buffer (pH 8.0) containing 1% SDS and 1% 2-mercaptoethanol (2-ME), and mixed with 0.25 U endo F (glycopeptidase F free; Boehringer Mannheim Biochemica) in 100 mM phosphate buffer (pH 6.1) containing 50 mM EDTA, 1% NP-40, 0.2% SDS and 1% 2-ME. The mixtures were incubated overnight at 37°C and then proteins were precipitated by adding 30 μ l of 50% trichloroacetic acid (TCA).

Immunofluorescence staining and flow cytometry

Cells suspended in APBS containing 0.1% bovine serum albumin and 0.1% NaN_3 were incubated for 1 hr on ice with 2.5 μ g/ml of XT-1 mAb, washed twice, and then incubated for 1 hr with the FITC-labeled anti-mouse IgG goat antibody (TAGO, Inc.). Control samples were incubated with FITC-labeled reagent alone. The stained cells were observed under a fluorescence

microscope with epiillumination or analysed with a EPICS-C cell sorter (Coulter Electronics) as described previously [5].

RESULTS

To characterize the molecular nature of the XTLA-1 antigen, radioiodinated thymocyte and splenocyte lysates from J strain frogs were immunoprecipitated with XT-1 mAb, and analysed by SDS-PAGE. Under nonreducing conditions, the immunoprecipitates from both thymocytes and splenocytes migrated as two bands of apparent molecular weight of 110 kilodalton (KD) and 120 KD (Fig. 1A). When the immunoprecipitated

materials were reduced with 2-ME and then electrophoresed, a single band of 120 KD could only be detected (Fig. 1B). Diagonal non-reducing and reducing SDS-PAGE of the same material revealed that the two peptide bands on non-reduced SDS-PAGE have the same mobility on reduced SDS-PAGE, forming two tandem spots corresponding to a molecular size of 120 KD on second dimension (Fig. 1C). To determine whether the immunoprecipitated peptides have N-linked glycans, immunoprecipitates were treated with endo F and then analysed by SDS-PAGE. As seen in Figure 2, the apparent molecular size of the 120 KD material was slightly reduced, indicating the presence of N-linked gly-

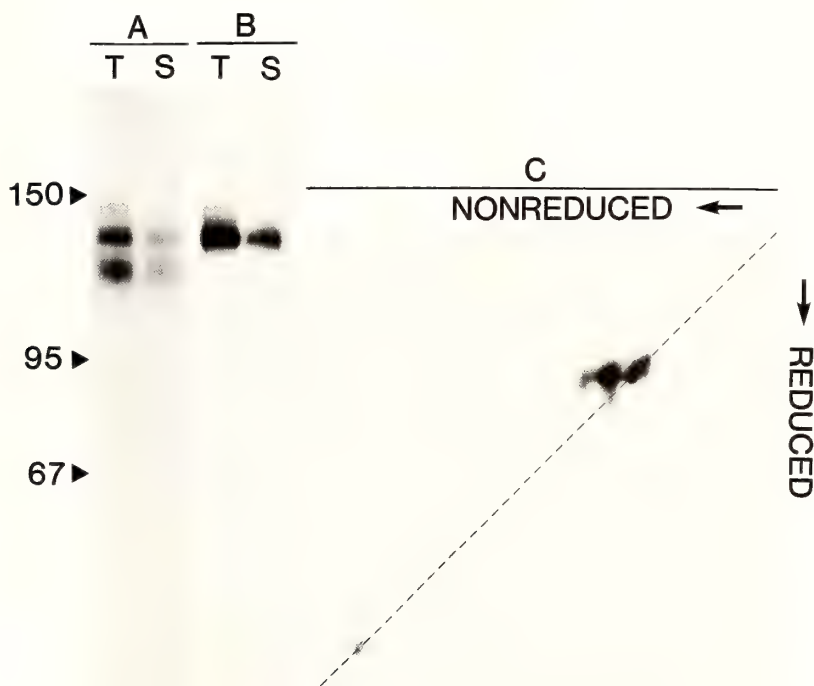


FIG. 1. Analysis of XTLA-1 antigen by one-dimensional SDS-PAGE under non-reducing (A) and reducing (B) conditions, and by two-dimensional non-reducing and reducing SDS-PAGE (C). Thymocytes (T) and splenocytes (S) from J strain *X. laevis* were radioiodinated, solubilized, and immunoprecipitated with XT-1 mAb followed by protein A-Sepharose CL-4B beads. For one-dimensional SDS-PAGE, immunoprecipitates were boiled in SDS sample buffer with (reduced) or without (nonreduced) 2-ME and electrophoresed on 7% polyacrylamide gels. For two-dimensional non-reducing and reducing SDS-PAGE, nonreduced immunoprecipitates from thymocyte lysates were run on 7% polyacrylamide tube gels for first dimension, gels were immersed in sample buffer containing 2-ME and then electrophoresed for second dimension. Electrophoresed gels were visualized by autoradiography. Broken line in Fig. C represents diagonal. Molecular size (KD) standards were run on same gels and represented with arrow heads.

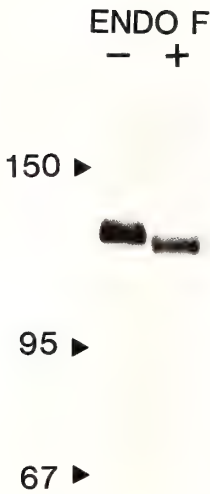


FIG. 2. Effect of endo F treatment on XTLA-1 antigen immunoprecipitated from radioiodinated J strain thymocytes. Immunoprecipitates were incubated overnight at 37°C with (+) or without (-) endo F; proteins were precipitated with TCA and subjected to reduced SDS-PAGE.

cans. For the further characterization of XTLA-1 antigen, immunoprecipitates from J thymocytes were analysed by two dimensional electrophoresis for isoelectric point and molecular size. As shown in Figure 3A, 120 KD peptide exhibited a charge heterogeneity near the acidic end of the gel (isoelectric point between pH 5.3-6.1). When the endo F-treated immunoprecipitates were analysed by two-dimensional electrophoresis under the same conditions, several spots with the same molecular size and the extensive charge heterogeneity (isoelectric point of pH 4.8-6.5) were identified (Fig. 3B).

The distribution of XTLA-1 antigen in several amphibian and non-amphibian species was examined by flow cytofluorometry with thymocytes and splenocytes after indirect immunofluorescence staining. Typical results of such analyses represented in Figure 4 show that more than 95% thymocytes and 20%-35% splenocytes from three *Xenopus* (*X. laevis*, *X. borealis* and LG15) were positive for fluorescence. The fluorescence intensity of positive cells in these histograms is similar, indicating the expression of approximately the same numbers of the determinants recognized by

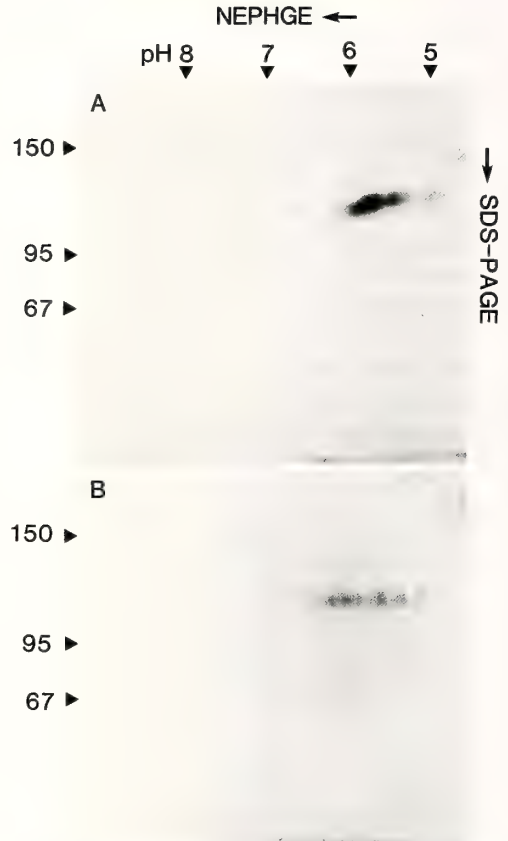


FIG. 3. Two-dimensional nonequilibrium pH gel electrophoresis (NEPHGE) and SDS-PAGE of XTLA-1 antigen immunoprecipitated from J strain thymocytes. Endo F-treated (B) and -nontreated (A) immunoprecipitates were separated by NEPHGE on first dimension, followed by second dimension reduced SDS-PAGE.

XT-1 mAb. As reported in the previous study on J strain *X. laevis* [5], early-larval thymectomy on these three toads resulted in depletion of fluorescence-positive lymphocyte population in spleen. Similar immunofluorescence analyses revealed that cells from the newt (*Cynopus pyrrhogaster*), frog (*Rana nigromaculata*), toad (*Bufo japonicus*), human, mouse, chicken and fish (Japanese medaka) were all negative for the expression of the determinants (data for the last four animals were not shown).

To examine whether the determinants identified by the flow cytofluorometry represent the same antigenic molecules, immunoprecipitation experi-

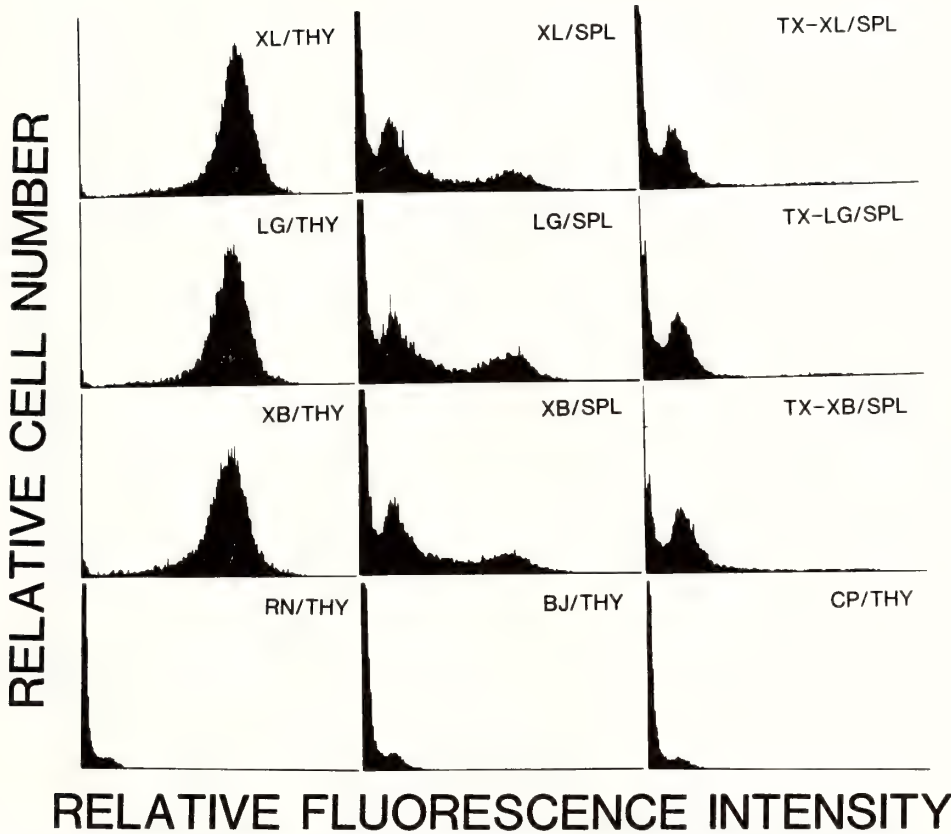


FIG. 4. Flow cytometry of thymocytes (THY) and splenocytes (SPL) from normal, and splenocytes from thymectomized (TX) J strain *X. laevis* (XL), LG15, *X. borealis* (B), *Rana nigromaculata* (RN), *Bufo japonicus* (BJ) and *Cynopus pyrrhogaster* (CP). Cells were stained by incubation with XT-1 mAb followed by FITC-labeled anti-mouse IgG goat antibody, and analysed with EPICS-C cell sorter.

ments were performed on radioiodinated thymocytes from J and K strain *X. laevis*, LG15 and *X. borealis*. The results showed that the molecules precipitated with XT-1 mAb from all these frogs were peptides with an identical molecular size of 120 KD (Fig. 5).

DISCUSSION

The present study described basic molecular nature and species distribution of the XTLA-1 antigen recognized by the XT-1 mAb. From the results of SDS-PAGE and two-dimensional electrophoresis, the XTLA-1 antigen seems to be glycoprotein consisting of a single polypeptide, reduced form of that has an apparent molecular size of 120 KD and isoelectric point between pH

5.3-6.7. Endo F-treatment of the XTLA-1 antigen resulted in minor but distinct reduction of the apparent molecular size, indicating that the XTLA-1 molecule has N-linked glycans. In addition, the fact that the endo F-treated XTLA-1 antigen still showed an extensive charge heterogeneity as revealed by two-dimensional electrophoresis suggests the presence of additional (O-linked?) glycans. On SDS-PAGE, non-reduced XTLA-1 antigen ran as two bands of apparent molecular size of 110 KD and 120 KD, both of these peptides have an identical mobility on reduced SDS-PAGE. They may reflect different forms of the 120 KD membrane peptide that has some 2-ME sensitive structures, such as intra-peptide chain disulfide bonds. Alternatively, the molecular conformation of the antigen might

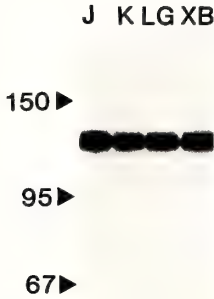


FIG. 5. Reduced SDS-PAGE of XTLA-1 antigens immunoprecipitated from thymocytes of J (J) and K (K) strain *X. laevis*, LG15 (LG) and *X. borealis* (XB).

be partially damaged during the extraction and immunoprecipitation procedures.

The XTLA-1 antigen could be detected on lymphocytes from three *Xenopus* (*X. laevis*, *X. borealis* and *X. laevis* × *X. gilli* hybrid LG15), but not on those from other amphibian and nonamphibian species examined. In the previous paper [5], we failed to detect XTLA-1 antigen on spleen cells from K and A strain frogs by immunofluorescence using hybridoma culture supernatants. But, as shown in the present paper, the high titer ascites or a purified IgG fraction consistently stains splenic T cells from these frogs, suggesting the use of culture supernatants could give misleading results. Immunoprecipitated antigens from the thymocyte lysates of these three toads seems to be an identical 120 KD peptide as analysed by SDS-PAGE. Since XTLA-1 positive spleen cells in these frogs were depleted by early-larval thymectomy, XTLA-1 antigen would be a T cell-specific cell surface antigen shared by these three *Xenopus*. Recent studies showed that *X. borealis* and LG series of cloned frogs provide excellent experimental models to study the developmental and genetical aspects of the immune system [4, 15]. The XTLA-1 antigen as a T cell marker in these animals should prove useful for studying the T cell development and function.

For some years, substantial efforts have been made with a minimum success to produce reagents that can identify cell surface markers specific to the functional lymphocyte subpopulations in *Xenopus* (reviewed in [16]). Thus, XTLA-1 antigen described in the present paper is the only known T cell marker, although surface Ig and MHC class II antigen have been established as markers of B cells and antigen-presenting cells [17, 18]. On the other hand, several T cell-specific antigens have recently been identified in teleost and amphibian species by using monoclonal or polyclonal antibodies [19–21]. The molecular nature of these antigens has, however, not been characterized. Mansour and Cooper [19] suggested the presence of an equivalent of thy-1 antigen, a well-characterized mammalian T cell marker, in *Rana pipiens*. The present XTLA-1 antigen is, however, different from the thy-1-like antigen reported in *R. pipiens* in the aspects of tissue distribution [5] and molecular nature. That is, as mammalian thy-1 antigen the thy-1-like antigen has molecular weight of less than 30 KD and distributes in the nervous tissues as well as on the T cell surface. Together with the results of species distribution studies, XTLA-1 antigen seems to have no direct relationship to the mammalian thy-1 antigen.

ACKNOWLEDGMENT

I thank Drs. Hirokawa and Maruyama, Tokyo Metropolitan Institute of Gerontology, for providing the use of their laboratory facilities, and Dr. Ishikawa for the help in gel electrophoresis. This work was supported in part by Grant No. 60440100 from the Japanese Ministry of Education, Science and Culture.

REFERENCES

- 1 Tompkins, R., Volpe, E. P. and Reinschmidt, D. C. (1980) Origin of hemopoietic stem cells in amphibian ontogeny. In "Development and Differentiation of Vertebrate Lymphocytes". Ed. by J. D. Horton, Elsevier/North-Holland, Amsterdam, pp. 25–34.
- 2 Flajnik, M. F., Horan, P. K. and Cohen, N. (1983) A flow cytometric analysis of the embryonic origin of lymphocytes in diploid/triploid chimeric *Xenopus laevis*. *Dev. Biol.*, **104**: 247–254.
- 3 Maeno, M., Todate, A. and Katagiri, C. (1985) The localization of precursor cells for larval and adult

- hemopoietic cells in *Xenopus laevis* in two regions of embryos. *Dev. Growth Differ.*, **27**: 137-236.
- 4 Maeno, M., Tochinal, S. and Katagiri, C. (1985) Differential participation of ventral and dorsolateral mesoderms in the hemopoiesis of *Xenopus*, as revealed in diploid-triploid or interspecific chimeras. *Dev. Biol.*, **110**: 503-508.
 - 5 Nagata, S. (1985) A cell surface marker of thymus-dependent lymphocytes in *Xenopus laevis* is identifiable by mouse monoclonal antibody. *Eur. J. Immunol.*, **15**: 837-841.
 - 6 Nagata, S. (1986) Development of T lymphocytes in *Xenopus laevis*: Appearance of the antigen recognized by an anti-thymocyte mouse monoclonal antibody. *Dev. Biol.*, **114**: 389-394.
 - 7 Nagata, S. (1986) T cell proliferative responses of *Xenopus* lymphocyte subpopulations separated on anti-thymocyte monoclonal antibody coupled to sepharose beads. *Dev. Comp. Immunol.*, **10**: 259-264.
 - 8 Tochinal, S. and Katagiri, Ch. (1975) Complete abrogation of immune responses to skin allografts and rabbit erythrocytes in the early thymectomized *Xenopus laevis*. *Dev. Growth Differ.*, **17**: 383-394.
 - 9 Nakamura, K. (1985) Lethal graft-versus-host reaction induced by parental cells in the clawed frog, *Xenopus laevis*. *Transplantation*, **40**: 393-397.
 - 10 Kobel, H. R. and Du Pasquier, L. (1975) Production of large clone of histocompatible fully identical clawed toads (*Xenopus*). *Immunogenetics*, **2**: 87-91.
 - 11 Laemmli, U. K. (1970) Cleavage of structural proteins during the assembly of the head of the bacteriophage T4. *Nature*, **227**: 680-685.
 - 12 O'Farrell, P. Z., Goodman, H. M. and O'Farrell, P. H. (1977) High resolution two dimensional electrophoresis of basic as well as acidic proteins. *Cell*, **12**: 1133-1141.
 - 13 Allison, J. P., McIntyre, B. W. and Bloch, D. (1982) Tumor specific antigen of murine T lymphoma defined with monoclonal antibody. *J. Immunol.*, **129**: 2293-2300.
 - 14 Elder, J. H. and Alexander, S. (1982) Endo-N- β -acetylglucosaminidase F: endoglycosidase from *Flabobacterium meningosepticum* that cleaves both high-mannose and complex glycoproteins. *Proc. Natl. Acad. Sci., USA.*, **79**: 4540-4544.
 - 15 Bernard, C. C. A., Bordmann, G., Blomberg, B. and Du Pasquier, L. (1981) Genetic control of T helper cell function in the clawed toad *Xenopus laevis*. *Eur. J. Immunol.*, **11**: 151-155.
 - 16 Flajnik, M. F., Hsu, E., Kaufman, J. F. and Du Pasquier, L. (1987) Biochemistry, tissue distribution and ontogeny of surface molecules detected on *Xenopus* hemopoietic cells. In "Differentiation Antigen in Lymphohemopoietic Tissues". Ed. by M. Miyasaka and Z. Trnka, Marcel Dekker, Inc., New York, pp. 387-419.
 - 17 Bleisher, P. A. and Cohen, N. (1981) Monoclonal anti-IgM can separate T cell from B cell proliferative responses in the frog, *Xenopus laevis*. *J. Immunol.*, **127**: 1549-1555.
 - 18 Kaufman, J. F., Flajnik, M. F., Du Pasquier, L. and Riegert, P. (1985) *Xenopus* MHC class II molecules. I. Identification and structural characterization. *J. Immunol.*, **134**: 3248-3257.
 - 19 Mansour, M. H. and Cooper, E. L. (1984) Purification and characterization of *Rana pipiens* brain thymol glycoprotein. *J. Immunol.*, **132**: 2515-2523.
 - 20 Secombes, C. J., Van Groningen, J. J. M. and Egbert, E. (1983) Separation of lymphocyte subpopulations in carp *Cyprinus carpio* L. by monoclonal antibodies: Immunohistochemical studies. *Immunology*, **48**: 165-175.
 - 21 Amenomori, A. and Sugiyama, K. (1986) Lymphocyte markers in *Rana catesbeiana* detectable by mouse monoclonal antibodies. *Zool. Sci.*, **3**: 1010.

Temperature-dependence in Reaggregation of Cells Dissociated from Sea Urchin Embryos with Different Seasonal Growth

HIROSUKE FUJISAWA and SHONAN AMEMIYA¹

Biological Institute, Faculty of Education, Saitama University, Urawa-shi, Saitama 338, and ¹Misaki Marine Biological Station, University of Tokyo, Miura-shi, Kanagawa 238-02, Japan

ABSTRACT—We investigated the temperature optimal for the aggregation of cells of sea urchin embryos as well as for morphological change of the aggregates into embryo-like organisms. The species of sea urchin used in the present work were *Hemicentrotus pulcherrimus*, *Clypeaster japonicus* and *Anthocidaris crassispina* which have different breeding seasons. In each species the range of temperature optimal for the aggregation of dissociated blastula cells coincided with the range of temperature optimal for their normal development and the ranges corresponded to those of the temperature of the sea water during their breeding seasons. Factors related to the species-specific temperature sensitivity of the embryonic cells were discussed.

INTRODUCTION

Since Giudice [1] opened the way to experiments on the reconstitution of blastula-like organisms using single isolated cells of sea urchin embryos, these cells have proved to be one of the most suitable materials for studies on the mechanism of cell adhesion during early development. Much work has been done to elucidate the processes occurring during reconstruction by the dissociated embryonic cells both electron-microscopically [2, 3] and biochemically [4-10]. The precise mechanism of cell adhesion during the reconstruction process is, however, far from being clearly understood as yet. The process does not seem to be as simple as could be explained only by the occurrence of certain aggregation substances on the cell surface or in the culture media; rather, it appears to be an intricate combination of cellular activities [2]. In order to gain more evidence to confirm this view, we have examined the physiological conditions necessary for the process. This paper reports the effects of temperature on the aggregation of dissociated embryonic cells of sea urchins followed by their reconstitution into blas-

tula-like organisms.

MATERIALS AND METHODS

Sea urchins In this work we used three species of sea urchin, *Hemicentrotus pulcherrimus*, *Clypeaster japonicus* and *Anthocidaris crassispina*. These sea urchins have different breeding seasons: January through March for *H. pulcherrimus*, June through August for *C. japonicus* and *A. crassispina*. The sea urchins investigated in this experiment inhabit the tidal areas around the Misaki Marine Biological Station, Kanagawa Prefecture, on the Pacific coast of Japan (139°6' E, 35°2' N. L.).

Temperatures The temperatures of the sea water used for culturing sea urchin embryos and for incubating dissociated cells of sea urchin embryos were adjusted with an accuracy of ± 0.1 degree as read by a standard thermometer.

Embryos Eggs and sperm were obtained by pipetting 0.55 M KCl into the body cavity of sea urchins. The eggs of *H. pulcherrimus* were fertilized and cultured in normal sea water at 12°C while those of *C. japonicus* and *A. crassispina* were treated at 20°C.

Preparation of single isolated blastula cells After being washed with calcium-free

sea water three times, blastulae were suspended in 0.44 M sucrose-1 mM EDTA-10 mM Tris-HCl buffer, pH 8.0, and dissociated into single cells by gentle pipetting according to the method of Giudice [1]. The temperatures of the calcium-free sea water and the buffer were the same as those used for incubation.

Culture of single isolated blastula cells The single cells thus obtained were suspended in 25 ml of normal sea water at a density of 1.5×10^6 cells per ml. Each of the cell suspensions was incubated at various temperatures ranging from 2° to 35°C. Each suspension was gently stirred with a glass blade at 80 rpm.

Measurement of aggregation of single isolated blastula cells At scheduled time intervals, an aliquot of each cell suspension was transferred to a hemacytometer plate and the total number of particles including single cells and cellular aggregates of various sizes was counted. The aggregation rate was defined as an index $(1 - N_p/N_t)$, where N_t is the total number of cells and N_p that of particles in a constant volume of cell suspension. Since the total number of particles decreases as the aggregation proceeds to form larger-sized aggregates, this value was considered to reflect the aggregation rate.

Drugs Cytochalasin B was purchased from Aldrich Chemical Co., Ltd. This antibiotic was dissolved in dimethylsulfoxide (DMSO) at a concentration of 5 mg/ml and stored at 4°C. Prior to incubation of the dissociated sea urchin embryonic cells, 25 μ l of the solution or DMSO alone were added to 25 ml of normal sea water to give a final cytochalasin B concentration of 5 μ g/ml of sea water.

Colchicine was purchased from Wako Chemicals Co., Ltd. The drug was used at a concentration of 5 μ M in normal sea water.

RESULTS

Effect of temperature on the aggregation of dissociated blastula cells

Sea urchin blastulae were successfully dissociated into single cells by Giudice's method [1]. The single cells prepared as described above started to

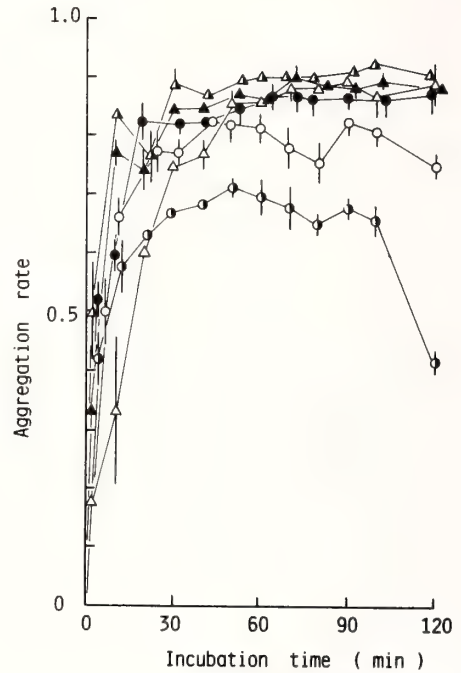


FIG. 1. Time course changes in the aggregation rate upon culturing dissociated embryonic cells of *Hemicentrotus pulcherrimus* at temperatures of 2°C (open triangle), 10°C (solid triangle), 15°C (semi-solid triangle), 20°C (solid circle), 25°C (open circle), and 30°C (semi-solid circle). Each point represents the average of triplicate determinations and the vertical bar indicates the standard error of those values.

aggregate immediately upon resuspension in normal sea water. Figure 1 shows the time course of the aggregation rate of dissociated *Hemicentrotus pulcherrimus* blastulae cells at various temperatures. Aggregation indices is plotted against incubation time (min). An increase in the rate indicates progress of aggregation of single cells. Curves indicating the changes occurring in the value of the rate were different at different temperatures. The cells cultured at 25° and 30°C continued to aggregate within the first 50 min of incubation, but after this time the aggregated cells showed gradual redissociation. Differences in the rate at different temperatures were apparent after 60 min of incubation. The aggregation rates were high at 2°, 10° and 20°C.

This result, shown in Figure 1, means that the optimal range of temperature for the aggregation

of *H. pulcherrimus* blastula cells lies above 2°C and below 25°C. At 2°C, however, the cell-to-cell contact in aggregates of the dissociated blastula cells of *H. pulcherrimus* remained loose and no sign of further morphological change into blastula like organisms was observed even after 4 days of culture.

The aggregates formed at temperatures ranging from 10° to 20°C changed morphologically within one day on the initial form showing loose intercellular contact and random cellular orientation into blastula-like aggregates with tight intercellular adhesion and regular cellular orientation. These aggregates ordinarily showed regeneration of cilia and the formation of a blastocoel, as reported by Giudice [1] and Amemiya [3]. The majority of aggregates were observed to develop into pluteus-like structures, as reported by Giudice [1]. The

aggregates formed at 2°C did not undergo such morphological changes as those described above. Figures 2 and 3 show similar results observed for the dissociated blastula cells of *C. japonicus* and *A. crassispina*, respectively. The aggregation rate after 60 min of incubation were high at temperatures ranging from 10° to 30°C for embryos of these sea urchins, indicating that the optimal temperature for aggregation of their dissociated cells lies within this range. Compared with the optimal range for cells of *H. pulcherrimus*, the optimal range for blastula cells of *C. japonicus* and *A. crassispina* was apparently higher than that for blastula cells of *H. pulcherrimus*. As for *C. japonicus* and *A. crassispina*, cell aggregates redissociated gradually after one day of culture at the lower temperature as well as at 10°C.

Table 1 shows the ranges of temperature opti-

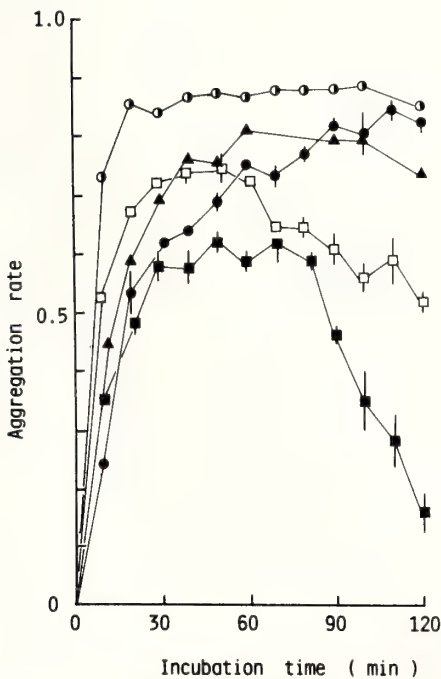


FIG. 2. Time course changes in the aggregation rate upon culturing dissociated embryonic cells of *Clypeaster japonicus* at temperatures of 10°C (solid triangle), 20°C (solid circle), 30°C (semi-solid circle), 35°C (open square) and 40°C (solid square). Each point is the average of triplicate determinations, the vertical bar being the standard error of those values.

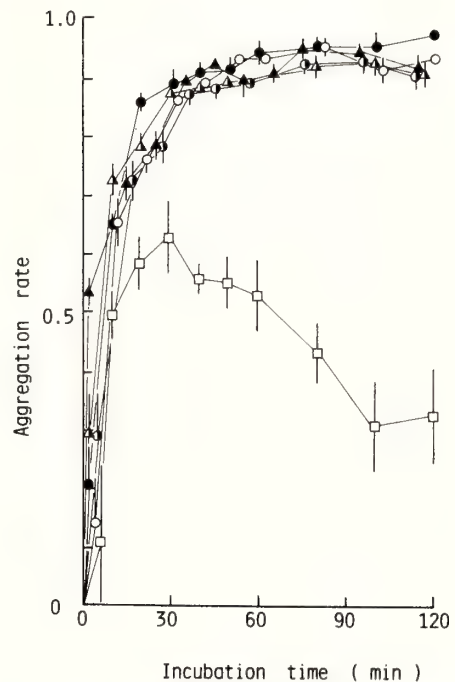


FIG. 3. Time course changes in the aggregation rate upon culturing dissociated embryonic cells of *Anthocidaris crassispina* at temperatures of 10°C (solid triangle), 15°C (semi-solid triangle), 20°C (solid circle), 25°C (open circle), 30°C (semi-solid circle), and 35°C (open square). Each point shows the average of triplicate determinations and the vertical bar depicts the standard error of those values.

TABLE 1. Ranges of optimal temperature for development of the three species of sea urchin and the ranges of sea water temperature in their spawning seasons

Species	Range of optimal temperature for development (°C)	Range of sea water temperature in the spawning seasons (°C)
<i>Hemicentrotus pulcherrimus</i>	4–23	10–17
<i>Clypeaster japonicus</i>	17–29	19–25
<i>Anthocidaris crassispina</i>	16–29	19–27

mal for normal development of these three species of sea urchin. The upper and the lower limits of temperature optimal for the development as shown in Table 1 indicate that embryos cultured at a temperature above the upper limit and below the lower limit were unable to develop into normal plutei without the occurrence of a significant proportion of deformed individuals. We confirmed that dissociated cells cultured at a temperature above the upper limits were able to aggregate but that they were unable to maintain the state of

aggregation.

Cells redissociated at a temperature above the upper limit of the optimal range were able to reversibly reaggregate when the temperature was reduced to the optimal one as shown in Figure 4. Dissociated cells from the blastula of *C. japonicus* cultured at 35°C were able to reaggregate again when the temperature reverted back to the optimal one (20°C) within half an hour of incubation. Upon culturing the cells at this higher temperature for periods longer than one hour, however, the cells showed a tendency to lose the capacity to reaggregate, even when the temperature was changed back to the optimal one.

In this experiment we were able to discriminate morphologically two phases in the process of aggregation. The first phase was one of mere aggregation with random loose intercellular contact, while the second phase induced compact aggregation with tight cell adhesion capable of forming an embryo-like structure. The first phase could be observed even at temperatures below or above the optimum, while the second phase only occurred at a temperature within the optimal range specific for each individual species.

Effects of cytochalasin B and colchicine on the aggregation of dissociated blastula cells

At 12°C, the optimal temperature for *H. pulcherrimus* embryos, single cells dissociated from the sea urchin blastulae aggregated in the presence of cytochalasin B (Fig. 5). The aggregates effected by cytochalasin B, however, were unable to adhere tightly to form a compact spherical ones, and hence could not develop into blastula-like ones. These aggregates gradually redissociated after being incubated for longer than four hours and finally reverted back to single cells. The aggrega-

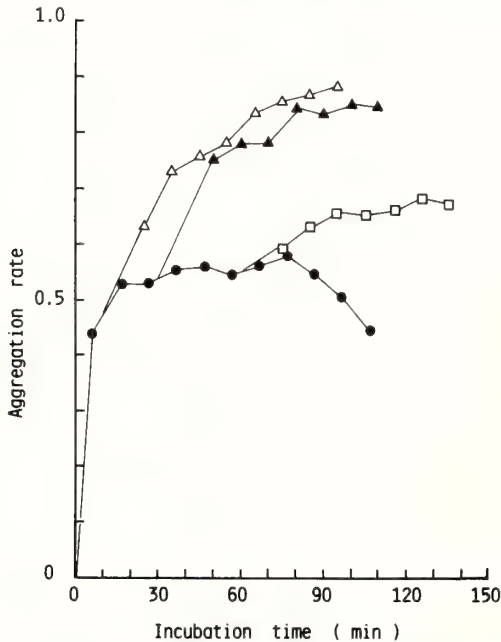


FIG. 4. Capability of reaggregation of the embryonic cells of *Clypeaster japonicus* after lowering the temperature from 35°C to 20°C. The cells were incubated at 20°C after being heated at 35°C for 10 min (△), 30 min (▲), and 60 min (□). Solid circle (●) shows the aggregation rate of the cells incubated continuously at 35°C.

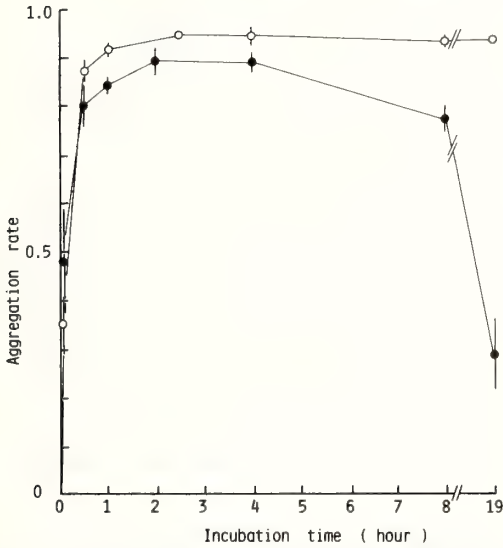


FIG. 5. Effect of cytochalasin B on the aggregation of embryonic cells dissociated from blastula of *Hemicentrotus pulcherrimus*. Concentration of cytochalasin B was $5 \mu\text{g/ml}$ of sea water. Dimethylsulphoxide (DMSO) was also added at the concentration of 0.1% in the sea water. This concentration of DMSO was non-effective to the cell aggregation. ○: control. ●: in the presence of cytochalasin B. Each point and vertical bar represents the average of triplicate determinations and the standard error of those values, respectively.

gates themselves, however, were unable to show further morphological change into compact spherical aggregates and hence did not develop into a blastula-like form. In contrast, these aggregates redissociated gradually into single cells after incubation in the presence of the drug for more than four hours. Thus it was clarified that cytochalasin B affects only the second phase of aggregation, suggesting that microfilaments are only involved in the morphogenetic change occurring in the second phase of aggregation.

The sea water added with cytochalasin B also contained DMSO at a concentration of 0.1%. However, this concentration of DMSO was shown not to produce any effect on these aggregation processes of dissociated cells.

The first phase of aggregation was also unaffected by colchicine. The aggregates, however, were unable to undergo morphogenetic change into a compact form followed by development into

a blastula-like form after being cultured for longer than four hours in the presence of colchicine. The aggregates remained in the initial state of loose intercellular contact throughout the culture period. This result suggests that the microtubule system is involved in the second phase of aggregation.

DISCUSSION

In the present work we confirmed that the optimal range of temperatures for aggregation of dissociated cells of sea urchin embryos is species specifically determined. Only the cells cultured at an optimal temperature can form aggregates with tight cell adhesion, change into blastula-like organisms which regenerate cilia and blastocoel and develop further into pluteus-like ones. At temperatures above the upper limit or below the lower limit of the range of temperature optimal for normal development, dissociated cells of sea urchin could aggregate, but the aggregates remained as loose-contacted ones without morphological changes into compacted spherical blastula-like organisms. Redissociation was usually observed after temporal aggregation when the cells were cultured at high temperature. Redissociation after temporal aggregation, though more gradual than that at high temperature, was also observed at 2°C in blastula of *C. japonicus* and *A. crassispina* whose breeding seasons are summer. We do not know why redissociation occurred after a brief time of incubation at higher temperatures. It is clear that the redissociation cannot be ascribed to low activity of the cytoskeleton since cytochalasin B could not cause such redissociation at brief time of incubation. A similar result has been reported in chick embryonic cells. Moscona [11] showed that the highest aggregation rate of retinal and of hepatic cells of chick embryos was achieved at 38°C , the temperature optimal for these embryos. He also noticed that at 15°C the formation of aggregates was prevented. Steinberg [12] also reported the prevention of aggregation by dissociated epidermal cells of chick embryo at 6.5°C . They observed the inability of formation of aggregates into compacted spherical ones with tight cellular adhesion at low temperatures. Temporal

formation of aggregates which remain in loose contact or redissociate after long incubation is thought to be possible at a low temperature since Curtis [13] reported that the cells dissociated from 5-day chick embryos were able to aggregate at 3°C although the aggregation rate was lowered. McClay and Baker [14] have already showed in dissociated neural retinal cells of chick embryo that the aggregation process is subdivided into at least two different phenomena: the reentering the population of cells and the adhesion itself. According to them both phenomena were sensitive to low temperature (4°C). We were also able to discriminate light microscopically two serial phases in the reaggregation in sea urchin embryonic cells. The first phase of aggregation is the formation of aggregates like clusters of single dissociated cells. In this phase cells adhere loosely and randomly to each other. Dissociated embryonic cells can form cluster-like loose aggregates in this first phase independently on thermal condition. The second phase is the formation of spherical compact aggregates with tight cell adhesion followed by the morphological change into blastula- and further pluteus-like organisms. The aggregates cannot develop into the second phase at a temperature outside the range optimal for normal embryogenesis. We confirmed that thermal condition for the reaggregation into reconstruction of embryo-like organisms is almost the same as that for normal development. Difference of the breeding seasons of sea urchins among different species in the same locality is thus thought to be explained partly by the species specifically determined temperature sensitivities of their embryogenesis.

In addition, we found that cells redissociated at a temperature over the upper limit of optimal temperature could reversibly reaggregate when the temperature was lowered to the optimal one. This reversibility, however, was lost after incubation longer than one hour at higher temperature. The reason why the cells redissociate finally at higher temperature is not certain.

These results also imply that the process of cellular aggregation does not depend merely on interactions among cells through the so-called cementing substance and divalent cations such as calcium and/or magnesium [5, 6, 8] or aggregation

promoting proteins [7, 9, 10]. The so-called cementing substance and/or divalent cations seems to be involved rather in the first phase of aggregation of dissociated embryonic cells than the second phase, since the first phase of aggregation is independent of temperature while attainment of the second phase can be observed only in the range optimal for normal embryogenesis. The synthesis of some cell surface glycoproteins [4, 15, 16] has been reported to be essential for reassociation of dissociated embryonic cells. We think that the synthesis of such substances is necessary for the second phase of aggregation because the aggregation was not affected but morphogenetic change of aggregates was arrested in the presence of some inhibitors of protein synthesis such as puromycin, ethionine [4] and cycloheximide (unpublished data).

Stage-specific adhesion or aggregation has been reported in sea urchin embryos [9, 10] as well as in amphibian embryos [17]. The present results are concerned only with the embryos at the mesenchymal blastula stage. We are now examining the aggregation of these sea urchin embryonic cells in other stages and the effect of temperature on the aggregation.

The activity of some cytoskeletal systems of microfilaments and/or microtubules is responsible for the second phase of aggregates [3, 18]. Present work showed that cytochalasin B, as well as colchicine, completely inhibited the compaction of the aggregates and hence the following morphological change into blastula-like organisms, which was in accordance with the result of Weiss using Ehrlich ascites cells [19, 20]. Cytoskeletal activities are known to be also involved in lectin-mediated cellular aggregation [21]. Microvilli have been reported to be important for aggregation of embryonic cells of sea urchin [22, 23] and other cells [19, 20, 24]. Microvilli are related to cytoskeletal activities [25], therefore the morphogenetic changes in the second phase, especially tight compaction of aggregates, may be aided with these cell surface structures. Electron microscopic investigations are now in progress to test the involvement of these structures in the aggregation and compaction of dissociated sea urchin embryonic cells. Fluidity of plasma membranes of aggrega-

ting embryonic cells may be another important factor for the second phase of aggregation. The temperature dependence of aggregation, especially of the second phase, seems to be well explained by this factor. Several pieces of direct evidence for the involvement of the fluidity in temperature-dependent cell agglutination have been obtained by modifying plasma membrane lipid composition or by alteration of proportion between saturated and unsaturated fatty acids [26–31]. Little evidence has been reported on species specific temperature dependent microfilament activity as yet. Therefore we think that possible candidate for explaining species specific temperature dependence of embryonic cell aggregation of these sea urchins with different breeding seasons is species-specific difference of plasma membrane fluidity of their embryonic cells. We are now attempting to confirm the possibility of relationship between the membrane property and the temperature dependence of aggregation.

ACKNOWLEDGMENTS

We wish to express our sincere thanks to Prof. H. Terayama and Prof. H. Katayama for their advice. We also thanks Dr. Y. Ichihara, Dr. S. Hattori, Dr. H. Kawasaki, Messrs. H. Kubo, M. Matsuda, S. Sone, T. Shinkai, M. Yoshikuni, Y. Ishida, Y. Kihira, T. Ishimori, Mrs. M. Toride, Misses T. Ohara, K. Ikeda, M. Ito, and S. Arai for their technical assistances.

REFERENCES

- Giudice, G. (1962) Restitution of whole larvae from disaggregated cells of sea urchin embryos. *Dev. Biol.*, **5**: 402–411.
- Giudice, G. (1967) Electron microscopic study of the reaggregation of cells dissociated from sea urchin embryos. *Dev. Biol.*, **5**: 91–101.
- Amemiya, S. (1971) Further studies on the relationship between cilium formation and cell association in sea urchin embryos. *J. Fac. Sci. Univ. Tokyo*, **IV**, **12**: 241–258.
- Giudice, G. (1965) The mechanism of aggregation of embryonic sea urchin cells; a biochemical approach. *Dev. Biol.*, **12**: 233–247.
- Kondo, K. and Sakai, H. (1971) Demonstration and preliminary characterization of reaggregation-promoting substances from embryonic sea urchin cells. *Dev. Growth Differ.*, **13**: 1–14.
- Kondo, K. (1973) Cell-binding substances in sea urchin embryos. *Dev. Growth Differ.*, **15**: 201–216.
- Noll, H., Matranga, V., Cascino, D. and Vittorelli, G. (1979) Reconstitution of membranes and embryonic development in dissociated blastula cells of the sea urchin by reinsertion of aggregation-promoting membrane proteins extracted with butanol. *Proc. Natl. Acad. Sci. U. S. A.*, **76**: 288–292.
- Tonegawa, Y. (1973) Isolation and characterization of a particulate cell-aggregation factor from sea urchin embryos. *Dev. Growth Differ.*, **14**: 337–351.
- Oppenheimer, S. B. and Meyer, J. T. (1982) Isolation of species-specific and stage-specific adhesion promoting component by disaggregation of intact sea urchin embryo cells. *Exp. Cell Res.*, **137**: 472–475.
- Oppenheimer, S. B. and Meyer, J. T. (1982) Carbohydrate specificity of sea urchin blastula adhesion component. *Exp. Cell Res.*, **139**: 451–455.
- Moscona, A. (1961) Rotation-mediated histogenetic aggregation of dissociated cells. *Exp. Cell Res.*, **22**: 455–475.
- Steinberg, M. S. (1962) The role of temperature in the control of aggregation of dissociated embryonic cells. *Exp. Cell Res.*, **28**: 1–10.
- Curtis, A. S. G. (1963) Effect of pH and temperature on cell reaggregation. *Nature*, **200**: 1235–1236.
- McClay, D. R. and Baker, S. R. (1975) A kinetic study of embryonic cell adhesion. *Dev. Biol.*, **43**: 109–122.
- Grunz, H. (1969) Hemmung der Reaggregation dissoziierter Amphibienzellen durch Inhibitoren der RNS- und Protein Synthese. *Wilhelm Roux' Archiv.*, **163**: 184–196.
- Moscona, A. (1961) Effect of temperature on adhesion to glass and histogenetic cohesion of dissociated cells. *Nature*, **190**: 408–409.
- Suzuki, A. S., Ueno, T. and Matsusaka, T. (1986) Alteration of cell adhesion system in amphibian ectoderm cells during primary embryonic induction: changes in reaggregation pattern of induced neurectoderm cells and ultrastructural features of the reaggregate. *Roux's Arch. Dev. Biol.*, **195**: 85–91.
- Weiss, L. (1972) Studies on cellular adhesion in tissue culture. XII. Some effects of cytochalasins and colchicine. *Exp. Cell Res.*, **74**: 21–26.
- Weiss, L. (1967) Studies on cell deformability. III. Some effects of EDTA on sarcoma 37 cell. *J. Cell Biol.*, **33**: 341–347.
- Weiss, L. and Subjek, J. R. (1974) Interactions between the peripheries of Ehrlich ascites tumor cells as indicated by the binding of colloidal iron hydroxide particles. *Int. J. Cancer*, **13**: 143–150.
- Smith, S. B. and Revel, J. P. (1972) Mapping of concanavalin A binding sites on the surface of several cell types. *Dev. Biol.*, **27**: 434–441.

- 22 Spiegel, M. and Spiegel, E. (1979) The morphology and specificity of cell adhesion of echinoderm embryonic cells. *Exp. Cell Res.*, **117**: 261-268.
- 23 Spiegel, M. and Spiegel, E. (1977) A scanning electron microscopical study of early sea urchin reaggregation. *Exp. Cell Res.*, **108**: 413-420.
- 24 O'Neill, C. H. (1968) An association between viral transformation and forssman antigen detected by immune adherence in cultured BHK 21 cells. *J. Cell Sci.*, **3**: 405-422.
- 25 Loor, F. (1976) Cell surface design. *Nature*, **264**: 272-276.
- 26 Wood, R. and Falch, J. (1974) Lipids of cultured hepatoma cells: II. Effect of media lipids on cellular phospholipids. *Lipids*, **8**: 702-710.
- 27 Jacobs, R. A. and Majerus, P. W. (1973) The regulation of fatty acid synthesis in human skin fibroblasts. *J. Biol. Chem.*, **248**: 8392-8401.
- 28 Wisnieski, B. J., Williams, R. E. and Fox, C. F. (1973) Manipulation of fatty acid composition in animal cells grown in culture. *Proc. Natl. Acad. Sci. U. S. A.*, **72**: 3669-3673.
- 29 Williams, R. E., Wisnieski, B. J., Rittenhouse, H. G. and Fox, C. F. (1974) Utilization of fatty acid supplements by cultured animal cells. *Biochemistry*, **13**: 1969-1977.
- 30 Horwitz, A. F., Hatten, M. E. and Burger, M. M. (1974) Membrane fatty acid replacements and their effect on growth and lectin-induced agglutinability. *Proc. Natl. Acad. Sci. U. S. A.*, **71**: 3115-3119.
- 31 Rittenhouse, H. G., Williams, R. E., Wisnieski, B. and Fox, C. F. (1974) Alterations of characteristic temperatures for lectin interactions in LM cells with altered lipid composition. *Biochem. Biophys. Res. Commun.*, **58**: 222-228.

Probable Participation of Mitochondrial Ca^{2+} Transport in Calcification of Spicules and Morphogenesis in Sea Urchin Embryos

KEIKO MITSUNAGA, YUKIO FUJINO¹ and IKUO YASUMASU²

Department of Biology, School of Education, Waseda University, 1-6-1 Nishiwaseda, Shinjuku-ku, Tokyo 160, and ¹Department of Pharmacology Teikyo University School of Medicine, 2-11-1 Kaga, Itabashi-ku, Tokyo 173, Japan

ABSTRACT—In embryos of the sea urchin, *Hemicentrotus pulcherrimus*, kept with ruthenium red or 2, 4-dinitrophenol in a period between the mesenchyme blastula and the pluteus corresponding stage, formation of calcified spicules was blocked at their concentrations to inhibit $^{45}\text{Ca}^{2+}$ uptake in isolated mitochondria. The ATP level slightly decreased in embryos kept with 2, 4-dinitrophenol but was hardly changed in those kept with ruthenium red. These compounds also inhibited spicule rod formation in cultured micromere-derived cells. This indicates that these compounds exert an effect directly on primary mesenchyme cells to block CaCO_3 deposition in the cells. Ca^{2+} uptake in mitochondria, known to be blocked by these compounds, probably participates in intracellular Ca^{2+} transport for spicule calcification. In embryos kept with these compounds, pluteus arm formation was also blocked, though quasi-normal archenterons were produced in embryos. Excess Ca^{2+} concentrations in the cells due to inhibition of Ca^{2+} uptake in mitochondria may result in a blockage of pluteus arm formation.

INTRODUCTION

Recently, we reported that Ca^{2+} influx through Ca^{2+} channels across plasma membrane is made electrosilent in all cell lineages of sea urchin embryos by coupled transport of anions [1-3]. In spicule forming cells, such as mesenchyme cells in embryos, those isolated by the procedure of Harkey and Whiteley [4] and in cultured micromere-derived cells obtained according to the method of Okazaki [5], Ca^{2+} thus carried into cells is transported into skeletal vacuoles, in which spicules are produced [6], and utilized as a main mineral material for their production [7]. Main mineral component of spicules in sea urchin embryos is known to be CaCO_3 [7] and a huge amount of CaCO_3 is produced in these spicule forming cells. In these cells, the turnover rate of

Ca^{2+} in cytoplasm is certainly higher than in the other cell lineages.

In these spicule forming cells, with a high rate of Ca^{2+} turnover, as well as in the other cell lineages, cytosolic Ca^{2+} level should be kept at an adequate concentration to maintain physiological activities of cell functions. It is well known that Ca^{2+} is one of important regulators of many cell functions. Probably, in the cells of sea urchin embryos, cytosolic free Ca^{2+} level is not only regulated by its uptake and release in endoplasmic reticulum but also by Ca^{2+} transport in mitochondria in a similar manner to the other cell types [8-13]. Indeed, in sea urchin eggs, inhibition of Ca^{2+} uptake in mitochondria by an uncoupler of oxidative phosphorylation results in an elevation of cytosolic Ca^{2+} level [14], in the same manner as in the other type of cells [15, 16]. When Ca^{2+} uptake in mitochondria is inhibited, cytosolic free Ca^{2+} level may increase especially in spicule forming cells with a high rate of Ca^{2+} turnover in cytoplasm. High level of cytosolic Ca^{2+} , which may be

Accepted August 13, 1987

Received July 27, 1987

² To whom requests of reprints should be addressed.

favorable for Ca^{2+} transport into skeletal vacuoles from cytoplasm in spicule forming cell, is expected to cause excess stimulation of Ca^{2+} -dependent cell functions to result in an abnormal development of embryos.

In the present study, we studied effects of ruthenium red, an inhibitor of ATP-dependent, H^+ -gradient mediated Ca^{2+} uptake in mitochondria [8, 17, 18], reported to elevate intracellular free Ca^{2+} level [19, 20], and 2, 4-dinitrophenol (DNP), an uncoupler of oxidative phosphorylation causing discharge of H^+ -gradient to block uptake of Ca^{2+} in mitochondria, on morphogenesis especially on the spicule formation in sea urchin embryos.

MATERIALS AND METHODS

Handling of gametes

Matured animals were collected at Tsushima Island and Sagami Bay and kept in a temperature-controlled sea water tank until use. Gametes of the sea urchin, *Hemicentrotus pulcherrimus*, were obtained by injection of 0.5 M KCl into the body cavity. Eggs were washed with artificial sea water (ASW) three times and inseminated by adding an adequate amount of sperm. Then, the eggs were washed twice with ASW and cultured at 20°C with gentle stirring by a motor-driven propeller.

Isolation and culture of micromeres

Micromeres were isolated at the 16-cell stage as described by Kitajima and Matsuda [21] and cultured at 20°C in ASW containing 4% horse serum, according to the procedure described by Kitajima and Okazaki [22].

Treatment of embryos and micromere-derived cells with ruthenium red and DNP

Stock solutions of ruthenium red (100 mM) and DNP (5 mM) dissolved in distilled water were added to embryo culture 15 hr after fertilization at 20°C and to micromere-derived cell culture at 15 hr of culture. The embryos and the micromere-derived cells were kept for another 30 hr in the presence of these compounds and then the photographs were taken. Less than 10 μl stock solutions

of these chemicals were added to 2 ml culture. Addition of 10 μl distilled water did not exert any effect on spicule formation and other morphogenesis in the culture. In some cases, stock solutions of these compounds dissolved in ASW were used in place of those dissolved in distilled water.

Calcium amount in spicules isolated from embryos

Spicules were isolated from embryos according to the procedure described previously [2]. Calcium content in the spicule fraction was analyzed using an atomic-absorption spectrophotometer (Hitachi 170-50A; Hitachi Ltd., Tokyo, Japan) as described previously [2].

Relative length of pluteus arm and archenteron

The lengths of embryos along pluteus arms and along archenteron were measured on photographs of the embryos treated with ruthenium red or DNP. Length of pluteus arm was calculated by subtraction of the length along archenteron from that along the arm and relative value was expressed as percentage of the length in normal embryos. The length of archenteron was also measured on photographs of the embryos. The relative length of archenteron in these treated embryos was also expressed as percentage of archenteron length in normal embryos. These lengths were measured on 30 embryos. The length of spicule in cultured micromere-derived cells was also measured on photographs obtained with a polarized-light microscope. When a spicule had branches, the sum of the length of branches was regarded as the length of this spicule. Spicule lengths in 30 clusters of micromere-derived cells in a culture were measured and these values were expressed as μm per cell.

Ca^{2+} uptake in mitochondria

Mitochondrial fraction was obtained from embryos at 35 hr after fertilization at 20°C (the prism stage). Embryos were collected by hand-driven centrifuge and were washed twice with ice cold 0.6 M sucrose solution containing 5 mM EDTA, 10 mM MgCl_2 and 10 mM Tris-HCl, pH 7.2 (homogenizing medium). Embryo suspension in the homogenizing medium was transferred to glass homogenizer and homogenized in an ice bath

with a motor-driven Teflon pestle. The homogenate was centrifuged at $1,000\times g$ for 10 min and resultant supernatant was again centrifuged at $8,000\times g$ for 20 min. The obtained pellet was washed once and suspended in the homogenizing medium without EDTA. This suspension was used as a crude mitochondria fraction. Reaction mixture in $200\ \mu\text{l}$ contained $5\ \mu\text{M}$ CaCl_2 , $5\ \mu\text{Ci/ml}$ $^{45}\text{CaCl}_2$, $0.3\ \text{M}$ KCl , $5\ \text{mM}$ MgCl_2 , $10\ \text{mM}$ phosphate buffer, pH 7.2, $10\ \text{mM}$ Tris-HCl, pH 7.2, $1\ \text{mM}$ ATP, $1\ \text{mM}$ ADP, $0.5\ \text{mM}$ succinate, $5\ \mu\text{M}$ cytochrome *c*, and $10\ \mu\text{l}$ mitochondria suspension (about $5\ \text{mg}$ protein ep./ml) in the homogenizing medium from which EDTA was omitted. The reaction was started at 20°C by adding mitochondria suspension. After 5 min incubation, it was terminated by adding 1 ml of ice cold $0.3\ \text{M}$ KCl solution containing $5\ \text{mM}$ MgCl_2 , $50\ \mu\text{M}$ CaCl_2 and $10\ \text{mM}$ Tris-HCl, pH 7.2. Then, this suspension was filtered through Millipore filter (HAWP02500, Millipore Corp., Ma, USA) and the filter was washed three times in the cold with the medium used for termination of the reaction. The filter was dried *in vacuo* and analyzed for radioactivity by a liquid scintillation spectrometer (Aloka LSC 700, Aloka, Tokyo, Japan). ^{45}Ca radioactivity, obtained following simultaneous additions to the reaction mixture of mitochondrial suspension and the solution with which the reaction was terminated, was subtracted from the values thus obtained. The rate of Ca^{2+} uptake is expressed as cpm of ^{45}Ca radioactivity per mg protein of mitochondrial fraction per 5 min. Protein was determined by the method of Lowry *et al.* [23], using bovine serum albumin as the standard.

ATP level in embryos

The embryos, washed once with ice cold artificial sea water and suspended in ice cold $0.6\ \text{M}$ sucrose solution, were centrifuged at $10,000\times g$ for 10 min. The embryo pellet obtained was diluted with 5 volumes of ice cold 5% perchloric acid and homogenized by Polytron (PT10-35, Kinematica GmbH, Switzerland). To the homogenate of embryos, one tenth volumes of $1\ \text{M}$ triethanolamine was added and the homogenate was centrifuged for 30 min at $15,000\times g$. The resultant

precipitate was analyzed for protein and the supernatant was neutralized with saturated K_2CO_3 in an ice-bath. After heavy white precipitate was centrifuged off, the supernatant was analyzed for ATP by the enzymatical methods [24], described in detail in a previous paper [25].

Chemicals

Ruthenium red and cytochrome *c* were purchased from Sigma Chemical Co., Mo., USA. 2,4-Dinitrophenol (DNP) was obtained from Kanto Chem. Co., Tokyo, Japan. Nicotinamideadenine dinucleotide phosphate, hexokinase, glucose-6-phosphate dehydrogenase (used for ATP determination), $\text{Na}_2\text{-ATP}$ and ADP were the products of Boehringer Mannheim, Federal Republic of Germany. $^{45}\text{CaCl}_2$ was purchased from the Radiochemical Centre, Amersham, Bucks, U. K. Artificial sea waters (ASW) were the products of Jamarin Laboratory, Osaka, Japan.

RESULTS

As shown in Figure 1, sea urchin embryos kept with ruthenium red at above $20\ \mu\text{M}$ from the mesenchyme blastula stage (15 hr after fertilization at 20°C) became abnormal spherical ones (Fig. 1B-E) having no pluteus arms and quasi-normal archenteron, when control embryos (Fig. 1F) became well developed plutei (45 hr after fertilization). Embryos kept with ruthenium red were considerably dark, probably because of ruthenium red-stained cells. This compound is known to bind with polysaccharides on cell surface [26, 27]. In embryos kept with ruthenium red at $20\ \mu\text{M}$, at which formation of pluteus arms was completely blocked, irregular tri-radiate spicules were observed in embryos with a polarized light microscope (Fig. 1b). The spicules became smaller in relation to the concentration of ruthenium red (Fig. 1a-d) and were hardly observed in embryos kept with this compound at above $150\ \mu\text{M}$ (Fig. 1e).

In embryos kept with DNP at 100 and $200\ \mu\text{M}$, pluteus arms (Fig. 2A, B) and spicules (Fig. 2a, b) were markedly shorter than in control embryos (Fig. 1F, f). DNP at $200\ \mu\text{M}$ inhibited growth of spicule and pluteus arm more strongly than at 100

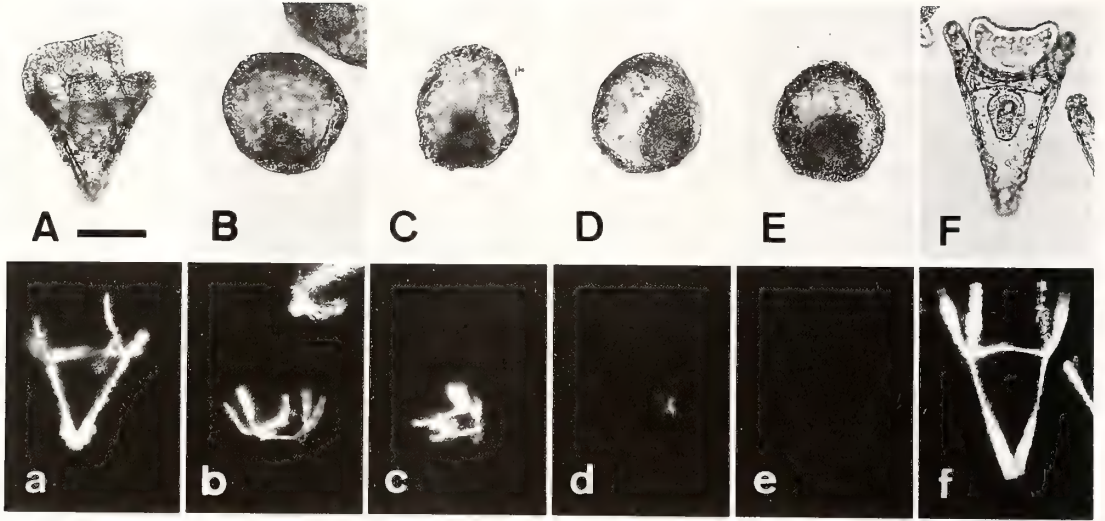


FIG. 1. Embryos treated with ruthenium red. Ruthenium red was added to the culture medium 15 hr after fertilization at 20°C (the mesenchyme blastula stage). Embryos, kept with ruthenium red at 10 μ M (A), 20 μ M (B), 40 μ M (C), 100 μ M (D) and 150 μ M (E), were photographed 45 hr after fertilization (the pluteus corresponding stage). Normal pluteus is shown in F. Photographs marked with (A-F) and (a-f) are those observed with a light and a polarized-light microscope, respectively. Bar shows 100 μ m.

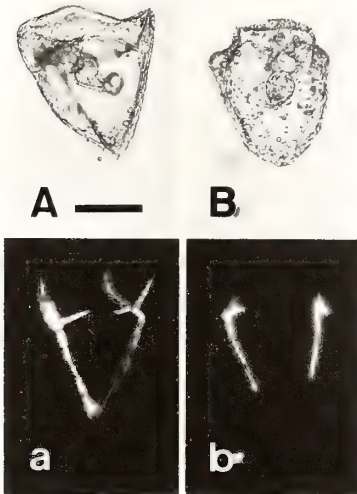


FIG. 2. Embryos treated with 2,4-dinitrophenol (DNP). Treatment of embryos with DNP was performed in the same manner as described for the ruthenium red-treatment in the legends of Fig. 1. The embryos were treated with 100 μ M (A) and 200 μ M DNP (B). Spicules observed with a polarized-light microscope in the same embryos shown in A and B are shown in a and b, respectively. Bar shows 100 μ m.

μ M (Fig. 2). However, these were not completely blocked by DNP even at 1 mM (photograph not shown).

Figure 3 shows the effects of ruthenium red (Fig. 3A) and DNP (Fig. 3B) on calcium deposition in spicules, growth of pluteus arms and of archenteron. Embryos at the mesenchyme blastula stage (15 hr after fertilization), in which any spicules, pluteus arms and archenterons had not been formed yet, were cultured for another 30 hr at 20°C in the presence of ruthenium red or DNP. Then, the calcium amount in spicules, the length of pluteus arms and the size of archenteron were measured. Hence, these values indicate growth of these structures in embryos during developmental period between 15 and 45 hr after fertilization.

As shown in Figure 3A, ruthenium red caused a slight decrease of calcium amount in the spicules at 10 μ M and a marked decrease at concentrations above 50 μ M. The calcium amount in spicules became close to zero at above 75 μ M. The growth of pluteus arms was inhibited by ruthenium red at above 10 μ M and was completely blocked at above 20 μ M. Strong inhibition of pluteus arm formation by ruthenium red occurred at lower concentrations than those to cause complete inhibition of spicule

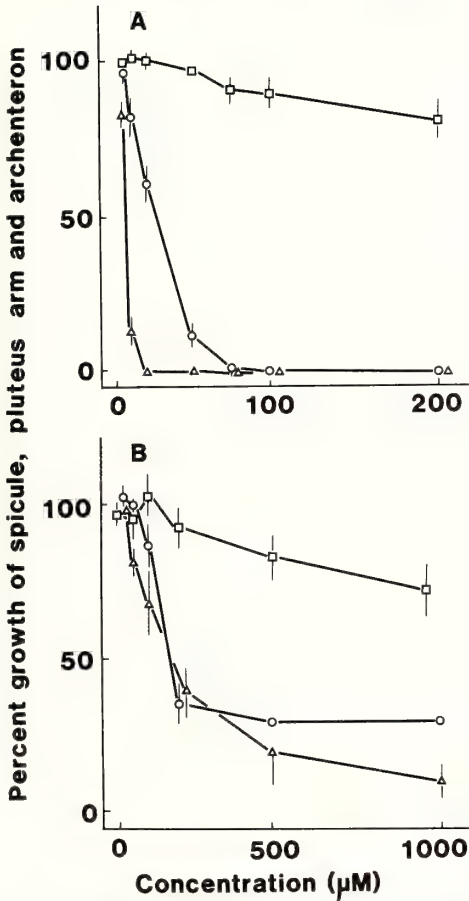


FIG. 3. Effects of ruthenium red and DNP on calcium deposition in spicules, growth of pluteus arms and of archenteron. Ruthenium red (A) and DNP (B) were introduced to embryo culture 15 hr after fertilization, being kept at 20°C. Embryos were cultured for another 30 hr. Calcium content in spicule fraction, length of pluteus arms and of archenterons were measured as described in Materials and Methods. Percentages of calcium contents in spicules of embryos thus treated with these compounds to those of normal embryos, shown with open circles (○), are the means of three experiments. Calcium contents in spicules of control embryos obtained in three experiments were 2.42, 2.63 and 2.39 μmol/mg embryo protein, respectively. Percentages of length of pluteus arms and archenteron in thus treated embryos to those in control ones, shown with open triangles (△: pluteus arm) and open squares (□: archenteron), are the means of three experiments, in which those in 30 embryos are measured in all embryo cultures, respectively. Vertical bar indicates SE. Fifteen hr after fertilization, embryos did not have any spi-

calcification. The size of archenteron hardly decreased at concentrations of ruthenium red lower than 75 μM and became considerably small at higher concentrations. Sensitivity of archenteron formation to ruthenium red is markedly lower than that of spicule formation.

DNP, at above 100 μM, caused a decrease in the calcium amount of spicules (Fig. 3B). The calcium amount of spicules in embryos treated with DNP at 200 μM was about 30% of the control embryos and did not decrease further even at 1 mM. Growth of pluteus arm was considerably inhibited by DNP at above 50 μM and was strongly blocked at above 200 μM (Fig. 3B). As far as examined, complete inhibition of pluteus arm formation and CaCO₃ deposition (spicule rods) was not obtained by DNP. The length of archenteron in the embryos kept with DNP at lower concentrations than 200 μM was almost the same as in the normal ones and became slightly short at above 500 μM (Fig. 3B). Inhibition of archenteron formation by DNP occurs at markedly higher concentrations than those to exert maximum inhibitory effect on spicule calcification and pluteus arm formation.

As shown in Figure 4, calcified spicule formation in cultured micromere-derived cells was inhibited by ruthenium red (B) and DNP (C). Ruthenium red and DNP were added at 15 hr of culture, at which spicule formation in the cultured cells had not been initiated yet. Photographs were taken at 45 hr of culture when well-developed spicules were observed in the control culture (A). Ruthenium red and DNP did not inhibit outgrowth of pseudopodial cables (shown with arrow heads in Fig. 4). These compounds seem to inhibit directly CaCO₃ production in the cables. As shown in Figure 5, the length of spicule became short in cultured micromere-derived cells at the concentration ranges of ruthenium red and DNP to block calcified spicule formation in embryos.

As shown in Figure 6, an increase in the length of spicule rod occurred in cultured micromere-derived cells in a period between 20 and 30 hr of culture and then, was followed by less steep

cules, pluteus arms and archenterons. Hence, these values measured 45 hr after fertilization indicate growth of these embryonic organs in this period of development.

increase in its length. This increase was instantly inhibited by adding 75 μM ruthenium red at 15, 20, 30 and 40 hr of culture. Even after cultured micromere-derived cells have been furnished with an ability to form spicule rods, these compounds are able to inhibit production of CaCO_3 . The same was observed using DNP (500 μM) in place of ruthenium red (data not shown).

As shown in Figure 7, the rate of $^{45}\text{Ca}^{2+}$ uptake in mitochondria isolated from embryos at the prism stage (35 hr after fertilization) decreased in the presence of these compounds. $^{45}\text{Ca}^{2+}$ uptake was evidently inhibited by DNP at above 50 μM and almost completely at above 200 μM (B). $^{45}\text{Ca}^{2+}$ uptake in mitochondria was also inhibited by ruthenium red at the concentrations higher than 20 μM and complete inhibition was obtained at

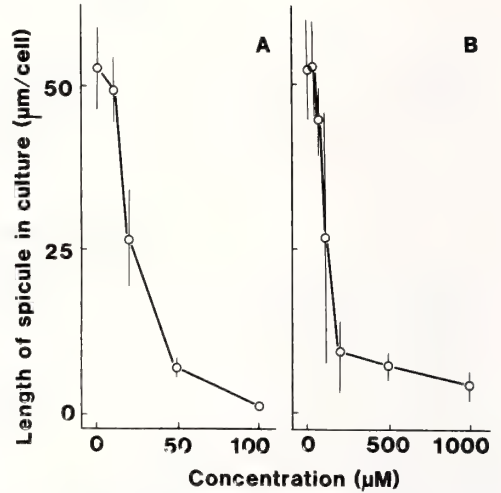


FIG. 5. Effect of ruthenium red and 2, 4-dinitrophenol (DNP) on growth of spicule rods in cultured micromere-derived cells. At 15 hr of culture, ruthenium red (A) and DNP (B) were added to the culture of isolated micromeres. Length of spicule rod (corresponding to its growth) was measured at 45 hr of culture as described in Materials and Methods. Each value shows the mean \pm SE of three different experiments.

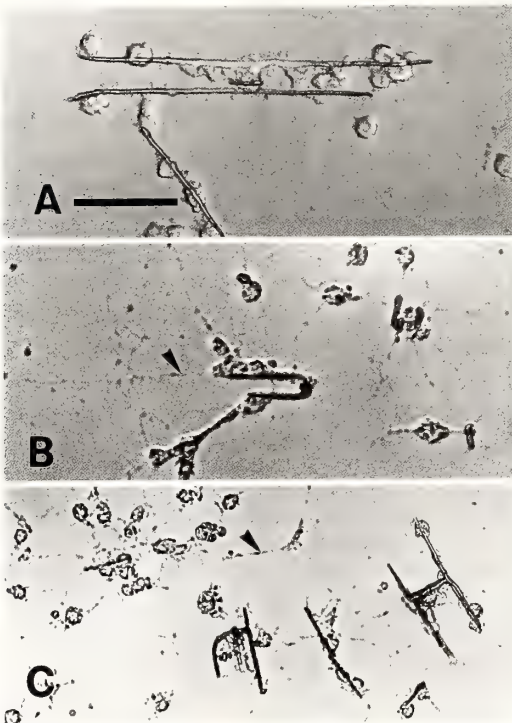


FIG. 4. Effect of ruthenium red and 2, 4-dinitrophenol (DNP) on calcified spicule formation in cultured micromere-derived cells. Ruthenium red (B, 25 μM) and DNP (C, 150 μM) were added to the culture at 15 hr of culture at 20°C. Cells were photographed at 45 hr of culture. Control culture is shown in A. Arrow head indicates pseudopodial cable. Bar shows 50 μm .

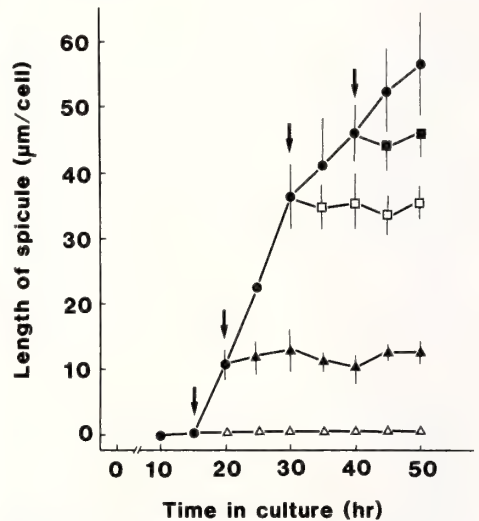


FIG. 6. Effect of ruthenium red on the growth of spicule rods in cultured micromere-derived cells. Ruthenium red at 75 μM was introduced at 15 (Δ), 20 (\blacktriangle), 30 (\square) and 40 hr (\blacksquare) of culture to these descendant cells of isolated micromeres. Arrows indicate the times of adding ruthenium red. Control culture is shown by using solid circles (\bullet). The values shown were means of 90 cell clusters measured in different 3 cultures. Bar shows SE.

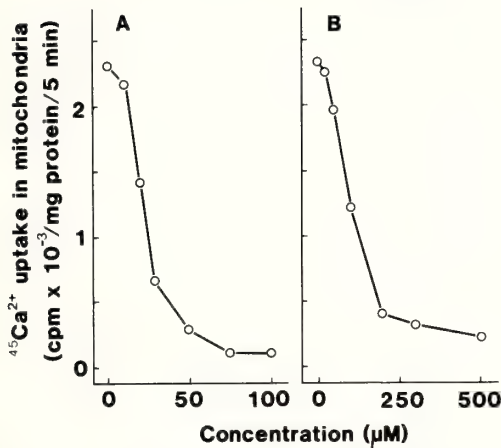


FIG. 7. Inhibition of Ca^{2+} uptake in mitochondria isolated from the embryos at the late gastrula stage by ruthenium red and 2, 4-dinitrophenol (DNP). Mitochondria fraction was obtained from embryos at the prism stage (35 hr after fertilization, being kept at 20°C). $^{45}\text{Ca}^{2+}$ uptake in mitochondria in the presence of ruthenium red (A) or DNP (B) was measured as described in Materials and Methods.

above $50 \mu\text{M}$ (A). Concentration ranges of these compounds to inhibit Ca^{2+} uptake in mitochondria were almost the same as those to inhibit calcified spicule formation in embryos and in cultured micromere derived cells.

The ATP level in embryos at the late gastrula stage was $13.9 \pm 2.4 \text{ nmol/mg protein}$. The levels in embryos at the late gastrula corresponding stage, having been kept with $500 \mu\text{M}$ DNP and $100 \mu\text{M}$ ruthenium red for 10 hr, were 10.5 ± 4.1 and $14.1 \pm 4.0 \text{ nmol/mg protein}$, respectively. In the embryos kept with DNP, the ATP level is not so low as expected. The ATP level in DNP-treated embryos may be maintained by glycolysis system. The level in ruthenium red-treated cells was as high as in control embryos. These suggest that the inhibition by these compounds of calcified spicule formation, as well as growth of pluteus arm and archenteron, is not due to a shortage of ATP.

DISCUSSION

In the present study, it was found that ruthenium red inhibited spicule formation in cultured cells derived from micromeres of sea urchin

embryos but did not block outgrowth of pseudopodial cables along which spicule rods were to be produced. These indicate that the inhibition of spicule rod formation by ruthenium red does not result from failure of outgrowth of pseudopodial cables. It was also observed that spicule rod formation was inhibited by ruthenium red even after spicule formation had been initiated. This indicates that spicule formation is inhibited by ruthenium red in the cells having been furnished with an ability to produce spicule rods. The inhibition of spicule rod formation by ruthenium red does not seem to result from possible blockage of mesenchyme cell differentiation into spicule forming cells but is probably ascribed to direct inhibition of several reactions in CaCO_3 production.

Ruthenium red is an inhibitor of ATP-dependent, H^+ -gradient mediated Ca^{2+} uptake in mitochondria [8, 17, 18]. Inhibition of spicule rod formation by this compound suggests that Ca^{2+} uptake in mitochondria participates in spicule formation. Indeed, DNP, an uncoupler of oxidative phosphorylation to cause a discharge of H^+ -gradient in mitochondria, also inhibited spicule rod formation in a manner essentially similar to ruthenium red. These compounds inhibited $^{45}\text{Ca}^{2+}$ uptake in mitochondria isolated from sea urchin embryos. The blockage of spicule rod formation occurred in almost the same concentration ranges of ruthenium red and DNP for the inhibition of Ca^{2+} uptake in mitochondria. These suggest that Ca^{2+} transport in mitochondria participates in spicule formation or CaCO_3 deposition.

DNP is also well known to make electron transport through mitochondrial respiratory chain uncoupled to oxidative phosphorylation, to cause a failure of ATP production in mitochondria. Decrease in ATP level certainly reduces the rates of ATP-dependent reactions in spicule formation, such as active ion transport across the membrane catalyzed by Cl^- , HCO_3^- -ATPase [28, 29] and H^+ , K^+ -ATPase [30]. In the embryos kept with DNP, as well as ruthenium red, however, the ATP level was almost the same as in control embryos.

Failure of Ca^{2+} uptake caused by ruthenium red and DNP in mitochondria probably results in an

increase in cytosolic Ca^{2+} level. Also in sea urchin eggs, an uncoupler of oxidative phosphorylation has been found to cause a marked increase in cytosolic free Ca^{2+} level [14]. Ca^{2+} uptake through Ca^{2+} channels is reportedly high in its rate in cells with low cytosolic free Ca^{2+} [31]. Hence, a high level of cytosolic free Ca^{2+} probably causes a decrease in Ca^{2+} influx into cells, with which Ca^{2+} , a main material for the spicule rod formation, is supplied from external sea water. Indeed, in spicule forming cells as well as in the other cells of sea urchin embryos, Ca^{2+} uptake into cells is blocked by ruthenium red [2, 3], though this compound is known to exert any inhibitory effect on Ca^{2+} channels. However, high level of cytosolic Ca^{2+} , which is assumed to be rather favorable for Ca^{2+} transport into skeletal vacuoles across their membrane, does not seem to be maintained, if Ca^{2+} is utilized for spicule rod formation. Thus, low rate of Ca^{2+} uptake through Ca^{2+} channels in spicule forming cells rather results from the inhibition by these compounds of spicule formation. Uptake of Ca^{2+} in mitochondria, seems to be indispensable for Ca^{2+} supply to skeletal vacuoles across their membrane in spicule forming cells. Condensation of Ca^{2+} may occur in mitochondria to supply high concentration of Ca^{2+} into skeletal vacuoles.

Ruthenium red is also known to inhibit Ca^{2+} -ATPase in plasma membrane, a Ca^{2+} pump [32, 33]. If the inhibition of Ca^{2+} pump in skeletal vacuoles by ruthenium red occurs in spicule forming cells, supply of Ca^{2+} into skeletal vacuoles may be blocked to cause a failure of CaCO_3 deposition in the vacuoles. However, DNP, which does not inhibit this ATPase, considerably blocks spicule formation. These may be a reason why ruthenium red exerts stronger inhibitory effect on spicule formation than DNP, but it is unlikely that the inhibition of spicule formation by these compounds is solely due to inhibition of Ca^{2+} transport by a Ca^{2+} pump in skeletal vacuole membrane.

Ruthenium red also exerted strong inhibitory effects on morphogenesis other than spicule formation in embryos. In embryos kept with ruthenium red, pluteus arm formation was completely inhibited at concentrations lower than

those for complete blockage of spicule formation. Also in DNP treated embryos, pluteus arm formation was inhibited more strongly than spicule formation, though their complete inhibition was not obtained at the concentrations of DNP examined in the present study. These suggest that the blockage of pluteus arm formation by these compounds does not result from the failure of spicule rod formation. Ruthenium red and DNP, causing an increase in cytosolic Ca^{2+} , probably result in excess stimulation of Ca^{2+} -dependent enzymes. Excess stimulation of these enzymes may change cell functions to cause a failure of pluteus arm formation. It has also been found that embryos develop to abnormal ones with poor pluteus arms, no spicules and quasi-normal archenterons in the presence of Ca^{2+} antagonists [1, 2, 28], which probably reduced cytosolic free Ca^{2+} . Low cytosolic Ca^{2+} probably prevents Ca^{2+} -dependent enzymes from the stimulation. It is likely that abnormal activities of Ca^{2+} -dependent cell functions, either being excessively stimulated by ruthenium red and DNP or remaining unstimulated in the presence of Ca^{2+} antagonists, fail to support morphogenesis such as pluteus arm formation.

On the other hand, archenteron formation was hardly inhibited by ruthenium red and DNP. The same is found in embryos kept in the presence of Ca^{2+} antagonists [1, 2, 28]. Archenteron is formed in blastocoel in which spicules are also produced. Spicule formation in cultured micromere-derived cells was inhibited by ruthenium red and DNP, as well as by Ca^{2+} antagonists [28], at almost the same concentrations for its inhibition in embryos. Hence, concentrations of these compounds in blastocoel are assumed to be almost the same as in media surrounding embryos. Archenteron can be constructed with cells in which Ca^{2+} -dependent cell functions are excessively stimulated or remain quite low in their activities, though the cells with adequate activities of Ca^{2+} -dependent cell functions are necessary for the formation of pluteus arms and spicules. Contribution of Ca^{2+} -dependent reactions to morphogenesis may be quite low in the formation of archenteron as compared to that in pluteus arm formation. One of Ca^{2+} -dependent reactions to support the mor-

phogenesis may be protein kinase C. Several observations to support the assumption mentioned above will be reported elsewhere.

ACKNOWLEDGMENTS

This work was supported by Grants-in-Aid for Scientific Research (Nos. 60223028 and 61304009) from the Ministry of Education, Science and Culture, Japan.

REFERENCES

- Mitsunaga, K., Fujino, Y., Fujiwara, A. and Yasumasu, I. (1984) Anion transport participates in spicule calcification of sea urchin embryos. *Dev. Growth Differ.*, **26**: 375, Abstract A33.
- Yasumasu, I., Mitsunaga, K. and Fujino, Y. (1985) Mechanism for electrostatic Ca^{2+} transport to cause calcification of spicules in sea urchin embryos. *Exp. Cell Res.*, **159**: 80–90.
- Fujino, Y., Mitsunaga, K. and Yasumasu, I. (1985) Inhibition of $^{45}\text{Ca}^{2+}$ uptake in the eggs and embryos of the sea urchin, *Anthocidaris crassispina*, by several calcium antagonists, anion transport inhibitor and chloride transport inhibitors. *J. Exp. Zool.*, **235**: 281–288.
- Harkey, M. A. and Whiteley, A. H. (1980) Isolation, culture, and differentiation of echinoid primary mesenchyme cells. *Wilhelm Roux Arch. Dev. Biol.*, **189**: 111–122.
- Okazaki, K. (1975) Spicule formation by isolated micromeres of the sea urchin embryo. *Am. Zool.*, **15**: 567–581.
- Gibbins, J. R., Tilney, L. G. and Porter, K. R. (1969) Microtubules in the formation and development of the primary mesenchyme in *Arbacia punctulata*. I. The distribution of microtubules. *J. Cell Biol.*, **41**: 201–226.
- Inoue, S. and Okazaki, K. (1977) The development of an elaborate crystalline skeleton within the transparent embryo of the sea urchin provides a model for the shaping of hard mineralized tissues such as shell and bone. *Sci. Am.*, **236**: 82–92.
- Moore, C. L. (1971) Specific inhibition of mitochondrial Ca^{2+} transport by ruthenium red. *Biochem. Biophys. Res. Commun.*, **42**: 298–305.
- Thorne, R. F. W. and Bygrave, F. L. (1974) The role of mitochondria in modifying the cellular ionic environment. *Biochem. J.*, **144**: 551–558.
- Landry, Y. and Lehninger, A. L. (1976) Transport of calcium ions by Ehrlich ascites-tumor cells. *Biochem. J.*, **158**: 427–438.
- Carafoli, E. and Crompton, M. (1978) The regulation of intracellular calcium by mitochondria. *Ann. N. Y. Acad. Sci.*, **307**: 269–284.
- Rasmussen, H. and Gustin, M. C. (1978) Some aspects of the hormonal control of cellular calcium metabolism. *Ann. N. Y. Acad. Sci.*, **307**: 391–402.
- Carafoli, E. (1986) Membrane transport in the cellular homeostasis of calcium. *J. Cardiovasc. Pharmacol.*, **8**: suppl. 8, s3–s6.
- Eisen, A. and Reynolds, G. T. (1985) Source and sinks for the calcium released during fertilization of single sea urchin eggs. *J. Cell Biol.*, **100**: 1552–1527.
- Brinley, F. J., Tiffert, T., Scarpa, A. and Mullins, L. J. (1977) Intracellular calcium buffering capacity in isolated squid axons. *J. Gen. Physiol.*, **70**: 355–384.
- Baker, P. F. and Singh, R. (1981) Influence of vanadate on calcium fluxes and net movement of calcium in intact squid axons. *Biochim. Biophys. Acta*, **646**: 450–456.
- Vasington, F. D., Gazzotti, P., Tiozzo, R. and Carafoli, E. (1972) The effect of ruthenium red on Ca^{2+} transport and respiration in rat liver mitochondria. *Biochim. Biophys. Acta*, **256**: 43–54.
- Reed, K. C. and Bygrave, F. L. (1974) The inhibition of mitochondrial calcium transport by lanthanides and ruthenium red. *Biochem. J.*, **140**: 143–155.
- Baker, P. F., Knight, D. E. and Umbach, J. A. (1985) Calcium clamp of the intracellular environment. *Cell Calcium*, **6**: 5–14.
- Rigoni, F. and Deana, R. (1986) Ruthenium red inhibits the mitochondrial Ca^{2+} uptake in intact bovine spermatozoa and increases the cytoplasmic Ca^{2+} concentration. *FEBS Lett.*, **198**: 103–108.
- Kitajima, T. and Matsuda, R. (1982) Specific protein synthesis of sea urchin micromeres during differentiation. *Zool. Mag.*, **91**: 200–205.
- Kitajima, T. and Okazaki, K. (1980) Spicule formation in vitro by the descendants of precocious micromere formed at the eight-cell stage of sea urchin embryo. *Dev. Growth Differ.*, **22**: 265–279.
- Lowry, O. H., Rosebrough, N. J., Farr, A. L. and Randall, R. J. (1951) Protein measurement with the Folin phenol reagent. *J. Biol. Chem.*, **193**: 265–275.
- Lamprecht, W. and Trautschold, I. (1963) Adenosine-5'-triphosphate. Determination with hexokinase and glucose-6-phosphate dehydrogenase. In "Methods of Enzymatic Analysis". Ed. by H. U. Bergmeyer, Acad. Press., N. Y., pp. 265–267.
- Yasumasu, I., Asami, K., Shoger, R. L. and Fujiwara, A. (1973) Glycolysis of sea urchin eggs. *Exp. Cell Res.*, **80**: 361–371.
- Gustafson, G. T. and Pihl, E. (1967) Histochemical application of ruthenium red in the study of mast cell ultrastructure. *Acta Path. Microbiol. Scand.*, **69**: 393–403.
- Gordon, M., Fraser, L. R. and Dandekar, P. V.

- (1974) The effect of ruthenium red and concanavalin A on the vitelline surface of fertilized and unfertilized rabbit ova. *Anat. Rec.*, **181**: 95-112.
- 28 Mitsunaga, K., Makihara, R., Fujino, Y. and Yasumasu, I. (1986) Inhibitory effects of ethacrynic acid, furosemide, and nifedipine on the calcification of spicules in cultures of micromeres isolated from sea-urchin eggs. *Differentiation*, **30**: 197-204.
- 29 Mitsunaga, K., Fujino, Y. and Yasumasu, I. (1986) Change in the activity of Cl^- , HCO_3^- -ATPase in microsome fraction during early development of the sea urchin, *Hemicentrotus pulcherrimus*. *J. Biochem.*, **100**: 1607-1615.
- 30 Mitsunaga, K., Fujino, Y. and Yasumasu, I. (1987) Probable role of allylthiocyanate-sensitive H^+ , K^+ -ATPase in spicule calcification in embryos of the sea urchin, *Hemicentrotus pulcherrimus*. *Dev. Growth Differ.*, **29**: 57-70.
- 31 DiPolo, R. (1979) Calcium influx in internally dialyzed squid giant axons. *J. Gen. Physiol.*, **73**: 91-113.
- 32 Watson, E. L., Vincenzi, F. F. and Davis, P. W. (1971) Ca^{2+} -activated membrane ATPase: Selective inhibition by ruthenium red. *Biochim. Biophys. Acta*, **249**: 606-610.
- 33 Tsuruo, T., Iida, H., Tsukagoshi, S. and Sakurai, Y. (1981) Prevention of vinblastine-induced cytotoxicity by ruthenium red. *Biochem. Pharmacol.*, **30**: 213-216.

Spawning of Three Intraspecific Groups of the Ascidian, *Halocynthia roretzi* (Drasche), in the Wild, and Fertilization among Them

TAKAHARU NUMAKUNAI, ZEN-ICHIRO HOSHINO¹ and SHOGO KAJIWARA

Marine Biological Station, Tohoku University, Asamushi, Aomori 039-34,
and ¹*Department of Biology, Faculty of Education,*
Iwate University, Ueda, Morioka 020, Japan

ABSTRACT—Spawning seasons and spawning times of three intra-specific groups of the ascidian, *Halocynthia roretzi*, were observed in the wild. They released gametes at the same time as in the laboratory. One of them, which spawns in April in the laboratory, spawned in the middle of December. This was caused by low sea water temperature in the laboratory. Experimentally, fertilization among the three Types was possible, and the resulting embryos gave rise to normal young adults. Experimental results and observations of spawning in the wild suggest the possibility of cross fertilization between Type A and Type C.

INTRODUCTION

We have reported of the ascidian, *Halocynthia roretzi*, that in Mutsu Bay there are three intraspecific groups (Types A, B and C), which have different spawning seasons and spawning times [1, 2]. The November, Type A spawning occurs in the morning, and the late October to mid-November, Type B spawning occurs in the evening, while the April, Type C group spawns at noon. We had previously investigated their spawning behavior under continuous light conditions, external characteristics and distribution in the bay, and allogeneic cellular reactions by blood cells [3-5]. During these investigations, we found that the most conspicuous difference was in spawning behavior under continuous light conditions, leading us to question whether these three types would spawn in the wild as they do in the laboratory. The survey of gamete release in the wild revealed that Types A and B have the same spawning season and time in the wild as they do in the laboratory, whereas Type C showed gamete release at a different season from that of the laboratory. Our observations in the wild being: Type A animals begin to

release their gametes near the end of Type B spawning season; Type C animals begin to spawn near the end of Type A spawning season, leading to a spawning season overlap. In addition, we discovered a location in the bay where Type C animals begin to spawn around noon, before Type A animals have completed their gamete discharge. These observations and the fact that many specimens are difficult to classify them into a definite type because of variations in their external characteristics [4] motivated us to investigate the degree of cross fertilization among these three groups. Here we report new observations on spawning and the possibility of cross fertilization among three groups in the wild.

MATERIALS AND METHODS

Spawning in the wild

Since the spawning seasons in the laboratory varied a little from year to year, we extended our period of observation in the wild from 1981 to 1985. From August to November, adults of each Type were collected by scuba diving at several locations in the bay and were kept in an aquarium supplied with running sea water. After gamete release started by these laboratory animals, we

dived to observe the spawning of each Type in the wild. When gamete release was recorded in the wild, these animals were brought into the laboratory to see if they would continue the discharge as in the wild.

Fertilization and young adult formation

To obtain gametes of the three Types at the same time, animals of Types A and B were kept at a low temperature (7°C) until Type C animals began to spawn. Some Type B animals were kept under continuous light at low temperatures to secure gametes in the morning [3]. After Type C animals began to spawn, the animals of Types A and B which had been kept at low temperatures were transferred to warm sea water (13°C) the day before the gametes were desired. After gamete discharge, the eggs were separated from the sperm suspension by filtration through nylon mesh (gauge=0.25 mm), and the sperm suspension was used for insemination. Fertilization was confirmed by observing the expansion of the perivitellin space. Developing embryos were kept at 13°C until they hatched out of the chorion. They were examined just before hatching to distinguish abnormal from normal embryos. Actively swimming larvae were selected and kept in plastic dishes to observe young adult formation. After attaching to the dishes and completing metamorphosis, the young adults were kept in aquaria supplied with running sea water until July. To test for the possibility of fertilization between Types A

and B in the wild, gametes of Type A discharged in the morning by natural spawning were kept at 13°C (sea water temperature in the wild) until evening when Type B animals started to release their gametes. Fertilization between them was checked as described above. This was possible because *H. roretzi* is strictly self sterile.

RESULTS

Spawning in the wild

In late October, we observed some Type B animals attached to rocks at 10–20 meters, starting to release gametes at 4.00 p.m. In mid-November, Type A animals began to spawn at 9.30 a.m. At that time, Type B animals were collected and brought into the laboratory where we found they continued to release a small quantity of gametes in the evening of the same day and for several days after. At 10.300 a.m. on November 21, 1984, we found three animals in the wild with typical Type C external characteristics discharging gametes, although no other Type C animals were spawning. These three animals were brought into the laboratory for observation, where they continued to spawn in the morning for several days more, as did the Type A animals previously mentioned.

By mid-December, some Type A animals were still spawning around noon, although gamete release was not as vigorous as at the peak of the spawning season. At one location in the bay, Type

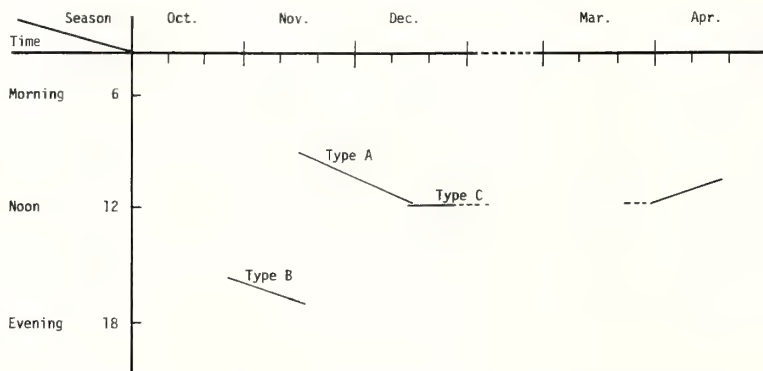


Fig. 1. Spawning seasons and spawning times in the wild. Type C begins to spawn in the middle of December, and the spawning season is prolonged to the following April by low sea water temperature.

TABLE 1. Fertilization among three Types

Sperm Type	A			B			C		
Egg Type	A	B	C	A	B	C	A	B	C
No. of eggs:									
Fertilized	335	342	334	351	361	344	356	332	365
Unfertilized	0	0	0	0	0	0	0	0	0
No. of larvae:									
Normal	252	269	295	300	308	292	285	274	207
Abnormal	83	73	39	51	53	52	71	58	58

Fertilization among three Types was completely successful. No significant difference was observed between cross fertilization among three Types and fertilization within the same Type.

TABLE 2. Fertilization between Type A and Type B

Sperm Type	A	A	B	A	B
Egg Type	A	A	B	B	A
Insemination time	11.00	17.30	17.30	17.30	17.30
Fertilized	384	84	373	117	364
Unfertilized	0	301	0	254	0

Eggs of Type A animals discharged in the morning were fertilized by Type B sperm later in the day.

C animals living in close proximity to Type A animals started releasing their gametes before Type A animals had stopped discharging theirs. These animals of Types A and C were brought into the laboratory and kept at the same temperature as in the wild. They all spawned as in the wild.

Observations made of the spawning seasons and spawning times of Types A, B, and C animals are summarized in Figure 1.

Fertilization, development and post-metamorphic growth

The experiments were repeated several times; the results of a typical experiment are shown in Table 1. As shown in the table, all the eggs were successfully fertilized regardless of the combination. Most embryos gave rise to normal larvae with active swimming movement, but some developed into larvae with bent tails. No significant differences were observed when evaluating the results of cross fertilization among the three groups and fertilization within the same group (Table 1).

Further cross fertilization experiments were made between Types A and B in mid-November. Eggs of Type A animals discharged in the morning were fertilized by Type B sperm later in the day (Table 2). In this experiment, we discovered that Type A sperm could not fertilize Type B eggs, but when Type A eggs were inseminated with Type B sperm, all of the eggs were fertilized and developed normally.

The actively swimming larvae obtained were transferred to plastic dishes. Some larvae resorbed the tail on the water surface, which were discarded. All the larvae that were able to attach to the plastic dishes gave rise to young adults, and survived up to July, having grown to 1.8 mm.

DISCUSSION

In this study, it was confirmed by scuba diving that animals of three groups (Types A, B and C) discharged their gametes at the same time in the wild as they did in the laboratory, exception made for the three animals found in November, 1984,

with Type C characteristics and whose spawning was observed in the morning. However, a big difference of spawning season was found between Type C animals in the wild and in the laboratory. We previously reported that Type C animals in the laboratory began to spawn in April and that they could release their gametes at any time from January to March if they were kept in warm sea water [2, 3]. The apparent reason for the observed difference seemed to be the sea water temperature. In the laboratory, surface sea water is supplied and its temperature is easily affected by air temperature. When we dived in mid-December, the sea water temperature at depths of 10 to 20 meters was 10°C and that of the water in the laboratory was 8°C; the air temperature fluctuated approximately between 5°C to -4°C. In this season, Type C animals fail to spawn in the laboratory, if they are not kept in warm sea water (higher than 10°C). By March, the sea water temperature had gradually decreased to 3°C. However, from mid-March, it gradually increased until it reached 10°C in April and Type C animals began to spawn. During January, February and March we collected Type C animals which had been reared by fishermen and found that their gonads varied from year to year, depending on the sea water temperature. In mid-January (1981), the gonads of Type C animals were empty, indicating the end of the spawning season. In early April of 1985 and 1986, we found that Type C animals had fully matured gonads and were able to release gametes when treated with warm sea water.

Soon after Type C animals in the wild reach spawning season in mid-December, the sea water temperature begins to decrease. If it reaches too low a temperature before all the gametes have been released, the spawning season is prolonged until the following April when sea water temperature gradually increases again.

Experimentally, fertilization within these three groups (Types A, B and C) was possible and the embryos gave rise to normal young adults. Because we found that there were many animals which were difficult to assign to a group, and that three animals with typical characteristics of Type C were releasing their gametes in the morning of November 21, 1984, the question of cross fertiliza-

tion among the groups in the wild arises. The fertilization of Type A eggs by Type C sperm seems to be the most probable explanation, since we observed sperm release of Type C animals before Type A animals had ended gamete release. As shown in Table 2, Type A eggs released in the morning were completely fertilized by Type B sperm released in the evening. But in the wild, it seems plausible that Type A eggs have a better chance of being fertilized by Type A sperm than Type B sperm. It is interesting to note that genetically compatible *Corella* species are maintained as discrete species by an 8 minute difference in spawning time [6]. If, however, our supposition is correct, it is strange that there are more animals that are difficult to classify as either Type B or Type C than there are animals difficult to confirm as either Type A or Type C. In order to clear up this problem, it is necessary to obtain mature animals by cross fertilization.

In the laboratory, we have not yet been able to get fully mature adults from either the cross or the intra-group fertilizations. Recently, we have been successful in rearing them in the laboratory for about a year. It would seem that at least two years are necessary to harvest mature animals from embryos. In the near future, we are hoping that these young adults will provide offspring able to give us the information needed to formulate more precise conclusions.

ACKNOWLEDGMENT

We are grateful to Prof. C. Lambert for critical reading of manuscript. We also thank Mr. T. Mayama, Mr. S. Tamura and Mr. M. Washio for scuba diving with us.

REFERENCES

- 1 Numakunai, T. and Hoshino, Z. (1973) Biology of the ascidian, *Halocynthia roretzi* (Drasche), in Mutsu Bay. I. Differences of spawning time and external features. Bull. Mar. Biol. Stat. Asamushi, Tohoku Univ., **14**: 191-196.
- 2 Numakunai, T. and Hoshino, Z. (1974) Biology of the ascidian, *Halocynthia roretzi* (Drasche), in Mutsu Bay. II. One of the three Types which has the spawning season and time different from two others. Bull. Mar. Biol. Stat. Asamushi, Tohoku Univ., **15**: 23-27.

- 3 Numakunai, T. and Hoshino, Z. (1980) Periodic spawning of three Types of the ascidian, *Halocynthia roretzi* (Drasche), under continuous light conditions. *J. Exp. Zool.*, **212**: 381–387.
- 4 Numakunai, T., Hoshino, Z. and Hori, R. (1981) Biology of the ascidian, *Halocynthia roretzi* (Drasche), in Mutsu Bay. III. Distribution and external characteristics of three Types. *Annot. Zool. Japon.*, **54**: 230–239.
- 5 Fuke, M. and Numakunai, T. (1982) Allogeneic cellular reactions between intra-specific types of a solitary ascidian, *Halocynthia roretzi*. *Dev. Comp. Immunol.*, **6**: 253–261.
- 6 Lambert, G., Lambert, C. and Abbot, D. P. (1981) *Corella* species in the American Pacific Northwest: distinction of *C. inflata* Hunstman, 1912 from *C. willmeriana* Herdman, 1898 (Asciacea, Phlebobranchia). *Can. J. Zool.*, **59**: 1493–1504.

Normal Stages of Development in the Lamprey, *Lampetra reissneri* (Dybowski)

YUTAKA TAHARA

Department of Biology, Osaka Kyoiku University,
Tennojiku, Osaka 543, Japan

ABSTRACT—A series of normal stages of embryonic development in the lamprey, *Lampetra reissneri* (Dybowski) is presented. The developmental processes from the ovulated but unfertilized egg to the ammocoete larva just before burrowing are divided into 31 stages using as identifying criteria of the stages the externally visible changes such as the appearance of structural changes, the beginning of movements and the body size. The age is determined in terms of an average time at which the stages occur at a temperature of 15°C. The stages and developmental tempos of *Lampetra reissneri* are compared with those of *Petromyzon marinus* reported by Piavis.

INTRODUCTION

Studies on embryonic development of the Lamprey have been attracting the attention of embryologists because of the phylogenetic position of this animal group. There is a good deal of literature on this subject. That consists mainly of descriptions of the separate phases in morphogenesis; for instance, the cleavage [1, 2], gastrulation [3-6] or the formation of the head [7, 8], the heart [9], the pronephros [10] and the blood vessels [13].

Around the middle of this century the Great Lakes fisheries suffered a threat of disaster which originated in the increase in the number of parasitic lamprey, *Petromyzon marinus*. Among the research programs aimed at controlling this menace, Piavis took charge of examining the effects of temperature on embryonic development in this species [11]. He also carried out a staging of embryonic development of the materials because the determination of standard stages was considered to be essential to a better understanding of the results of the experiments [11, 12]. Piavis subdivides the developmental processes, from the ovulated but unfertilized egg to the first stage of ammocoete larva, into 19 stages.

In Japan Hatta published a series of papers which dealt with the morphological descriptions on the development of one of the Japanese species of the Lamprey¹ [3-5, 9, 10, 13]. However, he did not attempt to establish the developmental stages of his materials. The present work deals with the staging of the embryonic development of *Lampetra reissneri* (Dybowski) from the ovulated but unfertilized egg to the ammocoete larva just before burrowing. It intends to put this standard to use someday for the experimental studies of embryogenesis of the lamprey.

MATERIALS AND METHODS

The sexually matured adults were collected in one of the brooks which flow into Lake Utonai near Sapporo City in Hokkaido during the breeding seasons of 1981 and 1982. Fertilized eggs were obtained by artificial insemination. The testis was taken out from a male and sperm was kept in a dry form in a petri dish until used. Ovulated eggs were allowed to extrude on a sheet of filter paper which was laid on a petri dish and moistened with water. Fertilization was accomplished by diluting dry

¹ In his 1891 paper [3], Hatta wrote his material was *Petromyzon planeri* or a variety of it, but in 1901 paper [13] *Lampetra mitsukurii* Hatta, and in others [4, 9, 10] only *Petromyzon*.

sperm in tap water and adding the sperm suspension to eggs. Immediately after the addition of sperm, filtered tap water was added and the filter paper was taken away. Embryos were reared in the petri dish kept at 15°C.

The developmental stages were determined mainly by externally visible changes such as the appearance of structural changes, the beginning of muscle contraction and the body size (Figures 1–4). The age was defined in terms of an average time at which the stages occurred at a temperature of 15°C. Internal changes were also observed histologically on sections of each stage of embryos. For histological preparations, embryos were fixed in Zenker acetic for 5 hr, serially sectioned at 7 μ m and stained with borax carmin and Pikro-Blauschwarz.

DEVELOPMENTAL STAGES

Stage 0. Age 0 hr. Ovulated, unfertilized egg. Piavis 0

Egg is creamy-white and oval in shape with narrow animal pole region. It is surrounded by vitelline coat to which sticky substance attaches. Size about 0.8×0.6 mm.

Stage 1. Age 0.07 hr after fertilization. Polar cone. Piavis 1

Animal pole region becomes flat and perivitelline space appears. Extrusion of a polar cone at depressed polar region.

Stage 2. Age 0.3 hr. Polar spot. Piavis 1

Polar cone is absorbed into egg cytoplasm leaving behind a polar spot. Egg becomes gradually spherical. Size about 1.0 mm.

Stage 3. Age 6.5 hr. Two cells. Piavis 2

Beginning of first cleavage. Cleavage furrow appears at animal pole and extends towards vegetal pole. Egg divides into two blastomeres with approximately equal size.

Stage 4. Age 11.5 hr. Four cells. Piavis 3

Second cleavage furrow appears at animal pole. Division occurs meridionally producing four blastomeres with approximately equal size.

Stage 5. Age 15.5 hr. Eight cells. Piavis 4

Third cleavage begins. Cleavage furrow appears horizontally in general, meridionally in eggs of some batches. Blastomeres in animal hemisphere

are smaller than those in vegetal.

Stage 6. Age 20 hr. Twelve to sixteen cells. Piavis 5

External: Fourth cleavage begins in animal hemisphere. Cleavage furrows appear meridionally or horizontally depending upon cleavage type in stage 5.

Internal: Blastomeres arrange themselves in one cell thick. Segmentation cavity appears.

Stage 7. Age 24 hr. Twenty-four to thirty-two cells. Piavis 6

Fifth cleavage furrows appear in blastomeres of animal hemisphere.

Stage 8. Age 28 hr. Morula. Piavis 7

Sixth cleavage begins in animal hemisphere.

Stage 9. Age 32 hr. Early blastula. Piavis 8

External: Seventh cleavage begins in animal hemisphere. Animal half makes smooth surface, vegetal half being still rough.

Internal: Segmentation cavity enlarges and blastocoel arises. The roof of blastocoel is composed of two cell layers and floor of three cell layers.

Stage 10. Age 48 hr. Mid blastula. Piavis 8

External: Blastocoel becomes visible from outside through its thin and translucent roof.

Internal: Blastocoel further expands, roof of which is composed of three cell layers and floor of five to seven cell layers.

Stage 11. Age 58 hr. Late blastula. Piavis 8

Roof of blastocoel becomes much thinner and transparent. Vegetal hemisphere makes smooth surface. Embryo becomes spherical in shape with smooth surface.

Stage 12. Age 3 days. Dorsal cone; Gastrula I. Piavis 8

External: In majority of embryos one or two conical protuberances (dorsal cones) appear in the dorsal subequatorial region. Blastocoel becomes larger and expands below equator. A groove appears at boundary between thin roof of blastocoel and thick vegetal yolk mass.

Internal: Roof and lateral wall of blastocoel become two cell thick. A vertical slit arises between outer thin layer and inner yolk cell mass on dorsal side.

Stage 13. Age 3 $\frac{1}{6}$ days. Brow-shape blastopore; Gastrula II. Piavis 9

External: A groove of brow-shape blastopore appears above the dorsal cone. Boundary groove bends towards animal pole on dorsal side.

Internal: Roof and lateral wall of blastocoel become one cell thick. The vertical slit becomes deeper on dorsal side. It appears also on lateral and ventral sides.

Stage 14. Age 3 $\frac{1}{2}$ days. Hemi-circular blastopore; Gastrula III. Piavis 9

External: Blastopore becomes hemi-circle, horseshoe or Δ -shape. Blastocoel becomes smaller than the preceding stage. Boundary groove bends nearly vertical.

Internal: Archenteron makes first appearance due to advancement of mesoderm invagination.

Stage 15. Age 4 days. Elliptical blastopore; Gastrula IV. Piavis 9

External: The groove of blastopore becomes elliptical in shape. Blastocoel becomes much smaller, still visible in anterior part of embryo. Both anterior and posterior ends of embryo become taper.

Internal: Archenteron elongates forming a narrow tube. Its roof is composed of mesodermal cells of two-cell thick.

Stage 16. Age 4 $\frac{1}{2}$ days. Flat dorsal lip; Gastrula V. Piavis 9

External: Dorsal blastopore lip becomes flat. Blastocoel can not be seen from outside. Posterior end of embryo protrudes.

Internal: Blastocoel becomes vestigial, still visible on antero-ventral side of embryos. Notochord begins to differentiate at the posterior part of archenteron roof. Ventral yolk cells are still uncovered.

Stage 17. Age 5 days. Neural groove; Neurula I. Piavis 10

External: Formation of neural plate. A neural groove appears in the middle of the neural plate. Its length is about one fourth of circumference of embryo.

Internal: Archenteron further elongates and reaches anterior end of embryo where it forms foregut. Yolk cells are mostly covered by epidermis.

Stage 18. Age 5 $\frac{1}{4}$ days. Neural folds; Neurula II. Piavis 10

External: Elevation of neural folds on both

sides of the neural groove. Neural groove elongates up to about one third of circumference of embryo.

Internal: Neural anlage starts sinking under epidermis. Notochord begins to separate from somitic mesoderm in trunk region. Mesodermal sacs appear in archenteron of the head region.

Stage 19. Age 6 days. Elevation of neural folds; Neurula III. Piavis 10

External: Neural folds further elevate and a deep neural groove is formed between them. It elongates up to about one half of circumference of embryo.

Internal: Segmentation begins in somitic mesoderm. Endodermal cells cover the archenteron roof in trunk region.

Stage 20. Age 6 $\frac{1}{4}$ days. Neural rod; Neurula IV. Piavis 11

External: Neural folds contact and fuse in the dorsal midline. Anterior end of embryo begins to protrude. Swelling of foregut region. Body length is about 1.3 mm in crown-rump.

Internal: Neural rod is formed and covered by epidermis. Notochord entirely separates from somitic mesoderm. Endodermal cells cover the archenteron roof in its total length.

Stage 21. Age 7 $\frac{1}{2}$ days. Head protrusion I. Piavis 12

External: Head protrudes in front of yolk mass, being about 0.3 mm in length. Appearance of cheek-like swellings on both sides of head.

Internal: Neural rod expands at its anterior-most part. The first visceral pouch attaches to epidermis. Appearance of the second visceral pouch. Liver diverticulum appears. Formation of proctodaeum. Anterior end of notochord separates from prechordal plate. The anteriormost myotomes separate from foregut wall and prechordal plate. Lateral plates are formed in trunk region.

Stage 22. Age 8 days. Neural tube; Head protrusion II. Piavis 13

External: Head further protrudes making an acute angle against yolk mass. It is about 0.4 mm in length, yet shorter than height of yolk mass. Proboscis-like sharpening of anterior end of head. A neck appears between cheek-like swellings and yolk mass.

Internal: A longitudinal slit appears in the nerve cord and the neural tube is formed. Mesectodermal cells increase in head region. Formation of auditory placodes and infundibulum. Separation of the first myotome from the second. Lateral plate is formed in head region at the third myotome level.

Stage 23. Age 9 days. Stomodaeum; Head protrusion III. Piavis 13

External: A stomodaeum appears as a longitudinal slit-like invagination. The cheek-like swellings fuse in the ventral midline. Formation of auditory pits. Head and neck elongate up to about 0.7 mm in length, nearly equal to height of yolk mass. Embryo becomes a comma-like shape. Anus points forward. About 25 segments are formed in the somite. Somitic muscles start contraction.

Internal: Formation of optic vesicles, optic stalks, lens placodes and ganglion placodes. The second visceral pouch attaches to epidermis. Formation of coelom. Differentiation of heart forming cells, sclerotome, dermatome and myoblasts.

Stage 24. Age 11 days. Nasal pit; Hatching. Piavis 13–14

External: Head and neck elongate up to about 1.0 mm in length. Appearance of a nasal pit. Through transparent skin the second to the fourth visceral pouches, endostyle, pericardial coelom, liver and pronephros become visible. Elevation of dorsal fin. Embryos start hatching during this stage.

Internal: Formation of lens cones and auditory vesicles. Fore-, mid- and hindbrain become discernible due to formation of epiphysis and fold in cerebral commissure. The fourth visceral pouch appears. Formation of tubular heart, endocardium, epimyocardium, dorsal and ventral aorta, pronephric tubules and collecting ducts. Appearance of blood cells and primordial germ cells. Notochordal cells begin to vacuolize.

Stage 25. Age 12 days. Heart beat; Tailbud I. Piavis 14

External: Heart starts beating. The stomodaeum becomes a transverse slit-like invagination. Formation of the second to the sixth visceral pouch. Elongation of trunk. Tailbud makes first

appearance. All embryos hatch out during this stage. Body length 3.5–4.0 mm.

Internal: Formation of optic cups. Separation of lens vesicles from epidermis. Appearance of external naris and nasal cavity. Differentiation of white matter in central nervous system. Formation of the seventh visceral pouch. Folding of endostyle. Appearance of pronephric arteries.

Stage 26. Age 16 days. Melanophores; Tailbud II. Piavis 15

External: Melanophores appear first in head, subsequently in trunk region. Appearance of hemoglobin in blood cells. Trunk becomes straight. Anus points ventralward. Body length 4.5–5.0 mm.

Internal: Ectodermal layer of oral plate disappears. Formation of the fifth to the eighth visceral pouches and blood vessels in the first to the fourth gill arches. Obliteration of midgut lumen. Liver starts folding. Sinus venosus, auricle, ventricle and trunks arteriosus differentiate in the heart.

Stage 27. Age 18 days. Eye spots; Tailbud III. Piavis 15

External: Pigmentation occurs in retinae. Upper lip expands anteriorly and laterally. External naris shifts towards anterior. The eighth visceral pouch becomes visible. Trunk becomes straight. Larvae start swimming. Body length 5.5–6.0 mm.

Internal: Formation of hypophysial sac. Endodermal layer of oral plate disappears and mouth opens. A pair of velum is formed. Differentiation of gall bladder and bile duct in liver. Gill filaments begin to arise in anterior pairs of gill arches. Blood vessels appear in the fifth gill arch and in typhrosome. Cilia appear in nephrostomes.

Stage 28. Age 22 days. Velum beating. Piavis 16

External: Velum starts beating. Upper lip further expands and oral hood is formed. Gill pores start contraction movement. Oral cirri appear. External naris further shifts anterodorsally. Melanophores increase in number in trunk. Tip of the tail points backward. Anal tube elongates. Body length 7.0 mm.

Internal: Lens vesicles become flat. Formation of definitive lumen throughout intestine. Gill filaments appear on six gill arches, from the first to the sixth. Blood vessels are formed in all eight

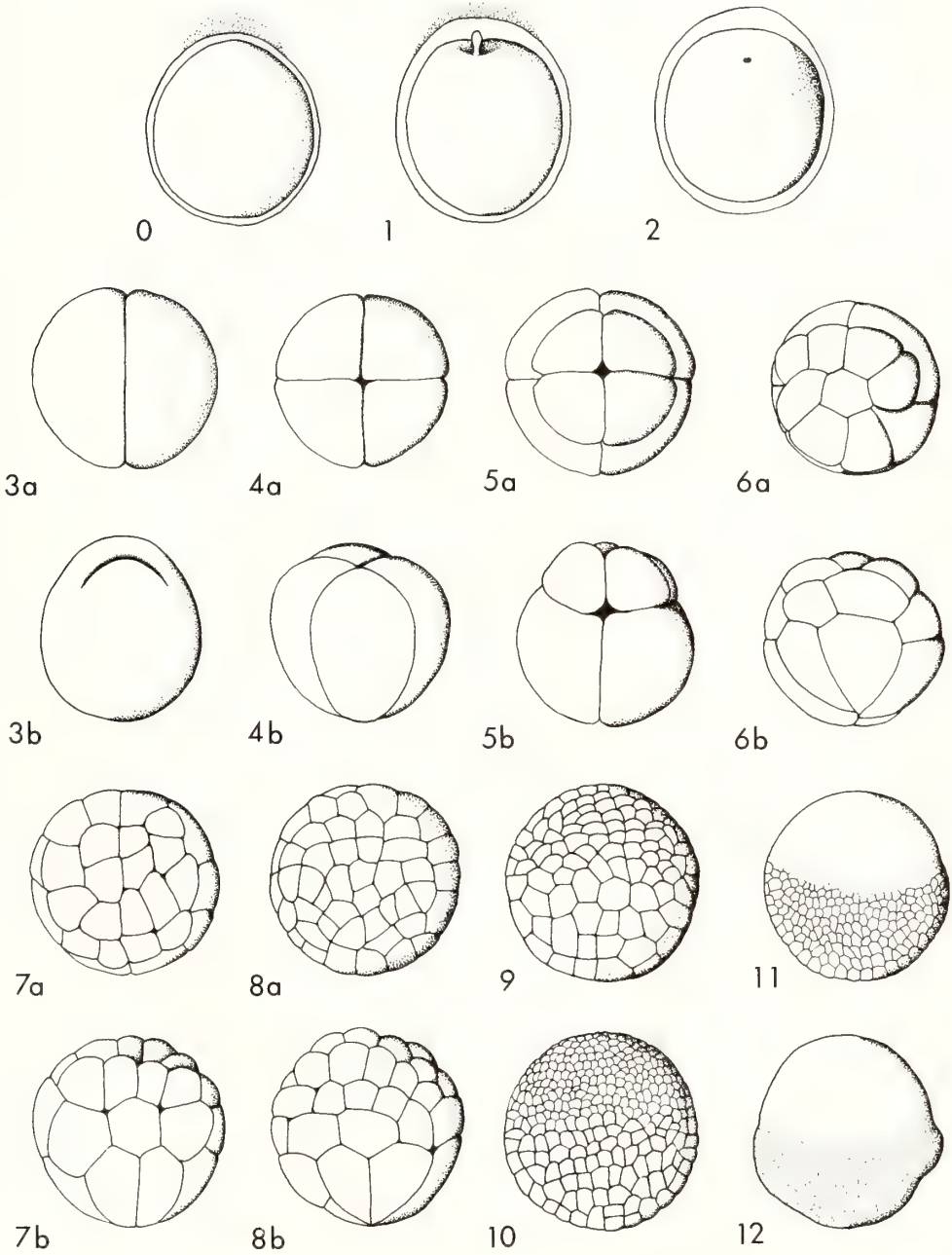


FIG. 1. Before fertilization and Stages 1-12.

0, Ovulated, unfertilized egg; 1, Polar cone; 2, Polar spot; 3, Two-cell; 4, Four-cell; 5, Eight-cell; 6, Twelve to sixteen-cell; 7, Twenty-four to thirty-two-cell; 8, Morula; 9, Early blastula; 10, Mid blastula; 11, Late blastula; 12, Dorsal cone, Gastrula I.

0 and 1, View from lateral side; 2, View from lateral and slightly animal pole side; 3a-8a, View from animal pole; 3b and 4b, View from lateral and slightly animal pole side; 8b and 9-12, View from lateral side.

Magnification 0 and 1, $\times 30$; 2-12, $\times 25$.

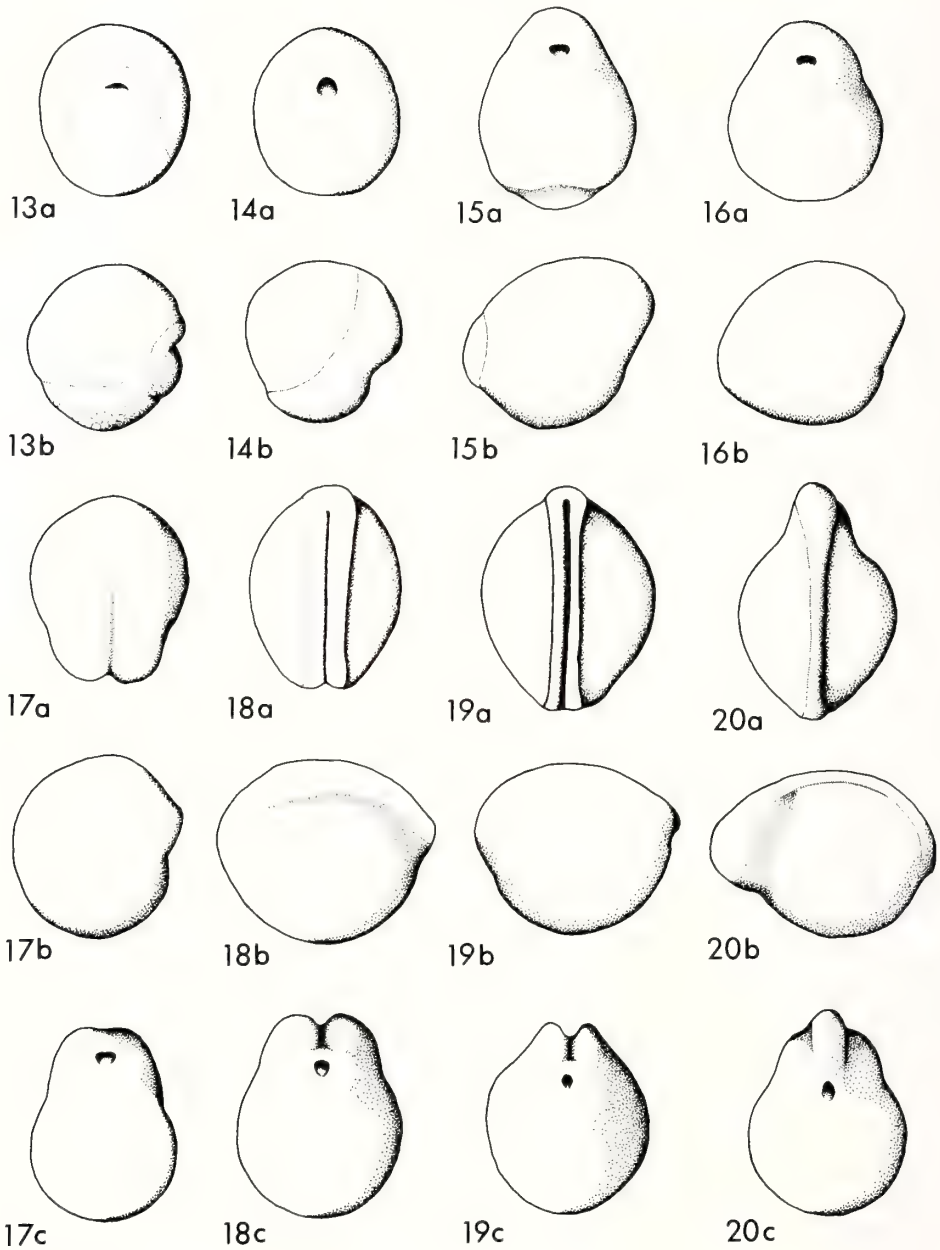


FIG. 2. Stages 13-20.

13, Brow-shape blastopore, Gastrula II; 14, Hemi-circular blastopore, Gastrula III; 15, Elliptical blastopore, Gastrula IV; 16, Flat dorsal lip, Gastrula V; 17, Neural groove, Neurula I; 18, Neural folds, Neurula II; 19, Elevation of neural folds, Neurula III; 20, Neural rod, Neurula IV.

13a-16a, View from posterior, slightly ventral side; 13b-20b, View from left side; 17a-20a, View from dorsal side; 17c-20c, View from posterior side.

Magnification 13-16, $\times 19$; 17-19, $\times 25$; 20, $\times 23$.

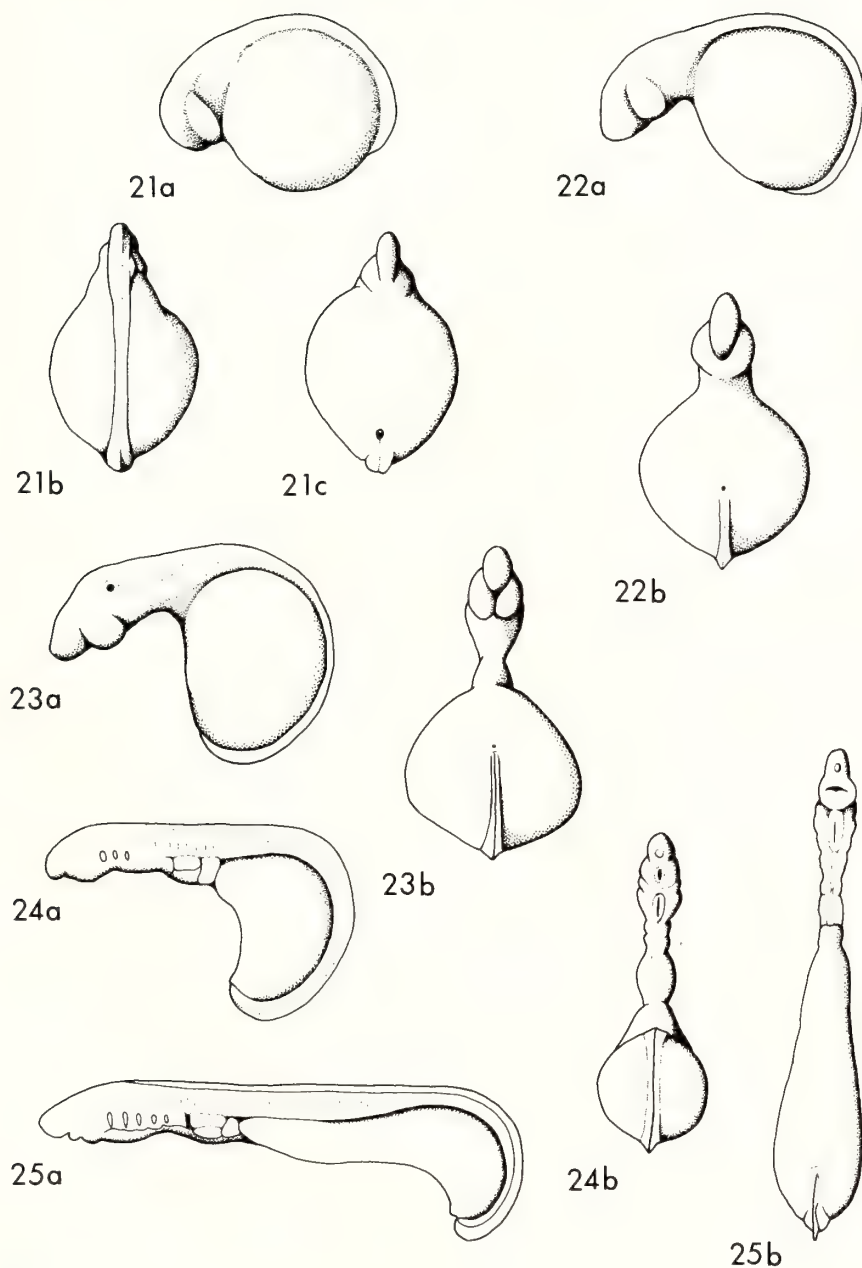


FIG. 3. Stages 21-25.

21, Head protrusion I; 22, Neural tube, Head protrusion II; 23, Stomodaeum, Head protrusion III; 24, Nasal pit, Hatching; 25, Heart beat, Tailbud I.

21a-25a, View from left side; 21b, View from dorsal side; 21c and 22b-25b, View from ventral side.

Magnification 21 and 22, $\times 23$; 23, $\times 25$; 24 and 25, $\times 17$.

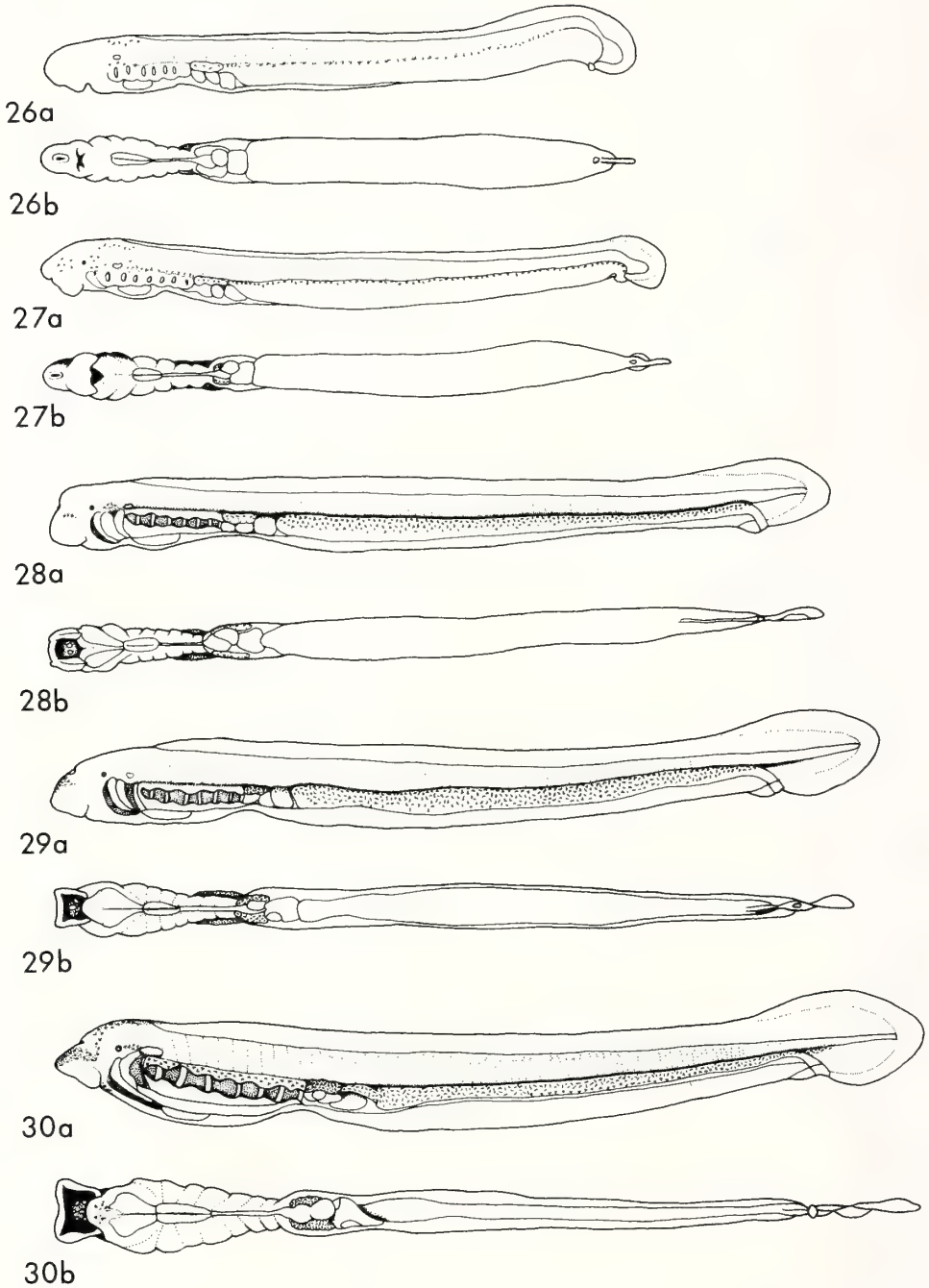


FIG. 4. Stages 26-30.

26, Melanophore, Tailbud II; 27, Eye spots, Tailbud III; 28, Velum movement; 29, Greenish bile; 30, completion of digestive tract, Earliest ammocoete larva. 26a-30a, View from left side; 26b-30b, View from ventral side.

Magnification 26, $\times 17$; 27 and 28, $\times 16$; 29, $\times 15$; 30, $\times 13.5$.

pairs of gill arches. Appearance of septum in endostyle. Irridescent pigment cells appear.

Stage 29. Age 24 days. Greenish bile. Piavis 17

External: Greenish bile appears in gall bladder. Oral hood expands. External naris arrives on dorsal side. Opening of all seven pairs of external gill pores. Irridescent pigment cells increase. Body length 8.0 mm.

Internal: Appearance of cerebral hemispheres. Cilia appear in hypophysial sac. Gill filaments are formed on all eight pairs of gill arch.

Stage 30. Age 31 days. Completion of digestive tract; The earliest stage of ammocoete larvae. Piavis 18

External: Remnants of digested yolk are extruded from anus and formation of digestive tract completes. Oral cirri increase in number. Oesophagus becomes visible on left side due to torsion of liver and "stomach" (anterior intestine). Body length 9–9.5 mm.

Internal: Appearance of cilia in dorsal ridge, hypopharyngeal groove, endostyle and oesopha-

TABLE 1. A comparison of subdivision of the stages in *L. reissneri* with that in *P. marinus*

Developmental phases	Subdivision of stages in	
	<i>L. reissneri</i>	<i>P. marinus</i>
	Stages	Stages
Ovulated, unfertilized egg	0	0
Fertilized, uncleaved egg	1–2	1
Cleavage	3–8	2–7
Blastulation	9–11	8
Gastrulation	12–16	8–9
Neurulation	17–20	10–11
Head protrusion	21–23	12–13
Hatching larva	24	13–14
Post-hatched larva	25–30	15–18
Total number of stages	31	19

TABLE 2. A comparison of the time after fertilization required to reach at the twelve stages in *L. reissneri* (at 15°C) with that in *P. marinus* (18.4°C)

Stages	<i>L. reissneri</i>	<i>P. marinus</i>
Two-cell (T3, P2)*	6.5 hr	2 hr
Eight-cell (T5, P8)	15.5 hr	10 hr
Morula (64-cell; T8, P7)	28 hr	19 hr
Blastula (T10, P8)	48 hr	24 hr
Gastrula (T13, P9)	78 hr	64 hr
Neural plate (T17, P10)	5 days	4 days
Head protrusion (T21, P12)	7½ days	6 days
Hatching (T24, P14)	11 days	10 days
Melanophore (T26, P15)	16 days	13 days
Eye spots (T27, P16)	18 days	15 days
Gall bladder (T29, P17)	24 days	17+ days
Completion of digestive tract (T30, P18)	31 days	33 days

* T3 and P2 mean Tahara's stage 3 and Piavis's stage 2, respectively.

gus. Gill filaments further elongate. Formation of brush border on intestinal epithelium. Typhrosole protrudes into intestinal lumen.

DISCUSSION

Since the present work is aimed at serving the students of developmental biology of the lamprey embryos, the division of the early phases of embryogenesis are made much more detailed than the staging of *Petromyzon marinus* presented by Piavis [11, 12]. In Table 1 the staging in *Lampetra reissneri* is compared with that of *P. marinus*.

Based on the present observations it may be concluded that the shape and size of the unfertilized egg, the mode of cleavage, the aspects of structural and functional changes as well as the developmental tempos in *L. reissneri* bear a close resemblance to those in *P. marinus*. The time required to reach at the twelve stages in the both species of lamprey is compared in Table 2. It can be thought that the early development proceeds in an approximately equal tempo in the two species if one takes account of the difference in the temperature at which the embryos are reared.

ACKNOWLEDGMENT

I wish to express my sincere gratitude to Professor Ch. Katagiri of Hokkaido University for his kind help in this study. I also thank Dr. T. Fujii of Ryukyu University for providing the lamprey embryos and also for collecting the adults.

REFERENCES

- 1 Glaesner, L. (1910) Studien zur Entwicklungsgeschichte von *Petromyzon fluviatilis*. I. Furchung und Gastrulation. Zool. Jahrb. Abt. Anat., **29**: 139-190.
- 2 Veit, K. (1957) Einige Beobachtungen über die ersten Furchungsgeschritte bei *Petromyzon planeri*. Morphol. Jahrb., **98**: 1-34.
- 3 Hatta, S. (1891) On the formation of germinal layers in *Petromyzon*. J. Coll. Sci. Imp. Univ. Tokyo, **5**: 129-147.
- 4 Hatta, S. (1907) On the gastrulation in *Petromyzon*. J. Coll. Sci. Imp. Univ. Tokyo, **21**: 1-44.
- 5 Hatta, S. (1915) The fate of the peristomal mesoderm and the tail in *Petromyzon*. Annot. Zool. Japon., **9**: 49-62.
- 6 Selys-Longchamps, M. de (1910) Gastrulation et formation des feuillettes chez *Petromyzon planeri*. Arch. Biol., **25**: 1-75.
- 7 Veit, O. (1939) Beiträge zur Kenntnis des Kopfes der Wirbeltiere. III. Beobachtungen zur Frühentwicklung des Kopfes von *Petromyzon planeri*. Morphol. Jahrb., **84**: 86-107.
- 8 Damas, H. (1944) Recherches sur la développement de *Lampetra fluviatilis* L. Contribution à l'étude de la céphalogenèse des vertébrés. Arch. Biol., **55**: 1-284.
- 9 Hatta, S. (1897) Contribution to the morphology of cyclostomata. I. On the formation of the heart in *Petromyzon*. J. Coll. Sci. Imp. Univ. Tokyo, **10**: 225-237.
- 10 Hatta, S. (1900) Contribution to the morphology of cyclostomata. II. The development of pronephros and segmental duct in *Petromyzon*. J. Coll. Sci. Imp. Univ. Tokyo, **13**: 311-425.
- 11 Piavis, G. W. (1961) Embryological stages in the sea lamprey and effect of temperature on development. Fishery Bull. Fish Wildl. Serv. U. S., **61**: 111-143.
- 12 Piavis, G. W. (1971) Embryology. In "The Biology of Lampreys". Ed. by M. W. Hardisty and I. C. Potter, Academic Press, London, pp. 361-400.
- 13 Hatta, S. (1901) Über die Entwicklung des Gefäßsystems des Neunauges, *Lampetra mitsukurii* Hatta. Zool. Jahrb. Abt. Anat., **44**: 1-257.

Analysis of Oral Replacement by Scanning Electron Microscopy and Immunofluorescence Microscopy in *Tetrahymena thermophila* during Conjugation

MINORU TSUNEMOTO, OSAMU NUMATA¹, TOSHIRO SUGAI²
and YOSHIO WATANABE^{1,3}

Department of Biology, Joetsu University of Education, Joetsu, Niigata 943,

¹Institute of Biological Sciences, University of Tsukuba,

Tsukuba, Ibaraki 305, and ²Department of Biology,

Ibaraki University, Mito, Ibaraki 310, Japan

ABSTRACT—The process of oral replacement in *Tetrahymena* during conjugation has not so far been elucidated, mainly because the oral regions of a conjugating pair are hidden by the cell-cell junction in their proximate anterior which makes observation difficult. To analyze in detail the process of the oral replacement, a newly devised technique for deciliation and pair detachment was used in the present study in combination with scanning electron microscopy and immunofluorescence microscopy for tubulin. Oral replacement during conjugation was found to proceed synchronously, so that we could classify the process into 12 stages including 6 regressive and 6 reformation stages: Regression of the old oral apparatus occurred in the order of membranelles 1, 2, 3 (M1, M2, M3) and the undulating membrane (UM). After this, the paired cells approached a virtually astomatous state, and then, reformation of the oral apparatus at the pre-existing area started from the right ends of each membranelle. The regressive processes are considerably different from those of oral replacement observed in cells under amino acid deprivation, although the oral reorganization in amino acid-starved cells and that in conjugating cells are both called “oral replacement”. The discrepancy may be due to the difference in stage-specific cellular events between abortive division under amino acid deprivation and conjugation.

INTRODUCTION

Studies on the serial morphological changes involved in oral neof ormation in *Tetrahymena* have presented many important clues for understanding the mechanisms of cell division [1–5] and synchrony induction [1–3, 6–8]. This is because oral neof ormation can be considered to be a stage-specific indication of the cellular events underlying the metabolic changes, physiological changes and the changes of gene expression during the division cycle. During this cycle, the pre-existing anterior oral apparatus is also known to show stage-specific regressive and remodeling

changes [3]. Other than these division cycle-dependent oral changes, much more extensive regression and reformation of the anterior oral apparatus has been known to occur under certain physiological conditions without being accompanied by cell division [3]. This phenomenon is referred to as “oral replacement”, and is observed, for example, in cells cultivated in an amino acid-free medium [6] and in cells during conjugation [3]. In the former case, the process of oral replacement has been well studied by Frankel [6] and Frankel and Williams [3], using the synchronous rounding (abortive division) system developed by us [9–11]. In the latter case, however, the process of oral replacement has not been made clear, because of the difficulty in studying the oral regions of the conjugating pairs which are hidden by the cell-cell junction.

Accepted July 1, 1987

Received May 22, 1987

³ To whom requests of reprints should be addressed.

We have previously shown that *Tetrahymena* intermediate filament protein (49K protein) [12–14] plays a crucial role in the oral morphogenesis preceding binary fission in *Tetrahymena* [15]: Although the 49K protein is localized in the so-called posterior connectives of the functional oral apparatus, dissociation of the 49K protein from the oral apparatus occurs concurrently with the regression of the old oral apparatus which is prerequisite to the oncoming oral reorganization at the predividing stage, and reassociation of the 49K protein occurs a short time before the completion of the functional new and old oral apparatuses. The correspondence of oral structural change to the occurrence of the 49K protein urged us to investigate the localization of the protein in the oral apparatus of *Tetrahymena* cells during conjugation. In a preliminary experiment, we observed that the 49K protein disappeared from the oral apparatus at an early phase of conjugation and reappeared in the apparatus after the separation of conjugating pairs. Thus, *Tetrahymena* cells are assumed to undergo oral replacement (extensive regression and reformation of the pre-existing oral apparatus) during conjugation.

In the present study, by using scanning electron microscopy (SEM) and immunofluorescence microscopy for tubulin, we have attempted to observe the oral structures of the cells of conjugating pairs detached artificially. We here describe the temporal sequence of oral replacement during conjugation, which differs from that of the oral replacement previously observed in cells cultivated in an amino acid-free medium [3, 6].

MATERIALS AND METHODS

Tetrahymena thermophila mating types I and III of strain B were axenically cultivated at 26°C in a proteose-peptone medium containing 1% proteose peptone, 0.5% yeast extract and 0.87% dextrose [10].

Synchronous conjugation of *Tetrahymena* was induced by a modification of the method of Sugai and Hiwatashi [16] as follows. Cells of the *T. thermophila* mating types I and III were washed three times with an NKC solution containing 0.2% NaCl, 0.008% KCl, and 0.012% CaCl₂, and then

resuspended in NKC at a concentration of approximately 4×10^5 cells/ml. Eight ml of the cell suspension was incubated at 26°C for 16–18 hr. Conjugation was elicited by mixing the cell cultures of the two mating types. After 1 hr at 26°C, mating cells were separated into individual cells again by a centrifugation at 100 g for 2 min at 0°C. The cells were resuspended in 4 ml of NKC and incubated at 26°C. The onset of pair formation is well synchronized in this treatment, so the time of the resuspension was considered to be the starting point (0 time) of conjugation. To obtain a population with a much higher conjugation rate, we gently diluted the mating mixture with NKC at 25 min and then carefully discarded the supernatant containing free swimming non-pairing cells, since the mating pairs tended to gather on the bottom of the culture dish. Thus, we were always able to obtain a high rate of synchronous conjugation with a pair rate of nearly 95%.

For SEM, 3 ml-samples were withdrawn from the conjugation culture at desired intervals. First, deciliation of living cells was carried out as follows. Cells collected by a light centrifugation were suspended in 0.5–0.8 ml of 12.5 mM dibucain (pH 6.5) and stirred gently with a capillary for 1–2 min. The suspension containing deciliated and detached cells was quickly mixed with 1 ml of 2% glutaraldehyde in 0.1 M phosphate buffer (pH 7.0) for pre-fixation and immediately centrifuged. The cells in the pellet were then loosened and post-fixed with 2 ml of 2% glutaraldehyde in 0.1 M phosphate buffer for 30 min. Next, the fixed cells were washed with the phosphate buffer and dehydrated in a series of acetone (50–70–90–99.5–100%) and in isoamyl acetate, followed by drying at the critical point. Specimens were coated with gold before they were observed with a scanning electron microscope (JEOL T-100). By using this procedure, a considerable number of conjugating pairs could be separated throughout the conjugation process. Therefore, we mainly observed the oral structures of such detached cells.

A rabbit antiserum specific for *Tetrahymena* 49 K protein used in this paper was the same as that used in our previous papers [14, 15]. For immunofluorescence staining materials, Nonidet P-40-extracted conjugating pairs were prepared as

described by Goodenough [17] and air-dried on slides. These slides were treated with anti-49K protein antiserum (diluted 1:160 in phosphate-buffered saline, PBS) and then rhodamine-conjugated goat anti-rabbit IgG (diluted 1:200 in PBS, Miles). The macro- and micronuclei were stained with 0.5 $\mu\text{g/ml}$ of DAPI (4', 6-diamidino-2-phenylindole dihydrochloride).

Polyclonal anti-tubulin antiserum was produced in a male rabbit using highly purified tubulin prepared from ciliary axoneme by two-dimensional polyacrylamide gel electrophoresis [18]. Affinity purification of this antiserum was performed by the method of Talin *et al.* [19]. The specificity of the antiserum was shown by the immunoblotting technique of Towbin *et al.* [20]. Deciliated conjugating pairs were air-dried on slides. The slides were fixed with 2.5% paraformaldehyde in PBS for 5 min at room temperature, and subsequently with acetone for 30 sec at -20°C . After washing in PBS, the slides were treated with 0.1 M glycine in PBS for 30 min at room temperature. For staining, these slides were treated with anti-tubulin antiserum (diluted 1:100 in PBS) and then fluorescein isothiocyanate (FITC)-conjugated goat anti-rabbit IgG. The staining of the nuclei was done in the same way as with the anti-49K protein.

RESULTS

Relation among oral immunofluorescence for 49K protein, food uptake activity and formation of conjugating pairs

To assess the occurrence of oral replacement during conjugation, we investigated the localization of 49K protein within cells during conjugation by using the indirect fluorescent antibody technique. As shown in Figures 1–3, τ -shaped oral fluorescence suddenly disappeared as the formation of pairs proceeded at the early phase of conjugation. During the middle stage of conjugation, immunofluorescence for 49K protein showed very interesting distribution relevant to the behavior of germ nuclei as reported in our previous paper [21]. At the late phase of conjugation, τ -shaped oral immunofluorescence reappeared after

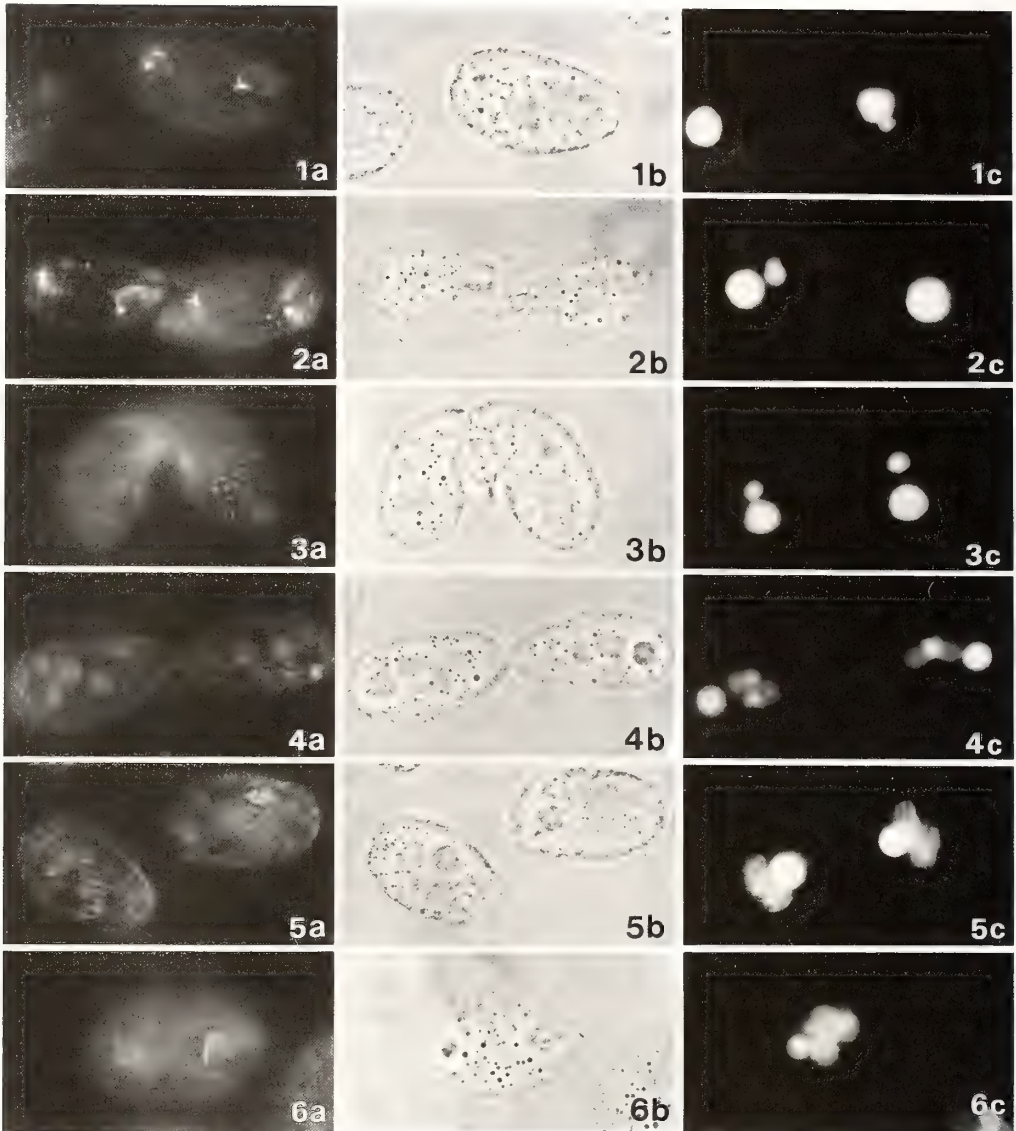
paired cells became naturally detached from each other (Figs. 4–6).

Next we investigated the percentages of cells having τ -shaped oral fluorescence and those of cells capable of uptaking carbon particles as a function of time after the start of conjugation. As shown in Figure 7, at the early phase of conjugation, curves representing both the percentages of cells with oral fluorescence and of cells with food uptake activity decreased simultaneously and sharply in a mirror-image fashion as the percentage of pair formation increased. In contrast to this, at the late phase of conjugation, curves representing both the ratios of cells with oral fluorescence and of cells with food uptake activity increased again nearly correspondingly with the decrease of paired cell ratio. The result strongly suggests that oral replacement occurs synchronously during conjugation. Consequently, we tried to analyze the oral structural changes in detail by SEM.

Scanning electron microscopic observation of sequential changes in oral structure during conjugation

We observed various kinds of SEM images of the oral apparatus in the course of synchronous conjugation. These images were classified into 12 stages according to both the temporal sequence of their occurrence and the characteristics of the oral structures. Stages 1–6 are regressive stages and stages 7–12 are reformation ones (The durations of each stage are shown in the abscissa of Fig. 7). The characteristics of each oral replacement stage are schematically shown using diagrams (Fig. 8). Each diagram was produced from several SEM images of the same stage. For reference, we also show typical SEM images as representatives of each stage (Figs. 9–20). Although the oral replacement process during conjugation is complex and involves many sequential and parallel events, the following descriptions can be made for each stage.

Stage 1: At the time of mixture of complementary mating types, the oral apparatuses of the cells are intact and functional (designated as stage 1) and are essentially the same as those of interphase cells during exponential growth: The oral apparatus consists of complete membranelles



FIGS. 1-6. Immunofluorescence localization of 49K protein in the oral apparatus of cells at an early phase and late phase of conjugation.

FIG. 1. A cell in costimulation stage just after mixing two cultures of complementary mating-type cells. Note that the τ -shaped region of the oral apparatus fluoresces.

FIG. 2. A pair-forming cell at very early stage of conjugation. Oral fluorescence is still evident.

FIG. 3. A pair taken from a conjugating culture at 1.5 hr after mixing. Note that the τ -shaped fluorescence disappears from the conjugating pair.

FIG. 4. A conjugating pair at the late stage of conjugation. Oral fluorescence has not yet reappeared.

FIG. 5. Exconjugants immediately after detachment from conjugating pairs. Oral fluorescence is still obscure.

FIG. 6. An exconjugant at the end of conjugation. Note the obvious τ -shaped fluorescence in the oral apparatus.

a, immunofluorescence image of a selected cell or conjugating pair; b, its phase contrast image; c, its nuclear state as revealed by DAPI staining. b and c are cited in aid of judging the stage of each cell shown in a. All $\times 1400$.

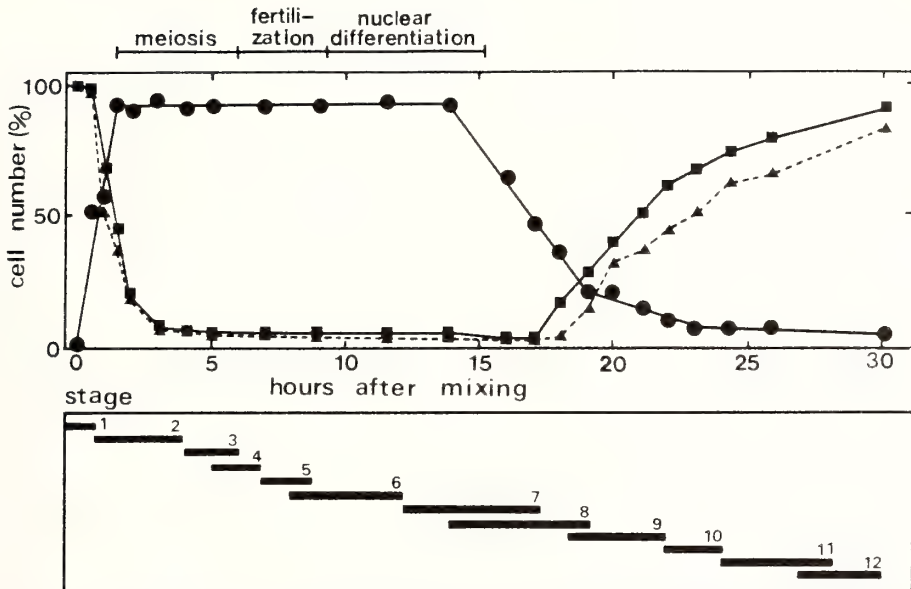


FIG. 7. Oral immunofluorescence for 49K protein and food uptake activity in *Tetrahymena thermophila* during conjugation. Ordinate, percentages of cells or pairs having τ -shaped oral immunofluorescence (■—■), percentages of cells or pairs capable of uptaking carbon particles when the cells were incubated in 2% India ink for 5 min (▲---▲), or percentages of conjugating pairs (●—●); abscissa, time (hr) after mixing the cells of complementary mating types. On the upper part of the figure, durations of germ nuclear events are shown for reference. As described later, oral replacement was observed during conjugation. The oral morphological changes involved in oral replacement were classified into 12 stages. The duration of each stage (from stage 1 to stage 12) is shown with a bar and stage number in the lower abscissa for the sake of convenience.

1, 2 and 3 (M1, M2 and M3), the undulating membrane (UM), the oral rib, and the buccal cavity (Figs. 8 and 9).

Stage 2: About 1.5 hr after the cultures were mixed, a sign of regression (resorption) in the oral apparatus began to appear. Several ciliary stubs of the first and second rows of M1 and of the first row of M2 (see legend for Fig. 8) disappeared from the animal's left side (Figs. 8 and 10).

Stage 3: About 4 hr after the cultures were mixed, disappearance of ciliary stubs from the left sides of M1 and M2 proceeded further than in stage 2. At this stage, the striation of oral rib became somewhat unclear (Figs. 8 and 11).

Stage 4: About 6 hr after the cultures were mixed, the oral regions of the conjugating pairs became smaller in size. Half of the ciliary stubs of M3 disappeared from its left side. In addition, the disappearance of ciliary stubs of M1 and M2 proceeded still further. At this stage, the striation

of the oral rib became unclear and the buccal cavity became smaller and shallower as compared to stages 1–3 (Figs. 8 and 12).

Stage 5: About 7–8 hr after the cultures were mixed, the buccal cavity became more shallower than in stage 4, so that the oral region itself became dish-like in shape. At this stage, only 12–18 ciliary stubs remained in the three membranelles, and the ciliary stubs of the UM disappeared progressively (Figs. 8 and 13).

Stage 6: About 8–12 hr after the cultures were mixed, the oral region became its smallest in size, being nearly completely flat, and its surface was smooth as if it was covered with a membrane. At this stage, the UM ciliary stubs were absent and only about 10–12 ciliary stubs presumably consisting of sculpturing portions remained in the approximately triangle-shaped oral region (Fig. 8). Figure 14 shows the early phase of this stage.

Stage 7: This oral stage was observed in con-

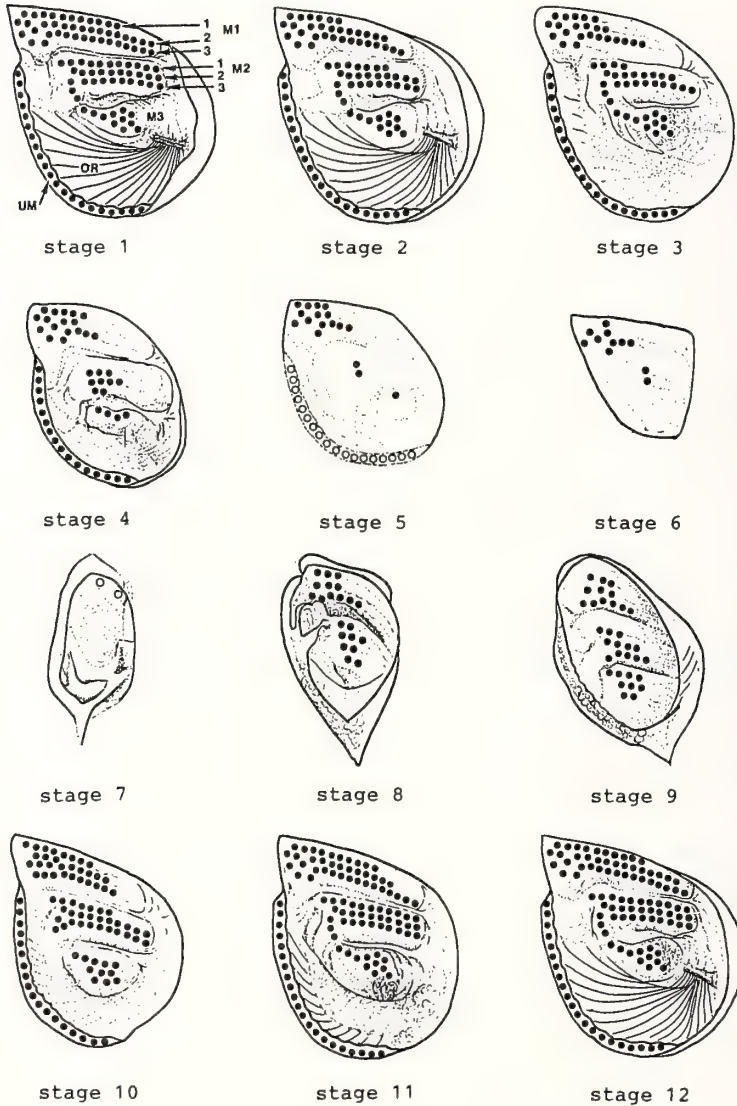
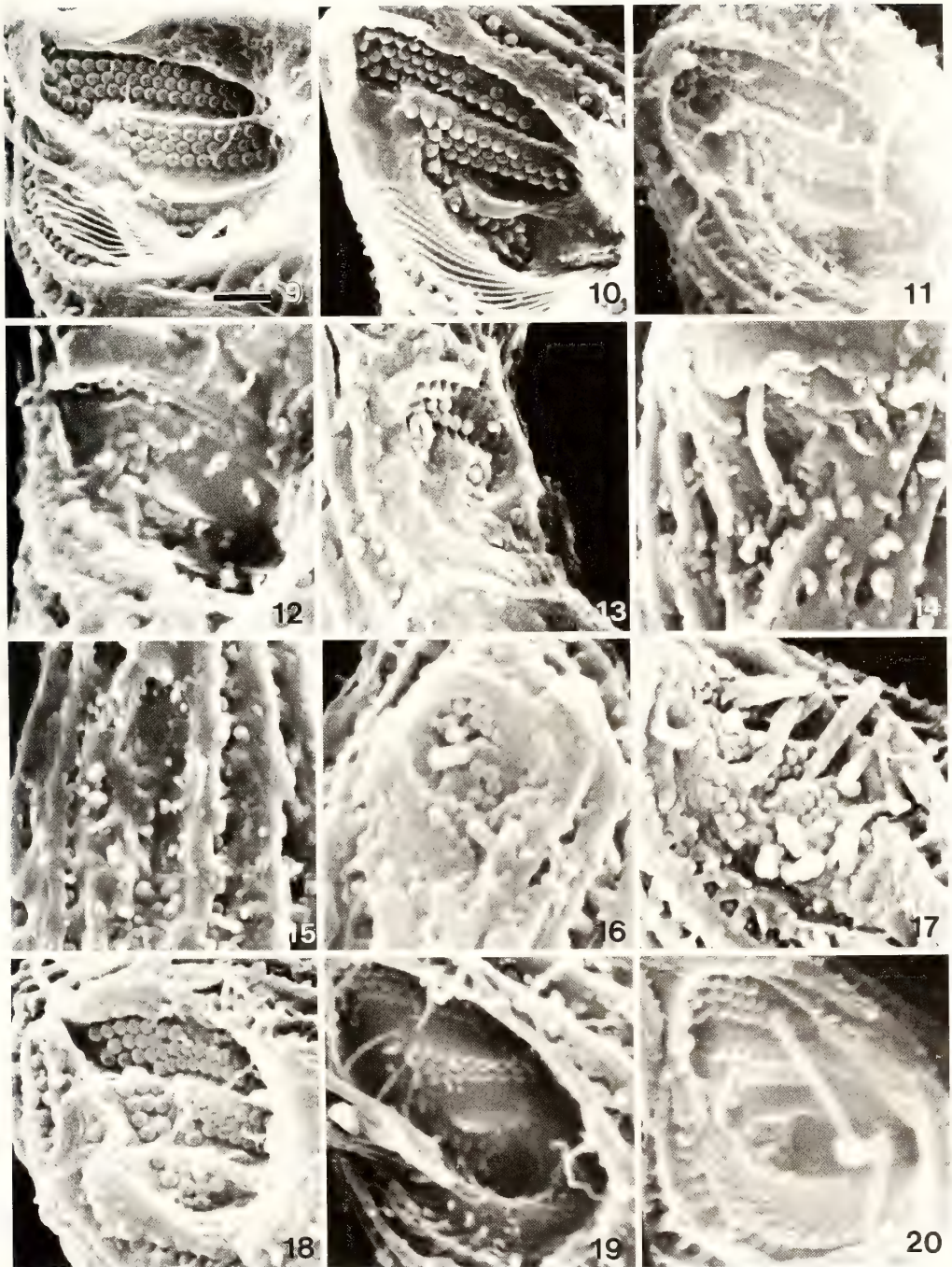


FIG. 8. Schematic figures from SEM images of 12 stages of the oral replacement in *Tetrahymena thermophila* during conjugation.

Closed circles represent ciliary stubs and open circles represent basal body-like bulges. The upper and lower directions of all diagrams correspond to the animal's anterior and posterior, respectively. The reader's left corresponds to the animal's right (in the text, the direction from the animal's side is used). Membranelles 1, 2, 3 (M1, M2, M3), undulating membrane (UM), oral rib (OR) are shown in the diagram of stage 1. The ciliary stub rows within the membranelles are here numbered in an anterior-to-posterior order for the sake of convenience. Unciliated basal bodies were difficult to observe in our preparation, so the UM was drawn as a single row.

jugating cells 12–17 hr after the cultures were mixed. Although no significant structure was observed inside the oral region except for the presence of a few cilia, the oral image seemed to

show signs of entering into the reforming process: The oral region began to sink inside again and the circumference of the oral region (especially at the right side) bulged (Figs. 8 and 15).



FIGS. 9–20. SEM micrographs of oral replacement in *Tetrahymena thermophila* during conjugation. Each micrograph is presented as a representative of each stage of oral replacement illustrated in Fig. 8. Correspondence of micrographs to the stages of oral replacement is as follows. Fig. 9, stage 1; Fig. 10, stage 2; Fig. 11, stage 3; Fig. 12, stage 4; Fig. 13, stage 5; Fig. 14, stage 6; Fig. 15, stage 7; Fig. 16, stage 8; Fig. 17, stage 9; Fig. 18, stage 10; Fig. 19, stage 11; Fig. 20, stage 12. For the structural features of respective stages, see *Results*. Magnifications of all micrographs are the same, and the bar in Fig. 9 indicates 1 μm .

Stage 8: About 14–19 hr after the cultures were mixed, reorganization of M1 and M2 began to occur from the right sides of each membranelle. In these membranelles, rearrangements of ciliary stubs proceeded in the order of the third, second and first rows. At this stage, the depth of the buccal cavity was nearly the same with the width of the oral apparatus. A few ciliary stubs were observed in the region corresponding to the right end of the incipient M3. In the bulged oral peripheral zone corresponding to the presumptive UM or its posterior area, we sometimes observed small bulges gathering, suggesting the presence of unarranged and unciliated basal body distribution as in usual stomatogenesis (Figs. 8 and 16).

Stage 9: About 17–22 hr after the cultures were mixed, organization of M3 proceeded in addition to that of M1 and M2. Alignment of the ciliary stubs in the UM was seemingly completed at this stage (Figs. 8 and 17).

Stage 10: About 22–24 hr after the cultures were mixed, M3 and M2 were reorganized nearly completely, but the left side of the first row of M2 was sometimes incomplete. As for M1, ciliary stub rearrangement at the left side remained incomplete, especially in the first and second rows of this membranelle. So-called sculpturing was not clearly recognizable yet. At this stage, the UM was completely formed and the oral size became larger, being comparable to the functional oral apparatus, but striation of the oral rib was still somewhat unclear (Figs. 8 and 18).

Stage 11: This oral stage was observed in the detached exconjugants 24–28 hr after the cultures were mixed. Reorganization of M1, M2, and M3 and sculpturing of the right parts of each membranelle were completely finished, and the buccal cavity deepened more than in stage 10. Striation of the oral rib became clear partly between the surface and a flat stair present inside the buccal cavity (Figs. 8 and 19).

Stage 12: The oral rib of this stage was fully striated and the oral pharynx was well formed. Thus, all replacement processes of the oral region expected in an exconjugant were completed (Figs. 8 and 20). The oral structure of this stage is, therefore, essentially the same as that of stage 1. However, the numbers of ciliary stubs of the left

side of M1 tended to be reduced as compared with those of stage 1, presumably due to the influence of long-term starvation.

Sequential changes of oral structures during conjugation as revealed by anti-tubulin immunofluorescence

To back up the results obtained by SEM observation, we investigated the localization of basal bodies in the oral apparatus at various stages of synchronous conjugation, using indirect immunofluorescence microscopy for anti-tubulin antiserum. The specificity of the antiserum was analyzed by immunoblotting technique (Fig. 21). Two immunofluorescence bands at a molecular weight of about 55K were observed, proving that the antiserum recognized α - and β -tubulin specifically among the proteins contained in *Tetrahymena* cilia. Furthermore, the relationship between sequential changes in oral structure and

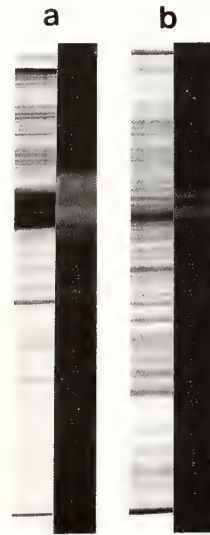


FIG. 21. Specificity of anti-tubulin antiserum. *Tetrahymena* cilia (a) and total cells (b) were electrophoresed on a sodium dodecyl sulfate (SDS) polyacrylamide gel and blotted onto a nitrocellulose strip. The strip was subjected to immunoreaction with anti-tubulin serum followed by reaction with fluorescein-labeled 2nd antibody. Coomassie Blue stain (left) and the corresponding immunoblot (right) of SDS-polyacrylamide gels are presented in pairs.

nuclear events during conjugation was revealed by fixed cells double-stained with FITC-conjugated antibody and DAPI (Figs. 22–32).

At stage 1, the organization of basal bodies was intact in the oral apparatus (Fig. 22a). We observed food vacuole formation at this stage (Fig. 22d). Stages 2 and 3 correspond to meiotic prophase. During these stages, several basal bodies in M1 and M2 disappeared from the left to the right in the order of first, second and third rows (Figs. 23a and 24a). At stage 4, the two main nuclear events, meiosis and fertilization, occurred. At this stage, the regression of basal bodies of M1 and M2 proceeded further and the basal bodies of UM disappeared progressively from the lower left to the upper right (Fig. 25a). At stage 5, the fertilization nuclei underwent two mitotic divisions. At this stage, SEM observation revealed that only 12–18 ciliary stubs remained in the three membranelles, and that ciliary stubs of UM disappeared progressively (Figs. 8 and 13). On the other hand, immunofluorescence microscopic observation showed that many basal bodies of the three membranelles and UM still remained (Fig. 26a). These results imply that the basal bodies of three membranelles and UM separated from the cell membrane and sank into cytoplasm. At stage 6, the mitotic products of the fertilization nucleus differentiated into new micro- and macronuclei (Fig. 27c, 27d). At this stage, the ciliary stubs of the UM and M3 were absent (Fig. 14) and only about 20–25 basal bodies remained in M1 and M2 (Fig. 27a).

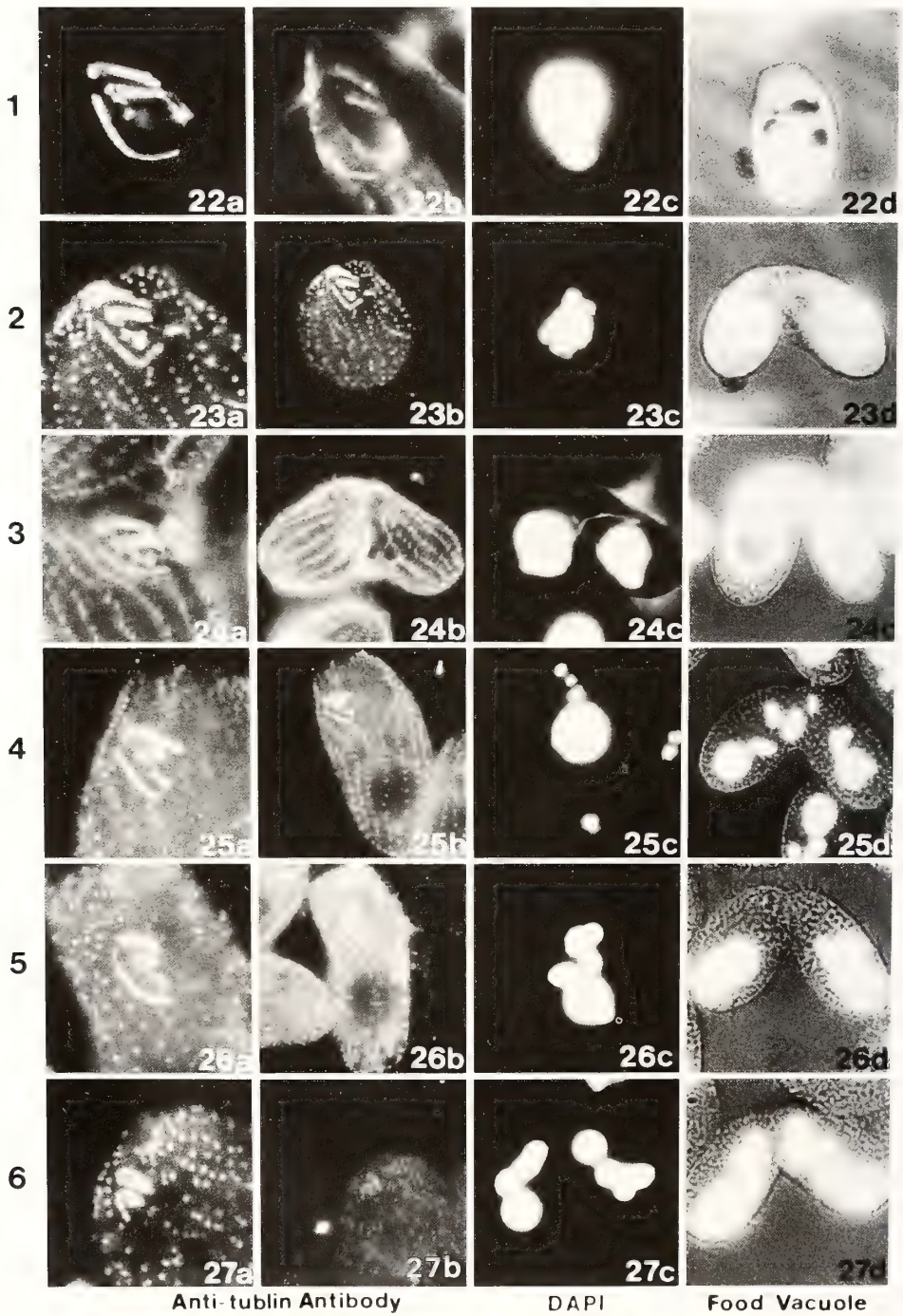
At stage 7, an oral primordium was first observed between the somatic ciliary rows (Fig. 28a). At stage 8, reorganization of M1 and M2 began to occur from the right sides of each membranelle and unarranged basal bodies were observed in the region corresponding to the incipient M3 (Fig. 29a). At stage 9, the both M1 and M2 coincidentally extended to the left and a small M3 appeared. A double row of the basal bodies of the UM organized itself along the right margin of the three membranelles (Figs. 29a and 30a). At stage 10, the basal bodies of M1, M2 and M3 were arranged into a rectangular formation within each membranelle. At this stage, the UM was nearly completely formed and the oral size

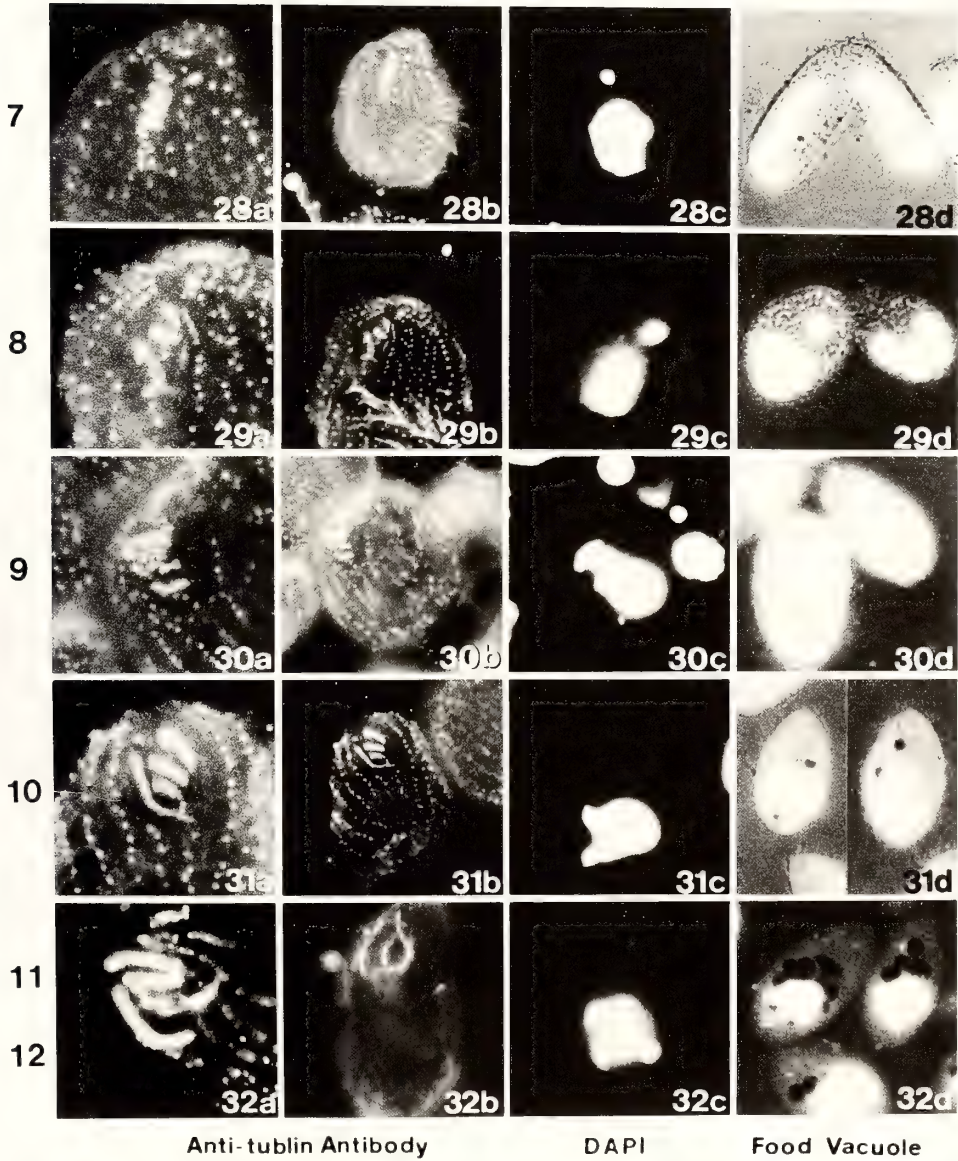
became larger (Figs. 18 and 31a). At the stages 11 and 12, reorganization of M1, M2, and M3 and the sculpturing of the right parts of each membranelle were completely finished (Fig. 2a).

During the stages 7 and 8, each conjugant contained two new macronuclei and two new micronuclei. At stage 9, the exconjugants of a pair separated from each other. At the stages 10 through 12, the cells recommenced food uptake.

DISCUSSION

In *Tetrahymena*, the oral primordium is known to develop at an equatorial site of the cell in usual exponential growth and to become the anterior new oral apparatus of the posterior division product. The process has been extensively studied by using the silver impregnation method in either or both light microscopy [1, 3–5] and SEM [22–25]. However, under certain conditions [6, 26–30], oral replacement is known to occur. One of the conditions eliciting oral replacement is the condition for inducing conjugation [3]. In this regard, it is only known that the oral apparatus of a conjugating pair in *Tetrahymena* remains intact at the very early phase of conjugation, but the exconjugants are astomatous [3]. However, details of how the old oral apparatuses are resorbed and the new ones later appear have not so far been elucidated. In *Paramecium tetraurelia*, oral replacement during conjugation seems to be sustained under the long-term control of micronuclear genes [31, 32]. More than 20 years ago, we found that *Tetrahymena* cells exhibited synchronous rounding and abortive synchronous division, by subjecting amino acid-starved cells to the ordinary heat treatment for synchronization [9–11]. By using this system, Frankel [6] demonstrated that the synchronous rounding cells performed oral replacement synchronously. According to the detailed observation on the oral replacement by Frankel and Williams [3] and Frankel [6], (i) resorption of the old oral apparatus occurs in the order of UM, M3, M2 and M1, and (ii) concurrently with the resorption of the old oral apparatus, oral neof ormation occurs in the order of M1, M2, M3 and UM. The latter neof ormation sequence is shown to be much the same as the sequence





FIGS. 22–32. Relations among the alignment of basal bodies, the nuclear events and food vacuole formation during conjugation. a, immunofluorescence localization of tubulin in the oral region. Each basal body could be seen by using this method. b, immunofluorescence localization of tubulin in the whole cell. Cells in a and b are the same except for the ones in Fig. 22 and Fig. 32. c, DAPI-stained nuclei of the same cell shown in b. d, food uptake activity and nuclear events of cells and pairs corresponding to the stages of a. At each point, an aliquot of culture was mixed with an equal volume of 1% India ink and incubated for 5 min at 26°C. The cells were fixed with an equal volume of 5% formaldehyde in PBS and stained with 10 µg/ml DAPI. Since cells seen in Fig. 22d, Fig. 31d and Fig. 32d had taken India ink into the food vacuoles, the food vacuoles were observed as black particles in the cells. In the left sides of photos a, b, c, d, stage numbers classified are given.

observed in oral neof ormation during division, except that only the forming site is different.

The above-mentioned sequences are different in some points from the sequences of oral replacement during conjugation demonstrated in the present paper (Figs. 8–32). The major differences found in the process of conjugation are: (i) Resorption of the old oral apparatus occurs in the order of M1, M2, M3 and UM; (ii) Resorption and neof ormation of the oral apparatus occur not concurrently but rather independently in the order of resorption and neof ormation; (iii) There exists a nearly astomatous state, although a very small oral area is recognized without significant surface structures. On the other hand, neof ormation occurs in nearly the same order as that observed in synchronous rounding. These differences are presumably due to a difference in cellular events between conjugation and abortive division. Thus, it is noteworthy that, although oral regression and reformation observed in conjugation and in abortive division are both called oral replacement, the detailed processes differ in some points from each other. To our knowledge, this paper is the first report describing in detail the oral morphological changes during conjugation in *Tetrahymena*.

Concerning the biological function of *Tetrahymena* intermediate filament protein, 49K protein, we previously emphasized its role in the oral morphogenesis in binary fission cells [15]. The same is true for the oral morphological change during conjugation (Figs. 1–7). The intermediate filament protein is dissociated from the oral apparatus at an early phase of conjugation, which may trigger the regression of the old oral apparatus. Then, the protein plays important roles in various germ nuclear events, such as meiosis, selection of functional meiotic products, transfer of pronucleus, and zygote formation [32]. After this, the protein reassociates with the immature oral apparatus, and may cause the oral apparatus to become a functional one (Figs. 4–7). It follows from these findings that the 49K protein is indispensable for the various processes during conjugation and is multifunctional.

REFERENCES

- 1 Frankel, J. (1962) The effects of heat, cold, and p-fluorophenylalanine on morphogenesis in synchronized *Tetrahymena pyriformis* GL. C. R. Trav. Lab. Carlsberg, **33**: 1–52.
- 2 Frankel, J. (1965) The effect of nucleic acid antagonists on cell division and oral organelle development in *Tetrahymena pyriformis*. J. Exp. Zool., **159**: 113–148.
- 3 Frankel, J. and Williams, N. E. (1973) Cortical development in *Tetrahymena*. In "Biology of *Tetrahymena*". Ed. by A. M. Elliott, Dowden, Hutchinson, and Ross, Stroudsburg, Pennsylvania, pp. 375–409.
- 4 Holz, G. G., Jr., Scherbaum, O. H. and Williams, N. E. (1957) The arrest of mitosis and stomatogenesis during temperature-induction of synchronous division in *Tetrahymena pyriformis*, mating type 1, variety 1. Exp. Cell Res., **13**: 618–621.
- 5 Williams, N. E. and Frankel, J. (1973) Regulation of microtubules in *Tetrahymena*. I. Electron microscopy of oral replacement. J. Cell Biol., **56**: 441–457.
- 6 Frankel, J. (1970) The synchronization of oral development without cell division in *Tetrahymena pyriformis* GL-C. J. Exp. Zool., **173**: 79–100.
- 7 Frankel, J. (1964) Cortical morphogenesis and synchronization in *Tetrahymena pyriformis* GL. Exp. Cell Res., **35**: 349–360.
- 8 Frankel, J. (1964) The effects of high temperatures on the pattern of oral development in *Tetrahymena pyriformis* GL. J. Exp. Zool., **155**: 403–436.
- 9 Tamura, S., Toyoshima, Y. and Watanabe, Y. (1966) Mechanism of temperature-induced synchrony in *Tetrahymena pyriformis*. Analysis of the leading cause of synchronization. Jpn. J. Med. Sci. Biol., **19**: 85–96.
- 10 Watanabe, Y. (1963) Some factors necessary to produce division conditions in *Tetrahymena pyriformis*. Jpn. J. Med. Sci. Biol., **16**: 107–124.
- 11 Watanabe, Y. (1971) Mechanism of synchrony induction. I. Some features of synchronous rounding in *Tetrahymena pyriformis*. Exp. Cell Res., **68**: 431–436.
- 12 Numata, O., Yasuda, T., Hirabayashi, T. and Watanabe, Y. (1980) A new fiber-forming protein from *Tetrahymena pyriformis*. Exp. Cell Res., **129**: 223–230.
- 13 Numata, O., Yasuda, T., Ohnishi, K. and Watanabe, Y. (1980) *In vitro* filament formation of a new fiber-forming protein from *Tetrahymena pyriformis*. J. Biochem., **88**: 1505–1514.
- 14 Numata, O. and Watanabe, Y. (1982) *In vitro* assembly and disassembly of 14-nm filament from *Tetrahymena pyriformis*. The protein component of

- 14-nm filament is 49,000-dalton protein. *J. Biochem.*, **91**: 1563–1573.
- 15 Numata, O., Hirono, M. and Watanabe, Y. (1983) Involvement of *Tetrahymena* intermediate filament protein, a 49K protein, in the oral morphogenesis. *Exp. Cell Res.*, **148**: 207–220.
- 16 Sugai, T. and Hiwatashi, K. (1974) Cytologic and autoradiographic studies of the micronucleus at meiotic prophase in *Tetrahymena pyriformis*. *J. Protozool.*, **21**: 542–548.
- 17 Goodenough, U. W. (1983) Motile detergent-extracted cells of *Tetrahymena* and *Chlamydomonas*. *J. Cell Biol.*, **96**: 1610–1621.
- 18 Hirabayashi, T., Tamura, R., Mitsui, I. and Watanabe, Y. (1983) Investigation of actin in *Tetrahymena* cells. A comparison with skeletal muscle actin by a devised two-dimensional gel electrophoresis method. *J. Biochem.*, **93**: 461–468.
- 19 Talin, J. C., Olmsted, J. B. and Goldman, R. D. (1983) A rapid procedure for preparing fluorescein-labeled specific antibodies from whole antiserum: Its use in analyzing cytoskeletal architecture. *J. Cell Biol.*, **97**: 1277–1282.
- 20 Towbin, H., Staehelin, T. and Gordon, J. (1979) Electrophoretic transfer of proteins from polyacrylamide gels to nitrocellulose sheets: Procedure and some applications. *Proc. Natl. Acad. Sci. U. S. A.*, **76**: 4350–4354.
- 21 Numata, O., Sugai, T. and Watanabe, Y. (1985) Control of germ cell nuclear behaviour at fertilization by *Tetrahymena* intermediate filament protein. *Nature*, **314**: 192–194.
- 22 Buhse, H. E., Jr., Stamler, S. J. and Corliss, J. O. (1973) Analysis of stomatogenesis by scanning electron microscopy in *Tetrahymena pyriformis* strain W during synchronous cell division. *Trans. Am. Microsc. Soc.*, **92**: 95–105.
- 23 Williams, N. E. and Bakowska, J. (1982) Scanning electron microscopy of cytoskeletal elements in the oral apparatus of *Tetrahymena*. *J. Protozool.*, **29**: 382–389.
- 24 Bakowska, J., Nelsen, E. M. and Frankel, J. (1982) Development of the ciliary pattern of the oral apparatus of *Tetrahymena thermophila*. *J. Protozool.*, **29**: 366–382.
- 25 Jerka-Dziadosz, M. and Frankel, J. (1979) A mutant of *Tetrahymena thermophila* with a partial mirror image duplication of cell surface pattern. I. Analysis of the phenotype. *J. Embryol. Exp. Morphol.*, **49**: 167–202.
- 26 Albach, R. A. and Corliss, J. O. (1959) Regeneration in *Tetrahymena pyriformis*. *Trans. Am. Microsc. Soc.*, **78**: 276–284.
- 27 Buhse, H. E., Jr. (1966) Oral morphogenesis during transformation from microstome to macrostome and macrostome to microstome in *Tetrahymena vorax* strain V₂ type S. *Trans. Am. Microsc. Soc.*, **85**: 305–313.
- 28 Buhse, H. E., Jr. (1967) Microstome-macrostome transformation in *Tetrahymena vorax* strain V₂ type S induced by a transforming principle, stomatin. *J. Protozool.*, **14**: 608–613.
- 29 Frankel, J. (1964) Morphogenesis and division in chains of *Tetrahymena pyriformis* GL. *J. Protozool.*, **11**: 514–526.
- 30 Roque, M., de Puytorac, P. and Savoie, A. (1970) Caractéristiques morphologiques et biologiques de *Tetrahymena bergeri* sp. nov., cilié hyménostome tétrahyménien. *Protistologica*, **6**: 343–351.
- 31 Ng, S. F. and Newman, A. (1984) The role of the micronucleus in stomatogenesis in sexual reproduction of *Paramecium tetraurelia*: conjugation of amiconucleates. *Protistologica*, **20**: 517–523.
- 32 Ng, S. F. and Newman, A. (1985) The macronuclear anlage does not play an essential role in stomatogenesis in conjugation in *Paramecium tetraurelia*. *Protistologica*, **21**: 391–398.

Comparative Effects *in vitro* of *Myxine*, *Squalus*, Avian and Mammalian Insulins on DNA-Synthesis in 3T3 Mouse Fibroblasts

WILHELM ENGSTRÖM, EVA DAFGÅRD
and STURE FALKMER

*Department of Tumour Pathology, Karolinska Institutet, Karolinska
Hospital, S-104 01 Stockholm, Sweden*

ABSTRACT—Five kinds of natural insulins, namely those obtained from the Atlantic hagfish, the spiny dogfish, turkey, pig, and man, failed to stimulate quiescent serum-starved 3T3 fibroblasts to re-enter the cell cycle. However, after addition of epidermal growth factor (EGF) four of the insulins enhanced its mitogenic effect. Turkey insulin was found to be the most potent, followed in this respect by the porcine and human insulins. Dogfish insulin only exerted a limited, but nevertheless significant, effect on the EGF-treated quiescent cells. In contrast, no permissive effect was observed by the hagfish insulin. In trying to explain these differences in the growth promoting effects of the five insulins as due to their amino-acid sequences in the receptor-binding regions of their molecules, it was concluded that any sequential arrangement in the B22-B26 positions seems not to be a prerequisite to exert a permissive effect on EGF-induced DNA-replication in mammalian fibroblasts.

INTRODUCTION

The evolution of hormones and growth factors has resulted in so-called polypeptide hormone families where the amino acid sequences are so similar that it is reasonable to assume that a joint ancestor molecule exists for all members [1]. The insulin family consists of the hormone relaxin and the growth factors NGF (nerve growth factor) and the IGFs (insulin like growth factors) [2, 3]. A comparison of their amino-acid sequences and their X-ray crystallographic appearance suggests that the ability to attain an insulin-like tertiary molecular structure—the so called insulin fold—has been retained [3]. The insulin and IGF molecules have also retained a few surface residues in common which mediate their interactions with insulin and type I receptors. In contrast, their ability to form dimers, hexamers, bind antibodies and interact with type II receptors has not been universally retained in evolution [4]. From an evolutionary point of view it has been proposed

that insulin and its relatives stem from a common precursor molecule which was encoded for by a gene that underwent duplication about 600 million years ago [1]. The subsequent gene duplication which led to diversion into insulin, relaxin, NGF, IGF I and IGF II may have taken place about 300 million years ago, when mammals appeared on earth [5]. In the present study we have compared the effects of insulins representing different stages in evolution on DNA-synthesis in a target cell line of fibroblastic origin (viz Swiss mouse 3T3 cells; cf.[6]). When these cells are starved to quiescence in low serum, they cannot be stimulated to resume proliferation by addition of human or porcine insulin only [7]. However, when 3T3 cells are concomitantly exposed to another mitogenic factor, viz EGF (epidermal growth factor), insulin exerts a substantial permissive effect on DNA-synthesis [8]. We report in this study that insulins from different species differ in their capacity to enhance the mitogenic effect of EGF. Differences in their amino acid sequences in the receptor-binding region cannot explain these differences in biological activity between insulins from different phyla and species.

MATERIAL AND METHODS

Growth factors and hormones

EGF was purchased from Collaborative Research Inc. (Waltham, MA., USA). Porcine and human insulins were purchased from Sigma Co. (Stockholm, Sweden). Turkey insulin was a kind gift from Dr. Steve Wood, Department of Crystallography, Birkbeck College, Malet Street, London, U. K.: Dogfish and hagfish insulins were prepared in our laboratory (cf. [9, 10]).

Cell culture

Swiss mouse 3T3 cells, obtained from Flow laboratories, Stockholm, Sweden, were maintained in monolayer cultures in NUNC 10 ml tissue culture bottles. The stock cultures were grown in humidified 5% CO₂/95% air mixture in Dulbecco's modified Eagle's medium (DMEM), supplemented with 10% (v/v) foetal calf serum, 50 units penicillin/ml and 50 µg streptomycin/ml and never allowed to reach confluency. For transfer, the cells were treated with 0.25% trypsin (w/v) in Tris-buffered saline, containing 0.5 mM EDTA for 2–3 min at 37°C. The stock cultures were passaged by seeding 3,000 cells/cm² culture bottle area and transferring them every third day. For experimental purpose, 3,000–4,000 cells/cm² were seeded in Petri dishes containing a glass coverslip in the bottom in DMEM and 10% (v/v) serum.

Autoradiography

DNA-synthesis was estimated by incorporating 0.5 µCi ³H-thymidine (Amersham; 56 mCi/mmol) per ml medium into TCA-unprecipitable material. At the end of each experiment, the cultures were washed twice in 0.9% NaCl (w/v) solution, fixed in 95% ethanol for at least 24 hr and maintained in an air dried state until autoradiography was performed. Before the film (Kodak AR10 stripping film) was applied, the cells were treated in 5% (w/v) TCA at 4°C for 5 min and then washed for 20 min in running tap water to remove non-incorporated thymidine. After 7 days' exposure, the autoradiograms were developed with Kodak D19 developer (4 min at 18°C), briefly rinsed in

water, fixed in Kodak acid X-ray fixative with hardener (5 min at 18°C), washed in running cold tap water for 20 min and routinely stained in haematoxylin and eosin. The percentage of cells that had initiated DNA-synthesis during the experimental period was determined by counting at least 500 cells in the light microscope.

RESULTS AND DISCUSSION

Figure 1 summarizes the effects of insulin on DNA-synthesis in quiescent serum starved 3T3-fibroblasts grown in sparse cultures. It was found that none of the five insulins obtained from the Atlantic hagfish (*Myxine glutinosa*), the spiny dogfish (*Squalus acanthias*), turkey, pig and man exerted any significant effects on DNA-synthesis in

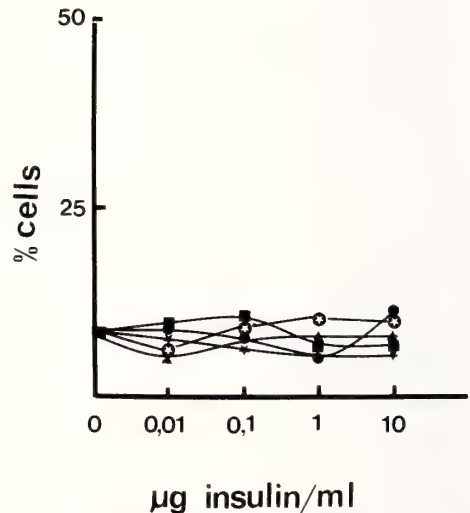


FIG. 1. Effect of five kinds of natural insulins on DNA-synthesis in quiescent serum starved mouse 3T3 fibroblasts *in vitro*. The cells were starved to quiescence for 48 hr in 0.1% serum. DMEM supplemented with various concentrations of *Myxine* (●), *Squalus* (★), turkey (■), porcine (▲), or human (○) insulin, was added. Cells, continuously exposed to 0.1% serum, were used as an internal control. The cells were maintained in the experimental media for 24 hr in the presence of 0.5 µCi ³H-thymidine per ml medium. The proportion of cells that had initiated DNA-synthesis was determined by autoradiography. The results clearly demonstrate that neither of the five insulins stimulated DNA-synthesis in quiescent 3T3 cells when added as the sole macromolecular supplement.

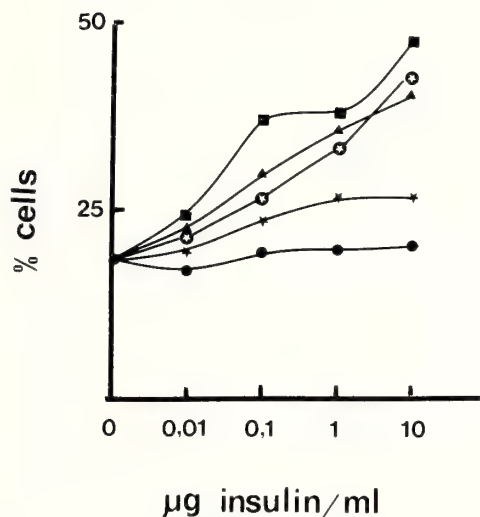


FIG. 2. The permissive effect of five kinds of natural insulins (as described in legend to Fig. 1) on EGF-stimulated quiescent 3T3 fibroblasts. Experiments were performed as shown in Fig. 1 but now the insulins were added together with 10 ng EGF/ml medium. The results show that turkey, porcine, human and *Squalus* insulins exerted a permissive effect on EGF-treated quiescent 3T3 fibroblasts. In contrast *Myxine* insulin failed to augment the stimulatory effects of EGF in this situation.

this target cell type. This is in marked contrast to human IGF I or IGF II that both increase the proportion of ^3H -thymidine-labelled cells up to three times under similar experimental conditions (Dafgård *et al.*, unpublished data). Figure 2 illustrates the permissive effects of insulins of the same five species as in Figure 1 on DNA-synthesis in serum-starved cells concomitantly exposed to

another growth factor, viz EGF. The results show that the maximum mitogenic effect was achieved by adding turkey insulin together with EGF. A lower, but nevertheless substantial, permissive effect was achieved by porcine or human insulin. When *Squalus* insulin was added, the percentage of labelled cells was approximately half of that achieved by EGF and turkey insulin. In contrast, *Myxine* insulin only exerted a minor and statistically insignificant effects in combination with EGF.

The inability of insulin alone to induce DNA-replication in mouse 3T3 fibroblasts has previously been reported [8, 11]. However, mammalian insulin, added together with EGF, is known to enhance the mitogenic effect on these cells many-fold [7, 8, 11]. Furthermore, it has been demonstrated that Swiss mouse 3T3 cells, unlike for instance human glia cells, require a multiple set of growth factors and hormones for proliferation under serum-free conditions [12]; in a pilot study we observed that some kinds of natural insulin seemed to exert a permissive rather than a primarily mitogenic effect [13]. A similar permissive effect of *Squalus* insulin on platelet derived growth factor-stimulated 3T3 fibroblasts was reported by Bajaj [14]. This lack of effect of insulin on mitogenesis in 3T3 fibroblasts is somewhat puzzling since all 3T3-clones hitherto examined express functional insulin receptors [15]. We have found that insulins from four different species that exhibit an identical amino acid sequence in the B22–B26 receptor binding region, differ completely in their permissive effect on DNA-synthesis in EGF-treated quiescent 3T3-cells (Table 1). Even

TABLE 1. Comparison of the amino acid sequences of insulin and insulin like growth factors in positions B22–B26 which comprises the insulin receptor binding region

B-chain	22	23	24	25	26
Human	Arg	Gly	Phe	Phe	Tyr
Porcine					
Turkey					
<i>Squalus</i>	Lys			Tyr	
<i>Myxine</i>					
hIGF I				Tyr	Phe
hIGF II				Tyr	Phe

Data from [3].

though differences in binding characteristics have been reported [16], it is conceivable that binding of insulin to the insulin receptor is not conditional for progression towards S-phase [8]. Nor can the substitution of B25-Phe with B25-Tyr, as in *Squalus* insulin, fully explain these differences in biological activity, since it evoked a lesser effect than for instance IGF I and IGF II on EGF-treated 3T3-cells (Dafgård *et al.*, unpublished data). It is tempting to propose that the permissive effect of insulin on EGF-treated 3T3-fibroblasts involves an initial binding of insulin to some other membrane receptor. One possible candidate is the type 1 receptor [17] which in many respects resembles the insulin receptor [18]. Consideration of the affinity of insulin to the type 1 receptor is, however, more difficult in the absence of extensive binding data. Notwithstanding, it has been demonstrated that *Squalus*, turkey and porcine insulins displace radiolabelled IGF I from target cells in a dose-dependent manner (Dafgård and Rees, unpublished data). It is, therefore, conceivable that the observed effects on mitogenesis are more dependent on binding to the type 1 receptor than to the insulin receptor. The type 2 receptor is probably not involved in the mitogenic signalling since insulin cannot bind—even with low affinity—to this receptor [19]. The exact relationship between EGF and insulin action is not known, but a similar synergistic effect between these two growth factors has been observed in human embryonic corneal stromal cells [20], indicating that this phenomenon is not unique to the 3T3 fibroblastic cell line. It remains, however, to be shown how other biological effects on the cell cycle, as effects on cellular enlargement, are mastered by insulin from different phyla [21]. These experiments are currently in progress.

ACKNOWLEDGMENTS

This study was generously supported by the Swedish Medical Research Council (Project No. 12X-718), the Swedish Diabetes Association, the Stockholm Cancer Society and the Robert Lundberg memorial fund. E. D. was the recipient of a British Council Scholarship at Department of Crystallography, Birkbeck College, London.

REFERENCES

- 1 Blundell, T. L. and Humbel, R. (1980) Pancreatic hormone families. *Nature*, **287**: 781-787.
- 2 Rindeknecht, E. and Humbel, R. (1976) Polypeptides with non-suppressable insulin like and cell growth promoting activities in human serum. Isolation, chemical characterization and some biological properties of forms I and II. *Proc. Natl. Acad. Sci. USA*, **73**: 2365-2369.
- 3 Dafgård, E., Bajaj, M., Honegger, A. M., Pitts, J., Wood, S. and Blundell, T. L. (1985) The conformation of insulin like growth factors. *J. Cell. Sci.*, **Suppl. 3**: 53-64.
- 4 Rechler, M. M. and Nissley, S. P. (1985) The nature and regulation of the receptors for insulin like growth factors. *Ann. Rev. Physiol.*, **47**: 425-442.
- 5 Froesch, E. R. and Zapf, J. (1985) Insulin like growth factors and insulin. *Comparative aspects*. *Diabetologia*, **28**: 485-493.
- 6 Larsson, O., Dafgård, E., Engström, W. and Zetterberg, A. (1986) Immediate effects of serum depletion on dissociation between growth in cell size and cell division in proliferating cells. *J. Cell. Physiol.*, **127**: 267-273.
- 7 Zetterberg, A., Engström, W. and Larsson, O. (1982) Growth activation of resting cells. *Ann. N. Y. Acad. Sci.*, **397**: 130-147.
- 8 Zetterberg, A., Engström, W. and Dafgård, E. (1984) The relative effects of different types of growth factors on DNA-replication, mitosis and cellular enlargement. *Cytometry*, **5**: 368-375.
- 9 Bajaj, M., Blundell, T. L., Pitts, J. E., Wood, S. P., Tatnell, M. A., Falkmer, S., Emdin, S. O., Gowan, L. K., Crow, H., Schwabe, C., Wollmer, A. and Strassburger, W. (1983) Dogfish insulin. Primary structure, conformation and biological properties of an elasmobranchial insulin. *Eur. J. Biochem.*, **135**: 535-542.
- 10 Emdin, S. O., Steiner, D. F., Chan, S. J. and Falkmer, S. (1985) Hagfish insulin; Evolution of insulin. In "Evolutionary Biology of Primitive Fishes". Ed. by R. E. Foreman, A. Gorbman, J. M. Dodd and R. Olsson, Plenum Press, New York, pp. 363-370.
- 11 Jimenez de Asua, L., O'Farrel, M., Clingan, D. and Rudland, P. S. (1976) Temporal sequences of hormonal interactions during the prereplicative phase of quiescent cultured 3T3 fibroblasts. *Proc. Natl. Acad. Sci. USA*, **74**: 3845-3849.
- 12 Shipley, G. D. and Ham, R. G. (1983) Multiplication of Swiss 3T3 cells in a serum free medium. *Exp. Cell Res.*, **146**: 249-260.
- 13 Falkmer, S., Dafgård, E. and Engström, W. (1986) Phylogeny of insulin - primitive insulins and the cell cycle. *Chemica Scripta*, **26B**: 209-212.

- 14 Bajaj, M. (1984) Ph. D.-thesis, Birkbeck College, London.
- 15 Murphy, R. F., Powers, S., Verderame, M., Cantor, C. R. and Pollack, R. (1982) Flow cytofluorometric analysis of insulin binding and internalization by Swiss 3T3-cells. *Cytometry*, **2**: 402-406.
- 16 Emdin, S. O., Sonne, O. and Gliemann, J. (1980) Hagfish insulin; The discrepancy between binding affinity and biological activity. *Diabetes*, **29**: 301-303.
- 17 Massague, J. and Czech, M. P. (1982) The subunit structures of two distinct receptors for insulin like growth factors I and II and their relationship with the insulin receptor. *J. Biol. Chem.*, **257**: 5048-5055.
- 18 Gammeltoft, S. (1984) Insulin receptors. *Physiol. Rev.*, **64**: 1321-1377.
- 19 Czech, M. P., Massague, J., Yu, K., Oppenheimer, C. L. and Mottola, C. (1984) Subunit structures and actions of the receptors for insulin and the insulin like growth factors. In "The Importance of Islets of Langerhans for Modern Endocrinology". Ed. by K. Ederlin and I. Scholtholt, Raven Press, New York, pp. 41-53.
- 20 Hyldahl, L. (1986) Studies on the human embryonic cornea. Ph. D.-thesis, Karolinska Institutet, Stockholm.
- 21 Falkmer, S., Dafgård, E., El-Salhy, M., Engström, W., Grimelius, L. and Zetterberg, A. (1985) Phylogenetical aspects on islet hormone families. *Peptides*, **6**: 315-320.

Effects of Long-term Progesterone Treatment on Synchronized Ovulation in Guinea Pigs

HIDEO UEDA, TADASHI KOSAKA and KAZUAKI W. TAKAHASHI¹

Toxicology Division, Institute of Environmental Toxicology, Suzuki-cho 2-772, Kodaira-shi, Tokyo 187, and ¹Department of Laboratory Animal Science, Nippon Veterinary and Zootechnical College, Kyonan-cho 1-7-1, Musashino-shi, Tokyo 180, Japan

ABSTRACT—Long-term effects of progesterone implants at different stages of the estrous cycle on synchronized ovulation were studied in guinea pigs. Females were subcutaneously implanted with Silastic tubing which contained crystalline progesterone for 7, 14, and 21 days (groups A, B and C) on day 0, 5, 10, and 15 of vaginal opening. The mean number of days to vaginal opening and leucocytic influx into vaginal smears in groups B and C were significantly less than those of group A ($P < 0.05$ and 0.01 , respectively). The length of leucocytic influx in the groups treated with progesterone took mostly 6 days, the mode day, following removal of the progesterone; number of animals showing results on this mode day ranged from 38% (9/24) in group A to 79% (19/24) in groups B and C. No significant differences in the mean number of days to vaginal opening or leucocytic influx were seen among subgroups given progesterone implants at different stages of the estrous cycle. Ovulation was observed in all animals sacrificed on the day of leucocytic influx into the vaginal smear. These findings indicate that long-term implantation of progesterone tubing, greater than 14 days, given at any estrous stage to female guinea pigs induces the synchronized ovulation within 5–6 days after the removal of progesterone tubing.

INTRODUCTION

Reproductive efficiency of guinea pigs for experimental animals is less than that of another kind of rodents; length of estrous cycles and gestation period in guinea pigs are 3 to 4 times longer and litter size 1/2 to 1/4 times less than those of rats, mice or hamsters. It is difficult to obtain the guinea pigs at a uniformed age or quality, which is needed for performing the toxicological study of chemicals or larger sized study at a scheduled time. So, synchronizing the estrous cycles of guinea pigs is one direction for researching how to control a scheduled supply with good uniformity. Progesterone treatment for synchronization of the estrous cycle has been widely used. In rats [1, 2], hamsters [3–5], and guinea pigs [6], a single injection of progesterone has caused either postponed or advanced ovulation depending on what stage of

the estrous cycle it was administered. The effect of long-term progesterone treatment on the estrous cycle has been studied in sheep [7], cattle [8] and swine [9, 10]. Woody *et al.* [11] reported that in guinea pigs, multiple injections of progesterone dissolved in oil for 6 days reduced the average length of estrous cycles. Recently, continuous progesterone treatment by subcutaneous implants instead of multiple injections of progesterone dissolved in oil has been used because of its ability to maintain a constant steroid supply to target organ [12]. We investigated, therefore, how many days were needed for receiving progesterone implants and/or what stage of the estrous cycle these implants were given at to be effective in inducing synchronized ovulation following influx of leucocytes into vaginal smears in guinea pigs.

MATERIALS AND METHODS

Adult female guinea pigs of the Hartley strain at 3–4 months of age (weight 575–925 g) were used.

They were provided with commercial pellets (GB-1: Funabashi Farm Co., Ltd.) and tap water *ad libitum*. Room temperature was maintained at 20–24°C, relative humidity at 45–65 %, photoperiod at 14-hr light and 10-hr darkness (light on at 5:00 a.m. and off at 7:00 p.m.) and ventilation at 12 times an hour. Vaginal closure membranes and vaginal smears were examined once a day until removal of the progesterone implant, and twice a day (morning and evening) thereafter. Vaginal opening was determined to be positive when the vaginal membrane was fully ruptured. The first day of vaginal opening was designated as day 0 of vaginal opening. The influx of leucocytes into the vaginal smear after the appearance of cornified cells in the sample was observed under a light microscope. At this time, the animals were

sacrificed in order to examine the state of ovulation. The number of ova ovulated was confirmed by direct observation of ova in the oviduct and uterus and by the appearance of the corpora lutea; color, size, and elevation from the ovarian surface were noted. The average duration of estrous cycle recorded before the beginning of this experiment was 17.5 days (range: 14–21 days).

Females received a subcutaneous implant (Silastic tubing, 1.0 cm long, 0.4 cm i.d.) of pure crystalline progesterone (Sigma Co. Ltd., Lot No. 73F-0198) for 7 days (group A), 14 days (group B), or 21 days (group C). The control group (group D) received empty Silastic tubing. Each group was divided further into four subgroups according to the stage at which the progesterone implant was to be received. Subcutaneous im-

TABLE 1. Effects of progesterone on vaginal opening and leucocytic influx into the vaginal smear

Group	Treatment		No. of animals examined	Days to vaginal opening after removal of Silastic tube (Mean±S.D.)	Days to leucocytic influx into the vaginal smear after removal of Silastic tube (Mean±S.D.)
	Implantation period (days)	Day of estrous cycle when Silastic tube was inserted			
A	7	0	6	5.8±1.6	8.8±1.5
		5	6	5.5±1.4	7.7±2.0
		10	6	4.0±0	6.3±0.8
		15	6	4.5±2.1	7.5±2.6
		Average			5.0±1.6
B	14	0	6	3.8±1.5	5.8±0.4
		5	6	3.5±1.2	6.0±0
		10	6	4.2±0.8	5.8±0.4
		15	6	4.3±0.5	5.5±0.5
		Average			4.0±1.0*, #
C	21	0	6	4.0±0	5.7±0.5
		5	6	3.8±0.4	6.0±0
		10	6	3.7±1.0	6.0±0.6
		15	6	4.3±0.8	5.8±0.4
		Average			4.0±0.7*, #
D (Control)	21	0	3	14.0±1.7	16.3±2.1
		5	3	9.7±1.5	11.3±2.1
		10	3	3.3±2.9	4.7±3.2
		15	3	4.3±6.7	6.3±6.7
		Average			7.8±5.5

*, **: Significantly different from group A at the 5% and 1% levels of probability, respectively.

#: Significantly different from group D at the 5% level of probability.

plants were given as follows: subgroup a, on day 0; subgroup b, on day 5; subgroup c, on day 10; subgroup d, on day 15 of vaginal opening. Removal of Silastic tubing was carried out at 16:00 hr–18:00 hr under ether anesthesia.

Results were analyzed statistically using the Mann-Whitney U test and Kruskal-Wallis H test.

RESULTS

Vaginal opening was not observed in any animals treated with progesterone implants during the implantation period. After removal of the Silastic progesterone tubing, the mean days to vaginal opening in the groups treated for 14 and 21 days was significantly less than that in the control group and the group exposed for 7 days ($P < 0.05$, Table 1). The mean days to leucocytic influx into vaginal smears following removal of progesterone tubing was 7.6 ± 1.9 days in group A, 5.8 ± 0.4 days in group B, 5.9 ± 0.4 days in group C, and 9.7 ± 5.9 days in group D (Table 1). The mean length of time to leucocytic influx following vaginal opening in the groups treated for 14 and 21 days (groups B and C) were also significantly reduced compared with the control group (group D, $P < 0.05$) and the group treated for 7 days (group A, $P < 0.01$). No significant differences in the mean length of time to vaginal opening and leucocytic influx were found among subgroups treated with progesterone on day 0, 5, 10, and 15 of vaginal opening.

Figure 1 shows the variation in the day of leucocytic influx into vaginal smears after the progesterone removal. The length of time to leucocytic influx in the control group (group D) varied widely, while those in the progesterone treated groups took mostly 6 days, the mode day, after Silastic tubing removal. Among the groups treated with progesterone, the number of animals showing results on this mode day (at 6 days) ranged from 38% in group A (9/24) to 79% in groups B and C (19/24).

Fresh ova in the oviduct were seen in all animals sacrificed on the day of leucocytic influx into the vaginal smear with the exception of one of 24 females in group A and two of 12 females in group D, whose ova were, however, seen in the uterus (Table 2). The mean number of ova seen in

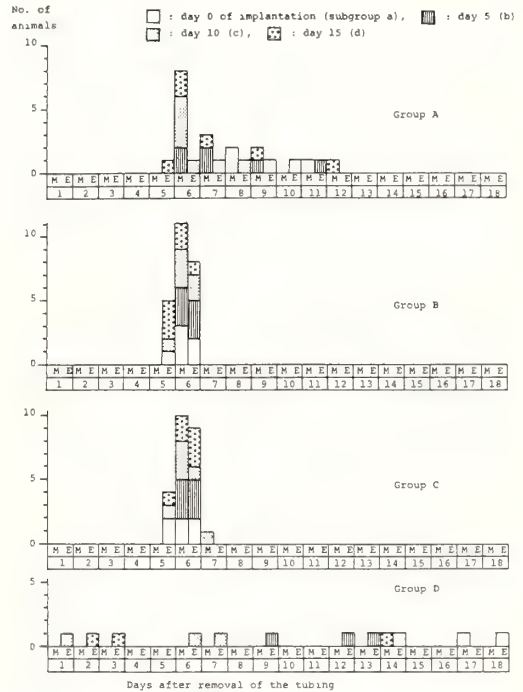


FIG. 1. Day of leucocytic influx into the vaginal smear after removal of the progesterone-filled (Groups A–C) or empty (Group D) tubing in the guinea pigs. M: 08:00–09:00 hr, E: 17:00–18:00 hr

oviduct was not significantly different among any of the groups.

DISCUSSION

The influx of leucocytes into the vaginal smear following the appearance of fully cornified cells has been considered to be the end of vaginal estrus [13], and an indication of ovulation [14, 15]. In these studies, all animals sacrificed on the first day of leucocytic smear showed ovulation. Our data confirmed that this smear pattern was a sign of ovulation in cyclic female guinea pigs.

As the agent for the synchronization or the alteration of estrous cycle, progesterone administration has been extensively used in many species of animals [7–10]. Single or multiple injections of progesterone given at different stage of the estrous cycle in guinea pigs induced prolongation of ovulation depending on the stage of administration [6, 16]. In guinea pigs, the timing of ovulation

TABLE 2. Results of ovulation test at the day of leucocytic influx into the vaginal smear after removal of the progesterone-filled (Groups A-C) or empty (Group D) tubing in the guinea pigs

Group	Treatment		No. of animals examined	No. of animals showing ovulation		No. of ova in oviduct (Range)
	Implantation period (days)	Day of estrous cycle when Silastic tube was inserted		Ova in oviduct	Ova in uterus	
A	7	0	6	6		4.2 (3-5)
		5	6	5	1	4.0 (2-5)
		10	6	6		4.0 (3-5)
		15	6	6		4.0 (3-5)
B	14	0	6	6		4.2 (4-5)
		5	6	6		4.3 (3-5)
		10	6	6		3.7 (3-4)
		15	6	6		4.3 (3-6)
C	21	0	6	6		4.5 (4-5)
		5	6	6		4.2 (3-5)
		10	6	6		4.3 (4-5)
		15	6	6		4.3 (4-5)
D (Control)	21	0	3	1	2	4.0 (4)
		5	3	3		3.3 (3-4)
		10	3	3		4.7 (4-5)
		15	3	3		4.0 (3-5)

after progesterone injection seems to be regulated by the stage of the estrous cycle at which the progesterone was administered. Induction of ovulation in guinea pigs by other hormones requires injection at some fixed time during the estrous cycle [17-21]. However, the present data revealed that effect of long-term progesterone treatment on inducing the synchronized ovulation following leucocytic influx was independent on the stage of the estrous cycle at which progesterone implants were given.

Here, we have shown that long-term progesterone treatment for 14 and 21 days was effective in inducing ovulation within 5-6 days after the removal of the progesterone implant. Tso and Tam [22] reported that approximately 5 days elapse between onset of luteolysis and ovulation in guinea pigs. Perhaps the removal of the progesterone implants provides the same function as the onset of luteolysis which in turn halted the suppression of gonadotropins caused by chronic progesterone treatment, resulting in synchronized

ovulation within 5-6 days. These findings indicate, therefore, that long-term implantation of progesterone tubing, greater than 14 days, given at any estrous stage of female guinea pigs induces the synchronized ovulation within 5-6 days after the removal of progesterone tubing.

Present study resulting in the synchronized ovulation in female guinea pigs gives first step to control a scheduled supply of animals with good uniformity. However, the following step has been remained: whether the animals synchronously ovulated using this method have normal reproductive activities, i. e. copulation, pregnancy, parturition, and lactation.

ACKNOWLEDGMENT

The authors are grateful to Dr. Y. Shirasu, Toxicology Division, Institute of Environmental Toxicology, Tokyo, for his valuable advice and suggestions during this study.

REFERENCES

- 1 Everett, J. W. (1944) Evidence in the normal albino rat that progesterone facilitates ovulation and corpus luteum formation. *Endocrinology*, **34**: 136-137.
- 2 Everett, J. W. (1948) Progesterone and estrogen in the experimental control of ovulation time and other features of the estrous cycle in the rat. *Endocrinology*, **43**: 389-405.
- 3 Leuter, L. A., Ciaccio, L. A. and Lisk, R. D. (1970) Progesterone: Regulation of estrous cycle, ovulation and estrous behavior in the golden hamster. *Endocrinology*, **86**: 1287-1297.
- 4 Reuter, L. A. and Lisk, R. D. (1973) A biphasic effect of progesterone on ovulation in the hamster. *Fed. Proc.*, **32**: 230.
- 5 Greenwald, G. S. (1977) Exogenous progesterone: Influence on ovulation and hormone levels in the cyclic hamster. *J. Endocrinol.*, **73**: 151-155.
- 6 Joslyn, W. D., Wallen, K. and Goy, R. W. (1976) Advancement of ovulation in the guinea-pig with exogenous progesterone and related effects on length of the oestrous cycle and life span of the corpus luteum. *J. Endocrinol.*, **70**: 275-283.
- 7 O'Mary, C. C., Pope, A. L. and Casida, L. E. (1950) The use of progesterone in the synchronization of the estrual periods in a group of ewes and the effect on their subsequent lambing records. *J. Anim. Sci.*, **9**: 499-503.
- 8 Christian, R. E. and Casida, L. E. (1948) The effects of progesterone in altering the estrous cycle of the cow. *J. Anim. Sci.*, **7**: 540.
- 9 Ulberg, L. C., Grummer, R. H. and Casida, L. E. (1951) The effects of progesterone upon ovarian function in gilts. *J. Anim. Sci.*, **10**: 665-671.
- 10 Baker, L. N., Ulberg, R. H. and Casida, L. E. (1954) Inhibition of heat by progesterone and its effect on subsequent fertility in gilts. *J. Anim. Sci.*, **13**: 648-657.
- 11 Woody, C. O., First, N. L. and Pope, A. L. (1967) Effect of exogenous progesterone on estrous cycle length. *J. Anim. Sci.*, **26**: 139-141.
- 12 Biegon, A., Parsons, B., Krey, L. C., Kamel, F. and McEwen, B. S. (1983) Behavioral and neuroendocrine effects of long-term progesterone treatment in the rat. *Neuroendocrinology*, **37**: 332-335.
- 13 Donovan, B. T. and Lockhart, A. N. (1972) Light and the timing of ovulation in the guinea-pig. *J. Reprod. Fertil.*, **30**: 207-211.
- 14 Young, W. C., Myers, H. I. and Dempsey, E. W. (1933) Some data from a correlated anatomical, physiological and behavioristic study of the reproductive cycle in the female guinea pig. *Am. J. Physiol.*, **105**: 393-398.
- 15 Hermreck, A. S. and Greenwald, G. S. (1964) The effects of unilateral ovariectomy on follicular maturation in the guinea pig. *Anat. Rec.*, **148**: 171-176.
- 16 Ginther, O. J. (1967) Length of estrous cycle and size of corpus luteum in guinea pigs and sheep treated with progesterone at different days of the estrous cycle. *Am. J. Vet. Res.*, **30**: 1975-1978.
- 17 Reed, M. and Hounslow, W. F. (1971) Induction of ovulation in the guinea pig. *J. Endocrinol.*, **49**: 203-211.
- 18 Donovan, B. T. and Lockhart, A. N. (1972) Gonadal hormones and the control of ovulation in the guinea pig. *J. Endocrinol.*, **55**: 599-607.
- 19 Rawson, J. M. R., Galey, C. I., Weinberg, L. C. and Hodgson, B. J. (1979) Effect of gonadotropins on follicular development, ovulation, and atresia in the mature guinea pig. *Hormone Res.*, **10**: 25-36.
- 20 Terranova, P. F. and Greenwald, G. S. (1981) Increased ovulation rate in the cyclic guinea pig after a single injection of an antiserum to LH. *J. Reprod. Fertil.*, **61**: 37-42.
- 21 Garza, F., Shaban, M. A. and Terranova, P. F. (1984) Luteinizing hormone increases the number of ova shed in the cyclic hamster and guinea pig. *J. Endocrinol.*, **101**: 289-298.
- 22 Tso, E. C. and Tam, W. H. (1977) The effect of continuous treatment with prostaglandin F-2 α on oestrous cycle length and corpus luteum regression in hysterectomized guinea-pigs. *J. Reprod. Fertil.*, **50**: 335-336.

Neuroendocrine Regulation of the Development of Seasonal Morphs in the Asian Comma Butterfly, *Polygonia c-aureum* L.: Difference in Activity of Summer-morph-producing Hormone from Brain-extracts of the Long-day and Short-day Pupae

KATSUHIKO ENDO, TADAKATSU MASAKI and KANJI KUMAGAI¹

Environmental Biology Laboratory, Biological Institute, Faculty of Science, and ¹Biological Institute, Faculty of Liberal Arts, Yamaguchi University, Yamaguchi 753, Japan

ABSTRACT—Seasonal morphs of the butterfly, *Polygonia c-aureum* L., were shown to be determined by a factor producing summer morphs (SMPH). The factor, which was extracted with 2% NaCl from the brains of *Polygonia* pupae, but unsuccessful with acetone or 80% ethanol, was thought to be a peptide hormone. The factor present in the 2%-NaCl extracts was precipitated by ammonium sulfate at 80% saturation. The summer-morph-producing activity was evaluated by injecting extracts containing a sufficient amount of the factor into the abdomen of 0-day-old pupae of autumn-morph producers. The recipients showed a dose-dependence in response to the factor (manifestation of characteristics of summer morphs). The factor was present in the pupal brains of both summer-morph and autumn-morph producers (LD- and SD-pupae). The quantity of SMPH present in the brains of 0-day-old pupae of autumn-morph producers seemed to be larger than in those of summer-morph producers of the same age. Sexual differences in the quantity of the factor also seemed to exist in the summer-morph producers. Furthermore, the SMPH-activity was detected from the brain-extracts of *Papilio xuthus*, *Lycaena phlaeas daimio* and *Bombyx mori*.

INTRODUCTION

The Asian comma butterfly, *Polygonia c-aureum* L., exhibits seasonal dimorphism, i. e. summer and autumn morphs (Fig. 1). The seasonal-morph development is governed by photoperiod and temperature during the larval stage as has been reported in previous papers [1, 2].

The physiological mechanism underlying the photoperiodic control of seasonal-morph determination was shown to involve a factor producing summer morphs (SMPH). The neurosecretory cells responsible for the factor are present in the pars intercerebralis of the brain. The factor is then conveyed along the axons and released into the hemolymph from the corpora cardiaca and/or corpora allata in the early pupal stage [3, 4].

The present study was designed to establish

methods of extraction of the factor showing SMPH-activity and of bioassay using *Polygonia* pupae. The study was extended to see whether or not the quantity of the factor varies according to the sex of the donors or to photoperiodic conditions under which the donors developed from the egg stage. Subsequently, some preliminary experiments were carried out to assess whether or not the factor showing SMPH-activity is present in the brain of other lepidopteran insects.

MATERIALS AND METHODS

Animals Eggs and larvae of the butterflies, *P. c-aureum*, *Papilio xuthus* and *Lycaena phlaeas daimio*, and those of the silkworm, *Bombyx mori*, were held in two kinds of transparent plastic containers (ϕ 9×5 cm³ or 19×13×5 cm³) and were exposed to either a long-day photoperiod alternating 16-hr light and 8-hr dark periods (16L-8D) or a short-day photoperiod of 8L-16D

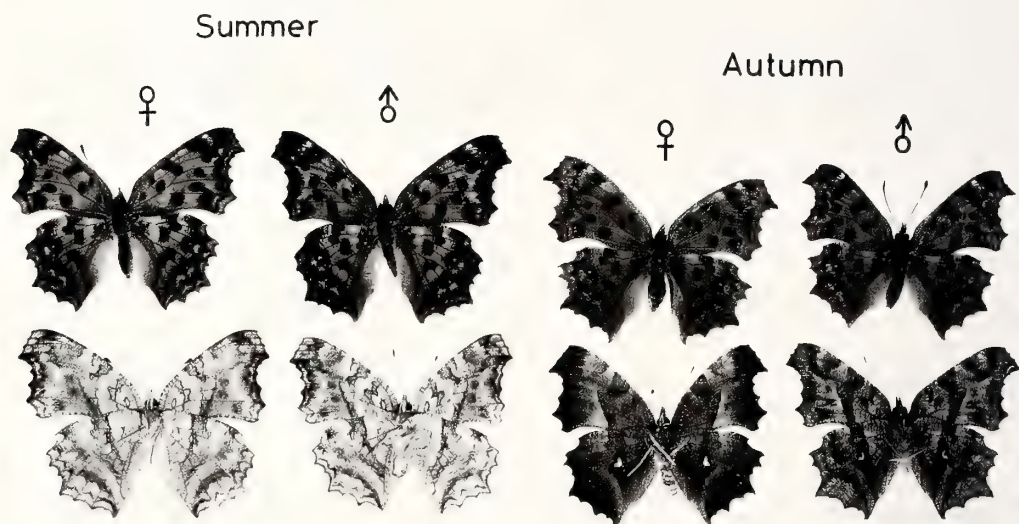


FIG. 1. Female and male butterflies of summer and autumn morphs. Butterflies in the upper row show the wing patterns of the dorsal side, whereas those in the lower row show the wing patterns of the ventral side.

at 20°C and 25°C. The larvae of *P. c-aureum* were fed on leaves of *Humulus japonicus*, whereas those of *P. xuthus*, *L. phlaeas daimio* and *B. mori* were fed on leaves of *Fagara ailanthoides*, *Rumex acetosa* and *Morus tiliaefolia*, respectively.

The rearing containers were placed in a cabinet with temperatures of either 20°C or 25°C and were illuminated by two 20-W white fluorescent tubes, which were controlled by a 24-hr time-switch. During the light period, the light-intensity was about 500 lux.

Under long-day conditions at 20°C and 25°C, larvae and pupae of *P. c-aureum* all developed into summer morphs, whereas under short-day conditions, they all developed into autumn morphs without exception.

Larvae and pupae developed from the egg stage under long-day conditions are referred to hereafter as LD-larvae and LD-pupae, whereas those developed under short-day conditions are referred to as SD-larvae and SD-pupae.

Extraction of SMPH Brains were obtained from 0-day-old *Polygonia* pupae (4–12 hr after larval-pupal ecdysis), and pharate pupae of *Papilio* and *Lycaena*, by dissection in saline (0.9% NaCl). Brains of the silkworm, *B. mori*, were also obtained in the same manner. One hundred brains from each species were grouped and stored at –85°C. Each 100-brain sample was homogenized in acetone (500 μ l \times 2) with a Teflon homogenizer at ice-bath temperature and was dried to powder under reduced pressure at room temperature (about 25°C). Then the sample was washed in 80% ethanol (100 μ l \times 2) and extracted with 2% NaCl (50 μ l \times 3) at ice-bath temperature. At each step insoluble materials were separated by centrifugation at 12,000 \times g for 30 min at 5°C. A supernatant of 2% NaCl was added with 84 mg of ammonium sulfate (80% saturation) to precipitate the factor and the precipitate was dissolved in distilled water to give an extract of 2%-NaCl. Washings with acetone and 80% ethanol were dried under re-

duced pressure at room-temperature and the residues were redissolved in saline (acetone and 80%-ethanol extracts).

Bioassay of SMPH-activity Five μ l of the sample containing the extract of 1- to 20-brain equivalents was injected into the abdomen of

0-day-old female *Polygonia* SD-pupae (4–12 hr after larval-pupal ecdysis). In controls, the 0-day-old female *Polygonia* SD-pupae were injected with saline containing 2.8 mg/5 μ l of ammonium sulfate (40% saturation) or distilled water. The injection was made through the ventro-

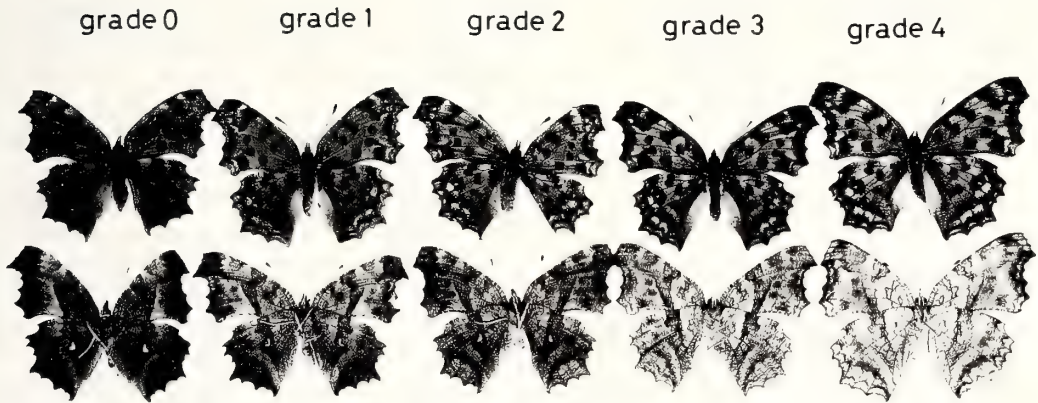


FIG. 2. Wing patterns of the female butterflies of each grade of summer-morphs (grades 0–4), upon which bioassay of summer-morph-producing hormone was performed. The butterflies arranged in the upper row show the wing patterns of the dorsal side, whereas those in the lower row show the wing patterns of the ventral side.

TABLE 1. Criteria for seasonal-morph classification on the basis of ventral-side wing color

Grades	Morphs	Characteristics
0	autumn	Ventral sides of the wings are mostly covered with dark-brown scales and dark-yellow scales are present only on the basal region of the wings.
1	autumn	Ventral sides of the wings are mostly covered with dark-brown scales, but dark yellow scales appear in the peripheral regions of the wings.
2	intermediate	A thick/dark-brown stripe remains on the ventral sides of the wings, but the other regions are mostly covered with light-brown scales.
3	summer	Ventral sides of the wings are mostly covered with dark-yellow scales, but a thick/brown stripe remains.
4	summer	The thick stripe becomes light brown and the other regions are mostly covered with dark-yellow scales.

lateral/intersegmental region between the 6th and the 7th abdominal segments.

On the day of emergence, the female butterflies were examined for the characteristics of summer morphs and classified into one of grades 0-4. An average grade score (AGS) for summer morphs was obtained from the response of 6-20 insects, the classification being based on a gradient of the color of the ventral side of the wings (Fig. 2, Table 1). Female butterflies of grade 0 and 1 were regarded as autumn morphs, those of grade 3 and 4 were regarded as summer morphs, and there were also intermediates of grade 2.

RESULTS

SMPH-activity in the brain-extracts of 0-day-old LD- and 0-day-old SD-pupae of P. c-aureum

Brain-extracts of 2% NaCl, acetone and 80% ethanol were provided from 0-day-old LD- and 0-day-old SD-pupae, and 5 μ l, containing the extract of 10-brain equivalents, were injected into the abdomen of 0-day-old female SD-pupae. For the control groups, the injection was made with either saline containing ammonium sulfate of 40% saturation (ca. 2.8 mg/5 μ l) or distilled water.

When 2%-NaCl extracts of the brains of LD-pupae were applied to 0-day-old female SD-pupae, the majority (24 out of 30) of the recipients responded and developed into summer or intermediate morphs. On the other hand, the recipient SD-pupae injected with acetone or 80%-ethanol brain-extract developed into autumn morphs of grade 0, as did the untreated controls and SD-pupae treated with either saline containing 2.8 mg/5 μ l of ammonium sulfate or distilled water (Table 2).

Similar results were also obtained by the injection with brain-extracts of 0-day-old SD-pupae. All SD-pupae receiving the 2%-NaCl extract of the brains of SD-pupae developed into summer morphs (grade 3 and 4). They recorded an AGS of 3.9 (average grade score for summer morph). They were judged as having more eminent characteristics of summer morphs than those injected with 2%-NaCl brain-extracts of LD-pupae (AGS 2.3). In contrast, the recipients of either acetone or 80%-ethanol brain-extracts of 0-day-old LD-pupae developed into autumn morphs of grade 0 (Table 2).

The results indicated that a factor showing the SMPH-activity is present in the brains of both 0-day-old SD- and 0-day-old LD-pupae of *P.*

TABLE 2. Effects of the brain-extracts of *Polygonia* pupae on the development of seasonal morphs

Source of extracts and extractants	No.	No. of butterflies classified into grades:					AGS
		0	1	2	3	4	
Control pupae							
Untreated	20	20	0	0	0	0	0.0
Distilled water	20	20	0	0	0	0	0.0
Saline (0.9% NaCl)	20	20	0	0	0	0	0.0
Saline containing 2.8 mg of (NH ₄) ₂ SO ₄	20	20	0	0	0	0	0.0
LD-pupae							
2% NaCl	30	2	4	9	12	3	2.1
Acetone	7	7	0	0	0	0	0.0
80% ethanol	22	22	0	0	0	0	0.0
SD-pupae							
2% NaCl	21	0	0	0	2	19	3.9
Acetone	19	19	0	0	0	0	0.0
80% ethanol	27	23	4	0	0	0	0.1

Each recipient injected with an extract of 10-brain equivalents.

c-aureum. The factor could be extracted with 2% NaCl and precipitated by adding ammonium sulfate at 80% saturation. However, the factor could not be extracted with acetone or 80% ethanol.

Dose-dependence of SMPH-activity in the 2%-NaCl extracts of the brains of LD- and SD-pupae (0-day-old)

Brain-extracts were made with 2% NaCl from 0-day-old LD- and 0-day-old SD-pupae and 5 μ l were injected into the abdomen of 0-day-old female SD-pupae. During these injections, the SD-pupae of each of the groups received a different dose of brain-extract (0- to 20-brain equivalents).

As is summarized in Figure 3, the recipient SD-pupae showed dose-dependent responses in AGS with brain-extracts of both LD- and SD-pupae. The dose eliciting a half response (AGS 2) was obtained by an extract containing 3-brain equivalents of SD-pupae. For a full response (AGS 4), the recipients required doses of extract larger than 10-brain equivalents. When injecting brain-extract of LD-pupae, the recipients required approximately 2-fold larger doses than with extracts of SD-pupae; the dose eliciting a half response (AGS 2) was obtained by an extract containing 5-brain equivalents of LD-pupae, but a dose of 20-brain equivalents was still insufficient for the induction of a full response (AGS 4).

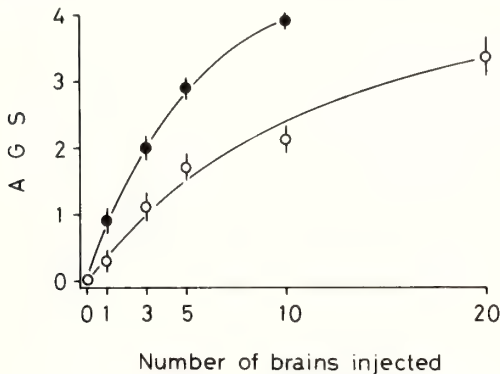


FIG. 3. Dose-response curves of SMPH obtained in the brain-extracts of 0-day-old SD- (solid circles) and 0-day-old LD-pupae (open circles). Each point depicts the AGS score (average grade score for summer morphs) with a standard error (thin vertical line) of about 20 females.

The results indicate that the quantity of factor in the brains of autumn-morph-producers (0-day-old SD-pupae) is approximately 2-fold larger than the factor in the brains of summer-morph-producers of the same age. However, the SMPH-rich brain of the autumn-morph-producer (0-day-old SD-pupa) does not seem to contain a sufficient amount of factor to produce a summer-morph butterfly (grade 4) from the pupa of an autumn-morph-producer (SD-pupa).

Sexual differences in the SMPH-activity of the brain-extracts of LD- and SD-pupae (0-day-old)

To clarify whether or not a sexual difference is present in the SMPH-activity of brain-extracts of LD- and SD-pupae, brain-extracts were made with 2% NaCl from 0-day-old male and 0-day-old female SD-pupae and precipitated by adding ammonium sulfate to 80% saturation. The precipitate was suspended in distilled water and 5 μ l containing the precipitate of 5-brain equivalents was injected into the abdomen of 0-day-old female SD-pupae. Brain-extracts were also made from male and female LD-pupae of the same age and 5-brain equivalents were injected into female SD-pupae in the same manner.

The brain-extract of female SD-pupae was found to show approximately the same relative SMPH-activity as the brain-extract of male SD-pupae. The recipient SD-pupae injected with extract of either male or female SD-pupae developed into summer-morph and intermediate-morph butterflies in addition to a few autumn-morph ones. They recorded AGS scores of 1.6 (male extract) and 1.5 (female extract) (Table 3).

Sexual differences in SMPH-activity were present in the brain-extracts of 0-day-old LD-pupae. The extract made from the brains of male LD-pupae showed a high SMPH-activity (AGS 1.5), almost corresponding to the activity of SMPH-rich extracts of the brains of SD-pupae (AGS 1.6 in male extract and AGS 1.5 in female extract). In contrast, the SMPH-activity of the brain-extract of female LD-pupae (AGS 0.6) was significantly lower than the SMPH-activity obtained with the brain-extract of male LD-pupae (Table 3).

The results indicate that a large amount of factor showing SMPH-activity is present in the brains of

TABLE 3. Sexual differences in the SMPH-activity of the brain-extracts of *Polygonia* long-day and short-day pupae

Source of extracts	No.	No. of butterflies classified into grades:					AGS
		0	1	2	3	4	
LD-pupae males	13	2	5	6	0	0	1.3
females	14	6	8	0	0	0	0.6
SD-pupae males	10	2	2	5	1	0	1.5
females	14	0	7	5	2	0	1.6

Each recipient was injected with an extract of 5-brain equivalents.

both male and female SD-pupae (0-day-old). In the brains of LD-pupae (0-day-old), however, sexual differences exist with regard to the quantity of factor; the amount present in the brains of 0-day-old male LD-pupae is approximately twice the amount present in the brains of female LD-pupae of the same age.

SMPH-activity in brain-extracts of other lepidopteran species

To assess whether or not factor showing SMPH-activity is present in the brains of other lepidopteran insects, brains were obtained from pharate pupae of two species of butterflies, *P. xuthus* and *L. phlaeas daimio*. The brains were homogenized in acetone, washed in 80% ethanol, extracted with 2% NaCl, and precipitated by adding ammonium sulfate to 80% saturation. Then the precipitate or

residue of evaporated washings (acetone and 80% ethanol) was dissolved in saline and 5 μ l containing the precipitate (or residue) of 20-brain equivalents was injected into the abdomen of female SD-pupae (0-day-old). Extracts were also made from the brains of diapause-egg producers (LD) of the silkmoth, *B. mori*, and 20-brain equivalents were injected into the abdomen of 0-day-old SD-pupae in the same manner.

Each 2%-NaCl extract made from the brains of *Papilio pharate-pupae* and *Lycaena pharate-pupae* showed SMPH-activity (AGS 0.9 and 0.6) when the extract was injected into the abdomen of *Polygonia* female SD-pupae (0-day-old). The majority of the recipient pupae injected with 2%-NaCl brain-extracts of pharate pupae of either *Papilio* or *Lycaena* produced butterflies having some characteristics of summer morphs. Howev-

TABLE 4. SMPH-activity in the brain-extracts of three species of lepidopteran insects

Source of extracts and extractants	No.	No. of butterflies classified into grades:					AGS
		0	1	2	3	4	
<i>Papilio xuthus</i> (pharate pupae)							
2% NaCl	10	3	5	2	0	0	0.9
80% ethanol	10	10	0	0	0	0	0.0
<i>Lycaena phlaeas daimio</i> (pharate pupae)							
2% NaCl	10	1	9	0	0	0	0.9
80% ethanol	10	10	0	0	0	0	0.0
<i>Bombyx mori</i> (adults)							
2% NaCl	9	0	0	2	3	4	3.2
80% ethanol	6	2	3	1	0	0	0.8

Recipient SD-pupae injected with an acetone brain-extract all developed into autumn morphs of grade 0.

er, the recipient SD-pupae injected with acetone extract or 80%-ethanol extract of the brains of *Papilio* or *Lycaena* pharate pupae did not show any response and developed into autumn morphs of grade 0 (Table 4).

Positive data were obtained by injection of two of the extracts (2% NaCl and 80% ethanol) made from the brains of the silkworm, *B. mori*. The recipient SD-pupae injected with 2% NaCl brain-extract developed into summer or intermediate morphs, whereas those injected with 80%-ethanol extract developed into butterflies having some characteristics of summer morphs (grades 1 and 2). They recorded AGS scores of 3.2 (2%-NaCl extract) and 0.9 (80%-ethanol extract), respectively, but the recipients of the acetone brain-extract all developed into autumn morphs of grade 0.

The results indicate that a factor showing the same SMPH-activity as the cerebral factor of *P. c-aureum* is present in the brains of three species of lepidopteran insects (*P. xuthus*, *L. phlaeas daimio* and *B. mori*). The factor can be extracted with 2% NaCl and precipitated by adding ammonium sulfate to 80% saturation as observed in the case of the factor of *P. c-aureum*. The SMPH-activity present in the brains of the silk-moth, *B. mori*, is approximately six times greater than the activity present in the brains of *Papilio* (or *Lycaena*) pharate pupae and is almost comparable to the activity of SMPH-rich brains of 0-day-old SD-pupae.

DISCUSSION

Summer-morph butterflies of *P. c-aureum* were shown to be produced by a neurosecretory factor (SMPH) which is secreted in the early pupal stage in summer-morph producers [3, 4]. The factor was present in the brains of both 0-day-old LD- and 0-day-old SD-pupae in this butterfly. It is thought to be a peptide hormone, since it was extracted with 2% NaCl but not with acetone or 80% ethanol. This theory is further supported by the fact that it was precipitated by raising the concentration of ammonium sulfate to 80% saturation.

Although we failed to evaluate the SMPH-activity remaining in the aqueous part of the ammonium-sulfate precipitation (80% saturation),

it appears to be negligible. One half of the SMPH-activity originally present in the brain-extracts (2% NaCl) was precipitated by raising the saturation of ammonium sulfate from 50% to 65% (unpublished data).

When the factor showing SMPH-activity is deprived from hemolymph in the early pupal stage, *Polytonia* pupae are thought to develop into autumn-morph butterflies [1, 3, 4]. It has been determined that SMPH-deprivation occurs in SD-pupae and the deprived state is thought to be achieved mainly by suppressing the secretion of the factor. On the other hand, in LD-insects, both production and secretion of the factor may be enhanced by long days. A large amount of factor is thought to be conveyed along axons, secreted into hemolymph hours following larval pupal ecdysis and it is believed that SMPH-activity remaining in the brains of 0-day-old LD-pupae becomes lower than one-twentieth the SMPH-activity required for summer-morph development.

In addition, sexual differences were present in the SMPH-activity of the brain-extracts of 0-day-old LD-pupae (Table 3). However, in LD-pupae, both male and female brains produce an equally large amount of the factor and are thought to secrete it into hemolymph until the hemolymph-titer of the factor satisfies an essential level for summer-morph development. Therefore, all LD-pupae succeed in developing into summer morphs. In contrast, *P. c-aureum* has an apparent sexual dimorphism in autumn morphs. It may be that females having darker colored wings than those of males as autumn morphs require an exposure to a higher titer of the factor than the males in the development of light-color-winged summer morphs. The high-titer flux is thought to be achieved by females secreting a larger quantity of the factor than males.

In *Papilio* and *Lycaena*, mechanisms underlying the photoperiodic control of seasonal morphs—spring and summer morphs—were also shown to involve a neuroendocrine factor (SMPH?) which is secreted from the brains of summer-morph producers in the pharate-pupal stage [5, 6].

The factor (?) was extractable with 2% NaCl from the brains of *Papilio* and *Lycaena* pharate-pupae, but not with acetone and 80%-ethanol, as

observed in the factor of *P. c-aureum*. The brains of the silkmoth, *B. mori*, were found to contain factor showing SMPH-activity in *P. c-aureum* and was able to be extracted with 2% NaCl and 80% ethanol. The brain-extract of the silkmoth was estimated to have a SMPH-activity six-times higher than the brain-extracts of *Papilio* (or *Lycaena*) pharate-pupae (Table 4).

We were unable to provide any evidence as to whether or not the factor extracted from the brains of *Papilio* and *Lycaena* pharate-pupae plays an essential role in the summer-morph development of these insects. However, we have concluded that a factor (peptide hormone?) showing the same effects as the *Polygonia* SMPH is present in the brains of several other lepidopteran insects and that the quantity may vary depending on the insect species from which the brains are obtained.

ACKNOWLEDGMENT

The authors wish to express their sincere gratitude to Professor A. Okajima and to Professor Y. Chiba of Yamaguchi University for advice and valuable suggestions during the course of this work. This work was supported in part by a grant from the Ministry of

Education, Science and Culture of Japan (No. 6154052).

REFERENCES

- 1 Fukuda, S. and Endo, K. (1966) Hormonal control of the development of seasonal forms in the butterfly, *Polygonia c-aureum* L. Proc. Japan Acad., **42**: 1082-1087.
- 2 Hidaka, T. and Takahashi, H. (1967) Temperature condition and maternal effect as modifying factor in the photoperiodic control of seasonal forms in *Polygonia c-aureum* (Lepidoptera, Nymphalidae). Annot. Zool. Japon., **40**: 200-204.
- 3 Endo, K. (1972) Activation of corpora allata in relation to ovarian maturation in the seasonal forms of the butterfly, *Polygonia c-aureum* L. Dev. Growth Differ., **14**: 263-274.
- 4 Endo, K. (1984) Neuroendocrine regulation of the development of seasonal forms of the Asian comma butterfly, *Polygonia c-aureum* L. Dev. Growth Differ., **26**: 217-222.
- 5 Endo, K. and Funatsu, S. (1985) Hormonal control of seasonal morph determination in the swallowtail butterfly, *Papilio xuthus* L. (Lepidoptera: Papilionidae). J. Insect Physiol., **31**: 669-674.
- 6 Endo, K. and Kamata, Y. (1985) Hormonal control of seasonal-morph determination in the small copper butterfly, *Lycaena phlaeas daimio* Seitz. J. Insect Physiol., **31**: 701-706.

Sexual Maturation in Female Wild Mice: Combined Effect of Adults' Urinary Chemosignals and Minimum Time of Exposure to Stimulus Substances for Bringing the Effects

SUBHASH C. PANDEY and SHEO D. PANDEY

Department of Zoology, Christ Church College, Kanpur, India

ABSTRACT—Young females exposed to urine of adult males attained puberty earlier than those exposed to urine of adult females. The puberty accelerating property of the male urine was masked when mixed with the urine of females either in ratio of 1:1 or 2:1. Further, puberty acceleration was initiated only when the young females were exposed to male urine for a minimum of 6 days. However, the puberty delay in subject females was not apparent by 6 days but was effectuated only after a long exposure of 9 days to female urine

INTRODUCTION

The age of puberty in mammals is thought to be determined by genetic factors and is specific for a particular species [1]. In addition to hereditary control over the onset of puberty, other factors such as nutrition and social stimuli also play an important role in scheduling the onset of puberty within the range of ages limited by heredity [2]. First oestrus is accelerated in young female mice caged with adult males relative to control females housed alone [3]. This effect is due to a male urinary pheromone [4] which acts synergistically with social cues associated with the physical presence of the male [5]. Several workers have replicated much of the accelerating effect by exposing the females to the urine collected from adult males [6-8].

In contrast to the ability of the adult male to accelerate sexual maturation in juvenile female mice, a pheromone of female origin is known to delay the maturation in the same sex [9]. McIntosh and Drickamer [10] reported that the delay of puberty in young female mice also occurs by exposure to urine collected from grouped adult females. Urine from socially isolated females is without effect on the time of puberty. However,

bladder urine of females invariably contains the maturation-delaying chemosignal irrespective of social condition [10].

Our laboratory studies have revealed that puberty in young female wild mice is also susceptible to social influences similar to its laboratory cousin. The causative factors are contained in urine of the adult individuals. The puberty-delaying chemosignal is released in the urine of females after housing them together for 15 days and a daily exposure of subject females to chemosignal, at least for 2 hr is needed for effective delay of puberty to occur [11]. The purpose of this study was to determine: (i) what is the resultant effect, if both puberty accelerating and delaying chemosignals are mixed, and (ii) how long the young females must be treated with these chemosignals for bringing about their respective effects.

MATERIALS AND METHODS

The experiments were carried out on wild mice, *Mus musculus domesticus*. The animals used in these experiments were wild trapped as the species usually avoids breeding in the laboratory. Mice weighing 12-16 g were used as adults while females of 4-5 g body weight were employed as youngs in the experiments. All animals were maintained in the laboratory at 28-34°C temperature with natural light-dark hours and fed on a diet

consisting of soaked Bengal gram (*Cicer arietinum*), boiled rice and milk. Water was supplied *ad libitum*. Young females were housed individually in galvanised steel cages, 34×18×14 cm, and were exposed to urine of adults as described in experiments I and II. The adult females were grouped in colony cages (30×30×30 cm) at a density of 10 mice/cage for 30 days before urine collection. The males remained isolated in steel cages for the same period. The urine was collected by placing the mice over a petridish and gently squeezing the abdomen, and diluted in distilled water, 1:9. A drop (0.5 ml) of diluted urine was applied on external nares of the subject females with the help of a small paintbrush twice daily at 9.00 and 17.00 hr.

Young subject females were examined daily from the start of experiment until the occurrence of vaginal perforation. Starting on the day of vaginal perforation, a vaginal lavage was taken daily and examined under microscope to determine the stage of the oestrous cycle, using the criteria of Bronson *et al.* [12] and Rugh [13]. The vaginal smears were examined until the occurrence of first oestrus. The data were analysed by one way analysis of variance.

Experiment I

To see the combined effect of male and female urinary chemosignals on puberty, 25 individually housed young females weighing 4.4 ± 0.28 g were randomly divided into 5 groups (5 mice/group). They were painted daily on their external nares

with water (control, group I) or urine from males (group II) or urine from females (group III) or mixed urines from males and females (1:1, group IV; 2:1, group V). The treatments continued till the occurrence of first vaginal oestrus.

Experiment II

In this experiment minimum time of exposure to stimulus substances for bringing the effects on puberty was observed. The experiment consisted of two parts. In one part, young females were exposed to male urine while in other part they were exposed to female urine. In each part there were 5 groups, each having 5 randomly selected young mice weighing 4.2 ± 0.23 g. Females in group I were treated with water for 12 days (control). The urine treatment was given for 3 days (group II), 6 days (group III), 9 days (group IV) or 12 days (group V). Vaginal smears were examined from all subjects until the occurrence of first vaginal oestrus.

RESULTS

Experiment I

Sexual maturation in young females as assessed by the time taken in occurrence of first vaginal oestrus was delayed by exposure to mixed urines in the same manner as if they were exposed to urine of adult females. Ages of first oestrus observed in groups III, IV and V were not significantly different with each other (C. D. = 2.08). Onset of

TABLE 1. Effect of exposure to urines collected from adult individuals or their mixtures on sexual maturation of young females (n=5/group)

Group	Treatment	Mean time (in days) taken for first vaginal oestrus to occur
I	Painted with water (control)	29.2±0.66
II	Painted with urine from adult males	21.2±0.63
III	Painted with urine from adult females	36.2±0.58
IV	Painted with male-female urine (1:1)	35.2±0.77
V	Painted with male-female urine (2:1)	34.6±0.46
		F=80.9**
		d.f.=4, 20
		C.D. at 5%=2.08

Means connected with same vertical line are at par at 5% level of significance.

TABLE 2. Exposure of young females (n=5/group) to stimulus substances for different duration and its effect on pubertal onset

Group	Treatment	Mean time (in days) taken for the occurrence of first vaginal oestrus in subject females exposed to water or to urine from	
		Male donors	Female donors
I	12 days exposure to water (control)	30.2±0.52	29.2±0.78
II	3 days exposure to urine	29.0±0.63	30.4±0.69
III	6 days exposure to urine	21.6±0.83	32.4±0.92
IV	9 days exposure to urine	20.2±0.51	35.8±0.52
V	12 days exposure to urine	20.6±0.45	36.4±0.60
		F=49.3**	F=16.2**
		d.f.=4, 20	d.f.=4, 20
		C.D. at 5%=2.05	C.D. at 5%=2.34

Means connected with same vertical line are at par at 5% level of significance.

puberty in females exposed to urine of adult males was significantly earlier ($P<0.01$) than those exposed to urine of adult females. The puberty accelerating effect of male urine was completely masked by female urine (even when the latter constituted only one third of the total mixed urine) as the young females exposed to mixed urines attained sexual maturity significantly later ($P<0.01$) than the control females (Table 1).

Experiment II

The time taken for the onset of puberty in females treated with male urine for 3 days was not significantly different from that of control (group I). By contrast, the first oestrus in females treated with male urine for 6 days occurred significantly earlier than control or 3 day-treated females. There was no significant difference in onset of puberty (i.e., occurrence of first oestrus) among females of groups III, IV and V treated with male urine for 6, 9 and 12 days respectively (Table 2).

In the second part of the experiment, the subjects treated with female urine for 3 or 6 days matured at about the same time at which the control ones. The occurrence of first oestrus was significantly delayed in females of group IV (9 days treatment). No further delay in puberty was observed by increasing the day of treatment (group V).

DISCUSSION

Following conclusions are derived from the foregoing pair of experiments: (1) The maturation-delaying chemosignal of female origin can override the male urinary factor causing puberty acceleration in young females. (2) Young females require exposure of, at least, 6 days to male urine or 9 days to female urine for puberty acceleration or delay to occur.

Investigations of the factors causing acceleration or delay in puberty in females have been focussed on laboratory strains of mice [3, 4, 7, 14]. Experiments conducted in our laboratory on wild mice have revealed that onset of puberty in females is a labile phenomenon in this species which is regulated by adults' chemosignal. Bronson and Maruniak [5] have reported that in addition to chemical stimuli, tactile cues also play some role in male-induced acceleration in young females. In an attempt to isolate the active fraction of urine accelerating puberty, it was shown that the substance is androgen dependent, heat labile and apparently associated with the protein fraction of the urine [15]. Jemiolo *et al.* [16] have recently synthesized and tested the analogs (2-(sec-butyl)-4, 5-dihydrothiazole and dehydro-exobrevicomin) of the male urinary factors involved in the Whitten effect in mice. How the acceleratory effect of male urine is suppressed by

female urine is not clear; the finding clearly indicate the high potency of female chemosignals in regulating puberty in juvenile females. It is to emphasize here that, though the male chemosignal is not effective over delaying substance of female origin, the former evokes the puberty accelerating process in prepubertal females by comparatively shorter exposure (Table 2).

Stimulatory and inhibitory pheromonal influences on puberty in juveniles living in population can not be examined separately because they are exposed to urine deposited by both males and females. One signal could overwhelm the other or two could be balanced in their action. Drickamer [17] reported that the inhibitory effect of the urine from grouped females takes precedence over urine source(s) that accelerates puberty. The sensitivity of juvenile females to the delay chemosignal from grouped females even in the presence of acceleratory signals from the males suggests that retardation of puberty may play an important role in modulating population growth. Massey and Vandenberg [18] while working on natural populations of mice, found that urine collected from females in dense population delayed puberty in test females; urine collected from females in sparse population failed to retard pubertal onset.

Drickamer [19] has reported that 4–7 days of treatment with urine containing the delay chemosignal is required for puberty delay to occur in laboratory mice. The wild *Mus* varies with its laboratory cousin as it requires a longer treatment, at least, of 9 days for puberty retardation. However, the puberty accelerating chemosignal of male origin is effective only by 6 days treatment. It seems that at low population density (when delaying chemosignal does not operate) male chemosignal accelerates the pubertal onset in juvenile females and promotes the population growth. When the density is increased, the females start retarding the sexual maturation in juvenile females. This phenomenon does provide a natural force for dispersal of individuals in a natural population. The shorter exposure time to male chemosignal for bringing the effect facilitates the quick propagation of the species.

ACKNOWLEDGMENT

Authors are grateful to the Department of Science and Technology, India for financial support and Council of Scientific and Industrial Research, New Delhi for a Senior Research Fellowship to SCP.

REFERENCES

- 1 Stone, C. P. and Barker, R. C. (1940) Change of the age of puberty in albino rats by selective mating. *Proc. Soc. Exp. Biol. Med.*, **44**: 48–50.
- 2 Vandenberg, J. G. (1983) Social factors controlling puberty in the female mouse. In "Hormones and Behaviour in Higher Vertebrates". Ed. by J. Balthazart, E. Prove and R. Gilles, Springer-Verlag, Berlin, pp. 342–349.
- 3 Vandenberg, J. G. (1967) Effect of the presence of a male on the sexual maturation of female mice. *Endocrinology*, **81**: 345–349.
- 4 Vandenberg, J. G. (1969) Male odour accelerates female sexual maturation in mice. *Endocrinology*, **84**: 658–660.
- 5 Bronson, F. H. and Maruniak, J. A. (1975) Male-induced puberty in female mice: evidence for a synergistic action of social cues. *Biol. Reprod.*, **13**: 94–98.
- 6 Cowley, J. J. and Wise, D. R. (1972) Some effects of mouse urine on neonatal growth and reproduction. *Anim. Behav.*, **20**: 499–506.
- 7 Colby, D. R. and Vandenberg, J. G. (1974) Regulatory effects of urinary pheromones on puberty in the mouse. *Biol. Reprod.*, **11**: 268–279.
- 8 Drickamer, L. C. and Murphy, R. X. (1978) Female mouse maturation: effects of excreted and bladder urine from juvenile and adult males. *Dev. Psychobiol.*, **11**: 63–72.
- 9 Vandenberg, J. G., Drickamer, L. C. and Colby, D. R. (1972) Social and dietary factors in the sexual maturation of female mice. *J. Reprod. Fertil.*, **28**: 397–405.
- 10 McIntosh, T. K. and Drickamer, L. C. (1977) Excreted urine, bladder urine and the delay of sexual maturation in female house mice. *Anim. Behav.*, **25**: 999–1004.
- 11 Pandey, S. C. and Pandey, S. D. (1986) Stimulus exposure time and period of grouping of donors required for the release of pheromonal cues delaying puberty in young female wild mice. *Zool. Sci.*, **3**: 687–690.
- 12 Bronson, F. H., Dagg, C. P. and Snell, G. D. (1966) Reproduction. In "Biology of Laboratory Mouse". Ed. by E. L. Green, McGraw Hill Book Co., New York, 2nd ed., pp. 187–204.
- 13 Rugh, R. (1968) *The Mouse; its Reproduction and*

- Development. Burgess Publ. Co., Minneapolis.
- 14 Drickamer, L. C. (1974) Sexual maturation of female house mice: Social inhibition. *Dev. Psychobiol.*, **7**: 257-265.
 - 15 Vandenberg, J. G., Whitsett, J. M. and Lombardi, J. R. (1975) Partial isolation of a pheromone accelerating puberty in female mice. *J. Reprod. Fertil.*, **43**: 515-523.
 - 16 Jemiolo, B., Harvey, S. and Novotny, M. (1986). Promotion of the Whitten effect in female mice by synthetic analogs of male mouse urinary constituents. *Proc. Natl. Acad. Sci. USA.*, **83**: 4576-4579.
 - 17 Drickamer, L. C. (1982) Acceleration and delay of first vaginal oestrus in female mice by urinary chemosignals: dose levels and mixing urine treatment sources. *Anim. Behav.*, **30**: 456-460.
 - 18 Massey, A. and Vandenberg, J. G. (1980) Puberty delay by a urinary cue from female house mice in feral populations. *Science*, **209**: 821-822.
 - 19 Drickamer, L. C. (1977) Delay of sexual maturation in female house mice by exposure to grouped females or urine from grouped females. *J. Reprod. Fertil.*, **51**: 77-81.

Sexual Interference in the Alpine Newt, *Triturus alpestris* (Amphibia, Urodela, Salamandridae)

PAUL A. VERRELL¹

Department of Biology, The Open University, Milton Keynes, U.K.

ABSTRACT—This paper describes sexual interference (a form of intermale competition) in the alpine newt, *Triturus alpestris*. When a male encounters a female already engaged in courtship, he may interfere with the courting male's attempts to inseminate her. The rival displays to the female and may inseminate her himself. The courting male may respond to sexual interference by displaying to the rival and leading him away from the female; this behavior can be interpreted as sexual defense. Females can be multiply inseminated as a consequence of sexual interference, although they frequently flee from competitively interacting males. Sexual interference in *T. alpestris* appears to be less complex than that of the congeneric smooth newt, *T. vulgaris*.

INTRODUCTION

Competition between males for access to females is ubiquitous in the animal kingdom, and is an important selective agent in the evolution of both morphological and behavioral characters of males [1, 2]. The nature of such competitive interactions within any one species depends, at least in part, on its mode of fertilization. In the majority of urodele amphibians, fertilization is internal but sperm transfer is indirect; a spermatophore is usually deposited on the substrate during the latter stages of courtship [3]. In many urodele species, the male does not physically sequester the female during the spermatophore deposition and transfer stage of courtship, and the pair are thus susceptible to attention from other males at this time. If a male encounters a pair already engaged in courtship, he may interfere with the efforts of the courting male to inseminate the female. Such sexual interference has been described in a number of urodele species [4-7] and, in many, the interfering male mimics behavior normally shown by a sexually responsive

female as the courting male initiates the latter stages of courtship. The interferer may, for example, stimulate the tail of the courter tactually, causing the latter to deposit a spermatophore which will not be picked up by a female. The interferer may then deposit a spermatophore of his own, with which the female can become inseminated. By adopting this strategy of sexual interference by female mimicry, the interfering male may obtain an insemination without first investing in a period of courtship display [4-7].

Newts of the European genus *Triturus* exhibit courtship behavior in which there is very little physical contact between partners [8]. In the smooth newt, *T. vulgaris*, sexual interference by female mimicry is commonly seen between males in the laboratory [7]. It also occurs in natural populations during those parts of the breeding season when sexually responsive females are fewest in number [9, 10]. Field observations indicate that similar intermale behavior occurs in the crested newt, *T. cristatus* [11; Verrell, unpubl. data]. Sexual interference in the alpine newt, *T. alpestris*, is described in the present paper, and is compared with that exhibited by congeneric newts.

Accepted July 21, 1987

Received June 27, 1987

¹ Present address: Allee Laboratory of Animal Behavior, Department of Biology, University of Chicago, 940 East 57th Street, Chicago, Illinois 60637, U.S.A.

MATERIALS AND METHODS

The alpine newts used in this study were taken from two introduced populations in southern

England (one in Sussex, the other in Northamptonshire). The species occurs naturally in the northwestern part of mainland Europe [12]. Five males and five females were obtained from each population, and all of these newts remained in breeding condition during the course of this study (i.e. the males had well-developed secondary sexual characters and the females were gravid with eggs).

In the laboratory, the newts were maintained in single-sex aquaria measuring $32 \times 30 \times 30$ cm. Food was provided *ad libitum*, and consisted of *Tubifex* and chopped earthworms (*Lumbricus*). The water in these aquaria was neither filtered nor aerated, and ranged in temperature from 15 to 20°C. The photoperiod to which the newts were exposed was made to track the natural (Milton Keynes) light-dark cycle.

All observations were made during spring 1986 in an aquarium measuring $32 \times 30 \times 30$ cm, floored with gravel overlaid with fine sand. The water in the aquarium was neither filtered nor aerated, and ranged in temperature from 18 to 22°C.

A female and two males were placed in the aquarium at approximately 17:00 hr, and all interactions between the three individuals were recorded on videotape (Panasonic video tape recorder VTR-NV-8030) for a continuous period of about 14 hr, using a timelapse facility (recording interval 0.18 sec, as against 0.02 sec for normal speed). A total of 15 trios were recorded in this way, the trios consisting of unique combinations of individuals drawn from the available pool of newts. In addition, five pairs were placed together and their behavior recorded (as described above) in order to gain a first-hand impression of the normative courtship of this species.

RESULTS

Sexual behavior between single males and females

A brief account is given, for comparison, of the sexual behavior of single male and female pairs of *T. alpestris* (for more detailed descriptions, see [8, 13–15]).

The courtship of *T. alpestris* differs markedly from that of congeneric newts. After a period of

“orientation”, during which the male attempts to assume a position in front of the female, there follows a long period of “static display”. During this period, the male remains stationary in front of the female and “fans” his tail towards her. Fanning is a single, stereotyped tail movement which produces water currents which probably stimulate the female tactually and olfactorily, carrying secretions produced by glands in the cloaca of the male. Provided the female does not flee during static display, the male then turns away from her and initiates spermatophore deposition and transfer behavior. The male “creeps” in front of the female, quivering his tail, and after a few seconds, deposits a spermatophore on the substrate in front of her. Although the female often nudges at the base of the male’s tail with her snout to elicit spermatophore deposition, such tactile stimulation seems less necessary in *T. alpestris* than it is in other newts (Verrell, personal observation). The male then “creeps-on” away from the female for a distance of about one body-length and turns to block her path as she follows him. This ends the first sequence of the courtship encounter. The sperm mass may or may not be picked up in the cloaca of the female at this time. The male may then creep again, thus initiating a second sequence of spermatophore deposition and transfer behavior. This usually occurs without the male reverting to an intervening period of display. As many as three spermatophores may be deposited during a single courtship encounter (i.e., three sequences may be completed).

Sexual interference

Fifty three discrete sexual encounters involving interactions between males were extracted from the videotape records for the 15 trios whose behavior was recorded (mean ± 1 SD number of encounters per trio was 3.5 ± 1.7). In all of these encounters, one male, hereafter called “the courter”, began to court the female. The other male was thus given the status of “the rival”. Close inspection of the videotape records revealed seven basic behavior patterns which occur in the context of competitive sexual encounters. These are as follows:

- 1) *Rival approaches pair*: the rival moves

towards a male and female already engaged in courtship. His first response on contact is usually to nudge either or both of the courting newts with his snout.

2) *Rival displays to female*: the rival fans his tail in the direction of the female.

3) *Rival displays to courter*: the rival fans his tail in the direction of the courter; either of the males may initiate display, which may be mutual.

4) *Rival creeps*: by creeping in front of the female, the rival initiates spermatophore deposition and transfer behavior.

5) *Female stays*: the female remains with the rival, following him as he moves into creep-on.

6) *Female leaves*: the female moves away from the two males. Her action appears to be deliberate, and she remains on the substrate some distance from the males. Moving away of this type is not immediately followed by the female ascending to the water surface in order to breathe.

7) *Males leave*: the courter and rival move away from the female, fanning towards one another as they go.

Figure 1 summarizes the frequency with which rival males were observed to proceed from one stage of a competitive sexual encounter to another. Of the 53 approaches made by rivals towards courting pairs, 40 (75.5%) were made after the female had completed one prior courtship sequence with the courter, 9 (17%) after she had completed two sequences and 4 (7.5%) after the

completion of three prior sequences. Forty out of the 53 (75.5%) encounters terminated when either the female or males left after a period of fanning display. In only 11 (21%) encounters did the rival male creep in front of the female, and in only 4 of these did the female remain with the rival during creep-on. In none of these encounters did the female nudge the rival's tail before he entered creep-on, suggesting that if he deposited a spermatophore, he did so in the absence of tactile stimulation. Unfortunately, the optical resolution of the video equipment used in this study was not sufficiently high to record the presence or absence of a spermatophore on the substrate. Therefore, it is concluded that only 4 (7.5%) of the 53 competitive sexual encounters observed potentially could have resulted in the insemination of the female by the rival male.

The rival appeared to assess the behavior of the courter during an encounter, as judged by the behavior he exhibited towards a courting pair. Consider the courtship behavior of *T. alpestris* as consisting of two phases: static display and spermatophore deposition and transfer (creep and creep-on). There are thus two types of behavior available to each male in a trio. In 31 encounters in which the courter was displaying, the rival responded with his own display in 28 (90%) and creeping in front of the female in 3 (10%). In 22 encounters in which the courter was creeping, the rival also crept in 8 (36%) and displayed in 14 (64%). The rival male was significantly more likely to display himself when the courter was also displaying ($\chi^2=20.16$, $P<0.001$), but not more likely to creep himself when the courter was also creeping ($\chi^2=1.64$, $P>0.1$).

Sexual defense

In the face of sexual interference of the form described above, the courting male is expected to retaliate with behavior patterns whose function is to defend the female [4, 5]. Subtle alterations in the temporal patterning of the courter's behavior were not monitored during this study, although they may play an important role in sexual defense [7]. More obvious behavioral responses which might function in the context of sexual defense were observed. First, 28% of all competitive

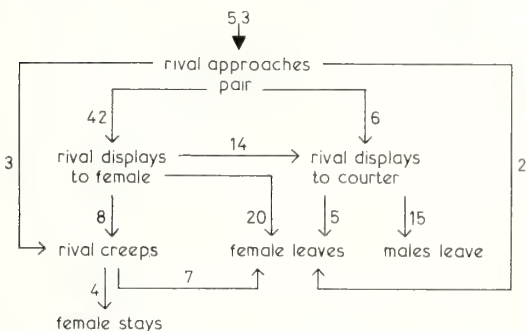


FIG. 1. Sequence diagram showing the frequency of behavioral transitions during competitive sexual encounters between trios consisting of two male and one female *Triturus alpestris*. See text for further information and for detailed descriptions of the behavior patterns involved.

encounters terminated when the courter and rival moved away from the female, displaying to one another (see Fig. 1). Of the 15 encounters in which this occurred, the courter initiated the move in 11 (73%) cases. Secondly, during one encounter, the courter appeared to lead the female away from the rival by moving backwards away from her as he displayed: she followed him. This action closely resembled "retreat display" seen in the smooth newt (see Discussion).

DISCUSSION

When a male alpine newt encounters a female already engaged in courtship, he may interfere with the efforts of the courting male to inseminate his partner. As shown in Figure 1, the rival usually initiates such interference by displaying to the female, which may then lead him to display to the courter. Most competitive sexual encounters break down at this point, either because the female moves away from the males or because the males leave the female. If the female remains close to the rival as he displays, he may initiate spermatophore deposition and transfer behavior. From a position close to the female, the rival creeps, apparently waiting for her to touch his tail with her snout. Even if such stimulation is not provided, a spermatophore may be deposited. Because spermatophores could not be seen on the substrate, definite instances of deposition and pick up could not be determined. However, as judged by the behavior of the rival, it is concluded that the probability of insemination by the rival as a consequence of sexual interference was no greater than 7.5%. Sexual interference in *T. alpestris* can thus be considered a "side-payment" conditional mating strategy [16–18]. Individuals pursue a primary, high-gain strategy of courtship, but will accept lower gains by adopting the subsidiary strategy of sexual interference should opportunities for the latter arise (see also [7]).

Female *T. alpestris* had always completed at least one sequence of courtship with the courter prior to the approach of the rival. It is thus likely that sexual interference will sometimes lead to the insemination of the female by both of the males attending her (first the courter, then the rival).

Rafinski [19] found that a high proportion (17 out of 18) of female alpine newts collected in the field laid clutches which showed multiple paternity (as determined by electrophoretic analysis). Multiple insemination due to sexual interference may be responsible for at least some instances of multiple paternity in this species. Multiple insemination may also lead to sperm competition, another manifestation of competition between males. Sperm competition has been demonstrated only in one species of plethodontid salamander [20], but is likely to occur in many species, including newts [21].

Sexual interference in *T. alpestris* differs markedly from that observed in the smooth newt, *T. vulgaris*, the only congener for which detailed descriptive data are available. In the latter species, a rival male seldom expends time and energy in displaying to a female already engaged in courtship [7], and usually interferes just as the courter initiates creep. By interposing himself between the partners, the rival nudges the courter's tail (female mimicry), causing him to deposit a profitless spermatophore, and then creeps himself [7]. In *T. alpestris*, most competitive sexual encounters begin with the rival displaying to the female (Fig. 1). If the encounter continues long enough for the courter to creep, the rival does not mimic female behavior by nudging his tail before creeping himself. These two major differences suggest that the sexual interference behavior of *T. vulgaris* is more derived than that of *T. alpestris*; the former involves less expenditure of energy by the rival and occurs at a time when the courter is "locked" into the relatively stereotyped behavior which follows spermatophore deposition [7, 22]. In addition, the observed probability of successful insemination by a rival is 20% in *T. vulgaris* [7], compared with a lower predicted maximum of 7.5% for *T. alpestris*.

Another reason why the sexual interference behavior of *T. alpestris* seems less derived than that of *T. vulgaris* concerns the apparent absence of well-defined sexually defensive behavior in the former species. Such behavior functions to defend the courting male against the deleterious effects of interference [4, 5]; interference and defense are expected to coevolve as a competitive arms race [23]. In *T. vulgaris*, the most obvious response of a

courting male to the threat of interference is to increase the duration of the "retreat display" stage of courtship. Verrell [7] interpreted this increase as an attempt to draw the female away from the rival male. Retreat display is absent from the repertoire of *T. alpestris*, and aside from one instance of behavior that could be interpreted as leading, the only other behavior that could be considered as defensive in function is male-male display. As discussed above, most instances of male-male display were initiated by the courter and resulted in both males moving away from the female. In the laboratory, this ended the courtship encounter, but in the field the courter may return to the female having driven the rival away. Field observations of mating behavior in natural alpine newt populations are needed to test this hypothesis.

One important similarity between *T. alpestris* and *T. vulgaris* concerns the response of the courting female to sexual interference. In the latter species, the female often flees as soon as the rival approaches and is thus lost to both males [7]. This seems to be as much a function of the density of males in her vicinity as of the behavior of those males [24]. A similar aversion is apparent in female *T. alpestris*; in only 11 (20.75%) of the 53 encounters did the female stay long enough for the rival to creep, and in no cases did she stay long enough for the rival to creep more than once.

Comparative analysis of the sexual behavior of newts in the genus *Triturus* led Halliday [8] to propose a tentative phylogeny of this taxon. The single tail display (fan) and absence of retreat display in *T. alpestris* suggest that its courtship is closer to that of the ancestral type than are the more derived courtship behavior patterns of other, well-studied species (*T. vulgaris*, *T. helveticus* and *T. cristatus*). I suggest that the rather unstructured nature of sexual interference in *T. alpestris*, as described in this paper, is further evidence that the behavior of this species is less derived than that of its congeners. Detailed studies of competitive interactions between male newts in other *Triturus* species are needed to provide a proper test of this hypothesis.

ACKNOWLEDGMENTS

This work was supported financially by grants from the Open University Research Committee and the National Science Foundation (BSR 8506766). I am most grateful to Trevor Beebee and Kenneth Blackwell for kindly lending me the alpine newts. I also thank Lynne Houck, Norah McCabe, Steve Arnold, Tim Halliday and Chris Raxworthy for helpful discussion and comments on the manuscript.

REFERENCES

- 1 Darwin, C. (1871) *The Descent of Man and Selection in Relation to Sex*. John Murray, London.
- 2 Wilson, E. O. (1975) *Sociobiology: The New Synthesis*. Belknap Press, Harvard, Massachusetts.
- 3 Salthe, S. N. (1967) Courtship patterns and the phylogeny of the urodeles. *Copeia*, **1967**: 100-117.
- 4 Arnold, S. J. (1976) Sexual behavior, sexual interference and sexual defense in the salamanders *Ambystoma maculatum*, *Ambystoma tigrinum* and *Plethodon jordani*. *Z. Tierpsychol.*, **42**: 247-300.
- 5 Arnold, S. J. (1977) The evolution of courtship behavior in New World salamanders with some comments on Old World salamandrids. In "The Reproductive Biology of Amphibians". Ed. by D. H. Taylor and S. I. Guttman, Plenum Press, New York, pp. 141-183.
- 6 Verrell, P. A. (1983) The influence of the ambient sex ratio and intermale competition on the sexual behavior of the red-spotted newt, *Notophthalmus viridescens* (Amphibia: Urodela: Salamandridae). *Behav. Ecol. Sociobiol.*, **13**: 307-313.
- 7 Verrell, P. A. (1984) Sexual interference and sexual defense in the smooth newt, *Triturus vulgaris* (Amphibia, Urodela, Salamandridae). *Z. Tierpsychol.*, **66**: 242-254.
- 8 Halliday, T. R. (1977) The courtship of European newts. An evolutionary perspective. In "The Reproductive Biology of Amphibians". Ed. by D. H. Taylor and S. I. Guttman, Plenum Press, New York, pp. 185-232.
- 9 Verrell, P. and Halliday, T. (1985) Reproductive dynamics of a population of smooth newts, *Triturus vulgaris*, in southern England. *Herpetologica*, **41**: 386-395.
- 10 Verrell, P. A. and McCabe, N. R. Field observations of the sexual behaviour of the smooth newt, *Triturus vulgaris vulgaris* (Amphibia: Salamandridae). *J. Zool.*, London. (In press)
- 11 Zuiderwijk, A. and Sparreboom, M. (1986) Territorial behaviour in crested newt *Triturus cristatus* and marbled newt *T. marmoratus* (Amphibia, Urodela). *Bij. Dierkunde*, **56**: 205-213.

- 12 Steward, J. W. (1969) The Tailed Amphibians of Europe. David and Charles, Newton Abbot, England.
- 13 Finkler, W. (1923) Analytical studies on the factors causing sexual display in the mountain newt (*Triturus alpestris*). Proc. R. Soc. Lond., Ser. B, **95**: 356-364.
- 14 Meissner, K., Rohler, E. and Rohler, L. (1983) Zur Balz des Bergmolches, *Triturus alpestris*: 1. Aqu. Terr., **6**: 210-213.
- 15 Meissner, K., Rohler, E. and Rohler, L. (1983) Zur Balz des Bergmolches, *Triturus alpestris*: 2. Aqu. Terr., **7**: 245-248.
- 16 Dawkins, R. (1980) Good strategy or evolutionarily stable strategy? In "Sociobiology: Beyond Nature/Nurture?". Ed. by G. W. Barlow and J. Silverman, Westview Press, Colorado, pp. 331-367.
- 17 Davies, N. B. (1982) Alternative strategies and competition for scarce resources. In "Current Problems in Sociobiology". Ed. by King's College Sociobiology Group, Cambridge Univ. Press, Cambridge, pp. 363-380.
- 18 Dunbar, R. I. M. (1982) Intraspecific variations in mating strategy. In "Perspectives in Ethology, Vol. 5". Ed. by P. P. G. Bateson and P. H. Klopfer, Plenum Press, New York, pp. 385-431.
- 19 Rafinski, J. (1981) Multiple paternity in natural populations of the alpine newt, *Triturus alpestris* (Laur.). Amphibia-Reptilia, **2**: 282.
- 20 Houck, L. D., Tilley, S. G. and Arnold, S. J. (1985) Sperm competition in a plethodontid salamander: preliminary results. J. Herpetol., **19**: 420-423.
- 21 Halliday, T. R. and Verrell, P. A. (1984) Sperm competition in amphibians. In "Sperm Competition and the Evolution of Animal Mating Systems". Ed. by R. L. Smith, Academic Press, New York, pp. 487-508.
- 22 Halliday, T. R. (1974) Sexual behavior of the smooth newt, *T. vulgaris*. J. Herpetol., **8**: 277-292.
- 23 Dawkins, R. and Krebs, J. R. (1979) Arms races between and within species. Proc. R. Soc. Lond., Ser. B, **205**: 489-511.
- 24 Verrell, P. A. (1984) Responses to different densities of males in the smooth newt, *Triturus vulgaris*: "one at a time, please". J. Herpetol., **18**: 482-484.

Land Hermit Crabs from the Ryukyus, Japan, with a Description of a New Species from the Philippines (Crustacea, Decapoda, Coenobitidae)

YUKIO NAKASONE

*Biological Laboratory, College of Education, University
of the Ryukyus, Okinawa 903-01, Japan*

ABSTRACT—Six species of land hermit crabs are now known from Japan. Of them *Coenobita brevimanus* and *C. violascens* are recorded from Japan for the first time. *C. purpureus* and *C. violascens* hitherto synonymized with *C. perlatus* and *C. cavipes*, respectively, are valid. These species are redescribed and discussed in more detail. *C. pseudorugosus* is described and illustrated as a new species on the basis of the specimens from the Philippines.

INTRODUCTION

In the Indo-West Pacific region, the genus *Coenobita* is represented by ten valid species [1-6]: *C. rugosus* H. Milne Edwards, 1837; *C. purpureus* Stimpson, 1858; *C. perlatus* H. Milne Edwards, 1837; *C. cavipes* Stimpson, 1858; *C. violascens* Heller, 1862; *C. brevimanus* Dana, 1852; *C. scaevola* (Forskål, 1775); *C. spinosus* H. Milne Edwards, 1837; *C. carnescens* Dana, 1852; *C. longitarsis* De Man, 1902. Among these species, *C. purpureus* and *C. violascens* have hitherto been treated as the synonym of *C. perlatus* and *C. cavipes*, respectively. In our recent study, however, comparison of the specimens from the Ryukyus reveals that they are valid species; Miyake [7] had already separated *C. purpureus* from *C. perlatus*.

The specimens from the Ryukyus were collected from the Miyako and the Yaeyama Islands during the ecological and distributional studies of land hermit crabs in Okinawa Prefecture, except *C. perlatus*, although this species has also been reported from Kuroshima, the Yaeyama Islands by Miyake [7].

The specimens collected from Cebu I., the Philippines were also examined and revealed to belong to an undescribed species of the genus

Coenobita. However, this species has been not reported from the Ryukyus.

The objectives of the present paper are to provide information on land hermit crab species in Japan, and to resurrect the synonym of some species, as well as to describe a new species of *Coenobita*.

Coenobita pseudorugosus n. sp. (Figs. 1A-H and 2)

Material examined: Holotype, male (SL=Shield Length, 12.37 mm). Paratypes, 15 males (SL=7.29-12.13 mm), 22 non-ovigerous females (SL=5.63-10.75 mm), Cebu I., the Philippines, Apr. 30, 1986, T. Higa leg.

Diagnosis: Rostrum small and triangular. Ocular acicle broad basally, triangular and terminating in a small spine. Antennular basal segment with very produced laminar portion proximally and vertical margin of its lamina making an obtuse angle with upper margin of segment. Palm of left cheliped with an oblique series of seven to ten up-standing laminar teeth on upper part of outer surface; lower margin of propodus nearly straight in distal half and not four-cornered in an external form. Outer surfaces of dactylus and propodus of left third leg flat, smooth and separated from dorsal surface by a well-marked longitudinal crest. Right coxa of fifth legs in male produced into an

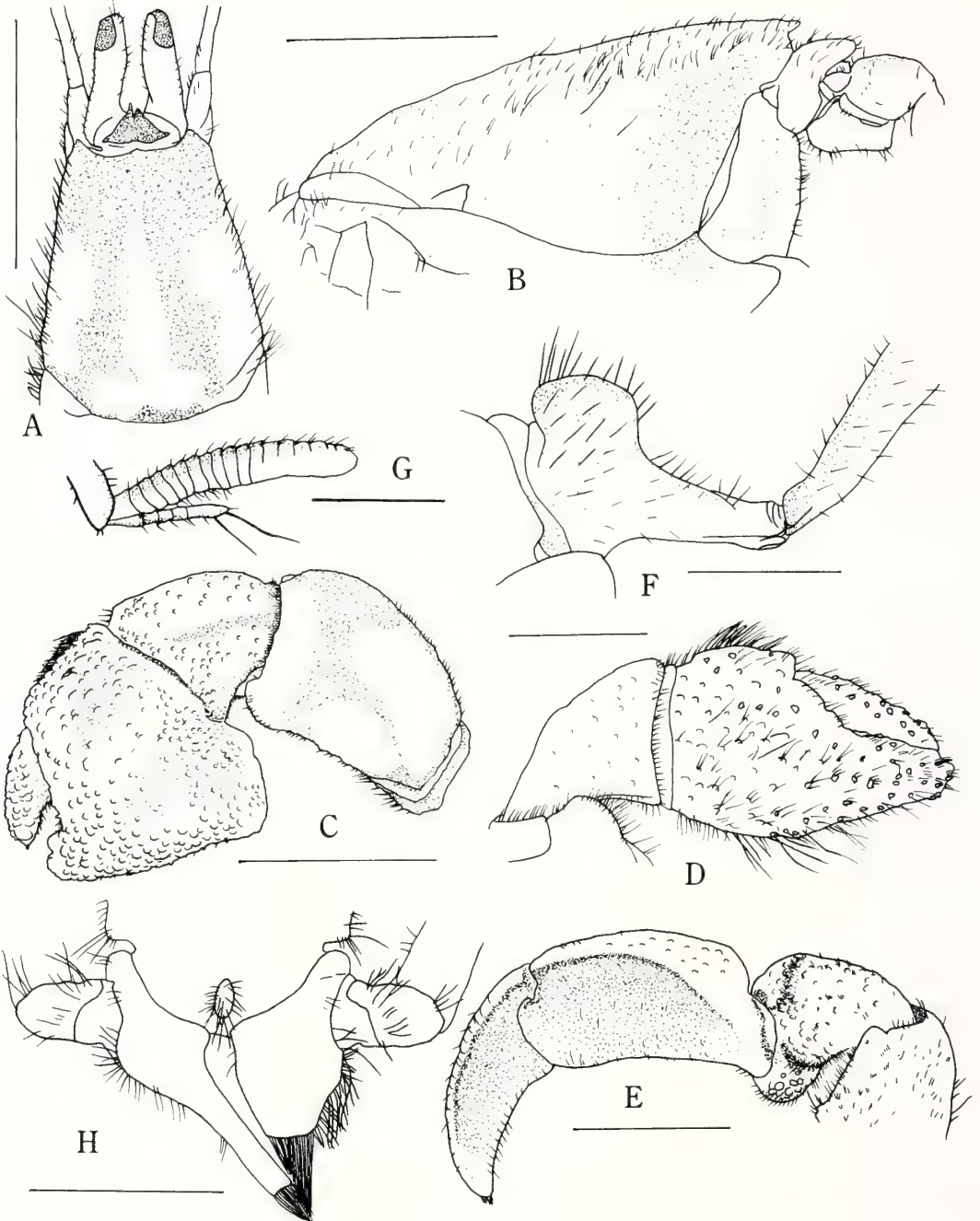


FIG. 1. *Coenobita pseudorugosus* n. sp., male, paratype (SL=11.3 mm). A, shield and some cephalic appendages, dorsal view; B, shield and antennal segments, lateral view; C, left cheliped; D, chela and carpus of right cheliped; E, left third leg, lateral view; F, basal segment of antennule; G, flagella of antenna; H, sternite and coxae of male fifth legs. Scale bars indicate 10 mm for A, C, E, 5 mm for B, D, H, and 2.5 mm for F and G.

elongate tube, always longer than left one.

Description: Shield usually longer than broad, narrower anteriorly; anterior margin between rostrum and lateral projections concave; rostrum small and triangular; dorsal surface with scattered granules on anterior and lateral portions; and lateral margins setose.

Ocular acicle broad basally, triangular and terminating in a small spine. Ocular peduncle compressed, reaching nearly to two-thirds the length of ultimate segment of antennal peduncle.

Antennular basal segment with very produced laminar portion proximally and vertical margin of its lamina making an obtuse angle with upper margin of segment; small flagellum of antennule reaching nearly to one-half length of large one. Antennal acicle fused with second segment of its peduncle.

In left chelipeds (Fig. 2) palm with an oblique series of seven to ten up-standing laminar teeth on upper part of outer surface; lower margin of propodus nearly straight in distal half and not four-cornered in an external form; palm with scattered round granules in addition to oblique teeth on outer surface, numerous especially on its lower portions; both fingers also with numerous round granules on outer surfaces; inner surface of palm strongly elevated in middle part and covered with large scale-like tubercles; movable finger with corneous-tipped granules on inner surface. In

small cheliped fingers and palm with corneous-tipped granules and setae on outer surfaces.

In left third leg (Fig. 1E) outer surfaces of dactylus and propodus flat, smooth and separated from dorsal surface by a well-marked longitudinal crest; walking legs except left third leg with setae on lower margin of each segment. In male coxae of fifth legs of both sides produced ventrally, unequal, and right coxa produced into an elongate tube, always longer than left one; its tube turning to the left and curved ventrally.

Coloration: Small individuals with a broad dark brown transverse band at anterior one-third of shield and two longitudinal stripes of the same color on posterior portion. Large individuals sometimes with two dark brown patches behind anterior margin of shield. Side walls of shield with a dark brown transverse band on anterior part. Ventral surface of ocular peduncle dark brown. Palm of left cheliped with a longitudinal white stripe on middle portion and the other part dark-brownish. Dactyli of left second and third legs each with a dark brown patch at proximal part. Propodus of left third leg with a broad dark brown band on middle portion; propodi of other legs with a white band at distal one-fourth, other area dark-brownish. Carpi of first and third legs with a longitudinal dark brown stripe; meri with dark brown ring distally.

Distribution: Known only from the type locality.

Remarks: *C. pseudorugosus* is most closely related to *C. rugosus*, but is distinguishable from the latter by the following characters. In *C. pseudorugosus* the lower margin of the propodus of the large cheliped is nearly straight for the distal half and the palm is, therefore, not four-cornered in an external form, while the palm of *rugosus* has an obtuse corner and is thus four-cornered in an external form; the palm of the present species is dark-brownish, lacking a distinct large patch of dark brown on the outer surface, but that of *rugosus* has a distinct large patch of dark brown. In all the specimens of the male, the right sexual tube is distinctly longer than the left one, while in a great number of the specimens of *rugosus* examined, the right sexual tube is almost equal in length to the left, or the right is slightly longer than the left.

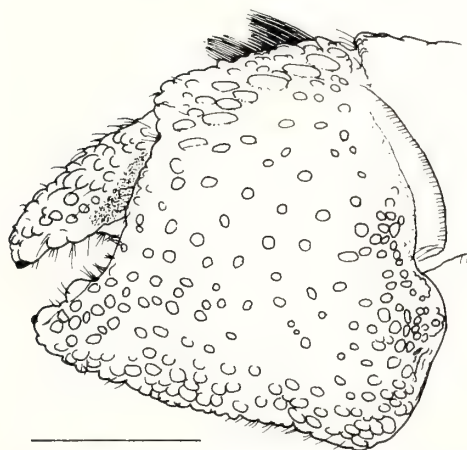


FIG. 2. *Coenobita pseudorugosus* n. sp., male, para-type (SL=11.3 mm). Enlargement of chela of the same cheliped as Fig. 1C. Scale 5 mm.

Coenobita rugosus H. Milne Edwards
(Figs. 3A-G and 9A)

Coenobita rugosa H. Milne Edwards [2], p. 241.

Coenobita rugosus: Alcock [9], p. 143, pl. 14, fig. 3, 3a;
Ball and Haig [15], p. 89; Miyake [7], p. 115, pl. 39,
fig. 1; Yu [12], p. 61, pl. 1, fig. D.

Material examined: I have treated a large number of individuals during the ecological and distributional studies of the species in Okinawa Prefecture.

Distribution: Widely distributed in the Indo-West Pacific region. In Japan this species is recorded from Chichijima and Anijima Islands in

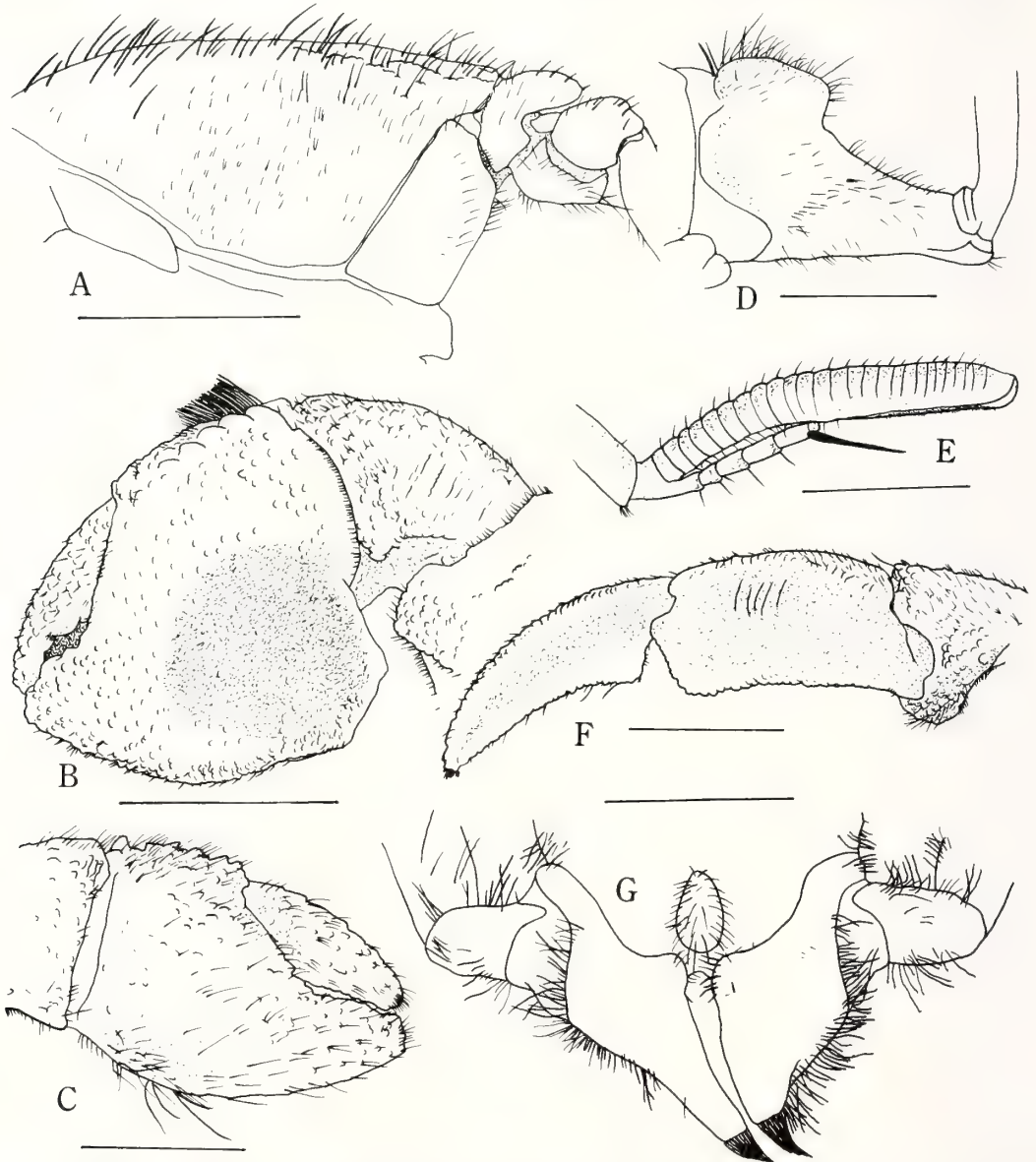


FIG. 3. *Coenobita rugosus* H. Milne Edwards, male. A, shield and antennal segments, lateral view; B, chela and carpus of left cheliped; C, chela of right cheliped; D, basal segment of antennule; E, flagella of antenna; F, left third leg; G, sternite and coxae of male fifth legs. Scales 10 mm for B and F, 5 mm for A, C and G, 3 mm for D, 2.5 mm for E.

the Bonin Islands [19], Amami-Oshima, Okinoerabujima and Yoronjima Islands in the Amami Islands [20] and from each island of Okinawa Prefecture except Kitadaitojima Island [17, 18, 21].

Remarks: This species is very abundant in Okinawa Prefecture. A great number of individuals are transported from Okinawa to Japan mainland as "pets" together with *C. purpureus* and *C. cavipes*. It is known that the transportation have been started since 1934 [22].

Coenobita purpureus Stimpson

(Figs. 4A-F and 9B)

Coenobita purpurea Stimpson [4], p. 83; Stimpson [23], p. 198.

Coenobita perlata var. *purpurea*: Bouvier [24], pp. 148-150.

Coenobita purpureus: Miyake [7], p. 221.

Material examined: I have examined a large number of individuals during the ecological and distributional studies of this species in Okinawa Island.

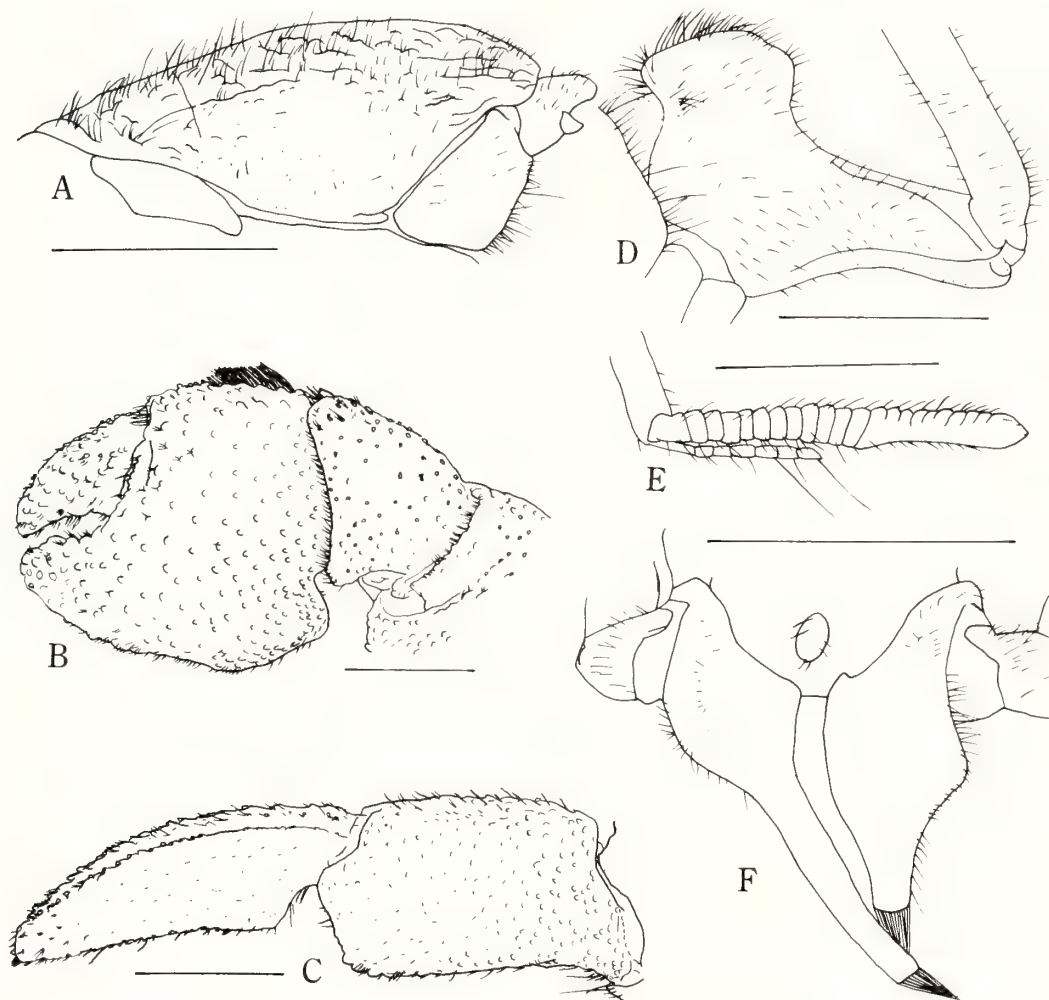


FIG. 4. *Coenobita purpureus* Stimpson, male. A, shield and antennal segments, lateral view; B, chela and carpus of left cheliped; C, left third leg; D, basal segment of antennule; E, flagella of antennule; F, sternite and coxae of male fifth legs. Scales 10 mm for A-C and F, 5 mm for D and E.

Description: Shield narrower anteriorly, strongly swollen just behind front; dorsal surface with numerous scattered granules on anterior, posterior and lateral portions; lateral margins of shield with setae.

Ocular peduncle compressed and reaching nearly to median part of ultimate segment of antennal peduncle.

Small flagellum of antennule reaching nearly to median part of large one. Antennal acicle fused with second segment of its peduncle.

Palm of left cheliped with an oblique series of up-standing four to five laminar teeth on upper part of outer surface; upper portion of palm with numerous scattered granules other than oblique teeth on outer surface, but lower portion with small granules and nearly smooth; both fingers with scattered granules on outer surface.

In left third leg outer surfaces of dactylus and propodus smooth, separated from dorsal surfaces by a well-marked longitudinal crest; outer surface of propodus not flat, but slightly swollen in midline.

In male coxae of fifth legs of both sides produced ventrally, unequal and right coxa produced into an elongate tube, usually longer than left one; its tube turning to the left and curved ventrally.

Coloration: Small individuals generally of cream color and large ones of purple color.

Distribution: In Japan this species is recorded from Chichijima, Hahajima, Anijima, Hirajima, Mukaijima and Kitaiwojima Islands in the Bonin Islands [19], the Ohsumi Peninsula and Biro I. in southern Kyushu, Tanegajima, Yakujima, Nakanojima and Takarajima Islands in the Tokara Islands, Amami-Ohshima, Kakeromajima, Kikaijima, Tokunoshima, Okinoerabujima and Yoronjima Islands in the Amami Islands [20], and from many islands in the Ryukyu Islands [17, 18, 21].

Remarks: The present species has been treated as the synonym of *C. perlatus* H. Milne Edwards by some authors since Henderson [25]. However, Bouvier [24] recognized this species as a variety of *C. perlatus*, but Terao [11] treated it as the synonym of *C. rugosus*. Miyake [7] resurrected *C. purpureus* from *C. perlatus* in the key to the Japanese species of *Coenobita*, but he did not give the colored illustration of the species. This species

is easily separated from *C. perlatus* by the coloration, the shape of the palm of the large chela, the shape of dactylus and propodus of the left third leg, and by the shorter right sexual tube. This species grows to a large size as in *C. perlatus*.

This species is very abundant in the Amami and the Okinawa Islands [17, 20, 21], but it is not so abundant in the southern Ryukyus [18]. I have treated and observed a great number of specimens during the ecological investigations of the present species [21]. *C. purpureus* is without doubt a valid species.

Coenobita perlatus H. Milne Edwards
(Figs. 5A–F and 9C)

Coenobita perlata H. Milne Edwards [2], p. 242.

Coenobita perlata: Fize and Serène [10], p. 24, fig. 3C, fig. 4; Yaldwyn and Wodzicki [13], p. 12.

Coenobita perlatus: Alcock [9], p. 145, pl. 14, fig. 2, 2a; Miyake [7], p. 115, pl. 39, fig. 2; Haig [16], p. 124.

Material examined: Male (SL=24.74 mm), Kitaiwojima I., the Bonin Islands, Aug. 1986, Kimura Johnson leg.

Distribution: Widely distributed in the Indo-West Pacific region. In Japan this species is known from Chichijima, Kitaiwojima and Minamitorishima Islands in the Bonin Islands [19] and from Kuroshima Island in the Yaeyama Islands [7].

Remarks: This species was first reported from Japan by Miyake [7]. His specimen was a single male and collected from Kuroshima Island by Dr. Imafuku in 1979 (Miyake, pers. commun.), but the specimens of this species were not collected since 1979. I had an opportunity to examine a male specimen from Kitaiwojima Island. According to Yaldwyn and Wodzicki [13], the juvenile specimen of 8 mm in the carapace length is creamy-white in general color and had red bands on the carpi of the chelipeds and walking legs, but the juvenile specimens of the same size of *C. purpureus* have no red bands. The question is whether *C. perlatus* reported by De Haan [26] from Kagoshima (=Satsuma) and Ryukyu is a genuine *perlatus* species, because *C. perlatus* had never been found anywhere in Kagoshima and Okinawa Prefectures after 1979 [17, 18, 20].

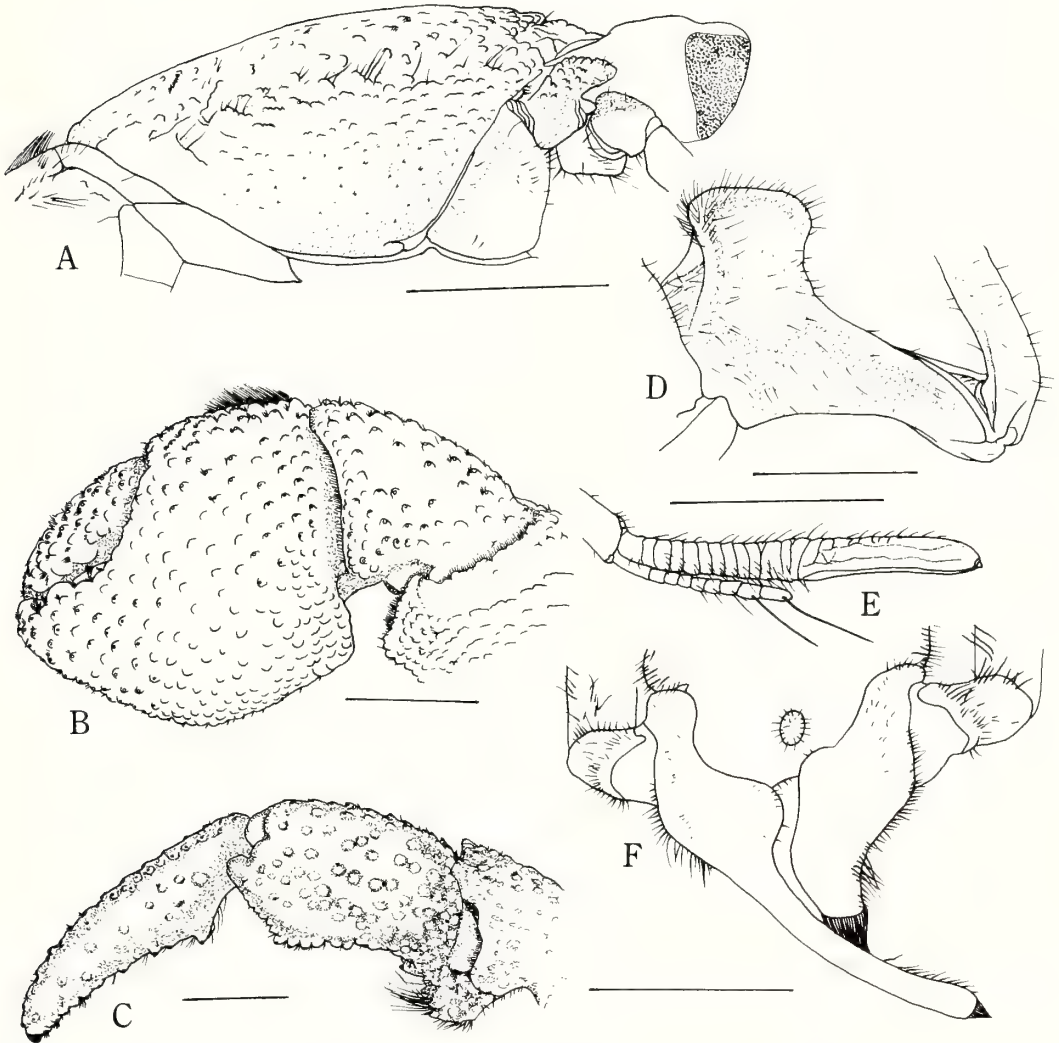


FIG. 5. *Coenobita perlatus* H. Milne Edwards, male. A, shield and antennal segments, lateral view; B, chela and carpus of left cheliped; C, left third leg; D, basal segment of antennule; E, flagella of antennule; F, sternite and coxae of male fifth legs. Scales 10 mm for A–D and F, 5 mm for E.

***Coenobita cavipes* Stimpson**
(Figs. 6A–F and 9D)

Coenobita cavipes Stimpson [4], p. 245; Stimpson [23], p. 200.

Coenobita cavipes: Alcock [9], p. 146, pl. 14, fig. 1; Fize and Serène [10], p. 30, fig. 3B, fig. 5A–C, pl. I, 4, 6.

Material examined: I have examined a number of individuals during the ecological studies of this species.

Distribution: Widely distributed in the Indo-West Pacific region. In Japan this species is known from Chichijima and Anijima Islands in the Bonin Islands [19], Okinoerabujima and Yoronjima Islands in the Amami Islands [20] and from many islands in the Ryukyu Islands except Akajima, Ikemajima and Nanbokudaitojima Islands [17, 18].

Remarks: This species has been confused with *C. violascens* Heller by some authors. The type locality was Loo Choo (Ryukyu) [4] and Bouvier

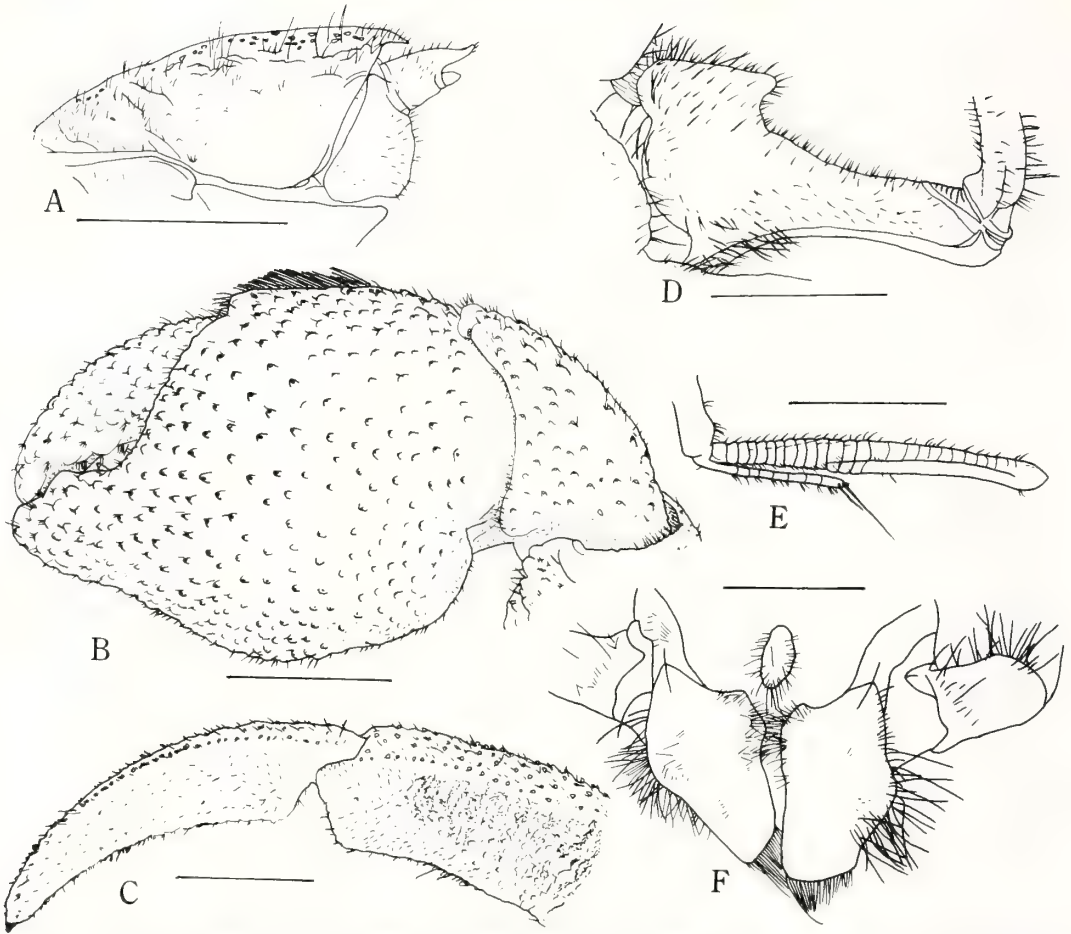


FIG. 6. *Coenobita cavipes* Stimpson, male. A, shield and antennal segments, lateral view; B, chela and carpus of left cheliped; C, left third leg; D, basal segment of antennule; E, flagella of antennule; F, sternite and coxae of male fifth legs. Scales 10 mm for A-C, 5 mm for D-F.

[24] and Fize and Serène [10] gave one locality name "Chine" in the distribution. This name "Chine" is a dialect and is now called "Kin", which is located in the central part of Okinawa mainland.

Coenobita violascens Heller
(Figs. 7A-F and 9E)

Coenobita violascens Heller [6], p. 524; Heller [27], p. 82, pl. 7, fig. 1.

Material examined: Two males (SL=4.16, 19.66 mm), 3 females (SL=6.81-16.09 mm), Hosozaki, Kohamajima I., the Yaeyama Islands, Aug. 4, 1986, K. Shimamura leg.; female (SL=17.38 mm), Ikemajima I., the Miyako Is-

lands, Sept. 12, 1986, M. Toyama leg.; male (SL=14.02 mm), 4 females (SL=14.19-19.14 mm), estuary of Shiira river, Iriomotejima I., the Yaeyama Islands, Jan. 16, 1987, Y. Nakasone leg.; male (SL=13.43 mm), 3 females (SL=9.51-14.11 mm), Cebu I., the Philippines, Apr. 30, 1986, T. Higa leg.

Description: Shield narrower anteriorly and slightly convex behind front; dorsal surface with scattered granules and punctations; tip of anterolateral margin of shield produced into a spinule which is white in the distal half.

Ocular acicle long and pointed. Ocular peduncle compressed, reaching almost to median part of ultimate segment of antennal peduncle. Small

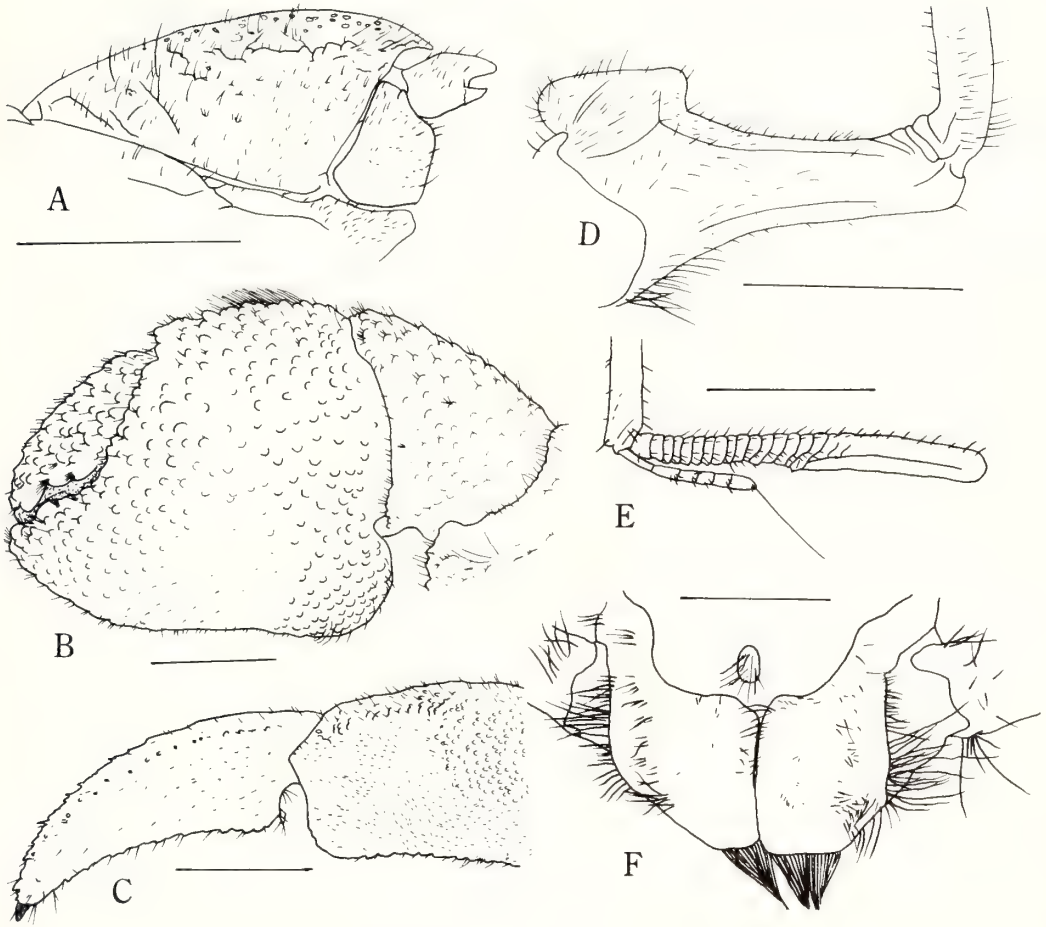


FIG. 7. *Coenobita violascens* Heller, male. A, shield and antennal segments, lateral view; B, chela and carpus of left cheliped; C, left third leg; D, basal segment of antennule; E, flagella of antennule; F, sternite and coxae of male fifth legs. Scales 10 mm for A-C, 5 mm for D-F.

flagellum of antennule small, shorter and not reaching to basal part of aesthetasc pad of large flagellum. Antennal acicle fused with second segment of its peduncle.

In left cheliped palm without an oblique series of up-standing teeth on upper part of outer surface; upper half portion of palm with numerous scattered granules, and lower half few granules, nearly smooth and with a distinct large patch of dark brown on outer surface; lower margin of palm straight or concave in middle portion and its proximal part (proximal lower margin near carpus) strongly produced into a lobe-like projection; both fingers violascent.

In left third leg outer surface of propodus nearly smooth and separated from dorsal surface by a well-marked longitudinal crest; inner margin of propodus strongly projecting inwards, and concave; a longitudinal ridge on ventral surface of propodus very small, indistinct. Second and third legs with numerous tufts of long stiff setae.

In male, coxae of fifth legs of both sides thick and short. A sternal protuberance between both coxae very small.

Coloration: Whole body except abdomen violascent, but showing light lavender to dark violet by individuals.

Distribution: Nicobar Islands; Cebu I., the

Philippines. In Japan this species is known from Ikemajima Island in the Miyako Islands and Ishigakijima, Kohamajima, Taketomijima, Iriomotejima, Yonagunijima Islands in the Yaeyama Islands [17, 18].

Remarks: This species is distinguished from *C. cavipes* by having the straight or concave lower margin of the palm of the left chela, by the violascent fingers of the left chela, by having the strongly projecting inner margin and the conspicuously concave inner surface of the left third leg propodus, by having a very small sternal protuberance between the coxae of the fifth legs of both sides, by the violascent body coloration, and by inhabiting mainly bay and estuary. In the juveniles the dactyli and propodi of the second and third legs are red brownish, and the ocular peduncle has a longitudinal dark brown stripe on the ventral surface and the other part is red brownish. Their juveniles are abundantly found near mangrove forest in Ishigakijima I., the Yaeyama Islands and they are easily distinguished from the juveniles of *C. cavipes* by the coloration of both the walking legs and the ocular peduncles and by the morphological difference of the propodus of the left third leg.

This species has been treated as the synonym of *C. compressus* and *C. cavipes* by Miers [28], De Man [5] and Fize and Serène [10], but it seems that *C. violascens* is distinctly a separate species. The specimens from the Philippines are easily distinguished from *C. cavipes*.

Coenobita brevimanus Dana
(Figs. 8A–G and 9F)

Coenobita clypeata var. *brevimanus* Dana [3], p. 473; Dana [8], pl. 30, fig. 4b.

Coenobita clypeata: Alcock [9], p. 142, pl. 15, fig. 1, la; Fize and Serène [10], p. 7, fig. 1A–C, pl. I, 1.

Coenobita hilgendorfi Terao [11], p. 338; Yu [12], p. 61, pl. 1, fig. C.

Coenobita brevimanus: Rathbun [14], p.314; Ball and Haig [15], p. 88; Haig [16], p. 124.

Coenobita brevimana: Yaldwyn and Wodzicki [13], p. 11.

Material examined: Three males (SL=15.37–18.15 mm), female (SL=15.89 mm), Ishigakijima I., the Yaeyama Islands, Dec. 4, 1985, Y. Naka-

sone leg. Male (SL=21.99 mm), Ishigakijima I., Sept. 11, 1986, M. Toyama leg. Two males (SL=13.58, 17.95 mm), Ikemajima I., the Miyako Islands, July 30, 1986, H. Iraha leg. Female (SL=17.07 mm), ovigerous female (SL=16.42 mm). Ikemajima I., Sept. 12, 1986, M. Toyama leg.

Distribution: Widely distributed in the Indo-West Pacific region. In Japan this species is now known from many islands in the Miyako and the Yaeyama Islands except Irabujima and Shimojijima Islands [17, 18].

Remarks: Until 1955, *Coenobita clypeatus* and *C. hilgendorfi* had been used as the scientific name of this species by many authors except some ones. Rathbun [14] used the name of *C. brevimanus* for specimens from the Indo-West Pacific for the first time.

In Japan, some individuals of this species were for the first time found within a forest near seashore in Ishigakijima Island on 4 December, 1985 and also collected from Ikemajima Island. This species is now distributed only in the southern Ryukyus. The animals were active within the forest in the daytime and they produced sound such as "Kukku, Kukku..." when they are caught. They mainly used *Turbo (Marmarostoma) argyrostomus* (Linné) as their host shell and one ovigerous female was collected in early September.

KEY TO THE SEVEN SPECIES OF
COENOBITA

- I. Antennal acicle fused with second segment of its peduncle; ocular peduncle strongly compressed; a brush of hairs on inner upper margins of palms of both chelipeds.
 - A. An oblique series of up-standing laminar teeth on upper part of outer surface of left palm; right coxa of fifth legs of male narrower than left one, tubular.
 - a. Outer surface of propodus of left third leg separated from dorsal surface by a well-marked longitudinal crest.
 1. Palm of left cheliped four-cornered in an external form; outer surface of propodus of left third leg flat; right coxa almost equal in length to left one, or slightly longer than

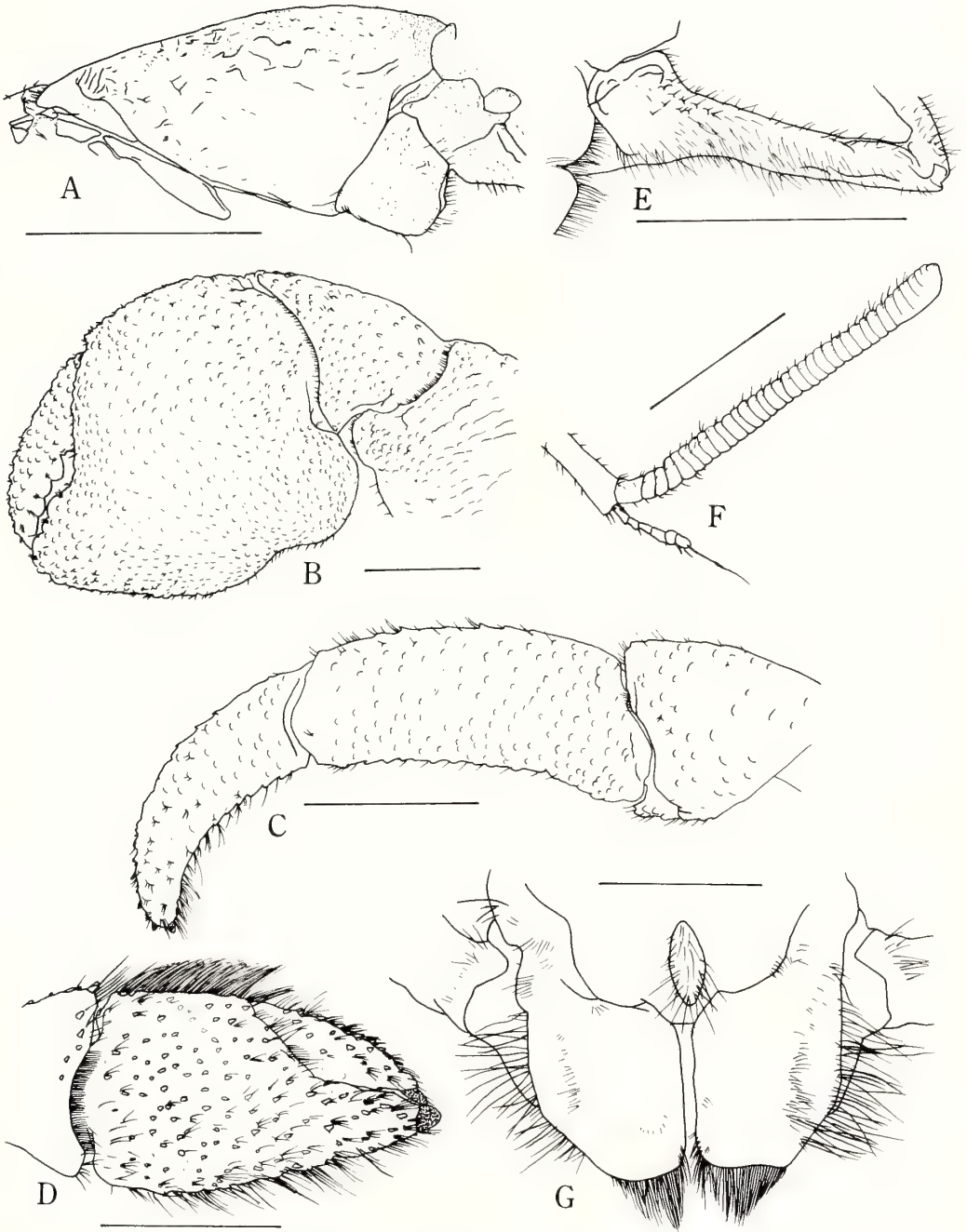


FIG. 8. *Coenobita brevimanus* Dana, male. A, shield and antennal segments, lateral view; B, chela and carpus of left cheliped; C, left third leg; D, chela of right cheliped; E, basal segment of antennule; F, flagella of antenna; G, sternite and coxae of male fifth legs. Scales 10 mm for A-E, 5 mm for F and G.

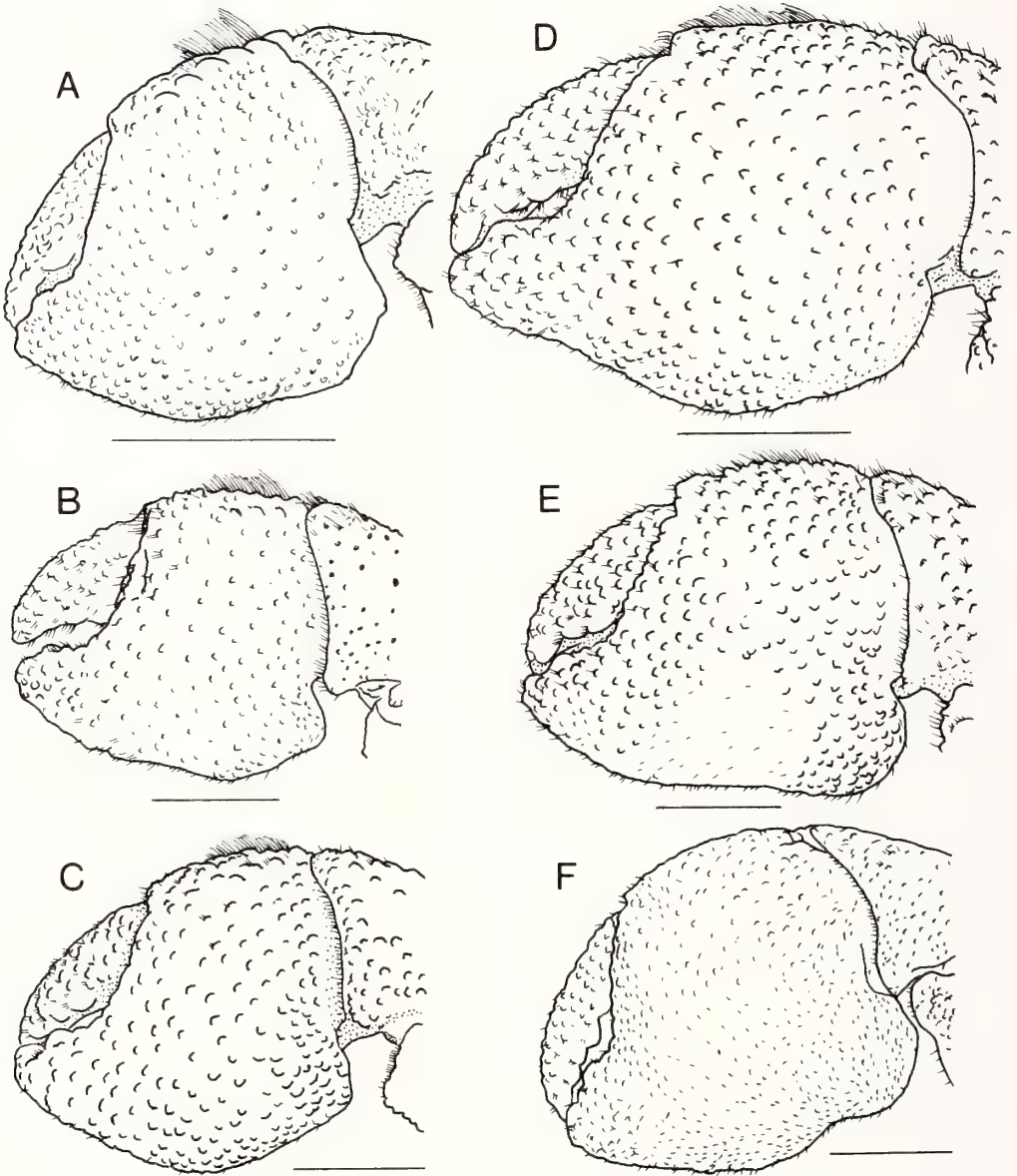


FIG. 9. Comparison of external forms of chelae. A, *Coenobita rugosus*; B, *C. purpureus*; C, *C. perlatus*; D, *C. cavipes*; E, *C. violascens*; F, *C. brevimanus*. Scales 10 mm for A-F.

- left*rugosus*
- 2. Palm of left cheliped not four-cornered in an external form; outer surface of propodus of left third leg flat; right coxa produced into an elongate tube, always longer than left one ...*pseudorugosus* n. sp.
- 3. Outer surface of propodus of left third leg

- not flat, slightly swollen in midline; coxae of fifth legs of both sides produced ventrally, unequal and right coxa produced into an elongate tube, usually longer than left one..... *purpureus*
- b. Outer surface of propodus of left third leg not separated from dorsal surface by a

longitudinal crest.

4. Outer surface of propodus of left third leg convex and with scattered white tubercles; right coxa produced into a long curved tube..... *perlatus*
- B. No oblique series of up-standing laminar teeth on upper part of outer surface of left palm; coxae of fifth legs of both sides thick and short.
5. Lower margin of left palm with an obtuse corner in middle portion; inner margin of propodus of left third leg not strongly projecting inwards and inner surface almost flat; a longitudinal ridge on ventral surface of propodus well-developed, distinct; a sternal protuberance between both coxae of fifth legs large *cavipes*
6. Lower margin of left palm straight or concave in middle portion; inner margin of propodus of left third leg strongly projecting inwards and inner surface strongly concave; a longitudinal ridge on ventral surface of propodus very small, indistinct; a sternal protuberance between both coxae of fifth legs very small *violascens*
- II. Antennal acicle not fused with second segment of its peduncle; ocular peduncle not compressed; a brush of hairs on inner upper margin of palm of right cheliped only *brevimanus*

ACKNOWLEDGMENTS

I am very grateful to Dr. S. Shokita, Department of Marine Sciences, University of the Ryukyus, Mr. M. Toyama, Cultural Administration Section, Okinawa Prefectural Office of Education, and Mr. K. Shimamura, Yaeyama Senior High School, for providing specimens for the present study. I am indebted to Dr. S. Miyake, Emeritus Professor of Kyushu University, for valuable advice and encouragement. Most of this work was made by a support of Agency for Culture Affairs, the Ministry of Education, Science and Culture of Japan.

REFERENCES

- 1 Lewinsohn, Ch. (1969) Die Anomuren des Roten Meeres (Crustacea Decapoda: Paguridea, Galatheidea, Hippidea). Zoologische Verhandeling-

en, Leiden, **104**: 1-213, pls. 1-2.

- 2 Milne Edwards, H. (1837) Histoire naturelle des Crustacés, comprenant l'anatomie, la physiologie et la classification de ces animaux, Vol. 2. Roret, Paris, pp. 1-531.
- 3 Dana, J. D. (1852) Crustacea. United States Exploring Expedition during the years 1838, 1839, 1840, 1841, 1842..., Vol. 13, Part 1. C. Sherman, Philadelphia, pp. 1-685.
- 4 Stimpson, W. (1858) Prodromus descriptionis animalium evertibratorum...VII. Crustacea Anomura. Proc. Acad. nat. Sci. Philadelphia, **10**: 225-252.
- 5 Man, J. G. De (1902) Die von Herrn Professor Kükenthal im Indischen Archipel gesammelten Decapoden und Stomatopoden. Abh. Senckenb. naturf. Ges., **25**: 467-929, pls. 19-27.
- 6 Heller, C. (1862) Neue Crustaceen gesammelt während der Weltumsegelung der K. K. Fregatte Novara. Zweiter vorläufiger Bericht. Verhandl. k. k. zool.-bot. Gesellsch. Wien, **12**: 519-528.
- 7 Miyake, S. (1982) Japanese Crustacean Decapods and Stomatopods in Color. Vol. I. Macrura, Anomura and Stomatopoda. Hoikusha Publishing Co., Ltd., Osaka, pp.1-261. (In Japanese).
- 8 Dana, J. D. (1855) Crustacea, Atlas. United States Exploring Expedition during the years 1838, 1839, 1840, 1841, 1842..., Vol. 14. C. Sherman, Philadelphia, pp. 1-27, pls. 1-96.
- 9 Alcock, A. (1905) Catalogue of the Indian Decapod Crustacea in the Collection of the Indian Museum. Part II. Anomura. Fasciculus I. Pagurides. Indian Museum, Calcutta. pp. i-xi, 1-197, pls. 1-16.
- 10 Fize, A. and Serène, R. (1955) Les Pagures du Viêt-nam. Institut Océanographique, Nhatrang, note 45. pp. i-ix, 1-228, pls. 1-6.
- 11 Terao, A. (1913) A catalogue of hermit-crabs found in Japan (Paguridea excluding Lithodidae), with descriptions of four new species. Annot. Zool. Japon., **88**: 355-391.
- 12 Yu, H. P. (1985) Notes on the land hermit-crabs (Crustacea, Decapoda, Coenobitidae) from Lan-yu Island in the Southern Taiwan. J. Taiwan Museum, **38**: 59-64, pl. 1.
- 13 Yaldwyn, J. C. and Wodzicki, K. (1979) Systematics and ecology of the land crabs (Decapoda: Coenobitidae, Grapsidae and Gecarcinidae) of the Tokelau Islands, Central Pacific. Atoll Res. Bull., **235**: 1-53, figs. 1-6.
- 14 Rathbun, M. J. (1910) Decapod crustaceans collected in Dutch East India and elsewhere by Mr. Thomas Barbour in 1906-1907. Bull. Mus. comp. Zool., Harvard, **52**: 305-317, pls. 1-6.
- 15 Ball, E. E. Jr. and Haig, J. (1972) Hermit crabs from Eastern New Guinea. Pacific Science, **26**: 87-107.
- 16 Haig, J. (1984) Land and freshwater crabs of the

- Seychelles and neighbouring islands. In "Biogeography and Ecology of the Seychelles Islands". Ed. by D. R. Stoddart, Dr W. Junk Publishers, pp. 123-139.
- 17 Toyama, M. and Kurozumi, T. (1987) Geographical distribution of the genus *Coenobita* in Okinawa Prefecture. In "A Report on the Distribution and Ecology of Land Hermit Crabs in Okinawa Prefecture". Okinawa Prefectural School Board, pp. 200-203. (In Japanese).
 - 18 Shimamura, K. (1987) Ecological studies of land hermit crabs in the Yaeyama Islands. In "A Report on the Distribution and Ecology of Land Hermit Crabs in Okinawa Prefecture." Okinawa Prefectural School Board, pp.61-118. (In Japanese).
 - 19 Sukanuma, H., Tachikawa, H. and Masuda, M. (1987) Report on the habitats of the land hermit crabs in the Bonin Islands. Tokyo Metropolitan School Board, pp. 1-98. (In Japanese).
 - 20 Saisho, T. and Suzuki, H. (1987) An urgent study on the distribution and ecology of land hermit crabs, genus *Coenobita*, in Kagoshima Prefecture. Kagoshima Prefectural School Board, pp. 1-64. (In Japanese).
 - 21 Nakasone, Y. (1987) Ecological studies of land hermit crabs in the southern part of Okinawa Island. In "A Report on the Distribution and Ecology of Land Hermit Crabs in Okinawa Prefecture". Okinawa Prefectural School Board, pp. 16-60. (In Japanese).
 - 22 Toyama, M. (1987) Gathering land hermit crabs as resources. In "A Report on the Distribution and Ecology of Land Hermit Crabs in Okinawa Prefecture". Okinawa Prefectural School Board, pp. 219-224. (In Japanese).
 - 23 Stimpson, W. (1907) Report on the Crustacea (Brachyura and Anomura) collected by the North Pacific Exploring Expedition, 1853-1856. *Smithson. misc. Collns.*, **49**: 1-240, pls. 1-26.
 - 24 Bouvier, E. L. (1890) Révision des Cénobites du Muséum. *Bull. Soc. philom. Paris*, **2**: 143-150.
 - 25 Henderson, J. R. (1888) Report on the Anomura collected by H. M. S. Challenger during the years 1873-76. Report on the scientific results of the voyage of H. M. S. Challenger during the years 1873-76... *Zoology*, Vol. 27. pp. i-ix, 1-221, pls. 1-21.
 - 26 Haan, W. De (1849) Crustacea. In "Fauna Japonica". Ed. by P. F. von Siebold, *Lugduni Batavorum*, pp. 197-243.
 - 27 Heller, C. (1865) Crustaceen. In "Reise der österreichischen Fregatte "Novara" um die Erde, in den Jahren 1857, 1858, 1859, unter den Befehlen des Commodors B. von Wüllerstorff-Urbair, *Zool.*, Vol. 2. pp. 1-280, pls. 1-25.
 - 28 Miers, E. J. (1880) Crustacea Anomura and Macrura (except Penaeidea). On a collection of Crustacea from the Malaysian Region. Part III. *Ann. Mag. nat. Hist.*, (5) **5**: 370-384. pls. 14, 15.

[COMMUNICATION]

Direct Evidence for Axopodial Fusion Preceding Cell-to-cell Contact in a Heliozoan *Echinosphaerium*

TAKAKO NISHI¹, MAKOTO KOBAYASHI³, MAMI ISOMURA,
HIDEKI ISHIDA² and YOSHINOBU SHIGENAKA

*Laboratories of Physiology and Cell Biology, Faculty of Integrated Arts
and Sciences, Hiroshima University, Hiroshima 730, Japan*

ABSTRACT—In a heliozoan *Echinosphaerium*, the electrical interactions between two organisms during the process of cell fusion were studied physiologically. The electron-microscopical observations were also made to examine the connection of axopodia of the two organisms. Results showed that the two organisms interacted electrically through their axopodia before the two cell bodies began to fuse.

INTRODUCTION

The large heliozoan, *Echinosphaerium*, frequently shows a characteristic type of cell fusion, termed plasmogamy, which is not preceded by the encystation and thus considered as an asexual phenomenon [1-3]. Vollet and Roth [3] have observed that the cell fusion can be induced only if the treatments are used causing large amounts of new cell-surface membrane to be formed in the presence of divalent cations.

In a Japanese heliozoan strain *Echinosphaerium akamae*, the cell fusion was found to occur between two approaching organisms even at normal cultural conditions [4]. The fusion process has then been studied in relation to the axopodial degradation [5] and the cell membrane fluidity [6]. The timing and process of the fusion of cell

membranes, however, have not been investigated in detail.

Electrophysiologically, the activities of protozoan cell membranes have been studied in many species in relation to the excitability, conduction and the movement of cilia or flagella [7, 8], but very few investigations have been done on the membrane characteristics during the cell fusion of two organisms.

In the present study, the electrical connections between two organisms during the process of cell fusion have been pursued physiologically, and the electron-microscopical observations have also been made especially on the axopodia of just-approaching organisms. Both physiological and morphological studies have shown that the axopodial fusion precedes the fusion of cell bodies themselves.

MATERIALS AND METHODS

The large multinucleated heliozoan, *Echinosphaerium akamae* [9], was cultured at $20 \pm 1^\circ\text{C}$ in 0.01% Knop solution containing 0.24 mM $\text{Ca}(\text{NO}_3)_2$, 0.14 mM KNO_3 , 0.058 mM MgSO_4 and 0.11 mM KH_2PO_4 . One or two grains of boiled wheat were added to each 15 ml of the culture medium. Small ciliates and flagellates such as *Tetrahymena*, *Colpidium* and *Chilomonas* were also added to the medium as food. Subculturing was carried out at 2-week intervals.

Prior to physiological experiments, the organisms were transferred from the culture medium to

Accepted August 6, 1987

Received July 3, 1987

¹ Present address: Department of Physiology, School of Medicine, Kagoshima University, Kagoshima 890, Japan.

² Present address: Department of Biology, Faculty of Science, Shimane University, Matsue 690, Japan.

³ To whom reprints should be requested.

the physiological saline solution in an experimental chamber. The saline solution was composed of 1 mM KCl, 1 mM CaCl₂, 1 mM MgCl₂ and 5 mM tris (hydroxymethyl) aminomethane, the pH being adjusted to 7.2 by HCl. The experimental chamber was set up on the stage of an inverted microscope through which observation and photographing of the organisms were made. When a pair of organisms came close to each other, a microelectrode, filled with 3 M KCl and having resistances of 15 to 30 M Ω , was inserted into each organism for recording membrane potential.

The heliozoan *Echinospaerium* showed a remarkable hyperpolarization, 15 to 20 mV in amplitude and several hundreds msec in duration, correlated with the contraction of contractile vacuole, termed H-CV [10]. The electrotonic spread of H-CV as well as of an electric potential caused by a current injection into one of the paired organisms was employed for determining of the degree of electric coupling between the two organisms. The electrical data were stored in a data recorder (Sony, DFR 3515) and displayed on an ink-writing recorder (Nihon-Kohden, RJG 4024).

For electron microscopy, the two just-approaching organisms were fixed with glutaraldehyde and osmium tetroxide fixatives by the method of Shigenaka *et al.* [11]. The fixed samples were then rinsed briefly, dehydrated, and embedded into a low viscosity embedding medium [12]. Ultra-thin sections were prepared with a glass knife loaded onto a Porter-Blum ultra-microtome (type MT-1) and stained with 3% uranyl acetate in 50% ethanol for 10 min and Reynolds' lead citrate stain [13] for 3 min. The sections were observed with a transmission electron microscope (JEOL, JEM-100S) operating at 80 or 100 kV and photographed using electron-microscopic films (Fuji, type FG).

RESULTS AND DISCUSSION

According to Shigenaka and Kaneda [5], the process of cell fusion in heliozoans can be divided into the following four stages; stage A before the tip-to-tip contact of axopodia, stage B until the contact of axopodial tip to the partner's cell

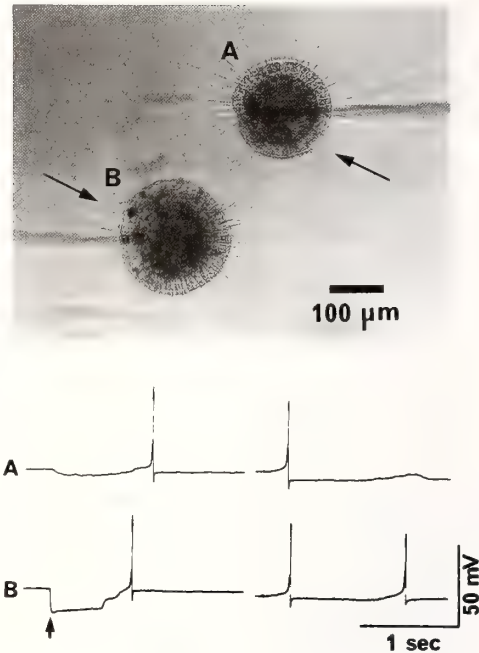


FIG. 1. Two organisms of *Echinospaerium akamae* and records of their membrane potential. Upper photograph shows a pair of organisms at the early stage C of cell fusion. Arrows indicate the contractile vacuoles. A and B in the lower tracings show the membrane potential recorded from the individuals A and B of the upper photograph, respectively. An arrow shows the onset of H-CV.

surface, stage C until the cell-to-cell contact, and stage D until the completion of fusion of the cell bodies. In a pair of just-approaching organisms at the stage A, any electrical signals in one organism were not detected in its partner. At the stage B, the electrotonic potential elicited by current application or H-CV in one organism was also recorded in the paired cell. On the contrary, action potentials, which developed spontaneously or by current injection, rarely conducted to the partner even at the late stage B. At the stage C, however, the conducted action potentials originated in one organism could also be recorded in the partner's cell membrane.

Upper photograph of Figure 1 shows a pair of organisms at the early stage C, in which some axopodia touched to the partner's cell surface while the two cell bodies are still about 120 μ m apart from each other. A and B in the lower

tracings of Figure 1 show the membrane potential recorded from the organisms A and B of the upper photograph, respectively. It is obvious that an H-CV produced in organism B was electrotonically spread to A. The coupling ratio, which is a ratio of the amplitude of spread H-CV in organism A to that of H-CV in B, was about 0.2. An action potential appeared after H-CV and spontaneous action potentials conducted or not case by case. In the cases shown at the right in Figure 1, a spontaneous action potential elicited in A conducted to B. The conduction velocity, calculated

from the distance between two electrodes divided by the time interval between two action potentials, was about 3 mm/sec. On the contrary, an action potential elicited in B did not conduct to A with leaving a slow small depolarization.

Summarizing these electro-physiological results, the coupling ratio was 0.1 to 0.3 at the stage B and early stage C, 0.4 to 0.5 at the late stage C, and 1.0 at the stage D. The ratio 1.0 means that the two cells are isopotential. At the late stage C and stage D, almost all action potentials elicited in one cell conducted to its partner. These results show that

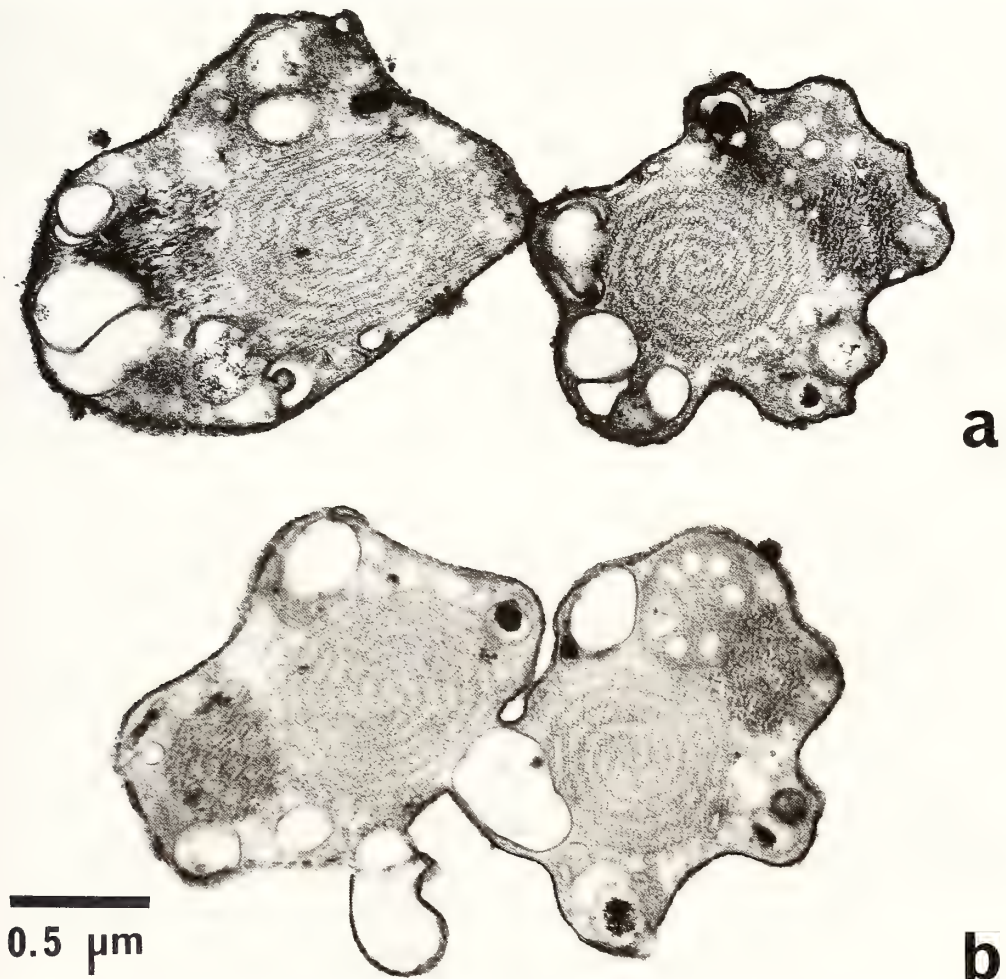


FIG. 2. Electron micrographs of just-attaching (a) and fusing (b) axopodia from a pair of individuals. Note that the coiling direction of axonemal microtubules in the two adjacent axopodia is different from each other. $\times 37,000$.

both the electrotonic spread of potential responses and the conduction of action potentials can occur through the membrane of axopodia before two cell bodies begin to fuse.

We examined a great number of ultra-thin sections of just-approaching organisms, especially at the early stage C. Two adjacent axopodia were seen as if they were just-attaching and fusing as shown in Figure 2. It is necessary to determine if these axopodia were of the same individual or the two different ones. We found that the coiling direction of axonemal microtubules was always the same in every axopodia of one organism, i.e., it was clockwise if the axonemal microtubules were viewed from the axopodial base to the tip. As shown in Figure 2, in the two just-attaching or fusing axopodia, the coiling direction was different from each other. This indicates that they were derived from the two different individuals, respectively.

The present study has revealed the degree of electrical coupling between two organisms during the cell fusion and has shown that the two organisms have electrical interactions through their axopodia before the two cell bodies begin to fuse. Observations through electron microscope have presented a strong evidence supporting the

physiological findings.

REFERENCES

- 1 Barrett, S. M. (1958) *J. Protozool.*, **5**: 205-209.
- 2 Vollet, J. J., Roth, L. E. and Davidson, M. (1972) *J. Cell Biol.*, **55**: 269a.
- 3 Vollet, J. J. and Roth, L. E. (1974) *Cytobiologie*, **9**: 249-262.
- 4 Shigenaka, Y., Ogura, T. and Maruoka, T. (1976) *Zool. Mag.*, **85**: 65-69.
- 5 Shigenaka, Y. and Kaneda, M. (1979) *Annot. Zool. Japon.*, **52**: 28-39.
- 6 Shigenaka, Y., Maruoka, T., Toyohara, A. and Suzaki, T. (1979) *Annot. Zool. Japon.*, **52**: 163-178.
- 7 Naitoh, Y. (1982) In "Electrical Conduction and Behavior in 'Simple' Invertebrates". Ed. by G. A. B. Shelton, Clarendon Press, Oxford, pp. 1-48.
- 8 Podesta, R. B. (1982) *Membrane Physiology of Invertebrates*, Marcel Dekker, Inc., New York.
- 9 Shigenaka, Y., Watanabe, K. and Suzaki, T. (1980) *Annot. Zool. Japon.*, **53**: 103-119.
- 10 Nishi, T., Kobayashi, M. and Shigenaka, Y. (1986) *J. Exp. Zool.*, **239**: 175-182.
- 11 Shigenaka, Y., Roth, L. E. and Pihlaja, D. J. (1971) *J. Cell Sci.*, **8**: 127-152.
- 12 Spurr, A. R. (1969) *J. Ultrastruct. Res.*, **26**: 31-43.
- 13 Reynolds, E. S. (1963) *J. Cell Biol.*, **17**: 208-212.

[COMMUNICATION]

An Established Marine Fish Cell Line with High Plating Efficiency

NORIAKI EBITANI and TOSHIYUKI KUBO¹

*Biological Laboratory, North Shore College, Atsugi 243, and
¹Biological Laboratory, Sophia University, Tokyo 102, Japan*

ABSTRACT—A fibroblast-like cell line with a high plating efficiency was established from the fins of a marine teleost fish, *Sebastes marmoratus*. The cells, designated SMF, have been subcultured over 300 passages. SMF cells have grown well in TC-medium 199 supplemented with 2.28 g/l NaCl and 15% FBS at 25 °C. The modal chromosome number was 99, while that of primary cells was 48. Plating efficiency of SMF cells was over 70% when 200–400 cells were inoculated in a 25 cm² flask with a tight cap.

A fish cell line with a high plating efficiency is a very useful material for *in vitro* studies of the effects of radiations, chemical mutagens and other environmental agents on fish cells.

Since the report of Clem *et al.* [1] on a cell line derived from fins of the yellow-striped grunt, a number of fish cell lines have been established. However, the cell lines derived from marine teleost fish have so far been compared in number with that from fresh water teleost fish [2, 3].

The plating efficiencies of several fish cell lines have been reported to be less than 10% [2, 4], but Shima *et al.* [5] have established a cell line derived from the goldfish with a plating efficiency of approximately 20%. Plating efficiency in the fish cell lines is however much lower than in the mammalian cell lines.

The purpose of the present study was to obtain a cell line with a high plating efficiency from marine teleost fish for studying the effects of several chemical mutagens contained in sea water.

We have established a cell line from a scorpion fish, *Sebastes marmoratus*, with a plating efficiency of over 70% and was designated SMF. Some characteristics of clones obtained from SMF cells will be reported in a subsequent paper.

MATERIALS AND METHODS

The scorpion fish, *Sebastes marmoratus*, caught in Sagami Bay, Japan on 28 February 1983, was used in the present study. The individual, from which the cell line was established, was a female and 20 cm in total length.

All of the fins were excised just above the muscled areas in the field. They were placed in chilled calcium and magnesium free marine phosphate buffered saline containing 0.197 M NaCl (M-PBS⁻) supplemented with 10% calf serum, 400 IU penicillin/ml (Meiji Seika, Tokyo, Japan), 200 µg streptomycin/ml (Meiji Seika) and 10 IU nystatin/ml (GIBCO). After 24 hr, these fins were immersed in Dakin's solution for 3 min and then washed three times with saline containing antibiotics for 10 min each. The washed fins were minced into small pieces and all the fins from a single fish were transferred to a flask containing 30 ml of 0.25% trypsin (1:250, Difco) solution in M-PBS⁻. After stirring at low speed with a small magnetic bar at 25°C for 15 min, the trypsin solution was discarded and replaced with another aliquot. The fluid was harvested 20 min later and more trypsin solution was added to the tissue. This procedure was repeated three times. At each harvest, calf serum was added to it to give a

concentration of 10% and stored in ice bath. The harvests were filtered through lens papers and centrifuged at 1,000 rpm for 5 min at 10°C. The supernatant was decanted and the cells were resuspended in culture medium. The cells were inoculated at the concentration of 300 cells in 1 mm² of a Corning 75 cm² culture flask with a tight cap and kept at 25°C.

The culture medium used in the present study was TC-199 (GIBCO) supplemented with 2.28 µg NaCl/ml, fetal bovine serum (FBS) (GIBCO), 200 IU penicillin/ml, 100 µg streptomycin/ml and 5 IU nystatin/ml. The medium was changed every third or fourth day by renewal of one-half of the old medium. Subculture was carried out by routine procedure.

Chromosome preparations were made, employing the air-drying technique. After the metaphases were arrested with colchicine, cells were harvested by trypsinization. Cells were treated with potassium chloride (0.075 M) for 15 min, fixed soon thereafter with methanol-acetic acid (3:1) and air dried. Chromosomes were stained with 6% Giemsa (in 1/15 M phosphate buffer) solution.

Plating efficiency was estimated by the following procedure. From 25 to 400 cells were inoculated in a Corning 25 cm² culture flask with a tight cap containing 5 ml of the conditioned medium and kept at 25°C. After incubation for 14 days, cells were fixed with methanol and stained with 6% Giemsa solution. The number of colonies, containing more than 50 cells were counted.

RESULTS AND DISCUSSION

Morphology and growth The cells from the fins of *Sebastes marmoratus* continued to proliferate for more than 1,000 days with 300 passages. The population doubling time was about 40 hr. The morphology of primary cells and SMF cells at 203 PDN is shown in Figure 1. Although primary cells were fibroblast-like and arranged regularly, SMF cells were crisscrossed.

The optimal concentration of FBS supplemented in the culture medium for cell growth was tested at 25°C. In each flask, 200 cells per mm² were inoculated. The results are presented in

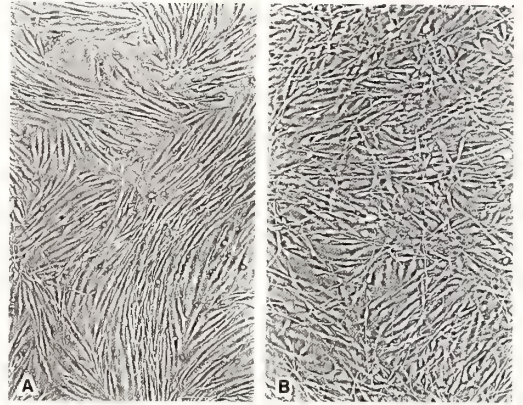


FIG. 1. Phase-contrast photomicrograph of primary cells (A) and SMF cells at 203 PDN (B). $\times 50$.

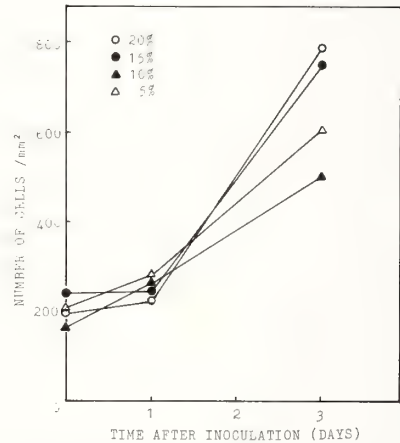


FIG. 2. Effect of concentration of fetal bovine serum on cell growth at 25°C.

Figure 2. The best growth was obtained at a concentration of 20% FBS. Hardly any difference could be demonstrated between the results at 15% and 20% FBS. The growth at concentrations of 5 and 10% FBS was delayed considerably.

For determining the optimal temperature for cell growth, the flasks containing 200 cells per mm² were incubated at 15, 20, 25 and 30°C in the medium with 15% FBS. The results are shown in Figure 3. At 25°C, the growth of cells was extremely high and cells increased to almost 650 per mm² at the third day of culture. Growths of cells at other temperatures were lower. These results suggest that 25°C may be physiologically optimum for marine fish cells.

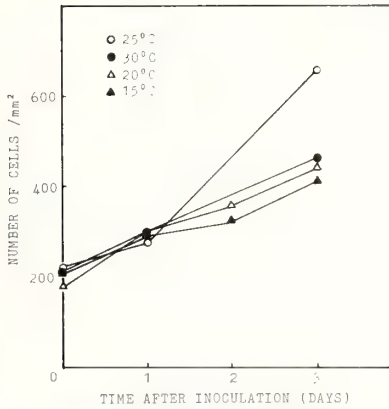


FIG. 3. Growth curves of SMF cells at 15, 20, 25 and 30°C.

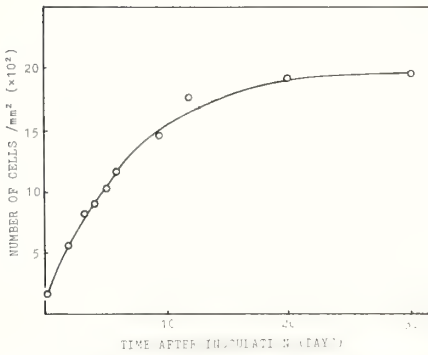


FIG. 4. Growth curve of SMF cells at 25°C.



FIG. 5. Photomicrograph of chromosomes of a primary cell (A) and a SMF cell at 203 PDN (B). $\times 400$

Taking these results into consideration, SMF cells were continued to culture at 25°C in the medium containing 15% FBS. The growth curve of SMF cells is shown in Figure 4. The saturation density of SMF cells was 1.9×10^3 cells per mm^2 and the contact inhibition of cell growth worked well.

For long-term storage of SMF cells, $3-4 \times 10^6$ cells were suspended in one milliliter of fresh culture medium supplemented with 12% DMSO and cryopreserved at -196°C . The viability of the thawed cells stored for 10 months was around 60%.

Distribution of chromosome number Chromosomes are rather small in size. Figure 5 (A and B) show the chromosomes of a primary cell and a SMF cell at 203 PDN. The distribution of chromosome number of primary cells and SMF cells at 146 and 203 PDNs is summarized in Figure 6.

The modal chromosome number of primary cells was $2n=48$ and the karyotype was comprised of one pair of metacentric and 23 pairs of acrocentric chromosomes. This result is consistent with that of

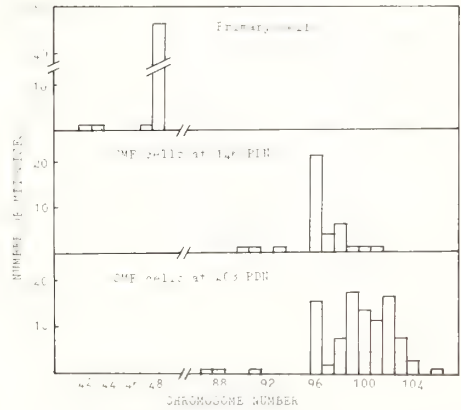


FIG. 6. Distribution of chromosome numbers in primary cells and SMF cells at 146 and 203 PDN.

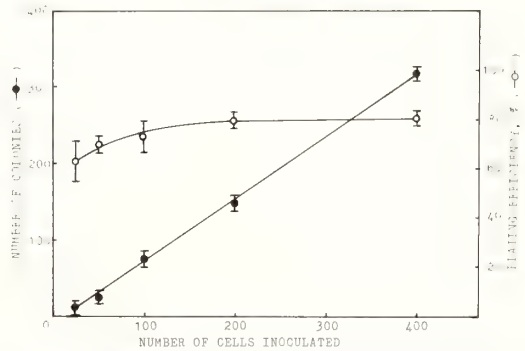


FIG. 7. Number of colonies and plating efficiency of SMF cells at 237 PDN. Results are given as mean \pm standard deviation.

Nishikawa *et al.* [6]. The chromosome number of SMF cells differed from those of primary cells.

At 146 PDN, the major distribution of chromosome numbers of SMF cells ranged from 96 to 98. Their modal number was 96 and more than 60% of the cells had 4N number. Their karyotype was composed of 4 metacentric and 92 acrocentric chromosomes.

At 203 PDN, SMF cells showed a wide range in the major distribution of chromosome numbers, which were from 87 to 106. Their modal number was 99 and cells with 96 and 102 chromosomes were predominant. Their karyotype was composed of 4 metacentric and acrocentric chromosomes.

In view of these results, the transition in chromosome distribution from a diploid mode to a subtetraploid mode is likely to take place through a tetraploid phase. The doubling of chromosome set occurs probably in the early passages by endomitosis and then the loss or gain of acrocentric chromosomes is assumed to have taken place progressively. Wolf and Quimby [7] stated that the fish cell lines for which chromosome number had been determined were all heteroploid and attainment of the potential for indefinite subculturing was usually accompanied by alternation in heteroploid chromosome constitution.

Colony formation and plating efficiency

The colony forming ability of SMF cells was tested by counting the number of colonies on the 14th day after inoculation. The results were presented in Figure 7. When 200–400 cells per flask were inoculated, the plating efficiencies of SMF cells were 80, 83 and 72% at 233, 237 and 248 PDNs respectively.

Only a very few reports have been made in the colony forming ability of fish cell lines. On the cell

line derived from a goldfish, Suyama and Etoh [4] reported that the plating efficiency was around 10%, when 2,000 or more cells per dish were inoculated. Shima *et al.* [5] reported that the plating efficiency of cell lines derived from the same species was about 20% at 183 or more PDNs. As for marine teleost fish cell lines, Clem *et al.* [1] reported that the plating efficiency of the cell line derived from the yellow-striped grunt was less than 1%.

In comparison with these results, SMF cells cultured in the conditioned medium have a much higher plating efficiency. This high plating efficiency makes it possible to obtain clones from somatic cells of the marine teleost fishes.

ACKNOWLEDGMENTS

The authors thank Prof. S. Nadamitsu of Hiroshima Women's University for his invaluable advice during the conduct of the present experiments.

REFERENCES

- 1 Clem, L. W., Moewus, L. and Sigel, M. M. (1961) *Proc. Soc. Exp. Biol. Med.*, **108**: 762–766.
- 2 Wolf, K. and Quimby, M. C. (1969) In "Fish Physiology". Ed. by W. S. Hoar and D. J. Randall, Academic Press, New York and London, Vol. 3, pp. 253–305.
- 3 Fryer, J. L., Yusha, A. and Pilcher, K. S. (1965) *Ann. N. Y. Acad. Sci.*, **126**: 566–586.
- 4 Suyama, I. and Etoh, H. (1979) *Zool. Mag. (Tokyo)*, **88**: 321–324.
- 5 Shima, A., Nikaido, O., Shinohara, S. and Egami, N. (1980) *Exp. Gerontol.*, **15**: 305–314.
- 6 Nishikawa, S., Honda, M. and Wakatsuki, A. (1977) *J. Shimonoseki Univ. Fish. (Japan)*, **25**: 187–191.
- 7 Wolf, K. and Quimby, M. C. (1962) *Science*, **135**: 1065–1066.

[COMMUNICATION]

**Female Heterogametic Sex-determination in *Xenopus laevis*
as Reconfirmed by Repeated Diploid Gynogenesis**TOSHIHIRO NAKAMURA¹¹*Zoological Institute, Faculty of Science, Hokkaido
University, Sapporo 060, Japan*

ABSTRACT—Diploid gynogenetic production of offspring was repeated for 4 generations in *Xenopus laevis*. Analyses of the resulting sex phenotypes in these progenies supported the hypotheses that (a) the female is heterogametic (ZW), (b) a recombination between sex-determination genes and the centromere occurs with high frequency, and (c) homogametic (WW) females are highly fertile.

INTRODUCTION

Although the South African clawed frog *Xenopus laevis* lacks sex-chromosome dimorphism, the female heterogamety (ZW) of this animal has been demonstrated on the basis of mating experiments with sex-reversed frogs [1-4]. Mating of sex-reversed genetic males with normal males gives rise to all male offspring [2]. Conversely, mating of sex-reversed genetic females with either normal females or sex-reversed genetic males yields offspring with the sex ratio of 3 (female): 1 (male) or of 1:1, respectively [3]. These results are explained on the basis of the presence of both heterogametic (ZW) and homogametic (WW, "super") genotypes in the female phenotype, while phenotypic males are homogametic (ZZ). The viability and fertility of homogametic super-females have recently been demonstrated in studies on the progeny of first diploid gynogenesis [5].

The behavior of sex-determination genes was

examined during our efforts to establish a histocompatible *Xenopus laevis* colony by repeated gynogenetic propagation [6, 7], as described below.

MATERIALS AND METHODS

The females of *Xenopus laevis* (Daudin) were induced to ovulate by injecting human chorionic gonadotropin (Gonadotropin; Teikoku Zoki, Tokyo) into the dorsal lymph sac. For mating experiments, inbred J strain males [8] were used. Gynogenetic diploid animals were obtained as described previously [6, 9]. Briefly, eggs were inseminated by UV-irradiated (5,400-7,200 erg/mm²) J sperm, followed by a cold shock for 15 min at 2°C between 12 and 30 min after insemination for suppressing the second polar body emission. Previous analyses [8] proved that under these conditions the participation of sperm genome is totally eliminated and the resulting normally developing individuals are all diploid. The lack of sperm-derived genome was also confirmed by an acute response against J skin grafts in metamorphosed animals [6, 7]. Larvae were fed boiled alfalfa leaf powder or mashed green peas, and metamorphosed animals were fed chopped liver or a commercial fish meal (Oriental Yeast Ind., Tokyo), three to six times a week. All animals were reared in aquaria at 23±0.5°C.

The sex of progeny was identified morphologically or functionally as early as one year after fertilization.

Accepted June 17, 1987

Received April 27, 1987

¹ Present address: Nippon Institute for Biological Science, 2221-1 Shinmachi, Ohme, Tokyo 198, Japan.

RESULTS AND DISCUSSION

Gynogenetic F_1 progeny produced from four randomly selected outbred females (A–D in Table 1) comprised 92.0 to 100% females. Starting from three gynogen F_1 mothers (A1, B1 and B2), gynogenetic propagation was repeated to produce F_2 – F_4 progeny. As summarized in Table 1, all F_2 – F_4 offspring from the A1 mother were females, whereas F_2 and F_3 progeny from B line mothers included a small proportion (<16.7%) of males.

These results may be explained in the context of a female heterogametic system operated by one locus per genome [4], as follows. Upon gynogenetic propagation, if there is no recombination between a putative sex-determinant locus and the centromere, only homogametic females (WW) and males (ZZ) will be obtained [cf., 6, 10, 11]. However, recombination at the pertinent locus should give rise to heterogametic (ZW) females, yielding females and males in a ratio dependent on the rate of recombination. In this respect, the occurrence of 92.0 or 92.3% females in the gynogenetic F_1 generation (offspring of A and C in Table 1) is not much different from the rate of

83.3% (ZW+WW) expected theoretically on the basis of the maximum frequency of recombination (66.7% ZW) in the pertinent locus in gynogenetic offspring [11, 12]. The hypothesis that there is a relatively high frequency of recombination of the sex-determination gene is tenable in view of the appearance of males in gynogens F_2 and F_3 derived from putatively heterogametic (ZW) mothers (B1 and B2 in Table 1). The rate of the appearance of females (83.3–94.7%) in gynogens F_1 – F_3 in this study is quite similar to the previously reported values of 80.7% [5] and 86.0% [13] obtained in F_1 gynogens from outbred animals.

Gynogenetic progeny of line A frogs was characteristic in that all 286 F_2 – F_4 frogs were consistently female (Table 1), suggesting that they were homogametic (WW). To prove their homogamety, three randomly selected F_3 frogs (A111, A112 and A113) and an F_4 frog (A1111) were mated with J males. More than 500 (J×line A) hybrids thus obtained were all females (Table 2). The heterogamety (ZW) of these females was supported by the result that a high proportion of males appeared when a (J×A111) hybrid frog was mated with a J male (Table 2). In contrast to the fertility of

TABLE 1. The number of offspring and the ratio of females in gynogenetically produced F_1 – F_4 frogs

Generation	Mother ^a	Number of offspring	
		female (%)	male
F_1	A	23 (92.0)	2
	B	4 (100.0)	0
	C	12 (92.3)	1
	D	6 (100.0)	0
F_2	A1	120 (100.0)	0
	B1	18 (94.7)	1
	B2	8 (88.9)	1
F_3	A11	46 (100.0)	0
	B11	5 (83.3)	1
	B12	3 (100.0)	0
F_4	A111	49 (100.0)	0
	A112	37 (100.0)	0
	A113	34 (100.0)	0

a, A–D, different outbred females; numbers, the lineage relationship of A and B progeny, e.g., B11 and B12 are progeny of B1.

TABLE 2. The number and the ratio of females and males in the offspring produced by mating of gynogenetic progeny with J males

Mother	Father	Number of offspring	
		female (%)	male (%)
A111 ^a	J	178 (100.0)	0 (0)
A112	J	151 (100.0)	0 (0)
A113	J	78 (100.0)	0 (0)
A1111	J	106 (100.0)	0 (0)
(JxA111) ^b	J	32 (58.2)	23 (41.8)

a, A111–A113 indicate F₃ gynogen derived from F₂ gynogen A11; A1111, F₄ gynogen derived from F₃ gynogen A111.

b, one female progeny derived from mating of A111 with one J male.

putative homogametic (WW) gynogenetic diploid females, all females produced by refrigerating W eggs after fertilization with unirradiated sperm were sterile, apparently due to their triploid (ZWW or WWW) state (data not shown).

In conclusion, our results not only support the previous notion that the female of *Xenopus laevis* is heterogametic (ZW), but also show that the recombination between this gene(s) and the centromere occurs in rather high frequency. Furthermore, consistent with Colombelli *et al.* [5], stable and highly fertile lines of WW super-females are easily obtained by gynogenetic propagation. Although it has been shown that the sex-determination locus is not linked with the major histocompatibility complex [7], it would be worthwhile to determine the linkage between the sex-determining genes and already identified genes in this species [13].

ACKNOWLEDGMENT

This study was supported in part by Grant-in-Aid for Scientific Research No. 60440100 from the Ministry of Education, Science and Culture of Japan. The author expresses appreciation to Drs. Ch. Katagiri and S. Tochinai for their guidance and help in preparing the manuscript, and to T. Enami and H. Ohinata for their

collaboration in producing gynogens.

REFERENCES

- 1 Chang, C. Y. and Witchi, E. (1955) Proc. Soc. Exp. Biol. Med., **89**: 150–152.
- 2 Chang, C. Y. and Witchi, E. (1956) Proc. Soc. Exp. Biol. Med., **93**: 140–144.
- 3 Mikamo, K. and Witchi, E. (1963) Genetics, **48**: 1411–1421.
- 4 Mikamo, K. and Witchi, E. (1966) Cytogenetics, **5**: 1–19.
- 5 Colombelli, B., Thiebaud, Ch. H. and Muller, W. P. (1984) Mol. Gen. Genet., **194**: 57–59.
- 6 Nakamura, T., Kawahara, H. and Katagiri, Ch. (1985) Zool. Sci., **2**: 71–79.
- 7 Nakamura, T., Sekizawa, A., Fujii, T. and Katagiri, Ch. (1986) Immunogenetics, **23**: 181–186.
- 8 Katagiri, Ch. (1978) Dev. Comp. Immunol., **2**: 5–14.
- 9 Kawahara, H. (1978) Dev. Growth Differ., **20**: 227–236.
- 10 Nace, G. W., Richards, C. M. and Asher, J. H., Jr. (1970) Genetics, **66**: 349–368.
- 11 Asher, J. H., Jr. (1970) Genetics, **66**: 370–391.
- 12 Volpe, E. P. and Dasgupta, S. (1962) J. Exp. Zool., **151**: 287–302.
- 13 Reinschmidt, D., Friedman, J., Hauth, J., Ratner, E., Cohen, M., Miller, M., Krotoski, D. and Tompkins, R. (1985) J. Hered., **76**: 345–347.

[COMMUNICATION]

Medaka Hatching Enzyme Consists of Two Kinds of Proteases which Act Cooperatively

SHIGEKI YASUMASU, ICHIRO IUCHI and KENJIRO YAMAGAMI

*Life Science Institute, Sophia University, Kioicho,
Chiyoda-ku, Tokyo 102, Japan*

ABSTRACT—Intensive fractionation of hatching liquid of the medaka, *Oryzias latipes*, by repeating Toyopearl HW-50 Superfine gel filtration chromatography in alkaline buffers gave rise to five fractions of proteases ultimately. In terms of some characteristics of the enzymes such as the choriolytic activity relative to the proteolytic activity, and the chromatographic behavior expressed as the ratio of the effluent volume for each fraction to the total column volume (V_e/V_t), the enzymes of these five fractions could be classified into two groups; one was a protease with high choriolytic activity and V_e/V_t of 0.80–0.83 (high choriolytic enzyme, HCE), and the other was a protease with low choriolytic activity and V_e/V_t of 0.47–0.48 (low choriolytic enzyme, LCE). When both enzymes were combined together, they showed a marked synergistic choriolytic activity. This fact strongly suggests that HCE and LCE participate in actual choriolysis cooperatively.

The hatching enzyme of various animal species is secreted from the hatching embryo into the perivitelline space, participates in breakdown or solubilization of an egg envelope, and is released into the medium after the egg envelope became soluble [1–4].

Physical heterogeneity or polymorphism of the hatching enzyme(s) has been reported so far, implying that the enzyme with a similar activity in the hatching liquid is separated into some fractions representing different molecular weights or different electric charges on some fractionation procedures such as gel filtration chromatography or zone electrophoresis. Such heterogeneity has been

ascribed to a probable difference in the state of association of one and the same enzyme with some concomitant heterologous substances [5–9]. However, it is dubious, at present, whether the hatching enzyme is a single enzyme or an enzyme system in which multiple enzymes with different properties participate in egg envelope digestion.

It was suggested that the association of the enzyme with any heterologous substances might be canceled by repeating gel filtration column chromatography in an alkaline buffer [6]. The present report describes the presence of two different types of proteases in the hatching liquid of medaka as revealed by repeating Toyopearl gel filtration chromatography in an alkaline buffer system. Both enzymes are considered to be responsible for natural choriolysis (egg envelope digestion), as a synergistic solubilization of chorion (egg envelope) occurred when both enzymes were applied together to the isolated chorion.

MATERIALS AND METHODS

The fertilized eggs of the orange-red variety of the medaka, *Oryzias latipes*, were used as materials. The embryos were cultured in the medium (10mM NaCl–1 mM NaHCO_3) containing penicillin G (K-salt, 100 units/ml, Meiji Seika Co.) and streptomycin sulfate (100 $\mu\text{g/ml}$, Meiji Seika Co.) until the time of hatching. The culture medium was refreshed every other day. The hatching liquid, the culture medium in which the larvae hatched out, was filtered and used as the enzyme source.

Determination of enzyme activity Throughout the experiment, the enzyme activity was expressed in terms of two kinds of activities, i. e., proteolytic activity (P.A.) and choriolytic activity (C.A.). P.A. was determined in the standard method using casein (Hammarsten, Merck) as substrate and expressed in terms of the increase in absorbance of the supernatant of the deproteinized reaction mixture at 280 nm (ΔOD_{280}) [10]. C.A. was determined following two different methods. One was the turbidimetric method using fine fragments of chorion as substrate and the activity was expressed as increase of transmission at 610 nm of the reaction mixture (ΔT_{610}) as reported previously [11]. The other was a method by which the amount of peptides solubilized from chorion fragments was determined: Twenty mg of coarse fragments of chorion was incubated with the enzyme in 1 ml of reaction mixture (50 mM Tris·HCl–10 mM NaCl, pH 7.5) at 30°C with continuous shaking. After the reaction was stopped by adding 1 ml of 30 mM ethylenediamine tetraacetate (EDTA) [10], the amount of the solubilized peptides in the supernatant was determined in terms of the absorbance at 280 nm (ΔOD_{280}).

Column chromatography The hatching liquid derived from 10,000–15,000 hatching larvae was added by solid ammonium sulfate to 60% saturation, allowed to stand for 1 hr and then centrifuged at 10,000 rpm for 20 min to sediment the precipitates. The precipitates were solubilized by suspending in about 10 ml of 5 mM Tris·HCl–5 mM NaCl (pH 8.5) and dialyzing against the same buffer for 1–2 hr. The clear solution thus obtained was applied onto a Toyopearl HW–50 Superfine (Toyo Soda) column (1.5×91 or 2.6×78 cm) equilibrated with the same buffer and eluted at a flow rate of 14 ml/hr or 24 ml/hr. At this step, four peaks of proteolytic activity, Pa (1), Pa (2), Pa (3) and Pa (4), were obtained. Further fractionation of Pa (1), and the combination of the other three peaks, Pa (2, 3, 4) was performed by repeating the ammonium sulfate precipitation, followed by Toyopearl HW–50 Superfine gel filtration chromatography in 50 mM NaHCO₃–Na₂CO₃ (pH 10.2). All the procedures described above were carried out at 0–4°C. The elution pattern of protein was depicted on the basis of absorbance at 280 nm.

RESULTS AND DISCUSSION

Toyopearl HW–50 Superfine column chromatography of the ammonium sulfate precipitate of the hatching liquid in a slightly alkaline buffer (pH 8.5) produced four proteolytically active peaks, Pa (1), Pa (2), Pa (3) and Pa (4) (Fig. 1–a). Among them, the void volume peak, Pa (1), contained a large amount of chorion digest. The second peak was characterized by its having very low choriolytic activity as compared with the proteolytic activity. The rechromatography of Pa (1) on the same column in an alkaline buffer (pH 10.2) shifted the effluent position of the activity backward and gave rise to two proteolytically active fractions as shown in Figure 1–b; one was an irregular peak of activity, Pa (1)–1, and the other was a single sharp peak, Pa (1)–2. Pa (1)–1 was found to include two proteases: When Pa (1)–1 was rechromatographed in the alkaline buffer (pH 10.2) as before, it was separated again into two sharp peaks of proteolytic activity, Pa (1)–1–1 and Pa (1)–1–2 (Fig. 1–c).

Pa (2, 3, 4) also could be separated by rechromatography on the Toyopearl HW–50 Superfine column in the alkaline buffer (pH 10.2) into two fractions, each of which represented a single sharp peak of proteolytic activity (Fig. 1–d).

After all, the intensive fractionation of the hatching liquid by repeating Toyopearl HW–50 Superfine column chromatography in the alkaline buffer gave rise to five sharp peaks of proteolytic activity, Pa (1)–1–1, Pa (1)–1–2, Pa (1)–2, Pa (2, 3, 4)–1 and Pa (2, 3, 4)–2, each of which could not be fractionated further. These five fractions could be classified into two groups in terms of the choriolytic activity relative to the proteolytic activity and their chromatographic behavior expressed as V_e/V_t , where V_e is the effluent volume for each fraction and V_t is the total column volume [12]. As shown in Table 1, the enzymes in Pa (1)–1–1 and Pa (2, 3, 4)–1 are considered to belong to one group, as they are characterized by low choriolytic activity as compared with the proteolytic activity ($CA/PA=0.63-1.21$) and by a low value of V_e/V_t (0.47–0.48). The enzymes in Pa (1)–1–2, Pa (1)–2 and Pa (2, 3, 4)–2 seem to belong to the other group, as they have very high choriolytic activity ($CA/PA=30.47-48.05$) and exhibit higher V_e/V_t .

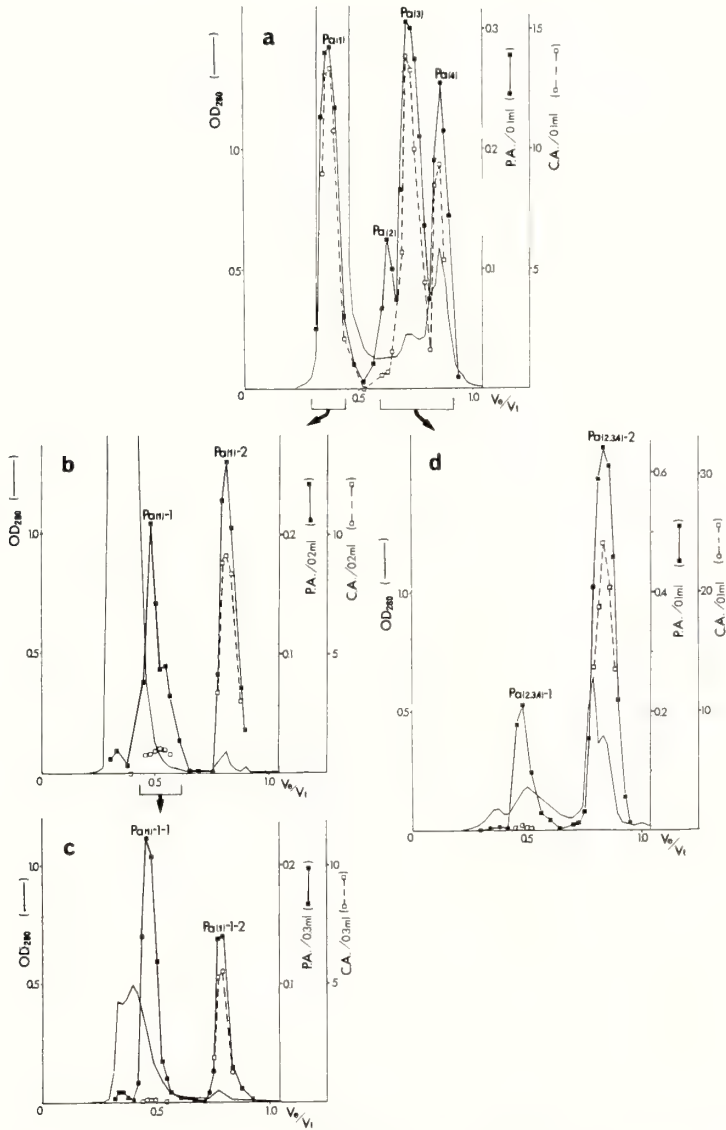


FIG. 1. Fractionation of proteolytic enzymes in the hatching liquid of medaka by Toyopearl HW-50 Superfine gel filtration column chromatography. (a) Ammonium sulfate (60% saturation) precipitate of the hatching liquid (16,000 larvae eq.) was fractionated at pH 8.5 (5mM Tris-HCl-5 mM NaCl). (b) Pa(1) in (a) was collected, added by ammonium sulfate (60% saturation) and the precipitate was collected, dissolved and chromatographed at pH 10.2 (50 mM NaHCO₃-Na₂CO₃). (c) Pa (1)-1 in (b) was collected, precipitated by ammonium sulfate (60% saturation) and rechromatographed at pH 10.2. (d) Pa (2), Pa(3) and Pa (4) in (a) were combined and added by ammonium sulfate (60% saturation) to obtain precipitates. Pa (2, 3, 4) thus obtained was chromatographed at pH 10.2. Column size and the volume of each tube were 2.6×78 cm and 8.6 ml, respectively in (a) and (b), and 1.5×91 cm and 3.4 ml, respectively in (c) and (d). —: Protein amount. ■—■: Proteolytic activity determined using casein as substrate [cf. 10], □---□: Choriolytic activity determined by turbidimetry [cf. 11].

TABLE 1. Choriolytic activity relative to proteolytic activity and chromatographic behavior of various fractions of proteases obtained from the hatching liquid of medaka by repeated Toyopearl HW-50 gel filtration chromatography

Fraction (ml)*	Choriolytic activity ($\Delta T_{610}/5 \text{ min}/30^\circ\text{C}$)	Proteolytic activity ($\Delta OD_{280}/30 \text{ min}/30^\circ\text{C}$)	C.A./P.A.	V_e/V_t
Pa(1)-1-1 (0.35)	0.14	0.223	0.63	0.47
Pa(1)-1-2 (0.40)	6.99	0.197	35.48	0.81
Pa(1)-2 (0.30)	8.50	0.279	30.47	0.80
Pa(2, 3, 4)-1 (0.15)	0.25	0.206	1.21	0.48
Pa(2, 3, 4)-2 (0.10)	16.00	0.333	48.05	0.83

C.A./P.A. is expressed simply in terms of the ratio of the choriolytic activity to the proteolytic activity. V_e/V_t refers to retention of each enzyme fraction to the column. * Volume of the fraction used as the enzyme solution.

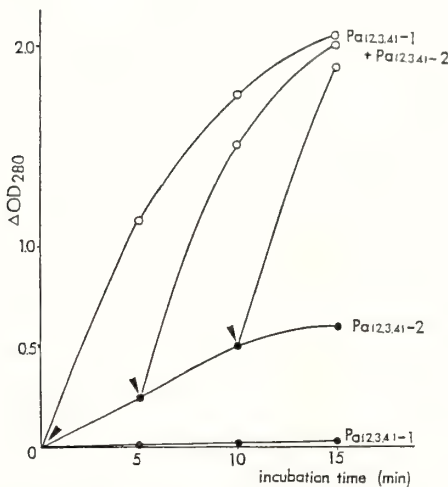


FIG. 2. Cooperative choriolytic action of two kinds of proteolytic enzymes fractionated from the hatching liquid of medaka. Pa (2, 3, 4)-1 and Pa (2, 3, 4)-2 refer to LCE and HCE, respectively. The choriolytic activity (C. A.) was determined by the second method described in Materials and Methods. The amounts of both enzymes used were approximately equivalent in terms of their proteolytic activity toward casein ($\Delta OD_{280}/30^\circ\text{C}/30 \text{ min}=0.4$). Arrow-head indicates the time when Pa (2, 3, 4)-1 was added to the incubated mixture of chorion fragments and Pa (2, 3, 4)-2.

value (0.80-0.83) in common. Thus, the proteolytic enzymes in the hatching liquid of medaka seem to be classified ultimately into two types of

enzymes; low choriolytic enzyme (LCE) and high choriolytic enzyme (HCE). It is considered that a large part of Pa (2) and Pa (4) in Figure 1-a correspond to LCE and HCE, respectively, from the values of V_e/V_t . Moreover, it is highly probable that LCE and/or HCE in the form complexed with some other substances are eluted as Pa (1) and Pa (3).

As shown in Figure 2, when LCE of Pa (2, 3, 4)-1 and HCE of Pa (2, 3, 4)-2 were applied together to the chorion, a marked synergistic choriolysis occurred, while LCE, if applied singly, exerted no significant choriolytic activity. Essentially the same results were obtained when Pa (1)-1 was used for LCE, and either Pa (1)-2 or Pa (1)-1-2 was used for HCE. Thus, making a distinction among the enzymes in those fractions was possible also from their roles in choriolysis. Recently both LCE and HCE have been obtained in homogeneous forms and found to be distinct from each other in some physical chemical characteristics. Their biochemical properties will be reported in the following papers.

Proteolytic enzyme in the hatching liquid of medaka has been fractionated by Sephadex G-75 column chromatography (pH 8.5) into two fractions, PI and PII, [6, 11] and they seem to correspond to Pa (1) and Pa (2, 3, 4), respectively, in the present experiment. Each of Pa (1) and Pa (2, 3, 4) includes both LCE and HCE. Therefore,

a previous view that the polymorphic hatching enzyme of medaka is a single and the same enzyme [6] should be corrected according to the present results, which strongly suggest that the hatching enzyme of medaka is an enzyme system composed of two distinct enzymes, HCE and LCE, acting cooperatively. In the present experiment, a previous presumption that a proteolytic enzyme without clearing (choriolytic) activity might be present in the hatching liquid of medaka [11] was verified.

ACKNOWLEDGMENT

This work was partly supported by a Grant-in-Aid for Scientific Research from the Ministry of Education, Science and Culture, Japan.

REFERENCES

- 1 Bourdin, J. (1926) *C. R. Soc. Biol.*, **95**: 1242-1243.
- 2 Ishida, J. (1936) *Annot. Zool. Japon.*, **15**: 453-457.
- 3 Cooper, K. W. (1936) *Proc. Natl. Acad. Sci., USA.*, **22**: 433-434.
- 4 Yamamoto, M., Iuchi, I. and Yamagami, K. (1979) *Dev. Biol.*, **68**: 162-174.
- 5 Barrett, D., Edwards, B. F., Wood, D. B. and Lane, D. J. (1971) *Arch. Biochem. Biophys.*, **143**: 261-268.
- 6 Yamagami, K. (1975) *J. Exp. Zool.*, **192**: 127-132.
- 7 Ogawa, N. and Ohi, Y. (1968) *Zool. Mag. (Tokyo)*, **77**: 151-156.
- 8 Ohi, Y. and Ogawa, N. (1970) *Zool. Mag. (Tokyo)*, **79**: 17-18.
- 9 Schoots, A. F. M., Sackers, R. J., Overkamp, P. S. G. and Denucé, J. M. (1983) *J. Exp. Zool.*, **226**: 93-100.
- 10 Yamagami, K. (1973) *Comp. Biochem. Physiol.*, **46B**: 603-616.
- 11 Yamagami, K. (1972) *Dev. Biol.*, **29**: 343-348.
- 12 Ackers, G. K. (1975) In "The Proteins". Ed. by H. Neurath and R. L. Hill, Academic Press, New York, Vol. 1, pp. 1-94.

[COMMUNICATION]

Corpuscles of Stannius of *Clarias batrachus* in Response to 1, 25 Dihydroxyvitamin D₃ Administration

AJAI K. SRIVASTAV and SHYAM P. SRIVASTAV

Department of Zoology, University of Gorakhpur,
Gorakhpur-273 009, India

ABSTRACT—Administration of 1, 25 dihydroxyvitamin D₃ (1, 10 or 50 U/100 g bw) to the catfish, *Clarias batrachus* for 10 days activated the corpuscles of Stannius.

INTRODUCTION

The corpuscles of Stannius (CS) secrete hypocalcemic factor(s). This is evident by a rise in serum calcium level after removal of CS which is corrected by administration of CS extract [1]. A PTH-like substance (parathyrin) has recently been localized immunocytochemically in the eel CS [2]. Lafeber *et al.* [3] have reported parathyroid hormone-like effects of rainbow trout Stannius products on bone resorption of embryonic mouse calvaria.

Although vitamin D₃ is abundantly present in fish liver, its role in calcium homeostasis has been emphatically denied [4]. Recently, it has been reported that vitamin D₃ and its metabolites induce hypercalcemia in fishes [5-8]. Moreover, Srivastav *et al.* [9] have also reported hyperactivity of CS after vitamin D₃ treatment. In the present study we have investigated the effects of 1, 25 dihydroxyvitamin D₃ (1, 25 (OH)₂D₃) on the CS of the freshwater catfish, *Clarias batrachus*.

MATERIALS AND METHODS

Adult male specimens of *Clarias batrachus* (21-25 cm, 65-90 g) were collected locally and acclima-

tized to the laboratory conditions for one week prior to use. They were then divided into four groups (A, B, C and D). Fish of all the groups were kept in identical all-glass aquaria, each containing eight liters of tap water (renewed daily). Only six fish were kept in each aquarium and they were not fed during the experiment.

Fish from all the groups (A-D) were given daily intramuscular injections of the following treatments for 10 days:

Group A: 0.1 ml/100 g bw of vehicle (ethanol)

Group B: 1 U of 1, 25 (OH)₂D₃/100 g bw

Group C: 10 U of 1, 25 (OH)₂D₃/100 g bw

Group D: 50 U of 1, 25 (OH)₂D₃/100 g bw

In all cases, the injection volume was 0.1 ml/100 g bw.

Six fish from each group were anesthetized with MS 222 (Sandoz Ltd., Basle) 2 hr after the last injection on the 1st, 3rd, 5th and 10th day of the experiment. Blood samples were collected by the sectioning of caudal peduncle. Blood samples from the non-treated (normal) specimens were also taken before the start of the experiment. After clotting of the blood the sera were separated by centrifugation at 3500 rpm and analysed for serum calcium level according to Trinder's [10] method.

After the collection of blood samples, the CS along with the adjoining portion of the kidney, were extirpated from the fish and fixed in Bouin's fluid and Zenker's formol. After routine processing in graded series of alcohols and clearing in xylene, tissues were embedded in paraffin. Serial sections were cut at 4-6 μm and stained with

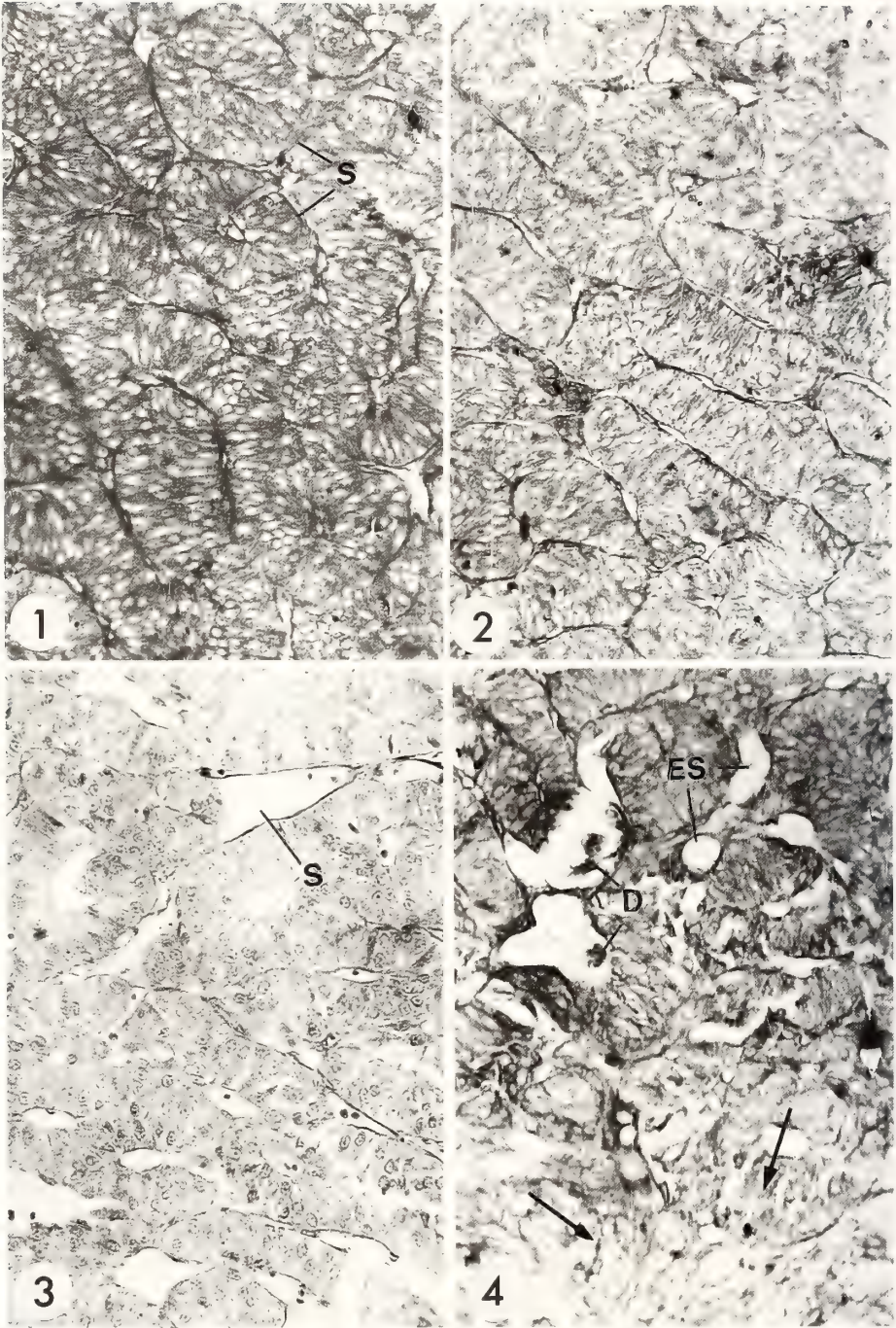


FIG. 1. CS of vehicle-treated fish showing the arrangement of corpuscular cells along septa (S). AF $\times 400$.
 FIG. 2. CS of fish from group B displaying decreased stainability of corpuscular cells after 10 days of treatment. AF $\times 400$.
 FIG. 3. CS of fish from group C exhibiting dilatation of sinusoids (S) after 5 days of treatment. HE $\times 400$.
 FIG. 4. CS of fish from group D depicting empty spaces (ES), cell debris (D) and loss of cellular arrangement (arrows) after 10 days of treatment. AF $\times 400$.

hematoxylin-eosin (HE) and aldehyde fuchsin (AF).

The nuclear diameter was measured with the aid of an ocular micrometer. Each nucleus was measured along its long and short axes and mean value was calculated. From each group 300 nuclei were measured (fifty nuclei from each specimen) at every interval.

Differences in the serum calcium level and nuclear diameter among different groups were analysed by Student's *t*-test.

RESULTS

The changes in the serum calcium levels and corpuscular cell nuclear size of groups A-D at various intervals have been summarised in Table 1.

In normal specimens, CS are enveloped by a thin connective tissue sheath from which a number of septa extend into the gland. The corpuscular cells are arranged along these septa (Fig. 1). Each cell possesses a distinct nucleus and homogenous cytoplasm; however, the cell boundaries are not distinct. There is only one cell type. When stained with HE, the cytoplasm of corpuscular cells is eosin-positive. However, the granules are not discernible by this stain. After AF staining, cytoplasm of corpuscular cells exhibits positive response and displays many coarse AF-positive

granules which are densely aggregated around the nucleus.

In group B (1 U/100 g bw of 1, 25 (OH)₂D₃), there is no change in the corpuscular cells until day 5. On day 10, the nuclear size increases (Table 1) and there is decreased stainability of corpuscular cells (Fig. 2).

In group C (10 U/100 g bw of 1, 25 (OH)₂D₃), the corpuscular cells show a progressive increase in nuclear size from day 5 to day 10 (Table 1). There is a progressive sinusoidal dilatation and decreased stainability of corpuscular cells from day 5 onwards (Fig. 3).

In group D (50 U/100 g bw of 1, 25 (OH)₂D₃) there is an increase in nuclear size (Table 1), decreased stainability of corpuscular cells and dilatation of sinusoids on day 3. These responses are exaggerated on day 5. Also, there is noticed degeneration of certain cells. The nuclear size of intact cells shows a further increase (Table 1). On day 10, the AF stainability of corpuscular cells increases. The degenerative changes are at their peak - the cells loose their arrangement, the empty spaces and cell debris become conspicuous (Fig. 4).

DISCUSSION

The present study reveals that the activity of CS is affected quite perceptibly on treatment with

TABLE 1. Serum calcium (mg/100 ml) and nuclear size (μ m) of corpuscular cells of different groups (A-D) after various intervals

Days	Group A	Group B	Group C	Group D
1 Serum Ca	10.42 ± 0.11	10.32 ± 0.23	10.68 ± 0.14	10.76 ± 0.23
Nuclear size	4.32 ± 0.04	4.29 ± 0.03	4.36 ± 0.02	4.34 ± 0.06
3 Serum Ca	10.36 ± 0.21	10.94 ± 0.17	11.30 ± 0.24 ^a	11.92 ± 0.27 ^c
Nuclear size	4.29 ± 0.03	4.33 ± 0.03	4.42 ± 0.06	4.48 ± 0.06 ^b
5 Serum Ca	10.28 ± 0.19	11.60 ± 0.13 ^c	13.48 ± 0.31 ^d	14.06 ± 0.21 ^d
Nuclear size	4.34 ± 0.04	4.46 ± 0.05	4.85 ± 0.04 ^d	4.96 ± 0.03 ^d
10 Serum Ca	10.32 ± 0.21	11.82 ± 0.25 ^c	13.08 ± 0.27 ^d	13.56 ± 0.32 ^d
Nuclear size	4.28 ± 0.05	4.75 ± 0.06 ^b	5.02 ± 0.05 ^d	5.19 ± 0.04 ^d

Each value represents mean ± S.E. of six specimens.

a, b, c and d indicate significant responses compared to group A: P < 0.05, < 0.02, < 0.01 and < 0.001, respectively.

In normal fish, serum level of calcium was 10.25 ± 0.16 mg/100 ml and nuclear size of corpuscular cells was 4.21 ± 0.03 μ m.

different doses of 1, 25 (OH)₂D₃ which is expressed by the decreased stainability and nuclear hypertrophy of corpuscular cells and sinusoidal dilatation. These changes have been considered as indications of the hyperactivity of the gland [9, 11]. The hyperactivity of the corpuscular cells suggests an increased synthesis and release of hypocalcemic factor(s) to combat the elevated serum calcium levels caused by 1, 25 (OH)₂D₃ treatment. The degeneration of the corpuscular cells can be attributed to their overactivation in response to perpetual hypercalcemic challenge. Degeneration due to hyperactivity has also been reported by Hiroi [12] and Srivastav *et al.* [9].

Although Lopez *et al.* [13] failed to get any change in CS activity in eels following 1, 25 (OH)₂D₃ treatment, the present study clearly indicates that this metabolite affects the activity of CS in *C. batrachus*. The failure of Lopez *et al.* [13] in not observing any change in CS could be explained as they have sacrificed their specimens 24 hr after the last injection of 1, 25 (OH)₂D₃ (in their experiments only two injections of 1, 25 (OH)₂D₃ were given at 0 and 48 hr and the fish were killed 72 hr after the first injection). It may be possible that by this time the changes in CS may have been recovered.

ACKNOWLEDGMENTS

One of us (AKS) is thankful to Sandoz Ltd., Basle for generous gift of MS 222 and U. G. C., New Delhi for financial assistance.

REFERENCES

- 1 Kenyon, C. J., Chester Jones, I. and Dixon, R. N. B. (1980) *Gen. Comp. Endocrinol.*, **41**: 531-538.
- 2 Lopez, E., Tisserand-Jochem, E. M., Eyvuem, A., Milet, C., Hillyard, C., Lallier, F., Vidal, B. and MacIntyre, I. (1984) *Gen. Comp. Endocrinol.*, **53**: 28-36.
- 3 Lafeber, F. P. J. G., Schaefer, H. I. M. B., Herrmann-Erlee, M. P. M. and Wendelaar Bonga, S. E. (1986) *Endocrinology*, **119**: 2249-2255.
- 4 MacIntyre, I., Colston, K. W., Evans, I. M., Lopez, E., Macauley, S. J., Peignoux-Deville, J., Spanos, E. and Szelke, M. (1976) *Clin. Endocrinol., Suppl.* **5**: 85.
- 5 Swarup, K. and Srivastav, S. P. (1982) *Gen. Comp. Endocrinol.*, **46**: 271-274.
- 6 Srivastav, A. K. (1983) *J. Fish Biol.*, **23**: 301-303.
- 7 Swarup, K., Norman, A. W., Srivastav, A. K. and Srivastav, S. P. (1984) *Comp. Biochem. Physiol.*, **78B**: 553-555.
- 8 Fenwick, J. C., Smith, K., Smith, J. and Flik, G. (1984) *Gen. Comp. Endocrinol.*, **55**: 398-404.
- 9 Srivastav, S. P., Swarup, K. and Srivastav, A. K. (1985) *Cell. Mol. Biol.*, **31**: 1-5.
- 10 Trinder, P. (1960) *Analyst*, **85**: 889-894.
- 11 Olivereau, M. and Olivereau, J. (1978) *Cell Tissue Res.*, **186**: 81-96.
- 12 Hiroi, O. (1970) *Bull. Fac. Fish. Hokkaido Univ.*, **21**: 179-192.
- 13 Lopez, E., Peignoux-Deville, J., Lallier, F., Colston, K. W. and MacIntyre, I. (1977) *Calcif. Tissue Res., Suppl.* **22**: 19-23.

[COMMUNICATION]

Translocation of ^{45}Ca from the Endolymphatic Sacs to the Bone in *Rana nigromaculata*MASAKO FUJIMORI¹, YUICHI SASAYAMA and CHITARU OGURO²*Department of Biology, Faculty of Science, Toyoma University, Toyama 930, Japan*

ABSTRACT—In the frog, *Rana nigromaculata*, intra-arterially administered ^{45}Ca was incorporated into all tissues and organs within 2 hr. The endolymphatic sacs showed the highest level of incorporation, followed by bones. After 4 days, bone was the only tissue that showed significant increase in ^{45}Ca deposition in comparison with the situation after 2 hr. In all other tissues and organs including the endolymphatic sacs, the values of incorporation were significantly lower than those after 2 hr. From these results, it was concluded that the endolymphatic sacs serve as a temporary depot tissue for calcium, which then moves chronically to the bones.

INTRODUCTION

The ultimobranchial gland (UB) of the frog contains calcitonin which evokes hypocalcemia and hypophosphatemia in rats [1-3]. This is supported by the facts that in several anuran species, substances in the ultimobranchial cells crossreact with anticalcitonin antisera [4-6].

It has been reported that in *Rana nigromaculata*, removal of the UB markedly reduces the calcium content in the endolymphatic sacs [7]. Moreover, administration of calcitonin promotes an uptake of ^{45}Ca into the endolymphatic sacs, but produces no effect on the calcium kinetics in other tissues and organs [7]. Thus, calcitonin seems to be a promoter of calcium storage in the endolymphatic sacs in frogs.

The present report describes the fate of ^{45}Ca

incorporated into the endolymphatic sacs at various times after administration.

MATERIALS AND METHODS

Adult males of *Rana nigromaculata*, 15-40 g bw, were used in the present study. They were collected in the suburbs of Toyama City during spring and summer. The frogs were kept in tapwater (Ca 1.7, Mg 0.6, Na 1.0, K 0.2 mg/100 ml) which had been allowed to stand for a long period.

The sciatic artery of anesthetized frogs was cannulated using polyethylene tubing (PE 10, Clay Adams) for the administration of ^{45}Ca and calcitonin (synthetic salmon calcitonin, dissolved in 0.6% NaCl adjusted to pH 4.6 with HCl).

Each frog received calcitonin (50 mU/50 μl /10 g bw) via the cannula. Thirty min later, ^{45}Ca (8 $\mu\text{Ci}/50 \mu\text{l}/10 \text{ g bw}$) was administered through the same cannula. Five frogs were killed 2 hr afterwards and 30 different tissues and/or organs were dissected out and ^{45}Ca radioactivity in each was measured. Another 5 frogs were killed 4 days afterwards and treated in the same way as the 2-hr frogs.

RESULTS

The results obtained are shown in Figure 1. This figure shows the levels of ^{45}Ca activity in the endolymphatic sacs, femur, vertebrae, cartilage, skin and some other soft tissues and organs. Levels in some soft tissues and organs which

Accepted August 6, 1987

Received July 15, 1987

¹ Present address: Fukumitsu Senior High School, Toyama 939-16, Japan.

² To whom reprints should be addressed.

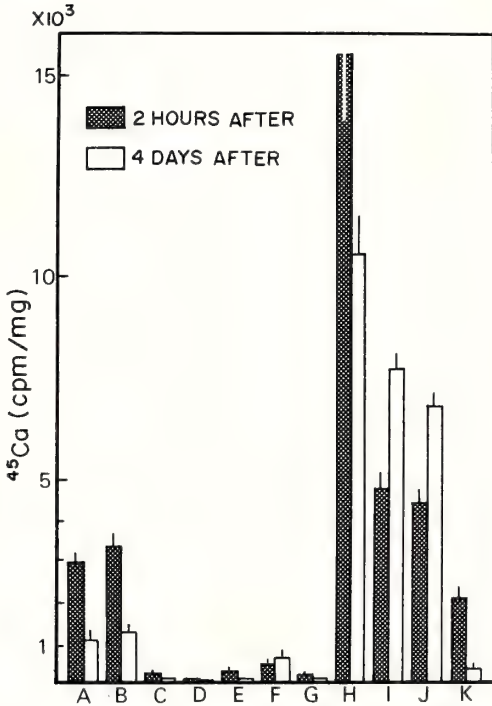


FIG. 1. ⁴⁵Ca activity in various tissues and organs of *Rana nigromaculata* 2 hr and 4 days after intra-arterial administration of ⁴⁵Ca. A, Skin (ventral). B, Skin (dorsal). C, Kidney. D, Muscle. E, Stomach. F, Gallbladder. G, Liver. H, Endolymphatic sacs. I, Femur. J, Vertebrae. K, Cartilage.

showed a similar tendency to the values shown in the figure are excluded.

Two hours after ⁴⁵Ca administration, all samples examined showed a certain level of ⁴⁵Ca activity. The endolymphatic sacs showed the highest activity (15,530 cpm/mg tissue), followed by the femur and vertebrae (4,848 and 4,351 cpm/mg tissue, in that order). Skin (dorsal and ventral) and cartilage showed fairly high values, whereas ⁴⁵Ca activity in the other samples was very low.

Four days after ⁴⁵Ca administration, radioactivity values in all tissues and organs, including the skin and cartilage, had decreased significantly except for the bones and gallbladder. However, the increased activity level in the gallbladder was not statistically significant. The activity levels in the endolymphatic sacs, femur and vertebrae were 10,643, 7,695 and 6,346 cpm/mg tissue, respectively. The increases in the levels for the femur

($P < 0.001$) and vertebrae ($P < 0.001$) and the decrease in the level for the endolymphatic sacs ($P < 0.05$) were significantly different from the values obtained 2 hr after ⁴⁵Ca administration.

Thus, the only portion for which ⁴⁵Ca activity was increased after 4 days was the bones, in comparison with the level 2 hr after ⁴⁵Ca administration.

DISCUSSION

It has been previously reported that in *Rana nigromaculata*, ultimobranchialectomy (UBX) brings about a decrease in calcium content only in the endolymphatic sacs, whereas other organs show no response [7]. Furthermore, salmon calcitonin promotes ⁴⁵Ca incorporation into the endolymphatic sacs but not into other tissues [7]. From these results and other indirect evidence [8, 9], it was concluded that the function of the UB is to promote calcium incorporation into the endolymphatic sacs through calcitonin secretion.

However, nothing has been known about the long-term fate of ⁴⁵Ca incorporated into the endolymphatic sacs.

⁴⁵Ca activity was decreased in the majority of tissues and organs after 4 days in comparison with the situation after 2 hr. Moreover, it was remarkable that ⁴⁵Ca incorporated into the endolymphatic sacs was also decreased as in the other soft tissues and organs. It seems, therefore, that the function of calcitonin is rather transient and not long-lasting.

The only portion in which ⁴⁵Ca activity increased was bone. The increase in activity in the femur was 63% and that in the vertebrae was 46%. These levels are in marked contrast to the decrease observed in the endolymphatic sacs. These results clearly show that ⁴⁵Ca incorporated into the endolymphatic sacs under the specific influence of calcitonin was translocated into the bones within several days.

It has previously been reported that the endolymphatic sacs accumulate a calcium salt which is utilized for skeletal ossification during metamorphosis when the larvae do not feed [10, 11]. It has been suggested that the UB of frog larvae promotes the accumulation of calcium in the

endolymphatic sacs at this stage [12].

It is concluded from the present results that in adult anurans one of the functions of the endolymphatic sacs is to serve as a temporary depot tissue for calcium, facilitating subsequent calcium supply to the bones.

ACKNOWLEDGMENTS

The present study was supported in part by Grants-in-Aid for Scientific Research from the Ministry of Education, Science and Culture of Japan (No.60440006) and the Tamura Foundation for the Encouragement of Science and Technology.

REFERENCES

- 1 Oguro, C., Nagai, K.-I., Tarui, H. and Sasayama, Y. (1981) *Comp. Biochem. Physiol.*, **68A**: 95-97.
- 2 Oguro, C. and Sasayama, Y. (1985) In "Current Trends in Comparative Endocrinology". Ed. by B. Loft and W. N. Holmes, Hong Kong Univ. Press, Hong Kong, pp. 839-841.
- 3 Oguro, C., Nogawa, H., Nagai, K.-I. and Sasayama, Y. (1986) *Zool. Sci.*, **3**: 663-668.
- 4 Van Noorden, S. and Pearse, A. G. E. (1971) *Histochemie*, **26**: 95-97.
- 5 Treilhou-Lahille, F., Jullienne, A., Aziz, M., Beaumont, A. and Moukhtar, M. S. (1984) *Gen. Comp. Endocrinol.*, **53**: 241-251.
- 6 Sasayama, Y., Oguro, C., Yui, R. and Kambegawa, A. (1984) *Zool. Sci.*, **1**: 755-758.
- 7 Oguro, C., Fujimori, M. and Sasayama, Y. (1984) *Zool. Sci.*, **1**: 82-88.
- 8 Robertson, D. R. (1969) *Gen. Comp. Endocrinol.*, **12**: 479-490.
- 9 Robertson, D. R. (1972) In "Calcium, Parathyroid Hormone and the Calcitonins". Ed. by R. V. Talmage and P. L. Munson, Excerpta Medica, Amsterdam, pp. 21-28.
- 10 Guardabassi, A. (1960) *Z. Zellforsch.*, **51**: 278-282.
- 11 Pilkington, J. P. and Simkiss, K. (1966) *J. Exp. Biol.*, **45**: 329-341.
- 12 Robertson, D. R. (1971) *Gen. Comp. Endocrinol.*, **16**: 329-341.

[COMMUNICATION]

Morphological Observations of the Large Intestine in the Common Vole, *Microtus arvalis* Pallas

HAJIME AMASAKI, MASAYUKI DAIGO, and NORIFUMI MEGURO¹

Department of Veterinary Anatomy, Nippon Veterinary and Zootechnical College,
1-7-1 Kyonan-cho, Musashino-shi, Tokyo 180, and ¹Itoh Equine Clinic,
2-2 Katsushima, Shinagawa-ku, Tokyo 140, Japan

ABSTRACT—In forty common voles, *Microtus arvalis* Pallas, the morphology and physiology of the large intestine (without the rectum) was observed and analyzed.

As a result, we found the large intestine to consist of five segments: 1) the caecum, 2) the cranial region of the proximal colon, 3) the caudal region of the proximal colon, 4) the medial colon and 5) the distal colon. These were determined according to the mesenterial attaching pattern, the arterial supplying system and the mucous epithelial surface structure.

The level of total volatile fatty acid (VFA) and level of water consistency in the digestive contents of the anatomically defined segments may correspond with digestive and absorptive functions.

INTRODUCTION

Previously, investigators have examined the vole, *Microtus montebelli*, which has a compound stomach (with the forestomach) and a well-developed large intestine (with the caecum and colon) for fermentative chambers [1-5]. These functions in the vole are similar to those of the forestomach in ruminant animals [5, 6]. Recently, a morphological investigation was also conducted on the caecum and proximal colon of the vole, *Microtus agrestis* [7].

This paper presents some morphological and physiological observations of the large intestine (without the rectum) in the common vole, *Microtus arvalis* Pallas.

MATERIALS AND METHODS

Forty mature common voles, *Microtus arvalis* Pallas, were used for morphological and physiological observation. These voles were given to us from the Department of Veterinary Physiological Chemistry of the Nippon Veterinary and Zootechnical College. Fifteen were used for macro-anatomical observations of the mesenterial attaching pattern and the vascular supplying system, and five for scanning electron microscopical (SEM) observation of the epithelial surface structure. Each specimen used for SEM investigation was fixed in Zamboni-solution. After fixation, they were dried to the critical point (HITACHI, HCO-1). They were coated with gold using a vacuum evaporating ion coater (NEVA, FTM-112), and observed by SEM (JSM-S25, Mk 2).

The remaining 20 animals were used for physiological analysis of total volatile fatty acid (VFA) levels, which consisted of acetic acid, propionic acid and butyric acid, and the level of water consistency in the digestive contents in each part of the large intestine. The level of total VFA of the digestive contents was determined using gas-chromatography (SHIMAZU, GC-6AM), and the level of water consistency of the digestive contents was determined using the drying chamber.

RESULTS AND DISCUSSION

Snipes [7, 8] reported that the large intestine of

Microtus agrestis can be defined as three segments, M1, M2 and M3. In our investigation on the common vole, *Microtus arvalis* Pallas, the same

result was observed. Namely, part M1 consisted of the caecum and proximal colon covered with the caecal mesentery, which continued from the ileo-

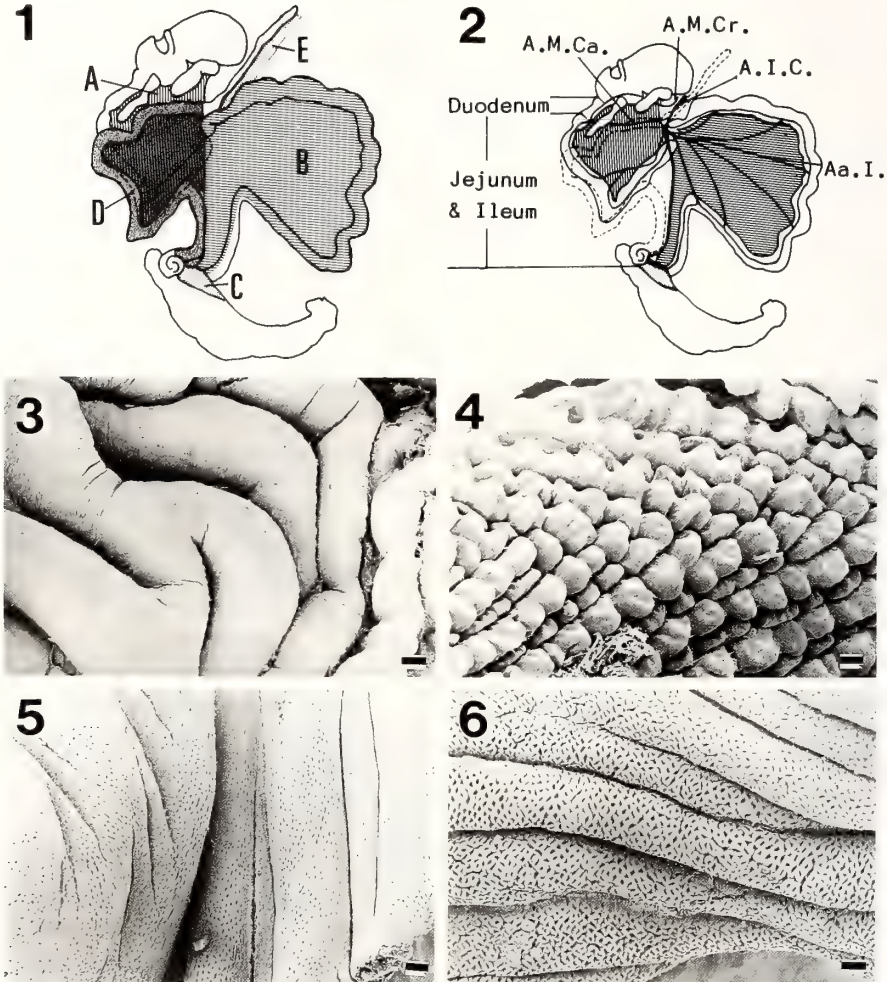


FIG. 1. Schematic diagram of the division in the large intestine (without the rectum) according to the mesenterial attaching pattern. A: Proximal part of the small intestinal mesentery covering over the duodenum and the proximal jejunum. B: Distal part of the small intestinal mesentery covering over the distal jejunum and the ileum. C(M1): Proximal part of the large intestinal mesentery covering over the caecum and the proximal colon. D(M2): Medial part of large intestinal mesentery covering over the medial colon. E(M3): Distal part of large intestinal mesentery covering over the distal colon and the rectum.

FIG. 2. Schematic diagram of the vascular supplying system in the intestine. A. M. Cr.: Cranial mesentery artery. A. M. Ca.: Caudal mesentery artery. A. I. C.: Ileo-colic artery. Aa. I.: Ileal arteries.

FIG. 3. Mucous epithelial surface in part S1. Well developed mucous folds are observed on the epithelial surface. Bar: 100 μm .

FIG. 4. Mucous epithelial surface in part S2. V-shaped mucous folds are made by many continuous papillae. Bar: 100 μm .

FIG. 5. Mucous epithelial surface in part S3. V-shaped mucous folds are disappearing caudally. Bar: 100 μm .

FIG. 6. Mucous epithelial surface in part S4. The longitudinal folds appear on the epithelial surface. Bar: 100 μm .

caecal mesentery. Part M2 was the medial colon covered with the colic mesentery. Part M3 was the distal colon covered with the caudal intestinal mesentery, which was attached to the dorsal abdominal wall (Fig. 1).

In *Microtus agrestis*, Snipes [7, 8] described the colon as being divided into four segments (A1, A2, A3 and A4) according to the vascular supplying system. In our investigation, part A1 was the most proximal colon from the ileo-caecal orifice to the centripetal gyri. The colic branch of the ileo-caecal

artery, which was the branch from the cranial intestinal artery, dispersed into part A1. Part A2 was the caudal region of the proximal colon from the centripetal gyri to the cranial colic flexure. The right colic artery, which was the branch from the cranial intestinal artery, dispersed into part A2. Part A3 was the medial colon. The medial colic artery, which was the branch from the cranial intestinal artery, dispersed into part A3. Part A4 was the distal colon. The caudal intestinal artery dispersed into part A4. Meanwhile, the caecal

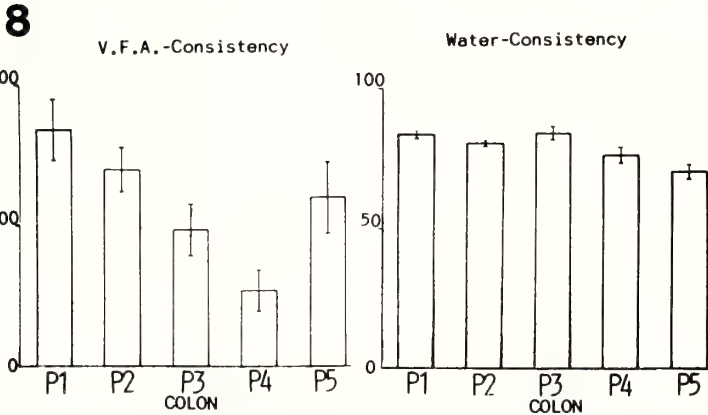
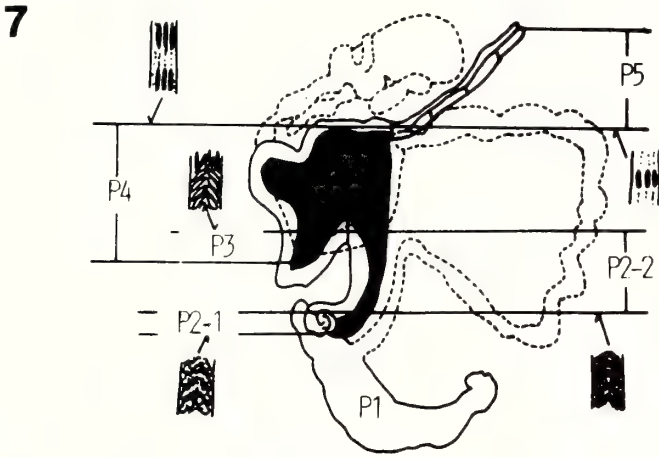


FIG. 7. Schematic diagram of the division of the large intestine (without the rectum) in the common vole, *Microtus arvalis* Pallas, according to our anatomical investigations. P1: Caecum, which consists of parts M1, A1 and S1. P2: Proximal colon (1), which consists of parts M1, A1, S1 and S2. P3: Proximal colon (2), which consists of parts M2, A2, S2 and S3. P4: Medial colon, which consists of parts M2, A3 and S4. P5: Distal colon, which consists of parts M3, A4 and S4.

FIG. 8. The level of total VFA and the level of water consistency of the digestive contents in the anatomically defined segments of the large intestine. Mean with standard error. (N=10; mmole/dl for the level of VFA, % for the level of water consistency).

branch of the ileo-caecal artery, which was the branch of the cranial intestinal artery, dispersed into the caecum (Fig. 2). The caecum added to part A1.

As for the epithelial surface structure observed by SEM, the colon was divided into four segments (S1, S2, S3 and S4). The epithelial surface structure of part S1 had well-developed mucous folds, which had similar structures to those of the caecum (Fig. 3). In part S2, V-shaped mucous folds consisted of continual small papillae (Fig. 4). In part S3, these folds gradually disappeared approaching the caudal region (Fig. 5). In part S4, the longitudinal folds appeared on the epithelial surface (Fig. 6). These findings were nearly the same as those reported by Behmann [1].

In view of the above findings, the large intestine (without the rectum) may be divided into five segments by mesenterial attaching pattern and vascular supplying system. The epithelial surface structure was included into above divided segments of the large intestine. Part 1 is the caecum which consists of parts M1, A1 and S1. Part 2 is the cranial region of the proximal colon which consists of parts M1, A1, S1 and S2. Part 3 is the caudal region of the proximal colon which consists of parts M2, A2, S2 and S3. Part 4 is the medial colon which consists of parts M2, A3, and S4. Part 5 is the distal colon which consists of parts M3, A4 and S4 (Fig. 7).

Analyses of the levels of total VFA and water consistency were conducted on the digestive contents in each segment of the large intestine. In part

1, the level of total VFA in the digestive contents was higher than in all the other parts. The level of VFA tended to decrease going from part 1 to part 4. In part 4, the level of the VFA was about 1/3 of that of part 1 (Fig. 8). The VFA may be produced and absorbed well in the caecum and the proximal colon (part 1 and part 2). However, the level of VFA increased in part 5. Meanwhile, the level of water consistency in the digestive contents merely tended to decrease caudally (Fig. 8). High levels of VFA in part 5 may actually be the reason for the produce of VFA in the fecal mass. The peripheral zone of the fecal mass might be dried. VFA may be producing at the core zone of the fecal mass. It is possible that VFA is increased at the fecal mass of the distal colon (part 5).

The fecal mass began formation in the medial colon, and were completely formed in the distal colon.

REFERENCES

- 1 Behmann, H. (1973) *Z. wiss. Zool.*, **186**: 173–298.
- 2 Golley, F. B. (1960) *J. Mammal.*, **41**: 89–99.
- 3 Kajigaya, H. and Goto, N. (1980) *J. Mammal. Soc. Jpn.*, **8**: 171–180.
- 4 Kurohmaru, M., Nishida, T. and Mochizuki, K. (1981) *Jpn. J. Vet. Sci.*, **43**: 887–899.
- 5 Obara, Y. and Goto, N. (1980) *Jpn. J. Zootech. Sci.*, **51**: 393–396.
- 6 Sugawara, M. (1982) *Jpn. J. Zootech. Sci.*, **53**: 400–405.
- 7 Snipes, R. L. (1979) *Anat. Embryol.*, **157**: 181–203.
- 8 Snipes, R. L. (1979) *Anat. Embryol.*, **157**: 329–346.

INSTRUCTIONS TO AUTHORS

ZOOLOGICAL SCIENCE publishes contributions, written in English, in the form of (1) Reviews, (2) Articles, and (3) Communications of material requiring prompt publication. A *Review* is usually invited by the Editors. Those who submit reviews should consult with the Editor-in-Chief or the Managing Editor in advance. *Articles* of less than 6 printed pages and *Communications* less than 3 printed pages will be published free of charge. Charges will be made for extra pages (7,000 yen/page). A *Communication* cannot exceed 4 printed pages. No charge will be imposed for invited reviews up to 15 printed pages. No free reprints of Articles and Communications are available. To the author of an invited review 50 reprints are provided gratis. Submission of papers from nonmembers of the Society is welcome. However, page charges (7,000 yen/page) will be made to nonmembers.

A. SUBMISSION OF MANUSCRIPT

The manuscript should be submitted in triplicate, one original and two copies, each including all illustrations. Rough copies of line drawings and graphs may accompany the manuscript copies, but the two copies of continuous-tone prints (photomicrographs, etc.) should be as informative as the original. The manuscript should be sent to:

Dr. SEIICHIRO KAWASHIMA, Managing Editor,
ZOOLOGICAL SCIENCE, Zoological Institute,
Faculty of Science, Hiroshima University,
1-1-89 Higashisenda-machi, Naka-ku,
Hiroshima 730, Japan.

B. CONDITIONS

All manuscripts are subjected to editorial review. A manuscript which has been published or of which a substantial portion has been published elsewhere will not be accepted. It is the author's responsibility to obtain permission to reproduce illustrations, tables, etc. from other publications. Accepted papers become the permanent property of ZOOLOGICAL SCIENCE and may not be reproduced by any means, in whole or in part,

without the written consent of both the Zoological Society of Japan and the author(s) of the article in question.

C. ORGANIZATION OF MANUSCRIPT

The desirable style of the organization of an original paper is as follows: (1) Title, Author(s) and Affiliation (2) Abstract (3) Introduction (4) Materials and Methods (5) Results (6) Discussion (7) Acknowledgments (8) References (9) Tables (10) Illustrations and Legends (11) Footnotes. The author is not obliged to adhere rigidly to this organization. He or she may modify the style when such modification makes the presentation clearer and more effective. In a *Communication*, combination of some of these sections is recommended. There is no restriction on the style of review articles.

D. FORM OF MANUSCRIPT

Manuscripts should be typewritten and double spaced throughout on one side of white type-writing paper with 2.5 cm margins on all sides. Abstract not exceeding 250 words, tables, figure legends and footnotes should be typed on separate sheets. All manuscript sheets must be numbered successively. The use of footnotes to the text is not recommended.

1. Title page

The first page of manuscript should contain title, authors' names and addresses of university or institution, abbreviated form of title (40 characters or less, including spaces), and name and address for correspondence. Authors with different affiliations should be identified by the use of the same superscript on name and affiliation. If one or more of the authors has changed his or her address since the work was carried out, the present address(es) to be published should be indicated in a footnote. In addition, a sub-field of submitted papers to be used as heading of an issue may be indicated in the first page. Authors are encouraged to choose one of the following: physiology, cell biology, molecular biology, genetics, immunology, biochemistry,

developmental biology, reproductive biology, endocrinology, behavior biology, ecology, phylogeny, taxonomy, or others (specify). However, the Editors are responsible for the choice and arrangement of headings.

2. Introduction

This section should clearly describe the objectives of the study, and provide enough background information to make it clear why the study was undertaken. Lengthy reviews of past literature are discouraged.

3. Materials and Methods

This section should provide the reader with all the information that will make it possible to repeat the work. For modification of published methodology, only the modification needs to be described with reference to the source of the method.

4. Results

Results should be presented referring to tables and figures, without discussion.

5. Discussion

The Discussion should include a concise statement of the principal findings, a discussion of the validity of the observations, a discussion of the findings in the light of other published work dealing with the same subject, and a discussion of the significance of the work. Redundant repetition of material in Introduction and Results, and extensive discussion of the literature are discouraged.

6. Statistical analysis

Statistical analysis of the data using appropriate methods is mandatory and the method(s) used must be cited.

7. References

References should be cited in the text by an Arabic numeral in square parentheses and listed at the end of the paper in numerical order. For example:

- 1 Takewaki, K. (1931) Oestrus cycle of female rat in parabiotic union with male. *J. Fac. Sci. Imp. Univ. Tokyo, Sec. IV*, 2: 353-356.
- 2 Shima, A., Ikenaga, M., Nikaido, O., Takabe, H. and Egami, N. (1981) Photoreactivation of ultraviolet light-induced damage in cultured fish cells as revealed by increased colony forming ability and decreased content of pyrimidine dimers. *Photochem. Photobiol.*, 33: 313-316.

- 3 Hubel, O. and Wiesel, T. N. (1986) The functional architecture of the striated cortex. In "Physiological and Biochemical Aspects of Nervous Integration". Ed. by F. D. Carlson, Prentice-Hall, New Jersey, pp. 153-161.

- 4 Campbell, R. C. (1974) *Statistics for Biologists*. Cambridge Univ. Press, London, 2nd ed., pp. 59-61.

Titles of cited papers may be omitted in Reviews and Communications. The source of reference should be given following the commonly accepted abbreviations for journal titles (e.g., refer to 'International List of Periodical Title Abbreviations'). The use of "in preparation", "submitted for publication" or "personal communication" is not allowed in the reference list. "Unpublished data" and "Personal communication" should appear parenthetically following the name(s) in the text. Text citations to references with three or more authors should be styled as, e.g., Everett *et al.* [7].

E. ABBREVIATIONS

Abbreviations of measurement units, quantity units, chemical names and other technical terms in the body of the paper should be used after they are defined clearly in the place they first appear in the text. However, abbreviations that would be recognized by scientists outside the author's field may be used without definition, such as SD, SE, DNA, RNA, ATP, ADP, AMP, EDTA, UV, and CoA. The metric system should be used for all measurements, and metric abbreviations (Table)

Table. Abbreviations for units of measure which may be used without definition

Length:	km, m, cm, mm, μm , nm, pm, etc.
Area:	km^2 , m^2 , cm^2 , mm^2 , μm^2 , nm^2 , pm^2 , etc.
Volume:	km^3 , m^3 , cm^3 , mm^3 , μm^3 , nm^3 , pm^3 , kl, liter (always spellout), ml, μl , nl, etc.
Weight:	kg, g, mg, μg , ng, pg, etc.
Concentration:	M, mM, μM , nM, %, g/l, mg/l, $\mu\text{g/l}$, etc.
Time:	hr, min, sec, msec, μsec , etc.
Other units:	A, W, C, atm, cal, kcal, R, Ci, cpm, dB, v, Hz, lx, $\times\text{g}$, rpm, S, J, IU, etc.

should, in general, be expressed in lower case without periods.

F. PREPARATIONS OF TABLES

Tables should only include essential data needed to show important points in the text. Each table should be typed on a separate sheet of paper and must have an explanatory title and sufficient explanatory material. All tables should be referred to in the text, and their approximate position indicated in the margin of manuscript.

G. PREPARATION OF ILLUSTRATIONS

All figures should be appropriately lettered and labelled with letters and numbers that will be at least 1.5 mm high in the final reproduction. Note the conventions for abbreviations used in the journal so that usage in illustrations and text is consistent. All figures should be referred to in the text and numbered consecutively (Fig. 1, Fig. 2, etc.). The figures must be identified on the reverse side with the author's name, the figure number and the orientation of the figure (top and bottom). The preferred location of the figures should be indicated in the margin of the manuscript. Illustrations that are substandard will be returned, delaying publication. Illustrations in color may be published at the author's expense.

1. Line drawings and graphs

Original artwork of high quality, glossy prints mounted on appropriate mounting card (less than 25×38 cm) should be submitted for reproduction. Author(s) may indicate size preference by making on the back of figures, such as "Do not reduce", "Two-column width" (no wider than 14.5 cm), or "One-column width" (no wider than 7 cm). Lines must be dark and sharply drawn. Solid black, white, or bold designs should be used for histograms. Xerox or any other copying mean may be used for the two review copies.

2. Continuous-tone prints

Three sets of continuous-tone prints (photomicrographs, etc.) must be submitted. One set for reproduction should be mounted on appropriate mounting card, and the other two for reviewers may be unmounted prints. Xerox or similar copies of photomicrographs are not acceptable for review purposes. The continuous-tone prints should be submitted preferably at the exact magnification which is to be used in the published papers and trimmed to conform to the page size (in no case should it exceed 14.5×20 cm). Press-on numbers should be applied to the lower right corner of individual prints. Letters (a, b, c, etc.) should be used for multiple parts of a single figure. If important structures will be covered by use of the lower right corner, identification may be applied in the lower left corner.

Reproduction of color photographs will have to be approved by the Editors. The extra costs of color reproduction will be charged to the authors.

3. Figure legends

Each figure should be accompanied by a title and an explanatory legend. The legends for several figures may be typed on the same sheet of paper. Sufficient detail should be given in the legend to make it intelligible without reference to the text.

H. PROOF AND REPRINTS

A galley proof and reprint order will be sent to the submitting author. The first proofreading is the author's responsibility, and the proof should be returned within 72 hours from the date of receipt (by air mail from outside Japan). The minimum quantity for a reprint order is fifty. Manuscript, tables and illustrations will be discarded after the editorial use unless their return is requested when the manuscript is accepted for publication.

ERRATUM

In the Contents on the back-cover of Vol. 4, No. 5, 1987, the authors' names of the article entitled 'Geotactic behavior in *Paramecium caudatum*. II. Geotaxis assay in a population of the specimens' were incorrectly printed.

'Taneda, K.' should read 'Taneda, K., S. Miyata and A. Shiota'.

Development Growth & Differentiation

Published by

the Japanese Society of Developmental Biologists

The journal is devoted to the publication of original papers dealing with any aspects of developmental phenomena in all kinds of organisms, including plants and micro-organisms. Papers in any of the following fields will be considered: developmental genetics, growth, morphogenesis, cellular kinetics, fertilization, cell division, dormancy, germination, metamorphosis, regeneration and pathogenesis, at the biochemical, biophysical and analytically morphological levels; reports on techniques applicable to the above fields. At times reviews on subjects selected by the editors will be published. Brief complete papers will be accepted, but not preliminary reports.

Members of the Society receive the Journal free of charge. Subscription by institutions is also welcome.

Papers in Vol. 30, No. 1. (February, 1988)

1. **REVIEW:** A. FUJIWARA, K. SUDOH and I. YASUMASU: Activation of sea urchin eggs by halothane and its inhibition by dantrolene.
2. S. Pine and R. FLICKINGER: Base composition of poly (A⁺) nuclear RNA of frog embryo and friend erythroleukemia cells.
3. Y. Maeda: Changes of the endocytotic activities during the cell cycle of *Dictyostelium* cells.
4. H. Shimizu, N. NORO and R. MATSUDA: Micromere differentiation in the sea urchin embryo: Expression of primary mesenchyme cell specific antigen during development.
5. R. Matsuda, T. Kitajima, H. Ohinata, Y. Katoh and T. HIGASHINAKAGAWA : Micromere differentiation in the sea urchin embryo: Two-dimensional gel electrophoretic analysis of newly synthesized proteins.
6. D. E. Chandler and V. D. VACQUIER: Phorbol myristate acetate induces the phosphorylation of plasma membrane-associated proteins in sea urchin eggs.
7. K. Ueno, Y. Hiramoto, S. Hayashi and H. KONDOH: Introduction and expression of recombinant β -galactosidase genes in cleavage stage mouse embryos.
8. M. Okamoto: Inhibition of lens regeneration by nickel subsulfide in the Japanese common newt, *Cynops pyrrhogaster*.
9. M. Yamashita: A fine structural study of the fertilization process of the jellyfish *Cladonema uchidai*.
10. P. Guerrier, I. Néant and P. CLÉDON: Urea-induced meiosis reinitiation in oocytes of the starfish *Marthasterias glacialis*.

Development, Growth and Differentiation (ISSN 0012-1592) is published bimonthly by The Japanese Society of Developmental Biologists, Department of Biology, School of Education, Waseda University, Tokyo 160, Japan. 1988: Volume 30. Annual subscription U. S. \$ 110.00 including air speed delivery except Japan. Application to mail at second class postage rate is pending at Jamaica, NY 11431, U. S. A.

Outside Japan: Send subscription orders and notices of change of address to Academic Press, Inc., Journal Subscription Fulfillment Department, 6277 Sea Harbor Drive, Orlando, FL 32887, U. S. A. Send notices of change of address at least 6-8 weeks in advance. Please include both old and new addresses. U. S. A. POSTMASTER: Send changes of address to *Development, Growth and Differentiation*, Academic Press, Inc., Journal Subscription Fulfillment Department, 6277 Sea Harbor Drive, Orlando, FL 32887, U. S. A.

In Japan: Send nonmember subscription orders and notices of change of address to Business Center for Academic Societies Japan, 16-3, Hongo 6-chome, Bunkyo-ku, Tokyo 113, Japan. Send inquiries about membership to Business Center for Academic Societies Japan, 4-16, Yayoi 2-chome, Bunkyo-ku, Tokyo 113, Japan.

Air freight and mailing in the U. S. A. by Publications Expediting, Inc., 200 Meacham Avenue, Elmont, NY 11003, U. S. A.

NARISHIGE

THE ULTIMATE NAME IN MICROMANIPULATION

OUR NEW MODELS MO-102 and MO-103
MAKE PRECISION MICROMANIPULATION SO EASY!

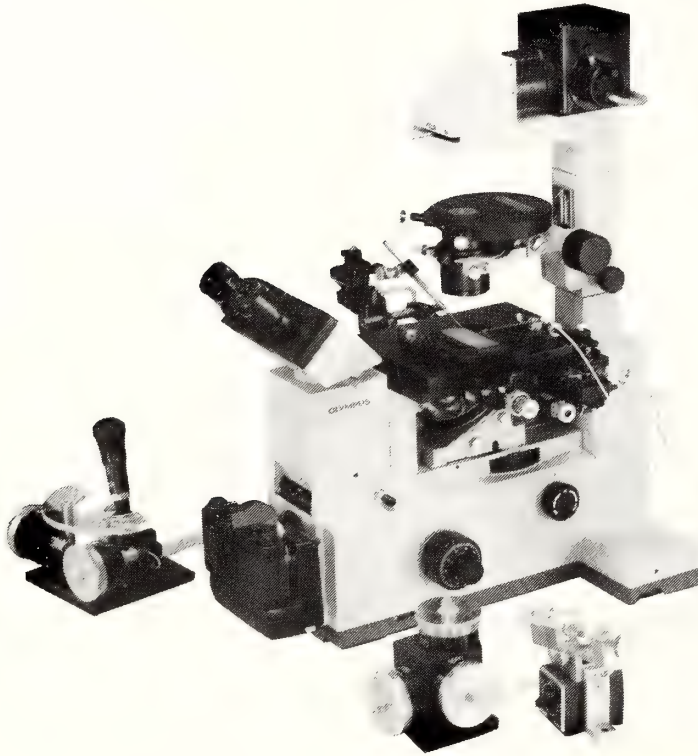


(Photo: by courtesy of Olympus Optical CO., LTD.)

SOME FEATURES of MO-102 and MO-103:

- * The manipulator head is so small that it can be mounted directly on the microscope stage. There is no need for a bulky stand.
- * Hydraulic remote control ensures totally vibration-free operation.
- * 3-D movements achieved with a single joystick.

Micromanipulators Microelectrode pullers Stereotaxic instruments

NARISHIGE
JAPAN

**NARISHIGE SCIENTIFIC INSTRUMENT
LABORATORY CO., LTD.**

4-9-28, Kasuya, Setagaya-ku, Tokyo 157 JAPAN
Telephone: 03-308-8233 Telex: NARISHG J27781

(Contents continued from back cover)

munofluorescence microscopy in *Tetrahymena thermophila* during conjugation 119

Yasumasu, S., I. Iuchi and K. Yamagami: Medaka hatching enzyme consists of two kinds of proteases which act cooperatively (COMMUNICATION) 191

Endocrinology

Engström, W., E. Dafgård and S. Falkmer: Comparative effects *in vitro* of *Myxine*, *Squalus*, avian and mammalian insulins on DNA-synthesis in 3T3 mouse fibroblasts 133

Ueda, H., T. Kosaka and K. W. Takahashi: Effects of long-term progesterone treatment on synchronized ovulation in guinea pigs 139

Endo, K., T. Masaki and K. Kumagai: Neuroendocrine regulation of the development of seasonal morphs in the Asian comma butterfly, *Polygonia c-aureum* L.: Difference in activity of summer-morph-producing hormone from brain-extracts of the long-day and short-day pupae 145

Srivastav, A. K. and S. P. Srivastav: Corpuscles of Stannius of *Clarias batrachus* in response to 1, 25 dihydroxyvitamin D₃ administration (COMMUNICATION) 197

Fujimori, M., Y. Sasayama and C. Oguro: Translocation of ⁴⁵Ca from the endolymphatic sacs to the bone in *Rana nigromaculata* (COMMUNICATION) 201

Morphology

Amasaki, H., M. Daigo and N. Meguro: Morphological observations of the large intestine in the common vole, *Microtus arvalis* Pallas (COMMUNICATION) 205

Behavior Biology

Pandey, S. C. and S. D. Pandey: Sexual maturation in female wild mice: Combined effect of adults' urinary chemosignals and minimum time of exposure to stimulus substances for bringing the effects 153

Verrell, P. A.: Sexual interference in the alpine newt, *Triturus alpestris* (Amphibia, Urodela, Salamandridae) 159

Taxonomy

Nakasone, Y.: Land hermit crabs from the Ryukyus, Japan, with a description of a new species from the Philippines (Crustacea, Decapoda, Coenobitidae) 165

Instructions to Authors 209

Erratum 212

ZOOLOGICAL SCIENCE

VOLUME 5 NUMBER 1

FEBRUARY 1988

CONTENTS

REVIEWS

- de Pomerai, D. I.: The transdifferentiation of neural retina into lens *in vitro* 1
- Tsuneki, K.: The neurohypophysis of cyclostomes as a primitive hypothalamic center of vertebrates 21

ORIGINAL PAPERS

Physiology

- Azuma, K.: Hypersensitivity after offset of adapting light in vertebrate photoreceptors 33
- Takei, Y., J. Okubo and K. Yamaguchi: Effects of cellular dehydration on drinking and plasma angiotensin II level in the eel, *Anguilla japonica* 43
- Nishi, T., M. Kobayashi, M. Isomura, H. Ishida and Y. Shigenaka: Direct evidence for axopodial fusion preceding cell-to-cell contact in a heliozoan *Echinospaerium* (COMMUNICATION) 179

Cell Biology

- Zama, N. and H. Katow: A method of quantitative analysis of cell migration using a computerized time-lapse videomicroscopy 53
- Iwasaki, S. K. Miyata and K. Kobayashi: Fine structure of the filiform papillar epithelium from the tongue of the frog, *Rana nigromaculata* 61
- Ebitani, N. and T. Kubo: An established marine fish cell line with high plating efficiency (COMMUNICATION) 183

Biochemistry

- Suzuki, T., R. Muramatsu, T. Kisamori and T. Furukohri: Myoglobin of the shark *Galeus nipponensis*: Identification of the exceptional amino acid replacement at the distal (E7) position and autoxidation of its oxyform 69

Genetics

- Nakamura, T.: Female heterogametic sex-determination in *Xenopus laevis* as reconfirmed by repeated diploid gynogenesis (COMMUNICATION) 187

Immunology

- Nagata, S.: T cell-specific antigen in *Xenopus* identified with a mouse monoclonal antibody: Biochemical characterization and species distribution 77

Developmental Biology

- Fujisawa, H. and S. Amemiya: Temperature-dependence in reaggregation of cells dissociated from sea urchin embryos with different seasonal growth 85
- Mitsunaga, K., Y. Fujino and I. Yasumasu: Probable participation of mitochondrial Ca^{2+} transport in calcification of spicules and morphogenesis in sea urchin embryos 93
- Numakunai, T., Z. Hoshino and S. Kajiwara: Spawning of three intraspecific groups of the ascidian, *Halocynthia roretzi* (Drasche), in the wild, and fertilization among them ... 103
- Tahara, U.: Normal stages of development in the lamprey, *Lampetra reissneri* (Dybowski) 109
- Tsunemoto, M., O. Numata, T. Sugai and Y. Watanabe: Analysis of oral replacement by scanning electron microscopy and im-
- (Contents continued on inside back cover)

INDEXED IN:

Current Contents/LS and AB & ES,
Science Citation Index,
ISI Online Database,
CABS Database

Issued on February 15

Printed by Daigaku Printing Co., Ltd.,
Hiroshima, Japan

Vol. 5 No. 2

QL
1
Z864
NH

April 1988

ZOOLOGICAL SCIENCE

An International Journal

PHYSIOLOGY
CELL and MOLECULAR BIOLOGY
GENETICS
IMMUNOLOGY
BIOCHEMISTRY
DEVELOPMENTAL BIOLOGY
REPRODUCTIVE BIOLOGY
ENDOCRINOLOGY
BEHAVIOR BIOLOGY
ENVIRONMENTAL BIOLOGY
ECOLOGY and TAXONOMY

published by **Zoological Society of Japan**

distributed by **Business Center for Academic Societies Japan**
VSP, Zeist, The Netherlands

ISSN 0289-0003

ZOOLOGICAL SCIENCE

The Official Journal of the Zoological Society of Japan

Editor-in-Chief:

Hideshi Kobayashi (Tokyo)

Managing Editor:

Seiichiro Kawashima (Hiroshima)

Assistant Editors:

Takeo Machida (Hiroshima)

Sumio Takahashi (Hiroshima)

Kazuyoshi Tsutsui (Hiroshima)

The Zoological Society of Japan:

Toshin-building, Hongo 2-27-2, Bunkyo-ku,

Tokyo 113, Japan. Tel. (03) 814-5675

Officers:

President: Nobuo Egami (Tsukuba)

Secretary: Hideo Namiki (Tokyo)

Treasurer: Tadakazu Ohoka (Tokyo)

Librarian: Shun-Ichi Uéno (Tokyo)

Editorial Board:

Howard A. Bern (Berkeley)

Walter Bock (New York)

Aubrey Gorbman (Seattle)

Horst Grunz (Essen)

Robert B. Hill (Kingston)

Yukio Hiramoto (Chiba)

Susumu Ishii (Tokyo)

Yukiaki Kuroda (Mishima)

Koscak Maruyama (Chiba)

Roger Milkman (Iowa City)

Hiromichi Morita (Fukuoka)

Kazuo Moriwaki (Mishima)

Tokindo S. Okada (Okazaki)

Andreas Oksche (Giessen)

Hidemi Sato (Nagoya)

Hiroshi Watanabe (Shimoda)

Mayumi Yamada (Sapporo)

Ryuzo Yanagimachi (Honolulu)

ZOOLOGICAL SCIENCE is devoted to publication of original articles, reviews and communications in the broad field of Zoology. The journal was founded in 1984 as a result of unification of Zoological Magazine (1888-1983) and *Annotationes Zoologicae Japonenses* (1897-1983), the former official journals of the Zoological Society of Japan. ZOOLOGICAL SCIENCE appears bimonthly. An annual volume consists of six numbers of more than 1000 pages including an issue containing abstracts of papers presented at the annual meeting of the Zoological Society of Japan.

MANUSCRIPTS OFFERED FOR CONSIDERATION AND CORRESPONDENCE CONCERNING EDITORIAL MATTERS should be sent to:

Dr. Seiichiro KAWASHIMA, Managing Editor, Zoological Science, Zoological Institute, Faculty of Science, Hiroshima University, 1-1-89 Higashisenda-machi, Naka-ku, Hiroshima 730, Japan, in accordance with the instructions to authors which appear in the first issue of each volume. Copies of instructions to authors will be sent upon request.

SUBSCRIPTIONS. ZOOLOGICAL SCIENCE is distributed free of charge to the members, both domestic and foreign, of the Zoological Society of Japan. To non-member subscribers within Japan, it is distributed by Business Center for Academic Societies Japan, 6-16-3 Hongo, Bunkyo-ku, Tokyo 113. Subscriptions outside Japan should be ordered from the sole agent, VSP, Utrechtseweg 62, 3704 HE Zeist (postal address: P. O. Box 346, 3700 AH Zeist), The Netherlands. Subscription rates will be provided on request to these agents. New subscriptions and renewals begin with the first issue of the current volume.

All rights reserved. No part of this publication may be reproduced or stored in a retrieval system in any form or by any means, without permission in writing from the copyright holder.

© Copyright 1988, The Zoological Society of Japan

[Publication of Zoological Science has been supported in part by a Grant-in-Aid for Scientific Publication from the Ministry of Education, Science and Culture, Japan.]

OBITUARY

**Kiyoshi Takewaki (1905-1988)**

Emeritus Professor Kiyoshi Takewaki of the University of Tokyo died at the age of 82 on the 16th of January 1988 after a long period of unconsciousness. His death was due to bronchial pneumonia originating in a traffic accident on the 12th of April 1987. Until the time of accident, Professor Takewaki had been healthy and vigorous. We feel great regret at the loss of this distinguished zoologist as well as an eminent endocrinologist. All that is left to us is to cherish his memory.

Kiyoshi Takewaki was born on the 1st of March 1905 at Toyama City in the middle of the Honshu on the Japan Sea. As a primary school boy, he was watching a water-scorpion in the evening of a summer day, and was deeply impressed by this beautiful scene of nature. He wrote later about this moment of beauty in a book "Mizukamakiri wa tobu (A Water-Scorpion Flies)". This esthetic impression exerted a long-lasting influence on his study and taste. He loved arts and crafts, mainly pictures, and occasionally he himself painted scenes from nature. In research, he maintained his naturalist's mind, being always modest before nature as well as in evaluation of his own results.

In 1922, he entered the Fourth High School, Science Course, at Kanazawa, and finished the Course after 3 years. Before leaving high school, he told his teacher about his choice of future occupation as zoologist. The teacher was greatly astonished at hearing this unexpected idea, because Takewaki always had the best record in the school. After a while, the teacher just said "It's impossible to live that way".

In 1925, he was admitted to the Zoological Institute of the Faculty of Science at the Imperial University of Tokyo. During his university student period, he wrote four short papers based on his observations of insects, although his full-fledged studies did not begin until after his graduation in 1928.

Here, Emeritus Professor Naohide Yatsu of the Imperial University of Tokyo should be mentioned in order to understand why Takewaki began to study endocrinology. Yatsu went to the United States the

year after graduation from the Imperial University (1900) to enter graduate school at Columbia University. He was strongly impressed there by Prof. Jacques Loeb's lectures, and recognized the importance of experimental zoology. After he obtained Ph. D. in 1905, Yatsu moved to the Stazione Zoologica of Naples, then came back to the Imperial University as lecturer (1907), and became associate professor (1909). Yatsu made efforts to develop experimental zoology, but met with stout resistance to his attempted innovation. So, he moved as professor of the Department of Anatomy at Keio University in 1919. However, he was finally called back to be professor at the Imperial University in 1922, where again he began to develop experimental zoology. During a period of "Sturm und Drang" in the Imperial University of Tokyo, Yatsu introduced the technique of parabiosis into experimental zoology in an attempt to elucidate the balance of sex hormones in rats (1916). These efforts marked the commencement of experimental endocrinology in Japan.

In 1928, Takewaki was added as assistant (instructor) at Yatsu's laboratory and first encountered rats and mice as the experimental animals which he used for more than 50 years thereafter. His first study on rats was to examine the state of various blood cells following gonadectomy (1929), but the second study on parabiosis between intact and gonadectomized rats became the origin of his life work on the endocrinology of reproduction (1931). In 1933-1935, his subject of study shifted to the transplanted testis and ovary in intact, senile, unilaterally or bilaterally gonadectomized and cryptorchidized rats. In this period he also published two papers on the state of the testis transplanted into intact and gonadectomized lizards, a pioneer study in comparative endocrinology. He also studied changes in the mouse adrenal glands following treatments with gonadotropic extract from human pregnancy urine.

The influences of castration, hysterectomy, pregnancy, pseudopregnancy and testis-implantation on the ovary and adrenal cortex were then examined in rats and mice (1936-1940). He obtained the degree of D. Sc. in 1936, and became an associate professor in 1938. At this time, he used not only rats but also other species of animals for experiments. He examined changes in the kidney and genital tract after removal of gonads and hypophysis in the snake, *Natrix tigrina tigrina*. He also studied the relationship between gonads and sex character in the isopod crustacean, *Armadillidium vulgare* and hormonal control of the molting in the canary in cooperation with Hideshi Kobayashi (1941-1947). Takewaki became professor in 1947. As the 1940's were a severely difficult period for scientists in Japan, it was inevitable for Takewaki to reduce his work on mammals. After 1949, however, he again took up enthusiastically his studies in rats and mice, especially on the relationship between gonads and hypophysis. During this period of his research renaissance, he spent several months (in 1954) in Prof. C. R. Moore's laboratory at University of Chicago. In 1955-1961, his interests were concentrated on the negative and positive feedback mechanisms between hypothalamo-hypophyseal and gonadal systems. For elucidation of these mechanisms he examined changes in intrasplenic ovarian grafts in gonadectomized rats. Neonatal treatments of rats with steroid hormones were carried out in connection with the study of sex differentiation. In cooperation with his associates, he also studied the relationship between gonads and adrenals in rats, the actions of sinus gland hormones in shrimps, and the hypophyseal control of reproductive functions in fishes.

The Third International Symposium on Comparative Endocrinology was held from June 5 to 11 in 1961 at Oiso, Japan. As the chairman of the international organizing committee, Takewaki led this symposium to a highly successful conclusion, resulting in an immeasurably strong impact on young zoologists studying the general and comparative endocrinology in Japan, especially since this symposium was one of the earliest international meetings held in Japan after the war.

In 1962-1965, he studied the permanent alteration of hypothalamo-hypophysio-gonadal system in persistent-estrous or -diestrous rats treated neonatally with sex hormones. He also worked on the genesis and nature of testicular tumors in rats.

Thus, Takewaki succeeded in advancing the experimental endocrinology he had inherited from Yatsu, contributing greatly to our understanding of the hormonal control of structure and function of

reproductive organs. He also carried out comparative studies of reproductive phenomena in several animal species, laying the stage for the later flourishing of comparative endocrinology in Japan.

Takewaki was a man of action. Until 70 years of age, he came to the laboratory before 8 a.m. every day, even on Sundays, and began his day by taking care of his animals. His speed of lecturing was very fast in order to convey as much knowledge as possible to students in a limited amount of time. He also rapidly reviewed the many manuscripts sent to him by investigators.

Takewaki retired from the University of Tokyo in 1965, but never wanted to spend his days in retirement from research. He continued his studies of sex phenomena in rats for the next five years, as professor at Tokyo Women's University. In 1970, he was invited to be a professor at Kawasaki Medical College in Kurashiki City, Okayama Prefecture, where he worked energetically with Dr. Yasuhiko Ohta, mainly on the uterine response to hormones under various physiological conditions in rats. He was elected a member of the Japan Academy in 1975, and expended great efforts in editing its Proceedings to the last. After he retired from the Medical College in 1976, he came back to Tokyo, and enjoyed travelling, reviewing papers, appreciating various works of art, giving lectures at Atomi Women's University (as a part-time lecturer), collecting insects around his cottage near Mt. Kurohime, Nagano Prefecture, for the rest of his life.

Thus, Professor Kiyoshi Takewaki continued his efforts as an investigator until the end of his active life. His academic publications totalled more than 200, and his students and followers more than 50. He was a rather reserved professor, who provided a powerful stimulating influence on the research activity of his students by his deeds rather than by his words.

We can expect that Kiyoshi Takewaki's unflagging pioneer's spirit that originated with Yatsu will continue to be sustained by the many zoologists who follow him.

NOBORU TAKASUGI

Department of Biology
Yokohama City University

REVIEW

Female Reproduction in Malacostracan Crustacea

JEAN-JACQUES MEUSY and GENEVIÈVE G. PAYEN

*Laboratoire de Physiologie de la Reproduction, Equipe
Neuroendocrinologie des Crustacés, Université Pierre
et Marie Curie et C. N. R. S., UA 040555
4, place Jussieu, Bâtiment A, F-75252
Paris Cedex 05, France*

CONTENTS

Introduction	218
I. Early steps of oogenesis and previtellogenesis	219
A. Chronology and cytology	219
B. Regulation	220
1. Mechanisms of oocyte differentiation	220
2. Maintenance of the germinative zone	221
3. Oocyte growth until puberty	221
II. Vitellogenesis	221
A. Vitellogenesis process	221
1. General considerations	221
2. Origin of vitellogenin	222
3. Vitellogenin uptake by vitellogenic ovaries	223
a) Transformation and role of the follicle envelope	223
b) Vitellogenic oocyte and endocytosis mechanism	224
4. From vitellogenin to vitellin: a processing?	224
5. Vitellogenin synthesis and vitellogenin level in haemolymph as means for monitoring vitellogenesis	226
6. Timing of the reproductive cycle: duration and relation with the molting cycle	227
B. Vitellogenesis control	229
1. Inhibitory control by VIH (Vitellogenesis Inhibiting Hormone)	229
a) The X organ-sinus gland complex	229
Eyestalked species	
Eyestalkless species	
b) Ways of action	230
Control of vitellogenin synthesis	
Control of vitellogenin uptake by the oocytes	
c) Extraction and purification of VIH	231
d) Latest data on VIH	231
2. Stimulatory control	233
a) Neurohumoral factors	234
b) Vitellogenin Stimulating Ovarian Hormone (VSOH)	234
c) Ecdysteroids	234
d) Juvenoids	235
e) Ovary-stimulating factor from males	237

3.	Effect of other substances	237
a)	Androgenic hormone	237
b)	Vertebrate hormones	237
c)	"Queen-substance" of honeybees	238
4.	Environmental factors and vitellogenesis	238
a)	Light and temperature	238
b)	Other factors	238
5.	Parasitism and vitellogenesis	240
III.	Oocyte maturation	240
IV.	Ovulation	242
V.	Oocyte activation	243
A.	Meiosis reinitiation of metaphase I-arrested oocytes	243
B.	Fertilization potential	243
C.	Cortical reaction	244
VI.	Oviposition	245
VII.	Sex characteristics associated to sperm storage, mating and egg incubation	245
A.	Genital duct	246
B.	External sex characteristics	246
1.	Differentiation	246
2.	Regulation of development	248
VIII.	Sex recognition and mating behavior	249
	References	250

INTRODUCTION

As in most organisms, the series of complex events that render the female germ cell of crustaceans capable of conjugation with the spermatozoon evolves over a long period which extends from the time of oogenic differentiation to the final maturation of the oocyte.

It is now well-known that the study of female reproduction falls into five main areas: 1) the mechanism of ovarian differentiation, 2) the sequence of morphological steps leading to vitellogenesis, oocyte maturation and activation, 3) the endocrine regulation of the onset, completion and maintenance of these different steps, 4) the influence of external factors such as photoperiod, temperature, ionic concentration of sea water on the female gametogenesis, 5) the events that follow mate selection and allow a specific response of the oocyte surface to the spermatozoon for a successful fertilization. Then, the normal growth of the embryo is ensured during incubation, a period of the life span of the female that is associated with the development of external sex characteristics and the secretion of pleopod tegumental glands in some species.

We must point out that the major phenomena that characterize crustacean oogenesis and its

regulation need to be known not only for the goal of basic research but also for the benefit of the aquaculture field. Achieving control of reproduction is often identified as a major problem that prevents the potential of shrimp farming from becoming a profitable industry. Thus, for their economical interest, a number of research programs are now devoted to the Decapoda, one of the three most-studied Malacostraca orders beside the Amphipoda and Isopoda.

A few general features related to the knowledge of malacostracan reproduction are recalled hereafter:

1. With the exception of Oxyrhyncha crabs which become sexually mature after a terminal molt, as the majority of insects, most malacostracan Crustacea continue to molt after puberty.

2. In peracarids and natantian decapods, spawning is obligatorily preceded by a molt and, during the period of genital activity, the number of spawnings varies according to the species.

3. Except for penaeid prawns that are free-spawners, malacostracans incubate their eggs. As a matter of fact, the time interval between each spawning is always longer than the time of egg incubation.

4. In species in which the development comprises larval stages, an ovigerous female carries

around several thousands of small sized-eggs (about 250 μm of diameter in the blue crab), whereas in species with abbreviated (direct) development a hundred or less eggs of larger size (about 3500 μm of diameter in the European crayfish) are incubated. Indeed, the loss of eggs due to predators or unfavorable environmental conditions as particularly encountered by the eggs of penaeids, is considerably reduced in malacostracans which have an abbreviated development and spawn in protected areas.

In this paper, we have tried to recapitulate the known processes undergone by the oocyte in order to acquire the capacity to generate the species. As in most animals, the sequence of major morphological transformations that occur during crustacean oogenesis includes the differentiation and the evolution of oogonia into primary oocytes that undergo previtellogenesis, vitellogenesis and meiotic maturation. Then, activation follows fertilization and spawning, physiological events that permit the completion of gametogenesis.

We have included the main features of the sex characteristics associated to the evolution of the female gamete as well as the regulation of these morphological events by hormonal and environmental factors. At last, the adjacent aspects related to sex recognition and mating behavior are briefly surveyed.

It must be noticed that the most intensely investigated aspect of oogenesis concerns the vitellogenesis. The term "vitellogenesis" will be employed in this review in the way it is the most frequently found in the literature referring to the reproductive physiology of egg laying animals, i.e., as synonymous with "secondary vitellogenesis" [1]. We shall see (Section II, A, 1) that this conspicuous event corresponds to a combination of extra- and intra-oocytic yolk production. Therefore, all previous steps called "previtellogenesis" and "primary vitellogenesis" by Dhainaut and De Leersnyder [1], as well as Charniaux-Cotton [2, 3] and Zerbib [4] can be grouped into a previtellogenic phase. Moreover, it is necessary to be aware that the term "maturation" often found in aquaculture publications with the meaning of "ovarian growth" must be avoided for it corresponds to the resumption of meiosis following

vitellogenesis (cf. Section III).

I. EARLY STEPS OF OOGENESIS AND PREVITELLOGENESIS

A. Chronology and cytology

The early steps of malacostracan oocyte growth were chiefly studied in the amphipod *Orchestia gammarella* and in few decapods from ultrastructural observations [1, 2, 4, 5; reviews in 3, 6, 7].

The undifferentiated gonad of young genetic females forms the germinative zone of the ovary. This structure that resembles a network in which each gonium is completely surrounded by mesodermal cells [8] persists the whole life of the female. Oogonial mitoses take place exclusively in the germinative zone [9].

In gonochoristic decapods, differentiation of the ovary is characterized by a precocious functioning of the germinative zone, i.e., by a precocious initiation of oogenesis as compared with spermatogenesis. Therefore, in the European crayfish, *Pontastacus leptodactylus leptodactylus*, oogenesis begins during the third postembryonic stage, while at the seventh stage the testes contain gonidia not yet engaged in spermatogenesis. A similar delay between male and female gametogenesis also occurs in crabs and in the penaeid shrimp *Penaeus japonicus* [10–12].

In Talitridae amphipods, there seems to be a slight precocity in oogenesis in comparison with spermatogenesis. Such a precocity is clearly visible in males whose testes display an ovarian region.

Some oogonia leave *continually* the germinative zone [13] by a mechanism as yet unknown and rapidly enter prophase of the first meiotic division up to diakinesis. Then, they become primary oocytes with condensed chromosomes which appear in synaptonemal complexes at the ultrastructural level. The decondensation of chromosomes is accompanied by marked cytoplasmic changes such as an accumulation of free ribosomes and the differentiation of a rough endoplasmic reticulum (RER). These phenomena characterize the beginning of the previtellogenesis. Mesodermal tissue forms around each oocyte a follicle multilayered epithelium. Follicle cells are

connected with one another by desmosome-like cell junctions and are themselves held by hemidesmosomes on the *basal lamina* [14]. When endogenous glycoproteins accumulate in the numerous RER vesicles, oocytes carry out the "endogenous vitellogenesis" [1]. Simultaneously, the oocytes acquire a vitelline envelope and their surface becomes irregular with the formation of short microvilli and a few micropinocytotic vesicles. Oocytes grow continuously until they reach a diameter typical for the species. Oogenesis stops at the end of this step in young females and during genital rest in puberal females [15, 16]. As a general rule, female genital puberty is realized when a one layered-epithelium surrounds for the first time each fully grown previtellogenic oocyte (cf. Section II, A).

B. Regulation

1. Mechanisms of oocyte differentiation and onset of oogenesis

The hypothesis of a spontaneous ovarian differentiation, or ovarian autodifferentiation, of the gonadal rudiment in the absence of diffusing androgenic hormone (AH) was stated for the first time by Charniaux-Cotton [17]. This hypothesis was based on the observation of a precocious development of an anterior ovarian region before the onset of spermatogenesis in the gonads of males of *Orchestia mediterranea*, Talitridae amphipods (rudimentary hermaphroditism). Gonidia of the anterior region are less subjected to the AH – the androgenic glands (AG) are located posteriorly – and differentiate into oocytes that acquire follicle cells and grow until the end of previtellogenesis. Posteriorly to this region, gonidia give rise to the various stages of spermatogenesis. Experimental proofs of an ovarian autodifferentiation in amphipods were then obtained in *O. montagui* after ablation of the AG by Charniaux-Cotton and Ginsburger-Vogel [18] and in *Talitrus saltator* after implantation of testes into males of *O. gammarella* from which AG have been removed [19]. In *O. gammarella*, the transformation of testes into ovaries is possible if the testes are protected from the action of AH, before the onset

of spermatogenesis that occurs at the second intermolt. This is accomplished by implantation of gonads from young males into females. If implanted before the beginning of spermatogenesis, the young testes can develop into ovaries; if implanted later, the testes do not transform but instead degenerate [20].

Ovarian autodifferentiation has been also demonstrated in the oniscoid isopod *Helleria brevicornis* following implantation of undifferentiated gonads deprived of AG rudiments [21].

Among decapods, the proterandric hermaphroditic shrimps, such as *Pandalus borealis* and *Lysmata seticaudata*, give a good proof of the ovarian autodifferentiation (review in [22]). Thus, when the AG degenerate at the time of sex-reversal, or after their ablation (andrectomy) during the male phase, oogenesis spreads into the gonad. Another proof of ovarian autodifferentiation has been obtained in the shrimp *Macrobrachium rosenbergii* [23]. In young males in which the gonads contain only gonidia, andrectomy is followed by differentiation of normal ovaries with oocytes in previtellogenesis and development of oviduct rudiments.

Several natural data confirm the inherent tendency of gonidia in genetic females or males to effect oogenesis. Thus, female gametogenesis appears not only in the gonad rudiment of young males of several Talitridae, as *O. mediterranea* and *O. cavimana* [24], but also in the testes of mature males of gonochoristic decapods. For instance, the testes of the crayfish *Pontastacus leptodactylus leptodactylus*, exhibit oogenesis of variable intensity during genital rest. At this time, when the AG are very small, spermatogenesis stops and oocytes sometimes appear in different parts of the testes [11]. Thus, oogenesis may occur in some testicular acini as soon as the gonidia receive an insufficient quantity of AH, or none at all. It results in the formation of normal primary follicles but this oogenesis always stops at the end of previtellogenesis (cf. Section II, B, 3, a).

To summarize, ovarian differentiation of the gonadal rudiment is an autodifferentiation. It concerns oogenesis from gonidia to the end of previtellogenesis and takes place spontaneously in the absence of any hormone, female or male. This

proves the “emerging inherent tendency to develop into an ovary” as in mammals ([25], p. 39).

Initiation of oogenesis does not appear to be controlled by a neurohormone. In crabs, it is not accelerated by removal of eyestalks from larvae and from very young females, whereas a neurohormone from eyestalks regulates the initiation of spermatogenesis, through its moderating control of the AG [26, 27].

2. Maintenance of the germinative zone

The germinative zone of the ovary, in contrast to that of the testis, does not require the presence of a neurohormone for its maintenance. Thus, in the shrimps *Palaemon serratus* and *Crangon crangon*, after cauterization of the median zone of the protocerebrum or culture of isolated ovaries, the gametogenic activity of the germinative zone persists [28–30]. Likewise, sacculinid rhizocephalans, through contact and at some distance, cause the destruction of neurosecretory regions of the host crabs in both sexes. However, the germinative zone of parasitized female crabs is not modified, while the one of parasitized males degenerates [31, 32].

3. Oocyte growth until vitellogenesis

As already mentioned, oogenesis up to the end of previtellogenesis is a continuous phenomenon. Some studies have shown that the continuous phase of oogenesis is regulated by a moderating neurohormone. In the juvenile freshwater crab *Eriocheir sinensis*, ablation of the eyestalks brings on an increase in the synthesis of DNA in the germinal cells that is expressed by an increase in the number of oogonial mitoses and in the number of oocytes entering into prophase of meiosis [33]. Molting hormone interferes little in oogonial mitoses and in previtellogenesis, as is shown by the ablation of Y-organs from the juvenile and prepuberal crabs [34]. Thus, small quantities of ecdysone which remain in serum after the ablation seem sufficient to allow a normal oogenesis in these destalked crabs.

On the other hand, when Y-organ and eyestalks are removed simultaneously, most of the previtellogenic oocytes degenerate. It appears that repeated injections of 20 OH-ecdysone are necessary

to restore a normal previtellogenic growth in the destalked crabs [34].

Ablation of eyestalks in 1-year-old female *Paratelphusa hydrodromous*, during their post-oviposition period, seems to accelerate previtellogenesis, leading to an early vitellogenesis. At that time, the ovaries normally show empty follicles. This result is given as an argument in favor of an inhibitory control of previtellogenesis by eyestalks [35].

The protein synthesizing capacity of previtellogenic ovaries of *Uca pugilator* has been tested for 24 hr *in vitro*. In presence of neuroendocrine tissues such as eyestalk or thoracic ganglion, as well as cyclic AMP (10^{-6} M), the rate of incorporation of radioactive leucine into protein by the ovary is inhibited [36]. Since cyclic AMP appears to mimic eyestalk tissue (well-known to have an inhibitory effect on oocyte growth, as recalled in Section II, B, 1), the decrease in protein synthesis is attributed by the authors to “changes in cyclic nucleotide levels”. No clear interpretation concerns the inhibitory effect of the thoracic ganglion. The lack of a specific component from the medium would explain this unexpected effect occurring instead of the stimulation observed *in vivo*.

II. VITELLOGENESIS

A. Vitellogenesis process

1. General considerations

Vitellogenesis is the step of the crustacean reproduction during which oocytes accumulate a large amount of yolk, especially – but perhaps not exclusively – by internalization of an extraovarian precursor named vitellogenin. It affects synchronously all the elder oocytes, i.e., all the oocytes which have reached the end of previtellogenesis. Such a process is common to many groups other than Crustacea particularly in insects, amphibians, fishes and birds. From several aspects, vitellogenesis is a very important step of the female reproduction:

—Most of the endocrine controls on reproduction known at the present time apply on vitellogenesis.

—Contrary to previtellogenesis, vitellogenesis is

not a continuous process: it is inhibited during non-breeding season and, for some species, in artificial conditions. So, it is easy to understand that the aquaculture services play a special attention to the control of vitellogenesis mechanisms.

—The ability to carry out vitellogenesis is the criterium on which the puberty concept was built in female crustaceans.

Crustacean vitellogenin is a high molecular weight protein associated with lipidic, glucidic and carotenoid prosthetic groups to which very few studies have been devoted.

When vitellogenesis takes place, the presence of carotenoids linked to vitellogenin brings on a bright color of the ovary in most species. So, it is quite easy to know, without dissecting the animals, whether vitellogenesis has begun in the species whose exoskeleton is transparent, such as most prawns and shrimps.

2. Origin of vitellogenin

The existence in the haemolymph of vitellogenic females of a "female-specific-protein" – the early name for vitellogenin when the physiological significance of this protein was not firmly stated – was reported for the first time in Crustacea by Frentz [37] in the crab *Carcinus maenas*. This observation and the role of vitellogenin in the vitellogenesis process as the major precursor of yolk was confirmed in several other species during the following years [38–43 for review].

The site of vitellogenin synthesis in Crustacea was known quite lately and the question is not yet completely elucidated. The first hypotheses concerned the hepatopancreas [44] and were supported by the early observations on the transit of carotenoid pigments from this organ to the ovaries (e.g., [45]). However, nothing suggested that the proteinic part of vitellogenin has the same origin than the carotenes associated with it.

Kerr [46] cultured different tissues and organs from the crab *Callinectes sapidus* – muscle, heart, hepatopancreas, total haemolymph and serum – in the presence of ^{14}C -leucine and analyzed the protein released in the medium by column chromatography and electrophoresis. The author found some suggestion for the hemocytes as site of vitellogenin synthesis but the results did not seem

conclusive.

In *Uca pugilator* and *Libinia emarginata* Wolin *et al.* [47] reported a complete immunochemical identity between vitellogenin and a protein from the hepatopancreatic extract. Nevertheless, haemolymph could have contaminated the extract. Recently, Paulus and Laufer [48], using immuno-histochemical technics for the study of the crabs *Libinia emarginata* and *Carcinus maenas*, localized vitellogenin in hepatopancreatic specialized cells they called vitellogenocytes. According to the authors, these cells are contained in small haemal sinuses between the hepatopancreatic tubules and can be found in association with some other tissues, especially connective tissue. They may be similar to the adipocytes which are considered by other authors as the site of vitellogenin synthesis ([63], see further).

Lui *et al.* [49–51] incubated ovaries of the crayfish *Procambarus* sp. and of the crab *Pachygrapsus crassipes* in a ^3H -leucine medium or a mixture of tritiated amino acids up to 48 hr. After denaturation and electrophoresis, they demonstrated that radioactivity was present in the main polypeptide subunits of *Procambarus* vitellogenin and in all the three subunits of that of *Pachygrapsus*; so they concluded that the ovaries are the source of vitellogenin. Unfortunately, the authors have not cultured other organs than ovaries as controls. Using similar methods to those of Lui *et al.*, Eastman-Reks and Fingerman [52] drawn the same conclusion about the ovary of the crab *Uca pugilator*. As the preceding authors, they did not attempt to incubate other tissues. In the kuruma prawn, *Penaeus japonicus*, Yano and Chinzei [53] reported also that "ovary is the site of vitellogenin synthesis". These authors incubated ovaries and hepatopancreas – but no fat body – in Ringer solution containing labeled amino acids. Protein synthesized by the ovary and precipitated with anti-vitellin serum was shown by electrophoresis and fluorography to consist of two polypeptides corresponding to the components of vitellogenin. No immunoreactive material was found in the hepatopancreas and its incubation medium.

Some ultrastructural studies of the vitellogenic oocyte gave indications in favor of both intra- and extraoocytic sources of yolk (in the spider crab,

Libinia emarginata, the isopod, *Oniscus asellus*, the terrestrial hermit crab, *Coenobita clypeatus*, [54–56]).

In an amphipod Crustacea, *Orchestia gammarella*, Junéra *et al.* [57] showed that vitellogenin synthesis did not stop immediately after bilateral ovariectomy, as would be the case if the ovaries were the site – or, more precisely, the exclusive site – of vitellogenin synthesis: it only stopped 5 to 8 days after the operation for reasons which will be discussed further on (cf. Section II, B, 2, b). In 1980, Picaud and Souty using double diffusion technique and autoradiography, demonstrated that fat body from *Porcellio dilatatus* incubated with a ^{14}C -leucine medium synthesized vitellogenin. Junéra and Croisille [58] and Croisille and Junéra [59] made the same inference in *O. gammarella* but, in this species, the *subepidermal* adipose tissue only seems to be involved in vitellogenin synthesis. In the shrimp *Palaemon serratus*, Meusy *et al.* [60] demonstrated also by immunohistochemistry the presence of vitellogenin in the same structures of the vitellogenic females; the hepatopancreas was not labeled. Similar results were obtained later in two other decapods, the penaeids *Penaeus japonicus* [61] and *Parapenaeus longirostris* [62].

The adipocytes from *O. gammarella* display ultrastructural modifications when vitellogenin synthesis takes place [63]. They acquire a well-developed rough endoplasmic reticulum, the space in the cell occupied by β -glycogen and lipid droplets significantly reduces and the vitellogenin is detectable in dense bodies by the peroxidase-antiperoxidase method. Furthermore, when vitellogenin synthesis stops following a total ovariectomy, the adipocytes acquire the ultrastructural features of non-vitellogenic or male adipocytes [64].

Though some of these studies are seemingly contradictory, it should be noted that, in some insects – *Drosophila* and few others –, not only fat body but also follicle cells of the ovary are able to synthesize vitellogenin [65–67]; such a possibility of a double origin of vitellogenic material may exist also in Crustacea or in *some orders* of Crustacea. Moreover, the results about “vitellogocytes” associated with the hepatopancreas

[48] and those about “adipocytes” may not be inconsistent, since these two cellular types would be homologous. Incubation of fat body, ovary and hepatopancreas is a very hazardous method since the maintenance of the integrity of these tissues/organs during the process is not reliable. Particularly with the hepatopancreas, the release of proteolytic enzymes into the incubation medium is difficult to avoid. So, an attractive approach of this problem would be to look for messenger RNA coding for vitellogenin in these various tissues/organs.

3. Vitellogenin uptake by vitellogenic ovaries

a) Transformations and role of the follicle envelope

At the onset of vitellogenesis, each oocyte is surrounded by a follicle envelope which comes from a *permanent* tissue: the follicle tissue from the eggs which have been laid is utilized again for setting up the new follicles [3, 68–71], except in the isopod, *Idotea balthica basteri*, in which it seems to degenerate just prior to oviposition [72]. At the beginning of vitellogenesis, a tubular network has been observed in the cells of the follicle envelope of four species of Palaemonidae (*Palaemon adspersus*, *Macrobrachium rosenbergii* [70, 73, 74], *Palaemonetes varians* and *Palaemon serratus* (Jugan, unpublished)). These tubules, characterized by a diameter of 0.15 μm , are bound by a single membrane and enclose a granular electron-dense material. They connect up all the extracellular compartments: haemolymph, intercellular spaces, space between the oocytes and the follicle epithelium. After incubation of ovaries in a peroxidase containing medium, the diaminobenzidine reaction product was seen in the tubular network and in all these compartments. Peroxidase penetrated also into the vitelline membrane and in some pinocytotic vesicles of the oocytes [73, 74]. The tubular network regresses at the end of vitellogenesis [70, 75]. This structure which has been also described in copepods [76], makes easier the passage of substances from haemolymph to vitellogenic oocytes.

In *Idotea balthica basteri*, where no tubular network has been described, some features seem to play the same role as in Palaemonidae shrimps:

the cells of the follicle envelope acquire oocyte oriented villi, tight junctions appear between follicle villi and oocyte microvilli, and the spaces between follicle cells become very wide [72].

Beside its role of interface, the follicle envelope has an endocrine function. Charniaux-Cotton [77, 78] has demonstrated in females of *O. gammarella* that the vitellogenic ovary controls a secondary sexual characteristic which is temporary and appears during vitellogenesis: the long ovigerous setae on oostegites, the role of which is connected with incubation. The follicle cells are presumably the source of this ovarian hormone, though this has not yet been established (cf. Section VII, B, 1 and 2).

b) Vitellogenic oocyte and endocytosis mechanism

At the beginning of vitellogenesis, microvilli develop towards the follicle cells [54, 55, 79, 80]. In *M. rosenbergii*, some of them have been described penetrating deeply in tubules of the follicle cells [73, 74]. A glycocalyx, or cell coat, covers the external surface of the microvilli. In addition to microvilli, macrovilli have been also observed in an amphipod, *O. gammarella* [80] and in some decapods ([81]; *Lysmata seticaudata*, Zerbib, unpublished). These micro- and macrovilli increase considerably the oocyte surface and probably its exchange ability.

Endocytotic vesicles, 100–140 nm in diameter, appearing at the surface of the cortical ooplasm, have been described in many species. In some of them, their content seems to be drained towards yolk spheres by a network of microcanalicules, 45–60 nm in diameter in *Orchestia gammarella* (Fig. 1) and in the crayfishes *Astacus astacus* and *A. leptodactylus*, [4, 81]. It has been demonstrated, by incubating oocytes in a horseradish-peroxidase containing medium [82, 83] or by using fluoresceine isothiocyanate conjugated vitellogenin [47] or tritiated vitellogenin [378], that these structures are related to an endocytotic – and not exocytotic – process. Recently, Jugan and Soyez [84] conjugated vitellin of *Macrobrachium rosenbergii* with colloidal gold and observed a labelling at the surface of the microvilli, on endocytotic vesicles and yolk spheres. Jugan [75], working on *M. rosenbergii* demonstrated that vitellogenin inter-

nalization in Crustacea is a receptor mediated process. The receptors have a high affinity ($K_D=3.5 \times 10^{-8}$) and are very numerous (about 10^{10} receptors per oocyte).

The yolk spheres grow in size by fusing together and are pushed towards the medullar ooplasm by those more recently formed. At the end of vitellogenesis, they take a polyhedric shape and measure up to about 40 μm (“yolk platelets”). It has been shown that yolk spheres contain a lipo-glyco-carotenoproteic material. Lipid droplets have been also observed during vitellogenesis, but the origin of their content still remains undetermined (cf. comments in: [6], pp. 472–473). The proteins and lipids represent the major enrichment of the ovaries during vitellogenesis ([85] cited in [6]).

The sequestration of vitellogenin by the oocytes is a *specific* feature of vitellogenesis. Nevertheless, a rough endoplasmic reticulum is still present during this phase and it seems likely that intraoocyte synthesis of proteinaceous material continues [4, 86–88]. Moreover, transfer of nuclear material to the ooplasm, as a possible prelude to protein synthesis, has been reported [89, 90]. As suggested by Adiyodi and Subramoniam [6], the relative emphasis on autosynthesis and heterosynthesis probably varies with species.

Some time *before* the end of vitellogenesis, microvilli (and also macrovilli in the species where they are present) regress and the endocytotic phenomena disappear (in the isopod *Idotea balthica*, [72] and in *M. rosenbergii*, (Jugan, personal communication)). The oocytes are overloaded with yolk spheres and lipid droplets, except in the cortical and perinuclear ooplasm. Cortical vesicles appear and seem to be related to the formation of the fertilization envelope (in *O. gammarella* [91]). For Goudeau and Lachaise working on *Carcinus maenas* [92], these cortical granules would originate from the “endogenous yolk” (cf. Section V, C).

4. From vitellogenin to vitellin: a processing?

When vitellogenin, previously termed “female specific protein”, enters the oocytes, it is usually named vitellin (or lipovitellin). With a historical regard, it seems that these two different names

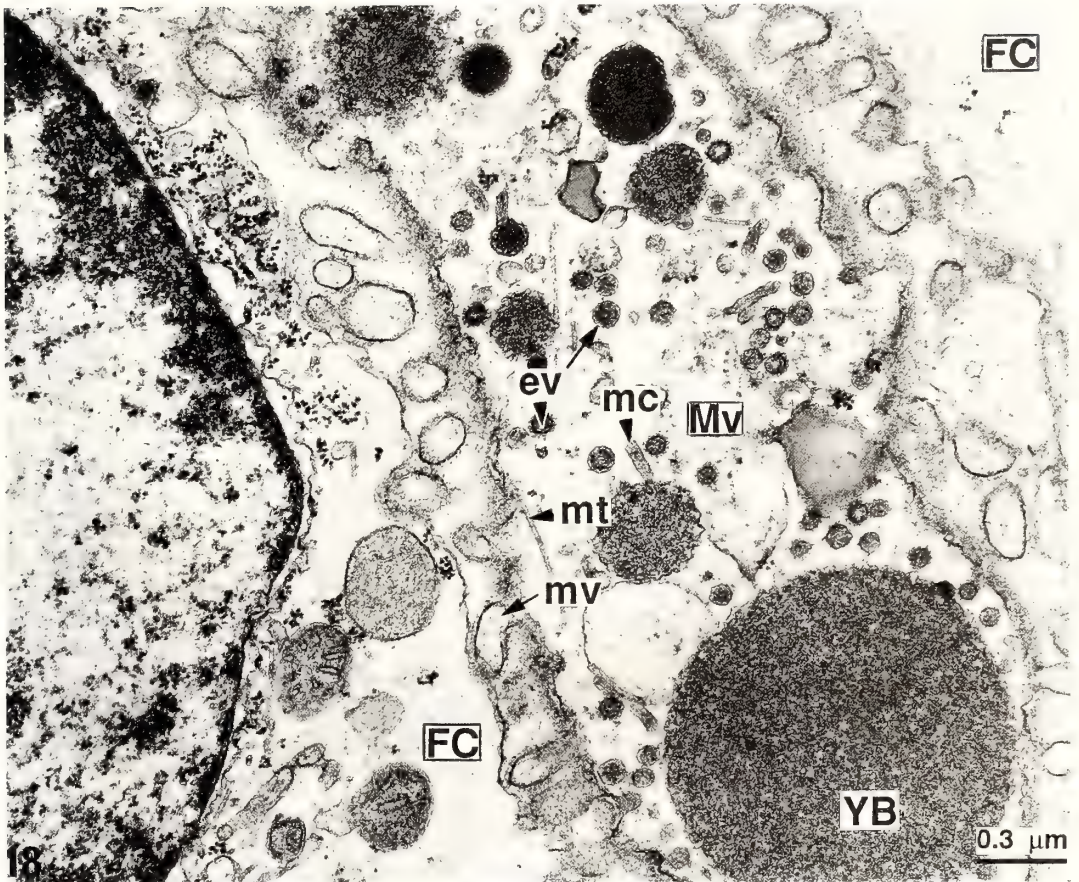


FIG. 1. Active endocytosis during vitellogenesis in the amphipod, *Orchestia gammarella*, and relationship between the oocyte and the follicle cells (FC) (courtesy of C. Zerbib).

ev: endocytotic vesicles; FC: follicle cells; mc: microcanalicules; mt: microtubules; Mv: macrovilli; mv: microvilli; YB: yolk body.

referred principally to the two compartments, haemolymph and oocytes, where these substances were found. Little was known about the chemical structure of vitellogenin and vitellin respectively.

The "female specific protein" of the haemolymph, i.e., vitellogenin, was initially characterized as an electrophoretically slow moving protein [37]. In the following years, the relation of vitellogenin to vitellogenesis was firmly established (cf. for review [93]). The presence of associated lipids (Sudan Black staining), carbohydrates (PAS positiveness) and carotenoids (pigment extraction and absorption spectrum study) was demonstrated and vitellogenin was consequently identified as a lipo-glyco-carotenoprotein (e.g., the early works:

in the crabs *Paratelphusa hydrodromous* [39], *Carcinus maenas* [94] and *Callinectes sapidus* [42]). The carotenoids give a bright color – varying according to the species – to the vitellogenin and vitellin and, consequently, to the vitellogenic oocytes. They are provided by the food and are not synthesized by the animal itself. It seems probable that they have a screening function against light (review in [95]; [96]). The molecular weight (MW) of the vitellogenin in Crustacea was reported in the amphipod *O. gammarella*: 397 ± 27 kD [57], and in the isopod *Porcellio dilatatus*: 315 ± 54 kD [97].

Vitellin, the major constituent of yolk, is also a lipo-glyco-carotenoprotein. It contains between 28

and 35% of lipids [98, 99] and about 4.8% of sugars [100]. On the basis of double-diffusion tests or related techniques, no immunological difference between vitellogenin and vitellin has ever been demonstrated in any species [42, 47, 99, 101–106].

The MW of vitellin is not very different from that of vitellogenin in the species where both have been determined [57, 97, 107]. The amino acid composition of the vitellin of some species has been established ([50, 51, 99, 107–109]; the results are compared in the review [6]), but no comparison with vitellogenin is available; so, these data bring no indication on a possible processing. Treatment of the vitellin by denaturing agents revealed in several species the presence of two polypeptide subunits with close MW of about 100 kD (*Palaemon adspersus*, *Uca pugilator*, *Homarus gammarus*, *Macrobrachium rosenbergii* [52, 96, 110, 111]; *Penaeus japonicus*, MW not determined [53]) or less (*Parapenaeus longirostris*, 45 and 66 kD, [106]). In the prawn, *Macrobrachium rosenbergii*, the vitellogenin and the vitellin have been both studied and exhibited the same two subunits of 84 and 92.2 kD MW [111]. In some other species, numerous fractions have been visualized (*O. gammarella*, *Procambarus* sp., *Squilla mantis*, *Penaeus japonicus* [50, 107, 112–114], but it seems probable that only few of them are native polypeptide subunits.

Although the possibility of a processing of the vitellogenin when, or after, entering the oocytes has been considered, especially with regard to the proteinic part of this yolk precursor, few informations are yet available. It is likely that vitellogenin and vitellin, if not identical, are very closely related substances.

5. Vitellogenin synthesis and vitellogenin level in haemolymph as means for monitoring vitellogenesis

A first attempt to know whether there is a close relation between the vitellogenesis process and the vitellogenin metabolism was carried out by injecting tritiated leucine to vitellogenic females of *Orchestia gammarella* at various steps of the reproductive cycle [115, 116]. The diagram (Fig. 2a) shows that the amount of radiolabeled vitellogenin in the haemolymph is growing from the

beginning to the 3/4 of the cycle, though endocytosis is maximal during this period (except at the very beginning of the cycle). This amount falls down during the last quarter of the cycle, though endocytosis, as seen by electron microscopy in several species (*Idotea balthica basteri* [72], *Palaemonetes varians* and *Macrobrachium rosenbergii* (Soyez and Jugan, personal communication)), become negligible at this period.

This result has been confirmed by *in vitro* incorporation of ^{14}C -leucine by the fat body of an isopod, *Idothea balthica basteri* (Fig. 2b)[117]. In addition to this statement, a diurnal rhythm of vitellogenin release was observed *in vivo* in another isopod, *Porcellio dilatatus* [118]. Other haemolymphatic and ovarian proteins seem also to be subjected to circadian variations [119–121].

In the lobster, *Homarus americanus*, where the reproductive cycle is not easy to study because it lasts about one year or more, it has been shown that the level of circulating vitellogenin, as measured by electrophoregram scanning, "is always highest well prior the maximum accumulation of yolk in the oocytes, and the levels dropped off markedly prior to oviposition" [105].

In the freshwater prawn, *Macrobrachium rosenbergii*, whose reproductive and molting cycles are short (about 3 weeks) and concomitant, as those of *O. gammarella*, an ELISA titration of circulating vitellogenin has shown that the vitellogenin level, very low at stages A and B, increases during stage C, i.e., during the period of intense uptake of vitellogenin by the oocytes, remains at a high level during stages D_0 – D_1 and fall down thereafter, though vitellogenesis is not still achieved (Fig. 3) ([111]; Derelle and Meusy, unpublished data). At the end of the molting/reproductive cycles, before and just after exuviation, the vitellogenin level is very low again. It will go up after oviposition if a new vitellogenesis takes place again. It is noteworthy that during the period of rapid decrease of the vitellogenin level, the vitellogenic oocytes display no more endocytosis but, nevertheless, their vitellin content increases up to oviposition. This observation is an indication for a vitellin synthesis by the oocytes themselves.

These studies, carried out on various species, firmly established that vitellogenin synthesis and

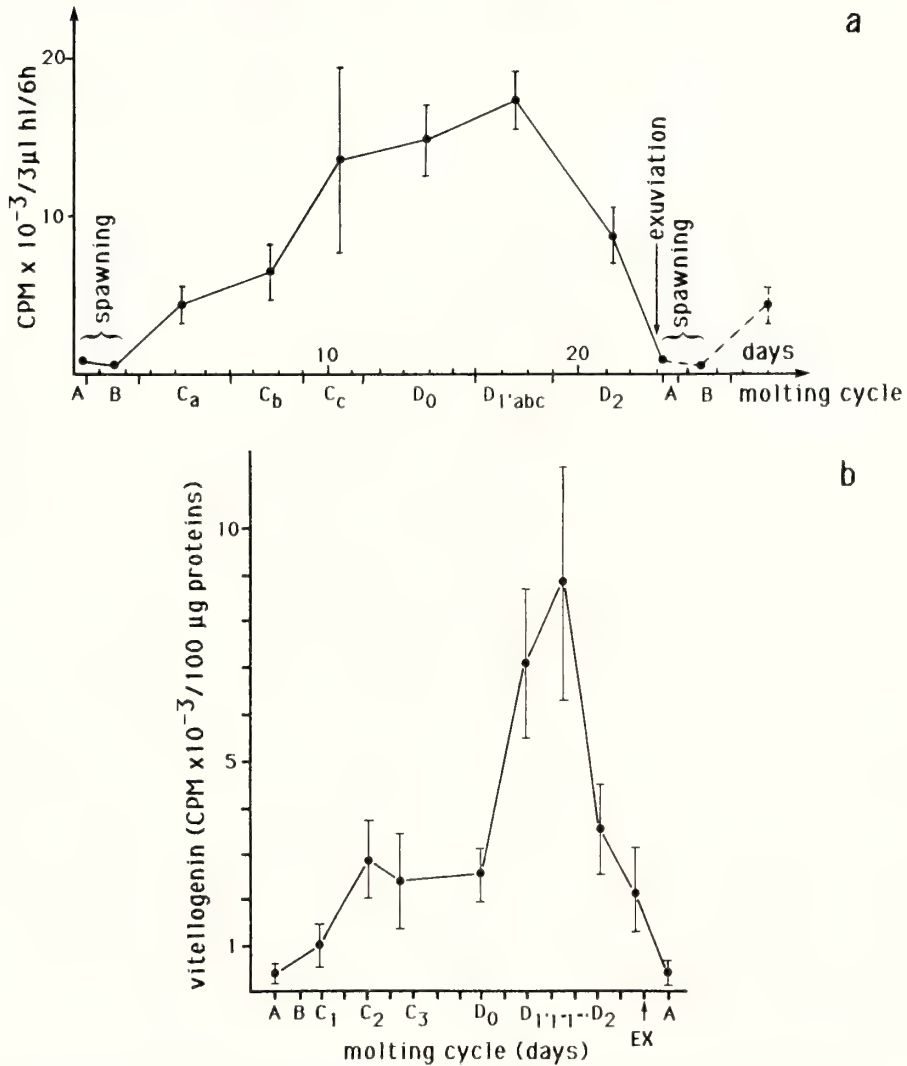


FIG. 2. (a) Vitellogenin synthesis in the amphipod, *Orchestia gammarella*, during the molting cycle.

Six hours before sampling of the haemolymph, the animals received an injection of 2.5 μCi of ^3H -leucine. The radioactivity of the vitellogenin was determined after separation by polyacrylamide gel electrophoresis of the serum proteins and corresponds to 3 μl of haemolymph (from [116, 347]).

(b) Relationship between the incorporation rates of ^{14}C -leucine by incubated fat bodies and the ovarian cycle (or molting cycle) of the isopod, *Idotea balthica basteri* (from [117]).

EX: exuviation.

vitellogenesis are closely correlated. Some important aspects of the mechanisms of control begin now to be elucidated.

6. Timing of the reproductive cycle: duration and relation with the molting cycle

The duration of the female reproductive cycle in

malacostracan Crustacea generally reduces when temperature increases and is very different from one species to another. For instance, it lasts about 3–4 weeks in the amphipod *Orchestia gammarella*, reared at the laboratory temperature, and in the prawn *Macrobrachium rosenbergii* at 27°C (observations made in our laboratory), several

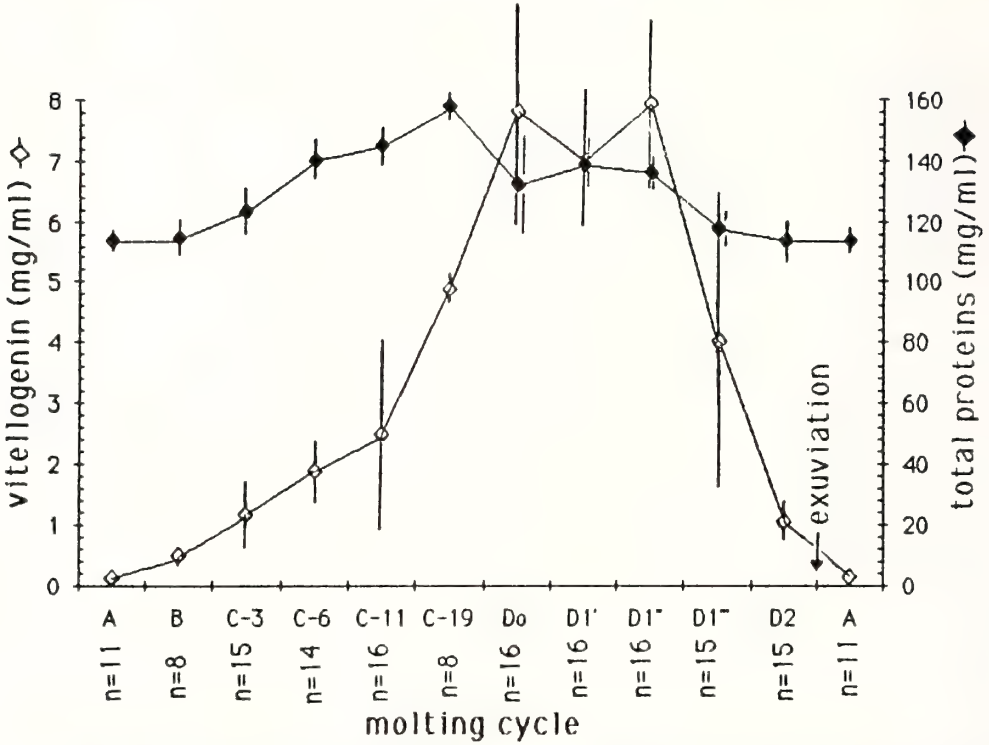


FIG. 3. Variations of circulating vitellogenin and total protein titres during the molting cycle in vitellogenic female prawns, *Macrobrachium rosenbergii*, of the same size. The titres of vitellogenin were determined by indirect ELISA and total proteins by Lowry's method (Derelle and Meusy, unpublished data). Bars: standard error of the mean; n: number of animals for each molting stage.

months in many species and about one or two years in the lobster, *Homarus americanus* [105, 122].

Various features can be found concerning the relation between vitellogenesis and molting cycle. In some species, vitellogenesis takes place during one intermolt and egg laying occurs just after the exuviation (for instance, in the amphipod, *O. gammarella* [123], the isopods, *Porcellio dilatatus* and *Idotea balthica* [124, 125], the decapods, *Lysmata seticaudata* and *M. rosenbergii* [16, 69]). In some other species, vitellogenesis can take place during more than one molting cycle, according to the season (for instance, in the decapods, *Palaemon serratus* and *Athyaephyra desmaresti* [126, 127]).

It is noteworthy that the molting cycle generally lasts a longer time during the reproductive season than during the genital resting period, because

vitellogenesis lengthens the cycle [123, 126].

In all these above malacostracans, egg laying takes place just after the exuviation. This is not the case of the crab, *Carcinus maenas*, whose vitellogenesis occurs only during the intermolt stage C₄ and which lays its eggs before premolt stages (D₀ to D₂), i.e., a long time before the exuviation [128]. In the crab, *Uca pugilator*, Webb [129] gives the following sequence of events: vitellogenesis - oviposition - incubation - hatching - molt. In the stone crab, *Menippe mercenaria*, several spawnings may occur within a single intermolt [130].

A very particular feature is that of few malacostracans which do not molt their whole life and become pubescent after their last molt, called "puberty molt" (cf. Section II, B, 2, d). In conclusion, the relationship between vitellogenesis and molting exhibits in Crustacea many different

features and seems to have supported a long and divergent evolution.

B. Vitellogenesis control

1. *Inhibitory control by VIH (Vitellogenesis Inhibiting Hormone)*

The first control to be known was inhibitory and its source is located in the central nervous system (cf. Fig. 4 for schematic representation of the main endocrine controls of vitellogenesis).

a) The X organ-sinus gland complex

Eyestalked species The works of Hanström, who discovered neurosecretory cells in the eyestalks of some species of stomatopods and decapods – the X organ or “Hanström’s organ” – and a connected neurohaemal organ – the sinus gland [131–133] –, marked the beginning of the

modern studies on crustacean endocrinology. At this time, the concept of neurosecretory cells was new: it was brought out only few years ago by Ernst Scharrer [134] from the observation of the hypothalamo-hypophyseal complex in Teleostei.

X organ is contained in the *medulla terminalis* of the optic lobes (protocerebrum), and consists of perikarya whose axons end in the sinus gland. The sinus gland, opalescent looking, is not really a gland but a neurohaemal organ. It stores and releases by exocytosis materials mainly from the X organ and contains no cell, except glial cells ([135–138]; review in [139]).

The role of the X organ-sinus gland complex was demonstrated by Panouse [140, 141], in the shrimp *Palaemon serratus*. This author observed that eyestalk ablation induces an acceleration of the molting cycle and a rapid growth of the ovary. He did not specify what stage of oogenesis was

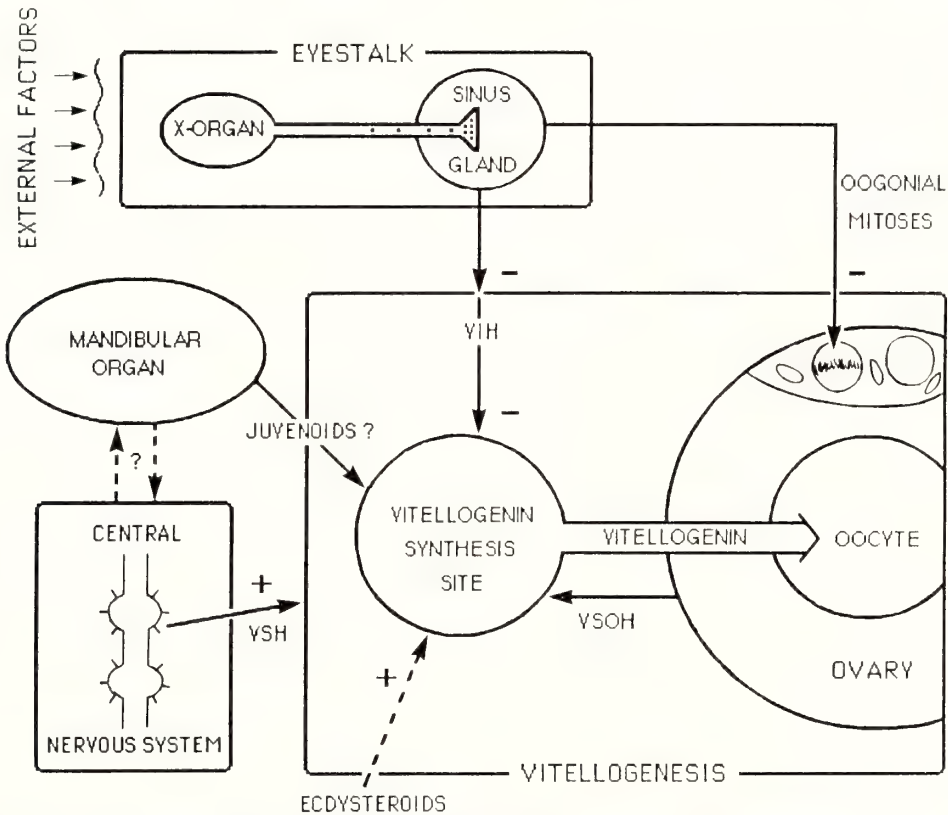


FIG. 4. Schematic representation of the main endocrine controls of oogenesis in malacostracans.

VIH: vitellogenesis inhibiting hormone; VSH: vitellogenesis stimulating hormone; VSOH: vitellogenesis stimulating ovarian hormone.

specially affected by this ablation and he thought that the two effects, on molting and ovogenesis, could result from the suppression of the same hormone ("anti-auxinic effect of the eyestalk hormone"). The results of Panouse's experiments, classically referred as "the Panouse effect", found their applying in aquaculture. In some species, the breeders do not carry out vitellogenesis in artificial conditions: a unilateral eyestalk ablation is usually practiced to trigger vitellogenesis [142]. A bilateral ablation is not required and has some disadvantages varying with species: for instance, it may shorten the life of the female and/or bring about some abnormalities of vitellogenesis [143, 347].

An extensive bibliography of the early works on the anatomy and physiological functions of the X organ-sinus gland complex is given in the book of Gabe [144] and a more recent review has been produced by Chaigneau [139].

It is noteworthy that eyestalk ablation often promotes either vitellogenesis or molting, according to the species, state of the ovaries, age of the animals, and temperature. The idea arises of a molting-vitellogenesis antagonism, though the real mechanism of this antagonism, hormonal or metabolic, remained unknown [35, 145, 146]. This hypothesis was backed up by the observation of the females of some Oxytrichina which molt during a limited part of their life and whose reproduction begins after the last molt and the degeneration of the Y-organ (molt organ): *Pisetaetraodon*, *Libinia emarginata* [147, 148].

While many other hormonal effects of the X organ-sinus gland complex were discovered and studied, i.e., on glucidic and lipidic metabolism, water balance, and chromatophores, most of the authors thought that vitellogenesis and molting are controlled by two distinct hormones, the Molt Inhibiting Hormone, MIH [149], and the Ovary Inhibiting Hormone, OIH [150]. The early ultrastructural observations of the sinus gland were in agreement with the hypothesis of several hormones (for review [139]), though the typing of the neurosecretion granules only took into account morphological criteria. It is clear enough that the number of granule types cannot be directly related to the number of alleged hormones. It is now established that the "Ovary Inhibiting Hormone"

acts mainly on vitellogenesis and is responsible for the sexual rest. So, the name of "Vitellogenesis Inhibiting Hormone" (VIH), proposed by Charniaux-Cotton and Touris [16], seems more adequate and precise.

Eyestalkless species The whitish and opalescent aspect of the sinus gland makes it quite easy to identify the gland in the vicinity of the optic lobes in eyestalkless species (review in [139]). In contrast, the identification of a structure homologous to X organ is much more difficult.

In the isopods which have no medulla terminalis, connections between neurosecretory cells of the brain and the sinus gland were found in *Porcellio dilatatus* [151], but the search for an X organ equivalent was mainly carried out by elective destruction of parts of the protocerebrum and optic lobes. Most authors located the source of VIH in the median part of protocerebrum (in *Idothea balthica* and *Ligia oceanica* [125, 152, 153]).

In the amphipod, *Orchestia gammarella*, electrocoagulation of the antero-medial part of the protocerebrum prevents the onset of vitellogenesis and this zone can be considered as stimulatory [116]. A VIH or a VIH-like substance seems to be secreted by some other part of the brain: a supernumerary brain grafted into females of this species inhibits vitellogenesis [154]. According to the author, the graft, which is deprived of external influences, would secrete continuously the inhibiting hormone. The concerned neurosecretory cells remain to be found in this order.

b) Ways of action

Control of vitellogenin synthesis When the concept of vitellogenin as the haemolymph precursor of vitellin became established, it appeared likely that the inhibitory action of VIH on vitellogenesis could act via the control of vitellogenin synthesis. Frenz [37] and Shade and Shivers [83] reported indications favorable to this hypothesis. Meusy *et al.* [60], injecting tritiated leucine to female shrimps, *Palaemon serratus*, showed that the ablation of eyestalks triggers vitellogenin synthesis. This result was confirmed and extended by *in vitro* experiments in the isopod, *Porcellio dilatatus*: extracts of sinus glands from non-vitellogenic females display a direct inhibitory

effect on vitellogenin synthesis by the fat tissue [155].

Control of vitellogenin uptake by the oocytes Unpublished observations on the amphipod, *O. gammarella*, by Meusy and Junéra suggested that the vitellogenin uptake might be hormonally controlled. Females do not usually lay eggs if mating has not occurred, for instance, in the absence of male. In this circumstance, a resorption of the non-laid oocytes is observed and, consequently, a very large amount of vitellin is detected in the haemolymph [101, 102]. Though vitellin could be used for a new vitellogenesis, in place of vitellogenin, as it has been proved by injecting radiolabeled vitellin in a vitellogenic female (Meusy, unpublished data), it happened that some of these females enter in the resting period, especially if the experiment was carried out at the end of autumn or at the beginning of winter. Similar observations were conducted on the prawn, *Macrobrachium rosenbergii*, when females were experimentally prevented from egg laying.

Direct evidence for a hormonal control of vitellogenin uptake by the oocytes of the prawn, *M. rosenbergii*, has been related by Jugan and Soyez [84]: a sinus gland extract inhibited the binding of colloidal-gold labeled vitellin on oocyte microvilli (Fig. 5). In preliminary studies using peroxidase-labeled vitellin, Jugan [75] reported that the affinity of VIH for the receptors to vitellin would be higher than that of the vitellin itself.

c) Extraction and purification of VIH

Though some other eyestalk hormones have been isolated in the seventies [156–158], the first attempt at purification of VIH was published only in 1981 by Bomirski *et al.* [159]. In a preliminary study, Klek-Kawinska and Bomirski [160] realized aqueous extracts of eyestalks of the shrimp, *Crangon crangon*, and tested their activity on destalked females of the same species. They found that the hormone is apparently absent during the early part of the breeding season. Later on, Bomirski *et al.* [159] dialysed, boiled and filtrated on Sephadex G-25 gel the eyestalk extracts from *Cancer magister* before testing them on destalked females of *Crangon crangon*. They concluded that VIH – they called GIH, i.e., Gonad Inhibiting Hormone –, is heat stable, dialyzable and has a

molecular weight of about 2000 Daltons. The thermostability was confirmed in the spiny lobster, *Panulirus argus* [146]. Quackenbush and Herrnkind [161], after extraction in phosphate buffer, pH 6.8, separated VIH and other peptides from the eyestalks of the spiny lobster, using Sephadex G-25 gel and bioassayed the fractions in eyestalkless female fiddler crabs, *Uca pugilator*. According to these authors, this neuropeptide has an apparent molecular weight near 5 kD and is different from the Molt Inhibiting Hormone, MIH, which did not induce gonadal inhibition. In a recent abstract, Quackenbush and Keeley mentioned a lighter MW for the GIH-VIH of the shrimp *Penaeus vannamei*: 3.3 kD [162].

More recently, Soyez *et al.* [163] extracted proteic material from isolated sinus glands of the lobster, *Homarus americanus*, with 0.1 N hydrochloric acid and purified the active factor by a two step reversed phase high performance liquid chromatography procedure. A bioassay, operated on destalked females of the shrimp, *Palaemonetes varians*, and an SDS-urea polyacrylamide gel electrophoresis revealed the presence of a single active peptide with a molecular weight between 7 and 8 kD. Some other peptides of similar molecular weight and with closely related elution time were partially characterized. Their amino-acid composition exhibits broad similarities (Soyez *et al.*, unpublished data).

d) Latest data on VIH

Recently, Meusy *et al.* [164] demonstrated that VIH from the lobster, *H. americanus*, is not strictly species specific from immunochemical criteria: the antibodies raised against the purified VIH from *H. americanus* crossreact in direct ELISA with sinus gland extracts from some other species (shrimps: *Palaemonetes varians* and *Palaemon serratus*; prawn: *Macrobrachium rosenbergii*; crab: *Carcinus maenas*) and not with that from several others (prawns: *Penaeus vanamei* and *P. monodon*; crayfishes: *Astacus leptodactylus* and *Orconectes limosus*; spiny lobster: *Jasus paulensis*). Immunocytochemical studies of the sinus gland of *H. americanus*, using the same antibodies and colloidal gold labelling, revealed that VIH is mainly localized in electron dense granules of medium size, 110–185 nm in diameter (Fig. 6).

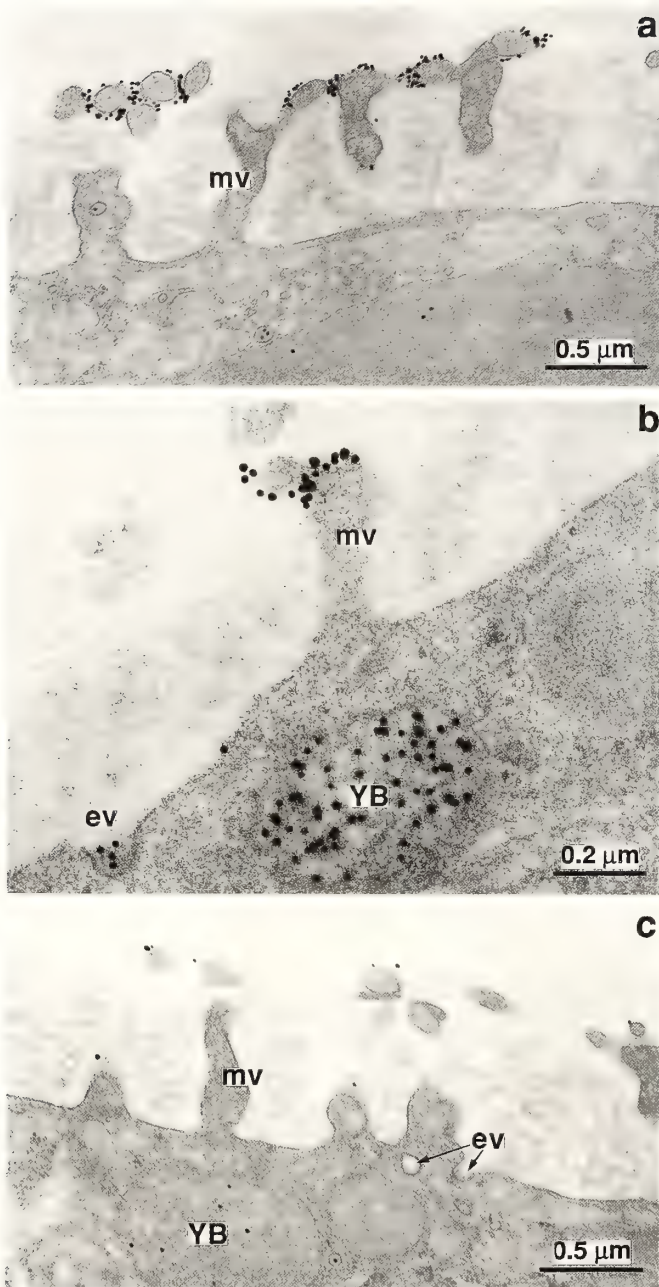


FIG. 5. Endocytosis in the prawn, *Macrobrachium rosenbergii*, as studied by incubation of vitellogenic oocytes in a medium containing colloidal gold conjugated vitellin (a, b). The effect on endocytosis of a sinus gland extract is shown (c). Microvilli (mv), endocytotic vesicles (ev) and yolk bodies (YB) are labeled. No significant labeling is observed in the presence of a sinus gland extract (courtesy of P. Jugan and D. Soyez).

Similar studies with an antiserum raised against the Crustacean Hyperglycemic Hormone (CHH) [165] have shown that this hormone, chemically related to VIH, is contained chiefly in large granules (170–260 nm) (Meusy *et al.*, unpublished results). So, the axonal endings, and consequently the neurosecretory perykaria, seem specialized, though the number of granule types recognized is below that of the neurohormones yet known. It is likely that the criteria, mainly morphological, used

for the typology of the secretory granules may not be satisfactory.

2. *Stimulatory control*

Many examples of hormonal antagonisms available in other groups, especially in mammals, suggested the possible occurrence of a vitellogenesis stimulating system in Crustacea. Moreover, following the opinion of some authors, the variable effect of eyestalk ablation on vitellogenesis, gener-

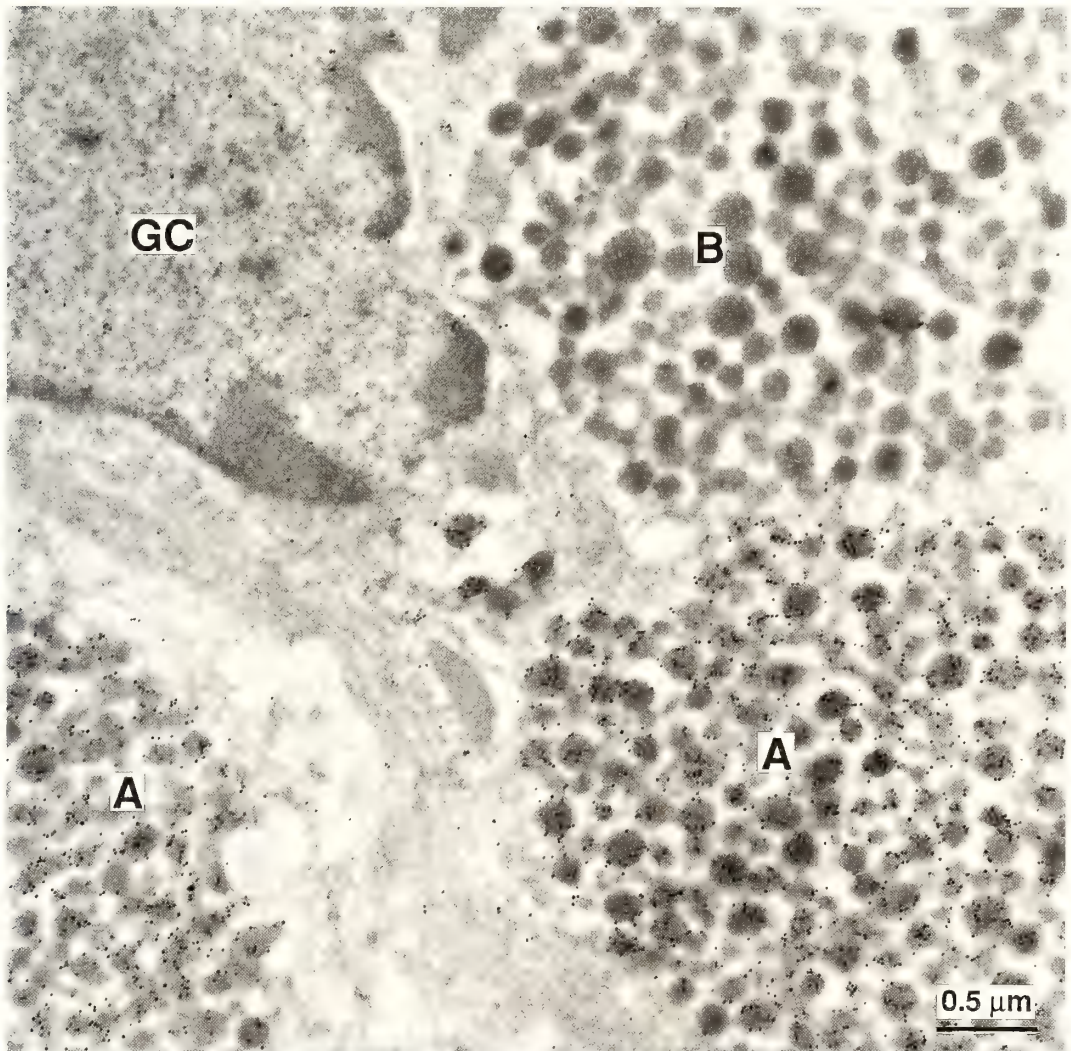


FIG. 6. Immunocytochemical (colloidal gold) staining of VIH in the sinus gland of the lobster, *Homarus americanus*, using a mouse serum against *H. americanus* VIH as primary antibody. The labeling is located on neurosecretory granules of medium size (A) (110–185 nm in diameter). The larger granules (B) (170–260 nm) are not labeled (from [164]).

ally stimulatory but dependent on the sexual condition of the female, the species and the environmental circumstances, seems to credit the hypothesis of an antagonistic control.

a) Neurohumoral factors

Though secretory cells have been described initially in the thoracic ganglia of crabs [166, 167], Otsu [168, 169] gave the first indications of a stimulatory control of vitellogenesis by substances issued from these structures: he observed a precocious development of the ovaries in the crab, *Potamon dehaani*, after implantation of thoracic ganglia. This result was confirmed in some other decapods [170–173].

Boiled aqueous extracts of thoracic ganglia from the fiddler crab, *Uca pugilator*, stimulated vitellogenesis in both intact and destalked crabs [36]. Takayanagi *et al.* [174] demonstrated *in vivo* and *in vitro* that aqueous extracts from not only thoracic ganglia but also brain have a positive effect on vitellogenesis in oocytes of the shrimp *Paratya compressa*. In the amphipod, *O. gammarella*, where the role of the thoracic ganglia has not been investigated until now, Blanchet-Tournier *et al.* [116] demonstrated that the antero-median part of the protocerebrum is stimulatory.

To conclude, the existence of an aqueous-soluble substance, secreted by nervous cells and having a stimulatory effect on vitellogenesis, seems established. However, the nature of this substance – perhaps a peptide –, its precise origin and the mechanism of its action remain to be studied.

b) Vitellogenin Stimulating Ovarian Hormone (VSOH)

As already mentioned (cf. Section I, B, 1), the ovary of Crustacea develops itself, i.e., its differentiation is not hormonally controlled [175, 176]. On the contrary, the testis – and the male secondary characters – are induced by the androgenic hormone secreted by the androgenic glands whose development is genetically induced [175].

If the testis is protected against the action of the androgenic hormone before the onset of spermatogenesis, it develops into an ovary (cf. Section I, B, 1). But the surgical suppression of the androgenic glands in *pubescent* males is generally

followed by the arrest of spermatogenesis and the degeneration of the testes only: vitellogenin synthesis, as well as oogenesis, do not take place. It has been demonstrated in *O. gammarella* that the implantation of an ovary is necessary for triggering vitellogenin synthesis [177].

On the other hand, the ovariectomy in vitellogenic females of *O. gammarella* is followed by the arrest of vitellogenin synthesis [177] and the fat body acquires the same features as the fat body of males and non-vitellogenic females [64]. This effect, considered alone, could be eventually explained by a feed-back regulation mechanism, as suggested by Picaud and Souty [178] for similar results obtained in females of the isopod, *P. dilatatus*. But the results of the preceding experiments performed on males of *O. gammarella* plead in favor of an ovary hormone. It might be possible that VSOH is the same hormone as the ovarian hormone controlling the ovigerous setae ([77, 78]; cf. Section VII, B). In the isopod, *Armadillidium vulgare*, vitellogenin synthesis is not ovary dependent [179].

Up to now, no other study has been carried out on VSOH which seems to play a similar role to that of estradiol-17 β in egg laying vertebrates.

c) Ecdysteroids

The Y-organs are responsible for molting [180] by secreting α -ecdysone, which is hydroxylated to the active hormone, 20 OH-ecdysone, also called β -ecdysone, ecdysterone or 20 β -hydroxyecdysone [181–185, 345].

Except the early works [186–190], several studies have shown that vitellogenesis cannot take place after Y-ectomy in the isopods, *Idotea balthica*, *Porcellio dilatatus* and *Armadillidium vulgare* [125, 191, 193], and in the amphipod, *Orchestia gammarella* [192]. Nevertheless, the relationship between 20 OH-ecdysone secretion and vitellogenesis is not easy to define. It has been demonstrated by radioimmunoassay that a high peak of ecdysteroids occurs in the haemolymph of various species before exuviation, during a short time of stage D₂ (or D₂–D₄) of the molting cycle (in the crab *Carcinus maenas*, in *O. gammarella*, in the shrimp, *Palaemon serratus* [194–197] and in the prawn, *Macrobrachium rosenbergii*, Derelle and Meusy, unpublished data). Vitellogenesis and

vitellogenin synthesis have begun a long time before this short increase of ecdysteroid level in haemolymph and cannot be directly related to this phenomenon (Fig. 7a and 7b). Moreover, molting and reproduction cycles are not synchronous in several Crustacea. The extreme instance is that of oxyrynch crabs whose Y-organs degenerate in males as well as in females and enter a terminal anecdyosis after the puberty molt [198, 199].

Further data on the effect of molting hormone on vitellogenesis have been brought on by studies on vitellogenin. Meusy *et al.* [192] have demonstrated that Y-ectomy in *O. gammarella* is followed by a decrease of the vitellogenin synthesis. In the isopod, *Porcellio dilatatus* [200], a decrease of the amount of the circulating vitellogenin was observed after Y-ectomy and this effect has been compensated by 20 OH-ecdysone injection to the animals. But administration of 20 OH-ecdysone to *non-operated* females of *O. gammarella* failed to trigger or stimulate the vitellogenin synthesis [201]. Furthermore, molting hormone is not necessary for an *in vitro* synthesis of vitellogenin by the fat body from female [202] or even male *P. dilatatus* [203], though an *in vivo* stimulatory effect has been reported in this species [200]. A stimulatory effect has been also reported on ovarian protein synthesis [348].

So, it is unlikely that the molting hormone plays a *specific* stimulatory effect on the vitellogenin synthesis and the vitellogenesis. Numerous studies carried out on insects seem to credit 20 OH-ecdysone with a stimulatory effect on several metabolisms, but not specifically on the vitellogenin synthesis which is controlled by juvenile hormone (the haematophagic insects, where 20 OH-ecdysone triggers vitellogenin synthesis after a blood meal, seem to be a particular feature).

The function and destiny of the ecdysteroids found in the ovaries of *O. gammarella* at the end of the vitellogenesis [196] and in the ovaries of *Carcinus maenas*, especially ponasterone A [204, 205], are still undetermined.

d) Juvenoids

Some authors have speculated that the juvenile hormone, JH, which regulates metamorphosis and gametogenesis in insects might also play a role in the physiology of crustaceans. Four approaches to

this topic were carried out by: 1) injecting juvenile hormone or analogs; 2) observing some structural similarities of the mandibular organs of Crustacea with the corpora allata of insects and steroid-producing cells; 3) implanting these mandibular organs in experimental animals; 4) identifying sesquiterpenoid compounds in haemolymph and mandibular organs.

Several authors have observed a chemosterilant effect of JH-I (on *Orchestia gammarella* [68]) or juvenile hormone analogs (on the mud crab, *Rhithropanopeus harrisi* [206], and on the immature spider crab, *Libinia emarginata* [207]). In these experiments, the addition of hormone increased the current haemolymphatic level to a supraphysiological state which might have toxic effects on the ovary. Similar results have been reported in insects ([208], p. 247), though the corpora allata, source of juvenile hormone in insects, are necessary for vitellogenin synthesis and vitellogenesis in most species [209].

The presence of corpora allata has never been pointed out in Crustacea but endocrine organs located in the vicinity of each mandible have been described by Le Roux [210] who postulated that these organs might have an endocrine function related to oogenesis. The ultrastructural features of the so-called mandibular organs showed analogies with steroid-producing cells [211–213] and corpora allata of insects [214].

The mandibular organs are controlled by the eyestalks, probably by a hormone from the sinus glands: they become hypertrophied after eyestalk ablation [211, 215]. Their involvement in vitellogenesis has been suggested in *Libinia emarginata*: mandibular organs from adult male spider crab were able to induce vitellogenesis when implanted in immature females [216].

After a preliminary work [217] in which the authors detected a juvenile hormone activity in two decapods, Laufer *et al.* [218] demonstrated the *in vitro* secretion of methylfarnesoate by the mandibular organs of *Libinia emarginata*. This compound is structurally and biologically related to JH-III, as a major product, and a very small amount of JH-III (1000 times less than methylfarnesoate). After eyestalk ablation, the secretion of methylfarnesoate was enhanced by at least two

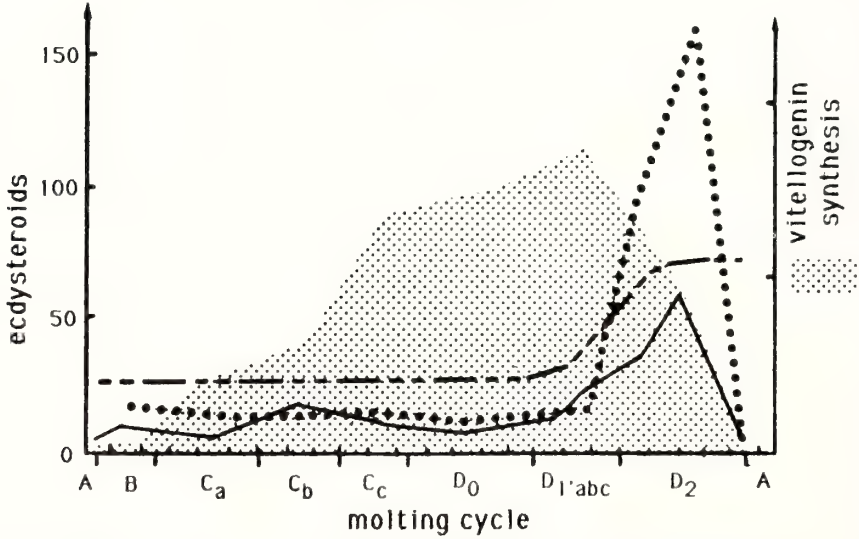
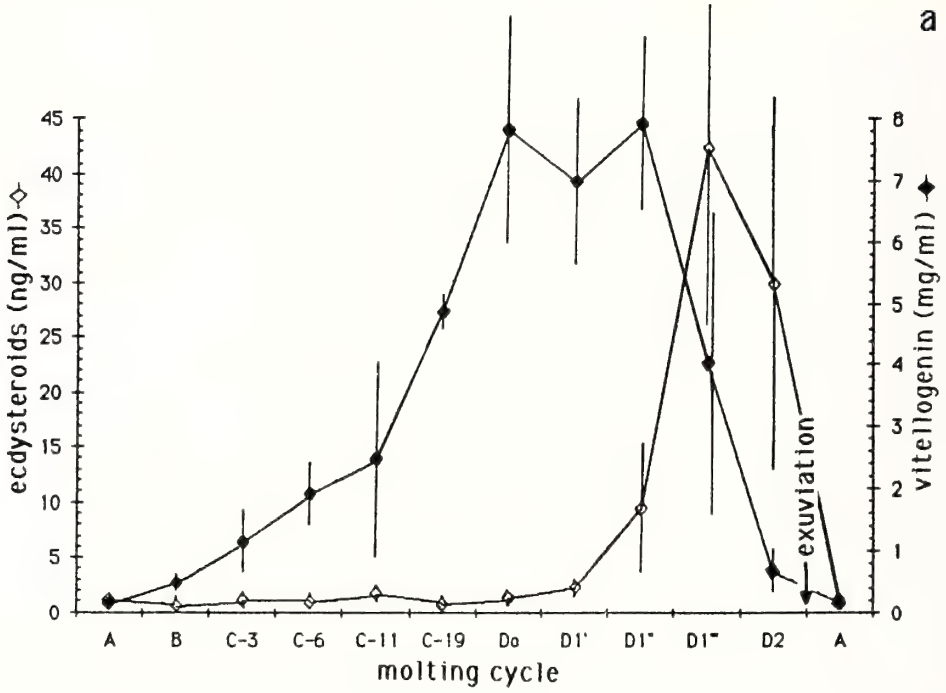


FIG. 7. (a) Evolution of the titres of circulating vitellogenin and ecdysteroids during the molting cycle in vitellogenic female prawns, *Macrobrachium rosenbergii*, of homogeneous size.

The titres of vitellogenin were determined by indirect ELISA and ecdysteroids by RIA (Derelle and Meusy, unpublished data).

Bars: standard error of the mean.

(b) Evolution of ecdysteroid titres and vitellogenin synthesis rate during the molting cycle of the female amphipod, *Orchestia gammarell* (data from [196]).

..... : vitellogenin synthesis (see Fig. 2.a).

..... : haemolymph ecdysteroids (pg eq. 20-OH ecdysone/ μ l haemolymph).

--- : ovarian ecdysteroids (pg eq. 20-OH ecdysone/mg ovary).

— : whole animal ecdysteroids (pg eq. 20-OH ecdysone/mg fresh weight).

folds. In the same species [219], haemolymph was found to contain 10 to 50 ng/ml of methylfarnesoate and 0.003 to 0.030 ng/ml of JH-III. The highest rate of methylfarnesoate in females was observed near the end of the ovarian cycle. The authors postulated a role of juvenoids in vitellogenesis, most likely mediated by the stimulation of vitellogenin synthesis.

It is noteworthy that the preceding studies have been carried out on *Libinia emarginata*, a crab exhibiting a *puberty molt* which is the last molt in its life [148]. Except the species belonging to the Oxyrhyncha's section, this feature is seldom observed in Crustacea. The reproductive physiology of such species seems more closely related to that of insects than to the majority of crustaceans. This conception seems supported by the very low level of methylfarnesoate in the haemolymph of the lobster *Homarus americanus*, a decapod which has also no puberty molt. This level is only of 1.3 ng/ml in *H. americanus* while it is of 55 ng/ml in *L. emarginata* [218]. Such a result was confirmed by the *in vitro* incubation experiments of the mandibular organs from several Brachyura and Macrura crustaceans.

The mandibular organ was also found to contain estradiol-17 β and progesterone [220] (cf. Section II, B, 3).

e) Ovary-stimulating factor from males

In the freshwater shrimp, *Paratya compressa*, vitellogenesis is delayed when females are reared in the absence of males [221]. An extract of the testis or the vas deferens is able to serve as substitute for males. According to the authors, the organs of mature male shrimps, particularly the testis or the vas deferens, would secrete an ovary-stimulating pheromone which accelerates ovarian development. The presence of males has a similar effect in the isopod, *Armadillidium vulgare*; moreover, the insemination lengthens the period of ovarian activity in this species [222].

3. Effect of other substances

Below are gathered several experiments with various substances from male Crustacea, as well as from insects and mammals. The androgenic hormone has been proved to be non-existent in females and the occurrence of other substances

acting on vitellogenesis is unknown or is a matter of discussion.

a) Androgenic hormone

As it has been demonstrated by Charniaux-Cotton (review in [175]), the androgenic gland develops only in males and controls the differentiation of the male sex. Therefore, the androgenic hormone cannot be considered as a *normal* factor controlling vitellogenesis. When the androgenic gland is implanted into females, the vitellogenin disappears from the haemolymph [223, 224], vitellogenesis stops and, in some species as *O. gammarella*, the ovary is transformed into a testis [123, 175]. More precisely, Junéra specified that synthesis in female *O. gammarella* ceased at the post-operative intermolt, or during the next following intermolt (personal communication). It is not clear whether the androgenic hormone inhibits vitellogenin synthesis directly or indirectly.

b) Vertebrate hormones

The idea that mammalian sexual hormones might be present and effective in Crustacea has led to some studies, especially on females. Bomirski and Klek-Kawinska [225] reported a positive effect of human chorionic hormone (HCG) on the ovary of the shrimp, *Crangon crangon*. After injection, they found this glycoprotein effective on vitellogenesis as well as on oögonia transformation into oocytes. The stimulation of vitellogenesis was confirmed by injection of HCG in the marine isopod, *Idotea balthica basteri*, and an increasing rate of vitellogenin synthesis and liberation was also observed [226]. This effect seems specific for vitellogenin since the rate of total protein synthesis was not modified.

A stimulatory effect of progesterone on the development of the oocytes of the penaeid prawn, *Parapenaeopsis hardwickii*, seemingly on vitellogenesis, was also reported [227].

An estrogenic activity was recognized for long time in tissues of the lobster, *Homarus americanus*, especially in eggs [228-230]. In the same species, Lisk identified the estrogenic activity to be estradiol-17 β and did not detect any estrone [346]. The presence of estrogen-like compound was also reported in the ovary of the shrimp, *Parapenaeus fissurus* [231]. Ollevier *et al.* [232], using mass spectrophotometry, identified five nonecdysteroid

steroids in the haemolymph of male and female *Astacus leptodactylus*: pregnenolone, 17 β -hydroxypregnenolone, testosterone, cholesterol and 6 β -hydroxyprogesterone. Recently, Couch *et al.* [220] found progesterone-like and estradiol-like immunoreactivity in the mandibular organ, green gland, hepatopancreas, ovary and serum of *H. americanus*. They showed that these steroids change in concentration in relation to the development of the ovary and suggested that estradiol-17 β , or one of its metabolites, could promote vitellogenesis in Crustacea as it acts in egg laying vertebrates. Further studies would be necessary to put forward well-stated hypotheses about the role of vertebrate-like hormones in Crustacea

c) "Queen-substance" of honeybees

It is known that the "queen-substance" of honeybees inhibits the development of the worker's ovaries and the production of further queens, probably through the inhibition of corpora allata growth (review in [233]). According to Carlisle and Butler [234], this substance shows an inhibitory effect on the development of the prawn's ovaries and, in a reciprocal way, the extract of sinus glands from *Palaemon serratus* inhibits the ovary development in worker honeybees. This result, which has not yet been confirmed, might indicate some chemical similarities between the "queen-substance" and VIH.

4. *Environmental factors and vitellogenesis*

Among environmental factors, photoperiodism and temperature were the most investigated (cf. [235], for review).

a) Light and temperature

Light seems the most prominent factor for controlling reproduction, but temperature seems to have also an effect, perhaps indirect (Table 1). As we could expect, light has various effects depending on the natural environment of the species, the history of the animal (i.e., the environmental conditions before the experiment), the stage of the ovary at the onset of the experiment, etc. For instance, vitellogenesis is induced by long day photoperiods in the southern amphipod, *Gammarus lawrencianus*, which produces sequential broods during spring and summer; in contrast, short day photoperiods promote vitellogenesis in another species, *Gammarus setosus*, which is found in high latitude and produces a single brood at the very beginning of the year [240]. Though it is undoubtful that environmental factors act on reproduction *via* VIH, perhaps together with some other neurohormones, the relationship between the receptors for environmental factors and the neurosecretory system remains to be studied.

b) Other factors

Extensive studies were carried out on aquacul-

TABLE 1. Effect of light and temperature on vitellogenesis and reproduction in malacostracans

Species	Author(s)	Factor(s)	Results
Amphipoda			
<i>Pontoporeia affinis</i>	Segerstrale (1970) [236]	Light	Constant light \rightarrow inhibition of gonad development. Decrease in illumination \rightarrow "maturation" process.
<i>Gammarus setosus</i>	Steel <i>et al.</i> (1977) [237]	Light	Short days \rightarrow acceleration of reproductive cycle. But the cycle is not completely controlled by photoperiod and cannot be stopped.
<i>Hyaella azteca</i>	de March (1977) [238]	Light and temperature	Long photophase \rightarrow reproduction (main factor). Temperature \rightarrow effect on the rate of all reproductive changes.
<i>Gammarus lawrencianus</i>	Steele (1981) [239]	Light	Short days \rightarrow resting stage.
<i>G. lawrencianus</i> and <i>setosus</i>	Steele and Steele (1986) [240]	Light	Short day photoperiods \rightarrow vitellogenesis in <i>G. setosus</i> \rightarrow opposite effect in <i>G. lawrencianus</i> .
<i>Gammarus lacustris</i>	de March (1982) [241]	Light	Decreased photophase \rightarrow reproduction.

TABLE 1. (Continued)

Species	Author(s)	Factor(s)	Results
Isopoda			
<i>Oniscus asellus</i>	McQueen and Steel (1980), Steel (1980) [242, 243]	Light and temperature	Long days → induction of reproduction (temp. affects molting and has no direct effect on reproduction). Seasonal periodicity in the responsiveness of females.
<i>Armadillidium vulgare</i>	Juchault <i>et al.</i> (1982) [244] Jassem <i>et al.</i> (1982) [377]	Light	Increased photophase over 12–14 h → reproduction.
Decapoda (Penaeidea)			
<i>Penaeus japonicus</i>	Laubier-Bonichon (1975, 1978) [245, 246]	Light and temperature	Long photophase (L=13.5–16 h) and high temp. (24–26°C) → stimulation of breeding.
Decapoda Astacidea			
<i>Cambarus</i>	Stephens (1952) [247]	Light	Dailylight periods (any duration) → periodic resorption of yolk. Continuous darkness → oocyte "maturation".
<i>Orconectes virilis</i>	Aiken (1969) [248]	Light and temperature	4–5 months of low temperature and constant darkness are necessary for complete "maturation" of the oocytes in lab. experiments.
<i>Procambarus clarkii</i>	Suko (1958) [249]	Light	Total darkness → effect depending on the initial stage of the ovary.
<i>Cambarellus shufeldtii</i>	Lowe (1961) [250]	Light and temperature	Increased photophase and temperature → acceleration of oocyte "maturation" and yolk resorption.
<i>Orconectes limosus</i>	Kracht (1972) [251]	Light and temperature	Artificial season able to promote anticipation of breeding, hatching and molting.
<i>Orconectes nais</i>	Armitage <i>et al.</i> (1973), Rice and Armitage (1974) [145, 252]	Light	Long-day photoperiod → inhibition of ovarian growth. Short-day photoperiod → acceleration of ovarian growth. Gonadal growth and molting are negatively related.
<i>Homarus americanus</i>	Nelson (1986) (+ earlier references from other authors) [253]	Light and temperature	In some populations: 2–3 months of short-days are necessary to condition the ovary for vitellogenesis following long-day onset. No requirement for European species (<i>H. gammarus</i>).
Decapoda Brachyura			
<i>Menippe mercenaria</i>	Cheung (1969) [130]	Temperature	Higher spawning frequency during hot months (even if the days are not the longest).
<i>Pachygrapsus marmoratus</i>	Pradeille-Rouquette (1976) [254]	Light	Long photophase → vitellogenesis only if the animals have been subjected to a short photophase before.
<i>Scylla serrata</i>	Nagabhushanam and Farooqui (1981) [255]	Light	Long-day photoperiod (14L: 10D or more) favours vitellogenesis.

ture species to improve the production of farming: for instance, about the composition of feeding pellets with the aim of promoting growth and/or vitellogenesis, about the density of population, nature and color of the substratum, and salinity.

Such applied investigations are generally reported in aquaculture journals.

Some other factors have been the matter of studies. For instance, noise, at the level of 30 dB, has a negative effect on female reproduction of the

sand shrimp *Crangon crangon* [256]. Lunar phases seem also to have an influence on reproduction: ovaries of the crabs, *Uca tangeri* and *U. terpsichores*, are the most highly developed around full moon [257–259].

5. Parasitism and vitellogenesis

In female decapods, parasitic infestation due to rhizocephalans leads to an atrophy of the ovaries chiefly due to an abortive vitellogenesis. Although such an effect was described in several crabs (*Macropodia rostrata*, *Carcinus mediterraneus*, *Pachygrapsus marmoratus* and *C. maenas*) [37, 260–262], the causes and the modalities of the gametogenesis impairment still remain not well known. A penetration of the rhizocephalan's root system across the ovarian wall and its close contact with the oocytes have been reported in *M. rostrata* parasitized by *Sacculina fraissei* as well as *C. maenas* and *C. mediterraneus* parasitized by *S. carcini* [32, 260].

In both *Carcinus*, the growth of oocytes does not progress beyond a diameter of 120 μm that corresponds to the end of previtellogenesis. Oocytes never develop further and do not reach an average size of 350 μm that is normally observed in vitellogenic ovaries of non-infested crabs. Preliminary ultrastructural studies indicate that this blocking is partly due to abnormality in the organization of the vitellogenic follicle: follicle cells remain at a certain distance from the oocytes, instead of surrounding them tightly as in healthy females. At their terminal evolution, oocytes agglomerate and then unite before being resorbed by hemocytes and some follicle cells, later on. This lysis phenomenon is quite comparable to the one that occurs following AG implantation into destalked females or topical application and ingestion of a juvenile hormone mimic [206, 263]. In both circumstances, there is no egg laying. Hormonal imbalances related to the presence of the parasite appear responsible for this inhibition [264]. A biochemical and immunochemical investigation of vitellin proteins from the ovary and haemolymph was recently performed in healthy and parasitized *C. maenas* [265]. This study shows that the ovarian development arrest would be due to an inhibition of the control of the vitellin

synthesis and vitellogenin uptake by the gonad. The vitellin proteins of *Sacculina* do not display any electrophoretic or immunochemical similarity to those from the host.

III. OOCYTE MATURATION

In malacostracans, the mechanism of oocyte maturation or meiotic maturation, i.e., meiotic resumption of the arrested-prophase I oocytes, occurs in the ovary and begins before fertilization. Very few histological descriptions have been devoted to this phenomenon. Beside those reported in some amphipods [266, 267], two recent cytological studies were carried out in *Orchestia gammarella*, and then in the prawn *Palaemon serratus* [268, 269]. They report the events which lead to the release of the first meiotic block and are closely linked in time with the preparation of the molting phenomena (Fig. 8).

The chronology of the cytological aspects has been recently established in *P. serratus* [270]. Initially arrested at prophase I, the oocytes resume meiosis when approaching stage D_{1-} of the molt cycle (4 to 5 days before molting). This premolt period is characterized by the following steps: nuclear envelope folding, nucleolar regression and dissociation, condensation of the chromosomes and beginning of the breakdown of the nuclear envelope. The germinal vesicle breakdown takes place at the D_{1-} -early D_2 stage, when the germinal vesicle still occupies a central position in the oocyte. Migration of the broken germinal vesicle that holds chromosomes occurs at the end of the D_2 stage, i.e., approximately 4 hr before exuviation. The divalent chromosomes that are not yet organized in a metaphase plate become visible at the oocyte surface, only 1–2 hr before the exuviation. They lay in a nucleoplasmic region devoid of nuclear envelope. The first meiotic spindle can be seen at the time of exuviation. The oocytes remain blocked at this stage of metaphase I until spawning.

To determine the exact stimulus that governs meiosis resumption, experimental studies have been conducted in *O. gammarella* and *P. serratus* [268, 269]. In *O. gammarella*, if exuviation is advanced by injection of 20 OH-ecdysone or de-

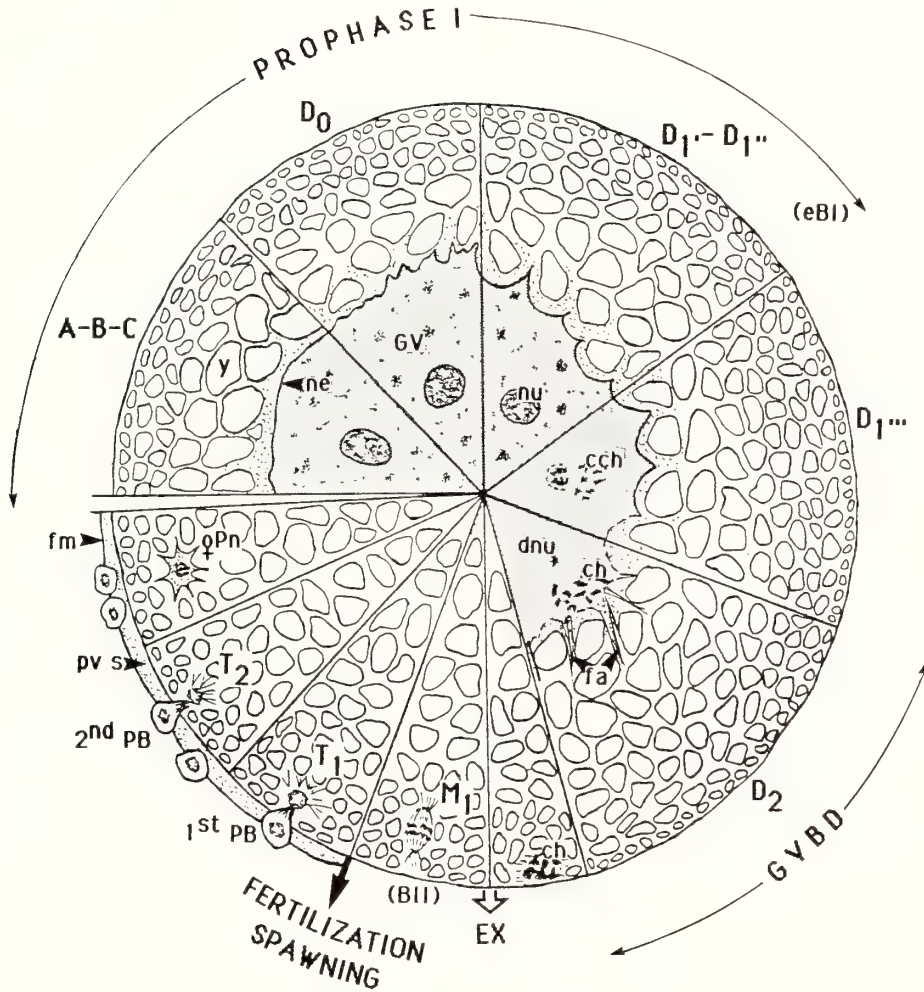


FIG. 8. Diagram showing the evolution of the nuclear apparatus during maturation and activation processes in the prawn *Palaemon serratus* (redrawn from [270]).

A, B, C, D₀, D₁, D₁', D₁'', D₂: stages of the molt cycle; cch: condensed chromosomes (ch); dnu: dissociation of nucleolus; EX: exuviation or maturation molt; eBl: end of the first blocking stage in prophase I; BII: second blocking in metaphase I (M1); fa: filamentous apparatus; fm: fertilization membrane; GV: germinal vesicle; GYBBD: germinal vesicle breakdown; ne: nuclear envelope; nu: nucleolus; 1st PB, 2nd PB: first, second polar bodies; pvs: perivitelline space; T1, T2: telophase 1 and 2; OPn: female pronucleus; y: yolk body.

layed by cauterization of the median zone of the protocerebrum, the two phenomena remain simultaneous only if the oocytes have reached a certain size (about 500 μm of diameter). Furthermore, if exuviation is blocked by Y-ectomy, no maturation occurs. In *P. serratus* meiotic reinitiation of prophase I blocked - oocytes is triggered if immature oocytes are incubated in presence of either 20 OH-ecdysone (10^{-6}M), or ponasterone A, or

ionophore A 23187 (5 μM in a normal or Ca^{2+} free seawater milieu). These results suggest that steroids are involved in meiotic maturation. To our knowledge the only comparable data in the other arthropod concern the insect *Locusta migratoria* [271]. Moreover, in the prawn, the treatment with ionophore indicates that steroid inducers may act via intracellular calcium. It is tempting to correlate Clédon's results with those that mention a high

concentration of ecdysteroids in the ovaries of the shore crab *Carcinus maenas* at the end of vitellogenesis (10^{-6} M compared to 10^{-8} M in the haemolymph), as well as in the eggs immediately after egg laying [204, 272]. If there exists a relationship between ecdysteroids and the resumption of meiosis, do steroids primarily at the level of oocyte membrane induce a cascade of events similar to those known in amphibian oocyte [273], or only after their entrance into the ooplasm where they accumulate?

IV. OVULATION

The process by which oocytes are expelled from the ovarian environment (ovarian spawning) has been rarely studied in crustaceans and must be distinguished as a separate process from oviposition that is the release of oocytes or eggs in the external milieu.

The only available description of ovulation has been carried out by Fauvel [274] in the prawn *Macrobrachium rosenbergii*. In this species, it occurs after ecdysis when the follicle epithelium retracts at the periphery of the ovary, i.e., when

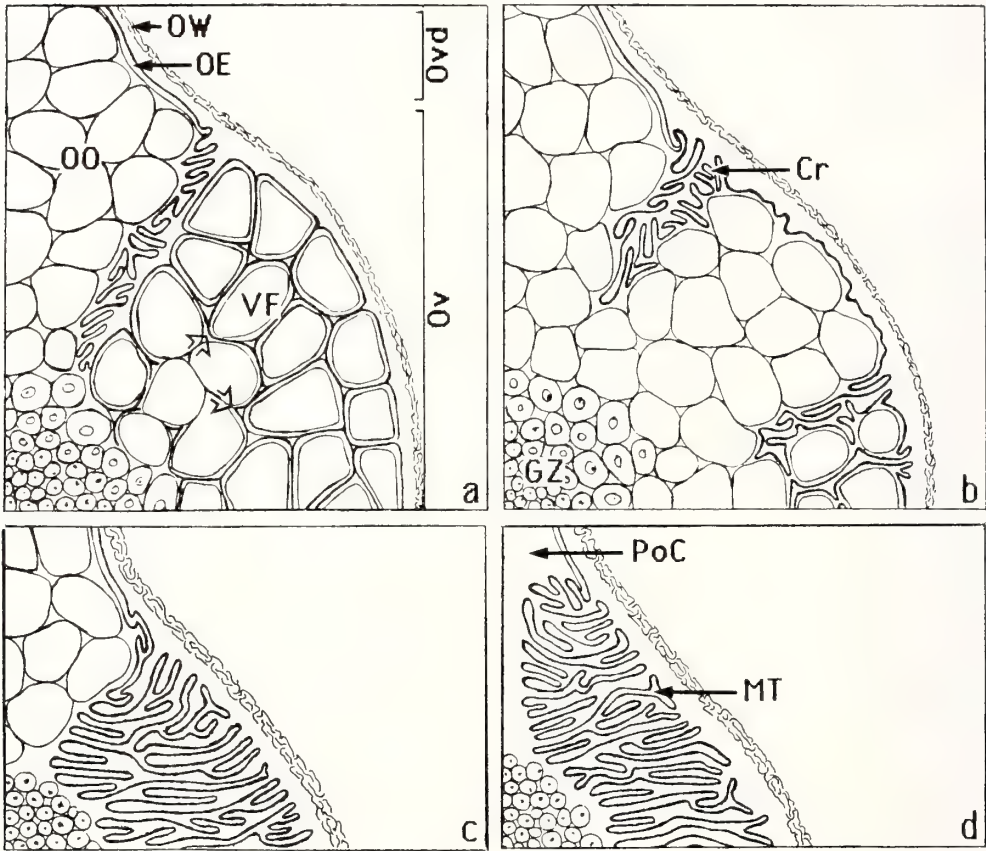


FIG. 9. Phases of ovulation in the prawn, *Macrobrachium rosenbergii* (adapted from [274]).

a. At the beginning of ovulation the follicle epithelium retracts from the vitellogenic oocytes (arrow) located near the oviduct (Ovd).

b. Course of ovulation. Retracted mesodermal tissue forms crests (Cr) between the ovulated oocytes (OO) at the periphery of the ovary (Ov).

c. and d. End of ovulation. The follicle tissue occupies the empty space left by the spawned oocytes.

MT: mesodermal (follicle) tissue; OE: oviducal epithelium; OW: ovarian wall; PoC: perioviducal cavity; VF: vitellogenic follicle; GZ: germinative zone.

the follicle envelope separates from the oocyte (Fig. 9). The retraction begins in an ovarian zone close to the oviduct. Then, crests of retracted mesodermal tissue are formed between the ovulated oocytes. At last, the follicle tissue occupies the empty space left by the spawned oocytes. This tissue, which always develops in continuity with the epithelium of the oviduct and remains in the peripheral region of the gonad, is used again for a new folliculogenesis. Although evidence of a direct hormonal intervention in ovulation has not yet been reported, we must mention that Matsu-moto [275] described an increased neurosecretory cell activity associated with ovulation in the crabs *Potamon*, *Sesarma*, *Neptunus* and *Chionocetes*. It is not sure that ovulation is used by the author with the above meaning.

V. OOCYTE ACTIVATION

Oocyte activation allows the completion of meiosis. It is characterized by the release of the second meiotic block which follows exuviation. It leads to both the extrusion of the polar bodies and the elaboration of the fertilization membrane. At last, the female pronucleus is formed, ready to fuse with the male pronucleus to make a zygote.

Among the sequence of morphological events that characterize fertilization and lead to the spermatozoon-oocyte association, we shall limit our interest to two aspects: 1) the fertilization potential, 2) the cortical reaction, i.e., the response of the oocyte plasma membrane to the spermatozoon penetration. Therefore, we do not describe the initial events of the gamete contacts and particularly the acrosome reaction that fits better in a review on male reproduction. Indeed, a number of well-documented papers dealing with this topic concern the decapods which show the particularity to have non-motile spermatozoa (cf. e.g., [276-281]).

A. Meiosis reinitiation of metaphase I - arrested oocytes

It is now well-known that oocytes of amphipods and several decapods are at the first meiotic metaphase at the time of spawning and meiosis resumes soon thereafter [266-269, 281-289].

Anaphase stage takes place in the spawned eggs. For a long time it has been uncertain whether spawning or fertilization triggers meiosis to complete. In order to elucidate this question, different experiments were undertaken on *Palaemon serratus*. It thus appears that the release of the second meiotic block can be obtained *in vitro*, in presence of an excess of extracellular calcium (10 to 30 mM), or KCl (60 mM), or ionophore A 23187 (5 μ M) [269]. As for the resumption of the first meiotic block, the stimulation by A 23187 requires the presence of Ca^{2+} . In addition, experimental fertilization performed *in vitro* indicates that in *P. serratus*, fertilization is responsible for the second meiotic resumption [269, 270]. However, other works carried out on the same prawn have shown that meiosis resumes when the egg comes into contact with seawater, independently of fertilization [288]. Investigations concerning a possible ionic control of activation have led to the conclusion that the presence of external Mg^{2+} , but not the external Ca^{2+} , is required for resumption of metaphase I in *P. serratus* oocytes. It is the change from the low Mg^{2+} environment of the ovary (10 mM) to the high Mg^{2+} of seawater (≥ 15 mM) that stimulates meiosis to resume. Therefore, activation occurs at spawning and does not require fertilization [289]. No indication yet concerns a possible role of extracellular Mg^{2+} for the spermatozoon-oocyte fusion.

An electrophysiological study completes the above results. It states that an increased oocyte membrane permeability to K^+ occurs at spawning in *P. serratus*. It is not dependent on fertilization but depends on the increase in external Mg^{2+} concentration at spawning. In other words, at spawning, the hyperpolarization of the oocyte membrane to K^+ only occurs in presence of a sufficient external Mg^{2+} concentration [289].

B. Fertilization potential

In contrast to various animal groups in which the electrical characteristics of oocytes at different steps of their development, including fertilization, have been described (cf. reviews [290, 291]), the electrical response to fertilization was evidenced quite recently in malacostracans. The investigations concern the crabs *Carcinus maenas* and *Maia*

squinado, and the lobster *Homarus gammarus* [287, 290, 291]. They show that the fertilization potential consists of a sustained hyperpolarization of the egg membrane (from -32 to -62 mV in the crabs). In these decapods, *in vitro* insemination revealed a sperm-triggered increase in the ionic permeability of the egg membrane which becomes selective for K^+ , whereas before insemination it was predominantly selective for Cl^- . This instantaneous shift that constitutes the fertilization potential seems to be promoted by a rise in cytoplasmic-free Ca^{2+} that might mediate the hyperpolarization. It occurs concurrently with the second meiotic reinitiation in the metaphase I-arrested oocytes. It must be pointed out that under natural conditions, the early events in crab fertilization take place internally in the female genital duct and sometimes in the lumen of the ovary [128, 280, 282, 292, 293], whereas the lobster oocytes are fertilized in the external environment [294]. It thus appears that the electrical response of the oocyte to fertilization may reflect a general property of reptantian Decapoda. As already pointed out (cf. Section V, A) in the prawn *Palaemon serratus* in which fertilization is external (the extruded oocytes pass over the spermatophore previously deposited by the male at mating), a similar increase in K^+ conductance of the oocyte membrane takes place at spawning. This increase is not dependent on fertilization, but depends on an increase in external Mg^{2+} concentration at spawning [289]. Until now, the egg's electrical response to fertilization remains to be explored in *Palaemon*.

C. Cortical reaction

The cortical reaction can be defined as one of the anatomical responses (besides the formation of the fertilization cone and the elaboration of the first polar body) of the oocyte developing an hyperpolarization response after insemination. However, this phenomenon may be also initiated after exposure to sea water.

The morphological events that occur in the cortex of eggs, i.e., the exocytosis of cortical granules into the perivitelline space and the transformation of the plasma membrane were investigated by means of scanning and transmis-

sion electron microscopy in the penaeid shrimps *Penaeus aztecus* and *P. setiferus*, and the shore crab *Carcinus maenas* [295–297]. A brief description of the cortical granules has been also reported in the amphipod *Orchestia gammarella* [4, 91]. We shall examine the cortical reaction process respectively in these three models, although it must be known that the elaboration of the fertilization envelope was described in detail in cirriped eggs [298].

During the cortical reaction, early fertilized *C. maenas* eggs maintained under *in vitro* conditions appear to release successively: 1) a fine granular material that accumulates in about 15 min on the inner face of the vitelline envelope [296] and, 2) a massive amount of ring-shaped elements which coalesce to give rise to a new thick coating underlying the vitelline envelope and represents most of the fertilization envelope. This phenomenon lasts about 7–8 hr. The ring-shaped elements come from egg cortical vesicles. It was established by Goudeau [297] that these elements and their enclosing vesicles originate in the endoplasmic reticulum from which they are released by direct endocytosis. The author considers that the ring-shaped elements are precursors common to the cortical exudate and to the endogenous yolk (cf. Section II, A).

The cortical reaction in the eggs of penaeids is unique with respect to: 1) the size of the cortical specializations (rods that are around $40 \mu\text{m}$ length for an egg diameter of about $270 \mu\text{m}$), 2) the rapid expulsion and dissipation of these elements in response to sea water, 3) the decrease in the egg volume after the reaction. The rods are always located perpendicular to the oolemma and composed of numerous tightly packed fibrillar structures. Each cortical rod lies within a partially membrane bound crypt and is separated from the external environment by a thin coat that completely surrounds the egg. As the rods are expelled in the sea water, a corona forms around the oocyte and then quickly dissipates. Simultaneously an extensive membrane vesiculation associated with cortical rod crypts become apparent around the entire egg surface and later forms a homogenous jelly. Mg^{2+} ions and a protease dependence of this jelly release have been demonstrated in *Penaeus*

and in another penaeid, *Sicyonia* [279, 281, 299].

In *O. gammarella*, cortical granules have been observed towards the end of vitellogenesis when the oocytes are no longer attached to the follicle tissue due to the retraction of the macro- and microvilli. At this period, the vitelline envelope becomes thick. The cortical granules are oval-shaped and measure 0.2–0.3 μm of mean diameter. They become visible when the microcanals and pinocytotic vesicles disappear. They display lamellae alternatively lucent and electron dense and are bound by an outer membrane. Glycoproteins have been detected. After fertilization, the cortical reaction consists of two steps. The first shows a fusion of the cortical granule membrane with the egg plasmic membrane, leading to the release of granule contents into the perivitelline space. During the second step, the vitelline envelope is elevated off the surface of the oocyte and acquires on its inner face an opacity that rapidly extends to the outer face. This opacity is concomitant with important modifications of the vitelline envelope that becomes the fertilization envelope. The origin of the cortical granules and the duration of the cortical reaction remain to be studied in this peracarid.

VI. OVIPOSITION

Generally, oviposition takes place when the environmental conditions are favorable for embryonic development. Thus, according to the geographical distribution of the species, oviposition is spread over a season or restricted to some months (cf. for review [235, 300]). In peracarids and some natantians, this phenomenon is usually preceded by a molt, whereas it is confined to intermolt in many brachyurans.

A few results concern the existence of a control of oviposition by an eyestalk factor. They have been obtained from diverse eyestalk-ablated decapods:

—In juvenile *Carcinus maenas* the operation leads to a precocious vitellogenesis and spawning may follow but, since the puberal form of the external sex characteristics is not completed, the eggs do not remain attached to the pleopods [301]. According to the author, a factor linked to the

presence of eyestalks would be involved in the development of the female external sex characteristics.

—Postmolt crabs, *Menippe mercenaria*, spawn precociously without undergoing accelerated ovarian development [130]. This may be an argument in favor of the fact that spawning and ovarian development would be controlled by different eyestalk hormones.

—However, in juvenile prawns *Penaeus japonicus*, oviposition never follows the accelerated vitellogenesis because the oocytes degenerate (Laubier and Bizot-Espiard, personal communication). Similarly, in the crabs *Rhithropanopeus harrisi* and *Paratelphusa hydrodromous* eyestalks would be necessary to the process of oviposition at time of the reproductive period [302, 303]. Moreover, the oviposition-inducing hormone would be released several days before spawning.

Environmental factors such as water temperature and photoperiod, probably channeled through the neuroendocrine system, seem also to affect oviposition, as has been shown in the crayfish *Orconectes virilis* [248, 304] and the crab *Pachygrapsus marmoratus* [285]. Synchronization of oviposition with specific tidal phases has been also reported in the stomatopods *Gonodactylus zaca* and *G. falcatus*. [305]. Spawning postures have been described for the spider crab *Chionocetes opilio* and the spiny lobster *Panulirus homarus* [306, 307].

In contrast to insects in which oviposition is a fully-studied event beginning shortly after mating (cf. review [308]), more thorough investigation is needed in crustaceans because this process occurs either after or before mating, depending on the considered species (cf. Section V, B).

VII. SEX CHARACTERISTICS ASSOCIATED TO SPERM STORAGE, MATING AND EGG INCUBATION

Among the female characteristics related to sperm storage, mating and egg incubation, one can distinguish specialized regions of the genital duct of species in which fertilization occurs internally and structural modifications of some body segments, as well as of different appendages.

A. Genital duct

The most original feature of the genital duct of some malacostracans is the spermatheca (seminal receptacle), a specialized area that receives the spermatophores in which spermatozoa are stored. The presence of spermatheca is essentially known in brachyurans. Study of the genital apparatus morphogenesis carried out in the crab *Rhithropanopeus harrisii* [11] reveals that, beginning at the fourth postlarval stage, one can determine in the female genital duct three distinct regions from the gonad to the sexual orifice, or vulva: an oviduct, a spermatheca and, distally, a vagina. This is in agreement with Hartnoll's description [309]. The oviducts shorten when the spermatheca develop. In puberal crabs, the cuticle lines the walls of the spermatheca. A scanning electron microscopy examination of the luminal wall of the genital duct of *Carcinus maenas* reveals that, at the level of the spermatheca, the epithelium and the cuticular covering form numerous parallel folds and differentiate two lateral pouches filled with stored spermatozoa [293]. Such an anatomical pattern explains sperm retention after mating for several successive reproductive periods separated by molts [310]. In addition, Anilkumar and Adiyodi [311] reported a cyclic synthetic activity of the spermatheca epithelial cells of the crab *Paratelphusa hydrodromous* in relation to the reproductive cycle.

The oviducal epithelium of the shore crab differentiates during the reproductive pre-molt period two distinct secretory zones that are supposed to be involved in the release of a sexual pheromone attracting the male for copulation. Another interpretation of Anghelou-Spiliotis and Goudeau [293] is that the secretions could have also a lytic function on the spermatophore walls. At last, when the oocyte is ready to be spawned, these substances could be involved in the modification of the chemical composition of the vitelline envelope.

B. External sex characteristics

The external sex characteristics only present in females and involved in specific functions are either permanent or temporary. The permanent

characteristics generally develop in the juvenile females. They are: 1) the shape of the last thoracic sternite which bears an external seminal receptaculum in caridean shrimps or a thelycum in penaeids, 2) the oostegites in some peracarids. The temporary characteristics include: 1) the sexual setae used for pairing, 2) the oostegites in some isopods, 3) the ovigerous setae (oosetae) of amphipods and decapods, 4) the brood chamber of Caridae. These last three characteristics are associated with the incubation of embryos.

1. Differentiation

As an example of permanent female characteristics we have chosen to describe the development of the oostegites that has been well-studied in the amphipod *O. gammarella* [123]. Oostegites appear as small outgrowths on the internal face of the coxae of the second gnathopod and pereopods 3, 4, and 5. At that time, the ovaries contain follicles with previtellogenic oocytes. The oostegites develop further at each molt and form the brood pouch or marsupium in the puberal female. During development of the oostegites in the young females, trichogenic matrices are set up. They form short setae (0.02 mm in length). Almost all amphipods possess four pairs of oostegites; however, this number can vary, as in Caprellidea, where only two pairs of oostegites are born by segments 3 and 4 [312]. In *O. gammarella*, during the reproductive season, a vitellogenesis occurs during each molt cycle, and spawning after each ecdysis. During stage D of the molt cycle, the trichogenic matrices form long setae (0.8 mm in length) which appear at ecdysis. These setae border the oostegites and ensure a good closing of the brood chamber. They are temporary sex characteristics associated with the incubation of embryos. They are replaced by short setae during the intermolt cycles without vitellogenesis [123].

Females of isopods also possess oostegites. These sexual appendages are permanent characteristics in *Ligia oceanica*, *Helleria brevicornis* and the aquatic species *Asellus aquaticus*, *Sphaeroma serratum* and *Idotea balthica* [125, 152, 313–315]. They acquire their functional form only at molts followed by egg laying and again take their non-functional form at the period of genital rest.

Their functional form can be considered as a temporary characteristic related to egg incubation. However this is not the case in the aquatic isopod, *Idotea balthica*, in which the functional form persists throughout the life span of the female. In Oniscidea, except Ligiidae and Tylidae, the presence of oostegites constitutes a temporary characteristic which only appears at time of the molts followed by egg laying and disappears at time of genital rest. In *I. balthica*, another temporary characteristic concerns the sexual setae born on the internal surface of the second pereopods which disappear at the molt preceding the first egg laying [125, 316].

The morphological modifications leading to the formation of the brood chamber in Caridea have been particularly studied in some Palaemonidae [317], *Atyaephyra desmaresti* [318] and *Macrobrachium rosenbergii* [23]. However, no correlation with the developing ovaries has been noted. The brood chamber is not permanent in some Palaemonidae. It disappears during genital rest. Indeed, coxopodites and sternites take again the juvenile form. No study concerns the trichogenic matrices. The brood chamber is formed by broadening of the sternites and lengthening of the coxopodites of the first three somites of the pleon. Basipodites enlarge and display a groove-like shape, with the concavity turned to the rear. An effective closing of the brood chamber is ensured by long plumose setae arranged in two rows on each basipodite. The eggs are attached to the ovigerous setae (oostegae) which are located on the internal edge of the basipodites. The newly laid eggs are guided to the seminal receptaculum by means of long setae both on the coxa of the pereopods 3, 4 and 5, and around the gonopores.

In female crabs, four pairs of unsegmented and hairless biramous pleopods develop from the third crab stage, on the second to the fifth abdominal segments. Segmentation of the endopodites, and exopodites generally precedes by one stage the appearance of tufts of hairs on the endopodites and of a setiferous fringe on the endopodites [11, 319]. In the crab *Pachygrapsus marmoratus*, as in caridean shrimps, oostegae develop on the pleopods and along the edge of the abdominal sternites at the molts that are followed by egg laying; the

oostegae disappear when the ovary is at rest [320]. These temporary characteristics appear for the first time during the molt preceding the first egg laying. In some species, such as *Carcinus maenas*, the abdomen acquires the female form (enlarging, curving inwards, and hairs on pleopods) at the puberty molt that occurs one or several molts before the first egg laying [301, 321]. The external characteristics acquire their definitive shape only at the final puberty molt in brachyurans that undergo a limited number of molts as the Majidae [322, 323], the Leucosiidae, and the Portunidae of the genus *Callinectes* [324, 325]. In the Majidae *Acanthonyx lunulatus* and *Libinia*, the first egg laying occurs immediately or sometime after the puberty molt [326, 327]. Indeed, in these two species, the first vitellogenesis begins respectively during the course of the last intermolt cycle and after puberty.

The mechanism that allows a newly laid egg to be attached to ovigerous setae has been studied in the crab *Carcinus maenas* [128, 328]. It involves the formation of a funiculus that originates from the two superimposed vitelline envelopes [92, 286].

Examination of the structure of the funiculus and of the morphological features of its binding to maternal egg-carrying setae revealed that the tip of the funiculus is coiled around the setae without adjunction of any additional attachment substance. Four concentric envelopes which are successively secreted by the ectodermal embryonic cells underneath the fertilization envelope have been detected during the embryo development. It is noteworthy that ponasterone A, an ecdysteroid present in high concentration, would be involved in the deposition of the embryonic envelopes [328].

In some species, special secretions of tegumental glands of the ventral abdomen seem to be used for attachment of eggs. For example, Mason [329] indicates that the oviposition posture leads to the formation of a water-filled cavity into which the eggs of the crayfish, *Pacifastacus leniusculus trowbridgii*, pass brushing across the glandular areas. Moreover, it has been noted in another crayfish, *Austropotamobius pallipes*, that the activity of these glands is possibly linked to egg growth [330].

At last, these glands would have also a role in dissolution of the spermatophore wall and transport of spermatozoa [329].

An ultrastructural analysis of the pleopod tegumental gland in the lobster, *Homarus americanus*, was recently carried out [331]. It completes a previous study in the same species by Aiken and Waddy [332]. The pleopods of both male and female lobsters contain rosette type glands. However, they are most abundant in females with well-developed ovaries. Two types of secretion seem to be produced continually. They would be involved in the hardening of the cuticle after molting and also in condensation and hardening of the outer egg coat during egg attachment to the ovigerous setae.

2. Regulation of development

An ovarian control of external female characteristics has been demonstrated in several peracarids. Such a control mechanism has been reported in various reviews [123, 333–336]. In decapods, attempts at surgical removal of the ovaries have not so far been successful and there is only an indirect proof of the existence of ovarian hormone(s) [337].

In *O. gammarella*, the ovaries control the permanent and temporary characteristics. The control of oostegites (permanent characteristic) has been studied by implantation of a young or fully-developed ovary into a male from which AG have been removed. In both circumstances, oostegites appear at the first or second postoperative molt. The follicle cells of previtellogenic oocytes seem to be the source of the ovarian hormone responsible for the formation of oostegites. Since this hormone is secreted throughout the life span of the female, Charniaux-Cotton and Payen [336] proposed to call it "Permanent Ovarian Hormone" (POH). The induction of oostegites by POH is irreversible: it persists in castrated females.

In some isopods, as *Idotea balthica* and *Ligia oceanica*, the oostegites differentiate in young females without the mediation of a hormone. In castrated females, the marsupium develops normally [125, 152, 316]. In addition, a marsupium develops in andrectomized males of *I. balthica* although the testes are not reversed into ovaries.

The experimental results obtained in *O. gammarella* and few isopods (*Armadillidium vulgare*, *Porcellionides pruinosus* and *Porcellio laevis*) [77, 338–340] show that the ovary secretes during vitellogenesis a hormone controlling the formation of the temporary external characteristics. Charniaux-Cotton and Payen [336] have called it "Temporary Ovarian Hormone" (TOH).

In *O. gammarella*, ovariectomy during the reproductive period is followed by replacement of ovigerous setae by juvenile setae [77]. Likewise, when a vitellogenic ovary is implanted into an andrectomized male, the induced oostegites acquire ovigerous setae. The follicle cells of the vitellogenic oocytes seem to be the source of TOH. The formation of ovigerous setae requires also the presence of molting hormone. During genital rest, when 20 OH-ecdysone acts alone, juvenile setae are formed. If the quantity of ovarian hormone does not attain a certain threshold, as after a partial ovariectomy, the elongation of the trichogenic matrices is only partial and, as a result, the length of the setae is intermediate. When molting and ovarian hormones are present, the matrices stretch out extensively and form ovigerous setae.

In *Armadillidium vulgare* and *Porcellio dilatatus*, the oostegites (temporary characteristic) never appear in ovariectomized females [338, 341, 342]. Reimplantation of a small ovarian portion induces the formation of an incomplete marsupium.

In decapods, in the absence of successful ovariectomies and implantations, the control of permanent female characteristics is not known. Temporary external characteristics appear to be controlled by vitellogenic ovaries, as in peracarids. Implantation of portions of early vitellogenic ovary into AG ablated male freshwater prawns *Macrobrachium rosenbergii* [337] results in the induction of female breeding characteristics as ovigerous and ovipositing setae and brood chamber. Indeed, these characteristics develop during vitellogenesis and disappear when the ovaries are resting. These relationships between the morphogenesis of the temporary characteristics and the course of vitellogenesis remain to be precised. However, it is worthy to note that the existence of an ovarian hormone controlling the external sexual character-

istics was suggested in the forties by some authors who studied the effects of parasitic or X-ray castration on the shrimp *Leander (Palaemon) serratus* [343]. Furthermore, at the same time, evidence of a correlation between ovarian and tegumental gland development was noted in the shrimp *Crangon crangon* and in the crayfishes *Cambarus virilis* and *C. rusticus* [304, 344].

VIII. SEX RECOGNITION AND MATING BEHAVIOR

As in nearly all phyla, recognition and attraction of a sexual partner to promote successful mating depends in malacostracans on a broadcast of identifying behaviors. The display patterns are mainly acoustic, visual, olfactory, tactile and chemical signals. Most of them have been reviewed separately or in their whole in some significant papers (cf. [235, 350–353]).

It must be pointed out that the diverse communication systems seem adapted to the various inhabited spatial localization. Thus, after the first experimental demonstration in the female crab *Portunus sanguinolentus* [379], crustacean sex pheromones inducing precopulatory behavior in the male have been detected in several aquatic species. (cf. for review [353]). Their stimulating effects predominate in small forms such as amphipods (cf. [354–356]), as well as in natantian and reptantian decapods which include large forms (shrimps, lobsters, crabs, etc.) (e.g., [357–360]). A synergistic effect between the pheromone released by the female, olfactory and visual stimuli of either or both sexes is also sometimes required for registering a positive response [361]. At last, among terrestrial and semi-terrestrial species, chemical cues emitted by females appear to be less important than visual, tactile and(or) acoustic signals from males [362, 363].

We have limited the scope of this section to recall the conditions that enable females to become attractive and receptive to males. The releasing and the possible producing site(s) of sex pheromones, as well as their nature and their target organs in the male are also briefly examined.

In addition to local climatic conditions that restrict the copulatory period, the female's attrac-

tiveness determining behavioral responses of the males is generally linked to its physiological state, i.e., its molting and ovarian development stages. In some Brachyura (Cancridae and Portunidae), some Astacidea and peracarids, a female is able to mate only when it is soft, shortly after ecdysis [355, 364, 365], while in other Brachyura (Majidae, Xanthidae and Gecarcinidae) mating involves intermolt (hard-shelled) females [364, 366–368]. Detailed informations concerning the ovarian developmental stage of females at the time of mating are lacking. In *Gammarus duebenii*, Hartnoll and Smith [356] mention that "ovarian ripeness" is one prerequisite of the female's attractiveness and that "ovarian condition and molt stage have a synergistic effect". Similar data were reported by Ducruet [355] in two other gammarids. However, unpublished works by Vilotte and Fontaine (cited in [353]) indicate that in *Scyllarus arctus* copulation occurs during previtellogenesis, while in *Carcinus maenas*, a female can remain attractive after exuviation (until A₂), when ovaries are engaged in vitellogenesis. Takayanagi *et al.* [371] identified an ovary-stimulating pheromone that would be released by male organs such as the testis or the vas deferens in the freshwater shrimp, *Paratya compressa*. In some crabs, we have already mentioned that sperm is stored for prolonged periods and can fertilize subsequent spawnings (cf. Section VII, A and for review [235] p. 224).

When a female attracts a male prior to its molt, as in *C. maenas*, presumably because this attraction is initiated pheromonally, the male usually guards her in a precopulatory embrace until she molts and copulation is possible [369]. In *Homarus americanus*, as in the crayfish *Austropotamobius pallipes*, the passive, or cooperative, reaction of the female when encountered by a male is considered as a pre-mating behavior [357, 365]. Likewise, in *Cardisoma armatum*, a semi-terrestrial crab, it is thought that courtship reduces aggressive tendencies in the female [368], but the cues used in sex recognition have not been investigated.

According to Hartnoll and Smith [372], there is no evidence for the production of a male stimulating pheromone in the urine of courted pre-molt female crab, *Cancer pagurus*. However, behavioral studies indicate that sex pheromone emission is

often associated with urine release from the female antennal gland (cf. reviews [350, 353, 359, 360]). The site of pheromone production is still not well known: Kamiguchi [373] described a sternal gland in female, *Palaemon paucidens*, and Bauchau [353] discovered in *C. maenas* an ectodermic gland more developed in females than in males. It opens in the ureter in the vicinity of the nephropore and seems well-suited to a pheromone release into urine. Information on the chemical nature of crustacean sex pheromones is scarce. Bauchau [353] reported that their molecular weight is ranging from 1000 to 10,000 daltons, according to the species. There are inconclusive data concerning ecdysone (or its derivative), serotonin or peptide as sex attractants ([374, 380], for review [353]). Chemoreceptor sensilla (aesthetascs) on the outer flagellum of antennules are involved in the detection of sex pheromones in several decapods ([353, 358, 375], for review [350]). It has been recently suggested that a hormonal modulation of pheromone-triggered courtship display behavior would exist in the blue crab, *Callinectes sapidus* [376].

ACKNOWLEDGMENT

We are grateful to Madeleine Martin and Daniel Soyey for their friendly assistance.

REFERENCES

- 1 Dhainaut, A. and De Leersnyder, M. (1976) Etude cytochimique et ultrastructurale de l'évolution ovocytaire du crabe *Eriocheir sinensis*. I. Ovogenèse naturelle. Arch. Biol., **87**: 261-282.
- 2 Charniaux-Cotton, H. (1978) L'ovogenèse, la vitellogénine et leur contrôle chez le Crustacé Amphipode *Orchestia gammarellus* (Pallas). Comparaison avec d'autres Malacostracés. Arch. Zool. exp. Gén., **119**: 365-397.
- 3 Charniaux-Cotton, H. (1980) Experimental studies of reproduction in Malacostraca Crustaceans. Description of vitellogenesis and of its endocrine control. In "Advances in Invertebrate Reproduction, 2". Ed. by W. H. Clark, Jr. and T. S. Adams, Elsevier, North Holland, pp. 177-186.
- 4 Zerbib, C. (1980) Ultrastructural observation on oogenesis in the Crustacea Amphipoda *Orchestia gammarellus* (Pallas). Tissue and Cell, **12**: 47-62.
- 5 Komm, B. S. and Hinsch, G. W. (1987) Oogenesis in the terrestrial hermit crab *Coenobita clypeatus* (Decapoda, Anomura). II. Vitellogenesis. J. Morphol., **192**: 269-277.
- 6 Adiyodi, R. G. and Subramoniam, T. (1983) Arthropoda-Crustacea. In "Reproductive Biology of Invertebrates. Vol. 1: Oogenesis, Oviposition, and Oosorption". Ed. by K. G. and R. G. Adiyodi, J. Wiley & Sons, Ltd., Chichester, New York, Brisbane, Toronto, Singapore, pp. 443-495.
- 7 Charniaux-Cotton, H. and Payen, G. (1988) Crustacean reproduction. In "Invertebrate Endocrinology, Vol. 2". Ed. by R. G. H. Downer and H. Laufer, Alan R. Liss, Inc., New York, pp. 279-304.
- 8 Meusy, J.-J. (1986) Ultrastructure de la zone germinative et des gonies du testicule et de l'ovaire d'*Orchestia gammarella* P. (Crustacé Amphipode). Ann. Sci. Nat., Zool. Biol. Anim., **10**: 101-116.
- 9 Meusy, J.-J. (1963) La gamétogenèse d'*Orchestia gammarella* Pallas, Crustacé Amphipode. Bull. Soc. Zool. Fr., **88**: 197-220.
- 10 Payen, G. G. (1973) Etude descriptive des principales étapes de la morphogenèse sexuelle chez un Crustacé Décapode à développement condensé, l'Écrevisse *Pontastacus leptodactylus leptodactylus* (Eschscholtz, 1823). Ann. Embryol. Morphog., **6**: 179-206.
- 11 Payen, G. G. (1974) Morphogenèse sexuelle de quelques Brachyours (Cyclométopes) au cours du développement embryonnaire, larvaire et postlarvaire. Bull. Mus. Nat. Zool., **209**: 201-262.
- 12 Laubier, A., Chim, L. and Payen, G. G. (1985) Morphogenèse sexuelle et régulation hormonale de l'activité génitale chez la crevette *Penaeus japonicus* en élevage. IFREMER, Actes de Colloques, n°1: 195-206.
- 13 Soyey, D. (1974) Etude comparée de l'activité prévitellogénétique pendant les saisons de repos génital et d'activité sexuelle chez le Crustacé Amphipode *Orchestia gammarellus* (Pallas). C. R. Acad. Sci., Sér. D, **278**: 1867-1870.
- 14 Rateau, J. G. and Zerbib, C. (1978) Etude ultrastructurale des follicules ovocytaires chez le Crustacé Amphipode *Orchestia gammarellus* (Pallas). C. R. Acad. Sci. Paris, Sér. D, **286**: 65-68.
- 15 Weitzman, M. C. (1966) Oogenesis in the tropical land crab *Gecarcinus lateralis* (Freminville). Z. Zellforsch., **75**: 109-119.
- 16 Charniaux-Cotton, H. and Touris, A. (1973) Contrôle de la prévitellogenèse et de la vitellogenèse chez la crevette hermaphrodite *Lysmata seticaudata* Risso. C. R. Acad. Sci. Paris, Sér. D, **276**: 2717-2720.
- 17 Charniaux-Cotton, H. (1959) Etude comparée du développement post-embryonnaire de l'appareil génital et de la glande androgène chez *Orchestia gammarella* et *Orchestia mediterranea* (Crustacés

- Amphipodes). Autodifférenciation ovarienne. Bull. Soc. Zool. Fr., **84**: 105–115.
- 18 Charniaux-Cotton, H. and Ginsburger-Vogel, T. (1962) Preuve expérimentale de l'autodifférenciation ovarienne chez *Orchestia montagui* Audouin (Crustacé Amphipode). C. R. Acad. Sci. Paris, **254**: 2836–2838.
- 19 Charniaux-Cotton, H. (1963) Démonstration expérimentale de la sécrétion d'hormone femelle par le testicule inversé en ovaire de *Talitrus saltator* (Crustacé Amphipode). Considération sur la génétique et l'endocrinologie sexuelle des Crustacés supérieurs. C. R. Acad. Sci. Paris, **256**: 4088–4091.
- 20 Hort-Legrand, C., Berreur-Bonnenfant, J. and Ginsburger-Vogel, T. (1973) Inversion expérimentale du testicule en ovaire par greffe dans la cavité péricardiale de femelles adultes, chez *Orchestia gammarella* Pallas (Crustacé Amphipode). C. R. Acad. Sci., Sér. D, **276**: 1891–1894.
- 21 Juchault, P. and Legrand, J.-J. (1964) Mise en évidence d'un inducteur sexuel mâle distinct de l'hormone adulte et contribution à l'étude de l'autodifférenciation ovarienne chez l'Oniscoïde *Helleria brevicornis*. C. R. Acad. Sci. Paris, **258**: 2416–2419.
- 22 Charniaux-Cotton, H. (1975) Hermaphroditism and gynandromorphism in malacostracan Crustacea. In "Intersexuality in the Animal Kingdom". Ed. by R. Reinboth, Springer-Verlag, Berlin and New York, pp. 91–105.
- 23 Nagamine, C. and Knight, A. W. (1980) Development, maturation, and function of some sexually dimorphic structures of the Malaysian prawn *Macrobrachium rosenbergii* (de Man) (Decapoda, Palaemonidae). Crustaceana, **392**: 141–152.
- 24 Graf, F. (1958) Développement post-embryonnaire des gonades et des glandes androgènes d'*Orchestia cavimana* (Heller) Crustacé Amphipode. Bull. Soc. Sci. Nancy, **17**: 223–261.
- 25 Ohno, S. (1979) Major Sex-Determining Genes, Springer-Verlag, Berlin and New York.
- 26 Payen, G., Costlow, J. D. and Charniaux-Cotton, H. (1967) Recherches sur le rôle de la neurosécrétion dans la différenciation sexuelle du Crabe *Callinectes sapidus* Rathbun. C. R. Acad. Sci., Sér. D, **264**: 2148–2151.
- 27 Payen, G., Costlow, J. D. and Charniaux-Cotton, H. (1969) Mise en évidence expérimentale de l'indépendance de la réalisation du sexe chez le Crabe *Rhithropanopeus harrisi* (Gould) à l'égard du complexe neurosécréteur organe de Hanström-glande du sinus. C. R. Acad. Sci. Paris, Sér. D, **269**: 1878–1881.
- 28 Touri, A. (1977) Données nouvelles concernant l'endocrinologie sexuelle des Crustacés Décapodes *Natantia* hermaphrodites et gonochoriques. I. Maintien des glandes androgènes et rôle de ces glandes dans le contrôle des gamétogenèses et des caractères sexuels externes mâles. Bull. Soc. Zool. Fr., **102**: 375–400.
- 29 Touri, A. (1977) Données nouvelles concernant l'endocrinologie sexuelle des Crustacés Décapodes *Natantia* hermaphrodites et gonochoriques. II. Maintien des gonies et évolution des gamétogenèses *in vivo* et *in vitro*. C. R. Acad. Sci. Paris, Sér. D, **284**: 2515–2518.
- 30 Touri, A. (1977) Données nouvelles concernant l'endocrinologie sexuelle des Crustacés Décapodes *Natantia* hermaphrodites et gonochoriques. III. Mise en évidence d'un contrôle neurohormonal du maintien de l'appareil génital mâle et des glandes androgènes exercé par le protocérébron médian. C. R. Acad. Sci. Paris, Sér. D, **285**: 539–542.
- 31 Rubiliani, C. and Payen, G. G. (1979) Modalités de la destruction des régions neurosécrétrices des Crabes *Carcinus maenas* (L.) et *C. mediterraneus* Czerniavsky infestés par la sacculine. Gen. Comp. Endocrinol., **38**: 215–228.
- 32 Rubiliani-Durozoi, M., Rubiliani, C. and Payen, G. G. (1980) Déroutement des gamétogenèses chez les Crabes *Carcinus maenas* (L.) et *C. mediterraneus* Czerniavsky parasités par la Sacculine. Int. J. Invertebr. Reprod., **2**: 107–120.
- 33 De Leersnyder, M. and Dhainaut, A. (1977) Action de l'épédonculation sur les premières étapes de l'ovogenèse d'*Eriocheir sinensis* H. Milne-Edwards (Crustacé Décapode Brachyoure). Etude cytologique et autoradiographique. Arch. Zool. Exp. Gen., **118**: 335–348.
- 34 De Leersnyder, M., Dhainaut A. and Porcheron, P. (1981) Influence de l'ablation des organes Y sur l'ovogenèse du crabe *Eriocheir sinensis* dans les conditions naturelles et après épédonculation. Gen. Comp. Endocrinol., **43**: 157–169.
- 35 Kurup, K. N. P. and Adiyodi, R. G. (1981) The programming of somatic growth and reproduction in the crab *Paratelphusa hydrodromous* (Herbst). Int. J. Invertebr. Reprod., **3**: 27–39.
- 36 Eastman-Reks, S. B. and Fingerman, M. (1984) Effects of neuroendocrine tissue and cyclic AMP on ovarian growth *in vivo* and *in vitro* in the fiddler crab, *Uca pugnator*. Comp. Biochem. Physiol., **79A**: 679–684.
- 37 Frenzt, R. (1960) Contribution à l'étude biochimique du milieu intérieur de *Carcinus maenas* Linné. Bull. Soc. Sci. Nancy, Nlle série, **19**: 1–176.
- 38 Descouturelle, G. and Frenzt, R. (1967) Etude par électrophorèse et immunoelectrophorèse des protéines d'extraits totaux et de l'hémolymphe d'*Atyaephyra desmaresti* Millet. Influence de l'ablation des pédoncules oculaires. Bull. Biol. Sci. Nancy, **6**: 259–270.

- 39 Adiyodi, R. G. (1968) Protein metabolism in relation to reproduction and moulting in the crab, *Paratellus hydrodromus* (Herbst): Part I. Electrophoretic studies on the mode of utilization of soluble proteins during vitellogenesis. *Indian J. Exp. Biol.*, **6**: 144–147.
- 40 Besse, G. and Mocquard, J.-P. (1968) Etude par électrophorèse des quantités relatives des protéines de l'hémolymphe d'individus normaux et de femelles castrées chez deux Crustacés Isopodes: *Porcellio dilatatus* Brandt et *Ligia oceanica*. *C. R. Acad. Sci. Paris, Sér. D*, **267**: 2017–2019.
- 41 Meusy, J.-J., Charniaux-Cotton, H. and Croisille, Y. (1969) Etude par électrophorèse chez *Orchestia gammarella* (Pallas) et *Orchestia mediterranea* Costa (Crustacés Amphipodes) des protéines de l'hémolymphe: comparaison entre les mâles, les femelles et les intersexués. *C. R. Acad. Sci. Paris, Sér. D*, **269**: 741–743.
- 42 Kerr, M. S. (1969) The hemolymph proteins of the blue crab, *Callinectes sapidus*. II. A lipoprotein serologically identical to oocyte lipovitellin. *Dev. Biol.*, **20**: 1–17.
- 43 Gibert, J. (1972) Synthèse bibliographique des recherches électrophorétiques sur les protéines des Crustacés. *Ann. Biol.*, **11**: 305–327.
- 44 Ceccaldi, H. J. and Martin, J.-L. (1969) Evolution des protéines de l'hémolymphe chez *Carcinus maenas* L. durant l'ovogenèse. *C. R. Soc. Biol.*, **163**: 2638–2641.
- 45 Abeloos, M. and Fisher, E. (1926) Sur l'origine et les migrations des pigments caroténoïdes chez les Crustacés. *C. R. Soc. Biol.*, **95**: 383–384.
- 46 Kerr, M. S. (1968) Protein synthesis by the hemocytes of *Callinectes sapidus*: a study of in vitro incorporation of ¹⁴C-leucine. *J. Cell Biol.*, **39**: 72a–73a.
- 47 Wolin, E. M., Laufer, H. and Albertini, D. F. (1973) Uptake of the yolk protein, lipovitellin, by developing crustacean oocytes. *Dev. Biol.*, **35**: 160–170.
- 48 Paulus, J. E. and Laufer, H. (1987) Vitellogenocytes in the hepatopancreas of *Carcinus maenas* and *Libinia emarginata* (Decapoda brachyura). *Int. J. Invertebr. Reprod. Dev.*, **11**: 29–44.
- 49 Lui, C. W., Sage, B. A. and O'Connor, J. D. (1974) Biosynthesis of lipovitellin by the crustacean ovary. *J. Exp. Zool.*, **188**: 289–296.
- 50 Lui, C. W. and O'Connor, J. D. (1976) Biosynthesis of lipovitellin by the crustacean ovary. II. Characterization of and in vitro incorporation of amino acids into the purified subunits. *J. Exp. Zool.*, **195**: 41–51.
- 51 Lui, C. W. and O'Connor, J. D. (1977) Biosynthesis of lipovitellin by the crustacean ovary. III. The incorporation of labeled amino acids into the purified lipovitellin of the crab *Pachygrapsus crassipes*. *J. Exp. Zool.*, **199**: 105–108.
- 52 Eastman-Reks, S. B. and Fingerman, M. (1985) *In vitro* synthesis of vitellin by the ovary of the fiddler crab, *Uca pugilator*. *J. Exp. Zool.*, **233**: 111–116.
- 53 Yano, I. and Chinzei, Y. (1987) Ovary is the site of vitellogenin synthesis in kuruma prawn, *Penaeus japonicus*. *Comp. Biochem. Physiol.*, **86B**: 213–218.
- 54 Hinsch, G. W. and Cone, M. V. (1969) Ultrastructural observations of vitellogenesis in the spider crab, *Libinia emarginata* L. *J. Cell Biol.*, **40**: 336–342.
- 55 Beams, H. and Kessel, R. G. (1980) Ultrastructure and vitellogenesis in the oocyte of the Crustacean, *Oniscus asellus*. *J. Submicrosc. Cytol.*, **12**: 17–27.
- 56 Komm, B. S. and Hinsch, G. W. (1985) Oogenesis in the terrestrial hermit crab *Coenobita clypeatus* (Decapoda, Anomura). I. Previtellogenic oocytes. *J. Morphol.*, **183**: 219–224.
- 57 Junéra, H., Zerbib, C., Martin, M. and Meusy, J.-J. (1977) Evidence for control of vitellogenin synthesis by an ovarian hormone in *Orchestia gammarella* (Pallas), Crustacea; Amphipoda. *Gen. Comp. Endocrinol.*, **31**: 457–462.
- 58 Junéra, H. and Croisille, Y. (1980) Recherche du lieu de synthèse de la vitellogénine chez le Crustacé Amphipode *Orchestia gammarella* (Pallas). Mise en évidence d'une activation de la synthèse protéique dans le tissu adipeux sous-épidermique des femelles en vitellogenèse secondaire. *C. R. Acad. Sci. Paris, Sér. D*, **290**: 703–706.
- 59 Croisille, Y. and Junéra, H. (1980) Recherches du lieu de synthèse de la vitellogénine chez le Crustacé Amphipode *Orchestia gammarella* (Pallas). Démonstration, à l'aide d'anticorps spécifiques, de la présence de vitellogénine dans le tissu adipeux sous-épidermique des femelles en vitellogenèse secondaire. *C. R. Acad. Sci. Paris, Sér. D*, **290**: 1487–1490.
- 60 Meusy, J.-J., Junéra, H., Clédon, P. and Martin, M. (1983) La vitellogénine chez un Crustacé Décapode Natantia, *Palaemon serratus* Pennant. Mise en évidence, comparaison immunologique avec les vitellines, site de synthèse et rôle des pédoncules oculaires. *Reprod. Nutr. Dév.*, **23**: 625–640.
- 61 Vazquez-Boucard, C. (1985) Identification préliminaire du tissu adipeux chez le Crustacé Décapode *Penaeus japonicus* Bate, à l'aide d'anticorps antilipovitelline. *C. R. Acad. Sci. Paris, Sér. III*, **300**: 95–97.
- 62 Tom, M., Goren, M. and Ovadia, M. (1987) Localization of the vitellin and its possible precursors in various organs of *Parapenaeus longirostris* (Crustacea, Decapoda, Penaeidae). *Int. J. Invertebr.*

- Reprod. Dev., **12**: 1–12.
- 63 Meusy, J.-J., Zerbib, C., Dacheux, F. and Dubois, M. P. (1983) Subcellular localization of vitellogenin in Crustacean adipocytes by the unlabelled antibody enzyme method. *Tissue and Cell*, **15**: 301–310.
- 64 Zerbib, C. and Meusy, J.-J. (1983) Electron microscopic observations of the subepidermal fat body changes following ovariectomy in *Orchestia gammarellus* (Pallas) (Crustacea: Amphipoda). *Int. J. Invertebr. Reprod.*, **6**: 123–127.
- 65 Wyss-Huber, M. and Lüscher, M. (1975) Protein synthesis in "fat body" and ovary of the physogastric queen of *Macrotermes subhyalinus*. *J. Insect Physiol.*, **21**: 1697–1704.
- 66 Gutzeit, H. O. (1980) Yolk synthesis in ovarian follicles of *Drosophila*. *Wihelm Roux's Arch.*, **189**: 221–224.
- 67 Brennan, M. D., Weiner, A. J., Goralski, T. J. and Mahowald, A. P. (1982) The follicle cells are a major site of vitellogenin synthesis in *Drosophila melanogaster*. *Dev. Biol.*, **89**: 225–236.
- 68 Charniaux-Cotton, H. (1974) Données nouvelles concernant la vitellogénèse des Crustacés Malacostracés obtenues chez l'Amphipode *Orchestia gammarellus* (Pallas): folliculogénèse à partir d'un tissu permanent; action du busulfan; action inhibitrice de l'hormone juvénile. *C. R. Acad. Sci. Paris, Sér. D*, **279**: 563–566.
- 69 Fauvel, C. (1981) Etude de l'ovaire de la Crevette d'eau douce *Macrobrachium rosenbergii* (de Man) au cours du cycle de reproduction. Première description de la folliculogénèse secondaire chez un Crustacé Décapode. *C. R. Acad. Sci. Paris, Sér. III*, **292**: 547–552.
- 70 Arcier, J.-M. and Bréhelin, M. (1982) Etude histologique et ultrastructurale du tissu folliculaire au cours des cycles de développement ovarien chez *Palaemon adspersus* (Rathke, 1837). *Arch. Biol.*, **93**: 79–97.
- 71 Charniaux-Cotton, H. (1985) Vitellogenesis and its control in Malacostracan Crustacea. *Am. Zool.*, **25**: 197–206.
- 72 Souty, C. (1980) Electron microscopic study of follicle cell development during vitellogenesis in the marine crustacean Isopoda, *Idotea balthica basteri*. *Reprod. Nutr. Dév.*, **20**: 653–663.
- 73 Jugan, P. and Zerbib, C. (1984) Follicle cell tubular system in the prawn *Macrobrachium rosenbergii*. A route for exchanges between haemolymph and vitellogenic oocytes. *Biol. Cell*, **51**: 395–398.
- 74 Meusy, J.-J., Jugan, P. and Zerbib, C. (1985) Les cellules folliculaires secondaires de la crevette *Macrobrachium rosenbergii* (Décapode Palaemonidé): mise en évidence d'un réseau tubulaire impliqué dans les échanges entre l'hémolymphe et l'ovocyte. *IFREMER, Actes de Colloques*, n°1: 207–216.
- 75 Jugan, P. (1985) Régulation de la croissance ovocytaire chez le Crustacé *Macrobrachium rosenbergii* (de Man). Démonstration d'une endocytose par récepteurs et approche du mode d'action de la neurohormone inhibitrice de la vitellogénèse. Thèse Doctorat, Univ. P. et M. Curie (Paris 6).
- 76 Blades-Eckelbarger, P. I. and Youngbluth, M. J. (1984) The ultrastructure of oogenesis and yolk formation in *Labidocera aestiva* (Copepoda: Calanoida). *J. Morphol.*, **179**: 33–46.
- 77 Charniaux-Cotton, H. (1953) Etude du déterminisme des caractères sexuels secondaires par castration chirurgicale et implantation d'ovaire chez un Crustacé Amphipode (*Orchestia gammarella*). *C. R. Acad. Sci. Paris*, **236**: 141–143.
- 78 Charniaux-Cotton, H. (1958) Contrôle hormonal de la différenciation du sexe et de la reproduction chez les Crustacés supérieurs. *Bull. Soc. Zool. Fr.*, **83**: 314–336.
- 79 Beams, H. W. and Kessel, R. G. (1963) Electron microscope studies on developing crayfish oocytes with special references to the origin of yolk. *J. Cell. Biol.*, **18**: 621–650.
- 80 Zerbib, C. (1973) Contribution à l'étude ultrastructurale de l'ovocyte chez le crustacé Amphipode *Orchestia gammarellus* Pallas. *C. R. Acad. Sci. Paris, Sér. D*, **277**: 1209–1212.
- 81 Zerbib, C. (1979) Etude ultrastructurale de l'ovocyte en vitellogénèse chez les Ecrevisses *Astacus astacus* et *A. leptodactylus*. *Int. J. Invertebr. Reprod.*, **1**: 289–295.
- 82 Zerbib, C. (1977) Endocytose ovocytaire chez le Crustacé Amphipode *Orchestia gammarellus* (Pallas). Démonstration par la peroxydase. *C. R. Acad. Sci. Paris, Sér. D*, **284**: 757–760.
- 83 Schade, M. L. and Shivers, R. R. (1980) Structural modification of the surface and cytoplasm of oocytes during vitellogenesis in the lobster, *Homarus americanus*. An electron microscope-protein tracer study. *J. Morphol.*, **163**: 13–26.
- 84 Jugan, P. and Soyeux, D. (1985) Démonstration in vitro de l'inhibition de l'endocytose ovocytaire par un extrait de glandes du sinus chez la Crevette *Macrobrachium rosenbergii*. *C. R. Acad. Paris, Sér. III*, **300**: 705–709.
- 85 Anilkumar, G. (1980) Reproductive physiology of female crustaceans. Ph. D. Thesis, Calicut University.
- 86 Kessel, R. G. (1986) Mechanism of protein yolk synthesis and deposition in Crustacean oocytes. *Z. Zellforsch. mikrosk. Anat.*, **89**: 17–38.
- 87 Ganion, L. R. and Kessel, R. G. (1972) Intracellular synthesis, transport and packaging of proteinaceous yolk in oocytes of *Orconectes immunis*.

- J. Cell Biol., **52**: 420-437.
- 88 Eurenien, L. (1973) An electron microscope study on the developing oocytes of the crab *Cancer pagurus* L. with special reference to yolk formation (Crustacea). Z. Morphol. Tiere, **75**: 243-254.
- 89 Adiyodi, R. G. (1969) Protein metabolism in relation to reproduction on moulting in the crab, *Paratelphusa hydrodromous*. Part III. RNA activity and protein yolk biosynthesis during normal vitellogenesis and under conditions of acute inanition. Indian J. Exp. Biol., **7**: 13-16.
- 90 Hinsch, G. W. (1970) Possible role of intranuclear membranes in nuclear-cytoplasmic exchange in spider crab oocytes. J. Cell Biol., **47**: 531-535.
- 91 Zerbib, C. (1975) Premières observations de granules corticaux dans l'ovocyte d'un Crustacé, l'amphipode *Orchestia gammarellus* (Pallas). C. R. Acad. Sci. Paris, Sér. D, **281**: 1345-1347.
- 92 Goudeau, M. and Lachaise, F. (1980) "Endogenous yolk" as the precursor of a possible fertilization envelope in a crab (*Carcinus maenas*). Tissue and Cell, **12**: 503-512.
- 93 Meusy, J.-J. (1980) Vitellogenin, the extraovarian precursor of the protein yolk in Crustacea: a review. Reprod. Nutr. Dév., **20**: 1-21.
- 94 Ceccaldi, H. J. (1967) Transport des pigments caroténoïdes dans l'hémolymphe de *Carcinus maenas* Linné. C. R. Acad. Sci. Paris, Sér. D, **161**: 1105-1110.
- 95 Ghidalia, W. (1985) Structural and biological aspects of pigments. In "The Biology of Crustacea, Vol. 9". Ed. by D. E. Bliss and L. H. Mantel, Academic Press, New York, pp. 301-394.
- 96 Zagalsky, P. F. (1985) A study of the astaxanthin-lipovitellin, ovoverdin, isolated from the ovaries of the lobster *Homarus gammarus* (L.). Comp. Biochem. Physiol., **80B**, 589-597.
- 97 Picaud, J.-L. (1978) Contribution à l'étude des propriétés physico-chimiques des protéines spécifiques femelles de *Porcellio dilatatus* Brandt (Crustacé Isopode, Oniscoïde). C. R. Soc. Biol., **172**: 299-303.
- 98 Wallace, R. A., Walker, S. L. and Hauschka, P. V. (1967) Crustacean lipovitellin. Isolation and characterization of the major high-density lipoprotein from the eggs of Decapods. Biochemistry, **6**: 1582-1590.
- 99 Fyffe, W. E. and O'Connor, J. D. (1974) Characterization and quantification of a crustacean lipovitellin. Comp. Biochem. Physiol., **47B**: 851-867.
- 100 Ceccaldi, H. J., Cheesman, D. F. and Zagalsky, P. F. (1966) Quelques propriétés et caractéristiques de l'ovoverdine. C. R. Soc. Biol., **160**: 587-590.
- 101 Meusy, J.-J. (1972) La gamétogénèse et la fraction protéique de l'hémolymphe spécifique du sexe femelle chez quelques Crustacés supérieurs: étude descriptive et rôle des glandes androgènes. Thèse Doctorat d'Etat, Univ. Paris 6, AO CNRS n° 6583, pp. 1-165.
- 102 Croisille, Y., Junéra, H., Meusy, J.-J. and Charniaux-Cotton, H. (1974) The female-specific protein (vitellogenic protein) in Crustacea with particular reference to *Orchestia gammarella* (Amphipoda). Am. Zool., **14**: 1219-1228.
- 103 Arcier, J.-M. and Tournamille, J. (1974) Recherches immunochimiques sur les protéines de vitellogenèse chez *Palaemon adspersus* (Rathke, 1837) (Crustacés Décapodes Natantia). C. R. Acad. Sci. Paris, Sér. D, **278**: 495-498.
- 104 Picaud, J.-L. (1978) Parentés antigéniques des protéines spécifiques femelles chez quelques Crustacés Isopodes. C. R. Soc. Biol., **172**: 320-324.
- 105 Byard, E. H. and Aiken, D. E. (1984) The relationship between molting, reproduction, and a female-specific protein in the lobster, *Homarus americanus*. Comp. Biochem. Physiol., **77A**: 749-757.
- 106 Tom, M., Goren, M. and Ovidia, M. (1987) Purification and partial characterization of vitellin from the ovaries of *Parapenaeus longirostris* (Crustacea, Decapoda, Penaeidae). Comp. Biochem. Physiol., **87B**: 17-23.
- 107 Vazquez-Boucard, C., Ceccaldi, H. J., Benyamin, Y. and Roustan, C. (1986) Identification, purification, et caractérisation de la lipovitelline chez un crustacé Décapode Natantia *Penaeus japonicus* (Bate). J. Exp. Biol. Ecol., **97**: 37-50.
- 108 Ceccaldi, H. J., Daumas, R. and Zagalsky, P. F. (1967) Comparaison des compositions en acides aminés des caroténo-lipoprotéines provenant d'ovaires de trois crustacés et d'un mollusque marin. C. R. Soc. Biol., **161**: 1111-1113.
- 109 Zagalsky, P. F. (1972) Comparative studies on the amino-acid compositions of some carotenoid-containing lipoglycoproteins and a glycoprotein from the eggs and ovaries of certain aquatic invertebrates. Comp. Biochem. Physiol., **41B**: 385-395.
- 110 Arcier, J.-M. and Bonami, J. R. (1979) Contribution à l'étude des lipovitellines chez *Palaemon adspersus* (Rathke, 1837). Arch. Int. Physiol. Biochim., **87**: 471-484.
- 111 Derelle, E., Grosclaude, J., Meusy, J.-J. and Martin, M. (1986) ELISA titration of vitellogenin in the freshwater prawn, *Macrobrachium rosenbergii*, with monoclonal antibody. Comp. Biochem. Physiol., **35B**: 1-4.
- 112 Meusy, J.-J. and Junéra, H. (1979) Analyse préliminaire de la composition en sous-unités polypeptidiques de la vitellogénine et des lipovitellines du Crustacé Amphipode *Orchestia gammarella* (Pallas) C. R. Acad. Sci. Paris, Sér. D, **288**: 1415-1418.

- 113 Junéra, H. and Meusy, J.-J. (1982) Vitellogenin and lipovitellins in *Orchestia gammarellus* (Pallas) (Crustacea, Amphipoda); labelling of subunits after *in vivo* administration of ^3H -leucine. *Experientia*, **38**: 252–253.
- 114 Marzari, R., Ferrero, E., Mosco, A. and Savoini, A. (1986) Immunological characterization of the vitellogenic proteins in *Squilla mantis* hemolymph (Crustacea, Stomatopoda). *Exp. Biol.*, **45**: 75–80.
- 115 Meusy, J.-J., Junéra, H. and Croisille, Y. (1974) Données sur la synthèse de la fraction protéique femelle chez *Orchestia gammarella* (Crustacé Amphipode), au cours de l'intermue et chez les femelles en repos sexuel. *C. R. Acad. Sci. Paris, Sér. D*, **279**: 587–590.
- 116 Blanchet-Tournier, M.-F., Meusy, J.-J. and Junéra, H. (1980) Mue et vitellogénèse chez le Crustacé Amphipode *Orchestia gammarella* (Pallas). Etude des effets de la destruction de la région antéro-médiane du protocérébrum sur la synthèse de la vitellogénine. *C. R. Acad. Sci. Paris, Sér. D*, **291**: 829–832.
- 117 Souty, C. and Picaud, J.-L. (1981) Vitellogenin synthesis in the fat body of the marine crustacean Isopoda, *Idotea balthica basteri*, during vitellogenesis. *Reprod. Nutr. Dév.*, **21**: 95–101.
- 118 Gohar, M., Souty, C. and Picaud, J.-L. (1982) Variations nyctémérales du taux des protéines hémolympatiques et de la libération de vitellogénine chez *Porcellio dilatatus* Brandt (Crustacé, Isopode). *Bull. Soc. Ecophysiol.*, **7**: 79–85.
- 119 Souty, C. (1983) Démonstration d'une alternance des pics de synthèse des fractions, respectivement endogène et exogène, du vitellus protéique chez l'Oniscoïde *Porcellio dilatatus* Brandt. *C. R. Acad. Sci. Paris, Sér. III*, **296**: 221–223.
- 120 Nakagawa, H. and Ceccaldi, H. J. (1985) Circadian variations of haemolymph lipoprotein of *Palaemon serratus*. *Biochem. Syst. Ecol.*, **13**: 345–348.
- 121 Vazquez-Boucard, C. G., Moureau, C. E. and Ceccaldi, H. J. (1985) Etude préliminaire des variations circadiennes des protéines de l'hémolymphe de *Penaeus japonicus* Bate. *J. Exp. Mar. Biol. Ecol.*, **85**: 123–133.
- 122 Aiken, D. E. and Waddy, S. L. (1976) Reproductive biology. In "The Biology and Management of Lobsters", Vol. 2. Ed. by J. S. Cobb and B. F. Phillips, Academic Press, New York, pp. 215–276.
- 123 Charniaux-Cotton, H. (1975) Croissance, régénération et déterminisme endocrinien des caractères sexuels d'*Orchestia gammarella* (Pallas), Crustacé Amphipode. *Ann. Sci. Nat. Zool. Biol. Anim.*, **19**: 411–559.
- 124 Legrand, J.-J. (1958) Induction de la maturité ovarienne et de la mue parturiale par la fécondation chez l'Oniscoïde *Porcellio dilatatus*. *C. R. Acad. Sci. Paris, Sér. D*, **247**: 754–757.
- 125 Reidenbach, J.-M. (1971) Les mécanismes endocriniens dans le contrôle de la différenciation du sexe, la physiologie sexuelle et la mue chez le Crustacé Isopode marin: *Idotea balthica* (Pallas). Thèse Doctorat d'Etat, Univ. Nancy I, AO CNRS n°: 4874, pp. 1–335.
- 126 Drach, P. (1955) Système endocrinien pédonculaire, durée d'intermue et vitellogénèse chez *Leander serratus* (Pennant), Crustacé Décapode. *C. R. Soc. Biol.*, **149**: 2079–2083.
- 127 Descouturelle, G. (1978) Influence de l'ablation des pédoncules oculaires sur la longévité, l'évolution ovarienne, et la durée du cycle d'intermue chez la Crevette d'eau douce *Atyaephyra desmaresti* Millet 1831. Etude des facteurs température, saison et sexualité. *Arch. Zool. exp. gén.*, **119**: 433–445.
- 128 Cheung, T. S. (1966) The interrelations among three hormonal-controlled characters in the adult female shore crab, *Carcinus maenas* (L.). *Biol. Bull.*, **130**: 59–66.
- 129 Webb, M. (1977) Eyestalk regulation of molt and vitellogenesis in *Uca pugilator*. *Biol. Bull.*, **153**: 630–642.
- 130 Cheung, T. S. (1969) The environmental and hormonal control of growth and reproduction in the adult female stone crab, *Menippe mercenaria* (Say). *Biol. Bull.*, **136**: 327–346.
- 131 Hanström, B. (1931) Neue Untersuchungen über Sinnesorgane und Nervensystem der Crustaceen. I. *Z. Morphol. Ökol. Tiere*, **23**: 80–286.
- 132 Hanström, B. (1933) Neue Untersuchungen über Sinnesorgane und Nervensystem der Crustaceen. II. *Zool. Jhb. Anat.*, **56**: 387–520.
- 133 Hanström, B. (1939) Hormones in Invertebrates, Oxford Univ. Press, London and New York.
- 134 Scharrer, E. (1928) Die Lichtempfindlichkeit blinder Elritzen (Untersuchungen über das Zwischenhirn der Fische). *Z. vergl. Physiol.*, **7**: 1–38.
- 135 Hodge, M. H. and Chapman, G. B. (1958) Some observations on the fine structure of the sinus gland of a land crab, *Gecarcinus lateralis*. *J. Biophys. Biochem. Cytol.*, **4**: 571–574.
- 136 Fingerman, M. and Aoto, T. (1959) The neurosecretory system of the dwarf crayfish, *Cambarellus shufeldtii*, revealed by electron and light microscopy. *Trans. Am. Microsc. Soc.*, **78**: 305–317.
- 137 Bunt, A. H. and Ashby, E. A. (1967) Ultrastructural study of the sinus gland in the crayfish, *Procambarus clarkii*. *Gen. Comp. Endocrinol.*, **9**: 334–342.
- 138 Meusy, J.-J. (1968) Précisions nouvelles sur l'ultrastructure de la glande du sinus d'un Crustacé

- Décapode Brachyoure, *Carcinus maenas* L. Bull. Soc. Zool. Fr., **93**: 291-299.
- 139 Chaigneau, J. (1983) Neurohemal organs in Crustacea. In "Neurohemal Organs in Arthropods". Ed. by A. P. Gupta, Charles C Thomas, Springfield, pp. 53-89.
- 140 Panouse, J. B. (1943) Influence de l'ablation des pédoncules oculaires sur la croissance de l'ovaire chez la crevette *Leander serratus*. C. R. Acad. Sci. Paris, **217**: 553-555.
- 141 Panouse, J. B. (1946) Recherches sur les phénomènes humoraux chez les Crustacés. L'adaptation chromatique et la croissance ovarienne chez la Crevette *Leander serratus*. Ann. Inst. Oceanogr. Monaco, **23**: 65-147.
- 142 Primavera, H. and Borlongan, E. (1978) Ovarian rematuration of ablated sugpo prawn *Penaeus monodon* Fabricius. Ann. Biol. Anim. Bioch. Biophys., **18**: 1067-1072.
- 143 Anilkumar, G. and Adiyodi, K. G. (1980) Ovarian growth, induced by eyestalk ablation during the prebreeding season, is not normal in the crab, *Paratelphusa hydrodromous*. Int. J. Invertebr. Reprod., **2**: 95-105.
- 144 Gabe, M. (1966) Neurosecretion. International Series of Monographs in Pure and Applied Biology, Zoology Division, Vol. 28, Pergamon Press.
- 145 Armitage, K. B., Buikema, A. L., Jr. and Willems, N. J. (1973) The effect of photoperiod on organic constituents and molting of the crayfish *Orconectes nais* (Faxon). Comp. Biochem. Physiol., **44A**: 431-456.
- 146 Quackenbush, L. S. and Herrnkind, W. F. (1981) Regulation of molt and gonadal development in the spiny lobster *Panulirus argus* (Crustacea: Palinuridae): effect of eyestalk ablation. Comp. Biochem. Physiol., **69A**: 523-527.
- 147 Vernet-Cornubert, G. (1960) Influence de l'ablation des pédonculaires sur la mue, la ponte et les caractères sexuels externes de *Pisa tetraodon* Pennant. Bull. Inst. Océanogr. Monaco, **1186**: 1-24.
- 148 Hinsch, G. W. (1972) Some factors controlling reproduction in the spider crab, *Libinia emarginata*, Biol. Bull., **143**: 358-366.
- 149 Passano, L. M. (1960) Molting and its control. In "The Physiology of Crustacea, Vol. 1". Ed. by T. H. Waterman, Academic Press, New York and London, pp. 473-536.
- 150 Carlisle, D. B. (1953) Studies on *Lysmata seticaudata* Risso (Crustacea Decapoda). V. The ovarian inhibiting hormone and the hormonal inhibition of sex-reversal. Pubbl. Staz. Zool. Napoli, **24**: 355-372.
- 151 Martin, G. (1982) Etude ultrastructurale de la régénération de la glande du sinus chez l'oniscoïde *Porcellio dilatatus* Brandt; données complémentaires sur l'origine des terminaisons de cet organe neurohémal. J. Physiol., Paris, **78**: 558-565.
- 152 Besse, G., Juchault, P., Legrand, J.-J. and Mocquard, J.-P. (1969) Contribution à l'étude de la physiologie sexuelle femelle de *Ligia oceanica* L. (Crustacé Oniscoïde). Différenciation des oostégites et contrôle neurohumoral de la maturation ovarienne. C. R. Acad. Sci. Paris., Sér. D, **269**: 733-736.
- 153 Mocquard, J.-P., Besse, G., Juchault, P., Legrand, J.-J., Maissiat, J. and Noulain, G. (1971) Contribution à l'analyse du contrôle neurohumoral de la croissance, de la mue et de la physiologie sexuelle mâle et femelle chez l'Oniscoïde *Ligia oceanica* L. (Crustacé Isopode). Ann. Embryol. Morphol., **4**: 45-63.
- 154 Blanchet-Tournier, M.-F. (1987) Mise en évidence d'une activité neurohormonale inhibitrice de la vitellogenèse chez l'amphipode *Orchestia gammarella*. Can. J. Zool., **65**: 1917-1922.
- 155 Gohar, M., Souty-Grosset, C., Martin, G. and Juchault, P. (1984) Mise en évidence d'une inhibition de la synthèse de la vitellogénine par un facteur neurohumoral (V.I.H.) chez le Crustacé Isopode terrestre *Porcellio dilatatus* Brandt. C. R. Acad. Sci. Paris, Sér. III, **299**: 785-787.
- 156 Ferlund, P. (1974) Structure of the red-pigment-concentrating hormone of the shrimp, *Pandalus borealis*. Biochim. Biophys. Acta, **371**: 304-311.
- 157 Kleinholz, L. H. (1976) Crustacean neurosecretory hormones and physiological specificity. Am. Zool., **16**: 151-156.
- 158 Huberman, A., Arechiga, H., Cimmet, A., De La Rosa, J. and Aramburo, C. (1979) Isolation and purification of a neurodepressing hormone from the eyestalks of *Procambarus bouvieri* (Ortmann). Eur. J. Biochem., **99**: 203-208.
- 159 Bomirski, A., Arendarczyk, M., Kawinska, E. and Kleinholz, L. H. (1981) Partial characterization of Crustacean gonad-inhibiting hormone. Int. J. Invertebr. Reprod., **3**: 213-219.
- 160 Klek-Kawinska, E. and Bomirski, A. (1975) Ovary-inhibiting hormone activity in shrimp (*Crangon crangon*) eyestalks during the annual reproductive cycle. Gen. Comp. Endocrinol., **25**: 9-13.
- 161 Quackenbush, L. S. and Herrnkind, W. F. (1983) Partial characterization of eyestalk hormones controlling molt and gonadal development in the spiny lobster *Panulirus argus*. J. Crust. Biol., **3**: 34-44.
- 162 Quackenbush, L. S. and Keeley, L. L. (1986) Vitellogenesis in the shrimp, *Penaeus vannamei*. Am. Zool., **26**: 56A.
- 163 Soyeux, D., Van Deijnen, J. E. and Martin, M. (1987) Isolation and characterization of a vitellogenesis inhibiting factor from sinus glands of the

- lobster, *Homarus americanus*. J. Exp. Zool., **244**: 479–484.
- 164 Meusy, J.-J., Martin, M., Soyey, D., van Deijnen, J. E. and Gallo, J.-M. (1987) Immunochemical and immunocytochemical studies of the crustacean Vitellogenesis Inhibiting Hormone (VIH). Gen. Comp. Endocrinol., **67**: 333–341.
- 165 Gorgels-Kallen, J. L. and Van Herp, F. (1981) Localization of Crustacean Hyperglycemic Hormone (CHH) in the X-organ sinus gland complex in the eyestalk of the crayfish, *Astacus leptodactylus* (Nordmann, 1842). J. Morphol., **170**: 347–355.
- 166 Enami, M. (1951) The source and activities of two chromatophorotropic hormones in crabs of the genus *Sesarma*. II. Histology of incretory elements. Biol. Bull., **101**: 241–258.
- 167 Matsumoto, K. (1958) Morphological studies on the neurosecretion in crabs. Biol. J. Okayama Univ., **4**: 103–176.
- 168 Otsu, T. (1960) Precocious development of the ovaries in the crab, *Potamon dehaani*, following implantation of the thoracic ganglion. Annot. Zool. Japon., **33**: 90–96.
- 169 Otsu, T. (1963) Bihormonal control of sexual cycle in the freshwater crab, *Potamon dehaani*. Embryologia, **8**: 1–20.
- 170 Gomez, R. (1965) Acceleration of development of gonads by implantation of brain in the crab, *Paratelphusa hydrodromous*. Naturwissenschaften, **9**: 216.
- 171 Gomez, R. and Nayar, K. K. (1965) Certain endocrine influences in the reproduction of the crab, *Paratelphusa hydrodromous*. Zool. Jb. Abt. Physiol., **71**: 694–701.
- 172 Hinsch, G. and Bennet, D. C. (1979) Vitellogenesis stimulated by thoracic ganglion implants into destalked immature spider crabs, *Libinia emarginata*. Tissue and Cell, **11**: 345–351.
- 173 Babu, O., Shyamasudari, E. T. and Rao, K. H. (1980) Correlative changes in neurosecretion and ovarian growth after bilateral ablation of eyestalks in the crab, *Menippe rumphii*. Indian J. Exp. Biol., **18**: 265–268.
- 174 Takayanagi, H., Yamamoto, Y. and Takeda, N. (1986) An ovary-stimulating factor in the shrimp, *Paratya compressa*. J. Exp. Zool., **240**: 203–209.
- 175 Charniaux-Cotton, H. (1960) Sex Determination. In "The Physiology of Crustacea, Vol. 1". Ed. by T. H. Waterman. Academic Press, New York and London, pp. 411–447.
- 176 Charniaux-Cotton, H. (1962) Preuve expérimentale de l'autodifférenciation ovarienne chez *Orchestia montagui* Audouin (Crustacé Amphipode). C. R. Acad. Sci. Paris, **254**: 2836–2838.
- 177 Junéra, H., Martin, M., Solari, A. and Meusy, J.-J. (1977) Détermination du poids moléculaire de la vitellogénine et des lipovitellines d'*Orchestia gammarella*, Crustacé Amphipode. C. R. Acad. Sci. Paris, Sér. D, **285**: 909–912.
- 178 Picaud, J.-L. and Souty, C. (1981) Approche quantitative de l'influence de l'ovariectomie sur la synthèse de la vitellogénine chez *Porcellio dilatatus* Brandt (Crustacé, Isopode). C. R. Acad. Sci. Paris, Sér. III, **293**: 479–482.
- 179 Souty-Grosset, C. and Juchault, P. (1987) Etude de la synthèse de la vitellogénine chez les mâles intersexués d'*Armadillidium vulgare* Latreille (Crustacé Isopode Oniscoïde): Comparaison avec les mâles et les femelles intactes ou ovariectomisées. Gen. Comp. Endocrinol., **66**: 163–170.
- 180 Echalier, G. (1959) L'organe Y et le déterminisme de la croissance et de la mue chez *Carcinus maenas* (L.), Crustacé Décapode. Ann. Sci. Nat. Zool., **1**: 1–59.
- 181 Kater, S. B. and Spaziani, E. (1971) Incorporation of cholesterol ¹⁴C into crab cholesterol pools and ecdysones as a function of the molting cycle. Am. Zool., **11**: 672.
- 182 Willig, A. and Keller, R. (1976) Biosynthesis of α - and β -ecdysone by the crayfish *Orconectes limosus* *in vivo* and by its Y-organs *in vitro*. Experientia, **32**: 936–937.
- 183 Chang, E. S., Sage, B. A. and O'Connor, J. D. (1976) The qualitative and quantitative determinations of ecdysones in tissues of the crab, *Pachygrapsus crassipes*, following molt induction. Gen. Comp. Endocrinol., **30**: 21–33.
- 184 Chang, E. S. and O'Connor, J. D. (1977) Secretion of α - and β -ecdysone by crab Y-organs *in vitro*. Proc. Natl. Acad. Sci., USA, **74**: 615–618.
- 185 Keller, R. and Schmid, E. (1979) *In vitro* secretion of ecdysteroids by the Y-organs and lack of secretion by mandibular organs of the crayfish following molt induction. J. Comp. Physiol., **130**: 347–353.
- 186 Arvy, L., Echalier, G. and Gabe, M. (1954) Modification de la gonade de *Carcinides maenas* L. (Crustacé Décapode) après ablation bilatérale de l'organe Y. C. R. Acad. Sci. Paris, **239**: 1853–1855.
- 187 Arvy, L., Echalier, G. and Gabe, M. (1956) Organe Y et gonade chez *Carcinides (Carcinus) maenas* L. Ann. Sci. Nat. Zool., **18**: 263–267.
- 188 Demeusy, N. (1959) Pédoncules oculaires, glandes de mue et appareil génital chez *Carcinus maenas* L. C. R. Acad. Sci. Paris, **248**: 2652–2654.
- 189 Demeusy, N. (1962) Observations sur la maturation ovarienne du crabe *Carcinus maenas* L. après ablation des glandes de mue chez les femelles adultes. Premiers résultats. C. R. Acad. Sci. Paris, **255**: 3062–3064.
- 190 Demeusy, N. (1962) Rôle de la glande de mue dans

- l'évolution ovarienne du crabe *Carcinus maenas* Linné. Cah. Biol. Mar., **3**: 37-56.
- 191 Besse, G. and Maissiat, J. (1971) Action de la glande de mue sur la vitellogénèse du Crustacé Isopode *Porcellio dilatatus* (Brandt). C. R. Acad. Sci. Paris, Sér. D, **273**: 1975-1978.
- 192 Meusy, J.-J., Blanchet, M.-F. and Junéra, H. (1977) Mue et vitellogénèse chez le Crustacé Amphipode *Orchestia gammarella* Pallas. II. Etude de la synthèse de la vitellogénine ("fraction protéique femelle" de l'hémolymphe) après destruction des organes Y. Gen. Comp. Endocrinol., **33**: 35-40.
- 193 Suzuki, S. (1986) Effect of Y-organ ablation on oocyte growth in the terrestrial isopod, *Armadillidium vulgare*. Biol. Bull., **170**: 350-355.
- 194 Andrieux, N., Porcheron, P., Berreur-Bonnenfant, J. and Dray, F. (1976) Détermination du taux d'ecdysone au cours du cycle d'intermue chez le crabe *Carcinus maenas*. Comparaison entre individus sains et parasités par *Sacculina carcini*. C. R. Acad. Sci. Paris, Sér. D, **283**: 1429-1432.
- 195 Lachaise, F., Lagueux, M., Feyerisen, R. and Hoffmann, J. A. (1976) Métabolisme de l'ecdysone au cours du développement de *Carcinus maenas* (Brachyura, Decapoda). C. R. Acad. Sci. Paris, Sér. D, **282**: 943-946.
- 196 Blanchet, M.-F., Porcheron, P. and Dray, F. (1979) Variations du taux des ecdystéroïdes au cours des cycles de mue et de vitellogénèse chez le Crustacé Amphipode *Orchestia gammarellus*. Int. J. Invertebr. Reprod., **1**: 133-139.
- 197 Baldaia, L., Porcheron, P., Coimbra, J. and Cassier, P. (1984) Ecdysteroids in the shrimp *Palaemon serratus*: relations with molt cycle. Gen. Comp. Endocrinol., **55**: 437-443.
- 198 Carlisle, D. B. (1957) On the hormonal inhibition of moulting in decapod Crustacea. II. The terminal anecysis in crabs. J. Mar. Biol. Assoc. U. K., **36**: 291-307.
- 199 Chaix, J.-C., Trilles, J.-P. and Vernet, G. (1976) Dégénérescence de l'organe Y chez les mâles pubères d'*Acanthonyx lunulatus* (Risso) (Crustacea, Oxyrhyncha). C. R. Acad. Sci. Paris, Sér. D, **283**: 523-525.
- 200 Souty, C., Besse, G. and Picaud, J.-L. (1982) Stimulation par l'ecdysone du taux hémolympatique de la vitellogénine chez le Crustacé Isopode terrestre, *Porcellio dilatatus* Brandt. C. R. Acad. Sci. Paris, Sér. III, **294**: 1057-1059.
- 201 Blanchet, M.-F., Junéra, H. and Meusy, J.-J. (1975) Mue et vitellogénèse chez *Orchestia gammarella* Pallas, Crustacé Amphipode: étude de la synthèse de la fraction protéique femelle après introduction d'ecdystérone. Experientia, **31**: 865-867.
- 202 Picaud, J.-L. and Souty, C. (1980) Démonstration par immunoautoradiographie de la synthèse de la vitellogénine par le tissu adipeux de *Porcellio dilatatus* Brandt (Crustacé, Isopode). C. R. Acad. Sci. Paris, Sér. D, **290**: 1019-1021.
- 203 Gohar, M. and Souty, C. (1983) Mise en évidence in vitro d'une synthèse et d'une libération de la vitellogénine dans le tissu adipeux mâle de *Porcellio dilatatus* Brandt (Crustacé Isopode terrestre). C. R. Acad. Sci. Paris, Sér. D, **297**: 145-148.
- 204 Lachaise, F. and Hoffmann, J. (1982) Ecdysteroids and embryonic development in the shore crab, *Carcinus maenas*. Hoppe-Seyler's Z. Physiol. Chem., **363**: 1059-1067.
- 205 Lachaise, F., Goudeau, M., Hetru, C., Kappler, C. and Hoffmann, J. A. (1981) Ecdysteroids and ovarian development in the shore crab, *Carcinus maenas*. Hoppe-Seyler's Z. Physiol. Chem., **362**: 521-529.
- 206 Payen, G. and Costlow, J. D. (1977) Effects of a juvenile hormone mimic on male and female gametogenesis of the mud-crab, *Rhithropanopeus harrisi* (Gould) (Brachyura: Xanthidae). Biol. Bull., **152**: 199-208.
- 207 Hinsch, G. W. (1981) Effects of juvenile hormone mimics on the ovary in the immature spider crab, *Libinia emarginata*. Int. J. Invertebr. Reprod., **3**: 237-244.
- 208 Slama, K., Romanuk, M. and Sorm, F. (1974) Insect hormones and bioanalogs. Springer-Verlag, Wien and New York, pp. 1-477.
- 209 Engelmann, F. (1983) Vitellogenesis controlled by juvenile hormone. In "Endocrinology of Insects, Vol. 1". Ed. by R. G. H. Downer and H. Laufer, Alan R. Liss Inc., New York, pp. 259-270.
- 210 Le Roux, A. (1968) Description d'organes mandibulaires nouveaux chez les Crustacés Décapodes. C. R. Acad. Sci. Paris, Sér. D, **266**: 1414-1417.
- 211 Bazin, F. (1976) Mise en évidence des caractères cytologiques des glandes stéroïdogènes dans les glandes mandibulaires et les glandes Y du crabe *Carcinus maenas* (L.) normal et épédonculé. C. R. Acad. Sci. Paris, Sér. D, **282**: 739-741.
- 212 Yudin, A. I., Diener, R. A., Clark, W. H., Jr. and Chang, E. S. (1980) Mandibular gland of the blue crab, *Callinectes sapidus*. Biol. Bull., **159**: 760-772.
- 213 Taketomi, Y. and Kawano, Y. (1985) Ultrastructure of the mandibular organ of the shrimp, *Penaeus japonicus*, in untreated and experimentally manipulated individuals. Cell. Biol. Int. Rep., **9**: 1069-1074.
- 214 Byard, E. H. and Shivers, R. R. (1975) The mandibular organ of the lobster, *Homarus americanus*. Cell Tissue Res., **162**: 13-22.
- 215 Le Roux, A. (1983) Réactions de l'organe mandibulaire à l'ablation des pédoncules oculaires chez

- les larves et les juvéniles de *Palaemonetes varians* (Leach). C. R. Acad. Sci. Paris, Sér. III, **296**: 697–700.
- 216 Hirsch, G. W. (1980) Effect of mandibular organ implants upon the spider crab ovary. Trans. Am. Microsc. Soc., **99**: 317–322.
- 217 Schneiderman, H. A. and Gilbert, L. I. (1958) Substances with juvenile hormone activity in Crustacea and other invertebrates. Biol. Bull., Woods Hole, Mass., **115**: 530–535.
- 218 Laufer, H., Landau, M., Borst, D. and Homola, E. (1986) The synthesis and regulation of methylfarnesoate, a new juvenile hormone for crustacean reproduction. In "Advances in Invertebrate Reproduction 4". Ed. by M. Porchet, J.-C. Andries and A. Dhainaut, Elsevier, North Holland, pp. 135–143.
- 219 Laufer, H., Borst, D., Baker, F. C., Carrasco, C., Sinkov, M., Reuter, C. C., Tsai, L. W. and Schooley, D. A. (1987) Identification of a juvenile hormone-like compound in a crustacean. Science, **235**: 202–205.
- 220 Couch, E. F., Hagino, N. and Lee, J. W. (1987) Changes in estradiol and progesterone immunoreactivity in tissues of the lobster, *Homarus americanus*, with developing and immature ovaries. Comp. Biochem. Physiol., **87A**: 765–770.
- 221 Takayanagi, H., Yamamoto, Y. and Takeda, N. (1986) Ovary-stimulating pheromone in the freshwater shrimp, *Paratyia compressa*. J. Exp. Zool., **240**: 397–400.
- 222 Jassem, W., Juchault, P. and Mocquard, J.-P. (1982) Déterminisme de la reproduction saisonnière des femelles d'*Armadillidium vulgare* Latr. (Crustacé, Isopode, Oniscoïde). V. Rôle du mâle dans le cycle de reproduction des femelles (induction et durée de la période reproduction). Ann. Sci. Nat. Zool., Paris, **4**: 195–201.
- 223 Besse, G., Juchault, P., Legrand, J.-J. and Mocquard, J.-P. (1970) Modification de l'électrophorogramme de l'hémolymphe des Oniscoïdes (Crustacés Isopodes) par action de l'hormone androgène. C. R. Acad. Sci. Paris, Sér. D, **270**: 3276–3279.
- 224 Meusy, J.-J., Junéra, H. and Croisille, Y. (1971) Recherche de la "fraction protéique femelle" dans l'hémolymphe des femelles d'*Orchestia gammarella* Pallas ayant subi une inversion expérimentale du sexe. C. R. Acad. Sci. Paris, Sér. D, **273**: 592–594.
- 225 Bomirski, A. and Klek-Kawinska, E. (1976) Stimulation of oogenesis in the sand shrimp, *Crangon crangon*, by human gonadotrophin. Gen. Comp. Endocrinol., **30**: 239–242.
- 226 Souty, C. and Picaud, J.-L. (1984) Effet de l'injection d'une gonadotropine humaine sur la synthèse et la libération de la vitellogénine par le tissu adipeux du Crustacé Isopode marin *Idotea balthica basterii* Audouin. Gen. Comp. Endocrinol., **54**: 418–421.
- 227 Kulkarni, G. K., Nagabhusanam, R. and Joshi, P. K. (1979) Effect of progesterone on ovarian maturation in a marine penaeid prawn *Parapenaeopsis hardwickii* (Miers, 1878). Indian. J. Exp. Biol., **17**: 986–987.
- 228 Donahue, J. K. (1948) Fluorimetric and biological determination of estrogens in the eggs of the American lobster (*Homarus americanus*). Proc. Soc. Exp. Biol. Med., **69**: 179–181.
- 229 Donahue, J. K. (1952) Studies on ecdysis in the American lobster (*Homarus Americanus*). I. The lobster egg as a source of estrogenic hormone. State of Maine Dept. of Sea and Shore Fisheries, Res. Bull., no. 8.
- 230 Donahue, J. K. (1957) Chromatographic identification of lobster estrogen. State of Maine Dept. of Sea and Shore Fisheries, Res. Bull., no. 28.
- 231 Jeng, S. S., Wan, W. C.-M. and Chang, C. F. (1978) Existence of an oestrogen-like compound in the ovary of the shrimp *Parapenaeus fissurus*. Gen. Comp. Endocrinol., **36**: 211–214.
- 232 Ollevier, F., De Clerck, D., Diederik, H. and De Loof, A. (1986) Identification of noncysteroid steroids in hemolymph of both male and female *Astacus leptodactylus* (Crustacea) by gas chromatography-mass spectrometry. Gen. Comp. Endocrinol., **61**: 214–228.
- 233 Doane, W. W. (1973) Role of hormones in insect development. In "Developmental Systems: Insects". Ed. by S. J. Counce and C. H. Waddington, Academic Press, London and New York, p. 436.
- 234 Carlisle, D. B. and Butler, C. G. (1956) The "queen substance" of honeybees and the ovary-inhibiting hormone of crustaceans. Nature, **177**: 276–277.
- 235 Sastry, A. N. (1983) Ecological aspects of reproduction. In "The Biology of Crustacea. Vol. 8". Ed. by F. J. Vernberg and W. B. Vernberg, Academic Press, New York, pp. 179–270.
- 236 Segerstrale, S. G. (1970) Light control of the reproductive cycle of *Pontoporeia affinis* Lindström (Crustacea Amphipoda). J. Exp. Mar. Biol. Ecol., **5**: 272–275.
- 237 Steele, V. J., Steele, D. H. and MacPherson, B. R. (1977) The effect of photoperiod on the reproductive cycle of *Gammarus setosus* Dementieva, 1931. Crustaceana, suppl. 4: 58–63.
- 238 De March, B. G. E. (1977) The effects of photoperiod and temperature on the induction and termination of reproductive resting stage in the freshwater amphipod *Hyaella azteca* (Saussure). Can. J. Zool., **55**: 1595–1600.
- 239 Steele, V. J. (1981) The effect of photoperiod on

- the reproductive cycle of *Gammarus lawrencianus* Bousfield. J. Exp. Mar. Biol. Ecol., **53**: 1-7.
- 240 Steele, V. J. and Steele, D. H. (1986) The influence of photoperiod on the timing of reproductive cycles in *Gammarus* species (Crustacea, Amphipoda). Am. Zool., **26**: 459-467.
- 241 De March, B. G. E. (1982) Decreased day length and light intensity as factors inducing reproduction in *Gammarus lacustris lacustris* Sars. Can J. Zool., **60**: 2962-2965.
- 242 McQueen, D. J. and Steel, C. G. (1980) The role of photoperiod and temperature in the initiation of reproduction in the terrestrial isopod *Oniscus asellus* Linnaeus. Can. J. Zool., **58**: 235-240.
- 243 Steel, C. G. (1980) Mechanisms of coordination between moulting and reproduction in the terrestrial Isopod Crustacea. Biol. Bull., **159**: 206-218.
- 244 Juchault, P., Jassem, W. and Mocquard, J.-P. (1982) Déterminisme de la reproduction saisonnière des femelles d'*Armadillidium vulgare* Latr. (Crustacé, Isopode, Oniscoïde). VI. Mise en évidence d'une photopériode critique permettant l'entrée en reproduction; modalités du maintien en reproduction. Ann. Sci. Nat. Zool., Paris, **4**: 203-210.
- 245 Laubier-Bonichon, A. (1975) Induction de la maturation sexuelle et ponte chez la crevette *Penaeus japonicus* Bate en milieu contrôlé. C. R. Acad. Sci. Paris, Sér. D, **281**: 2013-2016.
- 246 Laubier-Bonichon, A. (1978) Ecophysiologie de la reproduction chez la crevette *Penaeus japonicus*. Trois années d'expérience en milieu contrôlé. Oceanol. Acta, **1**: 135-150.
- 247 Stephens, G. C. (1952) Mechanism regulating the reproductive cycle in the crayfish, *Cambarus*. I. The female cycle. Physiol. Zool., **25**: 70-83.
- 248 Aiken, D. E. (1969) Ovarian maturation and egg-laying in the crayfish *Orconectes virilis*: influence of temperature and photoperiod. Can. J. Zool., **47**: 931-935.
- 249 Suko, T. (1958) Studies on the development of the crayfish. V. The histological changes of the developmental ovaries influenced by the condition of darkness. Sci. Rep. Saitama Univ., Sér. B, **3**: 67-78.
- 250 Lowe, M. E. (1961) The female reproductive cycle of the crayfish *Cambarellus shufeldti*: the influence of environmental factors. Tulane Stud. Zool., **8**: 157-176.
- 251 Kracht, D. (1972) Application de conditions hivernales et estivales, épédonculation et action d'une ecdystérone chez l'Ecrevisse femelle adulte *Orconectes limosus* R., pendant la période d'anecdysis: conséquence sur la ponte et sur la mue. C. R. Acad. Sci. Paris, Sér. D, **275**: 1677-1680.
- 252 Rice, P. R. and Armitage, K. B. (1974) The influence of photoperiod on processes associated with molting and reproduction in the crayfish *Orconectes nais* (Faxon). Comp. Biochem. Physiol., **47A**: 243-259.
- 253 Nelson, K. (1986) Photoperiod and reproduction in lobsters (*Homarus*), Am. Zool., **26**: 447-457.
- 254 Pradeille-Rouquette, M. (1976) Rôle de la photopériode dans la fonction de reproduction des femelles du crabe *Pachygrapsus marmoratus*. C. R. Acad. Sci. Paris, Sér. D, **282**: 199-201.
- 255 Nagabhushanam, R. and Farooqui, U. M. (1981) Photoperiodic stimulation of ovary and testis in the immature marine crab, *Scylla serrata* Forskal. Indian J. Mar. Sci., **10**: 396-398.
- 256 Lagardère, J.-P. (1982) Effets du bruit sur le métabolisme, la croissance et la reproduction de *Crangon crangon* (L.) (Décapode, Natantia). C. R. Acad. Sci. Paris, Sér. III, **294**: 425-428.
- 257 Von Hagen, H. O. (1962) Freilandstudien zur sexual und fortpflanzungs Biologie von *Uca tangeri* in Anadalousien. Z. Morphol. Oekol. Tiere, **51**: 611-725.
- 258 Von Hagen, H. O. (1970) Adaptations to the special intertidal level of habitat in Ocypodid crabs (Decapoda, Brachyura). Forma Functio, **2**: 361-413.
- 259 Zuker, N. (1976) Behavioral rhythms in the fiddler crab *Uca terpsichores*. In "Biological Rhythms in the Marine Environment". Ed. by P. J. De Coursey., Univ. of South Carolina, Carolina Press, Columbia, pp. 145-159.
- 260 Pérez, C. (1933) Processus de résorption phagocytaire des ovocytes dans l'ovaire chez les *Macropodia* sacculinées. C. R. Soc. Biol. Fr., **112**: 1049-1051.
- 261 Veillet, A. (1945) Recherches sur le parasitisme des Crabes et des Galathées par les Rhizocéphales et les Epicarides. Ann. Inst. Oceanogr. Paris, **22**: 193-341.
- 262 Cornubert, G. (1952) Influence de la Sacculine *Sacculina carcini* Thompson sur le Crabe *Pachygrapsus marmoratus* Fabricius. C. R. Acad. Sci. Paris, **234**: 1218-1220.
- 263 Payen, G. G. (1975) Effets masculinisants des glandes androgènes implantées chez la femelle pubère pédonclectomisée de *Rhithropanopeus harrisi* (Gould) (Crustacé Décapode Brachyoure). C. R. Acad. Sci. Paris, Sér. D, **280**: 111-115.
- 264 Rubiliani, C., Rubiliani-Durozoi, M. and Payen, G. G. (1980) Effets de la Sacculine sur les gonades, les glandes androgènes et le système nerveux central des Crabes *Carcinus maenas* (L.) et *C. mediterraneus* Czerniavsky. Bull. Soc. Zool. Fr., **105**: 95-100.
- 265 Andrieux, N., De Freschville, J. and Herberts, C. (1986) Etude des protéines vitellines de l'hémo-

- lymphe et de l'ovaire chez le Crustacé Décapode *Carcinus maenas*; incidence du parasite *Sacculina carcini* (Crustacé Rhizocéphale). *Can. J. Zool.*, **64**: 2279–2287.
- 266 Leroux, M.-L. (1933) Recherches sur la sexualité des Gammariens. *Bull. Biol. Fr. Berg.*, suppl. 16: 24–46.
- 267 Campbell-Parmentier, F. (1963) Vitellogenèse, maturation des ovocytes, accouplement et ponte en relation avec l'intermue chez *Orchestia gammarella* (Pallas), Crustacé, Amphipode, Talitridae. *Bull. Soc. Zool. Fr.*, **88**: 474–488.
- 268 Mathieu-Capderou, C. (1980) Relation entre la maturation ovocytaire et l'exuviation chez le Crustacé Amphipode *Orchestia gammarellus* (Pallas). *C. R. Acad. Sci. Paris, Sér. D*, **290**: 1495–1498.
- 269 Clédon, P. (1985) Analyse cytologique et expérimentale de la maturation et de l'activation de l'ovocyte de la Crevette *Palaemon serratus* (Crustacé Décapode Natantia). *C. R. Acad. Sci. Paris, Sér. D*, **301**: 317–322.
- 270 Clédon, P. (1986) Study on oocyte maturation and activation of the common prawn *Palaemon serratus* (Pennant): Relationship between oocyte maturation and the molt cycle cytological aspects. *Gamete Res.*, **13**: 353–362.
- 271 Lanot, R., Thiebold, J., Lagueux, M., Goltzene, F. and Hoffmann, J. A. (1987) Involvement of ecdysone in the control of meiotic reinitiation in oocytes of *Locusta migratoria* (Insecta, Orthoptera). *Dev. Biol.*, **121**: 174–181.
- 272 Lachaise, F. and Hoffmann, J. (1977) Ecdysone et développement ovarien chez un Décapode, *Carcinus maenas*. *C. R. Acad. Sci. Paris, Sér. D*, **285**: 701–704.
- 273 Maller, J. L. (1985) Oocyte maturation in amphibiens. In "Developmental Biology, A Comprehensive Synthesis. Vol. 1 Oogenesis. Ed. by L. W. Browder, Plenum Press, New York, London, pp. 289–311.
- 274 Fauvel, C. (1983) L'ovaire de *Macrobrachium rosenbergii* (De Man) (Crustacé Décapode) au moment de la ponte. Description de l'ovulation. *C. R. Acad. Sci. Paris, Sér. III*, **296**: 1053–1058.
- 275 Matsumoto, K. (1958) Neurosecretion in the thoracic ganglion of the crab, *Eriocheir japonicus*. *Biol. Bull.*, **106**: 60–68.
- 276 Brown, G. D. (1966) Ultrastructural studies of sperm morphology and sperm-egg interaction in the decapod *Callinectes sapidus*. *J. Ultrastruct. Res.*, **14**: 425–440.
- 277 Hinsch, G. W. (1971) Penetration of the oocyte envelope by spermatozoa in the spider crab. *J. Ultrastruct. Res.*, **35**: 86–97.
- 278 Talbot, P. and Chanmanon, P. (1980) Morphological features of the acrosome reaction of lobster (*Homarus*) sperm and the role of the reaction in generating forward sperm movement. *J. Ultrastruct. Res.*, **70**: 287–297.
- 279 Lynn, J. W. and Clark, W. H. (1983) A morphological examination of sperm-egg interaction in the freshwater prawn, *Macrobrachium rosenbergii*. *Biol. Bull.*, **164**: 446–458.
- 280 Goudeau, M. (1982) Fertilization in a crab. I. Early events in the ovary, and cytological aspects of the acrosome reaction and gamete contacts. *Tissue and Cell*, **14**: 97–111.
- 281 Clark, W. H., Yudin, A. I., Griffin, F. J. and Shigekawa, K. (1984) The control of gamete activation and fertilization in the marine Penaeidae *Sicyonia ingentis*. In "Advances in Invertebrate Reproduction. Vol. 3". Ed. by W. Engels, W. H. Clark, Jr., A. Fischer, P. J. W. Olive and D. F. Went, Elsevier, North Holland, pp. 459–472.
- 282 Binford, R. (1913) The sperm cells and the process of fertilization in the crab, *Menippe mercenaria*. *J. Morphol.*, **24**: 147–201.
- 283 Bloch, F. (1935) Contribution à l'étude des gamètes et de la fécondation chez les Crustacés Décapodes. *Trav. Station Zool. Wimereux*, **12**: 183–279.
- 284 Hoestlandt, H. (1948) Recherches sur la biologie de l'*Eriocheir sinensis* en France (Crustacé Brachyoure). *Ann. Inst. Oceanogr.*, **24**: 1–116.
- 285 Pradeille-Rouquette, M. (1976) Etude de la fonction de reproduction chez les femelles du crabe *Pachygrapsus marmoratus* (F.) et de différents facteurs qui lui sont liés. *Cah. Biol. Mar.*, **17**: 387–403.
- 286 Goudeau, M. and Lachaise, F. (1980) Fine structure and secretion of the capsule enclosing embryo in a crab (*Carcinus maenas*). *Tissue and Cell*, **12**: 287–308.
- 287 Goudeau, H., Kubisz, P. and Goudeau, M. (1984) Mise en évidence du potentiel de fécondation chez les Crustacés Décapodes Brachyours *Carcinus maenas* et *Maia squinado*. *C. R. Acad. Sci. Paris, Sér. III*, **299**: 167–172.
- 288 Goudeau, M. and Goudeau, H. (1986) Thè resumption of meiotic maturation of the oocyte of the prawn *Palaemon serratus* is regulated by an increase in extracellular Mg^{2+} during spawning. *Dev. Biol.*, **118**: 361–370.
- 289 Goudeau, M. and Goudeau, H. (1986) External Mg^{2+} is required for hyperpolarization to occur in ovulated oocytes of the prawn *Palaemon serratus*. *Dev. Biol.*, **118**: 371–378.
- 290 Goudeau, H. and Goudeau, M. (1985) Fertilization in crabs: IV. The fertilization potential consists of a sustained egg membrane hyperpolarization. *Gamete Res.*, **11**: 1–17.
- 291 Goudeau, H. and Goudeau, M. (1986) Electrical

- and morphological responses of the lobster egg to fertilization. *Dev. Biol.*, **114**: 325–335.
- 292 Spalding, J. F. (1942) The nature and formation of the spermatophore and sperm-plug in *Carcinus maenas*. *Q. J. Microsc. Sci.*, **83**: 399–422.
- 293 Anghelou-Spiliotis, A. and Goudeau, M. (1982) Analyse au microscope électronique à balayage de la paroi limitant la lumière du conduit génital de la femelle adulte de *Carcinus maenas* (L). *Crustacé Décapode Brachyoure. C. R. Acad. Sci. Paris, Sér. III*, **294**: 617–622.
- 294 Herrick, F. H. (1909) Natural history of the american lobster. *Bull. U. S. Bur. Fish.*, **29**: 149–408.
- 295 Clark, W. H., Lynn, J. W., Yudin, A. I. and Persyn, H. O. (1980) Morphology of the cortical reaction in the eggs of *Penaeus aztecus*. *Biol. Bull.*, **158**: 175–186.
- 296 Goudeau, M. and Becker, J. (1982) Fertilization in a crab. II. Cytological aspects of the cortical reaction and fertilization envelope elaboration. *Tissue and Cell*, **14**: 273–282.
- 297 Goudeau, M. (1984) Fertilization in a crab. III. Cytodifferentiation of vesicles enclosing ring-shaped elements involved in the cortical reaction. *Gamete Res.*, **9**: 409–424.
- 298 Klepal, W., Barnes, H. and Barnes, M. (1979) Studies on the reproduction of cirripedes. VII. The formation and fine structure of the fertilization membrane and egg case. *J. Exp. Mar. Biol. Ecol.*, **36**: 53–78.
- 299 Clark, W. H., Lynn, J. W. and Yudin, A. I. (1975) The cortical reaction in the egg of the Penaeid shrimp. *Int. Symp. on Reproductive Physiology of Invertebrates*, **1**: 21.
- 300 Adiyodi, R. G. (1985) Reproduction and its control. In "The Biology of Crustacea. Vol. 9". Ed. by D. E. Bliss and L. H. Mantel, Academic Press, New York, pp. 147–215.
- 301 Demeusy, N. (1958) Recherches sur la mue de puberté du Décapode Brachyoure *Carcinus maenas* Linné. *Arch. Zool. Exp. Gen.*, **95**: 253–491.
- 302 Bomirski, A. and Klek, E. (1974) Action of eyestalk on the ovary in *Rhithropanopeus harrisi* and *Crangon crangon* (Crustacea Decapoda). *Mar. Biol.*, **24**: 329–337.
- 303 Anilkumar, G. and Adiyodi, K. G. (1985) The role of eyestalk hormones in vitellogenesis during the breeding season in the crab, *Paratelphusa hydrodromous* (Herbst). *Biol. Bull.*, **169**: 689–695.
- 304 Stephens, G. C. (1952) The control of cement gland development in the crayfish, *Cambarus*. *Biol. Bull.*, **103**: 242–258.
- 305 Reaka, M. L. (1976) Lunar and tidal periodicity of molting and reproduction in stomatopod Crustacea: A selfish herd hypothesis. *Biol. Bull.*, **150**: 468–490.
- 306 Watson, J. (1970) Maturity, mating, and egg-laying in the spider crab, *Chionocetes opilio*. *J. Fish. Res. Board Can.*, **27**: 1607–1616.
- 307 Berry, P. F. (1970) Mating behavior, oviposition, and fertilization in the spiny lobster *Panulirus homarus* (Linnaeus). *Invest. Rep. Oceanogr. Res. Inst. Durban*, **24**: 1–16.
- 308 Engelmann, F. (1984) Reproduction in insects. In "Ecological Entomology". Ed. by C. B. Huffaker and R. L. Rabb, J. Wiley & Sons Inc., North-Holland, pp. 113–147.
- 309 Hartnoll, R. G. (1968) Morphology of the genital ducts in female crabs. *J. Linn. Soc. (Zool)*, **47**: 279–300.
- 310 Cheung, T. S. (1968) Trans-molt retention of sperm in the female stone crab, *Menippe mercenaria* (Say). *Crustaceana*, **15**: 117–120.
- 311 Anilkumar, G. and Adiyodi, K. G. (1977) Spermatheca of the freshwater crab, *Paratelphusa hydrodromous* (Herbst) in relation to the ovarian cycle. In "Advances in Invertebrate Reproduction, Vol. 1". Ed. by K. G. Adiyodi and R. G. Adiyodi, Peralam-Kenoth, Kerala, pp. 269–274.
- 312 Peyrot, S. and Trilles, J.-P. (1964) Recherches sur la sexualité et la glande androgène de *Caprella aequilibra* Say (Amphipode, Caprellidae). *Bull. Inst. Océanogr. Monaco*, **63**: 1–28.
- 313 Mead, F. (1963) Sur l'existence d'une cavité incubatrice complexe chez l'Isopode terrestre *Helleria brevicornis* Ebner. *C. R. Acad. Sci. Paris*, **257**: 775–777.
- 314 Balesdent, M.-L. (1964) Recherches sur la sexualité et le déterminisme des caractères sexuels de *Asellus aquaticus* Linné (Crustacé Isopode). Thèse Doctorat d'Etat, Univ. Nancy, pp. 1–231.
- 315 Daguerre de Hureaux, N. (1966) Etude expérimentale du rôle de quelques formations endocrines cérébrales chez *Sphaeroma serratum* (Crustacé Isopode). Thèse Doctorat d'Etat, Univ. Bordeaux, AO CNRS n°1036, pp. 1–115.
- 316 Tinturier-Hamelin, E. (1962) Sur un caractère de l'*Idotea balthica* (Pallas) (Isopode Valvifère) considéré jusqu'alors comme un caractère sexuel secondaire mâle. *Arch. Zool. Exp. Gen.*, **101**: 54–58.
- 317 Sollaud, E. (1923). Recherches sur l'embryogénie des Crustacés Décapodes de la sous-famille des Palaemonidae. *Bull. Biol. Fr. Belg.*, **5**: 1–234.
- 318 Descouturelle, G. (1971) Différenciation des caractères sexuels femelles chez la Crevette d'eau douce *Atyaephyra desmaresti* Millet (Crustacea, Decapoda, Natantia). *C. R. Soc. Biol.*, **169**: 1412–1416.
- 319 Shen, C. J. (1935) An investigation of the post larval development of the shore crab, *Carcinus maenas*, with special reference to the external

- secondary sexual characters. Proc. Zool. Soc. London, 1–33.
- 320 Vernet-Cornubert, G. (1958) Recherches sur la sexualité du crabe *Pachygrapsus marmoratus* Fabr. Arch. Zool. Exp. Gén., **96**: 101–276.
- 321 Veillet, A. (1945) Recherches sur le parasitisme des Crabes et des Galathées par les Rhizocéphales et les Epicarides. Ann. Inst. Paris, **22**: 193–341.
- 322 Teissier, G. (1933) Etude de la croissance de quelques variants sexuels chez *Macropodia rostrata*. Bull. Biol. Fr. Belg., **67**: 401–444.
- 323 Teissier, G. (1935) Croissance des variants sexuels chez *Maia squinado* L. Trav. Stn. Biol. Roscoff, **13**: 93–130.
- 324 Churchill, E. P. (1919) Life history of the blue crab. Bull. Bur. Fish. Wash., **36**: 93–134.
- 325 Van Engel, W. A. (1958) The blue crab and its fishery in the Chesapeake Bay. Pt. I. Reproduction, early development, growth and migration. U.S. Fish. Wild. Serv., Comml. Fish. Rev., **20**: 6–17.
- 326 Chaix, J.-C. (1979) Le cycle biologique et quelques aspects de la reproduction du Crabe Oxyrhynque *Acanthonyx lunulatus* (Risso, 1816) (Crustacea, Decapoda, Oxyrhyncha). Téthys, **9**: 17–22.
- 327 Hinsch, G. W. (1968) Reproductive behavior in the spider crab, *Libinia emarginata* (L.). Biol. Bull., **135**: 273–278.
- 328 Goudeau, M. and Lachaise, F. (1983) Structure of the egg funiculus and deposition of embryonic envelope in a crab. Tissue and Cell, **15**: 47–62.
- 329 Mason, J. C. (1970) Egg-laying in the western North American crayfish, *Pacifastacus trowbridgii* (Stimpson) (Decapoda, Astacidae). Crustaceana, **19**: 37–44.
- 330 Thomas, W. J. and Crawley, E. (1975) The glair glands and oosetae of *Austropotamobius pallipes* (Lereboullet). Experientia, **31**: 183–185.
- 331 Johnson, B. and Talbot, P. (1987) Ultrastructural analysis of the pleopod tegumental glands in male and female lobsters, *Homarus americanus*. J. Crust. Biol., **7**: 288–301.
- 332 Aiken, D. E. and Waddy, S. L. (1982) Cement gland development, ovary maturation, and reproductive cycles in the American lobster *Homarus americanus*. J. Crust. Biol., **2**: 315–327.
- 333 Charniaux-Cotton, H. (1965) Hormonal control of sex differentiation in invertebrates. In "Organogenesis". Ed. by R. De Haan and H. Ursprung, Holt, Rinehart and Winston, New York, pp. 701–740.
- 334 Charniaux-Cotton, H. (1972) Recherches récentes sur la différenciation sexuelle et l'activité génitale chez divers crustacés supérieurs. In "Hormones et Différenciation Sexuelle chez Invertébrés". Ed. by E. Wolff, Gordon and Breach, New York, pp. 128–178.
- 335 Legrand, J.-J. and Juchault, P. (1972) Le contrôle humoral de la sexualité chez les Crustacés Isopodes gonochoriques. In "Hormones et Différenciation Sexuelle chez les Invertébrés". Ed. by E. Wolff, Gordon and Breach, New York, pp. 179–213.
- 336 Charniaux-Cotton, H. and Payen G. (1985) Sexual differentiation. In "The Biology of Crustacea, Vol. 9". Ed. by D. E. Bliss and L. H. Mantel, Academic Press, New York, pp. 217–295.
- 337 Nagamine, C. and Knight, A. W. (1987) Induction of female breeding characteristics by ovarian tissue implants in androgenic gland ablated male freshwater prawns *Macrobrachium rosenbergii* (de Man) (Decapoda, Palaemonidae). Int. J. Invertebr. Reprod. Dev., **11**: 225–234.
- 338 Legrand, J.-J. (1955) Rôle endocrinien de l'ovaire dans la différenciation des oostégites chez les Crustacés Isopodes terrestres. C. R. Acad. Sci. Paris, **241**: 1083–1087.
- 339 Luca, V. and Patane, L. (1961) Ulteriori dati sul determinismo dei caratteri sessuali secondari negli Isopodi Oniscoidei (*Porcellio laevis* Latr.). Atti della Accad. Gioenia, Sc. Nat. Catania, **13**: 1–19.
- 340 Shimoizumi, M. (1964) Effects of ovariectomy on the oostegite formation in the Isopod Crustacean, *Porcellio pruinosus*. J. Gakugei, Tokushima Univ., **14**: 1–8.
- 341 Takewaki, K. and Nakamura, N. (1944) The effects of gonadectomy on the sex characters of *Armadillidium vulgare*, an isopod crustacean. J. Fac. Sci. Imp. Univ. Tokyo, **4**: 368–382.
- 342 Besse, G., Juchault, P. and Legrand, J.-J. (1968) Etude expérimentale du déterminisme des caractères sexuels externes chez des *Porcellio dilatatus* Brandt intersexués (Crustacés Isopodes terrestres). C. R. Soc. Biol., **162**: 2196–2200.
- 343 Callan, H. G. (1940) The effects of castration by parasites and X-rays on the secondary sex characteristics of prawns (*Leander* sp.). J. Exp. Biol., **17**: 168–179.
- 344 Lloyd, A. J. and Yonge, C. M. (1940) Correlation between egg-carrying setae and cement glands in decapod Crustacea. Nature, **146**: 334.
- 345 Bollenbacher, W. E. and O'Connor, J. D. (1973) Production of an ecdysone by crustacean Y-organs *in vitro*. Am. Soc. Zool., **13**: 1274.
- 346 Lisk, R. D. (1961) Estradiol-17 β in the eggs of the American lobster, *Homarus americanus*. Can. J. Biochem. Physiol., **39**: 659–663.
- 347 Dhainaut, A. and De Leersnyder, M. (1976) Etude cytochimique et ultrastructurale de l'évolution ovocytaire du crabe *Eriocheir sinensis*. II. Ovogenèse après ablation des pédoncules oculaires. Arch. Biol., **87**: 283–302.
- 348 Gohar, M. and Souty, C. (1984) Action temporelle

- d'ecdystéroïdes sur la synthèse protéique ovarienne in vitro chez le Crustacé isopode terrestre *Porcellio dilatatus* (Brandt). *Reprod. Nutr. Dév.*, **24**: 137–145.
- 349 Meusy, J.-J. and Charniaux-Cotton, H. (1984) Endocrine control of vitellogenesis in Malacostraca Crustaceans. In "Advances in Invertebrate Reproduction. Vol. 3". Ed. by W. Engels, W. H. Clark, Jr., A. Fischer, P. J. W. Olive and D. F. Went, Elsevier, North Holland, pp. 231–241.
- 350 Dunham, P. J. (1978) Sex pheromones in Crustacea. *Biol. Rev.*, **53**: 555–583.
- 351 Salmon, M. (1983) Courtship, mating systems, and sexual selection in decapods. In "Studies in Adaptation, The Behavior of Higher Crustacea". Ed. by S. Rebach and D. Dunham, John Wiley and Sons Inc., pp. 143–169.
- 352 Salmon, M. and Hyatt, G. W. (1983) Communication. In "The Biology of Crustacea. Vol. 7". Ed. by F. J. Vernberg and W. B. Vernberg, Academic Press, New York, pp. 1–40.
- 353 Bauchau, A. (1986) Sex pheromones in Crustacea. In "Advances in Invertebrate Reproduction. Vol. 4". Ed. by M. Porchet, J.-C. Andries and A. Dhainaut, Elsevier Science Publishers, North Holland, pp. 337–343.
- 354 Dahl, E., Emmanuelsen, H. and von Mecklenburg, C. (1970) Pheromone reception in the males of the amphipod *Gammarus duebeni* Lilljeborg. *Oikos*, **31**: 42–47.
- 355 Ducruet, J. (1973) Comportement sexuel spécifique et interspécifique chez les gammarus du groupe *pulex* (Crustacés Amphipodes). *C. R. Acad. Sci. Paris, Sér. D*, **276**: 1037–1039.
- 356 Hartnoll, R. G. and Smith, S. M. (1980) An experimental study of sex discrimination and pair formation in *Gammarus duebenii* (Amphipoda). *Crustaceana*, **38**: 254–264.
- 357 Atema, J. and Engstrom, D. G. (1971) Sex pheromone in the lobster, *Homarus americanus*. *Nature*, London, **232**: 261–263.
- 358 Kamiguchi, Y. (1972) Mating behavior in the freshwater prawn, *Palaemon paucidens*. A study of the sex pheromone and its effect on males. *J. Fac. Sci., Hokkaido Univ., Ser. VI, Zool.*, **18**: 347–355.
- 359 Eales, A. J. (1974) Sex pheromone in the shore crab *Carcinus maenas*, and the site of its release from females. *Mar. Behav. Physiol.*, **2**: 345–355.
- 360 Gleeson, R. A. (1980) Pheromone communication in the reproductive behavior of the blue crab, *Callinectes sapidus*. *Mar. Behav. Physiol.*, **7**: 119–134.
- 361 Teytaud, A. R. (1971) The laboratory studies of sex recognition in the blue crab, *Callinectes sapidus* Rathbun. *Sea Grant Tech. Bull., Univ. Miami Sea Grant Prog.*, **15**: 1–62.
- 362 Salmon, M. and Atsaiades, S. (1968) Visual and acoustic signalling during courtship of fiddler crabs (genus *Uca*). *Am. Zool.*, **8**: 623–639.
- 363 Bliss, D. E. (1979) From sea to tree: Saga of land crab. *Am. Zool.*, **8**: 355–392.
- 364 Hartnoll, R. G. (1969) Mating in the Brachyura. *Crustaceana*, **16**: 161–181.
- 365 Ingle, R. W. and Thomas, W. (1974) Mating and spawning of the crayfish *Austropotamobius pallipes* (Crustacea: Astacidae). *J. Zool., London*, **173**: 525–538.
- 366 Berry, P. F. and Hartnoll, R. G. (1970) Mating in captivity of the spider crab *Pleistacantha moseleui* (Miers) (Decapoda, Majidae). *Crustaceana*, **19**: 214–215.
- 367 Swartz, R. C. (1976) Agonistic and sexual behavior of the Xanthid crab, *Neopanope syi*. *Chesapeake Science*, **17**: 24–34.
- 368 Ameyaw-Akumfi, C. (1987) Mating in the lagoon crab *Cardisoma armatum* Herklots. *J. Crust. Biol.*, **7**: 433–436.
- 369 Berrill, M. and Arsenault, M. (1982) Mating behavior of the green shore crab *Carcinus maenas*. *Bull. Mar. Sci.*, Miami, **32**: 632–638.
- 370 Ducruet, J. (1982) Effets de l'ecdystérone sur la formation de couples et sur la vitellogenèse chez *Gammarus pulex* (L) et *Gammarus fossarum* Koch (Crustacés Amphipodes). *Pol. Arch. Hydrobiol.*, **29**: 307–317.
- 371 Takayanagi, H., Yamamoto, Y. and Takeda, N. (1986) Ovary-stimulating pheromone in the freshwater shrimp, *Paratya compressa*. *J. Exp. Zool.*, **240**: 201–207.
- 372 Hartnoll, R. G. and Smith, S. M. (1979) Pair formation in the edible crab (Decapoda, Brachyura). *Crustaceana*, **36**: 23–28.
- 373 Kamiguchi, Y. (1972) A histological study of the "sternal gland" in the female freshwater prawn, *Palaemon paucidens*, a possible site of origin of the sex pheromone. *J. Fac. Sci. Hokkaido Univ., Ser. VI, Zool.*, **18**: 356–365.
- 374 Seifert, P. (1982) Studies on the sex pheromone of the shore crab, *Carcinus maenas*, with special regard to ecdysone secretion. *Ophelia*, **21**: 147–158.
- 375 Gleeson, R. (1982) Morphological and behavioral identification of the sensory structures mediating pheromone reception in the blue crab, *Callinectes sapidus*. *Biol. Bull.*, **163**: 162–171.
- 376 Gleeson, R. A., Adams, M. A. and Smith, A. B. (1987) Hormonal modulation of pheromone-mediated behavior in a crustacean. *Biol. Bull.*, **172**: 1–9.
- 377 Jassem, W., Mocquard, J.-P. and Juchault, P. (1982) Déterminisme de la reproduction saisonnière des femelles d'*Armadillidium vulgare* Latr.

- (Crustac, Isopode, Oniscoïde). IV. Contribution à la connaissance de la perception du signal photopériodique induisant l'entrée en reproduction: mode de discrimination entre le jour et la nuit; longueurs d'onde actives. Ann. Sci. Nat. Zool., Paris, **4**: 85-90.
- 378 Zerbib, C. and Mustel, J.-J. (1984) Incorporation de la vitellogénine tritiée dans les ovocytes du Crustacé Amphipode *Orchestia gammarellus* (Pallas). Int. J. Invertebr. Reprod. Dev., **7**: 63-68.
- 379 Ryan, E. P. (1966) Pheromone: evidence in a decapod crustacean. Science, **151**: 340-341.
- 380 Gleeson, R. A., Adams, M. A. and Smith, A. B. (1984) Characterization of a sex pheromone in the blue crab, *Callinectes sapidus*: crustecdysone studies. J. Chem. Ecol., **10**: 913-921.

REVIEW

**Control of Prolactin and Growth Hormone
Secretion in Teleost Fishes**

RICHARD S. NISHIOKA, KEVIN M. KELLEY
and HOWARD A. BERN

*Department of Zoology and Cancer Research Laboratory, University of
California, Berkeley, CA 94720, U.S.A.*

INTRODUCTION

In teleost fish, hypothalamic fibers terminate in proximity to adenohypophysial (AH) cells of the pituitary, thereby circumventing a functional median eminence and a hypophysial portal system, structures considered to be both ancient and conservative in vertebrate evolution (see [1-3]). Thus, unlike the situation in most other vertebrates, teleosts have a more or less direct neural control of pituitary function. Although claims for a median eminence-portal system have been made for some teleostean species (see [4, 5]), the existence of such a system is generally considered absent from teleosts [2, 3, 6-8].

Two general classes of hypothalamic nerve fibers innervate the pituitary of all teleosts investigated to date: type A fibers, containing "elementary neurosecretory granules" (115-170 nm granule diameter) and generally considered to be peptidergic, and type B fibers, containing "large granulated vesicles" (45-95 nm granule diameter) and generally considered to be aminergic. A possible third type of hypothalamic fiber, however, is observed in *Oreochromis mossambicus* (tilapia) [9]; these "type C" fibers are similar to type A fibers, but are characterized by granules of intermediate size (90-145 nm granule diameter) with limiting membranes usually separated from the granule core. Type A fibers, because they are commonly observed leading into the neurohy-

pophysis (NH) and pars intermedia (PI) from the preoptic nuclei (PON), are believed to be concerned primarily with the secretion of neurohypophysial octapeptides and the control of the PI, whereas type B fibers, because they are commonly observed emanating from the nucleus lateralis tuberis (NLT) and ending in synaptic contact with the secretory cells of the pars distalis (PD), are believed to be more closely involved in the control of the PD [2, 6]. Type C fibers of tilapia are observed regularly in the hypothalamus and neurohypophysis, but no physiological function can be attributed to these fibers on the basis of morphological criteria alone [9]. More recently, however, physiological evidence of important peptidergic control of the PD has modified these early views; thus, type A (and possibly in tilapia, type C) control of PD function is considered in this review.

The focus of this review is the control of prolactin (PRL) and growth hormone (GH) secretion in teleosts, with primary emphasis on the tilapia; therefore, the hypothalamus and other parts of the brain will not be extensively discussed except as they relate directly to the material presented herein (for earlier reviews and articles of neural control of teleost adenohypophysial function, see [2-4, 6, 10-13]). Briefly, many different hypothalamic nuclei exist in teleosts, a number of which may be important in the control of AH function. Two nuclei previously mentioned have been particularly well studied: the PON and the NLT. The PON occurs in tilapia as layers of neurons alternating with layers of axonal processes

lying above the optic chiasma; in general, the cells of the PON are type A and can be divided into two groups, a ventral pars parvocellularis and a dorsal pars magnocellularis. Axonal processes from the PON converge mid-ventrally, progress along the NLT region into the pituitary, and become a part of the NH [2, 11, 13, 14]. The NLT, on the other hand, is usually present in teleosts as a pair of structures lying adjacent to the anterior and lateral regions of the base of the infundibular stalk from which, most commonly, type B fibers run in a main tract alongside type A (PON) fibers into the NH [1, 2, 10, 11, 14].

ANATOMICAL ASPECTS

The degree of directness of hypothalamic innervation of pituitary cells varies in the different regions of the pituitary, as well as among teleosts. In the case of the tilapia rostral pars distalis (RPD), hypothalamic fibers do not leave the NH but instead terminate on an adjacent basement

membrane (see [15, 16]). Similar observations have been made on *Fundulus heteroclitus* [17] and on *Carassius auratus* [18, 19]. As a consequence of this anatomical arrangement, chemical information from the brain must pass through the basement membrane, a layer of stellate cell processes, and also the adrenocorticotrophic hormone (ACTH) cells surrounding the neurohypophysial processes [15] (Fig. 1). Because of their direct contact with PRL cells, stellate cells and their processes may be involved directly in information transfer; perhaps stellate cells modulate movement of neurohormonal factors from the neurohypophysial nerve endings to the PRL cells located several cell layers away. The stellate cells may be equivalent to the tanycytes that link the third ventricle with the NH [20]. The role of the intervening layer of ACTH cells in information transfer, if any, is unknown, but a paracrine role for one or more proopiomelanocorticotropin products is possible (Fig. 1).

The anatomical basis for control of GH secre-

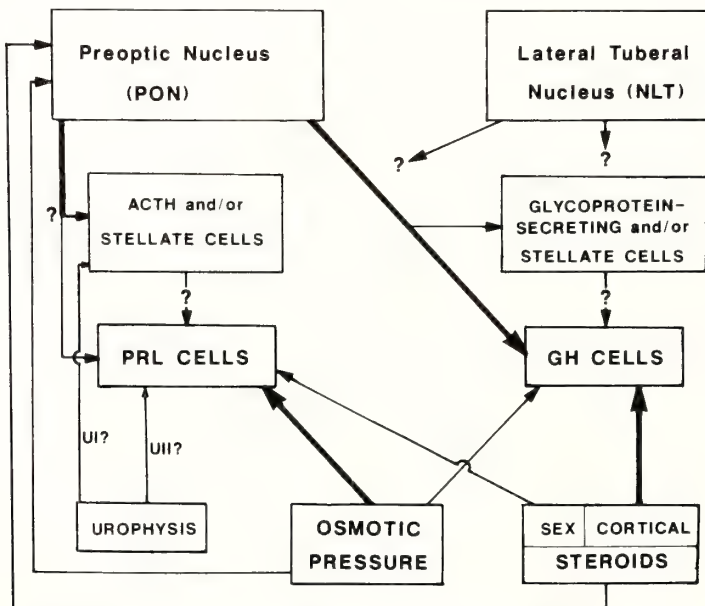


FIG. 1. Pathways for the control of PRL and GH secretion in tilapia. Thick lines (arrows) denote important pathways of control and thin lines indicate pathways of less importance. Question marks denote possible "paracrine" influences and less certain pathways. UI is a CRF-like peptide with possible influence on ACTH cells. UII shares an important tripeptide sequence with somatostatin and inhibits PRL but not GH secretion.

tion in tilapia parallels that for PRL. Unlike the indirect innervation seen in PRL cells, however, ultrastructural observations of the proximal pars distalis (PPD) indicate direct aminergic and peptidergic innervation of the GH cells by hypothalamic fibers [9] (Fig. 1). Fiber types A and B (and C?) are in close proximity to GH cells and often show synaptoid contacts; in addition, some appear to be in direct apposition to the cells of the PPD and PI [21].

Patterns of innervation similar to tilapia's, but with expected species differences, have been described for the goldfish (*C. auratus*) [18, 19], the killifish (*F. heteroclitus*) [17], the medaka (*Oryzias latipes*) [22], the molly (*Poecilia latipinna*) [20, 23], the longjawed mudsucker (*Gillichthys mirabilis*) [15], and the mullet (*Mugil cephalus*) [24].

In less advanced teleosts, such as eels and salmonids, there are noticeable differences in the innervation of the AH. In the European eel (*Anguilla anguilla*), the AH and NH are separated by a basement membrane as in other teleosts, but the penetration of the NH into the AH is not so extensive as is observed in the tilapia, the molly, and other more advanced teleosts, especially in the region of the PPD [2]. Furthermore, control of the PD is reported to be at least partially exerted via hypothalamic nerve endings on hypothalamic arteries in the rostral NH leading to the PD in the Atlantic salmon, *Salmo salar* [25] and brook trout, *Salvelinus fontinalis* [4].

Thus, although teleosts have in common a similar scheme for communication between the brain and the pituitary secretory cells (via direct innervation), there is much variation in the scheme among members of the vast taxonomic grouping termed "Teleostei".

HYPOTHALAMIC CONTROL

Early studies of pituitary transplantations that suggested control of PRL secretion in teleosts by a hypothalamic PRL release-inhibiting factor (PIF) (see [5, 10, 21, 26–29]), and other investigations that demonstrated a direct hypothalamic innervation of the teleost PD [2, 9, 15, 24, 30], prompted interest in the nature of hypophysiotropic factors operating in the hypothalamo-hypophysial area in

teleosts [31]. Indeed, many factors have now been implicated in the control of teleost PD function.

Aminergic factors

The role of catecholamines, especially dopamine (DA), in the control of pituitary function in vertebrate tetrapods is well documented; in fact, DA is considered by many to be the vertebrate PIF (cf. [32]). In teleosts, however, the nature of the innervation of the pituitary by aminergic fibers has been unclear. Initial studies described type B fibers either directly innervating the PRL cells in *G. mirabilis* [15, 33] and in *P. latipinna* [20] or ending on the adjacent membrane of the NH in tilapia [15]. However, when the formaldehyde-induced fluorescence technique for monoamines (a definitive method for the identification of catecholaminergic material [34]) is applied to the pituitary of tilapia [9] and *G. mirabilis* [35], none of the type B fibers initially observed in the NH fluoresces positively. Thus, in tilapia, *G. mirabilis*, and possibly other species, catecholamines appear to be absent from the pituitary. In *C. auratus*, however, using ³H-DA, type B fibers have been demonstrated going to and in close apposition to the basement membrane [36], a result supported by studies using a specific antibody against DA [37]. DA antiserum has also been used on the cyprinodont, *Cynolebias whitei*, to demonstrate DA-ergic fibers in the NH [38]. Furthermore, Halpern-Sebold *et al.* [39] have detected tyrosine hydroxylase-immunoreactivity in the hypothalamus and pituitary of *Xiphophorus maculatus*, particularly in the PRL cells. Serotonin, on the other hand, although not observed in fibers in the pituitary of *P. latipinna* using autoradiographic techniques [40], has not been demonstrated in the pituitary of *C. whitei* using serotonin antiserum [38].

Studies of the actions of aminergic factors on PRL secretion using physiological and pharmacological agents *in vitro* have demonstrated effects of DA, serotonin and adrenalins in various teleost species. An inhibitory effect of DA on PRL release is reported in the tilapia [41, 42], *P. latipinna* [23, 43], *G. mirabilis* [41], *C. auratus* [44], *A. anguilla* [45, 46], and *Salmo gairdneri* [47, 48]. In addition, endogenous levels of catechol-

amine presumably act to inhibit PRL secretion from the pituitary gland autotransplanted into the anterior chamber of the eye of *P. latipinna* [49]. Pharmacological agents that affect dopaminergic systems, as well as DA precursors, have been tested in various teleosts and have the expected actions based on mammalian studies; these agents (ergocryptine, 6-hydroxydopamine, L-dopa, reserpine, and various receptor antagonists) and their actions in teleosts are listed in Table 1. Serotonin, on the other hand, is stimulatory to PRL secretion *in vitro* in *S. gairdneri* [48] and in *A. japonica* [50]; in addition, injection of 5-hydroxytryptophan, a serotonin precursor, appears to activate PRL cells in the same species [48, 51]. Furthermore, the intraperitoneal injection of pargyline, a monoamine oxidase inhibitor, results in elevated brain serotonin concomitant with increased pituitary

PRL levels in *C. auratus* [52]. In contrast, parachlorophenylalanine, a tryptophan hydroxylase inhibitor, reduces hypothalamic serotonin content in *A. anguilla* [53] and in *S. gairdneri* [54]. The few studies on the role of adrenalin in the control of teleost PRL secretion are apparently contradictory. In *C. auratus*, epinephrine and norepinephrine increase adenylate cyclase activity in PD homogenates [55]. In *P. latipinna*, however, phenylephrine (α -adrenergic agonist) and isoproterenol (β -adrenergic agonist) inhibit PRL secretion *in vitro*; furthermore, the adrenergic blocking agents phentolamine and propranolol have no direct effect on PRL secretion, but oppose DA inhibition of PRL secretion *in vitro* [43].

Aminergic control of GH secretion in teleosts has received relatively little attention. In contrast to its inhibitory effect on PRL secretion, DA

TABLE 1. Factors affecting the dopaminergic control of prolactin secretion

Species	Dopamine	L-Dopa	Ergo-cryptine	Reserpine	6-HODA	Receptor antagonist
<i>Anguilla anguilla</i>						
45*		—	—		+	
140				?		
141		—				
142			—			
<i>Gillichthys mirabilis</i>						
41		—		+	+	
143				+		
<i>Heteropneustes fossilis</i>						
144				+		
<i>Mugil platanus</i>						
145				+	+	
<i>Poecilia latipinna</i>						
43	—					+
146		—			+	+
147			—			
<i>Salmo gairdneri</i>						
47	—					
48	—	—				+
<i>Oreochromis mossambicus</i>						
41	—					
42	—					
148					+	
<i>Xiphophorus helleri</i>						
147			—			

* Numbers under species names are references.

appears to be stimulatory to GH secretion in *C. auratus*; by using various agents administered intraperitoneally and intraventricularly, Chang *et al.* [56] have shown that DA may act centrally to stimulate GH secretion. Wigham *et al.* [43], however, report an *in vitro* inhibition of secretion of the putative GH in *P. latipinna* by DA, although this inhibition is not opposed by the specific DA antagonist 3, 4-dimethylphenylethylamine. Norepinephrine, on the other hand, may act directly to inhibit GH secretion in *C. auratus* [56]. In *P. latipinna*, however, the adrenergic blocker propranolol inhibits GH secretion, whereas phentolamine and other adrenergic pharmacological agents have no *in vitro* effect [43].

Peptidergic agents

The demonstration of a lack of aminergic fluorescence in the hypophysial area of tilapia and *G. mirabilis* raises questions about the nature of the PIF (and/or other factors) in these and other teleosts (see [57]). More recently, a role for somatostatin (SRIF) as an inhibitor of PRL secretion in teleosts has been investigated. By immunocytochemical techniques, SRIF-like material is observed in the brain of the catfish (*Heteropneustes fossilis*) [58] and *S. gairdneri* [59], and can be further localized to the hypothalamus and NH near the PD in *F. heteroclitus*, *G. mirabilis* [60], tilapia [60, 61], *P. latipinna* [62, 63], and in several other freshwater and seawater teleosts [64–67]. In addition, Batten [63] suggests that the SRIF-immunoreactive (IR) fibers in the pituitary of *P. latipinna* appear to correspond to a particular class of type A fibers: “type A2” identified by electron microscopy (EM) [20]. A similar situation exists in tilapia, where the SRIF-IR fibers in the NH appear to correspond well with the distribution of type C fibers as detected by EM.

In addition, immunocytochemical studies of the hypothalamo-hypophysial system following acute changes in environmental salinity offer further evidence for the role of SRIF in control of PRL secretion in tilapia [68]. Preliminary observations indicate that shortterm (up to 3 hr) transfer from SW to FW results in increased SRIF-IR in the cell bodies of the PON and decreased SRIF-IR in the neurohypophysial processes penetrating the RPD.

These observations suggest that transport of SRIF from the PON is inhibited in FW. The reciprocal transfer (FW to SW), on the other hand, is seen to deplete SRIF-IR in the cell bodies of the PON and increase SRIF-IR in the neurohypophysial fibers; furthermore, in SW-transferred tilapia, SRIF-IR is more prominent in the NH, and fibers containing SRIF-IR appear to penetrate the RPD more deeply than in FW-transferred tilapia. SRIF may be the significant PIF in tilapia based on its potent activity *in vitro*.

In tilapia, SRIF is inhibitory to PRL secretion *in vitro* [42, 69, 70], and this inhibitory effect is at least partially independent of any effects of SRIF on PRL synthesis [71]. In *P. latipinna*, SRIF inhibits total and newly-synthesized PRL secretion *in vitro* [72] and reduces synthetic activity of the PRL cells as detected by EM [73]. Coupled with observations on salmonids and eels that indicate less penetration of SRIF-IR hypothalamic fibers into the pituitary [66] as compared with more advanced teleosts, it is interesting that SRIF does not inhibit PRL secretion *in vitro* in *S. gairdneri* [48].

GH secretion is similarly inhibited by SRIF *in vitro* in *Anguilla japonica* [50]. In tilapia, SRIF inhibits GH secretion *in vitro* [70, 74], even in the presence of cortisol which stimulates GH secretion [75]. Helms *et al.* [76] have shown that SRIF is a more effective inhibitor of GH secretion in smaller (*ca.* 60 g) than in larger (*ca.* 120–180 g) tilapia. Using a perfusion system, Marchant *et al.* [77] have shown that SRIF (and SRIF-28) inhibit GH secretion in *C. auratus*; in the same study, however, it was found that catfish pancreatic SRIF-22 has no effect on GH secretion. Furthermore, injection of SRIF lowers plasma GH levels in *C. auratus* [78] as well as in *Oncorhynchus kisutch* [79].

A role for thyrotropin-releasing hormone (TRH) in the hypothalamic control of teleost PRL and GH secretion is supported by recent evidence. In *S. salar sebago*, TRH-IR is observed in the brain and pituitary [80]. TRH stimulates PRL secretion *in vitro* in *A. japonica* [50]. In *P. latipinna*, TRH stimulates PRL secretion *in vitro*, even in a hyperosmotic medium [72], and evidence of increased synthetic activity is observed by EM

[73]. Similarly, Prunet and Gonnet [81] have shown that TRH stimulates PRL secretion *in vitro* in a dose-dependent manner in *S. gairdneri*. Barry and Grau [82] have observed a stimulation of PRL secretion *in vitro* by TRH from pituitaries pretreated with 17β -estradiol. James and Wigham [48] have not observed an *in vitro* effect of TRH on PRL secretion in *S. gairdneri*; however, P. Prunet and F. Gonnet (personal communication) have shown that the addition of a protease inhibitor (e.g., Bacitracin) to the incubation medium prevents breakdown of TRH, allowing TRH to stimulate PRL secretion in a dose-related fashion in the same species.

The *in vitro* effects of vasoactive intestinal polypeptide (VIP) and peptide histidine isoleucine (PHI) have recently been examined in tilapia [83]. VIP and PHI are potent stimulators of PRL secretion in tetrapods *in vivo* and *in vitro* (cf. [84]), including in an amphibian [85]. In tilapia, however, the first non-tetrapod species in which VIP and PHI have been tested, both VIP and PHI inhibit PRL secretion *in vitro*; these two peptides have no effect, however, on GH secretion. Preliminary immunocytochemical observations suggest a moderate amount of VIP-IR, but no definitive PHI-IR, in the hypothalamo-hypophysial area of tilapia (R. S. Nishioka *et al.*, unpublished; see [83]). Such a discordant pattern of secretion between fish and mammal is not readily explainable, and studies are being conducted presently to gain some understanding of this phenomenon.

In tilapia, other peptide factors have been investigated for their *in vitro* effect on PRL and/or GH secretion. Urotensin II (UII), a dodecapeptide showing sequence similarity to SRIF (sharing an important tripeptide, Phe-Trp-Lys), inhibits PRL secretion, but does not have any significant effect on GH secretion [69, 70]. Recently, Kewish *et al.* (personal communication) have determined that growth hormone-releasing hormone (GHRH) stimulates GH release.

Peptidergic factors of potential importance in the control of teleost PRL and GH secretion are suggested by some immunocytochemical and other studies. Studies on gonadotropin-releasing hormone (GnRH; LHRH) in teleosts, for example, suggest a potentially important role for GnRH. In

S. gairdneri, immunoreactive GnRH is observed within telencephalic perikarya and in fibers passing to the pituitary stalk [86], whereas in *P. latipinna*, GnRH-IR fibers are observed in the NH leading toward and contacting the gonadotropes in the PPD [63] where GH cells are nearby. Similarly, Kah *et al.* [87] have detected GnRH-IR fibers going to the PPD of *C. auratus*. These anatomical studies of GnRH have prompted our interest in the potential effect of GnRH on tilapia PRL and GH secretion. Furthermore, inasmuch as gonadotropin-associated peptide (GAP), a segment of the GnRH precursor, belongs to the same family of peptides as VIP and PHI [84], we have begun investigation of the effects of this peptide (and some of its cleavage products) using our *in vitro* system (J. Planas *et al.*, unpublished). Corticotropin-releasing factor (CRF), as well, is observed in areas suggestive of a possible relation to PRL or GH secretion. In *C. auratus* and *Cyprinus carpio*, CRF-IR perikarya are observed in the PON and PVN, with fibers from them leading to the pituitary and ending anterior to the ACTH cells of the RPD [67]; the possibility of the intermingled PRL cells of the RPD being affected by such an innervation is suggested. Similar distributions of CRF-IR have been observed in *S. gairdneri* [88, 89] and *P. latipinna* [63]. Combined with the fact that some teleosts are known to secrete PRL while under stress (P. Prunet and M. Avella, personal communication), these CRF immunocytochemical data make further *in vitro* work desirable. Furthermore, urotensin I, a CRF-like peptide from the fish caudal neurosecretory system, and possibly also associated with the family of substances that includes VIP and PHI [84], is another conceivably important peptide factor, as there are claims for its presence in the brain in *Catostomus commersoni* [90]. Finally, in *P. latipinna*, fibers immunoreactive for the two neurohypophysial octapeptides, arginine vasotocin and isotocin, originate from separate preoptic perikarya and end near all AH cell types (except PRL cells) [63]; the possible interaction between neurohypophysial octapeptides which stimulate ACTH secretion *in vitro* in *C. auratus* [91], and the secretion of PRL and GH, is unknown in teleosts. Thus, several peptide factors of potential importance in the control of

teleost PRL and GH secretion merit further study.

EXTRAHYPOTHALAMIC CONTROL

In addition to hypothalamic factors, various extrahypothalamic factors also appear to control PRL and GH secretion in teleosts (see [3, 92–94]). These factors, which include medium osmotic pressure, sex steroids, corticosteroids and thyroid hormones, also appear to modulate the control of PRL and GH secretion.

Osmotic factors

In a pioneering study, Pickford and Phillips [95] demonstrated the important role of PRL in FW osmoregulation; subsequent investigations on numerous species of teleosts have substantiated the importance of PRL in FW adaptation (see [28, 92, 96–98]). There is general consensus that low osmotic pressure, characteristic of FW, is an important factor stimulating PRL secretion in euryhaline teleosts. Osmotic pressure and PRL secretion *in vivo* and *in vitro* are inversely related (Table 2).

The salmonids present an exceptional group

regarding the control of PRL secretion by osmotic pressure. In some salmonid species, it is difficult to demonstrate a direct relationship between osmotic pressure and PRL cell activity *in vitro*, but, in other salmonid species, the typical inverse relationship exists between osmotic pressure and PRL cell activity (Table 3). It has been suggested that this disparity may be due to the differences of the stage of development of the individuals used in a particular study [99]. Upon scrutiny of the studies listed in Table 3, there appears to be a tendency for decreased ability to regulate PRL secretion with advances in development; PRL cells of alevins, parr and smolts are responsive, whereas those of mature fish of some species are less responsive.

In addition, there appear to be differences in responses *in vivo* and *in vitro*. For example, PRL secretion *in vitro* from the PD of adult *O. keta* is unresponsive to variations in medium osmotic pressure [100], whereas plasma levels of PRL respond to changes in osmotic pressure *in vivo* [101]. These studies suggest that some factor in intact *O. keta* (possibly hypothalamic) is absent *in vitro*. On the other hand, Cook and van Over-

TABLE 2. Fishes showing inverse relationship between PRL cell activity and medium osmotic pressure and/or ion concentration

Species	Reference
<i>Anguilla anguilla</i>	105, 107, 108, 109, 149, 150
<i>A. japonica</i>	50, 111
<i>Aphanius dispar</i>	151, 152
<i>Carassius auratus</i>	18, 111, 153
<i>Cichlasoma biocellatum</i>	154
<i>Fundulus heteroclitus</i>	95, 155, 156
<i>Gasterosteus aculeatus</i>	157, 158
<i>Gillichthys mirabilis</i>	21, 41, 159
<i>Lebistes</i> sp.	160
<i>Mugil</i> sp.	30, 161
<i>Oreochromis mossambicus</i>	49, 97, 119, 126, 148, 162, 163, 164
<i>Oryzias latipes</i>	111, 165, 166
<i>Platichthys stellatus</i>	159
<i>Poecilia</i> sp.	20, 49, 107, 150, 168, 169, 170
<i>Tilapia</i> sp.	118
<i>Xiphophorus</i> sp.	171, 172, 173, 174, 175, 176, 177, 178, 179

TABLE 3. Prolactin cell activity at low osmotic pressure in salmonids based on various criteria

Species	Age	Response	Criterion	Reference
<i>Oncorhynchus keta</i> (chum salmon)	adult	+	RIA (plasma)	101
	adult	-	incubation	100
<i>O. kisutch</i> (coho salmon)	alevin	+	cytology	180
	fry	+	cytology	181
	smolt	+	cytology	99
	"yearling"	+	RIA (plasma & RPD)	182, 183
	parr/smolt	+	incubation	182
<i>Oncorhynchus nerka</i> (sockeye salmon)	smolt	-	cytology	114
	smolt	+	RIA (plasma)	103
	adult	-	cytology	102
<i>Salmo gairdneri</i> (rainbow trout)	adult	-	incubation	108
	"yearling"	+	RIA (plasma)	184
	"yearling"	- (?)	incubation	185

beeke [102] and McKeown and Leatherland [103] found no *in vivo* responsiveness in adult *O. nerka* subjected to different osmotic environments.

Thus, although it may be generally true that euryhaline teleosts can respond to osmotic pressure changes by altering PRL secretion, there are some exceptions to this rule among salmonids. Further study of this group is needed, with special attention to various life stages.

The catadromous *A. anguilla* [104-110] and *A. japonica* [100, 111] respond to lower osmotic pressure *in vivo* and *in vitro* by increasing PRL secretion at any stage of development. The anadromous *Gasterosteus aculeatus* has reduced PRL cell activity *in vivo* when exposed to FW containing Ca^{++} and Mg^{++} equal to that of SW [112]. Seasonal differences in PRL cell secretory cycle have been reported by Lam and Leatherland [113].

GH secretion, on the other hand, has received less attention regarding the influence of osmotic pressure. In two salmonid species, *O. nerka* [114] and *O. keta* [115], and in *P. latipinna* [116], there are no detectable changes in GH secretion *in vitro* in response to osmotic pressure changes of the medium. In *S. gairdneri*, however, large shortterm increases in the sodium content of the ambient medium inhibit GH secretion [108]. Similarly, in *A. anguilla*, high sodium medium inhibits and low sodium medium stimulates GH secretion *in vitro* [108]. These results are supported by cytological

studies of the GH cells in *A. anguilla* [104, 110, 117] and *A. japonica* [100, 111]. Furthermore, in two other tilapia species, *Tilapia grahami* and *T. alcalica*, the GH cells appear more active in fish acclimated to FW than in fish from African "soda" lakes [118]. However, Zambrano *et al.* [119] reported no ultrastructural changes in the GH cells of 20-30 g tilapia after transfer from SW to FW. In contrast, Helms *et al.* [76] have observed increased GH secretion *in vitro* in response to increased osmotic pressure in tilapia weighing *ca.* 60 g, but not in larger fish (*ca.* 120 g). The fact that GH has been shown to promote hypoosmoregulatory ability in salmonids (see [120] for references) suggests a possible role for GH in SW osmoregulation in these fish. At present, no generalization on the control of GH secretion by osmotic pressure is possible.

Hormones

Extrahypothalamic factors other than osmotic pressure have also been implicated in the control of PRL and GH secretion. Prolactin itself, by injection or as a result of uninhibited release from transplanted pituitaries, may have an inhibitory effect on *in situ* PRL cells (see [28]). Cortisol, which is believed to be a SW-adapting hormone in some teleosts, inhibits PRL secretion *in vitro* [49] and stimulates GH secretion *in vitro* [75, 76] in tilapia (Fig. 1). In contrast, cortisol is without effect on *in vitro* PRL secretion in *S. gairdneri* [48].

D, L-thyroxine inhibits GH release *in vitro* in *A. anguilla* [108], although triiodothyronine does not have any effects on *in vitro* GH secretion in tilapia ([75]; B. Kewish *et al.*, personal communication). 17β -Estradiol stimulates PRL synthesis [49] and promotes stimulation of secretion of PRL by TRH in tilapia [82]. Estradiol also stimulates PRL secretion in *A. japonica* [100]. In *C. auratus*, treatment of females *in vivo* with synthetic estrogen (ethinylestradiol) [111] or with 17β -estradiol [121] causes an increase in GH cell activity as detected by EM. Similarly, Young and Ball [122] found GH cells in *P. latipinna* strongly activated by 17β -estradiol treatment. B. Kewish *et al.* (personal communication) have recently tested methyltestosterone in male tilapia, and found no effect of this steroid *in vitro*. γ -Amino-n-butyric acid has also been tested in tilapia by Wigham *et al.* [49], and no effect on PRL secretion *in vitro* was observed.

Intracellular mediators

Although increased PRL secretion was once ascribed to a direct effect of low environmental Ca^{++} rather than to low osmotic pressure and/or Na^+ concentration in *G. aculeatus* by Wendelaar Bonga [112] and in tilapia by Wendelaar Bonga and van der Meij [123, 124], these authors subsequently proposed that their earlier conclusions of stimulation of PRL secretion by low cation levels *in vivo* may have resulted from an indirect effect of Ca^{++} concentration on gill permeability [125]. Furthermore, other workers have observed that PRL secretion *in vitro* is independent of physiological Ca^{++} concentration in tilapia [69, 97, 126], in *P. latipinna* [116], in *O. kisutch* [127] and in *S. gairdneri* (L. R. Johnston and T. Wigham, personal communication), provided a minimal level is present. MacDonald and McKeown [127] have found an optimal concentration of Ca^{++} for promoting PRL secretion *in vitro* in *O. kisutch*, and this concentration is roughly equal to the physiological levels of Ca^{++} found in the plasma of *O. nerka* [128].

Evidence for a role of Ca^{++} as an intracellular mediator of teleost PRL secretion is provided by various *in vitro* studies. For example, Taraskevich and Douglas [129] report that spontaneous secre-

tion of PRL from the RPD of the teleost *Alosa pseudoharengus* is associated with action potentials partly mediated by extracellular Ca^{++} . Similarly, exposure of tilapia PRL cells to a depolarizing concentration of K^+ elevates PRL secretion, presumably through the opening of Ca^{++} channels [130]. Further work on tilapia is in accord with these data: exposure of PRL cells to the Ca^{++} ionophore A23187 elicits increased PRL secretion, even in the presence of SRIF [69], and exposure of PRL cells to D600 (an organic Ca^{++} channel blocker), blocks K^+ -induced PRL elevation [130]. Interestingly, D600 does not have much effect on hypoosmotic medium-induced PRL secretion, suggesting that the effects of osmotic pressure on PRL release may be mediated by mechanisms different from those operating during chronic depolarization [130].

The mode of action of Ca^{++} in intracellular mechanisms is unclear, although a few studies suggest some particular roles for Ca^{++} . An action of Ca^{++} distal to its influx through a voltage-regulated channel may occur, as the use of Co^{++} , a competitive inhibitor of Ca^{++} in various calcium-mediated processes [131], suppresses PRL secretion induced by hypoosmotic medium in tilapia [130], as well as by K^+ -depolarizing medium (N. H. Richman and E. G. Grau, personal communication). On the other hand, *in vitro* exposure of the pituitary to chlorpromazine, a drug that may act on a Ca^{++} gate involving phosphatidyl inositol turnover [132–134] and that stimulates PRL secretion in mammals [135], simultaneously stimulates ^3H -PRL secretion and decreases $^{45}\text{Ca}^{++}$ accumulation in the coho salmon pituitary [136].

Post-receptor mechanisms utilizing the second messenger cAMP have been studied in teleost PRL cells by various groups. In tilapia, PRL secretion *in vitro* is stimulated by treatment with dibutyryl cyclic AMP (db-cAMP) alone, with 3-isobutyl-1-methylxanthine (IBMX, a phosphodiesterase inhibitor) alone, or with a combination of the two [69]. In *S. gairdneri*, db-cAMP stimulates both synthesis and release of PRL *in vitro* [47] and, in *O. kisutch*, db-cAMP stimulates synthesis, but not secretion, of PRL *in vitro* [136]. Similarly, L. M. H. Helms *et al.* (personal com-

munication) have stimulated PRL release with forskolin (adenylate cyclase stimulator) in tilapia, and L. R. Johnston and T. Wigham (personal communication) have demonstrated in *S. gairdneri* a db-cAMP stimulation of PRL synthesis, but not release, as well as a forskolin stimulation of PRL secretion and cAMP production. Recently, in preliminary studies on the striped bass (*Morone saxatilis*) in our laboratory, 8-bromo-cAMP, IBMX, and forskolin have proven to be equally stimulatory on PRL secretion *in vitro* (R. S. Nishioka *et al.*, unpublished).

A relationship between Ca^{++} and the adenylate cyclase-cAMP system, thought to possibly operate via Ca^{++} /calmodulin-induced cAMP formation [137-139], has not been studied directly in teleosts. However, MacDonald and McKeown [136] report a net $^{45}Ca^{++}$ accumulation in *O. kisutch* RPD tissue treated with db-cAMP, and Grau *et al.* [69] can reverse SRIF inhibition of PRL secretion by treatment with A23187, a calcium ionophore; thus, these studies suggest a relationship between Ca^{++} and cAMP, possibly via calmodulin, meriting further investigation.

PERSPECTIVES

As stated earlier, neuronal processes from the hypothalamus do not directly contact the PRL cells in tilapia. Generally, a layer of ACTH and stellate cell processes is interposed. It is possible that both these cell types play a "paracrine" role in stimulus transmission (Fig. 1). Since stellate cells with slender processes are closely apposed to PRL cells throughout the RPD of freshwater tilapia, their paracrine involvement could be substantial. Indeed, stellate cells with prominent processes stand out among the condensed PRL cells (under maximal inhibition) in seawater-adapted tilapia. Stellate cells and gonadotropic/thyrotropic cells could play a similar role in regard to GH secretion (Fig. 1).

The diversity of factors controlling PRL and GH secretion and release in tilapia and other teleosts is apparent in this review. It is possible that some of these molecules may have coincidental structural similarities in minor amino acid sequences and/or spatial configuration that may "fit" a particular

receptor. If this be true, then a substance foreign to the organism may cause a response in a fashion indistinguishable from that of a bonafide agent. Currently, many substances have been found to have inhibitory or stimulatory activity, but it is unlikely that all of these compounds originate from the hypothalamus of a teleost. On the other hand, redundancy of control may be built into these systems to allow separate maintenance of osmoregulatory, reproductive, and other physiological pathways.

The continued utilization of isolated RPD and PPD of teleosts in general for *in vitro* studies offers many advantages. PRL cells in the RPD and GH cells in the PPD are segregated into nearly homogeneous masses which are easy to dissect and convenient for use in incubation (or perfusion). These cell masses can be dissociated to provide uniform cell populations for a variety of studies. In addition, the secretory activity of PRL cells and some GH cells can be manipulated simply by altering the tonicity of the medium, thus facilitating the analysis of inhibitory and stimulatory control.

ACKNOWLEDGMENTS

We thank Professor Tetsuya Hirano and Dr. E. Gordon Grau for their helpful critique of this manuscript. Ms. L. M. H. Helms and Drs. P. Prunet, N. H. Richman and T. Wigham generously provided unpublished information for inclusion in this review. Support by the National Science Foundation (DCB 84-05249), by NOAA, National Sea Grant Program, Department of Commerce, under grant number NA80AA-D-00120, through the California Sea Grant College Program, and by the California State Resources Agency, project number R/F-101, has been essential to the research from our laboratory reported in this survey. The U.S. Government is authorized to reproduce and distribute for governmental purposes.

REFERENCES

- 1 Knowles, F. G. W. and Vollrath, L. (1966) *Phil. Trans. R. Soc. London, B*, **250**: 329-342.
- 2 Holmes, R. L. and Ball, J. N. (1974) *The Pituitary Gland: A Comparative Account*. Cambridge Univ. Press, London, pp. 1-397.
- 3 Ball, J. N. (1981) *Gen. Comp. Endocrinol.*, **44**: 135-170.

- 4 Henderson, N. E. (1969) *Gen. Comp. Endocrinol.*, **12**: 148–153.
- 5 Peter, R. E. (1973) *Am. Zool.*, **13**: 743–755.
- 6 Zambrano, D. (1972) *Gen. Comp. Endocrinol., Suppl.* **3**: 21–31.
- 7 Zambrano, D., Nishioka, R. S. and Bern, H. A. (1972) In “Brain-Endocrine Interaction. Median Eminence: Structure and Function”. Ed. by K. M. Knigge, D. E. Scott and A. Weindl, Karger, Basel, pp. 50–66.
- 8 Schreibman, M. P., Leatherland, J. F. and McKeown, B. A. (1973) *Am. Zool.*, **13**: 719–742.
- 9 Bern, H. A., Nishioka, R. S. and Nagahama, Y. (1974) In “Recherches Biologiques Contemporaines”. Ed. by L. Arvy, Imprimerie Vagner, Nancy, pp. 170–194.
- 10 Ball, J. N. and Baker, B. I. (1969) In “Fish Physiology”, Vol. 2. Ed. by W. S. Hoar and D. J. Randall, Academic Press, New York, pp. 1–110.
- 11 Perks, A. M. (1969) In “Fish Physiology”, Vol. 2. Ed. by W. S. Hoar and D. J. Randall, Academic Press, New York and London, pp. 111–205.
- 12 Peter, R. E. (1970) *Gen. Comp. Endocrinol.*, **14**: 334–356.
- 13 Dodd, J. M., Follett, B. K. and Sharp, P. J. (1971) In “Advances in Comparative Physiology and Biochemistry”. Ed. by O. Lowenstein, Academic Press, New York, Vol. 4, pp. 113–223.
- 14 Haider, S. and Sathyanesan, A. G. (1972) *Acta Anat.*, **81**: 202–208.
- 15 Bern, H. A., Zambrano, D. and Nishioka, R. S. (1971) In “Memoirs of the Society for Endocrinology”, No. 19. Ed. by H. Heller and K. Lederis, Cambridge Univ. Press, London and New York, pp. 817–822.
- 16 Sage, M. and Bern, H. A. (1971) *Int. Rev. Cytol.*, **31**: 339–376.
- 17 Betchaku, T. and Douglas, W. W. (1980) *Anat. Rec.*, **198**: 595–609.
- 18 Leatherland, J. F. (1972) *Can. J. Zool.*, **50**: 835–844.
- 19 Kaul, S. and Vollrath, L. (1974) *Cell Tissue Res.*, **154**: 231–249.
- 20 Batten, T. F. C. and Ball, J. N. (1977) *Cell Tissue Res.*, **185**: 409–433.
- 21 Nagahama, Y., Nishioka, R. S. and Bern, H. A. (1974) *Gen. Comp. Endocrinol.*, **22**: 21–34.
- 22 Aoki, K. and Umeura, H. (1970) *Endocrinol. Japon.*, **17**: 45–56.
- 23 Batten, T. F. C. and Ball, J. N. (1984) In “Current Trends in Comparative Endocrinology”, Vol. 1. Ed. by B. Lofts and W. N. Holmes, Hong Kong Univ. Press, Hong Kong, pp. 69–72.
- 24 Abraham, M. (1974) *Gen. Comp. Endocrinol.*, **24**: 121–132.
- 25 Fridberg, G. and Ekengren, B. (1977) *Can. J. Zool.*, **55**: 1284–1296.
- 26 Ball, J. N. (1969) In “Fish Physiology”, Vol. 2. Ed. by W. S. Hoar and D. J. Randall, Academic Press, New York, pp. 207–240.
- 27 Ball, J. N., Baker, B. I., Olivereau, M. and Peter, R. E. (1972) *Gen. Comp. Endocrinol., Suppl.* **3**: 11–21.
- 28 Ensor, D. M. (1978) *Comparative Endocrinology of Prolactin*. Chapman & Hall, London.
- 29 Ball, J. N., Batten, T. F. C. and Young, G. (1980) In “Hormones, Adaptation and Evolution”. Ed. by S. Ishii, T. Hirano and M. Wada, Japan Sci. Soc. Press, Tokyo/Springer-Verlag, Berlin, pp. 45–56.
- 30 Abraham, M. (1971) *Gen. Comp. Endocrinol.*, **17**: 334–350.
- 31 Crim, J. W., Dickhoff, W. W. and Gorbman, A. (1978) *Am. Zool.*, **18**: 411–424.
- 32 Ben-Jonathan, N. (1985) *Endocrine Rev.*, **6**: 564–589.
- 33 Zambrano, D. (1970) *Z. Zellforsch.*, **110**: 496–516.
- 34 Falck, B. (1962) *Acta Physiol. Scand.*, **56**, Suppl. 197: 1–25.
- 35 Swanson, D., Nishioka, R. S. and Bern, H. A. (1975) *Acta Zool. Stockholm*, **56**: 225–237.
- 36 Kah, O., Dubourg, P., Chambolle, P. and Calas, A. (1984) *Cell Tissue Res.*, **238**: 621–626.
- 37 Kah, O., Dubourg, P., Onteniente, B., Geffard, M. and Calas, A. (1986) *Cell Tissue Res.*, **244**: 577–582.
- 38 Ruijter, J. M., Steinbusch, H. W. M. and Joosten, H. W. J. (1984) *Neurosci. Letters, Suppl.* **18**: S96.
- 39 Halpern-Sebold, L. R., Margolis-Kazan, H., Schriebman, M. P. and Joh, T. H. (1985) *Proc. Soc. Exp. Biol. Med.*, **178**: 486–489.
- 40 Groves, D. and Batten, T. F. C. (1985) *Cell Tissue Res.*, **240**: 489–492.
- 41 Nagahama, Y., Nishioka, R. S., Bern, H. A. and Gunther, R. L. (1975) *Gen. Comp. Endocrinol.*, **25**: 166–188.
- 42 Wigham, T., Nishioka, R. S. and Bern, H. A. (1977) *Gen. Comp. Endocrinol.*, **32**: 120–131.
- 43 Wigham, T., Ball, J. N. and Ingleton, P. M. (1975) *J. Comp. Physiol.*, **B 104**: 87–96.
- 44 Peter, R. E. and McKeown, B. A. (1975) *Gen. Comp. Endocrinol.*, **25**: 153–165.
- 45 Olivereau, M. (1975) *Gen. Comp. Endocrinol.*, **26**: 550–561.
- 46 Olivereau, M., Aimar, C. and Olivereau, J. M. (1980) *Cell Tissue Res.*, **208**: 389–404.
- 47 McKeown, B. A., Jenks, B. G. and van Overbeeke, A. P. (1980) *Comp. Biochem. Physiol.*, **65B**: 705–709.
- 48 James, V. A. and Wigham, T. (1984) *Gen. Comp.*

- Endocrinol., **56**: 231-239.
- 49 Wigham, T. and Ball, J. N. (1977) *Gen. Comp. Endocrinol.*, **31**: 148-153.
- 50 Suzuki, R., Kishida, M. and Hirano, T. (1985) *Zool. Sci.*, **2**: 974.
- 51 Olivereau, M. and Olivereau, J. (1979) *Cell Tissue Res.*, **196**: 397-408.
- 52 Olcese, J. M., Hall, T. R., Figueroa, H. R. and de Vlaming, V. L. (1979) *Gen. Comp. Endocrinol.*, **38**: 309-313.
- 53 Olivereau, M. (1978) *Cell Tissue Res.*, **191**: 93-99.
- 54 Olcese, J., Figueroa, H., Hall, T. R., Yurgens, P., Kiebzak, G., Meyer, R. and de Vlaming, V. (1981) *Gen. Comp. Endocrinol.*, **43**: 462-466.
- 55 Deery, D. J. (1975) *Gen. Comp. Endocrinol.*, **25**: 395-399.
- 56 Chang, J. P., Marchant, T. A., Cook, A. F., Nahorniak, C. S. and Peter, R. E. (1985) *Neuroendocrinology*, **40**: 463-470.
- 57 Nishioka, R. S., Bern, H. A., Kelley, K. M., Grau, E. G., Rivas, R. and Young, G. (1986) *First Int. Congr. Neuroendocrinol.*, p. 65.
- 58 Vale, W., Ling, N., Rivier, J., Villareal, J., Rivier, C. and Brown, M. (1976) *Metabolism*, **35**: 1491-1494.
- 59 Dubois, M. P., Billard, R., Breton, B. and Peter, R. E. (1979) *Gen. Comp. Endocrinol.*, **37**: 220-232.
- 60 Grau, E. G., Nishioka, R. S., Young, G. and Bern, H. A. (1985) *Gen. Comp. Endocrinol.*, **59**: 350-357.
- 61 King, J. A. and Millar, R. P. (1979) *Endocrinology*, **105**: 1322-1329.
- 62 Batten, T. F. C., Groves, D. J., Ball, J. N., Cambre, M. L., Verdonck, W. A., Ollevier, F. and Vandesande, F. (1985) *Cell Tissue Res.*, **242**: 115-125.
- 63 Batten, T. F. C. (1986) *Cell Tissue Res.*, **244**: 661-672.
- 64 Kah, O., Chambolle, P., Dubourg, P. and Dubois, M. P. (1982) *C.R. Acad. Sci.*, **294**: 519-524.
- 65 Vigh-Teichman, K., Vigh, B., Korf, H. W. and Oksche, A. (1983) *Cell Tissue Res.*, **233**: 319-334.
- 66 Olivereau, M., Ollevier, F., Vandesande, F. and Olivereau, J. (1984) *Cell Tissue Res.*, **238**: 289-296.
- 67 Olivereau, M., Ollevier, F., Vandesande, F. and Verdonck, W. (1984) *Cell Tissue Res.*, **237**: 379-382.
- 68 Nishioka, R. S. (1987) Ph. D. Dissertation, Univ. Tokyo, Japan.
- 69 Grau, E. G., Nishioka, R. S. and Bern, H. A. (1982) *Endocrinology*, **110**: 910-915.
- 70 Rivas, R. J., Nishioka, R. S. and Bern, H. A. (1986) *Gen. Comp. Endocrinol.*, **63**: 245-251.
- 71 Grau, E. G., Ford, C.-A., Helms, L. M. H., Shimoda, S. K. and Cooke, I. M. (1987) *Gen. Comp. Endocrinol.*, **65**: 12-18.
- 72 Wigham, T. and Batten, T. F. C. (1984) *Gen. Comp. Endocrinol.*, **55**: 444-449.
- 73 Batten, T. F. C. and Wigham, T. (1984) *Cell Tissue Res.*, **237**: 595-603.
- 74 Fryer, J. N., Nishioka, R. S. and Bern, H. A. (1979) *Gen. Comp. Endocrinol.*, **39**: 244-246.
- 75 Nishioka, R. S., Grau, E. G. and Bern, H. A. (1985) *Gen. Comp. Endocrinol.*, **60**: 90-94.
- 76 Helms, L. M. H., Grau, E. G., Shimoda, S. K., Nishioka, R. S. and Bern, H. A. (1987) *Gen. Comp. Endocrinol.*, **65**: 48-55.
- 77 Marchant, T. A., Fraser, R. A., Andrews, P. C. and Peter, R. E. (1987) *Reg. Peptides*, **17**: 41-52.
- 78 Cook, A. F. and Peter, R. E. (1984) *Gen. Comp. Endocrinol.*, **54**: 109-113.
- 79 Sweeting, R. M. and McKeown, B. A. (1986) *Can. J. Zool.*, **64**: 2062-2063.
- 80 Jackson, I. M. D. and Reichlin, S. (1974) *Endocrinology*, **95**: 854-862.
- 81 Prunet, P. and Gonnet, F. (1986) *First Int. Congr. Neuroendocrinol.*, p. 114.
- 82 Barry, T. P. and Grau, E. G. (1986) *Gen. Comp. Endocrinol.*, **62**: 306-314.
- 83 Kelley, K. M., Nishioka, R. S. and Bern, H. A. (1988) *Gen. Comp. Endocrinol.*, (in press).
- 84 Said, S. I. (1986) *J. Endocrinol. Invest.*, **9**: 191-200.
- 85 Koiwai, K., Kikuyama, S., Seki, T. and Yanai-hara, N. (1986) *Gen. Comp. Endocrinol.*, **64**: 254-259.
- 86 Goos, H. J. T. and Murathanoglu, O. (1977) *Cell Tissue Res.*, **181**: 163-168.
- 87 Kah, O., Breton, B., Dulka, J. G., Nunez-Rodriguez, J., Peter, R. E., Corrigan, A., Rivier, J. E. and Vale, W. W. (1986) *Cell Tissue Res.*, **244**: 327-337.
- 88 Ollevier, F. and Verdonck, W. (1984) *Gen. Comp. Endocrinol.*, **54**: 433.
- 89 Verdonck, W. and Ollevier, F. (1984) *Gen. Comp. Endocrinol.*, **53**: 436.
- 90 Yulis, C. R., Lederis, K., Wong, K. L. and Fisher, A. W. F. (1986) *Peptides*, **7**: 79-86.
- 91 Fryer, J., Lederis, K. and Rivier, J. (1985) *Reg. Peptides*, **11**: 11-15.
- 92 Clarke, W. C. and Bern, H. A. (1980) In "Hormonal Proteins and Peptides", Vol. 8. Ed. by C. H. Li, Academic Press, New York, pp. 105-197.
- 93 Bern, H. A. (1983) *Am. Zool.*, **23**: 663-671.
- 94 Specker, J. L., Ingleton, P. M. and Bern, H. A. (1984) *Frontiers and Perspectives in Prolactin Secretion: A Multidisciplinary Approach*. Academic Press, New York, pp. 17-30

- 95 Pickford, G. E. and Phillips, J. G. (1959) *Science*, **130**: 454-455.
- 96 Hirano, T. and Mayer-Gostan, N. (1978) In "Comparative Endocrinology". Ed. by P. J. Gaillard and H. H. Boer, Elsevier/North Holland, Amsterdam, pp. 209-212.
- 97 Nicoll, C. S., Wilson, S. W., Nishioka R. S. and Bern, H. A. (1981) *Gen. Comp. Endocrinol.*, **44**: 365-373.
- 98 Loretz, C. A. and Bern, H. A. (1982) *Neuroendocrinology*, **35**: 292-304.
- 99 Nagahama, Y., Clarke, W. C. and Hoar, W. S. (1977) *Can. J. Zool.*, **55**: 183-198.
- 100 Suzuki, R. and Hirano, T. (1987) *Proc. 1st Congr. Asia and Oceania Soc. Comp. Endocrinol.*, pp. 335-336.
- 101 Hirano, T. (1985) *Aquaculture*, **45**: 375-394.
- 102 Cook, H. and van Overbeeke, A. P. (1969) *Can. J. Zool.*, **47**: 937-941.
- 103 McKeown, B. A. and Leatherland, J. F. (1973) *Z. Zellforsch.*, **140**: 459-471.
- 104 Olivereau, M. (1967) *Z. Zellforsch.*, **80**: 264-285.
- 105 Aler, O. M. (1971) *Acta Zool.*, **52**: 145-156.
- 106 Olivereau, M., Lemoine, A. M. and Dimovska, A. (1971) *Ann. Endocrinol.*, **32**: 271.
- 107 Ingleton, P. M., Baker, B. I. and Ball, J. N. (1973) *J. Comp. Physiol.*, **87**: 317-328.
- 108 Baker, B. I. and Ingleton, P. M. (1975) *J. Comp. Physiol.*, **100**: 269-282.
- 109 Benjamin, M. and Baker, B. I. (1978) *Cell Tissue Res.*, **191**: 161-170.
- 110 Hall, T. R. and Chadwick, A. (1978) *Gen. Comp. Endocrinol.*, **36**: 388-395.
- 111 Nagahama, Y. (1973) *Mem. Fac. Fish. Hokkaido Univ.*, **21**: 1-63.
- 112 Wendelaar Bonga, S. E. (1978) *Gen. Comp. Endocrinol.*, **34**: 265-275.
- 113 Lam, T. J. and Leatherland, J. F. (1969) *Gen. Comp. Endocrinol.*, **12**: 385-387.
- 114 Leatherland, J. I. and McKeown, B. A. (1974) *J. Comp. Physiol.*, **89**: 215-226.
- 115 Suzuki, R., Kishida, M., Ogasawara, T., Hasegawa, S. and Hirano, T. (1987) *Gen. Comp. Endocrinol.*, **68**: 76-81.
- 116 Batten, T. F. C., Young, G. and Ball, J. N. (1983) *Gen. Comp. Endocrinol.*, **51**: 113-130.
- 117 Olivereau, M. and Ball, J. N. (1970) *Mem. Soc. Endocrinol.*, **18**: 57-85.
- 118 Leatherland, J. F., Ball, J. N. and Hyder, M. (1974) *Cell Tissue Res.*, **149**: 245-266.
- 119 Zambrano, D., Clarke, W. C., Hajek, A., Sage, M. and Bern, H. A. (1974) *Acta Zool.*, **55**: 202-216.
- 120 Bolton, J. P., Collie, N. L., Kawauchi, H. and Hirano, T. (1987) *J. Endocrinol.*, **112**: 63-68.
- 121 Kaul, S. and Vollrath, L. (1974) *Cell Tissue Res.*, **154**: 211-230.
- 122 Young, G. and Ball, J. N. (1979) *J. Endocrinol.*, **83**: 30P.
- 123 Wendelaar Bonga, S. E. and van der Meij, J. C. A. (1980) *Gen. Comp. Endocrinol.*, **40**: 391-401.
- 124 Wendelaar Bonga, S. E. and van der Meij, J. C. A. (1981) *Gen. Comp. Endocrinol.*, **43**: 432-442.
- 125 Wendelaar Bonga, S. E., Löwik, C. J. M. and van der Meij, J. C. A. (1983) *Gen. Comp. Endocrinol.*, **52**: 222-231.
- 126 Grau, E. G., Nishioka, R. S. and Bern, H. A. (1981) *Gen. Comp. Endocrinol.*, **45**: 406-408.
- 127 MacDonald, D. J. and McKeown, B. A. (1983) *Can. J. Zool.*, **61**: 682-684.
- 128 Copp, D. H. and Ma, S. W. Y. (1981) In "Hormonal Regulation of Calcium Metabolism". Ed. by D. V. Cohn, R. V. Talmage and J. L. Matheus, Excerpta Medica, New York, pp. 298-306.
- 129 Taraskevich, P. S. and Douglas, W. W. (1978) *Nature*, **276**: 832-834.
- 130 Grau, E. G., Shimoda, S. K., Ford, C.-A., Helms, L. M. H., Cooke, I. M. and Pang, P. K. T. (1986) *Endocrinology*, **119**: 2848-2855.
- 131 Thaw, C. N., Geras Raaka, E. and Gershengorn, M. C. (1984) *Am. J. Physiol.*, **247**: C150.
- 132 Thompson, (1980) *The Regulation of Membrane Lipid Metabolism*. CRC Press, Boca Raton, pp. 1-218.
- 133 Michell, R. H. (1982) *Nature*, **296**: 492-493.
- 134 Axelrod, J. and Hirata, F. (1982) *Trends Pharmacol.*, **3**: 156-158.
- 135 Heindel, A. A. and Clement-Cormier, Y. C. (1981) *Endocrinology*, **108**: 310-317.
- 136 MacDonald, D. J. and McKeown, B. A. (1985) *Comp. Biochem. Physiol.*, **80A**: 553-557.
- 137 Sweennen, L. and Deneff, C. (1982) *Endocrinology*, **111**: 398-405.
- 138 Merritt, J. E., MacNeil, S., Tomlinson, S. and Brown, B. L. (1983) *Endocrinology*, **98**: 423-429.
- 139 Schettini, G., Cronin, M. J. and Macleod, R. M. (1983) *Endocrinology*, **112**: 1801-1807.
- 140 Olivereau, M. (1971) *Z. Zellforsch.*, **121**: 232-243.
- 141 Olivereau, M. and Lemoine, A. M. (1973) *C. R. Acad. Sci. Paris*, **276D**: 1325-1327.
- 142 Olivereau, M. and Lemoine, A. M. (1973) *C. R. Acad. Sci. Paris*, **276D**: 1883-1886.
- 143 Sage, M. (1970) *J. Exp. Zool.*, **173**: 121-127.
- 144 Sundararaj, B. I. and Nayyar, S. K. (1969) *Gen. Comp. Endocrinol.*, *Suppl.* **2**: 69-80.
- 145 Zambrano, D. (1975) *Cell Tissue Res.*, **162**: 551-563.
- 146 Wigham, T. and Ball, J. N. (1976) *J. Comp. Physiol.*, **110**: 135-143.
- 147 McKeown, B. A. (1972) *Experientia*, **28**: 675-676.

- 148 Zambrano, D., Clarke, W. C., Hawkins, E. F., Sage, M. and Bern, H. A. (1973/74) *Neuroendocrinology*, **13**: 284-298.
- 149 Olivereau, M. and Lemoine, A. M. (1972) *J. Comp. Physiol.*, **79**: 411-422.
- 150 Olivereau, M. (1966) *Am. Zool.*, **6**: 598.
- 151 Abraham, M., Dinari-Lavie, V. and Lotan, R. (1977) *Cell Tissue Res.*, **179**: 317-330.
- 152 Abraham, M. and Lotan, R. (1974) *Cell Tissue Res.*, **149**: 267-274.
- 153 Leatherland, J. F. (1972) *Can. J. Zool.*, **50**: 835-844.
- 154 Mattheij, J. A. M., Stroband, H. W. J. and Kingma, F. J. (1971) *Z. Zellforsch.*, **118**: 113-126.
- 155 Ball, J. N. and Pickford, G. E. (1964) *Anat. Rec.*, **148**: 358.
- 156 Emmart, E. W., Pickford, G. E. and Wilhelmi, A. E. (1966) *Gen. Comp. Endocrinol.*, **7**: 571-583.
- 157 Leatherland, J. F. (1970) *J. Endocrinol.*, **48**: xxxi-xxxii.
- 158 Leatherland, J. F. (1970) *Z. Zellforsch.*, **104**: 301-317.
- 159 Nagahama, Y., Nishioka, R. S. and Bern, H. A. (1973) *Z. Zellforsch.*, **136**: 153-157.
- 160 Ichikawa, T., Kobayashi, H., Zimmermann, P. and Müller, V. (1973) *Z. Zellforsch.*, **141**: 161-179.
- 161 Olivereau, M. (1968) *Z. Zellforsch.*, **87**: 545-561.
- 162 Dharmamba, M. and Nishioka, R. S. (1968) *Gen. Comp. Endocrinol.*, **10**: 409-420.
- 163 Clarke, W. C. (1973) *Can. J. Zool.*, **51**: 687-695.
- 164 Wendelaar Bonga, S. E., Flik, G., Löwik, C. W. G. M. and van Eys, G. J. J. M. (1985) *Gen. Comp. Endocrinol.*, **57**: 352-359.
- 165 Nagahama, Y. and Yamamoto, K. (1971) *Bull. Jpn. Soc. Sci. Fish.*, **37**: 691-698.
- 166 Utida, S., Hatai, S., Hirano, T. and Kamemoto, F. (1971) *Gen. Comp. Endocrinol.*, **16**: 566-573.
- 167 Ball, J. N. and Olivereau, M. (1965) *Am. Zool.*, **5**: 232-233.
- 168 Hopkins, C. R. (1969) *Tissue and Cell*, **1**: 653-672.
- 169 Ensor, D. M. and Ball, J. N. (1968) *Gen. Comp. Endocrinol.*, **11**: 104-110.
- 170 Ball, J. N. and Ingleton, P. M. (1973) *Gen. Comp. Endocrinol.*, **20**: 312-325.
- 171 Holtzman, S. and Schreiberman, M. P. (1972) *J. Exp. Zool.*, **180**: 187-196.
- 172 Schreiberman, M. P. and Kallman, K. D. (1966) *Gen. Comp. Endocrinol.*, **6**: 144-155.
- 173 Holtzman, S. and Schreiberman, M. P. (1971) *Am. Zool.*, **11**: 653-654.
- 174 Sage, M. (1968) *Gen. Comp. Endocrinol.*, **10**: 70-74.
- 175 Holtzman, S. (1973) Ph. D. Dissertation, City Univ. N. Y.
- 176 Sage, M. (1966) *J. Endocrinol.*, **34**: ix-x.
- 177 Holtzman, S. and Schreiberman, M. P. (1975) *Gen. Comp. Endocrinol.*, **25**: 447-455.
- 178 Holtzman, S. and Schreiberman, M. P. (1975) *Gen. Comp. Endocrinol.*, **25**: 456-461.
- 179 Holtzman, S. and Schreiberman, M. P. (1976) *Gen. Comp. Endocrinol.*, **30**: 234-237.
- 180 Leatherland, J. F. and Lin, L. (1975) *Can. J. Zool.*, **53**: 297-310.
- 181 McKeown, B. A. and Hazlett, C. A. (1975) *Can. J. Zool.*, **53**: 1195-1200.
- 182 Brewer, K. J. and McKeown, B. A. (1980) *J. Comp. Physiol.*, **140**: 217-225.
- 183 McKeown, B. A. and Brewer, K. J. (1978) In "Comparative Endocrinology". Ed. by P. J. Gailard and H. H. Boer, Elsevier/North-Holland Biomedical Press, Amsterdam, pp. 357-362.
- 184 Prunet, P., Boeuf, G. and Houdebine, L. M. (1985) *J. Exp. Zool.*, **235**: 187-196.
- 185 Gonnet, F., Prunet, P., Tonon, M. C., Dubourg, P., Kah, O. and Vaudry, H. (1988) *Gen. Comp. Endocrinol.*, **69**: 252-261.

A Possible Sugar Receptor Protein Found in the Labellum of the Blowfly, *Phormia regina*

MAMIKO OZAKI

*Department of Biology, College of General Education,
Kobe University, Nada, Kobe 657, Japan*

ABSTRACT—Previous physiological studies have suggested the existence of at least three functionally separated receptor sites in the labellar sugar receptor of the fly, called the pyranose (P site), the furanose (F site) and the third sites (T site), and that starch acts as a competitive inhibitor for the P site. I detected in this work a new candidate protein for the P site in the labellar extract by affinity electrophoresis with starch. The dissociation constant of the candidate protein-starch complex was estimated to be 0.7%, a value consistent with the electrophysiological estimate of the inhibition constant for starch on the sugar response. The stimulus sugars for the P site bound to the candidate protein in competition with starch. The dissociation constants of the candidate protein-sugar complexes were highly correlated with the electrophysiological constants defined as the sugar concentrations which give rise to half maximal responses. However, the stimulus sugars for the F site did not compete with starch for the candidate protein. The candidate protein was water insoluble and appeared to be located in the distal process and the cell body, but not in the axon, of the labellar chemosensory cell.

INTRODUCTION

Since the pioneering work of Dastoli and Price [1], repeated attempts have been made to identify sweet-taste receptor molecules in both vertebrates and invertebrates. However, no taste receptor proteins have been definitively identified yet, and biochemical studies on the sense of taste have met with only limited success.

In the fly, many behavioral and electrophysiological studies have suggested that the sugar receptor cell is sensitive to a broad spectrum of chemicals and that it has multiple receptor sites. At least three functionally separate receptor sites have been documented in the sugar receptor cell of the fleshfly [2-4]. They are the pyranose site (P site) sensitive to sucrose, maltose, D-glucose, L-fucose, etc., the furanose site (F site) sensitive to D-fructose, D-fucose, etc., and the third site (T site) sensitive to aliphatic carboxylate anions. As a working hypothesis, the P site was proposed to be identical with an α -glucosidase [5], but some inconsistencies have been reported for the hypothe-

sis [6]. I recently found that starch acts as a competitive inhibitor on the P site [7]*. Therefore, it was possible to detect a new candidate protein for the P site by affinity electrophoresis with starch. In this paper, I report on the identification of the candidate protein based on its affinity for starch or stimulus sugars and its location in the chemosensory cell.

MATERIALS AND METHODS

Sample preparation

Five to seven-day-old blowflies, *Phormia regina*, reared at 20-25°C and fed with 0.1 M sucrose were used. Living flies were anesthetized by cooling on ice, and the labella were cut at the distal end of the proboscis. Two hundred labella so obtained were frozen with a small volume of liquid nitrogen in a hand mortar. After the frozen labella were homogenized for 20 min, the homogenate was suspended in 0.1 ml of sample buffer (4.65 mM sodium barbiturate-HCl, 2% Triton X-100, 10%

glycerol, pH 6.8) and incubated at 4°C for 1 hr. The suspension was centrifuged at 3,000 rpm at 4°C for 10 min, and the supernatant was used as the sample extract. The extract of the proboscis without labellum was prepared in the same way to serve as control. To examine the water soluble fraction, the labellar homogenate was suspended in distilled water, incubated at 4°C for 1 hr, and centrifuged at 50,000 rpm at 4°C for 1 hr. The supernatant was then lyophilized and dissolved in the same buffer.

In addition, the labellum was separated into "labellar content" and the "labellar integument" following the method of Amakawa *et al.* [8]. Labella were gently sonicated, 150–200 at a time, in 5 ml of distilled water with a Tominaga model UR-150P ultrasonicator (25 kw output) on ice for 5 min. Subsequently, 500 "labellar integuments", or cuticle lobes, were collected and washed twice with distilled water. The extract was prepared in the same way as the whole labellum extract. The "labellar contents", which were washed out from the 500 labella into distilled water during sonication, were collected by lyophilization. They were then homogenized with 0.1 ml of sample buffer in a glass homogenizer on ice for 10 min and incubated at 4°C for 1 hr. The supernatant obtained following centrifugation at 3,000 rpm for 10 min was used as the sample extract.

Electron microscopy

For the scanning electron microscopy, whole labella or "labellar integuments" were fixed in 3% glutaraldehyde at 20°C for 1 hr, dehydrated through ethanol series and isoamylacetate, dried at the critical point of CO₂ with a Hitachi model HPC-2 dryer, and coated with gold by spattering with an Eiko model IB-3 ion-coater. They were then observed with Hitachi model S-430 scanning electron microscope.

For the transmission electron microscopy, whole labella or "labellar integuments" were fixed in 3% glutaraldehyde at 20°C for 1 hr and 2% osmium tetroxide on ice for 1 hr, dehydrated through ethanol series and propylene oxide, and embedded in Epon 812 resin. Sections were cut with a Porter-Blum model MT-1 ultramicrotome, double-stained with lead acetate and uranyl acetate

and observed with a Hitachi model H-300 electron microscope.

Affinity electrophoresis

As many different kinds of proteins are present in the blowfly labellum, it was difficult to detect a minor protein such as the sugar receptor protein in one-dimensional electrophoresis. Therefore, two-dimensional polyacrylamide gel electrophoresis, in which an affinity ligand was added to the running gel in the first dimension, was adopted. The gel system was similar to the Ornstein and Davis's stacking system [9, 10], except that Triton X-100 (2% at the final concentration) was added to the stacking (4.5% acrylamide) and running gels (7.5% acrylamide), and barbiturate buffers (stacking gel buffer: 9.3 mM sodium barbiturate-HCl, pH 6.7; running buffer: 91.1 mM sodium barbiturate-HCl, pH 8.9; electrode buffer: 41.1 mM sodium barbiturate-glycine, pH 8.3) were used instead of Tris buffers, which inhibit sugar responses [11]. Proteins were detected by the silver staining method of Oakley *et al.* [12]. The first dimensional electrophoresis was carried out with 10–20 μ l of the sample extract at 3 mA for 100 min in a disc gel (2 mm in diameter, 130 mm in length). The gel was removed into sample buffer, shaken at room temperature (20–25°C) for 1 hr, and loaded onto a slab gel (130×115×1 mm) for the second dimensional electrophoresis, carried out at 30 mA for 250 min. The composition of gels and buffers used in the two electrophoretic runs were similar except for the starch added in the first dimension. To evaluate the affinity of sugars for the candidate protein, stimulus sugar was added to the running gel, together with starch, in the first dimensional electrophoresis. During electrophoreses, the gel temperature measured through the glass tube or plate was 21±2°C, and the pH of the running gel was 9.4 immediately after the run.

Calculation of dissociation constant

Starch is a large polysaccharide molecule with no electric charge, which, when complexed with a protein, greatly retards the mobility of the protein during electrophoresis. Therefore, if the mobility of the protein, m_0 , decreases to m in the presence of starch of concentration $[I]$, the protein-starch

interaction can be expressed by the following equation [13]:

$$m_o/m = 1 + [I]/K_i \quad (1)$$

where K_i is the dissociation constant of protein-starch complex. Thus, the plot of m_o/m against $[I]$ yields a straight line with $[I]$ intercept at $-K_i$. Here the dissociation constant is expressed in % w/v because starch is polydisperse and therefore does not lend itself to the molarity measure.

On the other hand, stimulus sugars for the sugar receptor are much smaller than starch and have no electric charge so that the mobility of the protein-sugar complex is nearly the same as that of the free protein. Therefore, if the mobility, m , of a protein in the presence of starch becomes m' in the presence of both sugar (concentration, $[S]$) and starch (concentration, $[I]$), the protein-sugar interaction is given by the following equation [14]:

$$m'/(m_o - m') = K_i(1 + [S]/K_d)/[I] \quad (2)$$

where K_d is the dissociation constant of protein-sugar complex. Thus, the plot of $m'/(m_o - m')$ against $[S]$ gives a straight line intercepting the $[S]$ axis at $-K_d$. From Eqs. (1) and (2) it may be seen that if m' is equal to m , K_d is infinitely large. This means that the protein-sugar interaction through the starch binding center is negligible. That is, the protein migrates as if the gel contained only starch.

Assay of α -glucosidase

The α -glucosidase activity in the disc gel was assayed with *p*-nitrophenyl α -D-glucopyranoside (α -PNPG) [15]. After the electrophoresis in the first dimension, the disc gel was removed from the glass tube, and the running gel part was divided equally into 19 pieces (5 mm length). Each piece was incubated in the reaction mixture containing 10 mM α -PNPG in 0.5 ml of 0.1 M sodium citrate buffer (pH 6.0). After incubation at 27°C for 1 hr, the reaction was stopped by adding 2 ml of 0.5 M Tris-HCl (pH 9.0), and the absorbance of liberated *p*-nitrophenol was measured at 410 nm with the Shimadzu model UV-202 recording spectrophotometer.

Chemicals

Sucrose, maltose, D-glucose, D-xylose, L-

sorbose and D-fructose were purchased from Wako Pure Chemicals, Osaka, Japan. D- and L-fucose were obtained from Nakarai Chemicals, Ltd., Osaka Japan.

RESULTS

Affinity for starch

When two-dimensional electrophoresis of the labellar extract was carried out without starch, all proteins whose mobilities are different from each other migrated into a diagonal line on the slab gel, because each individual protein in the labellar extract showed the same mobility in the first dimension as in the second (Fig. 1a). When the electrophoresis was carried out with starch in the first dimension, however, a single spot was reproducibly found separated from the diagonal line. Figure 1b, c and d show that the mobility of this protein in the first dimension decreases with increasing concentration of starch in the running gel. In this way, a protein with affinity for starch was easily detected using this system. The values of m_o and m for the protein were directly measured on each gel (see Fig. 2b), and the ratio of mobilities, m_o/m , was plotted against the concentration of starch, $[I]$, to estimate the dissociation constant of the protein-starch complex, K_i , to be 0.7% (Fig. 2). The value is consistent with an electrophysiological estimate of the inhibition constant for starch at the P site of the sugar receptor at $22 \pm 2^\circ\text{C}$, i.e. around 0.6% [7]. The responsiveness of the fly to sugars is stable over a pH range of 3 to 10 [16]. Thus, these electrophoretic and electrophysiological estimates are comparable with each other.

Affinity for sugars

L- and D-fucose stimulate the P and the F sites, respectively [2], though they are neither metabolized in the blowfly [17] nor bind to the membrane-bound α -glucosidase in the blowfly labellum [6]. When electrophoresis was carried out in the presence of both D-fucose and starch, a protein spot was detected almost in the same position (Fig. 3c) as in the presence of starch alone (Fig. 3a). When L-fucose was added instead of D-fucose,

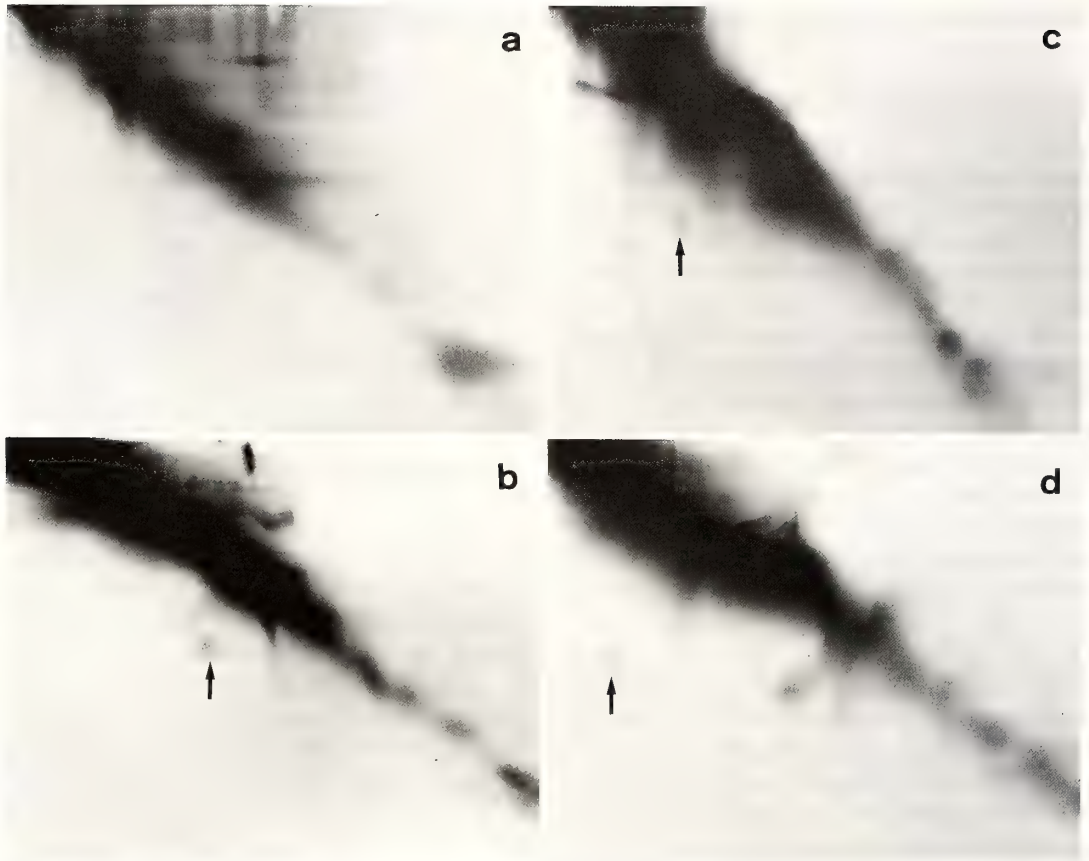


FIG. 1. Two dimensional affinity electrophoresis of the labellar extract: (a), 0%; (b), 0.5%; (c), 1%; (d), 2% starch in the first dimension. In Figs. 1 and 3, the origin of electrophoresis is the upper left-hand corner, and the proteins migrated toward the right and the bottom, respectively, in the first and the second dimensional electrophoreses (see Fig. 2b). The candidate protein spot is indicated by an arrow in each figure.

however, this spot was detected closer to the diagonal line (Fig. 3b). These results indicated that D-fucose did not compete with starch for the protein but L-fucose did. Thus, this protein is a possible sugar receptor molecule for the P site but not for the F site. Moreover, this new candidate protein very likely is different from α -glucosidase, since L-fucose does not bind to α -glucosidase [6]. Figure 4 shows the plot of the ratio $m'/(m_o - m')$ against the concentration $[S]$ of L- (a) and D-fucose (b), respectively. The calculated dissociation constant of the candidate protein-L-fucose complex was 254 mM, while that of the candidate protein-D-fucose complex was infinite.

Some other stimulus sugars for the P site were also examined, and the dissociation constants of

the complexes between the candidate protein and these sugars are listed in Table 1. These dissociation constants were calculated using Eq. (2) in Materials and Methods. For sucrose, maltose, D-glucose and D-fructose, the dissociation constants, K_d , were compared with the mid-point concentrations, K_b , defined as the concentration of stimulus which gives rise to half maximal electrophysiological responses. As seen in Table 1, the dissociation constant was 4-5 fold larger than the mid-point concentration for sucrose, maltose or D-glucose but infinitely larger than that for D-fructose.

Localization of the candidate protein

The water soluble fraction of labellum was

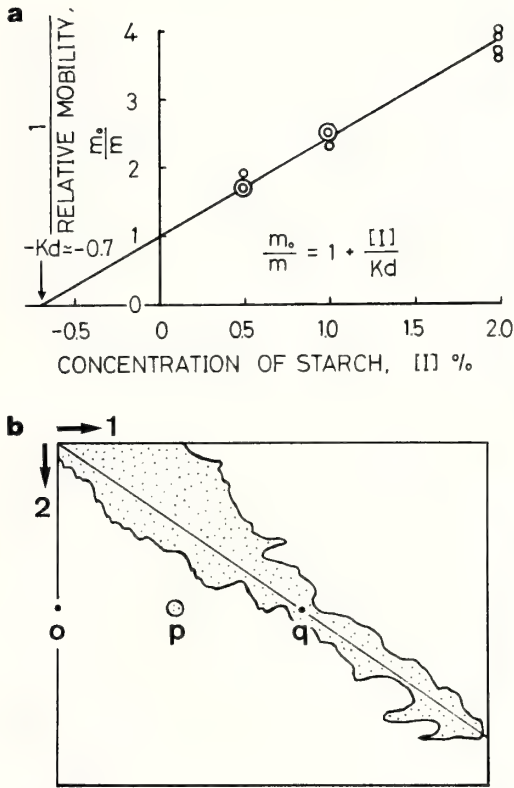


FIG. 2. (a) Determination of the dissociation constant of the candidate protein-starch complex by plotting the reciprocal of the relative mobility of the candidate protein, m_o/m , against the concentration of starch, $[I]$. (b) Illustration for the measurement of m and m_o . In the presence of starch, the candidate protein migrates to the position p . The position to which it would have migrated in the absence of starch, q , is estimated by extending the line op horizontally to the diagonal line defined by the protein stain (dotted area). When the protein stain appeared smeared in the central portion, the diagonal line was defined as that line from the origin of the electrophoresis to some distinguishable spots near the leading front of protein migration. The mobilities, m and m_o , are proportional to the distance op and oq , respectively.

FIG. 3. Comparison of affinity for the candidate protein between L- and D-fucose. (a) same electrophoretic pattern shown in Fig. 1d presented as no sugar control; (b) 0.2 M L-fucose plus 2% starch; (c) 0.2 M D-fucose plus 2% starch in the first dimension.

examined first for the presence of the candidate protein, but the candidate protein was not detected. The extract of the proboscis from which the labellum was removed also yielded negative results. These results suggested that the candidate protein was a labellum specific, membrane-bound protein. I attempted to determine in what part of

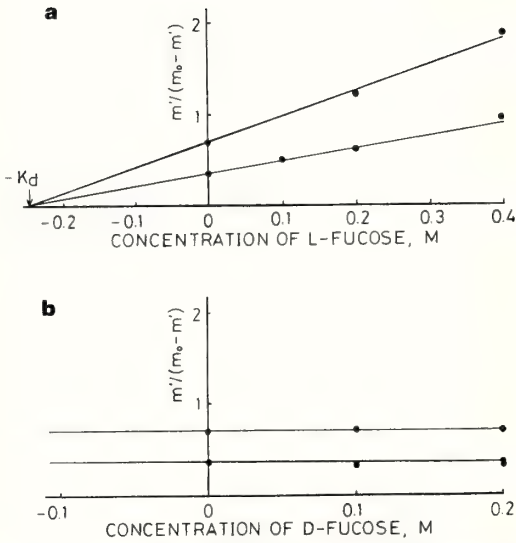


FIG. 4. Determination of the dissociation constant of the candidate protein-sugar complex by plotting $m'/(m_o - m')$ against the concentration of L-fucose (a) and D-fucose (b).

the sensory cell the candidate protein is located. Although the sensillum tip is especially rich in receptor membranes, they are too thin to cut and to collect. Therefore, I attempted to isolate the receptor membranes by sonication. Sonication separated the "labellar integument", which contained the receptor membranes, from the "labellar content", which consisted of the sensory cell bodies, labial nerve, supportive cells and connec-

tive tissues. In the intact labellum, the cell bodies of 4 chemosensory and a mechanosensory cells are surrounded by supportive cells at the base of each chemosensillum, and their axons extend into the labial nerve. In the "labellar integument", however, all these structures were completely removed, exposing the inside surface of the cuticle (Fig. 5a, c). Nevertheless, the chemosensilla were still attached to "labellar integument" preserving the membrane fragments in the inner lumen (Fig. 5d). These membrane fragments were thought to be derived from the distal processes of the chemosensory cells. In both the "labellar content" and the "labellar integument", the candidate protein was detected as a spot separated from the diagonal line, similar to the spot seen in Figure 1. Thus, the candidate protein seemed to be located in both the cell body and the distal process of the sensory cell.

α-Glucosidase

To examine the hypothesis that an α -glucosidase is the P site molecule, I compared the mobility of the α -glucosidase with that of the newly detected candidate protein in disc gel electrophoresis in the presence of varying concentration of starch. The α -glucosidase activity was always found at 30–35 mm from the origin regardless of the presence of starch, while the mobility of the new candidate protein decreased with increasing concentrations of starch (Fig. 6).

TABLE 1. Dissociation constant of candidate protein-sugar complex

Stimulu sugar	Site specificity ¹⁾	$K_d \pm S.D.$ (mM)	Test No.	$K_b \pm S.D.$ ²⁾ (mM)	Test No. ²⁾
sucrose	P	104 ± 25	4	21 ± 10	25
maltose	P	110 ± 20	2	26 ± 6	15
L-fucose	P	254 ± 21	5		
D-glucose	P	360 ± 25	4	83 ± 27	8
L-sorbose	P	575 ± 98	3		
D-xylose	P	1504 ± 596	2		
D-fructose	F	∞	4	53 ± 17	14
D-fucose	F	∞	5		

1): Shimada (1974), 2): Hara (1983)
 ∞, Calculated value is more than 10 M.

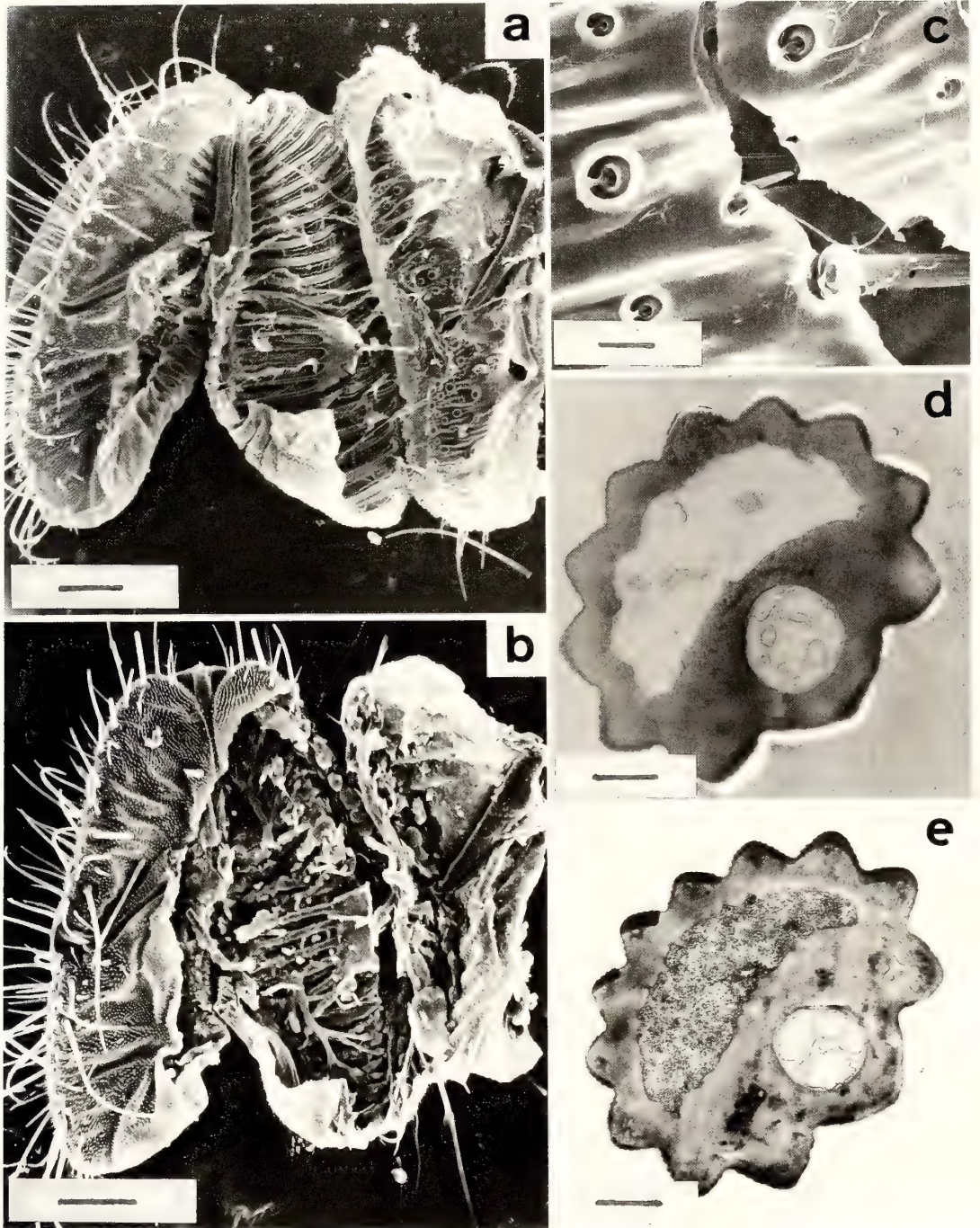


FIG. 5. Electron micrographs of "labellar integument" and intact labellum. (a) and (b), scanning electron micrographs of the internal appearance of labellar lobes of a "labellar integument" and an intact labellum, respectively; (c), scanning electron micrograph of the bases of chemosensilla seen from the inside of a "labellar integument". An attached sensillum can be seen through the crack in the cuticle; (d) and (e), cross sections of chemosensilla of the "labellar integument" and the intact labellum, respectively. Bars indicate 100 μm (a, b), 10 μm (c), and 1 μm (d, e).

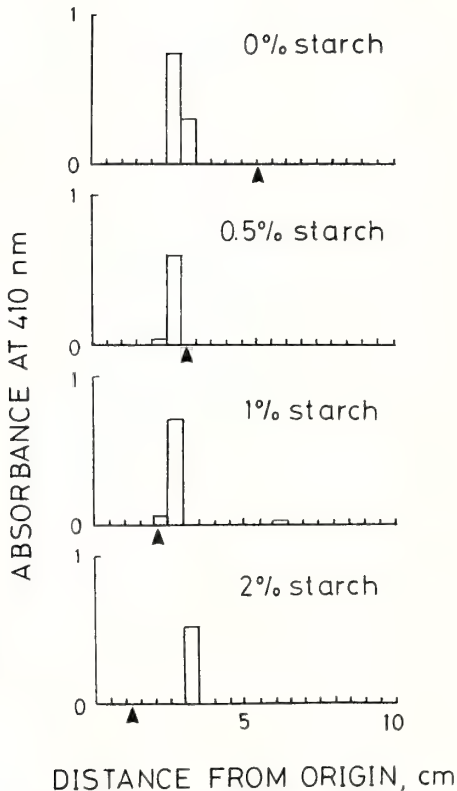


FIG. 6. Localization of α -glucosidase activity in the disc gel used in the first dimension under varying concentrations of starch. The ordinate indicates the α -glucosidase activity determined by the absorbance at 410 nm, and the abscissa shows the distance from the origin in the running gel. The location of the candidate protein in the disc gel was estimated by two dimensional electrophoresis (arrow heads).

DISCUSSION

Affinity electrophoresis

It has been thought that, in the taste receptor, the receptor-stimulus interaction is too weak and the quantity of the receptor protein is too small to detect or isolate the receptor protein. In the labellar sugar receptor of the fly, the P site-sucrose interaction is comparatively strong, but the dissociation constant of the P site-sucrose complex is still more than 0.01 M, according to Morita [18]. Such a weak interaction cannot be detected directly by any means other than affinity electrophoresis. For the application of affinity electrophoresis,

however, it is imperative that affinity ligand is water-soluble and immobile in the polyacrylamide gel. Starch becomes water-soluble when heated. Its molecular weight, estimated to be 10–100 times larger than that of the candidate protein, was expected to be large enough for it to be immobile in 7.5% polyacrylamide gel. The result shown in Figure 2 satisfied the linear relationship between m_o/m and $[I]$ demanded by Eq. (1), strongly suggesting that starch when complexed with the candidate protein was indeed immobile in the polyacrylamide gel. Thus, starch is a satisfactory affinity ligand and has already been used in affinity electrophoresis for phosphorylase [13, 14] or amylase [19]. As in the experiments on phosphorylase or amylase, the P site-starch interaction was strong enough to detect the P site molecule. Furthermore, the two dimensional electrophoresis technique applied here was very useful in isolating the protein of interest among many different kinds of protein.

As for the quantity of the receptor protein, Hansen and Wiczorek [20], on the basis of semi-quantitative calculation, estimated that 10^{-7} or 10^{-10} g of labellar sugar receptor protein can be obtained from 1,000 flies. The silver staining method of Oakley *et al.* [12] is sufficiently sensitive to detect protein density of 10^{-11} – 10^{-10} g/mm² on a gel plate. Since the candidate protein extracted from 20–40 flies made a visible spot about 2 mm diameter on the gel, at least 10^{-9} g of the candidate protein should be obtainable from 1,000 flies, consistent with the estimate of Hansen and Wiczorek [20].

Receptor-sugar interaction

The receptor-stimulus interaction is thought to be the primary process in the chemosensory transduction mechanism. The existence of the specific receptor molecule has not always been accepted in the case of salt, water or bitter taste reception [21]. In the case of sugar or amino acid reception, however, it is generally accepted that a specific receptor molecule mediates the receptor function [20, 21]. The electrophysiological analysis of the sugar receptor cell of the fly, in particular, is well developed, and the relation between the dissociation constant of the receptor-sugar com-

plex, K_d , and the mid-point concentration, K_b , is described [18] as follows:

$$K_d = K_b(sg/G + 1),$$

where s is the total receptor site; g , the conductance per activated site; G , the conductance across the receptor membrane in the resting state. Applying the electrophysiological data on the recovery process of the sucrose response to the above equation, Ninomiya *et al.* [23] obtained

$$\begin{aligned} sg/G &= 4 \text{ or} \\ K_d &= 5K_b. \end{aligned}$$

This is in good agreement with my result, i.e., $K_d = 4K_b$ (Table 1). These results may be interpreted in terms of amplification at the conductance level. That is, in the primary process of the chemosensory transduction in the sugar receptor of the fly, sucrose, maltose, D-glucose, etc., bind to the P site molecule, consisting of the candidate protein, according to their individual affinities, but the conductance change across the sugar receptor membrane uniformly gives 4 to 5-fold amplification of the sensitivity.

Table 1 shows the calculated dissociation constants, assuming the simple case that one molecule of starch or sugar binds to the P site molecule. Therefore, the calculated value for D-glucose is probably an overestimate because two glucose molecules are thought to bind to each P site molecule [24].

Location of the sugar receptor protein

The candidate protein was found in the "labellar content" and the "labellar integument" but not in the proboscis from which the labellum had been cut off. This suggested that the candidate protein is located in the cell body and the distal process but not in the axon of the labellar chemosensory cell. The P site molecule is probably synthesized in the cell body of the sugar receptor cell, transported to the distal process and concentrated in the receptor region at the tip. Recently, we suggested that the P site is located not only at the tip but also in the intermediate length of the distal process [23] and that a considerable number of receptor molecules for the P site exist in regions other than the receptor region of the sugar receptor cell [25].

Comparison with α -glucosidase

Many behavioral and electrophysiological studies have documented the stereospecificity of the P site for stimulus sugar [2, 7, 26], and it has been suggested that three successive equatorial hydroxyl groups in the chair form of the pyranose ring are essential for stimulation at the P site regardless of their position. Actually, all sugars which bind to the candidate protein have this essential structure and are stimulatory at the P site. As for starch, its glucopyranose residues do not have this essential structure, but it can compete with the stimulus sugars for the P site [7]. Although all stimuli which have been estimated behaviorally or electrophysiologically could not be investigated in the present work, the candidate protein showed binding specificity for several sugars and starch similar to that exhibited by the P site in behavioral or electrophysiological studies. However, L-fucose and starch do not bind to the labellar α -glucosidase. Thus, I conclude that this candidate protein is different from the α -glucosidase, and that it is rather likely to be the P site receptor molecule.

ACKNOWLEDGMENTS

I thank Dr. Taisaku Amakawa for letting me carry out this work in his laboratory as a research student. My thanks are also due to Professor Hiromichi Morita and Professor Tomiyuki Hara for the use of electron microscopes in their laboratories and Dr. Koichi Ozaki for his help with scanning electron microscopy. I also thank Professor Tsutomu Inoue for his invaluable advice on affinity electrophoresis, Dr. Fumio Hayashi for his general discussion and Professor W. L. Pak of Purdue University for kindly correcting and improving my English.

REFERENCES

- 1 Dastoli, F. R. and Price, S. (1966) Sweet-sensitive protein from bovine taste buds: Isolation and assay. *Science*, **154**: 905-907.
- 2 Shimada, I., Shiraishi, A., Kijima, H. and Morita, H. (1974) Separation of two receptor sites in a single labellar sugar receptor of the fleshfly by the treatment with p-chloromercuribenzoate. *J. Insect Physiol.*, **20**: 605-621.
- 3 Shimada, I. (1975) Two receptor sites and their relation to amino acid stimulation in the labellar

- sugar receptor of the fleshfly. *J. Insect Physiol.*, **21**: 1675–1680.
- 4 Shimada, I. and Isono, K. (1978) The specific receptor site for the aliphatic carboxylate anion in the labellar sugar receptor of the fleshfly. *J. Insect Physiol.*, **24**: 807–811.
 - 5 Hansen, K. (1969) The mechanism of insect sugar reception, a biochemical investigation. In "Olfaction and Taste, Vol. 3". Ed. by C. Pfaffmann, Rockefeller Univ. Press, New York, pp. 382–391.
 - 6 Nakashima, M., Enomoto, K., Kijima, H. and Morita, H. (1982) Discrepancy between the affinities of certain inhibitors for the membrane-bound α -glucosidases and those for the sugar receptor of the flies. *J. Insect Physiol.*, **12**: 579–585.
 - 7 Hara, M. (1983) Competition of polysaccharides with sugars for the pyranose and the furanose sites in the labellar sugar receptor cell of the blowfly, *Phormia regina*. *J. Insect Physiol.*, **29**: 113–118.
 - 8 Amakawa, T., Kijima, H. and Morita, H. (1975) Insoluble-glucosidase: Possible pyranose site of the sugar receptor of the labellar hairs of the blowfly, *Phormia regina*. *J. Insect Physiol.*, **21**: 1419–1425.
 - 9 Ornstein, L. (1964) Disc electrophoresis. I. Background and theory. *Ann. N. Y. Acad. Sci.*, **121**: 321–349.
 - 10 Davis, B. J. (1964) Disc electrophoresis. II. Method and application to human serum proteins. *Ann. N. Y. Acad. Sci.*, **121**: 404–427.
 - 11 Kawabata, K., Kijima, H., Shiraishi, A. and Morita, H. (1973) α -Glucosidase isozymes and the labellar sugar receptor of the fly. *J. Insect Physiol.*, **19**: 337–348.
 - 12 Oakley, B. R., Kirsch, D. R. and Morris, N. R. (1980) A simplified ultrasensitive silver stain for detecting proteins in polyacrylamide gels. *Anal. Biochem.*, **105**: 361–363.
 - 13 Takeo, K. and Nakamura, S. (1972) Dissociation constants of glucan phosphorylase of rabbit tissues studied by polyacrylamide gel disc electrophoresis. *Arch. Biochem. Biophys.*, **153**: 1–7.
 - 14 Takeo, K. and Nakamura, S. (1978) Dissociation constants of glucan phosphorylases to origo- and polyglucans studied by the affinity electrophoresis. In "Affinity Chromatography". Ed. by O. Hoffmann-Ostenhof, M. Breitenbach, F. Koller, D. Kraft and O. Scheiner, Pergamon Press, Oxford and New York, pp. 67–70.
 - 15 Halvorson, H. and Ellias, L. (1958) The purification and properties of an α -glucosidase of *Saccharomyces italicus*. *Biochem. Biophys. Acta*, **30**: 28–40.
 - 16 Shiraishi, A. and Morita, H. (1969) The effects of pH on the labellar sugar receptor of the fleshfly. *J. Gen. Physiol.*, **53**: 450–470.
 - 17 Hassett, C. C., Dethier, V. G. and Gans, J. (1950) A comparison of nutritive values and taste thresholds of carbohydrates for the blowfly. *Biol. Bull.*, **99**: 446–453.
 - 18 Morita, H. (1969) Electrical signs of taste receptor activity. In "Olfaction and Taste, Vol. 3". Ed. by C. Pfaffmann, Rockefeller Univ. Press, New York, pp. 370–381.
 - 19 Inoue, T. (1978) Affinity electrophoresis of α -amylase. *Physico-Chem. Biol.*, **22**: 135–138.
 - 20 Hansen, K. and Wieczorek, H. (1981) Biochemical aspects of sugar reception in insect. In "Biochemistry of Taste and Olfaction". Ed. by R. H. Cagan and M. R. Kare, Academic Press, New York, pp. 139–162.
 - 21 Kurihara, K., Miyake, M. and Yoshii, K. (1981) Molecular mechanisms of transduction in chemoreception. In "Biochemistry of Taste and Olfaction". Ed. by R. H. Cagan and M. R. Kare, Academic Press, New York, pp. 249–285.
 - 22 Cagan, R. H. (1981) Recognition of taste stimuli at the initial binding interaction. In "Biochemistry of Taste and Olfaction". Ed. by R. H. Cagan and M. R. Kare, Academic Press, New York, pp. 175–203.
 - 23 Ninomiya, M., Ozaki, M., Kashiwara, Y. and Morita, H. (1986) Destruction and reorganization of the receptor membrane in labellar chemosensory cells of the blowfly: Recovery of response to sugars after destruction. *J. Gen. Physiol.*, **87**: 1003–1016.
 - 24 Morita, H. and Shiraishi, A. (1968) Stimulation of the labellar sugar receptor of the fleshfly by mono- and disaccharides. *J. Gen. Physiol.*, **52**: 559–583.
 - 25 Ozaki, M., Ninomiya, M., Kashiwara, Y. and Morita, H. (1986) Destruction and reorganization of the receptor membrane in labellar chemosensory cells of the blowfly: Long lasting latent action of colchicine. *J. Gen. Physiol.*, **87**: 533–549.
 - 26 Hanamori, T., Shiraishi, A., Kijima, H. and Morita, H. (1974) Structure of effective monosaccharides in stimulation of the sugar receptor of the fly. *Chem. Senses Flavour*, **1**: 147–166.

Auditory Evoked Potentials Dynamically Related to Sleep-Waking States in Unrestrained Rats

YASUHISA OKANO, EDUARD DAVID¹, KAZUKI HONDA
and SHOJIRO INOUÉ²

Institute for Medical and Dental Engineering, Tokyo Medical and Dental University, Kanda-Surugadai 2-3-1, Tokyo 101, Japan and

¹Department of Physiology, University of Witten-Herdecke, D-5804 Herdecke, Federal Republic of Germany

ABSTRACT—Auditory evoked potentials (AEPs) to continuous click stimuli delivered at 1-s intervals were bipolarly recorded between the frontal and the fronto-parietal cortex in freely behaving rats throughout the first 3 hours of the light and the dark period. Dynamic changes in the middle and late latency components of AEPs were serially analyzed during slow wave sleep (SWS), paradoxical sleep (PS) and wakefulness (W). The sleep-waking stages affected greatly the latency of the first and second negative (N_1 and N_2) and positive (P_1 and P_2) waves. Especially during SWS, N_2 and P_2 dynamically changed: the deeper SWS, as evidenced by an elevated delta activity, was accompanied by the longer latency and the higher amplitude. The peak-to-peak voltage difference was maximal when delta-sleep occurred. During PS, AEPs remained quite stable, exhibiting a steady level of N_2 and P_2 amplitudes and no fluctuation of their latencies. During W, N_2 tended to decrease in amplitude and sometimes disappeared due to habituation to the stimuli. Significant circadian variations were found in the latency and amplitude of the middle and late AEP components. Thus, the state-dependent and time-of-day-dependent characteristics of AEPs might be utilized as a good indicator for sleep-vigilance scoring.

INTRODUCTION

An electroencephalogram (EEG) is universally adopted as an objective index for scoring the sleep-waking stages, which requires time-consuming analysis and a large storage space. Auditory evoked potentials (AEPs) can also provide an objective evaluation of the sleep-waking state in a more concise form. A definite change in the latency and/or amplitude of AEPs is known to occur during sleep-waking cycles in humans [1-11], cats [12-16] and rats [17, 18]. In the late components of AEPs, markedly increased amplitudes are observable during slow wave sleep (SWS) in animals or non-REM sleep in humans, although the early components equivalent to

brainstem evoked responses are considerably stable in humans [6, 19]. However, in these studies, attention was mainly focussed on the analysis and comparison of AEPs at a certain steady state of sleep-waking stages.

Since the conscious level of wakefulness (W) and the stages of sleep dynamically change as a function of time, a continuous time-course analysis of AEPs is of special interest. As far as the present authors know, Molnár *et al.* [15] noted that the peak latency of the latest negative component of AEPs shifts forward during the rapid eye movement phase of paradoxical sleep (PS) in cats; whereas Ujszászi and Halász [8] observed that the latency and amplitude of late components of AEPs show a considerable variety during stage 2 non-REM sleep in humans. The present paper deals with the first systematic approach to a dynamic aspect of AEP variations, both minute-to-minute and day-to-night, with special reference to the

Accepted August 20, 1987

Received July 18, 1987

² To whom requests of reprints should be addressed.

sleep-waking stages, i.e. SWS, PS and W, in freely behaving rats.

Since the rat is a multiphasic sleeper and a night-active animal, approximately two thirds of total sleep time are distributed in the light period under a 12-h light and 12-h dark schedule [20]. The duration of SWS and PS episodes is longer in the light period than in the dark period, while that of W episodes is shorter in the light period [21]. Hence the question arises as to whether circadian variation in the AEP components exist between the early phases of the light and the dark period. The experimental facts dealt with here indicate that this is really the case. The preliminary results are published elsewhere in abstract form [22–24].

MATERIALS AND METHODS

Seventeen male rats of the Sprague-Dawley strain, raised in our closed colony on a 12-h light and 12-h dark schedule (light period: 08:00–20:00 h) under a constant air-conditioned environment of $25 \pm 1^\circ\text{C}$ and $60 \pm 6\%$ relative humidity with free access to rat chow and water, were used. At the age of 60–90 days, animals weighing 300–450 g were anesthetized with sodium pentobarbital (50 mg/kg *i.p.*), placed on a stereotaxic apparatus and permanently implanted with three cortical electrodes for EEG and AEP recording, two nuchal electrodes for electromyogram (EMG) recording, and a silver plate on the skull as a reference electrode. The EEG-AEP electrodes were located on the surface of the frontal cortex (1.8 mm lateral to the central suture and 4.5 mm anterior to the bregma) and of the fronto-parietal cortex (3.7 mm lateral and 1.5 mm posterior, as above). EEG and AEP were bipolarly recorded between the two electrodes. The surgical procedure was the same as described in a previous paper [25].

The rats were individually housed in a special cylindrical cage which enabled continuous monitoring of EEG and EMG, and continuous auditory stimulation (Fig. 1). A slip-ring fixed above the cage guaranteed the free movement of the rats. Each cage was placed in a sound-proof, electromagnetically shielded chamber under the same environmental conditions as above. A week was

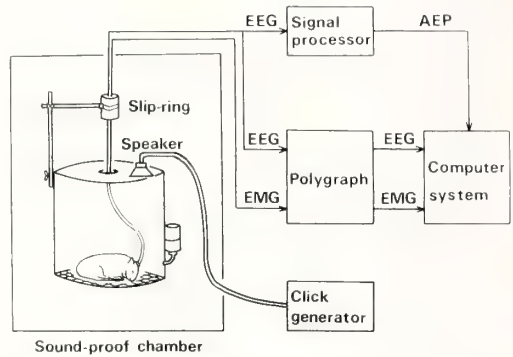


Fig. 1. Experimental system. For details, see text.

allowed for recovery from surgery before the experiment. Then EEG and EMG were polygraphically recorded, and SWS, PS and W were visually scored according to the routinized criteria [20]. After observing a steady circadian rhythmicity in sleep-waking amounts, auditory stimuli consisting of clicks were delivered at 1-s intervals through a speaker placed above the cage. The clicks were 0.1-ms square wave pulses, the intensity of which was adjusted to 70 dB above the noise level on the floor of the cage. Click stimuli were continuously given to the rats either between 08:00 h and 11:00 h or between 20:00 h and 23:00 h. Under continuous recordings of EEG and EMG, AEPs were collected from two out of the three cortical electrodes for averaging. Fifty AEPs were averaged at one time by a signal processor (7T17, NEC San-ei), stored in a floppy disk and simultaneously recorded on a plotter in the following 10 seconds. Hence each averaged AEP was recorded at 1-min intervals. Averaged AEPs were then analyzed with reference to the EEG-EMG defined sleep-waking stages and to the delta activity (0.5–3.5 Hz) of the EEG records which was filtered and integrated at 1-min intervals. For an analysis of circadian variations, AEPs recorded at the definite occurrence of SWS, PS and W in the 1-h period of either 08:00–09:00 h or 20:00–21:00 h were respectively compared and statistically analyzed by Student's *t*-test.

RESULTS

AEP components

Typical AEPs during SWS, PS and W in freely

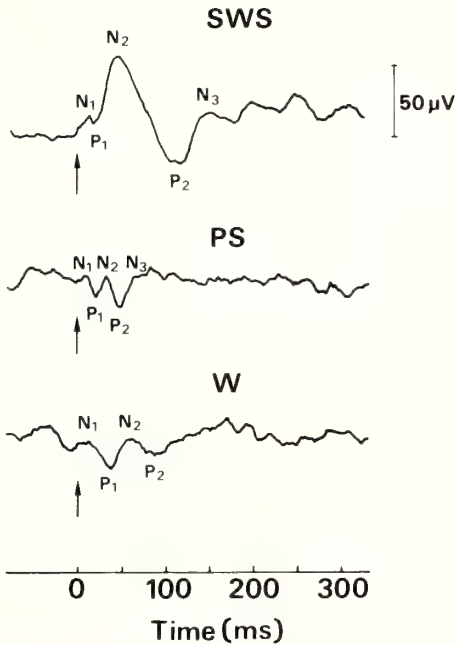


FIG. 2. A typical example of averaged AEPs with the definition of peaks during SWS, PS and W. The arrow indicates click stimuli.

behaving rats are shown in Figure 2. The waveforms were largely in accordance with those described in previous studies [17, 18]. The middle and late components of AEPs were composed of several positive and negative deflections in their waveforms. The peaks were designated as the first negative (N_1) and positive (P_1) waves, the second negative (N_2) and positive (P_2) waves, and so forth, according to their polarity and their sequence order. The waveform, the latency of peaks, and the peak-to-peak amplitude changed dynamically and were largely dependent on sleep-waking stages, as described below.

AEPs during SWS

In the typical waveform of an AEP during SWS, the first peaks, N_1 and P_1 , clearly appeared within 30 ms after the onset of click stimuli. The N_1 - P_1 amplitude was considerably small, never exceeding $10 \mu\text{V}$. Large N_2 and P_2 deflections then followed around 50 ms and 120 ms after the onset of click stimuli, respectively. Hence the difference between these peaks became very large, sometimes

exceeding $80 \mu\text{V}$, which was far greater than that during PS and W. Subsequent peaks (N_3 , P_3 , N_4 and P_4) were observable in a latency range from 110 to 200 ms (Fig. 2). The waveform of AEPs varied dynamically during the course of SWS (Fig. 3, right). Deep SWS, as evidenced by the elevated occurrence of delta activity, was characterized by a prolongation of N_2 and P_2 latencies and a profound increase in their amplitude. In contrast, the N_2 latency and amplitude declined in accordance with the reduction of delta activity (Fig. 3, left).

AEPs during PS

During PS, definite rises and falls in amplitude occurred three times within 100 ms after click stimuli (N_1 - N_3 and P_1 - P_3 , Fig. 2), and some rats exhibited 4th deflections (N_4 and P_4). All peak-to-peak amplitudes were smaller than those of SWS, never exceeding $30 \mu\text{V}$. Wave components were not clearly distinguishable later than 100 ms after stimulation. AEP components were characterized by their stability during the course of PS (Fig. 4). The latency of N_2 and P_2 showed little fluctuation. The N_2 - P_2 amplitude remained at a steady level. Sometimes, the duration of PS episodes was too short for a time-series analysis of successive AEPs, which were averaged at 1-min intervals.

AEPs during W

In the waking state, N_1 and P_1 appeared approximately 20 ms and 40 ms after click stimuli, respectively (Fig. 2). Subsequent wave components, N_2 and P_2 , occurred in the following 50 ms. No clear waveform was observable after then. Peak-to-peak amplitudes varied considerably, ranging from 5 to $40 \mu\text{V}$. The N_2 and P_2 tended to decrease their amplitude and often almost disappeared (Fig. 5, right). Television monitoring revealed that, during such a change, rats sometimes displayed definite behavior such as eating, drinking and grooming. N_2 and P_2 waves usually reappeared during the course of the same W episode. The N_1 and P_1 latency was relatively stable (Fig. 5).

Time-of-day-dependent variation in AEPs

AEPs in the early phase of the light period were compared to those of the dark period. Since

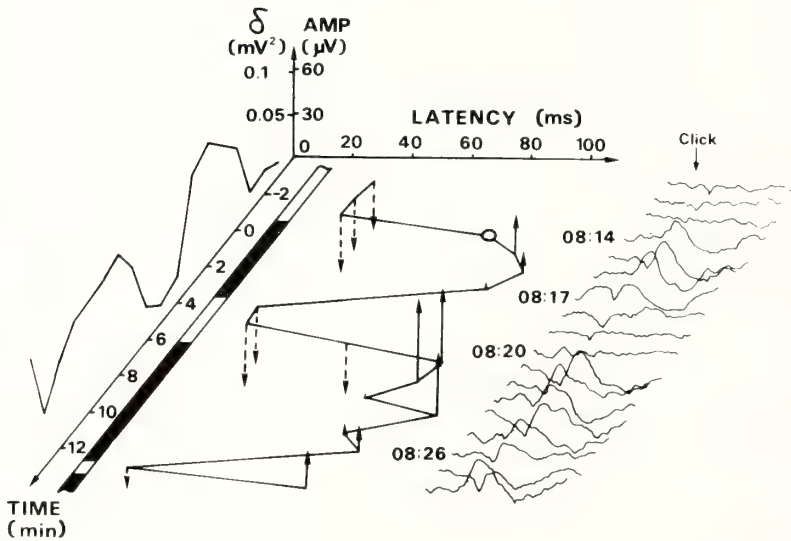


FIG. 3. A typical example of dynamic changes in the amplitude and latency of N_2 component of AEPs during SWS. The corresponding AEPs are shown at the right side. AMP (ordinate) means the difference between the reference N_2 amplitude at the initial SWS (indicated by an open circle) and that of the other AEPs. Increments and decrements in absolute values are expressed by arrows directed upward and downward, respectively. Sleep-waking stages are shown by an oblique column, in which SWS, PS (shown only in Fig. 4) and W are represented by black, dotted and white sections, respectively. The initial and final time of day is indicated for the main episodes. Integrated delta activity (δ) is shown at the left side.

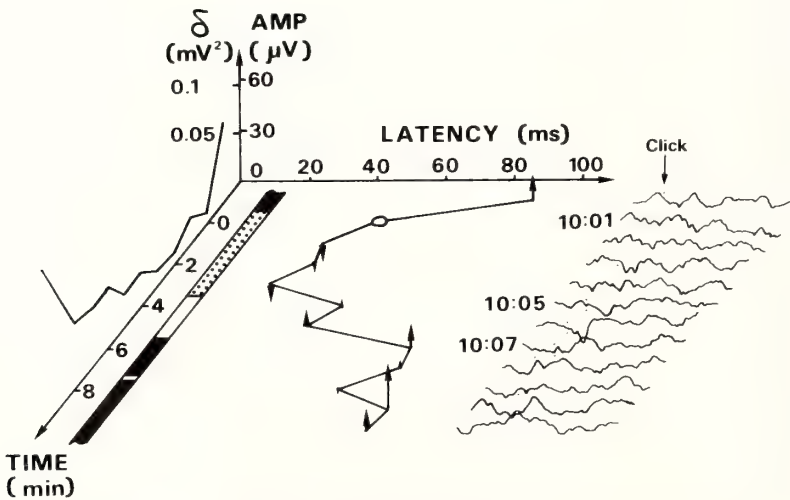


FIG. 4. A typical example of dynamic changes in the amplitude and latency of N_2 component of AEPs during PS. AMP (ordinate) means the difference between the reference N_2 amplitude at the initial PS (indicated by an open circle) and that of the other AEPs. For further explanations, see the legend of Fig. 3.

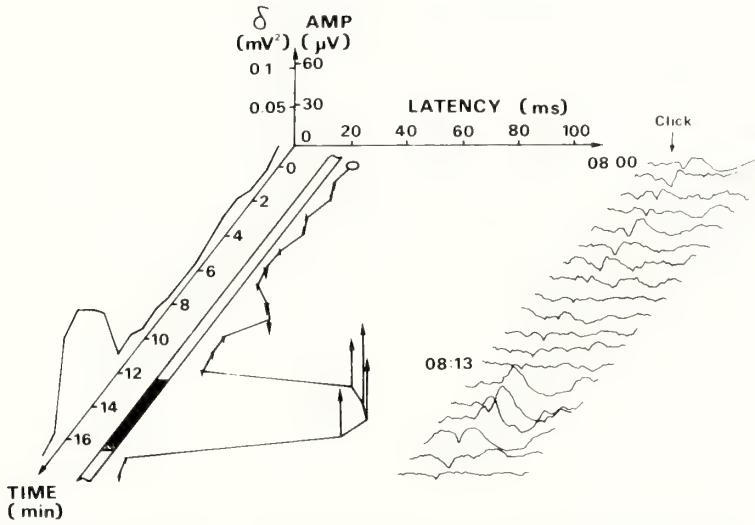


FIG. 5. A typical example of dynamic changes in the amplitude and latency of the P₂ component of AEPs during W. AMP (ordinate) means the difference between the reference P₂ amplitude at the initial W (indicated by open circle) and that of the other AEPs. For further explanations, see the legend of Fig. 3.

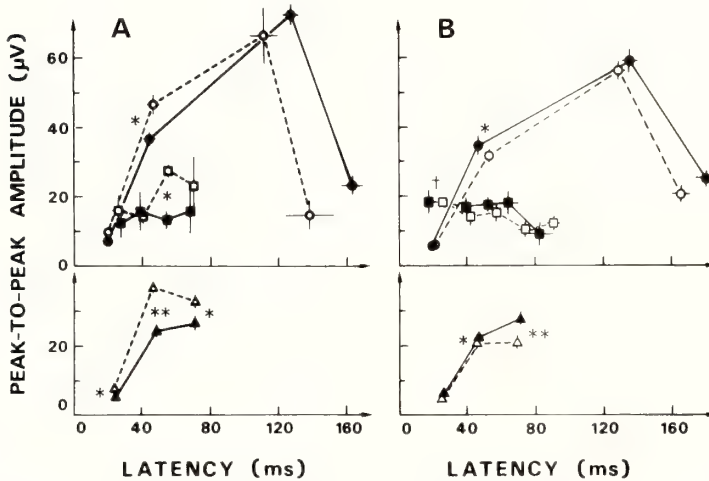


FIG. 6. The peak-to-peak amplitude and latency of AEP components as a function of the light-dark period and sleep-waking stages in two different rats A and B. Values are mean \pm SEM during the early light period (08:00–09:00 h, A: n=10 for SWS; n=3 for PS; n=24 for W, B: n=18 for SWS; n=4 for PS; n=7 for W) and the early dark period (20:00–21:00 h, A: n=16 for SWS; n=3 for PS; n=18 for W, B: n=11 for SWS; n=3 for PS; n=15 for W). Circles, squares and triangles indicate respectively SWS, PS and W, in which white and black signs mean respectively the light and the dark period. Peak-to-peak amplitudes are expressed in absolute values and arranged in sequence from left to right: the N₁–P₁ amplitude, the P₁–N₂ amplitude, the N₂–P₂ amplitude and the P₂–N₃ amplitude (shown only for PS in rat A). Asterisks indicate that the peak-to-peak amplitude difference between the light and the dark period was statistically significant at P<0.05 (*) and P<0.01 (**). A symbol (†) indicates that the latency difference between the light and the dark period was statistically significant at P<0.05.

individual variations were so large, no clear difference was found in average values from the results pooled for all animals. However, if data were individually processed for all AEPs during each state, a significant circadian variation was obtained from most of the rats. Figure 6 illustrates typical examples, in which the peak-to-peak amplitude and latency of AEP components showed significant differences between the light and the dark period.

During SWS, the differences in each peak-to-peak amplitude were apparent. In most cases, the P_1 - N_2 amplitude significantly differed between the two periods. The voltage difference ranged from 3 to 10 μV . The later components showed usually a larger difference which was insignificant due to considerable variations. The latency of P_2 and N_3 during nocturnal SWS was largely delayed by 5–20 ms in comparison with that during diurnal SWS. However, no statistical significance was detected because of large variations.

During PS, the circadian difference in the AEP parameters was rather small and statistically insignificant except for that of some components (for examples, Fig. 6A: the N_2 - P_2 amplitude significantly differed by 14 μV ; Fig. 6B: the N_1 latency significantly differed by 8 ms).

During W, the peak-to-peak amplitude of most AEP components significantly differed between the light and dark periods. The difference ranged from 2 to 15 μV . However, their latency exhibited little difference.

DISCUSSION

The middle and late components of AEPs in freely behaving rats exhibited state-dependent changes. It was found that minute-to-minute variations occurred in the waveform of AEPs during the course of W. In addition, our time series analysis first demonstrated that the latency and amplitude of the AEP components, especially during SWS, varied dynamically with close relation to the fluctuations in the EEG delta activity. Since the delta activity is regarded as a reliable indicator of deep sleep, it is likely that the AEP parameters might specifically indicate the time-course changes in the state of sleep-wakefulness.

The AEP activity in our rats was most prominent during the deep sleep stage. This was comparable to the previous reports in which auditory stimuli of a low frequency, up to 10 Hz, were given to cats [12–16] and rats [17,18]. It seems likely that in these animals, auditory inputs at a relatively low frequency may easily provoke a larger amplitude and a longer latency in the middle and late AEP components of AEPs during SWS than during PS and W.

The mechanism involved in this change remains unknown. There are several speculations. Firstly, Weitzman and Kremen [8] concluded that AEPs during sleep represents summed K complexes elicited from the auditory stimulation. Secondly, the chronic twitches of the middle ear muscles during PS are responsible for a reduction of auditory inputs, which eventually causes a reduction in the amplitude of AEPs [12, 13]. This assumption, however, is not confirmed by a later study [17]. Thirdly, a state-dependent change in body temperature may be considered. It is reported that heating and cooling of the body can respectively shorten and enlarge the latency and amplitude of auditory brainstem responses [26]. Since the early phase of an SWS episode generally accompanies a fall in body temperature [27], the slower middle and late latencies of AEPs during SWS might be accounted for by the lowered temperature, which accompanies a delayed synaptic transmission. Finally, the blockade of sensory information in neural circuits during W may be considered. Attention causes changes in the latency of late components of AEPs [28]. This was largely due to the habituation provoked by the inhibitory mechanism or the gating to the monotonous stimulation. Therefore, changes in attentive levels might reflect the amplitude fluctuations. In contrast, during SWS no attentive activity exists and the slow wave generator mechanism is predominant. This may result in an enlarged AEP waveform. At present no information is available to determine which possibility is most plausible.

In human studies, however, the results are conflicting; some investigators report a similar increase in peak amplitudes and a prolongation of their latencies in deep sleep stages [6, 8–11], whereas others report little changes depending on

the sleep-waking stages (see [29]); most authors refer to a reduced AEP activity during PS, while Ornitz *et al.* [5] demonstrated an enlarged waveform during PS. Furthermore, if auditory stimuli are given at sufficiently high frequency, up to 60 Hz, the amplitude changes are smaller during sleep than during waking [3, 4].

The present study first detected the diurnal and nocturnal differences in the amplitude and latency of the middle and late AEP components. In this connection, Hanada and Kawamura [30] noted that a clear circadian variation occurs in the amplitude of an early component of evoked potentials caused by electrical stimulation of the optic tract in rats. These facts may indicate the existence of a time-of-day-dependent change in the sleep-waking state. However, the existence of large individual variations in these AEP parameters may indicate that the differences between the light and dark periods reflected not only the rhythmicity derived from the circadian oscillator but also the variations in the behavioral situations in each rat, since an attentive behavior during W or an elevated delta activity during SWS might easily modify the AEP parameters.

Apart from the above discussions, the close correlation between the AEP parameters and the sleep-waking stages, especially during SWS, may suggest that the time-consuming sleep scoring based on polysomnography could be replaced or supplemented by the time-course analysis of AEPs. The latter technique seems to be simpler, more conventional and easier to define the dynamic state changes. Hence the AEP dynamics could be applied not only to the evaluation of sleepiness [31] but also to an objective sleep-vigilance scoring.

ACKNOWLEDGMENTS

E. David joined this study during his stay in Tokyo, which was sponsored by the Japan Society for the Promotion of Science, Tokyo, and the Deutscher Akademischer Austauschdienst, Bonn. S. Inoué partially prepared the manuscript during his stay in Herdecke, which was sponsored by the Alexander von Humboldt-Stiftung, Bonn. Both authors wish to express their gratitude for the sponsorship. This research was supported in part by Grant-in-Aid for Special Project Research of Endogenous Neuroactive Substances from

the Ministry of Education, Science and Culture of Japan (No. 60126002) to S. I.

REFERENCES

- 1 Buchsbaum, M., Gillin, J. C. and Pfefferbaum, A. (1975) Effect of sleep stage and stimulus intensity on auditory evoked responses. *Psychophysiology*, **12**: 707-712.
- 2 Erwin, R. and Buchwald, J. S. (1986) Midlatency auditory evoked responses: differential effects of sleep in the human. *Electroencephalogr. Clin. Neurophysiol.*, **65**: 383-392.
- 3 Linden, R. D., Campbell, K. B., Hamel, G. and Picton, T. W. (1985) Human auditory steady state evoked potentials during sleep. *Ear Hearing*, **6**: 167-174.
- 4 Linden, R. D., Picton, T. W., Campbell, K. B. and Hamel, G. (1985) Thresholds for auditory steady state evoked potentials during sleep. In "Sleep '84". Ed. by W. P. Koella, E. Rüter and H. Schulz, Gustav Fischer Verlag, Stuttgart, pp. 228-231.
- 5 Ornitz, E. M., Ritvo, E. R., Carr, E. M., Paniman, L. M. and Walter, R. D. (1967) The variability of the auditory evoked response during sleep and dreaming in children and adults. *Electroencephalogr. Clin. Neurophysiol.*, **22**: 514-524.
- 6 Osterhammel, P. A., Shallop, J. K. and Terkildsen, K. (1985) The effect of sleep on the auditory brainstem response (ABR) and the middle latency response (MLR). *Scand. Audiol.*, **14**: 47-50.
- 7 Ujszászi, J. and Halász, P. (1986) Late component variants of single auditory evoked responses during NREM sleep stage 2 in man. *Electroencephalogr. Clin. Neurophysiol.*, **64**: 260-268.
- 8 Weitzam, E. D. and Kremen, H. (1965) Auditory evoked responses during different stages of sleep in man. *Electroencephalogr. Clin. Neurophysiol.*, **18**: 65-70.
- 9 Williams, H. L., Marlock, H. C., Marlock, J. V. and Lubin, A. (1964) Auditory evoked responses and EEG stages of sleep. *Ann. New York Acad. Sci.*, **112**: 172-179.
- 10 Williams, H. L., Tepas, D. I. and Marlock, H. C., Jr. (1962) Evoked responses to clicks and electroencephalographic stages of sleep in man. *Science*, **138**: 685-686.
- 11 Yokoyama, T., Ryu, H., Uemura, K., Miyamoto, T., Yamamoto, T., Furuya, Y. and Nakajima, S. (1986) Middle latency auditory evoked potentials in awake and asleep. *Rinsho Noha*, **28**: 9-44.
- 12 Baust, W., Berlucchi, G. and Moruzzi, G. (1964) Changes in the auditory input in wakefulness and during the synchronized and desynchronized stages of sleep. *Arch. Ital. Biol.*, **102**: 657-674.

- 13 Berlucchi, G., Munson, J. B. and Rizzolatti, G. (1967) Changes in click-evoked responses in the auditory system and the cerebellum of free-moving cats during sleep and waking. *Arch. Ital. Biol.*, **105**: 118-135.
- 14 Chen, B. M. and Buchwald, J. S. (1986) Midlatency auditory evoked responses: differential effects of sleep in the cat. *Electroencephalogr. Clin. Neurophysiol.*, **65**: 373-382.
- 15 Molnár, M., Kormos, G. and Csépe, V. (1986) Laminar analysis of intracortical auditory evoked potentials during the wakefulness-sleep cycle in the cat. *Int. J. Psychophysiol.*, **3**: 171-182.
- 16 Winters, W. D. (1964) Comparison of the average cortical and subcortical evoked response to clicks during various stages of wakefulness, slow wave sleep and rhombencephalic sleep. *Electroencephalogr. Clin. Neurophysiol.*, **17**: 234-245.
- 17 Hall, R. D. and Borbély, A. A. (1970) Acoustically evoked potentials in the rat during sleep and waking. *Exp. Brain Res.*, **11**: 93-110.
- 18 Knight, R. T., Brailosky, S., Scabini, D. and Simpson, G. V. (1985) Surface auditory evoked potentials in the unrestrained rat: component definition. *Electroencephalogr. Clin. Neurophysiol.*, **61**: 430-439.
- 19 Campbell, K. B. and Bartoli, E. A. (1986) Human auditory evoked potentials during natural sleep: the early components. *Electroencephalogr. Clin. Neurophysiol.*, **65**: 142-149.
- 20 Honda, K. and Inoué, S. (1981) Effects of sleep-promoting substance on sleep-waking patterns of male rats. *Reports Inst. Med. Dent. Eng.*, **15**: 115-123.
- 21 Honda, K., Komoda, Y., Nishida, S., Nagasaki, H., Higashi, A., Uchizono, K. and Inoué, S. (1984) Uridine as an active component of sleep-promoting substance: its effects on the nocturnal sleep in rats. *Neurosci. Res.*, **1**: 243-252.
- 22 David, E., Inoué, S., Okano, Y., Honda, K. and Pfothenauer, M. (1986) Click-evozierte Potentiale im Schlaf- und Wachzustand; ein Vergleich zwischen Ratte und Mensch. *Biomed. Tech.*, **31**: suppl. 146.
- 23 Inoué, S., Okano, Y., Honda, K. and David, E. (1986) Auditory evoked potentials specific to sleep-waking stages in unrestrained rats. *Abstracts of 3rd Int. Evoked Potentials Symp.*, p. 125.
- 24 Okano, Y., Honda, K., David, E. and Inoué, S. (1986) Cortical auditory evoked potentials specific to the sleep-waking stages in unrestrained rats. *Abstracts of 1st Int. Congr. Neuroethol.*, p. 71.
- 25 Honda, K. and Inoué, S. (1978) Establishment of a bioassay method for the sleep-promoting substance. *Reports Inst. Med. Dent. Eng.*, **12**: 81-85.
- 26 Marsch, R. R., Yamane, H. and Potsic, W. P. (1984) Auditory brain-stem response and temperature: relationship in the guinea pig. *Electroencephalogr. Clin. Neurophysiol.*, **57**: 289-293.
- 27 Obál, F., Jr. (1984) Thermoregulation and sleep. *Exp. Brain Res., Suppl.* **8**: 157-172.
- 28 Polich, J. (1986) Attention, probability, and task demands as determinants of P300 latency from auditory stimuli. *Electroencephalogr. Clin. Neurophysiol.*, **63**: 251-259.
- 29 Mendel, M. I. (1980) Clinical use of primary cortical responses. *Audiology*, **19**: 1-15.
- 30 Hanada, Y. and Kawamura, H. (1984) Circadian rhythms in synaptic excitability of the dorsal lateral geniculate nucleus in the rat. *Int. J. Neurosci.*, **22**: 253-262.
- 31 Broughton, R. (1982) Performance and evoked potential measures of various states of daytime sleepiness. *Sleep*, **5**: 135-146.

The Anatomy and Physiology of the Stomatogastric Nervous System of *Squilla*. II. The Cardiac System

KENRO TAZAKI

*Biological Laboratory, Nara University of Education,
Takabatake, Nara 630, Japan*

ABSTRACT—A subsystem of the stomatogastric ganglion (STG) of the mantis shrimp, *Squilla oratoria*, which controls movements of the cardiac stomach was studied. Muscles of the cardiac stomach and their motor nerves leaving the STG are described. The paired anterior ventricular nerves and paired lateral ventricular nerves (lvn), which exit the STG, contain the motor axons that control muscular contractions of the cardiac stomach. One pair of superior oesophageal nerves (son) also carry motor axons. The lvn and son give rise to several peripheral nerves which innervate 8 identified muscles. Spontaneous motor activity recorded from the lvn and son (termed the cardiac cycle) has a long cycle period (ca. 10 sec) and consists of alternate firing of bursts by two motor neuron groups. Cardiac cycles similar to spontaneous ones are triggered by stimulation of afferent fibers entering the commissural ganglia. Four constrictor and 3 dilator motor neurons in the STG are identified. They are involved in sequential movements of the dorsal and lateral gastric walls of the cardiac stomach. The function of the cardiac cycle is described with reference to the maceration and transfer of food. It is compared to that of the posterior cardiac plate and pyloric cycle (pcp-pyloric cycle) which has been described previously. Comparisons are made of the cardiac systems in STG of stomatopods and decapods.

INTRODUCTION

The stomatogastric ganglion (STG) of decapods, a small, semi-autonomous nervous system, has been extensively studied as a model for the generation of patterned motor outputs [1, 2]. In the STG both individual cellular properties and neural networks can be analyzed. The lobster STG contains just over 25 identifiable motor neurons which innervate identified muscles of the cardiac and pyloric stomachs [3-5]. It produces cyclic patterned motor outputs having two distinct rhythms responsible for the sequential muscular contractions of the gastric and pyloric regions of the stomach, respectively [6, 7]. The gastric and pyloric cycles are modulated by the supra-oesophageal and commissural ganglia (CG) [8-10]. The cardiac dilator and constrictor neurons are identified in the lobster STG and oesophageal ganglion (OG), and their motor activity modulates

the pyloric cycle or coordinates it with the gastric cycle [11, 12].

The stomach in stomatopods is subdivided into the cardiac stomach, the posterior cardiac plate (pcp) and the pyloric stomach [14, 15]. The cardiac stomach is not equipped with a chewing apparatus such as the gastric mill ossicles of decapods. Most of the ossicles of the stomach form the pcp and pyloric systems of sieves and channels through which digested food moves. The muscles in the stomach and their sequential movements have been described by Kunze [15].

The anatomy and physiology of the stomatogastric nervous system of *Squilla* have been found to be similar to those of decapods [16]. Its gross anatomy was first described by Police [13]. The stomatogastric nervous system in stomatopods is basically similar to that in decapods. While the STG in decapods sends several unpaired and paired motor nerves to control the gastric mill and pyloric stomach, the paired lateral ventricular nerves (lvn) which leave the STG in stomatopods carry principal motor axons to innervate the

muscles of the pcp and pyloric stomach. Characteristics of the cyclic motor outputs observed in the lvn have been described previously in relation to the channel-opening function of the pcp and pyloric systems. The patterned motor outputs have been termed the pcp-pyloric cycle. The pcp-pyloric cycle of stomatopods is apparently homologous to the pyloric cycle in decapods although the neural circuits for its pattern generation remain to be analyzed. The pcp-pyloric cycle is also modulated by input fibers of the superior and inferior oesophageal nerves (son, ion). Cardiac motor activity controlling movements of the cardiac stomach is rarely observed to occur spontaneously in the semi-isolated preparation, but can be triggered or primed by stimulation of the son input fibers.

The present paper deals with the anatomy and physiology of the cardiac system of the stomatogastric nervous system of the mantis shrimp, *Squilla oratoria*. Muscles of the cardiac stomach and their motor nerves are described. The cyclic motor activity of the STG is shown to explain the sequential muscular contractions which control the functional movements of the cardiac stomach. Relations between the cardiac and pcp-pyloric systems primed by stimulation of the son are analyzed.

MATERIALS AND METHODS

The stomatogastric nervous system of a stomatopod, *Squilla oratoria*, was employed in this study. Animals were held in tanks of recirculated sea water at the temperature of 20°C. About 200 specimens were used for anatomical and physiological observations. Methods of dissection and recording were the same as those described in the previous paper [16].

Cardiac stomach

The cardiac stomach, which is a large cuticular sac serving to store ingested food, contains two pairs of ossicles [15]. The anteroventral cardiac ossicles (avc) lie along the anterior lateral margins of the ventral gastric wall (Fig. 1A). They act as supports for muscle attachment. The small posterior lateral cardiac ossicles lie in the posterior

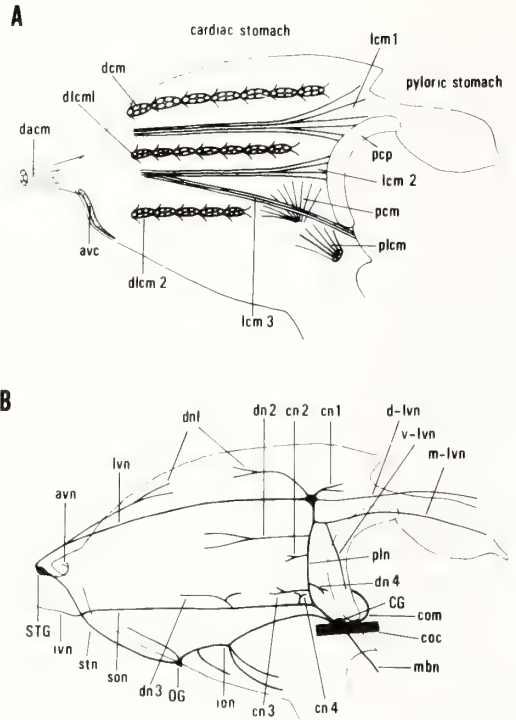


FIG. 1. A: Diagrammatic lateral view of musculature in the cardiac stomach. avc, anteroventral cardiac ossicle; pcp, posterior cardiac plate; dacm, dorsal anterior cardiac muscle; dcm, dorsal cardiac muscle; dlcml and dlc2, dorsolateral cardiac muscle; lcm1–lcm3, longitudinal cardiac muscle; pcm, posterior cardiac muscle; plcm, posterior lateral cardiac muscle.

B: Diagrammatic lateral view of the stomatogastric nervous system. The diagram shows peripheral nerve courses of the lvn and son. CG, commissural ganglion; OG, oesophageal ganglion; STG, stomatogastric ganglion; coc, circum-oesophageal connective; com, commissure; ion, inferior oesophageal nerve; ivn, inferior ventricular nerve; mbn, mandibular nerve; son, superior oesophageal nerve; stn, stomatogastric nerve; avn, anterior ventricular nerve; lvn, lateral ventricular nerve; d-lvn, dorsal lateral ventricular nerve; m-lvn, median lateral ventricular nerve; v-lvn, ventral lateral ventricular nerve; pln, posterior lateral nerve; cn1–cn4, cardiac constrictor nerve; dn1–dn4, cardiac dilator nerve.

lateral gastric wall anterior to the pcp (not shown), though their function is unknown. These two ossicles do not play a role of masticating ingested food. Kunze [15] has classified the muscles in the cardiac stomach into three groups: cardiac mus-

cles, longitudinal muscles and cardiac floor muscles. All of these muscles have been named, and the sequence of movements of the cardiac stomach after ingestion has been described. However, the functional anatomy of the muscles of the cardiac stomach has not been described in detail, and their origins and insertions remain obscure. The stomach muscles are divided into two groups: extrinsic muscles originating on the inner side of the exoskeleton and inserting on the stomach wall or ossicles, and intrinsic muscles having both attachments on the stomach wall itself [5]. Contractions of these individual muscles constrict or dilate different regions of the gastric wall. In this paper, the muscles in the cardiac stomach, which are innervated by motor nerves leaving the STG, have been identified (see *Anatomy* section).

Preparation

Two types of preparations were used in this study. The semi-intact preparation was made in order to record the spontaneous cardiac motor activity. After cutting away most of the appendages in the cephalothoracic region, the animal was immobilized, ventral side up, in the preparation box filled with saline. The ventral and lateral regions of carapace anterior to the mandibles were removed by cutting the extrinsic muscles thus exposing the cardiac stomach and the stomatogastric nervous system. The cardiac stomach moved rhythmically for two hours or more under these conditions. The lvn and son, which include motor axons controlling movements of the cardiac stomach, were drawn into suction electrodes. This preparation was also used to observe how the extrinsic and intrinsic muscles move the gastric wall.

The semi-isolated preparation, which consists of the gastric wall with the muscles, STG, OG and associated nerves, was employed to observe how motor nerves innervate identified muscles. Identification of the cardiac bursting units of the peripheral nerves was also made in this preparation: the son input fibers were stimulated by brief pulses with moderate intensity and frequency to activate rhythmic motor outputs from the STG. The semi-isolated preparation, including the CG, was used to study stimulus-induced cardiac motor

activity. The son input fibers were activated by stimulation of the afferent fibers of a mandibular nerve which enter the CG.

The saline used here was modified from that for *Squilla* developed by Watanabe *et al.* [17]. It had the following composition (in mmol/l): Na, 450; K, 15; Ca, 10; Mg, 20; Cl, 525; N-2-hydroxyethyl-piperazine-N'-2-ethanesulfonic acid (HEPES), 2. The saline was adjusted to pH 7.6. All experiments were done at room temperature (20–26°C).

RESULTS

Anatomy

Muscles The muscles of the cardiac stomach are shown diagrammatically in Figure 1A. Some of these muscles have been named by Kunze [15]. Some have not been previously identified, and are described later. All of these muscles are bilaterally symmetrical.

Four cardiac muscles are associated with medial movements of the dorsolateral gastric wall. The intrinsic longitudinal cardiac muscle 1 (lcm1) attaches to the dorsal gastric wall near the pcp and runs to the anterior region of the cardiac stomach. It serves to constrict the dorsolateral gastric wall. Two extrinsic muscles, which are antagonists of the lcm1, are the dorsal cardiac muscle (dcm) and the dorsolateral cardiac muscle 1 (dlcm1). The dcm originates on the dorsal carapace and inserts on the dorsal gastric wall. The dlcm1 originates on the lateral carapace and inserts on the dorsolateral gastric wall ventral to the lcm1. They dilate the gastric wall. The unpaired dorsal anterior cardiac muscle (dacm) is also an antagonist of the lcm1. The dacm originates on the anterior ventral carapace, and inserts on the anterior extremity of the cardiac stomach. Its contraction pulls the anterior gastric wall forward.

Six cardiac muscles are associated with medial movements of the lateral gastric wall which is medially folded to form the lateral cardiac fold (lcf). The intrinsic longitudinal muscles 2 and 3 (lcm2, lcm3) attach to the lcf. The lcm2 originates on the gastric wall at the lateral side of the pcp, and runs anteriorly. The lcm3 originates on the gastric wall at the ventral side of the pcp, and runs

anteriorly parallel to the lcm2. The lcm2 and lcm3 move the lateral gastric wall medially. The antagonists of the lcm2 and lcm3 are the dorso-lateral cardiac muscles 1 and 2 (dlcm1, dlcm2), respectively. The extrinsic dlcm2 originates on the lateral carapace where the dlcm1 attaches, and inserts on the ventrolateral gastric wall. The lcm2 and lcm3 are situated between the dlcm1 and dlcm2. The intrinsic posterior cardiac muscle (pcm) attaches to the lateral gastric wall at the ventral side of the pcp. The pcm serves to constrict the posterior lateral gastric wall in front of the pcp. The posterior lateral cardiac muscle (plcm) originates on the posterior lateral carapace, and inserts on the lateral gastric wall near the pcp. The plcm is an antagonist of the pcm.

Kunze [15] has described dacm, dcm, dlcm, pcm and plcm but not lcm1, lcm2 and lcm3. Besides these identified cardiac muscles, 2 intrinsic and 5 extrinsic muscles insert on the ventral gastric wall (not shown).

Innervation The stomatogastric nervous system and peripheral motor nerves are illustrated in Figure 1B. Most of the nerves are bilaterally paired. The anterior ventricular nerve (avn) leaves the STG a short distance posteriorly, carrying motor axons to the dacm. The lateral ventricular nerve (lvn) leaves the anterior end of the STG, and runs posteriorly along the lcm1 on the gastric wall, branching extensively at the region just anterior to the pcp. The dorsal, median and ventral lvn (d-lvn, m-lvn, v-lvn) supplies motor nerves to the muscles of the pcp and pyloric stomach [16]. The posterior lateral nerve (pln) connects the lvn with the son emerging from the CG which resides on the circumoesophageal connective (coc).

The lvn and son divide peripherally into two functional groups of motor nerves: cardiac constrictor nerves (cn) and cardiac dilator nerves (dn). Two branches emerging from the lvn run dorsally to innervate the anterior and posterior dcm. These nerves are named the dn1 because they innervate the same muscle. The cn1 branches from the lvn anterior to the pcp to innervate the lcm1. The pln gives rise to several branches. The dn2 is a long branch, traveling anteriorly to innervate the dlcm1. The cn2 and cn3 are short branches carrying motor axons to the lcm2 and lcm3,

respectively. The dn4 is a small branch which innervates the plcm. The son leaves the stomatogastric nerve (stn) posterior to the STG, and runs within the dlcm2, sending out the dn3 to it. The cn4 branches from the son near the pln to innervate the pcm.

The OG sends out several nerves. The ion connects the OG with the CG, and it branches extensively on the ventral gastric wall. These branches innervate intrinsic and extrinsic muscles which insert on the ventral gastric wall. They have not been examined in this study which is concerned with the motor activity of the STG relevant to the control of the muscles in the cardiac stomach.

Physiology

Cardiac cycle The dorsal and lateral gastric walls are moved by the sequential contractions of identified muscles. The patterned outputs that control movements of the cardiac stomach are provided by the motor axons which run in the avn, lvn and son. Recordings of spontaneous motor activity were made simultaneously from the lvn and son in semi-intact preparations. Movements of the cardiac stomach were observed by monitoring the motor activity. Spontaneous firing patterns of STG motor activity recorded from the lvn and son are shown in Figure 2. The cyclic motor outputs consisted of long-lasting bursts of alternately firing constrictor and dilator units (Fig. 2A). Bursts repeated at variable frequencies averaging about 5/min. The duration of bursts in the two units ranged from 3 to 15 sec. The impulse frequency in the constrictor units ranged from 30 to 120 Hz, and in the dilator units from 20 to 80 Hz. The initial units in the bursts leading to constriction of the gastric wall occurred simultaneously in the lvn and son. They were followed by dilator impulses. These patterned outputs are termed the cardiac cycle. There were variations of the motor activity of two units in these output nerves. In Figure 2B-D alternate silent periods in dilator and constrictor units are observed in the lvn or son. Such variations of the motor pattern seemed to be related to functional movements of the cardiac stomach (see later). Spontaneous cardiac cycles were rarely seen even in the semi-isolated preparation which included the CG and

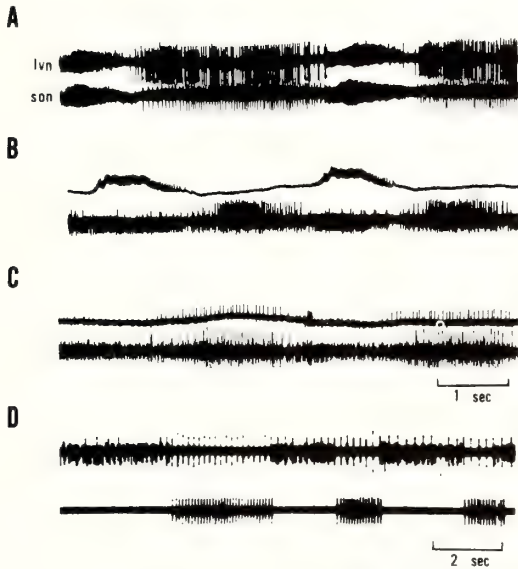


FIG. 2. Cyclic motor activity of the STG related to movements of the cardiac stomach. Spontaneous bursts were simultaneously recorded from the lvn and son. Initial bursts occurred in constrictor units, and were followed by those of dilator units. A: All constrictor and dilator burst units fired alternately. B-D: Either dilator or constrictor units were silent. In B and C displacements of the lvn trace are due to muscular contractions.

OG as well as the STG with associated nerves (similar to a combined preparation in the lobster: [1]). The avn was too small to permit monitoring impulses from it, but contraction of the dacm could be seen during bursting of dilator units.

The bursting pattern contributes to the sequential muscular contractions of the cardiac stomach. The burst units of the lvn and son observed by *en passant* recording correlate with those of their peripheral nerves invading various identified muscles. An example of such recordings is shown in Figure 3. The cardiac constrictor and dilator units are designated as CA and CD, respectively. The bursts of the lvn consist of two constrictor units. The bursting units of CA1 and CA2 are propagated to the cn1 and cn2, respectively (Fig. 3-A1, 2). Identification of these two units can be made by using the peripheral recording electrode for electrical stimulation of the axon to elicit an antidromic impulse in the lvn. The son also contains motor axons of two constrictor neurons.

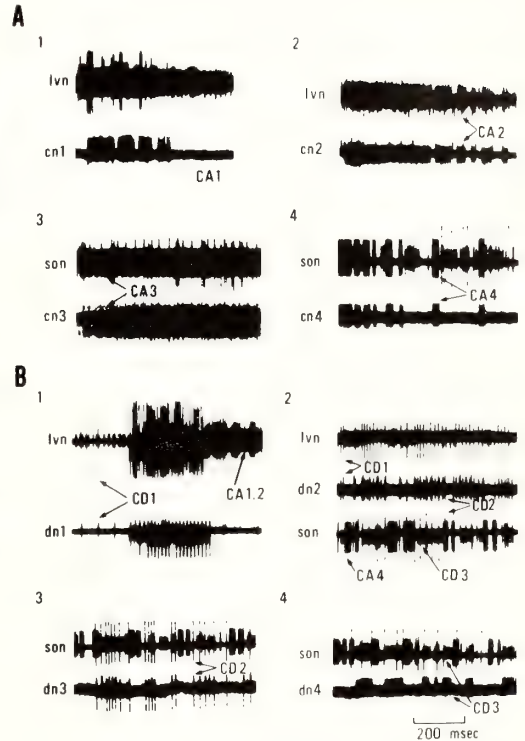


FIG. 3. Bursting units in peripheral nerves corresponding to those of the lvn or son. *En passant* recordings were made from the lvn or son at the region anterior to its ramification. The peripheral bursting units were recorded from nerve branches invading identified muscles. A: Burst firing of cardiac constrictor neurons (CA1-CA4). B: Burst firing of cardiac dilator neurons (CD1-CD3) (see text).

The long-lasting bursting unit of CA3 travels to the cn3 (Fig. 3-A3), and the short bursting unit of CA4 to the cn4 (Fig. 3-A4). The CA2 and CA3 neurons appear to discharge for a longer period than the CA1 and CA4 neurons. For the dilator units, the burst of large impulses in the lvn, which is attributed to CD1, is propagated to the dn1 (Fig. 3-B1). The dn2 contains two motor axons: one originates from the CD1 neuron, and the other from the CD2 neuron (Fig. 3-B2). Large impulses of CD2 unit in the son travel to the dn3 (Fig. 3-B3). The burst of small impulses of CD3 unit is propagated from the son to the dn4 (Fig. 3-B4). The size of impulses of the cardiac constrictor and dilator neurons extracellularly recorded from the lvn and son is relatively consistent: CD1 and CD2 are larger than CA, and CD3 is the smallest (Fig.

3-B1, 2).

The bursting patterns of motor outputs such as shown in Figure 2 are associated with movements of the cardiac stomach. The dorsolateral gastric wall is moved medially by contractions of the lcm1 and lcm2. The corresponding motor pattern is shown in Figure 2D. Two constrictor (CA1, CA2) and 2 dilator (CD1, CD2) neurons contribute to this movement. Medial movements of the posterior lateral gastric wall in front of the pcp are commanded by the CA3 and CA4 neurons, each causing contractions of the lcm3 and pcm. The motor pattern is shown in Figure 2C. During these two types of movements, ingested foods may be moved backward or forward in the cardiac stomach. Besides these movements, the dorsolateral and posterior lateral gastric walls are moved medially. The motor patterns shown in Figure 2A and B control these movements. The CA1 and CA2 neurons command constriction of the dorsolateral gastric wall, while the CA3 and CA4 neurons command constrictions of the lateral and posterior lateral gastric walls. During sequences of all these types of movements, ingested foods would be macerated into fine particles. Other types of patterned motor outputs are shown in Figure 5. These output patterns may control the pumping of digestive juices or the transfer of digested food between the cardiac and pyloric stomachs (see later).

Table 1 summarizes the present observations on motor neurons, location of axon, muscles inner-

vated and their functions. Although the precise number of neurons in the STG could not be determined, there seemed to be at least 7 motor neurons involved in the generation of the cardiac cycle.

Priming effect of input fibers via CG The son inputs induced dual effects on the motor activity of the STG: one input accelerated the pcp-pyloric cycle, and the other activated the cardiac cycle [16]. Cardiac cycles such as those seen during spontaneous activity (Fig. 1A) could be activated in the semi-isolated preparation by stimulating afferent fibers of the mandibular nerve with moderate intensity at 50 Hz, the highest frequency tested in this series of experiments (Fig. 4). Such stimulation activated the son input fibers via the CG. The pcp-pyloric cycle, which consisted of pyloric (PY) and pyloric dilator (PD) bursting units, repeated at a rate of about 2 Hz before stimulation. It disappeared gradually during stimulation, while the long-lasting cardiac cycle units were activated. The size of the PD and CD1 impulses is almost the same in this record. They can be distinguished by burst firing in the son which occurs simultaneously with the PD burst (see squares in Fig. 4). Initially, repetitive firing of the CD1 and CD2 neurons occurred in the lvn and son. It was followed by bursting of the CA1 and CA3 neurons. Bursting of the PY units in the lvn appeared to be accelerated during the high-frequency discharges of the CD1 neuron, and inhibited during the activity of the CA neurons

TABLE 1. Motor neurons of the cardiac cycle in the STG

Neuron	Location of axon	Muscle innervated	Function
Cardiac constrictor			constricts the gastric wall
CA1	lvn, cn1	lcm1	
CA2	lvn, cn2	lcm2	
CA3	son, cn3	lcm3	
CA4	son, cn4	pcm	
Cardiac dilator			dilates the gastric wall
CD1	lvn, dn1 lvn, dn2	dcm dlcm1	
CD2	son, dn2 son, dn3	dlcm1 dlcm2	
CD3	son, dn4	plcm	

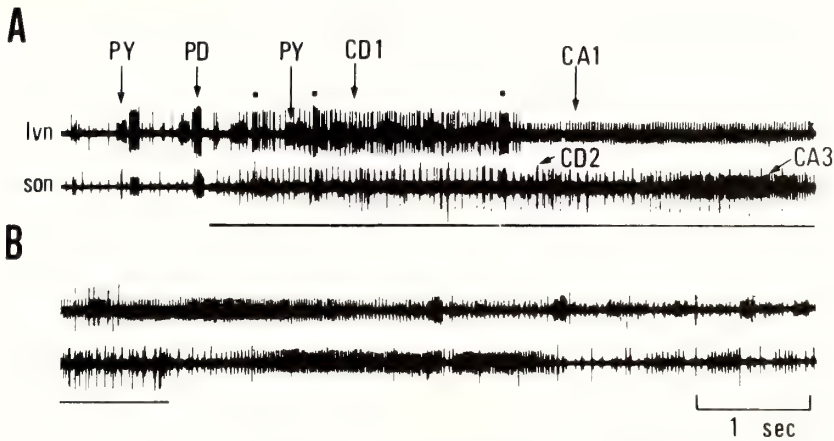


FIG. 4. Cardiac cycle triggered by son input fibers activated by repetitive stimulation of afferent fibers of the mandibular nerve entering the CG with moderate intensity at 50 Hz (marked by the underline). Records A–B are continuous recordings. A long-lasting cardiac cycle was activated during the stimulation. The CD1 and CD2 neurons fired initially, and thereafter the CA1 and CA3 neurons fired. PY, pyloric units; PD, pyloric dilator units. Bursts of PD occurred simultaneously with those in the son (see squares).

(Fig. 4A). Bursting of the CA neuron in the son was preceded by that in the lvn. Both continued after the cessation of stimulation (Fig. 4B). The priming effect was dependent on the stimulus frequency: the cardiac cycle became more obvious with increasing frequency. This observation suggests that some inputs from the CG may be necessary for activation of the cardiac cycle pattern generator.

Interaction of cardiac and pcp-pyloric cycles The function of the cardiac stomach is to macerate food and to transfer digested particles to the pyloric stomach. The pcp-pyloric cycle commands the opening and closing of the channels in the pcp and pyloric stomach [16]. Functional interactions between the cardiac and pcp-pyloric cycles were studied in the semi-isolated preparation. Modulation of the cardiac cycle by the pcp-pyloric cycle units was examined after cycling had been triggered by stimulation of son input fibers. An example is shown in Figure 5. Bursting of the CA1 and CA4 neurons was suppressed by bursting of the PY neurons (Fig. 5A, B). The CA and PY neurons fired alternately. The PY neurons provide the motor commands for movements of the ampulla in the pyloric stomach which forms the

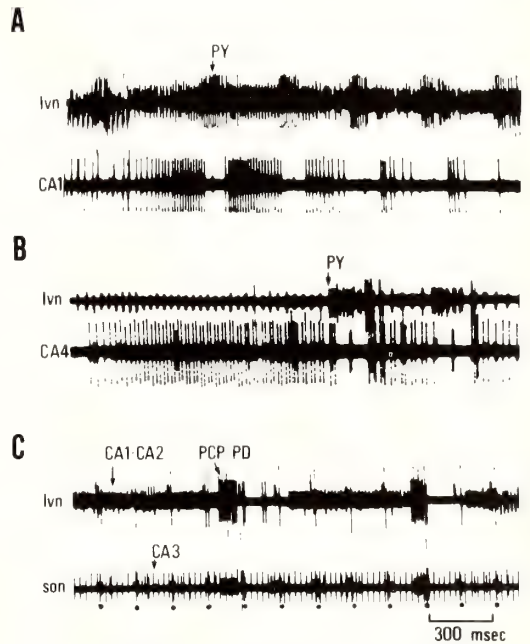


FIG. 5. Modulation of cardiac cycle units by pcp-pyloric cycle units. A, B: Bursts of CA1 and CA4 neurons were suppressed during bursting of PY neurons. C: Bursts of PCP and PD neurons suppressed bursting of CA1 and CA2 neurons. Bursting of CA3 neuron continued during bursting of PCP and PD neurons. Dots indicate individual stimuli given to the son.

channels leading to the midgut [16]. The CA1 and CA4 neurons control contractions of the *lcm1* and *pcm*, respectively. The results, therefore, indicate that constrictions of the dorsolateral and posterior lateral gastric walls near the *pcp* may not be occurring during constriction of the ampulla. In Figure 5C bursting of the CA1 and CA2 neurons recorded from the *lvn* was suppressed by that of the *pcp* neurons 1 and 2 (PCP1, PCP2) and PD neurons in the *pcp*-pyloric cycle. The PCP and PD neurons provide the motor commands for opening the *pcp* and cardio-pyloric channels. Bursting of the CA3 neuron, as recorded from the *son*, continued without inhibition from the PCP and PD neurons. The observations suggest that the CA neurons, which command constriction of the dorsolateral gastric wall of the cardiac stomach, may be inactivated during the opening of the *pcp* and pyloric channels to allow the transfer of suspensions of food particles from the cardiac to the pyloric stomach.

DISCUSSION

The stomatogastric nervous system in decapods has been widely used for research on the generation of rhythmic motor output pattern [1, 2]. We have introduced the stomatopod preparation, which lacks the gastric system found in the STG of decapods, to comparative neurophysiology of this nervous system [16]. In the previous paper, the *pcp*-pyloric system of *Squilla* was analyzed for comparison with the pyloric system in decapods, *Panulirus* and *Homarus*. In the present paper, the anatomy and physiology of the cardiac system in the STG of *Squilla* has been described. The cardiac ossicles located on the cardiac sac are not a chewing system like gastric mill ossicles in decapods [14, 15]. The food, partially masticated by the mandibles, is macerated by muscular contractions of the cardiac stomach with the aid of digestive juices that are pumped forward by the *pcp* and pyloric stomach [15, 16]. Four intrinsic muscles and 5 extrinsic cardiac muscles that constrict or dilate the dorsal and lateral gastric walls have been identified. All of these identified muscles are innervated by motor axons from the constrictor and dilator neurons in the STG.

Innervation

It is of interest to compare innervation of the muscles in the cardiac stomachs of stomatopods and decapods. Maynard and Dando [5] have described the detailed anatomy of muscles and nerves of the stomach in several decapods. In *Squilla* the *lvn* is the principal nerve carrying the motor axons which innervate the muscles of the *pcp* and pyloric stomach [16]. It was found that the *lvn* and, in addition, *son* are the principal nerves which contain motor axons both of the cardiac constrictor and dilator neurons of the STG. They divide peripherally into constrictor and dilator nerves supplying 8 identified muscles. One extrinsic muscle is doubly innervated. In *Panulirus*, on the other hand, the dorsal ventricular nerve contains most of motor axons from the STG which innervate the muscles of the gastric mill and pyloric stomach [1]. The anterior median nerve and median ventricular nerve (*mvn*) carry the motor axons of the cardiac constrictor neurons (AM and IC neurons) of the STG which innervate the muscles of the cardiac stomach and the muscles of the ventral cardiac ossicles (*cv2*) [1, 5, 11]. The motor innervation provided by the cardiac constrictor neurons in *Panulirus* is relatively simple, and differs from that in *Squilla*. In *Panulirus*, the *mvn* also contains a motor axon from the cardiac dilator neuron (VD neuron) which innervates the muscles of the ventral cardiac ossicles (*cv1*). The *cv1* and *cv2* muscles move the ventral gastric wall of the cardiac stomach in *Panulirus*: the one is homologous to the *plcm* in *Squilla*, and the other to the *pcm*. Four nerves carry motor axons of 2 cardiac dilator neurons (CD neurons) in *Panulirus* [11, 12]. Motor nerves branch from these nerves to innervate 7 extrinsic muscles: 5 muscles are innervated by the CD1, 4 muscles by the CD2, and thus 2 muscles receive a double innervation. The peripheral courses of the CD neurons in *Panulirus* appear complex compared to those in *Squilla*.

Cardiac cycle

Cardiac cycling occurred spontaneously in STG of semi-intact preparations (Fig. 2). The most notable characteristics of the cardiac cycle pattern, compared to the *pcp*-pyloric cycle pattern, are that

the burst duration is very long (over 10 times), the cycle rate is low, and the pattern is composed of only two alternately bursting groups. Although cardiac cycles did not occur spontaneously in the semi-isolated preparation, they could be produced by activation of the son inputs. These were activated via the CG by stimulation of afferent fibers (Fig. 4).

While the cardiac cycle is brought on by inputs from a higher center, the pcp-pyloric cycle is intrinsic to the STG, although it is modifiable [16]. The mechanism of cyclic pattern generation may be different for the two cycles. The cardiac cycle is generated by two groups of neurons. Four CA neurons and 3 CD neurons could be identified in the STG from the peripheral recordings (Fig. 3), but interactions present among them were not analyzed.

Comparison with the motor neurons of the cardiac system between stomatopods and decapods has been made as follows. In *Panulirus*, they have been described by Moulins and Vedel [11]. The CA1, CA2 and CA3 neurons are homologous to the AM neuron in *Panulirus*. These neurons control movements of the intrinsic muscles spread over the gastric wall. The CA4 neuron may be functionally homologous to the IC neuron in *Panulirus*. Both command constriction of the posterior lateral gastric wall. The CD3 neuron may be homologous to the VD neuron in *Panulirus*: the one is an antagonist of the CA4 neuron, and the other of the IC neuron. The VD and IC neurons are involved in the pyloric cycle [7]. The function of these neurons appears to be related to movements of both the cardiac and the pyloric stomachs, although their role in the pyloric cycle is unknown [6, 11]. Comparison of the phase relationships of the pcp-pyloric cycle in *Squilla* with those of the pyloric cycle in *Panulirus* suggests that the PCP1 (or PCP2) and PCP3 neurons, which control cardiac plate muscles, are homologous to the VD and IC neurons, respectively [16]. It is unknown whether the CA4 and CD3 neurons are involved in the pcp-pyloric cycle in controlling movements of these muscles. The CD1 and CD2 neurons in *Squilla* are certainly homologous to those in *Panulirus*. The two CD neurons in *Panulirus* exhibit complex functional properties

that contribute to the organization of the neural network taking part in motor commands [11, 12]. The cell body of CD1 is located in the OG, and that of CD2 in the STG. Furthermore, their peripheral nerve distributions are quite complex. Such complexity has not been observed in the 3 CD neurons of *Squilla*. Their cell bodies are located in the STG.

The functional movements of the cardiac stomach commanded by the cardiac cycle can now be described, although movements of the ventral gastric wall remain to be analyzed. Three of the four types of movements of the gastric wall described by Kunze [15] have been examined in this study. Four variations of spontaneous cardiac cycling are associated with them. The motor patterns shown in Figure 2D command medial movements of the dorsal and lateral gastric walls (termed the first phase by Kunze). The motor patterns which contribute to medial movements of the dorsal, lateral and posterior lateral gastric walls (the second phase) are illustrated in Figure 2A, B and C. Medial movements of the anterior dorsal gastric wall (the third phase) appear to be commanded by the motor pattern similar to that shown in Figure 2D, because the constrictor neurons in the son do not fire in this pattern. Maceration of ingested food may occur during these three phases while the pcp lateral channels are closed. Kunze [15] has seen the fourth phase which seems to occur sporadically. During this phase, digested food are transferred by simultaneous muscular contractions from the cardiac to the pyloric stomach through the pcp lateral and cardio-pyloric channels. Such food movements have not been examined in this study (see next section).

Functional relations between cardiac and pcp-pyloric cycles

It has been shown that once the cardiac cycle is activated by stimulation of the son input fibers, the pcp-pyloric cycle is suppressed [16]. On the other hand, it was found that the pcp-pyloric cycle units suppressed the cardiac cycle units: the PY neurons inhibited the CA1 and CA4 neurons (Fig. 5A, B); the PCP1, PCP2 and PD neurons also inhibited the CA1 and CA2 neurons (Fig. 5C). In both cycles

the units fired alternately. The CA1 and CA4 neurons control contractions of the lcm1 and pem, respectively, to bring the dorsolateral gastric wall medially in front of the pcp. Thus, the gastric wall can be tightly pressed to the dorsal floor of the pcp, resulting in blockade of the cardio-pyloric channel. The PY neurons command constrictions of the ampulla in the pyloric stomach, which cause a backflow of digestive juices to the cardiac stomach through the cardio-pyloric channel from the pyloric ampullary channels [15]. The inhibition of the cardiac constrictor neurons by the pyloric neurons probably makes the backflow possible. Figure 5C shows the pattern of motor outputs likely to represent the commencement of the transfer of digested food from the cardiac to the pyloric stomach: the CA neurons command constrictions of the gastric wall to force food suspensions backward, and the PCP and PD neurons command the opening of the pcp lateral and cardio-pyloric channels. In *Panulirus*, the CD neurons accelerate or inhibit the PD neurons [11]. Such modulation of the pcp-pyloric cycle by the cardiac cycle units appeared to be present in the *Squilla* STG (Fig. 4). However, the functional significance of such modulation is still unknown.

The present study has shown that the cardiac cycle of the STG in *Squilla*, as well as the pcp-pyloric cycle, is of special interest for studying the characteristics of central pattern generators. Differences between the two cycles have been described. The cardiac and pcp-pyloric systems also provide useful models for understanding the mechanism underlying the generation of rhythmic motor patterns. The cellular properties and neural networks of the two subsystems of the STG in stomatopods will be studied for comparison with those in decapods which have been well analyzed.

ACKNOWLEDGMENTS

The author is grateful to I. M. Cooke, J. A. Benson and M. W. Miller for critical review and suggestions on this manuscript; H. Fukuyama and M. Funahashi for technical assistance; to R. Miyamoto for illustrations. This work was supported in part by a Grant-in-Aid for Scientific Research from the Ministry of Education, Science and Culture of Japan (No. 59540460).

REFERENCES

- 1 Selverston, A. I., Russell, D. F., Miller, J. P. and King, D. G. (1976) The stomatogastric nervous system: structure and function of a small neural system. *Progr. Neurobiol.*, **7**: 215-290.
- 2 Wales, W. (1982) Control of mouth parts and gut. In "The Biology of Crustacea. Vol. 4. Neural Integration and Behavior". Ed. by D. Sandeman, and H. Atwood, Academic Press, New York, pp. 165-191.
- 3 Orlov, J. (1929) Über den histologischen Bau der Ganglien des Mundmagenervensystems der Crustaceen. *Z. Mikrosk.-Anat. Forsch.*, **8**: 493-541.
- 4 Maynard, D. M. (1966) Integration in crustacean ganglia. *Symp. Soc. Exp. Biol.*, **20**: 119-149.
- 5 Maynard, D. M. and Dando, M. R. (1974) The structure of the stomatogastric neuromuscular system in *Callinectes sapidus*, *Homarus americanus* and *Panulirus argus* (Decapoda, Crustacea). *Philos. Trans. R. Soc. Lond.*, **B268**: 161-220.
- 6 Maynard, D. M. (1972) Simpler networks. *Ann. NY. Acad. Sci.*, **193**: 59-72.
- 7 Hartline, D. K. and Maynard, D. M. (1975) Motor patterns in the stomatogastric ganglion of the lobster *Panulirus argus*. *J. Exp. Biol.*, **62**: 405-420.
- 8 Dando, M. R. and Selverston, A. I. (1972) Command fibres from the supraoesophageal to the stomatogastric ganglion in *Panulirus*. *J. Comp. Physiol.*, **78**: 138-175.
- 9 Russell, D. F. (1976) Rhythmic excitatory inputs to the lobster stomatogastric ganglion. *Brain Res.*, **101**: 582-588.
- 10 Russell, D. F. (1979) CNS control of pattern generators in the stomatogastric ganglion. *Brain Res.*, **177**: 598-602.
- 11 Moulins, M. and Vedel, J. P. (1977) Programmation centrale de l'activité motrice rythmique du tube digestif antérieur chez les Crustacés décapods. *J. Physiol. (Paris)*, **73**: 471-510.
- 12 Vedel, J. P. and Moulins, M. (1977) Functional properties of interganglionic motoneurons in the stomatogastric nervous system of the rock lobster. *J. Comp. Physiol.*, **118**: 307-325.
- 13 Police, G. (1909) Sul sistema nervoso viscerale della *Squilla mantis*. *Mitt. Zool. Sta. Neapel*, **19**: 144-148.
- 14 Reddy, A. R. (1935) The structure, mechanism and development of the gastric armature in Stomatopoda with a discussion as to its evolution in Decapoda. *Proc. Indian Acad. Sci.*, **B1**: 650-675.
- 15 Kunze, J. C. (1981) The functional morphology of stomatopod Crustacea. *Philos. Trans. R. Soc. Lond.*, **B292**: 255-328.
- 16 Tazaki, K., Miyatani, M. and Ando, F. (1986) The

anatomy and physiology of the stomatogastric nervous system of *Squilla*. I. The posterior cardiac plate and the pyloric systems. *J. Comp. Physiol.*, **159A**: 521–533.

- 17 Watanabe, A., Obara, S. and Akiyama, T. (1967) Pacemaker potentials for the periodic burst discharge in the heart ganglion of a stomatopod, *Squilla oratoria*. *J. Gen. Physiol.*, **50**: 839–862.

Ultrastructure and Physiological Response of Leucophores of the Medaka *Oryzias latipes*

MASATAKA OBIKA

Department of Biology, Keio University, Yokohama 223, Japan

ABSTRACT—Ultrastructure and physiological responses of leucophores in isolated scales of the medaka *Oryzias latipes* were studied. Many of the leucophores are in close association with overlying melanophores, and nerve fibers that run between the two cells frequently form synapses on both sides. This situation provides a very efficient way to conduct body lightening response, since the stimulation of single adrenergic fiber produces pigment aggregation in the melanophore and dispersion in the leucophore almost simultaneously. Although it appears to be rather infrequent, some nerve fibers enter into the cell body of leucophores. Spherical and tubular synaptic vesicles, and larger vesicles with an electron-dense central core are observed in single nerve fibers. Responses of leucophores are produced by selective migration of the pigment granules toward or away from the center of the cell. Numerous microtubules and 10 nm filaments run parallel to the long axis of the dendrites, though direct connection between these cytoskeletal elements and pigment granules has not been ascertained by electronmicroscopy. Pigment dispersion and aggregation proceed normally in the presence of cytochalasin B while colchicine and EHNA (erythro-9-3-(2-hydroxyonyl)adenine) potently inhibit pigment aggregation. NEM (N-ethylmaleimide) interferes with the pigment dispersion elicited by epinephrine. These results suggest that the intracellular movements of pigment granules in leucophores are microtubule-dependent.

INTRODUCTION

Leucophores in the integument of the medaka are generally found in close association with overlying melanophores to form the melanophore-leucophore combination. Pigment cells in this teleost are under the control of adrenergic nerves, and the prevailing alpha adrenergic receptors on melanophores make their pigment aggregate in response to nervous stimulation producing body lightening [1] while leucophores, which are predominantly controlled by beta adrenergic receptors respond to the same signal with pigment dispersal that also enhances body blanching by increasing light reflectance [2, 3]. Thus, the combination of these two types of pigment cells represents an exquisite example of dermal chromatophore unit [4] in fish integument. Studies on the physiological responses of leucophores have so far been carried out at light microscopic level, but the

ultrastructural basis of their responsiveness has not yet been clarified.

The present study deals with the ultrastructure of leucophore and melanophore-leucophore combination. Innervation of nerve fibers into leucophores and melanophore-leucophore combination is clearly shown for the first time. Leucophores contain numerous spherical pigmentary organelles that selectively migrate either centripetally or centrifugally upon aggregative and dispersive stimuli. Their cytoplasm possesses a moderately developed microtubule system in addition to 10-nm filaments. Pharmacological study indicates that the microtubule system, rather than actin-myosin system, is involved in the motile mechanism.

MATERIALS AND METHODS

Leucophores in the dermis of adult *Oryzias latipes* were used in this study. Scales were plucked from the anterior-dorsal region.

Electron microscopy

Scales were fixed in 2.5% glutaraldehyde in 0.1 M cacodylate buffer (pH 7.2) for 30 to 60 min at room temperature, post-fixed in 1% OsO₄ in the same buffer for 30 min at room temperature, dehydrated through a graded series of alcohol and embedded in epoxy resin. Ultrathin sections were stained with uranyl acetate and lead citrate and observed in a JEOL 100S electron microscope at the acceleration voltage of 80 kV.

Physiological responses and chemicals

Physiological and pharmacological studies were made on the materials from which overlying epidermis had been removed by a 30 min treatment in 0.25% collagenase (Worthington, type II) in a Ca-free teleost saline solution with gentle agitation. Response of leucophores was observed under a Nikon inverted microscope (Diaphot). Teleost saline solution contained 128 mM NaCl, 2.6 mM KCl and 1.8 mM CaCl₂ and buffered with 5 mM Tris-HCl at pH 7.2 [3]. Epinephrine (Sigma), theophylline (Tokyo Kasei), colchicine (Sigma), N-ethylmaleimide (NEM, Kokusan Kagaku,

Tokyo), 2, 4-dinitrophenol (Tokyo Kasei), potassium cyanide (Kokusan Kagaku), erythro-9- β -(2-hydroxynonyl)adenine (EHNA, Burroughs Wellcome) and synthetic teleost melanophore concentrating hormone (MCH), which was generously supplied by Dr. M. E. Hadley of University of Arizona, were dissolved directly in the saline solution at appropriate concentrations. Stock solution of cytochalasin B (Aldrich) was made in dimethylsulfoxide (DMSO) and diluted with saline immediately before use.

RESULTS

Morphology of leucophore and its association with melanophore

Although a few leucophores in the dorsal skin are found without having any obvious contact with other pigment cells, a large number of leucophores are observed immediately below overlying melanophores. The dendritic processes of melanophores occasionally extend downward and embrace the upper portion of leucophores. Figure 1 depicts an example where the structures like

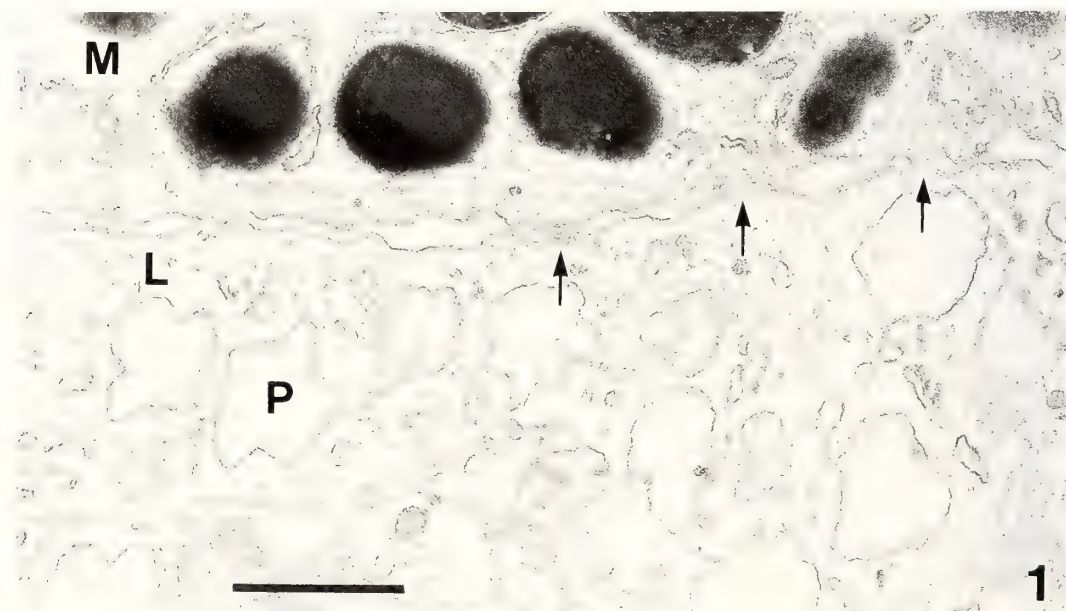


FIG. 1. Overlying melanophore (M) is in close contact with a leucophore (L) to form a melanophore-leucophore complex. Electron lucent vesicles in the leucophore (P) are pigmentary organelles characteristic of this cell type. Arrows indicate the sites where the pigment cells are closely attached. Bar represents 0.5 μ m.

intercellular bridge and the accumulation of dense materials on the membranes of both chromatophores are seen (arrows). Though the cells are very closely attached, there is no evidence that indicates the actual cytoplasmic connection between the two different types of chromatophores.

Innervation to melanophore-leucophore combination

Axons with putative synaptic vesicles of various morphology are frequent near the chromatophore combination. Many of them run in the intercellular space between melanophore and leucophore (Figs. 2 and 3) while some enter deeper into leucophores (Figs. 4 and 5). In any case, morphological specialization of pre- and postsynaptic membranes is not distinct. Synaptic vesicles are either spherical or tubular and contain moderately electron dense material. Some of the larger vesicles contain electron dense core. The diameter of smaller vesicles and tubules is about 40 nm while the larger ones with central electron dense core measure about 80 nm. These three types of synaptic vesicles occur in a single axonal fiber. Although melanophores have a relatively large number of synapses both on the outer (epidermal side) and lower (leucophore side) surfaces, axons on leucophores are rather infrequent compared with those locating on melanophores.

Morphology of leucophores with aggregated and dispersed pigment granules

Figure 6 depicts a typical profile of a leucophore with aggregated pigments. Central portion of the cell is occupied by an aggregate of spherical pigmentary organelles that contain some fuzzy, amorphous intravesicular substance. Pigmentary organelles are rather uniform in size (about 500 nm in diameter). The central cytoplasm contains ER, ribosomes, microtubules, 10-nm filaments and some other membrane-bound vesicles but mitochondria are always found in the dendritic processes. The dendrites are more or less flattened but retain their width after the withdrawal of the pigment. Smaller vesicles, mitochondria, a large number of ribosomes, 10 nm filaments and numerous microtubules aligned parallel to the long axis of the processes are prominent cytoplasmic

organelles in dendrites. Golgi complexes are frequent in their proximal portion. In cells with dispersed pigment, dendrites contain pigmentary organelles in addition to the larger vesicles in various size and morphology (Fig. 7). The origin and function of these larger vesicles are unknown, but they sometimes contain intravesicular material similar to that found in pigment granules. A few mitochondria are seen in the central portion of the cell, though the majority of them are densely populated in the proximal portion of the dendrites. Microtubules and 10-nm filaments are also abundant in this region. These findings indicate that chromatophore responses of the leucophores are produced by the change in the intracellular distribution of the pigmentary organelles.

The effects of chemicals on leucophore responses

EHNA Leucophores with their pigment aggregated in the saline solution responded to EHNA with pigment dispersion in a dose-dependent manner. This response was completely reversed by washing the specimens with physiological saline solution. At concentration of 30 μM , EHNA had no appreciable effect on aggregated leucophores, at 60 μM , however, it produced a slight pigment dispersal within 10 min. A 10 min incubation in 125 μM EHNA produced an almost full dispersion of leucophores in 10 min. In 500 μM or 1 mM, dispersal was induced within 5 min. Figure 8 shows an example where aggregated leucophores in saline solution (Fig. 8a) became dispersed after 20 min incubation in 1 mM EHNA (Fig. 8b). Subsequent perfusion with 10 μM epinephrine for 15 min in the presence of EHNA did not change their morphology in appreciable degrees (Fig. 8c). Further treatment of the cells with an aggregating agent, melatonin (1 $\mu\text{g}/\text{ml}$) for 25 min produced only a very minute response (Fig. 8d). The effect of EHNA was reversed by washing the scale in saline solution for 20 min and leucophores became punctate (Fig. 8e). These cells responded to epinephrine in 10 min as shown in Figure 8f.

Colchicine Most of the leucophores in isolated scales remained aggregated in physiological saline. Transfer of these scales into 1 to 5 μM

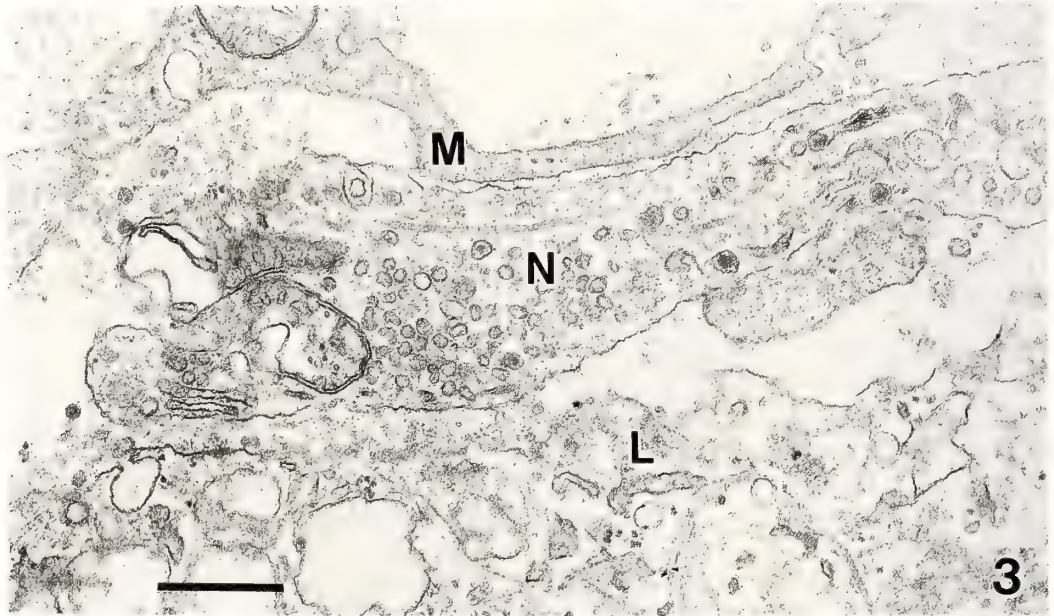
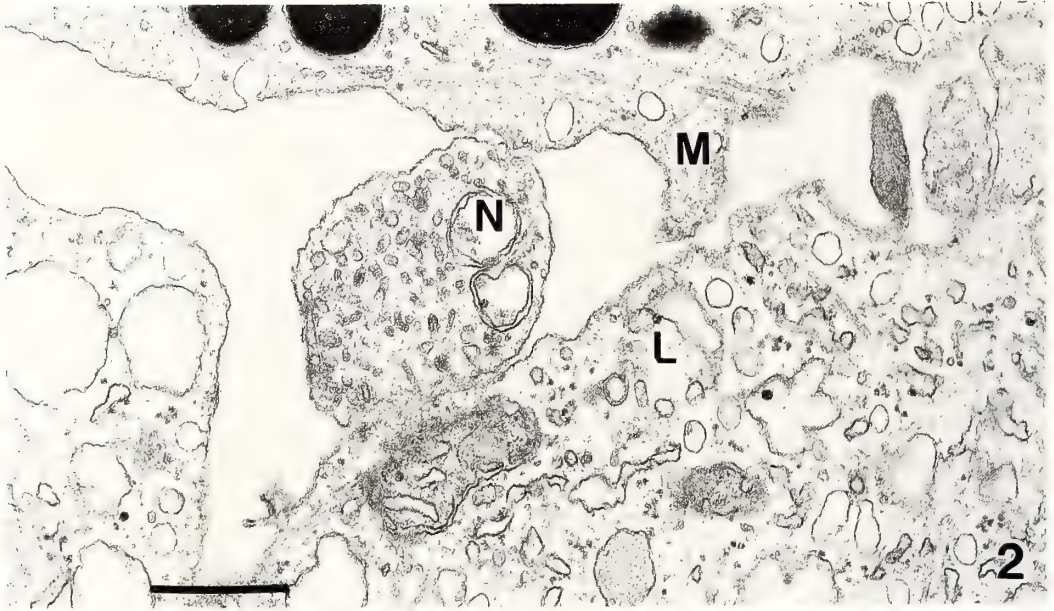
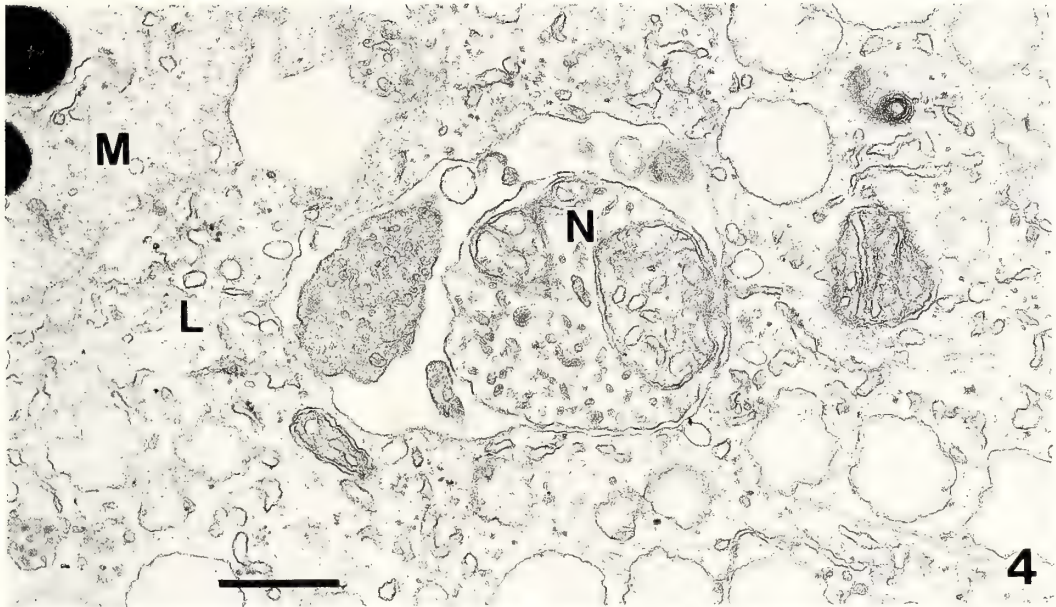


FIG. 2. A single nerve fiber (N) makes synaptic contacts with melanophore (M) and leucophore (L). Bar represents $0.5 \mu\text{m}$.

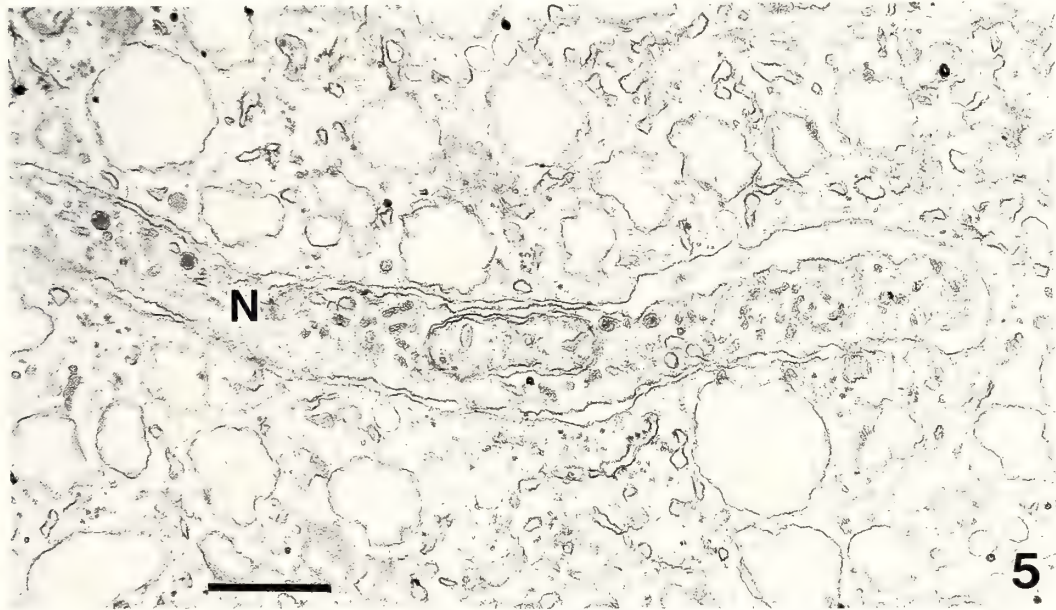
FIG. 3. A longitudinal section of a nerve fiber (N) between the dendrites of melanophore (M) and leucophore (L). Melanosomes are withdrawn from the dendrite. Synaptic vesicles of various size and morphology are seen. Ten nm filaments are found in leucophore. Scale bar represents $0.5 \mu\text{m}$.

colchicine produced a rapid dispersion of leucophores within a few minutes. Figure 9 shows leucophores in saline (Fig. 9a) and after 1 hr

incubation in 1 mM colchicine (Fig. 9b). Melatonin, epinephrine and theophylline all failed to elicit further response of leucophores in the



4



5

FIG. 4. Cross-sectional profile of a nerve fiber (N). The fiber is encircled by leucophore (L) membrane. Bar: 0.5 μm .

FIG. 5. Longitudinally sectioned nerve (N) found near the central portion of a leucophore. Bar: 0.5 μm .

presence of colchicine.

Cytochalasin B Leucophore responses are found to be totally insensitive to cytochalasin B. Specimens treated in 10 $\mu\text{g}/\text{ml}$ cytochalasin B (final concentration of DMSO was 0.25%) for up to 3 hr

responded normally to epinephrine with pigment dispersion. Removal of epinephrine produced leucophore reaggregation. Figure 10 shows a typical response of leucophores to cytochalasin B. Most of the leucophores in an isolated scale

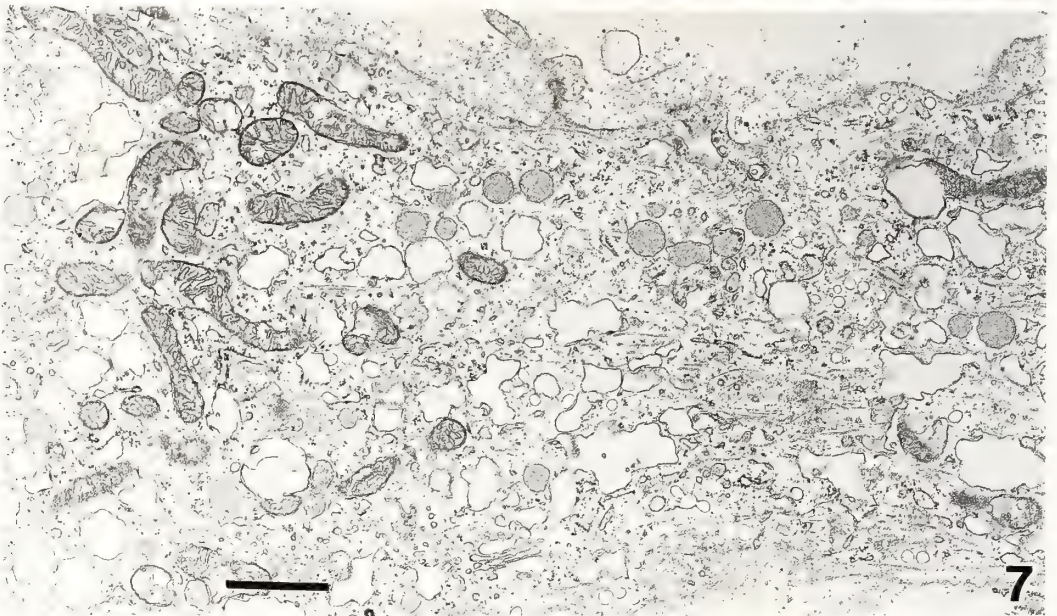
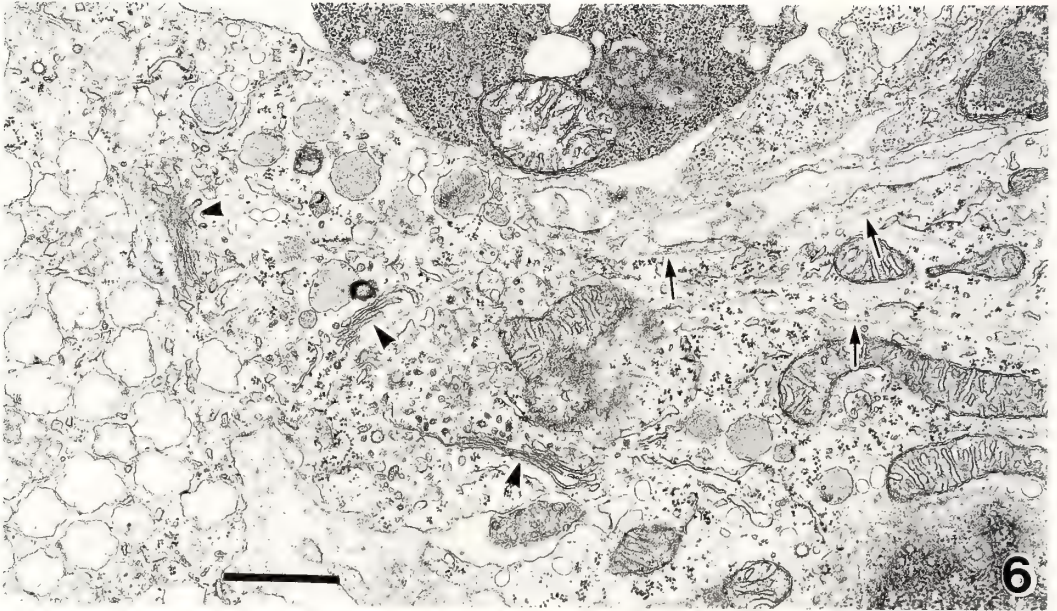


FIG. 6. Proximal portion of a dendrite of a leucophore with aggregated pigment. Pigment granules have migrated toward the cell center (far left), and the dendrite contains Golgi apparatus (arrowheads), mitochondria, microtubules (arrows) and other cytoplasmic organelles except pigment granules. Scale bar represents $1\ \mu\text{m}$.

FIG. 7. Proximal portion of a dendrite of a leucophore with dispersed pigment. Pigment granules and some larger vesicles are now present in the dendrite. Bar: $1\ \mu\text{m}$.

remained punctate in saline solution (Fig. 10a). Incubation in cytochalasin B for 2 hr did not change their shape (Fig. 10b) and the following

perfusion with the medium containing both epinephrine and cytochalasin B produced a prompt dispersal of the cells (Fig. 10c) within 7

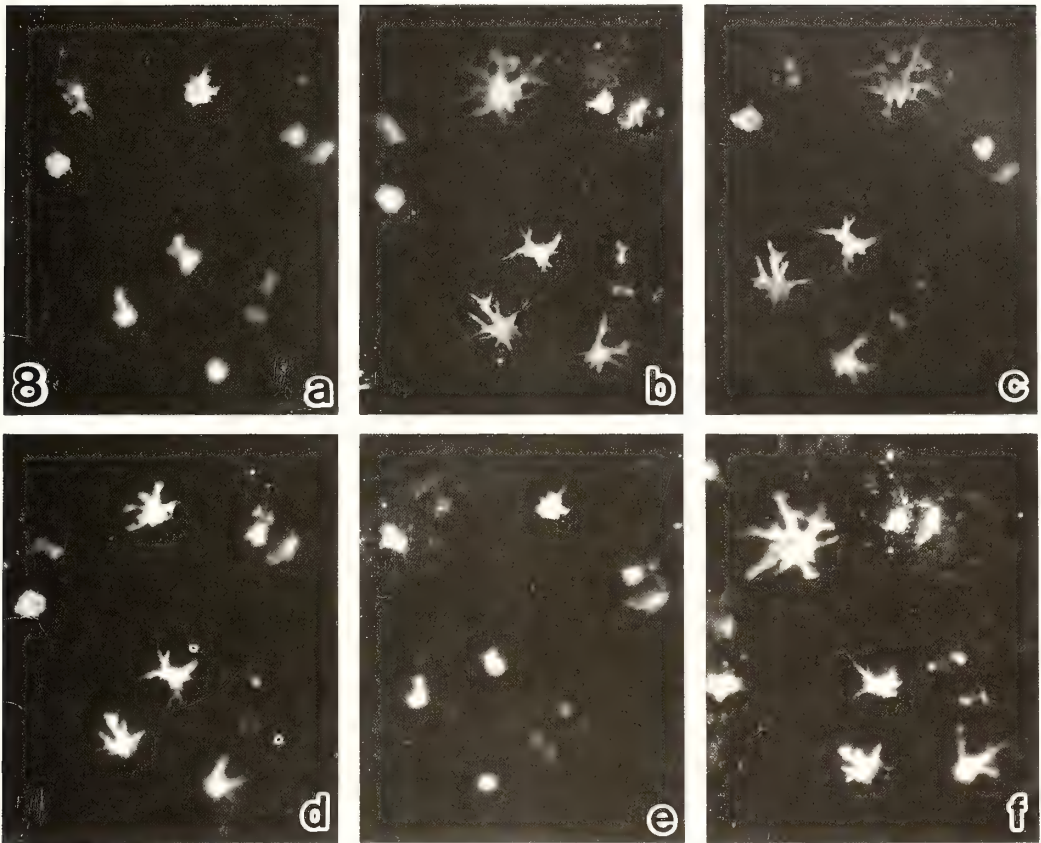


FIG. 8. Effect of EHNA on the physiological response of leucophores. Aggregated leucophores in the saline solution (a) became dispersed by a 20 min incubation in 1 mM EHNA (b). No further dispersion was induced by a 15 min treatment with $10 \mu\text{M}$ epinephrine (c). These cells did not respond to melatonin in appreciable degrees (d). The dispersive effect of the drug was completely reversed by washing in the saline (e), and the cells rapidly redispersed when treated with epinephrine (f). $\times 113$.

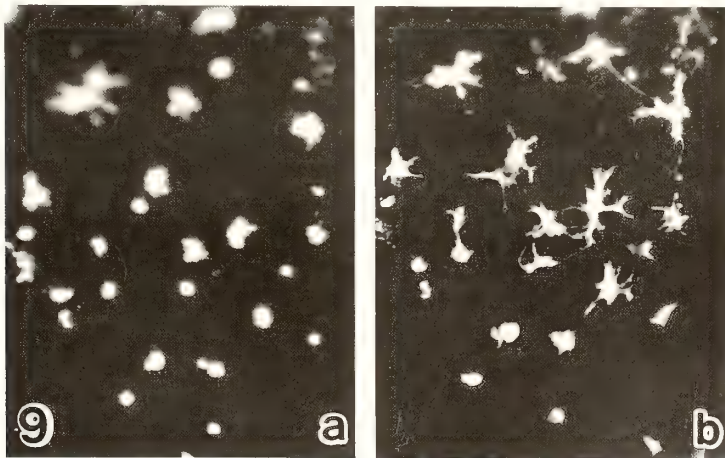


FIG. 9. Effect of colchicine. Aggregated leucophores in the saline solution (a) became dispersed by a 1 hr incubation in 1 mM colchicine (b). $\times 113$.

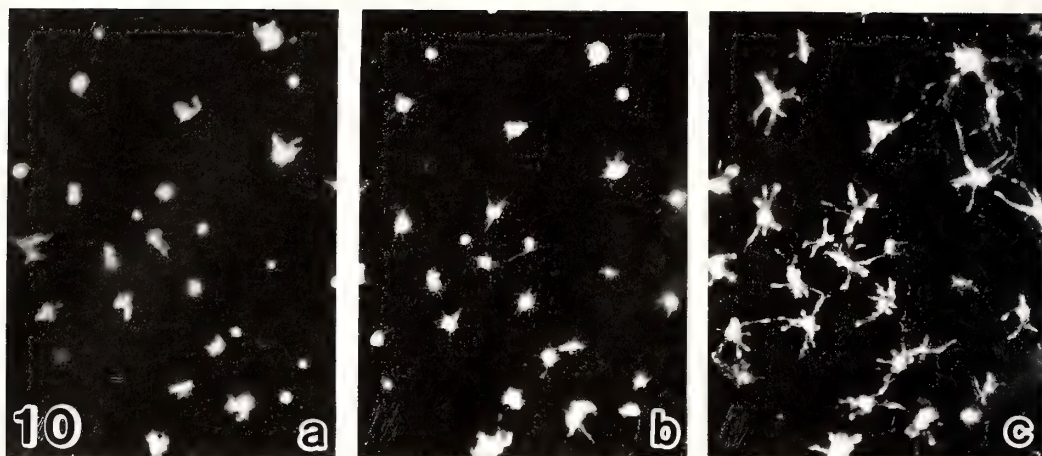


FIG. 10. Effect of cytochalasin B. Aggregated leucophores in the saline (a) remain aggregated during a 2 hr incubation in cytochalasin B (b). Rapid pigment dispersion was induced by epinephrine in the presence of cytochalasin B (c). $\times 113$.

min. Close observation of the dendritic processes of dispersed leucophores indicated that their tips were more inflated compared to those dispersed in the absence of cytochalasin B.

NEM NEM at concentrations between 0.1 to 2.5 mM potently inhibited epinephrine- or theophylline-induced pigment dispersion in leucophores. Application of the drug on dispersed leucophores (produced by theophylline-pretreatment) did not induce pigment aggregation either. This drug has also a very potent inhibitory effect on melanophore aggregation that is normally produced by epinephrine and MCH.

Potassium cyanide and dinitrophenol (DNP) When the isolated scales were incubated in KCN at 5×10^{-4} M for 40 to 60 min, dispersion of leucophores by epinephrine or theophylline was only partially inhibited. DNP at 1 mM potently inhibited leucophore dispersion by epinephrine and theophylline, but produced pigment aggregation when applied on dispersed leucophores. The effects of these metabolic inhibitors on leucophore responses were, however, not as prominent as those found on melanophores and xanthophores where the responses appear to be more susceptible to these chemicals.

Leucophore response to MCH

Leucophores with aggregated pigments produced by placing scales in physiological saline, or

those with dispersed state induced by theophylline treatment, were perfused with synthetic MCH (1 nM–1 μ M). Neither pigment dispersion nor aggregation was induced although the hormone was potent enough to produce full pigment aggregation in neighboring melanophores within a few minutes at the lowest concentration employed.

DISCUSSION

Membrane specialization of melanophore-leucophore junction

Although leucophores and melanophores of *Fundulus* are in close association as in the present species, no specialized junctional structure has been demonstrated in the earlier work [5]. In *Oryzias*, leucophores and melanophores appear to be more closely associated. Sometimes membranes of the two cells appeared to be tightly attached. Whether the association is simply holding the two cells together (tight junction) or it actually functions as electrical or metabolic coupling (gap junction) remains to be investigated.

Innervation into melanophore-leucophore combination

Pharmacological evidence indicates that leucophores of the medaka are under the control of beta adrenergic receptors [2, 3]. Since rhythmic

pigment granule aggregation and dispersion (pulsation) induced by Ba ions occur simultaneously but in opposite directions in a melanophore-leucophore combination, it has been suggested that the two chromatophores are innervated by the same nerve. Furthermore, the evidence is presented that xanthophores are also controlled by the same nerve, thus providing an efficient way to adapt the fish to its environmental background [6]. Since the early work of Ballowitz [7], innervation into fish melanophores has been studied repeatedly at light microscopic level (see [8, 9] for review). Adrenergic innervation to melanophores and erythrophores has also been demonstrated recently by light microscopic autoradiography [10–12]. At electron microscopic level, chromatophore-neural junctions have been described in the melanophores of *Fundulus* [13], *Chasmichthys* [14] and the angelfish *Pterophyllum* [15]. However, innervation to bright-colored chromatophores, i.e. xanthophores and leucophores, has not been studied at ultrastructural level. The present study clearly shows that the melanophore-leucophore combination is, in fact, innervated by a single nerve fiber as Iwata and his collaborators have concluded from their physiological studies [6]. The synaptic structure is rather indistinct, membrane specialization with pre- and postsynaptic densities being only occasionally observed. Synapses are frequently found on the epidermal side of melanophore membrane in addition to those found in melanophore-leucophore junctions. Sometimes fibers run deeper into melanophores or leucophores. Observation on serial sections indicates that nerve fibers form en passant synapses as has been shown in the angelfish melanophores [15].

Morphology of leucophore with aggregated and dispersed pigments

Ultrastructural observation revealed that, in contrast to the response of melanophores where the cytoplasm other than pigment granules translocates simultaneously [16, 17], aggregation or dispersion of leucophores is produced by a selective translocation of pigmentary organelles in the cytoplasm toward the centripetal or centrifugal direction. Very selective movement of pigment

granules conducted by a cytoskeletal meshwork has been reported in erythrophores [18]. In leucophores, however, direct association of the pigment granules with cytoplasmic microtubules or other cytoskeletal elements has not been demonstrated. Dendritic processes of a leucophore with aggregated pigments contain numerous microtubules, 10 nm filaments, free and membrane bound ribosomes, mitochondria and other membrane bound organelles but are entirely free of pigment granules. The central portion of the cell is, on the other hand, largely occupied by pigment granules but contains other cytoplasmic organelles in much less number compared to the peripheral region. Microtubules running parallel to the long axis of the dendrite are abundant while 10 nm filaments are more frequent near the central portion of the cell. Sometimes small bundles of 10 nm filaments were found at the boundary between the mass of pigment granules and the base of the dendrite. Mitochondria of leucophores, unlike those of melanophores that aggregate toward the perinuclear region during pigment aggregation, did not change their distribution pattern drastically during pigment migration. This suggests that the pigment migration in leucophores proceeds more gently and selectively, provided that mitochondria translocate passively in both cases.

Mechanism of pigment migration

EHNA, a dynein-ATPase inhibitor, made leucophore disperse at concentrations as low as 60 μ M. The effect was dose-dependent and was readily reversed by washing. Both in intact and detergent-treated, permeabilized preparations of *Fundulus* melanophores, EHNA at 2 mM blocked epinephrine-elicited pigment aggregation [19] and in melanophores of *Oryzias*, it inhibited epinephrine or MCH-induced melanosome aggregation at concentrations between 0.25 to 2 mM [20]. In *Holocentrus* erythrophores, the drug at 1 to 4 mM prevented the saltatory movement of pigment granules but epinephrine did induce pigment aggregation at slower rate than in untreated cells [21]. Thus, the response pattern of the leucophores to EHNA is similar to that observed in melanophores, though leucophores appear to be more sensitive to the inhibitor.

Kinesin, a microtubule-dependent motor molecule that supports anterograde axoplasmic transport of cytoplasmic particles [22, 23], is reported to be relatively resistant to the effect of EHNA [24] or NEM [23]. The movement of pigment granules within leucophores in centripetal and centrifugal directions was totally arrested by the presence of NEM, and centrifugal displacement of the granules was produced by EHNA. Although the effects of these drugs and those of uncouplers of oxidative phosphorylation may be partially due to the depletion of ATP, relatively high sensitivity of the leucophores to NEM and EHNA suggests the involvement of dynein-tubulin interaction in their responses, especially in pigment aggregation, as has been suggested in fish melanophores [19, 20] and melanoma cells [25]. The dispersive effect of colchicine is common to all types of *Oryzias* chromatophores but hardly reversible. Pigment dispersion in leucophores was induced rapidly in the presence of relatively low concentrations of the alkaloid. Cytoplasmic microtubules appear to be resistant to this drug, and a derivative of colchicine, lumicolchicine, which does not bind to tubulin also blocks pigmentary responses in melanophores in a similar manner as colchicine does [26]. These observations suggest that the site of action of colchicine is not restricted on cytoplasmic microtubules. The involvement of actin-myosin system in the pigment movements is not likely since the responses were insensitive to cytochalasin B.

It has recently been suggested that pigment dispersal and aggregation in fish xanthophores and melanophores are brought about by protein phosphorylation and dephosphorylation, respectively [27–30]. Though the mechanism of pigment translocation in leucophores remains to be ascertained from this point of view, induction of pigment dispersal by theophylline or dibutyl cyclic AMP [2] allows an assumption that the elevation of intracellular cyclic AMP level produces pigment dispersal in leucophores as well as in the other types of chromatophores.

REFERENCES

- Fujii, R. (1961) Demonstration of the adrenergic nature of transmission at the junction between melanophore-concentrating nerve and melanophore in bony fish. *J. Fac. Sci. Univ. Tokyo, Sec. IV*, **9**: 170–196.
- Obika, M. (1976) An analysis of the mechanism of pigment migration in fish chromatophores. *Pigment Cell*, **3**: 254–264.
- Iga, T., Yamada, K. and Iwakiri, M. (1977) Adrenergic receptors mediating pigment dispersion in leucophores of a teleost, *Oryzias latipes*. *Mem. Fac. Lit. Sci., Shimane Univ. Nat. Sci.*, **11**: 63–72.
- Bagnara, J. T., Taylor, J. D. and Hadley, M. E. (1968) The dermal chromatophore unit. *J. Cell Biol.*, **38**: 67–79.
- Menter, D. G., Obika, M., Tchen, T. T. and Taylor, J. D. (1979) Leucophores and iridophores of *Fundulus heteroclitus*: Biophysical and ultrastructural properties. *J. Morphol.*, **160**: 103–120.
- Iwata, K. S., Takahashi, T. and Okada, Y. (1981) Nervous control in chromatophores of the medaka. In "Phenotypic Expression in Pigment Cells". Ed. by M. Seiji, Univ. Tokyo Press, Tokyo, pp. 433–438.
- Ballowitz, E. (1893) Die Nervenendigungen der Pigmentzellen. *Z. wiss. Zool.*, **56**: 673–706.
- Parker, G. H. (1948) *Animal Colour Changes and their Neurohumours*. Cambridge Univ. Press, Cambridge.
- Bagnara, J. T. and Hadley, M. E. (1973) *Chromatophore and Color Change*. Prentice-Hall, N.J.
- Yamada, K., Miyata, S. and Katayama, H. (1984) Autoradiographic demonstration of adrenergic innervation to scale melanophores of a teleost fish, *Oryzias latipes*. *J. Exp. Zool.*, **229**: 73–80.
- Miyata, S. and Yamada, K. (1985) Pattern of adrenergic innervation to scale erythrophores of the swordtail, *Xiphophorus helleri*. *Zool. Sci.*, **2**: 49–57.
- Miyata, S. and Yamada, K. (1987) Innervation pattern and responsiveness of melanophores in tail fins of teleost. *J. Exp. Zool.*, **241**: 31–39.
- Bikle, D., Tilney, L. G. and Porter, K. R. (1966) Microtubules and pigment migration in the melanophores of *Fundulus heteroclitus* L. *Protoplasma*, **61**: 322–345.
- Fujii, R. (1966) A functional interpretation of the fine structure in the melanophore of the guppy, *Lebistes reticulatus*. *Annot. Zool. Japon.*, **39**: 185–192.
- Schliwa, M. (1976) Fine structure of nerve-melanophore contacts in the angelfish *Pterophyllum scalare*. *Cell Tissue Res.*, **171**: 381–387.
- Obika, M. (1976) Pigment migration in isolated fish melanophores. *Annot. Zool. Japon.*, **49**: 157–163.
- Schliwa, M. and Euteneuer, U. (1978) Quantitative analysis of the microtubule system in isolated fish melanophores. *J. Supramol. Struct.*, **8**: 177–190.

- 18 Byers, H. R. and Porter, K. R. (1977) Transformations in the structure of the cytoplasmic ground substance in erythrophores during pigment aggregation and dispersion. *J. Cell Biol.*, **75**: 541–558.
- 19 Clark, T. G. and Rosenbaum, J. L. (1982) Pigment particle translocation in detergent-permeabilized melanophores of *Fundulus heteroclitus*. *Proc. Natl. Acad. Sci. USA.* **79**: 4655–4659.
- 20 Negishi, S., Fernandez, H. R. C. and Obika, M. (1985) The effects of dynein ATPase inhibitors on melanosome translocation within melanophores of the medaka, *Oryzias latipes*. *Zool. Sci.*, **2**: 469–475.
- 21 Beckerle, M. C. and Porter, K. R. (1982) Inhibitors of dynein activity block intracellular transport in erythrophores. *Nature*, **295**: 701–703.
- 22 Vale, R. D., Reese, T. S. and Sheetz, M. P. (1985) Identification of a novel force-generating protein, kinesin, involved in microtubule-based motility. *Cell*, **42**: 39–50.
- 23 Vale, R. D., Schnapp, B. J., Mitchison, T., Steuer, E., Reese, T. S. and Sheetz, M. P. (1985) Different axoplasmic proteins generate movement in opposite directions along microtubules in vitro. *Cell*, **43**: 623–632.
- 24 Brady, S. T., Lasek, R. J. and Allen, R. D. (1985) Video microscopy of fast axonal transport in extruded axoplasm: A new model for the study of molecular mechanisms. *Cell Motility*, **5**: 81–101.
- 25 Ogawa, K., Hosoya, H., Yokota, E., Kobayashi, T., Wakamatsu, Y., Ozato, K., Negishi, S. and Obika, M. (1987) Melanoma dynein: evidence that dynein is a general “motor” for microtubule-associated cell motilities. *Eur. J. Cell Biol.*, **43**: 3–9.
- 26 Obika, M., Turner, W. A., Negishi, S., Menter, D. G. Tchen, T. T. and Taylor, J. D. (1978) The effects of lumicolchicine, colchicine and vinblastine on pigment migration in fish chromatophores. *J. Exp. Zool.*, **205**: 95–110.
- 27 Lynch, T. J., Taylor, J. D. and Tchen, T. T. (1986) Regulation of pigment organelle translocation. I. Phosphorylation of the organelle-associated protein p_{57} . *J. Biol. Chem.*, **261**: 4204–4211.
- 28 Lynch, T. J., Wu, B., Taylor, J. D. and Tchen, T. T. (1986) Regulation of pigment organelle translocation. II. Participation of a cAMP-dependent protein kinase. *J. Biol. Chem.*, **261**: 4212–4216.
- 29 Rozdzial, M. M. and Haimo, L. T. (1986) Reactivated melanophore motility: Differential regulation and nucleotide requirements of bidirectional pigment granule transport. *J. Cell Biol.*, **103**: 2755–2764.
- 30 Rozdzial, M. M. and Haimo, L. T. (1986) Bidirectional pigment granule movements of melanophores are regulated by protein phosphorylation and dephosphorylation. *Cell*, **47**: 1061–1070.

Conjugation in *Tetrahymena*: Its Relation to Concanavalin A Receptor Distribution on the Cell Surface

YOSHIKO SUGANUMA and HIROSHI YAMAMOTO¹

*Biological Laboratory, Nara Sahojogakuin College, Rokuyaon-Cho,
Nara 630, and ¹Department of Anatomy, Nara Medical University,
Kashihara, Nara 634, Japan*

ABSTRACT—Cell surface events during conjugation of *Tetrahymena thermophila* were studied by electron microscopic examination of ferritin conjugated concanavalin A (F-Con A). Small amounts of ferritin particles (F-particles) were bound to the surface of cells in the nutritional and starved states, but there were no large clusters of F-particles. In regions where F-particles were scanty, the ectoplasmic layer (epiplasm) was directly under the plasma membrane and no alveoli were observed. In contrast, in cells during co-stimulation, large clusters of F-particles were seen on the presumptive junctional area (PJA) formed after the onset of co-stimulation between the complementary mating types, and on the side walls of ectoplasmic ridges of the oral apparatus. In regions of large clusters of F-particles, there was a thick, dense ectoplasmic layer under the plasma membrane and no alveoli were seen. In conjugants, F-particles were seen not only on the smooth PJA but also in zones of gaps in the junctional area between the two conjugants. These findings suggest that the Con A binding glycocalyx is anchored to the ectoplasmic layer, a kind of cytoskeleton, under the plasma membrane.

INTRODUCTION

The protozoan ciliate *Tetrahymena* usually multiplies asexually by binary fission, but it can also reproduce sexually through conjugation. Conjugation can be induced artificially and distinguished into two successive processes: (i) an initiation process induced by removing nutrients from the culture medium, and (ii) a co-stimulation process which begins on mixing the two complementary mating types [1, 2]. Recent studies on the ultrastructure of cells during the conjugation process have shown that complementary mating type cells recognize each other during the co-stimulation period and then interact to form a presumptive junctional area (PJA) on the front side of the anterior region.

This PJA is a special area that has no particular subpellicular organelles. The co-stimulation period is followed by the conjugation period in which the cells pair at the sites of their PJAs.

Finally, the PJAs of the conjugated pairs partially fuse to form intercellular bridges [3, 4].

On the basis of these findings, the co-stimulation process in this protozoan ciliate can be regarded as the period for formation of a specialized membrane area, which may be important in cell recognition, cell adhesion, and final cell fusion. Glycocalyx on the surface of the plasma membrane is thought to be involved in cellular events such as differentiation, malignant transformation, and cell-cell adhesion [5].

Addition of concanavalin A (Con A) to cultured mammalian cells induces gathering of Con A receptors to form a cap-like structure [6]. Indeed, the conjugation process of *Tetrahymena*, which includes cell transformation, recognition and adhesion, is inhibited by Con A treatment [7, 8].

A previous report from this laboratory described ultrastructural changes in *Tetrahymena* during the process of PJA (SSA) formation [3]. In the present study, ferritin conjugated concanavalin A (F-Con A) was used to examine the distribution of Con A receptors on the cell surface of *Tetrahymena*.

MATERIALS AND METHODS

The two complementary mating types used were II and IV (strain B) of *Tetrahymena thermophila*, which were kindly provided by Dr. T. Sugai, Ibaraki University, Mito, Japan.

The ciliates were cultured axenically in growth medium (2% proteose peptone, 1% yeast extract, and 0.6% glucose) at 26°C. Late log phase ciliates (10^6 cells/ml) were harvested and washed three times with medium consisting of KCl (0.008%), NaCl (0.2%) and CaCl (0.012%) in redistilled

water with low speed centrifugation. Equal volumes of competent cells were mixed to induce subsequent conjugation.

For determination of the distribution of Con A receptors on the cell surface, a suspension of the cells was incubated with 25 $\mu\text{g/ml}$ of F-Con A (E. Y. Laboratories) for 20 min at 26°C. Then the cells were collected by centrifugation and washed twice with 0.2 M phosphate buffer, pH 7.4.

Specific binding of Con A to its receptors was confirmed in a control experiment using α -methylmannoside (20 mM).

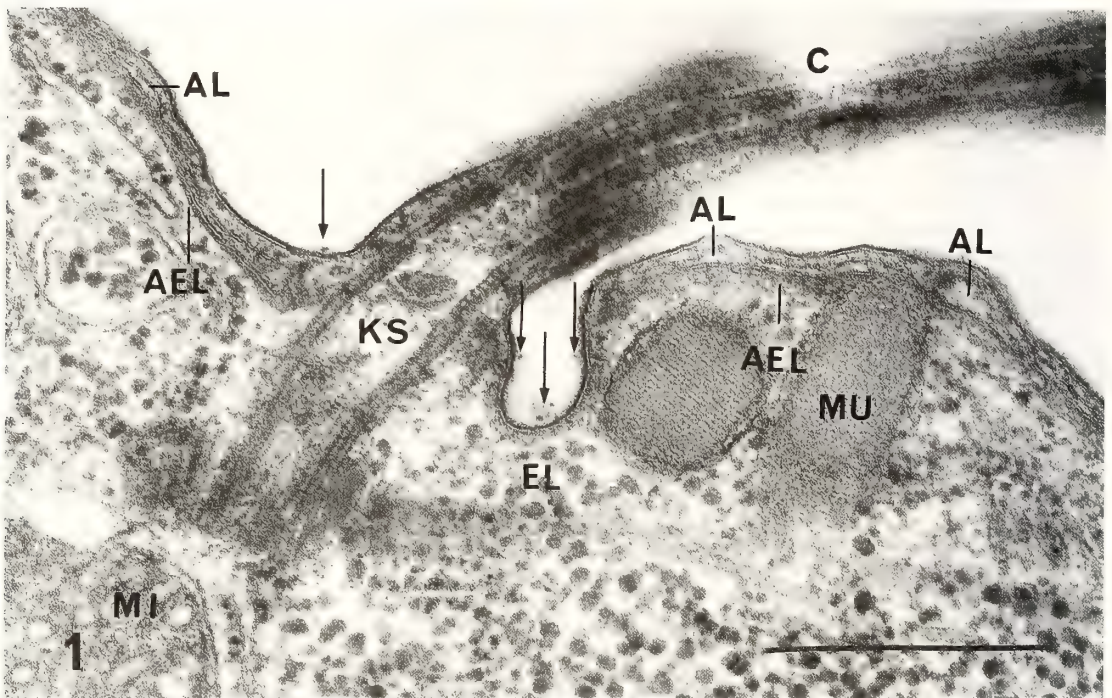


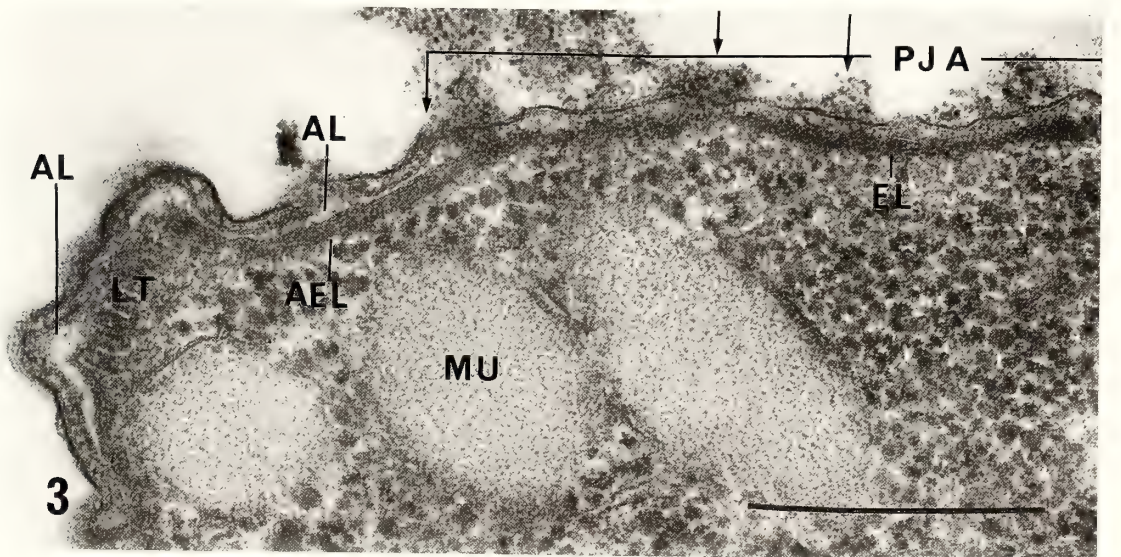
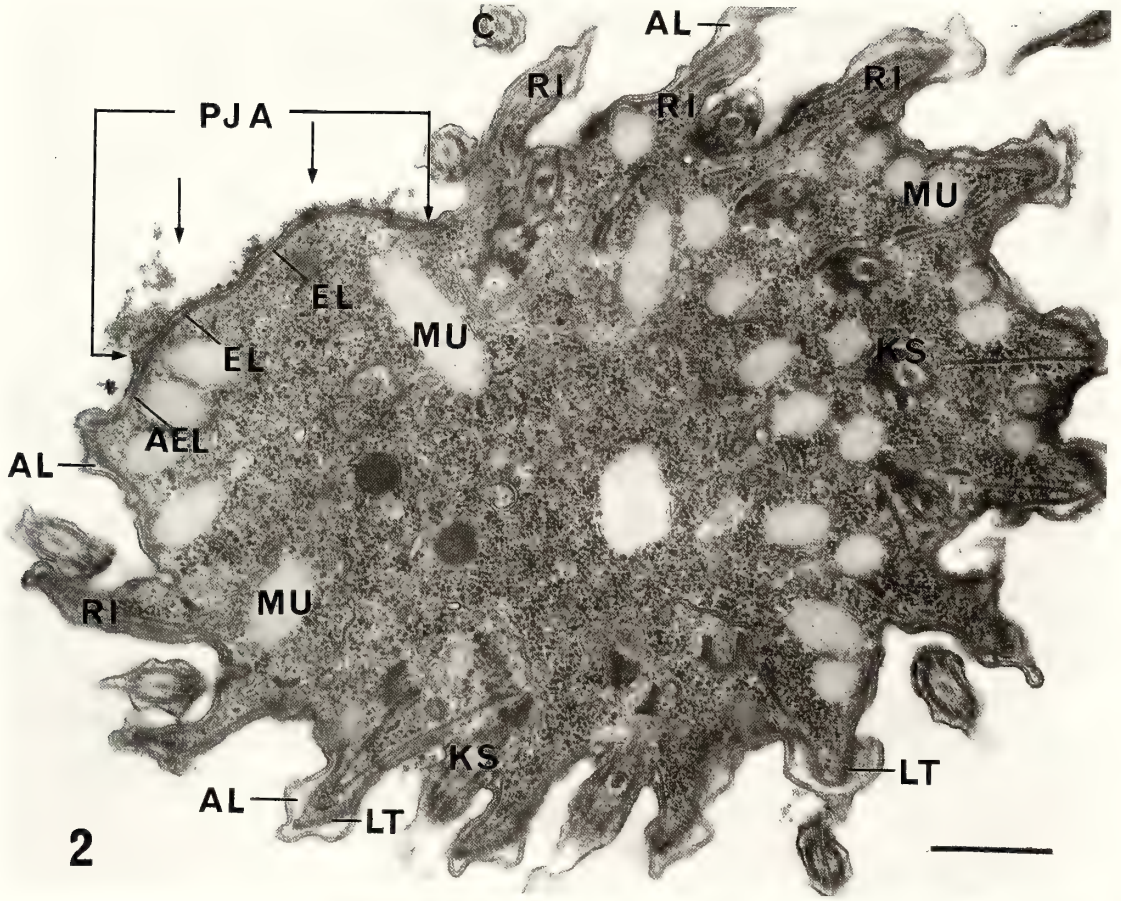
FIG. 1. Section of a starved cell after incubation for 20 min with F-Con A. A few ferritin particles (F-particles) can be seen at the bottom of the ectoplasmic grooves at the ciliary base (arrows). The plasma membrane in this area is directly above a thin ectoplasmic layer (EL). Scale bar: 0.5 μm .

FIGS. 1-7 are transmission electron micrographs of *Tetrahymena thermophila*.

AL: alveoli, AEL: inner alveolus ectoplasmic layer, AZM: adoral zone of membranelle, C: cilium, CI: cisterna, KS: kinetosome, LT: longitudinal tubule, MI: mitochondria, MU: mucocyst, RI: ectoplasmic ridge.

FIG. 2. Cross section through the upper part of the oral apparatus. The cells were mixed for 40 min, then incubated with F-Con A for 20 min. Numerous large clusters of F-particles can be seen on the surface of the plasma membrane of the smooth presumptive junctional area (PJA), but elsewhere there are few particles on the surface. Scale bar: 0.5 μm .

FIG. 3. Section of a closely adjacent part of the same cell as shown in Fig. 2. The EL in the PJA is connected with the inner alveolus ectoplasmic layer (AEL). Clusters of F-particles are found only on the plasma membrane of the PJA that is directly above the EL. Scale bar: 0.5 μm .



Samples for electron microscopy were collected by low-speed centrifugation and fixed for 30 min at 0°C in freshly prepared fixative consisting of a mixture of solutions of 0.6% glutaraldehyde, 2% osmium tetroxide, and 1.2% potassium bichromate (2:1:1, v/v) adjusted to pH 7.4 with 0.2 M phosphate buffer. Then they were dehydrated by rapid passage through a graded ethanol series and embedded in Epoxy resin containing Quetol 812 (11 g), DDSA (6 g) and MNA (5.8 g). Ultrathin sections obtained with an LKB ultratome were stained with 1% aqueous uranyl acetate and lead citrate and examined with a JEOL 100-C electron microscope.

OBSERVATIONS AND RESULTS

Tetrahymena cells are pear-shaped, and are covered with numerous ridges stretching along the

apex line. Cilia are arranged in a line along the ridges at the bottom. Cross sections, between the tip and upper edge of the oral apparatus of starved cells, have a highly undulating, ellipse-shaped profile. The region below the cytoplasmic membrane is mainly occupied by alveoli, kinetosomes, mucocysts, longitudinal tubules and other subpellicular organelles.

In the starved cell after incubation for 20 min with F-Con A (Fig. 1), a few F-particles are seen located exclusively around the ciliary base (arrows). In the areas where the F-particles are attached, there are no alveoli and an extremely thin ectoplasmic layer (EL) is seen directly below the cytoplasmic membrane. After co-stimulation for 40 min and additional incubation for 20 min with F-Con A, the unpaired cell has the profile of a highly undulating ellipse in cross section between the tip of the cell and the upper edge of the oral

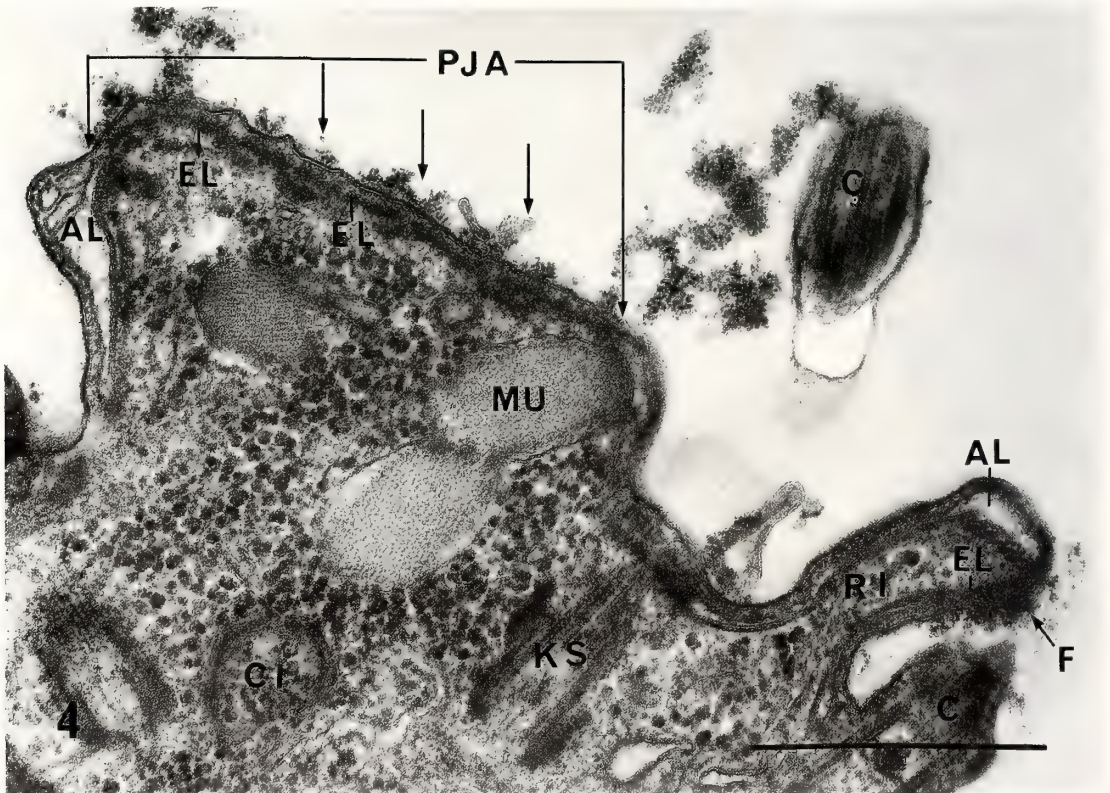


FIG. 4. Cross section through the adoral zone. Cells were mixed for 40 min and then incubated with F-Con A for 20 min. Large clusters of F-particles can be seen on the surface of the plasma membrane of the PJA (arrows) and on the side wall (F) of the ectoplasmic ridge (RI). Scale bar: 0.5 μ m.

apparatus (Figs. 2 and 3), like that of cells in the starved state (Fig. 1). But unlike during starvation the PJA appears during co-stimulation. A thick, dense EL appears under the cytoplasmic membrane of the PJA, and F-particles are only found on the surface that is directly above the EL, in areas of alveoli (AL), longitudinal tubules (LT) or cilia (C). The EL is seen as a single dense layer just beneath the cytoplasmic membrane of the PJA, whereas in areas around the PJA, it is displaced deep under the inner alveolus membrane (Figs. 2 and 3, AEL). The ectoplasmic layer is much thicker in cells in the co-stimulation period than in starved cells. Figure 4 shows a cross section through the adoral zone of an unpaired cell. There are numerous F-particles on the PJA (arrows) and

on the side wall (F) of the adjacent ridges (RI). The cytoplasmic membrane associated with F-particles is directly above the EL and there are no other subpellicular organelles in the cortical zone.

After co-stimulation for 60 min and incubation for 20 min with F-Con A (Figs. 5 and 6), cross sections through the junction area (JA) of conjugants shows that numerous F-particles are specifically distributed on regions of the PJA, that are not in contact, on the side walls of ridges (arrows) and in gaps between conjugant cells (Fig. 6, F). Figure 7 shows the PJA of a conjugant, without F-Con A incubation. The clear gap zone between the conjugant is filled with fine fibrous structures, possibly glycocalyx.

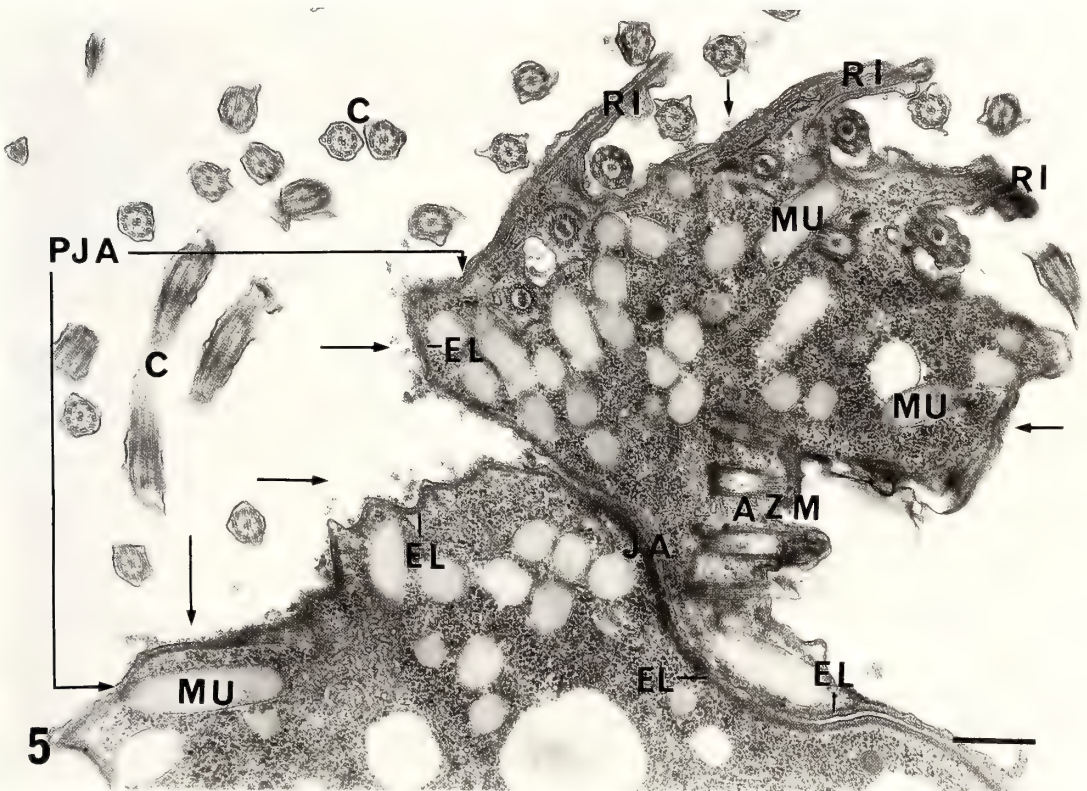


FIG. 5. Cross section through the junction area (JA) of a conjugant. The cells were mixed for 60 min, and then incubated with F-Con A for 20 min. Clusters of F-particles (arrows) can be seen on the surface of the PJA (arrows). Scale bar: 0.5 μ m.

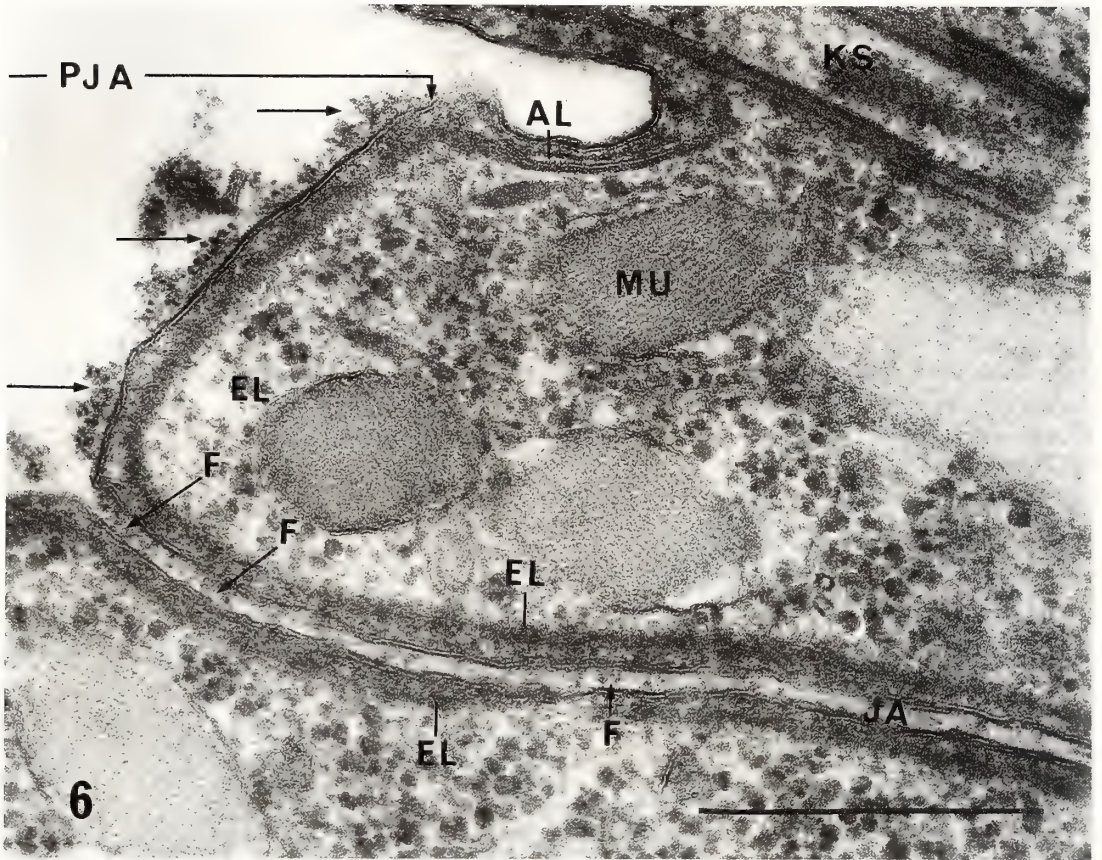


FIG. 6. Section of the junction area (JA) of conjugants. The cells were mixed for 60 min, and then incubated with F-Con A for 20 min. F-particles can be seen singly or in clusters on the surface of the PJA (arrows) and in the gap zone between the conjugants (F). Scale bar: $0.5 \mu\text{m}$.

FIG. 7. Section of the junction area of conjugants. The cells were mixed for 60 min. The gap zone between the conjugants (JA) contains many fine fibrous structures. Scale bar: $0.5 \mu\text{m}$.

DISCUSSION

The present study on the surface of the cytoplasmic membrane of *Tetrahymena* revealed the distributions of Con A receptors in starved and conjugation-induced cells. The relationship of the distribution of Con A receptors with that of substructures in the cortical zone is noteworthy.

The cortical zone of *Tetrahymena* contains various subpellicular organelles. The cytoplasmic membrane can be classified into the following three membrane areas according to differences in substructures in the cortical zone; (i) a ciliary area, (ii) a cortical area, and (iii) an area directly above the EL. The third type exhibits Con A binding activity specifically. During periods of nutrition and starvation, the third type is found only in restricted areas around ciliary bases and cell membranes that are directly above a thin EL.

There are only a few sparsely distributed F-particles bound to the surface of such areas, so their Con A binding activity may be extremely weak. In studies by fluorescence microscopy with FITC-Con A, no Con A binding activity was detected on the cell surface during starvation before mixing complementary mating types [4, 9]. Since there were so few Con A receptors at the ciliary bases, no FITC could be detected in these regions by fluorescence microscopy.

The most striking ultrastructural changes of the ectoplasm and cortex that occur after mixing starved complementary mating types are thickening of the EL under the inner-membrane of the alveoli and formation of PJAs [3]. Allewell and others [10] proposed that the co-stimulation period should be distinguished into an activation period and maturation period. Morphologically, the former corresponds to the period of thickening of the EL and the latter to the period of PJA formation. The EL under the inner-alveolus membrane, which has thickened and increased in electron density, is morphologically similar to the EL in the PJA, and may be of similar composition to the latter. Surface areas displaying structural similarities to PJA's are also found on the side walls of some cytoplasmic ridges in the cell tip near the adoral zone.

Numerous ferritin particles are attached as large

clusters to the outer surface of these special areas as well as to PJAs. After the co-stimulation period, cells can make contact with each other by forming PJAs. When the cells are in partial contact stage of conjugation, however, broad areas of PJAs around the junctional region of the one partner remain free from contact with PJAs of the other cell.

Changes in FITC-Con A binding patterns during the conjugation process were reported by Watanabe *et al.* [11, 12]. The changes in the fluorescence pattern they observed are similar to those in the F-Con A distribution pattern observed in the present study. The ring pattern of FITC-Con A described by Watanabe *et al.* may correspond to the present F-Con A distribution pattern in regions where PJA's of adjacent cells are not in contact.

From previous studies with inhibitors of protein synthesis, a special kind of protein was concluded to be synthesized during the co-stimulation period [13]. This protein was proposed to be a glycoprotein [14]. Watanabe *et al.* [11] found that changes in the Con A binding pattern are stopped or eliminated by cycloheximide. The striking thickening of the EL during the activation period may thus reflect an increase in structural protein in the EL during this period. The close relationship between the distribution of Con A receptors on the cell surface and morphological alterations of the EL under the cytoplasmic membrane strongly suggests that the structural protein(s) is bound to the Con A binding glycocalyx on the cytoplasmic membrane.

Since Con A receptors are rarely found in starved cells, the interaction between cells during the activation period is unlikely to be mediated by Con A receptors; rather, Con A receptors anchored to the EL are likely to play some role in adhesion during the maturation period.

REFERENCES

- 1 Bruns, P. J. and Brussard, T. B. (1974) Pair formation in *Tetrahymena pyriformis*, an inducible developmental system. *J. Exp. Zool.*, **188**: 337-344.
- 2 Bruns, P. J. and Palestine, R. F. (1975) Co-stimulation in *Tetrahymena pyriformis*. A developmental interaction between specially prepared cells. *Dev. Biol.*, **42**: 75-83.

- 3 Suganuma, Y., Simode, C. and Yamamoto, H. (1984) Conjugation in *Tetrahymena*: Formation of a special junction area for conjugation during the co-stimulation period. *J. Electron Microsc.*, **33**: 10–18.
- 4 Wolfe, J. and Grimes, G. W. (1979) Tip transformation in *Tetrahymena*: A morphogenetic response to interactions between mating types. *J. Protozool.*, **26**, 82–89.
- 5 Frazier, W. and Glaster, L. (1979) Surface components and cell recognition. *Ann. Rev. Biochem.*, **48**: 491–523.
- 6 Irimura, T., Nakajima, M., Hirano, H. and Osawa, T. (1975) Distribution of ferritin-conjugated lectins on sialidase-treated membranes of human erythrocytes. *Biochim. Biophys. Acta.*, **413**: 192–201.
- 7 Ofer, L., Levkovitz, H. and Loyter, A. (1976) Conjugation in *Tetrahymena pyriformis*. The effect of polylysine, concanavalin A and divalent metals on the conjugation process. *J. Cell Biol.*, **70**: 287–293.
- 8 Frisch, A., Levkovitz, H. and Loyter, A. (1977) Inhibition of conjugation in *Tetrahymena pyriformis* by concanavalin A. Binding of concanavalin A to material secreted during starvation and to washed cells. *Exp. Cell Res.*, **106**: 293–301.
- 9 Frisch, A. and Loyter, A. (1977) Inhibition of conjugation in *Tetrahymena pyriformis* by Con A. Localization of Con A-binding sites. *Exp. Cell Res.*, **110**: 337–346.
- 10 Allewell, N. M. and Wolfe, J. (1977) A kinetic analysis of the memory of a developmental interaction. Mating interactions in *Tetrahymena pyriformis*. *Exp. Cell Res.*, **109**: 15–24.
- 11 Watanabe, S., Toyohara, A., Suzaki, T. and Shigenaka, Y. (1981) The relation of concanavalin A receptor distribution to the conjugation process in *Tetrahymena thermophila*. *J. Protozool.*, **28**: 171–175.
- 12 Wolfe, J., Pagliaro, L. and Fortune, H. (1986) Coordination of concanavalin-A-receptor distribution and surface differentiation in *Tetrahymena*. *Differentiation*, **31**: 1–9.
- 13 Allewell, N. M., Oles, J. and Wolfe, J. (1976) A physicochemical analysis of conjugation in *Tetrahymena pyriformis*. *Exp. Cell Res.*, **97**: 394–405.
- 14 Van Bell, C. T. (1983) An analysis of protein synthesis, membrane proteins, and concanavalin A-binding proteins during conjugation in *Tetrahymena thermophila*. *Dev. Biol.*, **98**: 173–181.

Fine Structure of the Dorsal Tongue Surface in the Japanese Toad, *Bufo japonicus* (Anura, Bufonidae)

SHIN-ICHI IWASAKI and KAN KOBAYASHI

*Department of Anatomy, School of Dentistry at Niigata,
The Nippon Dental University, Niigata 951, Japan*

ABSTRACT—The ultrastructure of the epithelial cells and sensory organs of the dorsal surface of the tongue of *Bufo japonicus* were investigated by scanning electron microscopy. The specimens were prepared using a method designed to remove the extracellular material which normally adheres to the tongue's surface. Irregular undulant structures, or ridge-like papillae, which correspond to the filiform papillae of *Rana*, were compactly distributed over almost all of the dorsal surface of the tongue, while fungiform papillae were scattered amongst these ridge-like papillae. A round sensory disc was located on the top of each fungiform papilla. Lattice-work, which represented the outline of the boundary of each cell, was visible on the surface of each sensory disc. At higher magnification, we observed that the surface of almost every sensory disc was covered with a honeycomb structure, while a small number of cells with microvilli on their surfaces were scattered amongst them. Each sensory disc was encircled by a thin band of non-ciliated cells. Microridges were widely distributed on the epithelial cell surface of the ridge-like papillae. The observed micro-ornamentation of the lingual structure with its microridges and honeycomb structures may be related to the retention of mucus on the surface of the anuran tongue.

INTRODUCTION

Filiform and fungiform papillae are distributed on the dorsal surface of the anuran tongue. A round sensory disc is located on the top of each fungiform papilla. Electron microscopic studies of the structure of the sensory discs include those of Graziadei [1], Graziadei and DeHan [2], Düring and Andres [3] and Gubo *et al.* [4], all of whom reported that the entire surface of each sensory disc of the tongue is covered with microvilli. However, Jaeger and Hillman [5] described the cytoplasmic ridges of the associated cells of the sensory disc, as well as interspersed cells with microvilli. More recent studies [6, 7] have revealed that when mucus is almost completely removed, most of the surface of the sensory disc is covered with a honeycomb structure. It is possible that these conflicting observations reflect interspecific variations among the anuran species examined. We have attempted to ascertain whether

the honeycomb structure of the sensory disc occurs in the genus *Bufo* (Bufonidae) as well as in the frogs of the genus *Rana* (Ranidae).

In all but the most recent reports on studies of the anuran tongue [4, 6, 7], the fine structure of the surface of the filiform papillar cells has been neglected. The present study examines the structure of the surface of the ridge-like papillae in *Bufo japonicus*, since these structures may be analogous to the filiform papillae of *Rana*.

MATERIALS AND METHODS

Tongues from four male and three female adult Japanese toads, *Bufo japonicus*, were used in the present study. The toads were perfused from the heart with Karnovsky fixative [8] under anesthesia with MS-222. The tongues were then removed and fixation was continued by immersion in the same solution. After rinsing in 0.1 M cacodylate buffer, several specimens were postfixed in phosphate-buffered 1% osmium tetroxide solution [9] at 37°C for 2 hr and then treated with 8 N hydrochloric acid at 60°C for 30 min to remove

extracellular substances by acid hydrolysis. For use as controls, a few specimens were not subjected to the postfixation and treatment with acid. All of the specimens were then dehydrated, critical-point dried and coated by gold-ion sputtering. Finally, the specimens were examined under a

scanning electron microscope (Hitachi S-500, S-800).

RESULTS

When specimens were postfixed in 1% osmium

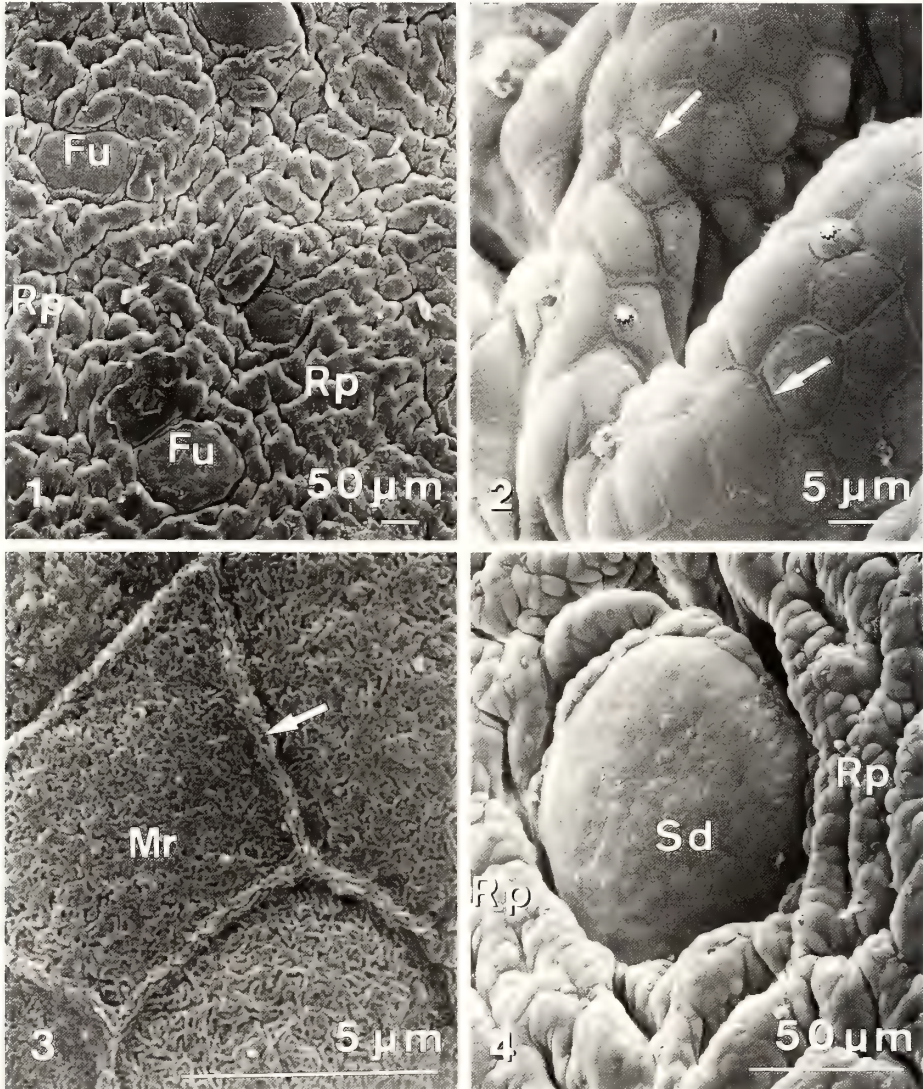


FIG. 1. Scanning electron micrograph of the central dorsal surface of the tongue of *Bufo japonicus*. Rp: ridge-like papillae, Fu: fungiform papillae.

FIG. 2. Ridge-like papillae from *Bufo japonicus*. Arrows show elevated intercellular borders. Asterisks indicate structures related to mucous secretion.

FIG. 3. Higher magnification of polygonal, non-ciliated cells of the ridge-like papilla in *Bufo japonicus*. Mr: microridges. Arrow shows elevated intercellular borders.

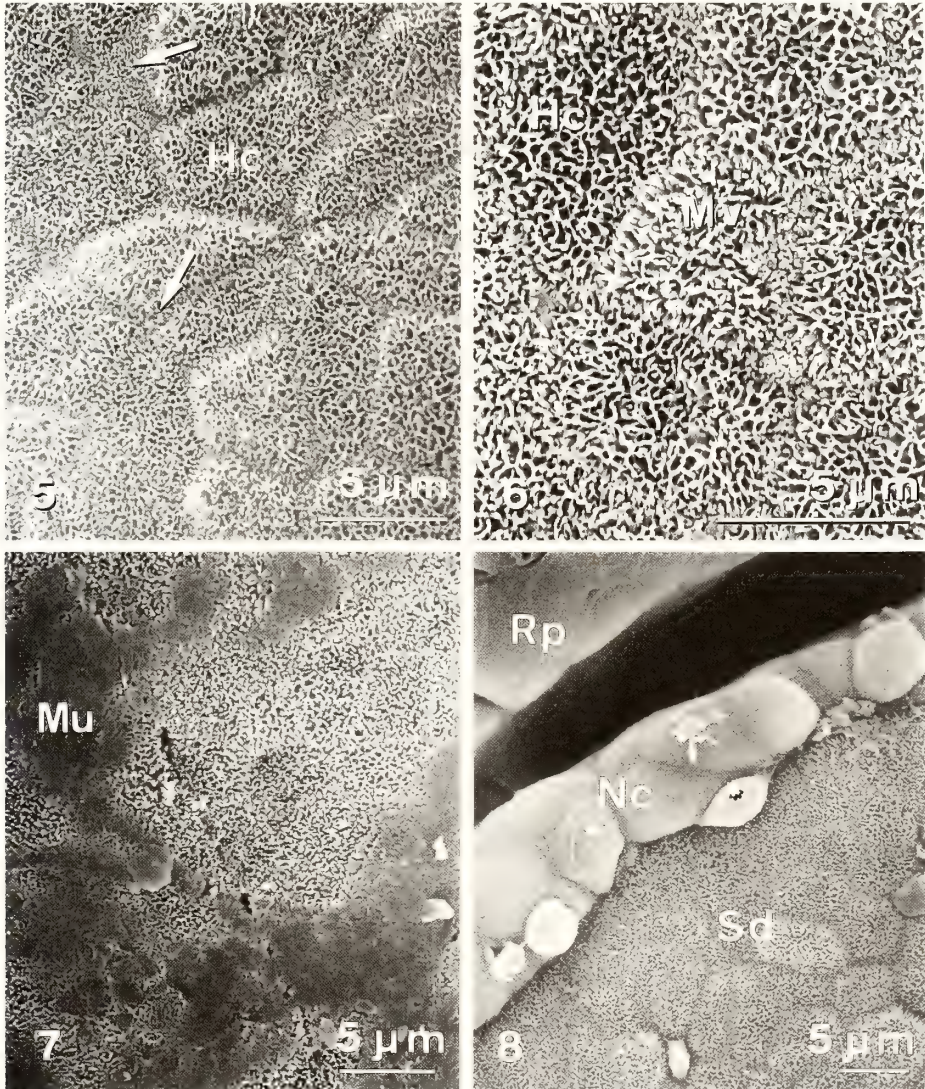
FIG. 4. Fungiform papillae from *Bufo japonicus*. Sd: sensory disc, Rp: ridge-like papillae.

tetroxide and treated with 8 N hydrochloric acid, extracellular substances were almost completely removed.

Irregular, undulant structures or ridge-like papillae are distributed in a compact arrangement over the entire dorsum of the tongue, except for its

anterior margin. Fungiform papillae, 100–150 μm in diameter, are scattered among the ridge-like papillae (Fig. 1).

The ridge-like papillae are 20–50 μm in width. They are covered with polygonal, non-ciliated cells, the borders of which are elevated (Fig. 2,



- FIG. 5. The surface of a sensory disc from *Bufo japonicus*. Hc: honeycomb structure. Arrows indicate microvilli.
 FIG. 6. Higher magnification of a sensory disc of the tongue of *Bufo japonicus*. Hc: honeycomb structure, Mv: microvilli.
 FIG. 7. Higher magnification of a sensory disc of the tongue of *Bufo japonicus*, without postfixation with osmium tetroxide and acid treatment. Mu: piled mucus.
 FIG. 8. Boundary region of a sensory disc and non-ciliated cell. Sd: sensory disc, Nc: non-ciliated cells, Rp: ridge-like papillae. Asterisks indicate structures related to secretion of mucus.

arrow). Mucus-secreting cells are scattered among these epithelial cells (Fig. 2, asterisks). At higher magnification (Fig. 3), fine plications, or microridges, are densely distributed on the surfaces of non-ciliated cells. The elevated intercellular borders are composed of bundles of such plications. In specimens which were not postfixed

with osmium tetroxide, the surfaces of the ridge-like papillae are obscured by mucus.

A sensory disc is located in the central area of the top of each fungiform papilla (Fig. 4). The surface of the disc has a latticework pattern which reflects the boundaries of the cells on the surface of the papilla. At higher magnifications of the

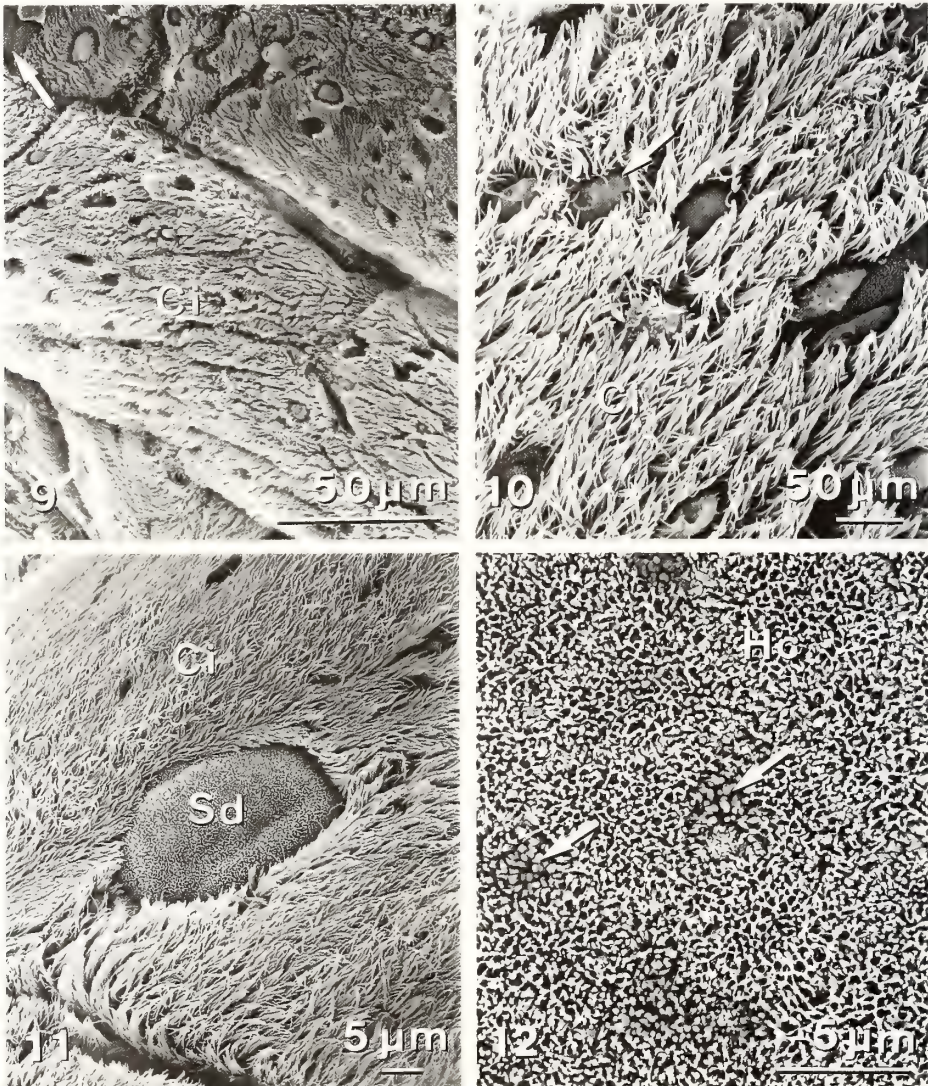


FIG. 9. Long ridges in the area near the apex. Ci: ciliated cells.

FIG. 10. Higher magnification of the long ridges in the area near the apex. Ci: ciliated cells. Arrow indicates the area without cilia.

FIG. 11. Sensory disc (Sd) in the area near the apex. Ci: ciliated cells.

FIG. 12. Higher magnification of a sensory disc in the area near the apex. Arrows indicate microrovilli. Hc: honeycomb structure.

sensory disc (Fig. 5), the cell surfaces resemble a honeycomb. Many processes, which are 0.1–0.3 μm long, are recognizable on the honeycomb-like structure. A few cells with microvilli are present among the honeycomb-like cells (Figs. 5 and 6). In specimens not subjected to postfixation and acid treatment, mucus forms a thin covering over the honeycomb framework of the cells (Fig. 7). Each sensory disc is surrounded by non-ciliated cells, which appear to be the same as those that form the ridge-like papillae (Fig. 8).

A series of long ridges about 1 mm in width are present on the anterior margin of the dorsal surface of the tongue in parallel with its anterior edge (Fig. 9). The surfaces of the long ridges are covered almost entirely by ciliated cells. Ridge-like papillae composed of non-ciliated cells are not found in this area. Non-ciliated areas are scattered on the surface of these ciliated cells (Fig. 10, arrow). Structures similar to the sensory discs on the top of fungiform papillae occur among the ciliated cells on the surfaces of these ridges (Fig. 11). At higher magnification, these discs appear to be identical to the discs described above (Fig. 12, compare with Fig. 6).

DISCUSSION

In several earlier reports [1–3], the surface of the sensory discs of the frogs, *Rana pipiens*, *Rana esculenta* and *Rana temporaria*, was described as being extensively covered with microvilli. In contrast, Jaeger and Hillman [5] described the cytoplasmic ridges of the associated cells of the sensory disc, as well as interspersed cells with microvilli in *Rana catesbeiana* and *Hyla arborea*. In our specimens of *Bufo japonicus* from which the mucus was removed, the greater part of the surface of each sensory disc was found to be covered with a latticework pattern similar to that which was demonstrated by us in two species of *Rana* namely *Rana catesbeiana* [6] and *Rana nigromaculata* [7]. As in *Rana*, most of the surface of each lingual sensory disc of *Bufo japonicus* is covered with a honeycomb-like texture of cell surfaces, which originate from “associated cells” designated by Graziadei and DeHan [2]. The honeycomb-like texture is completely coincident with the “cyto-

plasmic ridges” described by Jaeger and Hillman [5]. In the present study, thin processes were also recognized on the surface of the honeycomb-like textures, just as in the observation by Jaeger and Hillman [5]. They identified these structures as microvilli. However, we feel that these protrusions are too small to be considered microvilli. Microvilli, which are located between these “associated cells”, may derive from the “sensory cell” described by Key [10]. The honeycomb-like structures may play a role in the retention of water and other mucous fluid on the surface of the sensory disc. In addition, the possibility that the honeycomb-like structure has the same function as the taste hair is undeniable. On the other hand, it has been shown in a previous study [7] and in the present study that, when the mucus which covers the lingual surface is not completely removed, the remaining mucus may be transformed into various crystal structures during the drying of the specimens.

Among anurans, we were able to recognize some morphological differences in the tongues of two species of *Rana* [6, 7] and now can compare them to a species of *Bufo*, *Bufo japonicus*. In *Bufo japonicus*, the epithelium formed many ridge-like papillae, and the pores related to the secretion of mucus were not obvious on its surface, while in the two species of *Rana*, the epithelial surface formed many filiform papillae and there were many pores on its surface [6, 7]. In addition in *Bufo japonicus*, no ciliated cells were observed on the surface of the ridge-like papillae and on the surrounding areas of the sensory disc, while, in *Rana*, many ciliated cells were seen on the surface of the filiform papillae and the surrounding areas of the sensory discs. Structures and surface features which were somewhat similar to the ridge-like papillae in *Bufo*, were shown by Gubo *et al.* [4] in *Bombina variegata*. However, they did not describe these papillae in detail. The differences between anurans belonging to the varied genera may be ascribed to the local differentiation of function of the lingual mucosa.

In *Rana*, microridges were reported to be widely distributed on the non-ciliated cells of the filiform papillae [6, 7]. The present study of *Bufo japonicus* revealed that microridges are also present on

the non-ciliated cells of the ridge-like papillae. In our study of *Rana nigromaculata* using transmission electron microscopy [11], it appeared that a large fraction of the filiform papillar epithelial cells had both microridges on the free surface of cells and cellular processes on the surfaces which faced adjacent cells. Thus, the microridges may be the result of an altered pattern of arrangement of these cellular processes, which function as connecting structures between adjacent cells [12]. As suggested by Sperry and Wassersug [13], microridges may be important for holding mucus on the surface of the cells. Thus, the lingual microridges in *Bufo* may function to retain mucus on the dorsal surface of the tongue.

REFERENCES

- 1 Graziadei, P. P. C. (1969) The ultrastructure of vertebrate taste buds. In "Olfaction and Taste". Ed. by C. Pfaffmann, Rockefeller Univ. Press, New York, pp. 315-330.
- 2 Graziadei, P. P. C. and DeHan, R. S. (1971) The ultrastructure of frogs' taste organs. *Acta Anat.*, **80**: 563-603.
- 3 Düring, M. v. and Andres, K. H. (1976) The ultrastructure of taste and touch receptors of the frog's taste organ. *Cell Tissue Res.*, **165**: 185-198.
- 4 Gubo, G., Lametschwandtner, A., Simonsberger, P. and Adam, H. (1978) Licht- und raster-elektronenmikroskopische Untersuchungen an Gaumen und Zunge der Gelbbauchunke, *Bombina variegata* L. *Anat. Anz.*, **144**: 169-178.
- 5 Jaeger, C. B. and Hillman, D. E. (1976) Morphology of gustatory organs. In "Frog Neurobiology". Ed. by R. Linal and W. Precht, Springer-Verlag, Berlin, pp. 588-606.
- 6 Iwasaki, S. and Sakata, K. (1985) Fine structure of the lingual dorsal surface of the bullfrog. *Okajimas Folia Anat. Jpn.*, **61**: 437-450.
- 7 Iwasaki, S., Miyata, K. and Kobayashi, K. (1986) Studies on the fine structure of the lingual dorsal surface in the frog, *Rana nigromaculata*. *Zool. Sci.*, **3**: 265-272.
- 8 Karnovsky, M. J. (1965) A formaldehyde-glutaraldehyde fixative of high osmolality for use in electron microscopy. *J. Cell Biol.*, **27**: 137A-138A.
- 9 Millonig, G. (1961) Advantages of a phosphate buffer for OsO₄ solutions in fixation. *J. Appl. Physics*, **32**: 1637.
- 10 Key, E. A. (1961) Über die Endigungsweise der Geschmacksnerven in der Zunge des Frosches. *Arch. Anat. Physiol. wiss. Med.*, **28**: 329-349.
- 11 Iwasaki, S., Miyata, K. and Kobayashi, K. (1988) Fine structure of filiform papillar epithelium from the tongue of the frog, *Rana nigromaculata*. *Zool Sci.*, **5**: 61-68.
- 12 Krstić, R. V. (1979) Ultrastructure of the Mammalian Cell. Springer-Verlag, Berlin, pp. 238-239.
- 13 Sperry, D. G. and Wassersug, R. J. (1976) A proposed function for microridges on epithelial cells. *Anat. Rec.*, **185**: 253-258.

Fine Structure of the Iris Muscle in the Japanese Common Newt, *Cynops pyrrhogaster*, with Special Reference to Innervation

MITSUMASA OKAMOTO

*Department of Molecular Biology, Faculty of Science,
Nagoya University, Nagoya 464, Japan*

ABSTRACT—The localization and structure of the iridial muscles and associated nerves of the newt (*Cynops pyrrhogaster*) were examined by electron microscopy with some histochemical studies of catecholamine and acetylcholinesterase. The sphincter muscle, which was composed of pigmented smooth muscle cells, was located circumferentially in the pupillary margin of the iris. Sphincter muscle cells formed occasional close contacts with each other by protruding cellular processes. Numerous gap junctions and desmosomes were observed between anterior and posterior pigment epithelium of the iris, but not between muscle cells. Nerve endings formed varicosities and were composed of agranular vesicles and/or granular vesicles. There was no dilator muscle in this species. Prominent circumferential catecholamine fluorescence was observed in the pupillary margin. Acetylcholinesterase positive and negative muscle cells and nerve fibers were found within the sphincter muscle region.

INTRODUCTION

The iris sphincter and dilator muscles, known to be the iris muscle in the mammalian eye, change the size of the pupil and regulate the quantity of light. Studies on the iris muscles have been a fascinating subject from the standpoint of development and differentiation of the muscle, because these muscles are unique in that the sphincter muscle is the only vertebrate smooth muscle known to be derived from neuroectoderm [1-4] and the dilator muscle has myoepithelial characters [1, 5-6]. They are innervated by an autonomic nervous system [7-10], which is advantageous, in that we can easily detect the action of nerves through miosis and mydriasis of the eye. In addition to morphological studies on the iris muscle [1-6, 11-13], numerous pharmacological and electrophysiological reports have been made on this nervous system using various kinds of animals [14-20]. Studies on the fine structure of the iris muscle besides mammals have also been reported [21-24],

but only a few works have been undertaken on amphibian species [25-27].

On the other hand, it has been well known that the newt has a capacity for regeneration from the mid-dorsal margin of the iris after having extirpated an intrinsic lens. Numerous investigations at the light and electron microscopic level have been made on the process of lens regeneration (for review, see [28]). However, the iris muscle in the newt has so far received almost no attention in terms of the study of lens regeneration, although the sphincter muscle at the pupillary margin would appear to be closely relevant to lens regeneration.

There have been no reports on the fine structure of the iris muscle of the Japanese common newt, *Cynops pyrrhogaster* and no histochemical works on amphibian iridial muscles and nerves. Thus, in the present study, detailed investigations on the fine structure of the iris muscle and some histochemical studies on the iridial muscles and associated nerves were made in the adult *Cynops pyrrhogaster*. In addition, the present study also seeks to obtain basic information on the iris muscle, which presumably has some relevance to lens regeneration.

MATERIALS AND METHODS

Electron microscopy

Adult Japanese newts, *Cynops pyrrhogaster*, were kept in an aquarium at $21 \pm 2^\circ\text{C}$. Newts for experiments were decapitated and the isolated dorsal heads were prefixed at 4°C overnight in 3–6% glutaraldehyde in Hanks' solution diluted to 80% of the original concentration for newts. After rinsing with the buffer, iridocorneal complexes were isolated and postfixed in cold 1% osmium tetroxide in the buffer for 1 hr. The tissue fragments were then block stained with 0.5–1% aqueous uranyl acetate solution for 1 hr, washed, dehydrated in graded series of ethanol, and embedded in Epon. Sections were cut with a glass knife or a diamond knife with a Reichert ultramicrotome, collected on carbon-coated grids, stained with uranyl acetate and lead citrate, then examined by a JEOL 100C electron microscope at 80 KV.

Histochemical localization of catecholamines

The glyoxylic acid fluorescence technique [29] was employed with a slight modification for the newt iris. The isolated iris rings of the newts were immersed in 2% glyoxylic acid in 0.1–0.2 M Sørensen's phosphate buffer (pH 7.0) for 30 min. Samples were mounted on slides and air dried, then heated for 4 min on a hot plate at 100°C . Control samples were treated only with the buffer. The specimens were sealed in liquid paraffin and observed with fluorescence microscope.

Demonstration of acetylcholinesterase at the electron microscope level

For the demonstration of sites of acetylcholinesterase activity, the method of Karnovsky and Roots [30] modified by Tsuji [31] was employed with a slight modification for the newt iris. The specimens were fixed in 2% paraformaldehyde and 1.25% glutaraldehyde in 0.05–0.1 M Sørensen's phosphate buffer (pH 7.4) at 4°C for 2–3 hr and washed overnight in the buffer. After rinsing in 0.1 M acetate buffer (pH 6.2), the samples were placed in the incubation medium (1.7–8.5 mM acetylthicholine iodide, 0.1 M sodium acetate, pH 6.2, 0.01 M copper sulfate, 0.04 M glycine, and 0.04 M magnesium chloride) for 3 hr at room temperature. Thereafter, the tissues were rinsed twice in the acetate buffer and placed in 3% potassium ferricyanide solution for 30 min. All incubations were performed in the dark with gyration. After a rinse in the phosphate buffer, the tissues were processed for electron microscopy as previously described. Eserine (physostigmine), an inhibitor of cholinesterases, was used at the concentration of 10^{-4} M to detect the presence of nonspecific esterases. Tissue samples were preincubated for 15 min in an eserine solution, and placed in the incubation mixture containing an inhibitor at the same concentration.

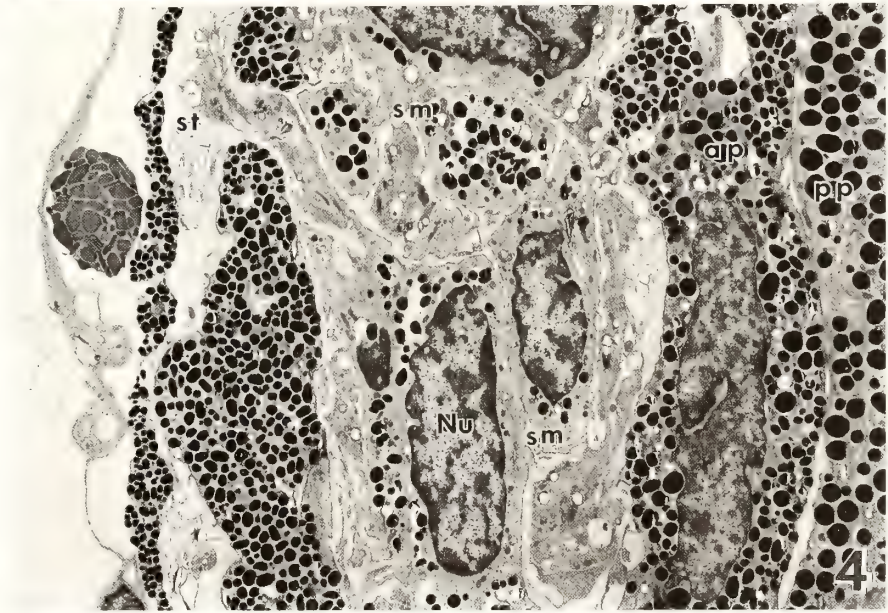
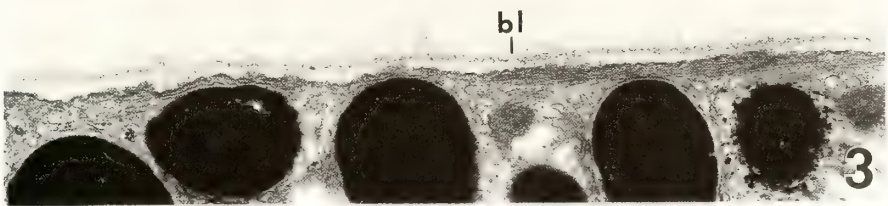
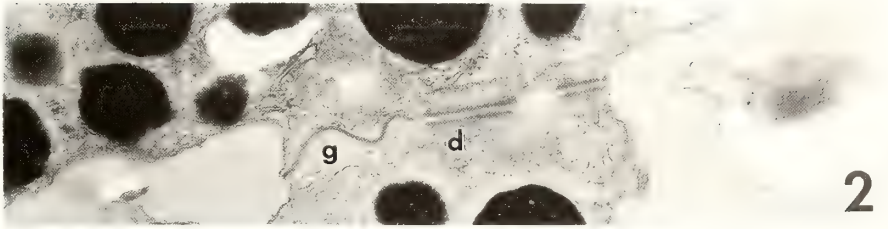
RESULTS

General features and localization of the iris muscle

The iris can be easily recognized as a three-

- FIG. 1. Meridional section of the iris. The stroma of the iris faces the cornea. Montage. Bar represents $20 \mu\text{m}$.
 FIG. 2. Junctions between anterior and posterior pigment epithelium. Both a gap junction and desmosomes are present side by side. $\times 23,000$.
 FIG. 3. A longitudinal section of the pigment epithelium. The surface of the pigment epithelium is surrounded by a basal lamina. $\times 23,000$.
 FIG. 4. A higher magnification of the sphincter muscle region shown in Fig. 1. The region is prominent with a scarcity of pigment granules within the cell. $\times 2,400$.
 FIG. 5. A horizontal section cut slightly obliquely to the iris diaphragm. The sphincter muscle cells are located parallel to each other and to the pupillary margin. $\times 1,300$.

FIGS. 1–16 are all electron micrographs. Abbreviations: st, stroma; ap, anterior pigment epithelium of the iris; pp, posterior pigment epithelium of the iris; sm, sphincter muscle; g, gap junction; d, desmosome; bl, basal lamina; Nu, nucleus; mf, myofilament; db, dense body; pr, polyribosome; fr, free ribosome; m, mitochondria; pg, pigment granule; ne, nerve ending; J, cell junction; col, collagen fiber; agv, agranular synaptic vesicle; gv, granular synaptic vesicle.



layered structure (Fig. 1). The most anterior layer is the stroma of an iris, which contains several cell types of mesenchymal cells and blood vessels. The iridial stroma is rather scanty compared with the other two layers. The next layer is the anterior pigment epithelium. It is laterally continuous with the pigment epithelium of the retina. It comprises a single layer of cells filled with melanin granules which are round to oval in profile, and about $0.6 \times 0.8 \mu\text{m}$ in diameter. The third layer is the posterior pigment epithelium. It is laterally continuous with the neural retina, also comprising a single layer of cells filled with round, relatively large melanin granules, about $1 \mu\text{m}$ in diameter. Numerous gap junctions and desmosomes can be found between the anterior and posterior pigment epithelium (Fig. 2). The anterior and posterior surfaces of the pigment epithelium are surrounded completely by a basal lamina (Fig. 3). The sphincter muscle cells are between the stroma and the anterior pigment epithelium (Fig. 4). They enclose a pupillary margin like a ring and are located parallel to each other and to the pupillary edge (Fig. 5). As the sphincter muscle cells have more scanty pigment granules than the surrounding pigment epithelial cells, their region can be easily recognized in the low magnification electronmicrograph (Figs. 1, 4 and 5).

Fine structure of iris muscle cells and associated nerve fibers

The individual sphincter muscle cells contain bundles of myofilaments along the long axis of the cell (Figs. 6 and 7). In cross section of the filament

bundles, thin (about 7 nm in diameter) and thick (about 20 nm in diameter) myofilaments can readily be identified (Fig. 8). Dense bodies or dense plaques were scattered throughout the bundles of myofilaments and on the cytoplasmic side of the plasmalemma (Fig. 6). Nuclei were slender in outline with many interdigitations along the nuclear envelope. Mitochondria, free ribosomes and polyribosomes were seen in the vicinity of the conglomerations of pigment granules and beneath the cell periphery. Average diameter of the pigment granules in the sphincter muscle cells was $0.5 \times 0.7 \mu\text{m}$; their size was consistent with those of the anterior pigment epithelium.

Many smooth-surfaced vesicles were interspersed along the plasmalemma (Figs. 6, 8 and 9). These vesicles have been called caveolae, plasmalemmal vesicles, or micropinocytotic vesicles in the cells of the smooth muscle. In Figure 9, we can easily identify the two different figures of caveolae. In sections tangential to the cell surface, the caveolae were seen in circles, but in vertical sections, they were seen in a flask-shaped invagination attached by a narrow neck region. Each sphincter muscle cell was surrounded by a basal lamina except the spots at which the muscle cells were closely adjacent (Figs. 6 and 10). The sphincter muscle cells usually formed close contacts with neighboring cells by protruding cytoplasmic processes. But no gap junctions and desmosomes were seen between muscle cells, in contrast to the junctions found between the anterior and posterior pigment epithelium. Collagen fiber or bundles of fibers were occasionally present in the

FIG. 6. A longitudinal section of the sphincter muscle cell. Myofilaments, dense body, pigment granules, caveolae, free and poly ribosomes are found within the cytoplasm. Each muscle cell is in close contacts with cellular processes. $\times 13,500$.

FIG. 7. A higher magnification of the myofilament bundle sectioned longitudinally to the bundle. Each myofilament is clearly discernible. $\times 37,000$.

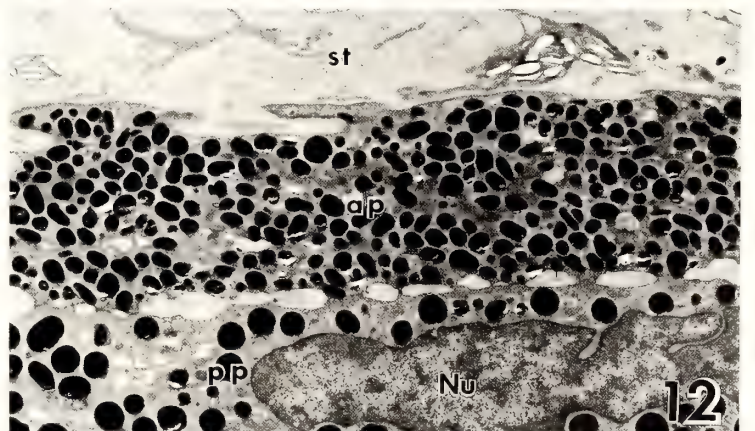
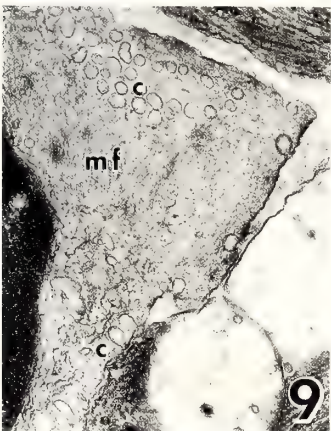
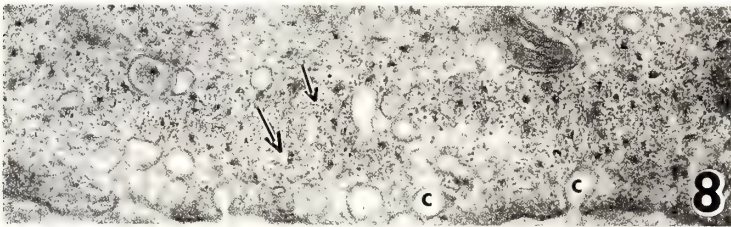
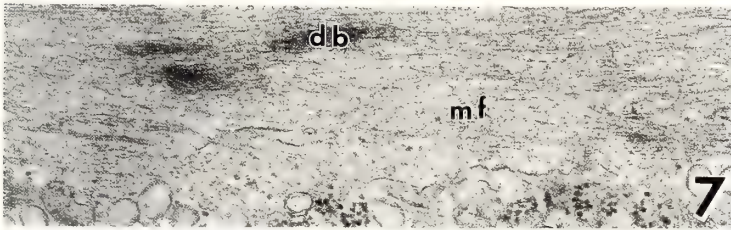
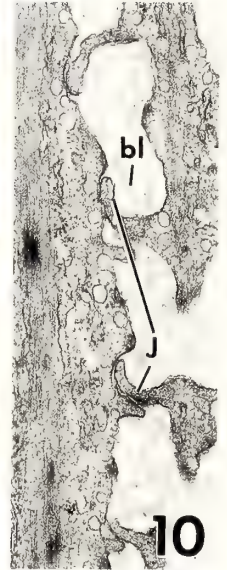
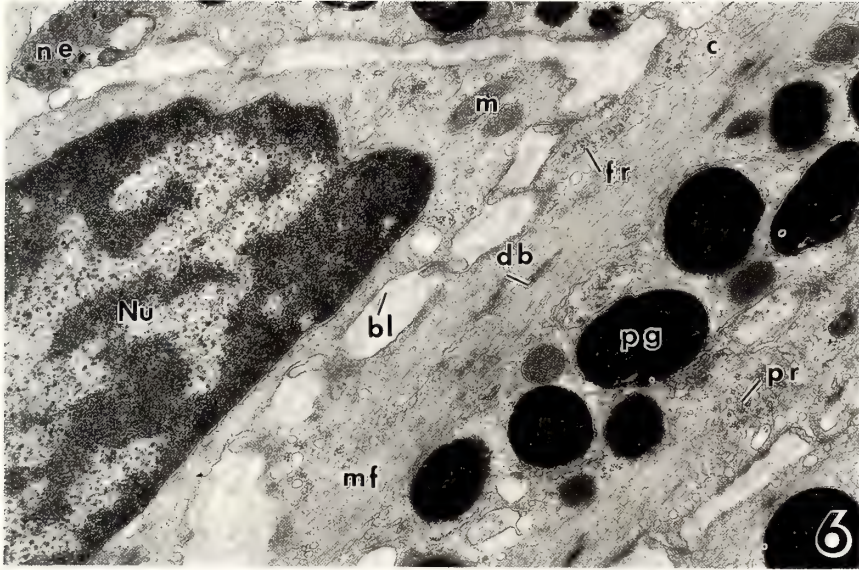
FIG. 8. A higher magnification of the myofilament bundle sectioned crossly to the bundle. Thick (large arrow) and thin (small arrow) myofilaments are prominent. Numerous caveolae are also found at the cell periphery. $\times 37,000$.

FIG. 9. Section cut partly tangential and partly longitudinal to the cell surface, showing crossly and longitudinally-sectioned caveolae, respectively. $\times 19,800$.

FIG. 10. The junction between two sphincter muscle cells. They closely contact each other with protruded cellular processes. $\times 18,150$.

FIG. 11. Collagen fiber or bundles of fibers scattering in the intercellular spaces of the sphincter muscles. $\times 66,300$.

FIG. 12. Meridional section of the iris situated between the sphincter muscle region and the root of the iris. There are no dilator muscles on the anterior pigment epithelium facing the iridial stroma. $\times 3,960$.



intercellular spaces (Fig. 11).

Mammalian dilator muscle is known to be situated peripheral to the sphincter muscle and to be continuous with the cell bodies of the anterior pigment epithelium [32]. The dilator muscle is therefore a partial specialization of cytoplasmic processes of the anterior pigment epithelium into the myoepithelium. The dilator processes in mammals are arranged in an overlapping manner somewhat like tiles on a roof. In the iris of *Cynops pyrrhogaster*, the dilator muscle could not be found even in detailed observations in the corresponding region of the mammalian dilator muscle (Fig. 12).

Large bundles of nerve fibers locating near the muscle cells were found at various places in the sphincter muscle region (Fig. 13). In cross and

longitudinal section of nerve fibers, microtubules and neurofilaments were seen along the long axis of the fibers. Nerve endings were found close to the muscle cells (Fig. 14). A cleft of about 5–10 nm between nerve membrane and muscle membrane was usually found, but in most examples, the area of contact between nerve endings and muscle cells did not show junctional specializations. Nerve endings which usually form varicosities contain agranular (40–60 nm in diameter) and/or granular (90–130 nm in diameter) synaptic vesicles (Figs. 15 and 16). Varicosities were roughly classified into two types. One is composed mostly of agranular vesicles of rather uniform diameter except the occasional existence of only few granular vesicles. Another is composed of granular, dense-cored vesicles and agranular, clear vesicles.

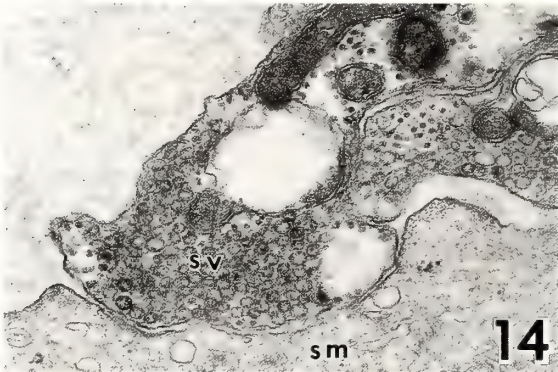
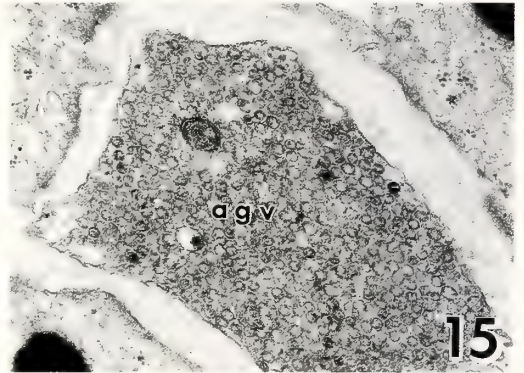


FIG. 13. Section showing dense innervation in the sphincter muscle region. $\times 6,435$.

FIG. 14. Adjacent contact of a nerve ending and a sphincter muscle cell. The nerve varicosity contains numerous agranular synaptic vesicles. $\times 29,500$.

FIG. 15. A nerve varicosity of agranular type. Almost all of the synaptic vesicles are composed of agranular vesicles. $\times 25,000$.

FIG. 16. A nerve varicosity of granular type. Agranular and granular vesicles are mixed in a varicosity. $\times 25,000$.

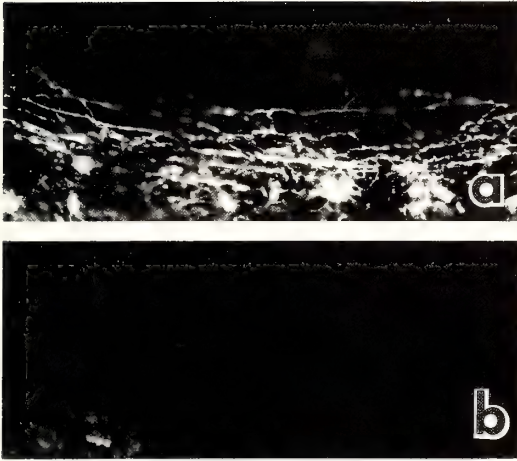


FIG. 17. Histochemistry of catecholamine in the pupillary margin. a, Fibrous catecholamine fluorescence is found circumferentially at the pupillary margin. b, No fluorescence at the pupillary margin is found in the buffer-treated sample. $\times 178$.

Localization of catecholamine and demonstration of acetylcholinesterase activities in iris muscle

The fluorescence micrographs of pupillary margin of the iris treated with glyoxylic acid are shown in Figure 17a. Fluorescence was prominent in fibrous structure circumferentially located at the pupillary margin. The fibers showed a knot-like structure in some places. No fluorescence was detectable in the buffer-treated samples (Fig. 17b). In samples treated with acetylthiocholine as the substrate of acetylcholinesterase, the enzymatic reaction product was observed randomly in the surface of the sphincter muscle cells (Fig. 18a). The precipitate also appeared randomly at nerve fibers and vesicle-filled varicosities. In addition to the presence of the acetylcholinesterase-positive cells and nerve fibers, there were some negative cells and nerve fibers associated with the surrounding muscle cells (Fig. 18b). They appeared to have the same features as eserine-treated samples (Fig. 18c).

DISCUSSION

Present study firstly demonstrated the localization and the detailed structure of the iris muscle in the Japanese common newt, *Cynops pyrrhogaster*.

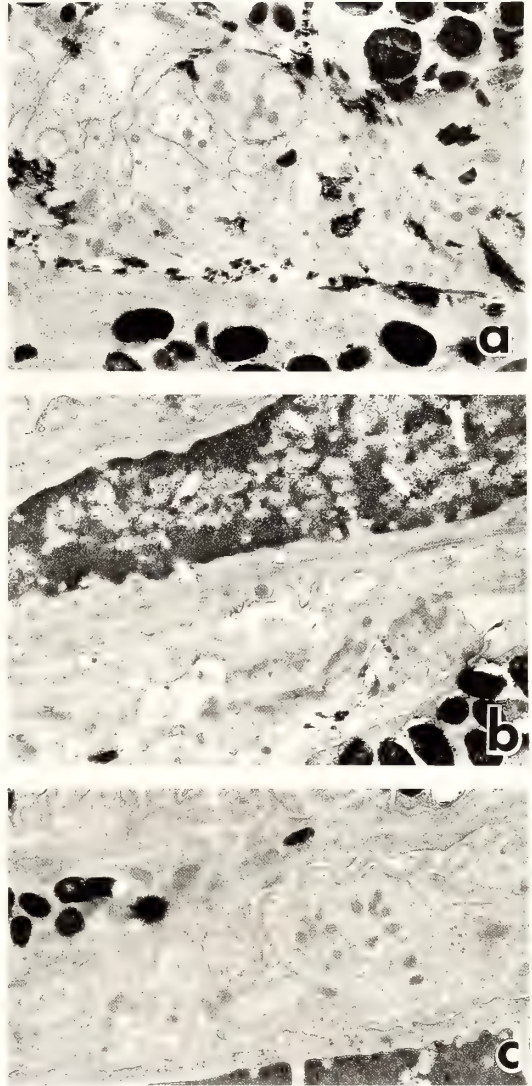


FIG. 18. Histochemistry of acetylcholinesterase in the sphincter muscle region. a, Acetylcholinesterase-positive muscles and nerve fibers are present in the samples treated with acetylthiocholine as the substrate. b, Acetylcholinesterase-negative muscles and nerve fibers are also found in the sample treated with the substrate. c, No reaction product is found in the eserine-treated samples. $\times 7,750$.

In addition, some histochemical studies on the localization of catecholamines and acetylcholinesterases were made in the iris muscle of the newt. The sphincter muscle is usually classified as the smooth muscle, even if its developmental

origin is very different from ordinary smooth muscle of mesodermal origin [32]. In contrast to the mammalian sphincter muscle, the iris muscle in the newt appears to maintain some characters of the pigment epithelium of the iris by including a considerable number of cytoplasmic pigment granules within the muscle cells even in adult age. The persistence of a considerable number of pigment granules within the muscle cells and the lack of the dilator muscle in *Cynops pyrrhogaster* are consistent with results in other amphibian species [25–27]. These results suggest an incomplete differentiation of the iris muscle in the amphibian eye.

The present results showed that the sizes of the pigment granules in the sphincter muscle cells were similar to those of the anterior pigment epithelium. But, in the American newt, *Taricha torosa*, the sizes of the pigment granules were similar to those of the posterior pigment epithelium [26]. Based on this observation, Tonosaki and Kelly [26] proposed the notion that the sphincter muscle was derived from the posterior pigment epithelium. On the other hand, in the grass frog, *Rana pipiens*, the pigment granules of the muscle cells were of an intermediate size of the anterior and the posterior pigment epithelium [27]. Thus, it seems not to be adequate to amplify the notion about the origin of the sphincter muscle obtained in *Taricha torosa* to all amphibian species.

It has been generally accepted in the mammalian eye that the iris sphincter or dilator muscles are innervated by excitatory cholinergic or adrenergic nerve fibers, respectively, and miosis or mydriasis is the result of contraction of these nerve fibers [33]. Then the question arises as to how miosis or mydriasis is caused in the newt eye which has no dilator muscle. Some suggestions will be provided in the present results and in those previously reported by others [12, 25]. Two types of varicosities were observed in nerve endings in the present study. Richardson [12] has described two types of nerve endings in the iris muscle of the rabbit, the first containing numerous small, agranular vesicles with an occasional large dense-cored vesicle, the second also with agranular vesicles, but mixed with a large number of dense-cored vesicles of two different types. He suggests that the first, associ-

ated with the sphincter, may be typical of cholinergic innervation; the second, associated with the dilator, typical of adrenergic innervation. The features of nerve endings found in the iris muscle of the rabbit were very similar to those in *Cynops pyrrhogaster*. However, in the *Cynops*, there is no dilator muscle.

Armstrong and Bell [25] found that the toad possesses no dilator muscle and the application of noradrenaline or sympathetic nerve stimulation causes pupillary dilation and acetylcholine or parasympathetic nerve stimulation produced pupillary constriction. From these results, they concluded that the sphincter muscle in the toad has a dual innervation. Based on the pharmacological and electrophysiological works, a dual innervation of the mammalian sphincter and dilator muscle has been postulated in various species including cat, rat, bovine, dog and human [14–20]. The present results may be explained by dual innervation of the sphincter muscle as in the toad. But it is also probable to postulate that both the sphincter and the dilator muscle are situated so to be mixed in the so-called mammalian “sphincter region.” The existence of acetylcholinesterase-positive and -negative muscle cells and nerve fibers in the “sphincter region” may support this idea. Because a dual innervation in only one type of the muscle makes it difficult to explain the mixed existence of acetylcholinesterase-positive and -negative muscles. Further examinations of the newt iris muscle will provide additional data to the above two possibilities. However, it is said that acetylcholinesterase is not always an appropriate marker for the cholinergic nerve [34] and it has been questioned that cholinergic and adrenergic nerve profiles can be identified by the morphological types of synaptic vesicles [35]. Thus, it seems necessary to further examine the autonomic nerves by immunoelectron microscopic studies using antibodies against the neurotransmitters or related enzymes to the metabolism of nervous system such as tyrosine hydroxylase and cholineacetyltransferase [34, 36].

Finally, as for relevance to lens regeneration, the present results disclosed the detailed structure of the iris muscle in the non-operated eyes before lentectomy. Thus, the behavior of the iris muscle

during lens regeneration is now under investigation, because it would be interesting to know whether the differentiated iris muscle cells situated at the dorsal marginal iris can be transformed into lens cells.

ACKNOWLEDGMENT

The author wishes to express his gratitude to Dr. Terumasa Komuro of Ehime University for his warm encouragement and helpful discussion.

REFERENCES

- 1 Tamura, T. and Smelser, G. K. (1973) Development of the sphincter and dilator muscles of the iris. *Arch. Ophthalmol.*, **89**: 332-339.
- 2 Ruprecht, K. W. and Wulle, K. G. (1973) Licht- und elektronenmikroskopische Untersuchungen zur Entwicklung des menschlichen Musculus sphincter pupillae. *Arbrecht v. Graefes Arch. klin. exp. Ophthalmol.*, **186**: 117-130.
- 3 Lai, Y.-L. (1972) The development of the sphincter muscle in the iris of the albino rat. *Exp. Eye Res.*, **14**: 196-202.
- 4 Imaizumi, M. and Kuwabara, T. (1971) Development of the rat iris. *Invest. Ophthalmol.*, **10**: 733-744.
- 5 Lai, Y.-L. (1972) The development of the dilator muscle in the iris of the albino rat. *Exp. Eye Res.*, **14**: 203-207.
- 6 Kelly, R. E. and Arnold, J. W. (1972) Myofilaments of the pupillary muscles of the iris fixed *in situ*. *J. Ultrastruct. Res.*, **40**: 532-545.
- 7 Laties, A. and Jacobowitz, D. (1964) A histochemical study of the adrenergic and cholinergic innervation of the anterior segment of the rabbit eye. *Invest. Ophthalmol.*, **3**: 592-600.
- 8 Csillik, B. and Koelle, G. B. (1965) Histochemistry of the adrenergic and cholinergic autonomic innervation apparatus as represented by the rat iris. *Acta Histochem.*, **22**: 350-363.
- 9 Malmfors, T. (1965) The adrenergic innervation of the eye as demonstrated by fluorescence microscopy. *Acta Physiol. Scand.*, **65**: 259-267.
- 10 Ivens, C., Mottram, D. R., Lever, J. D., Presley, R. and Howells, G. (1973) Studies on the acetylcholinesterase (AChE)-positive and -negative autonomic axons supplying smooth muscle in the normal and 6-hydroxydopamine (6-OHDA) treated rat iris. *Z. Zellforsch.*, **138**: 211-222.
- 11 Tousimis, A. J. and Fine, B. S. (1959) Ultrastructure of the iris: an electron microscopic study. *Am. J. Ophthalmol.*, **48**: 397-417.
- 12 Richardson, K. C. (1964) The fine structure of the albino rabbit iris with special reference to the identification of adrenergic and cholinergic nerves and nerve endings in its intrinsic muscles. *Am. J. Anat.*, **114**: 173-205.
- 13 Gabella, G. (1974) The sphincter pupillae of the guinea-pig: structure of muscle cells, intercellular relations and density of innervation. *Proc. R. Soc. Lond., B*, **186**: 369-386.
- 14 Narita, S. and Watanabe, M. (1981) Response of the isolated rat iris sphincter to cholinergic and adrenergic agents and electrical stimulation. *Life Sci.*, **29**: 285-292.
- 15 Narita, S. and Watanabe, M. (1982) Response of isolated rat iris dilator to adrenergic and cholinergic agents and electrical stimulation. *Life Sci.*, **30**: 1211-1218.
- 16 Schaeppi, U. and Koella, W. P. (1964) Innervation of cat iris dilator. *Am. J. Physiol.*, **207**: 1411-1416.
- 17 Schaeppi, U. and Koella, W. P. (1964) Adrenergic innervation of cat iris sphincter. *Am. J. Physiol.*, **207**: 273-278.
- 18 Suzuki, R., Oso, T. and Kobayashi, S. (1983) Cholinergic inhibitory response in the bovine iris dilator muscle. *Invest. Ophthalmol. Vision Sci.*, **24**: 760-765.
- 19 Yoshitomi, T., Ito, Y. and Inomata, H. (1985) Adrenergic excitatory and cholinergic inhibitory innervations in human iris dilator. *Exp. Eye Res.*, **40**: 453-459.
- 20 Yoshitomi, T. and Ito, Y. (1986) Double reciprocal innervations in dog iris sphincter and dilator muscles. *Invest. Ophthalmol. Vision Sci.*, **27**: 83-91.
- 21 Gabella, G. and Clarke, E. (1983) Embryonic development of the smooth and striated musculatures of the chicken iris. *Cell Tissue Res.*, **229**: 37-59.
- 22 Oliphant, L. W., Johnson, M. R., Murphy, C. and Howland, H. (1983) The musculature and pupillary response of the great horned owl iris. *Exp. Eye Res.*, **37**: 583-595.
- 23 Kuchnow, K. P. and Martin, R. (1970) Fine structure of elasmobranch iris muscle and associated nervous structures. *Exp. Eye Res.*, **10**: 345-351.
- 24 Reger, J. F. (1966) The fine structure of iridial constrictor pupillae muscle of *Alligator mississippiensis*. *Anat. Rec.*, **155**: 197-216.
- 25 Armstrong, P. B. and Bell, A. I. (1968) Pupillary responses in the toad as related to innervation of the iris. *Am. J. Physiol.*, **214**: 566-573.
- 26 Tonosaki, A. and Kelly, D. E. (1971) Fine structural study on the origin and development of the sphincter pupillae muscle in the west coast newt (*Taricha torosa*). *Anat. Rec.*, **170**: 57-74.
- 27 Nolte, J. and Pointner, F. (1975) The fine structure of the iris of grass frog, *Rana pipiens*. *Cell Tissue Res.*, **158**: 111-120.

- 28 Reyer, R. W. (1977) The amphibian eye, development and regeneration. In "Handbook of Sensory Physiology. VII/5: The Visual System in Vertebrates". Ed. by F. Crescitelli, Springer-Verlag, Berlin, pp. 309-390.
- 29 Lindvall, O. and Björklund, A. (1974) The glyoxylic acid fluorescence histochemical method: a detailed account of the methodology for the visualization of central catecholamine neurons. *Histochemistry*, **39**: 97-127.
- 30 Karnovsky, M. J. and Roots, L. (1964) A direct-coloring thiocholine method for cholinesterases. *J. Histochem. Cytochem.*, **12**: 219-221.
- 31 Tsuji, S. (1974) On the chemical basis of thiocholine methods for demonstration of acetylcholinesterase activities. *Histochemistry*, **42**: 99-110.
- 32 Fine, B. S. and Yanoff, M. (1979) *Ocular Histology*, Harper & Row Publishers, New York, 2nd ed., pp. 203-210.
- 33 Newell, F. W. (1986) *Ophthalmology: Principles and Concepts*, C. V. Mosby Company, St. Louis, 6th ed., pp. 274-282.
- 34 Pourcho, R. G. and Osman, K. (1986) Acetylcholinesterase localization in cat retina: a comparison with choline acetyltransferase. *Exp. Eye Res.*, **43**: 585-594.
- 35 Komuro, T., Baluk, P. and Burnstock, G. (1982) An ultrastructural study of nerve profiles in the myenteric plexus of the rabbit colon. *Neuroscience*, **7**: 295-305.
- 36 Thind, K. K. and Goldsmith, P. C. (1986) Ultrastructural analysis of synapses involving tyrosine hydroxylase-containing neurons in the ventral periventricular hypothalamus of the macaque. *Brain Res.*, **366**: 37-52.

***In vitro* Dimerization of I-protein, an A-I Junctional Component of Skeletal Muscle Myofibrils¹**

MAKOTO TSUNEOKA², KOSCAK MARUYAMA and KAZUYO OHASHI³

*Department of Biology, Faculty of Science,
Chiba University, Chiba 260, Japan*

ABSTRACT—Chicken myofibrillar I-protein, which was purified using ammonium sulfate precipitation and DEAE-cellulose column chromatography, was separated into two fractions by gel filtration, disc alkaline electrophoresis, or SDS polyacrylamide gel electrophoresis without SH reagents. These fractions consisted of 100,000 dalton and 50,000 dalton components. The amount of the high molecular weight component increased under the oxidizing conditions, while the amount of the low one increased when SH reagents were added. On the other hand, antiserum raised against 50,000 dalton component reacted with both of them, as revealed by immunoelectrophoresis. Therefore, it is concluded that I-protein dimerizes under oxidizing solutions. However, dimeric I-protein did not inhibit the ATPase activity of actomyosin *in vitro*, whereas monomeric I-protein did.

INTRODUCTION

I-protein is a myofibrillar protein which was isolated from chicken and rabbit striated muscles in 1977 [1-3]. The apparent molecular weight of I-protein, which was estimated from the migration rate of SDS polyacrylamide gel electrophoresis, is approximately 50,000 [1]. This protein is localized at the A-I junctional region of myofibrils in fresh myofibrils [4] and inhibits the ATPase activity of actomyosin *in vitro* [2].

In the process of chicken I-protein purification, we often found the coexistence of 100,000 dalton protein with I-protein in the I-protein fractions. We examined the form of I-protein in various solutions and found that the 100,000 dalton protein is a dimeric form of I-protein. It was observed that the inhibitory effect on actomyosin ATPase activ-

ity of these two forms of chicken I-protein were different.

MATERIALS AND METHODS

Preparation of I-protein and antiserum against I-protein

I-protein was prepared from chicken breast muscle according to the method described in a previous paper [1], using a DEAE-cellulose column. Antiserum against chicken I-protein was raised in a rabbit as mentioned before [4].

Electrophoresis

Disc alkaline electrophoreses of Tris-glycine buffer (pH 8.8) system were performed according to the method of Davis [5], using 10% acrylamide gel as separating gels (375 mM Tris-HCl, pH 8.8) and 4% acrylamide gel as stacking gels (125 mM Tris-HCl, pH 6.8). SDS polyacrylamide gel electrophoreses were carried out essentially according to Weber and Osborn [6], using 10% acrylamide gels with or without 2-mercaptoethanol (2-ME).

Determination of protein concentrations

Protein concentrations were determined by

Accepted October 20, 1987

Received August 11, 1987

¹ This work was supported by Grant-in-Aid for Scientific Research from the Ministry of Education, Science and Culture of Japan.

² Present address: Department of Physiology, Kansai Medical University, Fumizono-cho, Moriguchi, Osaka 570, Japan.

³ To whom reprint requests should be addressed.

means of biuret reaction or estimated from ultraviolet absorption at 280 nm and 260 nm in a Shimadzu spectrophotometer.

Immunoelectrophoresis

An immunodiffusion test of anti-I-protein antiserum against disc electrophoresed I-protein was carried out according to the method of Matsuda *et al.* [7]. A disc gel, on which I-protein was electrophoresed, was put on a slide glass and then 3 ml of 1% melted agarose containing 0.15 M NaCl and 20 mM sodium phosphate buffer, pH 7.2 was poured onto the slide glass. It was left for 30 min at room temperature. The agarose gel was grooved along the electrophoresed gel. Antiserum against I-protein was poured into the groove. This slide glass was placed in a moisture box overnight at room temperature. After dipped into PBS so as to remove soluble proteins, the slide glass was stained by 1% Amido Black in 7% acetic acid for 1 hr and subsequently destained by 4% acetic acid.

Oxidization and reduction of I-protein

Oxidized and reduced I-proteins were prepared according to the method described previously by Stewart [8]. I-protein was left for 2 hr at room temperature under an oxidizing condition: 1 M

NaCl, 25 mM sodium borate buffer (pH 9.3), and 25 mM CuCl_2 , or a reducing condition: 1 M NaCl, 25 mM sodium borate buffer (pH 9.3), 5 mM dithiothreitol (DTT). I-protein was also incubated in the same solution without CuCl_2 and DTT as control. Protein concentrations were finally adjusted to 0.2 mg/ml.

ATPase measurements

The ATPase activity of actomyosin was determined by measuring the amount of inorganic phosphate (Pi) liberated by the method of Tausky and Shorr [9]. The standard reaction mixture consisted of 43 mM KCl, 1 mM MgCl_2 , 1 mM ATP, and 10 mM Tris-HCl, pH 7.5. Incubation was carried out for 5–20 min at room temperature. The specific activity was given as μmoles of Pi split per mg of myosin per minute.

RESULTS

Monomeric and dimeric I-protein molecules coexisted in a solution

When a DEAE-cellulose column purified I-protein fraction [1] shown in Figure 1, a was applied onto the Sephadex G-200 column equi-

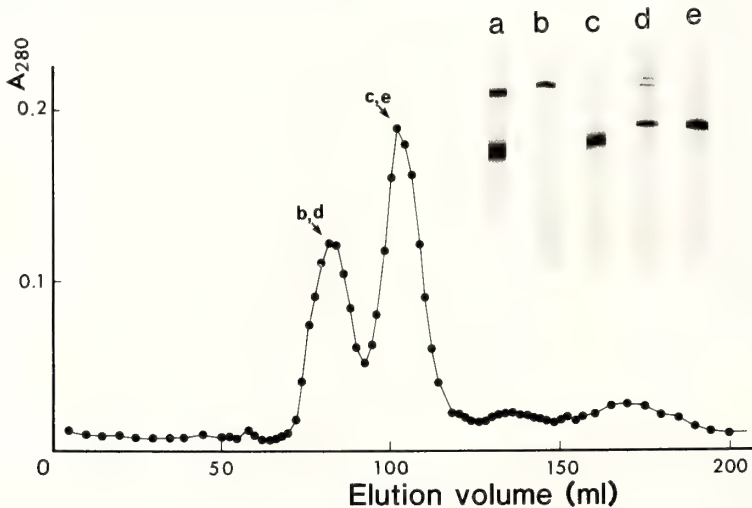


FIG. 1. Gel filtration chromatography of I-protein. Ion-exchange column purified I-protein was applied onto Sephadex G-200 column (1.8×90 cm). Fractionated proteins were electrophoresed by disc alkaline electrophoresis (a, b, c), or SDS-polyacrylamide gel electrophoresis with 2-ME (d, e). a; applied sample. b, d; protein eluted at 80 ml. c, e; protein eluted at 105 ml. Arrows indicate the electrophoresed fractions of b, d and c, e.

librated with 20 mM Tris-HCl, pH 7.5 and eluted with the same solution, the elution profile showed two peaks (Fig. 1). The first peak contained a protein of relatively low mobility by disc alkaline electrophoresis (Fig. 1, b) and a high mobility protein was eluted in the second peak (Fig. 1, c). These proteins in both peaks were electrophoresed with the same mobility on SDS polyacrylamide gels with 2-ME (Fig. 1, d, e). The ratio of the first peak to the second one calculated from the peak size was 5 : 8. Two protein bands on SDS polyacrylamide gels were electrophoresed at the positions of 100,000 dalton and 50,000 dalton proteins without any SH reagent (data are not shown). A small amount of two unidentified proteins, which molecular sizes were similar to that of 100,000 dalton protein, were contained in the first peak (Fig. 1, d).

Anti-I-protein antiserum reacted with both of the high and low mobility proteins

DEAE-cellulose column purified I-protein was electrophoresed on an alkaline disc gel. The gel was embedded in 1% agarose gel and reacted with anti-I-protein antiserum as described in Materials and Methods. A confluent immunoprecipitin line formed along the gel shows that the antiserum strongly reacted with both the high and the low mobility proteins of the same antigenicity (Fig. 2).

The ratio of the large molecular sized protein to the small one under a reducing condition differed from that under an oxidizing condition

Ion exchange column purified I-protein was incubated under oxidizing, reducing, or control conditions. The samples were electrophoresed in the system of Weber and Osborn without SH reagent. Each protein band stained with Coomassie Brilliant Blue R 250 was cut out and incubated overnight in 3 ml of 0.2% SDS and 0.2 M sodium phosphate buffer, pH 7.4, so as to extract the dye from acrylamide gel. The ratios of the large molecular sized protein were roughly estimated by measuring the absorbance of the dye solutions at 600 nm in a spectrophotometer. The sample left under an oxidizing condition contained more large molecular sized protein than the control sample. In the case of Figure 3, the ratio of the large

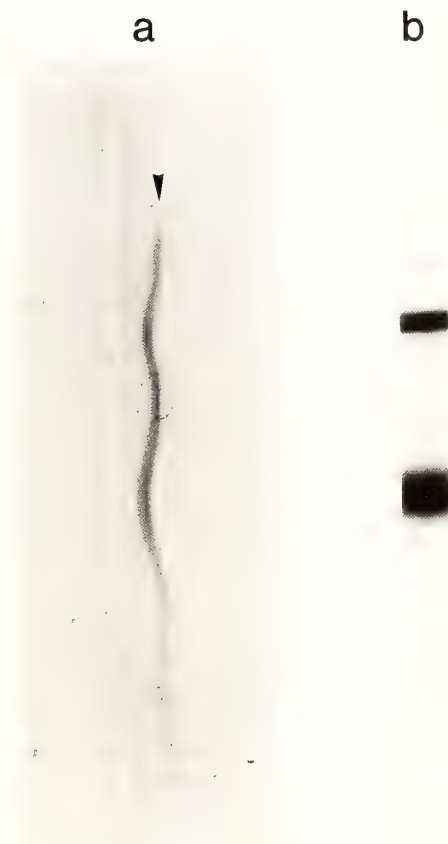


FIG. 2. Immunoelectrophoresis. Immunoelectrophoresis was carried out using 100 μ g of I-protein and anti-I-protein antiserum. a, immunoelectrophoretic profile. The arrow head shows an immunoprecipitin line. b, disc alkaline electrophoresis of I-protein.

molecular sized protein to the small one under an oxidizing condition was approximately 3 : 2 (Fig. 3, b), while the ratio of the control sample was 1 : 4 (Fig. 3, a). On the other hand, the sample under the reducing condition mainly contained the small molecular sized protein and did little large molecular sized one (Fig. 3, c). These two protein bands were electrophoresed at the position of 100,000 dalton and 50,000 dalton proteins. Therefore, it was concluded that these proteins were dimeric and monomeric I-proteins.

Dimeric I-protein possessed little inhibitory action on actomyosin ATPase activity

The inhibitory effects of I-protein in both

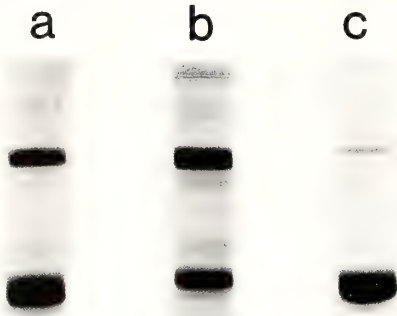


FIG. 3. SDS-polyacrylamide gel electrophoresis of oxidized and reduced I-protein. a, control I-protein. b, I-protein under an oxidizing condition. c, I-protein under a reducing condition.

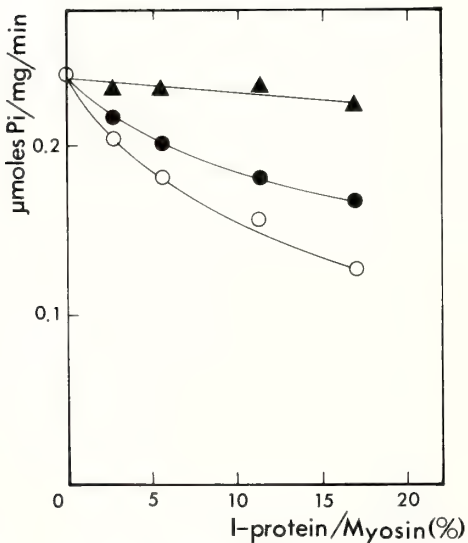


FIG. 4. The effect of dimeric or monomeric I-protein on the actomyosin ATPase. Ion-exchange column purified I-protein (○), dimeric I-protein (▲), or monomeric I-protein (●) was added to the actomyosin solution. The actomyosin ATPase was measured described in Materials and Methods.

dimeric and monomeric forms on actomyosin ATPase activity were examined (Fig. 4). Sephadex G-200 column fractionated dimeric and monomeric I-proteins (Fig. 1) were used. Reconstituted actomyosin was used. Final concentrations of myosin and actin were 0.8 mg/ml and 0.4 mg/ml, respectively. I-protein was added in various ratios to myosin. Dimeric I-protein hardly affected the actomyosin ATPase activity. Although the inhibitory action was lower than that of an original I-protein sample without gel-filtration, monomeric I-protein inhibited the actomyosin ATPase activity. Some denaturation of the protein during purification may account for the low inhibitory action of monomeric I-protein.

DISCUSSION

Ion exchange column purified I-protein usually contained both dimeric and monomeric molecules and the ratio of the two varied in each preparation. Dimeric I-protein usually increased with the lapse of time after preparation, even when stored at 0°C. In the present study, we showed that oxidization can account for the dimerization of I-protein. Dimerized I-protein was stable in a solution. Even an SDS solution containing 2-ME could not always dissolve the dimers into monomers in a short period incubation (data are not shown). However, the condition under which all monomeric I-protein molecules dimerize could not be specified.

Tropomyosin is a myofibrillar protein which also forms a dimer in a solution through disulfide bond [8]. Figure 3 shows that an oxidized I-protein solution contains more dimeric form and a reduced I-protein solution does more monomeric form. These results suggest that I-protein also forms a dimer through disulfide bond. It is assumed that I-protein may exist in a monomeric form under cellular circumstances. As is shown in Figure 4, dimeric I-protein lost the effect on the actomyosin ATPase activity while monomeric I-protein preserved. I-protein is localized at the A-I junctional region of myofibrils [4] and bind to myosin filaments *in vitro* [3]. These suggest that monomeric I-protein molecules bind to the both ends of thick filaments of myofibrils.

REFERENCES

- 1 Ohashi, K., Kimura, S., Deguchi, K. and Maruyama, K. (1977) I-protein, a new regulatory protein from vertebrate skeletal muscle I. Purification and characterization. *J. Biochem.*, **81**: 233–236.
- 2 Ohashi, K., Masaki, T. and Maruyama, K. (1977) I-protein, a new regulatory protein from vertebrate skeletal muscle II. Localization. *J. Biochem.*, **81**: 237–242.
- 3 Maruyama, K., Kunitomo, S., Kimura, S. and Ohashi, K. (1977) I-protein, a new regulatory protein from vertebrate skeletal muscle III. Function. *J. Biochem.*, **81**: 243–247.
- 4 Ohashi, K., Tsunocoka, M. and Maruyama, K. (1985) I-protein is localized at the junctional region of A-bands and I-bands of chicken fresh myofibrils. *J. Biochem.*, **81**: 1323–1328.
- 5 Davis, B. J. (1964) Disc electrophoresis – II. Method and application to human serum proteins. *Ann. N. Y. Acad. Sci.*, **121**: 404–427.
- 6 Weber, K. and Osborn, M. (1969) The reliability of molecular weight determination by dodecyl sulfate-polyacrylamide gel electrophoresis. *J. Biol. Chem.*, **244**: 4406–4412.
- 7 Matsuda, R., Obinata, T. and Shimada, Y. (1982) Types of troponin components during development of chicken skeletal muscle. *Dev. Biol.*, **82**: 11–19.
- 8 Stewart, M. (1975) Tropomyosin: Evidence for no stagger between chains. *FEBS Letters*, **53**: 5–7.
- 9 Taussky, H. H. and Shorr, E. (1953) A microcolorimetric method for the determination of inorganic phosphorus. *J. Biol. Chem.*, **203**: 675–681.

Oogenesis in the Medaka *Oryzias latipes* —Stages of Oocyte Development

TAKASHI IWAMATSU, TADAYUKI OHTA, EMIKO OSHIMA¹
and NORIYOSHI SAKAI²

Department of Biology, Aichi University of Education, Kariya 448, ¹Department of Breeding Research, Faculty of Agriculture, Nagoya University, Nagoya 464, and ²Laboratory of Reproductive Biology, National Institute for Basic Biology, Okazaki 444, Japan

ABSTRACT—An ovary of *Oryzias latipes* contains developing oocytes of various sizes and morphology during the breeding season. Formation of the egg membrane (chorion), changes in cell organelles and the volume of the developing oocyte as well as changes in follicle cells were investigated by ordinary light and electron microscopy. Basic morphological distinctions were primarily used to prepare a table of the developmental stages of *Oryzias latipes* oocytes. In addition to these distinctions, differences in proteins analyzed by SDS-polyacrylamide gel electrophoresis and the capacity for steroid production assayed by radioimmunoassay were examined in follicles at different stages. On the basis of these results, oogenesis is grossly classified into five phases (early and late previtellogenic phases, early and late vitellogenic phases and postvitellogenic phase) which are divided in detail into ten stages (Stage I–X) of oocyte development. The present classification of developing oocytes was compared with early ones by other investigators.

INTRODUCTION

In teleost fishes, many investigations on fine structures of the oocyte during oogenesis have been reviewed [1–3]. In the medaka, *Oryzias latipes*, developing oocytes have already been investigated [4–17]. Since these investigators fragmentally described developing oocytes with different viewpoints toward oogenesis, they have not always provided sufficient details on the defined developmental stages of oocytes that are required for various physiological and biochemical studies [18, 19] of medaka oocytes.

In order to establish a standard table of the developmental stages of medaka oocytes that can be used for cytological, physiological and biochemical studies, we investigated the characteristics of live and fixed follicles by light and electron microscopy and by a few biochemical methods, we also reviewed briefly the cytological and histologi-

cal observations by early investigators.

MATERIALS AND METHODS

Adult medakas, *Oryzias latipes* (orange-red type), used in the present investigation were obtained from a fish farm in Yatomi (Aichi Pref. Japan). They were kept in glass aquaria under artificial reproductive conditions (light 14 hr, 26–28°C) and fed mixed powders of shrimps and roasted wheat-grains at least three times a day.

To test the ability of large oocytes to mature in response to hormone stimulation, intrafollicular oocytes isolated as described elsewhere [20] were incubated for 10 hr (26°C) in culture medium (90% Earle's medium 199, Dainippon-seiyaku, Osaka, Japan) containing 17 α , 20 β -dihydroxy-4-pregnen-3-one (17 α , 20 β -diOHprog, 100 ng/ml). Ten to fifteen oocytes were incubated in 5 ml of culture medium in a sterilized glass Petri-dish. At the end of incubation, maturation of oocytes was determined by observing the breakdown of the germinal vesicle (GVBD) and the responsiveness to insemi-

nation. In the present study, the diluted Earle's medium 199 was supplemented with 30 mg/l penicillin G potassium (Meiji-seika, Tokyo, Japan) and 60 mg/ml streptomycin sulfate (Meiji-seika) and adjusted to pH 7.4 with 1 M NaHCO₃.

For light microscopic observations, some ovaries were fixed for 3–12 hr with Bouin's fixative or glutaraldehyde dissolved in regular saline buffered to pH 7.3 (4°C) with 0.1 M phosphate buffer. Fixed samples were dehydrated in a graded ethanol series and embedded in paraffin. Paraffin sections 7 μm in thickness were stained with Delafield's haematoxylin. For transmission electron microscopy, oocytes were fixed with modified Karnovsky's fixative (pH 7.3) for 12 hr and post-fixed in 1% solution of buffered (0.1 M phosphate buffer, pH 7.3) osmium tetroxide for 2 hr (4°C). These samples were rinsed in 0.1 M phosphate buffer and then embedded in epoxy resin. Examination of ultrathin sections stained with uranyl acetate and lead citrate was conducted with a JEM-100 B and a JEM-100 CX electron microscopes. Fixed and dehydrated samples shrank as in Table 1.

Follicles (80–90 per sample) of various sizes were homogenized in 10 mM Tris-HCl buffer (pH 6.8) at a ratio of 35 volumes of buffer to one volume of follicle or egg with 10 strokes of a teflon microhomogenizer. The homogenate was incubated for 3 min at 60°C, and was centrifuged at 1,000 *g* for 10 min (room temp.).

The supernatant was mixed with an equal volume of the sample buffer containing 2% SDS, β-mercaptoethanol, 20 mM Tris-HCl (pH 6.8) and 40% glycerin and incubated for 10 min at 60°C. It was then analyzed by SDS-polyacrylamide gel electrophoresis (SDS-PAGE). The protein samples (about 25 μg) prepared above were loaded on polyacrylamide gels (12%) containing 0.1% SDS, 0.0025% fresh ammonium persulfate, 0.00025% riboflavin, and 0.05% Temed. Gels were run at a

constant 10 A until the tracking dye (bromophenol blue) had reached the bottom of the gel, which took approximately 6.5 hr (20°C). A common electrophoresis buffer (0.1% SDS–0.05 M Tris–0.38 M glycine) was used. The gels were fixed for 10 hr in 45% methanol–10% acetic acid, stained for 6 hr with 0.05% Coomassie brilliant blue R-250 dissolved in the above solution, and destained by diffusion in 5% methanol–10% acetic acid for 6–12 hr. Molecular weights were determined after SDS-PAGE comparing log-relative electrophoretic mobilities (Log-Rm) of standard proteins as references: carbonic anhydrase, ovalbumin, albumin, phosphorylase, β-galactosidase and myosin (a MW-SDS-200 Kit from Sigma Chemicals, St. Louis, MO., USA).

17α, 20β-DiOHprog and estradiol-17β (E₂) were measured in conditioned culture medium (15 follicles/ml) with or without PMS (pregnant mare serum gonadotropin: Serotropin, Teikoku-zoki, Tokyo) by radioimmunoassay (RIA), as described in detail by Kagawa *et al.* [21] and Young *et al.* [22]. The samples of culture medium were assayed after extraction with five volumes of diethyl ether for 30 sec. The anti-E₂ and anti-17α, 20β-diOHprog sera were provided by Dr. Y. Nagahama. The level of cross reactivity of anti-E₂ serum, with E₂, estradiol-17α, estrone, estriol and testosterone was 100.0, 0.80, 3.20, 1.77 and 0.29%, respectively. The anti-17α, 20β-diOHprog serum was highly specific, cross-reacting less than 0.01% with most of a wide range of ovarian steroids such as progesterone (Δ⁴-pregnen-3, 20-dione), 17α-hydroxy-4-pregnen-3, 20-dione and 20β-hydroxy-4-pregnen-3-one. Only 17α, 20β-dihydroxy-5β-pregnan-3-one (2.4%) showed a cross reactivity above 1%. (2, 4, 6, 7-³H)E₂ and (1, 2, 6, 7-³H)17α, 20β-diOHprog were used as antigens. In the present radioimmuno-assay system, both E₂ and 17α, 20β-diOHprog standards of 20 pg/ml could be believably distinguished from the buffer blank with

TABLE 1. Change in size of follicles due to dehydration after fixation

Diameter (μm) of live follicles	<100	200	300	400	500–700	800–900	1100–1200
Bouin's fixative	< 66	152	267	356	450–630	720–810	880–960
Modified Karnovsky's fixative	< 75	164	264	364	460–644	728–818	979–1068

Numbers in the table indicate diameter (μm) of dehydrated follicles after fixation.

a 98% confidence limit, but for practical purposes, portions of media reading less than 30 pg/ml were considered to have nondetectable levels.

RESULTS

In a medaka during the reproductive season, an ovary contains oocytes in all phases of oogenesis (Fig. 1). Oocytes can be grossly divided into five phases and further into ten stages, based on major morphological characteristics of developing oocytes and follicles (Fig. 2). Figure 3 diagrammatically illustrates these stages, based on the present observations obtained using light microscope. Extracts of various sized follicles and eggs form numerous protein bands with SDS-PAGE (Fig. 4), which reveals some characteristic features. The capacity of follicles to produce E_2 and $17\alpha, 20\beta$ -diOHprog in response to gonadotropin stimulation is also different in follicles of different sizes

(Fig. 5). The developmental pattern of E_2 secretion by follicles is different from that of $17\alpha, 20\beta$ -diOHprog.

Early previtellogenic phase

Oocytes (Stages I and II of Fig. 3) in this phase (follicles approx. 20–90 μm) are the smallest growing oocytes in the ovary of spawning females. These oocytes usually form clusters in the peripheral region of the ovary.

Stage I (chromatin-nucleolar stage): This group of very small and transparent oocytes (follicles approx. 20–60 μm , Figs. 1A, 2 and 3), possesses poorly developed tubular endoplasmic reticulum (ER) and mitochondria. The roughly spherical nucleus with chromatin-threads with a network appearance has many spherical nucleoli, unlike that of the very small (about 10 μm) oogonia [6, 23] which have a large nucleolus in the nucleoplasm and aggregations of germinal dense bodies

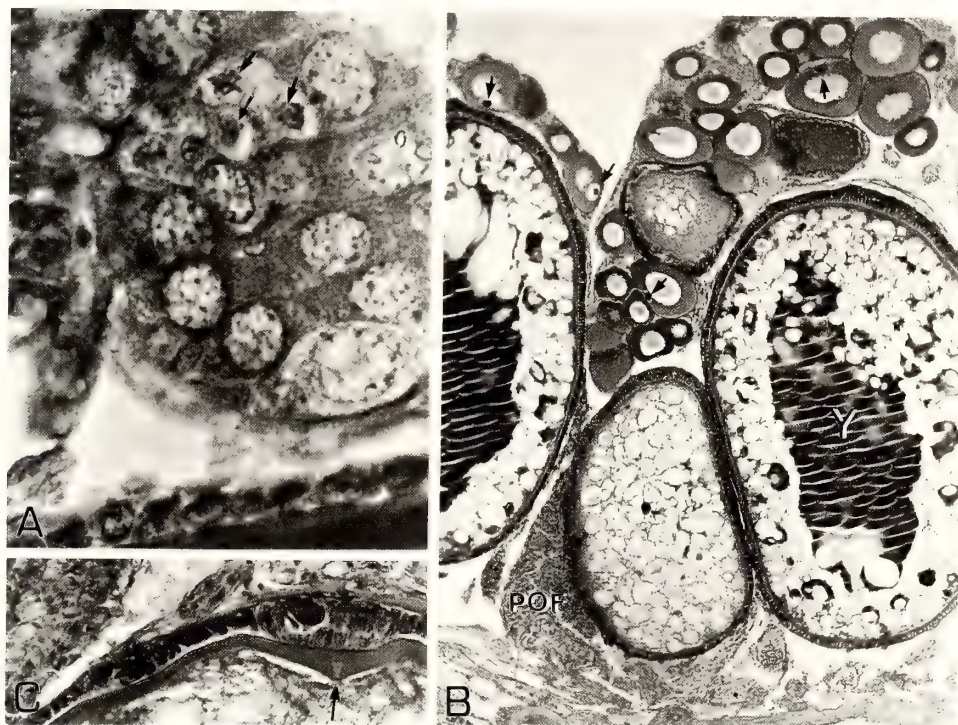


FIG. 1. Oocytes at the various stages of oogenesis in the *Oryzias* ovary.

A: Smallest oocytes at Stage I. $\times 600$.

B: A section of ovary during the spawning season. Note large yolky oocytes, postovulatory follicles (POF), and previtellogenic oocytes with a yolk nucleus (arrows). Y, yolk mass. $\times 150$.

C: Follicle layers and chorion at the animal pole side of an oocyte (micropyle, arrow). $\times 60$.

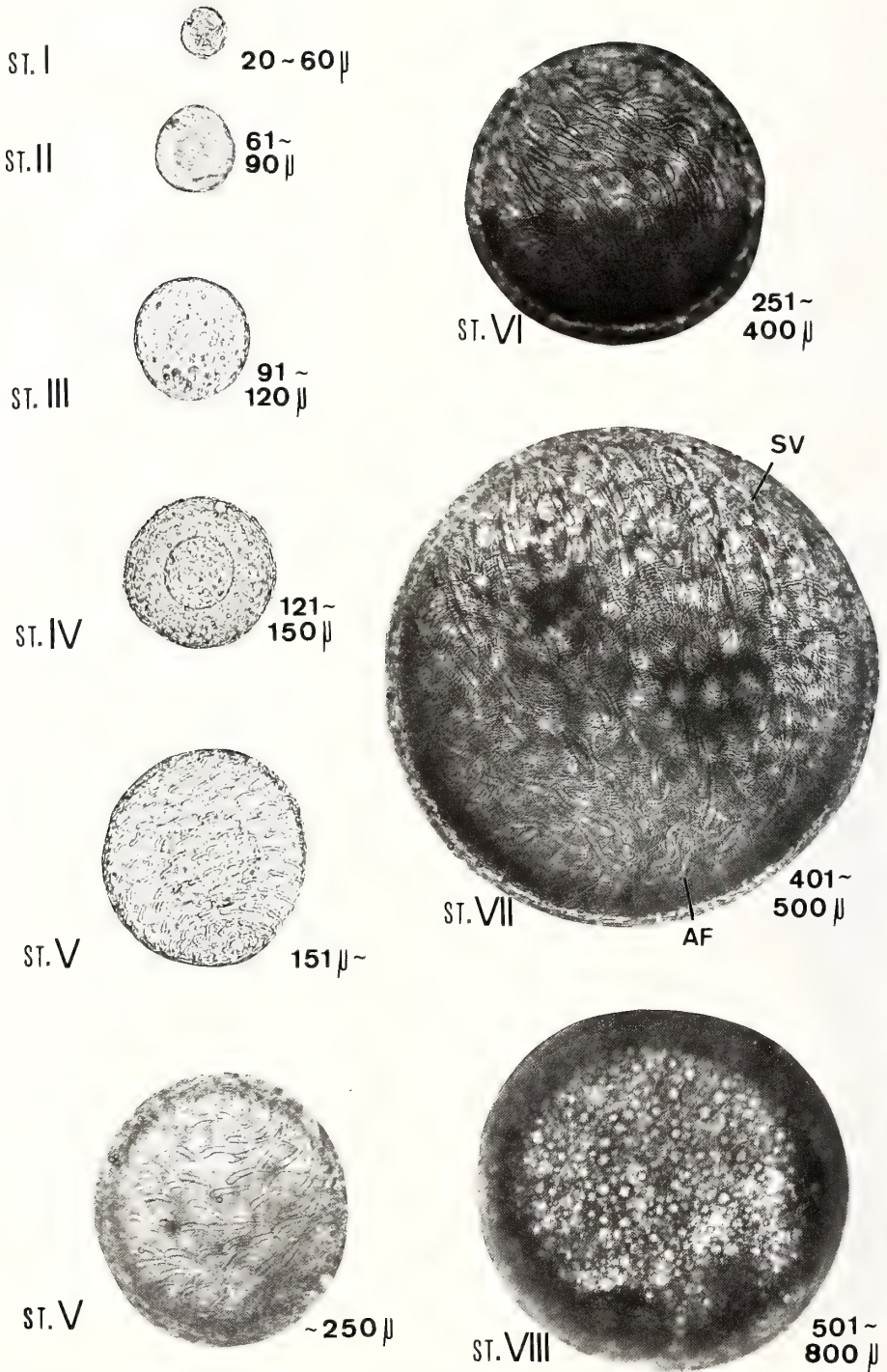


FIG. 2. Living follicles at various stages of oocyte development. Small- and medium-sized follicles (Stage I-VII). $\times 150$. Large-sized follicles (Stage VIII). $\times 80$. SV, short villi on the chorion; AF, attaching filaments on the chorion.

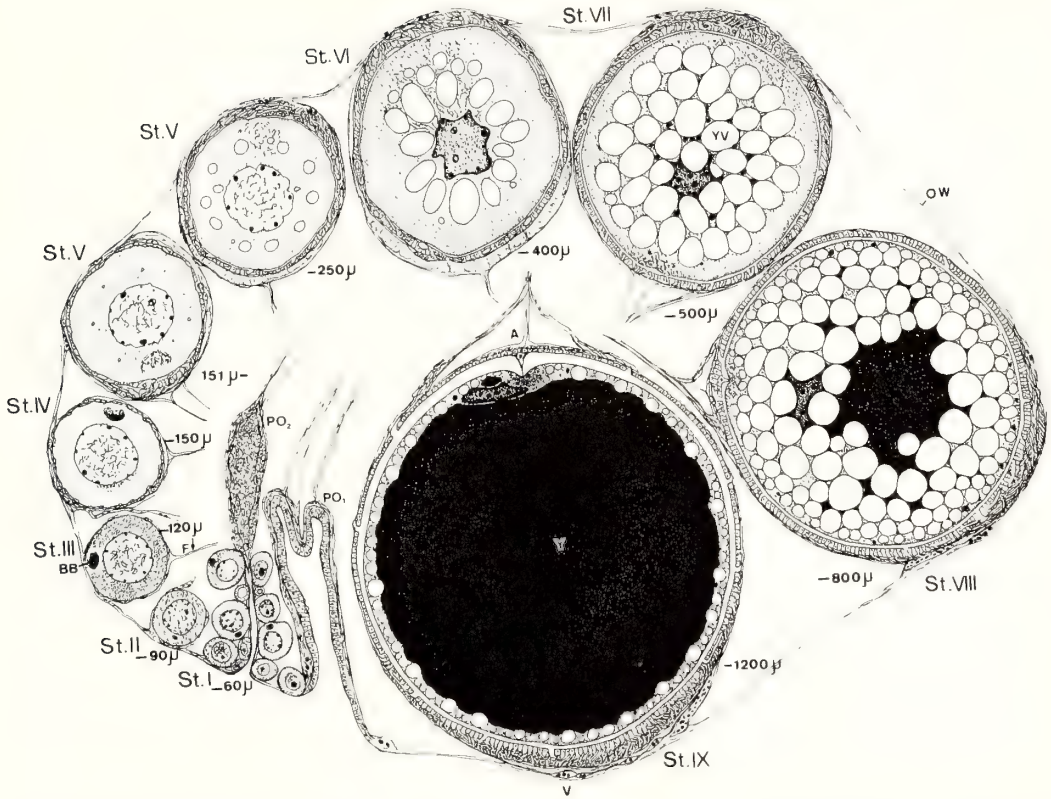
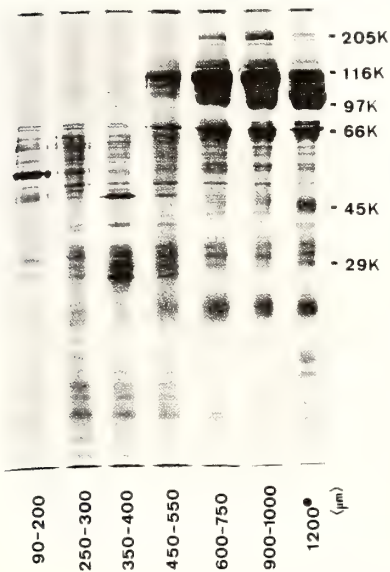


FIG. 3. Diagrammatic illustration of growing oocytes at various stages of oogenesis. OW, ovarian wall; PO₁, postovulatory follicle just after ovulation; PO₂, postovulatory follicle 24 hr after ovulation; A, animal pole; V, vegetal pole; Y, yolk mass; YV, yolk vesicle.



and mitochondria in the cytoplasm. Oocytes are covered with an extremely thin single layer of flattened follicle cells.

Stage II (perinucleolar stage): The small and transparent oocytes in the follicles vary from 61 μm to 90 μm in diameter (Fig. 2) and have a relatively large nucleus with many spherical nucleoli arranged in the peripheral region (Fig. 3) and haematoxylin-stainable cytoplasm containing a yolk nucleus (Balbiani's body, Fig. 1B). An electron-dense matrix free from cytoplasmic organelles is situated in the cortical region of the ooplasm (Fig. 6A). Mitochondria are arranged in the marginal region of the electron-opaque area of the cytoplasm that contains poorly developed

FIG. 4. SDS-polyacrylamide gel electrophoresis of extracts of various sized follicles and eggs. The size of the follicles and eggs (dot) is indicated at the bottom of each lane. Molecular weight values on the right indicate standard protein bands.

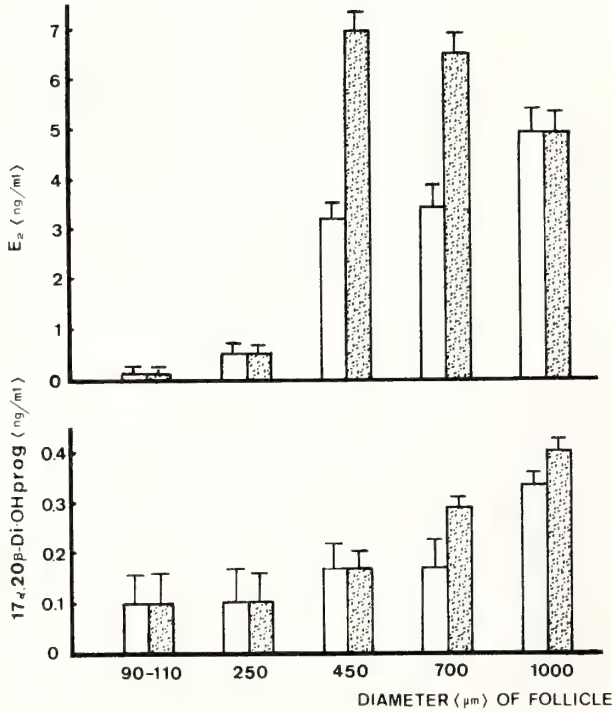


FIG. 5. Production of E_2 and $17\alpha, 20\beta$ -dihydroprog by follicles of various sizes. Follicles were incubated with (shaded columns) or without PMS. Twenty follicles were incubated in 1 ml of culture medium. The medium was collected for determination of E_2 and $17\alpha, 20\beta$ -dihydroprog by radioimmunoassay. Bars represent means \pm SE of four incubations.

tubular and smooth ER. The oocytes are covered with extremely flattened granulosa and thecal cells, which are separated by a basement membrane. Clustered microvillus-like projections increase on the restricted area of the oocyte surface facing the junctions of granulosa cells, which usually attach to each other by a number of desmosomes. Granulosa cells possess few microprojections, a small number of mitochondria, very poorly developed ER and flattened nuclei with a nucleolus.

Late previtellogenic phase (chorion-formation)

In this phase, follicles containing transparent oocytes (Fig. 2) vary in diameter from 91 μm to 150 μm (Stages III and IV of Fig. 3). The protein band pattern formed by SDS-PAGE is charac-

terized by 53 k M_r as a major band and 42 k, 63 k and 67 k M_r as minor bands (Fig. 4).

Stage III (chorion-rudiment stage): The oocytes in these follicles (91–120 μm , Figs. 2 and 3) exhibit rudiments of short villi prior to chorion formation. In the cortical cytoplasm, the electron-dense matrix (Fig. 6B) has already disappeared from the cortical region, in which mitochondria and tubular ER are located. The monolayer of granulosa cells is interconnected tightly and circumferentially with many well developed desmosomes (Fig. 6B). Thecal cells are separated from the granulosa cells 1–1.5 μm in width by a basement membrane. The cytoplasm of the oocytes has a large yolk nucleus (Fig. 1B) and is stained less intensely with haematoxylin.

Stage IV (attaching filament and oil-droplet

FIG. 6. Sections of ovarian follicles containing Stage II and Stage III oocytes. A: Oocyte (in a follicle about 65 μm in diameter) surrounded by a very thin follicular epithelium consisting of flattened granulosa (G) and thecal (T) cell layers which are separated by a basement membrane (B). Note that there are only a few microprojections from the surface of the oocyte (O). The cortical cytoplasm of the oocyte is electron dense (DL). $\times 6,600$. B: Oocyte (in a follicle about 100 μm in diameter) is surrounded by thick granulosa (G) and thecal (T) cell layers. Clusters of microprojections from the oocyte are found where adjacent granulosa cells joined by desmosomes (arrows) meet. Masses of long mitochondria are frequently observed. $\times 10,000$.

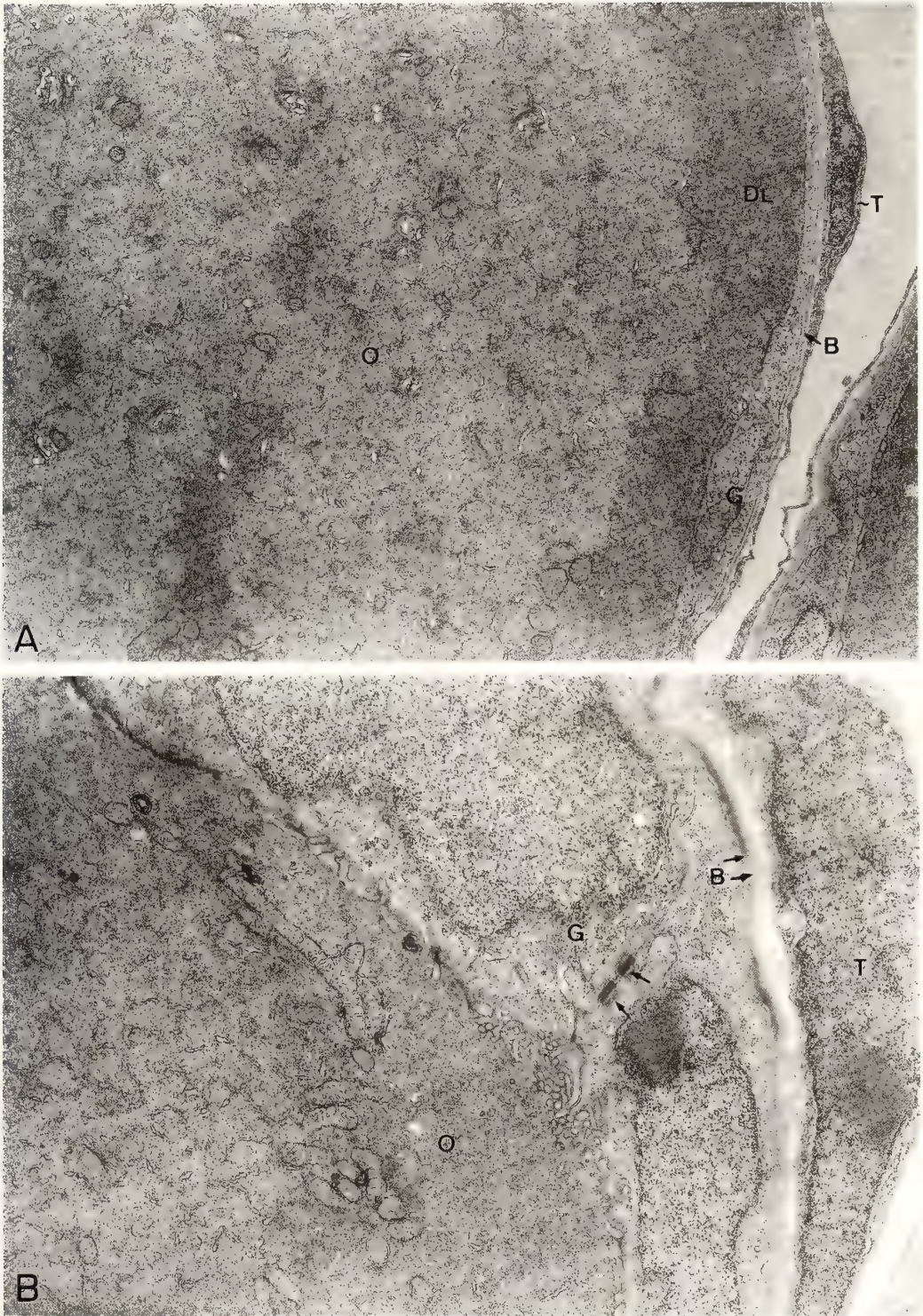


FIG. 6.

formation stage): The oocytes in these follicles (121–150 μm , Figs. 2 and 3) possess minute bumps as rudiments of short villi (Fig. 7A) on thin rudiments of chorion (about 0.1 μm in thickness) among ooplasmic projections (Fig. 7B). The oocyte surface possesses long microvillus-like projections among which very thin and electron-dense rudiments of the chorion have begun to appear. In the cortical region of the oocyte, scattered tubular ER, mitochondria (approx. 0.3–0.5 μm in diameter) and Golgi complexes have increased markedly in number (Fig. 7B). The oocytes belonging to this stage exhibit the differentiation of long chorion-villi (attaching filaments) at the vegetal pole region of the chorion (0.2–0.3 μm in thickness) and still possess the yolk nucleus (Fig. 1) in the cytoplasm. The most developed yolk nucleus consists of thread-like bodies [24], mitochondria, ER, Golgi lamellae, vesicles and multivesicular bodies (internal small vesicles, about 50 nm) (Fig. 8). Granulosa cells with desmosomes at intercellular junctions have become thicker than in the previous stage, and their cytoplasmic organelles such as mitochondria, ER and Golgi complexes have increased.

Early vitellogenic phase (pre-yolk formation stage)

The size of the oocytes markedly increases in this phase. The oocytes in those follicles (151–400 μm , Stages V and VI of Figs. 2 and 3) possess yolk vesicles forming from one to several layers and occupying the greater part of the cytoplasm. Minute fatty or oil droplets appear mainly in the deeper region of the cytoplasm at the end of this phase.

Stage V (early yolk vesicle stage): The oocytes in these follicles (151–250 μm) are characterized by the appearance of 1–2 layers of small vesicles which contain granular materials with a lower electron density than the surrounding cytoplasm. The yolk nucleus is obscure or not observed in the cytoplasm. Oil droplets appear adjacent to the

indented nuclear envelope. The nucleoplasm containing shortened lamp-brush chromosomes and ring-shaped nucleoli is deeply stained with haematoxylin. A new innermost layer has been found on the inside of the outermost layer of the chorion by deposition of electron-dense and amorphous material (0.2–0.6 μm in thickness) that is detectable as small vesicles in the vicinity of the oocyte surface (Fig. 9A). Numerous vesicular ER, lamella bodies [25] and mitochondria with minute electron-dense granules are distributed throughout the cortical cytoplasm of the oocytes (Fig. 9A). A special cell, presumably the micropylar cell, is observed among the granulosa cells with their desmosome junctions.

Stage VI (late yolk vesicle stage): The oocytes in these follicles (251–400 μm) before yolk formation have 2–6 layers of large yolk vesicles which occupy the greater part of the cytoplasm. Lipid granules are found in the perinuclear region and small yolk granules appear in the cytoplasm at the end of this stage. The protein band pattern is characterized by several bands (less than 20 k, 29 k, 37 k, 42 k, 53–80 k M_r ; Fig. 4). The nucleoplasm has a high affinity for haematoxylin and contains shortened chromosomes and ring-shaped nucleoli. As the oocyte enlarges, the innermost layer of the chorion thickens from 1.5 μm to 3 μm (Fig. 9B). Electron-lucent vesicles are seen in the cortical cytoplasm (Fig. 9B), probably blebbing inward as pinocytotic vesicles (see [10, 26]). Granulosa cells have developed rough ER, dilated smooth lamellae and lysosome-like bodies, and are in contact with ooplasmic projections via gap junctions. The ability to produce E_2 is first recognized in follicles of this stage, but these follicles do not increase their secretion of E_2 and $17\alpha, 20\beta\text{-diOHprog}$ in response to gonadotropin.

Late vitellogenic phase

In the oocytes within follicles (401–800 μm , Stages VII and VIII of Fig. 3) of this phase, yolk

FIG. 7. Follicles containing Stage IV and V oocytes. A: Follicle (about 125 μm in diameter, Stage IV) containing an oocyte that possesses bumps of short villi on the developing rudiment of the chorion. Note numerous microprojections derived from the oocyte at the oocyte-follicle cell interface. B, basement membrane; D, desmosome; G, granulosa cell; T, thecal cell. $\times 16,600$. B: Follicle (about 155 μm in diameter containing Stage V oocyte) showing formation of a very thin outermost chorion layer (COL) as an electron-dense layer. Mitochondria and Golgi complex (GO) are located at the peripheral region of oocyte (O). $\times 26,000$.

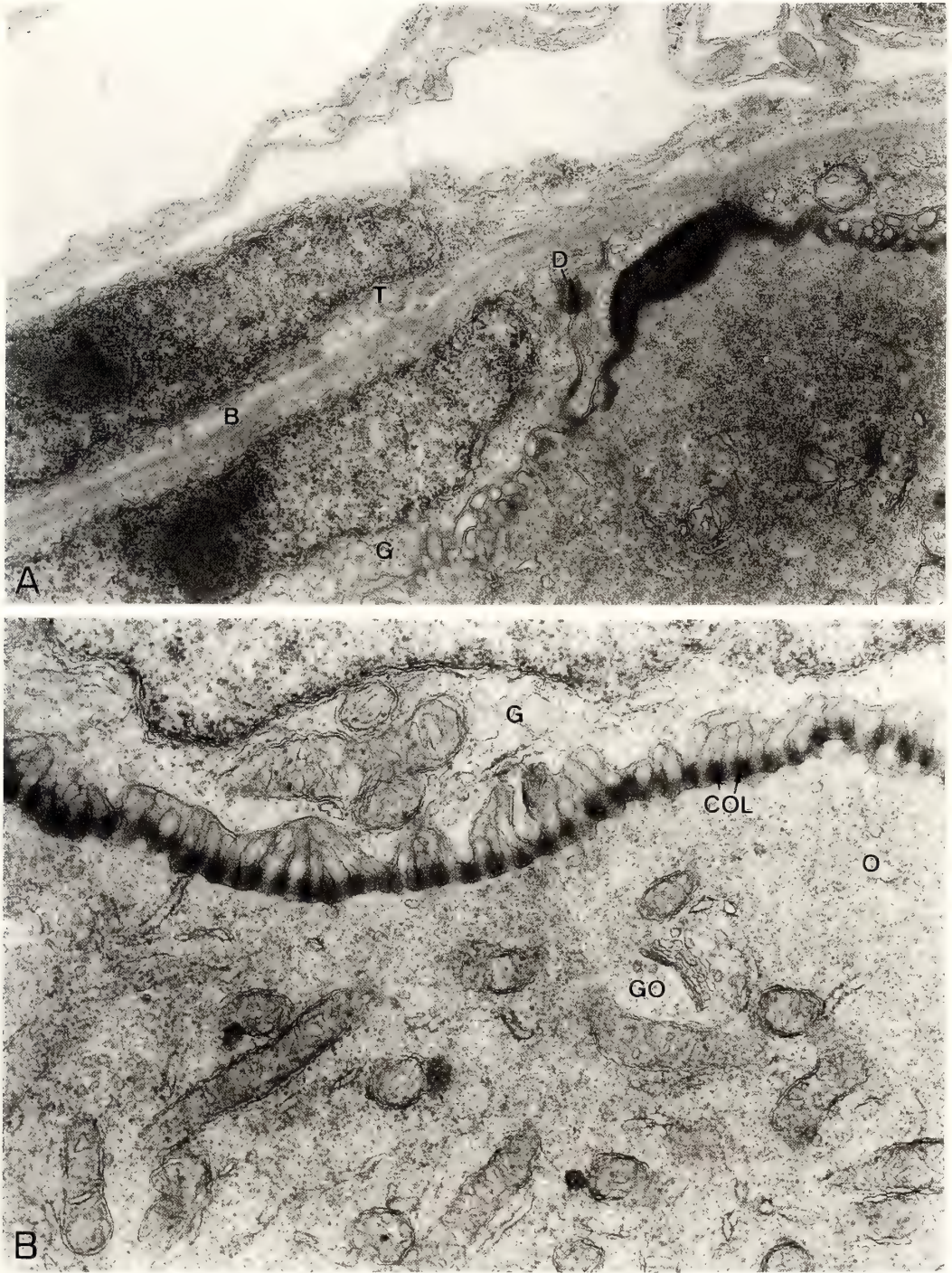


FIG. 7.

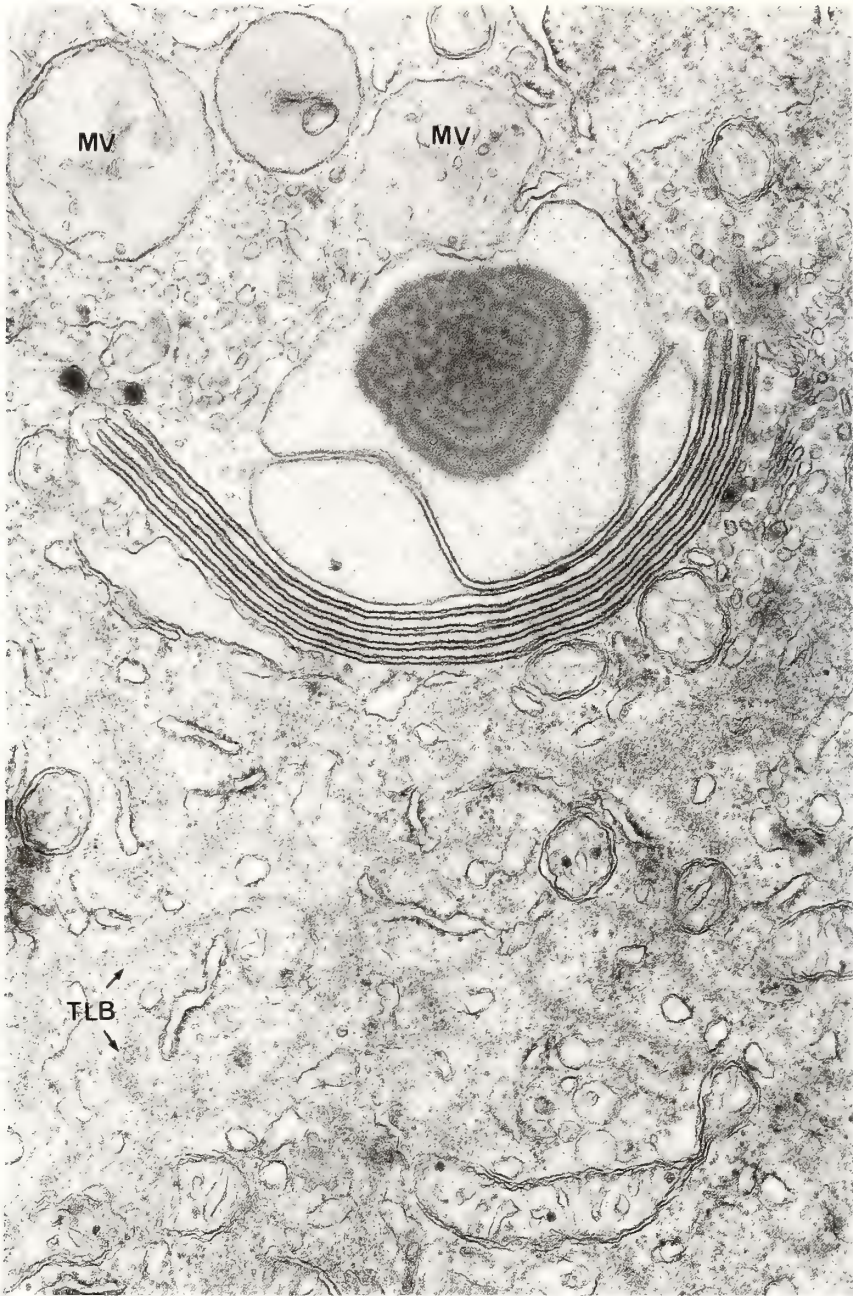


FIG. 8. Part of the yolk nucleus of an oocyte (in a follicle about $100\ \mu\text{m}$ in diameter) showing numerous thread-like structures (TLB), tubular endoplasmic reticulum, Golgi lamellae, small Golgi vesicles and primitive multivesicular bodies (MV). $\times 31,000$.

platelets first appear and fuse with each other to form yolk masses in the cytoplasm among yolk vesicles. Cytoplasmic inclusions are pushed toward the peripheral region of the oocyte as the

mass of yolk enlarges in the central part of the oocyte. The protein band pattern is characterized by the new appearance of 26 k, 27 k, 30 k, 32 k, 53 k, 78 k, 98–116 k (yolk proteins), 175 k and 205

k M_r bands and the disappearance of bands less than 20 k M_r .

Stage VII (early yolk formation stage): The oocytes in these follicles (401–500 μm , Fig. 2) enlarge rapidly as fusion of small yolk platelets to form yolk masses among yolk vesicles advances. Protein bands of 98 k–116 k and 175 k M_r first appear in this stage. The cortical cytoplasm contains a number of mitochondria, ER, yolk granules (YG), cortical alveoli (CA) and oil droplets (L) (Fig. 10A). A nearly formed micropyle (Fig. 1C) is easily recognized at the animal pole of the chorion. Cytoplasmic projections of oocytes are 0.2–0.3 μm in width, and their cytoplasmic matrix is more electron-dense than that of the follicle cell projections. At this stage, the egg nucleus (germinal vesicle) begins to migrate toward the animal pole where the chorion (about 5 μm in thickness) is thicker than at the vegetal pole region.

Gap junctions between granulosa cells (Fig. 10B) are observed. Follicles of this stage are most active in secreting E_2 and secrete slightly detectable ($P < 0.05$) 17α , 20β -diOHprog. Gonadotropin stimulates an apparent increase in E_2 secretion by follicles 450 μm in diameter, while it does not increase their 17α , 20β -diOHprog secretion (Fig. 5).

Stage VIII (late yolk formation stage): The oocytes which have formed a large yolk sphere in these follicles (501–800 μm , Figs. 1B and 2) show morphological differences between the animal and the vegetal poles. The chorion is thicker in the animal hemisphere than in the vegetal hemisphere, the micropyle is located at the animal pole, attaching filaments exist at vegetal pole (Fig. 1B), and the nucleus is located at the animal pole of the oocyte. The cortical ooplasm with the most elongated microprojections is filled with Golgi complexes, aligned ER, CA, yolk granules (YG) and ribosomes (Fig. 10D). Isolated these oocytes still fail to resume meiosis in response to maturation-inducing steroids (MIS; progesterone, or 17α , 20β -diOHprog) during incubation. Granulosa cells, which display pronounced mitochondria with well-developed tubular cristae and a dense matrix, actively produce E_2 and 17α , 20β -diOHprog. Production of these steroids is stimulated by gonadotropin ($P < 0.05$) (Fig. 5).

Postvitellogenic phase

The fully grown oocytes within preovulatory follicles (801–1200 μm) have the potential to initiate their maturation events in response to MIS. Follicles are capable of producing E_2 and 17α , 20β -diOHprog (Fig. 5).

Stage IX (maturation stage): The oocytes within the largest follicles (801–1200 μm) 0–24 hr before ovulation are capable of undergoing maturation when incubated with MIS. The oocytes approaching the resumption of meiosis clearly exhibit a large germinal vesicle in the vicinity of the micropyle. Before initiation of maturation, the cortical cytoplasm exhibits many mitochondria, annulate lamellae, rough ER and Golgi complexes (Fig. 11). In maturing oocytes the nucleus changes with GVBD leading to formation of the metaphase II spindle of meiosis. The first polar body is extruded at the animal pole. In the granulosa cells of this stage, the nucleus is located in the vicinity to the basement membrane (Fig. 12A). Marked features of the granulosa cells before initiation of oocyte maturation are mitochondria with highly developed tubular cristae and dense-matrix, many vacuoles among the Golgi complexes, transport vesicles and dilated ER (Fig. 12B). All cytoplasmic projections of both the oocyte and granulosa cells have withdrawn completely from the chorion by the time of ovulation. At the end of this stage, ovulation takes place: oocytes are squeezed from the vegetal pole side out of the follicular layers.

Stage X (postovulatory stage): Ovulated oocytes (eggs, approx. 1200 μm) exposing short villi and long attaching filaments on the chorion are in the ovarian lumen. Under the light microscope, the whole egg is semitransparent, and numerous cortical alveoli (CA, 0.4–40 μm) and oil droplets (1–50 μm) are visible throughout the entire egg surface, except for a restricted area at the animal pole. A few Golgi complexes and no annulate lamellae are observed in the cortical cytoplasm, as reported in previous notes [9, 27].

The protein band pattern is characterized by faint protein bands of 175 k and 205 k M_r , and reappearance of 20 k, 21 k and 45 k bands (Fig. 4).

DISCUSSION

The present study has summarized cytological and histological characteristics of developing oocytes of *Oryzias latipes* which were assigned to five phases and ten stages (Table 2). Phases were assigned from the viewpoint of vitellogenesis. The stages of oocyte development, which were classified on the basis of observations of changes in the nucleus and the cytoplasm, and of the formation of the egg membrane (chorion), were compared with those reported in early investigations (Table 3).

Oocytes less than 20 μm in diameter, which were designated as the chromatin-nucleus stage by Yamamoto and Yoshioka [17], seem to correspond to oogonia [23] with a large nucleolus and chromatin-threads in the nucleus. The perinucleolar stage (Pn) oocytes in the classification of Yamamoto and Yoshioka [17] are divided into Stage I (small oocytes less than about 20 μm with the nucleus displaying several nucleoli and chromatin-threads) and Stage II (slightly larger oocytes, which have a large nucleus with many perinucleoli, as in *Fundulus heteroclitus* [28]). Yamamoto [15] and the present study, which employed electron microscopy, also divided the stage A oocytes of an early classification [16] into two stages based on fine structural differences in the ooplasm. Our classification of the oocytes, based on changes in oocyte volume as well as cytoplasmic and nuclear morphology of oocytes surrounded by extremely flattened granulosa cells with well developed desmosomes, is as a whole consistent with the observations of Yamamoto [16]. Thus, the early previtellogenic phase before formation of the chorion is conveniently divided into Stage I (chromatin-thread stage) and Stage II (perinucleolus stage).

Concomitant with development of follicles, the growing oocytes in which the cytoplasm faintly

stains with haematoxylin can be distinguished from those of the previous stage. The late previtellogenic phase was established for two developmental stages of oocytes (Stages III and IV) with both the developing chorion and the most developed yolk nucleus present before formation of yolk vesicles. The present criterion for classification of these stages was the bipolar differentiation of the follicle, which was not studied in detail by any previous investigators. With advancing differentiation of the chorion, the egg polarity is recognized by appearance of attaching filaments on the chorion at the vegetal pole side in the vicinity of the yolk nucleus. Fine structural studies have revealed the yolk nucleus as an extensive aggregate of cell organelles such as thread-like bodies, mitochondria, Golgi complexes, smooth ER, vesicular bodies and plate structures. The thread-like bodies especially characterize the yolk nucleus [14]. Quite similar bodies in *Xenopus* oocytes (100 μm) have been described by Takamoto [24]. During the late phase of previtellogenesis, another typical feature is the most highly-developed lamp-brush chromosomes that possibly correlate with the most highly-developed yolk nucleus. In addition at this stage the maximal development of pinocytosis is seen at the oocyte surface, and the yolk precursors are actively incorporated. Yamamoto [16] and Yamakawa [13] assigned the yolk formation stage to oocytes that enlarged as yolk vesicles and mass increased.

The central zone of the cytoplasm has small yolk vesicles in the oocytes designated as being at the stage characterized by the dispersing yolk nucleus. The oocytes of Stage V are characterized by disappearance of the yolk nucleus and appearance of both a layer of yolk vesicles in the central part of the cytoplasm and two layers of the chorion. In addition to these features, other characteristics are appearance of oil droplets adjacent to the nucleus

Fig. 9. Follicles containing Stage V and VI oocytes. A: Follicle (about 200 μm in diameter) containing oocyte (Stage V) with thick outermost layer of the chorion. Microprojections from granulosa cells are observed at a low frequency. Arrows indicate electron-dense material. $\times 16,600$. *Inset*: Lamellar body in the ooplasm. $\times 32,000$. B: A part of the chorion of an oocyte at Stage VI. It consists of outermost (COL) and innermost (CIL) layers, into which microprojections (GP, from the granulosa cell; OP, from the oocyte) of both the oocyte (O) and the granulosa cell (G) insert. The granulosa cell surface is in contact with an ooplasmic projection (arrow heads). Arrows indicate small electron-lucent vesicles intact with the oocyte surface. $\times 20,000$.

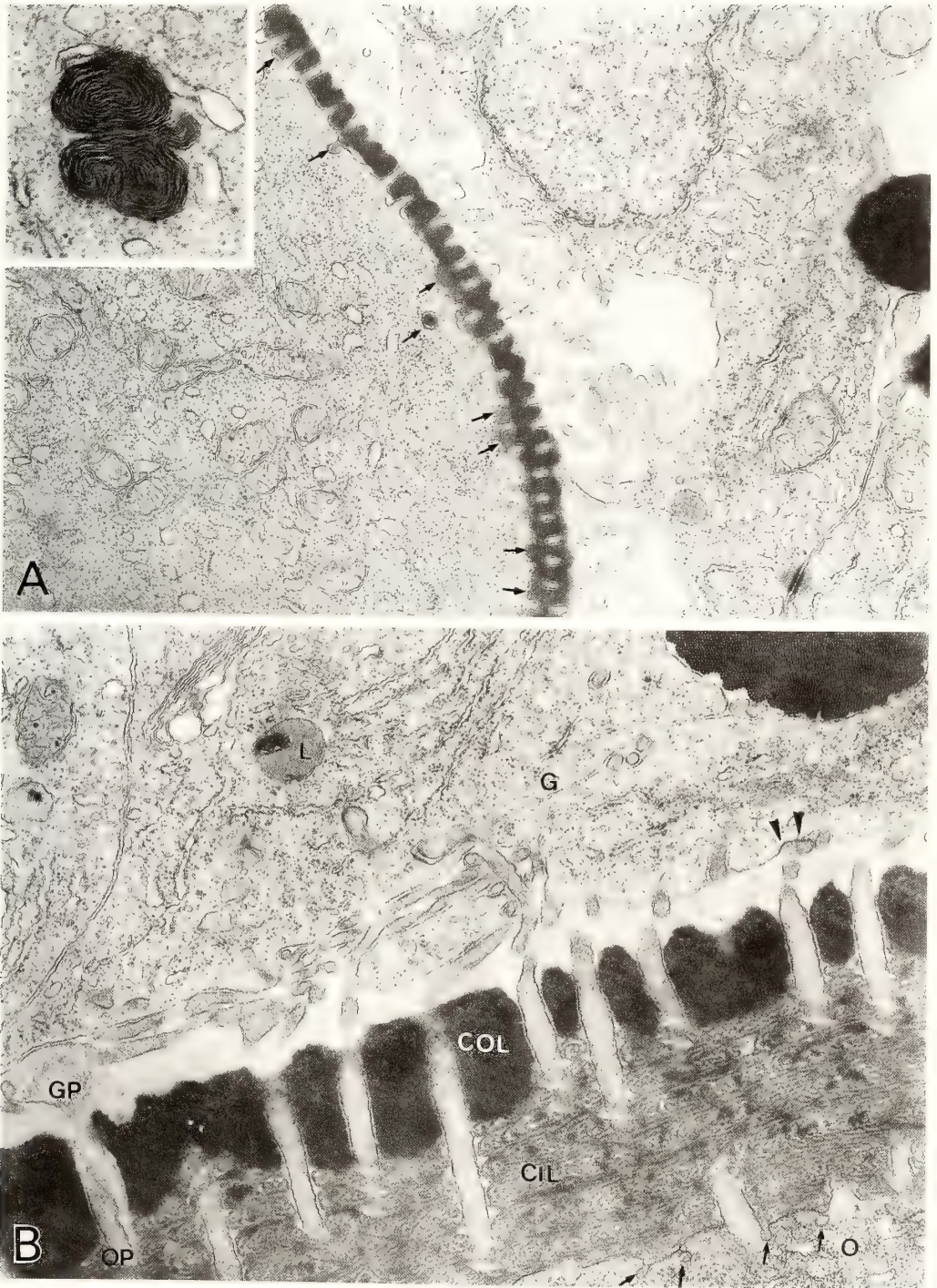


FIG. 9.

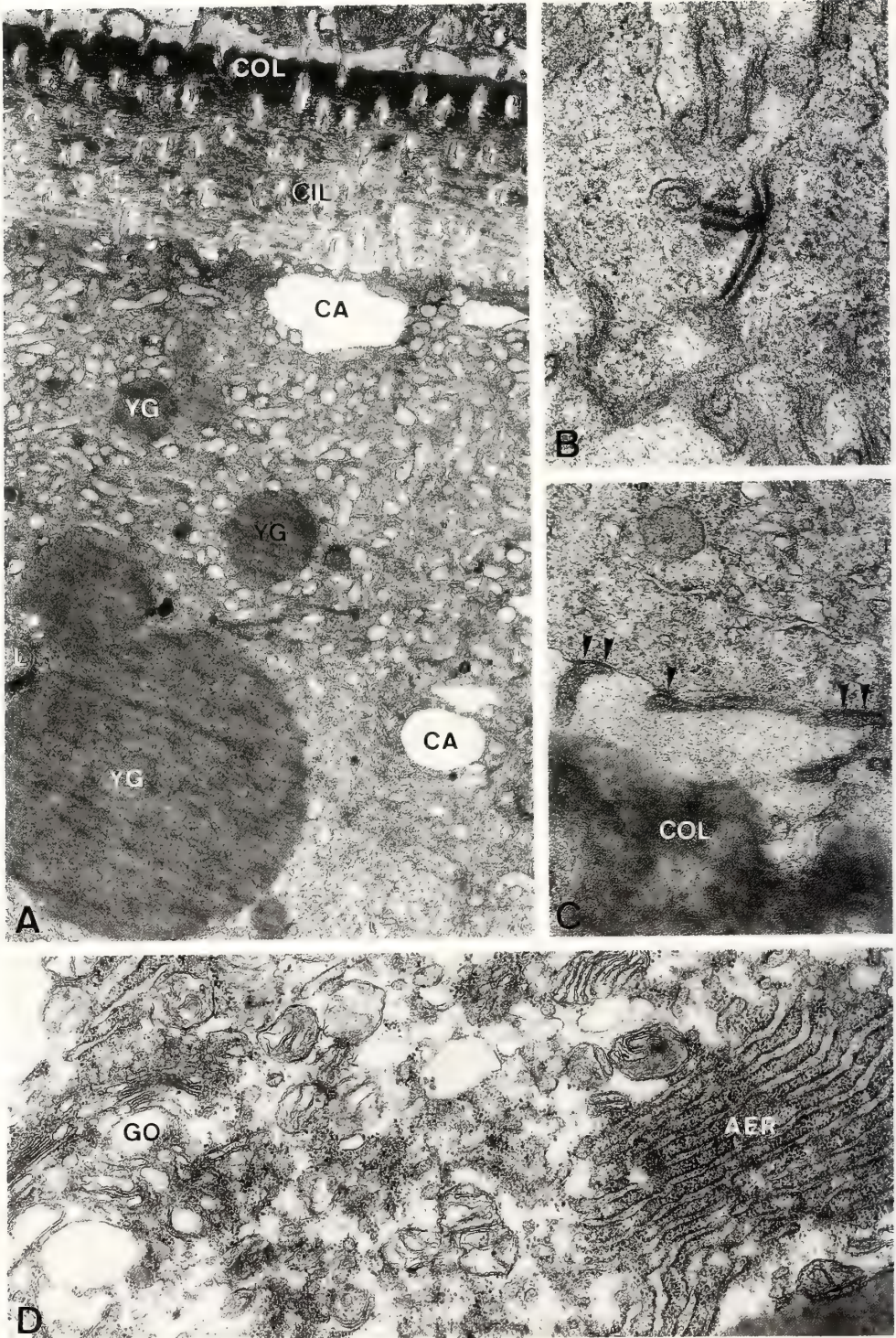


FIG. 10.



FIG. 11. Annulate lamellae in an oocyte at the maturation stage (Stage IX). Note the lamellae (AL) that are continuous at the end with lamellae of rough endoplasmic reticulum (ER). $\times 55,200$.

FIG. 10. Portions of follicles containing Stage VII and VIII oocytes. A: Cortical cytoplasm of Stage VII oocyte. Note ooplasmic inclusions such as cortical alveoli (CA), numerous mitochondria, yolk granules (YG) and oil droplet (L). $\times 7,000$. B: Gap junctions among granulosa cells surrounding Stage VII oocyte. $\times 44,800$. C: Gap junctions (arrow heads) between Stage VII oocyte microprojections (electron dense) and granulosa cell. $\times 25,700$. D: Cortical cytoplasm of Stage VIII oocyte. Note piled endoplasmic reticulum (AER) and many Golgi complexes (GO). $\times 23,100$.

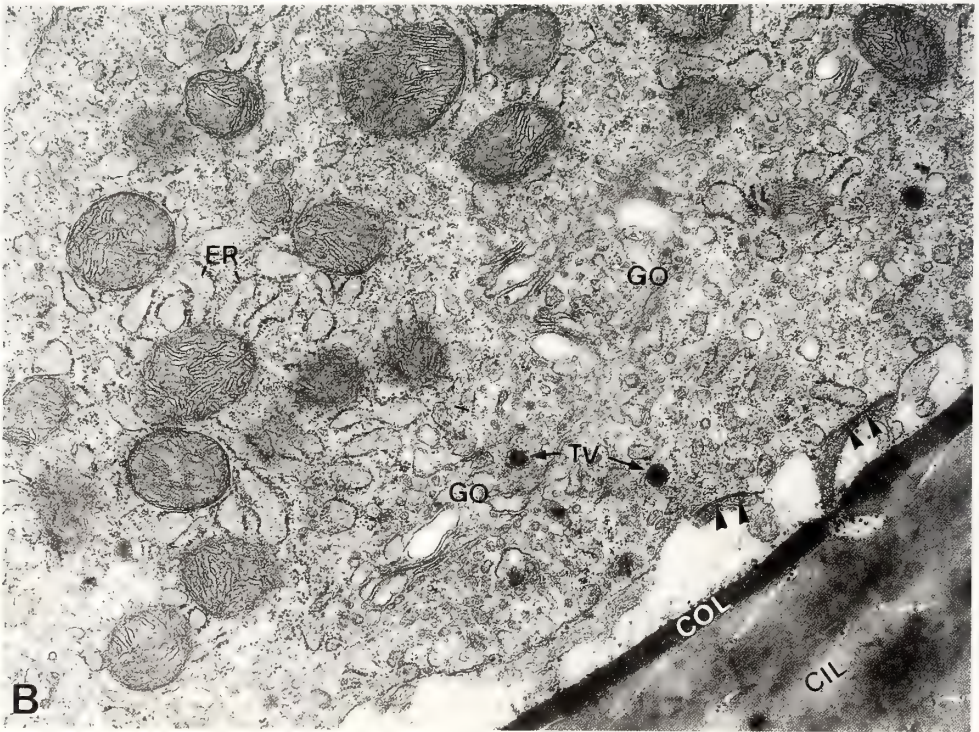
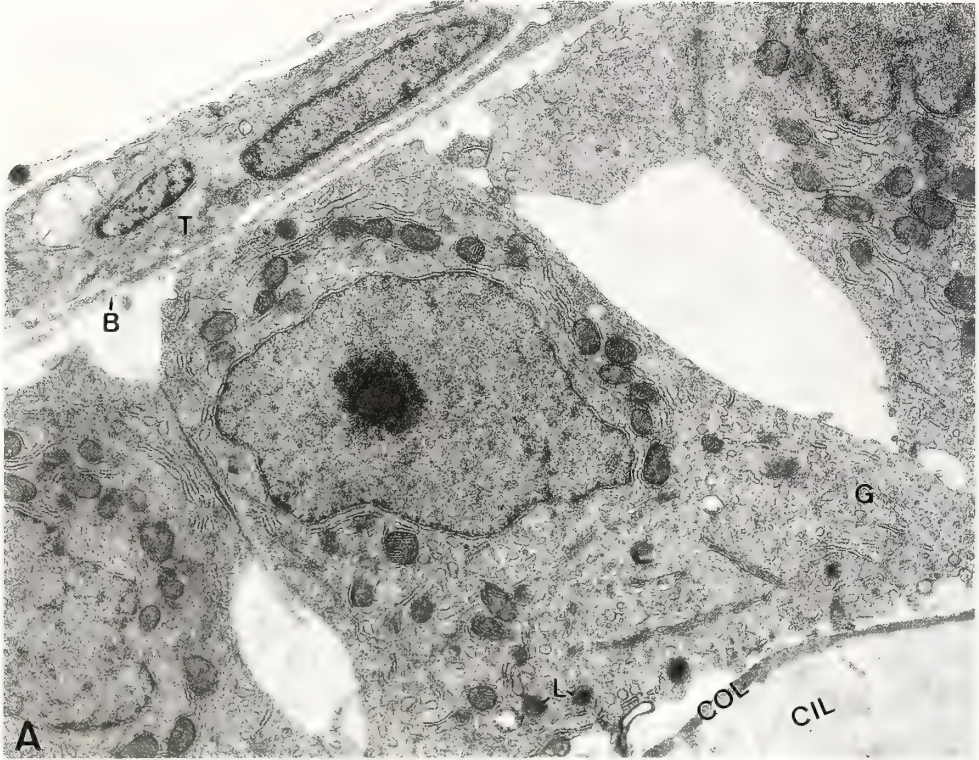


FIG. 12.

and ring-shaped nucleoli in the nucleoplasm. Our observations of Stage V oocytes are almost consistent with those reported by Yamamoto [14] in which irregularly shaped nucleoli become voluminous. At Stage V the two or more innermost layers are piled inside the outermost layer of the chorion. This mode of chorion formation has been proposed by Tesoriero [29]. The innermost layers are produced by the oocyte. Another characteristic of this stage is that yolk vesicles (or goutte claires, [30]), which contain PAS positive material [4, 13, 16, 31], are observed in the ooplasm. These vesicles correspond to the cortical alveoli (vesicles) in the mature egg. A change in the ER from a tubular to a vesicular form with ribosomes seems to reveal the beginning of active protein synthesis.

In hypophysectomized females [32], which are responsive to E_2 , the ovary contains only young oocytes earlier than those of this stage. Oocyte development beyond Stage V depends on stimulation by gonadotropin.

At the yolk vesicle stage of Yamamoto and Yoshioka [17], the oocytes that possess several layers of yolk vesicles in the cytoplasm are designated as Stage VI. In this stage, oocyte volume rapidly increases, but yolk globules (small yolk masses) are hardly observed. The oocytes in which small yolk globules appear between large yolk vesicles are designated as Stage VII, belonging to the late vitellogenic phase. The appearance of yolk globules is quite consistent with that of yolk proteins of 98–116 k M_r , as shown in *Fundulus* oocytes [33]. In this stage, small yolk masses are found in the peripheral region of the cytoplasm among yolk vesicles and numerous oil droplets.

Beyond this stage, oocytes in which the yolk mass has rapidly enlarged in the central region are designed as Stage VIII, as described by Yamamoto [16], Yamakawa [13] and Yamamoto and Yoshioka [17]. In these growing oocytes, there are markedly increased microprojections of the oocyte surface toward the granulosa cells through the

pore canals of the chorion, as well as projections of granulosa cells toward the oocyte surface. Gonadotropin stimulates an apparent increase in E_2 secretion by follicles of both Stages VII and VIII, but follicles of Stage VII do not secrete increased $17\alpha, 20\beta$ -diOHprog in response to gonadotropic stimulation while those of Stage VIII do. Thus, follicles containing oocytes of Stage VII are different from those of Stage VIII in their steroid synthesis capacities.

As the yolk mass enlarges, the yolk vesicles and the nucleus (germinal vesicle) shift toward the peripheral region of the oocyte and the nucleus are finally located at the cortical cytoplasm (the animal pole) near the micropyle. Most investigators have reported the late stage of yolk formation as the maturation stage. However, oocytes within follicles about 800 μm in diameter are the first that are able to respond to the MIS reinitiating meiosis [20]. Therefore, we assigned Stage VIII to large oocytes that have not yet obtained the capacity for resuming meiosis. During the maturation stage, the nuclei of the granulosa cells move from the side facing the chorion to the opposite side of the cell. Additionally, cytoplasmic protrusions of both the follicle cells and the oocyte into the chorion have shrunk and withdrawn. The oocytes rapidly enlarge up to about 1200 μm in diameter, primarily due to hydration [5, 34], and ovulate from the vegetal pole region [8].

ACKNOWLEDGMENTS

We are very thankful to Dr. Y. Nagahama, National Institute for Basic Biology, Okazaki, for supplying the antisera against steroids, and to Mr. T. Yokochi for his excellent technical assistance. We also wish to express our cordial thanks to Dr. C. A. Brown, Department of Pathology, School of Medicine, University of New Mexico, for her help in preparing the manuscript.

FIG. 12. Preovulatory follicles (about 900 μm in diameter). A: Special granulosa cells as progesterone-producing cells contain characteristic mitochondria with tubular cristae and dense matrix. L, lysosome-like body. $\times 6,600$. B: A portion of typical granulosa cell exhibits dilated Golgi lamellae (GO), endoplasmic reticulum and round mitochondria with many tubular cristae. Note gap junctions (arrow heads) between oocyte projections and granulosa cell. TV, transport vesicle. $\times 21,000$.

TABLE 2. Characteristics of the

Phase	Stage	Follicle size (μm)	General appearance	Nucleus	
Previtellogenic	Early	I	20 to 60	Centrally located and roughly spherical. Nucleoli and chromatin-threads with network appearance	
		II	61 to 90	Transparent cytoplasm and nucleus with round nucleoli clearly visible	Centrally located with peripheral nucleoli and thin lamp-brush chromosomes
	Late	III	91 to 120		Centrally located. Folded envelope. Voluminous nucleoli irregular in shape. Developed lamp-brush chromosomes
		IV	121 to 150	Transparent cytoplasm and nucleus with irregular shaped nucleoli clearly visible. Rudiments (bright spots) of short villi on chorion	Centrally located. Folded envelope. Voluminous nucleoli ring-shaped. Developed lamp-brush chromosomes
Vitellogenic	Early	V	151 to 250	Transparent cytoplasm and nucleus with ring-shaped nucleoli. Elongated short villi and attaching filaments on chorion	Folded envelope. Nucleoplasm strongly stainable with haematoxylin. Lamp-brush chromosomes thicker and shorter. Ring-shaped nucleoli
		VI	251 to 400	Transparent cytoplasm. Attaching filaments opaque in vegetal hemisphere	
	Late	VII	401 to 500	Attaching filaments opaque in vegetal hemisphere. Dark lipid granules in perinuclear region of cytoplasm filled with vacuoles (yolk vesicles) and oil droplets	Very irregular in shape. Displaced toward animal pole. Shortened chromosomes. Reduced in volume. Nucleoplasm strongly stainable with haematoxylin.
		VIII	501 to 800	Cortical alveoli (yolk vesicles) and oil droplets dimly visible in translucent cytoplasm surrounding yolk sphere	Located at animal pole. Condensed chromosomes massed in center of nucleoplasm
Post-vitellogenic	Maturation	IX	801 to 1200	Cortical alveoli and oil droplets clearly seen in light cortical cytoplasm. A large germinal vesicle visible near micropyle until resumption of meiosis	Apparent large vacuole within outer nuclear envelope at ovarian surface side. Nucleoli and nuclear envelope disappear with resumption of meiosis
	Ovulated	X	1200*	Projecting short villi and attaching filaments on chorion. Transparent and light cytoplasm clearly showing cortical alveoli and oil droplets	Second metaphase figure at animal pole in cortical cytoplasm

*Egg.

various stages of oocyte development

Cytoplasm	Chorion	Follicle cells
A few microvilli and small number of poorly developed ER and mitochondria	Absent	Extremely flat
Clusters of long microvilli (cytoplasmic projections). Yolk nucleus, a small number of mitochondria and ER. Electron-dense cortex	Absent	A single layer each of thecal and granulosa cells. Desmosomes developed between adjacent granulosa cells
Cytoplasmic projections evenly distributed on whole surface. Yolk nucleus, increased mitochondria and ER. Faintly stainable with haematoxylin	Outermost layer rudiments among cytoplasmic projections of oocyte. Short villi bumps appear	
Most developed yolk nucleus. Increased mitochondria in cortex. Faintly stainable with haematoxylin	Outermost layer (0.2–0.3 μm) rudiments among long cytoplasmic projections. Elongated short villi. Differentiation of attaching filaments	Granulosa cells thick at attaching filament side
Elongated cytoplasmic projections. Broken yolk nucleus and a single layer of small yolk vesicles	Outermost layer 0.2–0.6 μm in thickness. Two layers at end of this stage	Micropylar cell detectable
Very elongated cytoplasmic projections. Two to several layers of large yolk vesicles occupy most of cytoplasm. Lipid granules at perinuclear region and dense yolk granules	Outermost layer 0.5–0.6 μm and innermost layer 1.5–3 μm . Micropyle incomplete	Thick granulosa cells in vegetal hemisphere. E_2 production
Cytoplasmic projections irregularly contact with granulosa cells by gap junctions. Yolk vesicles fully occupy cytoplasm. Small yolk masses among yolk vesicles. Increased oil droplets	Thick in animal hemisphere. Outermost layer 0.6 μm and innermost layer about 4 μm	E_2 production responsive to gonadotropic stimulation
Most elongated cytoplasmic projections. Yolk vesicles and oil droplets aligned in a single layer in cortex. Central yolk mass occupies most of cytoplasm.	Very long attaching filaments at vegetal pole region, coiled around vegetal hemisphere. Ten μm in total thickness	$17\alpha, 20\beta\text{-DiOHprog}$ and E_2 production responsive to gonadotropic stimulation
Cortical alveoli (yolk vesicles), oil droplets, mitochondria, vesicular ER, Golgi complexes, annulate lamellae and multivesicular bodies in thin cortex	Cytoplasmic projections withdrawn at end of this stage	Nucleus located at side of basement membrane. Sifted off at end of this stage (micropyle open). E_2 and $17\alpha, 20\beta\text{-diOHprog}$ production
Transparent and light cytoplasm showing clearly cortical alveoli and oil droplets	Projecting short villi and attaching filaments on chorion. Innermost layers showing a stratiform state (12–14 layers)	Absent

TABLE 3. Comparison of the present classification of the stages of oocyte development with those of early investigations of *Oryzias latipes* oogenesis

		Stage										
(A)		I	II	III	IV	V	VI	VII	VIII	IX	X	
		20	60	90	120	150	250	400	500	800	1200	
(B)		A			B	C	D		E		F	
(C)		I			II				III		IV	
(D)		1	2		3		4	5			6	
(E)		Cn	Pn		Yv			Py	Sy	Ty	M	Re
(F)		A		B	C	C'	D					

- (A) The present classification
 (B) Yamamoto, T. S. (1955)
 (C) Yamakawa, Y. (1959)
 (D) Yamamoto, M. (1964)
 (E) Yamamoto, K. and Yoshioka, H. (1964)
 (F) Iwamatsu, T. (1973)

REFERENCES

- Guraya, S. S. (1986) *The Cell and Molecular Biology of Fish Oogenesis*. Karger, Basel & New York.
- Nagahama, Y. (1985) The functional morphology of teleost gonads. In "Fish Physiology, Vol. 9A". Ed. by W. S. Hoar, D. J. Randall and E. M. Donaldson, Academic Press, New York, pp. 223-275.
- Wallace, R. A. (1985) Vitellogenesis and oocyte growth in nonmammalian vertebrates. In "Developmental Biology, Vol. 1". Ed. by L. W. Browder, Plenum Press, New York, pp. 127-177.
- Aketa, K. (1954) The chemical nature and the origin of the cortical alveoli in the egg of the medaka, *Oryzias latipes*. *Embryologia*, **2**: 63-66.
- Hirose, K. (1972) The ultrastructure of the ovarian follicle of medaka, *Oryzias latipes*. *Z. Zellforsch.*, **123**: 316-329.
- Hogan, J. C. (1978) An ultrastructural analysis of "cytoplasmic markers" in germ cells of *Oryzias latipes*. *J. Ultrastruct. Res.*, **62**: 237-250.
- Iwamatsu, T. (1973) On changes of ovary, liver and pituitary gland of the sexually inactive medaka (*Oryzias latipes*) under the reproductive condition. *Bull. Aichi Univ. Educ. (Nat. Sci.)*, **22**: 73-88.
- Iwamatsu, T. (1974) The medaka as a teaching material. II. Oocyte maturation and fertilization. *Bull. Aichi Univ. Educ. (Nat. Sci.)*, **23**: 113-144. (In Japanese)
- Iwamatsu, T., Ohta, T., Nakayama, N. and Shoji, H. (1976) Studies of oocyte maturation of the medaka, *Oryzias latipes*. III. Cytoplasmic and nuclear changes of oocyte during *in vitro* maturation. *Annot. Zool. Japon.*, **49**: 28-37.
- Tesoriero, J. V. (1977) Formation of the chorion (zona pellucida) in the teleost, *Oryzias latipes*. I. Morphology of early oogenesis. *J. Ultrastruct. Res.*, **59**: 282-291.
- Tsukahara, J. (1971) Ultrastructural study on the attaching filaments and villi of the oocyte of *Oryzias latipes* during oogenesis. *Dev. Growth Differ.*, **13**: 173-180.
- Yamakawa, Y. (1959) Cytological studies on the oogenesis of the medaka, *Oryzias latipes*. Report I. Cytological observation of the oogenesis of *Oryzias latipes*. *Bull. Exp. Biol.*, **9**: 46-56. (In Japanese)
- Yamakawa, Y. (1959) Cytological studies on the oogenesis of the medaka, *Oryzias latipes*. Report II. Cytochemical studies on the oogenesis of *Oryzias latipes*. *Bull. Exp. Biol.*, **9**: 57-66. (In Japanese)
- Yamamoto, M. (1963) Electron microscopic studies on the oogenesis and early development of the teleost, *Oryzias latipes*. *Bull. Marine Biol. Station*

- Asamushi, Tohoku Univ., **9**: 211–216.
- 15 Yamamoto, M. (1964) Electron microscopy of fish development. III. Changes in the ultrastructure of the nucleus and cytoplasm of the oocyte during its development in *Oryzias latipes*. J. Fac. Sci. Univ. Tokyo, Sec. IV, **10**: 335–346.
 - 16 Yamamoto, T. S. (1955) Morphological and cytochemical studies on oogenesis of fresh water fish, medaka *Oryzias latipes*. Jpn. J. Ichthyol., **4**: 170–181. (In Japanese)
 - 17 Yamamoto, K. and Yoshioka, H. (1964) Rhythm of development in the oocyte of the medaka, *Oryzias latipes*. Bull. Fac. Fish. Hokkaido Univ., **15**: 5–19.
 - 18 Nakano, E. and Ishida-Yamamoto, M. (1968) Uptake and incorporation of labeled amino acids in fish oocytes. Acta Embryol. Morphol. Exp., **10**: 109–116.
 - 19 Tsusaka, A. and Nakano, E. (1965) The metabolic pattern during oogenesis in the fish, *Oryzias latipes*. Acta Embryol. Morphol. Exp., **8**: 1–11.
 - 20 Iwamatsu, T. (1978) Studies on oocyte maturation of the medaka, *Oryzias latipes*. VI. Relationship between the circadian cycle of oocyte maturation and activity of the pituitary gland. J. Exp. Zool., **206**: 355–364.
 - 21 Kagawa, H., Takano, K. and Nagahama, Y. (1981) Correlation of plasma estradiol-17 β and progesterone levels with ultrastructure and histochemistry of ovarian follicles in the white-spotted char, *Salvelinus leucomaenis*. Cell Tissue Res., **218**: 315–329.
 - 22 Young, G., Crim, L. W., Kagawa, H., Kambegawa, A. and Nagahama, Y. (1983) Plasma 17 α , 20 β -dihydroxy-4-pregnen-3-one level during sexual maturation of amago salmon (*Oncorhynchus rhodurus*): Correlation with plasma gonadotropin and *in vitro* production by ovarian follicles. Gen. Comp. Endocrinol., **51**: 96–105.
 - 23 Satoh, N. (1974) An ultrastructural study of sex differentiation in the teleost *Oryzias latipes*. J. Embryol. Exp. Morphol., **32**: 195–215.
 - 24 Takamoto, K. (1979) Electron-microscopic studies on the origin of the germinal cytoplasm. Stud. Hum. Nat., **13**: 29–59.
 - 25 Riehl, R. (1977) Konzentrische “Lamellen” in jungen Oocyten von *Noemacheilus barbatulus* (L.) (Teleostei, Cobitidae). Biol. Zbl., **86**: 523–528.
 - 26 Tesoriero, J. V. (1977) Formation of the chorion (zona pellucida) in the teleost, *Oryzias latipes*. II. Polysaccharide cytochemistry of early oogenesis. J. Histochem. Cytochem., **25**: 1376–1380.
 - 27 Iwamatsu, T. and Ohta, T. (1977) Fine structure of loach oocytes during maturation *in vitro*. Dev. Growth Differ., **19**: 213–226.
 - 28 Tokarz, R. E. (1978) Oogenical proliferation, oogenesis, and folliculogenesis in nonmammalian vertebrates. In “The Vertebrate Ovary”. Ed. by R. E. Johnes, Plenum Press, New York, pp. 145–179.
 - 29 Tesoriero, J. V. (1978) Formation of the chorion (zona pellucida) in the teleost, *Oryzias latipes*. III. Autoradiography of (³H) proline incorporation. J. Ultrastruct. Res., **64**: 315–326.
 - 30 Konopacka, B. (1935) Recherches histochimiques sur le développement des poissons. I. La vitellogenese chez le goujon (*Gobio fluviatillis*) et la carpe (*Cyprinus carpio*). Bull. int. Acad. pol. Sci. Lett. Ser. B. **1935**: 163–182.
 - 31 Masuda, K., Iuchi, I., Iwamori, M., Nagai, Y. and Yamagami, K. (1986) Presence of a substance cross-reacting with cortical alveolar material in “yolk vesicles” of growing oocytes of *Oryzias latipes*. J. Exp. Zool., **238**: 261–265.
 - 32 Iwamatsu, T. and Akazawa, Y. (1987) Effects of hypophysectomy and sex steroid administration on development of the ovary in *Oryzias latipes*. Bull. Aichi Univ. Educ. (Nat. Sci.), **25**: 63–71. (In Japanese)
 - 33 Wallace, R. A. and Selman, K. (1985) Major protein changes during vitellogenesis and maturation of *Fundulus* oocytes. Dev. Biol., **110**: 492–498.
 - 34 Wallace, R. A. and Selman, K. (1978) Oogenesis in *Fundulus heteroclitus*. I. Preliminary observations on oocyte maturation *in vivo* and *in vitro*. Dev. Biol., **62**: 354–369.

Morphological Features of Embryogenesis in *Drosophila melanogaster* Infected with a Male-killing Spiroplasma

SUMI TSUCHIYAMA-OMURA, BUNGO SAKAGUCHI¹, KATSUMI KOGA
and DONALD F. POULSON²

*Laboratory of Sericultural Science, Kyushu University,
Fukuoka 812, Japan, and ²Department of Biology, Yale
University, New Haven, Connecticut 06520, U.S.A.*

ABSTRACT—Morphological studies were conducted with *Drosophila melanogaster* embryos maternally infected with the 'sex-ratio' organism, a species of Spiroplasmas which specifically kill male zygotes. Abnormalities occurred at the stages from as early as cleavage or blastoderm to morphogenetic movements. The most remarkable feature was defective organization of the ventral nervous tissues, a result which fits well with that of previous mosaic analysis showing that the focal region of infection localizes at the ventral midline of the blastoderm.

INTRODUCTION

It has been rather long since the finding of an abnormal 'sex-ratio' (SR) condition in *Drosophila*, where females exceed males in number disturbing normal sex ratio of 1:1 (see ref. [1] for review). This trait is cytoplasmically inherited from generation to generation through ovaries and eggs [1-3]. Some of SR conditions have been proposed to be brought about by infectious, parasitic microorganisms [1] and finally it was demonstrated that the causal agent is a species of mycoplasma having a spiral form with a dimension of 4 to 8 μm in length and 0.1 to 0.2 μm in diameter [2]. This type of organism, although belongs to Spiroplasmas (cf. [3]), has often been called the sex-ratio organism and will be abbreviated as SRO. The SROs are found in the hemolymph of females of infected *Drosophila* strains and can be transferred to females of the same or other species by intra-abdominal injection, making non-SR strains into SR-ones [4]. Males are absent in the transferred as well as in the original SR strains, and this characteristic is accountable almost wholly through

mortality during embryogenesis [1].

We previously analyzed gynandromorph survivals in *D. melanogaster* having a maternally infected SRO line and suggested that the focus of action of the SRO locates in the close vicinity to the ventral midline [5]. In the present study, we observe by light and electron microscopes the SRO-infected zygotes of *D. melanogaster* at their embryonic stages and describe that the most markedly affected organ is in fact the ventral nervous system.

MATERIALS AND METHODS

Collection of eggs

The Oregon-R strain of *D. melanogaster* infected with the SRO of the *D. nebulosa* origin was used, since this heterologous combination has offered a stable and convenient investigation system [5]. Female adults of the infected Oregon-R strain aged 7 to 10 days after emergence were crossed to young males of Oregon-R strain and fed on yeast-enriched food for 3 days at 25°C. Eggs were deposited at 25°C onto filter paper, which had been dipped in a suspension of yeast and placed on an agar plate. The eggs were collected at intervals and washed with distilled water for

Accepted September 7, 1987

Received July 23, 1987

¹ To whom reprints should be requested.

several times to remove the debris of yeast and then treated outright or incubated until desired age. As a control, normal Oregon-R eggs were processed equally as described above.

Light microscopic observation of intact embryos

Eggs collected were allowed to develop for 24 hr at 25°C. Then they were counted for hatchability and, after deprived of the chorions by brief treatment with 3% sodium hypochlorite, were observed for the terminal abnormality under a phase-contrast microscope.

Another series of eggs were observed for the embryogenesis continuously. The chorions were removed as above. Then, young embryos undergoing cleavage mitosis were selected by the method according to Bownes [6], submerged in the *Drosophila* Ringer solution on a glass depression slide to allow development and subjected to inspection individually under a phase-contrast microscope.

Light microscopic observation of sectioned embryos

Dechorionated embryos at desired age were fixed in a mixture of 4 parts 95% ethanol, 1 part 50% acetic acid and 1 part formalin or 25% glutaraldehyde in 0.1 M phosphate buffer at pH 6.8 shaken with octane for 2–5 min. Vitelline membranes were removed with fine tungsten needles in the aqueous phase of the fixing mixture [7]. The fixed embryos were washed with 70% alcohol, dehydrated with a series of ethanol and finally with n-butyl alcohol. To facilitate observation, the eggs were stained *in toto* with 1% Eosine dissolved in 95% ethanol in the course of dehydration. The stained and dehydrated embryos were embedded in a solution of butoxyethanol and glycol methacrylate (Polysciences Inc., a JB-4 embedding kit) [8], sectioned with a Porter-Blum Sorvall MT-1 ultramicrotome at 2 μ m thickness, and stained with Giemsa solution (diluted with 0.12 M phosphate buffer, pH 7.4) for 20 min. The stained materials were mounted in Permunt and observed under a compound microscope.

Electron microscopic observation

Eggs were dechorionated, fixed and removed

from vitelline membranes as described above. The fixation was continued after removing vitelline membranes to make the total time of fixation 4 hr. The specimens were washed with sucrose-phosphate buffer of the same osmolarity as that of the fixative and allowed to stand overnight at 0°C, rapidly dehydrated in ethanol series and embedded in Epon 812. Embryos were sectioned at 60–150 nm thickness with a Porter-Blum Sorvall MT-1 ultramicrotome and stained with uranyl acetate and lead mixture. A JEM 7A type electron microscope was used for observation. Ovaries taken from female adults of the infected Oregon-R strain were fixed, embedded and sectioned followed by the observation for ultrastructure as above.

RESULTS

Hatchability and terminal abnormalities

The eggs of *D. melanogaster* maternally infected with the SROs from *D. nebulosa* had the hatchability of about 50% (Table 1). The resulting adults were found to be all females, and thus the unhatched embryos should mainly be males which were killed during embryogenesis. About one fifth of the unhatched eggs showed no sign of development as seen in Figure 1 a and were white in color, indicating early lethality or block of fertilization (Table 1). The majority of the unhatched eggs exhibited somewhat developed features (Fig. 1 b and c) and were brown in color, indicating late lethality (Table 1). Almost all the embryos of the late lethal group showed a common characteristic feature of morphology, with about one third of yolk mass at the posterior part and two thirds of cellular mass at the anterior part (see Fig. 1 b and c). The late lethal embryos had larval tissues in disordered arrangements at the cellular region (see below). Arrows show the yolk mass.

The results from continuous observation of embryos indicated that cessation of development occurred at the stages from cleavage mitosis to the early morphogenetic movements. The embryos which were abnormal at the cleavage stage never developed beyond the blastokinesis stage and later broke down as non-brown lethal embryos. These

TABLE 1. Hatchability and terminal phase of eggs of *D. melanogaster* infected with sex-ratio organisms^a

Strain	The number and percentage of eggs			Total
	hatched	unhatched		
		Early lethals or unfertilized ^b	Late lethals ^b	
SRO-infected	431 ^c (48%)	80 ^d (9%)	383 ^d (43%)	894
Control	581 ^c (93%)	26 ^d (4%)	18 ^d (3%)	625

a: Females of Oregon-R strain of *D. melanogaster* infected with the *D. nebulosa* SRO (or of the uninfected control) were aged 7 to 10 days after eclosion and crossed to males from Oregon-R. Eggs were collected at 1 or 2 hr intervals, incubated for 24 hr at 25°C, then the hatched individuals were counted and types of terminal abnormal embryos were estimated.

b: See text and Fig. 1.

c: The ratios of individuals developed into adults were about 94% (all females) for the SR-strain and about 45% females and 45% males for the control.

d: One might argue that the embryos of the SR-strain contain spontaneously occurring lethals as deduced from these data. Although this possibility could not be ruled out, the overall observation presented in this study may be reasonable because the SR-condition is clear-cut as shown in c and because we found the most common features out of several hundreds of specimens.



FIG. 1. Typical abnormal embryos infected with sex-ratio organisms. Dechorionated eggs were observed under a phase-contrast microscope as described in Materials and Methods. a) An early lethal embryo which stopped development at cleavage mitosis (aged 5 to 6 hr after oviposition). b) A late lethal embryo showing cellular mass at the anterior part and unused yolk mass at the posterior end (aged 20 to 22 hr after oviposition). c) A late lethal embryo with distinct larval tissues (aged 24 hr after oviposition). Scale, 100 μ m.

were typical early lethal embryos like that shown in Figure 1 a. Some embryos indicated their abnormality as the retardation of blastoderm formation. These embryos in time become anomalous in appearance and finally indistinguishable from those which showed their first abnormality during early morphogenesis. These were typical late lethal embryos like those shown in Figure 1 b and c.

Features of dying embryos

Samples taken at various times of embryogenesis were sectioned and inspected after staining for histology in relation to the stage or state the respective embryos were in (Table 2). During the first 2 hr of development after oviposition, difference between the SRO-infected embryos and the normal ones was seldom detected, and at 2 hr about 70% of the individuals were at the syncytial blastoderm stage. At the 3rd hr, infected samples showed significant delay of development, about 50% of which were still at the syncytial blastoderm stage and about 10% at cleavage mitosis (most of the normal embryos were already at or beyond the cellular blastoderm stage).

At 3 to 5 hr after oviposition, the delay became greater (data not shown), and some of abnormal embryos began to break down exhibiting energid-like cytoplasmic islands which seemed to begin to fall apart. These energid-like structures consisted of disturbed fibers (remnants of spindle fibers

and/or chromosomes?) as also seen in the SRO-infected *D. willistoni* embryos [9]. Some of other infected embryos were again at the cleavage stage or at the syncytial to cellular blastoderm stages.

As to the embryos which showed the first sign of abnormality at later stages beyond gastrulation, the deviation from the normal course of development was expressed as the appearance of unusual, necrotic type of cells. These cells were characterized by their strong stainability of the cytoplasm (dark blue with Giemsa), clear and large nucleus with a ring-shaped nucleolus-like structure and roundness of the cell surface under a light microscope. An electron microscopical appearance of this type of cells is seen in Figure 2. Autoradiographical study has suggested that these cells are inactive in RNA synthesis and protein synthesis (Tsuchiyama-Omura, unpublished data). They may therefore be a sort of retrograding cells. These occurred mainly in the neuroblast region 5–6 hr of the development (Fig. 3). As the SRO-infected embryos develop, such cells gradually increase in number also in the hypodermis, midgut or other tissues as well and coming to make a cluster.

More and more infected embryos were categorized as abnormal, even when they still did not reach the terminal features. At 9 hr after oviposition the cells constructing the hypodermis, neuroblast, ventral nervous system and mesodermal structures seemed to be somewhat disorderly intermingled with each other. During the succeed-

TABLE 2. Comparison of development between infected and control embryos^a

Time of observation	Strain	The number and percentage of eggs at the stage or state of					Total
		unfertilized	cleavage mitosis	syncytial blastoderm	cellular blastoderm	early gastrulation	
1±0.5 hr	SR	1 (1%)	68 (94%)	3 (4%)	0	0	72
	Control	1 (3%)	26 (72%)	3 (8%)	4 (11%)	2 (6%)	36
2±0.5 hr	SR	5 (10%)	7 (14%)	33 (66%)	5 (10%)	0	50
	Control	1 (4%)	5 (18%)	19 (68%)	3 (11%)	0	28
3±0.5 hr	SR	4 (4%)	7 (8%)	46 (52%)	23 (26%)	9 (10%)	89
	Control	4 (7%)	0	8 (13%)	31 (51%)	18 (30%)	61

a: Females of SRO-infected or control Oregon-R strains were crossed as described in Table 1 and eggs were collected at indicated times, sectioned and inspected light microscopically. There were significant differences between SRO-infected and control embryos by means of χ^2 -test in the 3rd-hr samples.



FIG. 2. Electron micrograph of a part of an embryo infected with sex-ratio organisms. An late lethal embryo at 10 hr old was taken to show a necrotic, retrograding cell (a dense and round cell in the center). Arrows point the SRO-like structures seen in the intercellular areas with low electron density. Scale, 1 μ m.

ing periods the hypodermic and mesodermal tissues followed the normal course of development, that is, the hypodermis thinned out dorsally at about 10 hr (Fig. 4), and the somatic visceral and pharyngeal muscles appeared from this time on. The salivary gland with or without contents (mucoprotein?) could also be found in most of the abnormal embryos. On the other hand, the region of ventral nervous system in SRO-infected embryos was shorter than normal even before the onset of shortening and little nerve fibers were found. Nevertheless, the brain was clearly identified at the ordinary place with normal configuration in most individuals. The fore- and hindgut looked quite normal, but the mid-ventral part of the midgut was disorganized having retrograding cells. Some of the latter tend to fall into the yolk mass which was abnormally concentrated in the center of an embryo (Fig. 4). The hypodermis

began to show the sign of cuticle secretion after the 12th hour which is the normal time course of uninfected embryos. The gonad-like structures were occasionally observed.

During the 11–14th hr after oviposition, the yolk mass began to extrude through the feeble and disorganized ventral nervous system leaving other tissues behind. After this incident, abnormal embryos could be easily recognized by the typical terminal phenotype of SRO-infected embryos. Following the extrusion of yolk, tissues seemed to develop autonomously; i.e. embryos from later samples showed more developed structures of tissues, although their interorganic arrangement was completely disturbed. This disturbance occurred increasingly as the time went, changing most of the abnormal embryos into the typical late lethal ones by the 20–22nd hr after oviposition. Figure 5 illustrates such features. The unabsorbed yolk

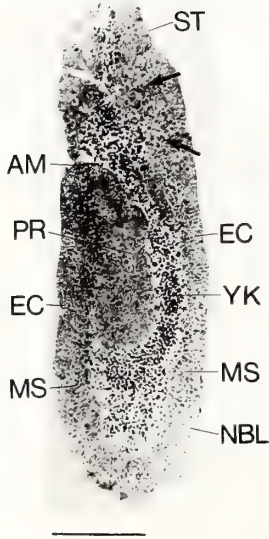


FIG. 3. Features of a 5 to 6 hr old embryo infected with sex-ratio organisms. A specimen was cut, stained and observed under a compound microscope as described in Materials and Methods. Arrows show necrotic cells. AM, amnion; EC, ectoderm; MS, mesoderm; NBL, neuroblast; PR, proctodaeum; ST, stomodaeum; YK, yolk mass. Scale, 100 μ m.

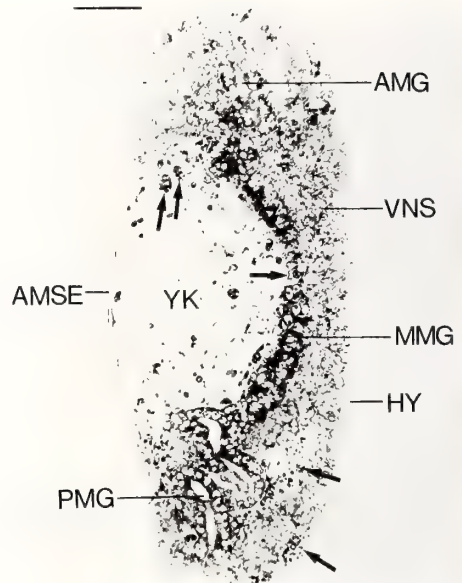


FIG. 4. Features of a 10 hr old embryo infected with sex-ratio organisms. A specimen was cut, stained and observed as described in Fig. 3. Arrows indicate retrograding cells in the midgut, hypodermis etc. AMG, anterior midgut; AMSE, amnioserosa; HY, hypodermis; MMG, middle midgut; PMG, posterior midgut; VNS, ventral nervous system; YK, yolk mass. Scale, 50 μ m.

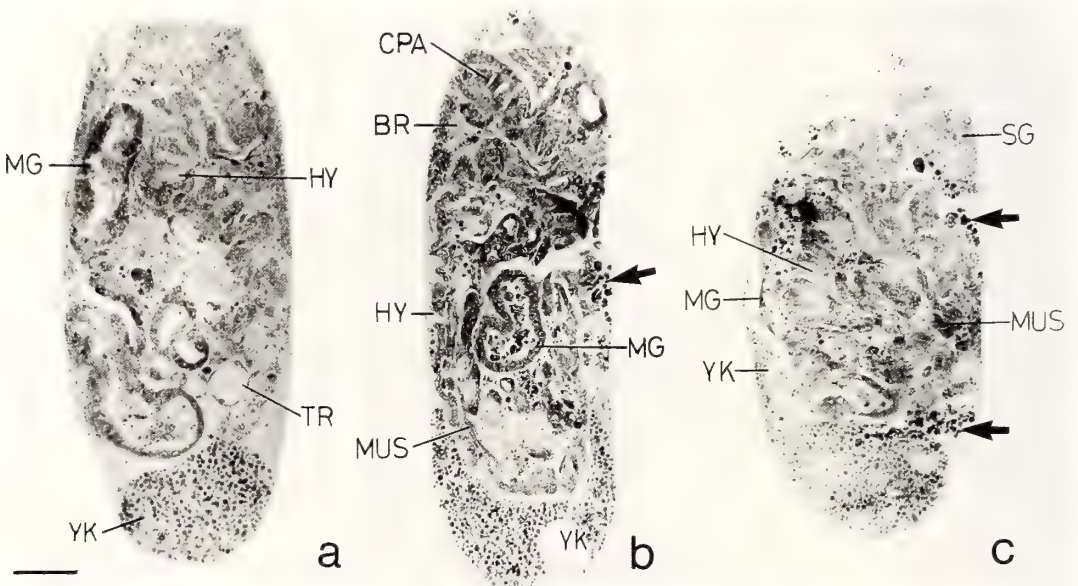


FIG. 5. Features of 22 to 25 hr old embryos infected with sex-ratio organisms. Specimens were cut, stained and observed as described in Fig. 3. a, b and c are from different individuals to show variety in arrangement of larval tissues from embryo to embryo. Arrows indicate necrotic cells. BR, brain; CPA, cephalopharyngeal apparatus; HY, hypodermis; MG, midgut; MUS, muscles; SG, salivary gland; TR, trachea; YK, yolk mass. Scale, 50 μ m.

resided at a posterior part (a, b and c) and sometimes at a lateral part (c) of the embryo. The tissue region gave an inside-out impression, with the hypodermis accompanying muscles almost at the central part. The midgut, trachea, cephalopharyngeal apparatus, brain, salivary gland, hypodermis and muscles were recognized, but most of them were located at unordered places (the number of cells which consist of each tissue seemed to be smaller than normal). The ventral nervous system was never found in a complete form; instead, the necrotic cells (arrows) were dispersed at the surface of the embryos.

Another remarkable status found in the present

study is the intercellular areas with low electron density as seen in Figure 2; these areas contained a number of peculiar structures pointed by arrows. We concluded the latter to be SROs from their form and their mode of existence. The intercellular spacing and the SRO-like structures were not detected in the specimens from normal embryos. Moreover, these curious features were very similar to those observable in the ovaries of SRO-infected *D. melanogaster* (Fig. 6 and Niki, personal communication). These may be the first electron microscopic observation of the SRO-like structures in the eggs and ovaries.

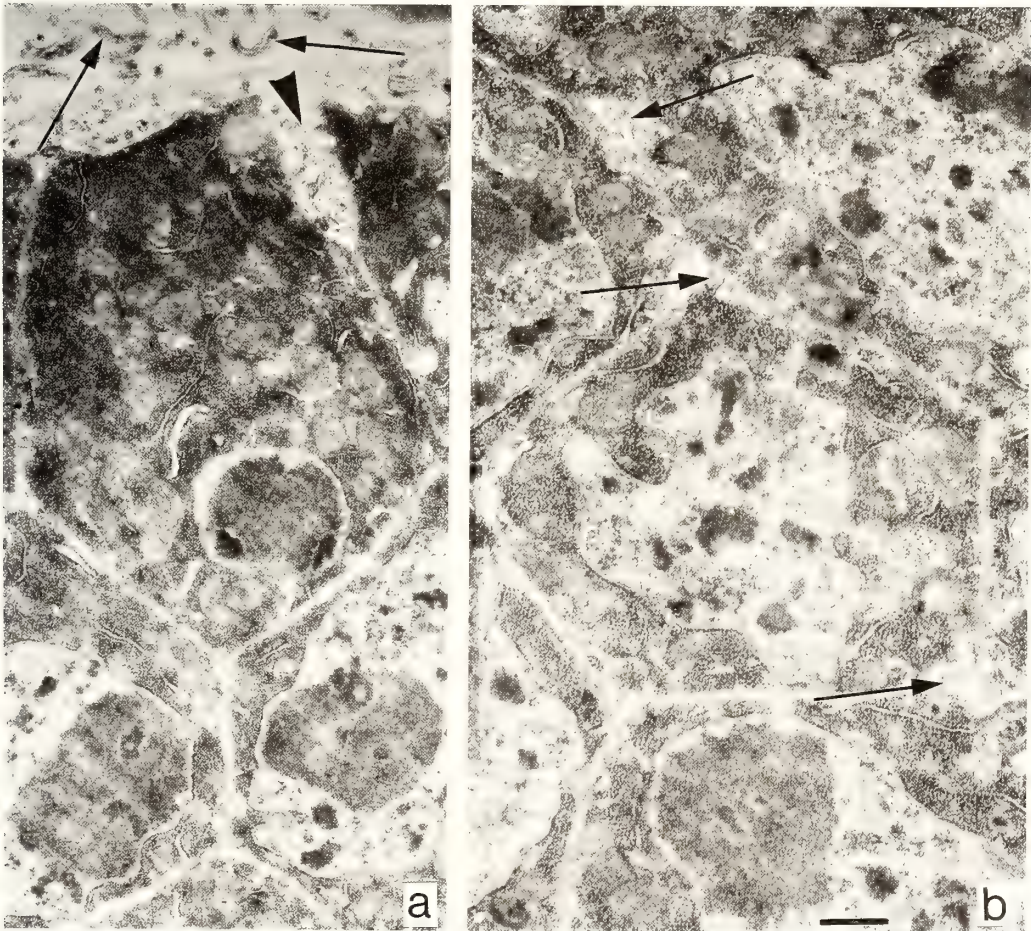


FIG. 6. Electron micrograph of parts of ovary infected with sex-ratio organisms. A female adult (Oregon-R) was dissected and the ovaries were taken. a) In upper side of the follicle cells a large number of SRO-like structures were observed (arrows) and some of them seem to invade between the follicle cells (arrowhead). b) SRO-like structures are seen in the area with low electron density between the follicle cells (arrows). Scale, 1 μ m.

DISCUSSION

In the SRO-infected strain, abnormalities may occur at different stages of embryogenesis. Nevertheless, in the large majority of the lethal embryos, the ventral nervous system was found to be the most severely affected organ. The occurrence of necrotic, seemingly degenerating cells in cluster must be in close association with the SRO infection, since in normally developing embryos of the control this type of cells were only occasionally found and never in cluster. These results in *D. melanogaster* were in agreement with those of the SRO-infected *D. willistoni* embryos [9].

Most tissues other than the ventral nervous system rather seemed to follow normal course of development in the SRO-infected strain although their arrangement in an embryo was highly abnormal. The ventral nervous system was never seen in a normal assembly by itself and the constituent cells became necrotic earlier than other cells. This apparent preference of the ventral nervous tissue in sensitivity to the SRO is compatible with the results of mosaic analysis of SRO-infected *D. melanogaster* [5] which indicated that the focus of SRO-lethal action included the ventral nervous system. Not only the SRO-lethal action but also many other embryonic lethalitys in *Drosophila* were shown to have their focal region at the ventral side of an embryo [10]. It should be mentioned here that our previous gynandromorph analysis has suggested the mesoderm also to be included in the target of SRO action [5] but in the present study this seemed not the case. The discrepancy may be owing to the difference in developmental stage of observation: The present study was done with embryos whereas the mosaic analysis with adults.

In addition to the major late lethal embryos, there also exist a minor group of SRO-lethal embryos, i.e. several percent of the total abnormal embryos stopped their development at the stages as early as cleavage or blastoderm, thus before the establishment of the ventral nervous system. We interpret the early mechanism of androcidal SRO action in terms of some perturbation due to the presence of the SRO. Such effects should be incurable by gene activation of the part of the

hosts, since female embryos with double dosage of X-chromosome-linked genes can escape from this lethal action [4]. The plausibility of the inference may be resolved by microinjection of the SRO into normal embryos.

The late effects of SRO-embryos might be explained by assuming that the ventral nervous system of the *Drosophila* embryo requires the expression of a large number of genes for its development and organization so that it is highly sensitive to disturbance owing to the hypothetical early SRO action. In support of this assumption is a preliminary observation by Nickla *et al.* [11], who indicated that a lethal mutation brings about the abnormalities at the ventral nervous system as well as the brain, although the genes concerned are known to be active in non-nervous tissues.

ACKNOWLEDGMENTS

This study was supported in part by a Grant-in-Aid for Scientific Research (No. 61480053) from the Ministry of Education, Science and Culture of Japan.

REFERENCES

- 1 Poulson, D. F. (1963) Cytoplasmic inheritance and hereditary infections in *Drosophila*. In "Methodology in Basic Genetics". Ed. by W. J. Burdette, Holden-Day, San Francisco, pp. 404-424.
- 2 Poulson, D. F. and Sakaguchi, B. (1961) Nature of "sex-ratio" agent in *Drosophila*. *Science*, **133**: 1489-1490.
- 3 Williamson, D. L. and Poulson, D. F. (1979) Sex ratio organisms (spiroplasmas) of *Drosophila*. In "The Mycoplasmas III". Ed. by R. F. Whitcomb and J. G. Tully, Academic Press, New York, pp. 175-208.
- 4 Sakaguchi, B. and Poulson, D. F. (1963) Interspecific transfer of the "sex-ratio" condition from *Drosophila willistoni* to *D. melanogaster*. *Genetics*, **48**: 841-861.
- 5 Tsuchiyama, S., Sakaguchi, B. and Oishi, K. (1978) Analysis of gynandromorph survivals in *Drosophila melanogaster* infected with the male-killing SR organisms. *Genetics*, **89**: 711-721.
- 6 Bownes, M. (1975) A photographic study of development in the living embryos of *Drosophila melanogaster*. *J. Embryol. Exp. Morphol.*, **33**: 789-801.
- 7 Zalokar, M. (1971) Fixation of *Drosophila* eggs without pricking. *Dros. Inf. Serv.*, **47**: 128-129.

- 8 Rice, T. B. and Garen, A. (1975) Localized defects of blastoderm formation in maternal effect mutants of *Drosophila*. *Dev. Biol.*, **43**: 277–286.
- 9 Counce, S. J. and Poulson, D. F. (1962) Developmental effects of the sex-ratio agent in embryos of *Drosophila willistoni*. *J. Exp. Zool.*, **151**: 17–31.
- 10 Hotta, Y. and Ishikawa, E. (1975) Mosaic analysis of lethal genes of *Drosophila*. *Protein, Nucleic Acid and Enzyme* (Kyoritsu Shuppan, Tokyo), **20**: 1234–1256. (In Japanese).
- 11 Nickla, H., Lilly, T. and McCarthy, A. (1980) Gene activity in the carnation-light synthetic lethal in *Drosophila melanogaster*. *Experientia*, **36**: 402–403.

Glandular Epithelium Induced from Urinary Bladder Epithelium of the Adult Rat Does Not Show Full Prostatic Cytodifferentiation

NAOYA SUEMATSU, HIROYUKI TAKEDA and TAKEO MIZUNO

*Zoological Institute, Faculty of Science, University of Tokyo,
Hongo, Tokyo 113, Japan*

ABSTRACT—Urinary bladder epithelium of the adult rat formed prostate-like glands, when combined with fetal urogenital sinus mesenchyme in culture and grafted beneath the renal capsule of male rat hosts. With the progression of the gland formation, the bladder epithelium lost its alkaline phosphatase activity and antigenicity against anti-functional bladder epithelium-antiserum. Like the normal prostate, the induced epithelium expressed acid phosphatase, nonspecific esterase and antigenicity against anti-human prostatic acid phosphatase-antiserum, but hardly expressed androgen receptors nor an antigen against anti-4-week prostate epithelium-antiserum. The SDS-PAGE patterns of total proteins in the induced glandular epithelium and in the normal epithelia of the urinary bladder and prostate revealed that the induced glandular epithelium loses some bands identified in the bladder epithelium and comes to express other bands similar to but not identical with those of the normal prostatic epithelium, suggesting that the induced gland does not differentiate as completely as the normal prostate, and this result is linked with extremely reduced androgen receptors in the induced epithelium.

INTRODUCTION

The prostate glands are one of the mammalian male accessory sex organs and develop from their rudiments in the urogenital sinus, which are recognized as epithelial buds projecting into the surrounding mesenchyme. Lasnitzki and Mizuno [1] have shown that the sinus epithelium requires both androgens and the sinus mesenchyme to form prostatic buds *in vitro*. The androgen receptors observed by steroid autoradiography [2] concentrate mainly in the sinus mesenchyme but are absent in the sinus epithelium until the lumen starts to be formed. It is likely, therefore, that the androgens stimulate first the sinus mesenchyme, and that the activated mesenchyme produces substances, which stimulate the epithelium to form buds, though their nature is yet unknown.

The urinary bladder epithelium could form prostatic glands when combined with the sinus mesenchyme [3]. Furthermore, the bladder epi-

thelium not only formed morphologically recognizable prostatic glands but also differentiated biochemically into prostatic glandular epithelium as assessed by protein profiles in two-dimensional gel electrophoresis [4].

In this paper we examined the nature of the prostate-like glands induced in the adult bladder epithelium and whether the induced glands accomplish full prostatic differentiation. The degree of cytodifferentiation was judged by the types and amount of proteins counted in slab gel electrophoresis and by immunochemistry of the tissue. Further an attempt was made to relate the type of cytodifferentiation to the presence or absence of androgen receptors.

MATERIALS AND METHODS

Animals and tissues

Inbred rats (Fischer 344, Charles River Japan Inc., Kanagawa) were mated during the night and copulation was confirmed by the presence of

spermatozoa in the vaginal smears on the following morning. Noon of the day was recorded as 0.5 days of pregnancy.

Urinary bladder and uterus were obtained from adult pregnant rats. Urogenital sinuses, rectums and stomachs were excised from 16.5-day male and female fetuses. Rudiments of the seminal vesicle were dissected out from 19.5-day male fetuses. The excised urogenital sinus was then separated into ventral and dorsal halves that develop ventral and dorsal lobes of the prostate respectively.

Collection of epithelium and mesenchyme

The adult bladder and uterus were treated with collagenase (Worthington Biochemical Corp., Code CLS) 0.03% in Tyrode's solution for 2 hr at 37°C and the fetal urogenital sinus, rectum, stomach and rudiments of seminal vesicle were treated with 0.06% collagenase for 30 min at 37°C. The collagenase-treated tissues were washed in 50% fetal bovine serum (FBS) in Tyrode's solution for 2 hr with three changes, and the epithelium was separated from the mesenchyme with two watchmaker's forceps under a stereomicroscope ($\times 20$).

Culture method

A small fragment of the epithelium was placed upon a piece of the mesenchyme put on a membrane filter (Millipore Corp., pore size 0.8 μm), which was put on a stainless grid placed in a glass dish filled with medium 199 with Earle's salts (GIBCO) containing 20% FBS to the level of the membrane filter, cultured in a CO₂ incubator (5% CO₂, 95% air, at 37°C) overnight and then the recombinant was grafted beneath the kidney capsule of syngeneic adult male hosts (8–20 weeks old) (designated as "in vivo cultivation"). After 3–5 weeks, the grafts were harvested for examination.

Enzyme histochemistry

Alkaline phosphatase The grafts were fixed in ice-cold 80% ethanol for 2 hr and embedded in paraffin (m.p. 46–48°C). The alkaline phosphatase was detected by the tetrazolium reaction [5] at pH 9.2–9.4.

Acid phosphatase and nonspecific esterase The grafts were fixed in ice-cold 4% paraformaldehyde

in 0.1 M phosphate buffer (pH 7.2–7.4) for 2 hr, washed overnight in several changes of 5% sucrose at 4°C and frozen in isopentane (–190°C) chilled with liquid nitrogen. The acid phosphatase was assessed by azo-coupling method [6] at pH 5, and the nonspecific esterase, by the azo-coupling method [7] at pH 5.

Immunohistochemistry

As the first ligands for the indirect immunofluorescence methods, the following antibodies were used: a rabbit polyclonal anti-human prostatic acid phosphatase-antibody (Miles-Yeda Ltd.), which stained patches of epithelial cells more intensely in the ventral prostate than in the dorsal one; mouse polyclonal anti-rat ventral or dorsal prostatic epithelium-antibodies of which antigen was homogenate of glandular cells of 4-week rat ventral or dorsal prostate respectively and the antibody was prepared in our laboratory according to the method of McKeehan *et al.* [8]; and a mouse polyclonal anti-rat urinary bladder epithelium-antibody prepared in our laboratory. Each antibody was applied to the sections of various tissues including urinary bladder, ventral and dorsal prostate, seminal vesicle, liver and kidney and thus confirmed to be specific to the tissues concerned.

Tissues were fixed in methanol (–20°C) for 30 min, replaced in ethanol (–20°C) for 30 min, embedded in Polyester wax (melting point 37°C, BDH Chemicals Ltd.), and sectioned at 6 μm . They were treated with the primary antibody for 1 hr at room temperature and exposed to second antibodies: Goat anti-rabbit IgG antibody (Miles) or goat anti-mouse IgG antibody (Cappel), both conjugated with fluorescein isothiocyanate. The sections were examined with an Olympus epifluorescence microscope (BH2–RFK). After observation, the sections were washed in phosphate-buffered saline and stained with haematoxylin-eosin (HX–E).

Steroid autoradiography

Tissues and grafts were labelled with [1, 2, 4, 5, 6, 7-³H] dihydrotestosterone and then subjected to the thaw-mount autoradiographic technique. The details of steroid autoradiographic techniques

have been described previously [2].

Polyacrylamide gel electrophoresis (PAGE) and immunoblotting

Tissues were treated with collagenase in Ca^{2+} , Mg^{2+} -free Tyrode's solution for 1.5 hr at 37°C , washed with gentle stirring in Ca^{2+} , Mg^{2+} -free Tyrode's solution for 30 min at room temperature. Then isolated glandular epithelial cells were pulverized in a stainless steel mill chilled with liquid nitrogen, dissolved in a SDS sample buffer including 5% (v/v) 2-mercaptoethanol and 2.3% (w/v) sodium dodecyl sulphate (SDS), and subjected to electrophoresis on a polyacrylamide 4/20 gradient gel with SDS (Daiichi Pure Chemicals Co.) according to Laemmli [9]. As molecular-weight markers, LMW calibration kit (Pharmacia) was used. After electrophoresis, proteins on the gels were either stained with silver or transferred electrophoretically to Durapore filters (Millipore) according to Towbin *et al.* [10]. The filters were then treated first with the antibody to be examined, and next with goat anti-mouse IgG antibody conjugated with horseradish peroxidase (Miles), washed, and treated with 4-chloro-1-naphthol in the presence of hydrogen peroxide.

RESULTS

Morphological differentiation There was no contamination with epithelial cells in the isolated urogenital sinus mesenchyme throughout the experiments examined in serial sections of the separated components (14 cases in total). All of the 17 homotypic recombinates composed of fetal ventral sinus epithelium and its mesenchyme developed fully differentiated ventral prostate glands with high secretory activity, when grown for 3.5 weeks beneath the kidney capsule of normal male hosts (Fig. 1), but all 5 recombinates failed to develop prostatic glands when grown in castrated male rats. Adult bladder epithelium recombined with fetal ventral sinus mesenchyme underwent morphological changes after *in vivo* cultivation in normal male hosts: after 1 week of cultivation, epithelial buds projected into the surrounding mesenchyme in 5 recombinates out of 5 (Figs. 2a and 2a'); after 2 weeks, lumina were formed in the



FIG. 1. A homotypic recombinant of fetal ventral sinus epithelium and its mesenchyme grown for 3.5 weeks in an adult male host. $\times 280$.

extended buds (Fig. 2b); after 3 weeks, prostate-like glands were formed, but they were lined with epithelium generally shorter than that found in the homotypic recombinates and were rich in stroma and poor in secretion (Fig. 2c) in all 37 recombinates. After 8 weeks, there was no further differentiation in all 8 recombinates (Fig. 2d). In the castrated male hosts, the bladder epithelium was maintained in the same state as at the onset of culture and no glands were formed in all 12 recombinates even in the presence of the sinus mesenchyme.

Mesenchymes of 16.5-day ventral and dorsal sinuses and of 19.5-day seminal vesicle induced prostate-like glands from the adult bladder epithelium, though the glands were morphologically different to some extent according to the kind of the recombined mesenchymes (Fig. 3a, b, and c), but fetal rectal mesenchyme did not. The other examined epithelia combined with fetal ventral sinus mesenchyme did not form any glandular structure even after 4 weeks' *in vivo* cultivation: In all 3 recombinates, adult uterine epithelium made only a tube; Fetal rectal epithelium formed a vesicle, with epithelium that developed many goblet cells in all 4 recombinates; Fetal stomach epithelium formed a vesicle, lined with mucous epithelium characteristic of the adult stomach epithelium in all 3 recombinates.

Functional differentiation The enzyme activities were seen to change during the prostate-like gland formation. The epithelium of the adult

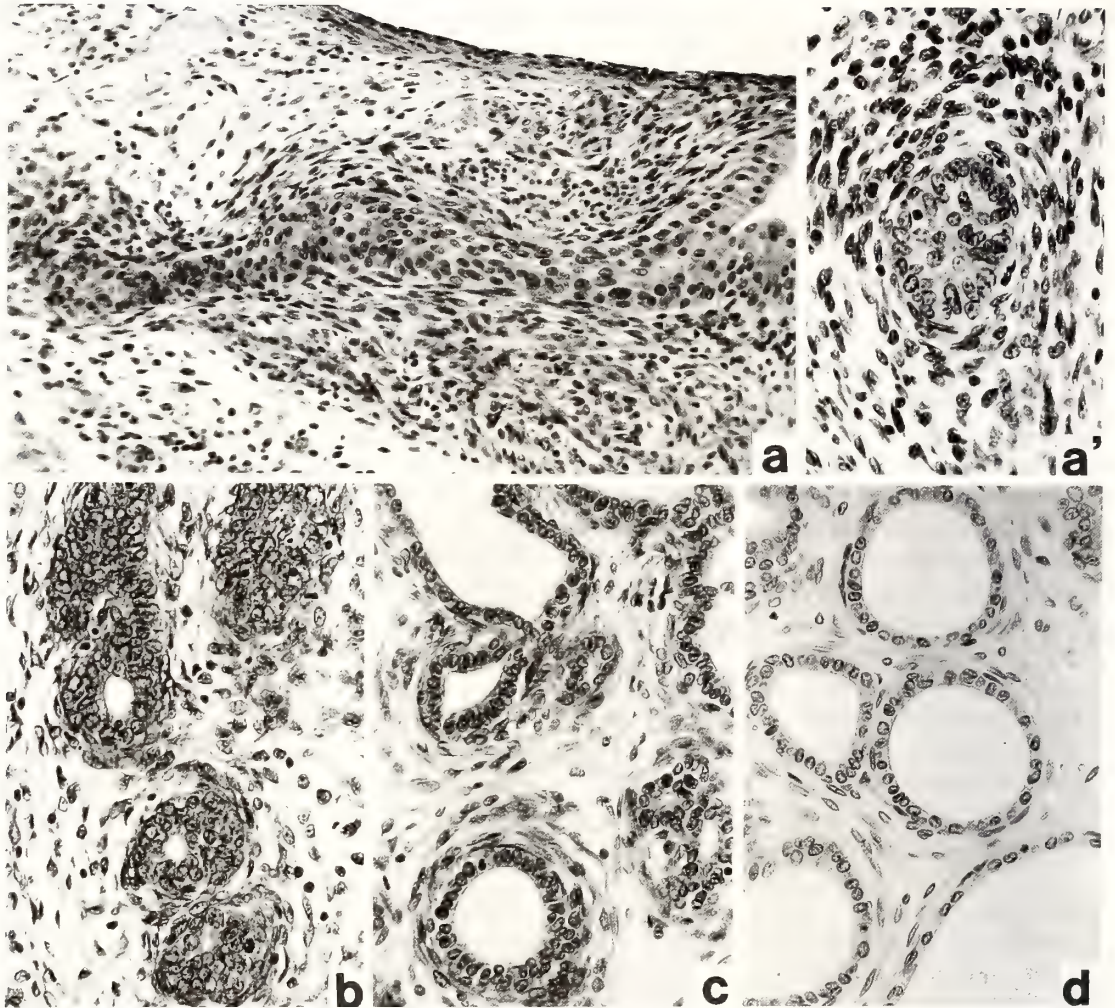


FIG. 2. Recombinates of adult bladder epithelium and fetal ventral sinus mesenchyme. (a) 1 week, $\times 215$; (b) 2 weeks, $\times 270$; (c) 3.5 weeks, $\times 270$; (d) 8 weeks, $\times 135$, cultured in adult male hosts. (a') A cross section of the epithelial bud as seen in (a), $\times 340$.

bladder was positive for alkaline phosphatase activity (Fig. 4a) and negative for both acid phosphatase (Fig. 4b) and nonspecific esterase (Fig. 4c) activities. In contrast, the glandular epithelium induced in the bladder epithelium by the fetal ventral sinus mesenchyme lost its alkaline phosphatase activity (Fig. 4d) but showed acid phosphatase (Fig. 4e) and nonspecific esterase (Fig. 4f) activities just like the acinar epithelium of the normal ventral prostate, which was negative for alkaline phosphatase (Fig. 4g) and positive for both acid phosphatase (Fig. 4h) and nonspecific

esterase (Fig. 4i). The stromal cells immediately adjacent to the acinar epithelium were positive for alkaline phosphatase both in the induced and normal prostatic glands. The glandular structure induced by the mesenchymes of fetal dorsal sinus and seminal vesicle showed similar histochemical features as those induced by the mesenchyme of the fetal ventral sinus. There was thus no difference between the heterotypic and homotypic recombinates as far as histochemical activities of these enzymes were concerned.

The immunohistochemical study also suggested

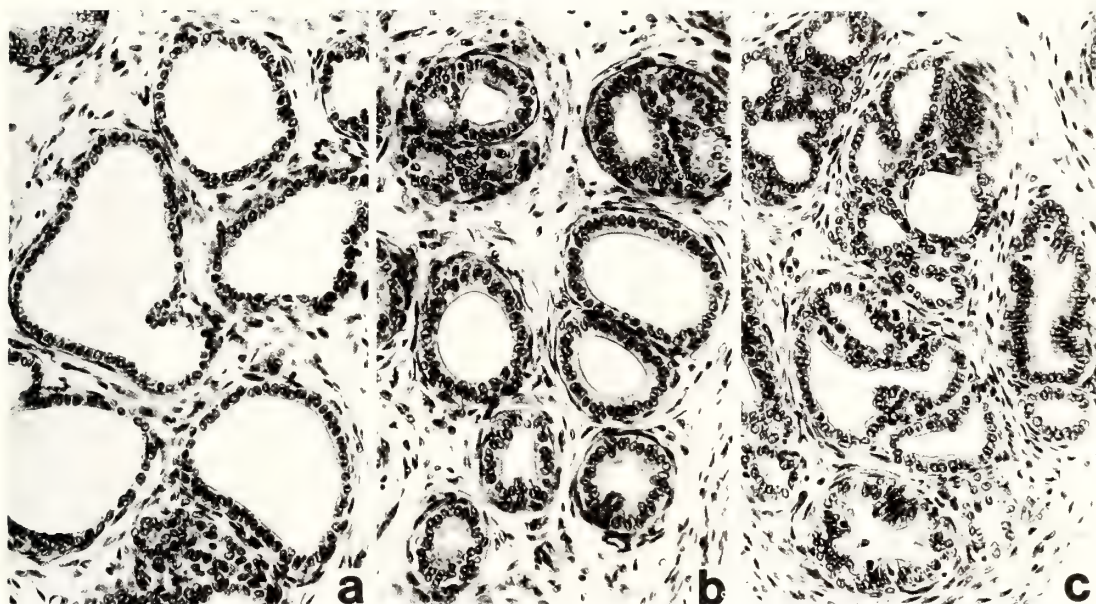


FIG. 3. Heterotypic recombinates of adult bladder epithelium and 16.5-day ventral sinus mesenchyme (a), dorsal sinus mesenchyme (b), or 19.5-day seminal vesicle mesenchyme (c) cultured in adult male hosts. $\times 215$.

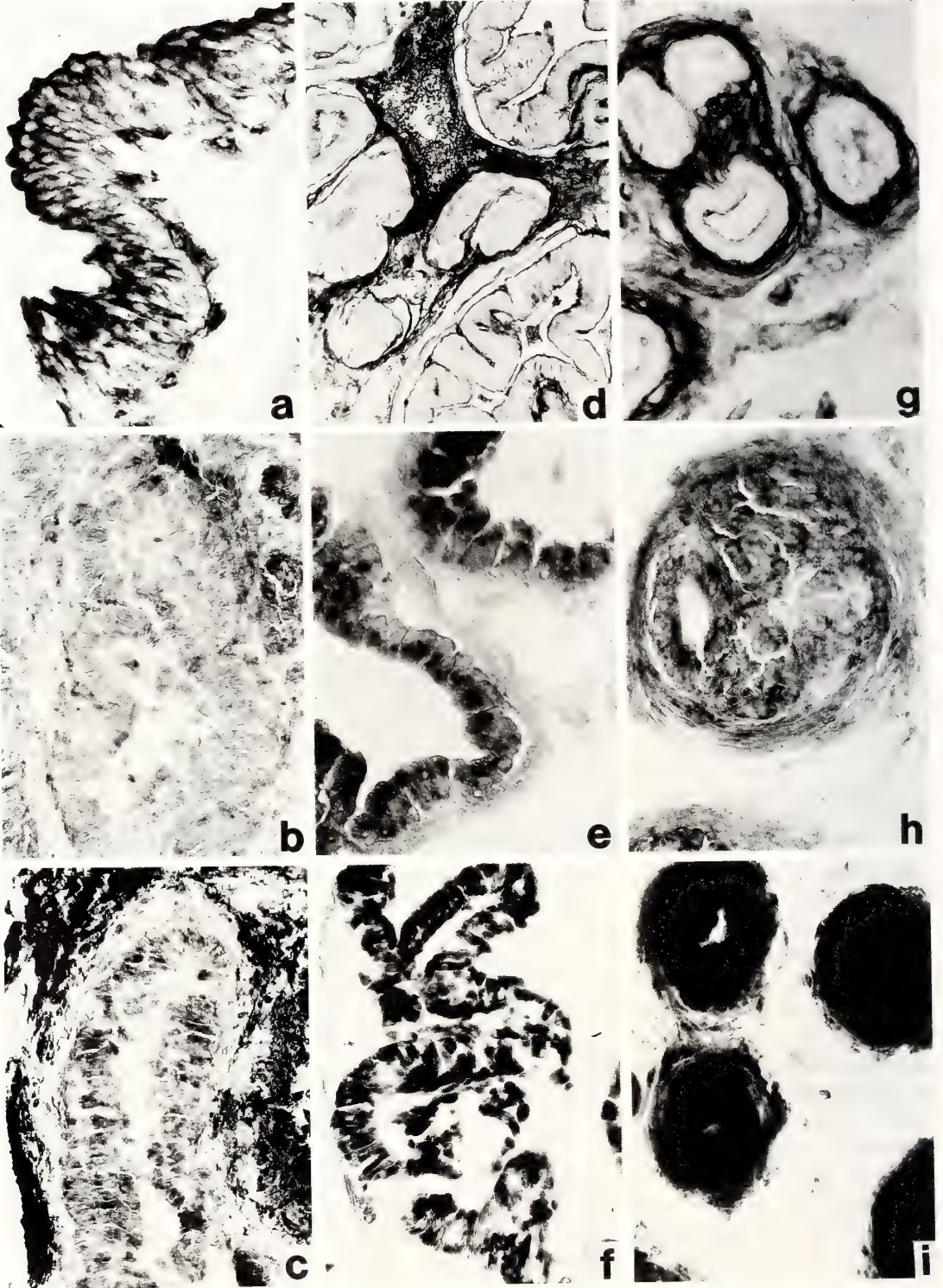
that heterotypic functional differentiation occurred in the induced glands. The bladder epithelium reacted with our anti-bladder epithelium-antiserum (Fig. 5) even after *in vivo* culture of 4 weeks as far as it maintained its original form seen at the time of recombination with sinus mesenchyme. The antigenicity against the antiserum was lost in the epithelium, when induced to form glandular epithelium (Fig. 6). This result suggests that the bladder epithelium dedifferentiated to express specific enzyme activities following the morphological gland formation.

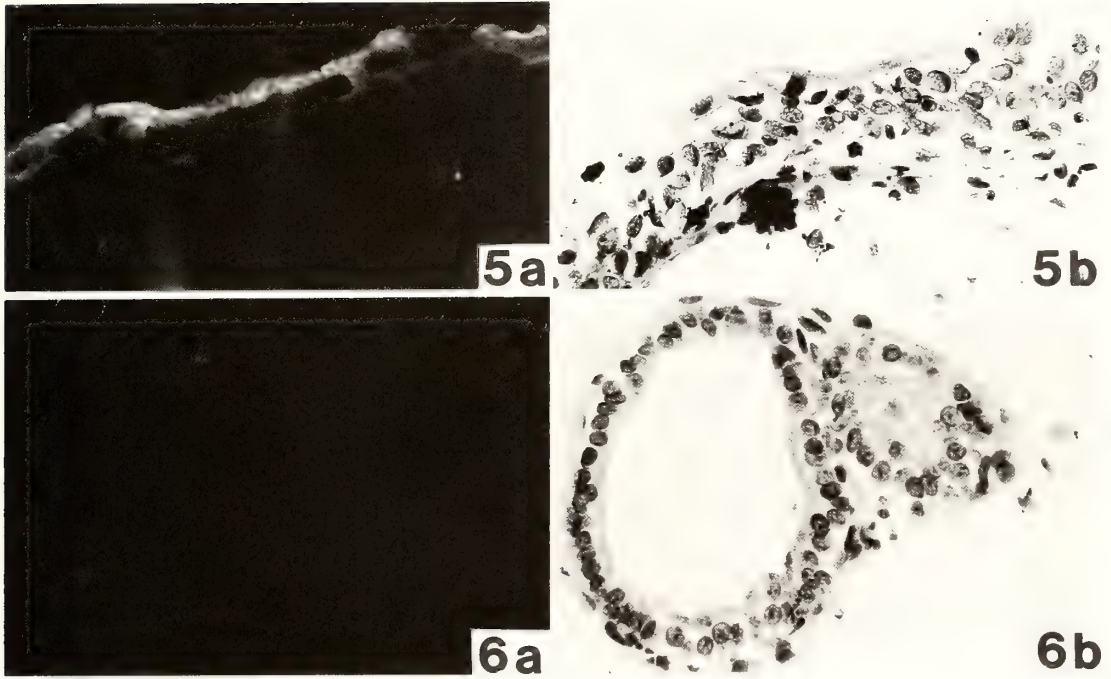
Most of the induced glandular epithelium was found to be positive against anti-human prostatic acid phosphatase-antiserum (Fig. 7), although some glandular cells as well as the normal counterparts were negative. Oddly enough it did not express antigenicity against the anti-ventral prostatic epithelium-antiserum (Fig. 8a), which intensely stained the normal ventral prostatic epithelium in the control explant (Fig. 8c) but only faintly the ventral prostate 5 days after castration (Fig. 8d). In the immunoblotting, the anti-ventral prostatic epithelium-antiserum recognized many types of proteins specific to the ventral prostatic epithelium (Fig. 9). The induced glandular epithelium did not

respond to anti-dorsal prostatic epithelium-antiserum, which reacted with the normal dorsal prostatic epithelium (Fig. 8e).

The steroid autoradiography showed heavy nuclear labelling with [^3H] dihydrotestosterone (DHT) in homotypic explants of sinus epithelium with its mesenchyme (Fig. 10a). In contrast, the glandular epithelium induced from bladder epithelium showed no preferential nuclear uptake of the steroid, but the surrounding mesenchymal cells showed heavily labelled nuclei in all 5 recombinates (Fig. 10b). In the competition experiments in which the tissues were incubated both with the radioactive steroid and with a 400-fold excess of unlabelled steroid, the uptake of radioactive steroid by nuclei was completely abolished.

We also compared the total proteins of the isolated glandular epithelial tissues with each other, which were separated by SDS-PAGE. The induced glandular epithelium differed qualitatively and quantitatively from the bladder epithelium but not from the ventral prostatic epithelium. The induced glandular epithelium lost the bladder epithelium-specific proteins (B, B', Fig. 11), and showed prostatic epithelial proteins (P, P'). Moreover the induced glandular epithelium ex-





FIGS. 5. and 6. Immunofluorescence with anti-bladder epithelium-antiserum (a) and HX-E (b) preparations of normal adult bladder (Fig. 5) and induced glands in the recombinates of adult bladder epithelium and fetal sinus mesenchyme (Fig. 6). $\times 270$.

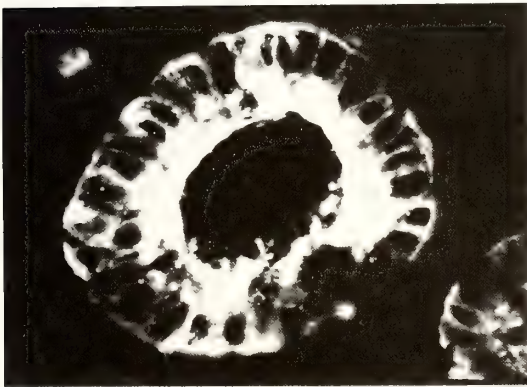


FIG. 7. Immunofluorescence with anti-human prostatic acid phosphatase-antiserum. The bladder epithelium-derived acinar epithelium showed intense reaction in the apical cytoplasm. $\times 480$.

pressed the ventral prostatic epithelial protein (V) but not the dorsal prostatic epithelial proteins (D, D'), even when the bladder epithelium was recombined with dorsal sinus mesenchyme.

DISCUSSION

In the present study, we found that in recombinates of fully differentiated adult rat bladder epithelium with sinus mesenchyme, cultured in the presence of androgens, the bladder epithelium formed prostate-like glandular epithelium. The stratified transitional bladder epithelium which is normally alkaline phosphatase positive changed to a simple columnar glandular epithelium, became alkaline phosphatase negative and acquired acid

FIG. 4. Histochemical assay of alkaline phosphatase (a, $\times 280$; d, $\times 140$; g, $\times 270$), acid phosphatase (b, $\times 140$; e, $\times 340$; h, $\times 270$) and nonspecific esterase (c, $\times 140$; f, $\times 250$; i, $\times 380$). Dark areas indicate the enzyme positive sites. The features of these histochemical markers expressed in the glandular epithelium induced in the recombinates composed of adult bladder epithelium and fetal ventral sinus mesenchyme (d, e, f) were similar to those of acinar epithelium of normal ventral prostate (g, h, i) but different from those of adult bladder epithelium (a, b, c).

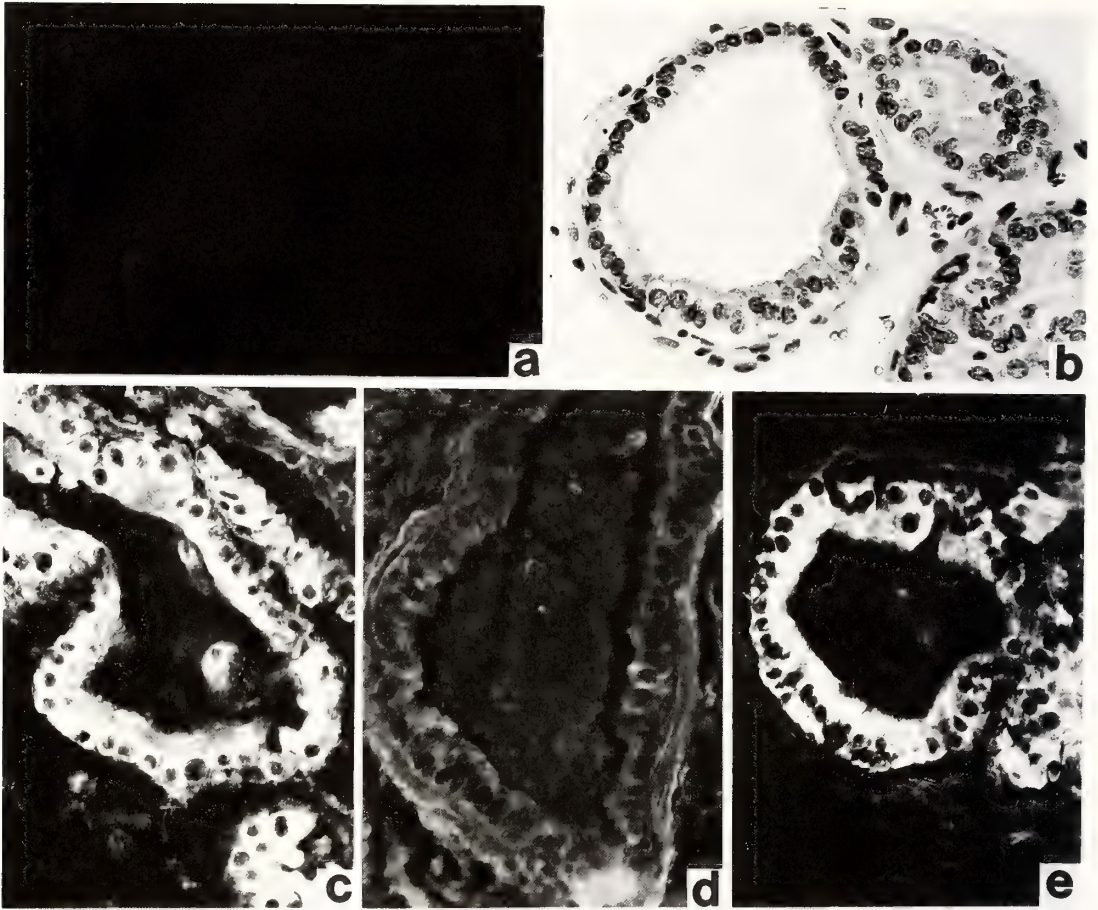


FIG. 8. Immunofluorescence with anti-ventral prostatic epithelium-antiserum of the induced glandular epithelium of bladder origin (a), ventral prostate gland in the control explant composed of sinus mesenchyme and its epithelium (c) and ventral prostate excised 5 days after castration (d). HX-E preparation (b) is the same with (a). Immunofluorescence with anti-dorsal prostatic epithelium-antiserum of normal dorsal prostate (e). $\times 270$.

phosphatase, nonspecific esterase and prostatic acid phosphatase antigen. Heterotypic morphogenesis has been reported in the studies of epithelio-mesenchymal interactions, but sometimes it was not accompanied by heterotypic cytodifferentiation [11, 12]. However, the present study revealed that cytochemical differentiation took place concomitant with heterotypic morphogenesis, and the mesenchyme played the decisive role both in the morphogenesis and in the cytodifferentiation of the epithelium.

The ventral-, dorsal- and coagulating-lobes of prostates develop from the urogenital sinus and the seminal vesicle, from the basal region of the

Wolffian ducts. Although they are similar in histological appearance, closer examination revealed differences among them. For instance, the acini of the ventral prostate are tightly packed in very small amounts of stroma and are lined with columnar epithelial cells that have basally located nuclei and a prominent supranuclear clear area that corresponds to the location of the Golgi apparatus, while the acini of the dorsal prostate are loosely distributed within large amounts of stromal tissue and are lined mainly with cuboidal epithelial cells with centrally placed nuclei and a supranuclear clear area as described by Jesik *et al.* [13].

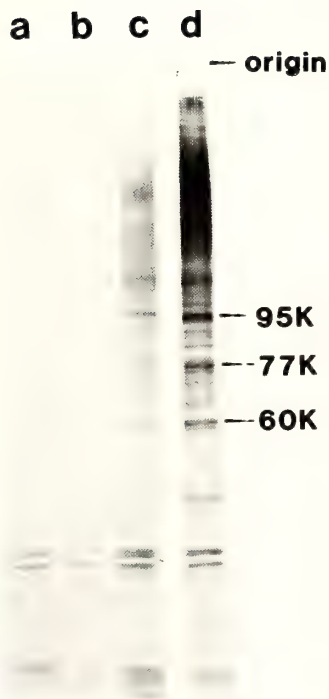


FIG. 9. Immunoblotting with anti-ventral prostatic epithelium-antisera after electrophoresis on the gel containing SDS of crude extract of adult bladder epithelium (a), glandular epithelium in the recombinates composed of adult bladder epithelium and fetal ventral sinus mesenchyme (b), glandular epithelium in the control explants of fetal ventral sinus epithelium and its mesenchyme (c) and normal ventral prostatic epithelium (d). Ten μg of protein were applied to each lane.

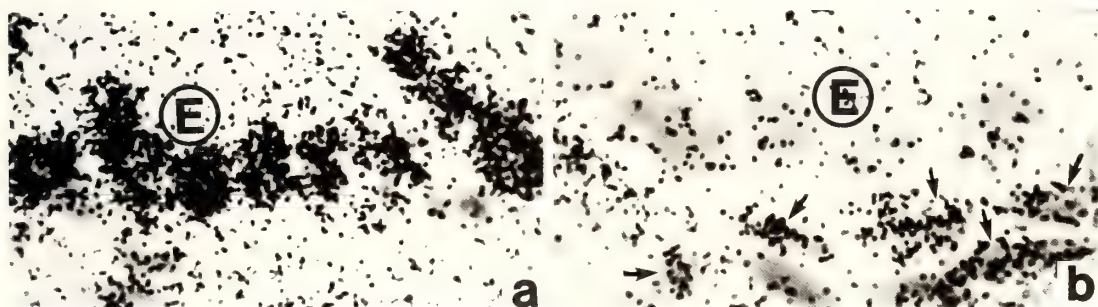


FIG. 10. Autoradiographs of explants incubated with ^3H DHT. Sections were stained with HX. The exposure period was 4 weeks. E, glandular epithelium. (a) Prostate gland formed in a control explant of fetal sinus. Epithelial cells exhibited intense nuclear labelling, while the intensity of labelling in the mesenchyme surrounding the epithelium is weaker. $\times 1350$. (b) Prostate-like gland induced in a recombine composed of adult bladder epithelium and fetal sinus mesenchyme. Epithelial cells showed no strong nuclear concentration of grains, while the mesenchymal cells immediately beneath the epithelium (arrows) showed heavy accumulation on nuclei. $\times 1350$.

Cunha *et al.* [3] showed that prostatic morphogenesis occurred in heterotypic recombinates of adult bladder epithelium and fetal sinus mesenchyme, but they did not mention which region of the sinus mesenchyme was used. In the present study, we used three precisely defined mesenchymal regions isolated from 16.5-day ventral and

dorsal sinus and from 19.5-day rudiments of seminal vesicle and found that our results agreed mostly with those of Cunha *et al.* except in a few details: In all grafts, glands rich in stroma and poor in secretion were formed, irrespective of the region of the mesenchyme used; When the sinus mesenchyme of the ventral or dorsal region was

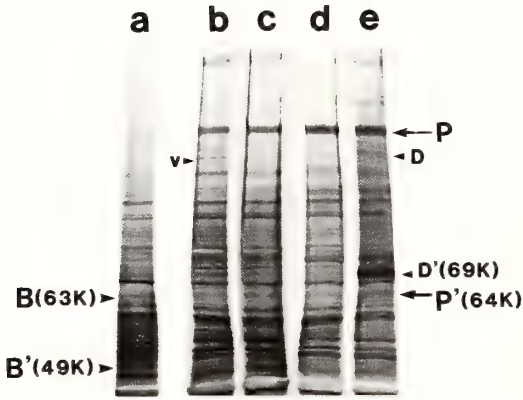


FIG. 11. SDS-electrophoretic patterns of proteins in adult bladder epithelium (a), acinar epithelium of recombinates composed of adult bladder epithelium and fetal ventral sinus mesenchyme (b) or fetal dorsal sinus mesenchyme (c), acinar epithelium of control grafts of ventral sinus (d) or dorsal sinus (e). Ten μ g of protein were applied to each lane. Both (b) and (c) lost proteins B, B' and expressed P, P', V but not D, D'.

used as an inductor, the acini formed in the recombinates resembled developing prostate in the histological character: the acini were loosely arranged within the supporting stroma and lined with cuboidal epithelial cells containing a centrally located round nucleus. When the mesenchyme of the seminal vesicle was used instead of the sinus mesenchyme, the acinus epithelium possessing long nuclei seen in the seminal vesicle was also induced (Fig. 3c).

Neubauer *et al.* [4] reported that the induced acinar epithelium in the recombinates composed of adult bladder epithelium and fetal sinus mesenchyme acquired androgen receptors but that the androgen binding activities were significantly lower than those of the adult ventral prostate. We assume that the androgen binding activities they detected in the experimental grafts lies principally in the stroma rather than the epithelium. Because our autoradiographic studies have shown that androgens scarcely bind to the induced glandular epithelium in the heterotypic recombinates but mainly to the stromal cells, particularly, those in the immediate vicinity of the epithelium (Fig. 10b). Similar results have been obtained with the epithelia of androgen-receptor defective *Tfm*

mice: the *Tfm* bladder epithelium as well as the sinus epithelium [14] formed prostate-like glands under the influence of normal sinus mesenchyme and expressed acid phosphatase and nonspecific esterase activities. It may, therefore, be assumed that the induced glandular epithelium is devoid of androgen receptors.

The function of the androgen receptors in the acinar epithelium is still uncertain. In adult ventral prostate glands excised 5 days after castration the reaction against anti-ventral prostatic epithelium-antiserum was significantly lowered (Fig. 8d), suggesting that the antibody recognized mainly the androgen-dependent proteins. Our results showed that the induced glandular epithelium possessed neither normal androgen receptors nor antigenicity against the anti-ventral prostatic epithelium-antibody. It seems, therefore, that the epithelial androgen receptors are necessary for the synthesis of androgen-dependent proteins responsible for epithelial function. When adult bladder epithelium was combined with dorsal sinus mesenchyme, the induced glandular epithelium did not possess D' (69 K)-protein specific to dorsal prostatic epithelium (Fig. 11). Though the molecular weight of D' is similar to serum albumin, serum contamination is never expected, because we did not use serum in the procedure of sample preparation, and D' is specific to the lane (e). This suggests that the androgen receptors also play an important role in the synthesis of lobe specific proteins.

It can be concluded that adult bladder epithelium is able to respond to the stimulation of androgen-activated sinus mesenchyme and loses the characteristic proteins for the bladder epithelium and forms glandular structures with newly induced enzyme activities similar to those of the normal prostate. The induced epithelium, however, is unable to attain full prostatic cytodifferentiation nor express lobe specificity due to a lack of normal androgen receptors.

ACKNOWLEDGMENTS

We thank Dr. Ilse Lasnitzki of the Strangeways Research Laboratory for constructive criticism and help in the preparation of the manuscript. This work was supported by a Grant-in-Aid from the Ministry of Education, Science and Culture of Japan.

REFERENCES

- 1 Lasnitzki, I. and Mizuno, T. (1977) Induction of the rat prostate gland by androgen in organ culture. *J. Endocrinol.*, **74**: 47–55.
- 2 Takeda, H., Mizuno, T. and Lasnitzki, I. (1985) Autoradiographic studies of androgen-binding sites in the rat urogenital sinus and postnatal prostate. *J. Endocrinol.*, **104**: 87–92.
- 3 Cunha, G. R., Fujii, H., Neubauer, B. L., Shannon, J. M., Sawyer, L. and Reese, B. A. (1983) Epithelial-mesenchymal interactions in prostatic development. 1. Morphological observations of prostatic induction by urogenital sinus mesenchyme in epithelium of the adult rodent urinary bladder. *J. Cell Biol.*, **96**: 1662–1670.
- 4 Neubauer, B. L., Chung, L. W. K., McCormick, K. A., Taguchi, O., Thompson, T. C. and Cunha, G. R. (1983) Epithelial-mesenchymal interactions in prostatic development. 2. Biochemical observations of prostatic induction by urogenital sinus mesenchyme in epithelium of the adult rodent urinary bladder. *J. Cell Biol.*, **96**: 1671–1676.
- 5 McGadey, J. (1970) Detection methods II. Hydrolases. Tetrazolium reaction. In "Enzyme Histochemistry (1979)". Ed. by Z. Lojda, R. Gossraw and T. H. Schiebler, Springer-Verlag, Berlin, pp. 61–63.
- 6 Lojda, Z. (1979) Detection methods II. Hydrolases. Simultaneous azo-coupling with esters of the naphthol AS series. In "Enzyme Histochemistry (1979)". Ed. by Z. Lojda, R. Gossraw and T. H. Schiebler, Springer-Verlag, Berlin, pp. 72–75.
- 7 Davis, B. J. and Ornstein, L. (1959) Detection methods II. Hydrolases. Simultaneous azo-coupling with 1-naphthyl acetate. In "Enzyme Histochemistry (1979)". Ed. by Z. Lojda, R. Gossraw and T. H. Schiebler, Springer-Verlag, Berlin, pp. 109–110.
- 8 McKeehan, W. L., Rosser, M. P., Glass, H. A. and Fast, D. (1980) Prostatic binding protein: An androgen-dependent marker for prostate epithelial cells. *Biochem. Biophys. Res. Commun.*, **95**: 674–681.
- 9 Laemmli, U. K. (1970) Cleavage of structural proteins during the assembly of the head of Bacteriophage T4. *Nature*, **227**: 680–685.
- 10 Towbin, H., Staehelin, T. and Gordon, J. (1979) Electrophoretic transfer of proteins from polyacrylamide gels to nitrocellulose sheets: Procedure and some applications. *Proc. Natl. Acad. Sci. USA*, **76**: 4350–4354.
- 11 Sakakura, T., Sakagami, Y. and Nishizuka, Y. (1979) Persistence of responsiveness of adult mouse mammary gland to induction by embryonic mesenchyme. *Dev. Biol.*, **72**: 201–210.
- 12 Yasugi, S. (1984) Differentiation of allantoic endoderm implanted into the presumptive digestive area in avian embryos. A study with organ-specific antigens. *J. Embryol. Exp. Morphol.*, **80**: 137–153.
- 13 Jesik, C. J., Holland, J. M. and Lee, C. (1982) An anatomic and histologic study of the rat prostate. *The Prostate*, **3**: 81–97.
- 14 Mizuno, T., Takeda, H. and Suematsu, N. (1986) Récepteurs d'androgènes de l'épithélium au cours de l'induction des glandes prostatiques à partir de l'épithélium du sinus urogénital de la Souris Tfm-mutant. *C. R. Soc. Biol.*, **180**: 593–595.

Development of an *in situ* Hybridization Method for Neurohypophysial Hormone mRNAs Using Synthetic Oligonucleotide Probes

SUSUMU HYODO, MAMORU FUJIWARA, SHIGERU KOZONO,
MORIYUKI SATO¹ and AKIHISA URANO

Department of Regulation Biology, Faculty of Science, Saitama University, Urawa, Saitama 338, and ¹Tokyo Research Laboratories, Kyowa Hakko Kogyo Co., Machida, Tokyo 194, Japan

ABSTRACT—Vasopressin (AVP) and oxytocin (OXT) mRNAs are highly homologous. We developed an *in situ* hybridization method to discriminate the AVP and the OXT mRNAs using synthetic 22mer deoxyoligonucleotides as probes which have several advantages over the use of cDNAs, e.g., highly specific, easy to obtain a designed probe, and easily accessible to cellular mRNAs. The probes were radiolabeled at the 5' ends with ³²P, applied to rehydrated paraffin sections of rat and/or toad hypothalami, and were visualized by autoradiography. RNase treatment before incubation with the probes and measurement of melting temperature showed that the probes actually paired with tissue RNAs. The specificity of hybridization signals was checked by the following tests: absorption test, competition test, a use of alternate probes complementary to the different regions of the same mRNA, cross species hybridization, and comparisons with the immunohistochemical localization of AVP and OXT in adjacent or the same tissue sections. These tests showed that the oligonucleotide probes specifically discriminate the AVP mRNA from the highly homologous OXT mRNA. Furthermore, cross species hybridization clarified that an oligonucleotide probe can discriminate nucleotide sequences which include 2 mismatching bases. The use of multiple probes complementary to different loci in the same mRNA showed not only the specificities of the hybridization signals, but also its usefulness to enhance hybridization signals.

INTRODUCTION

Arginine vasopressin (AVP) and oxytocin (OXT) are mammalian neurohypophysial hormones produced mainly in magnocellular neurons in the supraoptic (SON) and the paraventricular nuclei (PVN). They are released from neurosecretory terminals into blood capillaries in the neurohypophysis, and play important physiological roles, e.g., regulation of plasma osmolarity and blood pressure by AVP, and oxytocic action and stimulation of milk ejection by OXT. It is therefore important to examine expressions of AVP and OXT genes in magnocellular neurons in various physiological statuses. A recently developed *in situ* hybridization (ISH) method is the

most plausible candidate for this examination.

The structures of rat AVP and OXT genes recently clarified [1] show that the AVP mRNA and the OXT mRNA share an extremely homologous region, the exon B, the homology of which is about 95%. Since cDNAs can hybridize with mRNAs the homology of which is approximately 65% [2], the presence of the AVP mRNA has been detected with a spliced cDNA probe complementary to the glycoprotein encoding region which is not present in the OXT mRNA [3-7], while the OXT mRNA has been localized with a probe complementary to the 3'-end of neurophysin (NP) and the 3'-untranslated region [3]. A problem arising here is the occurrence of vasotocin (AVT) especially in fetal brains of mammals [8, 9]. A possibility that the cDNA probes hybridize with the AVT mRNA makes it difficult to apply the ISH method in a study of ontogeny of the

neurosecretory system. Moreover, the use of cDNA probes entirely depends on their availability that requires facilities for recombinant DNA techniques. One of possible ways to overcome these problems is the use of synthetic deoxyoligonucleotides as probes for ISH, the technique developed in our laboratory [10–12]. The use of oligonucleotides as probes for ISH further can have several advantages over the use of cDNAs, that is, highly specific [2, 13, 14], easy to obtain a designed probe, easy to prepare and to label in an ordinary laboratory [15] and easily accessible to cellular mRNAs [16–18].

We designed 22mer oligonucleotide probes to discriminate localization of AVP and OXT mRNAs in paraffin sections. We further revised our previous ISH protocol [10, 11] by checking each staining step. A fixative solution was also carefully screened to stain the same or adjacent tissue sections by both ISH and immunohistochemical methods, because demonstration of AVP and OXT is crucial for better understanding of their gene expressions. Specificity of the present method was confirmed by various tests including cross species hybridization with the mRNAs of toad neurohypophysial hormones, nucleotide sequences of which were recently determined by Nojiri *et al.* [19]. Through the specificity tests, we tried to elucidate technical limitations of the present method and to confirm its general applicability in gene expression studies of many other peptides and proteinaceous hormones.

MATERIALS AND METHODS

Preparation of tissue sections

Male Wistar-Imamichi rats (6–8 weeks old) and adult Japanese toads of both sexes captured in the autumn were obtained from commercial sources. They were killed by decapitation, and the hypothalamus and the pituitaries were rapidly taken out and immersed in fixative solutions at 4°C for 2 days. Since a preliminary experiment showed that fixation by perfusion markedly decreased hybridization signals, we preferred fixation of tissues by immersion. Fixatives tested were: Bouin's solution, modified Bouin's solution which does not

include acetic acid, 4% paraformaldehyde (PFA) in 0.05 M phosphate buffer (pH 7.3), a buffered solution containing 2% PFA and 1% glutaraldehyde (GLA), and that including 2% PFA, 1% GLA and 1% picric acid (PA). As is described in the Results section, the mixture of PFA, GLA and PA (PGP solution) yielded satisfactory results in both ISH and immunohistochemical staining among these fixatives. Therefore, the PGP solution was routinely used in the present study.

After fixation, the hypothalamus were washed in 70% ethanol at 4°C for 24 hr twice. They were then dehydrated through graded ethanols, and were embedded in paraplast. Serial transverse sections were cut at 8 or 10 μm , separated into several groups, and were mounted on gelatinized slides. Some hypothalamic tissues were washed in cold 0.05 M phosphate buffer (pH 7.3) after fixation, rapidly frozen in butanol cooled in dry ice-acetone, and were cut at 20 μm on a frozen microtome. They were also mounted on gelatinized slides.

Preparation of synthetic oligonucleotide probes

Four 22 mer oligonucleotide probes (Fig. 1) were synthesized by the phosphoramidite method [20] and were purified by polyacrylamide gel electrophoresis. They are complementary to the regions in the rat AVP mRNA encoding AVP (2–9) and AVP-NP (1–8), to that in the rat OXT mRNA encoding OXT-NP (1–8), and to that in the toad AVT mRNA encoding AVT (–1 to 7). They are thus referred to as AVP, AVP-NP, OXT-NP and AVT-OXT probes, respectively. The nucleotide sequence of AVT/OXT probe is exactly complementary to the corresponding region of OXT mRNA, while the nucleotide at position 9 of this probe is mismatched with the counterpart of AVP mRNA (*i.e.*, 95% homology). The AVP probe has 2 mismatching positions with the AVT mRNA (91% homology), and 6 mismatching positions with the OXT mRNA (73% homology). The AVP-NP and OXT-NP probes differ at 10 positions (55% homology). The homology of the corresponding region of toad mesotocin mRNA with the AVT-OXT probe is 77%, and that with the AVP probe is 73%.

The probes were labeled at the 5' ends with T4

AVP mRNA	Sig	AVP	AVP-NP	GP
		AVP(2-9)	AVP-NP(1-8)	
AVP		Cys Tyr Phe Gln Asn Cys Pro Arg Gly		
AVP mRNA	5'	UGC UAC UUC CAG AAC UGC CCA AGA GGA		3'
Probe		3' G AAG GTC TTG ACG GGT TCT CCT		5'
Template		AC TTC CAG AAC TGC		
AVP-NP		Ala Tyr Ser Asp Met Glu Leu Arg		
AVP-NP mRNA		GCC ACA UCC GAC AUG GAG CUG AGA		
Probe		GG TGT AGG CTG TAC CTC GAC TC		
OXT mRNA	Sig	OXT	OXT-NP	
			OXT-NP(1-8)	
OXT-NP		Ala Ala Leu Asp Leu Asp Met Arg		
OXT-NP mRNA		GCU GCG CUA GAC CUG GAU AUG CGC		
Probe		GA CGC GAT CTG GAC CTA TAC GC		
AVT mRNA	Sig	AVT	AVT-NP	GP
		AVT((-1)-7)		
AVT		Ala Cys Tyr Ile Gln Asn Cys Pro		
AVT mRNA		GCC UGC UAC AUC CAG AAC UGC CCC		
Probe		GG ACG ATG TAG GTC TTG ACG GG		

Fig. 1. Design of synthetic oligonucleotide probes in the present experiments. Nucleotide sequences of the probes are shown with those of the complementary mRNAs. Amino acid sequences encoded by the mRNA sequences are also shown. Numbers in parentheses indicate amino acid positions. Sig, signal peptide; NP, neurophysin; GP, glycoprotein.

polynucleotide kinase using [γ -³²P] ATP to a final specific activity of 4–6 × 10⁷ cpm/μg by the procedure of Maxam and Gilbert [15]. Radioactivity of the labeled probe was measured by liquid scintillation counting of Cerenkov radiation.

Procedure for in situ hybridization

After rehydration, tissue sections were treated with proteinase K (1 μg/ml; Sigma, type XI) in 0.1 M Tris buffer (pH 8.0) containing 50 mM EDTA at 37°C for 30 min, and were briefly washed in doubly deionized water at room temperature. They were then rinsed in 2 × SSC (1 × SSC contains 0.15 M NaCl and 0.015 M sodium citrate), preincubated in a hybridization buffer (0.9 M NaCl, 6 mM EDTA, 0.2% bovine serum albumin, 0.2% Ficoll, 0.2% polyvinylpyrrolidone and 100 μg/ml denatured salmon sperm DNA in 90 mM Tris buffer, pH 7.5) at room temperature for 1 hr, and were placed in a moist chamber. The radiolabeled oligonucleotide probe was diluted to 1 × 10⁴ cpm/μl in hybridization buffer, and 80 μl of the probe solution was applied to each slide glass. Sections were coverslipped, and were incubated at 30°C overnight. After removing coverslips in cold

6 × SSC, the sections were washed in 6 × SSC firstly at 4°C for 10 min, then at about 20°C for 20 min twice, and again at 4°C for 10 min. The sections were then dehydrated through graded ethanols (70, 90 and 100%) containing 0.3 M ammonium acetate and were air-dried. Thereafter, the sections were dipped in Sakura NR-M2 emulsion diluted 3:2 with 0.3 M ammonium acetate, air-dried for 30 min, and were exposed for 1 to 3 weeks. After development in Kodak D-19 and fixation, they were dehydrated and were coverslipped with Permount (Fisher).

Methodological checks

Proteinase treatment The proteinase treatment after rehydration has been considered to increase accessibility of the probes to tissue mRNAs. We examined whether the proteinase treatment actually increase hybridization signals in the rat hypothalamic sections fixed by PFA only and those fixed by the PGP solution.

Acetylation Acetylation of tissue sections was reported to decrease non-specific binding of probes, so that background could be reduced [21]. Therefore, proteinase treated rat tissue sections were immersed in freshly prepared 0.25 % acetic anhydride in 0.1 M triethanolamine buffer (pH 8.0) for 10 min prior to preincubation.

Effect of long-term storage of tissue sections Tissue sections from the same rats were separated into several groups, and were left unhydrated. They were kept in a desiccated box at a cool place. A group of tissue sections were periodically taken out, and the AVP mRNA was stained by ISH method during a period of more than 18 months.

Concentration of labeled probes Hybridization mediums containing different levels of probe concentrations between 5 × 10³ cpm/μl to 2 × 10⁴ cpm/μl were prepared, and were applied to tissue sections to determine an appropriate probe concentration.

Specificity tests for ISH

RNase pretreatment Sections treated with proteinase were incubated with ribonuclease (100 μg/ml; BDH Chemicals) in 0.1 M Tris-HCl (pH 7.5) at room temperature for 1 hr, and were washed in doubly deionized water. The sections

were then hybridized with labeled AVP-NP probe.

Estimation of melting temperature (T_m)
When a probe molecule is paired with the complementary mRNA region by hydrogen bonds, the T_m value experimentally determined was similar to those empirically determined and theoretically calculated [22]. As for oligonucleotide probes of around 20 bases, empirical T_m values for filter hybridization were between 50–60°C. An experimental T_m value was determined by modifying the washing procedure after incubation with the probes, that is, tissue sections were washed 6×SSC at a series of graded temperature (18–70°C) for 20 min after rinse in cold 6×SSC. The AVT/OXT probe was used in this experiment. In the hybridized rat sections, a 100 μm×100 μm square was settled in the OXT region of the PVN. The specific numbers of silver grains within the squares were determined, and were plotted to estimate graphically the T_m value after the logit transformation.

Absorption test A 14mer template oligonucleotide complementary to the AVP probe (Fig. 1) was synthesized, and a 20-fold amount was added to a hybridization medium so as to absorb the probe. Rat hypothalamic sections were incubated in this absorbed hybridization medium.

Competition test Rat hypothalamic sections were incubated in a hybridization medium containing the labeled AVP-NP probe and a 10-fold amount of unlabeled AVP-NP probe. A similar experiment was performed also for the OXT-NP probe. As the control of these competition tests, the unlabeled mismatching probes were added to the hybridization mediums, e.g., the unlabeled OXT-NP probe to the labeled AVP-NP probe and *vice versa*.

Use of different probes to the same mRNA
The AVP and AVP-NP probes were complementary to different regions in the same mRNA. The localization of the AVP probe was thus compared with that of the AVP-NP probe. In addition, the same amounts of labeled AVP and AVP-NP probes were mixed so as to keep the radioactivity of incubation medium at 1×10⁴ cpm/μl, and were applied to rat hypothalamic sections.

Cross species hybridization The limitation of the oligonucleotide probes to discriminate mismatching sequences was examined by using naturally occurring homologues of mRNAs of neurohypophysial hormones in the rat and the toad hypothalami. The AVP probe was applied to sections of the toad hypothalamus, and the resulting hybridization signals were compared to those obtained by use of the AVT/OXT probe. Meanwhile, the AVT/OXT probe was applied to sections of the rat hypothalamus.

Correspondence to immunohistochemical localization of neurohypophysial hormones The distributions of hybridization signals were compared with immunohistochemical localization of neurohypophysial hormones in the same or adjacent sections of the rat and toad hypothalami. For precise comparison, pairs of mirror image sections of the rat hypothalamus were utilized.

Immunohistochemistry

Tissue sections for immunohistochemistry were stained by the avidin-biotin-peroxidase complex (ABC) method using Vectastain ABC kit (Vector), the procedure of which was described elsewhere [11]. In the present study, rabbit anti-AVP (Bioproducts, batch #001) was diluted 1:32,000 with phosphate-buffered saline (PBS) containing 0.5% bovine serum albumin; and rabbit anti-OXT (a gift from Professor S. Kawashima, Hiroshima University) was diluted 1:20,000 with PBS. Since the anti-AVP antiserum cross-reacts completely with AVT, toad hypothalamic sections were stained with this antiserum as was described previously [23].

ISH and immunohistochemistry double staining
Tissue sections were first stained immunofluorescently with fluorescein-labeled avidin D (Vector; diluted 1:250 with bicarbonate-buffered saline, pH 8.2) that was replaced with ABC, photographed with a fluorescence microscope, and were processed for ISH. The use of an IgG-fractionated antiserum was required for this procedure. Otherwise, intensity of hybridization signals was markedly reduced probably by degradation of mRNAs by RNase in the serum.

Specificity tests of immunohistochemistry In addition to the specificity tests previously de-

scribed [11], tissue sections were stained with AVP and OXT antisera preabsorbed with antigen conjugated CNBr-Sepharose 4B (Pharmacia) columns. These tests confirmed the specificity of immunohistochemical stainings in the present study.

RESULTS

Autoradiographic silver grains that represent hybridization signals of the AVP, AVP-NP and OXT-NP probes were localized densely over the magnocellular neurons of the SON, the PVN, the circular nucleus, the anterior commissural nucleus

(ACN) and other accessory magnocellular nuclei in the rat hypothalamus (Figs. 2 and 3). The localization of AVP probe coincided with that of AVP-NP probe, while that of OXT-NP probe showed an independent pattern. The localization of hybridization signals was consistent with the immunohistochemical distribution of corresponding neurohypophysial hormones (Figs. 2 and 3). It was also true in the toad hypothalamus in which the AVT/OXT probe showed similar distribution to immunoreactive (ir) AVT in the magnocellular part of the preoptic nucleus (Fig. 5). In the rat hypothalamus, magnocellular neurons in the ven-

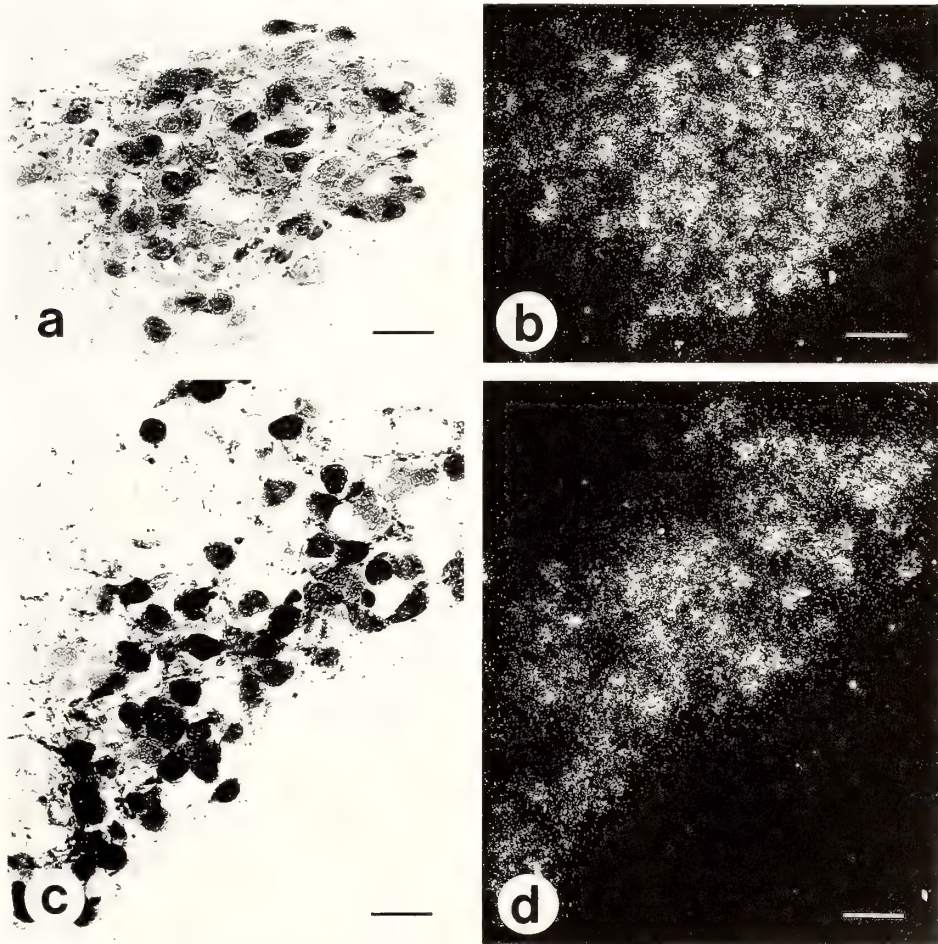


FIG. 2. Immunoreactive (ir) AVP (a) and OXT (c) neurons and hybridization signals of the AVP mRNA (b) and the OXT mRNA (d) in the paraventricular nucleus. Note parallel distribution of autoradiographic signals for the AVP mRNA (b) to AVP-ir neurons in mirror image section (a, counterstained with cresyl violet). Distribution of signals for the OXT mRNA (d) is also parallel to OXT-ir neurons in the adjacent section (c). Scale bar, 50 μ m.

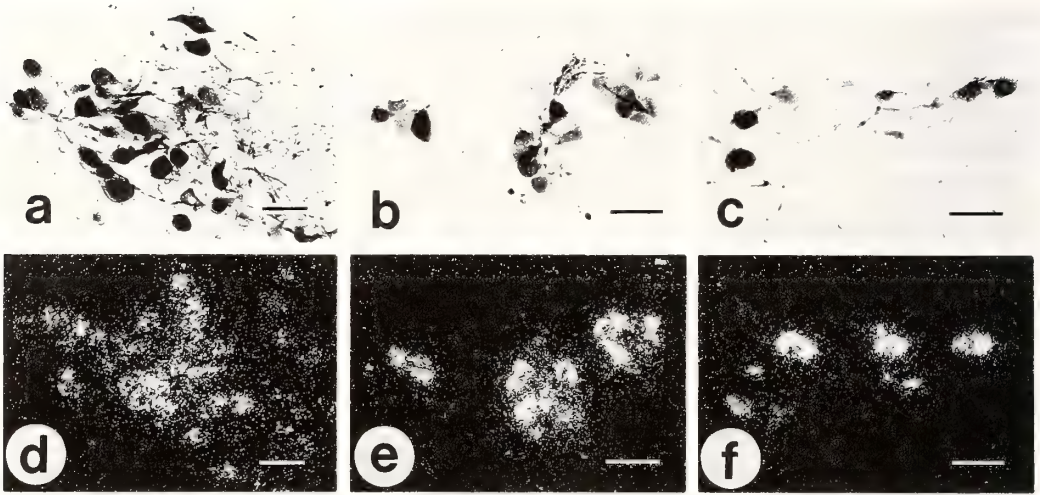


FIG. 3. Immunoreactive (ir) OXT (a) and AVP (b, c) neurons and hybridization signals of the OXT mRNA (d) and the AVP mRNA (e, f) in the anterior commissure nucleus (a, d), the circular nucleus (b, e), and the fornical nucleus (c, f). Autoradiographic signals for the OXT mRNA (d) are distributed parallel to OXT-ir neurons in the adjacent section (a). Signals for the AVP mRNA (e, f) are also distributed parallel to AVP-ir neurons in mirror image sections (b, c, counterstained with cresyl violet). Scale bar, 50 μ m.

tral region of the SON and the dorsolateral region of the PVN were mainly AVP-ir, coinciding well with the localization of the AVP and AVP-NP probes. While the dorsal region of the SON, the ventromedial region of the PVN and the ACN were composed of OXT-ir neurons, and the OXT-NP probe was localized in these regions (Figs. 2 and 3). However, noticeable hybridization signals were not detected in the suprachiasmatic nucleus and the parvocellular part of the PVN which

include AVP-ir parvocellular neurons. Hybridization signals were also not found in the median eminence and the pars nervosa, the terminal regions of neurosecretory fibers.

Preparation of tissue sections and methodological checks

Among the fixatives tested, 4% PFA gave the most intense hybridization signals in the rat hypothalamus (Table 1). The use of a PGP

TABLE 1. Comparison of fixatives for *in situ* hybridization (ISH) of the AVP mRNA and immunohistochemistry (IHC) of AVP in the rat hypothalamus

Fixatives	Proteinase treatment	ISH	IHC	
			001 ^(a)	1285 ^(b)
Bouin's solution	Yes	+	++	++
Bouin's without acetic acid	Yes	++	NT	++
4% PFA	No	++++	-	++
2% PFA+1% GLA	Yes	++	NT	NT
2% PFA+1% GLA+1% PA	Yes	+++	-	+
2% PFA+1% GLA+1% PA	No	+	+++	+++

PFA, paraformaldehyde; GLA, glutaraldehyde; PA, picric acid.

Note: -, not (or scarcely) stained; +, weakly stained; ++, moderately stained; +++, strongly stained; +++++, very strongly stained; NT, not tested.

^(a) Anti-vasopressin antiserum (Bioproducts, batch #001).

^(b) Anti-vasopressin antiserum (Bioproducts, batch #1285).

solution also yielded satisfactorily intense staining results, when tissue sections were treated with proteinase prior to incubation with labeled probes. Results of hybridization in frozen sections were similar to those in paraffin sections. These observations were consistent among the four oligonucleotide probes, while effects of fixation on immunohistochemical staining were rather complex, that is, stainabilities differed between the antisera utilized (Table 1). We are currently using the PGP solution with a proteinase treatment in the hybridization procedure.

The proteinase treatment of tissue sections fixed with the PGP solution markedly increased specific hybridization signals, although intensity of signals in 4% PFA fixed sections was not increased by this treatment.

Acetylation seemed to prevent not only non-specific background binding of labeled probes, but also their specific base-pairing with the complementary nucleotide sequences. Thus, we did not adopt this treatment in our method. On the other hand, the increase in probe concentration above 1×10^4 cpm/ μ l markedly augmented undesirable background. The probe concentration of 5×10^3 cpm/ μ l gave clearly identifiable specific hybridization signals, although the signals were weak. These results indicate that the probe concentration around 1×10^4 cpm/ μ l may be appropriate for the oligonucleotide-mRNA ISH method for neurohypophysial hormones.

The distributional pattern and intensity of hybridization signals in paraffin sections stored for up to 18 months were similar to those in the initial sections which were hybridized immediately after being cut.

Specificity tests

RNase pretreatment Hybridization signals in the magnocellular nuclei were almost completely diminished to the background level by the RNase pretreatment.

T_m When the temperature of washing after hybridization with the AVT/OXT probe was raised to 50°C, hybridization signals were apparently reduced. Signals were further decreased along with elevation of washing temperature, and at about 65°C, almost all signals were removed. The

value of T_m estimated from the plot (Fig. 4) was about 51°C for pairing between the AVT/OXT probe and the OXT mRNA.

Absorption and competition tests Addition of excess amounts of the synthetic template and the unlabeled probe to the hybridization mediums markedly reduced specific localization of silver grains. On the other hand, an excess amount of unlabeled mismatching probe did not change the localization and intensity of hybridization signals.

The use of alternate probes to the same mRNA Hybridization signals of the AVP and AVP-NP probes were localized in the same areas in the SON and the PVN. When the unlabeled AVP probe was added to the labeled AVP-NP probe and *vice versa*, hybridization signals were not altered. Furthermore, the application of mixed AVP and AVP-NP probes conspicuously increased hybridization signals (Fig. 6), showing that the AVP and the AVP-NP probes may not interact each other.

Cross species hybridization In the magno-

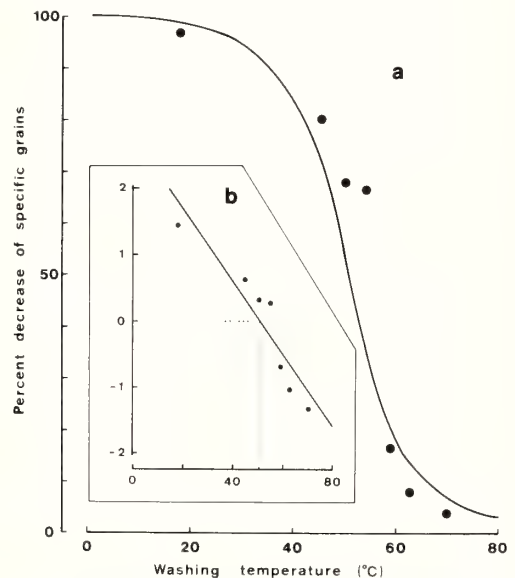


FIG. 4. T_m analysis for pairing of the AVT/OXT probe and the OXT mRNA by *in situ* hybridization. (a) Thermal denaturation of probe-mRNA duplexes. (b) Logit transformation and estimation of T_m value, showing that the value is about 51°C for pairing of the AVT/OXT probe and the OXT mRNA.

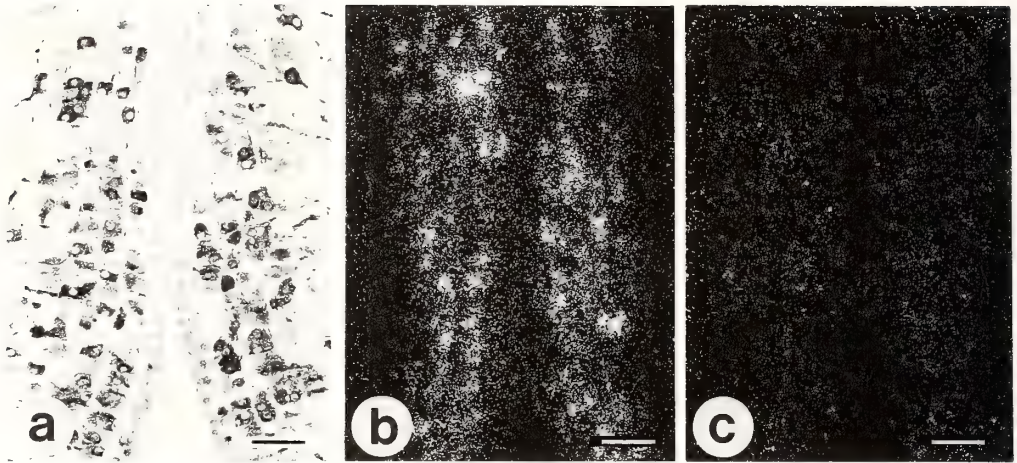


FIG. 5. Immunoreactive (ir) AVT neurons (a) and hybridization signals of the AVT mRNA in the magnocellular part of the toad preoptic nucleus (b, c). The AVT/OXT probe yielded intense hybridization signals (b), which are distributed parallel to AVT-ir neurons (a). In contrast, the AVP probe yielded only weak hybridization signals (c). Scale bar, 50 μm .

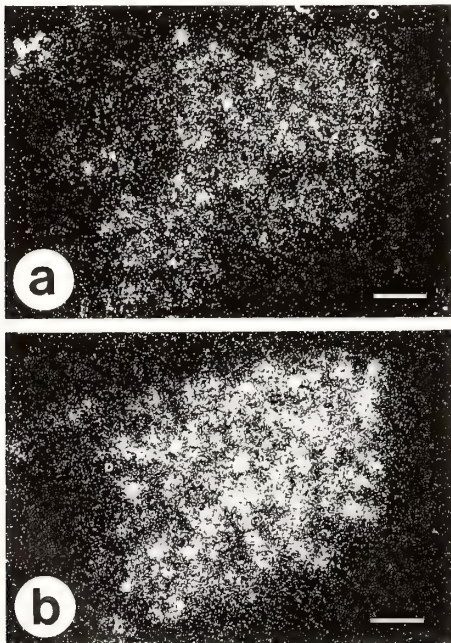


FIG. 6. *In situ* hybridization of the AVP mRNA with the AVP probe only (a) and the mixture of AVP and AVP-NP probes (b) in the paraventricular nucleus. Note that the density of silver grains by the mixed probe is higher than by the AVP probe only. Scale bar, 50 μm .

cellular part of the toad preoptic nucleus, the AVT/OXT probe yielded intense hybridization signals, while those given by the AVP probe were faint (Fig. 5). In contrast, in the rat hypothalamic sections, intensity of hybridization signals induced by the AVT/OXT probe was similar to that given by the AVP probe. The signals by the AVT/OXT probe were localized not only in the SON and the PVN regions where ir-OXT neurons are predominant, but also in the regions occupied by ir-AVP neurons with similar intensity to that seen in the OXT regions. The same result was obtained in another independent study on the hypothalamus of the ICR strain mouse (unpublished).

Distribution of ISH signals vs. that of AVP- and OXT-immunoreactivity As is described above, the distribution of hybridization signals was consistent with the immunohistochemical localization of related peptides. However, the intensity of hybridization signals did not necessarily correlate with that of immunoreactivity, as was reported previously [11]. Immunoreactive neurons were sometimes not labeled with the probe, and *vice versa*.

DISCUSSION

The present study showed that 22mer synthetic oligonucleotides as probes for mRNAs of neurohy-

pophysial hormones were localized in the hypothalamic magnocellular neurosecretory nuclei in the toad and the rat after ISH stainings. The distributions of the probes were consistent with those of immunoreactivities to related peptides, e.g., the AVP probe was localized in the dorso-lateral region of the PVN and the ventral region of the SON where ir-AVP neurons are predominant. However, suprachiasmatic neurons in which Uhl and Reppert [6] demonstrated intense hybridization signals for the AVP mRNA did not show noticeable hybridization signals in our study. Since the intense signals in the suprachiasmatic nucleus have been reported only by Uhl and Reppert, we consider that the above discrepancy is due to longer autoradiographic exposure time by them, judging from their published photographs.

The disappearance of hybridization signals after the RNase pretreatment and the estimated T_m value indicate that the oligonucleotide probes were actually paired with tissue RNAs by hydrogen bonds. Other specificity tests showed that the present probes specifically recognize the complementary nucleotide sequences in particular mRNAs. The consistency of the distribution of hybridization signals for AVP and OXT mRNAs with those of AVP and OXT immunoreactivities further supports the occurrence of specific base pairings between the probes and the related tissue mRNAs. The discrepancy in the distribution of hybridization signals and immunoreactivities at the cellular level must be considered with information concerning secretory activity of neurosecretory neurons [11]. We thus convince that the AVP and AVP-NP probes were hybridized with the rat AVP mRNA, the OXT-NP probe paired with the rat OXT mRNA, and the AVT/OXT probe recognized the toad AVT mRNA and the rat OXT and AVP mRNAs.

The cross species hybridization study clarified that the 22mer oligonucleotide probes discriminated nucleotide sequences which include mismatching bases at more than 2 positions, although one-point mismatching was not recognized. This result strongly supports a reliability of the present ISH method in the study of mRNAs for neurohypophysial hormones. Further, it suggests that the oligonucleotide-mRNA ISH technique is widely

applicable to studies of gene expressions for various peptides and proteinaceous hormones with high fidelity. The method may also be employable in detection of expressed genes concerning hereditary diseases.

Our present study showed that, as to the hypothalamic magnocellular neurons, the distribution of hybridization signals is coincide with that of immunohistochemical staining, indicating that the ISH method is sufficiently sensitive to study gene expression of neurohormones. Nonetheless, one of disadvantages in the ISH method using oligonucleotide probes is that labeling of multiple sites in a single probe molecule is rather difficult. The present result that an application of a mixture of the AVP and AVP-NP probes yielded a marked increase in specific signals suggests a solution for the above problem, since an interaction between the AVP and AVP-NP probes seems to be negligible. Thus, a use of mixed probes each of which recognized a different region in the same mRNA probably enhances hybridization signals, when an increase in the sensitivity of the oligonucleotide-mRNA ISH method is required.

ACKNOWLEDGMENT

The authors would like to thank Professor S. Kawashima, Hiroshima University, for providing the antiserum to oxytocin.

REFERENCES

- 1 Ivell, R. and Richter, D. (1984) Structure and comparison of the oxytocin and vasopressin genes from rat. *Proc. Natl. Acad. Sci. USA*, **81**: 2006-2010.
- 2 Lathe, R. (1985) Synthetic oligonucleotide probes deduced from amino acid sequence data. Theoretical and practical considerations. *J. Mol. Biol.*, **183**: 1-12.
- 3 McCabe, J. T., Morrell, J. I., Ivell, R., Schmale, H., Richter, D. and Pfaff, D. W. (1986) *In situ* hybridization technique to localize rRNA and mRNA in mammalian neurons. *J. Histochem. Cytochem.*, **34**: 45-50.
- 4 Sherman, T. G., McKelvy, J. F. and Watson, S. J. (1986) Vasopressin mRNA regulation in individual hypothalamic nuclei: a northern and *in situ* hybridization analysis. *J. Neurosci.*, **6**: 1685-1694.
- 5 Uhl, G. R., Zingg, H. H. and Habener, J. F. (1985)

- Vasopressin mRNA *in situ* hybridization: localization and regulation studied with oligonucleotide cDNA probes in normal and Brattleboro rat hypothalamus. *Proc. Natl. Acad. Sci. USA*, **82**: 5555–5559.
- 6 Uhl, G. R. and Reppert, S. M. (1986) Suprachiasmatic nucleus vasopressin messenger RNA: circadian variation in normal and Brattleboro rats. *Science*, **232**: 390–393.
 - 7 Wolfson, B., Manning, R. W., Davis, L. G., Arentzen, R. and Baldino, F., Jr. (1985) Co-localization of corticotropin releasing factor and vasopressin mRNA in neurons after adrenalectomy. *Nature*, **315**: 59–61.
 - 8 Pavel, S. (1975) Vasotocin biosynthesis by neurohypophysial cells from human fetuses. Evidence for its ependymal origin. *Neuroendocrinology*, **19**: 150–159.
 - 9 Pavel, S. (1980) Presence of relatively high concentrations of arginine vasotocin in the cerebrospinal fluid of newborns and infants. *J. Clin. Endocrinol. Metab.*, **50**: 271–273.
 - 10 Nojiri, H., Sato, M. and Urano, A. (1985) *In situ* hybridization of the vasopressin mRNA in the rat hypothalamus by use of a synthetic oligonucleotide probe. *Neurosci. Lett.*, **58**: 101–105.
 - 11 Nojiri, H., Sato, M. and Urano, A. (1986) Increase in the vasopressin mRNA level in the magnocellular neurosecretory neurons of water-deprived rats: *in situ* hybridization study with the use of synthetic oligonucleotide probe. *Zool. Sci.*, **3**: 345–350.
 - 12 Fujiwara, M., Hyodo, S., Sato, M. and Urano, A. (1985) Changes in vasopressin and oxytocin mRNA levels in the rat hypothalamus by oral hypertonic saline. *Zool. Sci.*, **2**: 990 (Abstract).
 - 13 Majzoub, J. A., Rich, A., van Boom, J. and Habener, J. F. (1983) Vasopressin and oxytocin mRNA regulation in the rat assessed by hybridization with synthetic oligonucleotides. *J. Biol. Chem.*, **258**: 14061–14064.
 - 14 Wallace, R. B., Shaffer, J., Murphy, R. F., Bonner, J., Hirose, T. and Itakura, K. (1979) Hybridization of synthetic oligodeoxyribonucleotides to $\Phi \chi$ 174 DNA: the effect of single base pair mismatch. *Nucleic Acids Res.*, **6**: 3543–3557.
 - 15 Maxam, A. and Gilbert, W. (1980) Sequencing end-labeled DNA with base-specific chemical cleavages. *Methods in Enzymology*, **65**: 499–560.
 - 16 Brahic, M. and Haase, A. T. (1978) Detection of viral sequences of low reiteration frequency by *in situ* hybridization. *Proc. Natl. Acad. Sci. USA*, **75**: 6125–6129.
 - 17 Lawrence, J. B. and Singer, R. H. (1985) Quantitative analysis of *in situ* hybridization methods for the detection of actin gene expression. *Nucleic Acids Res.*, **13**: 1777–1799.
 - 18 Moench, T. R., Gendelman, H. E., Clements, J. E., Narayan, O. and Griffin, D. E. (1985) Efficiency of *in situ* hybridization as a function of probe size and fixation technique. *J. Virol. Meth.*, **11**: 119–130.
 - 19 Nojiri, H., Ishida, I., Miyashita, E., Sato, M., Urano, A. and Deguchi, T. (1987) Cloning and sequence analysis of cDNAs for neurohypophysial hormones vasotocin and mesotocin for the hypothalamus of toad, *Bufo japonicus*. *Proc. Natl. Acad. Sci. USA*, **84**: 3043–3046.
 - 20 McBride, L. J. and Caruthers, M. H. (1983) An investigation of several deoxynucleoside phosphoramidites useful for synthesizing deoxyoligonucleotides. *Tetrahedron Lett.*, **24**: 245–248.
 - 21 Hayashi, S., Gillam, I. C., Delaney, A. D. and Tener, G. M. (1978) Acetylation of chromosome squashes of *Drosophila melanogaster* decreases the background in autoradiographs from hybridization with [¹²⁵I]-labeled RNA. *J. Histochem. Cytochem.*, **26**: 677–679.
 - 22 Kelsey, J. E., Watson, S. J., Burke, S., Akil, H. and Roberts, J. L. (1986) Characterization of proopiomelanocortin mRNA detected by *in situ* hybridization. *J. Neurosci.*, **6**: 38–42.
 - 23 Jokura, Y. and Urano, A. (1985) Projections of luteinizing hormone-releasing hormone and vasotocin fibers to the anterior part of the preoptic nucleus in the toad, *Bufo japonicus*. *Gen. Comp. Endocrinol.*, **60**: 390–397.

Effect of Hypothalamic Extract on the Prolactin Release from the Bullfrog Pituitary Gland with Special Reference to Thyrotropin-Releasing Hormone (TRH)

TATSUNORI SEKI, SAKAE KIKUYAMA¹ and MITSUO SUZUKI²

Department of Anatomy, Juntendo University School of Medicine, Bunkyo-ku, Tokyo 113, and ¹Department of Biology, School of Education, Waseda University, Shinjuku-ku, Tokyo 160, and ²Department of Physiology, Institute of Endocrinology, Gunma University, Maebashi 371, Japan

ABSTRACT—Acid extract of bullfrog hypothalami but not of rat hypothalami stimulated the release of prolactin (PRL) from the bullfrog pituitary gland *in vitro*. Since frog hypothalamus is known to contain thyrotropin-releasing hormone (TRH), a stimulator of PRL release, much more than rat hypothalamus, experiments were performed to determine whether PRL-releasing activity of the frog hypothalamic extract is derived from TRH it contains. PRL-releasing activity in the hypothalamic extract was nullified by incubation with bullfrog plasma. When the extract was fractionated on Sephadex G-25 chromatography, significant PRL-releasing activity was found in the fraction which is presumed to contain TRH. The activity of the hypothalamic extract was markedly reduced by co-incubation with IgG fraction separated from antiserum to TRH. These results indicate that TRH is one of the major PRL-releasing factors in the hypothalamic extract.

INTRODUCTION

Acid extract of the amphibian hypothalamus is known to stimulate the release of prolactin (PRL) from amphibian pituitary glands [1-3]. However, little is known about the identity of PRL-releasing factor in the hypothalamic extract. On the other hand, synthetic thyrotropin-releasing hormone (TRH) shows a potent PRL-releasing activity in amphibians [2, 4-7] as well as in mammals [8]. In amphibians, it is not clear whether TRH regulates TSH secretion. According to the results obtained by most of the investigators, there is no indication that synthetic TRH stimulates TSH release from amphibian pituitary gland [9-12], while some recent data pointed out the possibility that TRH induces TSH release in the amphibian [13]. It has been reported that hypothalamic TRH concentration is much higher in amphibians than in mammals [11, 14-16]. Immunohistochemical study of the bullfrog hypothalamus revealed that TRH

neurons exist in the hypothalamus and their axons terminate in the median eminence, suggesting that TRH neurons have a physiological role in the regulation of adenohipophyseal hormone release [16].

The present investigation was undertaken to ascertain whether the PRL-releasing activity in the hypothalamic extract is due to TRH. A preliminary report has been published elsewhere [3].

MATERIALS AND METHODS

Incubation of pituitary gland

Adult bullfrog (*Rana catesbeiana*) weighing 250-400 g were sacrificed by decapitation. The anterior pituitary gland was removed, weighed and hemisected. Two hemipituitaries were placed in a glass vial containing 200 μ l of 67% Eagle MEM (Nissui Seiyaku Co., Ltd., pH 7.4). The vials were incubated in a Dubnoff metabolic incubator in an atmosphere of 95% O₂-5% CO₂. After 1 hr of preincubation, the medium was replaced with fresh one containing a test substance. Incubation was

carried out for 8 hr at 25°C, since it was previously verified that bullfrog pituitaries incubated in the same condition as described above continue to release PRL until at least 28 hr at a linear rate [7].

Radioimmunoassay

PRL in the medium was measured by a homologous radioimmunoassay for bullfrog PRL developed in Yamamoto and Kikuyama [17].

Preparation of tissue extract

Fresh hypothalami were homogenized in cold 0.1 N HCl (50 μ l/hypothalamus) with a teflon homogenizer and centrifuged at 10,000 \times g for 30 min. The supernatant was neutralized with 1 N NaOH and recentrifuged. Acid extracts of frog cerebrum, frog neuro-intermediate lobe and rat hypothalamus were prepared in the same manner.

Inactivation of PRL-releasing activity of hypothalamic extract by frog plasma

Fifty microliters of the extract (one hypothalamic equivalent) was mixed with 50 μ l of bullfrog plasma or distilled water and incubated for 3 hr at 37°C. After incubation, PRL releasing activity of this mixture was tested.

Chromatography

Hypothalamic extract, derived from 200 hypothalamic fragments was filtered through Millipore filter (HAWP) and applied to a 1.5 \times 110 cm Sephadex G-25 column. Each fraction consisting of 3 ml was collected by eluting with 0.1 N acetic acid. ³H-TRH (1-proline-2, 3-H(N)-TRH, New England Nuclear) was also chromatographed to determine the position in which TRH is eluted. Fractions were assembled into three pools; fraction I (FI) eluted faster than TRH, fraction II (FII) eluted with TRH and fraction III (FIII) eluted later than TRH. The pooled fractions were lyophilized, dissolved in the incubation medium and tested for PRL-releasing activity.

Inactivation of PRL-releasing substance by IgG from anti-TRH serum

Immunoneutralization of hypothalamic TRH was performed by the use of IgG fraction from anti-TRH serum which had been prepared by

immunizing rabbit with TRH conjugated to bovine serum albumin according to the procedures described previously [18]. Protein A (Pharmacia Fine Chemicals) was combined with CNBr-activated Sepharose 4B (Pharmacia Fine Chemicals) by the method of Miller and Stone [19]. Anti-TRH serum or normal rabbit serum was applied to 0.8 \times 4.5 cm protein A-Sepharose column. The IgG fraction was dialyzed, lyophilized and dissolved in 50 mM Hepes buffer containing 0.7% NaCl (HBS). Hypothalamic extract was incubated with the solution of IgG from anti-TRH serum, from normal rabbit serum (NRS) or HBS at 4°C for 48 hr. After incubation, the medium was centrifuged. To test the PRL-releasing activity, aliquot of the supernatant was added to the medium in which pituitaries were placed. One milliliter of medium used for the test contained the extract from 0.2 hypothalamus which had been incubated with IgG obtained from 60 μ l of anti-serum or NRS. It has been ascertained that 1 μ l of the antiserum can inactivate nanogram quantities of TRH.

RESULTS

The response of bullfrog pituitaries to various doses of frog hypothalamic extract is shown in Figure 1. Hypothalamic extract, equivalent to 0.01–1 hypothalamic fragment stimulated the release of PRL from bullfrog pituitary gland in a dose-dependent manner. The dose of 0.1 and 1 hypothalamic equivalent per 1 ml medium caused a significant increase in the PRL release.

Effect of rat hypothalamic extract on the PRL release from the bullfrog pituitary gland was examined. No significant difference in the amount of PRL released into the medium was observed between the control medium (300 \pm 39 ng/mg pituitary) and the medium containing extract from one rat hypothalamus per milliliter (349 \pm 53 ng/mg pituitary).

PRL-releasing activities of extracts from the hypothalamus, cerebrum and neuro-intermediate lobe of the pituitary gland were shown in Figure 2. Addition of the extract from the hypothalamus or neuro-intermediate lobe to the medium significantly enhanced the release of PRL. The extract from

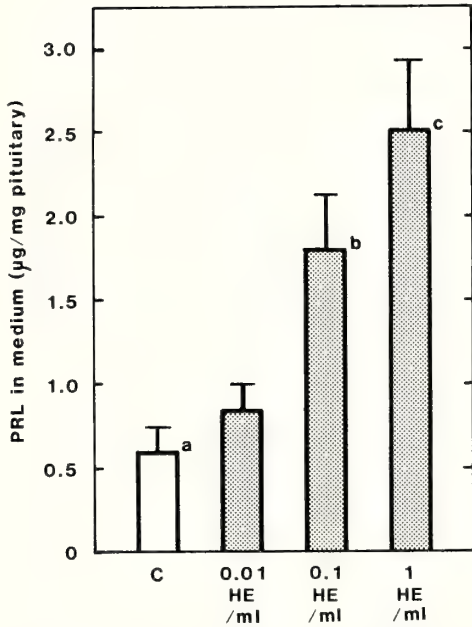


FIG. 1. Effect of various doses of hypothalamic extract (HE) on PRL release. One milliliter of medium contains acid extract from 0.01–1 hypothalamus. C, control medium. Each value represents mean \pm SEM for 7 determinations. Significance of difference (analysis of variance): a vs b, a vs c, $P < 0.001$.

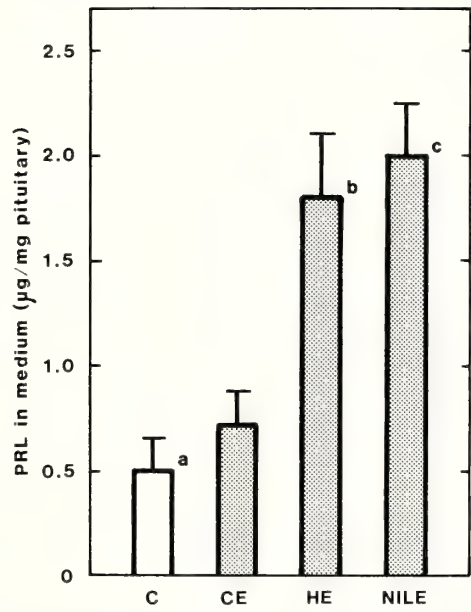
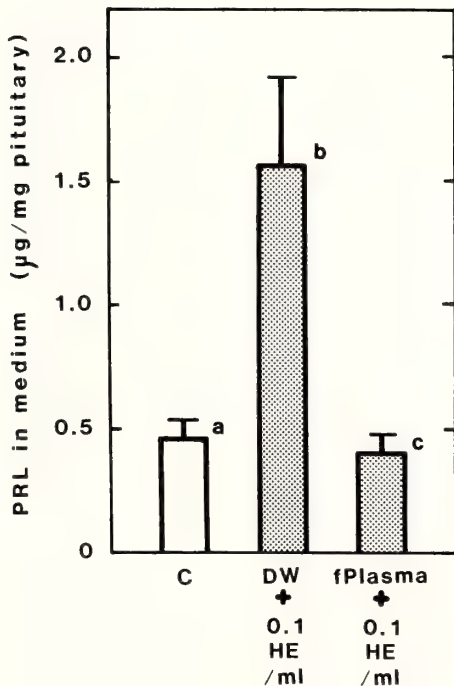


FIG. 2. Effect of extract of cerebrum (CE), hypothalamus (HE) and neuro-intermediate lobe (NILE) on PRL release. One milliliter of medium contains extract from 3 mg of each tissue. Each value represents mean \pm SEM for 7 determinations. Significance of difference (analysis of variance): a vs b, a vs c, $P < 0.001$.



the cerebrum caused a slight increase, but this increase was statistically not significant.

When the hypothalamic extract was incubated with bullfrog plasma, the PRL-releasing activity was completely lost (Fig. 3).

Figure 4 shows the profiles of Sephadex G-25 chromatography of the hypothalamic extract and the distribution of radioactivity of ^3H -TRH when chromatographed. Among the three pooled samples, FII exhibited a marked stimulatory effect on the PRL release, while FIII had no releasing activity and FI had a slight but not significant

FIG. 3. Effect of bullfrog plasma on PRL-releasing activity of bullfrog hypothalamic extract. One milliliter of medium contains extract from 0.1 hypothalamus subsequently incubated with distilled water (DW) or bullfrog plasma as described in Materials and Methods. Each value represents mean \pm SEM for 7 determinations. C, control medium. Significance of difference (analysis of variance): a vs b, a vs c, $P < 0.001$.

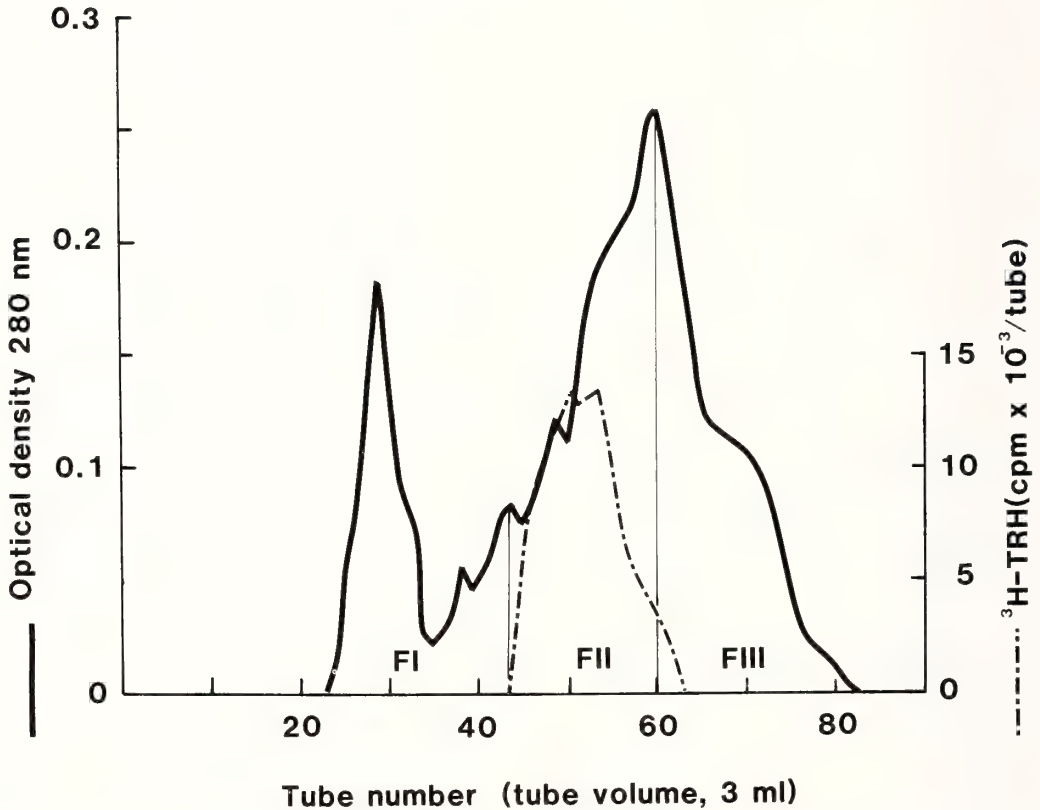


FIG. 4. Sephadex G-25 column (1.5×110 cm) chromatography of bullfrog hypothalamic extract and of ³H-TRH. Absorbance at 280 nm is denoted by the continuous line and radioactivity of ³H-TRH by the broken line.

releasing activity (Fig. 5).

Figure 6 shows the effect of immunoneutralization of TRH in the hypothalamic extract on the PRL release. Hypothalamic extract incubated with either IgG from NRS or HBS stimulated the PRL release. Incubation of the hypothalamic extract with IgG from anti-TRH serum considerably diminished the PRL-releasing activity of the hypothalamic extract.

DISCUSSION

It was demonstrated by the present experiment that the frog hypothalamic extract is effective in promoting PRL release from the bullfrog pituitary gland *in vitro*, while the rat hypothalamic extract is ineffective. It has also been reported that the frog hypothalamic extract stimulates the release of PRL from the rat pituitary gland [20]. These results

indicate that the effect of frog hypothalamic extract on the PRL release is predominantly stimulatory.

TRH is known to have a potent PRL-releasing activity in amphibians [2-6] as well as in mammals [8]. Among the three fractions separated from the bullfrog hypothalamic extract by Sephadex G-25 chromatography, the fraction (FII) which is presumed to contain TRH had the strongest PRL-releasing activity. In the present experiment, no attempt was made to eliminate PRL-inhibiting factors presumed to be present in the hypothalamic extract. Dopamine existing in the frog hypothalamus has been postulated to be a PRL-inhibiting factor [5, 21-25]. According to our test-run on Sephadex G-25 column, the monoamine was eluted later than TRH, indicating that dopamine will be included in FIII. Immunoneutralization of the hypothalamic extract

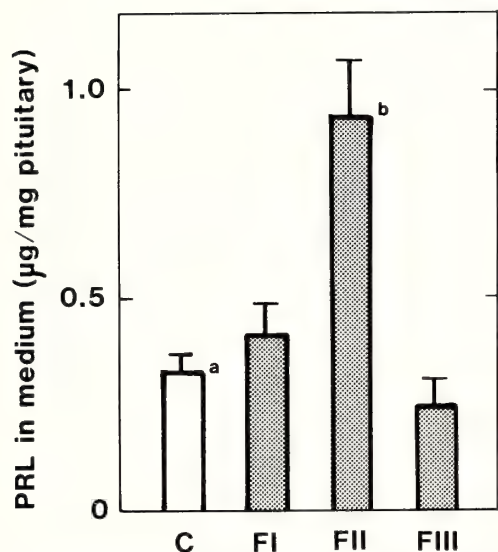


FIG. 5. Distribution of PRL-releasing activity among fractions obtained by gel-filtration of bullfrog hypothalamic extract on Sephadex G-25. One milliliter of medium contains each fraction derived from 0.1 hypothalamus. Each value represents mean \pm SEM for 7 determinations. Significance of difference (analysis of variance): a vs b, $P < 0.001$.

with IgG separated from anti-TRH serum resulted in a considerable degradation of PRL-releasing activity. These results strongly suggest that PRL-releasing activity in the hypothalamic extract is largely derived from TRH it contains. In perinatal rats, it has also been demonstrated that the PRL-releasing activity in the hypothalamic extract is attributable to the existing TRH [26].

The PRL-releasing activity of the hypothalamic extract was completely abolished by incubation with frog plasma. Preliminary study also revealed that NRS as well as anti-TRH serum inactivated the PRL-releasing activity of the hypothalamic extract. This may be the result of enzymatic degradation of substances bearing PRL-releasing activity. It is well known that TRH is degraded rapidly in the blood [27]. Accordingly, we used IgG fraction instead of antiserum for immunoneutralization.

The present experiment revealed that extract of neuro-intermediate lobe tissue possesses a marked PRL-releasing activity. Neuro-intermediate lobe tissue as well as the hypothalamus of bullfrogs

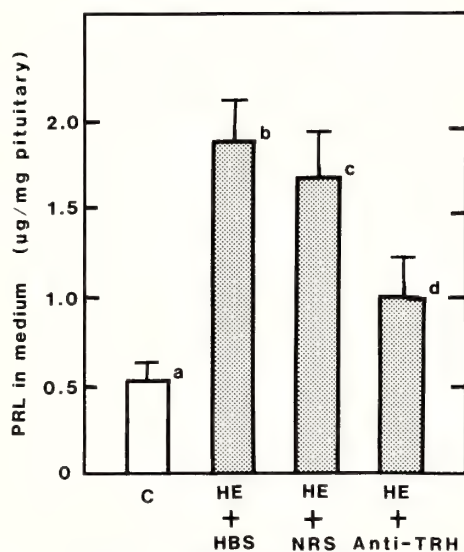


FIG. 6. Effect of immunoneutralization of hypothalamic TRH on PRL release. One milliliter of medium contains acid extract from 0.2 hypothalamus which had been subsequently incubated with 60 μ l of 50 mM HEPES buffer containing 0.7% NaCl (HBS), IgG from normal rabbit serum (NRS) or IgG from anti-TRH serum. Each value represents mean \pm SEM for 7 determinations. C, control medium. Significance of difference (analysis of variance): a vs b, a vs c, b vs d, c vs d, $P < 0.001$; a vs d, $P < 0.01$.

contains a considerable amount of TRH [15, 16]. Accordingly, the stimulatory effect of the extract from neuro-intermediate lobe may partly be due to TRH. In mammals, it has been reported that extract of posterior pituitary or hypophyseal stalk contains a PRL-releasing activity and that the substance in the extract is distinct from TRH [28-31].

In the present experiment, an excess amount of IgG from anti-TRH serum was applied for the immunoneutralization of TRH in the hypothalamic extract, taking into consideration of the TRH content in the bullfrog hypothalamus [16]. However, complete depression of PRL-releasing activity was not observed. This suggests the existence of PRL-releasing factors other than TRH in the frog hypothalamic extract. Several substances such as vasoactive intestinal peptide (VIP) and peptide histidine isoleucine (PHI) are known to stimulate PRL release from the pituitary gland

in amphibians [32] as well as in mammals [33–36]. Identification of other PRL-releasing substances in the bullfrog hypothalamus is under way.

ACKNOWLEDGMENTS

This work was supported by a Grant-in-Aid for Scientific Research from the Ministry of Education, Science and Culture, Japan and by a grant from Waseda University.

REFERENCES

- Hall, T. R. and Chadwick, A. (1979) Hypothalamic control of prolactin and growth hormone secretion in different vertebrate species. *Gen. Comp. Endocrinol.*, **37**: 333–342.
- Hall, T. R. and Chadwick, A. (1984) Effect of synthetic mammalian thyrotropin releasing hormone, somatostatin and dopamine on the secretion of prolactin and growth hormone from amphibian and reptilian pituitary glands incubated *in vitro*. *J. Endocrinol.*, **102**: 175–180.
- Seki, T. and Kikuyama, S. (1986) Possible involvement of thyrotropin-releasing hormone in the release of prolactin from the hypophysis of the bullfrog. In "Pars Distalis of the Pituitary Gland—Structure, Function and Regulation". Ed. by F. Yoshimura and A. Gorbman, Elsevier Science Publisher B. V., Amsterdam, pp. 247–249.
- Clemons, G. K., Russell, S. M. and Nicoll, C. N. (1979) Effect of mammalian thyrotropin-releasing hormone on prolactin secretion by bullfrog adenohypophyses *in vitro*. *Gen. Comp. Endocrinol.*, **38**: 62–67.
- Kikuyama, S. and Seki, T. (1983) Dopamine and serotonin control of prolactin release in bullfrog. In "Neuropeptides, Neurotransmitters and Regulation of Endocrine Processes". Ed. by E. Endroczi, Academiai Kiado, Budapest, pp. 317–324.
- Kühn, E. R., Kikuyama, S., Yamamoto, K. and Darras, V. M. (1985) *In vivo* release of prolactin in *Rana ridibunda* following an intravenous injection of thyrotropin-releasing hormone. *Gen. Comp. Endocrinol.*, **60**: 86–89.
- Seki, T. and Kikuyama, S. (1986) Effect of thyrotropin-releasing hormone and dopamine on the *in vitro* secretion of prolactin by the bullfrog pituitary gland. *Gen. Comp. Endocrinol.*, **61**: 197–202.
- Vale, W., Rivier, C. and Brown, M. (1977) Regulatory peptides of the peptides of the hypothalamus. *Ann. Rev. Physiol.*, **39**: 473–527.
- Etkin, W. and Gona, A. G. (1986) Failure of mammalian thyrotropin releasing factor preparation to elicit metamorphic response in tadpoles. *Endocrinology*, **82**: 1067–1068.
- Gona, A. G. and Gona, O. (1974) Failure of synthetic TRF to elicit metamorphosis in frog tadpoles or red-spotted newts. *Gen. Comp. Endocrinol.*, **24**: 223–225.
- Taurog, A., Oliver, C., Eskay, R. L., Porter, J. C. and McKenzie, J. M. (1974) The role of TRH in the neoteny of the Mexican axolotl (*Ambystoma mexicanum*). *Gen. Comp. Endocrinol.*, **24**: 267–279.
- Vandesande, F. and Aspeslagh, M. R. (1974) Failure of thyrotropin releasing hormone to increase ¹²⁵I uptake by the thyroid in *Rana temporaria*. *Gen. Comp. Endocrinol.*, **23**: 355–356.
- Darras, V. M. and Kühn, E. R. (1985) Increased plasma levels of thyroid hormones in a frog *Rana ridibunda* following intravenous administration of TRH. *Gen. Comp. Endocrinol.*, **48**: 469–475.
- Giraud, P., Gillioz, P., Conte-Devolx, B. and Oliver, C. (1979) Distribution de thyroliberine (TRH), α -melanocyte-stimulating hormone (α -MSH) et somatostatine dans les tissue de la Grenouille verte (*Rana esculenta*). *C. R. Acad. Sci. Paris, Ser. D.*, **228**: 127–129.
- Jackson, I. M. D. and Reichlin, S. (1974) Thyrotropin-releasing hormone (TRH): Distribution in hypothalamic and extra-hypothalamic brain tissues of mammalian and submammalian chordates. *Endocrinology*, **95**: 854–862.
- Seki, T., Nakai, T., Shioda, S., Mitsuma, T. and Kikuyama, S. (1983) Distribution of immunoreactive thyrotropin-releasing hormone in the forebrain and hypophysis of the bullfrog, *Rana catesbeiana*. *Cell Tissue Res.*, **233**: 507–516.
- Yamamoto, K. and Kikuyama, S. (1982) Radioimmunoassay of prolactin in plasma of bullfrog tadpoles. *Endocrinol. Japon.*, **29**: 159–167.
- Nishiyama, T., Heike, Y., Matsuzaki, T., Kawano, H., Daikoku, S. and Suzuki, M. (1983) Immunoreactive TRH-containing neurones in the rat hypothalamus. *Biomed. Res., Suppl.* **4**: 65–74.
- Miller, T. J. and Stone, H. O. (1978) The rapid isolation of ribonuclease-free immunoglobulin G by protein A-Sepharose affinity chromatography. *J. Immunol. Methods*, **24**: 111–125.
- Kühn, E. R. and Engelen, H. (1976) Seasonal variation in prolactin and TSH releasing activity in the hypothalamus of *Rana temporaria*. *Gen. Comp. Endocrinol.*, **28**: 277–282.
- Alonso-Bedate, M. and Delgado, M. J. (1983) Effects of prolactin and bromocriptine in *Discoglossus pictus* Otth (anuran amphibian) tadpoles. *Comp. Biochem. Physiol.*, **74A**: 763–772.
- Kikuyama, S. and Seki, T. (1980) Possible involvement of dopamine in the release of prolactin-like hormone from bullfrog pituitary gland. *Gen. Comp.*

- Endocrinol., **41**: 173–179.
- 23 Platt, J. E. (1976) The effects of ergocornine on the tail height, spontaneous and T₄-induced metamorphosis and thyroidal uptake of radioiodide in neonetic *Ambystoma tigrinum*. Gen. Comp. Endocrinol., **28**: 71–81.
- 24 Seki, T. and Kikuyama, S. (1979) Effect of ergocornine and reserpine on metamorphosis in *Bufo bufo japonicus* tadpoles. Endocrinol. Japon., **26**: 675–678.
- 25 Seki, T. and Kikuyama, S. (1982) *In vitro* studies on the regulation of prolactin secretion in the bullfrog pituitary gland. Gen. Comp. Endocrinol., **46**: 473–479.
- 26 Khorram, O., Depalatis, L. R. and McCann, S. M. (1984) Hypothalamic control of prolactin secretion during the perinatal period in the rat. Endocrinology, **115**: 1698–1704.
- 27 McKelvy, J. F. (1983) Enzymatic degradation of brain peptides. In "Brain Peptides". Ed. by D. T. Krieger, M. J. Brownstein and J. B. Martin, John Wiley & Sons, New York, pp. 117–134.
- 28 Boyd, III, A. E., Spencer, E., Jackson, I. M. D. and Reichlin, S. (1976) Prolactin-releasing factor (PRF) in porcine hypothalamic extract distinct from TRH. Endocrinology, **99**: 861–871.
- 29 Kokubu, T., Sawano, S., Shiraki, M., Yamasaki, M. and Ishizuka, Y. (1975) Extraction and partial purification of prolactin-release stimulating factor in bovine hypothalamus. Endocrinol. Japon., **22**: 213–217.
- 30 Szabo, M. and Frohman, L. A. (1976) Dissociation of prolactin-releasing activity from thyrotropin-releasing hormone in porcine stalk median eminence. Endocrinology, **98**: 1451–1459.
- 31 Yasuda, N., Yasuda, Y. and Greer, S. E. (1984) Heterogeneity of activity of the prolactin-releasing factor in the bovine hypothalamo-neurohypophysial complex. J. Endocrinol., **103**: 243–249.
- 32 Koiwai, K., Kikuyama, S., Seki, T. and Yanaihara, N. (1986) *In vitro* effect of vasoactive intestinal polypeptide and peptide histidine isoleucine of prolactin secretion by the bullfrog pituitary gland. Gen. Comp. Endocrinol., **64**: 254–259.
- 33 Kato, Y., Iwasaki, Y., Iwasaki, J., Abe, H., Yanaihara, N. and Imura, H. (1978) Prolactin release by vasoactive intestinal polypeptide in rats. Endocrinology, **103**: 554–558.
- 34 Ruberg, N., Rotsztein, W. E., Aranchibia, S., Beson, J. and Enjalbert, A. (1978) Stimulation of prolactin release by vasoactive intestinal peptide (VIP). Eur. J. Pharmacol., **51**: 319–320.
- 35 Samson, W. K., Lumpkin, M. D., McDonald, J. K. and McCann, S. M. (1985) Prolactin-releasing activity of porcine intestinal peptide (PHI-27). Peptides, **4**: 817–819.
- 36 Werner, S., Hulting, A. L., Hökfelt, T., Eneroth, P., Tatemoto, K., Mutt, V., Moroder, L. and Wunsch, E. (1983) Effect of the peptide PHI-27 on prolactin release *in vitro*. Neuroendocrinol., **37**: 476–478.

Morphology and Distribution of the Skin Glands in *Xenopus laevis* and Their Response to Experimental Stimulations

KEIKO FUJIKURA, SHINGO KURABUCHI¹, MASAHIRO TABUCHI
and SAKAE INOUE

*Department of Comparative Endocrinology, Institute of Endocrinology,
Gunma University, Maebashi 371, and ¹Department of Anatomy,
Nippon Dental University, Tokyo 102, Japan*

ABSTRACT—Four types of skin glands were observed in the skin of adult *Xenopus laevis*. Among them, the mucous and the granulated glands showed similar morphological characteristics with those previously reported. In this report, we made detailed description on the saccular gland (referred to as NP gland in the present study) of the male nuptial pad. The small granulated gland which has not been reported so far is also described. The granulated gland and the NP gland were observed to receive innervation inside the secretory compartments. The NP glands were only distributed in the nuptial pad of the male forelimb while the other three kinds of glands were widely distributed throughout the body surface. When the frogs were kept under waterless conditions, the mucous glands secreted a watery substance, the cross sectional area of the skin occupied by the mucous glands being reduced to 46–71% of the control. While, the granulated gland and the small granulated gland were less affected by the water deprivation. Evacuation of contents of the skin glands was recognized only in the mucous glands. After hypophysectomy, a significant decrease in the area of the NP glands occurred accompanied by the disappearance of the nuptial pad, while the mucous and the granulated glands were unchanged. A possible enhanced secretory activity of the small granulated glands was encountered after hypophysectomy. Isoproterenol induced the discharge of viscid white material from the contracted granulated gland both *in vivo* and *in vitro*, while other types of skin of glands seemed to be unchanged by this chemical.

INTRODUCTION

The skin glands of amphibians have been classified into major types, *viz.*, the granulated glands and the mucous glands, based mainly on light microscopic observations [1, 2]. The granulated glands are involved in protecting the body through their poisonous or irritating secretions in response to violent stimulation [3], while the mucous glands produce a watery secretion containing Na^+ and Cl^- that keeps the skin moist and controls its permeability [4]. Among the skin glands of *Xenopus laevis*, the granulated gland has been intensely investigated mainly due to interest in the biochemistry of its secretion. The granulated gland of *X. laevis* has been reported to contain

thyrotrophin releasing hormone, 5-hydroxytryptamine [5] and caerulein [6, 7]. Dockray and Hopkins [6] also reported that the dermal layer of the dorsal skin of *X. laevis* contains several kinds of glandular structures, but there was no description of gland other than the granulated and mucous glands.

During the course of the investigation of the nuptial pad of male *X. laevis* [8], two other types of skin glands could be differentiated. Berk [9] briefly described one of them as a simple saccular gland in the nuptial pad, and the other has not been possibly identified in any previous report cited. In the present paper we provide a classification of different types of skin glands of adult *X. laevis* after studying of fourteen regions all over the body surface of both sexes accompanied with a study of changes in these glands after exposing frogs to a waterless condition, hypophysectomy

and adrenergic stimulation. The possible relationship of these glands to the internal and environmental modifications is also discussed.

MATERIALS AND METHODS

Animals

The African clawed frogs *X. laevis* which were successively kept in our laboratory were used.

Light and electron microscopy

Excised skin pieces from frogs, after decapitation and pithing or under 0.5% ethyl m-aminobenzoate methanesulfonate anesthesia, were fixed with Bouin's fluid, processed routinely for light microscopy and stained with Mallory's trichrome. To study on the distribution of skin glands through the body surface, pieces of skin of about 2 cm square were excised from fourteen selected areas from both sexes as shown in Figure 3. To study the ultrastructure, skin pieces were fixed in 3% glutaraldehyde followed by postfixation with 1% osmium tetroxide and embedded in an Epon-Araldite mixture. The prepared ultra-thin sections were observed with HITACHI HS-8 and LEM 2000 electron microscopes.

Response of the skin glands to various experimental conditions

Dry milieu Adult frogs of various body weights were housed in separate containers without water (75–80% humidity and $21 \pm 0.5^\circ\text{C}$). Body weight was recorded every 24 hr exactly. At later stages of the experiment, pieces of skin in the central regions of ventral and dorsal sides were dissected out and processed for histological observation.

Hypophysectomy Adult males with well-developed nuptial pads were hypophysectomized. Frogs then were observed for macroscopic changes in their nuptial pads. Representative frogs were sacrificed on 12 and 40 days and at 15 months after the operation for histological observation. All quantitative measurements of the area, length and number of glands and of skin were carried out with an image analyzing apparatus (VIP, 121CH, Olympus Co., Japan).

Sympathomimetic stimulation The response of skin glands to isoproterenol was tested *in vivo* and *in vitro* as follows.

Experiment 1; For the *in vivo* study, 2 ml of isoproterenol (ISP) (Sigma) at a concentration of 2×10^{-2} M/100 g body weight was subcutaneously injected into the adult frogs.

Experiment 2; An *in vivo* study concerning the interruption of vascularization and innervation of skin pieces was done as follows. Pieces of dorsal skin about 1.5×1.0 cm in size were first cut completely free from their surroundings, and were then stitched into the same position as before. Seven days after the operations, the frogs were subcutaneously injected with ISP and their responses were observed.

Experiment 3; For *in vitro* study explants about 2 cm square were taken from the middle of the dorsal or ventral sides and were immersed in Ringer solution or TCM 199 solution for up to 14 days. Response of the freshly excised skin to ISP was first tested employing the solutions containing ISP in concentrations of 10^{-1} to 10^{-5} M. The pieces of skin incubated were transferred every other day to the solution containing 10^{-1} M ISP to examine their reactivity.

Noradrenaline (Sigma) was also used *in vivo* and *in vitro* study to test the reaction of the skin glands.

RESULTS

Morphological characteristics of the classified skin glands

Through the microanatomical observations of the skin from several regions of the body surface, the following four types of skin glands were identified.

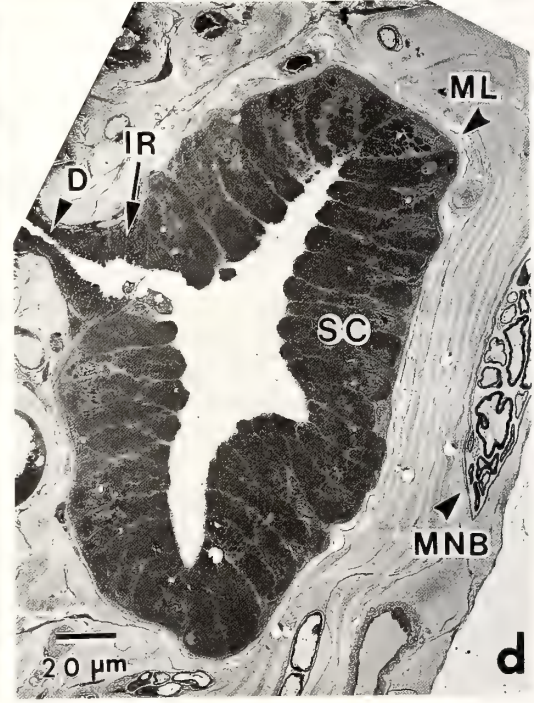
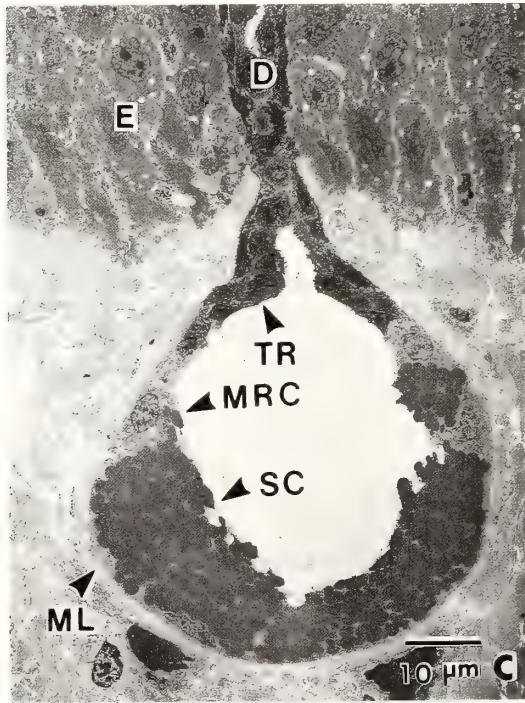
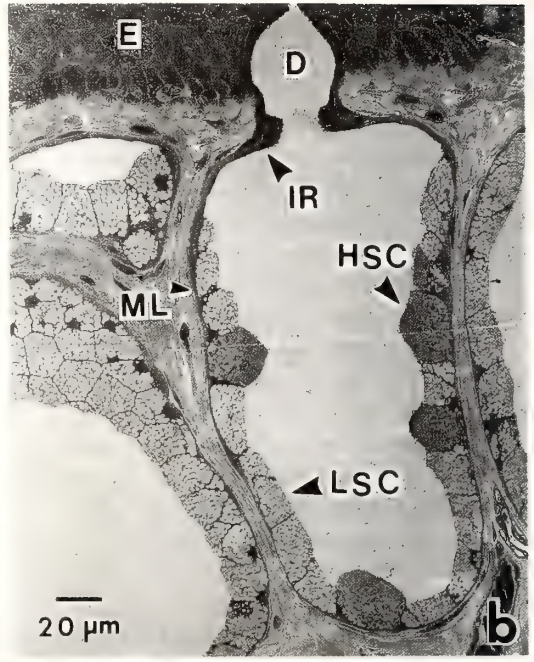
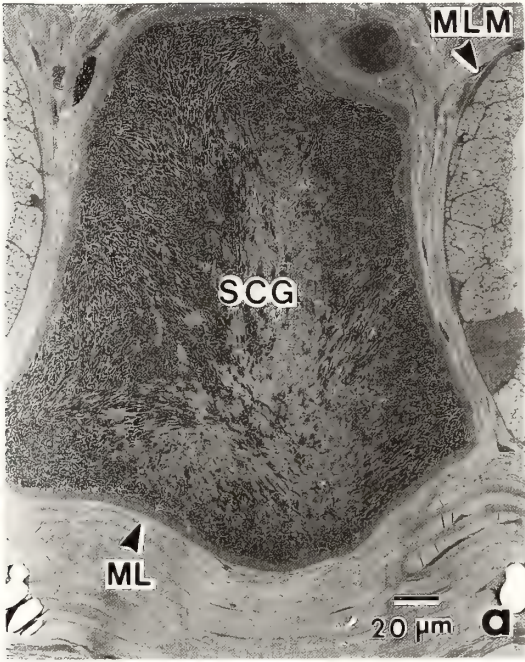
The granulated gland The granulated gland was composed of a secretory compartment, a duct and an intermediated region connecting them. This type of gland was largest of the four types of glands observed, ranging 150 μm up to 200 μm in height and 200 to 400 μm in diameter. Above all the dorsal side of a large-sized female observed had a group of the largest granulated glands, measuring from 350 to 450 μm in height and from 300 to 550 μm in diameter. The secretory compart-

ment consists of a syncytial sac surrounded by a myoepithelial cell layer (Fig. 1a). In a histological view of a gland which might be a median profile of a secretory compartment, there were observed twelve peripherally arranged nuclei profiles with their long axes parallel to the myoepithelial layer. The electron microscopic (EM) observations revealed that the secretory granules which occupy the greater part of the syncytial cell were elipsoidal in shape, measuring $2.7 \times 0.8 \mu\text{m}$ in average. These secretory granules were membrane-bounded and varied in electron density. Their contents were heterogeneous showing electron dense stripes randomly distributed and running parallel to the long axes of the granules (Fig. 7a, b, c). In the cytoplasm, well-developed rough ER and Golgi apparatus were observed surrounding the nucleus. In the area of the Golgi apparatus small dense granules were prominent, some of them appeared to be larger and membrane-bounded containing homogeneous substance, which might be a sign of the formation of secretory granules.

In the intermediate region between the secretory compartment and the excretory duct, two different types of small cells were observed. The cells located at the inner side, i.e. near the compartment, have a central large nucleus and distinct microvilli projecting into the ductal lumen with no secretory granules. On the other hand, the outer side cells were larger than the inner ones, interdigitated with each other and continued to the ductal cells. The excretory ducts of the glands were opened throughout its length onto the surface of the skin, and some secretory materials were occasionally found to remain in the ductal lumen. The duct was a bilayered structure whose cells are columnar, the outer cells being a little slenderer than the inner ones. The myoepithelial cells which completely envelop the secretory compartment are cuboidal in cross section and their width and height were about $7\text{--}9 \mu\text{m}$ and $4\text{--}6 \mu\text{m}$, respectively. The individual myoepithelial cells in longitudinal sections were found to face each other with indented cellular surface on which desmosomes were frequently seen. Thick myofilaments were distributed equally through the cytoplasm and the smooth ER were well developed in the peripheral cytoplasm

facing the secretory cells (Fig. 7a) or adjacent to the myoepithelial cells. Numerous pinocytotic vesicles were found along the plasma membrane of the myoepithelial cells, especially facing the secretory cell cytoplasm. Irregular finger-like projections from the secretory cells came close to the myoepithelial cells and desmosomes were found in these areas, especially in contracted cells (Fig. 7b). Extreme contractions of the myoepithelial layers of the granulated gland were always present in the biopsied specimens whose secretory products were expelled via the excretory ducts. Both myelinated and non-myelinated nerve bundles, capillaries and melanocytes were found in the subcutaneous connective tissue around the gland. In the vicinity of the granulated gland, nerve bundles were divided into small nerve branches and the non-myelinated nerve bundles were seen close to the glands. It was observed that these non-myelinated fibers run through the intercellular spaces between the adjacent myoepithelial cells and are distributed in the intercellular spaces between the myoepithelial cells and the secretory cells with a number of nerve ending structures on the surfaces of the myoepithelial cells or of the secretory cells (Fig. 2a). Occasionally these nerve endings were found to rest on the deeply concave surfaces of the secretory cells. No partial thickening like pre- or postsynaptic membrane could be found in these areas. Individual nerve endings were seen to contain a large number of small vesicles of the size of synaptic vesicles (about $50\text{--}60 \text{ nm}$), a few cored vesicles (about $100\text{--}150 \text{ nm}$) and mitochondria. The serially arranged pinocytotic vesicles along the surfaces of myoepithelial cells were frequently opened toward the intercellular spaces at places close to nerve ending structures.

The mucous gland The mucous gland was composed of a secretory compartment, a duct and an intermediate region between them (Fig. 1b). The glands of this type in the male under normal conditions measured approximately $125 \mu\text{m}$ in height and $184 \mu\text{m}$ in width. In cross sectional profile the secretory cells were found to be arranged in a monolayered or a multilayered pattern along the periphery of the secretory compartment, and in horizontal section they appeared somewhat pentagonal in shape. Most of



them were stained light blue with Mallory's triple stain and some were stained dense blue. With the EM, the structural cells of a compartment could be classified into two types, one appearing as a low density cell possessing granules of low electron density and the other a high density cell with electron-dense granules (Fig. 1b). The latter type had a strongly positive periodic acid-Schiff (PAS) reaction. The first type of secretory cells was found to be the prevailing type while the second type was less represented, forming only about one quarter of the total number of secretory cells in a compartment. With the EM, the clear granules were occasionally seen to be vacuolated square, pentagonal or round in shape measuring $2.4 \mu\text{m}$ along the longer axis and $1.7 \mu\text{m}$ along the shorter axis in average (Fig. 2b). Dark granules were not uniform, were of varied deformed eggplant shapes and contained irregular filamentous deposits that run roughly parallel to the long axis of the granules. They occasionally fused with each other. Numerous dark spots were also present in the granules. The nuclei of cells were situated basally and surrounded by a moderate number of rough ER. Many interdigitations and occasional desmosomes were found in the intercellular space between the neighbouring secretory cells. Toward the basal region of the excretory duct, the cell type in the secretory compartment changed abruptly. In this area the cells adjacent to the secretory cells were slender and elongated containing a moderate number of mitochondria with no secretory granules. This cell type was adjoined to a cell aggregation forming the base of the excretory duct (Fig. 1b). In this cell aggregation, the inner side cells which were adjoined to the ductal cells were small and columnar in shape. They possessed large nuclei and were provided with numerous microvil-

li. The outer side cells were elongated and almost the same size as the inner side cells. Well-developed interdigitations were observed between the inner and the outer side cells, occasionally with desmosomes. These cells were adjoined to the bilayered ductal cells of which the inner side cells were of small and columnar shape. The outer side cells were slightly larger than the inner side cells. Cornified ductal cells were continuation of the epidermal cornified layer. The myoepithelial cells surrounding the mucous gland were flat and elongated and not so thick as those of the granulated gland (Figs. 1b and 2a), measuring 0.6 to $0.8 \mu\text{m}$ in thickness which is about one tenth of that of granulated gland. The intercellular space between the secretory cells and the myoepithelial cells was of a simple appearance as compared with that of the granulated gland. Both myelinated and the non-myelinated nerve bundles were seen in the dermal connective tissue around the mucous glands (Fig. 2b). However, they did not pass through the intercellular space between the adjacent myoepithelial cells.

The small granulated gland The small granulated gland was also composed of a secretory compartment, a duct and an intermediate region between them (Fig. 1c). This gland has not been described in the literature cited so far. This type of gland was located close to the epidermal layer of the skin and was the smallest among the four types of skin glands observed in the present study. It averages $50 \mu\text{m}$ in height and $60 \mu\text{m}$ in width. The nuclei, rough ER and Golgi apparatus were confined to the base with a large amount of secretory granules occupying most of the cytoplasmic area. The secretory granules were of a uniform appearance and they became yellow with Mallory's stain. With the EM, the granules were

FIG. 1. Electron micrographs of four types of skin glands.

- a: A granulated gland showing the syncytial appearance of a secretory compartment and thick myoepithelial cell layer. On the right hand side of the figure, a thin myoepithelial cell layer of a mucous gland can be seen. SCG, secretory compartment of granulated gland; ML, muscle cell layer of granulated gland; MLM, muscle cell layer of a mucous gland.
- b: Mucous glands showing low density secretory cell (LSC) and high density secretory cell (HSC) intermediate region (IR) and excretory duct (D). E, epidermis; ML, myoepithelial cell layer.
- c: A small granulated gland showing secretory cell (SC), intermediate region with mitochondria-rich cells (MRC) and transition region (TR). D, secretory duct; ML, myoepithelial cell layer; E, epidermis.
- d: A NP gland showing secretory cells (SC), secretory duct (D) and intermediate region (IR). ML, myoepithelial cell layer; MNB, myelinated nerve bundle.

found to be electron-dense and spheroidal in shape with an average size of $1.9 \times 3.2 \mu\text{m}$, including the largest one that measured around $6 \mu\text{m}$ in diameter (Fig. 1c). This is the largest among the secretory granules of the four kinds of skin glands observed. In the intermediate region adjacent to the secretory cells, mitochondria-rich cells were observed adjoining the transition region of the excretory duct (Fig. 2c). Other than numerous mitochondria, these cells were characterized by their microvilli, large round nuclei and the cytoplasm free of secretory granules. The arrangement of cells at the transition region toward the excretory duct and that at the excretory duct were the same as those of the mucous gland. The myoepithelial cells discontinuously surrounded the secretory compartment. The myoepithelial cells of the small granulated

gland were wider than those of the mucous gland, but narrower than those of the granulated gland. The myelinated and non-myelinated nerve bundles were seen to have access to the gland, and the nervous structures which seemed endings or near the endings containing number of small vesicles and some cored vesicles, were occasionally observed in the area close to the basement lamina of the myoepithelial cells (Fig. 2c). However, no innervation was found in the intercellular space between the myoepithelial cells and the secretory cells.

NP gland NP glands were found only in the nuptial pad. The average size of the gland was $160 \mu\text{m}$ in width and $99 \mu\text{m}$ in height in a frog weighing about 43 g. This gland consists of a secretory compartment, a duct and an intermedi-

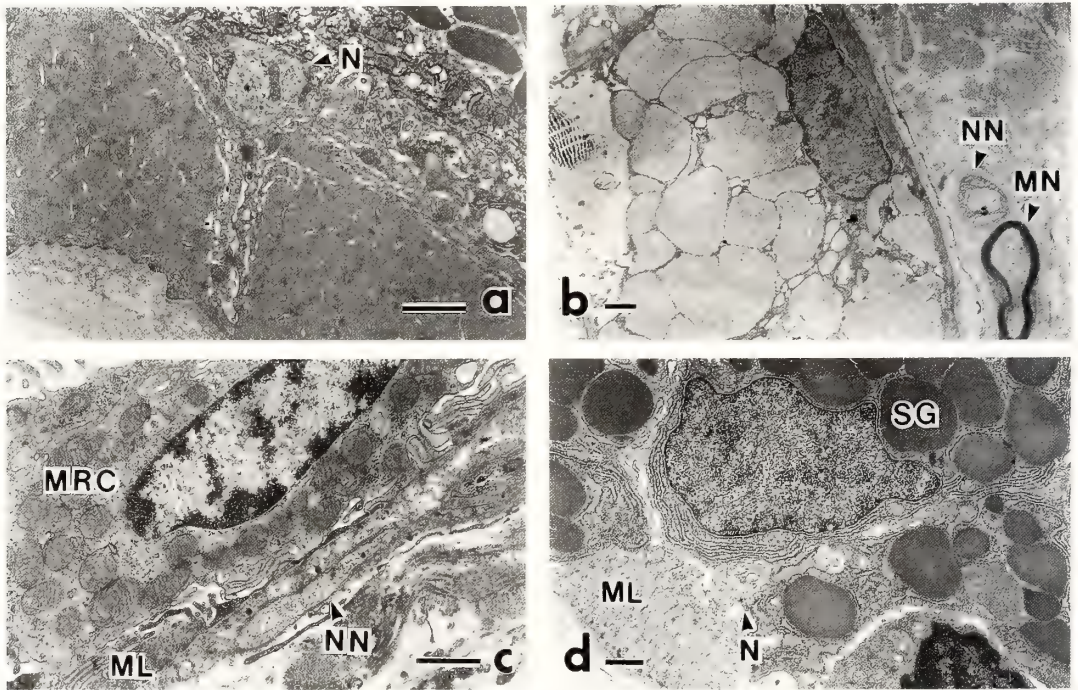


FIG. 2. Electron micrographs showing innervations in four types of skin glands.

- A nerve ending structure in the intercellular space between myoepithelial cell and secretory cell of a granulated gland. N, nerve ending.
- A profile of a mucous gland showing a secretory cell with clear vesicles, and a non-myelinated nerve bundle and a myelinated nerve with access to the secretory compartment. MN, myelinated nerve, NN, non-myelinated nerve.
- A small granulated gland showing a mitochondria-rich cell in a secretory compartment and non-myelinated nerves which face a thin myoepithelial cell layer (ML). MRC, mitochondria-rich cell.
- A NP gland showing secretory cells with large secretory granules (SG), a myoepithelial cell in longitudinal section (ML), and a nerve ending (N) surrounded by secretory cells.

ate region between them (Fig. 1d). The secretory compartment was composed of monolayered columnar secretory cells which were arranged in the bottom of the compartment. The average size of secretory cells was 38 μm in height and 7 μm in width. The secretory cells lodged with a large quantity of secretory granules and their nuclei were situated at the base. These granules were stained deep blue by Mallory's triple stain, and yielded a strong positive reaction to PAS. With the EM, profiles of well developed layered rough ER and Golgi apparatus were seen near the nucleus, and the apical part of the cells was provided with numbers of microvilli protruding into the lumen of the compartment. The adjacent

cells were interdigitated with each other with occasional desmosomes. In a profile of a secretory cell, there were observed 50 to 60 membrane-bounded granules which were homogeneous and mostly spheroidal in shape. In the areas of Golgi apparatus there were occasionally observed small granules of varied electron density, measuring $1.8 \times 1.2 \mu\text{m}$ in average, which seemed to be in a process of maturation. Some of these small granules were in shapes suggesting that secretory granules might also become larger by the fusion of small granules together. The glands were surrounded discontinuously with myoepithelial cells which were moderately developed as in the case of the small granulated gland. In the regions where

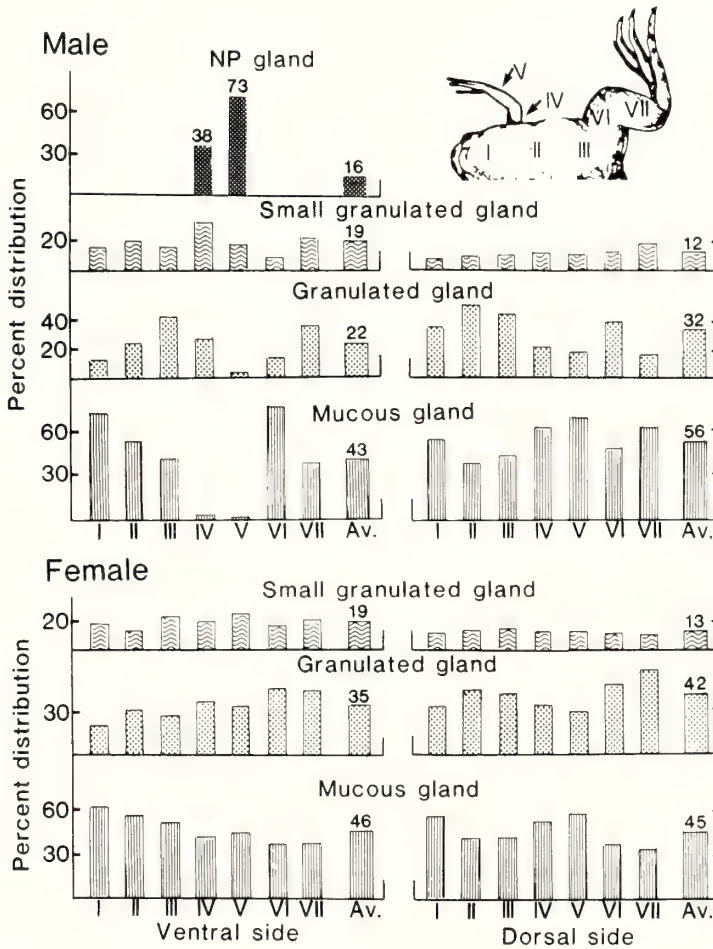


Fig. 3. Percent distribution of skin glands in selected regions of body surfaces. I-VII indicate areas selected for observations as shown in the right hand corner.

the secretory cells were not covered with myoepithelial cells, the basement lamina of the secretory cells directly faced the connective tissue surrounding the glands. In the connective tissue surrounding the NP glands, there were observed intense vascularizations. The terminal structures of the non-myelinated nerves were observed to rest on the surfaces of the secretory cells or the myoepithelial cells after passing through the intercellular space between the adjacent myoepithelial cells (Fig. 2d). Also the terminal structures were observed to make direct contact with the secretory cells at the place where the secretory cells had no myoepithelial cell covering.

Distribution of skin glands through the body surfaces The distribution of four types of skin glands in selected areas of the body surface of both male and female frogs is shown in Figure 3. Distribution is shown as the number of each skin gland as a percentage of the total number of skin glands counted in the area selected for study. In the male, the percentages of mucous glands, granulated glands, small granulated glands and NP glands were 43, 22, 19 and 16% on the ventral side and 56, 32 and 12% on the dorsal side, respectively, while in the female they were 46, 35 and 19% on the ventral side and 45, 42 and 13% on the dorsal side, respectively. The percentage distribution of NP glands was 73% at V and 38% at IV in the male. In the nuptial pad region occurrence of

mucous glands and the granulated glands was infrequent. No NP glands were found in other regions.

Changes in skin glands under the experimental conditions

1) Dry milieu

Figure 4 shows the decrease in body weight after keeping in a waterless condition. The percent reduction in body weight varied among the experimental frogs and the small-sized frogs were apt to show a larger reduction (32–34%) than the larger ones (21–34%). The skin pieces excised from the experimented frogs as well as the controls were subjected to histological studies to measure the heights of the skin and epidermis, sectional areas of the mucous glands, granulated glands and small granulated glands. In the control frogs, all these measurements in the females were larger than those in the males (Table 1). It is worth noting here that the area of the granulated glands on the dorsal side was about twice as great as that of those on the ventral side. When the frogs were kept in a waterless milieu for 3 days, all the measurements in the skin and the skin gland became smaller than those of the controls. The thickness of the skin became 73–83% of that of the controls, the epidermis 63–82%, and the areas of the mucous gland 29–54%, the granulated gland 63–80% and the small granulated gland 74–98%.

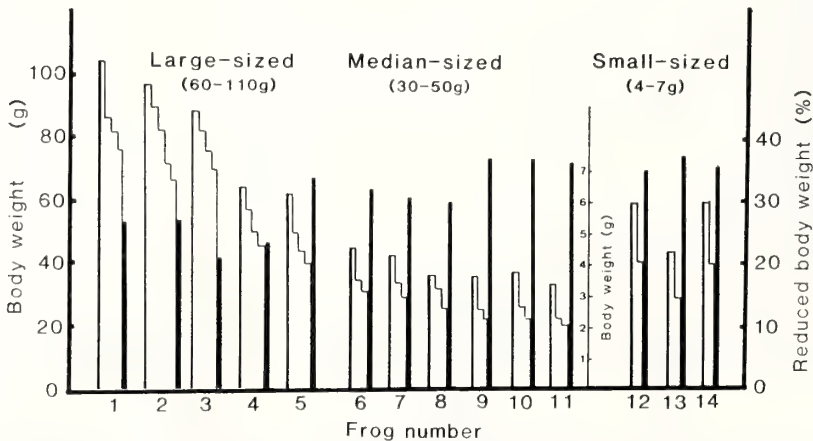


FIG. 4. Daily changes in body weight after keeping the animals under waterless conditions. Dark bars indicate reduced body weight as a percentage reduction as determined by final weighing. () indicates body weight of frogs.

TABLE 1. Measurement of skin and skin glands of *Xenopus laevis* kept in water (normal) and under waterless conditions

	Male						Female					
	Height of skin in μm			Areas of skin glands in μm^2			Height of skin in μm			Areas of skin glands in μm^2		
	Skin	Epi-dermis	Mucous	Granulated	Small granulated		Skin	Epi-dermis	Mucous	Granulated	Small granulated	
Normal	372 \pm 4 [†] (25)	56 \pm 1 (24)	10,999 \pm 433 (72)	25,125 \pm 953 (52)	Ventral side							
					1,743 \pm 206 (22)	568 \pm 7 (24)	110 \pm 2 (22)	22,741 \pm 1,506 (61)	76,821 \pm 4,151 (39)	3,221 \pm 579 (24)		
Waterless	289 \pm 6* (25)	35 \pm 1* (24)	4,079 \pm 222* (72)	19,652 \pm 1,374* (51)	Dorsal side							
					1,299 \pm 126 (23)	473 \pm 6* (24)	90 \pm 2* (21)	6,487 \pm 379* (59)	60,612 \pm 3,034* (49)	3,164 \pm 339 (19)		
Normal	544 \pm 4 (24)	55 \pm 1 (24)	17,304 \pm 876 (56)	55,935 \pm 3,122 (60)	Dorsal side							
					1,670 \pm 99 (23)	645 \pm 7 (24)	66 \pm 1 (23)	19,247 \pm 1,103 (56)	123,929 \pm 6,803 (58)	1,809 \pm 229 (20)		
Waterless	397 \pm 5* (25)	36 \pm 1* (23)	9,305 \pm 585* (73)	44,835 \pm 2,629* (62)	Dorsal side							
					1,484 \pm 178 (19)	520 \pm 6* (23)	55 \pm 2* (21)	8,418 \pm 637* (57)	77,811 \pm 4,885* (57)	1,515 \pm 126 (24)		

[†] Mean \pm S.E.

(): Number observed.

* Significant as compared with the control (P<0.01, with t-test).

The present study revealed that the area of the mucous gland showed the most remarkable reduction, especially in those on the ventral side (down to 37% in the male and 29% in the female). The sectional areas of their glands were reduced, and the evacuation of contents of the glands was also recognized histologically. In addition, low density cells in the compartment of the atrophied mucous gland seemed to be reduced in size more than high density cells. The granulated glands seemed to be unchanged.

2) Hypophysectomy

A significant decrease in the area of the NP gland occurred after hypophysectomy and the size of gland became about half that of the unoperated control frog, while the mucous, the granulated and the small granulated glands were unchanged (Table 2, Fig. 5a, b). On day 12 after hypophysectomy, the NP gland cell already showed a decrease in diameter, area and height (Table 3). Such regressed features were persisted in the specimens kept for 15 months after hypophysectomy (Fig. 5c). The area of the secretory cell nuclei was unchanged. The amount of secretory granules was

also decreased on day 12 and became much less on day 40 without recovery later. In association with regression of the NP gland, the numerous small epidermal spikes which specifically cover the nuptial pad area were rapidly decreased in number followed by complete disappearance in the 40 day specimens. There were often seen profiles of the small granulated gland which seemed to show active secretion through their distended excretory ducts which contained a considerable amount of secretory material. Such a histological view was unusual in other experimental series as well as in the controls.

3) Isoproterenol (ISP) application

Experiment 1: Within a minute after the injection of ISP, the recipient frogs started to react to ISP and in about 5 min the entire body surface was covered with milky and viscid secretory material expelled from the granulated glands. Histologically, evacuation of the contents of the glands occurred only in the granulated glands in which the myoepithelial layer showed remarkable undulation accompanied by hypertrophy in some places. The mucous gland and the small granulated gland were

TABLE 2. Effect of hypophysectomy on the areas of skin glands 40 days after the operation

Skin glands	Area of gland in μm^2 (Mean \pm S.E.)	
	Control	Hypophysectomy
Mucous	11,002 \pm 1,211 (71)	10,833 \pm 1,195 (61)
Granulated	15,686 \pm 2,089 (25)	13,352 \pm 1,559 (26)
Small granulated	2,794 \pm 441 (22)	2,975 \pm 233 (21)
NP	9,779 \pm 1,766 (9)	4,867 \pm 412 (6)*

(), number of glands observed.

* $P < 0.05$ with t-test.

TABLE 3. Morphological alterations in NP glands after hypophysectomy

Days after operation	Number of glands observed	Diameter (μm , Mean \pm S.E.)		Cross sectional areas (μm^2 , Mean \pm S.E.)			Height ⁺ of gland cell (μm)	Area ⁺ of nucleus (μm^2)
		long	short	Gland (a)	Lumen in compartment (b)	(a)-(b)		
0	23	99 \pm 2	160 \pm 6	12,549 \pm 881	1,877 \pm 216	10,671 \pm 718	30-55	25-34
12 days	28	84 \pm 3**	138 \pm 5	9,194 \pm 567*	2,715 \pm 359	6,478 \pm 409**	20-35	23-29
40	23	56 \pm 2**	130 \pm 7**	4,847 \pm 338*	1,478 \pm 284	3,369 \pm 290**	10-20	23-27
15 months	23	69 \pm 2**	116 \pm 5**	5,783 \pm 362**	3,407 \pm 355**	2,376 \pm 117**	5-20	26-32

* $P < 0.05$, ** $P < 0.01$, with t-test.

+ shows only ranges of measurements.

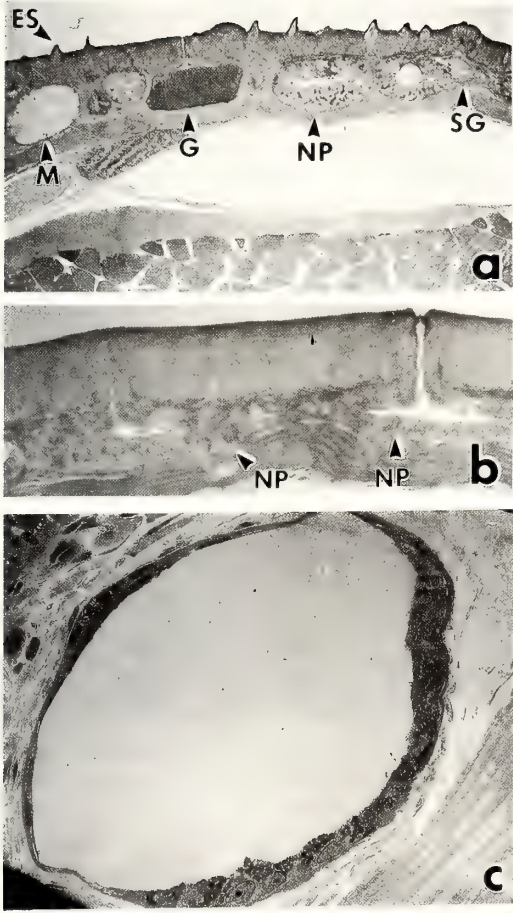


FIG. 5. Histological views of nuptial pads showing a control (a), and operated animals in 40 days (b) and 15 months (c) after hypophysectomy. $\times 53$ (a), $\times 145$ (b), $\times 470$ (c). ES, epidermal spike; NP, NP gland; M, mucous gland; G, granulated gland; SG, small granulated gland.

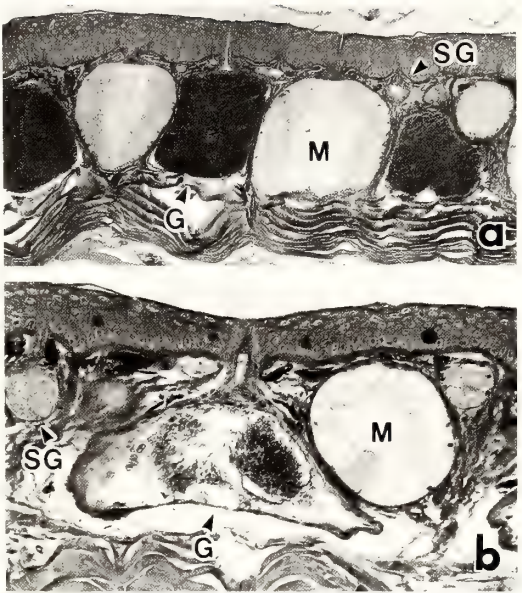


FIG. 6. Histological views of skin glands of a control skin (a) and of a skin affected 30 min after ISP injection (b). $\times 110$ (a), $\times 110$ (b). G, granulated gland; M, mucous gland; SG, small granulated gland.

unchanged (Fig. 6b).

Experiment 2: Upon injection of ISP, the operated skin areas on the backs of the frogs did not respond to a drug injected although the surrounding intact skin responded well in a way similar to that of normal frogs (Fig. 8). The operated skin area showed gradual response to injected ISP with time, following operation days. The central area of the operated skin pieces started to react weakly to the injected ISP by post-operative day 16. Approximately a half area of the operated skin piece was observed to respond to ISP on day 28.

Experiment 3: The skin pieces taken from the body surfaces showed results similar to that in the Experiment 2 when they were immersed in the physiological saline or medium containing ISP in concentrations ranging from 10^{-1} to 10^{-5} M. With the EM, 30 min after immersion in ISP solution (10^{-1} M), the intercellular space between the secretory cells and the myoepithelial cells was seen to be wider, and a large number of vascular structures appeared at the periphery of the secretory cells (Fig. 7d). Secretory granules were sparsely distributed (Fig. 7c). The fibrillar sarcoplasm of the myoepithelial cells had a condensed appearance. However, in the sarcoplasm facing the basal lamina of the secretory compartment, a number of small protrusions appeared in the specimens fixed 5 sec after ISP immersion (Fig. 7b). The higher the concentration of ISP applied the more rigorous was the response of the glands to it. The lower the concentration of ISP, the more time needed for the glands to respond and the weaker was their response. At a concentration of 10^{-5} M the reaction was obscure. These skin

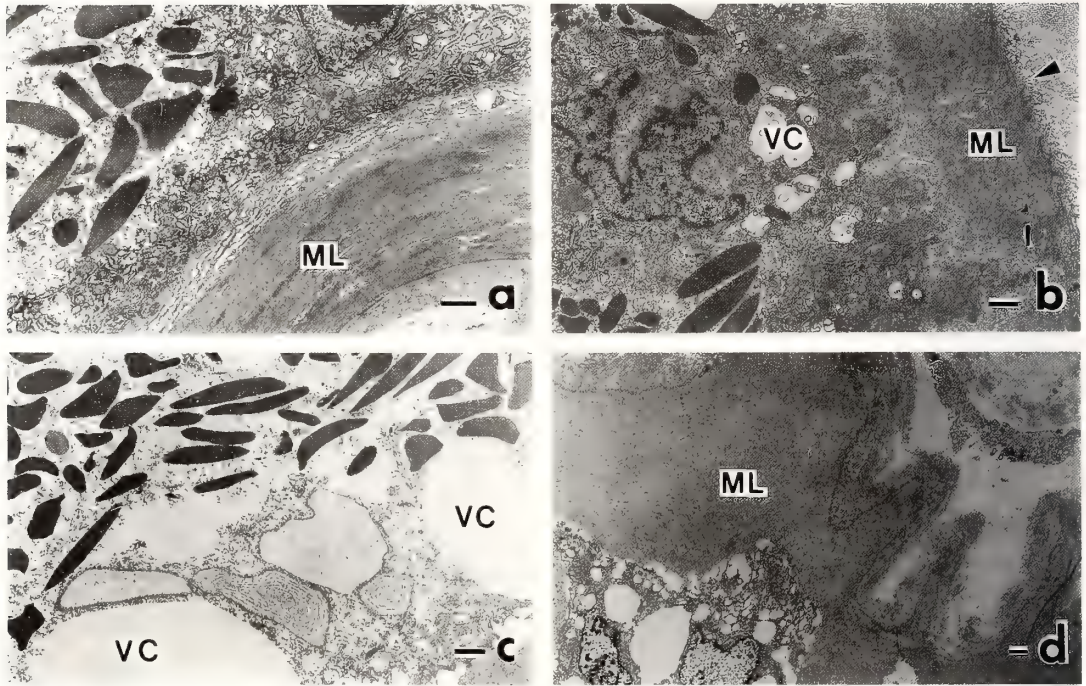


FIG. 7. Electron micrographs of granulated glands of a control (a), and 5 sec (b) and 30 min (c and d) after immersion in ISP solution. Arrow shows small sarcoplasmic protrusions. ML, myoepithelial cell layer; VC, vascular formations.

pieces were able to respond to ISP even after they were kept for as long as 14 days (Fig. 9). However, in this case the response occurred sporadically and not through the entire skin surface.

In vivo and *in vitro* application of noradrenaline at a concentration of 10^{-5} M was able to induce a discharge of secretion.

DISCUSSION

Classification of skin glands

The granulated and mucous glands have been reported to be the major types of the amphibian skin glands [1]. Mills and Prum [10] classified the mucous glands of *Rana pipiens*, *R. temporaria* and *R. catesbeiana* as mucous and seromucous glands on the basis of electron microscopic observations. According to this report the mucous gland has mitochondria-rich cells in the junctional area between the duct and the acinus while the seromucous gland has cells without granule in the same

region. Fox [11] introduced kinds of amphibian skin glands as poisonous, lumpy, callous, mucous, and so on. In *Salamandrina terdigitata*, three types of skin glands, that is the mucous, serous and the mixed type, have been described [12]. These indicate that the skin glands of amphibians vary in form, and the terminology for these glands has not been well established. In the case of the skin glands of *X. laevis*, most of the studies have been concentrated on the granulated gland due to the interesting biochemical nature of its secretion and a little has been elucidated about other type of skin glands, although it was reported that the dorsal skin of *X. laevis* contained several kinds of grandular structures opening via the epidermal ducts to the external surface [6]. In the present study, we were able to demonstrate four different types of skin glands in the body surface of adult *X. laevis*. These were the mucous, the granulated, the small granulated and the NP glands. It appeared that the small granulated gland and the NP gland as termed in the present report were different

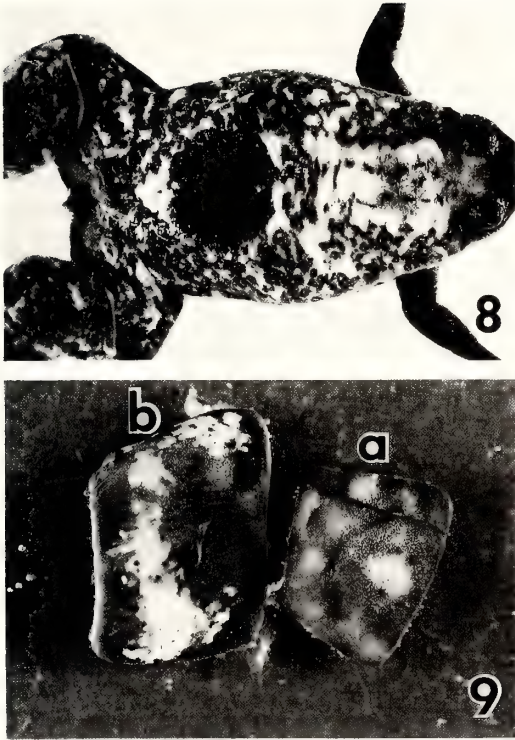


FIG. 8. Response of skin granulated glands about 5 min after the injection of ISP. No response is seen in the operated skin (Experiment 2) at the center of the back, 7 days post-operation. $\times 0.55$.

FIG. 9. Response of the *in vitro* granulated gland kept in medium 199 (a) and in physiological saline (b) for 12 days followed by immersing them in the media containing 10^{-1} M ISP for 5 min. $\times 2$.

types from the seromucous or mixed type which was described previously in other species, as well as from the mucous and the granulated glands of *X. laevis* in their morphology, and responses of glands to various types of stimulation will be mentioned later.

Distribution of skin glands

Except NP gland the other three types of skin glands are distributed throughout the body surface. The mucous gland and the granulated gland were found to be greater in number and larger in size. This is in agreement with a report by Sjöberg and Flock [13] on *R. temporaria* and *R. esculenta*. However, the NP gland was found to be distributed only in the male nuptial pads. According to

Berk [9], in the nuptial pad area there were only glands of a simple saccular type (NP gland) and no other glands were found in this area. However, in the present study it was found that the granulated and the mucous glands existed in the nuptial pad area although a few in number. Also quite a number of small granulated glands were observed in this area.

Stimulation of glands

The response of the mucous and the granulated glands to adrenergic agonists observed might be similar to that of the previous reports [4, 14, 15]. However, to what kind of stimulation the small granulated gland responds could not be clarified by the present experiment. We only found that some of the small granulated glands expelled much of their contents into the excretory ducts when the frogs were hypophysectomized. Many investigators have reported that some kinds of glands were present underneath the papillae in thumb pads of male frogs and newts [16–18]. However it has been still not certain whether skin glands in the area of thumb pads are the same or different from those of the common skin glands. As has already been reported, the development of the pads was dependent on the androgenic hormonal cycle [16–18], and the development of the nuptial pad was accompanied by the specially differentiated NP glands which occurred only in this area. It is still not certain, however, what kinds of substances are produced in NP gland and how this gland discharges its secretion upon what kind of stimulation. In our preliminary experiment using a pair of frogs in courtship, the nuptial pad of the male and the pieces of skin of the female biopsied during amplexus showed any noticeable histological changes. After hypophysectomy only this gland showed remarkable morphological regression of the secretory cells and this continued many days. Therefore the functional significance of NP gland is different from the mucous gland. The skin glands underneath the thumb pads in certain species have been classified as mucous glands [16–18]. Since the structural integrity of the NP glands is absolutely associated with the development of nuptial pad, this gland must have something to do with sexual behavior of the male frog, but this

remains unresolved in the present experiment.

The mucous glands lost their contents enormously when the frogs were kept in waterless conditions. The contents of other kinds of glands were unchanged, although their size became small due to possible loss of water in such abnormal conditions. The skin textures gradually evolved to adapt exterior circumstances [11] and in amphibians, ions and organic substances in water passively pass through the skin [19]. The watery substance of the mucous glands may be secreted first to keep well being of an individual under the present severe experimental circumstances. In normal physiological condition it was reported that an active ion-transport rather than secretion of cellular product occurred in the secretory cells of the mucous gland, and this mechanism was not elucidated [20, 21].

Numbers of biologically active peptides and biogenic amines, similar to those of mammalians, and alkaloids have been found in amphibian skins [3, 25]. High concentrations of thyrotrophic releasing hormone (TRH) and 5-hydroxytryptamine (5-HT) in the granulated glands of *X. laevis* and *R. pipiens* have been demonstrated [22]. Dockray and Hopkins [6] and others [23, 24] demonstrated a large amount of caerulein in the granulated gland of *X. laevis*. These substances (TRH, 5-HT and caerulein) were proved to be discharged following adrenergic stimulation [6, 25]. In the present experiment we employed isoproterenol (ISP), one of the sympathomimetic substances, to observe the response of the granulated gland in normal and experimentally treated skin. Benson and Hadley [14] reported that adrenaline and noradrenaline stimulated secretion of the contents of the granulated gland but ISP was ineffective when *R. pipiens* and *X. laevis* were subjected to *in vitro* treatment with various sympathomimetic agents in concentrations of 10^{-4} , 10^{-5} and 10^{-6} M. Holmes *et al.* [15] also observed the effectiveness of adrenaline and related substances in stimulating glandular secretion of *X. laevis* skin and they ranked their stimulative effectiveness as follows; adrenaline was most effective followed by noradrenaline and phenylephrine, while isoprenaline and salbutamol of adrenergic agonist were ineffective. However, we

were able to demonstrate that applications of ISP to *X. laevis* skin *in vivo* or *in vitro* caused positive responses. The secretion of a milky substance on their surfaces and changes in structures of the granulated glands occurred. Such an apparent difference between ISP effectiveness in the present series of experiments and others may not be due to the nature of the drug nor to a species specificity of the frogs employed but largely due to the concentrations of ISP applied. In the present series of experiments we applied ISP in concentrations 10^{-1} to 10^{-5} M, compared to 10^{-4} M, 10^{-5} M and 5×10^{-6} M in the experiments by Benson and Hadley [14] and 10^{-4} M and 10^{-5} M in the experiment by Holmes *et al.* [15]. Our experiment 2, in which ISP was applied to the frogs which had the detached and sewed skin pieces in their backs, the skin pieces operated on showed exceedingly retarded response to ISP in the early post-operative period followed by gradual recovery. This may be largely due to the degree of recovery of vascularization after the operation in which the vascularization of the operated skin pieces in the early phases of healing might not be sufficient to carry the amount of ISP needed for stimulation of gland secretion.

Innervations

In the present series of experiments, we also surveyed innervations of the glands studied. All the skin glands have been reported to be surrounded by myoepithelial cells either completely [26] or incompletely [27]. The innervations in the small granulated gland and the NP gland in the male nuptial pad have not been studied before. In the granulated gland and the NP gland we were able to demonstrate nerve fibers in the secretory compartments, while in the mucous gland and the small granulated gland the nerve fibers only came to have access to the glands outside the secretory compartments. Dockray and Hopkins [6] showed that nerve endings were present in the secretory compartment of the granulated gland of *X. laevis*, and Sjöberg and Flock [13] also reported a similar finding in the granulated gland of *R. temporaria* and *R. esculenta*. In mammalian species, it was also reported that similar types of innervations existed in the nasal gland in Guinea pig [28] and

the lacrimal gland of sheep [29]. The present results also suggest that neural influence may be exerted in the skin glands differently, according to the individual gland, since some glands received innervation on the inside of the secretory compartments while other glands were not innervated inside the secretory compartments but were only accessed by the nerve ending structures outside the secretory compartment. The excretion of the contents of the glands may occur mainly due to contraction of the myoepithelial cells. Histological signs of contraction of the myoepithelial cells were evident through the reports by Holmes and Balls [26] and the results of the present series of experiments. However, the present study demonstrates that there were also nerve endings resting on the surfaces of the secretory cells and occasionally in a deep place far from the surface of the myoepithelial cells. Therefore it is important to study the receptor sites for the sympathomimetic substances not only through the surface of the myoepithelial cells but also of the secretory cells with thorough studies on alternations of nerve endings and the structures of the secretory cell cytoplasm, to elucidate the cellular mechanism by which the contents of the granulated gland are expelled upon nervous stimulation.

REFERENCES

- Noble, G. A. and Noble, E. R. (1944) On the histology of frog skin glands. *Trans. Am. Microsc. Soc.*, **63**: 254-263.
- Joseph, W. and Vanable, J. R. (1964) Granular gland development during *Xenopus laevis* metamorphosis. *Dev. Biol.*, **10**: 331-357.
- Myers, C. W. and Daly, J. W. (1983) Dart-poison frogs. *Sci. Am.*, **248**: 96-105.
- Campantico, E., Guardabassi, A. and Torasso, L. (1978) Histological changes in *Xenopus laevis* Daudin adult specimens kept under dry conditions, then moved back to their natural aquatic environment. II. Skin, kidney and interrenal tissue. *Arch. Sci. Biol.*, **62**: 63-76.
- Bennett, G. W., Marsden, C. A., Clothier, R. M., Waters, A. D. and Balls, M. (1982) Co-existence of thyrotrophin releasing hormone and 5-hydroxytryptamine in the skin of *Xenopus laevis*. *Comp. Biochem. Physiol.*, **72C**: 257-261.
- Dockray, G. J. and Hopkins, C. R. (1975) Caerulein secretion by dermal glands in *Xenopus laevis*. *J. Cell Biol.*, **64**: 724-733.
- Wakabayashi, T., Kato, H. and Tachibana, S. (1985) Complete nucleotide sequence of mRNA for caerulein precursor from *Xenopus* skin: the mRNA contains an unusual repetitive structure. *Nucleic Acids Res.*, **13**: 1817-1828.
- Kurabuchi, S. and Inoue, S. (1981) Small spiny projections in the epidermis of the mature *Xenopus laevis*. *Annot. Zool. Japon.*, **54**: 182-190.
- Berk, L. (1939) Studies in the reproduction of *Xenopus laevis*. III. The secondary sex characters of the male *Xenopus*: The pads. *S. Afr. J. Med. Sci.*, **4**: 47-60.
- Mills, J. W. and Prum, B. E. (1984) Morphology of the exocrine glands of the frog skin. *Am. J. Anat.*, **171**: 91-106.
- Fox, H. (1986) The skin of Amphibia. In "Biology of the Integument. Vol. 2. Vertebrates". Ed. by J. Bereiter-Hahn, A. G. Matoltsy and K. Sylvia Richards, Springer-Verlag, Berlin, pp. 116-135.
- Delfino, G., Brizzi, R. and Calloni, C. (1982) Development of cutaneous glands in *Salamandrina terdigitata* (Lacépède, 1788) (Amphibia: Urodela); findings by light and electron microscopy. *Z. Mikrosk. Anat. Forsch.*, Leipzig, **96**: 948-971.
- Sjöberg, E. and Flock, Å. (1976) Innervation of skin glands in the frog. *Cell Tissue Res.*, **172**: 81-91.
- Benson, B. J. and Hadley, M. E. (1969) *In vitro* characterization of adrenergic receptors controlling skin gland secretion in two anurans *Rana pipiens* and *Xenopus laevis*. *Comp. Biochem. Physiol.*, **30**: 857-864.
- Holmes, C. H., Moondi, P. S., Rao, R. R. and Balls, M. (1977) *In vitro* studies on the effects on granular gland secretion in *Xenopus laevis* skin of stimulation and blockade of α and β adrenoreceptor of myoepithelial cells. *Cell Biol. Int. Rep.*, **1**: 263-270.
- Yoneyama, H. and Iwasawa, H. (1985) Annual changes in the testis and accessory sex organs of the bullfrog *Rana catesbeiana*. *Zool. Sci.*, **2**: 229-231.
- Iwasawa, H. and Asai, O. (1959) Histological observations on the seasonal change of testis and the thumb pad in the frog, *Rana nigromaculata*. *J. Fac. Sci., Niigata Univ.*, Ser. II., **2**: 213-219.
- Iwasawa, H. and Takasu, T. (1985) Study of thumb pad regions developed by the administration of testosterone in a young female of *Rana nigromaculata* with a supernumerary forelimb. *Jpn. J. Herpetol.*, **11**: 5-10.
- Lillywhite, H. B. (1971) Thermal modulation of cutaneous mucous discharge as a determinant of evaporative water loss in the frog, *Rana catesbeiana*. *Z. Vergl. Physiologie*, **73**: 84-104.
- Thompson, I. G. and Mills, J. W. (1981) Isopterenol-induced current changes in glands of frog

- skin. *Am. J. Physiol.*, **241**: C250–C257.
- 21 Thompson, I. G. and Mills, J. W. (1983) Chloride transport in glands of frog skin. *Am. J. Physiol.*, **244**: C221–C226.
- 22 Bennett, G. W., Balls, M., Clothier, R. H., Marsden, C. A., Robinson, G. and Wemyss-Holden, G. D. (1981) Location and release of TRH and 5-HT from amphibian skin. *Cell Biol. Int. Rep.*, **5**: 151–158.
- 23 Inselvini, M. (1975) First appearance of caerulein during the development of *Xenopus laevis*. *Gen. Pharmacol.*, **6**: 215–217.
- 24 Seki, T., Kikuyama, S. and Yanaihara, N. (1985) Development of caerulein producing cells in *Xenopus* skin gland during metamorphosis. *Zool. Sci.*, **2**: 980.
- 25 Mueller, G. P., Alpert, L., Reichlin, S. and Jackson, I. M. D. (1980) Thyrotrophin-releasing hormone and serotonin secretion from frog skin are stimulated by norepinephrine. *Endocrinology*, **106**: 1–4.
- 26 Holmes, C. and Balls, M. (1978) *In vitro* studies on the control of myoepithelial cell contraction in the granular glands of *Xenopus laevis* skin. *Gen. Comp. Endocrinol.*, **36**: 255–263.
- 27 Neuwirth, M., Daly, J. W., Myers, C. W. and Tice, L. W. (1979) Morphology of the granular secretory glands in skin of poison-dart frogs (Dendrobatidae). *Tissue and Cell*, **11**: 755–771.
- 28 Yamamoto, T. (1968) On the fine structure of the terminal portion of nasal gland in guinea pig, with special references to the interrelationship between glandular cells and nerve endings. *Arch. Histol. Jpn.*, **27**: 311–325.
- 29 Yamauchi, A. and Burnstock, G. (1967) Nerve-myoeepithelium and nerve-glandular epithelium contacts in the lacrimal gland of the sheep. *J. Cell Biol.*, **31**: 917–919.

Circadian Rhythms in Locomotor Activity of the Hagfish, *Eptatretus burgeri* II. The Effect of Brain Ablation

SADAKO OOKA-SOUDA, HIROSHI KABASAWA¹ and SEIICHIRO KINOSHITA^{2,3}

Atomi Gakuen Junior College, 1-5-2 Otsuka, Bunkyo-ku, Tokyo 112,

¹*Keikyū Aburatsubo Marine Park Aquarium, 1082 Koajiro, Misaki, Miura-shi, Kanagawa 238-02, and*

²*Misaki Marine Biological Station, University of Tokyo, 1024 Koajiro, Misaki, Miura-shi, Kanagawa 238-02, Japan*

ABSTRACT—The hagfish, *Eptatretus burgeri*, displays locomotor activity only during the first two thirds of the dark period under 12L: 12D (7:00–19:00 light, 19:00–7:00 dark), and shows a clear free-running rhythm under constant darkness. The altered activity in the animal, whose brain was surgically removed except for the medulla oblongata, assumed a peculiar pattern which can be described as follows: (1) The free-running rhythm in constant darkness disappeared. (2) Under 12L: 12D, motor activity in the dark period disappeared, and continuous activity was observed throughout the light period. (3) This continuous activity always appeared and remained throughout the light period in various light regimens and it seems to be a direct reaction to light.

INTRODUCTION

There are many reports concerning the localization of the circadian pacemaker. It has been suggested that it is in the optic lobes of the cockroach [1] and of the cricket [2], in the prothoracic gland of the moth [3] and in the eyes of a molluscan species [4]. In vertebrates, the suprachiasmatic nucleus of the rat [5], the pineal gland of the chick [6, 7], both the suprachiasmatic nucleus and the pineal gland of the house sparrow [8] and the pineal gland of the lamprey [9] are candidate tissues in which circadian pacemakers may be located. It is remarkable that the pineal gland is supposed to play an important role in circadian control in lower vertebrates. The hagfish, one of the most primitive vertebrates, belongs to the same vertebrate group in which the lamprey is also included. However, the hagfish is supposed not to have a pineal gland [10].

In the present study, as the first step in deter-

mining the localization of the circadian pacemaker in the animal, the effect of the brain ablation on motor activity patterns was investigated. Normally the animal shows a clear nocturnal rhythm under light-dark cycles and displays a free-running rhythm when placed in continuous darkness [11].

MATERIALS AND METHODS

The hagfish, *Eptatretus burgeri*, were collected by use of a trap containing sardines as bait. For experiments both males and females were used, because it is not possible to distinguish males from females on the basis of outer appearance. Furthermore, males and females are similar in their circadian rhythms.

The methods and procedures for recording the motor activity of the animals were described in a previous paper [11]. The water temperature was kept at 15°C, and no food was given throughout the experiment. All surgical operations were done while the animals were lightly anesthetized with MS 222. The animal was fixed on a plastic stage, and the skin and the fibrous connective tissue covering the brain were cut longitudinally along the median axis. The brain was removed with a

Accepted August 31, 1987

Received October 31, 1986

³ Present address: Saitama Medical School, 981 Kawakado, Moroyama-machi, Iruma-gun, Saitama 350-04, Japan.

pair of scissors. The connective tissue was replaced as it was originally, and the skin was sewn. Ten animals were subjected to a sham-operation. In them the skin and the fibrous connective tissue were cut but the brain was not disturbed. The animals were kept in a large aquarium under 12L:12D for two weeks prior to the recording of the behaviour in the experimental aquaria.

RESULTS

The intact animal clearly shows nocturnal swimming activity, which occurs only in the first two thirds of the dark period under 12L:12D (7:00–19:00 light, 19:00–7:00 dark), and it displays a distinct free-running rhythm under constant darkness [11]. In the sham-operated animal activity rhythms were the same as in the intact animals both in the light-dark cycle and in constant darkness (Fig. 1).

When the entire brain was removed, the animal immediately died. However, animals, in which the medulla oblongata was left intact, survived for at least two months. They were very active, swimming in a manner similar to the intact hagfish: swimming near the surface of the water and moving along the edges of the aquarium.

The activity pattern in the brain-ablated animal was very different from that in the sham-operated one; under 12L:12D, the activity did not occur in the dark period, but appeared continuously throughout the light period, and under constant darkness, intermittent activity with no circadian rhythm was recorded. Figure 2 showed one of the nine records from brain-ablated animals.

In Figure 3, various light-dark schedules were programmed for one brain-ablated animal. Similarly, activity was confined almost completely within light period under all the lighting conditions including 6L:6D and 77L. No transient activity was observed when the light-dark cycle was reversed.

DISCUSSION

Ueck and Kobayashi [12] searched unsuccessfully for a pineal gland in the hagfish, *Eptatretus burgeri*. It is of interest to find the location of the

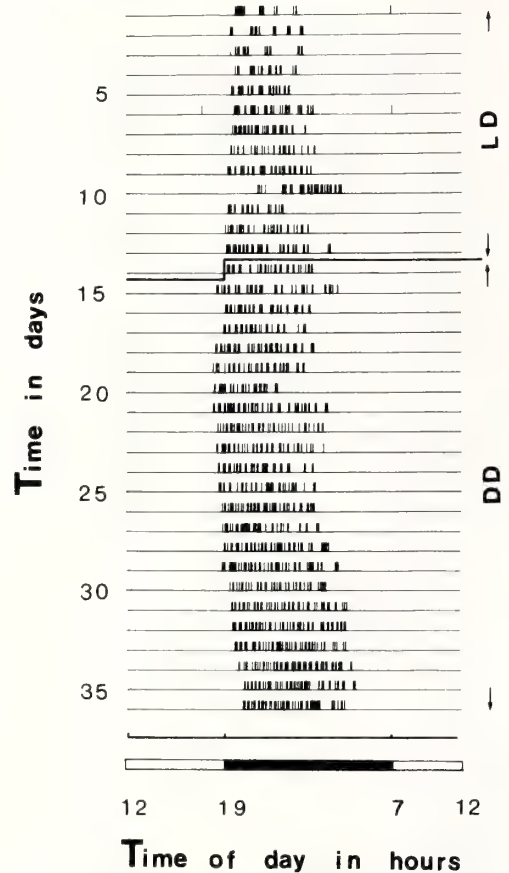


FIG. 1. Locomotor activity recorded for the sham-operated hagfish kept in 12L:12D and in constant darkness. The activity is indicated by the vertical marks on the time lines. The activity occurred only in the first two thirds of the dark period in 12L:12D and displays a distinct free-running rhythm in constant darkness. These activity patterns are fairly the same ones as those in an intact hagfish.

circadian pacemaker in an animal which has no pineal.

In the present study, we found that the circadian rhythm disappeared when the brain was removed, except for the medulla oblongata. This fact suggests that the circadian pacemaker may be in the brain. In these experiments locomotor activity was observed as the measurable result of the operations. Since the center controlling locomotor activity itself should exist in the brain and might be disturbed by our procedures then we cannot conclude definitively whether the circadian pacer-

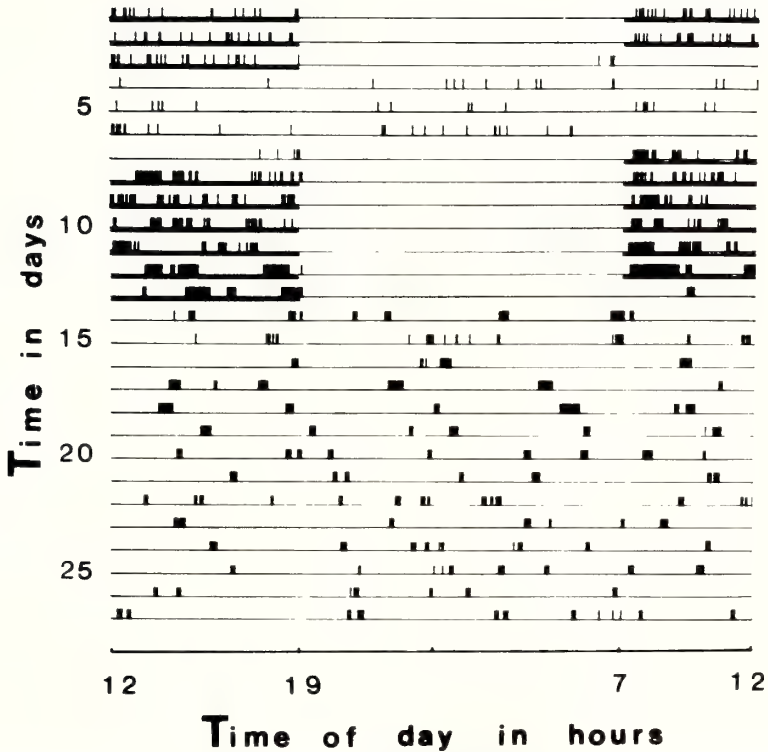


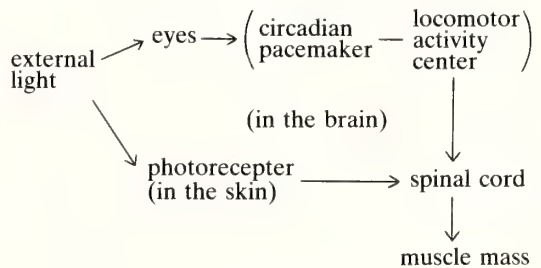
FIG. 2. Locomotor activity recorded for the operated hagfish kept in 12L:12D and in constant darkness. The underlines show the light period. In constant darkness, the free-running rhythm disappeared and intermittent activity were recorded throughout the period. In 12L:12D, the animal showed activity throughout the light period but none in the dark.

maker is located in the brain. Continuous swimming by animals lacking a fore- and mid-brain, however, argues that no essential motor control was impaired by the operation.

The characteristic response to light changed after removal of the fore- and mid-brain in this animal even though optic function was lost. Therefore, the locomotor activity stimulated by light stimuli probably was in response to a photoreceptor in the skin. Previous reports have established a photoreceptor in the skin of hagfish [13]. Light perceived through eyes has been supposed to control the nocturnal rhythm in intact hagfish because the nocturnal rhythm can not stay in dark period and free-runs after eye removal (unpublished data, Kabasawa and Ooka-Souda).

Accordingly, the following innervation scheme can be postulated in control of the locomotor

activity system in the hagfish.



ACKNOWLEDGMENTS

The authors wish to express their gratitude to Prof. A. Gorbman, University of Washington, for his help in preparing the manuscript.

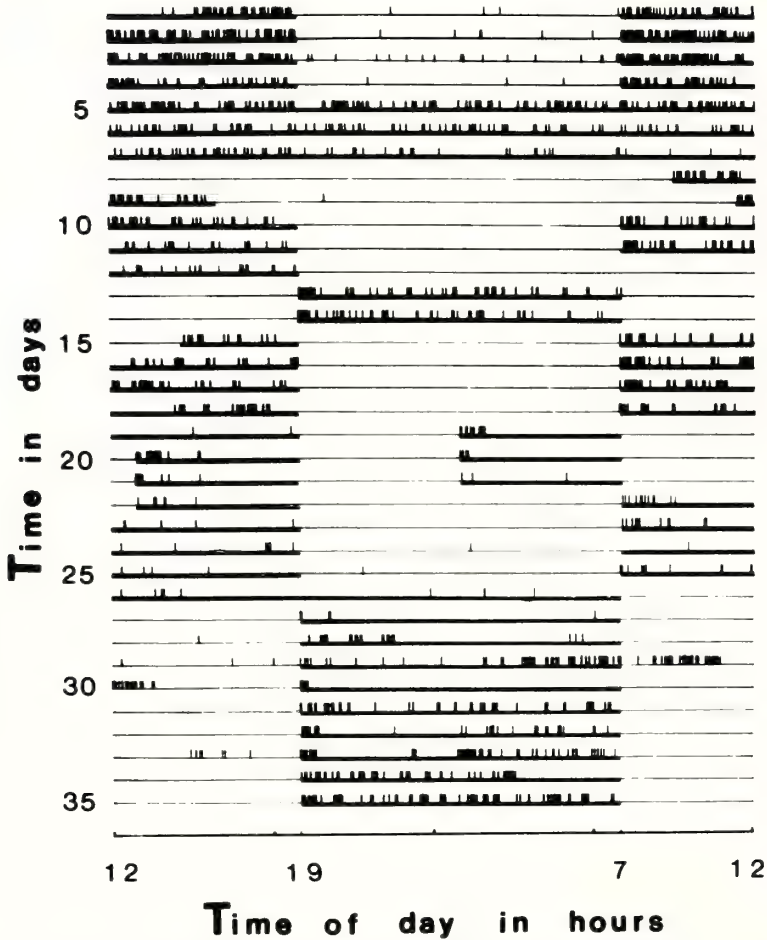


FIG. 3. Locomotor activity recorded for the operated hagfish kept under the various light-dark programs indicated. The brain-ablated animal which was under such time schedules as 12L: 12D, 77L, 21D, 12L: 12D, reversal of the 12L: 12D, 12L: 12D, 6L: 6D, 12L: 12D and reversal of the 12L: 12D successively alternatively behaved itself with light-active/dark-resting.

REFERENCES

- Page, J. L. (1982) Transplantation of the cockroach circadian pacemaker. *Science*, **216**: 73-75.
- Tomioka, K. and Chiba, Y. (1985) Circadian rhythm in the neurally isolated lamina-medulla-complex of the cricket, *Gryllus bimaculatus*. *J. Insect Physiol.*, **32**: 747-755.
- Mizoguchi, A. and Ishizaki, H. (1982) Prothoracic glands of the saturniid moth, *Samia cynthia racini*, possess a circadian clock controlling gut purge timing. *Proc. Natl. Acad. Sci. USA*, **79**: 2726-2730.
- Gene, B. D. and MeeMahon, D. G. (1984) Cellular analysis of the *Bulla* ocular circadian pacemaker system III. Localization of the circadian pacemaker. *J. Comp. Physiol. A*, **155**: 387-395.
- Inouye, S. T. and Kawamura, H. (1979) Persistence of circadian rhythmicity in a mammalian hypothalamic "island" containing the suprachiasmatic nucleus. *Proc. Natl. Acad. Sci. USA*, **76**: 5962-5966.
- Deguchi, T. (1979) A circadian oscillator in cultured cells of chicken pineal gland. *Nature*, **282**: 94-96.
- Takahashi, J. S., Hamm, H. and Menaker, M. (1980) Circadian rhythms of melatonin release from individual superfused chicken pineal glands *in vitro*. *Proc. Natl. Acad. Sci. USA*, **77**: 2319-2322.
- Takahashi, J. S. and Menaker, M. (1982) Role of the suprachiasmatic nuclei in the circadian system of the house sparrow, *Passer domesticus*. *J. Neurosci.*,

- 2: 815-828.
- 9 Morita, Y. and Samejima, M. (1984) Control of diurnal circadian locomotor rhythm by direct photosensory pineal organ. In "Animal Behavior: Neurophysiological and Ethological Approaches". Ed. by K. Aoki, S. Ishii and H. Morita, Japan Sci. Soc. Press, Tokyo/Springer-Verlag, Berlin, pp. 232-241.
 - 10 Quentin, B. (1963) The central nervous system. In "The Biology of Myxine". Ed. by A. Brodal and R. Fänge, Scand. Univ. Books, Oslo, pp. 50-91.
 - 11 Ooka-Souda, S., Kabasawa, H. and Kinoshita, S. (1985) Circadian rhythms in locomotor activity in the hagfish, *Eptatretus burgeri*, and the effect of reversal of light-dark cycle. *Zool. Sci.*, **2**: 749-754.
 - 12 Ueck, M. and Kobayashi, H. (1979) Neue Ergebnisse zu Fragen der vergleichenden Epiphysenforschung. *Verh. Anat. Ges.*, **73**: 961-963.
 - 13 Newth, D. R. and Rose, M. D. (1955) On the reaction to light of *Myxine glutinosa* L. *J. Exp. Biol.*, **32**: 4-21.

Circadian Rhythms in Locomotor Activity of the Hagfish, *Eptatretus burgeri* III. Hypothalamus: a Locus of the Circadian Pacemaker?

SADAKO OOKA-SOUDA and HIROSHI KABASAWA¹

Atomii Gakuen Junior College, 1-5-2 Otsuka, Bunkyo-ku, Tokyo 112,
and ¹Keikyu Aburatsubo Marine Park Aquarium, 1082 Koajiro,
Miura-shi, Kanagawa 238-02, Japan

ABSTRACT—By recording the locomotor activity rhythms of hagfish in which partial ablations in brain were made, this work was designed to determine the location of the circadian pacemaker. The characteristic rhythms were maintained in the absence of the optic tectum, but were lost in animal lacking the telencephalon or diencephalon. The telencephalon-diencephalon unit was more finely dissected for more precise localization. The rhythm still occurred without the upper or the lateral parts of this anatomical unit. Transecting the middle of the telencephalon had no effect on the rhythms displayed. These findings suggest that a crucial part (circadian pacemaker?) for the fish to be rhythmic may be in the ventromedial part of telencephalon-diencephalon, the hypothalamus, the frontal part of which extends under the telencephalon.

INTRODUCTION

The authors have demonstrated a clear circadian rhythm of the locomotor activity of the hagfish, *Eptatretus burgeri*, using an infra-red light-photocell system [1]. Attempts to determine the localization of the circadian pacemaker by surgical ablation have shown that the pacemaker may be in the brain anterior to the medulla oblongata [2]. In the present study, more precise examination was undertaken to identify more precisely the part of brain where the circadian pacemaker may be situated.

MATERIALS AND METHODS

All surgery was performed while the hagfish were lightly anesthetized by MS-222. Fixing the animal on a plastic stage, the skin and the fibrous connective tissue covering the brain were cut longitudinally along the median axis. Each part of the brain was removed with a pair of scissors. The connective tissue was replaced as it was originally

and the skin was sewn together. The operated animals were kept in a large aquarium under 12L:12D for one week prior to recording the activity in the experimental aquaria. The method and procedure for recording the activity of the animal have been described in the previous papers [1, 2]. The existence of locomotive rhythm was detected by observation of the distribution of activity records.

RESULTS

Figure 1 shows diagrammatically the locality of the brain where the surgical cuts were made. The effect of each type of operation on the locomotor activity is summarized in Table 1.

Animals without the optic tectum displayed a nocturnal rhythm under 12L:12D, and a free-running rhythm in constant darkness (Fig. 2).

Without either the telencephalon and anterior part of hypothalamus, or the diencephalon, activity was not rhythmic, but was irregularly intermittent under 12L:12D or under constant darkness (Figs. 3 and 4).

When the dorsal part of the telencephalon-diencephalon was cut out horizontally to the

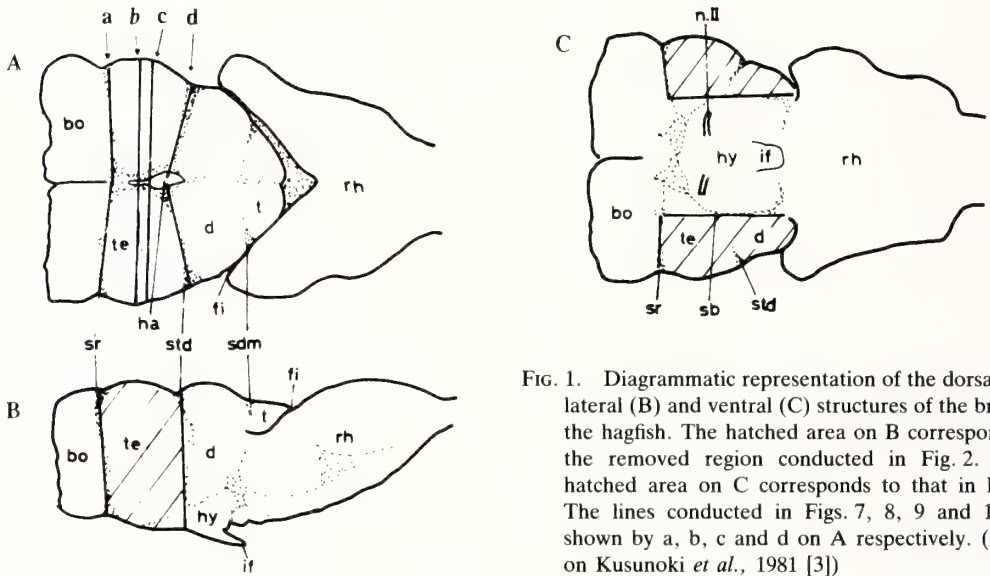


FIG. 1. Diagrammatic representation of the dorsal (A), lateral (B) and ventral (C) structures of the brain in the hagfish. The hatched area on B corresponds to the removed region conducted in Fig. 2. The hatched area on C corresponds to that in Fig. 6. The lines conducted in Figs. 7, 8, 9 and 10 are shown by a, b, c and d on A respectively. (Based on Kusunoki *et al.*, 1981 [3])

TABLE 1. Surgical operations in brain and their effects on locomotor activity rhythm in the hagfish

Removed parts and line-cuts in brain	Specimens tested, number	Free-running rhythm in constant darkness	Nocturnal rhythm in 12L:12D
telencephalon + frontal part of hypothalamus	8	—	—
diencephalon	9	—	—
optic tectum	3	+	+
dorsal part of (telencephalon + diencephalon)			
1/4	2	+	+
1/2	3	+	+
3/5	2	+	+
lateral halves of (telencephalon + diencephalon)	5	+	+*
line-cut at			
a	1	+	+
b	2	+	+
c	2	—	—
d	1	—	—

See Fig. 1 for surgical operations.

+; rhythm positive.

—; rhythm negative.

*+ the activity is not confined to the dark period.

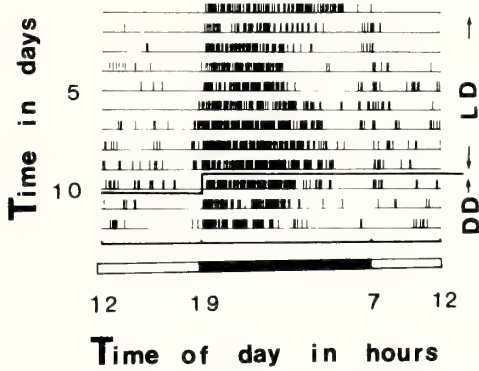


FIG. 2. Locomotor activity of the hagfish without the optic tectum kept under 12L:12D (7:00–19:00 light, 19:00–7:00 dark) and in constant darkness. The activity is indicated by the vertical marks on the time line. The operated hagfish shows activity in the dark period under 12L:12D, and exhibits, in constant darkness, the free running rhythm whose length is about 24 hr.

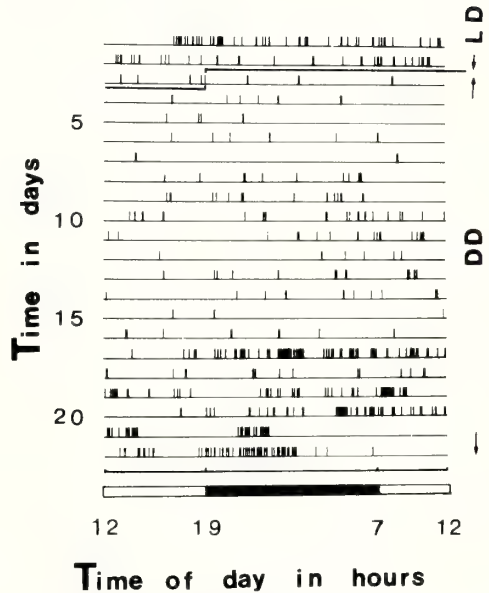


FIG. 4. Rhythm-negative activity without the diencephalon.

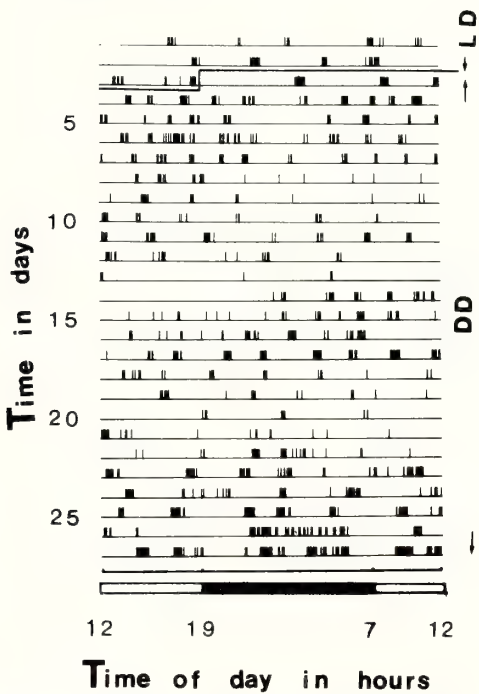


FIG. 3. Locomotor activity of the hagfish without the telencephalon (including the frontal part of hypothalamus) (see Fig. 1B). The operated hagfish shows intermittent activity both in 12L:12D and in constant darkness. This is suggestive of losing the rhythm without the tissues. The peripheral lighting conditions are the same as that explained in Fig. 2, and the following figures (Figs. 4–10) are also in the same.

depths of 1/4, 1/2 or 3/5, in all cases, the nocturnal rhythms appeared under 12L:12D and free running rhythms appeared under constant darkness (Fig. 5).

In absence of the lateral halves of the telencephalon-diencephalon, the rhythm appeared both under 12L:12D and under constant darkness. However, in the 12L:12D, the activity extended beyond the dark period and occurred even in the light period (Fig. 6). This phenomenon is similar to that in the eye ablation experiment (Kabasawa and Ooka-Souda, unpublished).

After lineal cuts across the full depth of the brain both at the border between the bulbus olfactorius and the telencephalon, and at the middle of the telencephalon, there was motor activity in the dark period under 12L:12D, and the activity pattern showed a free-running rhythm under constant darkness (Figs. 7 and 8). The cuts both anterior to the posterior large habenula and at the border between the telencephalon and the diencephalon caused intermittent activity both under 12L:12D and under constant darkness (Figs. 9 and 10).

From the results described above, it appears that the hypothalamus plays an important part in

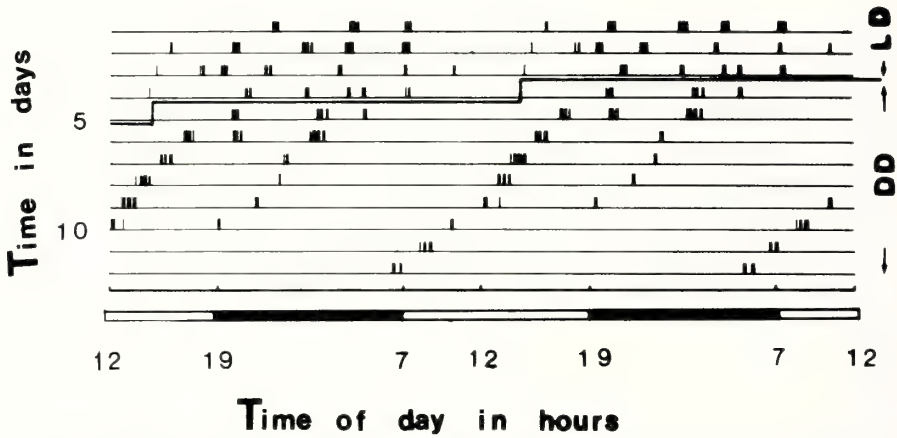


FIG. 5. Rhythm-positive activity without the upper part (3/5) of telencephalon-diencephalon. The original record is plotted twice.

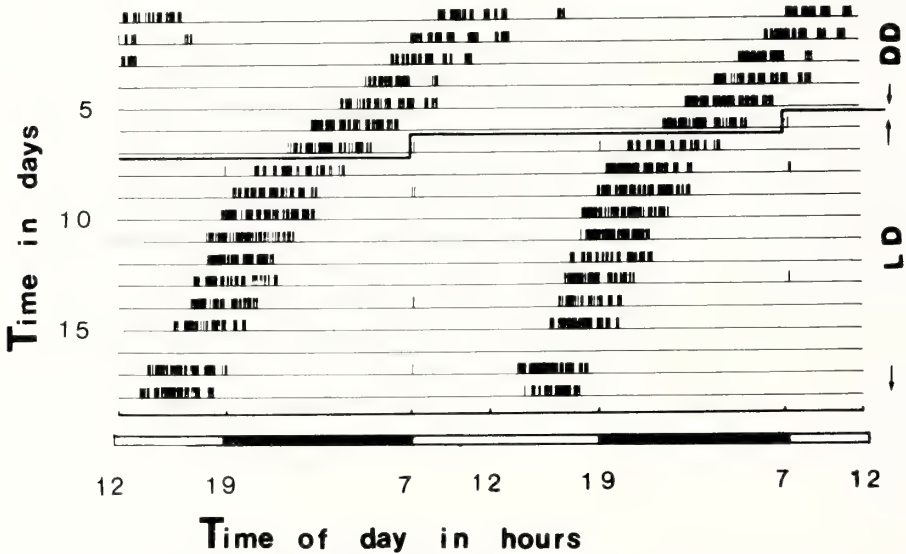


FIG. 6. Rhythm-positive activity without the lateral halves of the telencephalon-diencephalon (see Fig. 1C). In this case, the activity shows a free-running rhythm not only in constant darkness but also in 12L:12D.

circadian locomotor activity system, and it is possibly the locus for the circadian pacemaker function. As shown in Figure 1, the hypothalamus is located in the ventromedial part of the telencephalon-diencephalon and anteriorly it extended as far as the midline of the telencephalon. The results of the transectional experiments can be interpreted as meaning that the hypothalamus may include a circadian pacemaker.

DISCUSSION

There are many published reports concerning the localization of the circadian pacemaker in vertebrates. The suprachiasmatic nuclei of the rat [4], the pineal body of the chick [5], both the suprachiasmatic nuclei and the pineal body of the house sparrow [6, 7] and the pineal body of the lamprey [8] all have been proposed to be the sites

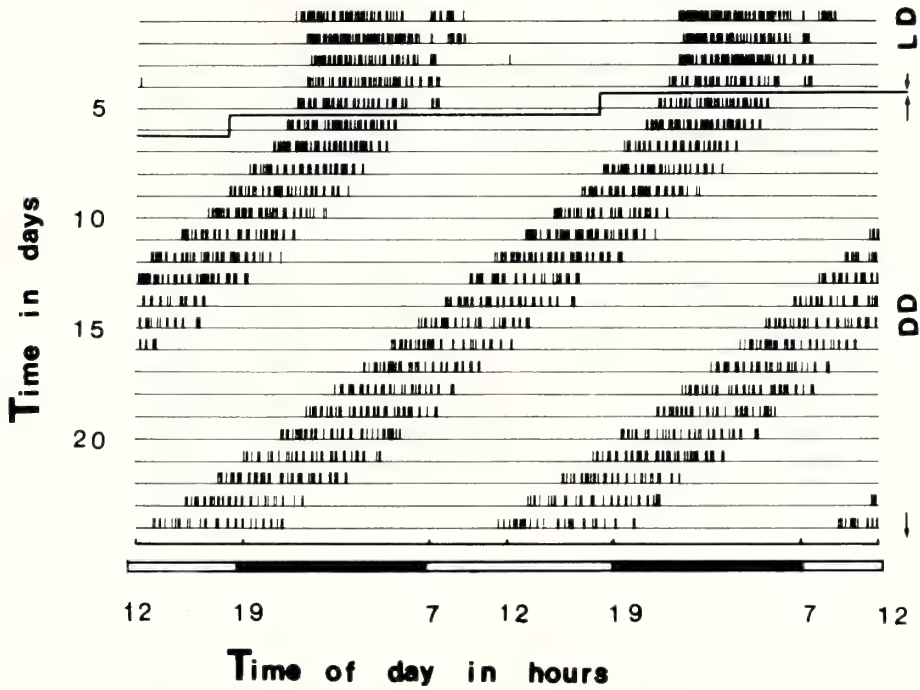


Fig. 7. Rhythm-positive activity with cutting across the border between the bulbus olfactorius and the telencephalon (see Fig. 1A, line a).

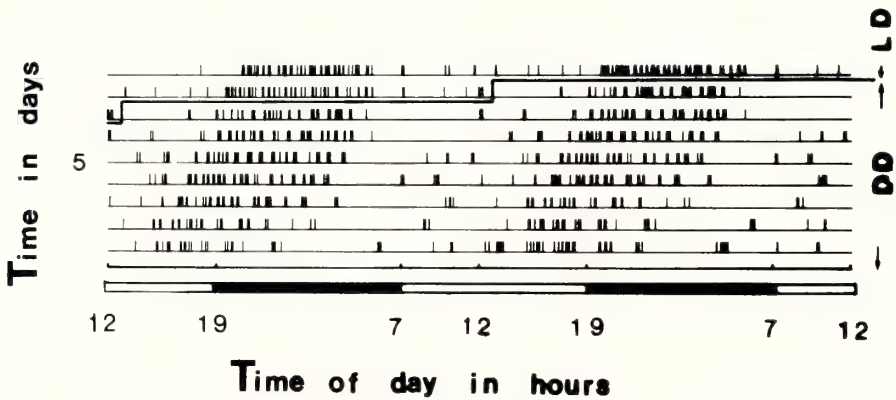


Fig. 8. Rhythm-positive activity with cutting across the middle of telencephalon (see Fig. 1A, line b).

of pacemaker function.

It has been reported that the hagfish has no pineal body [9]. In hagfish in which the dorsal part (3/5) of diencephalon was removed there still was a circadian rhythm in locomotor activity. Thus even if there was a pineal-equivalent tissue in the dorsal thalamus it would not seem to have a pacemaker

function. It is rare in lower vertebrates that the pacemaker is proposed to be situated in the hypothalamus. Continued efforts toward more precise localization of the hagfish circadian pacemaker in the hypothalamus using electrode lesion methods are in progress by the authors.

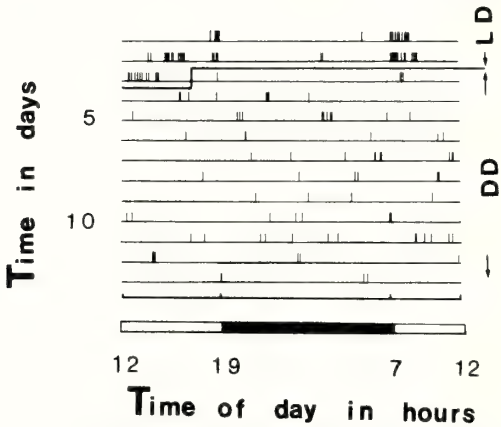


FIG. 9. Rhythm-negative activity with cutting across the front of the posterior habenula (see Fig. 1A, line c).

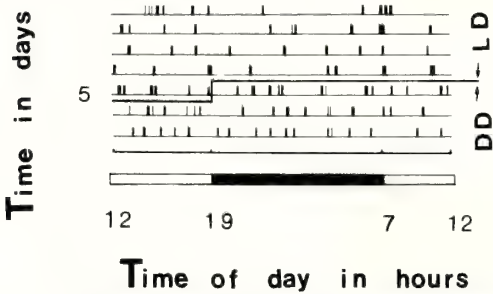


FIG. 10. Rhythm-negative activity with cutting across the border between the telencephalon and the diencephalon (see Fig. 1A, line d).

ACKNOWLEDGMENTS

All these experiments were performed at Misaki Marine Biological Station, University of Tokyo. The authors wish to express their gratitude to Prof. A. Gorbman, University of Washington, for his help in preparing the manuscript.

REFERENCES

- 1 Ooka-Souda, S., Kabasawa, H. and Kinoshita, S. (1985) Circadian rhythms in locomotor activity in the hagfish, *Eptatretus burgeri*, and the effect of reversal of light-dark cycle. *Zool. Sci.*, **2**: 749-754.
- 2 Ooka-Souda, S., Kabasawa, H. and Kinoshita, S. (1988) Circadian rhythms in locomotor activity in the hagfish, *Eptatretus burgeri*. II. The effect of brain ablation. *Zool. Sci.*, **5**: 431-435.
- 3 Kusunoki, T., Kadota, T. and Kishida, R. (1981) Chemoarchitectonics of the forebrain of the hagfish, *Eptatretus burgeri*. *J. Hirnforsch.*, **22**: 285-298.
- 4 Kawamura, H. and Inouye, S. (1979) Circadian rhythm in a hypothalamic island containing the suprachiasmatic nuclei. In "Biological Rhythms and their Central Mechanism". Ed. by M. Suda, O. Hayashi and H. Nakagawa, Elsevier/North-Holland Biomedical Press, Amsterdam, pp. 335-341.
- 5 Deguchi, T. (1979) Circadian oscillator in cultured cells of chicken pineal gland. *Nature*, **282**: 94-96.
- 6 Zimmerman, N. H. and Menaker, M. (1979) The pineal gland; A pacemaker within the circadian system of house sparrow. *Proc. Natl. Acad. Sci. U.S.A.*, **76**: 999-1008.
- 7 Takahashi, J. S. and Menaker, M. (1982) Role of the suprachiasmatic nuclei in the circadian system of the house sparrow, *Passer domesticus*. *J. Neurosci.*, **2**: 815-828.
- 8 Morita, Y. and Samejima, M. (1984) Control of diurnal and circadian locomotor rhythm by direct photosensory pineal organ. In "Animal Behavior: Neurophysiological and Ethological Approaches". Ed. by K. Aoki, S. Ishii and H. Morita, Japan Sci. Soc. Press, Tokyo/Springer-Verlag, Berlin, pp. 237-241.
- 9 Bone, Q. (1963) The central nervous system. In "The Biology of Myxine". Ed. by A. Brodal and R. Fänge, Scand. Univ. Books, Oslo, pp. 50-91.

Feeding Responses of Pacific Snappers (genus *Lutjanus*) to the Yellow-bellied Sea Snake (*Pelamis platurus*)

PAUL J. WELDON

*Department of Biology, Texas A & M University,
College Station, TX 77843, U.S.A.*

ABSTRACT—Previous studies indicate that Pacific fishes refuse to attack the yellow-bellied sea snake (*Pelamis platurus*). Visual and non-visual cues are thought to be used to identify this snake. Three species of Pacific snappers – *Lutjanus aratus*, *L. argentiventris*, and *L. guttatus* – were tested for reactions to pieces or extracts of *P. platurus*. Snappers presented with carcass pieces of a variety of stimulus animals regurgitated *P. platurus* more than others; one experiment was inconclusive. Snappers presented in darkness with pieces of stimulus animals attached to clips removed fewer *P. platurus* pieces than those of other species. Pieces of *P. platurus* skin were regurgitated more frequently, and removed from clips less frequently, than were pieces of skinned carcass or control animals. Large pieces (5.0 g) of *P. platurus* were regurgitated and rejected more often than were small pieces (1.3 g). Snappers regurgitated and rejected fish pieces treated with a chloroform:methanol extract of *P. platurus* more than pieces treated with solvent alone. This study indicates that snappers detect chemicals from this snake.

INTRODUCTION

The yellow-bellied sea snake (*Pelamis platurus*) is found from the west coast of Central America to the east coast of Africa [1]. Although predation pressure in tropical Pacific waters is notoriously intense [2], no species has been observed to eat this highly venomous, pelagic serpent. A couple of presumed predators (rather than scavengers) have regurgitated *P. platurus* [3, 4], but stomach content analyses of a variety of predatory fishes – 457 fishes representing 25 species from Panama [1], 186 dolphins (*Stenella* spp.) and 79 tuna (*Thunnus albacores*) from the eastern Pacific [5], approximately 1000 sharks (mostly *Carcharhinus falciformis*) from Baja California to Costa Rica (S. Kato, pers. comm.), and thousands of sharks from around Australia [6, 7] – failed to indicate this snake's remains. Heatwole [6] inspected 19 species of marine snakes in Australian waters for predator-induced injuries and found that *P. platurus* was the only amply represented species that lacked any sign of attacks by fishes. Wounds in *P.*

platurus from the eastern Pacific have been documented, but at least some of these appear to be man-made rather than caused by would-be predators [8].

Observations of the reactions of birds and predatory fishes to *P. platurus* indicate that this snake is avoided. Naive herons and egrets in Panama presented with several eels, a terrestrial snake, and *P. platurus* fled only from the latter [9]. A variety of teleost and elasmobranch fishes refused to attack *P. platurus* or regurgitated pieces of this snake if they were ingested [10].

The cues by which potential predators recognize sea snakes have not been studied systematically, but several authors suggest that the conspicuous yellow (ventral) and black (dorsal) coloration of *P. platurus* acts as an aposematic signal [1, 6, 10, 11]. Rubinoff and Kropach [10] state that other cues also may be involved since snake pieces were rejected by Pacific fishes even after the snakes' color patterns had been modified with marking pens, when snakes were skinned, and when snake pieces were wrapped in squid flesh. Rubinoff and Kropach [10] suggest that fishes identify snakes by chemical cues.

This study examines the feeding reactions of

Pacific snappers (*Lutjanus* spp.) to pieces of *P. platurus* and other animals, and tests the acceptability to the fishes of different sized *P. platurus* pieces and those from different body parts. In addition, the reactions of snappers to chemicals extracted from *P. platurus* are examined.

The *Lutjanus* species used in this study are found primarily on the continental shelf over rocky or sandy substrates [12], where they could encounter sea snakes. Adult *Lutjanus* spp. generally are non-specialized feeders [13, 14]; they therefore were deemed appropriate to test as potential predators of sea snakes. Since some of the snappers tested in this study fed regularly only in darkness (at night), the descriptions and results of diurnal and nocturnal feeding tests are given separately.

DIURNAL TESTS

Reactions to different species

Methods: Six mullet snappers, *Lutjanus aratus* (total lengths = 28–42 cm), were maintained together in an 18.0×6.6 m tank filled one meter deep with recirculating water. The mean water temperature in this and other tanks ranged from 27 to 29°C. These fish had been captive for at least one year, during which they were fed shrimp on an irregular schedule. They were fed shrimp each of two days before testing began.

Pieces of *P. platurus*; two fishes, *Tylosurus fodiator* and *Pomadasys panamensis*; and a squid, *Lolliguncula panamensis*, were presented to the snappers. The snakes used in this and in other experiments ranged from 34 to 62 cm (total lengths). Stimulus animals were sacrificed and kept frozen no more than two days before material from them was used, unless stated otherwise.

The stimulus animals were thawed and pieces, including integument and muscle, were cut from them (1.2–2.3 g). Pieces of squid were taken from the mantle. All pieces were wrapped in aluminum foil, kept frozen, and thawed at least 20 min before being presented to the fish.

Pieces of the stimulus animals were dropped one at a time to the snappers. If a piece was ingested and not regurgitated within one minute, the next

stimulus animal was presented. Observations on fish that regurgitated and reingested a piece were continued for an additional three minutes, beginning the moment the food was reingested. Fish that accepted a piece of stimulus animal after another fish had regurgitated it also were observed for an additional three minutes. Rejection was scored if a piece was ingested, regurgitated, and not consumed by any fish within three minutes of the last regurgitation. A session refers to the period during which the reactions of one or more fish to a piece of stimulus animal were observed.

The snappers were tested until a total of 30 pieces of each stimulus animal were consumed or regurgitated during tests over two consecutive days. Tests were conducted between 13:00 and 16:00 hr.

Results: *P. platurus* pieces were regurgitated 23 times during eight sessions; no other pieces were regurgitated and none were rejected. The Fisher exact-probability test indicates that regurgitations occurred during significantly more sessions with *P. platurus* pieces than with the other species ($P=0.002$).

Methods: Five yellow tail snappers, *L. argentiventris* (total lengths = 22–38 cm), and four spotted rose snappers, *L. guttatus* (19–36 cm), were maintained in a 4.4×4.0 m tank filled one meter deep with recirculating sea water. These fishes had been captive for 20 days before testing and were fed pieces of squid on each of three days before testing began.

The stimulus animals were *P. platurus*; two fishes, *Oligoplites mundus* and *Tylosurus fodiator*; and an octopus, *Octopus vulgaris*. Pieces of stimulus animals were prepared as described in the previous experiment.

Fishes were tested for four consecutive days between 12:00 and 14:00 hr, with responses to ten pieces of each stimulus animal scored per day.

Results: *P. platurus* pieces were regurgitated four times during three sessions; no other pieces were regurgitated and none were rejected. The Fisher exact-probability test fails to indicate that this trend is significant ($P>0.10$).

Responses to different sized *Pelamis* pieces

Methods: Five *L. argentiventris* tested in the previous experiment were kept together in a 4.4×4.0 m tank. They were fed shrimp each of two days before testing. Small (1.3 g) and large (5.0 g) pieces of *P. platurus* were freshly cut and presented to the snappers. Ten pieces each of small and large snakes were presented to the fish each day for three consecutive days between 10:00 and 11:00 hr. During these tests, fish sometimes approached the snake pieces, touched them with their snout, and moved away without ingesting them.

Results: The small pieces of *P. platurus* were regurgitated during one session; none were rejected. The large pieces were regurgitated or refused after snout contact during ten sessions; five were rejected. The Fisher exact-probability test indicates that large pieces were refused and rejected during significantly more sessions than were small pieces ($P < 0.005$ for both measures).

Acceptability of different *Pelamis* body parts

Methods: Five *L. argentiventris* were presented with pieces of the following parts of *P. platurus*: muscle (1.0–1.5 g), dorsal whole skin, ventral whole skin (0.9–1.6 g), and shed skin (0.7–1.2 g). The snakes from which the muscle and whole skin samples were obtained were decapitated, eviscerated, and their whole skin was cut away from the carcass. The dorsal (black) and ventral (yellow) skin were separated. Shed skins, pooled from several collected off the surface of the snakes' aquarium, were wrapped in aluminum foil and kept frozen. Each piece of shed and whole skin was folded and tied to present a compact morsel to the fish. Pieces of squid mantle (2.5 g) served as controls. A total of 12 pieces of each item was presented to the fish, six in each of two consecutive days. Tests were run between 12:00 and 13:00 hr.

Results: *P. platurus* shed skins were regurgitated 11 times during eight sessions; they were rejected in seven sessions. No other pieces were

regurgitated. The Fisher exact-probability test indicates that shed skins were regurgitated and rejected during significantly more sessions ($P < 0.002$ for both measures).

Methods: Four *L. guttatus*, maintained in a 4.4×4.0 m tank filled 2.2 m, were tested as described above, except that the fish *Vomer declivifrons* was used as the control animal. Six pieces of each item were presented, three in each of two consecutive days.

Results: The total number of sessions during which *P. platurus* dorsal, ventral, and shed skins were regurgitated (and total regurgitations) were 6 (7), 4 (10), and 4 (6), respectively. Rejection of these materials occurred during 6, 4, and 4 sessions respectively. No regurgitation was observed with either fish or *P. platurus* skinned carcasses. The Fisher exact-probability test indicates that, despite the small sample size, snake skins were regurgitated and rejected during more sessions than were pieces of fish or skinned snakes ($P < 0.05$ in all cases).

Responses to *Pelamis* extracts

Methods: Four *L. guttatus* (total lengths = 37–40 cm) were captured and maintained in a 9.0×6.6 m tank for one month before regularly accepting food (pieces of various fishes). They were fed fish three days before testing.

Fifteen snakes (total lengths = 34–36 cm) were cut into 5 cm pieces and placed into one liter of a chloroform:methanol (2:1 v/v) solution. The solution was heated (40°C) for several hours and filtered. The filtrate was placed over a water bath (60°C) on a rotary evaporator for 2 hr, after which an aqueous solution was poured off and saved. The remaining residue was dissolved in 150 ml of chloroform and kept 13 hr in an open glass beaker under ventilation to remove the solvent. A total of 0.31 g of residue remained after the chloroform had evaporated. This residue was redissolved in 25 ml of chloroform.

Strips of the integument and muscle of a fish (*Scomberomorus sierra*) were cut into 4.5 g pieces. The experimental pieces were soaked for 10 hr in

the aqueous snake extract solution and were injected with 0.5 ml of the chloroform-soluble carcass extract (some of which flowed out on to the surface). The control pieces were soaked in a distilled water:methanol solution (1:1 v/v) for 10 hr and injected with 0.5 ml of chloroform. Both experimental and control fish pieces were wrapped in aluminum foil and allowed to air-dry for 4 hr. They were kept refrigerated (4°C) for several days during tests.

Fish were presented with 5–7 items a day between 09:00 and 13:00 hr and were observed for one minute. If regurgitation and reingestion occurred, the session was extended for three minutes. A total of 17 pieces each of control and *Pelamis*-treated pieces were presented.

Results: The control pieces were regurgitated twice during one session; none were rejected. The *Pelamis*-treated pieces were regurgitated a total of 31 times during eight sessions and rejected in six sessions. The Fisher exact-probability test detects significantly higher rates of regurgitation ($P < 0.01$) and rejection ($P < 0.001$) with *Pelamis*-treated pieces.

NOCTURNAL TESTS

Reactions to different species

Methods: Seven *L. guttatus* (total lengths = 23–28 cm) were captured and maintained for one month in a 9.0 × 6.6 m tank filled to 1.1 m deep. These fish refused to eat pieces of fish offered to them during the day, but at night they accepted food attached to wooden clips suspended from a string immersed into their tank. The string (11 m) was tied at opposite ends along one side of the tank. A metal weight was attached to each of nine wooden clips, placed 60 cm apart on the string. The food items attached to the clips were situated from 20 to 100 cm from the floor of the tank during the test.

Pieces from three stimulus species were presented: *P. platurus*, *Octopus vulgaris*, and the fish, *Scomberomorus sierra*. Each piece (3.5 g) included the integument and underlying muscle tissue. Three pieces of each stimulus animal were

presented during each one hour session. The pieces were attached in a random order on the clips, the lights were extinguished, and the string was lowered into the water; fish, therefore, were not permitted visual access to the items.

After one hour, the string was raised out of the water, the lights were turned on, and the pieces remaining on the string were noted. Four consecutive sessions were run each of two nights, giving 24 presentations of each stimulus animal. All nocturnal tests were conducted between 20:00 and 02:00 hr.

Results: A total of 20, 6, and 1 pieces of *P. platurus*, octopus, and fish, respectively, remained attached to the clips. The χ^2 test indicates that significantly more snake pieces were left attached than were the other items ($P < 0.001$).

Reactions to marine and terrestrial snakes

The same fish, facilities, and protocol described in the previous test were used. Fish were presented with pieces (3.5 g) of *P. platurus*, western diamondback rattlesnakes (*Crotalus atrox*), and the fish, *Scomberomorus sierra*. The rattlesnakes were obtained in Nolan County, Texas. The carcasses of both *Pelamis* and *Crotalus* had been kept frozen (–70°C) for 5 months and shipped on dry ice. A total of 36 of each item was presented to snappers over three nights.

Results: A total of 31, 9, and 0 pieces of *P. platurus*, rattlesnake, and fish, respectively, remained attached to the clips. The χ^2 test indicates that significantly more *P. platurus* pieces were left attached than were the other items ($P < 0.001$).

Acceptability of different *Pelamis* body parts

The same fish, facilities, and protocol described in the previous two tests were used in this experiment. Fish were presented with pieces of *P. platurus* whole skin (1.4 g), skinned carcass (3.2 g), and a fish (*Epinephalus* sp.) (3.5 g). A total of 36 of each item was presented to snappers over three nights.

Results: A total of 24, 15, and 0 pieces of *Pelamis* skin, *Pelamis* carcass, and fish, respective-

ly, remained attached to the clips. The χ^2 test indicates significantly more pieces of skin were left attached than were pieces of snake carcass or fish ($P < 0.05$).

DISCUSSION

The reactions of *Lutjanus* spp. to the stimulus animals presented in this study indicate that *P. platurus* is least acceptable as food. Bullseye puffers (*Sphoeroides annulatus*) also rejected *P. platurus* more frequently than pieces of fishes or squid [8], as did spotted cabrillas (*Epinephelus analogus*) (Weldon, preliminary observation). These results agree with initial observations by Rubinoff and Kropach [10] on the rejection of this snake by numerous Pacific fishes.

Kropach [11] suggested that *Lutjanus* spp. attend to visual cues in avoiding *P. platurus*., *L. aratus* and *L. argentiventris* immediately and rapidly swim away from *P. platurus* introduced into their tanks, even when dead snakes coated with varnish were used (Weldon, preliminary observation). It seems likely that visual stimuli do elicit avoidance by snappers, but other cues may also be involved.

The reactions of fishes during the diurnal tests were scored if the items presented were contacted by the snout or taken into the oral cavity. Visual cues may have been discerned, but the decision to swallow or regurgitate these materials likely was based upon post-ingestive information of a chemical or mechanical nature. The results of the nocturnal experiments indicate that snappers discriminated between pieces of *P. platurus* and other animals under conditions where no visual information was available. The increased frequencies with which larger *P. platurus* pieces were regurgitated and rejected in tests with different sized pieces probably were due to mechanical difficulties encountered in swallowing.

MacLeish [15] describes an "underwater taste test" where Australian fishes regurgitated the carcass of a sea snake (not *P. platurus*). It has been unclear, however, whether the refusal of snakes by fishes is elicited by chemicals. The greater frequencies of regurgitation and rejection of fish pieces treated with *P. platurus* extract,

compared to those observed with solvent-treated controls, support the hypothesis that fish attend to chemicals to avoid ingesting this snake. The solubility of these substances suggests that they are lipoidal.

The results of the nocturnal test comparing fishes' reactions to *P. platurus* and the rattlesnake, *Crotalus atrox*, suggest that snappers discriminate between these species on the basis of non-visual cues. Tests of the reactions of fishes to extracts of various snakes are needed. While *P. platurus* appears to be relatively predator-free, other marine snakes occasionally are eaten by sharks [7, 16]. Whether snakes differ in palatability is unknown.

Pacific fishes, including *Lutjanus* spp., have been observed to reject *P. platurus* carcasses bereft of skin [1, 10]. No pieces of skinned *P. platurus* were regurgitated by the snappers in the diurnal tests here. *L. guttatus* rejected ventral, dorsal, and shed skins of *P. platurus*, and *L. argentiventris* rejected pieces of shed skin, which probably were recognized as inedible. The results of the nocturnal test with *L. guttatus* also indicate that whole snake skin is less acceptable than the skinless snake carcass. It is unclear whether the decision to regurgitate or eat different parts of *P. platurus* is based upon chemical or mechanical cues since the materials used differ in texture and consistency. Tests of fishes' reactions to extracts from different body parts are needed to determine whether unpalatable chemicals are localized in the body of *P. platurus*.

ACKNOWLEDGMENT

I. Rubinoff generously offered facilities and logistical support for this research. K. Haworth, O. Vallarino, and A. Velarde provided expert field and laboratory assistance. S. Kato provided unpublished information on shark stomach contents. H. Drummond, D. R. Robertson, and I. Rubinoff made helpful comments on an earlier version of this manuscript, and R. Eaton typed it. This study was supported by grants from the Smithsonian Institution and the Whitehall Foundation.

REFERENCES

- 1 Kropach, C. N. (1973) A field study of the sea snake

- Pelamis platurus* (Linnaeus) in the Gulf of Panama. Ph. D. Diss., The City University of New York.
- 2 Vermeij, G. J. (1978) Biogeography and Adaptation: Patterns of Marine Life. Harvard University Press, Cambridge.
 - 3 Heatwole, H. and Finnie, P. E. (1980) Seal predation on a sea snake. *Herpetofauna*, **11**: 24.
 - 4 Pickwell, G. V., Bezy, R. L. and Fitch, J. E. (1983) Northern occurrences of the sea snake, *Pelamis platurus*, in the eastern Pacific, with a record of predation on the species. *California Fish Game*, **69**: 172–177.
 - 5 Perrin, W. F., Warner, R. R., Fiscus, C. H. and Holts, D. B. (1973) Stomach contents of porpoise, *Stenella* spp., and yellowfin tuna, *Thunnus albacores*, in mixed-species aggregations. *Fish. Bull.*, **71**: 1077–1092.
 - 6 Heatwole, H. (1975) Predation on sea snakes. In "The Biology of Sea Snakes". Ed. by W. A. Dunson, University Park Press, Baltimore, pp. 233–249.
 - 7 Lyle, J. M. and Timms, G. J. (1987) Predation on aquatic snakes by sharks from northern Australia. *Copeia*, **1987**: 802–803.
 - 8 Weldon, P. J. and Vallarino, O. (1988) Wounds on the yellow-bellied sea snake (*Pelamis platurus*) from Panama : Evidence of would-be predators? *Biotropica*, **20**: 298–301.
 - 9 Caldwell, G. S. and Rubinoff, R. W. (1983) Avoidance of venomous sea snakes by naive herons and egrets. *Auk*, **100**: 195–198.
 - 10 Rubinoff, I. and Kropach, C. (1970) Differential reactions of Atlantic and Pacific predators to sea snakes. *Nature*, **228**: 1288–1290.
 - 11 Kropach, C. (1975) The yellow-bellied sea snake, *Pelamis*, in the eastern Pacific. In "The Biology of Sea Snakes". Ed. by W. A. Dunson, University Park Press, Baltimore, pp. 185–213.
 - 12 Thomson, D. A., Findley, L. T. and Kerstitch, A. M. (1979) Reef Fishes of the Sea of Cortez. John Wiley & Sons, New York.
 - 13 Hobson, E. S. (1968) Predatory behavior of some shore fishes in the Gulf of California. *Bull. Sports Fish. Wildlife, Res. Rep.*, **73**: 1–92.
 - 14 Walford, L. A. (1937) Marine Game Fishes of the Pacific Coast from Alaska to the Equator. University of California Press, Berkeley.
 - 15 MacLeish, K. (1972) Diving with sea snakes. *Natl. Geogr.*, **141**: 565–578.
 - 16 Heatwole, H., Heatwole, E. and Johnson, C. R. (1974) Shark predation on sea snakes. *Copeia*, **1974**: 780–781.

Geographical Differentiation in Populations of Japanese Dace *Tribolodon hakonensis* Deduced from Allozymic Variation

NAOTO HANZAWA¹, NOBUHIKO TANIGUCHI²
and KEN-ICHI NUMACHI³

Ocean Research Institute, University of Tokyo, Minamidai, Nakano-ku, Tokyo 164,

²Laboratory of Aquatic Ecology, Faculty of Agriculture, Kochi University,

Nankoku, Kochi 783, and ³Otsuchi Marine Research Center, Ocean

Research Institute, University of Tokyo, Akahama, Otsuchi,

Iwate 028-11, Japan

ABSTRACT—Allozymic variation of Japanese dace *Tribolodon hakonensis* was examined at 20 loci in 17 populations derived from Hokkaido to Kyushu. Intrapopulation variability indicated by the proportion of loci polymorphic and heterozygosity was close to the standard levels in vertebrates. On the other hand, allelic frequencies at five loci of the twenty were remarkably different among populations, and even replacement of predominant alleles was observed. The extent of interpopulation differentiation was estimated by coefficient of gene differentiation (G_{st}) and genetic distance (D). Levels of these indices were remarkably high compared with the levels known among populations in many vertebrates. Based on a dendrogram, we classified the populations into three local groups; 1) Northern Group, 2) Southern Group, and 3) Lake Biwa Group. These results suggest that the populations of different local groups have been highly differentiated from each other and the differentiation is due to geographical isolation.

INTRODUCTION

The genus *Tribolodon* which belongs to the family Cyprinidae has a unique characteristic on distribution: it is widely distributed from the upper reaches of rivers to the coastal regions of the sea in Japan and adjacent countries. The other genera of Cyprinidae do not show such a wide distribution. Therefore fishes of *Tribolodon* have been extensively studied from the viewpoints of physiology [1] and ecology [2]. However, their taxonomy had been confused and greatly different among taxonomists [3-5], because the species of this genus have not been morphologically differentiated enough from each other. Our previous study using allozyme markers clearly showed that the four

species of *Tribolodon* classified by Nakamura [4] had been genetically differentiated enough as highly as the interspecific levels in vertebrates [6, 7]. Thus, biochemical analysis provided good information as for taxonomy. In addition, we examined *T. hakonensis* from the waters in Fukushima Pref. and Kochi Pref. in the previous work, and found the possibility that this species contained the highly differentiated populations [7].

In this work, we further analysed *T. hakonensis* collected at more locations from Hokkaido to Kyushu, evaluated the level of intraspecific variability and the extent of interpopulation differentiation, and discussed the evolutionary aspects in populations of *T. hakonensis*.

MATERIALS AND METHODS

Specimens

We collected a total of 883 specimens of *T.*

Accepted September 30, 1987

Received March 16, 1987

¹ Present address: Department of Cytogenetics, National Institute of Genetics, Mishima, Shizuoka 411, Japan.

hakonensis in 17 waters from Hokkaido to Kyushu. Sample locations are shown in Figure 1, and sample sizes are given in Table 3. Fish were caught at a single location within a few days by a gill net, a casting net, and angling, and were frozen by dry ice at once and stored under -20°C . In the Otsuchi, the Monobe, and the Shimanto Rivers, specimens were collected at a few locations, the upper reaches, and the lower reaches or the coastal regions of the sea, which were isolated by dums at present.

Electrophoretic analyses

Horizontal starch gel electrophoresis was performed upon drip from tissue samples as described by Numachi [8]. The following four buffer systems (Table 1) were used: CAPM (citric acid, 4-(3-aminopropyl)-morpholine), pH 6.0 described by Clayton and Tretiak [9]; CAEA (citric acid,

N-(3-aminopropyl)-diethanol-amine), pH 7.0 and CT (citric acid, tris), pH 8.0 described by Numachi *et al.* [10]; and TBE (tris, boric acid, EDTA), pH 8.7 described by Numachi [11]. The staining methods were according to Shaw and Prasad [12], and Taniguchi and Numachi [13]. The gels stained were washed and dried by the method of Numachi [14]. A list of proteins analysed, their abbreviations, E. C. numbers, locus designations, tissues, and buffers employed are shown in Table 1. Tissues of skeletal muscle, liver, heart, and blood were used. Mitochondrial and supernatant isozymes of AAT, IDH, MDH, and ME were discriminated.

Locus and allele designation followed Hanzawa *et al.* [15]. The most common alleles in the populations of the Northern Group were designated as 100 or -100, and the other alleles were designated by the relative differences in elec-

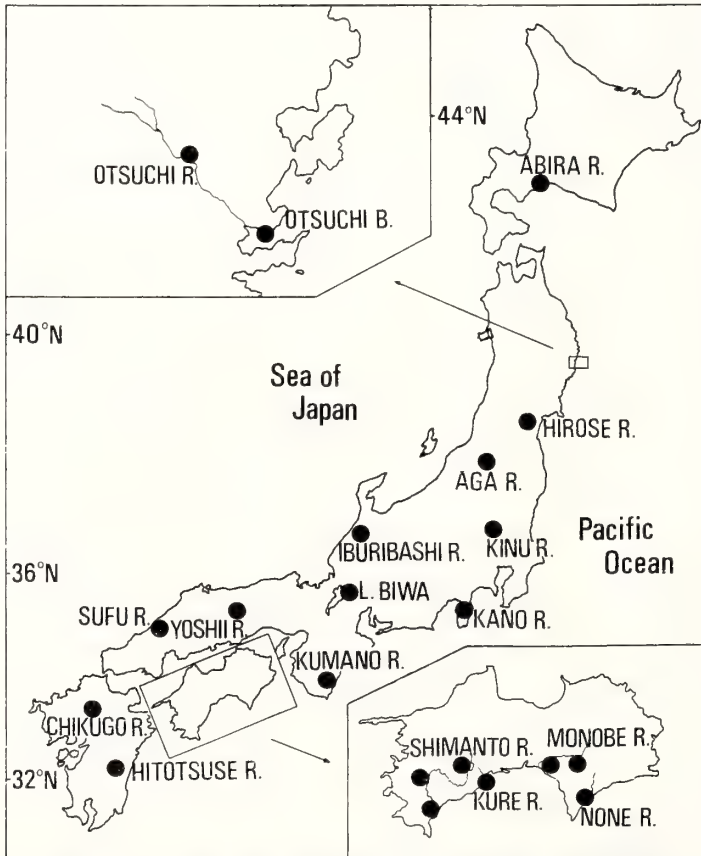


FIG. 1. The sites where specimens of *T. hakonensis* were sampled.

TABLE 1. Enzymatic and non-enzymatic proteins examined, locus designations, tissues, and electrophoretic buffers employed

Protein (Abbreviation; E.C. Number)	Locus	Tissue	Buffer
Aspartate aminotransferase (AAT; 2.6.1.1)	<i>m-Aat</i>	muscle	CT
Alcohol dehydrogenase (ADH; 1.1.1.1)	<i>Adh</i>	liver	CAEA
α -Glycerophosphate dehydrogenase (α -GDH; 1.1.1.8)	<i>α-Gdh-2</i>	liver	CAEA
Glucosephosphate isomerase (GPI; 5.3.1.9)	<i>Gpi-1</i>	heart	TBE
	<i>Gpi-2</i>	heart	TBE
Hemoglobin (HB)	<i>Hb-1</i>	blood	CT
	<i>Hb-2</i>	blood	CT
Isocitrate dehydrogenase (IDH; 1.1.1.42)	<i>s-Icd-1</i>	liver	CAEA
	<i>s-Icd-2</i>	liver	CAEA
Lactate dehydrogenase (LDH; 1.1.1.27)	<i>Ldh-1</i>	heart	CT
	<i>Ldh-2</i>	muscle	CT
	<i>Ldh-3</i>	liver	CT
Malate dehydrogenase (MDH; 1.1.1.37)	<i>s-Mdh-1</i>	muscle	CAPM
	<i>s-Mdh-2</i>	liver	CAPM
	<i>m-Mdh</i>	muscle	CAEA
Malic enzyme (ME; 1.1.1.40)	<i>s-Me</i>	muscle	CAEA
Phosphoglucomutase (PGM; 2.7.5.1)	<i>Pgm</i>	muscle	CAEA
6-Phosphogluconate dehydrogenase (6-PGD; 1.1.1.44)	<i>6-Pgd</i>	liver	CAEA
Sarcoplasmic protein (SP)	<i>Sp-2</i>	muscle	CAEA
	<i>Sp-3</i>	muscle	CAEA

trophoretic mobility of respective gene products with the reference allele, *100* or *-100*.

Statistical analyses

Amount of intrapopulational variability was evaluated by the proportion of loci polymorphic and heterozygosity. Degree of interpopulational differentiation was evaluated by coefficient of gene differentiation (G_{ST}) [16] and genetic distance (D) [17]. G_{ST} value, which is calculated based on average heterozygosity, indicates the degree of allelic differentiation over all populations. D value, which is calculated based on allelic frequencies, indicates the degree of differentiation between pairs of populations. Divergence time between the populations was estimated based on D value and gene substitution rate of 10^{-7} [16].

RESULTS

Intrapopulational variation

Twenty loci controlling 12 kinds of enzymatic

and nonenzymatic proteins were examined. The genetic control by 20 loci was mainly deduced from the phenotypes of different species and their hybrids [6, 7, 15]. Allozymic variation was found at 14 of the 20 loci in sample populations of *T. hakonensis*. Particularly, various polymorphisms were observed at 5 loci, *Adh*, *α -Gdh-2*, *Gpi-2*, *s-Mdh-2*, *6-Pgd*, and each allelic control was interpreted (Fig. 2). Deviations of observed number of phenotypes from their expectations under Hardy-Weinberg equilibrium were not significant in all sample populations except the upper reach of the Shimanto River (at *6-Pgd*, $P < 0.05$).

Intrapopulational variability of *T. hakonensis* indicated by proportion of loci polymorphic and heterozygosity was given in Table 2. The proportion of loci polymorphic ranged from 0.05 to 0.50, and the mean value indicated 0.22 ± 0.10 . Heterozygosity observed ranged from 0.019 to 0.085, and the mean value indicated 0.041 ± 0.019 . Levels of these two indices were similar among sample populations. Heterozygosity observed agrees with its expectation ($H^o/H^E = 1$).

TABLE 2. Estimates of genetic variability at 20 loci within populations of *T. hakonensis*

Location	Proportion of loci polymorphic	Heterozygosity		H ^O /H ^E
		(Observed; H ^O)	(Expected; H ^E)	
Abira R.	0.30	0.039	0.040	0.976
Otsuchi				
upper reach	0.20	0.019	0.020	0.950
Otsuchi Bay	0.30	0.028	0.028	1.000
Hirose R.	0.25	0.046	0.047	0.979
Kinu R.	0.50	0.069	0.075	0.922
Kano R.	0.30	0.072	0.081	0.889
Aga R.	0.25	0.035	0.037	0.952
Iburibashi R.	0.15	0.030	0.029	1.039
Yoshii R.	0.10	0.019	0.019	0.947
Sufu R.	0.20	0.023	0.021	1.098
Chikugo R.	0.15	0.033	0.033	1.014
L. Biwa	0.40	0.085	0.089	0.954
Kumano R.	0.25	0.072	0.074	0.970
None R.	0.15	0.034	0.030	1.125
Monobe R.				
upper reach	0.05	0.026	0.024	1.111
lower reach	0.15	0.029	0.024	1.212
Kure R.	0.10	0.028	0.031	0.917
Shimanto R.				
upper reach	0.25	0.050	0.059	0.848
middle reach	0.20	0.048	0.049	0.974
lower reach	0.20	0.042	0.042	1.000
Hitotsuse R.	0.20	0.034	0.034	1.003
	(0.22 ± 0.10)	(0.041 ± 0.019)		

Interpopulational differentiation

Gene constitution of sample populations collected at 21 locations in 17 waters from Hokkaido to Kyushu were compared (Table 3). Allelic frequencies among subpopulations within the same waters were very similar, and a significant deviation among allelic frequencies was not observed at all loci except *Adh* and α -*Gdh-2* in the Shimanto River population. These subpopulations were isolated by dums at present, and fish of the Otsuchi Bay was particularly the amphidromous type. However, gene constitution of these subpopulations within the same waters was thus very similar.

On the other hand, remarkable differences among populations derived from the different waters were found at five loci, *Adh*, α -*Gdh-2*,

Gpi-2, *s-Mdh-2*, *6-Pgd*. At *Adh* and α -*Gdh-2* of the five, predominant alleles of *100* in the populations of the Pacific coast of the northern Japan and of the coast of the Sea of Japan were replaced with the other alleles (*119* or *0*) in those of the Pacific coast of the southern Japan. Similarly, predominant allele of *100* at *6-Pgd* was replaced with *127* only in the Lake Biwa and the Kumano River populations. Population specific alleles with high frequencies were found, such as *176* at *Adh* in the Lake Biwa population and *-153* at *Gpi-2* in the Kumano River population.

The extent of interpopulational differentiation was evaluated by two kinds of indices, coefficient of gene differentiation (G_{ST}) and genetic distance (D). As for the Otsuchi, the Monobe, and the Shimanto River systems, specimens collected at

TABLE 3. Allelic frequencies for 14 loci in populations of *T. hakonensis*

Location	<i>m-Aat</i>			<i>Adh</i>			<i>a-Gdh-2</i>			<i>Gpi-1</i>				<i>Gpi-2</i>			<i>s-Idh-1</i>			<i>s-Idh-2</i>		
	-100	-62	100	100	119	176	0	100	169	79	91	100	118	-153	-100	-47	52	100	85	100	155	
Abira R.	0.988	0.013	0.726	0.274	0.000	0.000	0.000	0.977	0.023	0.000	0.000	1.000	0.000	0.000	0.941	0.059	0.023	0.977	0.000	1.000	0.000	
Otsuchi upper reach	0.938	0.063	1.000	0.000	0.000	0.000	0.000	1.000	0.000	0.000	0.050	0.950	0.000	0.000	0.913	0.088	0.000	1.000	0.000	1.000	0.000	
Otsuchi Ray	0.925	0.075	1.000	0.000	0.000	0.000	0.000	0.988	0.013	0.000	0.063	0.938	0.000	0.000	0.875	0.125	0.000	1.000	0.013	0.988	0.000	
Hirose R.	0.768	0.232	0.938	0.063	0.000	0.000	0.000	1.000	0.000	0.012	0.000	0.988	0.000	0.000	0.720	0.280	0.000	1.000	0.000	1.000	0.000	
Kinu R.	0.670	0.330	0.826	0.174	0.000	0.080	0.920	0.000	0.030	0.000	0.000	0.970	0.000	0.013	0.744	0.244	0.000	1.000	0.000	1.000	0.000	
Kano R.	0.829	0.171	0.600	0.400	0.000	0.000	1.000	0.000	0.000	0.000	0.000	1.000	0.000	0.000	0.925	0.075	0.000	1.000	0.000	0.975	0.025	
Aga R.	1.000	0.000	1.000	0.000	0.000	0.015	0.985	0.000	0.015	0.000	0.000	0.985	0.000	0.000	0.712	0.288	0.000	1.000	0.000	1.000	0.000	
Iburibashi R.	1.000	0.000	1.000	0.000	0.000	0.288	0.713	0.000	0.000	0.000	0.000	1.000	0.000	0.000	0.446	0.554	0.000	1.000	0.000	0.961	0.039	
Yoshii R.	1.000	0.000	0.962	0.038	0.000	0.207	0.793	0.000	0.000	0.000	0.000	1.000	0.000	0.000	1.000	0.000	0.000	1.000	0.000	1.000	0.000	
Sufu R.	1.000	0.000	0.864	0.136	0.000	0.093	0.907	0.000	0.000	0.000	0.000	1.000	0.000	0.000	0.988	0.012	0.000	1.000	0.000	1.000	0.000	
Chikugo R.	1.000	0.000	0.591	0.409	0.000	0.239	0.761	0.000	0.000	0.000	0.000	1.000	0.000	0.000	1.000	0.000	0.000	1.000	0.000	1.000	0.000	
L. Biwa	1.000	0.000	0.000	0.526	0.474	0.879	0.121	0.000	0.000	0.000	0.000	1.000	0.000	0.019	0.815	0.167	0.000	1.000	0.000	0.976	0.024	
Kumano R.	1.000	0.000	0.000	1.000	0.000	0.769	0.231	0.000	0.000	0.000	0.000	1.000	0.000	0.446	0.554	0.000	0.000	1.000	0.000	1.000	0.000	
None R.	1.000	0.000	0.090	0.910	0.000	0.875	0.125	0.000	0.000	0.000	0.000	1.000	0.000	0.000	1.000	0.000	0.000	1.000	0.000	1.000	0.000	
Monobe R.																						
upper reach	1.000	0.000	0.000	1.000	0.000	1.000	0.000	0.000	0.000	0.000	0.000	1.000	0.000	0.000	1.000	0.000	0.000	1.000	0.000	1.000	0.000	
lower reach	1.000	0.000	0.000	1.000	0.000	0.988	0.012	0.000	0.000	0.000	0.000	1.000	0.000	0.000	1.000	0.000	0.000	1.000	0.000	1.000	0.000	
Kure R.	1.000	0.000	0.000	1.000	0.000	0.914	0.086	0.000	0.000	0.000	0.000	1.000	0.000	0.000	1.000	0.000	0.000	1.000	0.000	1.000	0.000	
Shimanto R.																						
upper reach	1.000	0.000	0.000	0.838	0.163	0.563	0.438	0.000	0.000	0.000	0.000	0.988	0.013	0.000	1.000	0.000	0.000	1.000	0.000	1.000	0.000	
middle reach	1.000	0.000	0.000	1.000	0.000	0.650	0.350	0.000	0.000	0.000	0.000	1.000	0.000	0.000	0.975	0.025	0.000	1.000	0.000	1.000	0.000	
lower reach	1.000	0.000	0.000	1.000	0.000	0.788	0.213	0.000	0.000	0.000	0.000	0.988	0.013	0.000	0.988	0.013	0.000	1.000	0.000	1.000	0.000	
Hitotsuse R.	1.000	0.000	0.023	0.965	0.012	0.718	0.282	0.000	0.000	0.000	0.000	1.000	0.000	0.000	1.000	0.000	0.000	1.000	0.000	1.000	0.000	

TABLE 3. (Continued)

Location	Ldh-1			Ldh-2			Ldh-3			S-Mdh-2			s-Me			6-Pgd			Pgm			Sample size
	87	100	-11	100	-11	100	220	-188	-100	113	81	100	119	23	100	100	100	127	100	119	144	
Abira R.	0.000	1.000	0.000	1.000	0.000	1.000	0.000	0.000	1.000	0.000	0.000	1.000	0.000	0.000	1.000	0.907	0.093	1.000	0.000	0.000	0.000	43
Otsuchi upper reach	0.000	1.000	0.000	1.000	0.000	1.000	0.000	0.000	1.000	0.000	0.000	1.000	0.000	0.000	1.000	1.000	0.000	1.000	0.000	0.000	0.000	40
Otsuchi Bay	0.000	1.000	0.000	1.000	0.000	1.000	0.000	0.000	1.000	0.000	0.013	0.988	0.000	0.000	1.000	1.000	0.000	1.000	0.000	0.000	0.000	40
Hirose R.	0.000	1.000	0.000	1.000	0.000	1.000	0.000	0.000	1.000	0.000	0.012	0.988	0.000	0.000	1.000	1.000	0.000	1.000	0.000	0.000	0.000	41
Kinu R.	0.000	1.000	0.010	0.990	0.000	0.031	0.969	0.000	0.061	0.939	0.000	0.030	0.970	0.989	0.011	1.000	0.000	0.000	0.000	0.000	0.000	33
Kano R.	0.000	1.000	0.000	1.000	0.000	0.000	1.000	0.000	0.000	0.813	0.188	0.000	1.000	0.750	0.250	1.000	0.000	0.000	0.000	0.000	0.000	50
Aga R.	0.000	1.000	0.000	1.000	0.000	0.013	0.984	0.000	0.000	1.000	0.000	0.000	0.000	1.000	0.917	0.083	1.000	0.000	0.000	0.000	0.000	40
Ibaribashi R.	0.000	1.000	0.000	1.000	0.000	0.000	1.000	0.000	0.000	1.000	0.000	0.000	0.000	1.000	1.000	0.000	1.000	0.000	0.000	0.000	0.000	40
Yoshii R.	0.000	1.000	0.000	1.000	0.000	0.000	1.000	0.000	0.000	1.000	0.000	0.000	0.000	1.000	1.000	0.000	1.000	0.000	0.000	0.000	0.000	41
Sufu R.	0.000	1.000	0.000	1.000	0.000	0.000	1.000	0.000	0.000	1.000	0.000	0.000	0.000	1.000	0.952	0.048	1.000	0.000	0.000	0.000	0.000	43
Chikugo R.	0.000	1.000	0.000	1.000	0.000	0.000	1.000	0.000	0.000	1.000	0.000	0.000	0.000	1.000	0.989	0.011	1.000	0.000	0.000	0.000	0.000	44
L. Biwa	0.034	0.966	0.000	1.000	0.000	0.000	0.955	0.045	0.000	0.739	0.261	0.000	1.000	0.236	0.764	1.000	0.000	0.000	0.000	0.000	0.000	44
Kumano R.	0.000	1.000	0.000	0.947	0.053	0.000	1.000	0.000	0.000	0.255	0.745	0.000	1.000	0.167	0.833	1.000	0.000	0.000	0.000	0.000	0.000	47
None R.	0.000	1.000	0.000	1.000	0.000	0.000	1.000	0.000	0.000	0.875	0.125	0.000	1.000	1.000	0.000	1.000	0.000	1.000	0.000	0.000	0.000	40
Monobe R. upper reach	0.000	1.000	0.000	1.000	0.000	0.000	1.000	0.000	0.000	0.619	0.381	0.000	1.000	1.000	0.000	1.000	0.000	1.000	0.000	0.000	0.000	42
Monobe R. lower reach	0.000	1.000	0.000	1.000	0.000	0.000	1.000	0.000	0.000	0.683	0.317	0.000	1.000	0.988	0.012	1.000	0.000	1.000	0.000	0.000	0.000	41
Kure R.	0.000	1.000	0.000	1.000	0.000	0.000	1.000	0.000	0.000	0.413	0.588	0.000	1.000	1.000	0.000	1.000	0.000	1.000	0.000	0.000	0.000	40
Shimanto R. upper reach	0.000	1.000	0.000	1.000	0.000	0.000	1.000	0.000	0.000	1.000	0.000	0.000	1.000	0.711	0.229	0.975	0.013	0.975	0.013	0.013	0.013	40
Shimanto R. middle reach	0.000	1.000	0.000	1.000	0.000	0.000	1.000	0.000	0.000	1.000	0.000	0.000	1.000	0.700	0.300	0.975	0.025	0.975	0.025	0.025	0.025	40
Shimanto R. lower reach	0.000	1.000	0.000	1.000	0.000	0.000	1.000	0.000	0.000	1.000	0.000	0.000	1.000	0.675	0.325	1.000	0.000	1.000	0.000	0.000	0.000	40
Htotsuse R.	0.000	1.000	0.000	1.000	0.000	0.000	1.000	0.000	0.000	0.991	0.009	0.000	1.000	0.808	0.192	1.000	0.000	1.000	0.000	0.000	0.000	54

TABLE 4. Estimates of Nei's genetic distance between pairs of 17 populations of *T. hakonensis* based on allelic frequencies at 20 loci

	17	16	15	14	13	12	11	10	9	8	7	6	5	4	3	2
1 Abira R.	.053	.064	.092	.086	.063	.135	.095	.004	.002	.005	.022	.007	.005	.009	.008	.005
2 Otsuchi Bay	.081	.094	.120	.113	.087	.172	.123	.013	.003	.003	.014	.002	.014	.006	.003	—
3 Hirose R.	.082	.095	.121	.114	.089	.169	.123	.016	.007	.009	.011	.003	.014	.002	—	—
4 Kinu R.	.069	.080	.104	.097	.074	.152	.110	.014	.009	.011	.015	.008	.011	—	—	—
5 Kano R.	.050	.058	.080	.079	.061	.103	.079	.010	.010	.016	.032	.016	—	—	—	—
6 Aga R.	.083	.094	.123	.116	.090	.163	.115	.016	.005	.007	.005	—	—	—	—	—
7 Iburibashi R.	.080	.090	.113	.104	.081	.158	.108	.025	.018	.016	—	—	—	—	—	—
8 Yoshii R.	.062	.073	.095	.087	.065	.152	.102	.007	.001	—	—	—	—	—	—	—
9 Sufu R.	.059	.070	.095	.088	.065	.146	.100	.005	—	—	—	—	—	—	—	—
10 Chikugo R.	.031	.040	.062	.054	.035	.116	.076	—	—	—	—	—	—	—	—	—
11 L. Biwa	.035	.028	.052	.045	.045	.035	—	—	—	—	—	—	—	—	—	—
12 Kumano R.	.063	.055	.051	.060	.071	—	—	—	—	—	—	—	—	—	—	—
13 None R.	.004	.007	.012	.003	—	—	—	—	—	—	—	—	—	—	—	—
14 Monobe R.	.010	.012	.004	—	—	—	—	—	—	—	—	—	—	—	—	—
15 Kure R.	.022	.025	—	—	—	—	—	—	—	—	—	—	—	—	—	—
16 Shimanto R.	.001	—	—	—	—	—	—	—	—	—	—	—	—	—	—	—
17 Hitotsuse R.	—	—	—	—	—	—	—	—	—	—	—	—	—	—	—	—

the lower reach of each river were used for the comparison among populations. G_{ST} value which indicates the extent of differentiation of allelic frequencies over 17 populations was estimated to be 0.544.

D values which indicate the extent of differentiation between pairs of populations were shown in Table 5. D values between pairs of 17 populations ranged from 0.001 to 0.172. A dendrogram based on D values was further constructed to examine genetic relationships among the populations (Fig. 3). Three major clustering groups were discriminated on this dendrogram. Namely, the populations from the Abira River to the Kano River in the Pacific coast and from the Aga River to the Chikugo River in the coast of the Sea of Japan (including the Yoshii River in the side of the Inland Sea), those from the None River to the Hitotsuse River in the Pacific coast, and those of the Lake Biwa and the Kumano River formed each of the three clustering groups. We gave names to these local groups; 1) Northern Group, 2) Southern Group, and 3) Lake Biwa Group, respectively. From Table 5, D values between the Northern Group and the Southern Group ranged from 0.031 to 0.123 (0.081 on average). Similarly, the values

between the Northern Group and the Lake Biwa Group, and between the Southern Group and the Lake Biwa Group ranged from 0.076 to 0.172 (0.125 on average), and from 0.028 to 0.070 (0.051 on average), respectively. On the other hand, D

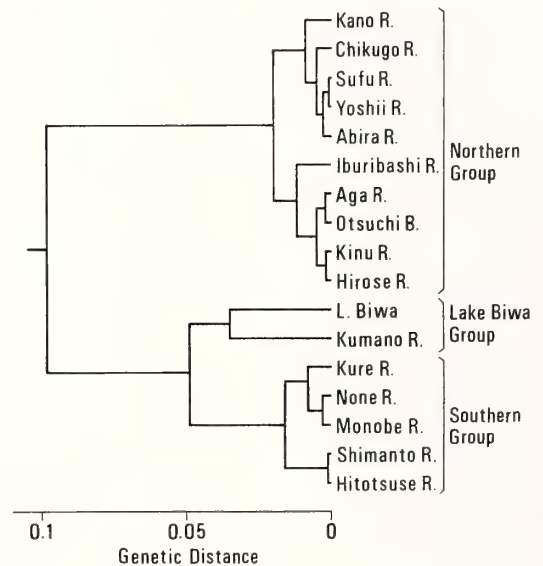


FIG. 3. A dendrogram based on Nei's genetic distance between pairs of 17 populations of *T. hakonensis*.

values between pairs of the populations within Northern, Southern, and Lake Biwa Groups ranged from 0.001 to 0.032 (0.010 on average), from 0.001 to 0.025 (0.010 on average), and 0.035, respectively. Thus, genetic distances between the local groups were considerably large compared with those within the groups.

DISCUSSION

Level of intrapopulational variability

Intrapopulational variability at protein level in various species of animals has been examined and that of fishes is close to the standard levels in vertebrates [18]. In the populations of *T. hakonensis*, proportion of loci polymorphic and heterozygosity were estimated to be 0.22 ± 0.10 and 0.041 ± 0.019 , respectively (Table 3). These values are close to the mean values of Ostariophysi (0.16 and 0.045) and are within the range of fishes [18]. Therefore, it is regarded that intrapopulational variability of *T. hakonensis* is close to the standard levels in vertebrates. At the same time, this suggests that most of the populations in *T. hakonensis* has been maintained without extreme reduction of their size.

Level of interpopulational differentiation

Allelic frequencies were remarkably different among populations of three local groups in *T. hakonensis* (Table 3) and the extent of their differentiation was estimated by two kinds of indices. These data were further compared with those obtained in various animals. G_{ST} value among the populations of *T. hakonensis* was estimated as 0.544. Nei [16] reported G_{ST} value among populations in wild mice as 0.119, and that among populations in horseshoe crabs as 0.072, respectively. Thus, level of G_{ST} value in *T. hakonensis* is several times as high as the levels hitherto reported. This reveals that most of genetic variation exists within populations in the animals hitherto examined, whereas a half of genetic variation exists among populations in *T. hakonensis*.

Mean genetic distance between populations of different local groups in *T. hakonensis* was esti-

mated as 0.051–0.125. Levels of genetic distance between local races or populations, and between subspecies of various vertebrates have been examined hitherto. Nei [16] reported D values between local races and between subspecies in wild mice as 0.010–0.024 and 0.194, respectively. In fish, D values between populations were reported as 0.001–0.006 for salmonid fish [19] and as 0.0007–0.0040 for red sea bream [20], and those between subspecies were reported as 0.11–0.19 for cyprinid fish, the genus *Campostoma* [21]. Thus, level of D values between populations of local groups in *T. hakonensis* is much higher than the levels between local races or populations hitherto reported, and is close to those between subspecies. These results are consistent with those of mitochondrial DNA, since mitochondrial genomes had been also highly differentiated among three populations of each local group [22]. Level of D values between populations within each local group of *T. hakonensis* is a little higher than or close to the levels hitherto reported.

In the other species of *Tribolodon*, *T. brandti* and *T. ezoe*, Sakai and Hamada [23] who examined populations from the waters of Hokkaido pointed out that allelic frequencies at a few loci were largely different from populations of Fukushima Pref. we had reported previously [7]. Hanzawa [24] estimated the genetic distance between these populations of two species based on allelic frequencies at 20 loci as 0.104 and 0.113, respectively. Thus, the high degree of interpopulational differentiation is also documented in the other two species of *Tribolodon*.

Geographical isolation of local groups

The extent of genetic differentiation among the local groups of *T. hakonensis* was remarkably high. Fishes of each local group of *T. hakonensis* are very similar in morphology. Nakamura [25] who examined morphological characters of *T. hakonensis* could not clearly show the regional differentiation, although he found slight differences among specimens collected from different regions in Japan. The present study on allozyme markers clearly showed the high degree of regional differentiation in the populations of *T. hakonensis*.

We considered two possibilities which could

explain the formation of these local groups. First is that any of populations of the local groups have undergone introgression and have accumulated genes derived from other related species. But, this is unlikely, because the local groups of *T. hakonensis* have been differentiated enough from the other species of *Tribolodon* at most of loci. Allelic differentiation between each local group of *T. hakonensis* and the other species of *Tribolodon* was observed at *m-Aat*, *s-Idh-1*, 2, *Ldh-1*, 3, *Pgm*, *Sp-2*, 3 [6, 7, 24]. On the other hand, allelic differentiation among the local groups of *T. hakonensis* independently occurred at the other 5 loci, *Adh*, α -*Gdh-2*, *Gpi-2*, *s-Mdh-2*, 6-*Pgd*. Therefore, we cannot interpret that the other related species had taken part in the interpopulational differentiation of *T. hakonensis*.

The second possibility, which is the most prob-

able, is that the populations of different local groups have been geographically isolated from each other since the time of the separation from their ancestral populations, and little gene flow has occurred among the populations of the groups. The dispersal of freshwater fishes is restricted by mountains, sea, etc., and regional differentiation occurs in their populations. Sakaizumi *et al.* [26] surveyed allozymic variation in Japanese wild populations of *Oryzias latipes*, and suggested that this case could be applied to interpopulational differentiation of this species because the boundary of the regions agreed well with watersheds or coastlines.

Distribution of the three local groups of *T. hakonensis* was shown in Figure 4. Their distribution shows distinct region specificity, and outline of their boundary agrees with watersheds or coast-

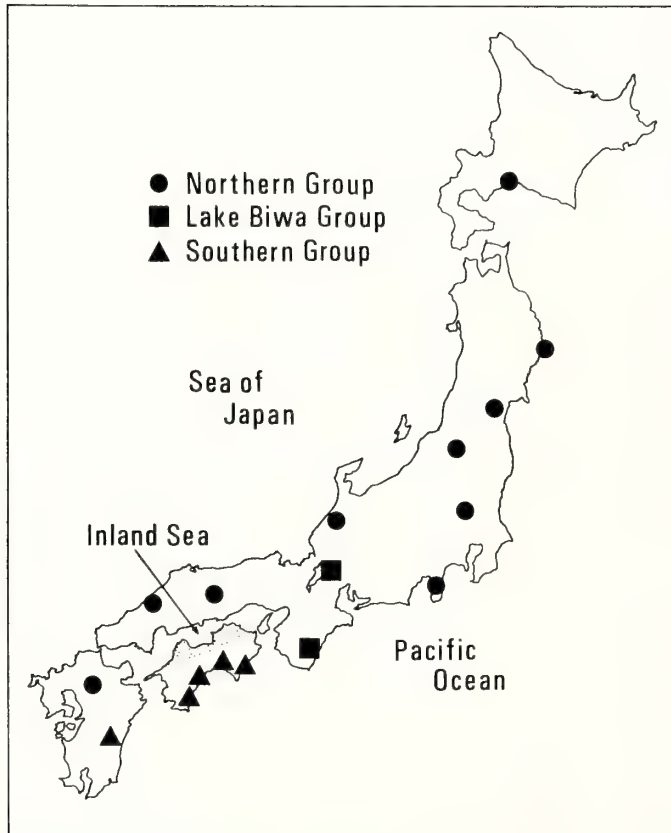


FIG. 4. Distribution of three local groups of *T. hakonensis*. *T. hakonensis* has not been originally distributed in the area designated by .

lines. In the Southern Group of *T. hakonensis*, northeastern part of the boundary agrees with the Shikoku mountains, because *T. hakonensis* has not been originally distributed in the side of the Inland Sea of Shikoku ([27], Mizuno, N., personal communication). The Sikoku mountains may have restricted the dispersal of the Southern Group from the side of the Pacific Ocean to that of the Inland Sea. The restriction of dispersal by the Shikoku mountains is also suggested from the fact that faunae of freshwater fishes are largely different between the side of the Inland Sea and that of the Pacific Ocean in Shikoku [27, 28]. Considering that the Yoshii River population in the side of the Inland Sea of Honshu belongs to the Northern Group, the boundary of the Northern Group may agree with the coastline of the Inland Sea. In this regard, we speculate that *T. hakonensis* of the Northern Group has extended their distribution from the side of the Sea of Japan to that of the Inland Sea through plains around the Chugoku mountains. The reasons why the Northern Group had not extended their distribution to Shikoku through the Inland Sea is now obscure. But, we speculate one of the reasons is that *T. hakonensis* hardly migrates out of bays or coastal regions, as mentioned in detail later. Further investigation in the side of the Inland Sea of Honshu and Shikoku will give any suggestion.

Lake Biwa group included two populations, but gene constitution of these populations was somewhat different (Table 3, Fig. 3). Lake Biwa population which showed the unique gene constitution (Table 3) also suggests the geographical isolation. Lake Biwa had been originated in the Pliocene epoch, and has been maintained as the independent waters surrounded by watersheds [29]. Many endemic species, subspecies and local races are distributed in this lake, and it is considered that they have been isolated within this lake and have been differentiated here. It is likely that *T. hakonensis* has been also isolated within the lake for a considerably long period of time and has been remarkably differentiated from the other populations.

As stated above, the restriction of dispersal by watersheds may have affected the formation of the local groups. However, this cannot explain the

reason why little gene flow is observed among the local groups although *T. hakonensis* can migrate through the sea regions. In this regard, we consider the following reasons. Though this species can migrate to the sea regions, it spawns in the middle reaches of rivers. This species is firmly dependent on the fresh waters, and may stay within bays or coastal regions without migrating to the open sea. Therefore, gene flow hardly occurs among populations of different local groups through the sea regions. This speculation is consistent with the observation that fish of this genus was distributed within the area of five meters in depth in Tokyo Bay [30]. Furthermore, this speculation may be supported by the observation that gene constitution of the amphidromous type of *T. hakonensis* was very similar to the landlocked type in the same waters (see Results). This observation suggests that the amphidromous type might have returned to its spawning ground in the middle reaches of the river without migrating to the other waters and had been mated with the landlocked type before these types were isolated by dums.

It is likely that the populations of different local groups have been geographically isolated from each other for a long period of time. Divergence time between three local groups based on Nei's genetic distance was estimated as approximately 200,000–600,000 years, and agreed with the divergence time based on the net nucleotide differences between mitochondrial DNA of three populations of each local group [22]. This time corresponds to the middle of diluvial epoch when the Japanese Islands had been strongly affected by ups and downs of the sea level with vicissitudes of glaciers and had connected with each other and the Asiatic Continent. It is likely that *T. hakonensis* had extended their distribution and that the local groups had been formed during this epoch. As for the dispersal and the differentiation of the local groups, we speculate as follows. Considering a fact that all of other related species of *Tribolodon* are distributed in the northern Japan and north of Japan at present, the ancestral population of *T. hakonensis* had been possibly distributed in or near these areas. First, the population of the Southern Group had extended their distribution to the

southern Japan and had begun to be genetically differentiated from the ancestral population. Secondly, a part of the population of the Southern Group had been isolated and the Lake Biwa group had been differentiated. On the other hand, the Northern Group had arisen from the ancestral population which had stayed in the north, and had extended its distribution rapidly. Further study as for specimens sampled at other waters will make sure this hypothesis.

ACKNOWLEDGMENTS

We are grateful to Drs. T. Kajiura (Ocean Research Institute, Univ. Tokyo) and A. Ochiai (Kochi Univ.) for their helpful discussions. We also thank T. Kobayashi (Ocean Research Institute, Univ. Tokyo) and M. Ogura for their kind help in calculation. We would like to thank Drs. A. Kijima (Tohoku Univ.), S. Seki (Kochi Univ.), Y. Iwatsuki (Univ. Tokyo), K. Uchida and T. Kawamura (Ocean Research Institute, Univ. Tokyo), S. Kimura (Kyushu Univ.), H. Sakai (Shimonoseki Univ. Fisheries), M. Maehata and M. Kuwahara (Biwako-Bunkakan), K. Narita (Fukushima Prefectural Inland Water Fisheries Experimental Station), K. Suzuki (Fukushima Prefectural Fisheries Experimental Station), A. Shikita (Ishikawa Prefectural Office), T. Tanaka (Okayama Prefectural Fisheries Extension Office), J. Yoshio (Shimane Prefectural Fisheries Experimental Station), and T. Yamasaki for their kind help in collection of specimens. This research was supported in part by a grant from the Itoh Ichthyological Foundation.

REFERENCES

- Mashiko, K., Jozuka, K. and Asakura, K. (1973) Different type chloride cells in the gills of *Tribolodon hakonensis* from Lake Ososesan-ko. Ann. Rep. Noto Mar. Lab., **13**: 33-37. (In Japanese)
- Tanaka, S. and Miyazaki, S. (1976) On the annual growth of Ugui, *Tribolodon hakonensis* and Maruta, *T. taczanowskii* in Zinzu River, Toyama Prefecture, central Japan. Physiol. Ecol. Jpn., **17**: 401-406. (In Japanese with English summary)
- Ikeda, H. (1938) Statistical observations on the species of the genus *Tribolodon* in Japan and some notes on their distribution. Sci. Rep. Tokyo Bunrika Daigaku, Sec. B, **3**: 163-192.
- Nakamura, M. (1963) Keys to the Freshwater Fishes of Japan Fully Illustrated in Colors. Hokuryukan, Tokyo, 3rd ed., pp. 127-129. (In Japanese)
- Onodera T. and Honnma, Y. (1976) Racial differentiation of the Japanese dace (genus *Leuciscus*) in the north-eastern Japan. Proc. Jpn. Soc. Syst. Zool., **12**: 65-77. (In Japanese with English summary)
- Hanzawa, N. and Taniguchi, N. (1982) Isoelectric focusing patterns of sarcoplasmic protein of the Japanese dace, genus *Tribolodon*. Rep. Usa Mar. Biol. Inst., Kochi Univ., **4**: 51-54. (In Japanese with English summary)
- Hanzawa, N. and Taniguchi, N. (1982) Genetic differentiation of the Japanese dace, genus *Tribolodon* collected from the waters of Fukushima Pref. Fish Genet. Breed. Sci., **7**: 26-30. (In Japanese)
- Numachi, K. (1971) Genetic polymorphism of α -glycerophosphate dehydrogenase in saury, *Cololabis saira* - I. Seven variant forms and genetic control. Bull. Jpn. Soc. Sci. Fish., **37**: 755-760.
- Clayton, J. W. and Tretiak, D. N. (1972) Amine-citrate buffers for pH control in starch gel electrophoresis. J. Fish. Res. Bd. Can., **29**: 1169-1172.
- Numachi, K., Nagahora, S. and Iwata, M. (1979) Genetic identification of hybrids between chum and pink salmon in the northwest Pacific. Rep. Otsuchi Mar. Res. Cent., Univ. Tokyo, **5**: 87-102. (In Japanese)
- Numachi, K. (1970) Polymorphism of malate dehydrogenase and genetic structure of juvenile populations in saury *Cololabis saira*. Bull. Jpn. Soc. Sci. Fish., **36**: 1235-1241.
- Shaw, C.R. and Prasad, R. (1970) Starch gel electrophoresis of enzymes - a compilation of recipes. Biochem. Genet., **4**: 297-320.
- Taniguchi, N. and Numachi, K. (1978) Genetic variation of 6-phosphogluconate dehydrogenase, isocitrate dehydrogenase, and glutamic-oxaloacetic transaminase in the liver of Japanese eel. Bull. Jpn. Soc. Sci. Fish., **44**: 1351-1355.
- Numachi, K. (1981) A simple method for preservation and scanning of starch gels. Biochem. Genet., **19**: 233-236.
- Hanzawa, N., Taniguchi, N. and Shinzawa, H. (1984) Genetic markers of the artificial hybrids between *Tribolodon hakonensis* and *T. sp.* (Ukeguchi-ugui). Otsuchi Mar. Res. Cent. Rep., Univ. Tokyo, **10**: 11-17. (In Japanese)
- Nei, M. (1975) Molecular Population Genetics and Evolution. North-Holland, Amsterdam and Oxford.
- Nei, M. (1972) Genetic distance between populations. Am. Natur., **106**: 283-292.
- Nevo, E. (1978) Genetic variation in natural populations: Patterns and theories. Theret. Pop. Biol., **13**: 121-177.
- Numachi, K. (1976) Genetics and genetic improvement of aquatic organisms. Marine Sciences, **8**: 7-14. (In Japanese with English abstract)
- Taniguchi, N., Fujita, M. and Akazaki, M. (1986) Genetic divergence and systematics in sparid fish from Japan. In "Indo-Pacific Fish Biology: Proceed-

- ings of the Second International Conference on Indo-Pacific Fishes". Ed. by T. Uyeno, R. Arai, T. Taniuchi and K. Matsuura, Ichthyol. Soc. Jpn., Tokyo, pp. 849–858.
- 21 Buth, D. G. and Burr, B. M. (1978) Isozyme variability in the cyprinid genus *Campostoma*. *Copeia*, **1978**: 298–311.
 - 22 Hanzawa, N., Yonekawa, H., and Numachi, K. (1987) Variability of mitochondrial DNA in Japanese dace, *Tribolodon hakonensis* (Cyprinidae). *Jpn. J. Genet.*, **62**: 27–38.
 - 23 Sakai, H. and Hamada, K. (1985) Electrophoretic discrimination of *Tribolodon* species (Cyprinidae) and the occurrence of their hybrids. *Jpn. J. Ichthyol.*, **32**: 216–224.
 - 24 Hanzawa, N. (1986) Biochemical genetic studies on the speciation in the Japanese dace, genus *Tribolodon*. Ph. D. Thesis, Univ. Tokyo, Tokyo, pp. 1–113. (In Japanese)
 - 25 Nakamura, M. (1969) Cyprinid Fishes of Japan. Studies on the Life History of Cyprinid Fishes of Japan. Special Publications, Res. Inst. Nat. Resources, No.4, Tokyo. (In Japanese with English summary)
 - 26 Sakaizumi, M., Moriwaki, K. and Egami, N. (1983) Allozymic variation and regional differentiation in wild populations of the fish *Oryzias latipes*. *Copeia*, **1983**: 311–318.
 - 27 Uematsu, T., Sunaga, T. and Kawada, H. (1979) Kagawa-ken no Tansuigo. *Dobutsu to Shizen*, **9**: 11–17. (In Japanese)
 - 28 Ochiai, A., Teraoka, K. and Hanzawa, N. (1979) A survey of freshwater fishes of Kochi Prefecture. *Res. Rep. Kochi Univ.*, **28**: 145–156. (In Japanese with English summary)
 - 29 Tomoda, Y. (1978) A new course in the study of organisms of the Lake Biwa I. *Michurin Seibutsugaku Kenkyu*, **14**: 60–92. (In Japanese with English summary)
 - 30 Kurata, Y. and Iimura, T. (1954) Injurious effects of *Tribolodon hakuensis hakuensis* (GUNTHER) on shell fish. *Saishu to Shiiku*, **16**: 233–235. (In Japanese)

The Larval Stages of Three Pagurid Crabs (Crustacea: Anomura: Paguridae) from Hokkaido, Japan

KOOICHI KONISHI and RODOLFO QUINTANA

*Zoological Institute, Faculty of Science, Hokkaido University,
Sapporo 060, Japan*

ABSTRACT—Complementary descriptions of laboratory-reared larvae are given for three hermit crabs from Hokkaido: *Pagurus middendorffii* Brandt, *P. geminus* McLaughlin, and *P. lanuginosus* De Haan. Larval characters of the present material were compared with those of the previous works and some differences were apparent. Morphological evidences suggest that Kurata's zoea II-IV stages of *P. middendorffii* reconstructed from plankton samples should be assigned to another allied species. The number of telsonal processes was constant (=7) in all zoeal stages of both *P. middendorffii* and *P. lanuginosus*.

INTRODUCTION

The family Paguridae of Hokkaido, northern Japan, contains approximately 15 species [1, 2], and the following four species are predominant in the anomuran population of the seashore in this area: *P. lanuginosus* De Haan, 1849, *Pagurus middendorffii* Brandt, 1851, *P. brachiomastus* (Thallwitz, 1892) and *P. geminus* McLaughlin, 1976. Although the larval stages of these four hermit crabs have been documented [3-6], knowledge on their larvae, however, remains incomplete. Kurata [3] reported four zoeal stages of *P. middendorffii*, reconstructed mainly from the plankton; the magalopa and early crab stages of this species are still unknown. Later he [4] also described the larval development of *P. geminus* (as *P. samuelis* (Stimpson)) reared in the laboratory, but information on several important larval characters, e.g. setation of maxillule, maxilla, and maxillipedal endopods was not given. The larvae of *P. lanuginosus* described from Korean waters [5], and those of our material show two unique features, i.e. constant number of telsonal processes and absence of mandibular palp throughout zoeal stages.

This paper provides: 1) a re-description of zoeal stages and the first descriptions of post-larvae of *P. middendorffii*, 2) complementary information on zoeal stages of *P. geminus* and *P. lanuginosus*, and 3) comparisons of larval characters between the present study and the previous works.

MATERIALS AND METHODS

The localities and the date of collection of ovigerous females, as well as the date of hatching of zoeas in each species are as follows: *P. middendorffii* (Muroan, Pacific coast, 6 May 1985; hatch out: 13 May 1985; Higashi-Shizunai, Pacific coast, 17 May 1984; hatch out: 21 May 1984), *P. geminus* (Oshoro, Sea of Japan, 20 July 1984; hatch out: 31 July 1984), and *P. lanuginosus* (Usujiri, Pacific coast, 8 May 1985; hatch out: 22 June 1985).

The methods for larval culture, dissection, drawings of the specimens and expression of setal arrangement were almost the same as in previous papers [6, 7] except slight modifications. The carapace length (= CL) of zoeas was measured from the tip of the rostral spine to the posterior margin of the carapace, laterally, and that of megalopas and first crabs (*P. middendorffii*) dorsally from the rostrum to mid-posterior point of the carapace. The present descriptions are pri-

mary based on notes made at the time of observation of the larval and postlarval appendages, and further, supplemented with figures prepared.

RESULTS

Rearing data

The megalopa of *P. middendorffii* was attained 24–26 days after hatching and the first crab appeared after 32–34 days [7].

Approximately 130 zoea I larvae of *P. lanuginosus* were reared and checked daily for alive, dead larvae and their exuviae in the laboratory. Duration of each larval stage was 4 to 5 days for stages I–III, and 6 to 7 days for stage IV. The zoea II appeared after 6 days of culture, zoea III after 10 days, zoea IV after 14 days, and megalopa after 21 days. Due to a lack of food during 1.5 days (15th–16th days), high mortality of zoeas III and IV was produced; it is probable that the megalopal stage is attained one or two days before. After 24 days, when most of larvae were in megalopal stage, 3 larvae of zoea IV remained without moulting, probably due to the lack of food. Rearing experiment was terminated 24 days after hatching, obtaining 25 megalopas of which 13 were fixed.

Only zoea I larvae of *P. geminus* were obtained from a single ovigerous female and no attempts were made to obtain the following stages.

Descriptions of larval stages

Pagurus middendorffii Brandt, 1851

First Zoea

Dimension: CL=1.31–1.36 mm (mean 1.34 mm).

Carapace (Fig. 1A): Surface smooth. Rostral spine slightly directed downward, reaching well beyond the antennule and antennal exopod. Postero-lateral spines short. Eyes sessile.

Antennule (Fig. 2A): Peduncle unsegmented, elongate, with 2 aesthetascs and 3 setules distally, and a subterminal, long plumose seta projecting beyond the aesthetascs.

Antenna (Fig. 2G, g): Biramous; endopod fused with peduncle, pointed distally, slightly shorter than the exopod (=scale). The latter distally projected as a stout spine, fringed with 5 long plumose setae and a distal shorter simple seta. A stout serrate spine emerging proximally near base of endopod.

Mandible (Fig. 3A): Both asymmetrical, slightly different in dentition. Incisor process stout, rather short. Molar process with several pointed teeth of different lengths and minute granules on inner surface.

Maxillule (Fig. 3G): Endopod 3-segmented, with setae arranged as 1, 1, 3 of which the proximal seta is very short. Basial¹ endite with 2 large stout spines, each spinulate distally, and 2 fine setae. Coxal endite single-lobed, with 5 plumose and 2 fine setae.

Maxilla (Fig. 4A): Endopod medially stepped, with 6 setae arranged into two groups as 2+4. Basial and coxal endites bilobed, with 5+4 and 5+4 setae respectively. Scaphognathite fringed with 5 soft plumose setae.

Maxilliped 1 (Fig. 5A): Endopod 5-segmented, with setae arranged as 3, 2, 1, 2, 4+I (I=dorsal plumose seta); segments 1–3 with 5–6, 8–10, and 6–8 setules on outer margin respectively. Exopod with 4 long natatory setae. Basis with 9 setae on inner margin.

Maxilliped 2 (Fig. 5G): Endopod 4-segmented, with 2 setae on segments 1–3 and 5 setae on distal segment of which one is dorsal. Five to six fine setules on dorsal margin of the segments 2–3. Exopod with 4 long natatory setae. Basis with 3 setae on inner margin, the distal setae very similar to those of segments 1–3.

Maxilliped 3 (Fig. 5L): Rudimentary, uniramous, unarmed.

Pereiopods (Fig. 1A): Rudimentary, visible laterally beneath the carapace.

Abdomen (Fig. 6A): Composed of 5 segments

¹ In a previous paper [8], Dr. R. W. Ingle (British Museum, Natural History, London, U.K.) has pointed out to one of us (R.Q.) that the adjective *basial* is preferable to "*basal*" as usually has been used, since *basial* is derived from *basis* whereas "*basal*" means "at the base of", and certainly is not specific in this sense.

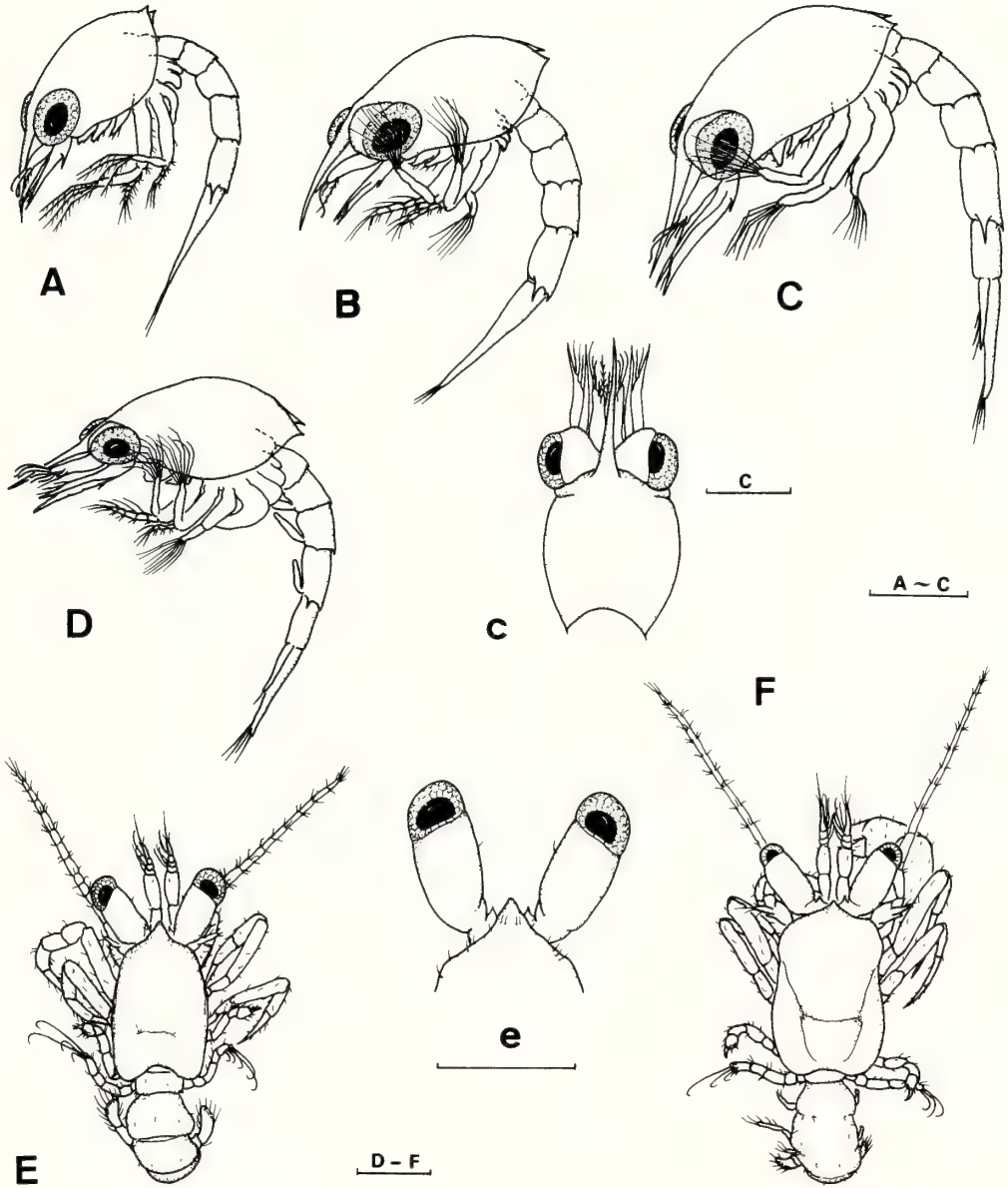


FIG. 1. *Pagurus middendorffii* Brandt, 1851. Whole specimens of zoeal stages I-IV (A-D), lateral view, megalopa (E) and first crab (F), dorsal view; c, zoea III, carapace in dorsal view; e, megalopa, anterior portion of carapace. Scale bars=0.5 mm.

and a telson. Posterior margin of each segment except the first, with 4-5 minute spines; segment 5 with well-developed acute posterolateral spines.

Telson (Fig. 6A): Elongate, posterior margin slightly convex, with 7+7 processes; outermost process a short stout spine, articulated at its base,

the second an inconspicuous fine seta, and the third to seventh are large setae, each finely setulose along margins. Anal spine present medio-ventrally.

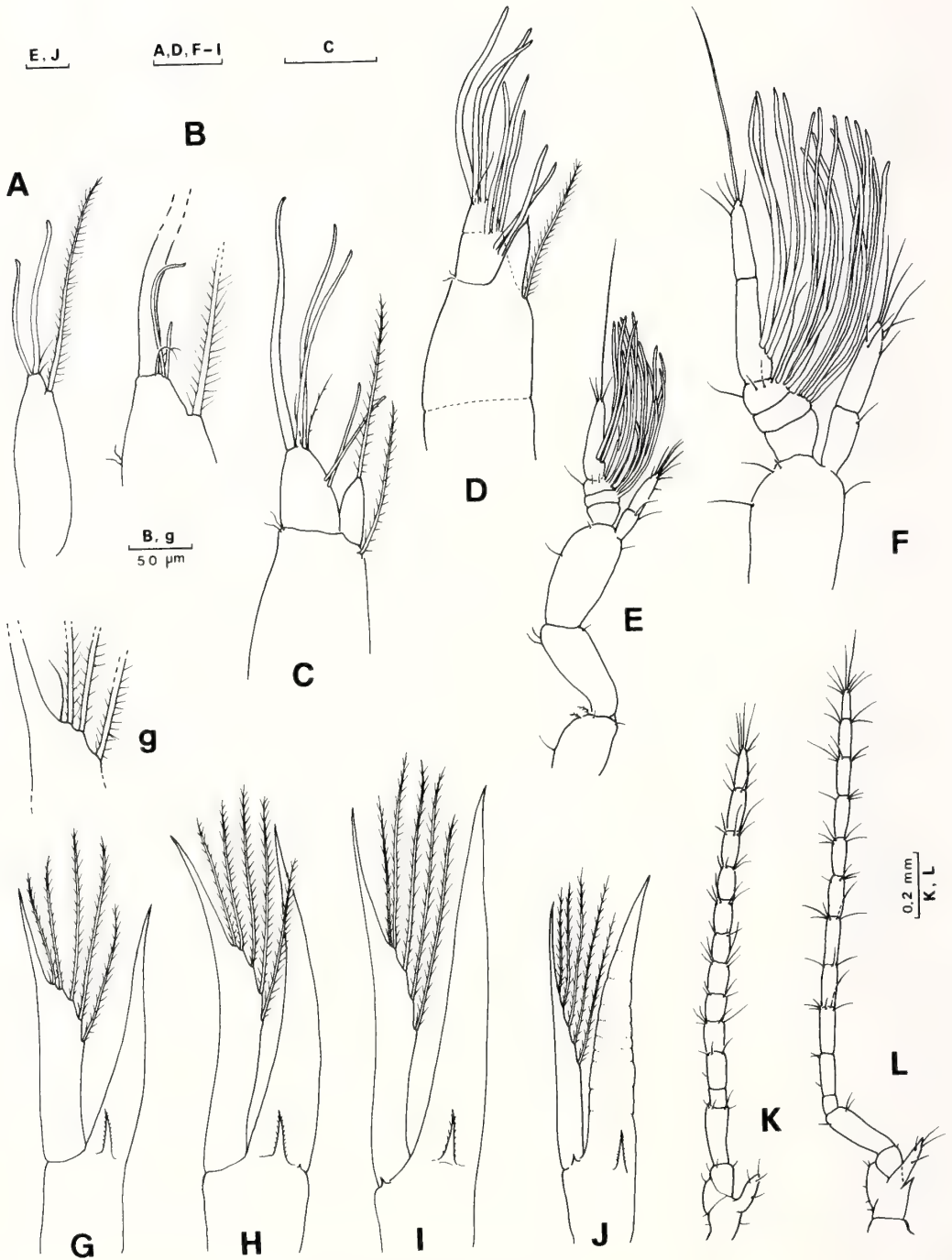


FIG. 2. *Pagurus middendorffii* Brandt, 1851. Antennules and antennae. A-F, antennule of zoea I-IV (A-D), megalopa (E) and first crab (F); G-L, antenna of zoea I-IV (G-J), megalopa (K) and first crab (L); g, detail of apical setae of antennal exopod of zoea I. Scale bars=0.1 mm, except for 50 μ m (B, g) and 0.2 mm (K, L).

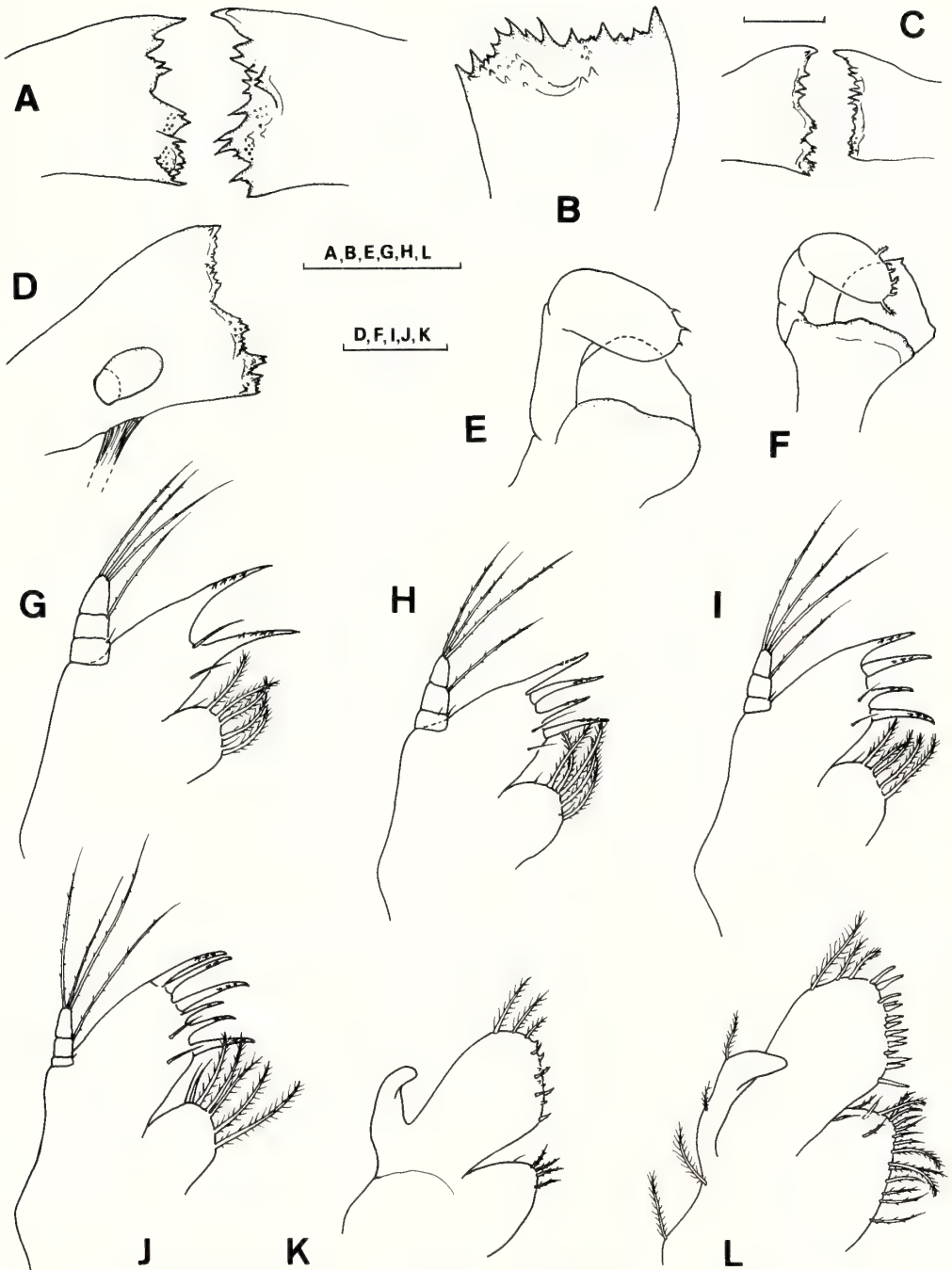


FIG. 3. *Pagurus middendorffii* Brandt, 1851. Mandibles and maxillules. A-F, mandibles of zoea I-IV (A-D), megalopa (E) and first crab (F); G-L, maxillule of zoea I-IV (G-J), megalopa (K) and first crab (L). Scale bars=0.1 mm.

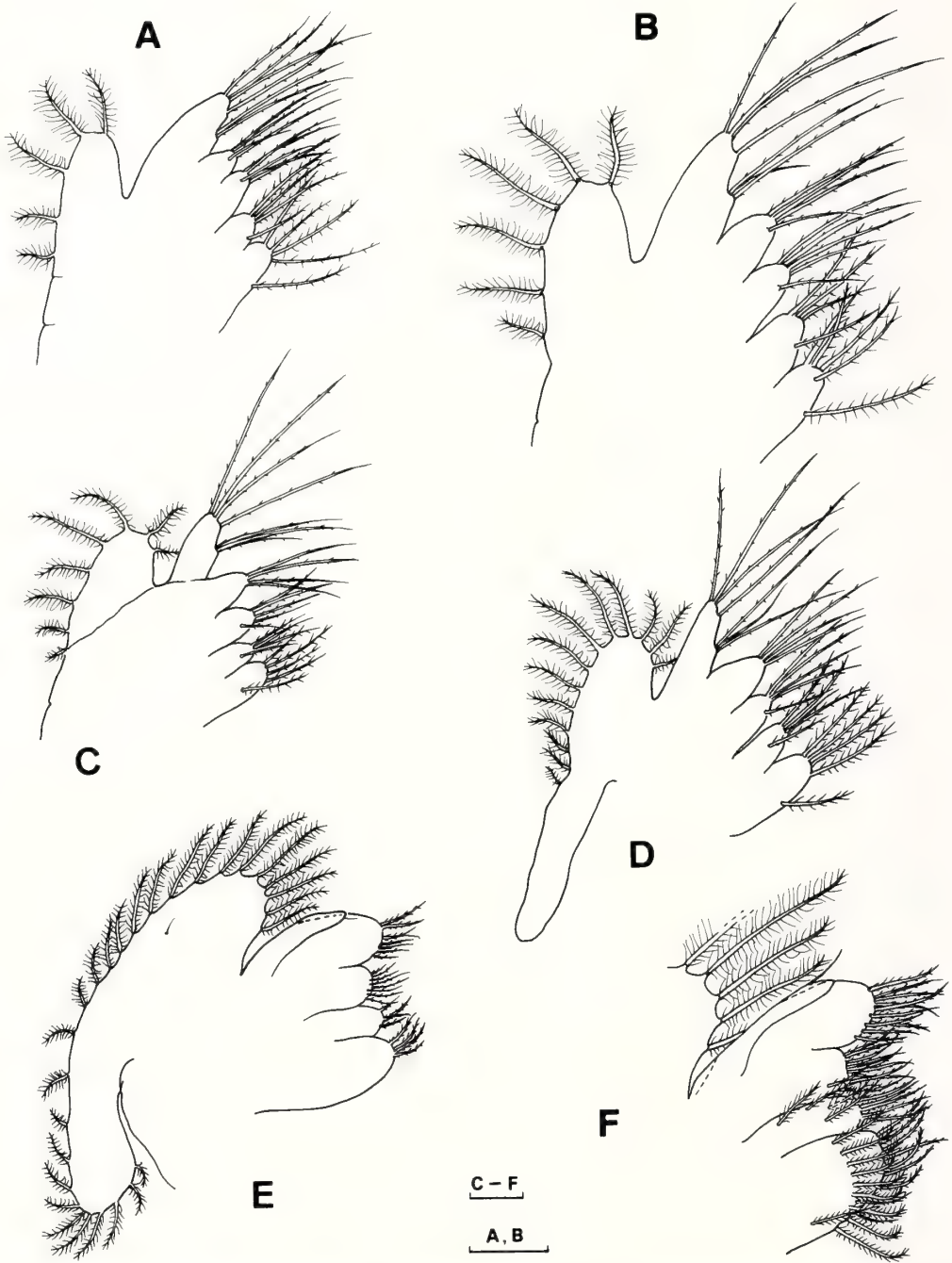


FIG. 4. *Pagurus middendorffii* Brandt, 1851. Maxilla of zoea I-IV (A-D), megalopa (E) and first crab (F). In F, scaphognathite partially drawn. Scale bars=50 μ m.

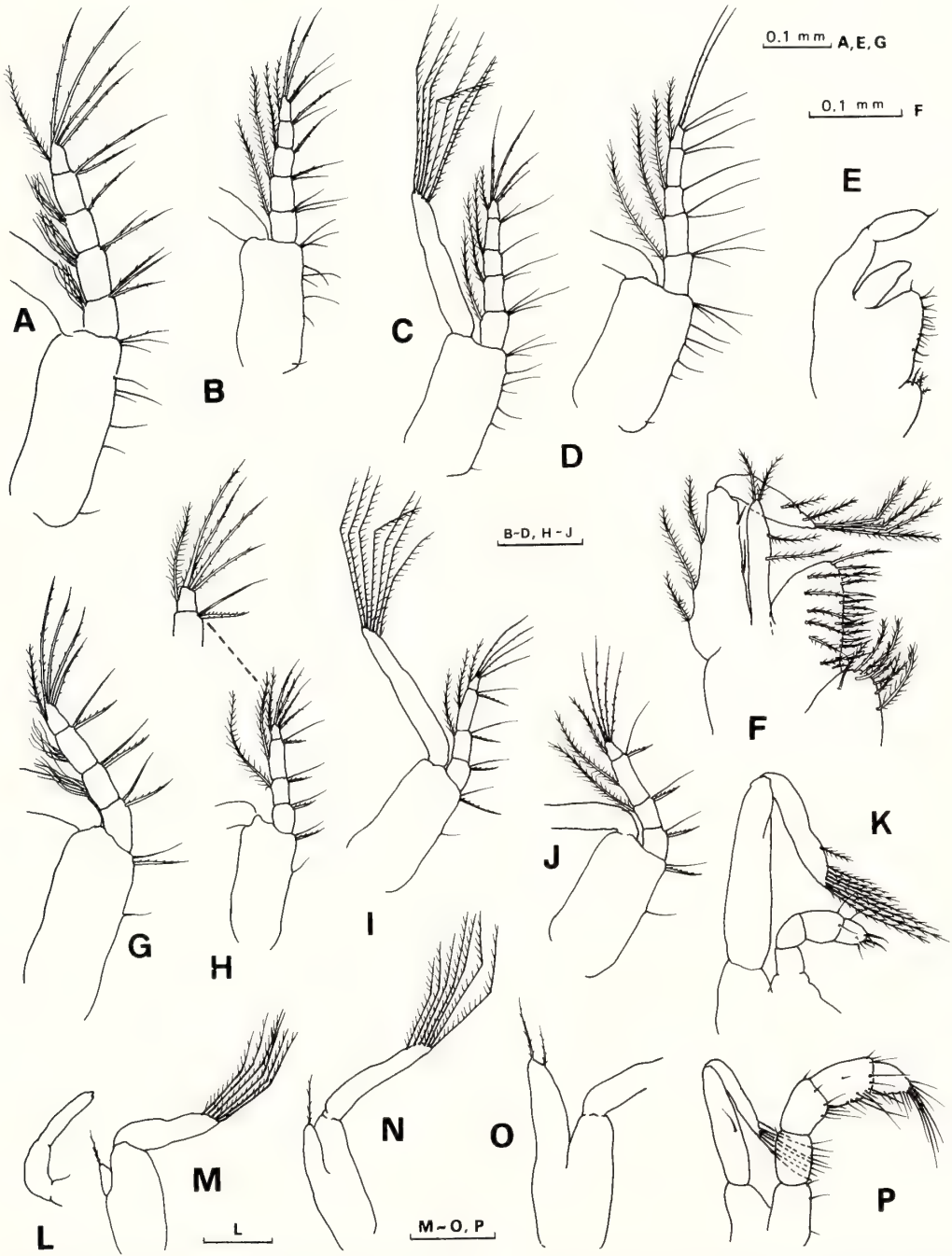


FIG. 5. *Pagurus middendorffii* Brandt, 1851. Maxillipeds. A-F, maxilliped 1 of zoea I-IV (A-D), megalopa (E) and first crab (F); G-K, maxilliped 2 of zoea I-IV (G-J) and of megalopa (K); L-P, maxilliped 3 of zoea I-IV (L-O) and of megalopa (P). Scale bars=0.2 mm, except for 0.1 mm.

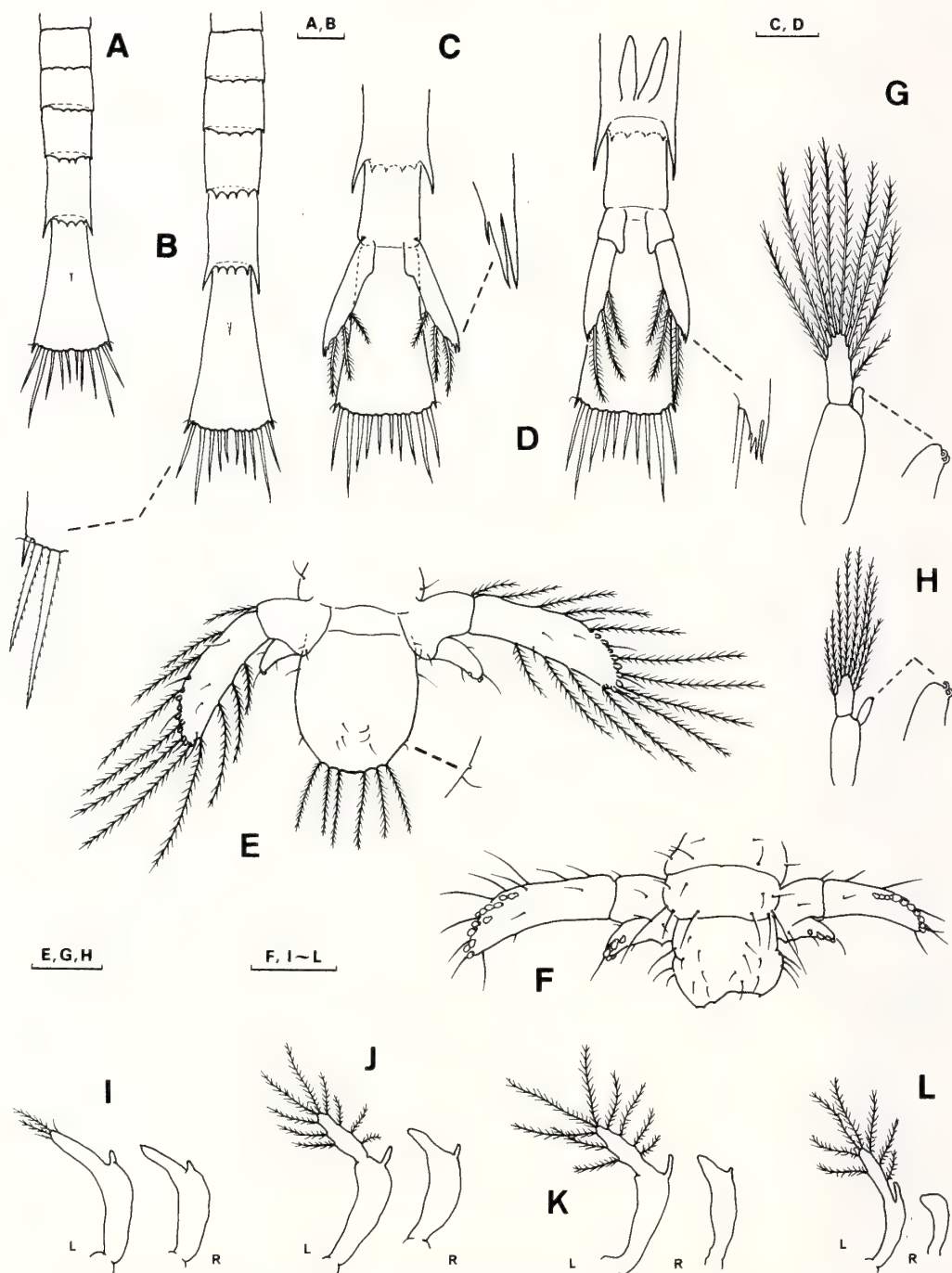


FIG. 6. *Pagurus middendorffii* Brandt, 1851. Abdomens and pleopods. A-D, abdomen and telson of zoeal stages I-IV; E, F, tail fan of megalopa (in ventral view) and of first crab (in dorsal view) respectively; pleopod 1 (G) and 4 (=last) (H) of the megalopa, each with a detail of distal hooked setae on endopod; I-L, pleopods 1-4 of the first crab (R= right pleopod; L= left pleopod). Scale bars=0.2 mm.

Second Zoea

Dimension: CL=1.48–1.54 mm (mean 1.51 mm).

Carapace (Fig. 1B): General morphology as in the previous stage. Eyes stalked.

Antennule (Fig. 2B): With 3 aesthetascs and 2 fine setae distally; the two shorter aesthetascs extremely fine, approximately 1/5 of the thick aesthetasc. Subterminal plumose seta not reaching the tip of the longest aesthetasc. Two fine setules on the opposite margin.

Antenna (Fig. 2H): Endopod as long as the exopod. Exopod with 5 plumose setae.

Mandible (Fig. 3B): Longer, but similar in dentition to the previous stage.

Maxillule (Fig. 3H): Endopod with 2, 1, 3 setae; basal two setae hardly observable, but some specimens showed only one minute seta. Basial endite with 4 spinulose stout spines (two articulated at their bases) and 2 fine setae. Coxal endite with 5 plumose and 2 minute setae.

Maxilla (Fig. 4B): Endopod stepped, with 3 (occasionally 2) medial, 1 subterminal and 3 terminal setae. Scaphognathite with 6 soft, plumose setae. The others unchanged.

Maxilliped 1 (Fig. 5B): Endopod 5-segmented, setation as 3, 2, 1, 2, 4, on the inner margin, plus 1 additional long plumose seta on the outer margin of all segments except the fourth one. Exopod with 7 natatory setae. Basis with 9 setae.

Maxilliped 2 (Fig. 5H): Endopod 4-segmented, setation as 2, 2, 2, 4 (rarely 3) on inner margin, plus additional long plumose seta on the outer margin of segments 2–4. Exopod with 7 natatory plumose setae. Basis with 3 setae.

Maxilliped 3 (Fig. 5M): Endopod vestigial, with a single seta apically. Exopod with 6 plumose setae.

Pereiopods (Fig. 7A): As rudimentary buds, unsegmented; first pereiopod broader, non-chelate.

Abdomen (Fig. 6B): Minute posterolateral spines on segments 2–4, well-developed spines on the segment 5. The others unchanged.

Telson (Fig. 6B): General morphology unchanged.

Third Zoea

Dimension: CL=1.74–1.86 mm (mean 1.82 mm).

Carapace (Fig. 1C): Larger, but similar to the previous stages in general morphology.

Antennule (Fig. 2C): Exopod with 3 subequal terminal aesthetascs and 2 additional medial aesthetascs. Endopod well developed, with 1 apical long plumose seta. Another similar seta near base of endopod, and 2 minute setae on the opposite margin.

Antenna (Fig. 2I): Endopod slightly longer than the exopod. The latter with 5 plumose setae as in the previous stage. An additional minute seta basally.

Mandible (Fig. 3C): Asymmetrical, slightly different in dentition. No palp at this stage.

Maxillule (Fig. 3I): Endopod with 1, 1, 3 setae. Basial endite unchanged. Coxal endite with 5 plumose and 1 fine setae.

Maxilla (Fig. 4C): Endopod with setation as 3 (rarely 2)+1+3. Scaphognathite with 8 marginal setae. The others unchanged.

Maxillipeds 1–3 (Fig. 5C, I, N): Setation unchanged. Endopod of maxilliped 3 longer than previous stage but not reaching the apical margin of basis.

Pereiopods (Fig. 7B): Rudimentary, unsegmented; pereiopod 1 chelate at tip. Pereiopods 2–3 as long as the cheliped.

Abdomen (Fig. 6C): A sixth segment is added; its posterior margin unarmed. Pleopods not present at this stage, but uniramous uropods emerging ventrally from the segment 6, each reaching approximately 2/3 of telson length. Uropod bifid apically, plus an additional inner spine subapically; distal inner border with 3 plumose setae.

Telson (Fig. 6C): Setation of 7+7 processes unchanged. Anal spine now absent.

Fourth Zoea

Dimension: CL=1.94–2.15 mm (mean 2.03 mm).

Carapace (Fig. 1D): Larger, but similar to the previous stages in general morphology.

Antennule (Fig. 2D): Peduncle indistinctly 3-segmented. Endopod unarmed distally. Outer

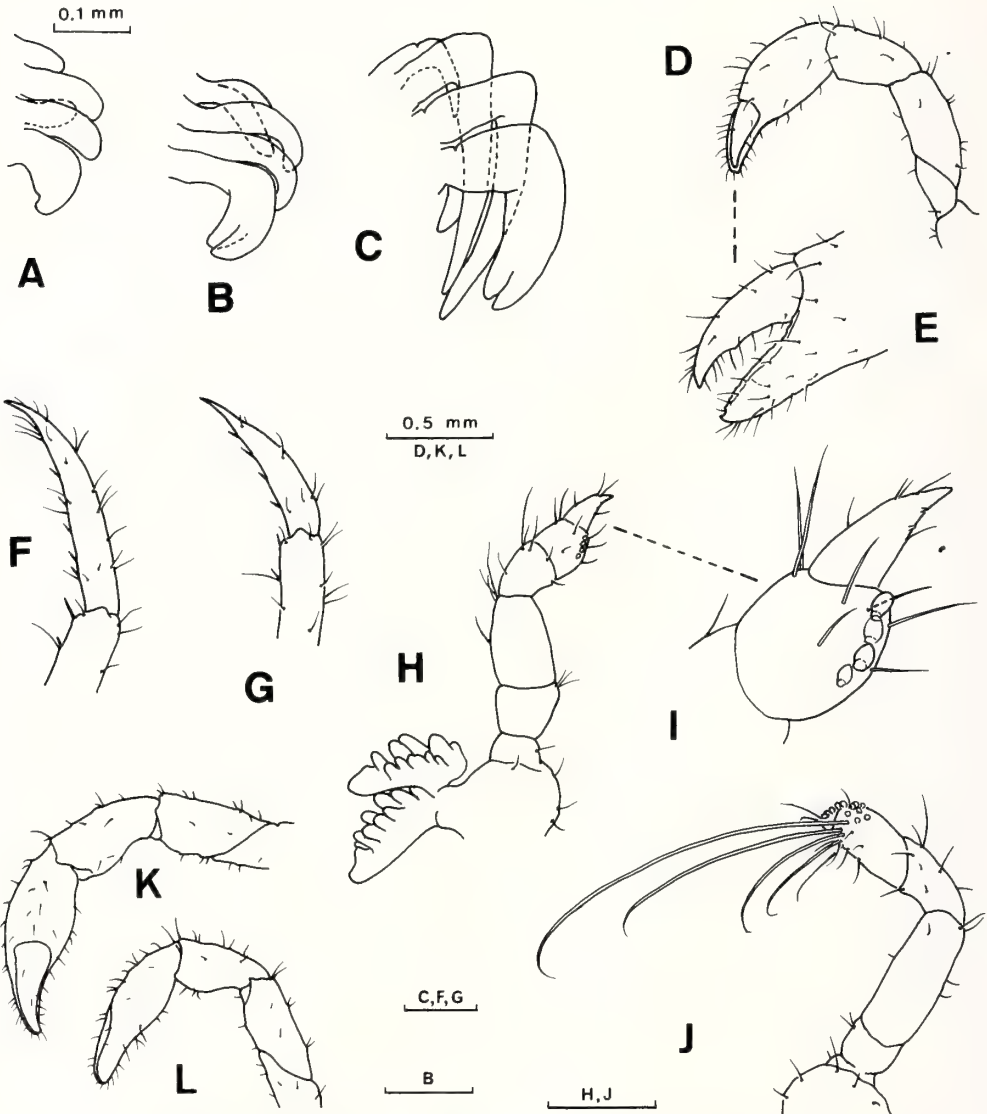


FIG. 7. *Pagurus middendorffii* Brandt, 1851. Pereiopods. A-C, rudiments of pereiopods of the zoea II-IV; D-J, pereiopods of the megalopa; D, right cheliped; E, detail of the chela; F-J, pereiopods 2-5, with a detail (I) of dactylus and propodus of the pereopod 4; K, L, right and left chelipeds of the first crab respectively. Scale bars=0.2 mm; others as indicated.

flagellum with 8 aesthetascs in total, arranged into three tufts.

Antenna (Fig. 2J): Endopod indistinctly segmented, more developed than the scale. Exopod with 5 setae on distal inner margin.

Mandible (Fig. 3D): Palp present as a soft unsegmented bud.

Maxillule (Fig. 3J): Basal endite with 6 stout spines and 2 inner setae. Coxal endite with 5 plumose and 2 simple setae.

Maxilla (Fig. 4D): Setations of endopod and basal endite unchanged. Proximal lobe of coxal endite with 5 setae; distal lobe with 4 or 5 setae. Scaphognathite with 13 plumose setae on margin,

projected posteriorly as a well-developed naked lobe.

Maxillipeds 1–2 (Fig. 5D, J): Both exopods with 8 plumose setae. The others unchanged.

Maxilliped 3 (Fig. 5O): Endopod well-developed, surpassing the basis in length, with 2 distal setae. Exopod with 8 natatory setae. Basis glabrous, as in the previous stages.

Pereiopods (Fig. 7C): Rudimentary, indistinctly segmented. Second and third pereiopods elongate, markedly longer than the cheliped.

Abdomen (Fig. 6D): With uniramous pleopods on segments 2–5; segment 6 with well-developed 2-segmented uropods. Endopod rudimentary, unarmed; exopod with 4 acute spines distally and 3 plumose setae on distal inner margin.

Telson (Fig. 6D): Setation as in the previous stage.

Megalopa

Dimensions: CL=1.06–1.16 mm (mean 1.12 mm); CW=0.64 mm.

Carapace (Fig. 1E, e): Oblong, zoeal rostral spine reduced to a blunt rostrum. Surface sparsely covered with minute setae. Ocular peduncles each with a minute acicle on inner basal margin.

Antennule (Fig. 2E): Peduncle 3-segmented. Inner flagellum slender, 2-segmented, with 2 on proximal and 8 setae on distal segments. Outer flagellum 4-segmented, with 7, 4, 3 aesthetascs on segments 2–4. Distal segment markedly longer than the total length of the 3 proximal segments, with 4 distal setae, one of which is longer than the entire outer flagellum.

Antenna (Fig. 2K): Peduncle 4-segmented, distal segment elongate. Flagellum composed of 11 segments, each (except the first one) with short setae on distal margin; distal segment with 8 terminal setae. Acicle (=exopod) emerging laterally from the peduncle and armed with 4 setae.

Mandible (Fig. 3E): Palp greatly developed, indistinctly 3-segmented, with 3 minute setae distally. Mandibular plate strong, margin slightly rounded.

Maxillule (Fig. 3K): Greatly modified from the previous stages. Endopod digitiform, unsegmented, unarmed. Basal endite with 3 plumose setae and 11–12 minute smooth spines. Coxal

endite with 5 setae.

Maxilla (Fig. 4E): Endopod unsegmented, with a single apical seta. Basal endite with 9 on the proximal and 8 setae on the distal lobes. Coxal endite with 4 setae on each lobe. Scaphognathite greatly expanded, with 27 setae on margin.

Maxilliped 1 (Fig. 5E): Greatly modified from the previous stages. Endopod digitiform, unsegmented, unarmed, 1/2 exopod length. Exopod 2-segmented, with a short simple seta distally. Basal endite broad, with 14–15 short setae. Coxal endite with 3–4 setae.

Maxilliped 2 (Fig. 5K): Endopod 4-segmented, with 2 on the penultimate and 7 setae on the distal segments. Exopod 2-segmented, proximal segment greatly developed, glabrous; distal segment with 8 plumose setae.

Maxilliped 3 (Fig. 5P): Different from the maxillipeds 1–2; endopod markedly longer than exopod, 5-segmented; each segment with numerous setae, profusely setose on distal segments. Exopod 2-segmented, proximal segment with a single seta medially; distal segment with 7 setae.

Pereiopods (Fig. 7D–J): Well-developed, sparsely covered with short setae. Right cheliped larger than the left one; cutting borders of fingers hardened, lacking acute teeth. Pereiopods 2–3 cylindrical, long, similar in length, dactyli acutely pointed. Inner margin of dactylus of pereiopod 2 armed with 6 spinules and additional setae. Pereiopod 3 with 4 spinules and additional setae; propodi with 2 spinules on inner margin distally. Pereiopod 4 reduced, flattened distally; propodus with 4 spatuliform setae, dactylus triangular, with 2 spinules on inner border and additional setae. Pereiopod 5 reduced, subchelate, with 7–9 spatuliform setae on propodus and 3–4 on dactylus. Five long setae emerging from the propodus, of which the longest one is as long as the entire pereiopod.

Abdomen (Fig. 1E): Subcylindrical, slightly asymmetrical, sparsely covered with short setae, 6-segmented. Segments 2–5 each with a pair of well-developed pleopods; segment 6 with uropods. Pleopods (Fig. 6G, H) each with 2 distal hooked setae on endopod. Pleopods 1–3 with 9 long plumose setae on exopod. Pleopod 4 (=last) with 8 plumose setae.

Uropods (Fig. 6E): Left uropod slightly larger

than right one. Endopod with 3 "corneous granules" (better called *spatuliform seta*, see [7]) and 3 setae. Exopod well-developed, armed with 9–10 spatuliform setae on outer distal margin, 12 (left) or 10 (right) long plumose setae on margins, and 4 simple setae placed alternately among the plumose setae. Additional setae as illustrated.

Telson (Fig. 6E): Symmetrical, longer than broad, posterior margin rounded, with a mid-posterior group of 6 (occasionally 7) plumose setae, 2 minute setae located laterally, and short setae on surface.

First Crab

Dimensions: CL=1.10–1.20 mm (mean 1.16 mm); CW=0.73 mm (measured at mid portion).

Carapace (Fig. 1F): Elongate, lateral margins subparallel, surface smooth and with moderate transverse depression dorsally; front short. Ocular peduncles large, each with 1 spine basally.

Antennule (Fig. 2F): Inner flagellum 2-segmented, with 1 on proximal and 8 setae on distal segments. Outer flagellum now 5-segmented, with a total of 15 aesthetascs arranged into three tufts, proximal segment unarmed; apical segment without aesthetascs, but armed apically with 5 setae of which one is extremely long.

Antenna (Fig. 2L): Peduncle 4-segmented (fourth segment the longest); second segment with a well-developed acicle and a stout spine. Flagellum composed of 11 segments, each except the first armed with setae.

Mandible (Fig. 3F): Palp 3-segmented, distal segment ovoid, with 7 short setae on outer margin. Cutting edge almost straight.

Maxillule (Fig. 3L): Endopod unsegmented, with 2 setae laterally and additional 2 setae basally. Basal endite with 3 plumose setae and 14–15 smooth spines. Coxal endite ovoid, with 16–18 setae.

Maxilla (Fig. 4F): Endopod slender, with a single subapical seta. Basal endite bilobed, each lobe with 10–11 setae. Coxal endite bilobed, proximal lobe with 19–20 rigid curved setae arranged transversely and marginally, distal lobe with a total of 9 setae. Scaphognathite fringed with 26–28 plumose setae.

Maxilliped 1 (Fig. 5F): Endopod unsegment-

ed, digitiform, armed with 4 setae. Exopod 2-segmented, proximal segment with 3 plumose setae on outer margin and 2 simple setae on inner margin; distal segment with 6 plumose setae. Basis profusely setose, with a total of 20–21 setae arranged transversely and marginally. Coxa with 7–8 setae.

Maxillipeds 2–3 (not drawn): Similar in morphology to those of the megalopal stage, but profusely setose at this stage, especially the endopod of maxilliped 3; distal segments with numerous rigid setae and spines.

Pereiopods: Similar to those of the previous stage (see Fig. 1F). Chelipeds (Fig. 7K, L) markedly different in size, right larger than left, each covered with short setae.

Abdomen (Fig. 1F): Subcylindrical, segmentation indistinct, sparsely setose. Pleopods on abdominal segments 2–5, rather placed ventrolaterally. Left pleopods longer than right ones, each armed with plumose setae on exopod as illustrated; right pleopods with reduced, unarmed exopod. However, other specimens examined exhibited another range of pleopodal variation, i.e., first pair reduced to a very short bud-like projection, left pleopods 2–4 with 9, 9, 8 plumose setae on exopod, respectively, but right pleopods markedly reduced to buds.

Uropods (Fig. 6F): Left uropod larger than right one. Endopod with 6 (left) or 4 (right) spatuliform setae. Exopod with 12 (left) or 10 (right) spatuliform setae and additional setae on surface and margins.

Telson (Fig. 6F): Posterior margin divided into unequal lobes by a shallow sinus; surface and margins with several setae as illustrated.

Pagurus geminus McLaughlin, 1976

First Zoea

Dimension: CL=1.09–1.15 mm (mean 1.13 mm).

Carapace (Fig. 8A, B): Surface smooth. Rostral spine slightly directed downward, not reaching the tip of antennal scale. Eyes sessile.

Antennule (Fig. 8C): Peduncle unsegmented, with 3 subequal aesthetascs and 2 fine setae

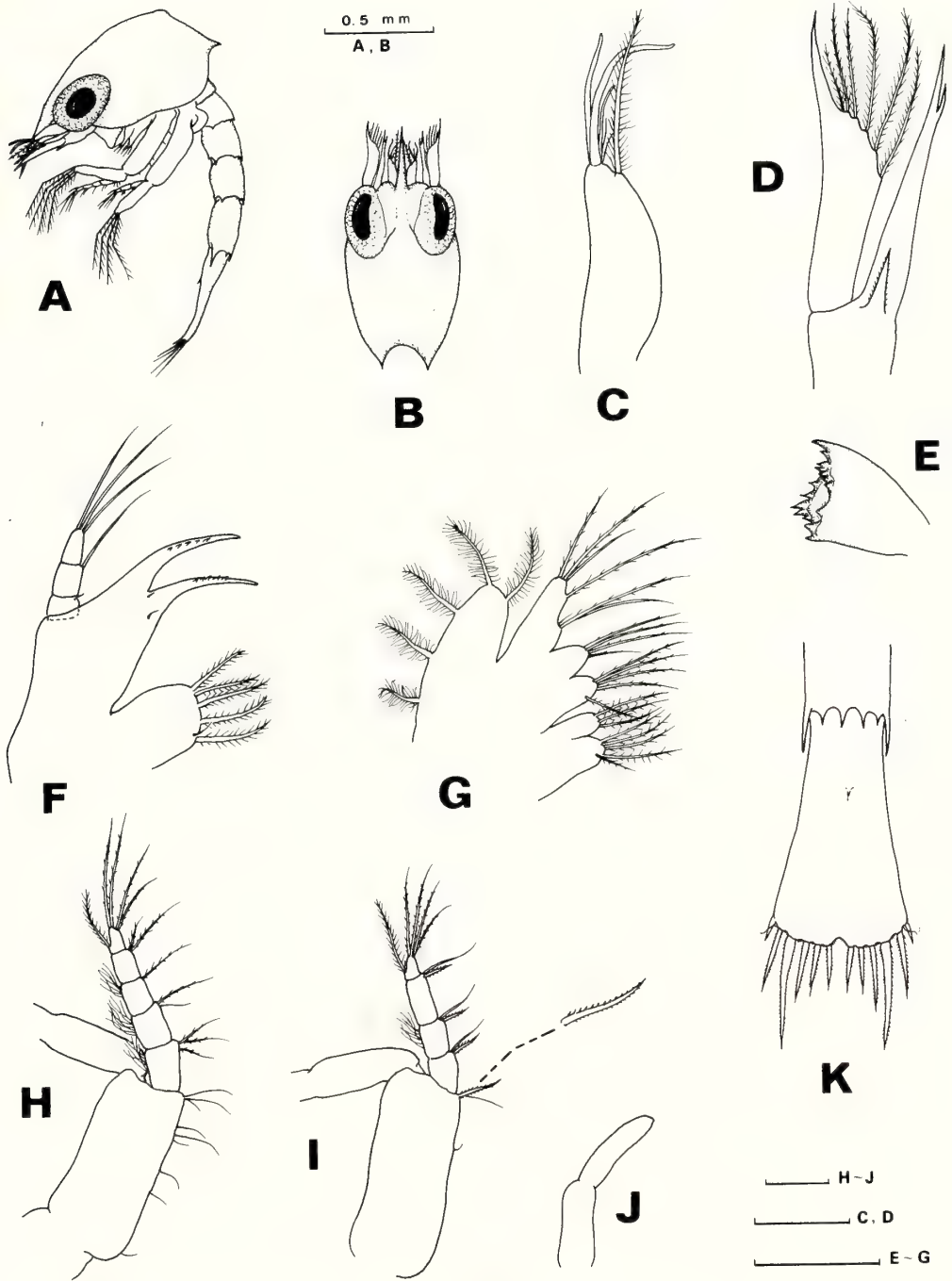


FIG. 8. *Pagurus geminus* McLaughlin, 1976. Zoea I. A, whole specimen, lateral view; B, carapace, antennules and antennae, dorsal view; C, antennule; D, antenna; E, mandible; F, maxillule; G, maxilla; H-J, maxillipeds 1-3; K, abdominal segment 5 and telson, dorsal view. Scale bars=0.1 mm, except for A and B.

distally, and subterminal, long plumose seta.

Antenna (Fig. 8D): Endopod bifid at tip, shorter than the exopod. Exopod distally pointed, with 6 plumose setae on inner distal half. A stout serrate spine near the base of endopod.

Mandible (Fig. 8E): Incisor process short, stout. Molar process with several acute teeth of diverse lengths.

Maxillule (Fig. 8F): Endopod 3-segmented, with 1, 1, 3 setae, the proximal a minute seta. Basial endite with 2 long curved stout spines and 2 minute inner setae. Coxal endite with 5 rigid plumose and 1 simple setae.

Maxilla (Fig. 8G): Endopod stepped medially, with 3+1+3 setae. Basial and coxal endites bilobed, with 5+4 and 5+3 setae respectively. Scaphognathite fringed with 5 soft plumose setae.

Maxilliped 1 (Fig. 8H): Endopod 5-segmented, setation as 3, 2, 1, 2, 4+I. Segments 1-3 with 6-7, 8, 5-7 very fine setules on outer margin respectively. Exopod with 4 long natatory setae. Basis with 9 setae along inner margin.

Maxilliped 2 (Fig. 8I): Endopod 4-segmented, setation as 2, 2, 2, 4+I. Segment 2 with 7-8 (rarely absent) fine setules dorsally. Exopod with 4 long, natatory setae. Basis with 3 setae marginaly, distal pair similar to setae of segments 1-3.

Maxilliped 3 (Fig. 8J): Rudimentary, uniramous, unarmed.

Pereiopods: Not observable at this stage.

Abdomen (Fig. 8K): Composed of 5 segments and a telson. Posterior margin of segments (except the first) with short spines. Posterolateral margins of fifth segment projected as stout spines.

Telson (Fig. 8K): Elongate, furcae apparent, each with 7 processes. Anal spine present medio-ventrally.

Pagurus lanuginosus De Haan, 1849

First Zoea

Dimension: CL=1.53-1.59 mm (mean 1.57 mm).

Carapace (Fig. 9A): With a pointed rostral spine, slightly directed downward; posterolateral edges projecting moderately backward, distally acute.

Antennule (Fig. 9B): Peduncle unsegmented, distally invested with 3 aesthetascs, of which two are similar in length and one is short, slender, and 2 fine setae. Subterminally with 1 long plumose seta.

Antenna (Fig. 9C): Endopod slightly longer than the scale. Scale distally pointed, with 5 plumose setae on distal half of inner margin. A single stout serrate spine emerging from base of endopod.

Mandible (not drawn): Incisor process stout. Molar process with several pointed teeth of different lengths and minute granules on inner surface. Additional shorter teeth between both processes.

Maxillule (Fig. 9D): Endopod 3-segmented, with setae arranged as 2, 1, 3, of which the proximal ones are very short and fine. Basial endite with 2 long stout non-articulated spines and 2 fine setae. Coxal endite with 4-5 long and 2 shorter setae.

Maxilla (Fig. 9E): Endopod indistinctly bilobed, with 2 setae medially and 3-4 setae distally. Basial and coxal endites bilobed with 5+4 and 6+4 setae respectively. Scaphognathite fringed with 5 plumose setae.

Maxilliped 1 (Fig. 9F): Endopod 5-segmented, with setal arrangement as 3, 2, 1, 2, 4+I on inner margin; segments 1-3 with very fine long setules on outer margin arranged as 5-6, 10-11, and 9-10 respectively. Exopod with 4 long, plumose, natatory setae. Basis with 9 setae on inner margin.

Maxilliped 2 (Fig. 9G): Endopod 4-segmented, with 2 setae on segments 1-3, and 5 setae on distal segment of which one is dorsal. Segments 2-3 each with 4-5 and 5-6 very fine setules on outer margin respectively. Basis with 3 setae, the distal pair very similar to those of segments 1-3.

Maxilliped 3 (Fig. 9H): Rudimentary, uniramous, unarmed.

Pereiopods: No rudiments of pereiopods at this stage.

Abdomen (Fig. 9A, I): Composed of 5 segments and a telson. Posterior margin of each segment with minute spines; posterolateral spines of the fifth segment well-developed.

Telson (Fig. 9I): Elongate, approximately 1.5 times its posterior width, slightly notched medial-

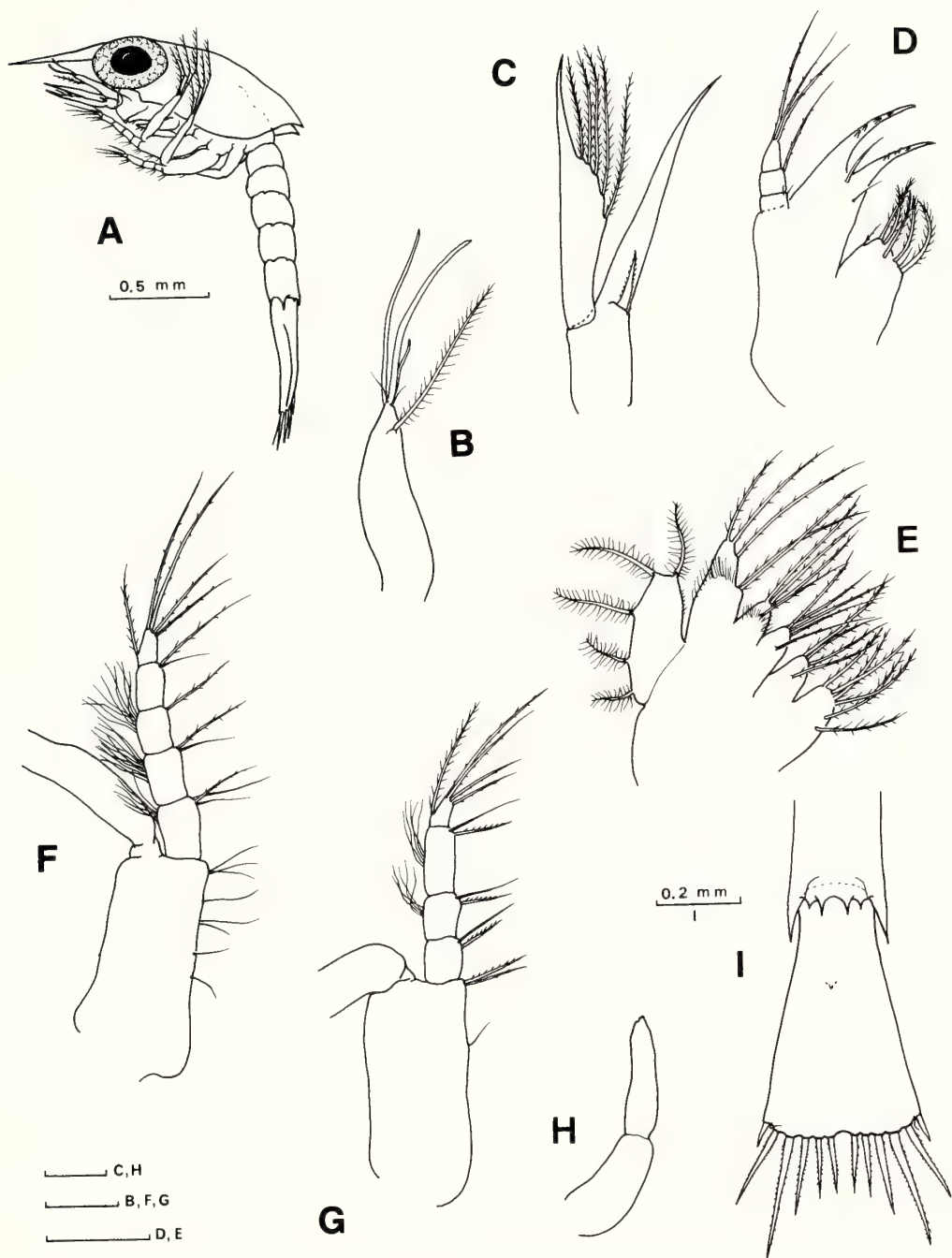


FIG. 9. *Pagurus lanuginosus* De Haan, 1894. Zoea I. A, whole specimen, lateral view; B, antennule; C, antenna; D, maxillule; E, maxilla; F-H, maxillipeds 1-3; I, abdominal segment 5 and telson, dorsal view. Scale bars = 0.1 mm, except for A and I.

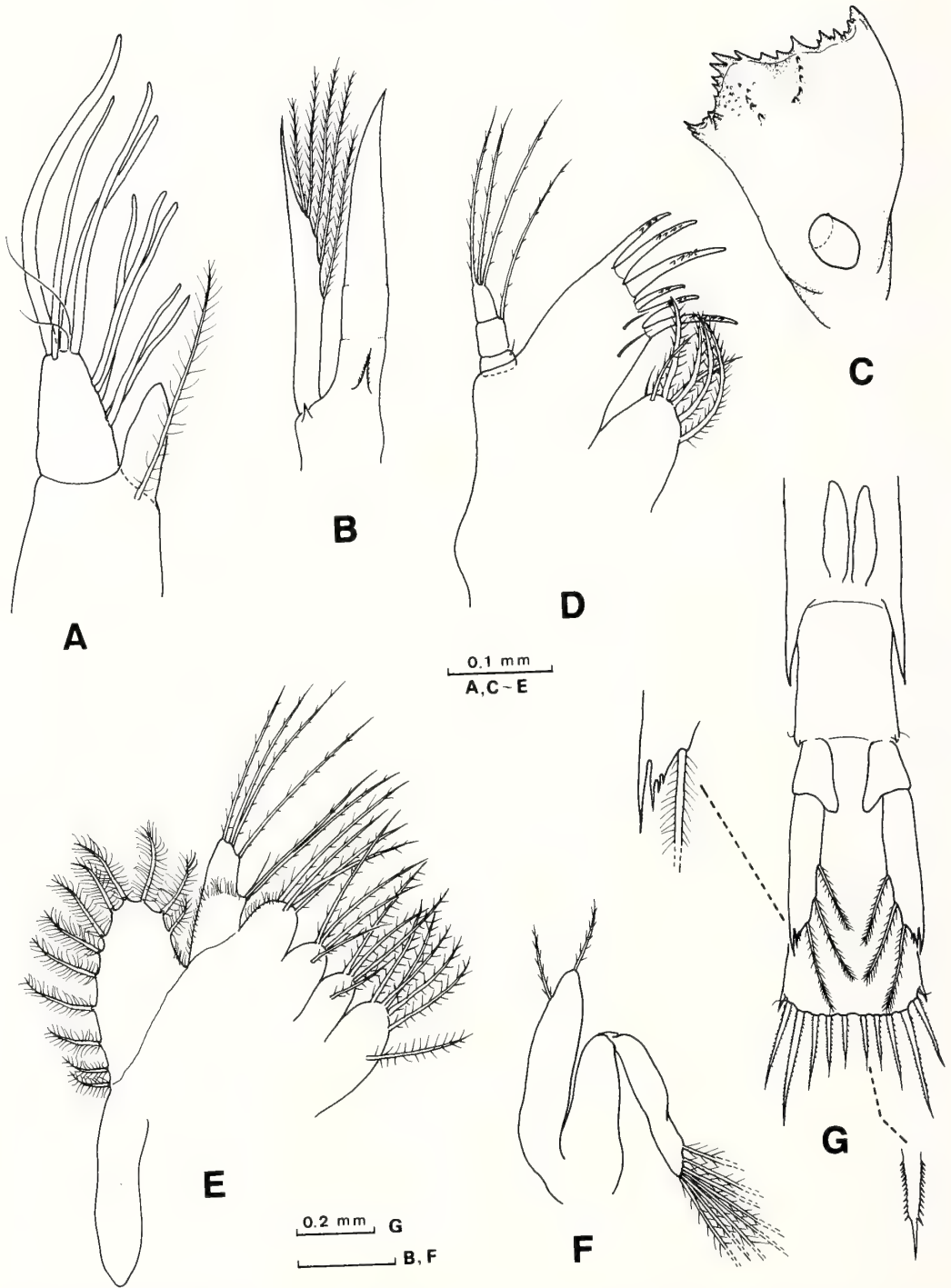


FIG. 10. *Pagurus lanuginosus* De Haan, 1849. Zoea IV. A, antennule (distal portion); B, antenna; C, mandible; D, maxillule; E, maxilla; F, maxilliped 3; G, last two abdominal segments and telson, ventral view, with details of distal portion of uropods and marginal seta. Scale as indicated.

ly. Posterior margin of each furca with 7 processes; outermost process a stout spine articulated to telson; second a fine seta (under high magnification it is seen as fringed with fine setules); third to seventh processes stout long setae (the fourth is the longest seta), each bearing setules along borders; processes 5–7 markedly pointed distally. Anal spine minute.

Fourth Zoea

Dimension: CL=1.90–2.12 mm (mean 2.03 mm).

Antennule (Fig. 10A): Endopod digitiform, unarmed. Outer flagellum indistinctly segmented, distally with 4 (rarely 3) aesthetascs and 2 fine setae, medially with 5 aesthetascs, arranged into two groups. A single, long plumose seta near base of endopod, and 2 fine setules on opposite margin. Segmentation distinct at level of endopod.

Antenna (Fig. 10B): Endopod thick, acute distally, slightly longer than scale. The latter with 5 plumose setae on inner margin. A stout serrate spine and a smaller smooth seta basally.

Mandible (Fig. 10C): Palp present as a soft unsegmented bud. Cutting border with several acute teeth.

Maxillule (Fig. 10D): Endopod 3-segmented, with 1, 1, 3 setae, the proximal seta very short and fine. Basal endite with 6 stout spines (some articulated at their bases) and 2 inner simple setae. Coxal endite with 6 rigid plumose and 1 simple setae.

Maxilla (Fig. 10E): Endopod stepped medially, with 3+1+3 setae. Basal and coxal endites bilobed, with 5+4 and 6+4 setae respectively. Scaphognathite composed of distal and proximal lobes, the former with 11–12 soft plumose setae and the latter unarmed.

Maxillipeds 1–2: Not dissected.

Maxilliped 3 (Fig. 10F): Endopod greatly developed, longer than protopod, with 1 terminal and 1 subterminal setae. Exopod 2-segmented, distal segment with 8 long natatory setae.

Abdomen (Fig. 10G): Composed of 6 segments and the telson. Uniramous, unarmed paired pleopods on abdominal segments 2–5; segment 6 with well-developed 2-segmented uropods. Endopod as a short unarmed projection. Exopod

elongate, with 4 pointed spines distally and 3 plumose setae on inner distal half.

Telson (Fig. 10G): Elongate, posterior margin almost straight, with 7 processes on each furca; processes 5–7 markedly acute distally. Anal spine absent.

DISCUSSION

Kurata [3] described the zoea I stage of *P. middendorffii* from laboratory-reared larvae, and assigned a series of planktonic zoeas II–IV to the same species. Morphological comparison of all zoeal stages between Kurata's and our study is shown in Table 1.

The larval characters of the zoea I stage are almost identical in both studies, whereas Kurata's zoeas II–IV of *P. middendorffii* are different from those of our entirely laboratory-reared material, e.g., even in important characters such as the maxillary scaphognathite and telsonal processes. This fact suggests that the specific identification was inadequate in his planktonic material. What species shall we attribute these planktonic zoeas to? Up to present, as shown in Table 2, the complete larval developments of 9 pagurid species from Japan except *P. trigonocheirus* have been described from laboratory-rearing which insures correct specific identification. Among them, zoeas of the following 4 species have 8+8 telsonal setation in the stages II–IV, as well as 3 setae on exopod of uropods in the III–IV stages: *P. brachiomastus*, *P. hirsutiusculus*, *P. dubius* and *P. geminus*. However, no zoea IV of these species has 14 marginal setae on the maxillary scaphognathite as in Kurata's material [3]. Larvae of the other allied species from Hokkaido, such as *P. ochotensis* [7] and *P. lanuginosus* (this study), are quite different from those of Kurata's "*middendorffii*", especially in the setations of antenna (exopod), maxilla (coxal endite), uropods (exopod), along with the marginal setation of the telson.

Other *Pagurus* species occurring in the coasts of Hokkaido [1, 2] are *P. hirsutiusculus* (Dana, 1851), *P. constans* (Stimpson, 1858), *P. gracilipes* (Stimpson, 1858), *P. pectinatus* (Stimpson, 1858), *P. trigonocheirus* (Stimpson, 1858), *P. dubius*

TABLE 1. Comparison of zoeal characters of *Pagurus middendorffii* between Kurata's [3] material and this study [*]

Characters	Zoea I		Zoea II		Zoea III		Zoea IV	
	Kurata	*	Kurata	*	Kurata	*	Kurata	*
Source of Material:	L	L	P	L	P	L	P	L
Carapace:								
length (mean; mm)	1.24	1.34	1.75	1.51	2.16	1.82	2.50	2.03
Antennule:								
aesthetascs	[2]**	2	2	3	4	5	9	8
endopod bud	[-]	-	-	-	+	+	+	+
endopod seta	[(1)]	(1)	(1)	(1)	1	1	-	-
Antenna:								
exopod setae	6	6	6	5	6	5	6	5
Mandible:								
bud of palp	-	-	-	-	-	-	+	+
Maxillule:								
coxal endite	[5]	7	[6]	7	[7]	6	[7]	7
basial endite	[2sp+1]	2sp+2	[4sp+1]	4sp+2	[4sp+1]	4sp+2	[6sp+1]	6sp+2
endopod	[1, 1, 3]	1, 1, 3	[1, 1, 3]	2, 1, 3	[1, 1, 3]	1, 1, 3	[1, 1, 3]	1, 1, 3
Maxilla:								
coxal endite	[4+3]	5+4	[5+4]	5+4	[5+4]	5+4	[5+4]	5+4 (5)
basial endite	[3+3]	5+4	[4+4]	5+4	[5+4]	5+4	[5+4]	5+4
endopod	[2+1+3]	2+1+3	[3+1+3]	3+1+3	[3+1+3]	3 (2)+1+3	[3+1+3]	3+1+3
scaphognathite	[5]	5	[6]	6	[10]	8	[14]	13
Mxp. 1, endopod:								
segment 1	[3+n]	3+n	[3+I]	3+I	?	3+I	?	3+I
segment 2	[2+n]	2+n	[2+I]	2+I	?	2+I	?	2+I
segment 3	[1+n]	1+n	[1+I]	1+I	?	1+I	?	1+I
segment 4	[2]	2	[2]	2	?	2	?	2
segment 5	[4+I]	4+I	[4+I]	4+I	?	4+I	?	4+I
Mxp. 2, endopod:								
segment 1	[2]	2	[2]	2	?	2	?	2
segment 2	[2+n]	2+n	[2+I]	2+I	?	2+I	?	2+I
segment 3	[2+n]	2+n	[2+I]	2+I	?	2+I	?	2+I
segment 4	[4+I]	4+I	[4+I]	4 (3)+I	?	4+I	?	4+I
Mxp. 3:								
endopod setae	-	-	1	1	?	1	?	2
Abdomen:								
pleopod	-	-	-	-	-	-	+	+
uropod setae	-	-	-	-	3	3	3	3
Telson:								
processes	7+7	7+7	8+8	7+7	8+8	7+7	8+8	7+7

** Data in brackets are estimated from illustrations. n: numerous, sp: spine, I: dorsal plumose seta, L: laboratory-reared, P: plankton, +: present, -: absent, ?: no data.

(Ortmann, 1892), and *P. rathbuni* (Benedict, 1892). But larval studies, except those of *P. hirsutiusculus* (see [9]), *P. dubius* (see [10]) and *P. trigonocheirus* (see [7, 11]) are unknown to refer to.

In the present study, there were conspicuous differences between the larvae of *P. geminus* and the other two species. The bifid character of

antennal endopod clearly distinguishes *P. geminus* from the other allied species [6]. Thus, two possibilities are suggested by the facts mentioned above: 1) Kurata's zoeas II-IV belong to another species whose larvae are unknown, 2) each zoeal stage of these planktonic larvae also may be assigned to different species, although this probability is more difficult to ascertain. At present, we

TABLE 2. Comparison of selected zoeal characters and their setation in known pagurid species from Japan

Species	Antenna (Z I)		Maxillule (Z I)	Maxilla		Uropod (Z III-IV)		Telson (Z II-IV)	Ref.
	exo.	endo.	endo.	(Z I) endo.	(Z IV) sca.	exo.	endo.	processes	
<i>Pagurus</i>									
<i>lanuginosus</i>	5	simple	1, 1, 3	3+1+3	12	3	+	7+7	[5, *]
<i>middendorffii</i>	6	simple	1, 1, 3	2+1+3	13	3	+	7+7	[*]
" <i>middendorffii</i> "	6	simple	1, 1, 3	2+1+3	14	3	+	8+8	[3]
<i>brachiomastus</i>	6	simple	1, 1, 3	3+1+3	12	3	+	8+8	[6]
<i>hirsutiusculus</i>	5	simple	0, 1, 3	3+1+3	12	3	+	8+8	[9]
<i>ochotensis</i>	7	simple	2, 1, 3	3+1+3	15-16	4-5	+	8+8	[7]
<i>dubius</i>	5	bifid	0, 1, 3	2+1+3	11	3	+	8+8	[10]
<i>geminus</i>	6	bifid	1, 1, 3	3+1+3	?	3	+	8+8	[4, *]
<i>trigonocheirus</i>	8	bifid	1, 1, 3	3+1+3	?	?	?	?	[7, 11]
<i>similis</i>	10	2 setae	1, 1, 3	3+3	11	7	2	8+8	[12]
<i>Labidochirus</i>									
<i>splendescens</i>	7	simple	1, 1, 3	3+1+3	17-18	7-8	0-1	8+8	[13]

endo.: endopod, exo.: exopod, sca.: scaphognathite, Z: zoea, Ref.: references, +: present, ?: no data, * this study.

have no complete larval information concerning about 40% of the Paguridae from Hokkaido. Future larval studies will answer the above cited question.

Most of pagurid zoeas exhibit 7 processes on each telsonal furca in the zoea I stage and a setation of 8+8 in the zoea II-IV stages. This led to generalize that all pagurid zoeal stages II-IV exhibit this setation [3, 13]. However, the first record of setation of 7+7 processes throughout zoeal stages was given for *P. lanuginosus* [5]; this setation is also consistent with our material (see Fig. 10G). The present descriptions of *P. middendorffii* also indicate that the previous presumption is not applicable to all known *Pagurus* zoeas.

An anal spine is present in only the zoeal stages I and II in most of known pagurid larvae. Additional specimens of zoea I stage of *P. brachiomastus* and *P. ochotensis*, although previously described [6, 7] were reexamined. The anal spine was minute and short in *P. geminus* and *P. lanuginosus*, moderate in *P. middendorffii*, but conspicuous in *P. brachiomastus* and *P. ochotensis*.

Besides the telsonal setation of 7+7, the zoeal stages II-IV of *P. middendorffii* and *P. lanuginosus* have characters common to both species. A

number of megalopal characters, especially the 6 telsonal plumose setae is shared by these species and also by *P. hirsutiusculus* [9]. Most of megalopas known from Japan exhibit 8 marginal setae [6].

Kurata [3] briefly described and distinguished 5 types of *Pagurus* megalopas by the length of antennal scale, cheliped ornamentation, rostrum length, and proportion of dactylus to propodus of pereopods II-III. It is now known that at least one of *Pagurus* megalopas belongs to a different genus, *Paguristes* [7], but the correct assignment of the remaining megalopas is still uncertain because of his brief descriptions and incomplete illustrations.

The present material of *P. lanuginosus* from Hokkaido differs in a few minor features from the larvae of the same species from Korea reported by Hong [5]. However, the most conspicuous difference is the presence of mandibular palp in all specimens of zoea IV from Hokkaido (see Fig. 10C), not observed by Hong. This palp is rather located basally, so it seems likely that Hong was probably unaware of its nature (his illustrations rather emphasized the dentition). It seems that the other minor differences can occur due to the extensive geographical range and different habitats

in which the adults and planktonic larvae of this species inhabit, i.e. Pacific coast, Hokkaido, and Pusan, Korea, including different laboratory conditions used. The first megalopas of *P. lanuginosus* were obtained after 21 days of culture, whereas in the Hong's study, these appeared after 31–32 days. Under the laboratory conditions of 18°C temperature and 31.5 ppt salinity, the duration of each zoeal stage was approximately 5–6 days in our study and 7–9 days in Hong's study (at 13.6°C and 33.67 ppt).

Although zoeas and megalopas of *P. lanuginosus* and *P. middendorffii*, sympatric species in the sublittoral of Hokkaido have a number of similar characters ([5], this study), the adults are so distinct that their larval resemblance may suggest some phylogenetic significance. In fact, adults of *P. lanuginosus* have hairy pereopods with scattered brownish spots ([15], our material), whereas those of *P. middendorffii* are smooth, without coloured spots ([16], our material).

ACKNOWLEDGMENTS

We are grateful to Prof. F. Iwata (Hokkaido University) for his encouragement and further reading of the manuscript. We also thank to the staff of the Usujiri Marine Biological Station for facilities to collect ovigerous females. The present study was partially carried out during the tenure of a Scholarship (R. Q.) awarded by the Ministry of Education, Science and Culture, Japan.

REFERENCES

- Igarashi, T. (1970) A list of decapod crustaceans from Hokkaido, deposited at the Fisheries Museum, Faculty of Fisheries, Hokkaido University. II. Anomura. Contrib. Fish. Mus. Fac. Fish. Hokkaido Univ., No. 12, 15 pp., 9 pls.
- Miyake, S. (1982) Japanese Crustacean Decapods and Stomatopods in Color. Vol. I. Macrura, Anomura and Stomatopoda. Hoikusha, Osaka. 261 pp., 56 pls. (In Japanese)
- Kurata, H. (1964) Larvae of decapod Crustacea of Hokkaido. 5. Paguridae (Anomura). Bull. Hokkaido Reg. Fish. Res. Lab., **29**: 24–48. (In Japanese, with English abstract)
- Kurata, H. (1968) Larvae of Decapoda Anomura of Arasaki, Sagami Bay—I. *Pagurus samuelis* (Stimpson)(Paguridae). Bull. Tokai Reg. Fish. Res. Lab., **55**: 265–269. (In Japanese, with English abstract)
- Hong, S. Y. (1969) The larval development of *Pagurus lanuginosus* de Haan (Crustacea, Anomura) reared in the laboratory. Bull. Kor. Fish. Soc., **2**: 1–15.
- Konishi, K. and Quintana, R. (1987) The larval stages of *Pagurus brachiomastus* (Thallwitz, 1892) (Crustacea: Anomura) reared in the laboratory. Zool. Sci., **4**: 349–365.
- Quintana, R. and Iwata, F. (1987) On the larval development of some hermit crabs from Hokkaido, Japan, reared under laboratory conditions (Decapoda: Anomura). J. Fac. Sci. Hokkaido Univ., Ser. VI, Zool., **25**: 25–85.
- Quintana, R. and Saelzer, H. (1986) The complete larval development of the edible crab, *Cancer setosus* Molina and observations on the prezoaeal and first zoeal stages of *C. coronatus* Molina (Decapoda: Brachyura, Cancridae). J. Fac. Sci. Hokkaido Univ., Ser. VI, Zool., **24**: 267–303.
- Fitch, B. M. and Lindgren, E. W. (1979) Larval development of *Pagurus hirsutiusculus* (Dana) reared in the laboratory. Biol. Bull., **156**: 76–92.
- Hong, S. Y. (1981) The larvae of *Pagurus dubius* (Ortmann) (Decapoda, Paguridae) reared in the laboratory. Bull. Natl. Fish. Univ. Busan, **21**: 1–11.
- Ivanov, B. G. (1979) A contribution to the biology of hermit crabs of the North Pacific. 2. The first larval stages of some species reared in the laboratory (Crustacea, Decapoda, Paguridae). Zool. Zhur., **58**: 977–985. (In Russian, with English abstract)
- Lee, B. D. and Hong, S. Y. (1970) The larval development and growth of decapod crustaceans of Korean waters. I. *Pagurus similis* Ortmann (Paguridae, Anomura). Publ. Mar. Lab. Pusan Fish. Coll., **3**: 13–26.
- Nyblade, C. F. and McLaughlin, P. A. (1975) The larval development of *Labidochirus splendescens* (Owen, 1839) (Decapoda, Paguridae). Crustaceana, **29**: 271–289.
- Pike, R. B. and Williamson, D. I. (1960) Larvae of decapod Crustacea of the families Diogenidae and Paguridae from the Bay of Naples. Pubbl. Staz. Zool. Napoli, **31**: 493–552.
- Miyake, S. (1978) The Crustacean Anomura of Sagami Bay. Biol. Lab. Imp. Household, pp. 1–200, 4 pls.
- McLaughlin, P. A. (1974) The hermit crabs (Crustacea Decapoda, Paguridea) of northwestern North America. Zool. Verhandl., **130**: 1–136.

Two New Hymenolepidid Cestodes, *Vampirolepis molani* sp. n. and *V. iraqensis* sp. n., from Iraqi Bats

ISAMU SAWADA and ABDUL L. MOLAN¹

Biological Laboratory, Nara Sangyo University, Sango, Nara 636, Japan and

¹Department of Biology, Education College, Salahaddin University, Arbil, Iraq

ABSTRACT—Two new hymenolepidid cestodes were found in bats collected at the various places in Iraq from October 1985 to November 1986. *Vampirolepis molani* sp. n. from *Pipistrellus kuhli* is related to but differs from *V. macrotesticulatus* Sawada, 1979, in the shapes of rostellar hooks and ovary. *V. iraqensis* sp. n. from *Taphazous nudiventris* is related to *V. taiwanensis* Sawada, 1984 and *V. hipposidera* (Lin, 1959) comb. n., but it differs from the former in the shapes of rostellar hooks, ovary and eggs, and from the latter in the length of rostellar hooks, the arrangement of testes and the shapes of ovary and eggs.

Cestode species parasitizing bats indigenous to Iraq have been entirely unknown up to the present. This study was conducted to clarify the cestode fauna of bats in Iraq.

MATERIALS AND METHODS

Total 123 bats, composed of two species, *Pipistrellus kuhli* (Natterer, 1819) and *Taphazous nudiventris* Cretzschmar, 1830, were collected from various parts in Iraq from October 1985 to November 1986, by the second author (Fig. 1).

The cestodes obtained from bats were fixed in 4% formalin and sent to the first author for identification. The cestodes removed out of formalin were washed in running water overnight. The morphological features of scoleces and eggs were examined without staining in this process. After being soaked in 45% acetic acid for about 5 hr for expanding, they were stored in 70% alcohol and then stained with alcohol-hydrochloride-carmin, dehydrated in alcohol, cleared in xylene, and mounted in Canada balsam. Measurements are given in millimeters.

RESULTS

Bats examined and cestodes obtained are shown in Table 1.

Vampirolepis Spassky, 1954

Vampirolepis molani sp. n.

(Figs. 2-4)

Of the 20 specimens of the bats, *P. kuhli*, caught



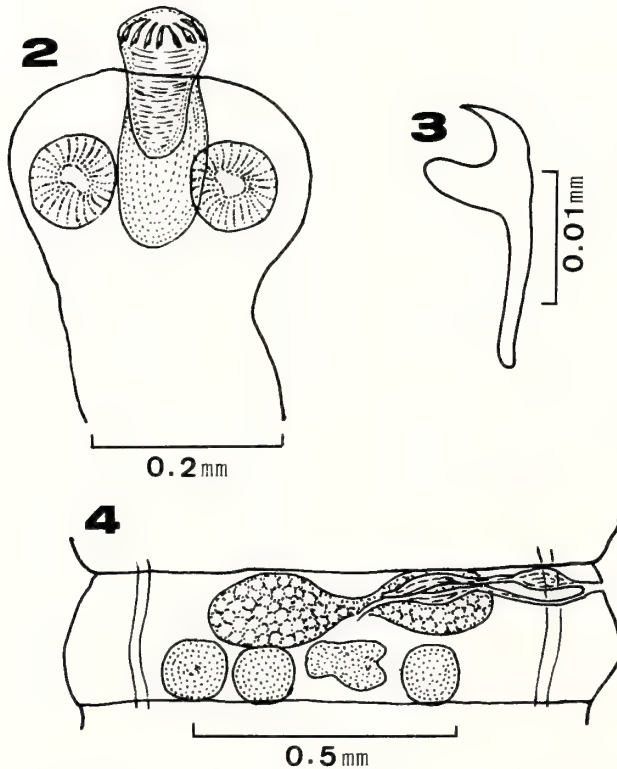
FIG. 1. Map showing the collection sites of bats. For locality numbers, see Table 1.

Accepted September 5, 1987

Received July 16, 1987

TABLE 1. Localities and dates of collection of bats and their cestode parasites in Iraq in 1985 and 1986

Host species Locality	Date	Number of bats			Cestode species
		examined	infected	%	
Vespertilionidae					
<i>Pipistrellus kuhli</i>					
(1) Arbil	Apr. 20, 1986	20	3	15	<i>Vampirolepis molani</i> sp. n.
(2) Kirkuk	Jul. 23, 1986	20	1	5	<i>V. molani</i>
(3) Sulaimaniah	Oct. 3, 1985	13	0	0	
(4) Diala	Oct. 4, 1985	12	0	0	
Emballonuridae					
<i>Taphozous nudiventris</i>					
(5) Babylon	Oct. 22, 1986	38	5	13	<i>V. iraqensis</i> sp. n.
(6) Basrah	Nov. 14, 1986	20	4	20	<i>V. iraqensis</i>



FIGS. 2-4. *Vampirolepis molani* sp. n. 2: Scolex. 3: Rostellar hook. 4: Mature proglottid, dorsal view.

at Arbil, on April 20, 1986, three were found infected with this cestode. All the cestode specimens obtained were fully mature but not gravid.

Description: Medium-sized hymenolepidid; worm length 58, maximum width 0.93. Scolex

0.189 in length and 0.259 in breadth across suckers, not sharply demarcated from strobila. Rostellum 0.133 long and 0.077 wide, armed with a single circle of 28 spanner-shaped hooks 0.021 long. Hook handle relatively long; guard strong,

round at its end, longer than blade, blade sharp at its end. Rostellar sac small, 0.217 long and 0.091 wide, extending to posterior edge of suckers. Suckers unarmed, round, 0.070–0.077 in diameter. Neck slender, 0.88 long and 0.21 wide. Numerous proglottids much broader than long.

Genital pores unilateral, located anterior 1/3 of proglottid margins. Testes three in number, round to oval, 0.098–0.105 by 0.119–0.126, arranged in a transverse row, one poral and two aporal, not in contact with longitudinal excretory canals laterally. Cirrus sac long and rather cylindrical, 0.154–0.161 long and 0.028 wide, occupied by internal seminal vesicle measuring 0.084–0.091 long and 0.028 wide. External seminal vesicle 0.119–0.040 by 0.028. Ovary transversely elongated, bilobate, 0.420–0.441 wide. Seminal receptacle dorsal to ovary, measuring 0.182–0.210 long and 0.025–0.035 wide. Vitelline gland lying just posterior to ovary, irregularly lobate, 0.126–0.133 by 0.077–0.091. Gravid and senile proglottids unknown.

Host: *Pipistrellus kuhli* (Natterer, 1819).

Site of infection: Small intestine.

Locality and date: Arbil, Iraq; April 20, 1986.

Type specimen: Holotype: NSU Lab. Coll. No. 8801. Paratypes: No. 8802.

Remarks: The present new species closely resembles *V. macrotesticulatus* Sawada, 1970 [1] from *Rhinolophus ferrumequinum nippon* in the number and length of rostellar hooks. However, it differs from *V. macrotesticulatus* in the shape of rostellar hooks (guard strong and blade remarkably curved vs. guard slim and blade gently curved) and the shape of ovary (distinctly bilobate vs. irregularly bilobate).

***Vampirolepis iraqensis* sp. n.**

(Figs. 5–8)

Of the 38 specimens of *T. nudiventris*, collected at Babylon, Iraq, on October 22, 1986, five were found infected with this cestode.

Description: Small-sized hymenolepidid; mature worms 30–50 in length; maximum width 0.9. Metamerism distinct, craspedote, margins serrate. Proglottids wider than long. Scolex 0.280 long and 0.245–0.294 wide, distinctly set off from neck region measuring 0.6 long and 0.12 wide. Rostel-

lum 0.063 long and 0.049 wide, armed with a single row of 24 spanner-shaped hooks measuring 0.018 long. Hook handle slender; guard round at its end, slightly shorter than blade; blade remarkably curved, sharp at its end. Rostellar sac pyriform, 0.147 long and 0.098 wide, not extending posterior to suckers. Suckers unarmed discoid, 0.077 in diameter.

Genital pores unilateral, located slightly posterior to middle of each proglottid margin. Testes three in number, round to subspherical, 0.049–0.060 by 0.053–0.056, arranged in form of triangle, one poral and two aporal. Cirrus sac, well developed, pyriform, 0.084–0.095 long and 0.028–0.035 wide. Internal seminal vesicle 0.060–0.063 long and 0.028–0.035 wide, occupying almost whole of cirrus sac. External seminal vesicle 0.042–0.049 long and 0.035–0.045 wide. Ovary distinctly trilobate, 0.105–0.112 wide. Vitelline gland irregularly lobate, lying just posterior to ovary, 0.049–0.060 by 0.039–0.042. Seminal receptacle saccated, 0.050–0.053 long and 0.042–0.053 wide, overlapping ovary. Uterus arising directly from ovarian lobes as a lobe sac, which is gradually enlarging, fulling whole available space in proglottids. Eggs oval, 0.049–0.056 in major axis and 0.035–0.039 in minor axis, surrounded by four thin envelopes. Outermost chorion thin; inner membrane with at each pole a round projection provided with polar filaments. Onchospheres subspherical, 0.021–0.025 by 0.025–0.028; embryonic hooks 0.018 long.

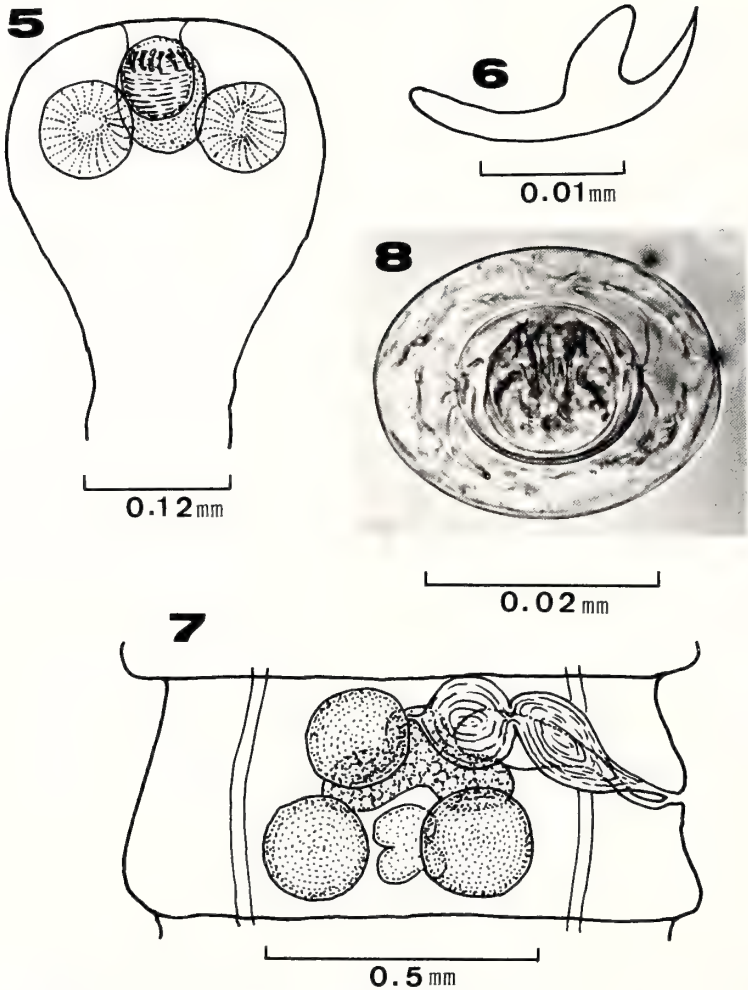
Host: *Taphazous nudiventris* Cretzschmer, 1830.

Site of infection: Small intestine.

Locality and date: Babylon, Iraq; Oct. 22, 1986.

Type specimen: Holotype: NSU Lab. Coll. No. 8803. Paratypes: 8804.

Remarks: *Vampirolepis iraqensis* sp. n. most closely resembles *V. taiwanensis* Sawada, 1984 [2] in the number and length of rostellar hooks, the location of genital pores and the arrangement of testes, and *V. hipposidera* (Lin, 1959) comb. n. [3, 4] in the shape of scolex, the number of rostellar hooks and the location of genital pores. However, this new species is distinguished from *V.*



FIGS. 5-8. *Vampirolepis iraqensis* sp. n. 5: Scolex. 6: Rostellar hook. 7: Mature proglottid, dorsal view. 8: Egg.

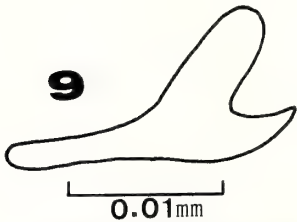


FIG. 9. Rostellar hook of *V. taiwanensis*.

taiwanensis by the shape of the rostellar hooks. The blade is longer than the guard, and the guard is slimmer (Figs. 6 and 9). The species can be separated also from *V. hipposidera* in the shorter rostellar hooks (0.018 vs. 0.021-0.024) and the

arrangement of testes (in a triangular form vs. in a transverse row). Furthermore, it differs from the two others in the shape of ovary (trilobate vs. transversely elongated), the thinner outermost chorion of eggs (thin vs. tough) and in the morphological feature of eggs (provided with polar filament vs. no polar filament).

REFERENCES

- 1 Sawada, I. (1970) Helminth fauna of bats in Japan VII. Bull. Nara Univ. Educ., 19: 73-80.
- 2 Sawada, I. (1984) Two new species of cestodes belonging to the genus *Vampirolepis* (Cyclophyllidea:

- Hymenolepididae) from cave bats in Taiwan. Zool. Sci., **1**: 327–331.
- 3 Lin Yu-Kwang (1959) Notes on a new cestode, *Hymenolepis hipposidera*, from the bat *Hipposideros pratii* Thomas, in Fukien, South China. J. Fukien Teacher's Coll., **2**: 185–193. (In Chinese with English summary)
- 4 Sawada, I. (1980) Helminth fauna of bats in Japan XXII. Annot. Zool. Japon., **53**: 194–201.

[COMMUNICATION]

Gene-Centromere Mapping for 5 Visible Mutant Loci in Multiple Recessive Tester Stock of the Medaka (*Oryzias latipes*)

KIYOSHI NARUSE, ATSUKO SHIMADA and AKIHIRO SHIMA

Zoological Institute, Faculty of Science, University of Tokyo, Bunkyo-ku, Tokyo 113, Japan

ABSTRACT—Five visible mutant loci used for development of the multiple recessive tester Medaka were mapped in relation to their centromeres by the use of the diploid gynogenetic technique. Under complete interference condition, gene-centromere distances were 2cM for *pl*, 13cM for *r*, 32cM for *b*, 40cM for *Da* and 48cM for *gu*, respectively. No joint segregations were observed between the following sets of loci; *b* with *pl*, *b* with *gu*, and *b* with *Da*. The frequency of 0.97 for the heterozygosity at the *gu* locus strongly suggested the presence of chiasma interference. That is, one cross-over most likely inhibited occurrence of another cross-over in the same interval on the chromosome arm carrying the *gu* locus.

INTRODUCTION

The multiple recessive tester stock homozygous for 5 loci was developed [1] to investigate the frequency and mechanism of radiation-induced [2] and/or chemically induced mutations in the fish *Oryzias latipes*. The loci used in this tester fish were *b* (colorless melanophores), *Da* (double anal fins), *gu* (reduced deposition of guanine in iridocytes), *pl* (no pectoral fins) and *r* (colorless xanthophores) [3]. All loci except *Da* were recessive [3]. The *r* locus was sex-linked [4] and others were autosomal [3].

We believe it important for further understanding of the basic biology of the Medaka as a laboratory animal to characterize these loci in terms of linkage relationship between different genes and between the gene and centromere. For

this purpose, we used diploid gynogenesis [5]. The phenotypes of diploid gametes in the Medaka, which were produced by blocking the second meiotic division of the eggs, i.e. by diploid gynogenesis, reflect the egg genotypes. Thus, using this gynogenesis linkage analyses in the Medaka were accomplished without backcrosses to double mutants or F_1 inbreeding.

MATERIALS AND METHODS

Genetic cross to obtain F_1 hybrids

In order to produce F_1 hybrids, females of the HB-12 inbred strain of the Medaka *Oryzias latipes* [6] were mated with males of the multiple recessive tester stock homozygous for the *b*, *pl* and *r* loci or *b*, *gu* and *r* loci [1]. F_1 hybrids with *Da*/+ and *b*/*B* were produced by crossing females of wild stock from Aomori (stock # 1) [7, 8] with males of multiple recessive tester stock homozygous for the *b* and *Da* loci.

Production of gynogenetic diploid Medaka

The method to produce gynogenetic diploid Medaka was described by Naruse *et al.* [5]. Briefly, unfertilized eggs were collected from F_1 hybrids using sham-mating method, and eggs thus obtained were fertilized with UV-irradiated genetically impotent Medaka sperm, and exposed to heat shock or hydrostatic pressure 2 to 3 min after insemination to block the second meiotic division [5]. The yield of gynogenetic diploid Medaka was

over 20% at hatching. The phenotypes of the gynogenetic diploid progeny were visually recognized using a stereoscopic microscope.

The judgement of phenotype of the *b* locus was performed 4 days after fertilization, those of *pl* and *gu* loci just after hatching. The phenotypes of the *Da* and *r* loci were judged at about one month after hatching.

Determination of gene-centromere distances

Recombination frequency (*X*) between a gene and its centromere can be estimated from the frequency (*Y*) of heterozygous diploid progeny gynogenetically obtained from heterozygous *F*₁ hybrids. But it was difficult or impossible to distinguish the heterozygotes from the homozygotes for wild type alleles with regard to the marker genes used for the production of the multiple recessive tester Medaka. So we assumed that the proportions of the homozygotes for mutant alleles and wild-type alleles were identical. Then the fraction of heterozygotes was obtained from the following formula:

$$Y = 1 - 2m$$

where *Y* = fraction of heterozygotes, and *m* = fraction of homozygotes for mutant alleles.

In order to convert *Y* to map distance (*X*) in cM between the gene and centromere, two formulas were used:

$$X = Y \times 100/2 \quad (1)$$

(with complete interference)

$$X = -[\ln(1 - Y)] \times 100/2 \quad (2)$$

(with zero interference)

The formula (1) was based on Morgan's summation formula (multiplication with 100 for conversion into cM unit and division by 2 because of using diploid gynogenesis), while formula (2) was in accordance with Haldane [9].

Linkage analysis using diploid gynogenesis

The analyses for joint segregation of two different genes were made by comparing the observed numbers of individuals with the numbers expected if the loci were inherited independently using 2 × 2 contingency table.

RESULTS AND DISCUSSION

Gene-centromere distance

Table 1 shows the gene-centromere distance under zero and complete interference condition, respectively. When the fraction of heterozygotes was small, map distance between the gene and centromere was almost the same under both conditions. On the other hand, under high heterozygous proportion, the map distances were largely different.

If the occurrence of cross-over is independent of each centromere, the maximum frequency of heterozygotes in gynogenetic diploids is expected to be 0.67 [10]. The frequency of 0.97 for the *gu* locus was significantly different (upper/lower 99% confidence limits: 0.983/0.932) from 0.67. This result suggests that exactly one cross-over occurred between the *gu* locus and the centromere. Such high frequency was not exclusive for the *gu* locus. Indeed in the Medaka the *Ldh-A* and *Amy* loci showed the high heterozygous fraction (1.00 for *Ldh-A* and 0.93 for *Amy*; Naruse and Shima, in preparation). Further, other species of fish with high heterozygous fractions were also reported (e.g., 1.00 for the *Sod* locus of rainbow trout, and 0.89 for *gol-1* gene of zebrafish) [11–13]. Thus, to obtain high heterozygous frequencies for some loci appeared not exceptional for the Medaka but rather frequent in fish. Our result also suggests that the chiasma interference is very high on the chromosome arm carrying the *gu* locus.

Considerable variations in heterozygous fractions were observed in the *b* locus. When maternal genotype was *b/B* (DO–AO), heterozygous fraction was low in comparison with other maternal genotype (0.47, 0.63 and 0.67). But the difference among these values were not statistically significant (95% confidence limit). Therefore, we summed up progeny numbers of each phenotypes to estimate the heterozygous fraction and gene-centromere distance for the *b* locus (Table 1).

To the best of our knowledge, there is only one paper on zebrafish (*Brachydanio rerio*) reporting gene-centromere distances of visible mutant loci which were comparable for the *b* locus of the Medaka [12]. Streisinger *et al.* [12] estimated

TABLE 1. Progeny phenotypes in gynogenetic diploid Medaka and gene-centromere distances

Locus	Maternal* genotype	Progeny phenotype		Heterozygous fraction	Gene-centromere distance	
		Mutant	Wild		Complete**	Zero***
<i>pl</i>	<i>pl</i> /(HB-PL)	278	303	0.04	2	2
<i>r</i>	<i>r</i> / <i>R</i> (HB-PL)	13	22	0.26	13	15
<i>b</i>	<i>b</i> / <i>B</i> (HB-PL)	107	474	0.63	32	50
	<i>b</i> / <i>B</i> (HB-GU)	58	289	0.67	33	55
	<i>b</i> / <i>B</i> (DO-AO)	14	39	0.47	24	32
		179†	802§	0.64#	32	51
<i>Da</i>	<i>Da</i> /(DO-AO)	5	48	0.81	40	83
<i>gu</i>	<i>gu</i> /(HB-GU)	6	341	0.97	48	175

* HB; HB-12 inbred strain, PL; multiple recessive Medaka with *b/b*, *pl/pl* and *r/r*, GU; multiple tester Medaka with *b/b*, *gu/gu* and *r/r*, DO; multiple tester Medaka with *b/b* and *Da/Da*, AO; wild stock collected from Aomori. (HB-PL) indicates crossing of females of HB-12 strain with males of PL stock.

** Heterozygous fraction $\times 100/2$.

*** $-\ln(1 - \text{Heterozygous fraction}) \times 100/2$ [9].

† Total number of mutants at the *b* locus.

§ Total number of wild type progeny at the *b* locus.

Calculated as $1 - 2 \times [179 / (179 + 802)]$.

gene-centromere distances of 44.5 cM for *gol-1* and 28.5 cM for *gol-2*, respectively. Our study gave 32 cM for the *b* locus in the Medaka. Thus, the gene-centromere distance of the *b* locus was rather similar to that of *gol-2* than *gol-1*. Obviously a simple comparison of distances does not allow to draw any conclusion about the extent of genome conservation among fishes without further accumulation of more information about linkages of not only the visible mutant loci but also the enzymatic polymorphic loci.

Linkage analysis using diploid gynogenesis

We tested joint segregation of the following sets of loci in gynogenetic diploid Medaka: *pl* with *b*; *gu* with *b*; *Da* with *b* (Table 2). The tests were made by comparing the observed numbers of individuals with the numbers expected if the loci were inherited independently using 2×2 contingency table. The results of all tests were nonsignificant ($\chi^2 = 3.08$ for the *pl* and *b* loci, 1.23 for the *gu* and *b* loci, and 1.98 for the *Da* and *b* loci, respectively). These results indicated that these loci were not closely linked, as suggested by segregation analysis using F_2 progeny [1].

TABLE 2. Linkage analysis in gynogenetic diploid Medaka

Genotype	Genotype	
	<i>gu/gu</i>	<i>gu</i> +/ and +/+
<i>b/b</i>	0 (0.99)*	58 (56.96)*
<i>b/B</i> and <i>B/B</i>	6 (4.91)*	283 (284.14)*
<i>b/b</i>	<i>pl/pl</i>	<i>pl</i> +/ and +/+
	43 (51.10)**	64 (55.80)**
<i>b/B</i> and <i>B/B</i>	235 (226.62)**	239 (247.47)**
<i>b/b</i>	<i>Da/Da</i>	<i>Da</i> +/ and +/+
	0 (1.3)***	14 (12.5)***
<i>b/B</i> and <i>B/B</i>	5 (3.7)***	34 (35.5)***

The number in parentheses is expected number if two loci were independent.

* $\chi^2 = 1.23$, $P > 0.05$, d.f. = 1.

** $\chi^2 = 3.08$, $P > 0.05$, d.f. = 1.

*** $\chi^2 = 1.98$, $P > 0.05$, d.f. = 1.

ACKNOWLEDGMENT

This study was supported by the subsidy from the Ministry of Education, Science and Culture, Japan as a part of the Project for Preservation of Medaka as a Gene Resource.

REFERENCES

- 1 Shimada, A., Shima, A. and Egami, N. (1988) *Zool. Sci.*, **5**: (in press).
- 2 Shima, A. and Shimada, A. (1988) *Mutation Res.*, (in press).
- 3 Tomita, H. (1982) *Medaka*, **1**: 7-9.
- 4 Aida, T. (1921) *Genetics*, **6**: 554-573.
- 5 Naruse, K., Ijiri, K., Shima, A. and Egami, N. (1985) *J. Exp. Zool.*, **236**: 335-341.
- 6 Hyodo-Taguchi, Y. (1980) *Zool. Mag.*, **89**: 283-301. (In Japanese)
- 7 Shima, A., Shimada, A., Komura, J., Isa, K., Naruse, K., Sakaizumi, M. and Egami, N. (1985) *Medaka*, **3**: 1-4.
- 8 Sakaizumi, M., Moriwaki, K. and Egami, N. (1983) *Copeia*, **1983**: 311-318.
- 9 Haldane, J. B. S. (1919) *J. Genet.*, **8**: 299-309.
- 10 Mather, K. (1935) *J. Genet.*, **30**: 53-78.
- 11 Thorgaard, G. H., Allendorf, F. W. and Knudsen, K. L. (1983) *Genetics*, **103**: 771-783.
- 12 Streisinger, G., Singer, F., Walker, C., Knauber, D. and Dower, N. (1986) *Genetics*, **112**: 311-319.
- 13 Churfass, N. B. (1977) *Genetika*, **14**: 599-604.

[COMMUNICATION]

**T Cell-specific XTLA-1 Antigens from *Xenopus laevis*
Tadpole and Froglet are not Identical**

SABURO NAGATA

*Tokyo Metropolitan Institute of Gerontology, Sakaecho 35-2,
Itabashiku, Tokyo 173, Japan*

ABSTRACT—T cell-specific XTLA-1 antigen molecules were immunoprecipitated from tadpoles and froglets of J strain *Xenopus laevis*, and analysed by gel electrophoresis. Both the tadpole and froglet XTLA-1 molecules have an apparent molecular size of 120 KD as analysed by SDS-PAGE. But, after deglycosylation with endo F glycosidase, the froglet XTLA-1 molecules show more extensive charge heterogeneity than the tadpole ones do on two-dimensional gels. The results suggest that the XTLA-1 molecules partially changes their structure during metamorphosis.

INTRODUCTION

During amphibian metamorphosis, profound biochemical transitions occur in association with the morphological and physiological changes. In erythrocytes, for example, there is a complete switch in hemoglobin from larval to adult type molecules. It has been demonstrated that such a switch in hemoglobin types results from a replacement in the blood of larval hemoglobin-producing erythrocytes by newly differentiating adult hemoglobin-producing cells [1]. Recently, evidences have been accumulated in *Xenopus* supporting that similar biochemical and functional transitions may occur in association with the shift of lymphoid cell types during metamorphosis (see review [2]).

The XTLA-1 antigen recognized by a mouse monoclonal antibody is the only thymus-dependent (T) cell-specific surface antigen that has so far been identified in *Xenopus*, and provides a useful marker for studying the development, dif-

ferentiation and function of the T cell system of this animal [3-5]. The XTLA-1 molecules immunoprecipitated from froglet thymocytes and splenocytes are glycoproteins of an apparent molecular size of 120 k dalton (KD) [5]. In the present study, the biochemical characterization was carried out on the XTLA-1 molecules immunoprecipitated from tadpoles as well as froglets. The results indicate that the tadpole XTLA-1 molecules have the same apparent molecular size as the froglet ones but differ in a charge heterogeneity, suggesting that the XTLA-1 molecules may partially change their structure during metamorphosis.

MATERIALS AND METHODS

Major histocompatibility complex (MHC) homozygous, partially inbred J strain *Xenopus laevis* were used. Mature females were injected with 300 U of human chorionic gonadotropin (Gonadotropin 1000; Teikoku Zoki Co.) to induce ovulation, and the eggs obtained were artificially fertilized in Steinberg's solution according to the method described previously [6]. Embryos and larvae were kept in aquaria and their developmental stages were determined by the Normal Table of Nieuwkoop and Faber [7]. The mouse monoclonal antibody, XT-1, was produced by the previously described method [5] and the IgG fraction of the hybridoma ascites, obtained by the affinity chromatography on a protein A-Sepharose CL-4B (Pharmacia) column, was used for immunoprecipitation.

Thymuses were dissected from tadpoles between stages 55–56 (35 days after the fertilization) and from froglets of 8 months in age, and the thymocyte suspensions were prepared in amphibian phosphate buffered saline. Cells from 50 tadpoles or 10 froglets were pooled and labeled with ^{125}I . Cell labeling, immunoprecipitation, digestion with endo F glycosidase (glycopeptidase F-free; Boehringer Mannheim Biochemica) and gel electrophoresis were carried out exactly as described previously [5].

RESULTS AND DISCUSSION

The lysates of radioiodinated thymocytes from tadpoles and froglets were immunoprecipitated by sequential incubations with the specific monoclonal XT-1 antibody and protein A-Sepharose CL-4B beads, and analysed by SDS-PAGE. The results showed that both tadpole and froglet XTLA-1 molecules run as a single band around an apparent molecular size of 120 KD (Fig. A), confirming the previous results on the adult molecules [5].

Since the endo F glycosidase-treated XTLA-1 molecules from froglet thymocytes were known to segregate into the characteristic pattern of spots on O'Farrell's two-dimensional gel electrophoresis, immunoprecipitates from tadpoles and froglets were digested with endo F glycosidase and then analysed by two-dimensional gel electrophoresis. As shown in the previous study [5], the deglycosylated froglet XTLA-1 molecules formed a number of spots (some are fused) with a slightly reduced molecular size near the acidic end of the gel (Fig. B). In contrast, the tadpole XTLA-1 molecules migrated into a more restricted charge heterogeneity under the same conditions, i.e., several relatively basic spots seen on the gel of the froglet antigen were not detected on that of the tadpole antigen. Endo F glycosidase was reported to remove both high-mannose and complex type glycans linked through asparagine to the peptide backbone [8]. The difference in charge distribution patterns between the tadpole and froglet XTLA-1 molecules observed here is, therefore, assumed to represent a difference in other linked glycans and/or amino acid compositions of the 120

KD glycopeptides.

During the metamorphosis of anuran amphibians, a profound reorganization occurs in the larval immune system as the tadpole changes its physiology, morphology and behavior. This reorganiza-

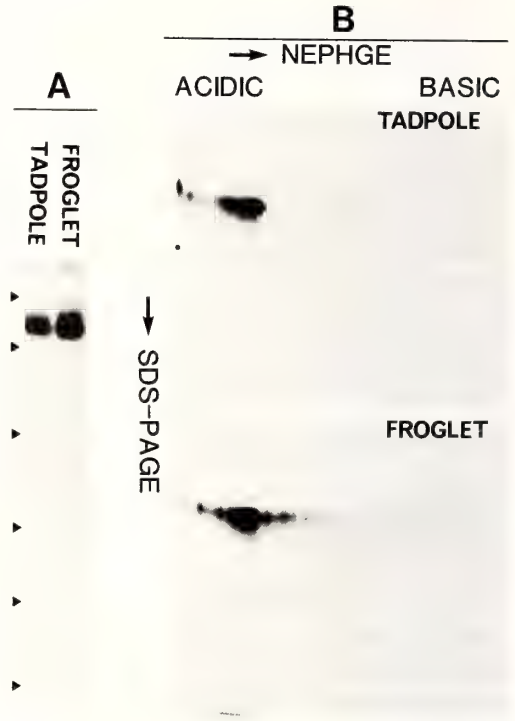


FIG. 1. Analysis of tadpole and froglet XTLA-1 molecules by SDS-PAGE (A) and O'Farrell's two-dimensional gel electrophoresis (B). Thymocytes from J strain tadpoles and froglets were radioiodinated, solubilized with lysis buffer containing 1% Nonidet P-40, and immunoprecipitated with XT-1 monoclonal antibody followed by protein A-Sepharose CL-4B beads. For SDS-PAGE, immunoprecipitates were boiled in SDS sample buffer containing 5% 2-mercaptoethanol and electrophoresed on 10% polyacrylamide gels. For two-dimensional gel electrophoresis, immunoprecipitates were deglycosylated with endo F glycosidase, and separated by nonequilibrium pH gel electrophoresis (NEPHGE) on first dimension. Electrophoresed tube gels were immersed in SDS sample buffer and then subjected to second dimension SDS-PAGE. Electrophoresed gels were visualized by autoradiography on X-ray films. Molecular size standards (150 KD, 94 KD, 67 KD, 43 KD, 30 KD and 20.1 KD) were run on the same gels and indicated with arrowheads in (A).

tion is suggested to involve a nearly complete replacement of lymphopoietic cells and a reorganization of the microenvironment where lymphocytes differentiate [2]. Thus, lymphopoietic cells in the early-larval thymus are replaced by precursor cells derived from a distinct compartment of the embryonic dorsal lateral plate mesoderm [9], so that the reconstituted lymphopoietic system may supply the froglet with adult type lymphocytes having "mature" immunological functions. Recently, it was demonstrated that the MHC class I molecules are not expressed on the lymphocyte surface until the metamorphic climax [10]. Although their function is remained to be clarified, the difference in two-dimensional gel patterns of the XTLA-1 molecules found in the present study might provide, as the MHC class I antigens, a marker to distinguish adult type T cells from larval type ones in *Xenopus*. Such a marker should prove useful in studying the cellular basis of the development of immune reactivity and tolerance during amphibian metamorphosis.

ACKNOWLEDGMENTS

This work was in part supported by the Grant-in-Aid (No. 60440100) from the Japanese Ministry of Education, Science and Culture.

REFERENCES

- 1 Dorn, A. R. and Broyles, R. H. (1982) Proc. Natl. Acad. Sci. USA., **79**: 5592-5596.
- 2 Flajnik, M. F., Hsu, H., Kaufman, J. F. and Du Pasquier, L. (1987) Immunol. Today, **8**: 58-64.
- 3 Nagata, S. (1985) Eur. J. Immunol., **15**: 837-841.
- 4 Nagata, S. (1986) Dev. Biol., **114**: 389-394.
- 5 Nagata, S. (1988) Zool. Sci., **5**: in press.
- 6 Moriya, M. (1976) J. Fac. Sci. Hokkaido Univ. Ser. VI, **20**: 272-276.
- 7 Nieuwkoop, P. D. and Faber, J. (1976) The Normal Table of *Xenopus laevis* (Daudin). North Holland Publ. Co., Amsterdam.
- 8 Elder, J. H. and Alexander, S. (1982) Proc. Natl. Acad. Sci. USA, **79**: 4540-4544.
- 9 Maeno, M., Tochinai, S. and Katagiri, C. (1985) Dev. Biol., **110**: 503-508.
- 10 Flajnik, M. F., Kaufman, J. F., Hsu, E., Manes, M., Parisot, R. and Du Pasquier, L. (1986) J. Immunol., **137**: 3891-3899.

[COMMUNICATION]

**Interspecific Transplantation of Developing Tissues
and Their Subsequent Differentiation in Flies**

PAKKIRISAMY SIVASUBRAMANIAN

*Department of Biology, University of New Brunswick,
Fredericton, New Brunswick, E3B 6E1, Canada*

ABSTRACT—Imaginal leg discs from the larvae of housefly, *Musca domestica* were cultured in the body cavity of the pupae of fleshfly, *Sarcophaga bullata*. The implanted discs were not rejected by the foreign species. On the contrary, they differentiated fully and completed metamorphosis in time according to their own developmental program. However, the tanning and hardening of the cuticle occurred along with that of the host after eclosion of the host fly. These developmental events are discussed in relation to the hormonal milieu of the host species.

INTRODUCTION

During the course of their development flies go through distinct stages such as larva and pupa before metamorphosing into adults. Several adult structures like the legs, wings, eyes, etc., differentiate in the pupal stage from groups of embryonic cells called imaginal discs. Simultaneously, the central nervous system (CNS) too undergoes considerable reorganization and establishes specific neural connections with the newly formed peripheral target tissues. A great deal of information is available with regard to the formation of specific nerve connections between the CNS and target tissues of the same species such as crickets [1], fleshflies [2] and fruitflies [3]. However, very little is known whether this specificity is restricted within a species or it extends beyond species boundaries. To explore this aspect of neuron-target interaction, developing tissues of

the housefly, *Musca domestica*, were cultured into the pupal body cavity of the fleshfly, *Sarcophaga bullata*, and this report describes the metamorphosis of such transplanted imaginal discs. The differentiation of transplanted CNS of the housefly has been reported elsewhere [4].

MATERIALS AND METHODS

The housefly, *Musca domestica*, and the fleshfly, *Sarcophaga bullata*, were cultured in the laboratory under constant conditions of temperature (25°C) and photoperiod (16L:8D). The housefly larvae were raised in an artificial diet containing milkpowder, wheat bran and sawdust, while the fleshfly maggots were fed with fresh beef liver.

Since the housefly is smaller in size with a shorter pupal life they were used as donors, while the larger fleshfly with longer pupal period served as hosts. The imaginal leg discs of mature 3rd instar larvae of *Musca domestica* were dissected in insect saline and implanted into freshly formed fleshfly prepupae. The transplantation method was based on the technique of Bhaskaran and Sivasubramanian [5] but slightly modified as described in Sivasubramanian and Nassel [2]. Of the total of 76 successful implants, 36 were recovered 6 days after the operation from the host pupa (total pupal period of donors) and 40 were recovered 12 days post operation after eclosion of the metamorphosed host flies. The tissues were examined as whole mounts.

RESULTS AND DISCUSSION

Housefly, the donor, is about half the size of the fleshfly, the host. The imaginal leg discs of the housefly being very small (0.55 mm long; 0.38 mm wide) compared to the volume of the host pupa (170 mm³) several discs could be cultured in the same host. Accordingly, 2–4 discs from housefly larvae were transplanted into the fleshfly pupae. The time taken to complete metamorphosis is also correspondingly shorter for housefly, i.e., 6 days as compared to 12 days for fleshfly. Therefore, the implanted leg discs were recovered from hosts 6 days after operation. As seen in Figure 1 the discs had fully metamorphosed in 6 days with well tanned bristles albeit in an uneverted condition because of their development inside the body cavity. However, the cuticle was still untanned. Figure 2 shows the metamorphosed leg discs recovered from an eclosed host fly (12 days post-operation). The cuticle of these legs were fully tanned.

Although insect imaginal discs are routinely cultured *in vitro* for understanding of hormonal control of growth [6], eversion [7], biochemistry of developmental events [8], etc., *in vivo* culture is the preferred method of developmental biologists looking into the aspects of determination [9], pattern formation [10], axonal projection [2, 11] etc. In the latter method, the discs from larval stages are transplanted into the metamorphosing stages (pupa) of the same species and examined at the completion of metamorphosis of the host. In this procedure, one of the limiting factors is the volume of the host which restricts the size and number of discs that can be cultured. This problem was solved as reported in this communication by using a larger species as host and a smaller one as a donor. The housefly discs not only survive but also complete their differentiation within the body cavity of fleshfly pupa.

Molting hormone ecdysone is an essential requirement for differentiation of imaginal discs, and, according to Wentworth *et al.* [12], there is an ecdysone peak in the host *Sarcophaga bullata* at the time of transplantation. Therefore, it is not surprising that the housefly discs complete metamorphosis within fleshfly pupae. Nevertheless, it is



FIG. 1. Metamorphosed leg discs. Two prothoracic leg discs recovered 6 days after transplantation showing fully tanned bristles. $\times 35$.

FIG. 2. Metamorphosed leg discs. Two prothoracic leg discs recovered from eclosed host flies 12 days after transplantation showing fully tanned cuticle. $\times 35$.

interesting to find that the transplanted discs follow their own inherent developmental timetable to complete differentiation. That is, within a period of 6 days they were fully differentiated with well tanned bristles whereas bristle tanning begins much later, 10 days after pupariation in the host species [13]. However, the cuticular tanning of the implants occurs simultaneously with that of the host cuticle (Fig. 2). Hardening and tanning of the cuticle is a critically timed event that is controlled by the neurohormone bursicon secreted soon after eclosion of the host fly [14] and therefore the housefly legs too undergo tanning after the eclosion of the host fly.

Thus, the *Sarcophaga* pupal body cavity acts as a suitable environment for the differentiation of housefly imaginal discs. The central nervous

system of larval housefly also undergoes complete metamorphic reorganization within the fleshfly pupa [4]. Such a system has the potential to be exploited for studies of neuronal specificity by means of *in vivo* culture of the CNS with the discs of the same or different species.

ACKNOWLEDGMENT

This study was supported by a grant from the Natural Sciences and Engineering Research Council of Canada.

REFERENCES

- 1 Murphey, R. K., Bacon, J. P., Sakaguchi, D. S. and Johnson, S. E. (1983) *J. Neurosci.*, **3**: 659-672.
- 2 Sivasubramanian, P. and Nassel, D. R. (1985) *J. Comp. Neurol.*, **239**: 247-253.
- 3 Schmid, H., Gendre, N. and Stocker, R. F. (1986) *Dev. Biol.*, **113**: 160-173.
- 4 Sivasubramanian, P. (1987) *J. Neurochem.*, **48** (suppl): S 59.
- 5 Bhaskaran, G. and Sivasubramanian, P. (1969) *J. Exp. Zool.*, **171**: 385-396.
- 6 Davis, K. T. and Shearn, A. (1977) *Science*, **196**: 1438-1440.
- 7 Millner, M. J. (1977) *J. Embryol. Exp. Morphol.*, **37**: 105-117.
- 8 Nishirua, J. T. and Fristrom, J. W. (1975) *Proc. Natl. Acad. Sci. USA*, **72**: 2984-2988.
- 9 Hadorn, E. (1965) *Brookhaven Symp. Biol.*, **18**: 148-161.
- 10 Bryant, P. J. (1975) *J. Exp. Zool.*, **193**: 49-78.
- 11 Stocker, R. F. and Schmid, H. (1985) *Experientia*, **41**: 1607-1609.
- 12 Wentworth, S. L., Roberts, B. and O'Conner, D. (1981) *J. Insect Physiol.*, **27**: 435-440.
- 13 Sivasubramanian, P. and Biagi, M. (1983) *Int. J. Insect Morphol. Embryol.*, **12**: 355-359.
- 14 Fraenkel, G. and Hsiao, C. (1965) *J. Insect Physiol.*, **11**: 513-556.

[COMMUNICATION]

Preference for Striped Backgrounds by Striped Fishes

YASUTOSHI KOHDA and MUNETAKA WATANABE

*Department of Biology, College of Liberal Arts and Sciences,
Okayama University, Tsushima, Okayama 700, Japan*

ABSTRACT—Six available species of freshwater fishes, two cross-striped, two lengthwise-striped and two non-striped ones, were exposed to vertically and horizontally striped backgrounds. The two cross-striped fishes preferred to rest at vertically striped sites over horizontally striped ones. One of the two lengthwise-striped fishes tended to rest at horizontally striped sites. These results imply that many striped fishes prefer resting at sites with stripes similar to their own. The behavior of one non-striped fish suggests that there may be a factor other than a fish's own stripes that causes preference of vertically striped sites.

INTRODUCTION

Cryptic animals must merge with their backgrounds [1, 2]. It is known that some cryptic animals choose resting places appropriate to their body colorations [3-5]. Kohda and Watanabe [6] showed that the freshwater serranid fish oyani-rami, *Coreoperca kawamebari*, which has cross stripes on its body, chooses to rest at vertically rather than horizontally striped sites.

Do cross-striped fishes other than the oyani-rami have the same preference? Do lengthwise-striped fishes prefer horizontally striped sites? Do non-striped fishes have any preference between vertically and horizontally striped sites? In the present study, we tested the preferences of six available species of freshwater fishes including the oyani-rami for striped sites.

MATERIALS AND METHOD

Ten individuals from each of six species were

used; two cross-striped fishes, *C. kawamebari* (7.8-8.8 cm in total length) and *Macropodus chinensis* (3.2-4.0 cm), two non-striped, *Carassius auratus* (6.3-8.0 cm) and *Acheilognathus limbata* (5.0-7.4 cm), and two lengthwise-striped, *Barbus titteya* (3.0-3.4 cm) and *Melanochromis auratus* (3.5-5.1 cm). The four former species were collected in Okayama Prefecture, Japan, while the latter two were obtained from a tropical-fish dealer.

As all the specimens were small, we used an experimental apparatus different from that used in our previous study [6]. Instead, we utilized a gray plastic tank 150×100×50 cm high (20 cm deep), which had two vertically striped and two horizontally striped shelters (Fig. 1B). Shelters were transparent plastic boxes (15×15×15 cm), which had three striped side walls and one open side, and were put on squares (25×20 cm) bordered by a light green line (Fig. 1A). The stripes were 2 mm black bands with 2 mm transparent intervals.

A fish was placed in the center of the tank, and the time the fish spent in each square was recorded for 30 min. The fish was left in the tank and the next day its position was recorded again for 30 min. Five of the ten fishes of each species were tested under one arrangement of shelters (Fig. 1B), and the other five were tested under the reverse arrangement. Preference for stripes by each species was tested by the two-tailed matched pairs signed test [7].

RESULTS AND DISCUSSION

In the first-day test, the two cross-striped species, *C. kawamebari* and *M. chinensis*, preferred

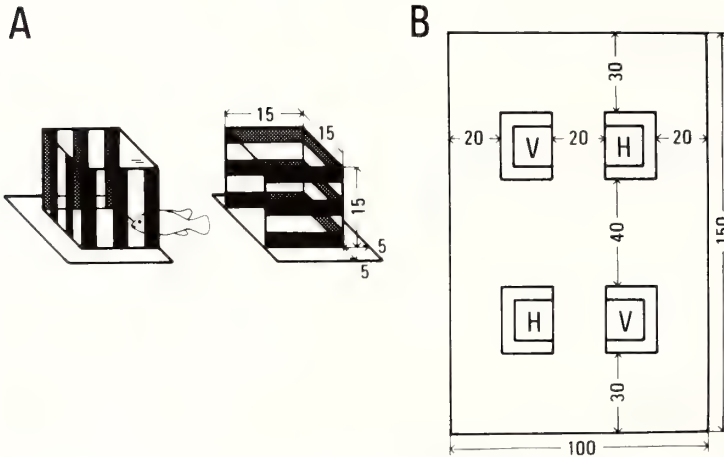
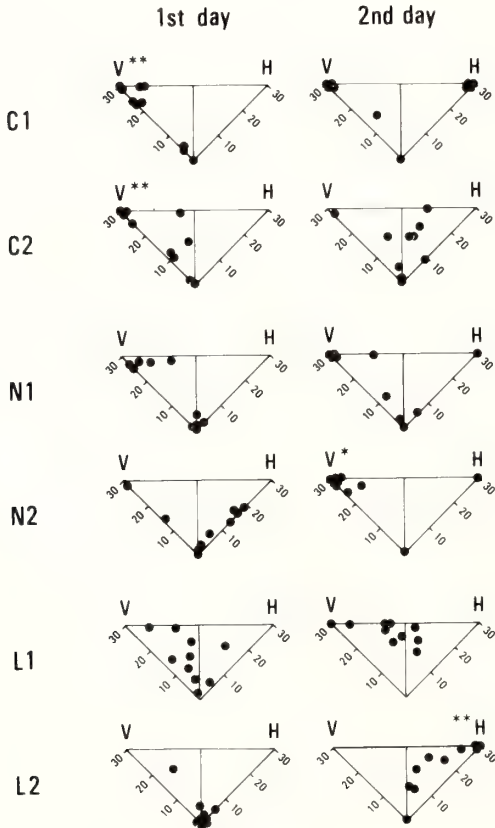


FIG. 1. Schematic representation of striped shelters and experimental apparatus.

(A) Striped shelters (15×15×15 cm) having three vertically or horizontally striped side walls and one open side were put on squares (25×20 cm) bordered by a light green line. The stripes were 2 mm black bands with 2 mm transparent intervals.

(B) One arrangement of striped shelters in the experimental tank (150×100×50 cm). V: vertically striped shelters, H: horizontally striped shelters. Half of the specimens were tested under this arrangement of shelters and the other half were tested under the reverse arrangement.



vertically striped zones to horizontally striped ones (both $r/n=0/9$, $P<0.01$) (Fig. 2). The two length-wise-striped and the two non-striped species showed no preference ($r/n=2/10$, $1/8$, $2/10$, $2/6$, all $P>0.05$).

In the second-day test, one of the two length-wise-striped fishes, *M. auratus*, preferred horizontally striped sites ($r/n=0/9$, $P<0.01$) (Fig. 2). One of the two non-striped fishes, *A. limbata*, showed a slight preference for vertically striped zones ($r/n=1/9$, $P<0.05$). The other four species showed no preference ($r/n=4/9$, $3/8$, $2/9$, $3/10$, all $P>0.05$).

On the first day, the specimens were unfamiliar

FIG. 2. The time that the fishes spent in the striped sites during the 30 min observation time. One dot represents the data of one specimen. The foot of the perpendicular from a dot on the V-axis is the time (min) spent in the vertically striped sites and the foot on the H-axis is the time spent in the horizontally striped sites. 1st day: the results of the tests immediately after placing the specimens into the experimental tank, 2nd day: the results after one-day of adaptation. C1: *Coreoperca kawamebari*, C2: *Macropodus chinensis*, N1: *Carassius auratus*, N2: *Acheilognathus limbata*, L1: *Barbus titteya*, L2: *Melanochromis auratus*. *: $P<0.05$, **: $P<0.01$.

with the experimental tank, and might have been frightened and thereby motivated to seek refuge. On the second day, they probably knew the geography in the tank, and their motivation to seek refuge was probably smaller than on the first day. No fish preferred the same striped zone on both days, but we can infer that the species which chose either zone on either day have a preference for that stripe.

Kohda and Watanabe [6] showed that the oyanirami, a cross-striped fish, prefers vertically striped sites and this was reconfirmed in the present study. The other cross-striped fish, *M. chinensis*, showed the same preference. A lengthwise-striped fish *M. auratus*, preferred horizontally striped sites. These three fishes tended to rest at shelters with stripes similar to their own. One lengthwise-striped fish, *B. titteya*, showed no preference. None of the four striped fishes showed a preference for stripes unlike their own. These results imply that many striped fishes prefer resting at sites similar to their own body stripes, thereby camouflaging themselves. Further studies with more striped species are needed to prove this hypothesis.

One non-striped species, *C. auratus*, showed no preference, and this result conforms to our hypothesis. However, the other non-striped one, *A. limbata*, showed a slight preference for vertical stripes over horizontal stripes on the second day.

This observation means that there may be a factor other than a fish's own stripes causing a preference for vertically striped sites. In order to determine what this factor is, we need to observe the behavior of many non-striped fishes that show a preference for vertical stripes and to find which character of these fishes correlates with their preference for vertical stripes.

ACKNOWLEDGMENTS

We wish to express our sincere thanks to Dr. Hiromi Iwagaki and Ms. Yurie Hiraoka Nakatsuka for their help in carrying out pilot experiments, and to Professor Susumu Ishii of Waseda University for advice concerning the statistical analyses.

REFERENCES

- 1 Wickler, W. (1986) *Mimicry in Plants and Animals*. McGraw-Hill, New York.
- 2 Edmunds, M. (1974) *Defence in Animals*. Longman, Harlow.
- 3 Ergene, S. (1950) *Z. vergl. Physiol.*, **32**: 530–551.
- 4 Kettlewell, H. B. D. (1955) *Nature*, **175**: 943–944.
- 5 Sargent, T. D. (1968) *Science*, **159**: 100–101.
- 6 Kohda, Y. and Watanabe, M. (1986) *Ethology*, **72**: 185–190.
- 7 Siegel, S. (1959) *Nonparametric Statistics for Behavioral Sciences*. McGraw-Hill, New York, pp. 68–75.

1988 MEETING OF THE AMERICAN SOCIETY OF ZOOLOGISTS
and
**AMERICAN MICROSCOPICAL SOCIETY, ANIMAL BEHAVIOR SOCIETY,
THE CRUSTACEAN SOCIETY, INTERNATIONAL ASSOCIATION OF ASTACOLOGY,
SOCIETY OF SYSTEMATIC ZOOLOGY, AND WESTERN SOCIETY OF NATURALISTS**

SAN FRANCISCO HILTON & TOWERS
SAN FRANCISCO, CALIFORNIA
DECEMBER 27 - 30

Housing Rates:

\$66 Single, Double, Triple & Quad

Call for Papers: April 1988

Abstract Deadline: August 8, 1988

For Oral and Poster Presentations

SYMPOSIA/WORKSHOPS:

Recent Developments in the Study of Animal Migration
Parasites and Sexual Selection

Evolving Concepts of Chemical Mediation: A Symposium in
Honor of Howard A. Bern

Marine Invertebrate Allorecognition and the Evolution of Immunity
Concepts of Efficiency in Biological Systems

Concepts of Adaptation in Aquatic Animals: Deviations from
the Terrestrial Paradigm

Cellular and Molecular Biology of Pattern Formation
Developmental Neurobiology of the Cnidaria

Antarctic Marine Biology

Chemical Factors that Influence the Settlement and Metamorphosis of Marine
Invertebrate Larvae

Cracking a Black Box: Field Inferences in the Ecology of Marine Invertebrate Larvae
Species and Evolution in Clonal Organisms

Biology of Nonmammalian Chordate Testis

A History of Regeneration Research

Science As A Way of Knowing — Cell and Molecular Biology

Sex Attraction, Mating Behavior and Insemination in the Crustacea

The Complete Biology of Giant Kelp

Workshop on Science Comes to California

Workshop on Research-Education at Small College and Universities: Quality Science on
a Frayed Shoestring

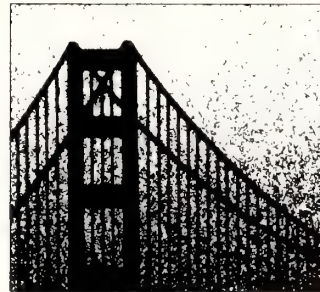
Hosted by the California Academy of Sciences
Daphne G. Fautin and Ralph I. Smith
Co-Chairpersons of the Local Arrangements Committee

SAN FRANCISCO

NUMEROUS SOCIALS, SPECIAL PROGRAMS
COMMERCIAL EXHIBITS
JOB PLACEMENT SERVICE

For more information, contact:

Mary Adams-Wiley, Executive Officer
American Society of Zoologists
104 Sirius Circle
Thousand Oaks, California 91360
Telephone: (805) 492-3585



1 9 8 8

Development Growth & Differentiation

Published by

the Japanese Society of Developmental Biologists

The journal is devoted to the publication of original papers dealing with any aspects of developmental phenomena in all kinds of organisms, including plants and micro-organisms. Papers in any of the following fields will be considered: developmental genetics, growth, morphogenesis, cellular kinetics, fertilization, cell division, dormancy, germination, metamorphosis, regeneration and pathogenesis, at the biochemical, biophysical and analytically morphological levels; reports on techniques applicable to the above fields. At times reviews on subjects selected by the editors will be published. Brief complete papers will be accepted, but not preliminary reports.

Members of the Society receive the Journal free of charge. Subscription by institutions is also welcome.

Papers in Vol. 30, No. 2. (April 1988)

11. **REVIEW:** T. KISHIMOTO: Regulation of metaphase by a maturation-promoting factor.
12. S. TANIMOTO and M. MORISAWA: Roles for potassium and calcium channels in the initiation of sperm motility in rainbow trout.
13. K. MIKAMI-TAKEI, A. FUJIWARA, and I. YASUMARU: The acrosome reaction induced by dimethylsulfoxide in sea urchin sperm.
14. T. KAWASHIMA and T. NAKAZAWA: Stimulation of protein synthesis in the mitochondria of sea urchin embryos before gastrulation.
15. G. CASAZZA, R. DE SAMTIS, and M. R. PINTO: Plasma membrane glycoproteins of *Ciona intestinalis* spermatozoa that interact with the egg.
16. M. YAMAGUCHI, T. NIWA, M. KURITA, and N. SUZUKI: The participation of speract in the acrosome reaction of *Hemicentrotus pulcherrimus*.
17. R. MORIYAMA and K. YANAGISAWA: Protein synthesis initiated by cell fusion in *Dictyostelium discoideum*.
18. A. M. MONTES and W. K. MORISHIGE: Lung-derived growth factors: Ontogenic shift in parahormone secretion in the perinatal rat lung.
19. J. C. LABBE, A. PICARD, and M. DOREE: Does the M-phase promoting factor (MPF) activate a major Ca^{2+} - and cyclic nucleotide-independent protein kinase in starfish oocytes?

Development, Growth and Differentiation (ISSN 0012-1592) is published bimonthly by The Japanese Society of Developmental Biologists, Department of Biology, School of Education, Waseda University, Tokyo 160, Japan. 1987: Volume 29. Annual subscription U. S. \$ 110.00 including air speed delivery except Japan. Application to mail at second class postage rate is pending at Jamaica, NY 11431, U. S. A.

Outside Japan: Send subscription orders and notices of change of address to Academic Press, Inc., Journal Subscription Fulfillment Department, 6277 Sea Harbor Drive, Orlando, FL 32887, U. S. A. Send notices of change of address at least 6-8 weeks in advance. Please include both old and new addresses. U. S. A. POSTMASTER: Send changes of address to *Development, Growth and Differentiation*, Academic Press, Inc., Journal Subscription Fulfillment Department, 6277 Sea Harbor Drive, Orlando, FL 32887, U. S. A.

In Japan: Send nonmember subscription orders and notices of change of address to Business Center for Academic Societies Japan, 16-3, Hongo 6-chome, Bunkyo-ku, Tokyo 113, Japan. Send inquiries about membership to Business Center for Academic Societies Japan, 4-16, Yayoi 2-chome, Bunkyo-ku, Tokyo 113, Japan.

Air freight and mailing in the U. S. A. by Publications Expediting, Inc., 200 Meacham Avenue, Elmont, NY 11003, U. S. A.

NARISHIGE

THE ULTIMATE NAME IN MICROMANIPULATION

OUR NEW MODELS MO-102 and MO-103
MAKE PRECISION MICROMANIPULATION SO EASY!

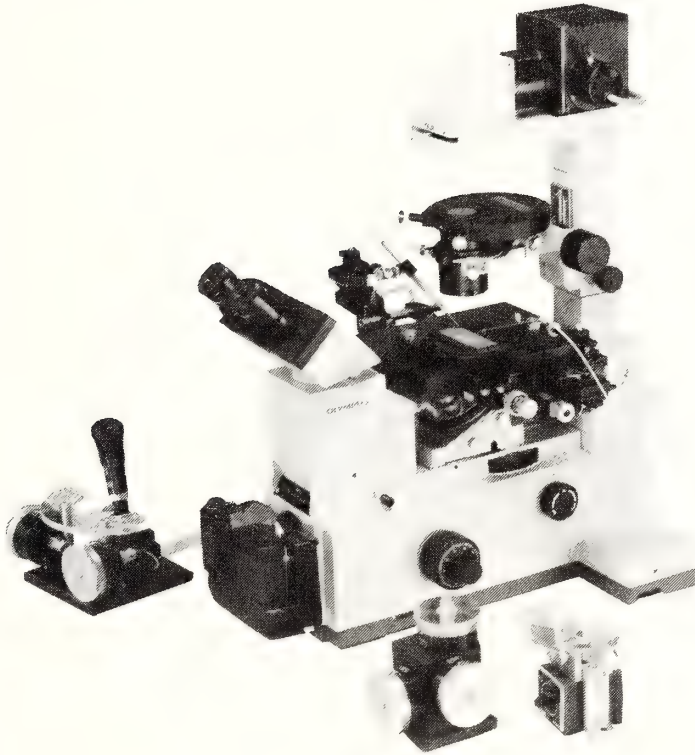


(Photo: by courtesy of Olympus Optical CO., LTD.)

SOME FEATURES of MO-102 and MO-103:

- * The manipulator head is so small that it can be mounted directly on the microscope stage. There is no need for a bulky stand.
- * Hydraulic remote control ensures totally vibration-free operation.
- * 3-D movements achieved with a single joystick.

Micromanipulators Microelectrode pullers Stereotaxic instruments



**NARISHIGE SCIENTIFIC INSTRUMENT
LABORATORY CO., LTD.**

4-9-28, Kasuya, Setagaya-ku, Tokyo 157 JAPAN
Telephone: 03-308-8233 Telex: NARISHG J27781

Sophisticated Balance between Safety and Centrifugation Capability without Compromise.

Centrifuge in
Integrated with A
Refrigerator

Extra-Quiet
Operation

Ease of Loading/
Unloading
The Rotors

Quick Start/
Quick Stop

High Quality

Triple Safety
Design

Corrosion
Resistance



**HIGH SPEED
REFRIGERATED
MICRO CENTRIFUGE**

MODEL MR-150

TOMY CORPORATION

1002 SOLEIL NARIMASU BLDG. 31-8. NARIMASU 1-CHOME,
ITABASHI-KU, TOKYO 175 JAPAN
TEL:(03)976-3411 TLX:02723111 TOMYCO J
CABLE:TOMYSHO TOKYO FAX:(GIII GII)(03)930-7010

TOMY SEIKO CO., LTD.

2-2-12. ASAHICHO NERIMA-KU. TOKYO 176 JAPAN
TEL:(03)976-3111

SOLE AGENT

MANUFACTURER

SPECIFICATIONS

Max. Speed :
15000 rpm
Max. Centrifugal Force
15050 G

(Contents continued from back cover)

hybridization method for neurohypophysial hormone mRNAs using synthetic oligonucleotide probes397

Seki, T., S. Kikuyama and M. Suzuki: Effect of hypothalamic extract on the prolactin release from the bullfrog pituitary gland with special reference to thyrotropin-releasing hormone (TRH)407

Morphology

Fujikura, K., S. Kurabuchi, M. Tabuchi and S. Inoue: Morphology and distribution of the skin glands in *Xenopus laevis* and their response to experimental stimulations415

Behavior Biology

Ooka-Souda, S., H. Kabasawa and S. Kinoshita: Circadian rhythms in locomotor activity of the hagfish, *Eptatretus burgeri*. II. The effect of brain ablation431

Ooka-Souda, S. and H. Kabasawa: Circadian rhythms in locomotor activity of the hagfish,

Eptatretus burgeri. III. Hypothalamus: a locus of the circadian pacemaker?437

Weldon, P. J.: Feeding responses of Pacific snappers (genus *Lutjanus*) to the yellow-bellied sea snake (*Pelamis platurus*)443

Kohda, Y. and M. Watanabe: Preference of striped backgrounds by striped fishes (COMMUNICATION)501

Ecology and Taxonomy

Hanzawa, N., N. Taniguchi and K. Numachi: Geographical differentiation in populations of Japanese dace *Tribolodon hakonensis* deduced from allozymic variation449

Konishi, K. and R. Quintana: The larval stages of three pagurid crabs (Crustacea: Anomura: Paguridae) from Hokkaido, Japan463

Sawada, I. and A. L. Molan: Two new-hymenolepidid cestodes, *Vampirolepis molani* sp. n. and *V. iraqensis* sp. n., from Iraqi bats483

ZOOLOGICAL SCIENCE

VOLUME 5 NUMBER 2

APRIL 1988

CONTENTS

Obituary 213

REVIEWS

Meusy, J.-J. and G. G. Payen: Female reproduction in malacostracan Crustacea 217

Nishioka, R. S., K. M. Kelley and H. A. Bern: Control of prolactin and growth hormone secretion in teleost fishes 267

ORIGINAL PAPERS

Physiology

Ozaki, M.: A possible sugar receptor protein found in the labellum of the blowfly, *Phormia regina* 281

Okano, Y., E. David, K. Honda and S. Inoué: Auditory evoked potentials dynamically related to sleep-waking states in unrestrained rats 291

Tazaki, K.: The anatomy and physiology of the stomatogastric nervous system of *Squilla*. II. The cardiac system 299

Obika, M.: Ultrastructure and physiological response of leucophores of the medaka *Oryzias latipes* 311

Cell Biology

Suganuma, Y. and H. Yamamoto: Conjugation in *Tetrahymena*: Its relation to concanavalin A receptor distribution on the cell surface 323

Iwasaki, S. and K. Kobayashi: Fine structure of the dorsal tongue surface in the Japanese toad, *Bufo japonicus* (Anura, Bufonidae) 331

Okamoto, M.: Fine structure of the iris muscle in the Japanese common newt, *Cynops pyrrhogaster*, with special reference to innervation 337

Genetics and Immunology

Naruse, K., A. Shimada and A. Shima: Gene-centromere mapping for 5 visible mutant loci in multiple recessive tester stock of the medaka (*Oryzias latipes*) (COMMUNICATION) 489

Nagata, S.: T cell-specific XTLA-1 antigens from *Xenopus laevis* tadpole and froglet are not identical (COMMUNICATION) 493

Biochemistry

Tsuneoka, M., K. Maruyama and K. Ohashi: *In vitro* dimerization of I-protein, an A-I junctional component of skeletal muscle myofibrils 347

Developmental Biology

Iwamatsu, T., T. Ohta, E. Oshima and N. Sakai: Oogenesis in the medaka *Oryzias latipes*—stages of oocyte development ... 353

Tsuchiyama-Omura, S., B. Sakaguchi, K. Koga and D. F. Poulson: Morphological features of embryogenesis in *Drosophila melanogaster* infected with a male-killing spiroplasma 375

Suematsu, N., H. Takeda and T. Mizuno: Glandular epithelium induced from urinary bladder epithelium of the adult rat does not show full prostatic cytodifferentiation 385

Sivasubramanian, P.: Interspecific transplantation of developing tissues and their subsequent differentiation in flies (COMMUNICATION) 497

Endocrinology

Hyodo, S., M. Fujiwara, S. Kozono, M. Sato and A. Urano: Development of an *in situ*

(Contents continued on inside back cover)

INDEXED IN:

Current Contents/LS and AB & ES,
Science Citation Index,
ISI Online Database,
CABS Database

Issued on April 15
Printed by Daigaku Printing Co., Ltd.,
Hiroshima, Japan

264
4
5 No. 3

June 1988

ZOOLOGICAL SCIENCE

An International Journal

SPECIAL ISSUE

ADVANCES IN CELL
DIVISION RESEARCH

published by Zoological Society of Japan

distributed by Business Center for Academic Societies Japan
VSP, Utrecht, The Netherlands

ISSN 0289-0003

ZOOLOGICAL SCIENCE

The Official Journal of the Zoological Society of Japan

Editor-in-Chief:

Hideshi Kobayashi (Tokyo)

Managing Editor:

Seiichiro Kawashima (Hiroshima)

Assistant Editors:

Takeo Machida (Hiroshima)

Sumio Takahashi (Hiroshima)

Kazuyoshi Tsutsui (Hiroshima)

The Zoological Society of Japan:

Toshin-building, Hongo 2-27-2, Bunkyo-ku,
Tokyo 113, Japan. Tel. (03) 814-5675

Officers:

President: Nobuo Egami (Tsukuba)

Secretary: Hideo Namiki (Tokyo)

Treasurer: Tadakazu Ohoka (Tokyo)

Librarian: Shun-Ichi Uéno (Tokyo)

Editorial Board:

Howard A. Bern (Berkeley)

Horst Grunz (Essen)

Susumu Ishii (Tokyo)

Roger Milkman (Iowa City)

Tokindo S. Okada (Okazaki)

Hiroshi Watanabe (Shimoda)

Walter Bock (New York)

Robert B. Hill (Kingston)

Yukiaki Kuroda (Mishima)

Hiromichi Morita (Fukuoka)

Andreas Oksche (Giessen)

Mayumi Yamada (Sapporo)

Aubrey Gorbman (Seattle)

Yukio Hiramoto (Chiba)

Koscaq Maruyama (Chiba)

Kazuo Moriwaki (Mishima)

Hidemi Sato (Nagoya)

Ryuzo Yanagimachi (Honolulu)

ZOOLOGICAL SCIENCE is devoted to publication of original articles, reviews and communications in the broad field of Zoology. The journal was founded in 1984 as a result of unification of Zoological Magazine (1888-1983) and *Annotationes Zoologicae Japonenses* (1897-1983), the former official journals of the Zoological Society of Japan. ZOOLOGICAL SCIENCE appears bimonthly. An annual volume consists of six numbers of more than 1000 pages including an issue containing abstracts of papers presented at the annual meeting of the Zoological Society of Japan.

MANUSCRIPTS OFFERED FOR CONSIDERATION AND CORRESPONDENCE CONCERNING EDITORIAL MATTERS should be sent to:

Dr. Seiichiro KAWASHIMA, Managing Editor, Zoological Science, Zoological Institute, Faculty of Science, Hiroshima University, 1-1-89 Higashisenda-machi, Naka-ku, Hiroshima 730, Japan, in accordance with the instructions to authors which appear in the first issue of each volume. Copies of instructions to authors will be sent upon request.

SUBSCRIPTIONS. ZOOLOGICAL SCIENCE is distributed free of charge to the members, both domestic and foreign, of the Zoological Society of Japan. To non-member subscribers within Japan, it is distributed by Business Center for Academic Societies Japan, 6-16-3 Hongo, Bunkyo-ku, Tokyo 113. Subscriptions outside Japan should be ordered from the sole agent, VSP, Utrechtseweg 62, 3704 HE Zeist (postal address: P. O. Box 346, 3700 AH Zeist), The Netherlands. Subscription rates will be provided on request to these agents. New subscriptions and renewals begin with the first issue of the current volume.

All rights reserved. No part of this publication may be reproduced or stored in a retrieval system in any form or by any means, without permission in writing from the copyright holder.

© Copyright 1988, The Zoological Society of Japan

[Publication of Zoological Science has been supported in part by a Grant-in-Aid for Scientific Publication from the Ministry of Education, Science and Culture, Japan.]

General Introduction to the Special Issue

on

Advances in Cell Division Research

The publication of special issues of *Zoological Science* was proposed by the Editorial Board and approved by the council of the Zoological Society of Japan in 1986. This special issue on "Advances in Cell Division Research", dedicated to Emeritus Professor Katsuma Dan, was suggested by Professor N. Egami, the former Editor-in-Chief and the present President of the Zoological Society and is issued with the full support of the Editorial Board of *Zoological Science*.

Emeritus Professor Dan is now 83 years old, yet he remains active and is working by himself on cell division of embryos of marine invertebrates at the Misaki Marine Biological Station. Since he began work on the surface potential of *Arbacia* eggs in the laboratory of the late Professor L. V. Heilbrunn, he has dedicated himself for almost 60 years to the study of cell division, which has profoundly influenced various areas of biological science.

Professor Dan graduated from the Department of Zoology of the Tokyo Imperial University (now the University of Tokyo) in 1929. He joined the late Professor Heilbrunn's laboratory at the University of Pennsylvania in December of 1930, and in 1934 he received the Ph. D. degree there. After returning to Japan he was appointed instructor at the Misaki Marine Biological Station of the Tokyo Imperial University. Two years later, he married Jean Clark of New Jersey. His well-known studies on the behavior of the cell surface during cleavage began after he returned to Japan in 1937 and continued until 1947. The series of his experiments became the basis for a proposed model for the mechanism of cytokinesis, the astral model that elucidates the role of the spindle elongation in the initial shrinkage during constriction of the cell (1943) (see the chapter by Professor Dan herein). Furthermore, his perforation experiments during this period (1943) beautifully demonstrated the fascinating rules of interactions between the mitotic apparatus and the egg cortex, which later contributed to the well-known concept of the "cleavage signal" proposed by Professor Daniel Mazia in 1961 in *The Cell*, III.

In 1943, he was appointed lecturer at the Tokyo Imperial University. In 1945 he was the last to leave the Misaki Marine Biological Station at the end of the war, when the Station was occupied by the American forces. He made great efforts to take the Station back from the Occupation forces, and on December 31, 1945, it was returned to the University of Tokyo. Professor Dan returned to the Station in the summer of 1946, starting a series of studies with Jean on the mechanism of unequal division (1947). Soon he was appointed full professor at the Tokyo Metropolitan University, with the strong support of Emeritus Professor Daigoro Moriwaki, the former president of the National Institute of Genetics at Mishima.

In 1950, he was awarded the Zoological Society of Japan Prize for his studies on the mechanism of cell division in marine eggs. With one of his students, Professor Shinya Inoue, he had the great success of observing birefringence of dividing cells for the first time (see the chapter by Professor Inoue). Soon he was invited to work on the mitotic apparatus with his longtime friend, Professor Daniel Mazia. They succeeded for the first time in isolating the mitotic apparatus and characterizing its protein components. This pioneering work has had a major influence on later investigations of the structure and function of the mitotic apparatus. Many of his colleagues can recall Professor Dan's memorable lecture on the isolated mitotic apparatus at the 1952 annual meeting of the Zoological Society.

Although he was reluctant to be an educational administrator, he was elected President of Tokyo Metropolitan University in 1965, and served until 1973, for an eight-year period that included the years of serious student unrest in Japan. During this period, he also served as President of the Zoological Society of Japan (1967–1972) and the Japanese Society of Developmental Biologists (1968–1972). After retiring from Tokyo Metropolitan University in 1973, he returned to his laboratory in the Misaki Marine Biological Station to work on the mechanism of unequal cleavage.

He was invested with the Second Order of Merit in 1976. Last year, he was named a Person of Cultural Merit in the annual Honors list for his long dedication to biological science. We are pleased to dedicate the chapters of this special issue to Emeritus Professor Dan Festschrift in honor of his long devotion to cell division research. Finally, I would like to express many thanks to Drs. D. Mazia, Y. Hiramoto, M. Yoneda, H. Sato and I. Mabuchi for their valuable collaboration in the organization and editorial works of this issue.

March 1988

HIKOICHI SAKAI

Mechanism of Equal Cleavage of Sea Urchin Egg: Transposition from Astral Mechanism to Constricting Mechanism

KATSUMA DAN¹

*Misaki Marine Biological Station, Koajiro, Miura-shi,
Kanagawa 238-02, Japan*

ABSTRACT—In past 40 years, there have been two opposing theories on the mechanism of cleavage for sea urchin eggs. One was the author's theory in which elongation of the spindle is a main source of force which is assisted by the presence of two asters. This will be called "astral mechanism". The other was Schroeder's constricting ring theory. He argues that the ring consists of bundles of actin fibers and by the contraction of these fibers, they pinch a cell into two equal halves.

The strong point of the astral mechanism is that it has quantitative verifications for the degree of equatorial shrinkage and also for the depth of forming furrow. Its shortcoming is that it works for only a few minutes at the beginning of cleavage. After the equatorial surface goes into a stretching phase, the theory no longer works. The strong point of the constricting mechanism is that it provides an ideal way to pinch a cell into two parts but its shortcoming is that the ring cannot be found as long as the egg remains spherical which means that a spherical cell can never start to cleave.

Emphasis of the present paper is to point out that both mechanisms are at work in a process of cleavage but they are activated in succession. Furthermore, by the author's analysis, it is possible to determine the time point of switching from the astral mechanism to the constricting mechanism.

HISTORICAL

Course of advancement of our knowledge on the mechanism of cell division of sea urchin egg can be divided into three steps.

Step 1

In 1943, the present author proposed a scheme for division of the sea urchin egg [1]. There, the author contended that the two asters have their astral rays crossing on the equatorial plane (see Fig. 4 of this paper). If these asters are pushed away from each other by an intervening and elongating spindle, the equatorial surface shrinks as indicated by coming closer of two marker particles. The degree of shrinkage of the equatorial surface and the depth of the deepening furrow can be accounted for semi-quantitatively by the scheme.

For convenience, this scheme will be called the astral mechanism.

However, after the beginning of furrowing, in a few minutes, the equatorial surface begins to stretch. Once this stage is reached, the proposed scheme no longer holds. In other words, the stage in which the astral mechanism is valid is restricted to the initial phase of the furrow formation, in spite of the fact that it is provided with semi-quantitative proofs.

Step 2

This step spans between 1953 to 1956. In 1953, Swann and Mitchison in England [2] and in 1956, Hiramoto in Japan [3] conducted two different experiments and arrived at closely similar conclusions.

The former workers tried to destroy the spindle rapidly by concentrated colchicine solutions and the latter worker tried to remove the spindle by sucking it in a capillary. Both groups reached a unanimous conclusion that if the spindle is de-

Accepted March 17, 1988

¹ Correspondence should be addressed to the following home address: 3-19-8 Kami-Yoga, Setagaya-ku, Tokyo 158, Japan.

stroyed or removed during metaphase, the egg remained spherical forever, but if operated at the ana- or telophase, the egg could cleave completely in spite of the absence of the spindle.

These experiments show that either the reaction of a dividing cell changes in the course of cell division or a new division mechanism comes into play in the latter half of the division process, although the above workers failed to pinpoint what was a real nature of the change.

Step 3

In 1972, by using the eggs of *Arbacia punctulata*, Schroeder discovered a special structure underlying the surface of cleavage furrow in thin sections by transmission electron microscopy [4]. Later he succeeded in identifying the structure as bundles of actin fibers running along the bottom of the furrow [5].

If the bundles of actin fibers encircle the bottom of the furrow, it is not hard to imagine that the bundle would contract and pinch the cell to complete separation. This offers a concrete way of pinching which Swann and Mitchison as well as Hiramoto alluded to before.

In passing, it must be mentioned that in 1965, Hiramoto injected a large amount of paraffin oil or sea water into the sea urchin egg which was about to divide. He reported that in spite of an enormous inflation of volume and shifting of the spindle to the cell periphery, the cleavage furrow appeared exactly at the place anticipated from the position of the spindle before the injection, the furrow dividing the inflated cell body exactly into two equal halves [6]. This experiment, however, is directed to a slightly different aspect of division process from those quoted above. It means that once a constricting ring is formed, its position cannot be shifted by inflating the cell volume.

ANALYSES

Concerning step 1

When the author's original work was done, it was during the World War II. As the result, various quantities (surface shrinkage, surface stretching, spindle length etc.) were measured on

camera lucida drawings. This must have sliced off reliability of the data in the eyes of readers. Besides, the distribution of the Journal in which the work was published was very limited at that time. For these reasons, new sets of data were collected.

A brief explanation of the author's scheme may be necessary here. When two kaolin particles are attached to the equatorial surface of the egg, the distance between them shrinks for first few minutes and then it begins to stretch. This behavior is specific to the equatorial surface and not shared by other regions of the egg surface (Figs. 1 and 2) [7]. This shrinkage begins with the onset of spindle elongation together with an elongation of the cell

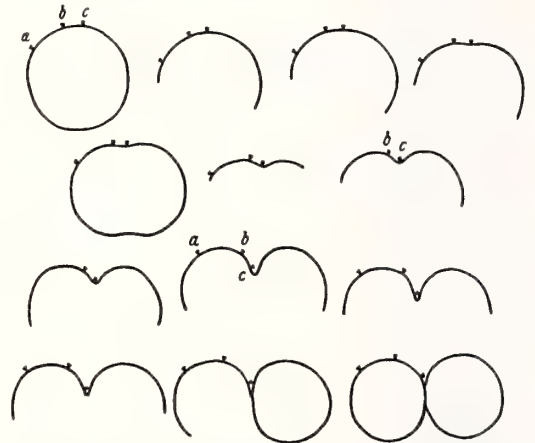


FIG. 1. A record of surface behavior of the egg of *Mespilia globulus* during cleavage as revealed by attaching marker particles. (Reproduced by permission of Protoplasma).

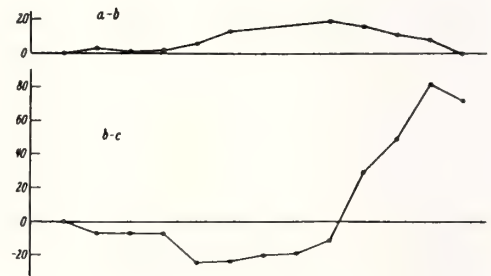


FIG. 2. Graphic presentation of the data of Fig. 1. A sharp contrast in behavior between the surface of the furrow and that of adjacent regions. (Reproduced by permission of Protoplasma).

body in the direction of the spindle axis (Fig. 3) [1].

Now the astral rays of the two asters are crossing on the equatorial plane (Fig. 4). Since the tips of the rays are anchored to the cortical gel (Fig. 1 in [3]), they are not free to move separately but they must move as a mass. When the astral centers are pushed away from each other by the elongation spindle, the loci of the tips of the rays will be as shown in Figure 5. It is obvious that while the equatorial surface is being pulled in toward the spindle, it shrinks at the same time.

Here, I would like to call attention of readers to the fact that the author applies the term "furrow" to the stage when a circular contour of the cell becomes flat as shown in Figure 5. In the literature, some people use the term only after an indentation appears on this flat surface.

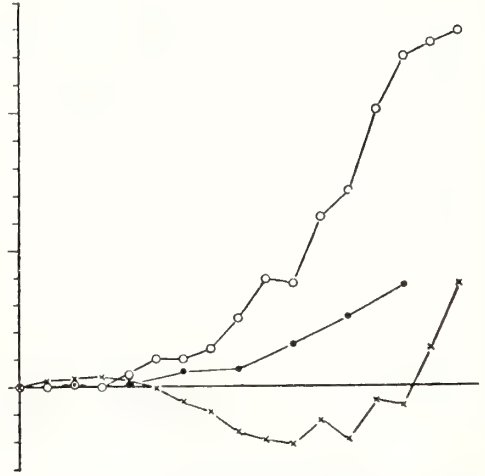


FIG. 3. Simultaneity among spindle (●) and cell body (○) elongation and shrinkage of furrow surface (×).

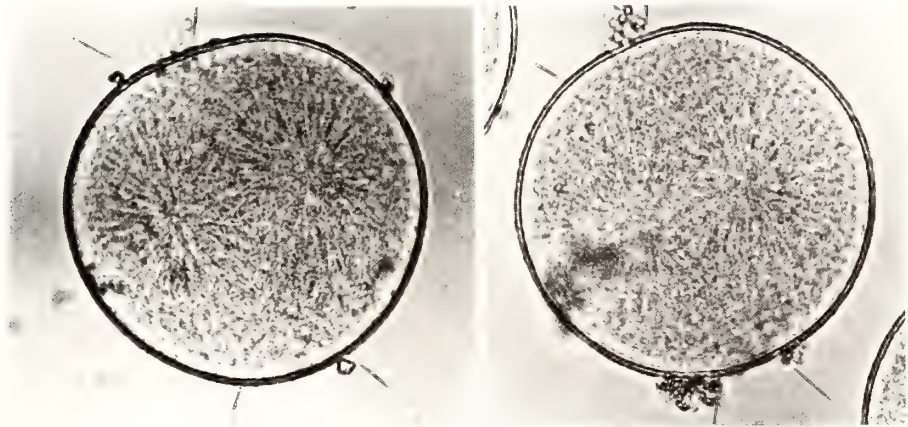


FIG. 4. Two examples of *Clypeaster* eggs just before cleavage. (Please ignore attaching particles). One can see crossing of the rays on the equatorial regions. The widest crossing ranges are indicated by a pair of lines outside the pictures. Since rays are radiating out from a center, it is extremely difficult to get clear images of crossing rays along their lengths. This drawback is compensated by flattening the cell or by moving focus up and down.

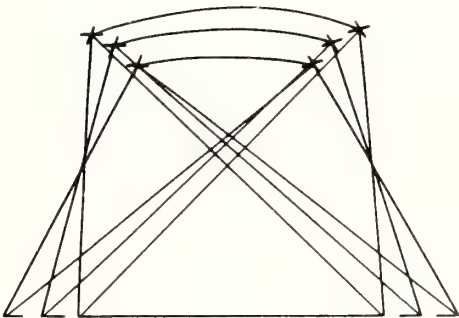


FIG. 5. Loci of the tips of crossing rays as astral centers are pushed away by elongating spindle. The equatorial surface shrinks as it is drawn in toward the spindle.

Going over to Figures 6 and 7, these are microphotographs of the eggs of *Clypeaster japonicus* with two particles of activated clay attached on the equatorial surface. In taking these photographs, special care was taken for the following conditions.

(a) Eggs should be selected in which the spindle is strictly parallel to the substratum so that it won't tilt during measurement. (b) Two attached particles must be situated roughly on the widest crossing range of the crossing rays (Fig. 4) If the

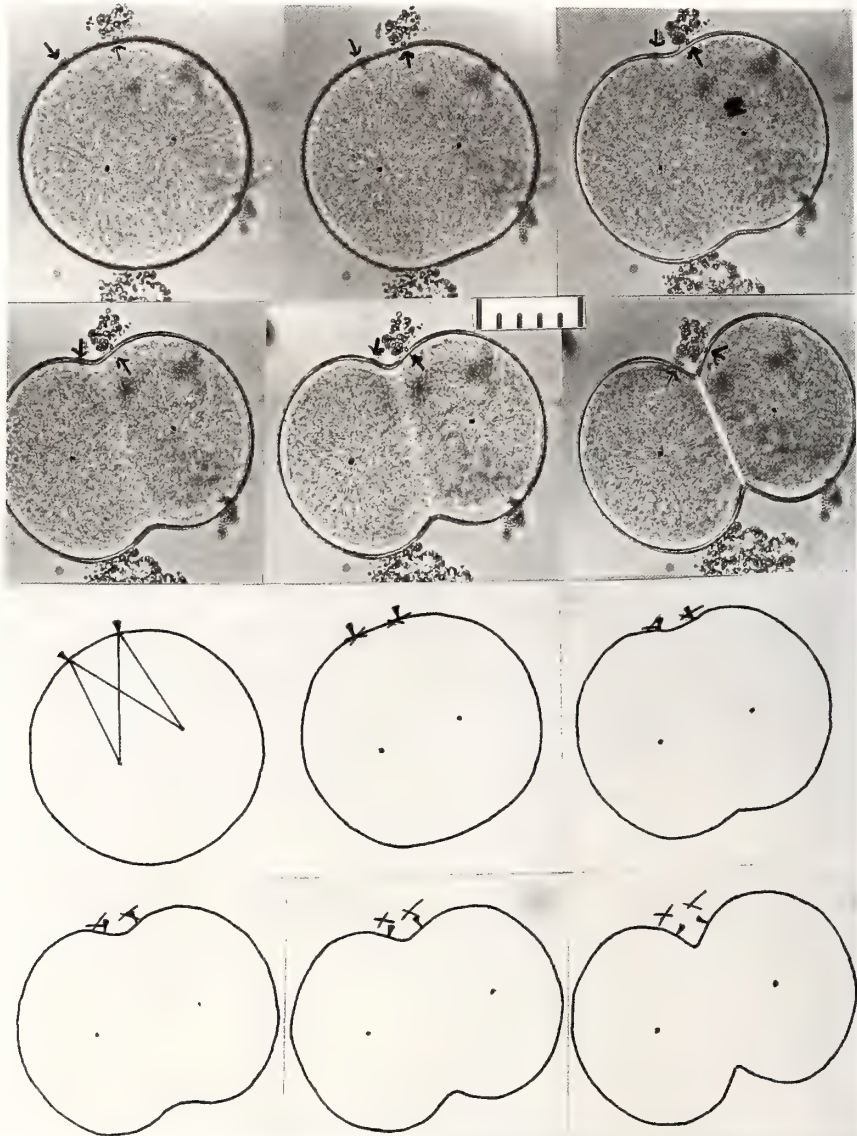


FIG. 6. An egg of *Clypeaster japonicus* in cleavage. (Times of photographing: 0'', 1'45'', 2'50'', 3'20'', 4'45'', 6'00'').

Two dots on upper furrow surface are attached clay particles. The distance between them reaches a minimum in the 3rd picture. Astral centers are separating owing to a push by the elongating spindle. (Smallest division of the scale is 10 μ m).

In explanatory drawing, clay particles are represented by arrow heads and positions of the particles anticipated by the author's theory (obtained by the methods in Fig. 5) are shown by X.

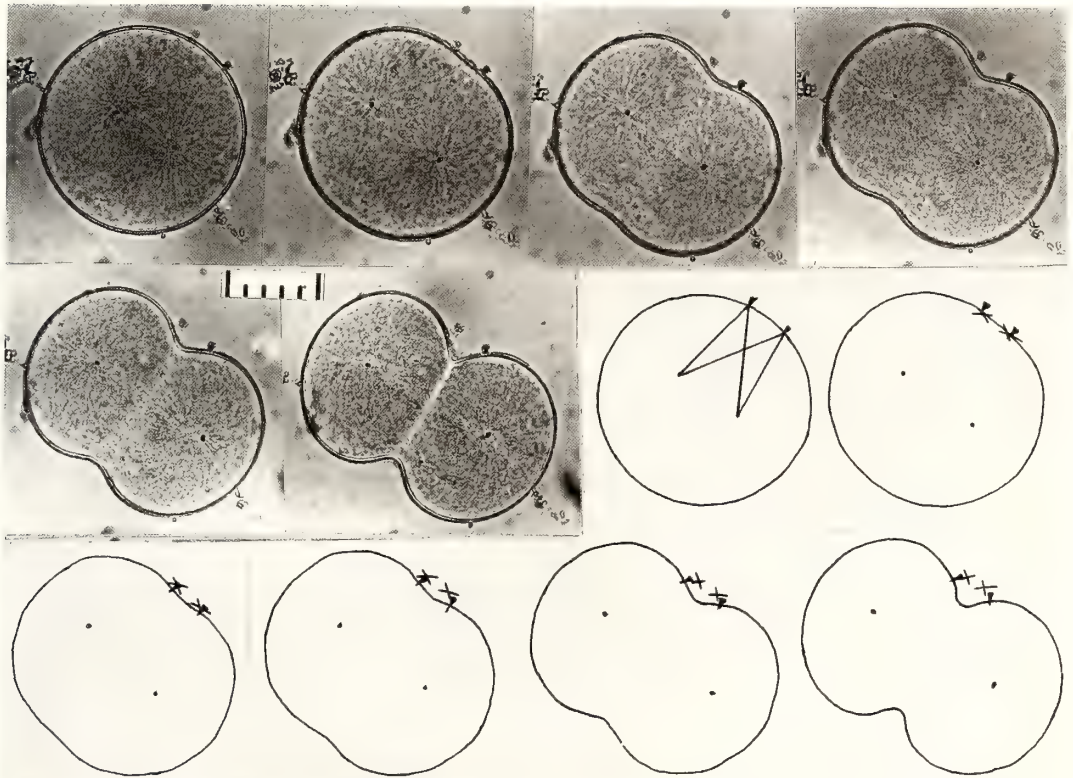


FIG. 7. Another example of the same experiment as Fig. 6. (Times of photographing: 0'', 3'00'', 4'30'', 5'00'', 5'30'', 6'30''). The astral rays are sharper here than Fig. 6. By the time constricting ring begins to work (4th–5th photos), crossing of the rays is no longer discernible and the rest of the rays are bending into a fountain figure as the result of push against the polar surface. (Smallest division of the scale is 10 μ m).

positions of the particles do not coincide with actual crossing range, good agreement between the degree of observed approach of the particles and the degree of calculated shrinkage by drawings of the intersection points cannot be expected [1]. The present author's crossing range could be a concrete basis for Rappaport's 'joint astral influence' [8]. (c) Camera must be sharply focussed on the two astral centers. Owing to the fact that particles are on the cell periphery, one tends to get an impression that sharp focussing on the cell contour is important, which, however, is not the case. Since the contour is being looked down upon tangentially from above, a slight up and down deviation of the image of the cell contour does not affect the calculation while slight errors in positioning of astral centers upsets the accuracy of the calculation to a large extent.

In the accompanying explanatory drawings of Figures 6 and 7, attaching particles are indicated by arrow heads and separating centers of the asters or the tips of the elongation spindle are shown by black dots. The particles, astral centers and cell contour are traced from the photographs. In the first explanatory figure, 4 segments of line are obtained by connecting the particles and the astral centers. These represent a pair of crossing rays and two non-crossing rays. From the second drawing on, keeping the lengths of the segments unchanged and using them as radii, 4 circles are drawn placing the centers of the circles at moving positions of the astral centers. Intersections of the circles are indicated by X. These X's show the positions where the particles would be by the astral mechanism.

Degrees of shrinkage of particle distance and

TABLE 1. Changes of the particle distance (P) and intersectional distance (D) in the egg shown in Fig. 6

Time	P		D	
	distance	%	distance	%
0''	*12.3 mm	100.0	*12.3 mm	100.0
1'00''	11.8	95.9	10.8	87.8
1'45''	*10.3	83.7	* 9.9	80.5
2'15''	10.2	82.9	10.2	82.9
2'50''	* 9.8	<u>79.7</u>	* 9.4	76.4
3'30''	*11.1	90.2	* 8.0	65.0
4'10''	12.9	104.9	7.5	61.0
4'45''	*13.0	105.7	* 6.9	55.1
5'20''	16.2	151.7	6.1	49.6
6'00''	*19.2	156.3	* 6.0	48.2

Series VII: 24.0°C, crossing angle 62°. Underlined numerals are minimum values. Asterisks are cases in Fig. 6.

those of the intersectional distance are shown in Tables 1 and 2 and plotted in Figures 8 and 9. In the Tables and Figures, all the data are given, among which cases illustrated in the photographs are indicated with asterisks.

Two features are obvious. (1) The distance between actual particles and that of the intersections decreases *pari pasu* until the end of the shrinkage phase of the equatorial surface. During the following stretching stage, although the intersections continue to come closer, particles move away from each other. (2) Roughly until this turning point (third drawing of Fig. 6, 3rd-4th drawings of Fig. 7) the intersection points fall on the contour line of the deepening furrow. Coincidence between the transition from shrinkage to stretching and the point of disparity between the positions of particles and intersections is almost perfect in Figure 6 but it is slightly off in Figure 7. However, on examining the data of Figure 7 closely, it is revealed that although the particle distance of the 8th point or the 4th drawing is certainly smaller than the preceding step, the difference between them is less than in previous steps (see Table 2 and Fig. 9). This may mean that an actual minimum must have happened between them, at some time during 30 second interval and the seeming minimum point must be representing very beginning of the stretching phase.

Repeating the conclusion once more, during the

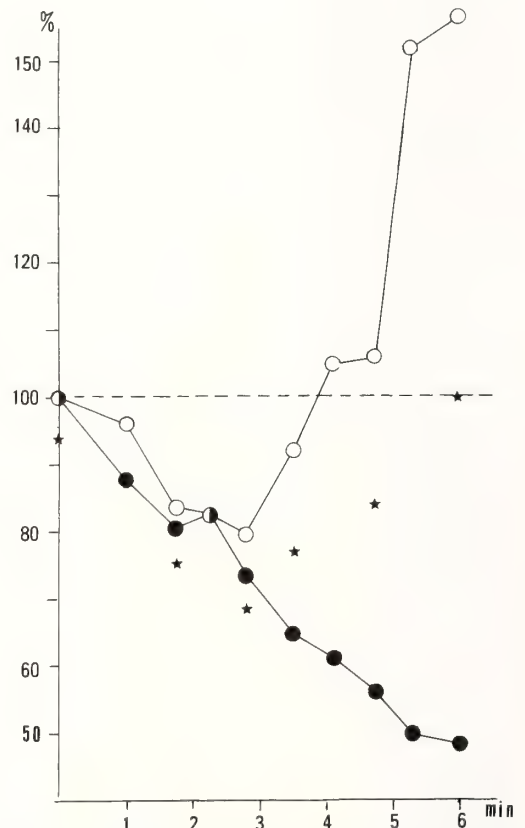


FIG. 8. A graph showing changes in distance of particles (open circles) and of intersections (filled circle) of the data of Fig. 6. Asterisks are cases shown in photographs.

TABLE 2. Changes in the particle distance (P) and intersectional distance (D) in the case shown in Fig. 7

Time	P		D	
	distance	%	distance	%
0''	*14.7 mm	100.0	14.7 mm	100.0
2'00''	14.1	95.9	14.1	95.9
2'30''	12.0	81.6	12.0	81.6
3'00''	*11.9	81.0	10.5	71.4
3'30''	11.0	74.8	10.5	71.4
4'00''	10.0	68.0	10.5	71.4
4'30''	* 9.1	61.2	9.0	61.2
5'00''	* <u>8.9</u>	<u>60.5</u>	8.0	54.4
5'30''	* 9.9	67.3	6.8	46.3
6'00''	12.6	85.7	7.0	47.6
6'30''	*12.9	87.8	6.9	46.9
7'00''	17.0	115.7	6.9	46.9

Series I: 24.5°C, crossing angle 58°. Underlined numerals are minimum values. Asterisks are cases shown in Fig. 7.

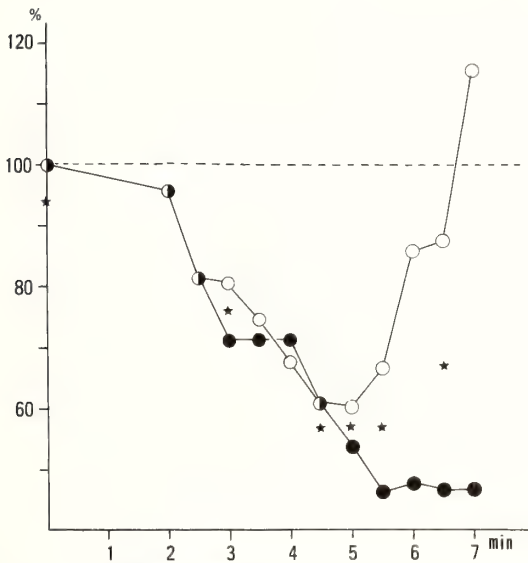


FIG. 9. A similar graph as Fig. 8 for the data of Fig. 7.

shrinkage phase of the equatorial surface, the astral mechanism can account for the degree of shrinkage quantitatively and it can also define the depth of the forming furrow. However, once the stretching phase of the equatorial surface begins, the behavior of the particles and the intersections diverge and the positions of the intersections begin to go outside of the furrow contour. In other

words, from this stage on, the actual furrow is always deeper than expected by the astral mechanism which, in turn, suggests that the constricting mechanism is being activated.

Concerning step 2

It was an important discovery that both English and Japanese investigators became aware of the fact that the cell behavior changes between metaphase and anaphase.

Since Swann and Mitchison were using a polarization microscope, they could discern the chromosome stage more or less [2]. On the other hand, since Hiramoto was using phase contrast optics, he could not see the condition of chromosomes [3]. The present author presumes that Hiramoto's criteria of meta- and anaphase were probably whether the cell was spherical or with a furrow. However, this bears a relation to a delicate point of discussion in the next section.

Concerning step 3

By the first impression, Schroeder's thesis sounds almost perfect, since he succeeded to identify the special structure underlying the cleavage furrow as bundles of actin fibers. To scrutinize his idea we must keep in mind a very crucial statement of his that the ring does not exist as long as the cell

remains spherical while it appears only after a furrow is formed (pp.422–425 in [4]). On the other hand, he also tries hard to show that the ring is present from the very beginning of furrow formation: 20 sec after the end of anaphase (pp. 422, 425, and Fig. 6 in [4]). Of course, we can understand his strong wish to make the ring appear as early as possible and to make it do the entire work of furrow formation, since the constricting mechanism is the only scheme he has in mind. At any rate, Schroeder's two statements even sound somewhat contradictory.

There are two papers reporting the absence of the constricting ring in early phase of nuclear division. Usui and Yoneda [9] showed a series of meridional thin sections of the eggs of *Hemicentrotus pulcherrimus* in early phase of mitosis. They concluded that until late telophase when a slight decrease in equatorial diameter is perceived, the ring is absent ([9], Fig. 3a). But in eggs 1 min after furrow formation a ring is there (Fig. 3b in [9]).

Yonemura and Kinoshita [10] obtained peeled cortices isolated by Vaquier's cortical lawn method [11] of *Clypeaster* eggs. They stained the cortices by phalloidin conjugated with nitrobenzoxadiazole to examine the distribution of F-actin. When cortices are prepared from telophase cells, they could recognize constricting rings as bands of F-actin, while they failed to find them when taken from anaphase cells. At any rate, the ring does not seem to exist through anaphase to the first half of telophase when the spindle elongation is taking place.

Actually the situation is more complicated than Schroeder's notion. By Rappaport's experiments, we now know that some time before actual formation of a furrow, a precursor or some basis of a future furrow is laid by induction by the asters [12]. That is to say that once the induction becomes completely effective, the presence of the asters is no longer required for the formation of the furrow. The time when this induction takes effect is 4 min before the appearance of the furrow in *Echinarachnius parma*. Comparable figures for Japanese sea urchins by Hamaguchi are of the same order of magnitude [13]. Taking advantage of this situation, Rappaport prepared a cylindrical egg in a glass capillary of 80 μm in diameter and after

leaving the mitotic apparatus at one place during effective time for the induction, he moved it to a new location in the egg. Thereby he succeeded in making furrows appear and regress more than 10 times in a single cell [14].

It was mentioned earlier that Schroeder confronted a very queer fact that he could not find the constricting ring unless the egg has already a furrow. Giving a direct expression, it means that spherical eggs can never start to cleave. This is a serious matter. If the induction story is superimposed on this fact, the situation becomes still more complicated. Facing such a complicated circumstance, the author feels that there may be a missing link in the story which has been overlooked so far. This link could be called an assembly-initiating factor and the factor could be the spindle elongation itself, as the result of which dormant induction effect is made apparent as a constricting ring. From the author's standpoint, the astral mechanism invariably precedes the constricting mechanism. In the past, people, not being aware of this fact, thought the asters offer sufficient and adequate explanation for furrow formation. When people use mitotic poisons to suppress cleavage, the author believes that the effects of the poisons are primarily on the spindle elongation and inhibition of furrow formation is a secondary result.

Then what is the merit of spindle elongation? (1) In our daily experience, under some adverse conditions, a shallow furrow which once appeared often regresses. Rappaport would say that, in this case, induction is inadequate or it is during latent period. But the period under consideration is the intervening time (4 min) between the induction and realization of the furrow. As far as this period is concerned, the author feels that it would be as likely as Rappaport's interpretation as to think that shallow furrow is formed by the elongation of the spindle and the next step of assembly of actin fibers is failing. Quoting Rappaport: the result indicates (Fig. 7) that in these cylindrical cells, a considerable portion of the increase in interastral distance takes place after the position of the furrow is fixed (p. 570 in [12]).

(2) From Rappaport's measurements [12], the strength of cleavage stimulus of the asters seems to decrease more or less proportionally to the dis-

tance between the aster and the cell surface. In general, in intact spherical eggs, presence of only one aster is considered to be inadequate to form a furrow [7, 15, 16]. However, even under this condition, by reducing the distance between the asters and cell surface, say, by making the cell cylindrical, the cell can divide. Under normal condition, while the cell remains spherical, asters lie closer to the polar surface than to the equatorial surface. But when the spindle elongates, the cell changes its shape to oblate or cylindrical, bringing the equatorial surface closer to the asters. This is exactly the same condition as Rappaport's experiment making cell cylindrical to make the asters and cell surface come to proximity in order to enhance interaction between them [15].

(3) The force of cleavage of sea urchin egg has been measured [18] and the figures are around 1.5

$\times 10^{-3}$ dyne. As long as the furrow keeps on constricting with this force, the efficiency of pinching will become greater as the diameter of the ring decreases. Stating it in the reverse way, at the beginning of constriction when the diameter of the ring is maximal, the efficiency of pinching is minimal. The astral mechanism comes into play at this moment as if it helps the constricting mechanism to start more easily. As a matter of fact, according to analysis of cleavage force in our other papers [19, 20], the time when the largest force is required is the initial stage of division when the egg goes off the spherical shape to an oblate form and the rest of the division process goes downhill forwise.

(4) Since an illustration in the paper of Yoneda and Dan [20] is very elucidating for the situation under discussion, it is partly reproduced here (Fig.

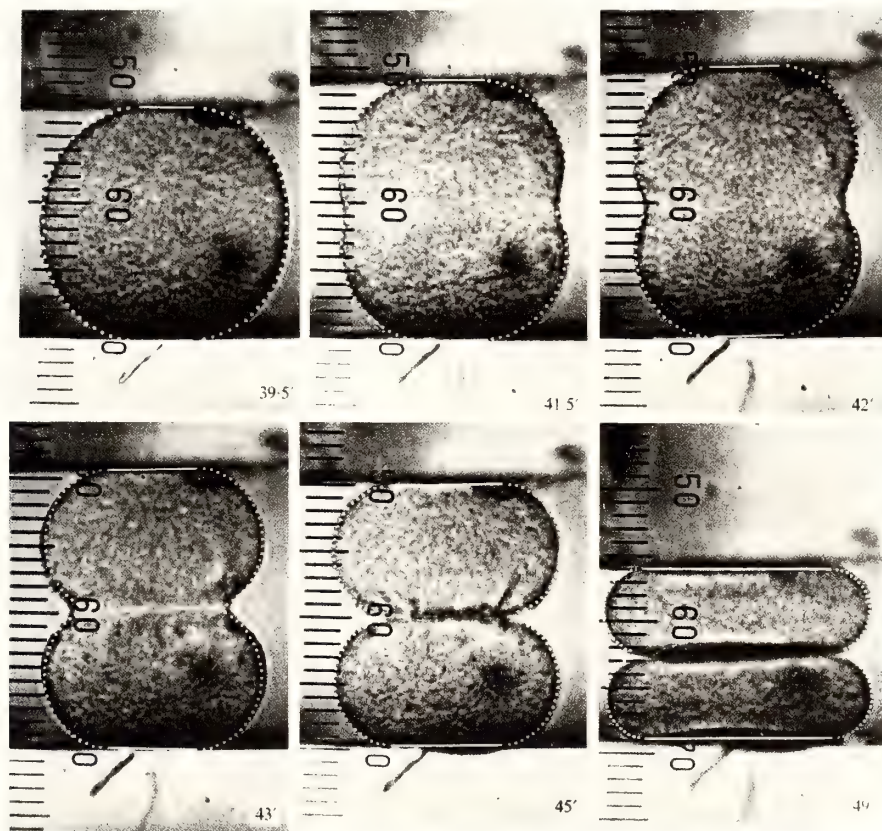


FIG. 10. An egg of *Temnopleurus hardwicki* compressed between two parallel glass plates with the spindle oriented vertically. Force of 2.7×10^{-3} dynes is applied continuously from above. The egg elongates against the force till the 3rd frame and then slackens. (reproduced by courtesy of J. exp. Biol.).

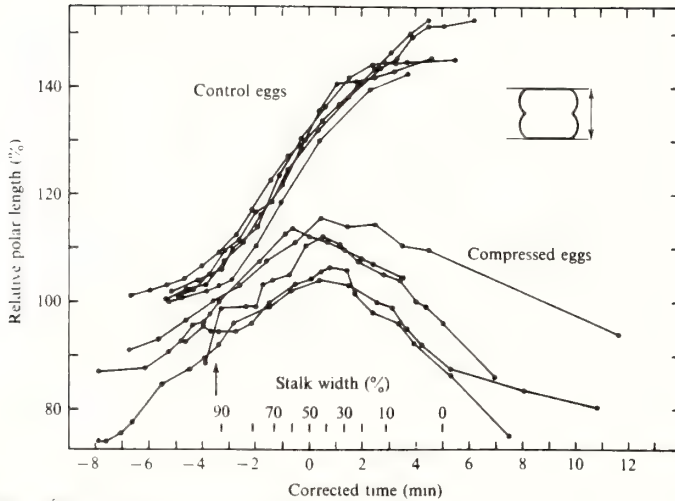


FIG. 11. Similar measurements as Fig. 10 for eggs of *Pseudocentrotus* with and without the weight. (by permission of J. exp. Biol.).

10). In this experiment, eggs of *Temnopleurus hardwicki* at about the time to divide are placed between two horizontal glass plates with the spindle oriented vertically. The lower glass plate is fixed unmovable while the upper plate is movable and can press on the egg. Force of 2.7×10^{-3} dynes is applied continuously throughout the observation.

It is clear that the egg elongates against the weight of 2.7×10^{-3} dynes until the third picture and then it slackens. The same situation is found in the eggs of *Pseudocentrotus depressus* (Fig. 11). In the light of the astral mechanism, this can be interpreted as showing that until the third photograph, cleavage furrow is being formed by the spindle elongation, namely astral mechanism and from the 4th on, the constricting ring begins to work. As a matter of fact, by comparing 3rd and 4th pictures of Figure 10, in the former, the blastomere surface is smooth and the tip of the furrow is roundish, while in the latter, the cell surface is beginning to wrinkle and the furrow tip is becoming pointed, showing it is being dragged by the constricting ring.

Comparing Figures 6 and 7 on one hand and Figure 10 on the other, a point of departure from the astral to constricting mechanism looks to have occurred somewhat later in the latter case than in the former examples. This may be because the

imposed pressure may have delayed the time of shifting from the astral to constricting mechanism in the latter case.

DISCUSSION

In the foregoing description, a point of interest is that the author's astral mechanism just fits into the complicated period. As the result, Schroeder does not have to worry about early appearance of the ring. Furthermore, although the ring is an ideal tool for pinching, the ring itself has no information as to in which direction it should be formed. The mitotic apparatus not only gives directional information by induction but also gives an impetus to the assembly of actin fibers. From this stage on, the ring carries out the rest of the cleavage process. In other words, the mitotic apparatus is a planner and the ring is an executer, so to speak. At any rate, the author thinks that both mechanisms are involved in cleavage process and a baton is handed over from astral to constricting mechanisms in early stage of the process.

REFERENCES

- 1 Dan, K. (1943) Behavior of the cell surface during cleavage. VI. On the mechanism of cell division. J. Fac. Sci. Tokyo Imp. Univ., Sec. 4, 6: 323-368.

- 2 Swann, M. M. and Mitchison J. M. (1953) Cleavage in sea-urchin eggs in colchicine. *J. exp. Biol.*, **30**: 506-514.
- 3 Hiramoto, Y. (1956) Cell division without mitotic apparatus in sea urchin eggs. *Exp. Cell Res.*, **11**: 650-656.
- 4 Schroeder, T. E. (1972) The constricting ring II. Determining its brief existence, volumetric changes and vital role in cleaving *Arbacia* eggs. *J. Cell Biol.*, **53**: 419-454.
- 5 Schroeder, T. E. (1975) Actin in dividing cells; contractile ring filaments bind heavy meromyosin. *Proc. Natl. Acad. Sci. USA*, **70**: 1688-1692.
- 6 Hiramoto, Y. (1965) Further studies on cell division without mitotic apparatus in sea urchin eggs. *J. Cell Biol.*, **25**: 161-168.
- 7 Dan, K., Yanagita, T. and Sugiyama, M. (1937) Behavior of the cell surface during cleavage. I. *Protoplasma*, **28**: 66-81.
- 8 Rappaport, R. (1975) Establishment and organization of the cleavage mechanism. In "Molecule and Cell Movement". Ed. by S. Inoué and R. E. Stephan, Raven Press, N. Y., pp. 287-304.
- 9 Usui, N. and Yoneda, M. (1982) Ultrastructural basis of the tension increase in sea-urchin eggs prior to cytokinesis. *Dev. Growth Differ.*, **24**: 453-465.
- 10 Yonemura, S. and Kinoshita, S. (1986) Actin filament organization in the sand dollar egg cortex. *Dev. Biol.*, **115**: 171-183.
- 11 Vacquier, V. D. (1975) The isolation of intact cortical granules from sea urchin eggs: calcium ions trigger granule discharge. *Dev. Biol.*, **43**: 62-74.
- 12 Rappaport, R. (1981) Cytokinesis: cleavage furrow establishment in cylindrical sand dollar eggs. *J. exp. Zool.*, **217**: 365-375.
- 13 Hamaguchi, Y. (1975) Microinjection of colchicine into sea urchin eggs. *Dev. Growth Differ.*, **17**: 111-117.
- 14 Rappaport, R. (1985) Repeated furrow formation from a single mitotic apparatus in cylindrical sand dollar eggs. *J. exp. Zool.*, **234**: 167-171.
- 15 Rappaport, R. (1986) Mitotic apparatus-surface interaction and cell division. *J. Inverteb. Reprod. Dev.*, **9**: 263-277.
- 16 Rappaport, R. (1965) Geometrical relation of cleavage stimulus in invertebrate egg. *J. Theoret. Biol.*, **9**: 51-66.
- 17 Hiramoto, Y. (1971) Analysis of cleavage stimulus by means of a micromanipulation of sea urchin eggs. *Exp. Cell Res.*, **68**: 291-298.
- 18 Rappaport, R. (1977) Tensiometric studies of cytokinesis in cleaving sand dollar eggs. *J. exp. Zool.*, **201**, Suppl. 3: 375-378.
- 19 Dan, K. (1963) Force of cleavage of the dividing sea urchin egg. *Symp. Int. Soc. Cell Biol.*, **2**: 261-276.
- 20 Yoneda, M. and Dan, K. (1972) Tension at the surface of the dividing sea-urchin egg. *J. exp. Biol.*, **57**: 575-587.

Mitotic Poles in Artificial Parthenogenesis: *A Letter to Katsuma Dan*

DANIEL MAZIA

*Hopkins Marine Station of Stanford University,
Pacific Grove, CA 93950, U.S.A.*

ABSTRACT—The two steps in the classical procedure for artificial parthenogenesis in the sea urchin egg are analyzed. Step I (typically a treatment with butyric acid) can be considered to be the turning-on of the cell cycle, as in normal fertilization. Early events such as Ca^{2+} release and elevation of intracellular pH lead into chromosome replication and a mitotic cycle. However, NONPOLAR MA are produced. The basic structure of the NONPOLAR MA is like that of a normal MA, but it can not make poles; chromosomes can not orient and can not separate and the egg can not divide.

Step II (typified by a treatment with hypertonic sea water) results in the production of a great variety of MA, mostly abnormal. MONOPOLAR MA, which orient and engage chromosomes, are common, but the half-spindles often fail to engage all the chromosomes. There are various MA which seem to be partially POLAR and partially NONPOLAR. BIPOLAR MA may be formed, but often these do not engage all the chromosomes. There are great variations of the poles: some make asters, some do not; some are compact, some are so flat that the chromosomes diverge in anaphase. If the eggs divide at all, the blastomeres are likely to be aneuploid. The fact that truly normal parthenogenetic development is rare is explained by the likelihood of aneuploidy.

The results are best interpreted in the light of Boveri's hypothesis that the maternal centrosome becomes disordered (but is not destroyed) in the maturation of the egg; it is restored to its active form by the parthenogenetic procedure. An explanation can be found in a linear model of the structure of the centrosome (Mazia, D. (1987) *Int. Rev. Cytol.*, **100**: 49–91). The linear model would allow for the *denaturation* of the centrosome in the unfertilized egg and its *renaturation* by the parthenogenetic procedures. The high incidence of abnormal poles would follow from the probability of errors in the refolding of the very long linear structure.

Dear Kady:

Our tribute is more than praise; it is thanks. My thanks go back very far — some 55 years. You were a graduate student, I was an ignorant undergraduate who had been accepted by our teacher, Lewis Victor Heilbrunn, into his laboratory family. I learned so much from you then and have learned much from you since; I learned a lot from your most recent paper. I want to tell you about some work that I have been doing over the last 10 years or so. Let me claim the right of old friendship to say what I have to say in the form of a letter to you. In a letter between friends, one may look more deeply into the past and imagine further

into the future than is welcome in a normal scientific publication.

The topic is artificial parthenogenesis, especially in the sea urchin egg. The letter has some of the elements of a review, but a personal letter does not require the citation of the larger literature. (The field began to languish so long ago that Albert Tyler's publication in 1941 [1] covers a major part of the literature). In this letter I also report original but hitherto-unpublished results of experiments that I have been doing over more than a decade. Mostly I will be trying to account for artificial parthenogenesis in the light of present views about the nature of the centrosome.

Others are free to read and cite this letter, although artificial parthenogenesis does not now interest many biologists. It was exciting and even

sensational before our time because the genesis of fatherless sea urchins by chemical means ("Chemische Entwicklungserregung", as Loeb [2] called it) defied the essential idea of fertilization. After that excitement was over, the intrinsic problem—the formation of a bipolar mitotic apparatus in an unfertilized egg—remained unsolved. The problem was hard to think about at a time when there was so much scepticism about the very "reality" of the mitotic apparatus and when cell biologists doubted the universal occurrence of centrosome.

An historian can trace the main ideas about artificial parthenogenesis back to two great cell biologists, Jacques Loeb and Theodor Boveri. (The two have been the subjects of interesting biographies [3, 4]). To say that they disagreed would be an understatement. Each simply dismissed the other's idea of the very nature of the problem. The outcome, viewed some 80 years later, was that each identified one part of the problem correctly but saw that part as the whole problem. Loeb's central thesis [2] was that the egg could be excited by changes of ions; thereby he minimized the role of the spermatozoon in fertilization. Boveri [5], who had discovered that the spermatozoon contributes the centrosomes which then provide the poles of the mitotic apparatus, responded to the challenge of parthenogenesis by hypothesis that: the parthenogenetic procedures resurrect the maternal centrosome, which had become disordered during the maturation of the egg.

Considering artificial parthenogenesis in the sea urchin egg as a two-step procedure I will consider how Loeb's point of view explains step I (activation by butyric acid or other means) and how Boveri's thoughts define Step II (restoration of mitotic poles by a treatment with hypertonic sea water).

When Jacques Loeb came here to Pacific Grove, to work in his little laboratory on Monterey Bay, not far from where I am now writing (in the Loeb Building of the Hopkins Marine Station), he was prepared by previous experience to study artificial parthenogenesis as a one step process. He expected to arouse development in unfertilized eggs of *Strongylocentrotus purpuratus* by a one-step

treatment with hypertonic sea water. The results were unsatisfactory, stimulating him to the chain of ingenious experiments that led to the two-step method.

The two steps of the procedure that was designated as the "improved method" are: Step I, a brief exposure to a dilute solution of butyric acid in sea water, after which the eggs were returned to sea water, and Step II, an interval of exposure to hypertonic sea water, at about $1.5\times$ the osmolarity of normal sea water. Many other agents can be substituted for butyric acid in Step I. My present favorite is CO_2 -sea water, artificial sea water made up in ordinary carbonated water. (Loeb had used CO_2 ; I can only guess why he preferred butyric acid). Different solutes could be used to raise the osmotic pressure in Step II. The method could not be completely standardized with respect to the timing of Step I and Step II; it called for trial-error sampling of the time of starting and the duration of exposure.

Nowadays we can understand Step I reasonably well. The broadest statement is that Step I turns on the Cell Cycle, which is repressed in unfertilized sea urchin eggs. Observations of the outcome of Step I assure us the chain of events is about the same as is found at fertilization: the membrane events that precede Ca^{2+} -release; the pH changes that follow the Ca^{2+} -release; the phosphorylations of nucleosides and the initiation of DNA replication that follows the pH changes, and the further cell cycle events that lead to the production of an MA. **The turning-on of these Cell Cycle events by agents other than sperm is Step I of the parthenogenetic procedure.** Nowadays, as we know more about the turning-on the Cell Cycle by weak acids, weak bases, IP_3 , Ca -ionophores, non-electrolytes, proteolytic enzymes, etc., etc., we have to be reminded that we do not yet know how the events are started by a spermatozoon.

It is confusing to speak of "parthenogenetic activation", as some writers do, because Step I does not bring about division and development. (It may do so in kinds of eggs in which both steps can be carried out in a single treatment). It was fortunate that Loeb moved to Pacific Grove, where he was forced to sort out the two quite different components of artificial parthenogenesis.

Step I, applied to unfertilized sea urchin eggs, leads to the formation of a NONPOLAR MA. The NONPOLAR MA is very different from a MONOPOLAR MA. We will define the NONPOLAR MA after we have described the MONOPOLAR MA. That may sound perverse, but the MONOPOLAR MA has taught us what a single true mitotic pole can do.

The NONPOLAR MA is seen in the living cells as a symmetrical aster; it was seen long ago by earlier workers on parthenogenesis. It can be isolated by methods of isolating MA. The fine structure resembles that of a normal MA, but the microtubules radiating from the center do not seem to engage the kinetochore in a normal way [6]. In the NONPOLAR MA, the chromosomes go through their cycle of condensation, splitting and recondensation. The split chromosome does not move apart. The chromosomes show no orientation (Fig. 1A). There is no polarity; no spindle or half-spindle can be distinguished from the monaster. Chromosomes are not separated and the completed cycle produces a single diploid nucleus. The cycle may be repeated, again forming a NONPOLAR MA with doubled numbers of chromosomes [7]. In modern language the NONPOLAR MA appears to be generated by an MTOC, but that MTOC can not function as a pole. **We will try the hypothesis that the NONPOLAR MA expresses the action of the degenerated (denatured) but still-existing maternal centrosome,** the survival of which was postulated by Boveri. Running ahead of my story, I can say that the center of the NONPOLAR MA contains centrosomal material, as judged by osmiophilic foci [6] and by staining with anticentrosomal antibody. (Heide Schatten and Gerald Schatten allow me to cite their unpublished finding).

The evidence from all the biochemical and cytological studies tells us that Step I starts up the Cell Cycle in unfertilized eggs. What we have seen of the NONPOLAR MA allows us to pursue the idea that the maternal centrosome persists in the mature unfertilized egg but is **incapable of functioning as a pole.**

In my experience, the definition of a pole became clear only from a closer study of the MONOPOLAR MA [8] and from consideration of other modern work on MONOPOLAR MA [9]. Working with sea urchin eggs, we can make large

numbers of monopolar MA by the “Mercaptoethanol Experiment” [10–13]. That useful stratagem traces back to the days when you and I were so fascinated by the role of thiol groups in the MA.

With correct timing of the period during which fertilized eggs are kept in beta-mercaptoethanol, we can persuade the eggs to divide into four blastomeres, each of which receives one centrosomal unit (monovalent) instead of the normal pair (bivalent) of centrosomal units. In the next cycle, each blastomere makes a MONOPOLAR MA; literally, there is one pole and there is clearly a half spindle [8]. In the following cycle, we see that the pole of the MONOPOLAR MA has doubled; now there is a bipolar MA and the blastomeres divide.

(The cycles of doubling and division of poles in the normal Cell Cycle are so precise! — and necessarily so for the success of cell reproduction. How can we reconcile the *normal* reproductive behavior of poles with the opinions that they can arise *de novo*, opinions that have been so influential in the literature of artificial parthenogenesis!)

The close study of the MONOPOLAR MA yields, I believe, a very clear idea of what a true pole can do. Without any interaction with a second pole the MONOPOLAR MA can (1) form a distinct half spindle; (2) gather the chromosomes at the “equatorial” edge of the half spindle; (3) orient and engage the chromosomes so that one kinetochore of a sister-pair points at the pole and makes connections to the pole; (4) carry out anaphase (or an equivalent change that results in the restoration of an interphase nucleus near the pole).

We will see that a MONOPOLAR MA is a likely outcome of Step II of the parthenogenetic procedure.

In trying to understand Step II, **it is helpful to realize that some of the literature exaggerates the success of the parthenogenetic methods,** at least with sea urchin eggs. As students, we may have received from textbooks the impression that the technique of artificial parthenogenesis is the equivalent of pushing a few buttons: carry out Step I and Step II and watch the nice plutei appear! As teachers, we have had to face disappointed students who tried the procedures in the laboratory. Perhaps some investigators (and species of eggs) have produced large numbers of normal embryos,

but careful observers, in the past [14] and more recently [15, 16] comment on the rarity of normal larvae and on the progressive attrition of the developing population. That is unfortunate for those who want to study orphan sea urchins. **The "bad" results turn out to be the most interesting to those of us who are trying to understand mitotic poles** — if we make the effort to diagnose the varied pathologies of the imperfect mitotic apparatus that we find in many eggs.

Boveri's proposed in 1901 [5] that the maternal centrosome is inactivated during the maturation of the sea urchin egg but remains and is reconstructed during the parthenogenetic procedures. In 1988, **I am adding the statement that the mature egg contains a *denatured* centrosome that can generate a NONPOLAR MA after Step I of the parthenogenetic procure. After Steps I and II, the centrosome can be *renatured* and can carry out the functions of pole. (The terms "denaturation" and "renaturation" anticipate the hypothesis that the centrosome is a fundamentally linear structure whose activity depends on its 3-dimensional conformation.)**

Extensive cytological studies show that the renaturation of the centrosomes is, most often, imperfect. The MA display an extravagant variety of abnormalities in the forms of the poles and in the engagement of the chromosomes by the poles. It becomes clear why perfect parthenogenetic development is so rare.

The variety of abnormalities is immense, but a

few examples tell the essential story.

(1) Many eggs do not make a pole at all; Step II has not worked. One sees only NONPOLAR MA (Fig. 1A) as they have been described earlier [e.g. 6, 7].

(2) In some cases a seemingly perfect MONOPOLAR MA is formed (Fig. 1C). The mitotic apparatus as a whole is seen as a single aster. The chromosomes are arranged on a metaphase plate on the boundary of a half-spindle.

(3) One sometimes sees MA that are intermediate (Fig. 1B) between the NONPOLAR (as in Fig. 1A) and the well-developed MONOPOLAR MA (Fig. 1C). The chromosomes are arranged on one sector of the spherical monaster, as though engaged to a very wide half-spindle.

(4) Studying many of the cases where MONOPOLAR MA are produced, one often sees MA in which some of the chromosomes are oriented on a plate (rather an arc, as is typical of the monopolar MA) on the virtual "equator" at the margin of a half spindle. Others can lie anywhere around the aster (Fig. 1D). Obviously the renaturation of the centrosome has been imperfect. To some degree, the such MONOPOLAR MA retains properties of a NONPOLAR MA as judged by the behavior of some of the chromosomes. Such defects are common and they predict the production of aneuploid blastomeres.

(5) The MA may be BIPOLAR to some degree. The common defects are not familiar from experi-

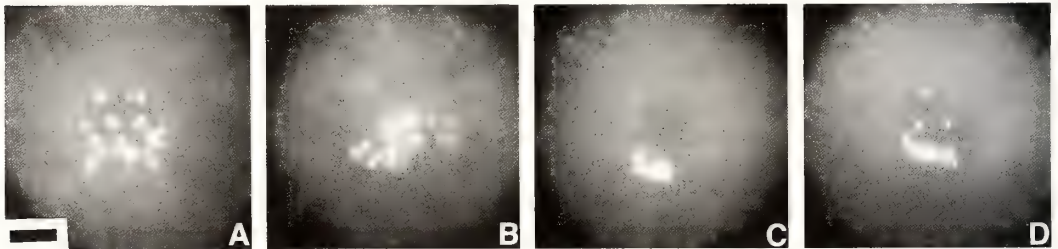


FIG. 1. The first mitotic phase after parthenogenetic treatment. The MA is a monaster; MTs arise from a single center.

A. NONPOLAR MA. Chromosomes arranged all around the monaster. **B.** Indication of formation of MONOPOLAR MA. Chromosomes arranged on side of the monaster, interpreted as a "metaphase" configuration on a wide half-spindle. Intermediate between A and C. **C.** Monopolar metaphase. **D.** MONOPOLAR MA in which some chromosomes are not engaged on metaphase plate.

These figures are fluorescence images of isolated MA stained for DNA with DAPI (4,6-diamidino-2-phenylindole). Haploid chromosome sets indicate that the eggs were in the first mitotic period after the parthenogenetic treatments. Bar=10 micrometers.

ence with sick MA in fertilized eggs. (My parthenogenetic MA are not sick; they are trying hard to make a good mitotic apparatus and are frustrated by the very improbability of the perfect renaturation of a centrosome.)

Figure 2 tells just about the whole story. Some of the chromosomes are engaged in a spindle and are going through a plausible anaphase. Other chromosomes are not engaged; they lie outside the spindle, experiencing a NONPOLAR mitosis. The photograph may or may not convince you of the observed fact that the chromosomes outside the spindle have split, as they should have done at the onset of anaphase. If you have noticed that one pole lacks an aster you are correct, although the evidence is clearer in Figure 3.

(6) Even when chromosomes are in a bipolar spindle, sister kinetochores may fail to make the right connections and are not always separated. One finds cases of non disjunction; sister chromosomes go to the same pole (Fig. 2).

(7) In many of the cases where bipolar MA are formed, the shapes of the poles may be strange. One may find no asters, or unequal asters or one pole with no aster. More interesting, in the light of the linear model of the centrosome that I will be proposing, are anaphases (Fig. 3A) or telophases

(Fig. 3B) which indicate that one group of chromosomes has *converged* toward a more compact pole while the other has moved on a *divergent* course, as though moving to a very flat pole. Such an image is incomprehensible if we think of a centrosome as a particle, but is reasonable according to the idea that a centrosome may have many shapes, depending on the folding of a long and linear fundamental structure [17, 18].

If interest in artificial parthenogenesis ever revives, the new devotees will have to think about the problem of timing. The first cell divisions in parthenogenetic embryos appear much later than they do in fertilized eggs. As shown in Figures 1 and 2, the timing of the chromosome cycle and of the provision of poles may be out of phase. The monopolar and more-or-less bipolar MA shown in Figures 1 and 2 both belong to the first mitotic cycle; chromosome numbers are haploid. Thus, at the same time on the chromosome clock, the poles have either failed to form (Fig. 1A); barely formed (Fig. 1B); formed as good MONOPOLAR (Fig. 1C); formed as a bad MONOPOLAR (Fig. 1D) or it may have started to make two poles, separated but usually pretty poor compared to normal poles. Eggs with good MONOPOLAR MA may go through another cycle to produce bipolar MA that distrib-

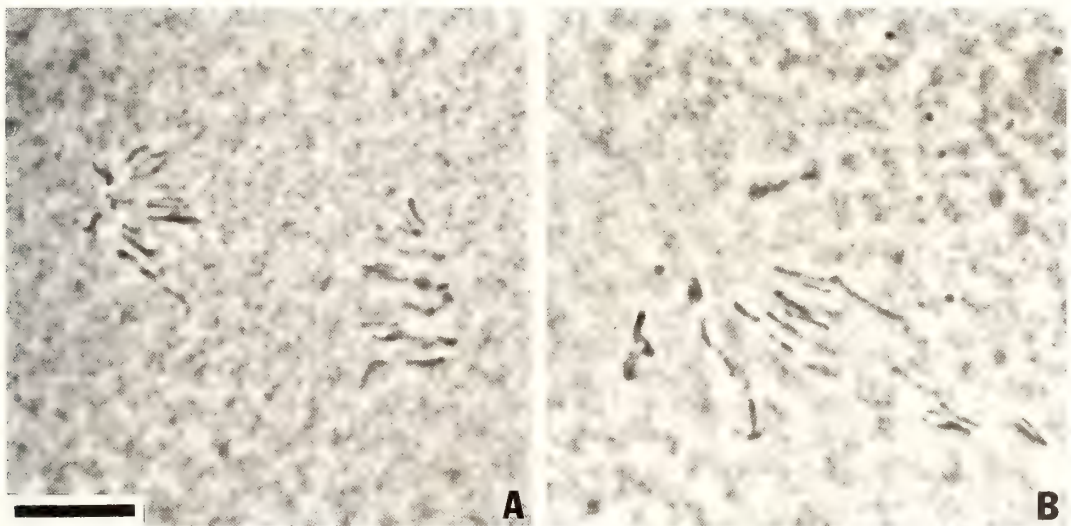


Fig. 2. Examples of defective bipolar MA in artificial parthenogenesis. Some chromosomes are not engaged in spindle; they have split but do not separate toward poles. Some of chromosomes on spindle appear double, indicating non-disjunction; sister chromosomes are going to same pole. Aceto-orcein squash preparations. Bar = 10 micrometers.

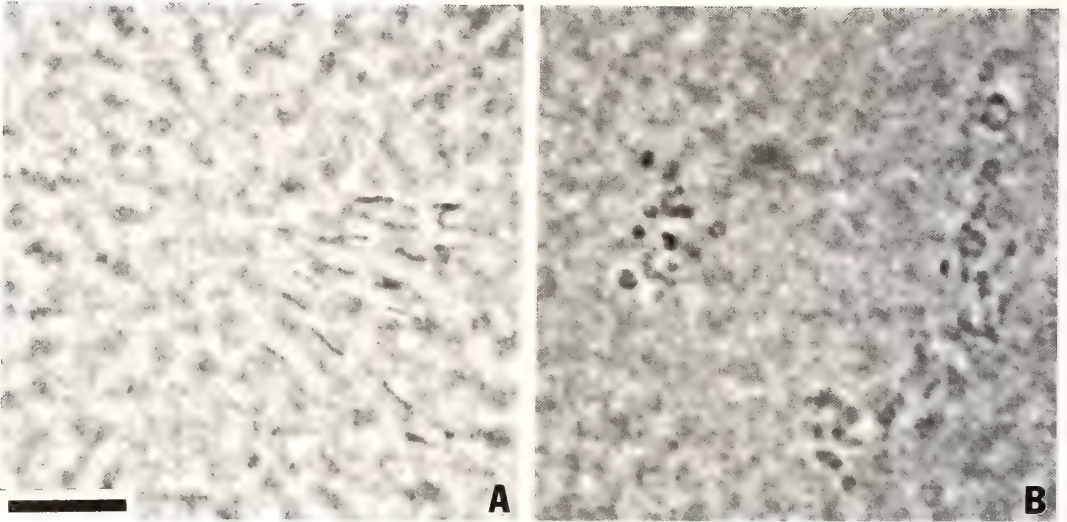


FIG. 3. Differences in shapes of poles. One group of chromosomes converges toward a compact pole while the other group diverges as though toward a very wide flat pole. The figures show rather extreme cases of this common occurrence. A. Anaphase. B. Telophase. Aceto-orcein squash preparations. Bar = 10 micrometers.

ute diploid complements of chromosomes. Then a gap in our information becomes evident. It arises from our habit of going home to dinner after a long day in the laboratory. A great many workers in this field must have had the same bad habit; they are content to report the numbers of "swimming embryos" seen on the next morning.

The observations I present above do explain why most of the parthenogenetic embryos develop so poorly. Aneuploidy is very likely. The aneuploidy will take its developmental toll progressively, as gene regulation becomes more important and the embryo can no longer depend on stored messages and modification of molecules in the cytoplasm.

A few papers in the literature describe the abnormal MA in artificial parthenogenesis. The paper of Wilson [14] and an excellent study by Marianne von Ledebur-Villiger [15] contain drawings that illustrate a number of the mitotic abnormalities I have presented as photographs. Von Ledebur-Villiger also made measurements of DNA content of parthenogenetic blastomeres which indicated the frequent occurrence of aneuploidy. My long study, from which I illustrate only a few examples, has been directed toward the varieties of defective poles as possible indications

of the process of renaturing centrosomes. The original concept of the centrosome as a "polar corpuscle" would not imply such flexibility.

We now see Step II as the restoration of MITOTIC POLES (mostly defective) in unfertilized eggs which would otherwise have produced a NONPOLAR MA. It would seem obvious that the effects of the hypertonic medium would arise from an increase in the internal concentration of ions or other solutes. That interpretation became doubtful with the discovery that Step II can be carried out by replacing normal cell water with D_2O . In my experience, D_2O does not work well with eggs of *Strongylocentrotus purpuratus* but sea water made up in D_2O is especially effective in experiments with *Lytechinus pictus*. (In a typical experiment, the eggs might be kept in sea water made up in concentrated D_2O between the 20th and 40th minute after Step I.) The eggs do not shrink, although cytoplasmic particles may aggregate into coarser clumps.

From what I have read, the behavior of electrolytes does not change so very much when the solvent is D_2O . So, one speculates that **the effects of hypertonic sea water depend less on the concentrations of intracellular solutes than they do on changes of the intracellular water.** The suspicion

would apply to the effects of hypertonic sea water as well as to those of D_2O . Hypertonic sea water at $1.5\times$ isosmolar would remove a great deal of the “free” water of the cell. At the very least, macromolecular—and even larger—units would become more crowded and interactive sites would come closer.

Speculation about water recalls the fate of theorists who, over the years, have indulged in special “cell water” (bound water, structured water) that is different from ordinary water. Cell water is an intoxicating beverage. At the moment, it is respectable to think about a role of more-structured water in the cell, thanks to the introduction of modern methods such as NMR. The time has come when colleagues are beginning to study changes of properties of water during the mitotic cycle in sea urchin eggs [20]. For my part, I do predict that the configuration of mitotic poles will become more explicable when we know more about cell water.

That is not a lot of progress from Boveri’s [5] comment (freely translated) that “...the transfer into the Loeb medium brings the egg protoplasm into a condition under which the egg centrosome can function. *If this explanation is correct then the effect of (hypertonic medium) has nothing in common with that of the spermatozoon, despite the same end-result*”.

The controversies about artificial parthenogenesis have played a large part in the evolution of our ideas about centrosomes. There can not be many questions more important than: **is the centrosome a universal, permanent, reproducing organ of the eucaryotic cell; or is it an agent that can be generated *de novo*?** A profound question, because the permanent, reproducing organ accounts logically for the fact that cells divide into two, generation after generation.

The centrosome was very much in decline at the time when we were students. The cytologists had failed to find it in many cells. The defect was not in their eyes, but in their erroneous preconception. **They were looking for a compact particle. The centrosome is not a particle.**

The closer study of artificial parthenogenesis directs us to a model of the centrosome. Reciprocally, the model helps us to understand the hap-

penings of parthenogenesis.

The model [17, 18] calls for a linear centrosome, very long in its extended form, more comparable in length to a chromosome than to a macromolecule. The thread (or ribbon) bears microtubule-initiating units; each unit determines the origin and the direction of a microtubule. The very long centrosome can fold in definite conformations; these conformations are expressed in the shapes of the microtubular structures they generate. The shapes of the centrosome change during the normal mitotic cycle [5, 17, 18]; correspondingly the shapes of poles change. The compact centrosomes at metaphase in sea urchin eggs generate pointed spindles, while the flattened centrosomes at late anaphase explain the more barrel-shaped spindles. The unusual shapes of poles that have been described above (Fig. 3A, 3B) would also be examples. Here I am citing facts, based on the resolution of centrosomes with the aid of anticentrosome antibodies as well as other criteria such as osmiophilia [11, 23].

Nowadays, anticentrosome antibodies are reassuring us that we can expect to find centrosome at mitotic poles in all kinds of cells and that the centrosomes are not necessarily compact particles and can change their shapes.

The model helps to explain some facts—and deficiencies—in the interpretation of artificial parthenogenesis as the renaturation of centrosomes.

(1) A deficiency—there is still no direct evidence for centrosomes in the mature unfertilized sea urchin egg. If a denatured centrosome is present, it may be present as a very much unraveled thread, too fine to have been resolved by the immunofluorescent staining reported so far.

(2) When a NONPOLAR MA results from the Step I treatment, it does seem to be organized by a centrosome. The centrosome is compact at this stage. It was identified originally by osmiophilic foci [6]. I am allowed to say that it can be identified with the help of anticentrosome antibodies (personal communication, H. and J. Schatten). It can still be considered to be a denatured centrosome; the postulated extended thread has collapsed into a randomly folded compact body that can not form a pole.

(3) Step II provides conditions for renaturation, but a *perfect* refolding of the extended thread will be rare. By the stage at which the cell cycle commands the formation of an MA, some regions of the centrosome may have the necessary configuration for MONOPOLAR behavior (generation of some sort of half-spindle) while other parts of the very large structure still can only function in the NONPOLAR mode.

The problem posed by the *cytasters* seem less formidable in the light of increasing experience. For the above description of the variants of the parthenogenetic MA, I used experiments in which there were no *cytasters*. In fact some of the MA observed had no asters at all—or asters could be unequal or poles could be very flat. The view that *cytasters* (generated *de novo*) are taking over the roles of mitotic poles does not describe what we actually see. In many cases where *cytasters* were present, they do not participate as poles. If mitotic poles came from *cytasters*, we would expect to find nice MONOPOLAR, BIPOLAR or MULTIPOLAR MA rather than the zoo of abnormal MA that is actually encountered.

There is no need to take your time with various explanations of *cytasters*. *Cytasters* may defy logic but they refuse to go away (I do not want to risk the seductions of Lawyer-Science in speaking to you who are a model of Scientist-Science.)

The idea of the linear centrosome invites experiments that test the ideas of its linearity, its native and denatured states and its expression as a mitotic pole. Indeed, we now have evidence that the conformation is sensitive to low temperatures [24]. In the experiments, the forms of the centrosomes were observed by staining with anticentrosome antibody. Fertilized eggs at a prometaphase stage were stored at 0°C. The centrosomes collapsed in a single compact mass. After return to normal temperature, the centrosome material unwound quickly as an irregular thread then reassociated to form a bipolar spindle with flat poles. The observation gives comfort to the hypothesis of the linear centrosome and some assurance that ideas about the unfolding and refolding of the centrosome thread can be defended.

As I reflect on centrosomes and mitotic poles and the fabrication of mitotic apparatus, I think of

your wonderful new work on unequal division, and memory goes back to 1952 and the first isolation of MA with unequal asters from clam eggs [25]. Your opinion that unequal asters can explain unequal division was a revelation to me then. Surely an unequal division that invokes an MA with asters of different size implies an MA whose poles are different. Therefore the centrosomes are different. What would you expect from experiments that look into differences in centrosomes at two poles of an MA? Can you imagine that differentiation seen in unequal divisions in cell lineages might be an expression of differentiation of centrosomes, manifested as differences of asters at the two poles of a decisive division?

If I were a better writer, I would know how to express every sentence of this letter as a question to you—?—, not as a statement... Then, I could be learning. We, your friends and your students and their students have been learning from you for half a century and it is we who are honored by this opportunity to thank you.

Your friend,

Daniel Mazia

ACKNOWLEDGMENT

I express my gratitude to Dr. Colin Pittendrigh, former Director of the Hopkins Marine Station, for calling me to Pacific Grove. It will be evident that much of the substance of this contribution comes out of collaborations with Dr. Neidhard Paweletz of the Deutsches Krebsforschungszentrum, Heidelberg and with Dr. Heide Schatten and Dr. Gerald Schatten, of the University of Wisconsin. The National Science Foundation to support my work through Grant DCB-8401901.

REFERENCES

- 1 Tyler, A. (1941) *Biol. Rev. Cambridge Philos. Soc.*, **16**: 291-335.
- 2 Loeb, J. (1909) *Die chemische Entwicklungserregung des tierischen Eies. (Kuenstliche Parthenogenese)*. Berlin, Julius Springer Verlag.
- 3 Baltzer, F. (1967) *Theodor Boveri; Life and Work*. (English translation by J. Oppenheimer). Univ. California Press, Berkeley.
- 4 Pauly, P. J. (1987) *Controlling Life*. Jacques Loeb

- and the Engineering Ideal in Biology. Oxford Univ. Press, New York.
- 5 Boveri, T. (1901) Zellen-studien IV. Ueber die Natur der Centrosomen. Fischer Verlag, Jena.
 - 6 Paweletz, N. and Mazia, D. (1979) Eur. J. Cell Biol., **20**: 37-44.
 - 7 Mazia, D. (1974) Proc. Natl. Acad. Sci., **72**: 690-693.
 - 8 Mazia, D., Paweletz, N., Sluder, G. and Finze, E.-M. (1981) Proc. Natl. Acad. Sci., **78**: 337-381.
 - 9 Bajer, A. S. and Mole-Bajer, J. (1979) In "Cell Motility: Macromolecules and Organelles". Ed. by S. Hatano, H. Ishikawa and H. Sato, Univ. Tokyo Press, Tokyo, pp. 569-592.
 - 10 Mazia, D., Harris, P. J. and Bibring, T. (1960) J. Biophys. Biochem. Cytol., **7**: 1-20.
 - 11 Paweletz, N., Mazia, D. and Finze, E.-M. (1984) Exp. Cell Res., **152**: 47-65.
 - 12 Sluder, G. (1978) In "Cell Reproduction". Ed. by E. R. Dirksen, D. M. Prescott and C. F. Fox, Academic Press, New York, pp. 563-570.
 - 13 Sluder, G. and Rieder, C. (1985). J. Cell Biol., **100**: 887-896.
 - 14 Wilson, E. B. (1901) Roux Arch. Entwicklungs-mech., **12**: 529-589.
 - 15 von Ledebur-Villiger, M. (1972) Exp. Cell Res., **72**: 285-308.
 - 16 Brandriff, B., Hinegardner, R. T. and Steinhardt, R. (1975) J. Exp. Zool., **192**: 13-24.
 - 17 Mazia, D. (1984) Exp. Cell Res., **153**: 1-15.
 - 18 Mazia, D. (1987) Int. Rev. Cytol., **100**: 49-92.
 - 19 Wilson, E. B. (1928) The Cell in Development and Heredity, 3rd. ed. Macmillan, New York.
 - 20 Schatten, H., Schatten, G, Mazia, D., Balczon, R. and Simerly, C. (1986) Proc. Natl. Acad. Sci., **83**: 105-109.
 - 21 Mazia, D. and Dan, K. (1952) Proc. Natl. Acad. Sci., **38**: 826-838.
 - 22 Mazia, D. (1975) Ann. N.Y. Acad. Sci., **253**: 7-13.
 - 23 Endo, S. (1980) Dev. Growth Differ., **22**: 509-516.
 - 24 Mazia, D., Schatten, H., Coffe, G., Szoেকে, E., Howard, C. and Schatten, G. (1987) J. Cell. Biol., **105**: no.4, part 2: 206a.
 - 25 Dan, K., Ito, S. and Mazia, D. (1952) Biol. Bull., **103**: 292.

The Living Spindle

SHINYA INOUÉ

Marine Biological Laboratory, Woods Hole, Massachusetts 02543, USA

ABSTRACT—Experience relating to earlier studies on the birefringence of the mitotic spindle and spindle fibers in living cells is first reviewed. This is followed by a description of the dynamic arrangement of microtubules in spindle fibers in living cells studied recently with high resolution video polarized light microscopy.

KD'S LAB

The urchin eggs had been collected, washed gently in a hand centrifuge, and mixed just minutes ago with a dilute sperm suspension. "What's the rate of fertilization?" KD (Dan-san, Dan-sensei, Professor Katsuma Dan) would ask. "75%? Better try another female," he'd say. "You'd just be kidding yourself if you worked with cells that aren't completely healthy." That was the way KD lived his science, and the way he trained the upstarts working in his laboratory.

The second floor laboratory at the Misaki Marine Biological Station, overlooking the waters of Aburatsubo and Moroisso Bay, was where so many of us were exposed to KD's challenges, to his way of biology, and to the enchantment of science. "The goddess of science is terribly jealous," he'd utter when he'd feel that we were not fully engaging our wits in carrying out an experiment. Or, he might even shout, "Try putting yourself in the animals' shoes!" when we'd missed accounting for a parameter that critically affected the organism or embryo.

Most of the time these criticisms seemed born more out of exasperation rather than as tongue lashing from a hard task master. Even those who felt cowed or rebellious at these words were working in KD's lab because that was simply what they wanted to do. They were neither paid assistants nor students who were required to be there. They were a school teacher, a brash graduate student, a junior colleague, or one just fascinated by biology;

anyone who cared enough to be there and who dared take on the challenge. That was the makeup of those who frequented KD's and Jean's laboratory in the early post-war days (ca. 1946–1949).

To Jean and KD who had survived the double hardships of raising a young family and keeping up research under the challenging conditions of the bombed-out nation, while coping with the complex adjustments of a couple whose countries were in mortal conflict, those post-war days brought forth incalculable strength, joy, and optimism. Their mood pervaded the Laboratory just returned to the Japanese biologists and students by the occupation forces (with KD's intervention: "The last one to go," now prominently featured at the MBL Library in Woods Hole).

KD's cramped lab, saturated with the scent of marine organisms, bustled with activity oblivious to, and actually challenged by, the absence of all but a few essential tools for research. Some mornings the marine scent would be taken over by the delectable aroma of buttered toast smeared with honey that Jean and KD would share with us. Jean would have rounded up the butter, and the honey had been spun from KD's own hives in Nagai.

In the lab, Kayo was raising miniature adult sand dollars from the four blastomeres she'd cut apart free hand, KD and Jean were busy writing up their papers on the role of spindle elongation in astral cleavage, Endo-san had given up his hardware business to explore fertilization, and I was tinkering with pieces of optics trying to visualize spindles in living sea urchin eggs following Runnström's (in fixed plant cells [1]) and Schmidt's [2]

earlier observations.

SPINDLE BIREFRINGENCE

With a mercury arc lamp and a pair of calcite prisms loaned us by Professor Koana rigged to the microscope, and with the window shades drawn tught, we finally caught glimpses of the football-shaped birefringence just before each division of the transparent *Clypeaster* and *Spirocodon* eggs. Those were the spindles that we had attempted to see at KD and Jean's home in Kudan during an airraid blackout (ca.1942).

There was no question that we could detect the spindle birefringence now, that was, until I readjusted the microscope (while observing the back aperture of the objective lens to maximize the extinction). What I'd believed would give us a much better image had made the spindle birefringence disappear altogether. "See, I told you to leave well enough alone," was KD's admonishment. Red-faced, I continued to tinker for another month before it dawned on me that the strain birefringence in the lens was not hindering us, but was in fact helping us visualize the weakly birefringent spindle. The lens was acting as a compensator and raising the contrast and field brightness!

Through such a hard lesson, how could one ever forget how helpful the bias retardation is [3]. As I learned then (and Michael Swann and Murdoch Mitchison were also finding out in Edinburgh half way around the globe [4]), a low retardation compensator not only allows us to measure the birefringence, but is indeed an indispensable friend for the biologist who is trying to visualize the orderly but dynamic alignment of just a few molecules in the living cell (Fig. 1). In retrospect, W. J. Schmidt in Giessen had figured this out a decade before us, but my poor performance in the three year German classes had ill-equipped me to grasp the important teachings in Schmidt's two classic volumes [2, 5].

JEAN'S HOMECOMING

From Jean who had just visited her homeland, there was doubly good news. As a present for KD, she had secured (with support from the American

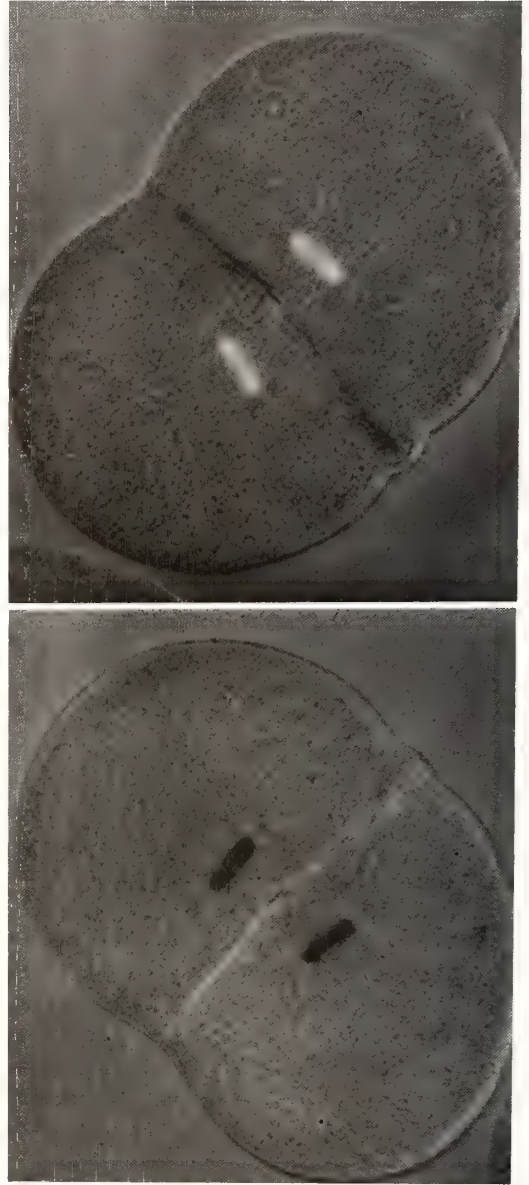


FIG. 1. Birefringence of dividing egg of a jellyfish *Spirocodon saltratrix*. The mitotic spindle and astral rays exhibit a longitudinally positive birefringence while the cell surface exhibits a tangentially negative birefringence. From Inoué and Dan [3].

Philosophical Society) one of the first phase contrast microscopes produced by Bausch and Lomb in Rochester, New York. She had also arranged that I apply to graduate school at Princeton, with a loan from her sister Peggy Chittick of Bridgeport,



FIG. 2. Birefringence of spindle fibers and fibrils in *Chaetopterus* oocyte. From Inoué [8].

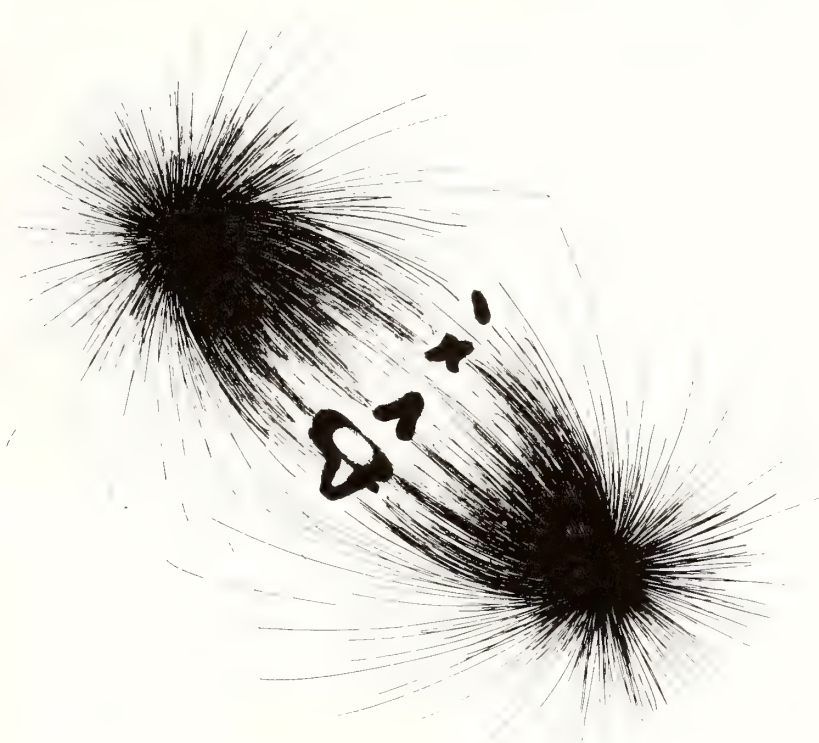


FIG. 3. Detailed structure of *Chaetopterus* spindle (Fig. 2) as I interpreted in 1951 [8].

Connecticut, to help finance the trip.

The phase microscope, as documented in KD's autobiography [6], led Jean back into the lime light of biology and to her discovery of the sperm acrosomal reaction [7]. I myself in the meantime had sped to Princeton, and to Woods Hole about which we had heard so much from KD and Jean.

SPINDLE FIBERS

With guidance and encouragement from my mentor Kenneth Cooper at Princeton and with help from the Osterhouts in Woods Hole, using a moderately improved polarizing microscope I was able to settle a 50-year controversy regarding the reality of spindle fibers and fibrils in intact living cells (Figs. 2-4, [8]). So entrenched was the idea that spindle fibers were invisible in living cells that E. B. Harvey, upon first seeing my time-lapse movies in the Lillie Auditorium asked, "Were

those cells alive?" She could not accept the fact that the dividing *Chaetopterus* and *Lilium* cells which distinctly showed the spindle fibers (owing to their weak but distinctly higher birefringence) were in fact alive!

Albert Tyler from Cal. Tach. was also at the MBL in Woods Hole those summers (1949-1950). At his suggestion, I looked into the effects of colchicine on spindle birefringence. In dilute colchicine protected from blue light, the birefringence of the metaphase-arrested *Chaetopterus* spindle faded away in just a few minutes. The chromosomal spindle fibers were the last to go. As they were disappearing, the fibers would shorten (without fattening) and pull the chromosomes and inner centrosome to the animal pole surface where the outer spindle pole was anchored [8, 9]. When colchicine was washed out, the spindle and its birefringence grew back.

This experience with colchicine, and later with

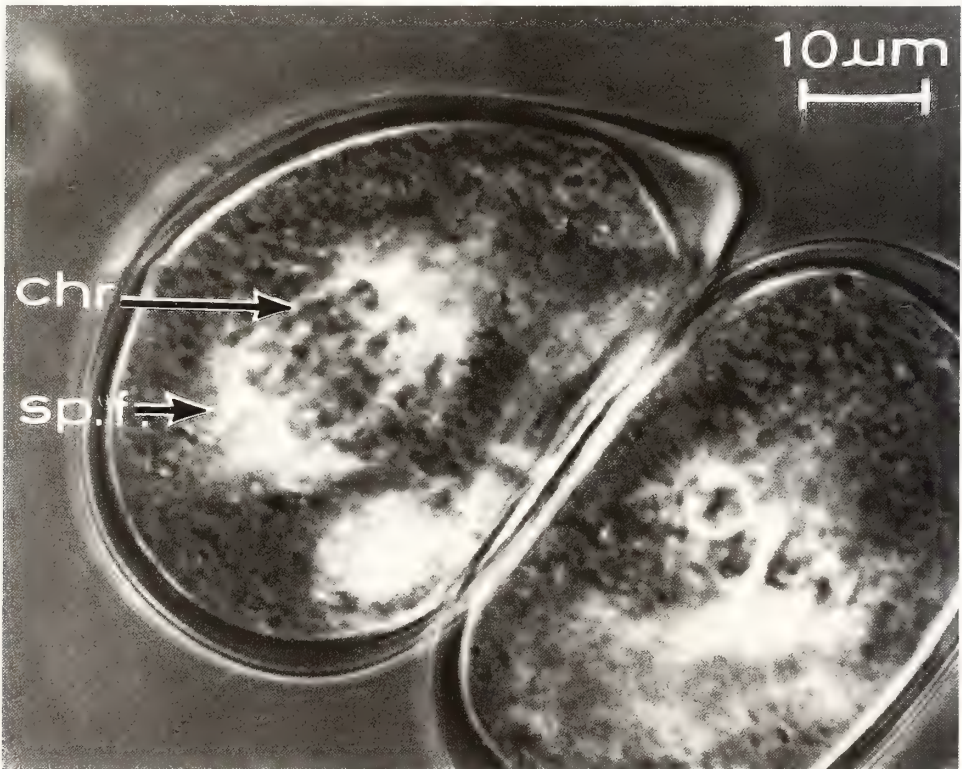


FIG. 4. Spindle fiber birefringence. Early anaphase in pollen mother cell of Easter lily. Chr: chromosome, spf: spindle fiber [8].

low temperature and high hydrostatic pressure, gave birth to the notion that spindle and astral fibers and their fibrils (later shown to be microtubules) could dynamically assemble from preformed subunits and grow, and that they could disassemble and shorten [10–12]. In other words, the spindle fibers and fibrils could polymerize and push, or depolymerize and pull [13].

ISOLATED SPINDLE

A few years after my early MBL days, KD was visiting Dan Mazia who had recently been appointed to the faculty at the University of California at Berkeley. Dan was a long standing friend of both KD's and Jean's from their Pennsylvania and Woods Hole days in the early 1930s. In the basement lab of the Medical School in Seattle where I was an Instructor at the University of Washington, I got an excited call from Dan who told me that he and KD had just figured out to isolate the mitotic apparatus [14]. Could he fly up with some samples to see if the isolates were birefringent? Next day Dan was bubbling with excitement at the reassuring sight under my polarizing scope, now significantly refined mechanically thanks to inputs from my colleague Wayne Thornburg and chairman Stan Bennett.

After establishing the positive birefringence of the isolated mitotic apparatus, Dan and I decided that the isolate's response to colchicine would reveal how native the isolates were. But, as the colchicine solution that we perfused had just reached the isolates under the slide, the microscope field and the room went completely dark. Fortunately we had already photographed several isolates before the power went out, but we had no clear answer regarding the sensitivity of the isolates to colchicine.

The inability of colchicine to affect the isolates (event those isolated according to more recent, gentler methods that yield spindles which depolymerize in the cold) still remains an enigma today. Once the conditions required to maintain colchicine sensitivity in the isolates are found, we will presumably also have found the conditions needed to reliably study anaphase movement in the isolates. Unlike striated muscle and cilia, the

mitotic structures have tenaciously refused to reveal their force-generating machinery.

VIDEO ENHANCEMENT

Many years later, KD and Kayo were visiting my laboratory at the MBL in Woods Hole. The scope was now equipped with a rectifier with a rectifier for DIC as well as for pol, and we could directly image the spindle in the somewhat opaque *Spisula* egg thanks to the contrast enhanced by video.

On his previous visit to the States, KD had worked together with Sus Ito from Harvard [15]. The two had isolated *Spisula* spindle with asymmetric asters and related these to their role in asymmetric cleavage. Now with time-lapsed, video-enhanced polarized light microscopy, we could directly follow the growth, migration, and striking oscillation of the spindle seeking its polar anchorage point [9, 16]

The dynamic behavior of the spindle, centrosomes, and asters, presumably reflecting the life-like extension and shortening of their microtubules, continues to amaze and challenge investigators (e.g., see [17, 18]). And as we improved the imaging capability of the microscope, the dynamic behavior of each individual microtubule became ever more evident.

In the next section of this paper, I shall describe some observations that Ted Salmon, Lynn Casimeris, and I made on dividing newt lung epithelial cells, using a recent version of the high extinction polarizing microscope. Despite KD's admonition, I had not, since those days at the Misaki Labs, been able to leave the microscope alone.

MICROTUBULE DYNAMICS IN SPINDLE FIBERS

The following observations were made with the high extinction polarizing microscope recently equipped with a fiber optic light scrambler [19; 20, Figs. III-11,12]. The scrambler provides a high intensity, uniform illumination that homogeneously fills the back aperture of the N.A. 1.35 rectified condenser (made by Nikon for Plan Apo objective lenses). Illuminated with this condenser, the video-enhanced image, formed with the new

(1987) series N.A. 1.4 Plan Apo objective lenses, gives a depth of field as shallow as $0.1\ \mu\text{m}$ in polarized light microscopy [21].

The newly available shallow depth of field (i.e., outstanding optical sectioning capability and very high axial resolution) was now coupled with the inherently high lateral resolving power and the further improved corrections just incorporated by Nikon and Zeiss in the new series 1.4 N.A. Plan Apochromatic objective lenses.

When the contrast of the faint polarized light image produced by this high resolution system was enhanced with video (analog output of Dage/MTI model 65 Newvicon camera digitally processed, in continuous background subtraction and 4-frame jumping average mode, with Universal Imaging's Image-1/AT [20, 22]), the behavior of individual microtubules and their bundles could be clearly captured in the live, newt (*Taricha granulosa*) lung epithelial cells (Figs. 5–8).

In early prometaphase of the *Taricha* cells, we

find a discrete, positively birefringent thread, about $1\ \mu\text{m}$ in diameter, attached to the kinetochore of each chromosome. According to Rieder's high voltage EM studies, the thread is a bundle of a dozen or so, tightly-packed, parallel microtubules [25]. Polewards, beyond the birefringent "bundle" or "cable", the microtubules splay apart from each other, then mix with polar microtubules as well as other kinetochore microtubules (Figs. 5 and 6). Each cable alternately grows and shortens with the progression of prometaphase, but on the whole they gradually shorten so that by the onset of anaphase few cables are present.

Throughout prometaphase to anaphase, short, very weakly birefringent "rods" appear and disappear stochastically throughout the spindle. The rods are regions of microtubules, including the kinetochore microtubules splayed poleward from the bundle, which transiently associate with other microtubules in parallel pairs over a few micron lengths. The transient lateral associations each last



FIG. 5. Prometaphase in newt lung epithelial cell [24]. See Fig. 6 for interpretation of this video-enhanced, high-resolution polarized light image.

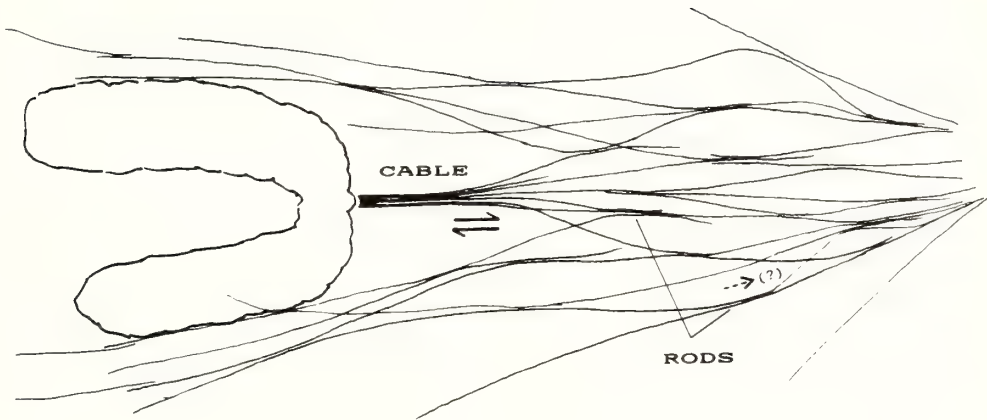


FIG. 6. Schematic of microtubule distribution and behavior as interpreted from dynamic playback of laser disk recordings of the video-enhanced, high-resolution polarized light images such as those in Figs. 5, 7, and 8 [23]. Note the remarkable similarity of this schematic to those by Nicklas *et al.* derived by another approach, i.e., serial thin section electron microscopy [27].



FIG. 7. Early anaphase of cell shown in Fig. 5 [23]. The birefringent cables are mostly gone and replaced by many short-lived birefringent rods. (See Fig. 6 for definition of cable and rod.)



FIG. 8. Telophase of the same cell in Figs. 5 and 7. In such very thin optical section, the density of microtubules is low enough so that individual microtubules are clearly imaged (arrow). ([23]; see [22, 24] on microtubule distribution in *Haemaphysalis* endosperm, observed in fixed cells stained with immuno-gold antitubulin, also with digitally enhanced high resolution polarized light microscopy).

for only a few seconds, but on the whole they form what could be considered a fringed micellar structure (Figs. 6 and 7).

According to these observations, what was called a chromosomal spindle fiber in the classical literature (e.g., see Schrader [26]), or that we observed with lower resolution in polarized light microscopy [8, 10, 13], turns out to be a mixture of kinetochore and non-kinetochore microtubules. The different microtubules in the chromosomal spindle fiber stochastically associate laterally with each other and presumably form an anastomosing, fringed micellar gel.

We believe that the fringed micelle structure, formed by the short-lived, dynamic lateral association between microtubules, explains the modest mechanical integrity of the whole spindle and of the chromosomal and other spindle fibers. It also accounts for their lability when repetitively teased

with a glass microneedle [27,28].

The dynamic fluctuation of microtubules due to transient lateral association (or zipping as the Bajers may prefer to call it), presumably together with the dynamic instability of the microtubules (see below), also accounts for the Northern lights flickering of spindle fiber birefringence that is seen at lower resolution [10].

AND NOW?

Given the dynamic lateral association coupled with the dynamic instability of microtubules (wherein each microtubule extends steadily until it suddenly undergoes rapid shortening as postulated by Tim Mitchison and Mark Kirschner [17] and observed under the light microscope by Horio and Hotani [29] and ourselves—see companion paper by Inoué [30]), it is no wonder that microtubules

exhibit complex life-like behavior.

In addition to the dynamic properties of the fibrillar microtubules themselves, also calcium-regulating vesicles, microtubule-associated proteins, and other factors modulate the stability of the microtubules in local parts within a living cell. Together they account for the dynamic, enigmatic behavior of the centrosomes, spindle fibers, and asters, which govern much organizational activity so crucial to the cell's survival and proper function.

In exploring these mysteries, on the one hand, the diversity of pattern expressed by different life forms may provide us with clues, by exaggerating or omitting some elements involved in the complex set of interactions (e.g., see [26, 31–33]).

On the other hand, we need to learn much more about the state of the microtubules and modifying factors, not only as isolated purified elements, but as they function *dynamically* and *locally* in intact living cells.

To this end, direct studies of living cells with the light microscope as a non-invasive, analytical probe should play increasingly important roles, especially when combined with video. Images with high lateral and axial resolution can provide better 3-dimensional insight (Fig. 8), and the video-enhanced contrast can reveal subtler changes in fine structure and molecular organization of living cells with reduced exposure to light [20].

We should also use the microscope more effectively to modify minute targeted regions in living cells, not only with UV or other high energy irradiation, but with wavelengths and energy levels selected to induce subtler chemical modifications [34–36]. Combined with a good choice of reagents that are activated or inhibited by those wavelengths, we can better probe for local factors that govern the intricate, dynamic organization of the living cell and its spindle.

ACKNOWLEDGMENT

This paper is dedicated to Professor Katsuma Dan on his 83rd birthday. I recall with great pleasure the support and challenges provided by KD, which started as early as 1941 when I was still a student at the Musashi Higher School. The recent work described here and preparation of the manuscript were supported by NIH grant R37 GM31617–06 and NSF grant DCB 8518672.

REFERENCES

- 1 Runnström, J. (1929) Über die Veränderung der Plasmakolloide bei der Entwicklungserregung des Seeigelleies. II. Protoplasma, **5**: 201–310, Fig. & Table 4.
- 2 Schmidt, W. J. (1937) Die Doppelbrechung von Karyoplasma, Zytoplasma und Metaplasma. Protoplasma-Monographien, Vol. 2. Gebrüder Borntraeger, Berlin.
- 3 Inoué, S. and Dan, K. (1951) Birefringence of the dividing cell. J. Morphol., **89**: 423–455.
- 4 Swann, M. M. (1951) Protoplasmic structure and mitosis. II. The nature and cause of birefringence changes in the sea-urchin egg at anaphase. J. Exp. Biol., **28**: 434–444.
- 5 Schmidt, W. J. (1934) Polarisationsoptische Analyse des submikroskopischen Baues von Zellen und Geweben. In "Handbuch der biologischen Arbeitsmethoden." Ed. by E. Aberhalden, Urban und Schwarzenberg, Berlin and Vienna, Sec. 5, Part 10, pp. 435–665.
- 6 Dan, K. (1987) "Uni toh kataru." (Dialogue with sea urchin.) Gakkai Shuppan Center, Tokyo.
- 7 Dan, J. C. (1954) Studies on the acrosome. II. Acrosome reaction in starfish spermatozoa. Biol. Bull., **107**: 203–218.
- 8 Inoué, S. (1953) Polarization optical studies of the mitotic spindle. I. The demonstration of spindle fibers in living cells. Chromosoma, **5**: 487–500.
- 9 Lutz, D. A., Hamaguchi, Y. and Inoué, S. (1988) Micromanipulation studies of the asymmetric positioning of the maturation spindle in *Chaetopterus* sp. oocytes. I. Anchorage of the spindle to the cortex and migration of a displaced spindle. Cell Motility and Cytoskeleton, in press.
- 10 Inoué, S. (1964) Organization and function of the mitotic spindle. In "Primitive Motile Systems in Cell Biology". Ed. by R. D. Allen and N. Kamiya, Academic Press, New York, pp. 549–598.
- 11 Inoué, S. (1981) Cell division and the mitotic spindle. J. Cell Biol., **91**: 131s–147s.
- 12 Inoué, S., Fuseler, J., Salmon, E. D. and Ellis, G. W. (1975) Functional organization of mitotic microtubules. Physical chemistry of the in vivo equilibrium system. Biophys. J., **75**: 725–744.
- 13 Inoué, S. and Sato, H. (1967) Cell motility by labile association of molecules. J. Gen. Physiol., **50**: 259–292.
- 14 Mazia, D. and Dan, K. (1952) The isolation and biochemical characterization of the mitotic apparatus of dividing cells. Proc. Natl. Acad. Sci., **38**: 826–838.
- 15 Dan, K. and Ito, S. (1984) Studies of unequal cleavage in molluscs. I. Nuclear behavior and anchorage of spindle pole to the cortex as revealed

- by isolation technique. *Dev. Growth Differ.*, **26**: 249–262.
- 16 Dan, K. and Inoué, S. (1987) Studies of unequal cleavage in molluscs. II. Asymmetric nature of the two asters. *Int. J. Invertebr. Reprod. Dev.*, **11**: 335–353.
 - 17 Mitchison, T. and Kirschner, M. (1984) Dynamic instability of microtubule growth. *Nature*, **312**: 237–242.
 - 18 Salmon, E. D., Leslie, R. J., Saxton, W. M., Karow, M. L. and McIntosh, J. R. (1984) Spindle microtubule dynamics in sea urchin embryos: Analysis using a fluorescein labelled tubulin and measurements of fluorescence redistribution after photobleaching. *J. Cell Biol.*, **99**: 2165–2174.
 - 19 Ellis, G. W. (1985) Microscope illuminator with fiber optic source integrator. *J. Cell Biol.*, **101**: 83a.
 - 20 Inoué, S. (1986) *Video Microscopy*. Plenum, New York.
 - 21 Inoué, S. (1988) Imaging of unresolved objects, superresolution, and precision of distance measurement, with video microscopy. In "Fluorescence Microscopy of Living Cells in Culture: Quantitative Fluorescence Microscopy: Imaging and Spectroscopy". Ed. by D. L. Taylor and Y.-L. Wang, *Methods in Cell Biology*, Vol. 30, Academic Press, New York. In press.
 - 22 Inoué, S. (1987) Video microscopy of living cells and dynamic molecular assemblies. *Applied Optics*, **26**: 3219–3225.
 - 23 Cassimeris, L., Inoué, S. and Salmon, E. D. (1988) Microtubule dynamics in the chromosomal spindle fiber: Analysis by fluorescence and high resolution polarization microscopy. *J. Cell Motil. Cytoskeleton*, in press.
 - 24 Inoué, S., Molè-Bajer, J. and Bajer, A. S. (1985) Three-dimensional distribution of microtubules in *Haemanthus* endosperm cell. In "Microtubules and Microtubule Inhibitors". Ed. by M. De Brabander and J. De Mey, Elsevier, Amsterdam, pp. 15–30.
 - 25 Rieder, C. and Bajer, A. S. (1977) Heat-induced reversible hexagonal packing of spindle microtubules. *J. Cell Biol.*, **74**: 717–725.
 - 26 Schrader, F. (1953) *Mitosis. The Movements of Chromosomes in Cell Division*. Columbia Univ. Press, New York, 2nd ed.
 - 27 Nicklas, R. B., Kubai, D. F. and Hays, T. S. (1982) Spindle microtubules and their mechanical associations after micromanipulation in anaphase. *J. Cell Biol.*, **95**: 91–104.
 - 28 Begg, D. A. and Ellis, G. W. (1979) Micromanipulation studies of chromosome movement. II. Birefringent chromosomal fibers and the mechanical attachment of chromosomes to the spindle. *J. Cell Biol.*, **82**: 542–554.
 - 29 Horio, T. and Hotani, H. (1986) Visualization of the dynamic instability of individual microtubules by dark-field microscopy. *Nature*, **321**: 605–607.
 - 30 Inoué, S. (1988) Manipulating single microtubules. *Protoplasma: Noburo Kamiya Festschrift*, in press.
 - 31 Bělař, K. (1926) Der Formwechsel der Protistenkerne. *Ergeb. Fortschr. Zool.*, **6**: 1–420.
 - 32 Inoué, S. and Ritter, H., Jr. (1978) Mitosis in *Barbulanympha*. II. Dynamics of a two-stage anaphase, nuclear morphogenesis, and cytokinesis. *J. Cell Biol.*, **77**: 655–684.
 - 33 Wilson, E. B. (1928) *The Cell in Development and Heredity*. Macmillan, New York, 3rd ed.
 - 34 Englemann, Th. W. (1882) Ueber Sauerstoffausscheidung von Pflanzenzellen im Mikrospektrum. *Bot. Zeitung*, **40**: 419–426.
 - 35 Aronson, J. and Inoué, S. (1970) Reversal by light of the action of N-methyl N-desacetyl colchicine on mitosis. *J. Cell Biol.*, **45**: 470–477.
 - 36 Hiramoto, Y., Hamaguchi, M. S., Nakano, Y. and Shoji, Y. (1984) Colcemid UV-microirradiation method for analyzing the role of microtubules in pronuclear migration and chromosome movement in sand-dollar eggs. *Zool. Sci.*, **1**: 29–34.

Measurement of Spindle Birefringence by the Optical Integration Method

YOSHITARO NAKANO¹ and YUKIO HIRAMOTO²

Biological Laboratory, Tokyo Institute of Technology, Tokyo 152, Japan

ABSTRACT—A method was developed to determine the total amount of birefringence within a given area in the field of a polarization microscope using photometry (optical integration method). By setting a Brace-Köhler compensator inserted in the optical path at 20° in reference to the crossed polarizer and analyzer axes, it was possible to integrate the phase retardation over an area in the specimen by measuring the light intensity passing through that area. Because the integral of the phase retardation along the cross line of the mitotic spindle is proportional to the number of microtubules in the cross-section that contains the cross-line in echinoderm eggs, the number of microtubules in the cross-section could be determined from the intensity of the light passing through a rectangular area crossing the spindle. Distribution of the number of microtubules in the cross-section of the spindle along its axis was determined at various stages of mitosis in eggs of the sand dollar, *Clypeaster japonicus*. Effects of Colcemid on the microtubule distribution in the mitotic spindle were determined by measuring the change in birefringence distribution in the spindle after application of seawater containing Colcemid to the egg in mitosis.

INTRODUCTION

The structure of the mitotic spindle has been examined by many investigators using polarization microscopy since Inoué [1] showed the presence of birefringent fibers in the mitotic spindle in living cells. Electron microscopic studies have shown that many microtubules are present parallel to the axis of the spindle and that spindle fibers observed by light microscopy are the bundles of microtubules. Sato *et al.* [2] concluded that the birefringence of a spindle isolated from a starfish oocyte is caused mainly by microtubules in the spindle, by making a quantitative comparison of the measured birefringence and form birefringence expected theoretically from the number of microtubules in the spindle determined by electron microscopy. Hiramoto *et al.* [3, 4] extended this conclusion to living sand dollar eggs by their quantitative analysis of the spindle birefringence, and concluded that

the number of microtubules in the spindle can be estimated by measuring the birefringence of the spindle in living cells. However, it took a full minute or so to obtain a single birefringence distribution in a cross-section using their method. An increase in the speed of measurement is required because the spindle structure changes considerably within this period.

In the present study, we devised a method to determine the integral of the birefringence phase retardation over an area in a microscopic field, where the retardation is not uniform, by measuring light intensity passing through that area by polarization microscopy (optical integration method). We succeeded in obtaining the distribution of microtubules in the spindle at various stages of first mitosis in sand dollar eggs whereby each measurement was possible within 10 sec.

OPTICAL INTEGRATION METHOD FOR POLARIZATION MICROSCOPY

We used a microscopic birefringence detection system described by Hiramoto *et al.* [3] to make birefringence measurements. The system consisted of a polarization microscope with a rectified

Accepted April 21, 1988

¹ Present address: Instruments Division, Nikon Corporation, Sakae-ku, Yokohama 244, Japan.

² To whom reprints should be requested at the following address: The University of the Air, Wakaba, Chiba 260, Japan.

condenser and rectified objectives, a system to illuminate a limited area in the specimen on the microscope stage with 546 nm monochromatic light, and a system to measure and display the intensity of light passing through a definite area at the center of the illuminated area. A Brace-Köhler compensator with 27.7 nm (0.319 radian) retardation for 546 nm monochromatic light was inserted between the crossed polarizer and analyzer in the optical path.

Hiramoto *et al.* [3] showed that the intensity of the light passing through the same microscopic birefringence detection system as used in the present study changed as expected from Jerrard's theoretical equation [5] when the compensator angle was changed. According to Jerrard [5], the intensity (I) of the light passing through the crossed polarizer and analyzer, between which a compensator plate and a birefringent specimen are inserted, is given by

$$I = I_0 \left[\sin^2 \frac{\delta_1}{2} \cos \delta_2 \sin^2 \gamma_1 + \frac{1}{2} (\sin \delta_1 \sin \delta_2 \sin 2\gamma_1) + \sin^2 \frac{\delta_2}{2} \right] \quad (1)$$

where I_0 is the intensity of the light emerging from the polarizer, γ_1 and δ_1 are the azimuth and the phase difference of the compensator plate, respectively, and γ_2 and δ_2 are those of the specimen whose axis is set at 45° to the polarizer axis (cf. [3]). In the present measurements where δ_1 was 0.319 radian,

$$I = I_0 [0.0252 \cos \delta_2 \sin^2 \gamma_1 + 0.157 \sin \delta_2 \sin 2\gamma_1 + \sin^2 (\delta_2/2)]. \quad (2)$$

As shown in this equation, the relation between I and δ_2 (retardation of the specimen) is not linearly related when γ_1 (azimuth of the compensator) is small. However, the relation approaches linear if the azimuth of the compensator is increased. The solid curve in Figure 1 indicates the theoretical relation between I and δ_2 when the compensator plate is set at 20° ($\gamma_1 = 0.349$ radian), in which I increases almost linearly as δ_2 increases at a rate of 0.126/nm.

This relation between I and δ_2 was confirmed by the following experiment. Chips of mica pre-

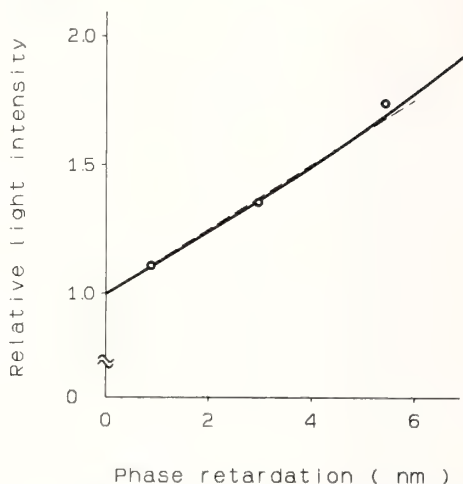


FIG. 1. Relation between the intensity of light passing through the specimen and its birefringence phase retardation in the optical system used.

Light intensity is expressed by the ratio to the light intensity of the background without birefringence. Solid line indicates the relation calculated from Jerrard's theoretical equation [5]. Circles indicate experimental results using mica chips. Broken line indicates the inclination of 0.13/nm retardation.

pared by grinding mica plates in a Waring blender and suspending them in water were put on the stage of the birefringence detection system. The light passing through the chips was determined at various points of uniform phase retardation. The retardation was determined at the same points by the ordinary extinction method (by finding the compensator angle in which light intensity becomes minimal). As shown by the open circles in Figure 1, the experimental results almost fit the theoretical curve. This implies that the phase retardation (δ_2) of the specimen can be determined from the ratio (x) of the intensity of the light passing through the specimen to the intensity of the light passing through the same area without birefringence by the equation

$$\delta_2 = (x-1)/0.126 = 7.9(x-1) \quad (\text{nm}). \quad (3)$$

Because the retardation in every part of the specimen is proportional to $x-1$ in it, the average phase retardation in an area where the retardation is uneven can be determined by the same method. The retardation can be integrated over a region from the total intensity of light passing through

that region using

$$B = (7.9 \times 10^{-7})a(x-1) \quad (4)$$

where B is the integral of the birefringence (in cm^3) over the region ($a \text{ cm}^2$ in area).

THE NUMBER OF MICROTUBULES IN THE SPINDLE OF SAND DOLLAR EGGS DURING MITOSIS

The number of microtubules at various points in the spindle at various stages of first mitosis was determined in eggs of the sand dollar, *Clypeaster japonicus* by the optical integration method mentioned above.

Principle of the determination of microtubule numbers in cross-section of the spindle

The birefringence of the spindle is mainly due to the form birefringence of microtubules aligned in parallel to the spindle axis in echinoderm eggs [2, 4]. According to Hiramoto *et al.* [4], the number of microtubules per unit cross-section of the spindle is proportional to the coefficient of birefringence of the spindle, and the total number of microtubules in the cross-section of the spindle in the living cell (N_L) is given by

$$N_L = (2.08 \times 10^{13})M_L \quad (5)$$

where M_L is the areal integral of the coefficient of birefringence over the cross-section of the spindle (in cm^2).

The areal integral of the coefficient of birefringence over the cross-section of the spindle, viz. the integral of the retardation along the cross-line of the spindle (M_L), can be determined from the intensity (I_S) of light passing through a rectangular area whose long sides cross the spindle perpendicularly and cover the spindle width.

Thus,

$$M_L = (7.9 \times 10^{-7})L(I_S/I_B - 1) \quad (6)$$

in which L is the length (in cm) of the long side of the rectangular area crossing the spindle and I_B is the intensity of light passing through an area in the background with the same size and the same absorption as the rectangular area crossing the spindle.

From Eqs. 5 and 6 the total number of microtubules (N_L) in the cross-section of the spindle is given by

$$N_L = (1.65 \times 10^7)L(I_S/I_B - 1) \quad (7)$$

Materials and procedure of measurement

Eggs were deprived of fertilization membranes and hyaline layers by treating with a 1 M urea solution for 1 min shortly after insemination and kept in Ca-free artificial sea water (Ca-free Jamarin-U; Jamarin Laboratory, Osaka). Shortly before the onset of mitosis, they were put into normal artificial sea water (ASW, Jamarin-U), and then placed on a poly-L-lysine-coated glass slide. Pieces of polyester film $60 \mu\text{m}$ in thickness were used as spacers, and a cover-slip was put over them. Because the eggs were compressed between the glass slide and cover-slip, most spindles in mitosis were oriented in parallel to the plane of the glass slide.

An egg at the onset of first mitosis was brought into the microscopic field of the birefringence detection system, and the spindle axis was oriented at 45° in reference to the polarizer axis. The azimuth of the compensator was set at 20° . A rectangular area ($18 \mu\text{m} \times 4 \mu\text{m}$) at the plane of the specimen was illuminated with 546 nm monochromatic light by inserting a rectangular window of an appropriate size at the plane conjugate to the specimen plane, in reference to the condenser lens so that the long sides of the window image might cross the spindle axis at right angles. The intensity of light passing through the rectangular window corresponding to $15 \mu\text{m} \times 1 \mu\text{m}$ at the center of the illuminated area was cast on the photocathode of a photomultiplier tube to measure the intensity of the light after passing through another window placed at the plane conjugate to the specimen plane in reference to the objective lens (cf. [3]).

A point on the extension of the spindle axis was brought to the center of the illuminated area at the beginning of measurement and the stage of the microscope was moved with a micromotor in the direction of the spindle axis at a speed of $5 \mu\text{m}/\text{sec}$ to record the intensity of light passing through the rectangular area crossing the spindle. The length

of the area ($15 \mu\text{m}$) was large enough to cover the spindle width. A single measurement of the change in light intensity along the whole spindle axis could be made within 10 sec or so. The intensity of light passing through the background (I_B in Eqs. 6, 7) was measured by setting the background at the center of the microscopic field or setting the spindle axis in parallel to the polarizer axis.

The numbers of microtubules in cross-section (N_L) at various positions along the spindle axis were obtained by substituting the intensity of light thus measured and the light intensity of the background for I_S and I_B in Eq. 8.

$$N_L = (2.5 \times 10^4) (I_S/I_B - 1) \quad (8)$$

which was obtained by substituting $1.5 \times 10^{-3} \text{ cm}$ ($15 \mu\text{m}$) for L in Eq. 7.

At each interval between successive measurements of birefringence, the glass slide was transferred to the stage of a differential interference microscope (Optiphot, Nikon) to take a micrograph of the same egg used in the birefringence measurement and then transferred back to the stage of the polarization microscope for the next measurement. In this way, the morphological processes of mitosis including the positions of chromosomes and centrosomes which were difficult to determine accurately by polarization microscopy could be recorded in the same egg.

Changes in microtubule distribution in the spindle during mitosis

Figure 2 shows a series of measurements of an egg in mitosis. In this egg, the distribution of the number of microtubules along the spindle axis was measured 7 times (a-g). The positions of the centrosomes at the center of the aster (circles) and those of the chromosomes (triangles) in this figure were obtained from differential interference micrographs taken during the intervals between successive birefringence measurements. The timing of birefringence measurements and differential interference microphotography is shown by horizontal arrows pointing to the time scale on the right. These records are similar to those in a previous report [4], although the method of measurement was greatly improved in the present

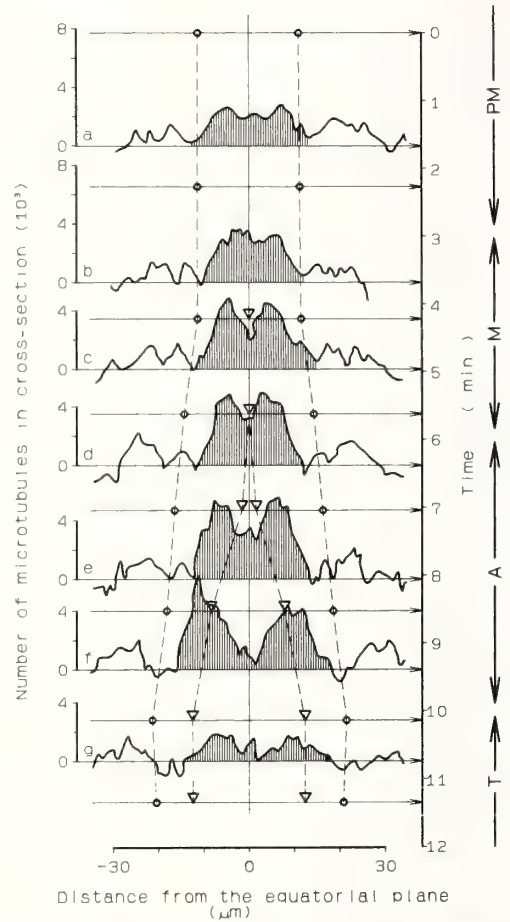


FIG. 2. Change in the distribution of microtubules in the spindle of a sand dollar egg at first mitosis.

Hatched area indicates the amount of microtubules. Circles indicate the positions of the centrosomes and triangles, the positions of the chromosomes. Time and stage of mitosis are indicated on the right side. Horizontal arrows indicate time of measurement. PM, M, A and T are prometaphase, metaphase, anaphase and telophase, respectively.

study.

The area of the hatched region in Figure 2, which is the integral of the number of microtubules along the spindle length from one end to the other, indicates the sum of the lengths of all microtubules contained in the spindle. It can be seen in Figure 2 that the amount of microtubules expressed by the sum of the lengths of microtubules increases in prometaphase, metaphase and early anaphase and decreases in late anaphase and telophase.

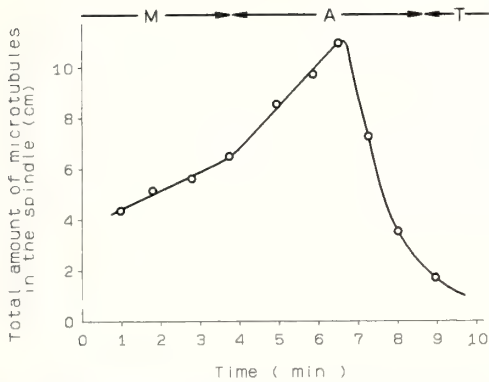


FIG. 3. Change in the total amount of microtubules in the spindle of a sand dollar egg at first mitosis. The total amount of microtubules is expressed by the sum of the lengths of all the microtubules. M, A, and T are metaphase, anaphase and telophase, respectively.

Figure 3 shows the change in the total amount (length) of microtubules in the spindle during mitosis from another egg. The above results indicate that formation and destruction of microtubules occur during mitosis in parallel to their translocation in the spindle.

Effect of Colcemid on the microtubule distribution in the spindle

Colcemid (N-methyl-N-desacetylcolchicine) is known to be an agent which can destroy microtubule structures. The effects of Colcemid on microtubule distribution in the spindle were examined by the optical integration method.

When the egg reached metaphase, ASW containing 10^{-5} – 10^{-6} M Colcemid (Sigma Chemicals, St. Louis, MO) was substituted for the medium of the egg on the glass slide by adding it at one edge of the cover-slip and placing a piece of filter paper at the opposite edge.

Figure 4 shows typical results. The hatched area in the figure a indicates the distribution of microtubules in the spindle in ASW and those in b–g are the microtubule distributions after ASW containing Colcemid (Colcemid-SW) was substituted for the medium. It was noted that both the microtubule number and the length of the spindle gradually decrease after the medium is replaced with Colcemid SW. It appears that the disassembly of

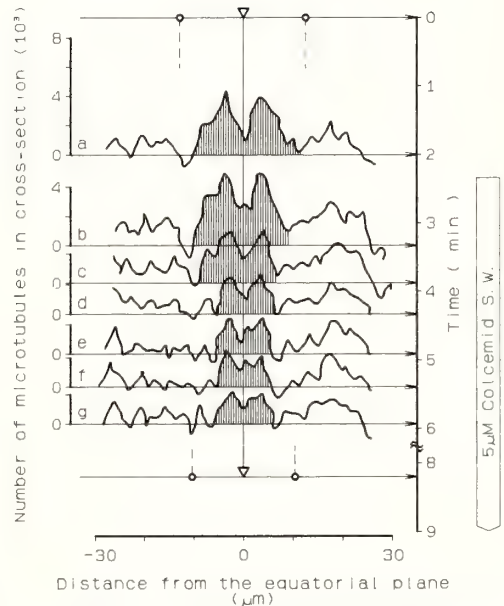


FIG. 4. Effect of Colcemid on the distribution of microtubules in the metaphase spindle of a sand dollar egg.

Circles indicate the positions of the centrosomes. Triangles indicate the position of chromosomes remaining in the equatorial plane of the spindle. Time of application of Colcemid-SW is indicated on the right side. Horizontal arrows indicate time of measurement.

microtubules is more conspicuous at the polar regions than at the central regions of the spindle. Chromosomes stay in the equatorial plane and the distance between the centrosomes decreases. This evidence suggests that the centrosomes are still attached to the spindle even after the disassembly of microtubules at the polar ends of the spindle.

DISCUSSION

Optical integration method

The optical integration method described in the present study is a simple method to determine the average or total birefringence phase retardation of a microscopic body when the axes of birefringence are parallel to one another and the intensity of birefringence is uneven. If the birefringence is regarded to be form birefringence due to the fibrous elements being aligned in the same direc-

tion as the mitotic spindle in echinoderm eggs, the total amount of fibrous elements in the body can be estimated by this method.

In using this method, the elimination of stray light coming from background is important because the background is quite bright owing to the large azimuth of the compensator. Limitation of the illuminated area by using a window inserted in the optical path for illumination may be effective in minimizing measurement errors due to background brightness (cf. [3]). The fact that the experimental results using mica chips fit so well with the theoretical curve expected from Jerrard's equation [5] may indicate that this method can be of practical use.

As shown by Eqs. 1 and 2, an increase in the azimuth of the compensator plate increases the linearity between the light intensity and the retardation of the specimen, while it decreases the ratio of the light intensity in the birefringent region to the light intensity in the background. We decided that the azimuth of the compensator plate should be set at 20° considering the fact that the linearity and the accuracy of the present experimental conditions depends on the strength of the birefringence of the specimen and the phase retardation of the compensator plate.

We demonstrated changes in the distribution and number of microtubules in the spindle under circumstances of normal division and immersion in seawater containing Colcemid, an agent inhibiting polymerization of tubulin into microtubules. We confirmed our previous results [4] on microtubule distribution in normal mitosis and presented more detailed data. By application of Colcemid-SW to the cell in mitosis, microtubules disappeared predominantly at the polar regions as compared with the equatorial regions of the spindle. This observation appears to contradict the idea that the depolymerization of microtubules at a steady state predominantly occurs at the plus ends of microtubules [6], because most of the spindle microtubules are oriented so that the plus ends point toward the equatorial region (cf. [7]). However, further studies on the mode of disassembly of microtubules

by Colcemid in living cells and more quantitative information on the dislocation of microtubules in Colcemid-treated cells are required for a detailed discussion of the effect of Colcemid on the microtubule structure of the spindle. Differences in stability between kinetochore microtubules and nonkinetochore microtubules to colchicine reported by Salmon *et al.* [8] should also be considered in this discussion.

ACKNOWLEDGMENT

This work was supported in part by a Grant-in-Aid for Scientific Research No. 61480019 from the Ministry of Education, Science and Culture, Japan awarded to Y. H.

REFERENCES

- 1 Inoué, S. (1952) The effect of colchicine on the microscopic and submicroscopic structure of the mitotic spindle. *Exp. Cell Res.*, **2** (Suppl.): 305-318.
- 2 Sato, H., Ellis, G. W. and Inoué, S. (1975) Microtubular origin of mitotic spindle form birefringence. Demonstration of the applicability of Wiener's equation. *J. Cell Biol.*, **67**: 501-517.
- 3 Hiramoto, Y., Hamaguchi, Y., Shôji, Y. and Shimoda, S. (1981) Quantitative Studies on the polarization optical properties of living cells. I. Microphotometric birefringence detection system. *J. Cell Biol.*, **89**: 115-120.
- 4 Hiramoto, Y., Hamaguchi, Y., Shôji, Y., Schroeder, T. E., Shimoda, S. and Nakamura, S. (1981) Quantitative Studies on the polarization optical properties of living cells. II. The role of microtubules in birefringence of the spindle of the sea urchin egg. *J. Cell Biol.*, **89**: 121-130.
- 5 Jerrard, H. G. (1948) Optical compensators for measurement of elliptical polarization. *J. Opt. Soc. Am.*, **38**: 35-59.
- 6 Horio, T. and Hotani, H. (1986) Visualization of the dynamic instability of individual microtubules by dark-field microscopy. *Nature (Lond.)*, **321**: 605-607.
- 7 Euteneuer, U. and McIntosh, R. (1981) Structural polarity of kinetochore microtubules in PtK₁ cells. *J. Cell Biol.*, **89**: 338-345.
- 8 Salmon, E. D., McKeel, M. and Hays, T. (1984) Rapid rate of tubulin dissociation from microtubules in the mitotic spindle *in vitro* measured by blocking polymerization with colchicine. *J. Cell Biol.*, **99**: 1066-1075.

In vivo Cytochemistry in Cell Division

YUKIHISA HAMAGUCHI

*Biological Laboratory, Tokyo Institute of Technology,
O-okayama, Meguro-ku, Tokyo 152, Japan*

INTRODUCTION

The movement of chromosomes during cell division and the dividing process of the cell have well been documented. The mitotic apparatus plays an important role in translocating chromosomes while the contractile ring plays an important role in dividing the cell. These two structures are fundamentally composed of two different cytoskeletal elements, i.e., microtubules in the mitotic apparatus and microfilaments in the contractile ring. These elements are too thin to be observed by ordinary light microscopy, although they can be observed individually by electron microscopy after fixation and staining. It is well-known through biochemical analysis that tubulin and actin are the principal constituents of microtubules and microfilaments, respectively, and that the dynamics of microtubules and microfilaments have been extensively investigated *in vitro*. However, the *in vivo* dynamics of these molecules in living cells have not yet been investigated to a satisfactory degree. It is not clear how the mitotic apparatus and the cleavage furrow are composed of microtubules and microfilaments, respectively, or how the motive force responsible for chromosome movement and dividing processes is generated in these structures during cell division (for a review, see [1]).

In vivo cytochemistry was introduced to supplement cytological and biochemical analyses by Taylor and Wang [2]. They injected fluorescently labeled actin into living cells and reported the incorporation of the exogenous actin into the microfilamentous structures in living cells [2]. In this brief review, I summarize results obtained by *in vivo* cytochemistry in the last ten years, from the time studies were first begun.

METHOD FOR *IN VIVO* CYTOCHEMISTRY

Procedures of *in vivo* cytochemistry are as follows (see [3, 4] for reviews).

1. Prepare a molecule having biological specificity
2. Label with probes
3. Purify a functional and optimally labeled conjugate
4. Characterize the labeled conjugate
 - a. probe/molecule ratio
 - b. site of labeling
 - c. check the functional activity of the conjugate *in vitro*
5. Microinject the labeled conjugate into living cells
6. Determine the functional activities *in vivo*

The molecules having biological specificity used in *in vivo* cytochemistry are divided into three groups: 1) cytoskeletal proteins, 2) antibodies against cytoskeletal proteins, and 3) agents specific to cytoskeletal proteins. Fluorescent probes are the most useful among the various probes because they are detectable in living cells by fluorescence microscopy. Since fluorescence conjugates are called fluorescent analogs, *in vivo* cytochemistry where fluorescent analogs are used is called fluorescent analog cytochemistry. In the past ten years, *in vivo* cytochemistry has become a useful tool mainly due to the improvements of two techniques, micromanipulation and video microscopy. Micromanipulation or microinjection was greatly advanced by the introduction of useful micromanipulators and the development of a method of microinjection [4-6]. The development of electronics has been of great significance, especially in digital image using video which can raise the luminescence of the microscopic image and enhance the contrast of the image [7, 8].

Using these fluorescent analogs, we can investigate the following functions of the cytoskeleton and cytoskeletal proteins *in vivo* by means of determining the functional activities *in vivo* as well as *in vitro* (for details, see the following sections).

1. Dynamic distribution
2. Local physiological characteristics such as polymerization and pH (fluorescence of fluorescein is pH-sensitive)
3. Molecular dynamics (assembly-disassembly equilibrium, dynamic redistribution, and diffusion constant)
4. Inhibition

CYTOSKELETAL PROTEINS

Mitosis

Tubulin is one of the proteins which has been investigated extensively by *in vivo* cytochemistry during mitosis because it is a conservative protein and can copolymerize with the endogenous tubulin in the injected cell. Rich sources of tubulin can be found in brains and sperm flagella. Less than 3% of the endogenous tubulin did not perturb mitosis or cleavage when injected into sea urchin eggs [9]. Travis *et al.* [10] first prepared native and fluorescent analogs of brain tubulin and microtubule-associated proteins; fluorescent analog of tubulin showed polymerizability and these fluorescent analogs showed affinity for unlabeled proteins. Keith *et al.* [11] reported that the fluorescent analog of tubulin was incorporated into the microtubular network in the cell even though the analogs of microtubule-associated proteins were not incorporated into the microtubules when injected into the living cell. In sea urchin eggs, the fluorescent analog of tubulin was incorporated into microtubular structures such as the mitotic apparatus and the sperm aster, and the distribution in the mitotic spindle of the labeled tubulin was coincident with the distribution of birefringence [9, 12, 13]. Even after the formation of the mitotic apparatus, tubulin was found to be incorporated within 20–30 sec of injection, and fluorescence redistribution occurred within this period after photobleaching in sea urchin eggs, indicating that tubulin in microtubules is quickly exchangeable with that in the cytoplasm

[14, 15]. Exchangeability in the mitotic cell was 18-fold more than that in the interphase cell [16]. The effects of microtubule depolymerizing agents such as colchicine and nocodazole, and microtubule stabilizing agents such as taxol on the mitotic apparatus were examined *in vivo* [14, 15, 17].

Mitchison and Kirschner [18] prepared biotinylated tubulin, which is not fluorescent but is visualized by electron microscopy using an antibody against biotin followed by a secondary antibody coupled to colloidal gold. Using this analog, Mitchison *et al.* [19] reported that astral microtubules incorporated the analog very rapidly, but, by contrast, kinetochore microtubules incorporated it at a slower rate at metaphase and not at all during anaphase.

Saxton and McIntosh [17], using the fluorescent analog of tubulin, showed that interdigitated microtubules in the interzonal region can undergo antiparallel sliding and therefore, that the mitotic spindle can elongate during anaphase. Hamaguchi *et al.* [15] also reported that the photobleached region moved poleward at the same rate as spindle elongation in metaphase and anaphase during fluorescence recovery after photobleaching (Fig. 1). However, Wadsworth and Salmon [14] reported that the translocation of the bleached region could not be detected at metaphase.

The injection of calcium-saturated calmodulin caused a significant shortening of the kinetochore and interpolar microtubules into which the fluorescent analog of tubulin had been incorporated but did not cause shortening of the astral microtubules. The spindle quickly recovered its normal form [20].

Calmodulin was extracted from brains and testes, purified, and labeled fluorescently. The fluorescent analog of calmodulin was also used to investigate the function of the protein in mitosis [21–24]. The fluorescent analog of calmodulin accumulated in the mitotic apparatus (Fig. 2), and bound to microtubules in a calcium-independent manner even though it usually binds to many enzymes in a calcium-dependent manner when it acts as a modulator protein [21]. The distribution of calmodulin is different from that of microtubules and dynein, although the role of calmodulin in mitosis might be imagined to regulate assembly

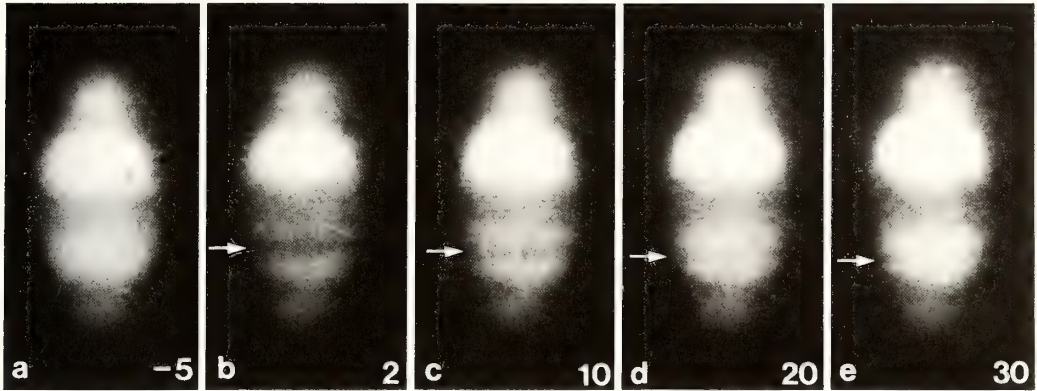


FIG. 1. A series of fluorescence micrographs of anaphase mitotic apparatus in which fluorescence was redistributed when the photobleached area (the arrow) was perpendicular to the spindle axis. The numbers in these micrographs represent the time (sec) after the end of photobleaching. The fluorescent analog of tubulin was injected into sand dollar eggs at prophase. (From Hamaguchi *et al.* [15] with the permission of Cell Struct. Funct.)

and disassembly of microtubules and/or dynein ATPase activity [21–23, 25, 26].

Scherson *et al.* [27] and Drubin and Kirschner [28] reported that tau protein and MAP2, microtubule associated proteins, were injected into living cells after labeling and were associated with microtubules, in contrast to the report by Keith *et al.* [11]. These proteins did not perturb mitosis and tau protein was found to induce tubulin assembly and to stabilize microtubules *in vivo* although they were not always involved in all types of cells [27, 28].

Cytokinesis

Rabbit skeletal muscle actin was first used in the study of fluorescent analog cytochemistry by Taylor and Wang [2, 29]. They reported that the fluorescent analog of actin was incorporated into microfilamentous structures in the cortex of sea urchin eggs for only a short period after fertilization when injected into unfertilized eggs [29]. This was, however, inconsistent with the biochemical and cytological analyses. Hamaguchi and Mabuchi [30] reinvestigated actin dynamics in the living cell during early development using sea urchin egg actin labeled with fluorescent probes which can modify two different groups of actin. Fluorescein-labeled actin was incorporated into microvilli and the cortex through cleavage. No difference was found in fluorescence between the region of the

cleavage furrow and the rest of the cortex, which indicates that as shown in biochemical and electron microscopical analyses [31, 32], microfilaments of the contractile ring are not newly synthesized from the cytoplasmic actin pool, but are reconstructed from the cortical microfilamentous network previously formed. Accumulated actin molecules in the cortex, which may be polymerized, may exchange quickly with diffusible cytoplasmic actin molecules because the fluorescence in the cortex quickly redistributed after photobleaching [30].

Fluorescent analogs of light chains of muscle myosin were injected into dividing cells [33, 34]. Myosin light chains were concentrated in the cleavage furrow, which suggests that fluorescent analogs of myosin light chains from muscle can be readily incorporated into non-muscle myosins and then used to follow the dynamics of myosin distribution in living cells.

The fluorescent analog of alpha-actinin isolated from sea urchin eggs or muscle was readily incorporated into the microfilamentous structures of the egg cortex although the localization of the fluorescent analog of egg alpha-actinin was distinct compared with that of the analog of muscle alpha-actinin [35]. The fluorescent layer at the cleavage furrow region seemed slightly thicker than that in the polar region. Just after the meiotic apparatus arrived at the cortical region of starfish oocytes, egg alpha-actinin accumulated in the region where

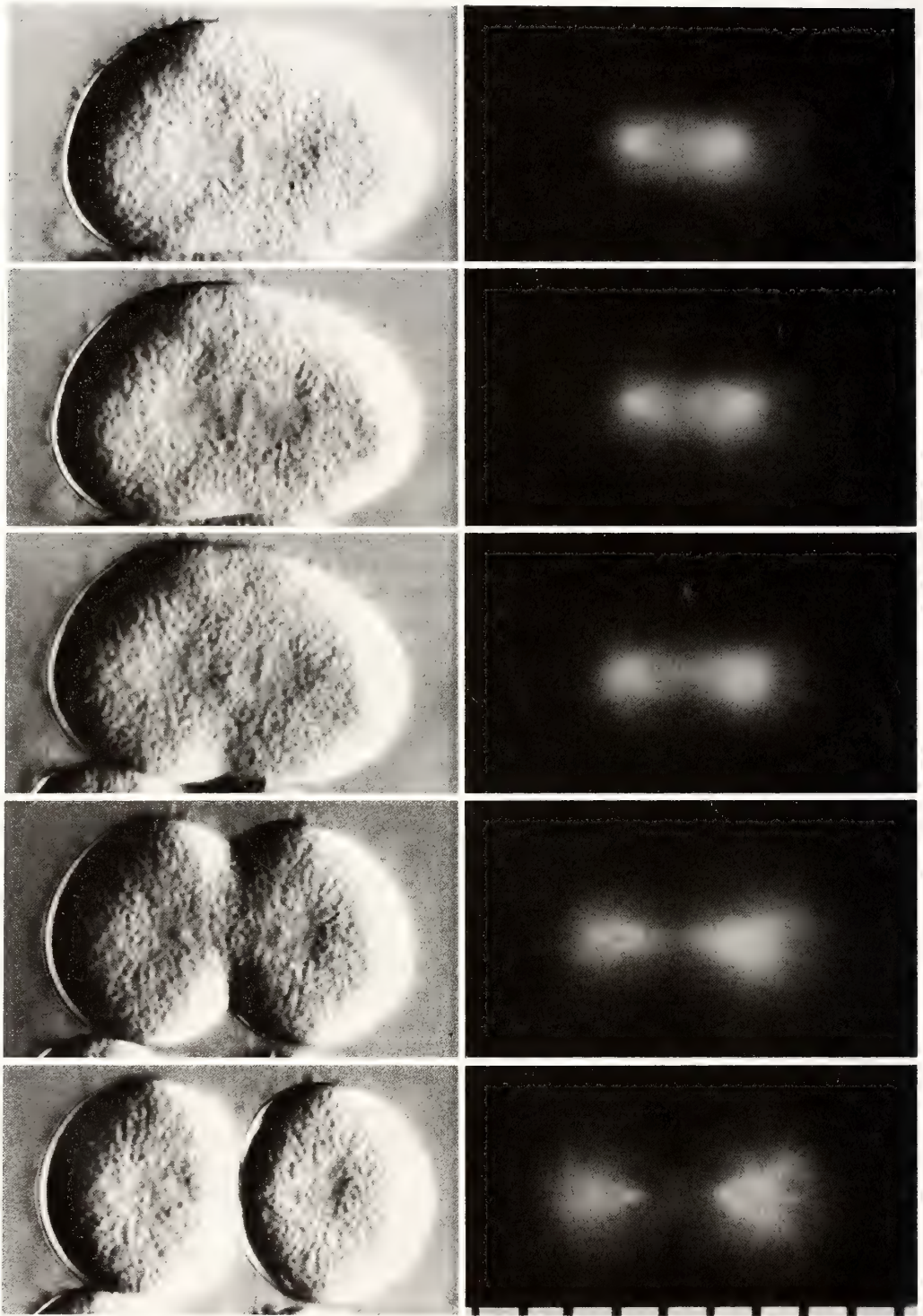


FIG. 2

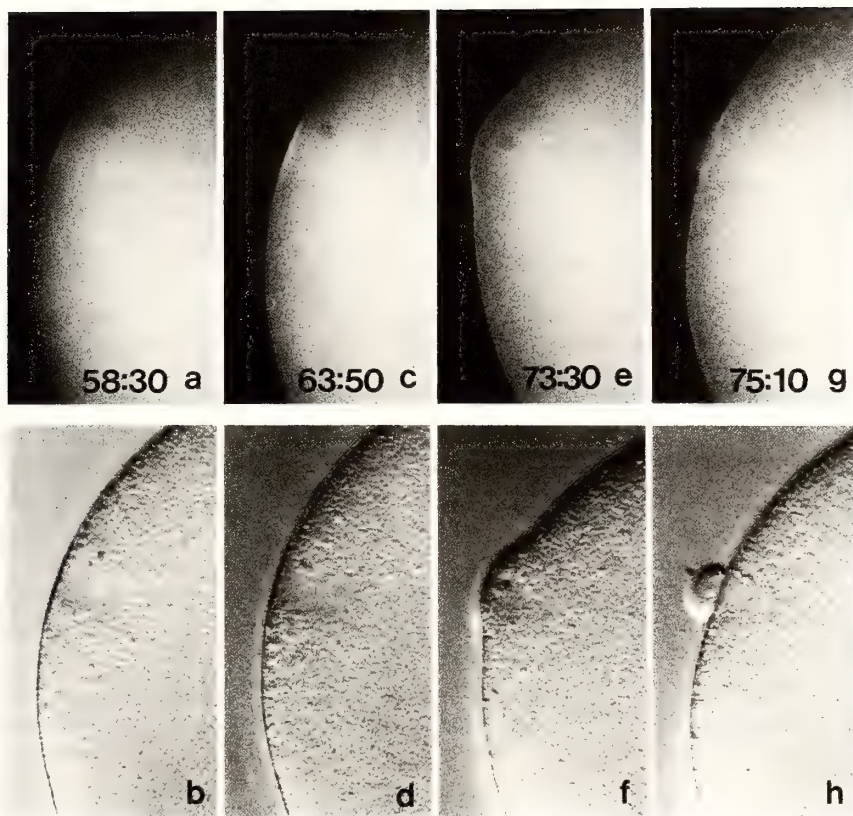


FIG. 3. Distribution of the fluorescent analog of egg alpha-actinin in a starfish oocyte during the first polar body formation. The numbers represent time (min: sec) after treatment with 1-methyladenine. The upper and lower rows are fluorescence and differential interference micrographs, respectively. (From Hamaguchi and Mabuchi [36] with the permission of Cell Motil. Cytoskeleton)

the polar body was expected to form, suggesting that the meiotic apparatus induces differentiation of the cortex so as to form a polar body (Fig. 3) [36].

Fluorescent analogs of tropomyosin and filamin, other microfilament-associated proteins, were incorporated into stress fibers of interphase cells but were not reported in dividing cells [37, 38].

ANTIBODIES AGAINST CYTOSKELETAL PROTEINS

Monoclonal antitubulin antibody (YL1/2) which

reacts specifically with tyrosinated alpha-tubulin was fluorescently labeled and injected into living cells [39, 40]. At lower concentrations, the antibody did not perturb cell division and was incorporated into the mitotic apparatus. At present, only one antibody mentioned above has been applied *in vivo*. However, since antibodies against different types of tubulin molecules have been obtained, the dynamic distribution corresponding to each type of tubulin molecule may be investigated [41-44]. Moreover, peptide antibodies are simple to prepare [45]. They are antibodies against short peptides whose sequence corresponds to the sequence

FIG. 2. Localization of the fluorescent analog of calmodulin in a blastomere during the 8-cell stage. Differential interference micrographs show the mitotic stage (left column) and fluorescence micrographs show calmodulin localization (right column). The fluorescent analog of calmodulin was injected into a fertilized egg at prophase. (From Hamaguchi and Iwasa [21] with the permission of Biomed. Res.)

of a part of a cytoskeletal protein. They react specifically with different molecules of cytoskeletal proteins even with different molecular sites of cytoskeletal proteins. Dynamic distribution and specific inhibition of each cytoskeletal protein may be investigated using these antibodies.

AGENTS SPECIFIC TO CYTOSKELETAL PROTEINS

Phallotoxins, toxic hepta-peptides from a mushroom, are filamentous-actin specific drugs [46]. Fluorescent analogs of phallotoxins which show no significant alteration in the binding capacity to filamentous-actin can be used to visualize actin containing cytoskeleton [47-49]. The fluorescent analog of phalloidin was injected into living eggs in order to investigate F-actin localization [49]. Fluorescein-labeled phalloidin became localized in the cortical layer of both unfertilized and fertilized eggs soon after injection. No difference was detected, however, in fluorescence between the region of the cleavage furrow and the rest of the cell cortex during cytokinesis, which is consistent with the results obtained using the fluorescent analog of actin. Distinct fluorescence was not detected in the mitotic apparatus, which indicates that microfilaments are not concentrated in the mitotic apparatus.

The fluorescent analog of colchicine, a tubulin binding agent, was used to visualize soluble tubulin, but not microtubules in fixed cells [50].

PERSPECTIVES

Further advancements in equipment and techniques for *in vivo* cytochemistry are outlined below.

The recent development of the scanning confocal light microscope [41] offers the advantages of greater resolution than that attained by conventional microscopy and improved rejection of out-of-focus noise which provides better optical sectioning of thick specimens such as living cells. Cytoskeletal elements can more easily and clearly be visualized by fluorescent analog using a scanning confocal light microscope as a fluorescence microscope.

Owing to advances in video microscopy, small granules have now become visible with differential interference microscopy [7, 52]. Small particles such as colloidal gold particles and bacteria are valuable tools with wide applicability to the study of the functions of cytoskeletal proteins within living cells [52, 53]. Gold particles coupled to a monoclonal antibody reacting with the alpha-subunit of tubulin stayed in an entirely fixed position in the cell after injection, which indicates that microtubule treadmilling does not seem to be involved in microtubule dynamics in the cell [52].

Phycobiliproteins, constituents of the light-harvesting apparatus of blue-green bacteria, red algae, and cryptomonads, can be used as fluorescent probes because they are highly fluorescent [54]. If fluorescent intensity greatly increases, detection of cytoskeletal elements may be improved. Oi *et al.* [54] reported on the various phycobiliprotein conjugates to a molecule having biological specificities such as phycoerythrin-immunoglobulin, phycoerythrin-protein A, and phycoerythrin-avidin conjugates. Local structural changes in cytoskeletal proteins can be determined *in vivo* if the fluorescent probe responsible for the condition of the cytoskeleton such as pyrene is used.

Fluorescence intensity of N-(1-pyrenyl)-iodoacetamide-labeled actin was enhanced by a factor of about 25 on polymerization [55].

In the near future, *in vivo* cytochemistry is expected to be applied to many different cytoskeletal proteins in various dividing cells using the improvements mentioned above, and may become an even more powerful technique in the study of cell division.

ACKNOWLEDGMENT

This review is dedicated to Professor Katsuma Dan on the occasion of his 83rd birthday. I wish to thank Dr. M. S. Hamaguchi for her valuable criticism.

This work was supported by Grants-in-Aid from the Ministry of Education, Science and Culture of Japan (61304008, 62300004, and 62540538).

REFERENCES

- 1 Ishikawa, H., Hatano, S. and Sato, H. (1985) Cell

- Motility: Mechanism and Regulation, Univ. Tokyo Press, Tokyo.
- 2 Taylor, D. L. and Wang, Y.-L. (1987) Molecular cytochemistry: Incorporation of fluorescently labeled actin into living cells. *Proc. Natl. Acad. Sci.*, **75**: 857-861.
 - 3 Taylor, D. L. and Wang, Y.-L. (1980) Fluorescently labeled molecules as probes of the structure and function of living cells. *Nature*, **284**: 405-410.
 - 4 Kreis, T. E. and Birchmeier, W. (1982) Microinjection of fluorescently labeled proteins into living cells with emphasis on cytoskeletal proteins. *Int. Rev. Cytol.*, **75**: 209-227.
 - 5 Hamaguchi, Y. (1986) Introduction to microinjection. *Saiho (Cell)*, **18**: 36-40. (in Japanese)
 - 6 Hiramoto, Y. (1984) Micromanipulation. In "Cell Biology". Ed. by T. Niizu and T. Okigaki, Maruzen Co. Ltd., Tokyo, pp. 277-297. (in Japanese)
 - 7 Inoué, S. (1986) Video Microscopy, Plenum Press, New York.
 - 8 Arndt-Jovin, D. J., Robert-Nicoud, M., Kaufman, S. J. and Jovin, T. M. (1985) Fluorescence digital imaging microscopy in cell biology. *Science*, **230**: 247-256.
 - 9 Hamaguchi, Y., Toriyama, M., Sakai, H. and Hiramoto, Y. (1985) Distribution of fluorescently labeled tubulin injected into sand dollar eggs from fertilization through cleavage. *J. Cell Biol.*, **100**: 1262-1272.
 - 10 Travis, J. L., Allen, R. D. and Sloboda, R. D. (1980) Preparation and characterization of native, fluorescently labeled brain tubulin and microtubule-associated proteins (MAPs). *Exp. Cell Res.*, **125**: 421-429.
 - 11 Keith, C. H., Feramisco, J. R. and Shelanski, M. (1981) Direct visualization of fluorescein-labeled microtubules in vitro and in microinjected fibroblasts. *J. Cell Biol.*, **88**: 234-240.
 - 12 Salmon, E. D., Leslie, R. J., Saxton, W. M., Karow, M. L. and McIntosh, J. R. (1984) Spindle microtubule dynamics in sea urchin embryos: Analysis using a fluorescein-labeled tubulin and measurements of fluorescence redistribution after laser photobleaching. *J. Cell Biol.*, **99**: 2165-2174.
 - 13 Hiramoto, Y., Hamaguchi, Y., Hamaguchi, M. S. and Nakano, Y. (1985) Roles of microtubules in pronuclear migration and spindle elongation in sand dollar eggs. In "Cell Motility: Mechanism and Regulation". Ed. by H. Ishikawa, S. Hatano and H. Sato, Univ. Tokyo Press, Tokyo, pp. 349-356.
 - 14 Wadsworth, P. and Salmon, E. D. (1986) Analysis of the treadmilling model during metaphase of mitosis using fluorescence redistribution after photobleaching. *J. Cell Biol.*, **102**: 1032-1038.
 - 15 Hamaguchi, Y., Toriyama, M., Sakai, H. and Hiramoto, Y. (1987) Redistribution of fluorescently labeled tubulin in the mitotic apparatus of sand dollar eggs and the effects of taxol. *Cell Struct. Funct.*, **12**: 43-52.
 - 16 Saxton, W. M., Stemple, D. L., Leslie, R. J., Salmon, E. D., Zavortink, M. and McIntosh, J. R. (1984) Tubulin dynamics in cultured mammalian cells. *J. Cell Biol.*, **99**: 2175-2186.
 - 17 Saxton, W. M. and McIntosh, J. R. (1987) Interzone microtubule behavior in late anaphase and telophase spindles. *J. Cell Biol.*, **105**: 875-886.
 - 18 Mitchison, T. J. and Kirschner, M. W. (1985) Properties of the kinetochore in vitro. I. Microtubule nucleation and tubulin binding. *J. Cell Biol.*, **101**: 755-765.
 - 19 Mitchison, T., Evans, L., Schulze, E. and Kirschner, M. (1986) Sites of microtubule assembly and disassembly in the mitotic spindle. *Cell*, **45**: 515-527.
 - 20 Keith, C. H. (1987) Effect of microinjected calcium-calmodulin on mitosis in PtK2 cells. *Cell Motil. Cytoskeleton*, **7**: 1-9.
 - 21 Hamaguchi, Y. and Iwasa, F. (1980) Localization of fluorescently labeled calmodulin in living sea urchin eggs during early development. *Biomed. Res.*, **1**: 502-509.
 - 22 Hamaguchi, Y. and Iwasa, F. (1982) Localization of fluorescently labeled calmodulin in living sand dollar eggs during early development. In "Biological Functions of Microtubules". Ed. by H. Sakai, H. Mohri and G. G. Borisy, Academic Press, Tokyo, pp. 199-210.
 - 23 Zavortink, M., Welsh, M. J. and McIntosh, J. R. (1983) The distribution of calmodulin in living mitotic cells. *Exp. Cell Res.*, **149**: 375-385.
 - 24 Luby-Phelps, K., Lanni, F. and Taylor, D. L. (1985) Behavior of a fluorescent analogue of calmodulin in living 3T3 cells. *J. Cell Biol.*, **101**: 1245-1256.
 - 25 Hisanaga, S., Tanaka, T., Masaki, T., Sakai, H., Mabuchi, I. and Hiramoto, Y. (1987) Localization of sea urchin egg cytoplasmic dynein in mitotic apparatus studied by using a monoclonal antibody against sea urchin sperm flagellar 21S dynein. *Cell Motil. Cytoskeleton*, **7**: 97-109.
 - 26 Hisanaga, S. and Pratt, M. M. (1984) Calmodulin interaction with cytoplasmic and flagellar dynein: Calcium-dependent binding and stimulation of adenosinetriphosphatase activity. *Biochemistry*, **23**: 3032-3037.
 - 27 Scherson, T., Kreis, T. E., Schlessinger, J., Littauer, U. Z., Borisy, G. G. and Geiger, B. (1984) Dynamic interactions of fluorescently labeled microtubule-associated proteins in living cells. *J. Cell Biol.*, **99**: 425-434.
 - 28 Drubin, D. G. and Kirschner, M. W. (1986) Tau protein function in living cells. *J. Cell Biol.*, **103**:

- 2739–2746.
- 29 Wang, Y.-L. and Taylor, D. L. (1979) Distribution of fluorescently labeled actin in living sea urchin eggs during early development. *J. Cell Biol.*, **82**: 672–679.
 - 30 Hamaguchi, Y. and Mabuchi, I. (1988) Accumulation of fluorescently labeled actin in the cortical layer in sea urchin eggs after fertilization. *Cell Motil. Cytoskeleton*, **9**: 153–163.
 - 31 Mabuchi, I., Hosoya, H. and Sakai, H. (1980) Actin in the cortical layer of the sea urchin eggs. *Biomed. Res.*, **1**: 417–426.
 - 32 Usui, N. and Yoneda, M. (1982) Ultrastructural basis of the tension increase in sea-urchin eggs prior to cytokinesis. *Dev. Growth Differ.*, **24**: 453–465.
 - 33 Mittal, B., Sanger, J. M. and Sanger, J. W. (1987) Visualization of myosin in living cells. *J. Cell Biol.*, **105**: 1753–1760.
 - 34 McKenna, N. M. and Wang, Y.-L. (1987) Localization and exchangeability of microinjected smooth muscle myosin LC₂₀ in living cells. *J. Cell Biol.*, **105**: 127a.
 - 35 Mabuchi, I., Hamaguchi, Y., Kobayashi, T., Hosoya, H., Tsukita, S. and Tsukita, S. (1985) Alpha-actinin from sea urchin eggs: Biochemical properties, interaction with actin, and distribution in the cell during fertilization and cleavage. *J. Cell Biol.*, **100**: 375–383.
 - 36 Hamaguchi, Y. and Mabuchi, I. (1986) Alpha-actinin accumulation in the cortex of echinoderm eggs during fertilization. *Cell Motil. Cytoskeleton*, **6**: 549–559.
 - 37 Wehland, J. and Weber, K. (1980) Distribution of fluorescently labeled actin and tropomyosin after microinjection in living tissue culture cells as observed with TV image intensification. *Exp. Cell Res.*, **127**: 397–408.
 - 38 Mittal, B., Sanger, J. M. and Sanger, J. W. (1987) Binding and distribution of fluorescently labeled filamin in permeabilized and living cells. *Cell Motil. Cytoskeleton*, **8**: 345–359.
 - 39 Wehland, J. and Willingham, M. C. (1983) A rat monoclonal antibody reacting specifically with the tyrosylated form of α -tubulin. II. Effects on cell movement, organization of microtubules, and intermediate filaments, and arrangement of Golgi elements. *J. Cell Biol.*, **97**: 1476–1490.
 - 40 Warn, R. M., Flegg, L. and Warn, A. (1987) An investigation of microtubule organization and functions in living *Drosophila* embryos by injection of a fluorescently labeled antibody against tyrosinated α -tubulin. *J. Cell Biol.*, **105**: 1721–1730.
 - 41 Thompson, W. C., Asai, D. J. and Carney, D. H. (1984) Heterogeneity among microtubules of the cytoplasmic microtubule complex detected by a monoclonal antibody to alpha tubulin. *J. Cell Biol.*, **98**: 1017–1025.
 - 42 Gundersen, G. G. and Bulinski, J. C. (1986) Distribution of tyrosinated and nontyrosinated α -tubulin during mitosis. *J. Cell Biol.*, **102**: 1118–1126.
 - 43 Piperno, G., LeDizet, M. and Chang, X.-J. (1987) Microtubules containing acetylated α -tubulin in mammalian cells in culture. *J. Cell Biol.*, **104**: 289–302.
 - 44 Lopata, M. A. and Cleveland, D. W. (1987) In vivo microtubules are copolymers of available β -tubulin isotypes: Localization of each of six vertebrate β -tubulin isotypes using polyclonal antibodies elicited by synthetic peptide antigens. *J. Cell Biol.*, **105**: 1707–1720.
 - 45 Bulinski, J. C. (1986) Peptide antibodies: New tools for cell biology. *Int. Rev. Cytol.*, **103**: 281–302.
 - 46 Wieland, T. (1977) Modification of actins by phallotoxins. *Naturwissenschaften*, **64**: 303–309.
 - 47 Wulf, E., Deboben, A., Bautz, F. A., Faulstich, H. and Wieland, T. (1979) Fluorescent phallotoxin, a tool for the visualization of cellular actin. *Proc. Natl. Acad. Sci. USA*, **76**: 4498–4502.
 - 48 Berek, L. S., Yocum, R. R., Nothnagal, E. A. and Webb, W. W. (1980) Fluorescence staining of the actin cytoskeleton in living cells with 7-nitrobenz-2-oxa-1, 3-diazole-phalloidin. *Proc. Natl. Acad. Sci. USA*, **77**: 980–984.
 - 49 Hamaguchi, Y. and Mabuchi, Y. (1982) Effects of phalloidin microinjection and localization of fluorescein-labeled phalloidin in living sand dollar eggs. *Cell Motil.*, **2**: 103–113.
 - 50 Albertini, D. F. and Clark, J. I. (1981) Visualization of assembled and disassembled microtubule protein by double label fluorescence microscopy. *Cell Biol. Int. Rep.*, **5**: 387–397.
 - 51 White, J. G., Amos, W. B. and Fordham, M. (1987) An evaluation of confocal versus conventional imaging of biological structures by fluorescence light microscopy. *J. Cell Biol.*, **105**: 41–48.
 - 52 De Brabander, M., Geuens, G., Nuydens, R., Moeremans, M. and De May, J. (1985) Probing microtubule-dependent intracellular motility with nanometre particle video ultramicroscopy (nanovid ultramicroscopy). *Cytobios*, **43**: 273–283.
 - 53 Hynes, T. R., Block, S. M., White, B. T. and Spudich, J. A. (1987) Movement of myosin fragments in vitro: Domains involved in force production. *Cell*, **48**: 953–963.
 - 54 Oi, V. T., Glazer, A. N. and Stryer, L. (1982) Fluorescent phycobiliprotein conjugates for analyses of cells and molecules. *J. Cell Biol.*, **93**: 981–986.
 - 55 Kouyama, T. and Mihashi, K. (1981) Fluorimetry study of N-(1-pyrenyl)iodoacetamide-labelled F-actin. *Eur. J. Biochem.*, **114**: 33–38.

Computed Profiles of Compressed Sea-Urchin Eggs with Elastic Membranes

MITSUKI YONEDA

*Department of Zoology, Faculty of Science, Kyoto University,
Kyoto 606, Japan*

ABSTRACT—A computer simulation was made for profiles of compressed sea-urchin eggs with various amounts of elasticity at their surfaces. Fluidity of cytoplasm and negligible bending stress of the surface were assumed *a priori*. Based on the profiles thus calculated, the relation of the force of compression and the degree of flattening was predicted and matched with the observed force and flattening of unfertilized eggs of *Hemicentrotus pulcherrimus*. The experimental data were shown to fit well with the calculated force-deformation curve on the assumption of non-elasticity at the surface. The possibility that the egg surface had an elasticity modulus of 10^3 dyne/cm² was precluded.

Whether the surface of sea-urchin eggs is elastic or not has been the subject of a debate between Hiramoto [1-5] and myself [6-8]. Both claims have emerged from experimental data on the force required to compress the egg by the "compression method" originally developed by Cole [9].

When an unfertilized sea-urchin egg with the diameter Z_0 is compressed between a pair of parallel plates with a known force (F), the thickness (Z) of the egg reaches an equilibrium within a few minutes. By measuring the thickness of a single egg under varying amounts of force, we can determine the relation of the force (F) and the thickness ($z=Z/Z_0$) as a "F-z curve" (Fig. 1).

Hiramoto adopted a mathematical procedure different from mine to calculate the tension (T) working at the egg surface from measured values of force (F). This gave rise to the differing views as to the physical nature of the egg surface; Hiramoto [1] converted the measured force into excess internal pressure $P=F/\pi D^2$ by measuring the radius (D) of the circle of cell surface in contact with the plates of compression (Fig. 1). By also measuring the radii of curvatures (R_1 and R_2) of the egg surface, he calculated the meridional and equatorial tensions (T_L and T_T) with two formulae,

$$\pi R_2^2 P = 2\pi R_2 T_L + F \quad \text{and} \quad P = T_L/R_1 + T_T/R_2.$$

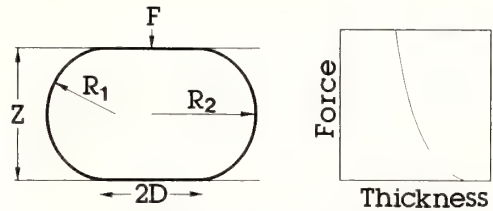


FIG. 1. Sea-urchin egg compressed to thickness (Z) between a pair of parallel plates under force (F) of compression. R_1 and R_2 are radii of the principal curvature of the egg surface at the equator. D is the radius of the circular area in contact with the plate. Typical curve of the force versus flattening of the egg is shown schematically to the right.

Both tensions were found to increase as the egg surface is stretched upon compression, which led him to claim the presence of elasticity at the egg surface.

The method I adopted equates the work of compression, $-FdZ$, with the work of stretching the surface, TdS . Hence $F=T(-dS/dZ)$, or

$$F = \pi T Z_0 (-ds/dz) \tag{1}$$

where $s=S/S_0$ is the total surface area (S) of the compressed egg divided by the initial surface area, $S_0 = \pi Z_0^2$. I calculated the tension (T) by eq. (1) employing an empirical expression of the surface area derived from measured Z , R_1 and R_2 , and found that the calculated tension now remains constant in spite of the change in surface area.

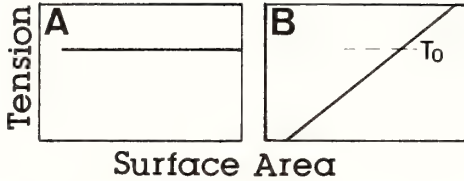


FIG. 2. Conceptual illustration of the relation between the tension and the degree of stretching of the egg surface. A: Non-elastic surface. The tension is independent of the surface area. B: Elastic surface. The tension increases upon surface stretching. T_0 is the initial tension when the egg is a sphere.

Thus I concluded that the egg surface is *not* elastic, a view diametrically opposite to Hiramoto's. Figure 2 is a conceptual illustration of the contrast between the calculated results.

Thus the debate has arisen as to the validity of both procedures. I feel that the term D used by Hiramoto will not be accurately measured because the "angle of contact" is close to 180° . Conversely, Hiramoto (1976) argues that "it is questionable whether $-ds/dz$ could be determined with a reasonable accuracy" because "increase in surface area dS by compression dZ is very small". Both Hiramoto and I have reinforced our own theories by supplementing with circumstantial evidence, which however, does not logically prove or disprove the validity of either calculation.

I [6, 7] earlier found an analytical solution for the profile of the compressed egg, assuming non-elasticity of the egg surface. The calculated contour coincided with the actual contour of the compressed egg. Calculated values of $-ds/dz$ were also consistent with those derived from measured geometrical parameters. The agreement between the calculation and observation, while supporting the view of non-elasticity of the egg surface, does not prove it however, since an elastic membrane may also show similar contours and similar values of $-ds/dz$.

I recently found a mathematical procedure to derive the profile of elastic shells by numerical calculation. The theoretical contour thus obtained provides a means of directly evaluating the unprocessed raw data of the force versus compression without relying upon the geometrical parameters of the egg, as presented here.

CALCULATION

Mathematical formulation

Since the profile of the compressed egg is axially symmetric, the problem is finding the meridian of the egg by numerical calculation. Four assumptions can be made: that 1) the volume of the egg remains unchanged upon compression, 2) the surface does not resist bending, 3) the inner cytoplasm is fluid, and 4) hydrostatic pressure inside the egg cytoplasm does not affect the egg shape. Based on these assumptions, the egg is looked upon as a thin elastic shell encircling incompressible fluid, to which the classical membrane theory of shells can be applied.

Two kinds of mathematical expressions for balance of forces are known to apply to the thin elastic shell loaded with external forces along the axis, as given by Timoshenko and Woinowsky-Krieger [10]. One is the familiar Laplace formula which relates the internal pressure P with the tensions (T_L and T_T) as

$$P = T_L/R_L + T_T/R_T \quad (2)$$

where T_L is the tension in the direction of the meridian (meridional tension) and T_T (transverse tension) is the tension in the direction perpendicular to T_L (Figs. 3 and 4). R_L is the radius of curvature of the meridian and R_T is the radius of curvature in the direction perpendicular to R_L and, by the theory of differential geometry, equal to the line segment normal to the meridian cut by the symmetry axis.

Another expression for axially loaded shell is

$$d/d\varphi (T_L X) - T_T R_L \cos \varphi + Y R_L X = 0$$

[eq. (f) on page 434 in Timoshenko and Woinowsky-Krieger [10]]. In the case of compressed shells, the term Y , expressing the force acting tangentially to the shell, is null. Defining the orthogonal coordinates ($x-y$) as shown in Figure 3 in which the line $x=0$ denotes the symmetry axis, we obtain $dX/d\varphi = R_L \cos \varphi$. Hence,

$$d/dX (X T_L) = T_T \quad (3)$$

The calculations to follow are to find the profile of the egg which satisfies both eqs. (2) and (3). To

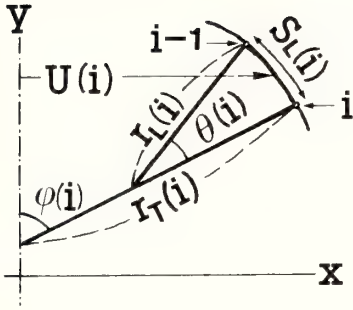


FIG. 3. Geometric parameters describing the compressed shell. Parameters R_L and R_T in eq. 2 correspond to $r_L(i)$ and $r_T(i)$ in this figure.

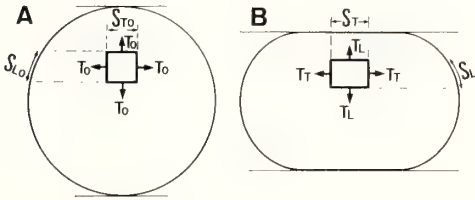


FIG. 4. Rectangular surface element. Its meridional (S_{L0}) and transverse (S_{T0}) dimensions in the spherical shell change to $S_L \times S_T$ upon compression. The initial tension working at element T_0 changes to T_L and T_T in the meridional and transverse directions, respectively.

begin with, let us suppose a rectangular surface element of the shell with the meridional and transverse dimensions S_{L0} and S_{T0} (Fig. 4A). When the shell is a sphere, the meridional and transverse tensions coincide at T_0 . Compression will change the dimension of the element to S_L and S_T (Fig. 4B). "Relative elongation" E_L and E_T of the element, are defined here as

$$E_L = (S_L - S_{L0})/S_{L0}, \quad E_T = (S_T - S_{T0})/S_{T0} \quad (4)$$

Denoting the thickness and Young's modulus of the shell by h and E respectively, T_L is given as

$$T_L = T_0 + \frac{E_L + sE_T}{(1 + E_L)(1 + E_T)} \cdot \frac{Eh}{1 - s^2}$$

where s is the Poisson ratio of the material of the shell and usually assigned with the value of 0.5 for rubbery materials. Now the term "elasticity index", $Q = Eh/(1 - s^2)/T_0$, which represents the magnitude of elasticity (E) relative to the initial

tension T_0 , is defined. Then, letting $t_L = T_L/T_0$,

$$t_L = T_L/T_0 = 1 + \frac{E_L + 0.5E_T}{(1 + E_L)(1 + E_T)} Q \quad (5)$$

Similarly, $t_T (= T_T/T_0)$ is calculated by

$$t_T = T_T/T_0 = 1 + \frac{E_T + 0.5E_L}{(1 + E_T)(1 + E_L)} Q \quad (6)$$

All parameters used in calculations are expressed in their relative values, $z = Z/Z_0$, $t_L = T_L/T_0$, $t_T = T_T/T_0$, $r_L = R_L/R_0$, $r_T = R_T/R_0$, $d = D/R_0$ and $p = P R_0/T_0$, where R_0 , Z_0 , T_0 are the initial radius, diameter and tension, respectively, when the shell is a sphere. Expressing eqs. (2) and (3) by these parameters, we have

$$p = t_L/r_L + t_T/r_T \quad (7)$$

and

$$d/dx(x t_L) = dt_L/dx + t_L = t_T \quad (8)$$

Starting profile

Calculation of the profile of the compressed shell was started by assuming a semicircular contour at the free surface, and by assigning a proper value of $d (= D/R_0)$ so that the volume encompassed by the shell retains the volume of the sphere with a unit radius. The boundary between the surface in contact with the plate and the free surface will be called "the border", hereafter.

Fine detail of the shell was described by positions in orthogonal co-ordinates of "nodes" which divide the meridian into 48 "segments" (Fig. 5). The nodes are serially numbered from 0 (pole) to

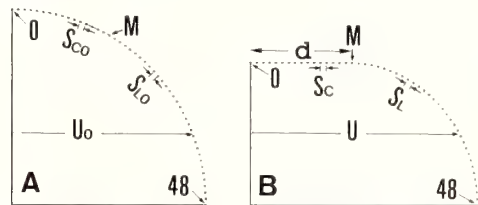


FIG. 5. Form of meridians of the initial (A) and compressed (B) shells defined by node nos. 00 to 48. The node at the border is "node M". Initial lengths of "segments" delimited by adjacent nodes are S_{C0} (at the contacting surface) and S_{L0} (at the free surface). On compression, they change to S_C and S_L , respectively. U_0 and U are the position on the X-coordinates of the center of the segment.

48 (equator). Initially, they were properly spaced along the surface of the compressed shell so as to allocate either one of the nodes on the border. This is denoted by node M. Initial spacing of the nodes is S_C on the surface contacting the plate and S_L on the free surface (Fig. 5B). Such a distribution of the nodes on the compressed shell was transcribed back to the initial sphere, accommodating the spacing to different meridional lengths between the compressed and spherical shells, so that the spacing among nodes 0 to M (S_{C0}) and the spacing among nodes M to 48 (S_{L0}) retain the ratio S_C/S_L .

The original positions of the center of each segment on the X-coordinate (U_0 in Fig. 5) in the sphere varies among segments and is expressed as $U_0(i)$ ($i=0$ to 48). The corresponding value for the position in the compressed profile is $U(i)$. Due to the axial symmetry of the shell, the ratio $U(i)/U_0(i)$ is numerically equal to S_T/S_{T0} (cf. eq. (4)) which is the rate of stretching of the rectangular element shown in Figure 4 along the transverse direction. In routine calculations, E_T was given as $U(i)/U_0(i)$.

The nodes 0 to M at the contacting surface were defined by their positions in orthogonal coordinates as $x(i)$ and $y(i)$, but nodes M+1 to 48 at the free surface were primarily defined by $r_L(i)$ and $\theta(i)$ for convenience in calculation, and $x(i)$ and $y(i)$ for $i=M+1$ to 48 were given successively by $r_L(i)$ and $\theta(i)$ (see Fig. 3), starting from node M (border) as

$$\begin{aligned}\varphi(i) &= \varphi(i-1) + \theta(i) \\ x(i) &= x(i-1) + r_L(i) [\sin \varphi(i) - \sin \varphi(i-1)] \\ y(i) &= y(i-1) + r_L(i) [\cos \varphi(i) - \cos \varphi(i-1)]\end{aligned}$$

$S_L(i)$ is directly obtained as $\theta(i)r_L(i)$.

Iteration for fine adjustment of the profile

The compressed shell was defined in the foregoing section by rather arbitrary parameters under given flattening ($=z$) and elasticity index (Q). This is the starting model to be examined for local balance of forces.

First, the rates of stretching (E_L and E_T) of each segment obtained by eq. (4) were used to calculate the local tensions $t_L(i)$ and $t_T(i)$ by eqs. (5) and (6). The pair of $t_L(i)$ and $t_T(i)$ determined for each segment was then examined as to whether they

satisfy both eqs. (7) and (8), which are two fundamental expressions of the balance of forces in elastic shells under compression, by calculating imbalance between the lefthand and righthand sides of the equations under given $t_L(i)$ and $t_T(i)$. According to the amount of the imbalance, necessary adjustments were made for parameters $r_L(i)$, $\theta(i)$, or d to improve the profile of the shell. Iteration of the adjustment is explained in the Appendix. The whole procedure was repeated using the renewed parameters $r_L(i)$, $\theta(i)$ and d until the calculated profile substantially satisfied the conditions predicted by eqs. (7) and (8).

RESULTS

The profile of the shells under a given degree (z) of compression is determined by the elasticity index $Q = Eh/(1-s^2)/T_0$ as the only parameter. Hiramoto (1963) calculates Young's modulus (E) for the surface membrane of unfertilized eggs of *Hemicentrotus pulcherrimus* as 1.2×10^3 dyne/cm² when the membrane thickness (h) is 3.1 μ m, and the initial tension T_0 is 0.032 dyne/cm. These values give the value of Q as 16. The calculations were, therefore, made of the profile of a shell compressed from $z=0.90$ down to 0.40, and assigned with varying elasticity indices (Q) ranging from 0 (no elasticity) to 16. The results are summarized in Table 1 and show the geometrical parameters of the compressed shell. In real eggs, the force (F) of compression is counterbalanced by the force $F = \pi PD^2$ due to internal pressure (P), and since πPD^2 can be written as $(pd^2/2)\pi T_0 Z_0$, the value of $pd^2/2$ in Table 1 is identical to $(-ds/dz)$ in eq. (1). The present values of $pd^2/2$ for $Q=0$ were found to coincide with $-ds/dz$ (not shown here) derived in a previous paper [11] by an analytical solution of the profile.

Typical examples of the contour of the shell under compression (z) in 4 steps for $Q=0$ and 16 are drawn in Figure 6. The contours in the presence of elasticity (shown by circles) tend to become flatter near the equatorial surface than the contour in the absence of elasticity (lines), resulting in a diminished largest diameter of the shell. Conversely, the contours of the elastic shell exhibit steeper curvatures at the region near the boundary

TABLE 1. Geometric parameters of elastic shells under compression

z	u	d	p	pd ² /2	z	u	d	p	pd ² /2
Q = 0					Q = 5				
.90	1.022	0.215	2.046	0.047	.90	1.018	0.247	2.080	0.063
.85	1.038	0.284	2.082	0.083	.85	1.031	0.325	2.153	0.113
.80	1.057	0.350	2.125	0.130	.80	1.048	0.397	2.254	0.177
.75	1.079	0.416	2.178	0.188	.75	1.069	0.466	2.387	0.259
.70	1.104	0.484	2.243	0.262	.70	1.093	0.534	2.562	0.365
.65	1.132	0.554	2.321	0.356	.65	1.122	0.602	2.788	0.505
.60	1.166	0.628	2.417	0.476	.60	1.156	0.672	3.080	0.696
.55	1.205	0.708	2.536	0.635	.55	1.196	0.746	3.458	0.963
.50	1.250	0.794	2.683	0.846	.50	1.243	0.826	3.950	1.348
.45	1.304	0.890	2.869	1.136	.45	1.299	0.915	4.596	1.924
.40	1.370	0.997	3.110	1.546	.40	1.365	1.016	5.453	2.815
Q = 1					Q = 10				
.90	1.021	0.222	2.053	0.050	.90	1.015	0.270	2.112	0.077
.85	1.037	0.293	2.096	0.090	.85	1.027	0.354	2.225	0.139
.80	1.055	0.361	2.151	0.140	.80	1.043	0.430	2.385	0.221
.75	1.076	0.428	2.220	0.203	.75	1.063	0.501	2.602	0.326
.70	1.101	0.495	2.306	0.283	.70	1.087	0.568	2.889	0.465
.65	1.130	0.566	2.414	0.386	.65	1.116	0.633	3.264	0.654
.60	1.163	0.639	2.549	0.520	.60	1.151	0.699	3.751	0.916
.55	1.202	0.718	2.720	0.700	.55	1.191	0.768	4.388	1.293
.50	1.248	0.803	2.936	0.946	.50	1.239	0.843	5.222	1.853
.45	1.303	0.897	3.214	1.293	.45	1.296	0.927	6.325	2.715
.40	1.368	1.003	3.578	1.800	.40	1.364	1.024	7.798	4.085
Q = 2					Q = 16				
.90	1.020	0.229	2.060	0.054	.90	1.013	0.291	2.152	0.091
.85	1.035	0.302	2.110	0.096	.85	1.024	0.381	2.315	0.167
.80	1.053	0.371	2.177	0.149	.80	1.039	0.460	2.551	0.269
.75	1.074	0.438	2.262	0.271	.75	1.058	0.531	2.873	0.404
.70	1.099	0.506	2.370	0.303	.70	1.082	0.596	3.297	0.585
.65	1.128	0.576	2.507	0.416	.65	1.111	0.658	3.850	0.832
.60	1.161	0.649	2.682	0.564	.60	1.146	0.719	4.570	1.182
.55	1.201	0.726	2.904	0.766	.55	1.188	0.783	5.513	1.691
.50	1.247	0.810	3.189	1.047	.50	1.237	0.854	6.755	2.461
.45	1.301	0.903	3.560	1.451	.45	1.294	0.934	8.404	3.665
.40	1.367	1.008	4.047	2.053	.40	1.363	1.028	10.614	5.610

z: thickness, u: largest diameter, d: radius of contacting area,
 p: internal pressure, Q: elasticity index, $Eh/(1-s^2)/T_0$

than does the non-elastic shell. The calculated radius of the area of contact increased as Q increased. This character of the elastic shell was qualitatively identical to the behaviour of a real

tennis ball filled with water under compression [7], when the value of Q was expected to be much higher than 16.

Such a definite and systematic dissimilarity be-

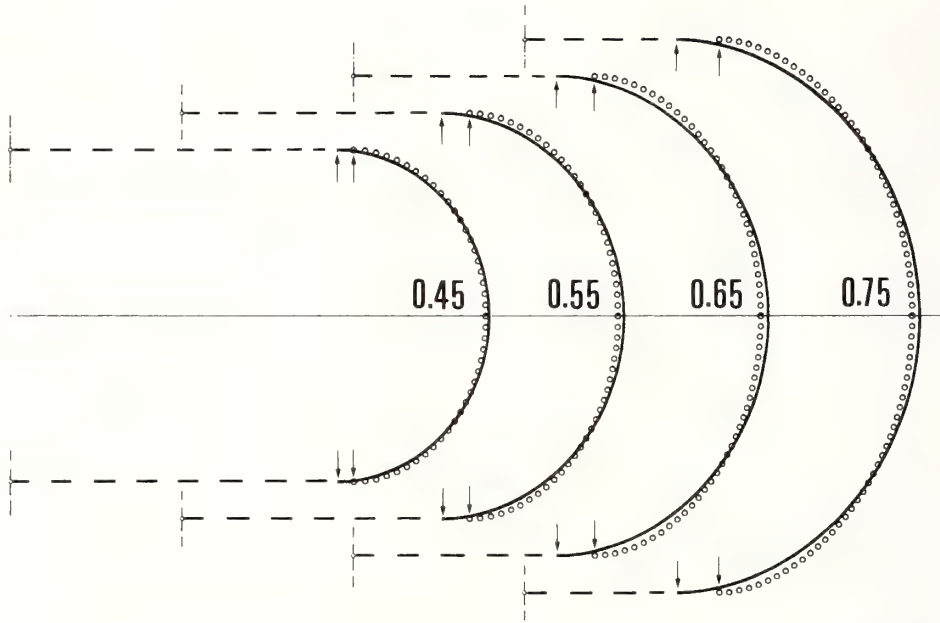


FIG. 6. Calculated contours of elastic and non-elastic shells. Numerals indicate relative thickness (z). Short dot-dash lines indicate the axes of the shells. Solid lines: Non-elastic surface ($Q=0$). Circles: Elastic surface ($Q=16$). Arrows point to the border between the contacting and free surface.

TABLE 2. Force of compression measured in unfertilized eggs of *Hemicentrotus pulcherrimus* (assembled by Prof. Yukio Hiramoto)

Relative thickness (Z)	0.90	0.80	0.70	0.60
Force of compression (F) ($\times 10^{-4}$ dyne)	0.90	2.25	4.60	8.75

tween the two contours is, however, not very large. As is evident from Table 1, the largest diameters differ, at the most, by only 2% (at $z=0.70$). Matching these contours with the actual contour of the real eggs would require high-quality pictures of several numbers of sea urchin eggs under compression before a fair judgement could be formed.

Yet Table 1 provides another means of testing the presence or absence of elasticity by using the values of $pd^2/2$ as a proportionality factor for predicting the force of compression (F). Prof. Yukio Hiramoto of the University of the Air kindly supplied me with his data on the force required to compress unfertilized eggs of *Hemicentrotus pulcherrimus* (Table 2). The calculated values of $pd^2/2$ for each degree of compression were multi-

plied by a certain factor (mathematically equal to T_0Z_0) so as to get the best fit for the data (Fig. 7). As in the case of matching contours, here, too, the predicted forces of compression of elastic and non-elastic shells were not very different, both fitting substantially well with the observed data. This is not entirely unexpected, however. In such a range ($z \geq 0.6$) of mild compression, the surface is only slightly stretched and the elasticity, if any, will not largely affect the issue.

Data presented in my earlier paper [6] will now be utilized since it includes 50 readings on 11 unfertilized eggs of *Hemicentrotus pulcherrimus* (Table 3) covering the range of compression down to 0.485. For each egg, the force of compression at $z=0.75$ was estimated by proper intrapolation of measured forces, as indicated in Table 1 under the

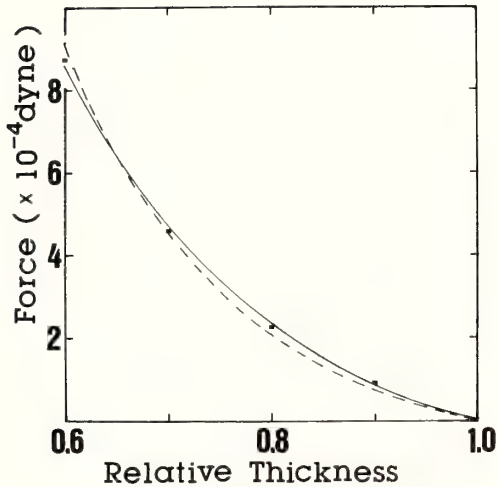


FIG. 7. Calculated force-deformation curves fitted to observed force (dots) at $z=0.90$ to 0.60 . Data obtained from Prof. Yukio Hiramoto. Solid line: Non-elastic ($Q=0$) surface. Broken line: Elastic surface ($Q=16$).

column "F₇₅". To even out the variation among eggs, the measured forces were normalized so that the estimated values of F₇₅ would come to unity. The normalized forces were plotted on a logarithmic scale against the degree of flattening (Fig. 8) in order to critically examine the F-z curve rather than the absolute values of force. The calculated force for the shells with or without elasticity ($Q=0$ and 16) were similarly normalized to have a unit force at $z=0.75$ and also plotted on the logarithmic scale. A substantial divergence in the calculated forces between elastic and non-elastic shell was noted. Plots of measured forces are now scattered around the theoretical curve for $Q=0$ (solid line) and favors the claim of non-elasticity of the membrane. Owing to the nature of logarithmic plotting, the points representing small forces for mild compression ($z=0.75$ to 0.9) are widely scattered, yet they are located closer to the solid line ($Q=0$) than to the broken line ($Q=16$). Both calculated curves happen to be quite linear on a logarithmic

TABLE 3. Force of compression (F) and thickness (Z) measured in unfertilized eggs of *Hemicentrotus pulcherrimus*

Egg							F ₇₅	Z ₀
1	0.20 (.900)	0.53 (.795)	1.16 (.680)	1.66 (.595)	2.21 (.550)	3.27 (.485)	0.68	93.0
2	0.26 (.860)	0.64 (.725)	0.90 (.665)	1.58 (.570)	2.50 (.495)		0.53	94.0
3	0.64 (.780)	1.15 (.680)	1.79 (.580)	2.56 (.530)			0.68	98.0
4	0.38 (.845)	0.92 (.715)	1.56 (.630)	2.27 (.575)			0.75	97.5
5	0.15 (.855)	0.62 (.735)	0.89 (.645)	1.35 (.590)	1.81 (.535)		0.49	97.0
6	0.48 (.830)	0.99 (.725)	1.52 (.665)	2.13 (.605)			0.84	95.5
7	0.33 (.825)	0.56 (.720)	0.85 (.670)	1.61 (.570)			0.51	93.5
8	0.20 (.870)	0.43 (.770)	0.70 (.705)	1.05 (.645)	1.51 (.605)	2.10 (.560)	0.58	92.0
9	0.31 (.840)	0.67 (.735)	1.00 (.650)	1.63 (.570)	2.33 (.510)		0.55	93.0
10	0.32 (.860)	0.59 (.760)	1.20 (.650)	2.02 (.580)			0.66	97.0
11	0.29 (.780)	0.67 (.665)	0.95 (.600)				0.37	95.0

Taken from the data presented in [6]. Upper rows: Force in 10^{-3} dyne. Lower rows in parentheses: Relative thickness ($z=Z/Z_0$). Force to compress the egg to $z=0.75$ estimated by proper intrapolation is shown under "F₇₅". Z₀: initial diameter(μm).

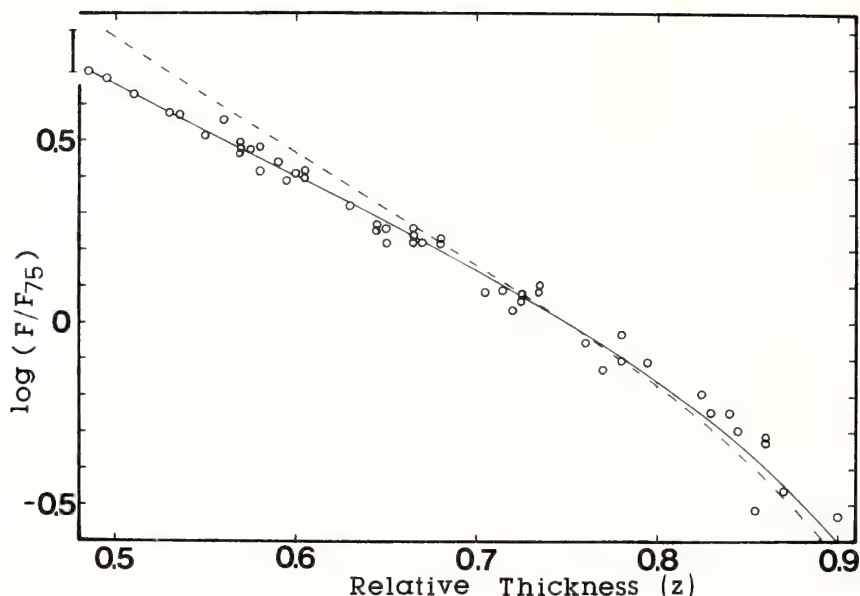


FIG. 8. Data measured at $z=0.90$ to 0.485 and the calculated forces for $Q=0$ (solid line) and $Q=16$ (broken line) are plotted on a logarithmic scale against the relative thickness, and normalized so that the values at $z=0.75$ ("F₇₅") come to unity. The scale bar at the upper-left corner indicates a 30% change of force.

TABLE 4. Calculated slopes of the $\log F-Z/Z_0$ curve

Q	0	1	2	5	8	12	16
slope	-2.60	-2.66	-2.72	-2.85	-2.95	-3.04	-3.12

Calculated force at $z=0.75, 0.70, 0.65, 0.60, 0.55, 0.50$ were linearized.

scale in the low range of $z (<0.75)$. The slopes of the $(\log F)-z$ curves are shown in Table 4. On the other hand, the slope of the linear regression curve for 36 points (in common logarithm) measured in the range of z from 0.75 to 0.48 was found to be -2.57 . The error variance $S^2=(S_{yy}-S_{xy}^2/S_{xx})/(n-2)$ of the slope was 0.00065 where the "sums of products", S_{xx} , S_{xy} and S_{yy} were 0.178 , -0.459 and 1.202 , respectively, and $n=36$. Based on these parameters, the probable range of the slope is -2.57 ± 0.17 ($t\sqrt{S^2/S_{xx}}=2.7 \times 0.061=0.17$) at $p < 0.01$. Comparison with the calculated slopes precludes the possibility that the surface of unfertilized sea-urchin eggs has elasticity index as high as 16 , or the Young's modulus of 10^3 dyne/cm² as claimed by Hiramoto [1]. A small amount of elasticity up to $Q=2$ is marginally probable, but making a distinction between non-elasticity and elasticity as low as $Q=2$ (Young's modulus of 10^2

dyne/cm²) appears very difficult using experimental data from the compression method. Thus, the data presented do not support the presumption of elasticity.

REMARKS

The present paper reports success in calculating the profile of spherical shells with given elasticity, which could serve to simulate deformed animal cells. The present calculation was based on simplifying assumptions. Among them, the assumptions that there is no bending stress in the membrane and that the inner cytoplasm is fluid should be kept in mind when simulating the calculated profile with living cells. As for unfertilized eggs of the sea-urchin, I earlier estimated that the bending stress of the membrane would be negligible in the compression experiment [6]. Measurement of the

viscoelasticity of the cytoplasm of unfertilized sea-urchin eggs by Hiramoto [12] indicates that deformation of the cytoplasm will not create any permanent stress. Thus, I believe that the present calculation will apply at least to unfertilized sea urchin eggs.

Although the present study precluded the presence of elasticity as high as 10^3 dyne/cm² based on Hiramoto's calculation, there are still two sets of data which seem to contradict my claim of non-elasticity. One is the observation of Hiramoto [2] on centrifuged sea-urchin eggs, and the other is my own experience with highly compressed sea-urchin eggs [13]. Critical examinations of these data have not yet been performed.

ACKNOWLEDGMENT

I wish to express my gratitude to Prof. Yukio Hiramoto of the University of the Air who kindly provided me with his data on the compression experiment. I also thank Prof. Susumu Ishii of Waseda University for instructing me on the statistical analysis of measured and calculated slopes of $F-z$ curves. This work was supported in part by a grant from the Ministry of Education, Science and Culture of Japan (61304008, 61490016).

APPENDIX: DETAILS OF THE ADJUSTMENTS

The parameters of the shell were modified by the following five kinds of adjustments.

1) Pressure adjustment (by eq. (7))

The internal pressure $p(i)$ to be held by each segment was calculated by eq. (7) using $t_L(i)$ and $t_T(i)$. The calculated pressures for segments $M+1$ to 48 were averaged. Based on the premise of uniform pressure in egg cytoplasm (cf. assumption 4 given earlier), the value of $r_L(i)$ for each segment was modified so that the calculated pressures $[p(i)]$ would come closer to their average. Throughout this adjustment, $\theta(i)$ was also modified to compensate for the change in $r_L(i)$ so that $S_L(i) [=r_L(i)\theta(i)]$ remains unchanged with the hope that the balance of tensions, which is largely susceptible to change in the length of the segment (S_L), is not drastically disturbed.

2) Tension adjustment at the free surface (by eq. (8))

In numerical calculation, the value dt_L/dx in eq.

(8) was replaced by $t_L(i+1)-t_L(i)$ divided by $(x(i+1)-x(i-1))/2$. The balance of forces at each node ($M+1$ to 48) was examined by putting $t_L(i)$, $t_T(i)$, and $x(i)$ into eq. (8). According to the imbalance thus detected, the position of each node ($M+1$ to 48) was shifted along the meridian by modifying $\theta(i)$ to improve the balance.

3) Tension adjustment at the contacting surface (by eq. (8))

The tension balance at each node on the contacting surface was adjusted in a procedure similar to adjustment 2 except that the modification was made to $x(i)$ ($i=1$ to $M-1$), instead of $\theta(i)$.

4) Tension adjustment at the border (by eq. (8))

Separate adjustments of the tension balance for the contacting and free surfaces (adjustments 2 and 3) will concentrate the imbalance at the border (node M) where the contacting and free surfaces meet. Since the two segments neighboring the border are assigned different resting lengths, S_{C0} and S_{L0} , the adjustment at the border was achieved by shifting the position of node M along the surface of the initial sphere, which involves reciprocal changes in S_{C0} and S_{L0} with the accompanying modification of E_L , t_L and t_T . This results in reducing the imbalance between the two segments at the border. This adjustment of the resting lengths induces a subtle disturbance of the balance in all but one (border) nodes which are carried over to subsequent iterations.

5) Volume adjustment

Adjustments 1 and 2 usually change the calculated volume of the shell. To return it to its initial volume, a certain factor was multiplied to all sets of $r_L(i)$ at the nodes $M+1$ to 48, and $x(i)$ of nodes 1 to M . A modification of the radius d of the contacting surface is performed for this occasion.

The iteration consisting of these 5 separate adjustments, each involving a negative feedback of imbalances to the original parameters $r_L(i)$, $\theta(i)$ and d , was repeated several times until a) the pressures calculated for all segments became uniform within 0.01%, b) tension imbalances between any adjacent segments became less than 0.1% and c) deviation of the volume from unity became less than 10^{-5} . The chief difficulty encountered in such a scheme of "multiple adjustments" was that any

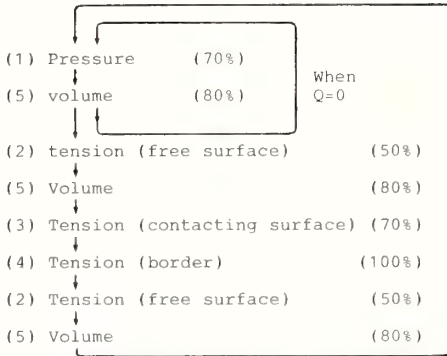


FIG. 9. Iteration of adjustments. Percentages in parentheses are the rate of negative feedback to parameters.

one of the adjustments (pressure, for example) often tended to amplify the imbalance of other aspects (tension for example) resulting in a never-ending oscillation of the calculated profile, even when only moderate changes were imposed on original parameters in a single step of adjustment by limiting the rates of feedback to low levels. A scheme for a successive sequence of adjustments which modified the profile steadily and quickly to its equilibrium was fortunately found after several trials. Figure 9 is the final version of present iteration in which the adopted rates of negative feedback are specified in percentages.

Numerical calculations were automatized by a computer program called "ELAS", written in Basic and adapted to a personal computer (Hitachi S1-40).

REFERENCES

- Hiramoto, Y. (1963) Mechanical properties of sea urchin eggs. I. Surface force and elastic modulus of the cell membrane. *Exp. Cell Res.*, **32**: 59-75.
- Hiramoto, Y. (1976) Observations and measurements of sea urchin eggs with a centrifuge microscope. *J. Cell. Physiol.*, **69**: 219-230.
- Hiramoto, Y. (1970) Rheological properties of sea urchin eggs. *Biorheology*, **6**: 201-234.
- Hiramoto, Y. (1976) Mechanical properties of sea urchin eggs. III. Visco-elasticity of the cell surface. *Dev. Growth Differ.*, **18**: 377-386.
- Hiramoto, Y. (1987) Evaluation of cytomechanical properties. In "Cytomechanics". Ed. by J. Bereiter-Hahn, O. R. Anderson and W.-E. Reif, Springer, Berlin. pp. 31-46.
- Yoneda, M. (1964) Tension at the surface of sea-urchin eggs. A critical examination of Cole's experiment. *J. Exp. Biol.*, **41**: 893-906.
- Yoneda, M. (1973) Tension at the surface of sea urchin eggs on the basis of 'liquid drop' concept. *Adv. Biophys.*, **4**: 153-190.
- Yoneda, M. (1976) Temperature-dependence of the tension at the surface of sea-urchin eggs. *Dev. Growth Differ.*, **18**: 387-389.
- Cole, K. S. (1932) Surface force of the *Arbacia* egg. *J. Cell. Comp. Physiol.*, **1**: 1-9.
- Timoshenko, S. and Woinowsky-Krieger, S. (1970) *Theory of Plates and Shells*, McGraw-Hill, New York, 2nd ed., pp. 434.
- Yoneda, M. (1986) The compression method for determining the surface force. *Methods Cell Biol.*, **27**: 421-434.
- Hiramoto, Y. (1969) Mechanical properties of the protoplasm of the sea urchin egg. I. Unfertilized egg. *Exp. Cell Res.*, **56**: 201-208.
- Yoneda, M. (1980) Tension at the highly stretched surface of sea urchin eggs. *Dev. Growth Differ.*, **22**: 39-47.

Effect of Hexyleneglycol on Meiotic Division of Starfish Oocytes

WAKAKO YAMAO and TAIKO MIKI-NOUMURA

*Department of Biology, Ochanomizu University,
Ohtsuka, Tokyo 112, Japan*

ABSTRACT—Following 1-methyladenine treatment, maturing oocytes of the starfish, *Asterina pectinifera*, were transferred to sea water containing 2.5% hexyleneglycol (HG). After 20–30 min, the meiotic apparatus (MA), at first clearly visible as a tiny point close to the cell membranes, began to increase in size. After a time, most of the larger MA became situated perpendicular or parallel to the cell membranes, but in the case of a few oocytes near the cell center. The diameter of the aster of the isolated MA at metaphase of HG-treated oocytes two or three times longer than that in the control experiment. Depending on its particular location in the oocytes during maturation, the larger MA induced three different events during meiotic division: giant polar body formation, unilateral furrowing in most oocytes, and equal cell division in a few oocytes. The frequency of these events depended upon when the oocytes were transferred to HG–SW during maturation.

Based on these findings, we attempted to present an explanation for the events induced by HG. When maturing oocytes were transferred to HG–SW, HG diffused gradually into them, stabilizing the migrating MA in its particular position during maturation, and causing its size to increase through the reassembly of microtubules around it. The larger MA may cause the meiotic division of oocytes to change, leading to the subsequent inducement of the above three events, depending on their particular location in the oocytes during maturation.

INTRODUCTION

Mazia and Dan in 1952 [1] were the first to succeed in isolating the mitotic apparatus (MA) from synchronous dividing sea urchin eggs, and confirmed the MA to be a rigid structure which appears and then disappears during mitosis. They accomplished this in two steps: light fixation of dividing cells by application of cold ethanol and dispersion of cytoplasm around the MA with detergents.

After several attempts, Kane [2] finally devised a simple one-step isolation method, treating a synchronous culture of dividing sea urchin eggs with 1 M (12.8%) hexyleneglycol (HG), maintaining pH at 6.4. He reported that various non-sulfur containing six-carbon glycols could be used for the isolation. Rebhun and Sawada [3] found that the volume and birefringence of the MA of sea urchin eggs increases with the addition of HG at meta-

phase. In their study of the effect of HG on MA, Endo *et al.* [4] recently found that the MA of sea urchin eggs in sea water containing 5% HG, possesses a surprisingly large number of microtubules conspicuously uniform in length.

Studying the polymerization process of porcine brain tubulin in the presence of HG, we recently found that HG promotes microtubule polymerization, shifting the equilibrium between microtubules and tubulin to the polymer side, and accelerating the initial velocity of the polymerization (Yamao and Miki-Noumura, unpublished data).

In consideration of the above, we attempted to bring about some change in the polar body formation of starfish oocytes by HG, since HG stabilizes MA [2] and induces an increase in the volume and birefringence of MA [3]. Using starfish oocytes, HG was first noted to cause additional microtubules to reassemble around the meiotic apparatus (MA), causing it to become much larger than that in the control. Depending on the particular posi-

tion of MA in the oocytes during maturation, the larger MA induced the occurrence of three distinct events during meiotic division: formation of a giant polar body, unilateral furrowing or equal cell division.

MATERIALS AND METHODS

Materials

A starfish, *Asterina pectinifera*, was used, and a sea urchin, *Hemicentrotus pulcherrimus*, was used for a preliminary experiment.

Immature oocytes of the starfish were prepared by treating the ovaries with Ca-free artificial sea water (CaFSW), in order to remove follicular envelopes. The oocytes were pooled and suspended in sea water (SW) at 17°C, after washing several times with CaFSW. More than 95% of these isolated oocytes were intact and immature.

Sea urchin eggs were obtained by injecting 0.5 M KCl into the body cavity. Shedded eggs were suspended in SW at about 18°C, after washing several times with SW.

Hexyleneglycol (HG) treatment

The isolated immature oocytes were suspended in SW containing 5×10^{-6} M 1-methyladenine (1-MeAde) to induce meiosis. After various set periods, from 20 to 50 min, equal volumes of SW containing 5% hexyleneglycol were added to the suspended SW of the oocytes. The oocytes were cultured continuously in it. To observe the polar body formation clearly, the fertilization membranes were sometimes elevated, by treating the oocytes with 10 mM caffeine for 5 min, before suspending in 1-MeAde-SW. Such a 5 min treatment in caffeine was confirmed not to induce a parthenogenetic response, only the elevation of the membrane, as reported by Obata and Nemoto [5]. Observation took place under a phase-contrast (XF-ph) and a high sensitivity polarizing differential (recti-Nomarski, HPO) microscope (Nikon Optical Co., Tokyo). The phase-contrast microscope was equipped with a Nikon PFMB camera, and photographs were taken on Neopan F film (Fuji Co., Tokyo) with an exposure time of 1/4–1/30 sec.

Isolation of meiotic apparatus (MA)

We have used the word "MA" here for the meiotic apparatus of starfish oocytes, because Dan and co-workers used "MA" for meiotic apparatus of *Spisula* oocytes in their papers [6].

Two methods, using hexyleneglycol (HG) or glycerol/DMSO, were used for isolation of the MA, as described previously [2, 4]. Compositions of the isolation medium were as follows: HG isolation medium (15% (V/V)HG, 1 mM EGTA, 10 mM KH_2PO_4 , pH 6.2) and glycerol/DMSO-isolation medium (1 M glycerol, 10% (V/V) DMSO, 1 mM EGTA, 0.5 mM MgCl_2 , 1% (V/V) Nonidet P-40, 10 mM MES pH 6.2).

Oocytes at the desired stage were collected by low-power centrifugation washed twice with ten volumes of 1 M dextrose, to favor dispersion of cytoplasm. The pellet of oocytes was suspended in ten volumes of the isolation medium. The suspension was shaken up and down several times in a centrifugal tube to disperse cytoplasm around the MA. The isolated MA was then collected by low-power centrifugation.

RESULTS

Observation under a phase-contrast microscope

Confirmation was first made on the effects of hexyleneglycol (HG) by using fertilized sea urchin eggs, as previously reported by Endo *et al.* [4]. When fertilized eggs reached prometaphase or metaphase in the first cleavage, they were transferred to artificial sea water containing 5% HG (HG-SW). After 15 min in HG-SW, a clear zone appeared around the mitotic apparatus (MA) of prometaphase eggs, encircling the MA and causing its width to increase with time (Fig. 1a). The two asters of the metaphase MA became larger (Fig. 1b), and could be discerned more clearly. They appeared to become slightly separated from each other during the 15 min in HG-SW. The two larger asters apparently consisted of two larger monasters side by side, resembling a pair of glasses (Fig. 1c). Based on these observations, we next attempted to bring about some changes in the polar body formation of starfish oocytes using HG.

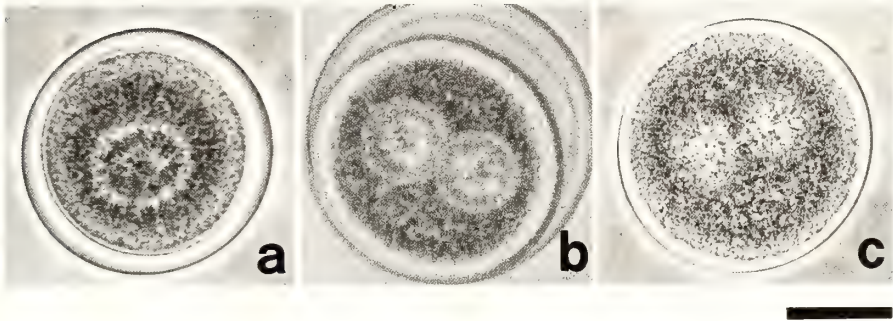


FIG. 1. Fertilized sea urchin (*Hemicentrotus*) eggs.
 a. 15 min after suspension in 5% HG-SW at prometaphase.
 b. 15 min after suspension in 5% HG-SW at metaphase.
 c. 30 min after suspension in 5% HG-SW at metaphase.
 Phase-contrast micrographs. Bar represents 100 μm .

As is already known, immature oocytes of starfish start meiosis in sea water within 20 min at 20°C, following the addition of 1-methyladenine (1-MeAde). The germinal vesicles in the oocytes begin to break down in 1-MeAde-SW and then disappear. The first polar body is formed after 70–80 min (Fig. 2a, b), and the second one, 110–120 min after 1-MeAde treatment.

In this experiment, the concentration of HG in SW was determined to be 2.5%, after various concentrations from 1 to 10% HG had been added to the SW. The oocytes were transferred to 2.5% HG-SW after 40 min of 1-MeAde treatment. Each oocyte possessed a tiny meiotic apparatus (MA) which could initially be clearly discerned as a small point under a phase-contrast microscope. In about 15 min, the MA of HG-treated cells

became distinct and larger, with its orientation and shape quite evident (Fig. 3a). The oocytes in the control had a smaller MA situated close to the cell membranes and visible as a clear point. After 30 min, the larger MA of HG-treated oocytes appeared to consist of two larger asters, side by side, resembling a pair of glasses, as was also noted in HG-treated eggs of the sea urchin. The larger MA was situated close to the cell membranes, and apparently attached to the cell cortex. The long axis of the MA was directed parallel or perpendicular to the cell membranes (Fig. 3b, c).

When the long axis of the MA became perpendicular to the cell membranes (Fig. 3d), the larger MA then continued to grow and after about 70–80 min, extruded a giant polar body, which was about 10–18 μm in diameter. Its length was about two or

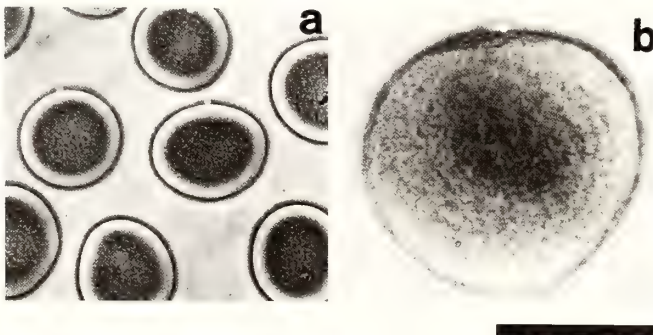


FIG. 2. Polar body formation of the oocytes in the control experiment. Extruded polar body in control experiment about 60 min after 1-MeAde treatment. a: lower magnification, b: higher magnification. Phase-contrast micrographs. Bar represents 100 μm .

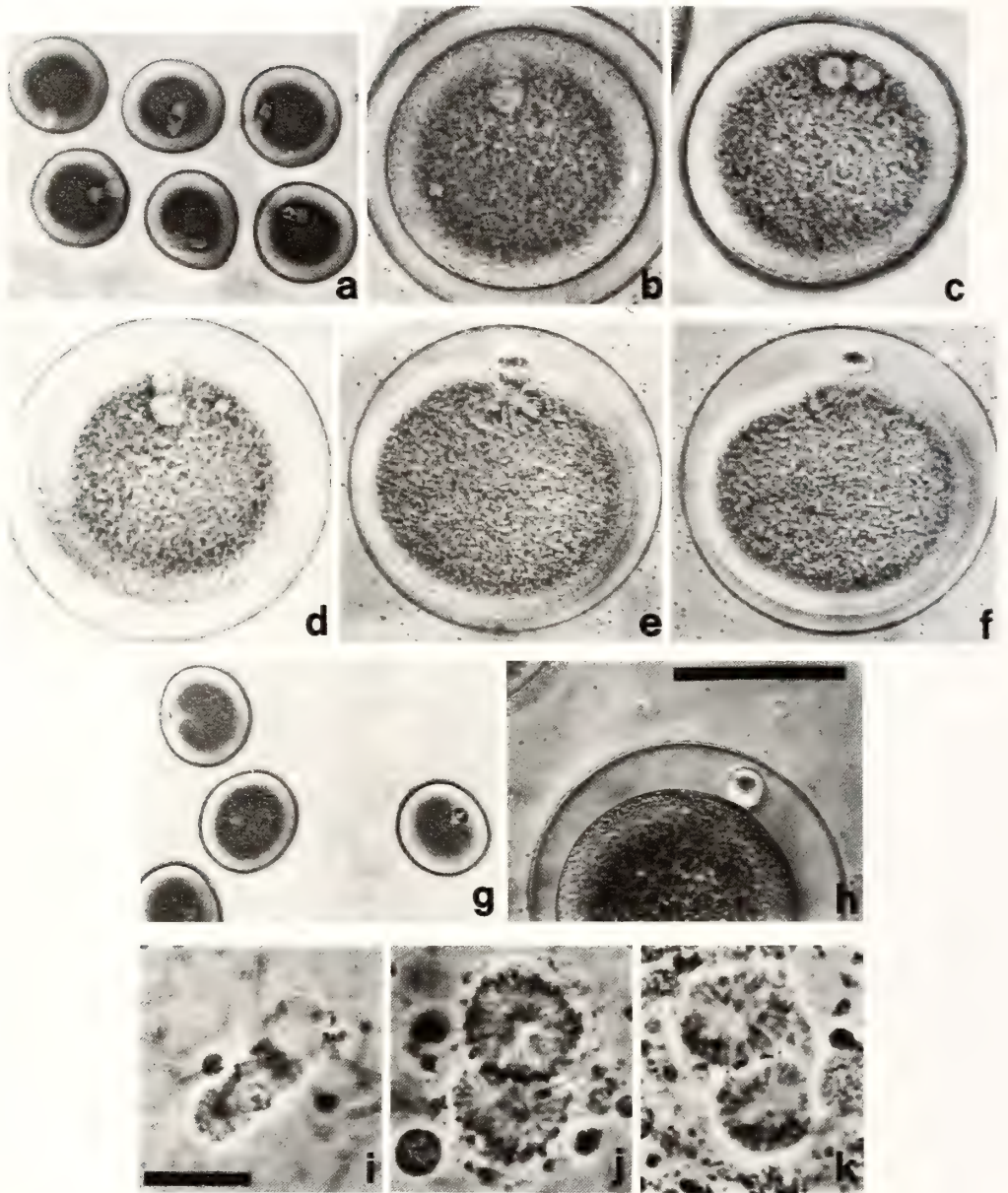


FIG. 3. Polar body formation of the oocytes suspended in 2.5% HG-SW. Giant polar body extruded from the oocytes. a: 30 min after HG-SW treatment. b: 30 min. Larger MA oriented perpendicular to the cell membrane. c: 30 min. Larger MA oriented parallel to the cell membrane. d-f: Extrusion process, d: 40 min, e: 90 min, f: 140 min, g and h: 180 min, after HG-SW treatment. Bar represents 100 μ m, which is shown for photos at higher magnification. Phase-contrast micrographs.

i-k: Isolated meiotic apparatus (MA) from starfish oocytes. i: MA in the control experiment. j and k: Larger MA isolated from HG-treated oocytes. Bar represents 20 μ m. Phase-contrast micrographs.

three times that of the control (compare Fig. 3g, h and Fig. 2a, b). Immediately beneath the extruded polar body, one larger aster continued to remain and never disappeared (Fig. 3e, f). In no case did a HG-treated oocyte extrude a second polar body, in contrast to the control oocytes.

For a comparison of the MA in HG-treated and control oocytes, MA were isolated from both sources as described in "Methods". The MA in the control consisted of a spindle body and two smaller asters after 40 min in 1-MeAde. In some cases, a normal aster about $6\ \mu\text{m}$ in diameter was present on one side. The other aster had its flattened end on astral rays attached by some vesicles or membrane (Fig. 3i). MA isolated from HG-treated oocytes exhibited well-developed asters on both sides of the spindle, which was about 9 to $10\ \mu\text{m}$ in diameter, and increased to about $20\ \mu\text{m}$ after 30 min of HG-SW treatment. The MA appeared to be comprised of a spindle body and two larger asters of the same diameter (Fig. 3j, k). The aster with its flattened end on the astral rays could not be found in the MA of HG-treated oocytes.

With its long axis parallel to the cell membranes,

MA continued to grow, and the cell surface immediately above the middle point of the MA gradually became concave (Fig. 4A). The concavity progressed more on one side with time, in a manner similar to the cleavage furrowing of medusa (*Spirocodon*) eggs. The two well-developed asters were situated just under the concave cell surface on both sides of the furrow region (Fig. 4B, C). Unilateral furrowing did not divide the oocytes completely, and later, the furrow sometimes ceased to be apparent.

The MA was often situated near the cell center of HG-treated oocytes, but the reason is unknown at present. It continued to grow, becoming much larger than previously observed in giant polar body formation and unilateral furrowing. The MA consisted of two larger asters. The chromosomes were observed near the equator region, and sometimes formed vesicles or lumps. The cell surface over the middle of the MA along the long axis became concave on both sides (Fig. 4D, E). The cleavage furrow became deeper on both sides of the cell surface, often constricting the oocytes equally (Fig. 4F). Each divided cell contained a

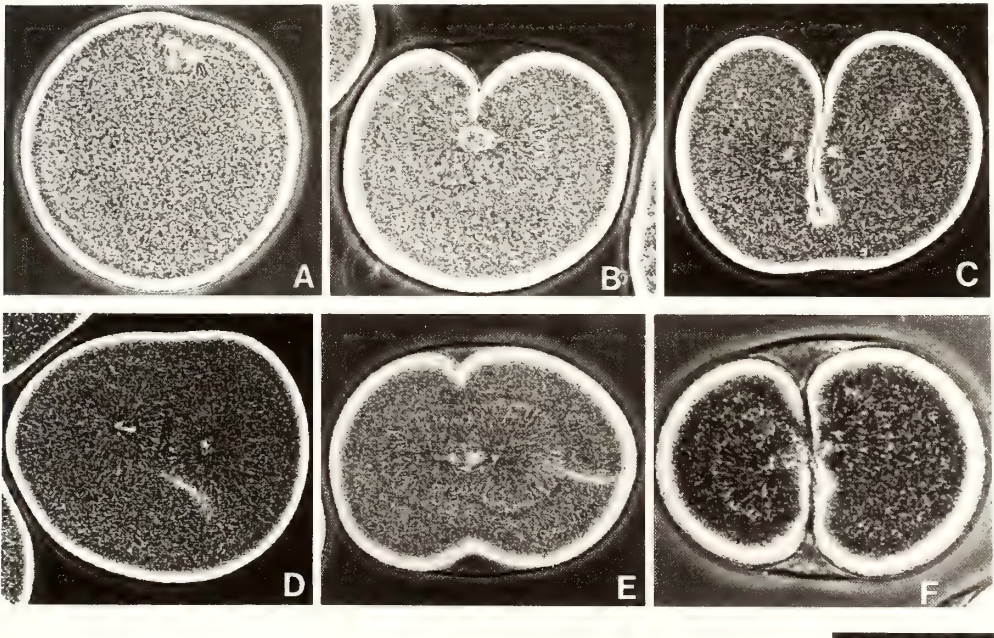


FIG. 4. A-C, Unilateral furrowing of the oocytes suspended in HG-SW. A: 50 min, b: 100 min, c: 140 min after suspension in HG-SW. D-F, Equal cell division of oocytes suspension in HG-SW. D: 120 min, E: 200 min, F: 230 min, after suspended in HG-SW. Bar represents $100\ \mu\text{m}$. Phase-contrast micrographs.

well-developed larger MA, with vesicles or lumps of chromosomes. The MA failed to disappear even upon completion of division. The two equally divided cells ceased to undergo further division.

Time course of events in HG-treated starfish oocytes

Following HG-SW treatment of oocytes during maturation, the following three events were observed to occur: formation of a giant polar body, unilateral furrowing and equal cell division. When the oocytes were transferred to HG-SW after 40 min of 1-MeAde treatment, HG at 2.5% in SW induced formation of a giant polar body after 80 min of 1-MeAde treatment. The frequency of occurrence of this event was measured every 10 min. Using 100 oocytes, we found that it was 85% at 100 min, decreasing to 20% at 130 min. It increased again, reaching 40% at 160 min. Unilateral furrowing first began after 80 min, and reached a maximal value of 30% at 200 min. It decreased again at 240 min. Equal cell division was first noted at 160 min and gradually occurred in 5% of the oocytes at 200 min. These decreases in frequency of occurrence with time may possibly have resulted from recovery to the beginning state, due to the incomplete division of the giant polar body or incomplete unilateral furrowing. When the oocytes started constricting again, the occurrence of a giant polar body formation and unilateral furrowing peaked for a second time.

In order to further examine the above events, we studied the effects of HG-SW on oocytes,

extending the time of HG treatment from 20 to 50 min. The procedure is shown in Figure 5. The relationship between the frequency of these events and time in HG-SW is illustrated in Figure 6. The frequency was maximal at about 100 min and 140–160 or 200 min following 1-MeAde treatment. The increasing and decreasing trends were essentially the same as those of the control during meiotic division, corresponding to the formation of first and second polar bodies, in spite of some delay in HG-treated oocytes. It thus appeared that the cycle of maturation division may possibly exert some effect on the occurrence of these events which were induced by HG. The frequency of giant polar body formation depended on the particular time at which the oocytes were subjected to HG-SW treatment. Later treatment resulted in a higher frequency. When oocytes were transferred to HG-SW after 50 min of 1-MeAde treatment, polar body formation occurred in about 90% of the oocytes, while transfer after 20 min reduced it to about 40% during a period of 100 min. Essentially the same results occurred at 140–150 min, when the second peaks or second maximal values were observed. As shown in Figure 6a, transfer at 50 min resulted in a frequency of about 90%, but only 5–8% at 20 min.

Unilateral furrowing was maximal or peaked two times, at 100 and 200 min, the latter exceeding the former. A transfer time of 30 min following 1-MeAde-SW treatment resulted in a frequency of 40%, while at 50 min, the frequency was 20% at

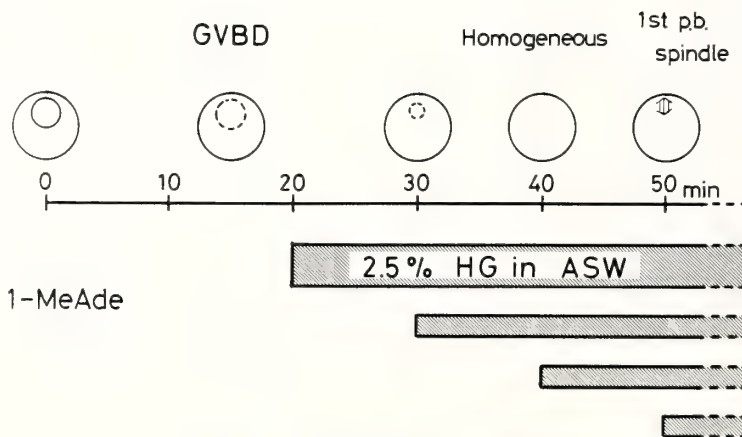


FIG. 5. The experimental procedure.

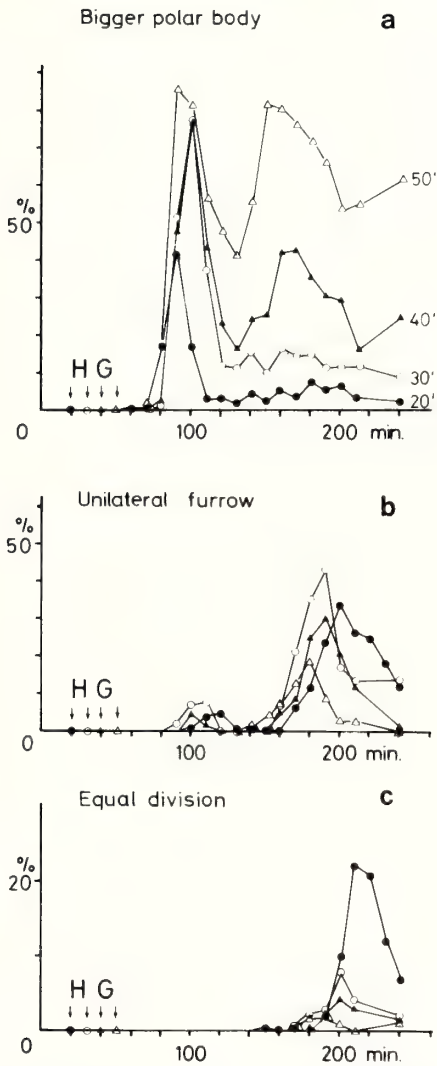


FIG. 6. Time course of frequency of three changes induced by HG. The oocytes were transferred to HG-SW at various time, from 20 to 50 min after 1-MeAde treatment. ● 20 min, ○ 30 min, ▲ 40 min, △ 50 min after 1-MeAde treatment. Arrows indicate the transferring time of the oocytes to HG-SW. Ordinate: Frequencies (%) of each event. Abscissa: Time (min) after 1-MeAde treatment. a: Giant polar body formation. b: Unilateral furrowing. c: Equal cell division.

the second peak during 200 min (Fig. 6b). The equal division peaked only once at 200 min. It attained a maximum of 20% during 200 min, as a result of a transferring time of 20 min, but only 2–3% at 50 min, as shown in Figure 6c. The frequen-

cies of both unilateral furrowing and equal division were greater with early HG-SW treatment, but polar body formation was more frequent with later treatment. The frequencies of these events seem to be a function of the time of HG-SW treatment. In spite of the considerable deviation due to incomplete meiotic synchronization in starfish oocytes, the relationship is adequately apparent. That is, greater unilateral furrowing and equal division resulted from earlier HG-SW treatment, while later treatment induced more frequent giant polar body formation.

Next, the occurrence of these events was observed in the HG-treated oocytes at 40 min following 1-MeAde treatment, to determine which events occurred when the MA was in a certain location or with a certain orientation in the oocytes. About sixty oocytes were continuously observed under a recti-Nomarski microscope (a high sensitivity polarizing differential interference contrast microscope). The position of the MA in oocytes was found by measuring its distance from the center of the oocytes after determining the focal plane. In order to represent where the MA situates in the oocyte, the sphere of oocyte was divided into two parts. The radius of the oocyte was expressed as 0% at the center and 100% at the cell surface. One area of the oocyte was occupied by radius from 0% to 50%, and another area, by radius from 50% to 100%. In about 90% of the oocytes, the MA was situated near the cell surface, i.e., in the area occupied by 50–100% radius of an oocyte to the cell surface. Unilateral furrowing and giant polar body formation were observed in 90% of the oocytes situated in that area. In a few cases, the MA was found near the center of the oocytes, that is, in the area occupied by 0–50% radius from the cell center, reaching 5–7%. The location of the MA in the oocytes was substantially consistent with the frequencies of the three events, and thus may be closely related.

DISCUSSION

Effects of hexyleneglycol on the MA

At meiotic division, the MA could be clearly seen as a tiny point close to cell membranes in

starfish oocytes under a phase-contrast microscope. It grew with time, with its long axis perpendicular to the cell membranes. The small area of the cell cortex to which the astral rays were attached, appeared as being pushed out; it was finally extruded as a polar body at the first meiotic division. Based on a study of *Spisula* oocytes, Dan [6] has proposed that "anchorage" of the spindle to the cortex at its one pole is a common phenomenon in the unequal division of polar body formation.

As shown in "Results", when the oocytes were transferred to HG-SW after 1-MeAde treatment, three distinct events occurred as a result: giant polar body formation, unilateral furrowing and equal cell division. Observation of HG-treated oocytes indicated that the MA at metaphase grew in size. The extruded polar body had a diameter of about 10–18 μm , which was two or three times that of a normal polar body. The MA at the time of unilateral furrowing and equal cell division was much larger than that in the control. Although not investigated in detail by electron microscopy, the astral rays in the MA appeared similar to those of the MA in sea urchin eggs. In Figure 4D and E, the MA has a remarkable number of microtubules very fine in appearance. The asters contained many microtubules of uniform length, thus constituting a layer or membrane surrounding the MA in dividing cells. The two large asters in the MA had the appearance of a pair of glasses, surrounded by a clear distinct zone. This was also observed in sea urchin eggs by Endo *et al.* [4]. HG-SW induced growth of the MA by causing the number of microtubules around it to increase. In fact, a preliminary study of HG-effects on tubulin polymerization of porcine brain, indicated that HG shifts the equilibrium between the microtubules and tubulin to the polymer side and further accelerates the initial velocity of the polymerization (Yamao and Miki-Noumura, unpublished data). This shows HG to be the cause for the greater number of microtubules of uniform length around the MA in dividing cells, possibly by rapid organization of many microtubule nucleating center around the MA, to induce additional microtubule assembly, and to shift the equilibrium between tubulin and the microtubules to the poly-

mer side.

Time course of the three events in oocytes induced by HG-SW

The following events were induced by 2.5% HG in SW: giant polar body formation or unilateral furrowing in most of the oocytes, and equal cell division in a few cases. The frequency initially increased, reached a plateau, decreased and then increased again, as shown in Figure 6. The time course of this increase and decrease was essentially in agreement with that of meiotic division, the first and the second polar body formations. The cell cycle of oocyte maturation may have some effect on the time course of these events.

As described in "Results", in most cases, the long axis of the MA was directed parallel or perpendicular, close to the cell membranes after a break-down of the germinal vesicles. In 90% of the oocytes, the MA was close to the cell membranes, in spite of the perpendicular or parallel long axis orientation. Giant polar body formation and unilateral furrowing were also induced in these oocytes. Unilateral furrowing was maximal at 30 min after 1-MeAde treatment. Equal division was so at 20 min, and giant polar body formation at 50 min. Although incompletely synchronous meiosis in the starfish oocytes may possibly bring about a time deviation in the occurrence of each event, the order of occurrence appeared to be, equal division, unilateral furrowing, and giant polar body formation. This order suggests the location and orientation of the MA after a break-down of the germinal vesicles. It is initially parallel to the cell membranes and then becomes perpendicular to them. In the former case, it would grow in size through the action of HG, followed by inducement of the unilateral furrow at the cell cortex in the middle of the MA. In the latter case, the increase in size of the MA would possibly cause extrusion of a giant polar body, attached with astral rays to the small area of cell cortex. In about 5% of the oocytes, the MA may be situated near the cell center and may not migrate to the cell surface following the break-down of germinal vesicles. The MA may become larger at the cell center, thus inducing a furrow in the middle of the oocytes, and causing them to divide in half.

In this present experiment, HG diffused gradually into the oocytes following their transfer to HG-SW, and stabilized the migrating MA *in situ*. Furthermore, HG promoted reassembly of microtubules in oocytes and resulted in greater growth of the MA which may be the possible cause of the three distinct events. The results of the present research are presented schematically in Figure 7, although nothing definite can be said about equal division owing to the low frequency of its occurrence. E. B. Wilson's book, *The Cell in Development and Heredity*, presents figures describing MA orientation during meiosis [7], which are consistent with the present ideas concerning the MA during

meiosis in starfish oocytes. As mentioned above, Dan has proposed that the migration of the meiotic spindle to the cell cortex and its becoming situated close to it are phenomena that occur in the case of polar body formation, based on observation of the meiotic division of *Spisula* oocytes [6]. However, we have so far been unable to directly observe the migration of the MA to the cell cortex after the break-down of germinal vesicles in starfish oocytes. Examination of the processes of meiotic division of starfish oocytes through electron microscopy should provide further clarification of this phenomenon.

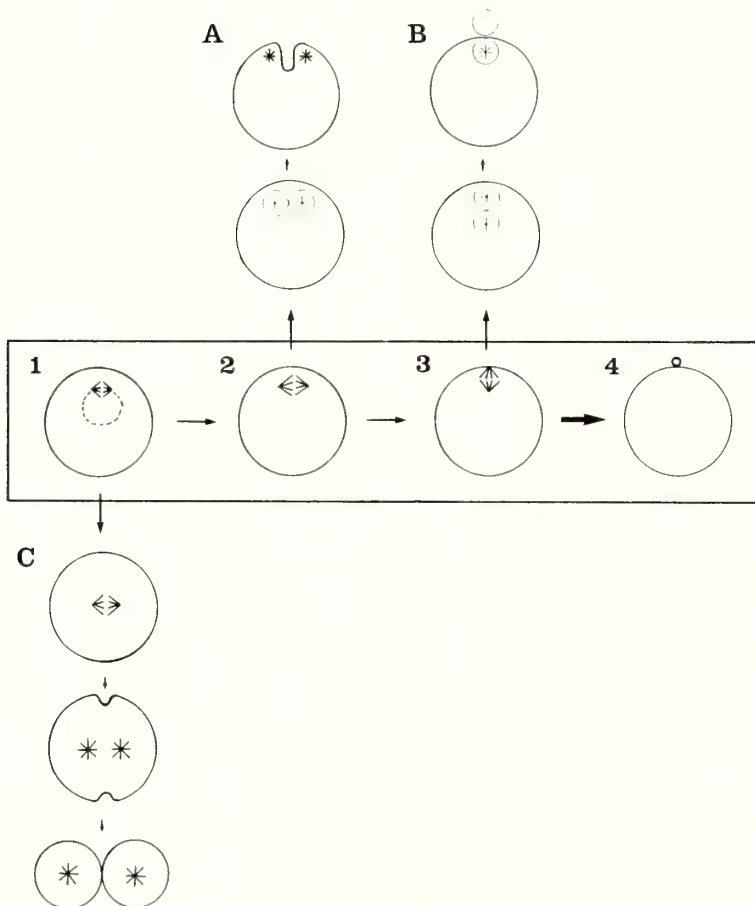


FIG. 7. Proposed explanation of our results. Normal maturation process is shown by 1-4, enclosed in the box. A-C: Events induced by HG. A: Unilateral furrowing. B: Formation of a giant polar body. C: Equal cell division.

ACKNOWLEDGMENTS

We thank Miss Atsuko Hanayama for her kind help in preparing this manuscript. Thanks are also due to the staff of Tateyama Marine Laboratory, Ochanomizu University, for providing facilities and materials for this study. This work was supported in part by a Grant-in-Aid for scientific research from the Ministry of Education, Science and Culture, Japan.

REFERENCES

- 1 Mazia, D. and Dan, K. (1952) The isolation and biochemical characterization of the mitotic apparatus of dividing cells. *Proc. Natl. Acad. Sci.*, **38**: 826-838.
- 2 Kane, R. (1962) The mitotic apparatus: Isolation by controlled pH. *J. Cell Biol.*, **12**: 47-55.
- 3 Rebhun, L. I. and Sawada, N. (1969) Augmentation and dispersion of the *in vitro* mitotic apparatus of living marine eggs. *Protoplasma*, **68**: 1-22.
- 4 Endo, S., Toriyama, M. and Sakai, H. (1983) The mitotic apparatus with unusually many microtubules from sea urchin eggs treated by hexyleneglycol. *Dev. Growth Differ.*, **25**: 307-314.
- 5 Obata, C. and Nemoto, S. (1984) Artificial parthenogenesis in starfish eggs: Production of parthenogenetic development through suppression of polar body formation by methylxanthines. *Biol. Bull.*, **166**: 525-536.
- 6 Dan, K. and Ito, S. (1984) Studies of unequal cleavage in Molluscs: I. Nuclear behavior and anchorage of a spindle pole to cortex as revealed by isolation technique. *Dev. Growth Differ.*, **26**: 249-262.
- 7 Wilson, E. B. (1925) *The Cell in Development and Heredity*, Macmillan, New York, pp. 498-503.

Gamete Interactions and Sperm Incorporation in the Nemertean, *Cerebratulus lacteus*

FRANK LONGO, WALLIS H. CLARK, JR.¹ and GERTRUDE W. HINSCH²

Department of Anatomy, University of Iowa, Iowa City, IA 52252, ¹Bodega Marine Laboratory, University of California, P.O. Box 247, Bodega Bay, CA 94923, and ²Department of Biology, University of South Florida, Tampa, FL 33620, U.S.A.

ABSTRACT—Light and electron microscopic observations have been carried out with *Cerebratulus* gametes prior to and immediately following sperm-egg fusion. *Cerebratulus* eggs released into sea water underwent germinal vesicle breakdown and a massive exocytosis of cortical vesicles concomitant with the elevation of a chorion. Contact of the sperm with the egg surface induced the acrosome reaction. This was followed by gamete membrane fusion which occurred between the acrosomal process and an egg microvillus. Although the base of the microvillus involved in gamete fusion enlarged to permit entry of the spermatozoon, a fertilization cone failed to form and actin filaments did not accumulate at the site of sperm incorporation. Morphological changes in the egg cortex and extracellular coverings, that might be involved with a block to polyspermy, were not apparent.

INTRODUCTION

Sperm and eggs of the nemertean worm, *Cerebratulus lacteus*, are released from male and female animals into their respective burrows. Currents then carry the gametes into the open sea water where fertilization takes place [1]. Fertilization of *Cerebratulus* eggs can also be achieved in the laboratory as animals are easily maintained in sea water aquaria and gametes may be collected as described by Kume and Dan [2] and Costello *et al.* [3]. Eggs dissected from animals are in the germinal vesicle stage and if fertilized become polyspermic. If left uninseminated in sea water, however, the germinal vesicle breaks down and a chorion lifts from the surface of the egg. Eggs fertilized at this stage are monospermic [2]. Wilson [4] noted that a "favorable character" of *Cerebratulus* eggs for cleavage studies is the absence of a fertilization membrane. The lack of a morphological correlate that might be involved with a block to polyspermy is in agreement with recent observations by Kline *et al.* [5] who demonstrated electrical changes in the plasma membrane of *Cerebratulus* eggs that

are involved in polyspermy prevention.

The structure and chemistry of *Cerebratulus* sperm have been enigmas. Afzelius [6] described a distinct acrosome in the sperm of the nemertine, *Malacobdella grossa*. The presence of an acrosome in *Cerebratulus* sperm, however, could not be morphologically substantiated by Olds and Austin [7] nor could Metz [8] demonstrate sperm lysins even though eggs possess a heavy investing layer (chorion).

Considering the features of this evolutionary distinctive organism [9] and its gametes, it is surprising that *C. lacteus* has not been used more extensively for investigations of fertilization and embryogenesis. In light of this paucity of information, we have carried out observation on *Cerebratulus* gametes prior to and immediately following sperm-egg fusion.

MATERIALS AND METHODS

Collection of Gametes *Cerebratulus lacteus* were generously provided by Drs. Douglas Kline and Laurinda Jaffe. Methods for handling adults and obtaining gametes were as described by Costello *et al.* [3]. Eggs were obtained from 0.5 to

1.0 cm segments cut from the posterior end of female worms. The segments were cut several times in sea water to release eggs which were then collected with a Pasteur pipette, filtered through cheesecloth and suspended in 50 ml sea water until fertilized.

Sperm were obtained from a 0.5 to 1.0 cm segment cut from the posterior end of a male worm just prior to insemination. The segment was suspended in 2 ml sea water and cut to release sperm. Sperm were diluted to a final concentration of about 1:10,000 for insemination.

Electron Microscopy Segments from the posterior end of female worms, unfertilized eggs suspended in sea water for 1 to 60 min and inseminated ova were fixed in 3% glutaraldehyde in sea water at 4°C for 1 hr. Fixed specimens were washed in sea water overnight, post-fixed in 0.5% OsO₄ in sea water at 4°C for 1 hr, dehydrated with ethanol and embedded in Spurr's embedding medium [10]. Thin sections stained with uranyl acetate and lead citrate were examined with a Philips EM 300 transmission electron microscope.

Fluorescence Microscopy Fertilized eggs were fixed for 1 hr at 4°C with 3% paraformaldehyde in sea water, washed for 2 hr in sea water containing 50 mM NH₄Cl, and rinsed for 5 min in 0.1% Triton X-100 in sea water. To visualize the DNA of incorporated sperm nuclei, inseminated eggs were stained for 30 min at 37°C in 10 μm Hoechst 33342 (Sigma) in phosphate-buffered saline (2.9 mM NaH₂PO₄, 7 mM Na₂HPO₄ and 136.9 mM NaCl, pH 7: PBS) and washed three times in PBS. Filamentous actin was localized in Hoechst-stained zygotes with rhodamine-

phalloidin [11]. Specimens were stained in 0.5 μg/ml rhodamine-phalloidin for 30 min, rinsed three times in PBS, and mounted in 90% glycerol. Preparations were observed with a Nikon inverted microscope fitted with an epifluorescence attachment.

RESULTS

Structure of the Egg Cortex and Extracellular Matrix

The cortices of ovarian eggs, which were at the germinal vesicle stage of meiosis, were filled with yolk granules and numerous vesicles containing a filamentous material (Fig. 1). The plasma membranes of these eggs were reflected into numerous microvilli (Fig. 1) that projected into a narrow (0.3–0.4 μm) perivitelline space; consequently, the microvilli were bent and usually only seen in cross and oblique section. The extracellular layers of eggs consisted of a thin envelope or chorion, composed of filamentous material, and immediately superficial to this layer, a jelly layer. The innermost region of the jelly layer was composed of filamentous material that formed a coarse reticulum; this graded into a region containing a more dispersed material.

Egg Changes on Exposure to Sea Water

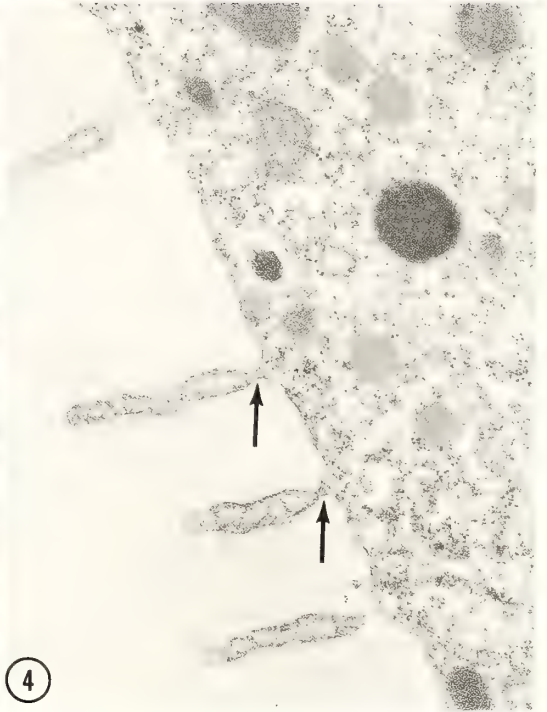
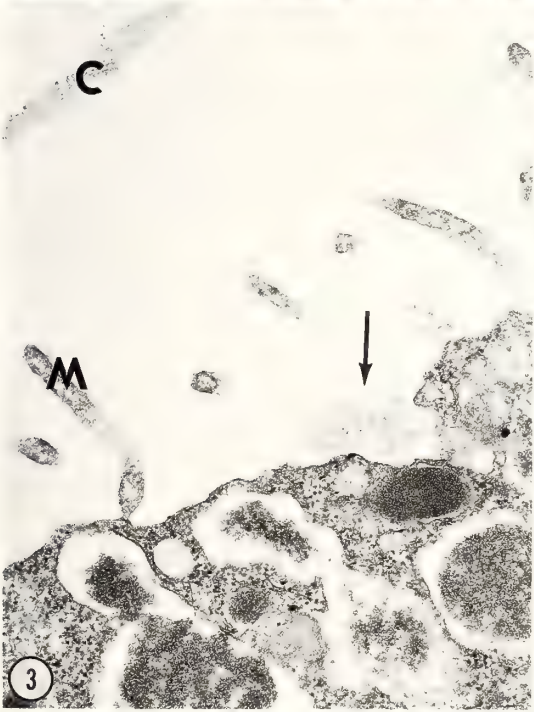
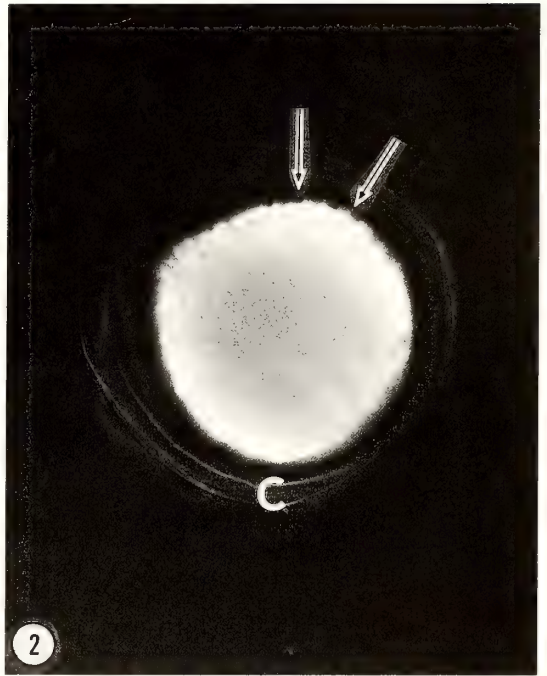
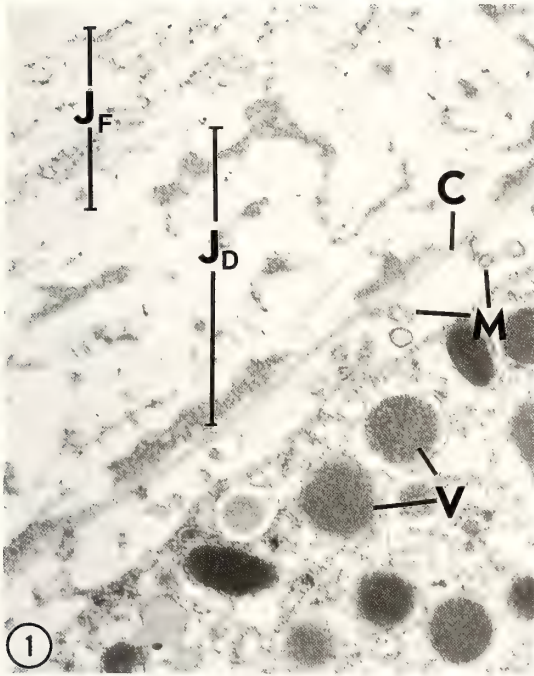
When *Cerebratulus* eggs were exposed to sea water, they initiated germinal vesicle breakdown; meiotic maturation progressed to metaphase I and then arrested. Concomitantly, changes in the egg cortex and extracellular layers took place. The jelly layer expanded and the chorion elevated enlarging the perivitelline space (Figs. 2 and 3).

Fig. 1. Section of an ovarian *Cerebratulus* egg. The cortex is projected into microvilli (M) and filled with numerous vesicles (V) that are released upon the egg's exposure to sea water. Extracellular structures associated with the egg's surface include a chorion (C) and a jelly layer consisting of a dense internal reticulum (J_D) and a more flocculent outer region (J_F). × 15,000.

Fig. 2. Nomarski micrograph of an egg exposed to sea water depicting the elevation of its chorion (C) and numerous scalloped structures along its surface which represent regions of dehiscing vesicles (arrows). × 310.

Fig. 3. Section of an egg exposed to sea water in which the jelly layer has swollen (not depicted); the chorion (C) has elevated and vesicles within the cortex have begun to exocytose (arrow). In contrast to microvilli (M) of ovarian eggs, those of ova released into sea water project at more-or-less right angles from the egg surface. × 19,000.

Fig. 4. Cortex of an egg 60 min after its exposure to sea water which lacks the numerous vesicles found in ovarian specimens. Typically the bases of microvilli that project from the egg surface are constricted (arrows). × 29,000.



This elevation accompanied the exocytosis of vesicles contained within the egg's cortex. The release of these vesicles appeared to be random, in groups, and involved extensive portions of the egg surface (Fig. 2). By 15 min virtually all of the vesicles had exocytosed and the egg cortex was essentially devoid of such structures (Fig. 4). With the elevation of the chorion and expansion of the perivitelline space, microvilli became erect and oriented perpendicular to the egg surface. Structurally, microvilli at this stage were approximately $1 \mu\text{m}$ in length by $0.2 \mu\text{m}$ in diameter. Characteristically, the bases of microvilli were constricted to a region $0.05 \mu\text{m}$ in diameter. Internally, the microvilli lacked a prominent microfilamentous core (Fig. 4).

Sperm Structure

Cerebratulus sperm consisted of a distinct head, mitochondrial-middle piece and flagellum. The head was a tapering crescent-shaped structure, approximately $16 \mu\text{m}$ in length, containing an acrosome and nucleus (Fig. 5). The nucleus, which made up most of the sperm head, consisted of uniformly electron dense chromatin.

The acrosome was an elongated ellipsoid about $1 \mu\text{m}$ in length by $0.3 \mu\text{m}$ in diameter (Figs. 6 and 7). Its posterior aspect was invaginated to form a fossa approximately $0.2 \mu\text{m}$ deep. Within the fossa and the space separating the acrosome and nucleus was accumulation of electron dense, postacrosomal material.

The middle piece of the sperm possessed four mitochondria ($2 \mu\text{m}$ in length by $0.5 \mu\text{m}$ in diameter), which were situated in depressions along the base of the nucleus (Figs. 8 and 9). Approximately one third the length of the mitochondria extended posteriorly, surrounding a cytoplasmic compartment in which were found the proximal and distal centrioles (Fig. 8).

The proximal centriole was situated partially in a fossa at the posterior end of the sperm nucleus (Fig. 8). The distal centriole was oriented perpendicular to the proximal; only its anterior region was situated within the space circumscribed by the mitochondria. The portion of the distal centriole which was not surrounded by mitochondria was associated with nine pericentriolar processes that

projected from its triplet tubular wall and terminated in thickened tips (Figs. 8 and 10). In cross section the nine pericentriolar processes defined a wheel-like structure that marked the anterior margin of the sperm tail (Fig. 10).

Sperm-Egg Interaction and the Acrosome Reaction

Examination of living specimens revealed that sperm were capable of swimming in and out of the perivitelline space, i.e., through the chorion that surrounded the egg. During its transit through the chorion the acrosome remained intact (Figs. 11 and 12). An acrosome reaction did not occur until the sperm apex came into contact with an egg microvillus (Fig. 13). Fusion of the sperm plasmalemma and acrosome membrane occurred at the apex of the sperm head, thereby releasing the acrosomal contents (Fig. 13). An acrosomal process formed via the inversion of the former acrosomal membrane and the modification of postacrosomal substance. The acrosomal processes in specimens that appeared to have just undergone the acrosome reaction were associated with some filamentous material (Figs. 13 and 14). This material joined the acrosomal process to the egg surface.

Gamete Fusion and Sperm Incorporation

Gamete fusion occurred via the tip of the acrosomal process and a microvillus (Fig. 15). Interestingly, the base of the microvillus involved in gamete membrane fusion enlarged before the contents of the spermatozoon moved through it, into the egg cortex (Fig. 15). Other than an enlargement of the base of the microvillus involved in gamete fusion, no other specializations of the egg cortex were found in association with the incorporating sperm, e.g., the appearance of microfilament bundles and a fertilization cone (Fig. 16; see also Figs. 20–22). In addition to an absence of fertilization cone formation in metaphase I eggs, immature, germinal vesicle oocytes also failed to develop such a cortical specialization (Figs. 17–19).

When inseminated eggs were treated with rhodamine-phalloidin there was a general diffuse staining throughout the cytoplasm indicating the presence of filamentous actin (Figs. 23 and 24).

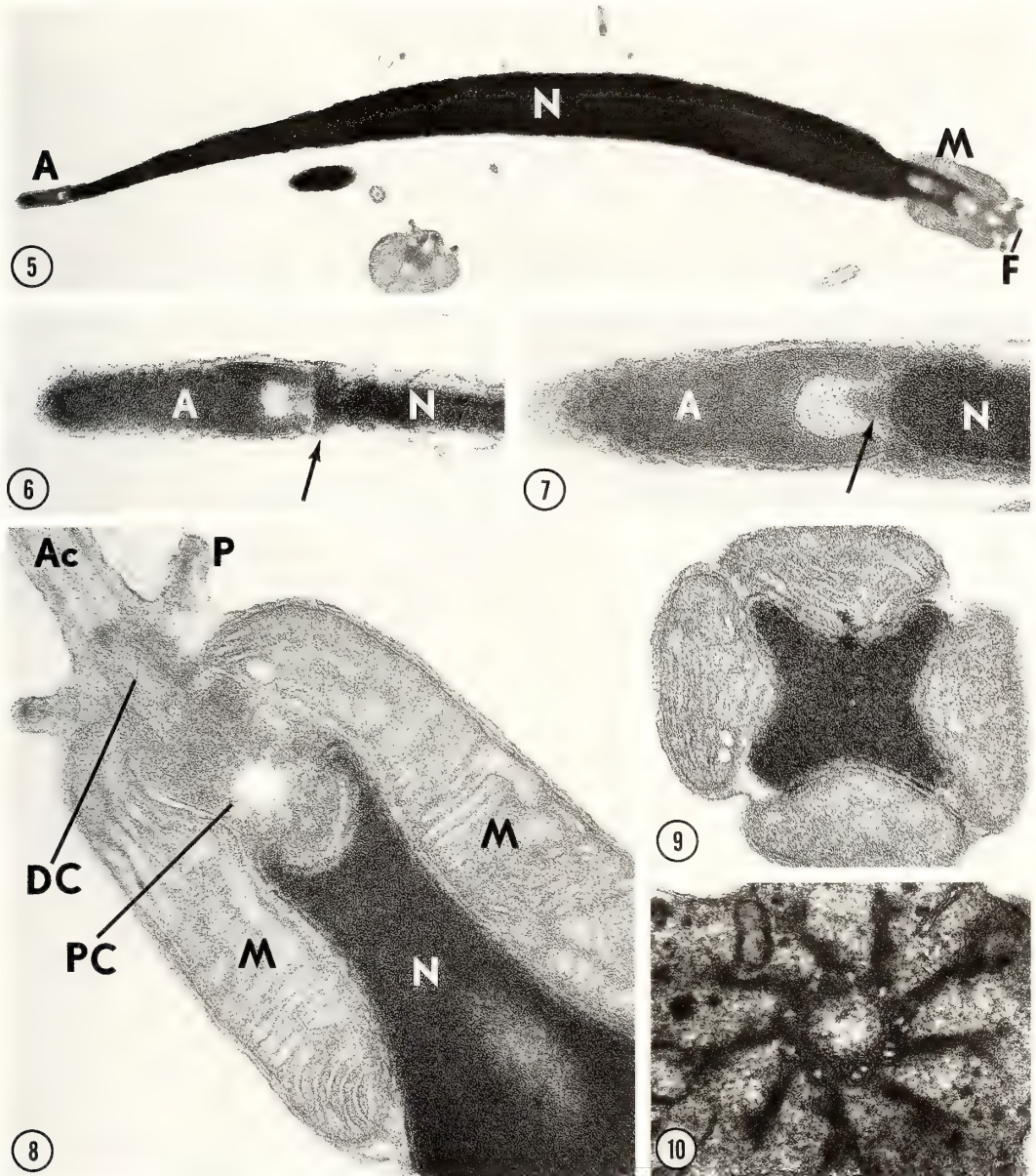


FIG. 5. Longitudinal section of a *Cerebratulus* sperm depicting its crescent-shaped nucleus (N), acrosome (A), mitochondria (M) and proximal elements of the flagellum (F). $\times 9,000$.

FIGS. 6 and 7. Longitudinal sections through the acrosome (A) and anterior of the sperm nucleus (N). Between these two organelles is some electron dense material (arrows) that surrounds the anterior aspect of the nucleus and projects into a small fossa at the posterior of the acrosome. Fig. 6, $\times 37,000$; Fig. 7, $\times 59,000$.

FIGS. 8 and 9. Longitudinal- and cross-sections of *Cerebratulus* sperm along the region of the middle piece. The anterior aspect of the four mitochondria (M) fit into shallow invaginations along the posterior of the sperm nucleus (N). The posterior aspect of the mitochondria define a compartment which contains two centrioles. The proximal centriole (PC) is located in a shallow fossa at the posterior of the nucleus. Just posterior to the proximal centriole is the distal (DC) from which the axonemal complex (Ac) and pericentriolar processes project (P). Figs. 8 and 9, $\times 28,000$.

FIG. 10. Cross section of a spermatozoon at the level of the distal centriole. Nine pericentriolar processes, which project from the distal centriole, are depicted. $\times 40,000$.

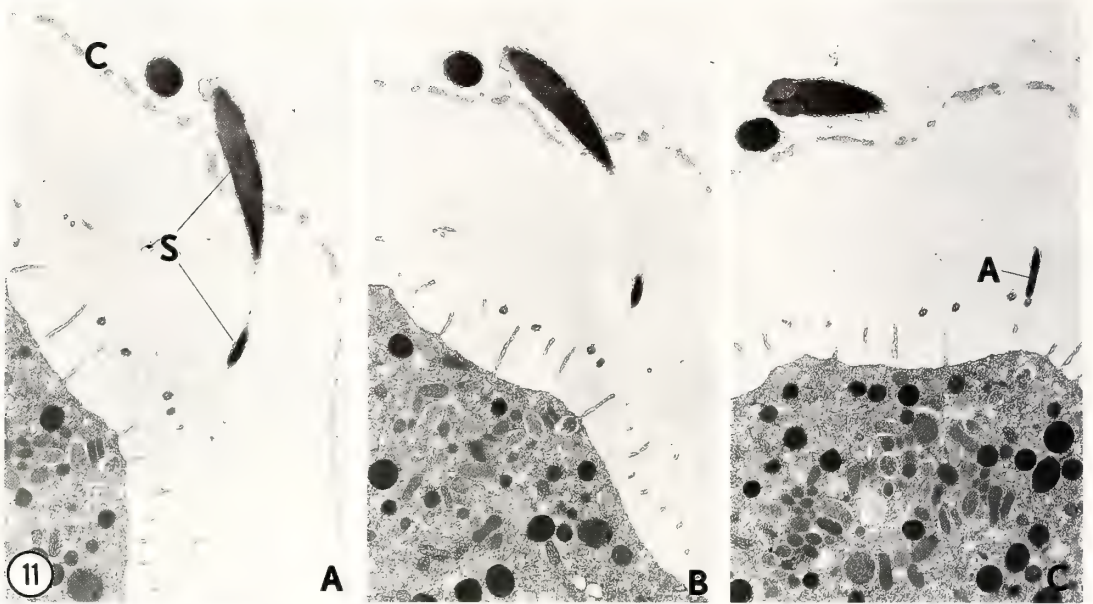


FIG. 11A-C. Serial sections of a sperm (S) traversing the chorion (C) which has lifted from an egg surface. The intact acrosome (A) of this specimen is depicted in Figs. 11C and 12. $\times 2,900$.

An accumulation of rhodamine-phalloidin staining was not observed in association with the incorporated spermatozoon.

Once fusion had taken place the entire cytoplasmic contents of the sperm moved into the cortical ooplasm (Figs. 20 and 21). The sperm flagellum extended from the surface of the egg (Fig. 22). In the present study we were unable to determine the eventual fate of this structure. It is interesting to note, however, that the tips of the sperm pericentriolar processes were closely associated with the zygote plasmalemma (Fig. 22).

DISCUSSION

Other than recent investigations of the electrical properties of eggs following insemination and aspects of protein synthesis during early development [12, 13], *Cerebratulus* have been little used for contemporary studies of fertilization processes. The present observations provide structural features of gamete interactions leading to the acrosome reaction, sperm-egg fusion and sperm incorporation in the nemertean, *Cerebratulus*. These results amplify much earlier light microscopic studies in this phylogenetically unusual organism and have a direct bearing on fertilization mecha-

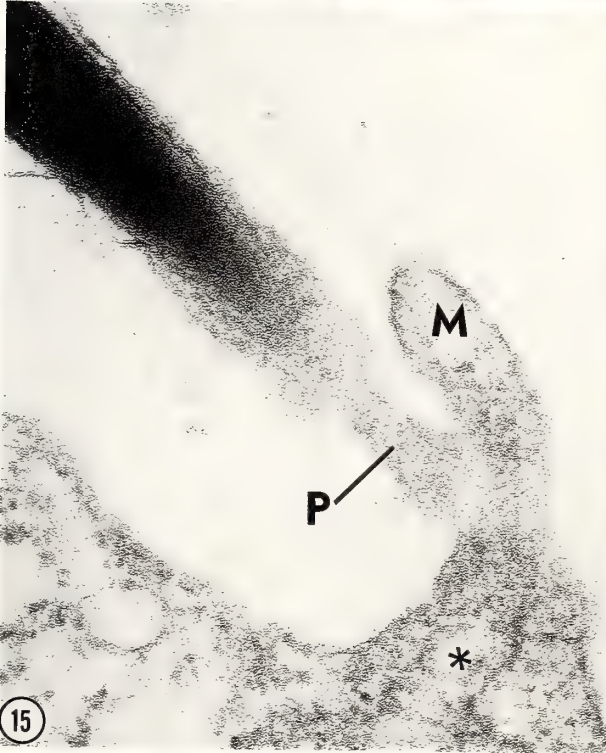
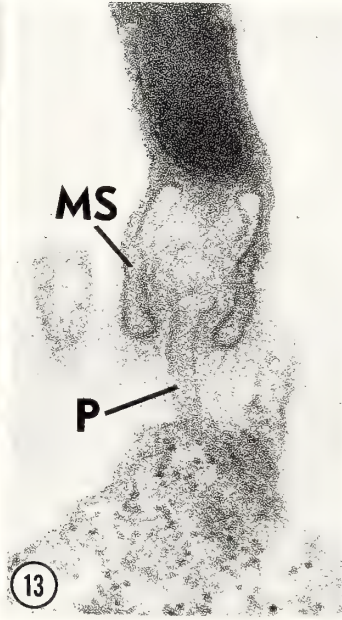
FIG. 12. Anterior aspect of the sperm shown in Fig. 11C which has penetrated the chorion surrounding an egg. The acrosome (A) is intact. $\times 20,500$.

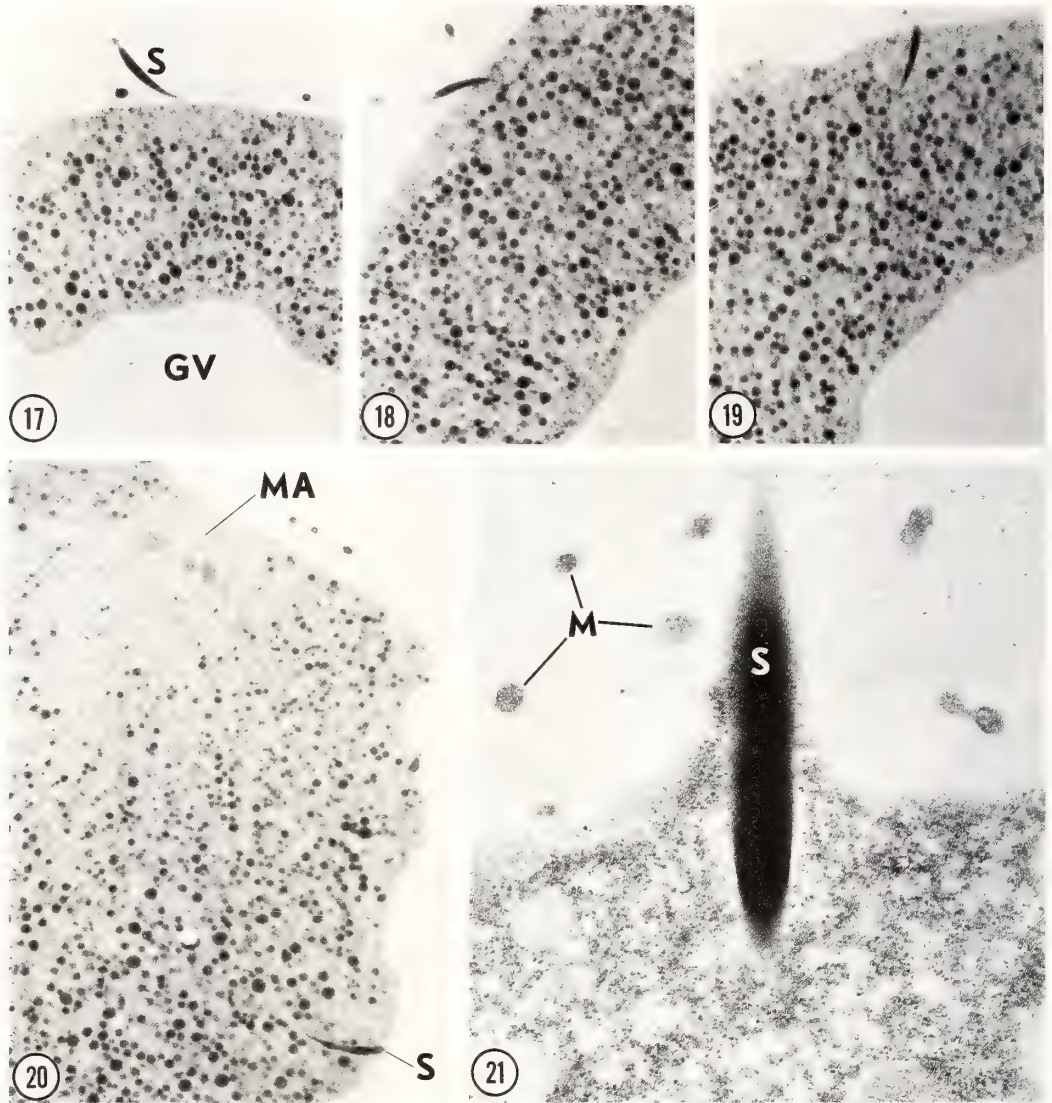
FIG. 13. Anterior aspect of a spermatozoon that has contacted the surface of an egg and has undergone the acrosome reaction. The membranous sleeves (MS), that consist of the outer acrosomal membrane and the plasmalemma, partially surround the forming acrosomal process (P). Some filamentous material joins the acrosomal process and the egg surface. $\times 41,000$.

FIG. 14. Anterior aspect of a sperm in contact with an egg microvillus (M) via its acrosomal process (P). $\times 52,000$.

FIG. 15. Sperm that is in the process of fusion with an egg. Gamete fusion occurs at the tip of the acrosomal process (P) and an egg microvillus (M). Gamete fusion results in slight enlargement at the base of the microvillus (*). $\times 41,000$.

FIG. 16. Fused sperm and egg. The site of cytoplasmic continuity of the sperm and egg is depicted by the arrow. $\times 33,500$.





FIGS. 17 to 19. Stages of sperm incorporation (S) into germinal vesicle (GV) containing eggs. An elevation of egg cytoplasm, a fertilization cone and characteristically observed at the site of gamete fusion in other organisms, e.g., sea urchins, fails to form in inseminated, immature *Cerebratulus* eggs. $\times 750$.

FIGS. 20 and 21. Eggs inseminated at metaphase I of meiosis in which sperm incorporation is not associated with the formation of a projection of cytoplasm, the fertilization cone. MA, meiotic apparatus; M, microvilli; S, incorporated sperm. Fig. 20, $\times 750$; Fig. 21, $\times 27,000$.

nisms in other organisms.

Eggs *Cerebratulus* eggs are enveloped by distinct extracellular coats, a chorion and a jelly layer. Upon exposure to sea water the chorion lifts from the surface of the egg. The concomitant dehiscence of cortical vesicles with the elevation of

the chorion suggests that these two processes may be linked. That is, the vesicle contents may become hydrated upon dehiscence thereby expanding the perivitelline space and lifting the chorion. A similar mechanism has been shown to be involved in the elevation of the vitelline layer to form the fertilization membrane in sea urchins

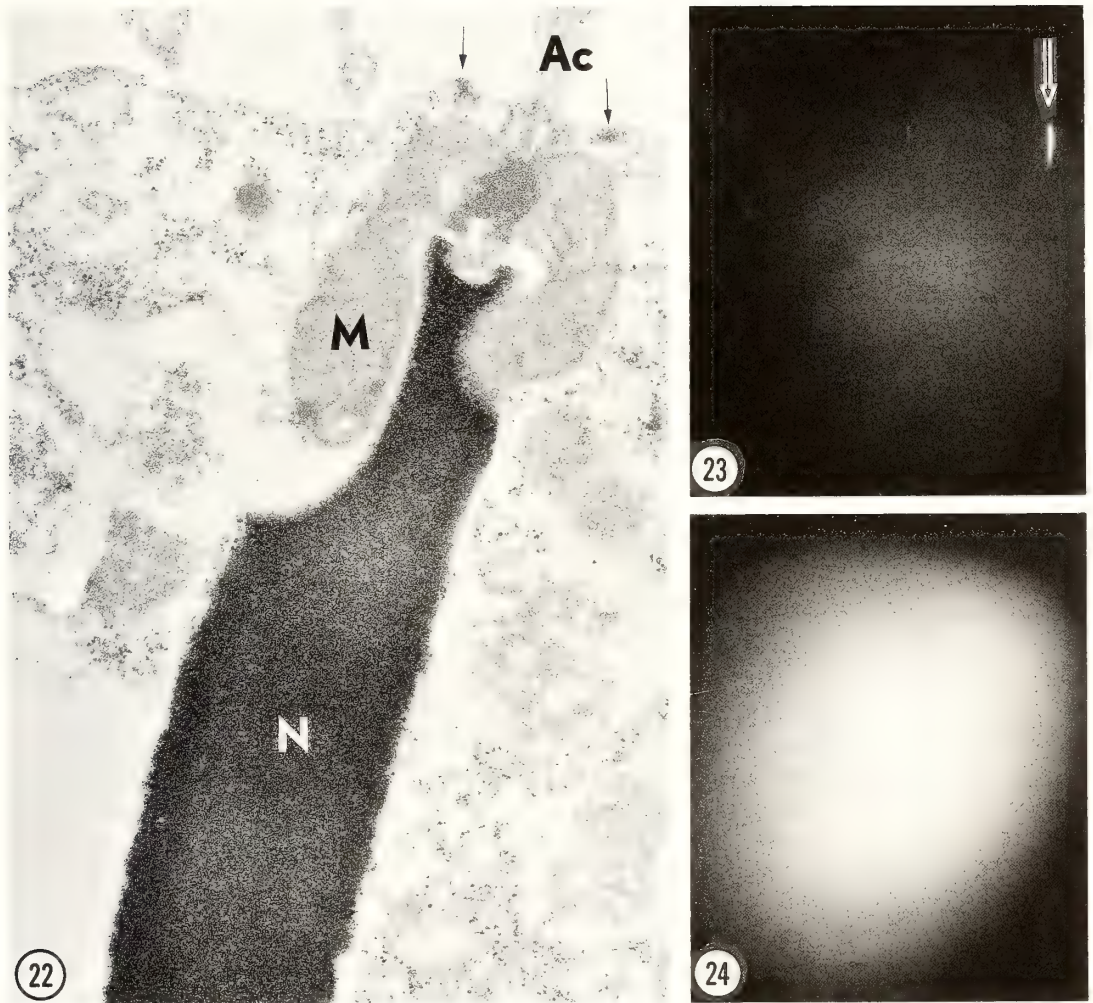


FIG. 22. Cortex of an inseminated egg depicting the posterior aspect of an incorporated sperm nucleus (N), mitochondria (M), and axonemal complex (Ac). The surface of the egg immediately superficial to the incorporated sperm does not show signs of fertilization cone formation. Portions of the incorporated pericentriolar processes are shown at the arrows. $\times 28,000$.

FIGS. 23 and 24. Fluorescence micrographs of an inseminated egg stained with Hoechst for DNA (Fig. 23) and rhodamine-phalloidin for filamentous actin (Fig. 24). The inseminated egg shows a diffuse staining for filamentous actin; specific rhodamine-phalloidin-staining in the vicinity of the incorporated sperm nucleus (arrow) is not apparent. The maternal chromatin is out of the plane of focus in Fig. 23. $\times 450$.

[14].

Unlike sea urchins, however, the elevation of the chorion does not occur as a result of sperm-egg interaction nor does the elevated chorion act as a barrier to sperm. Sperm were seen to move through this structure with apparently little effort [see also 5]. Sperm-egg fusion is not associated with a cortical reaction in this species. Structural

changes, at the site of sperm incorporation or along other regions of the egg cortex that might be involved with a block to polyspermy, were not observed. These data are in agreement with morphological observations of Kline *et al.* [5] who also demonstrated a rapid positive-going shift in membrane potential coincident with insemination. They suggest that this change in potential acts as a

block to polyspermy which lasts for approximately 60 min in *Cerebratulus*.

Sperm The general structure of the sperm of *Cerebratulus* resembles that observed in the nemertean, *Malacobdella grossa* [6]. Elaborate pericentriolar processes radiate from the distal centrioles of *Cerebratulus* sperm; structures similar to those described in other species [15]. In the sperm of *Malacobdella* these structures are described as radiating "rods" that terminate in an electron dense annulus [6]. In *Hydactinia* sperm, the elements that project from the distal centriole contain actin [15].

The acrosome of *Cerebratulus* sperm consists of a vesicle and distinct subacrosomal fossa containing electron dense postacrosomal material. The organization of this material is morphologically similar to that described for sperm of *Malacobdella* [6]. We have observed the acrosome reaction in *Cerebratulus* sperm and it is functionally similar to that observed in other invertebrate sperm [16, 17]. Interestingly, the acrosome reaction in *Cerebratulus* does not take place when sperm swim through the jelly coat and chorion. Instead, this reaction is induced by an association of the sperm with the egg surface. In every instance examined, acrosome reacted sperm were found in close association with egg microvilli, suggesting that a microvillus-sperm interaction leads to the release of acrosomal contents and the formation of an acrosomal process. It is interesting to note that Metz [8] was unable to demonstrate sperm-lysins in *Cerebratulus*. If in fact lysins are required for sperm penetration through the chorion one would expect their release prior to/during chorion passage by the sperm. In addition, sperm attachment and fusion with the egg occurs at a microvillus, the latter apparently induces the resumption of meiotic maturation [3]. A similar sperm-egg relationship has also been described for *Chaetopterus* [18].

Sperm Incorporation The present observations substantiate and extend previous light microscopic studies [19-21] demonstrating that sperm incorporation in *Cerebratulus* is not accompanied by the formation of a fertilization cone in either germinal vesicle or metaphase I eggs.

Sperm incorporation in sea urchin germinal vesicle (immature) eggs is distinguished by the formation of extremely large fertilization cones in contrast to those formed by mature (pronuclear) ova [22].

Prior to sperm-egg interaction, microvilli possess constricted bases and do not appear to have a distinctive microfilamentous core. Although the base of the microvillus involved in gamete fusion enlarges slightly, the formation of a cytoplasmic projection, as observed in sea urchin and other invertebrates and vertebrates [22], does not occur in *Cerebratulus*. In other species that have been studied, namely sea urchins and mice [23-25], actin filaments accumulate in the cytoplasm surrounding the entering sperm. In sea urchins the accumulation of microfilaments is believed to be derived from the *in situ* polymerization of monomeric actin [26, 27], which in turn aggregate to form large bundles that are organized with the same polarity [28]. Such an accumulation of filamentous actin in *Cerebratulus* zygotes was not detected either by rhodamine-phalloidin staining or electron microscopy.

These observations indicate that fertilization cone formation and the accumulation of filamentous actin are not obligatory for sperm incorporation. They are similar to previous investigations of fertilized sea urchin eggs treated with cytochalasins [23, 25]. When sea urchin eggs are treated with cytochalasins immediately after gamete fusion, fertilization cone formation and actin polymerization fail to occur. Nevertheless, the sperm nucleus and mitochondria enter the egg cortex and male pronuclei form [23]. The inhibition of microfilament and fertilization cone formation in sea urchin zygotes treated with cytochalasins also suggests that these processes are coupled [see 28], i.e., fertilization cone formation is dependent upon actin polymerization [22, 27]. The absence of fertilization cone formation in *Cerebratulus* may result from a failure of actin to polymerize and accumulate in the region of sperm incorporation. The results presented here and those employing sea urchin zygotes treated with cytochalasins [22, 25] beg the question of possible mechanisms involving the movement of the sperm contents into the egg cortex.

ACKNOWLEDGMENTS

This paper is dedicated to Professor Katsuma Dan, an international scientist whose many outstanding research contributions have had major influences in cellular and developmental biology.

The authors wish to thank Drs. Laurinda Jaffe, Douglas Kline and Frederick Griffin for the contribution of their time and valuable discussions during the course of this study. The assistance of Ms. Susan Cook and the typing of Ms. Tena Perry are gratefully acknowledged. This investigation was supported by funds from the NIH (F.J.L.) and National Sea Grant College Program, Department of Commerce, under grant number NA95AA-D-SG140 project number R/A-61 (W.H.C.).

REFERENCES

- 1 Wilson, C. B. (1900) The habits and early development of *Cerebratulus lacteus* (Verrill). A contribution to physiological morphology. *Q. J. Microsc. Sci.*, **43**: 97-198.
- 2 Kume, M. and Dan, K. (1968) *Invertebrate Embryology*. Nolit Publishing House, Belgrade, Yugoslavia.
- 3 Costello, D. P., Davidson, M. E., Eggers, A., Fox, M. H. and Henly, C. (1957) *Methods for Obtaining and Handling Marine Eggs and Embryos*. Lancaster Press, Inc., Lancaster, PA.
- 4 Wilson, E. B. (1903) Experiments on cleavage and localization in the nemertine egg. *Arch. Entwicklungsmech.*, **16**: 411-460.
- 5 Kline, D., Jaffe, L. and Tucker, R. P. (1985) Fertilization potential and polyspermy prevention in the egg of the nemertean, *Cerebratulus lacteus*. *J. Exp. Zool.*, **236**: 45-52.
- 6 Afzelius, B. (1971) The spermatozoon of the nemertine, *Malacobdella grossa*. *J. Submicrosc. Cytol.*, **3**: 181-192.
- 7 Olds, P. J. and Austin, C. R. (1967) Entry of *Cerebratulus* spermatozoa into *Echinarachnius* eggs. *Biol. Bull.*, **133**: 477.
- 8 Metz, C. B. (1957) Specific egg and sperm substances and activation of the egg. In "Beginnings of Embryonic Development". Ed. by A. Tyler, R. C. Von Borstel and C. B. Metz. *Am. Assoc. Adv. Sci.*, Washington, D.C., pp. 23-69.
- 9 Barnes, R. D. (1980) *Invertebrate Zoology*. Saunders, Philadelphia, PA.
- 10 Spurr, A. K. (1969) A low viscosity epoxy resin embedding medium for electron microscopy. *J. Ultrastruct. Res.*, **26**: 31-43.
- 11 Wieland, T. and Faulstich, H. (1978) Amatoxins, phallotoxins, phallolysin and antamanide: The biologically active components of poisonous *Amanita* mushrooms. *CRC Crit. Rev. Biochem.*, **5**: 185-260.
- 12 Candelas, G. and Monroy, A. (1968) Protein synthesis during maturation and early development of the egg of *Cerebratulus lacteus*. *Exp. Cell Res.*, **52**: 664-667.
- 13 Kline, D., Jaffe, L. A. and Kado, R. T. (1986) A calcium-activated sodium conductance contributes to the fertilization potential in the egg of the nemertean worm *Cerebratulus lacteus*. *Dev. Biol.*, **117**: 184-193.
- 14 Schuel, H. (1978) Secretory function of egg cortical granules in fertilization and development. A critical review. *Gam. Res.*, **1**: 299-382.
- 15 Kleve, M. G. and Clark, W. H. (1980) Association of actin with sperm centrioles: Isolation of centriolar complexes and immunofluorescent localization of actin. *J. Cell Biol.*, **86**: 87-95.
- 16 Dan, J. C. (1967) Acrosome reaction and lysins. In "Fertilization, vol. 1". Ed. by C. B. Metz and A. Monroy. Academic Press, New York., pp. 237-293.
- 17 Tilney, L. G. (1975) The role of actin in nonmuscle cell motility. In "Molecules and Cell Movement". Ed. by S. Inoué and R. E. Stevens. Raven Press, New York., pp. 339-388.
- 18 Anderson, W. A. and Eckberg, W. R. (1983) A cytological analysis of fertilization in *Chaetopterus peramentaceus*. *Biol. Bull.*, **165**: 110-118.
- 19 Yatsu, N. (1904) Experiments on the development of egg fragments in *Cerebratulus*. *Biol. Bull.*, **6**: 123-136.
- 20 Yatsu, N. (1909) Observations on ookinesis in *Cerebratulus lacteus* Verrill. *J. Morphol.*, **20**: 353-401.
- 21 Chambers, R. (1933) The manner of sperm entry in various marine ova. *J. Exp. Biol.*, **10**: 130-141.
- 22 Longo, F. J. (1987) *Fertilization*. Chapman and Hall, New York.
- 23 Longo, F. J. (1980) Organization of microfilaments in sea urchin (*Arbacia punctulata*) eggs at fertilization: Effects of cytochalasin B. *Dev. Biol.*, **74**: 422-433.
- 24 Maro, B., Johnson, M. H., Pickering, S. J. and Flach, G. (1984) Changes in actin distribution during fertilization of the mouse egg. *J. Embryol. Exp. Morphol.*, **81**: 211-257.
- 25 Cline, C. A. and Schatten, G. (1986) Microfilaments during sea urchin fertilization: fluorescence detection with rhodaminyl phalloidin. *Gam. Res.*, **14**: 277-291.
- 26 Spudich, A. and Spudich, J. A. (1979) Actin in Triton-treated cortical preparations of unfertilized and fertilized sea urchin eggs. *J. Cell Biol.*, **82**: 212-226.
- 27 Cline, C. A., Schatten, H., Balczon, R. and Schatten, G. (1983) Actin-mediated surface motility during sea urchin fertilization. *Cell Motility*, **3**: 513-

- 524.
- 28 Tilney, L. G. and Jaffe, L. A. (1980) Actin, microvilli, and the fertilization cone of sea urchin eggs. *J. Cell Biol.*, **87**: 771-782.

Centrosomes, Centrioles and Post-translationally Modified Microtubules during Fertilization

HEIDE SCHATTEN, CATHY HOWARD, GÉRARD COFFE,
CALVIN SIMERLY and GERALD SCHATTEN

*Integrated Microscopy Resource for Biomedical Research, University of Wisconsin,
1117 West Johnson Street, Madison, WI 53706, U.S.A.*

I. INTRODUCTION

Fertilization requires an elaborately choreographed sequence of motions, all of which are effected by rearrangements of the cytoskeleton (review in [1]). The first example of an alteration of the cytoskeleton is found in the sperm as the microfilaments of the acrosomal process assemble ([2-5] for review). This occurs while the microtubules in the sperm axoneme are sliding and bending to produce the waveform motion which propels the sperm through the insemination fluid ([6, 7] for review).

Once the sperm contacts and binds to the egg surface (review in [8, 9]) microfilaments at the egg cortex (reviewed by [10]) as well as actin binding proteins including fodrin [11] serve a critical role in the physical incorporation of the sperm in some, but not all [12], fertilization systems. The fertilized egg surface erupts with elongated microvilli (reviewed by [13]) and clathrin-coated endocytosis has been observed by Fisher and Rebhun [14].

As the sperm nucleus decondenses into the male pronucleus (reviewed by [15, 16]), typically a monastral array of microtubules, the sperm aster, assembles. The sperm astral microtubules perform the crucial role of uniting the male and female pronuclei. In many fertilization systems the two pronuclei fuse during interphase, though in some systems such as mammals ([17] for review) and ascidians [18], the pronuclei do not fuse during interphase. Instead the male and female chromatin condense into individual chromosome sets at prophase of first mitosis. The completion of ferti-

lization, signalled by the intermingling of the parental genomes is formally achieved at metaphase of first mitosis when the chromosomes are aligned on the metaphase plate.

Since most eggs are fertilized as oocytes rather than as mature pronucleate eggs (reviewed by [19]), the functioning of microtubules during the completion of meiotic maturation and the motility of cortical microfilaments in the constriction of the polar bodies must also be included in a consideration of cytoskeletal reorganization during fertilization.

The foundation for the elucidation of cytoskeletal activity during fertilization has already been laid, and it is now possible to begin a molecular characterization of the responsible proteins and the post-translational modifications of these molecules throughout the cell cycle. The objectives of this chapter are to evaluate the composition, behavior and mode of inheritance of the centrosome, to investigate the status of the centriole during fertilization and to consider post-translational modifications of α -tubulin during meiosis, fertilization and mitosis.

II. CENTROSOMES

A. Paternal Inheritance of Centrosomes

The centrosome is the structure which specifies the configurations of assembling microtubules, and in doing so, defines cell polarity either by shaping mitotic spindle axes or by controlling the organization of the interphase microtubule array. Boveri [20] recognized the central importance of the centrosome and proposed that the centrosome is one

of the vital components contributed by the sperm to the egg at fertilization. In this view, the egg loses its centrosomes during oogenesis and therefore cannot normally organize a bipolar mitotic spindle after artificial activation. By the paternal contribution of centrosomes, the fertilized egg is able to first organize the microtubules comprising the monastral sperm aster, and after duplication, the bipolar mitotic apparatus.

While this classic view of centrosomal inheritance was well documented by Boveri's hematoxylin images, the ability to directly trace centrosome configurations has only recently been rediscovered. Calarco-Gillam *et al.* [21] found an autoimmune serum which reacts specifically with pericentriolar material and this serum has been used to investigate centrosome shape in a wide variety of somatic and germ cells ranging from plants [22] to eggs and embryos of sea urchins [23] as well as mice [21, 23, 24]. Recently a mouse monoclonal antibody to a 68 kD protein has been shown by Schatten *et al.* [25] to react specifically with centrosomes from sea urchin eggs and embryos. This monoclonal antibody may well overcome many of the limitations of routine availability and sufficient quantity necessary for a more complete characterization of the centrosome.

The organization of the centrosome during fertilization and first division in sea urchins is shown in Figure 1. The unfertilized egg does not bind the monoclonal antibody to the 68 kD antigen. However one or two spots are usually found at the base of the sperm head, and this material is introduced to the egg at sperm incorporation. As the microtubules of the sperm aster develop, the

centrosome is found as a compact sphere at the center of the aster and adjacent to the male pronucleus (Fig. 1A). It then spreads around the decondensing male pronucleus, forming into an arc (Fig. 1B) and it enlarges and spreads to opposing poles of the zygote nucleus by the streak stage (Fig. 1C).

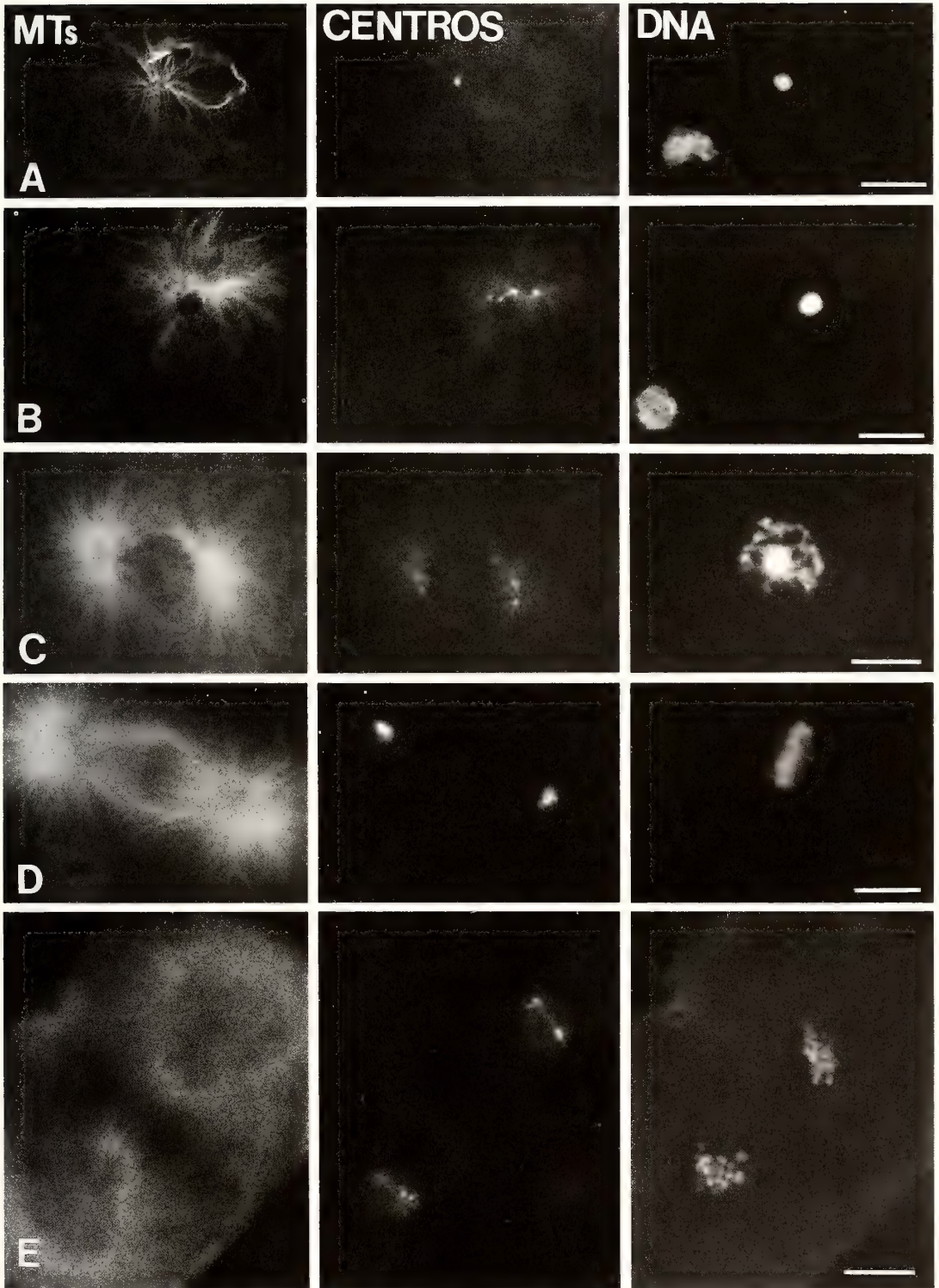
The centrosome undergoes a characteristic change in shape during mitosis. At prophase and metaphase, the centrosomes are compact spheres (Fig. 1D). By anaphase the centrosomes flatten (Fig. 1E). At telophase the centrosomes enlarge into large ovoid structures; the direction of spreading is perpendicular to the axis of the first mitotic axis and parallel with the axes for the next mitosis.

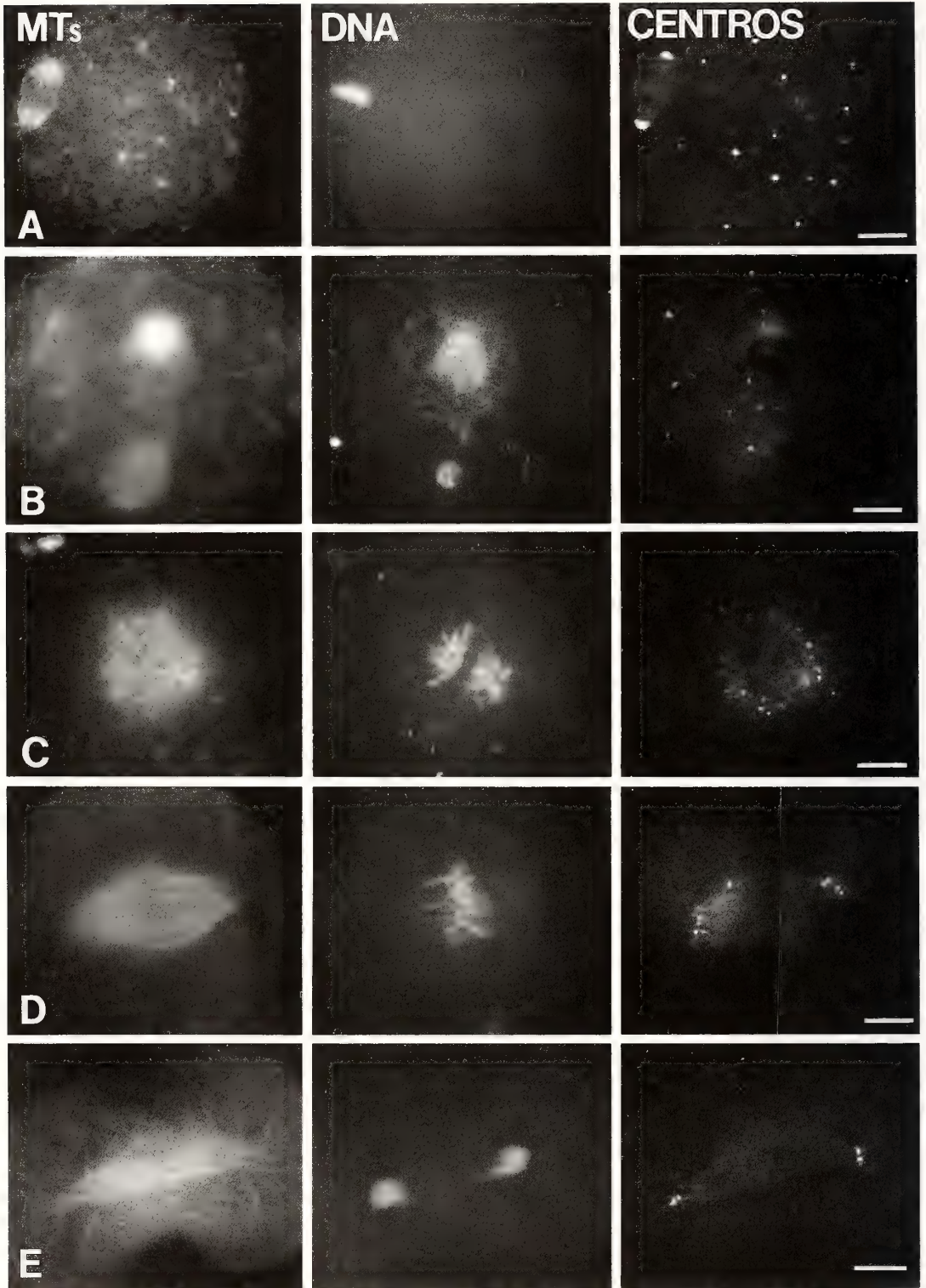
Evidence that the centrosome is contributed by the sperm at fertilization is rather strong in a wide variety of animals. In systems as diverse as ctenophores [26] through amphibians [27] a monastral sperm aster is organized from a site adjacent to the sperm nucleus and few other microtubules are observed after the loss of the second meiotic spindle. Antitubulin immunofluorescence microscopy in sea urchins [28–30], clams [31] and ascidians [18] provide more direct evidence that microtubules are predominantly organized around the sperm centrosome after fertilization. However mammalian fertilization may not follow this pattern.

B. The Question of Maternal Inheritance of Centrosomes in Mammals

The observation that microtubules in fertilized mouse eggs were organized by numerous cytoplasmic sites first leads to the suggestion that the origins of the microtubule organizing centers

Fig. 1. Centrosomes during sea urchin fertilization and division. At fertilization the centrosome is introduced into the egg by the sperm and it is detected here with a monoclonal antibody to *Drosophila* intermediate filament protein. Initially the centrosome is quite compact and in tight association with the male pronucleus (A). It organizes the radially symmetric sperm aster. Later (B), the centrosome disperses into an arc and the sperm aster enlarges. At the end of first interphase (C), at 60 min post-insemination, the centrosome separates in two; asters are associated with each centrosome. At metaphase (D), the centrosomes are quite compact, as the characteristic mitotic spindle with well elaborated asters and a fusiform spindle develops. The metaphase chromosomes are aligned at the spindle equator. During the remainder of the mitotic cycle, the centrosomes expand and enlarge in the direction perpendicular to the spindle axis (E). The asters enlarge as microtubules clear from the astral centers. The separated chromosomes decondense into karyomeres, which will fuse to reconstitute the blastomere nuclei. B–E are triple stained for microtubules (MTs; left), centrosomes (CENTROS; middle) and DNA (DNA; right). A: double stained for microtubules and DNA with a corresponding centrosome image at the same stage. *Lyttechinus pictus*. Bars: 10 μ m. A, D and E: reprinted, with permission, from [55].





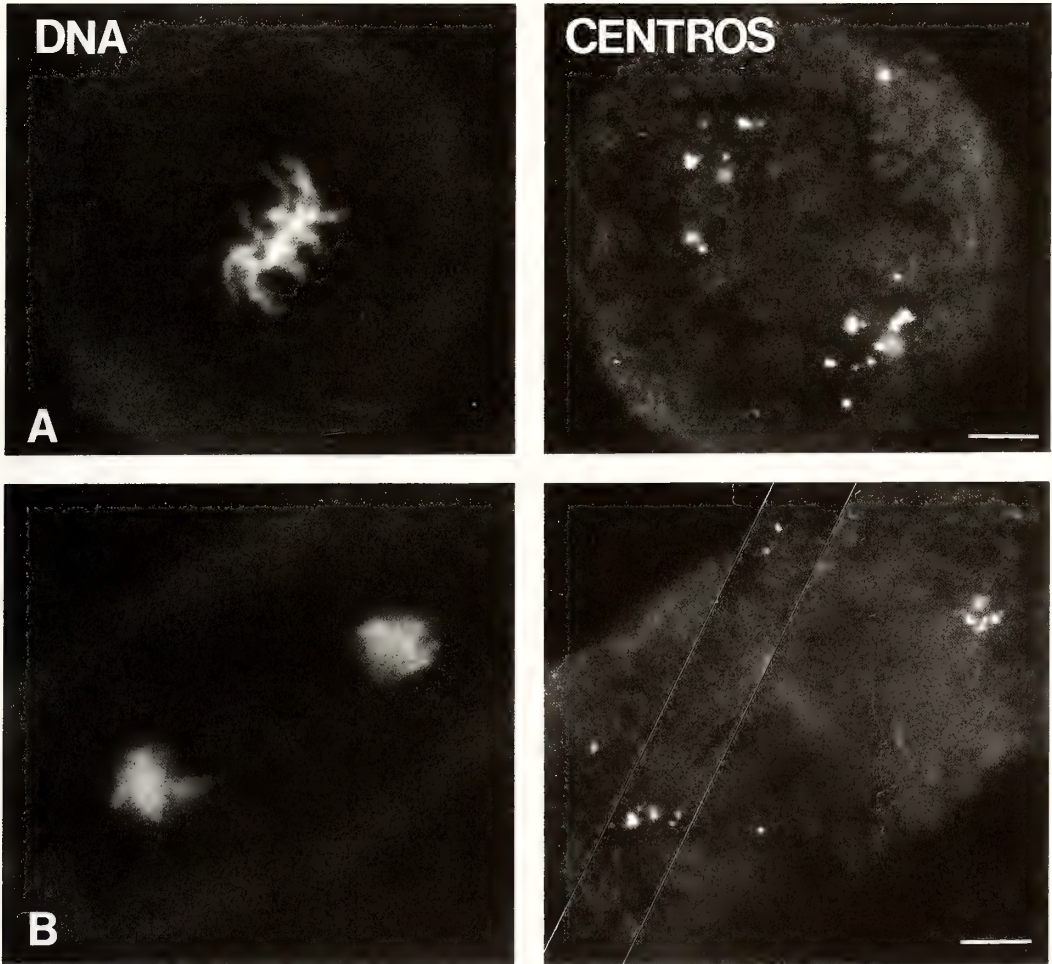


FIG. 3. Centrosomes in parthenogenetically activated mouse oocytes. The centrosomes in parthenogenetically activated mouse oocytes behave in the same fashion as those during normal fertilization. At the time for mitotic prometaphase (A) they aggregate to form a bipolar barrel-shaped spindle and by telophase they separate and move to the poleward faces of the blastomere nuclei (B). These observations support the hypothesis that the centrosome in this mammal is maternally inherited. Images are double stained for DNA (left) and centrosomes (right). Bars: 10 μ m.

FIG. 2. Centrosome during mouse fertilization and division. The unfertilized mouse oocyte, which is ovulated arrested at second meiotic metaphase, displays numerous centrosomal foci in addition to those found at the poles of the meiotic spindle (A). Each centrosomal focus is associated with a microtubule-containing cytaster. The centrosome does not appear to be contributed by the sperm at fertilization and instead these maternal centrosomal foci associate with each pronucleus during interphase (B). They duplicate by the completion of first interphase and at prophase (C) aggregate and move towards the cell center in apposition with the condensing chromosomes. At metaphase (D), the centrosomes are positioned to form broad spindle poles and a barrel-shaped anastral spindle emerges. At telophase (E), the centrosomes are found on the poleward faces of the decondensing blastomere nuclei. All images are triple stained for microtubules (MTs: left), DNA (DNA: middle) and centrosomes (CENTROS: right). Bars: 10 μ m. Reprinted, with permission, from [12].

(MTOCs) in this mammal did not follow the expected pattern [32]. By the use of the autoimmune serum reactive with centrosomes [21], Schatten *et al.* [32] hypothesized that the mouse centrosome is maternally inherited.

This hypothesis was based on the observations that mouse sperm did not react with this autoimmune serum, while numerous cytoplasmic foci were detected in the unfertilized oocyte. Each centrosomal focus organized a cytaster, detectable with antitubulin labeling, and larger foci were associated with larger asters (Fig. 2A). After sperm incorporation, when a single prominent sperm aster is expected, the mouse egg displays numerous cytoplasmic asters, each with their own centrosomal particles (Fig. 2B). The incorporated sperm nucleus does not appear to be associated with any centrosomal particles initially. The male pronucleus associates with the cytoplasmic centrosomal particles at the same time as the female pronucleus associates with them. It is likely that there is an attraction of centrosomes for interphase nuclear surfaces, and that this interaction contributes to the motions which result in pronuclear apposition. At the end of first interphase (Fig.

2C), the centrosomal particles aggregate near the condensing chromatin at the cell center.

First mitosis in the mouse is quite unusual. Instead of the typical fusiform mitotic spindle with associated asters, the mouse spindle at metaphase is often barrel-shaped and devoid of asters (Fig. 2D). It is more reminiscent of a plant cell spindle [33, 34] than that expected in animal cells. This observation is reinforced by the fact that the mouse spindle at first mitosis is organized in the apparent absence of functional centrioles [32]. This topic of centrioles is considered in the next section.

The hypothesis that the centrosomes are maternally inherited in mice can be experimentally tested. One prediction is that parthenogenetically activated unfertilized oocytes should contain all the information necessary to form a normal bipolar mitotic apparatus: the centrosomes which serve as the mitotic poles should not require any paternal contribution. In Figure 3, mouse oocytes parthenogenetically activated by ethanol are found to organize normal bipolar mitotic spindle (Fig. 3A, B) which divide the eggs from one into two at a frequency of greater than 50%. This is quite

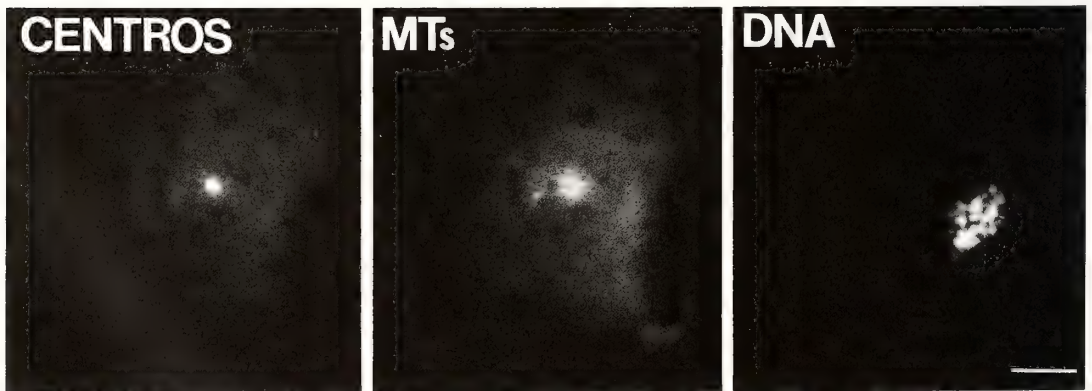
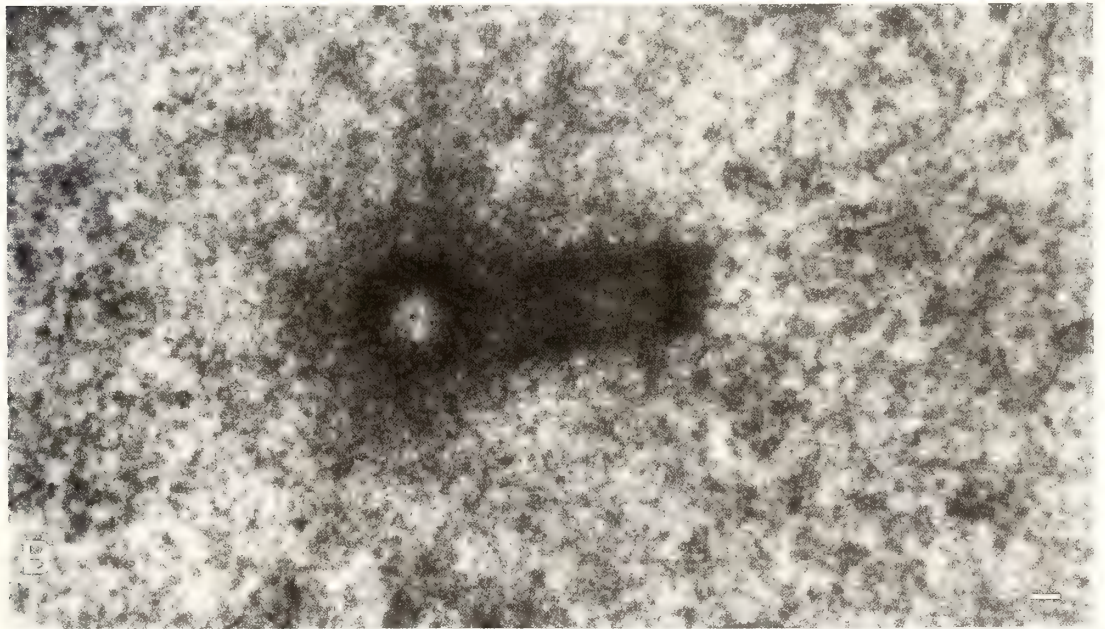
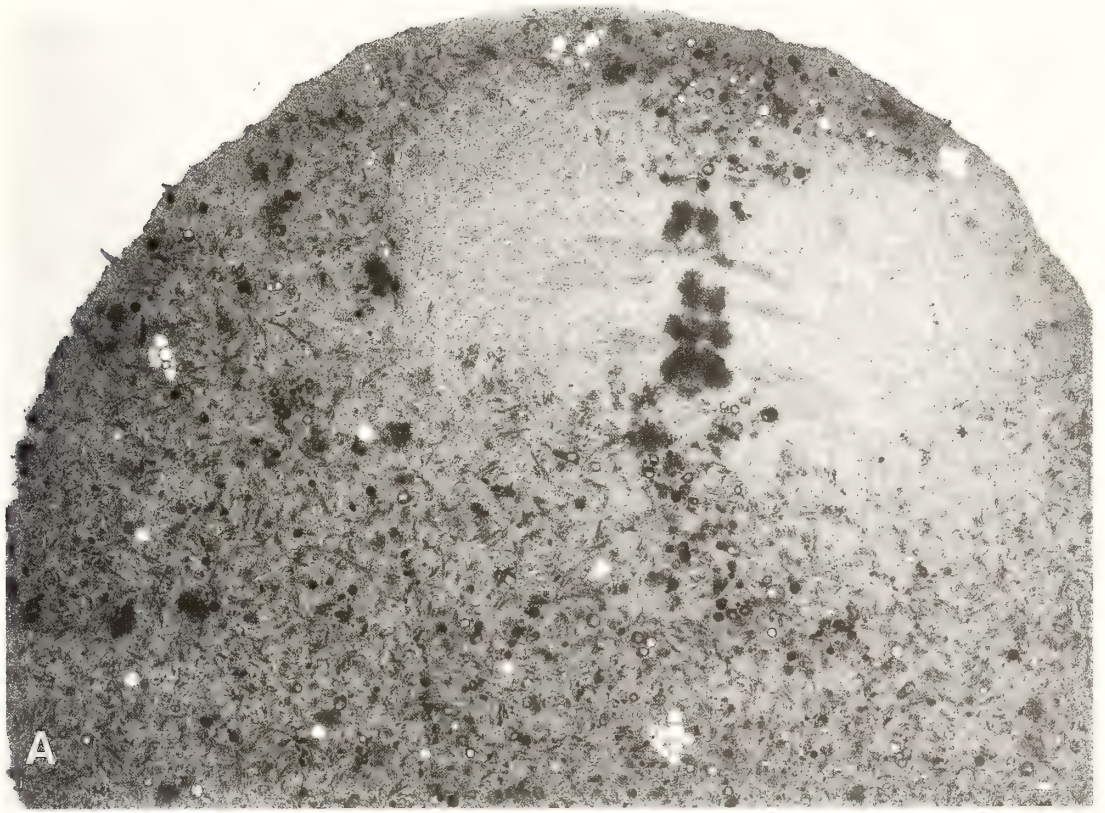


FIG. 4. Aggregation of the sea urchin centrosomes at prometaphase into a single particle. When sea urchin eggs are transferred to ice temperatures at prometaphase, the two centrosomes aggregate into a single compact particle. After recovery from the cold for only 30 sec, a monaster of microtubules is observed. The chromosomes remain condensed, but separate from the compact centrosome. Triple stained for centrosomes (CENTROS: left), microtubules (MTs: middle) and DNA (DNA: right). Bar: 10 μm .

FIG. 5. Centriole appearance during mouse embryogenesis. Centrioles are not found in unfertilized oocytes (A) or in blastocysts as studied with 0.5 μm sections using high voltage electron microscopy. The centrosomes appear as dense osmiophilic material at the spindle poles. By seven-days after mating, centrioles are found at spindle poles (B). The centrioles which appear at this stage have the typical orthogonal pattern of 9+0 triplet microtubules. Bars: A: 1 μm , B: 100 nm.



unlike the situation in lower animals in which parthenogenesis can occur but the spindles that emerge are typically irregular and only rarely bipolar.

C. Physical Treatments Modify Centrosome Configurations

Since the shape of the centrosome is critical in the establishment of a microtubule array, it is of great importance to understand the forces which direct centrosome shape and positioning. A recent collaborative effort has discovered the remarkable effect of physical treatments on centrosome shape [35]. In Figure 4, centrosomes are demonstrated to collapse on each other due to the effects of prolonged cold treatments. Sea urchin eggs at prometaphase, when the two mitotic centrosomes are rather condensed, are incubated for over eighteen hours at 0°C. The microtubules of the mitotic apparatus largely disassemble, the chromosomes remain in their condensed state, and the two centrosomes coalesce into one compact particle. This observation suggests that centrosome shape might well be altered by physical treatment, much in the same way that the state of chromosome condensation can be modified.

III. CENTRIOLES

A. Centriole Appearance in Mouse Embryogenesis

Centrioles are thought to follow a pattern similar to centrosomes during gametogenesis: they are retained at spermatogenesis and lost during oogenesis. High voltage electron microscopy

(HVEM) by Rieder *et al.* [36] demonstrates elegantly the progressive loss of centrioles during maturation in starfish oocytes.

The absence of centrioles in mouse oocytes was first shown by Szöllösi *et al.* [37]. Wooley and Fawcett [38] noted the absence of centrioles in rat sperm. HVEM observations (Fig. 5) confirm the finding that centrioles are absent in unfertilized mouse oocytes and show the dense osmiophilic material at the poles of the meiotic spindle characteristic for centrosomes (Fig. 5A). In light of the unusual "plant-like" shape of the first mitotic apparatus, the ultrastructure of the spindle poles was examined [32]. Surprisingly a structure similar to the sperm centriole was found in association with the remnants of the sperm axoneme, but centrioles were not observed at the spindle poles. This leads to the suggestion that the first mitotic spindle in the mouse is organized in the absence of centrioles. This suggestion raises questions about the functions of centrioles in animal cells as well as their mode of inheritance and timing of appearance during embryogenesis.

To address this latter question, mouse embryos and fetuses were fixed and processed for HVEM at progressively later stages. The advantages of million volt high-voltage electron microscopy for this investigation includes the ability to locate centrioles in thick sections more rapidly than would be possible with conventional thin sections studied with transmission electron microscopy. At all stages until seven days after mating, quite late in fetal development, centrioles have not been located. At this time, centrioles are found in a few cells and it appears that centrioles emerge slowly and asynchronously during mouse development

FIG. 6. Acetylated α -tubulin antibody localization during completion of second meiosis. At ovulation, mouse oocytes are arrested at metaphase (A); tyrosinated α -tubulin antibody (YL1/2) staining reveals microtubules of the anastral barrel-shaped spindle and small cytoplasmic asters heavily decorated (B) while the acetylated α -tubulin antibody only weakly recognizes the polar ends of the spindle (C). At anaphase (D), the chromosomes begin migrating to their respective poles; tyrosinated α -tubulin antibody (YL1/2) and acetylated α -tubulin antibody are indistinguishable in their recognition of the spindle and forming interzonal microtubules (E and F). By late telophase (G), the midbody connecting the polar body with the egg proper has replaced the spindle apparatus and is equally recognized by both α -tubulin (H) and acetylated α -tubulin antibodies (I). Note, however, that acetylated α -tubulin antibody does not stain the cytoplasmic asters during meiosis (I). In addition to the meiotic midbody, the sperm axoneme remains acetylated during interphase (J and K). All images triple labeled for DNA, glutamate (H) or tyrosinated (B, E) α -tubulin antibody, and acetylated α -tubulin antibody. DNA (left panel), rat or rabbit antitubulin antibody (center panel), and acetylated α -tubulin antibody (right panel) on metaphase, anaphase, and late telophase of meiosis in the mouse. Bars: 10 μ m.

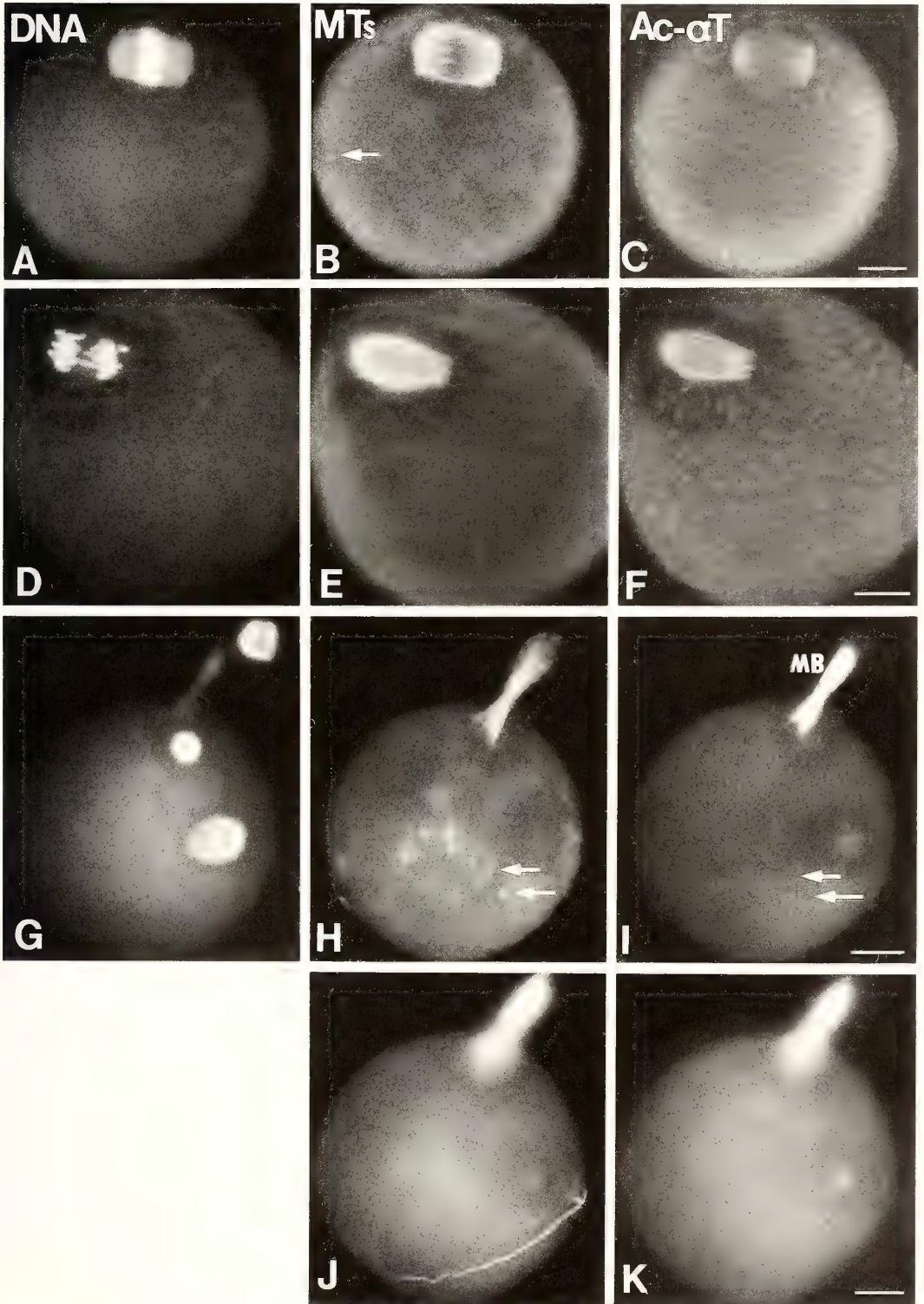


(Fig. 5B). Magnuson and Epstein [39] have described the appearance of centrioles in cultured mouse blastocysts at approximately six days after mating.

IV. POSTTRANSLATIONAL MODIFICATIONS OF α -TUBULINS

A. Modifications and Their Implications for the Fertilization Process

Microtubules are composed primarily of heterodimer subunits of α -tubulin and β -tubulin, as well as numerous microtubule associated proteins (MAPS; reviewed by [40]). Recently it has been shown that tubulin can be post-translationally modified in a few ways including the acetylation of lysine in α -tubulin [41–44], and by the removal and later readdition of the carboxyterminal tyrosine of α -tubulin [45–48] referred to as detyrosination and tyrosination.

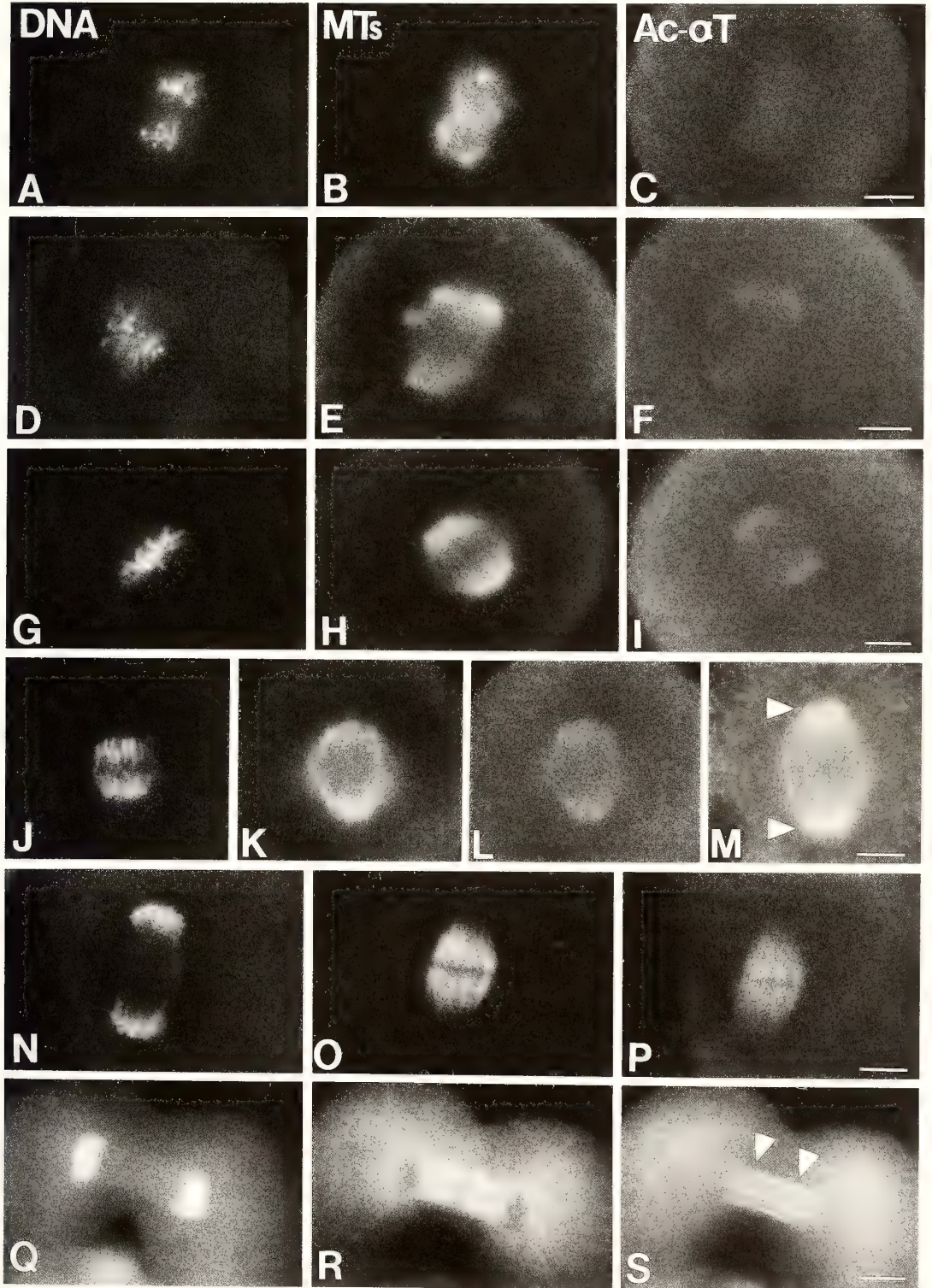
The mouse oocyte at fertilization presents a useful model for exploring the mechanisms responsible for the new appearance of some microtubules and the selective disappearance or stabilization of others. The oocytes are ovulated arrested at second meiotic metaphase and the resumption of meiosis occurs upon activation. New cytoplasmic microtubules proliferate after sperm entry during interphase. The microtubules comprising the incorporated sperm axoneme and the meiotic spindle disassemble with the exception of those destined to form the midbody between the oocyte and the second polar body [32].

B. Acetylation

α -Tubulin in the microtubules of mouse oocytes and embryos is acetylated and detyrosinated in a specific spatial and temporal sequence. In unfertilized oocytes, which are arrested at second meiotic metaphase (Fig. 6A; DNA: Hoechst dye 33258 DNA fluorescence), comparisons of total microtubule image (Fig. 6B; MTs: microtubules) with the binding pattern of acetylated- α -tubulin antibody (Fig. 6C; Ac- α -T: acetylated- α -tubulin) show that the acetylated form is found primarily at the spindle poles though weaker staining is noted throughout the spindle; the cytoplasmic asters (Fig. 6B; arrows) are not acetylated. At meiotic anaphase (Fig. 6D), the spindle microtubules (Fig. 6E) are heavily decorated with the acetylated antibody (Fig. 6F). At the completion of second meiosis (Fig. 6G), when cytasters (Fig. 6H; arrows) and the midbody between the oocyte and second polar body are apparent, only the midbody is acetylated (Fig. 6I; MB: midbody).

The mouse sperm axoneme contains acetylated- α -tubulin, expected from the studies of Piperno and Fuller [44] who investigated sperm from several species, including mammals. After sperm incorporation and during the phases of pronuclear development and apposition, the axoneme retains its ability to bind the antibody to acetylated- α -tubulin (Fig. 6J and 6K). The midbody which resulted from the completion of second meiosis retains its ability to bind the acetylated- α -tubulin antibody. However comparisons of the total tubulin image (Fig. 6H) with that for acetylated- α -

FIG. 7. Acetylated α -tubulin localization during first mitosis. DNA (left panel), affinity purified porcine brain antitubulin antibody (middle panel), and acetylated α -tubulin (right panel) from prophase through telophase in mouse oocytes. At prophase, the male and female chromatin condense separately (A) as each pronucleus is enveloped by a sheath of microtubules (B); this dense array of microtubules is not acetylated (C). By prometaphase, the chromatin has fully condensed (D), the nuclear membranes have disappeared, and the mitotic spindle begins to take shape (E). Acetylated α -tubulin antibody is weakly localized around the developing spindle poles (F). By metaphase, the fertilization process has concluded with the intermingling of the fully condensed male and female chromatin (G) and the formation of a barrel-shaped spindle (H); however, the acetylation of the spindle remains weak at the poles (I). At early anaphase (J and K), there is a dramatic increase in acetylation of the spindle microtubules, particularly at the spindle poles (M). By late anaphase (N) the polar microtubules appear to lose their affinity for the acetylated- α -tubulin antibody and instead, interzonal microtubules become labeled (O and P). At telophase each daughter cell has a monaster of microtubules extending from the nuclear surface of each chromatin mass towards the cell surface as well as an association with the mitotic midbody (Q and R); only the midbody is acetylated (S). All images are triple-labeled for DNA, total tubulin and acetylated α -tubulin antibody except M, which is a single stained image of acetylated- α -tubulin at anaphase. Bars: 10 μ m.



tubulin (Fig. 6I) demonstrates that the microtubules comprising the numerous cytasters in the oocyte are not acetylated (arrows: Fig. 6I).

The meiotic midbody remains acetylated throughout the remainder of first interphase. The incorporated sperm axoneme is frequently found to splay into several fibers towards the completion of the first cell cycle.

First mitosis follows a pattern similar to the second meiotic division. At prophase, only the meiotic midbody binds the acetylated antibody strongly. At prometaphase and metaphase (Fig. 7A, D and G), a barrel shaped mitotic spindle emerges (Fig. 7B, E and H) and the acetylated- α -tubulin stains the polar microtubules weakly (Fig. 7F and I). At anaphase (Fig. 7J) most of the fibers are acetylated with an abundance of the polar microtubules (Fig. 7M: arrowheads). At telophase (Fig. 7N), interzonal microtubules (Fig. 7O) destined to form the mitotic midbody are found to be acetylated (Fig. 7P). After first division (Fig. 7Q), microtubules (Fig. 7R) are found in the monasters extending from the blastomere nuclei to the opposing cell surfaces as well as the interzonal microtubules which will form the midbody. Only the forming midbody microtubules (Fig. 7S; arrowheads) are acetylated.

At the second meiotic and first mitotic divisions, the microtubules surrounding the centrosomes are acetylated at metaphase and there is an increase in acetylation of all spindle microtubules at anaphase: this pattern is not observed precisely during later mitoses. The two-cell mouse embryo which has an interphase array of microtubules binds the acetylated α -tubulin antibody only at the mitotic midbody. Midbodies, however, remain acetylated at these later development stages.

To study the pattern of acetylation of α -tubulin at higher resolution, high voltage electron microscopy was performed on extracted oocytes with immunogold (Fig. 8). At meiotic metaphase, the majority of the acetylated microtubules are found

at the spindle poles with only sparse detection of acetylated microtubules within the spindle proper. Figure 8A is a low magnification HVEM image of a meiotic spindle at metaphase. In Figure 8B, at higher magnification, acetylated microtubules are detected by immunogold labeling. In contrast only sparse acetylation is found on the microtubules at the spindle equator (Fig. 8C).

C. Detyrosination

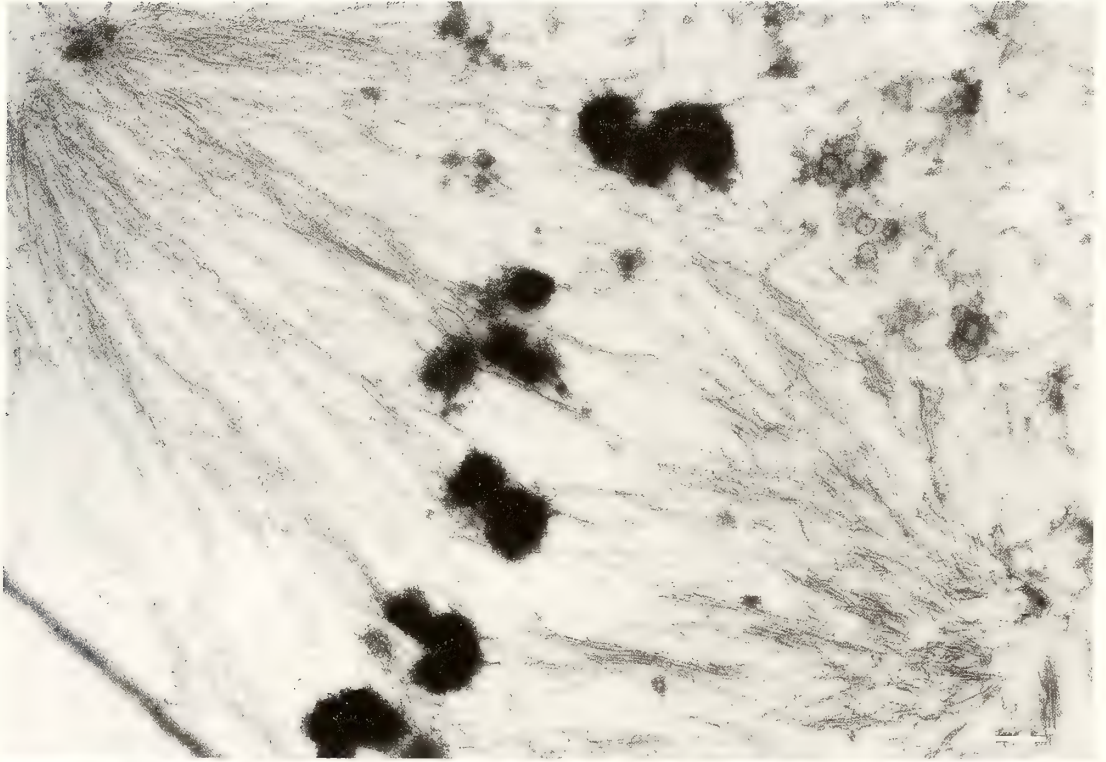
Microtubules can also be post-translationally modified by the loss of the carboxyterminal tyrosine amino acid residue from α -tubulin [45, 46, 48]. Detyrosinated microtubules appear to be older, more stable microtubules and in the mouse oocyte, the sperm axoneme is found to be the only class of microtubules which is uniquely detected with a rabbit affinity purified antibody to detyrosinated- α -tubulin (courtesy of Dr. Bulinski). Eichenlaub-Ritter *et al.* [49] have examined the pattern of detyrosinated microtubules in ageing mouse oocytes and showed the presence of both types of α -tubulin.

All the other classes of microtubules, including the meiotic and mitotic spindles, the meiotic and mitotic midbodies, the cytasters in meiotic and mitotic cytoplasm and the interphase microtubule complex all appear to be composed of a mixture of tyrosinated and detyrosinated microtubules. The images obtained from a global analysis of fixed material do not yet address the question of instantaneous turnover and dynamics of individual microtubules, a problem which awaits improvements in imaging technologies for cells as large as oocytes and embryos.

V. CONCLUSIONS AND FUTURE PROSPECTS

These studies comparing the origins of centrosomes and centrioles during fertilization and the post-translational modifications of α -tubulin have

FIG. 8. Immuno-gold labeling of acetylated- α -tubulin with high voltage electron microscopy. Meiotic spindle microtubules in unfertilized mouse oocytes at metaphase are primarily acetylated at the spindle poles (A). The microtubules in the middle of the spindle including those at the kinetochores are less heavily acetylated. B: High magnification image showing heavy labeling of immunogold against acetylated- α -tubulin along the microtubules at the centrosomes. C: The microtubules at the spindle equator are only weakly acetylated at metaphase. Bars: 100 nm.



several implications regarding the manner in which microtubule arrays are organized and stabilized.

Microtubule configurations appear to be specified by the combination of labile, actively growing microtubules emanating from the centrosome and stable, perhaps older microtubules which are post-translationally acetylated or detyrosinated. For example in the two-cell mouse egg (Fig. 7), the midbody microtubules are acetylated and stable to cold or drug treatments. In contrast the monastral microtubules extending from the centrosomes on the polar faces of the blastomere nuclei are deacetylated, sensitive to cold and drug treatments, and are likely the result of rapid turnover due to the dynamic instability of growing microtubules [50]. Perhaps the stabilization of certain microtubules by post-translational acetylation or detyrosination assists in the generation of persistent architecture without the energetic costs of maintaining an array of microtubules involving the constant equilibrium between assembly and disassembly.

Centrosomes appear to be paternally inherited in most all animals: animals ranging from coelenterates to lower vertebrates including fish and amphibians. In the mouse evidence is accumulating supporting the theory that centrosomes are of maternal origin. If studies on other mammals support this conclusion, then the evolutionary question as to when and why centrosomes switched from a paternal pattern to a maternal one must be posed.

Perhaps the typical pattern of paternal inheritance is designed to ensure biparental fertilization. The requirement for the sperm centrosome would decrease the likelihood of successful natural parthenogenesis, if for example the second polar body is not properly extruded. This idea is supported by studies on artificial activation [51]; most metabolic processes are properly initiated, including DNA synthesis (reviewed by [52]), but without the sperm centriole the egg cannot form a mitotic apparatus and divide.

If this is correct, why then might mammals violate this seemingly sensible scheme? Abnormal fertilization and embryogenesis in mammals represent a significant risk to the mother, a risk which is not found in any other class of animals. Perhaps to

reduce this jeopardy, mammalian reproduction switched from a reliance on biparental centrosomal contributions to one needing biparental chromosome contributions. This idea is well supported by the elegant studies of Surani and Barton [53] demonstrating that fertilized eggs with two maternal or two paternal pronuclei cannot develop to term and by Sapienza *et al.* [7] which extends these observations on the molecular differences between sperm and egg DNA.

If a strict requirement for biparental genomic contributions became the norm in mammals, then the requirement to maintain fidelity to the sperm centrosome could be relaxed. Perhaps the sperm might contribute some centrosomal material, perhaps the egg could also contribute: oogenesis might not destroy centrosomes and spermatogenesis might not necessarily retain them. In this manner, one prediction might be that in some mammals either or both parent could contribute centrosomes and there might be heterogeneity among various mammalian species. Evidence to support this is emerging from the studies of Kola and Trounson [54]; human oocytes polyspermicallly fertilized *in vitro* divide in a pattern not predicted from studies on invertebrates or mice.

While it is tempting to indulge in these speculations, answers supporting or refuting some assumptions are possible to obtain. The events during parthenogenesis, when the paternal contribution is lacking, or polyspermy, when the paternal contribution is multiplied, will likely provide important evidence. Future studies on other rodents and non-rodent mammals may confirm the homogeneity among mammalian species and investigations on birds and reptiles will help fill some evolutionary gaps.

In conclusion, the centrosomes and centrioles are paternally inherited in most animals. However the mouse and perhaps other mammals violate this scheme: centrosomes appear to be of maternal origin, and centrioles emerge only late in fetal development probably also from maternal sources. Microtubule patterns are generated not only by the discriminating positioning of centrosomes, but also by the selective post-translational acetylation and detyrosination of α -tubulins. The rapid discoveries on the molecular basis of microtubule dynamics

will undoubtedly result in an even greater understanding on the role, regulation and mechanisms of force generation of the microtubule-mediated motions at fertilization.

ACKNOWLEDGMENTS

It is indeed our pleasure to acknowledge all of our wonderful colleagues and collaborators who have contributed to various aspects of this research. These investigators include Drs. David Asai, Harald Biessmann, Chloe Bulinski, Peter Cooke, Daniel Mazia, Ester Szöke and Marika Walter. We are also grateful for the technical assistance of Kathleen Johnson and Cody Martin. The research reviewed here was funded by research grants from the National Institutes of Health. The IMR in Madison is an NIH Biomedical Research Technology Resource.

REFERENCES

- Schatten, G. (1982) Motility during fertilization. *Int. Rev. Cytol.*, **79**: 59-163.
- Garbers, D. L. (1988) The regulation of spermatozoan function by the egg. In "The Molecular Biology of Fertilization". Ed. by H. Schatten and G. Schatten, in press. Academic Press, New York.
- Lardy, H. and San Agustin, J. (1988) Caltrin and Calcium regulation of sperm activity. In "The Cell Biology of Fertilization". Ed. by H. Schatten and G. Schatten, in press. Academic Press, New York.
- Schackman, R. (1988) Ionic regulation of the sperm acrosome reaction and stimulation by egg-derived peptides. In "The Cell Biology of Fertilization". Ed. by H. Schatten and G. Schatten, in press. Academic Press, New York.
- Tilney, L. (1976) The polymerization of actin. II. How non-filamentous actin becomes nonrandomly distributed in sperm: Evidence for the association of this actin with membranes. *J. Cell Biol.*, **69**: 51-72.
- Gibbons, I. R. (1981) Cilia and flagella of eukaryotes. *J. Cell Biol.*, **91**: 107S-124S.
- Sapienza, C., Peterson, A. C., Rossant, J. and Balling, R. (1987) Degree of methylation of transgenes is dependent on gamete of origin. *Nature*, **328**: 251-254.
- Ruiz-Bravo, N. and Lennarz, W. J. (1988) Receptors and membrane interaction during fertilization. In "The Molecular Biology of Fertilization". Ed. by H. Schatten and G. Schatten, in press. Academic Press, New York.
- Shur, B. D. (1988) Galactosyltransferase as a recognition molecule during fertilization and development. In "The Molecular Biology of Fertilization". Ed. by H. Schatten and G. Schatten, in press. Academic Press, New York.
- Longo, F. J. (1988) Egg cortical architecture. In "The Cell Biology of Fertilization". Ed. by H. Schatten and G. Schatten, in press. Academic Press, New York.
- Schatten, H., Cheney, R., Balczon, R., Cline, C., Simerly, C. and Schatten, G. (1986) Localization of fodrin during fertilization and early development in sea urchins and mice. *Dev. Biol.*, **118**: 457-466.
- Schatten, H., Schatten, G., Mazia, D., Balczon, R. and Simerly, C. (1986) Behavior of centrosomes during fertilization and cell division in mouse oocytes and in sea urchin eggs. *Proc. Natl. Acad. Sci. USA.*, **83**: 105-109.
- Schroeder, T. (1981) Interrelations between the cell surface and the cytoskeleton in cleaving sea urchin eggs. In "Cytoskeletal Elements and Plasma Membrane Organization". Ed. by G. Poste and G. L. Nicolson, Elsevier/North Holland, Amsterdam, pp. 170-216.
- Fisher, G. W. and Rebhun, L. I. (1983) Sea urchin egg cortical granule exocytosis is followed by a burst of membrane retrieval via uptake into coated vesicles. *Dev. Biol.*, **99**: 456-472.
- Poccia, D. (1988) Reactivation and remodelling of the sperm nucleus following fertilization. In "The Molecular Biology of Fertilization". Ed. by H. Schatten and G. Schatten, in press. Academic Press, New York.
- Zirkin, B. R., Perreault, S. D. and Naish, S. J. (1988) Formation and function of the male pronucleus during mammalian fertilization. In "The Molecular Biology of Fertilization". Ed. by H. Schatten and G. Schatten, in press. Academic Press, New York.
- Austin, C. R. (1965) Fertilization. Prentice Hall, New Jersey.
- Sawada, T. and Schatten, G. (1988) Anti-tubulin indirect immunofluorescence microscopy of Ascidian eggs during fertilization and early development. *Cell Motil. Cytoskeleton*, in press.
- Rothschild, L. V. (1956) Fertilization. Methuen Publ., London.
- Boveri, Th. (1900) Zellen-Studien IV. Ueber die Natur der Centrosomen. Fischer, Jena, Germany.
- Calarco-Gillam, P. D., Siebert, M. C., Hubble, R., Mitchison, T. and Kirschner, M. (1983) Centrosome development in early mouse embryos as defined by an autoantibody against pericentriolar material. *Cell*, **35**: 621-629.
- Wick, S. M. (1985) Immunofluorescence microscopy of tubulin and microtubule arrays in plant cells. *Cell Biol. Int. Rep.*, **9**: 357-371.
- Schatten, G., Schatten, H., Spector, I., Cline, C., Paweletz, N., Simerly, C. and Petzelt, C. (1986) Latrunculin inhibits the microfilament-mediated

- processes during fertilization, cleavage and early development in sea urchins and in mice. *Exp. Cell Res.*, **166**: 191–208.
- 24 Maro, B., Howlett, S. K. and Webb, M. (1985) Non-spindle microtubule organizing centers in metaphase-II arrested mouse oocytes. *J. Cell Biol.*, **101**: 1665–1672.
- 25 Schatten, G., Simerly, C., Asai, D., Szöke, E., Cooke, P. and Schatten, H. (1987) Acetylation and detyrosination of α -tubulin in microtubules during mouse fertilization, mitosis and early development. *J. Cell Biol.*, **105**: 258a.
- 26 Carre, D. and Sardet, C. (1984) Fertilization and early development in *Beroë ovata*. *Dev. Biol.*, **105**: 188–195.
- 27 Klymkowsky, M. W. (1988) Cytoskeletal reorganizations during amphibian fertilization and early development. In "The Cell Biology of Fertilization". Ed. by H. Schatten and G. Schatten, in press. Academic Press, New York.
- 28 Balczon, R. and Schatten, G. (1983) Microtubule-containing detergent extracted cytoskeletons in sea urchin eggs from fertilization through cell division: Antitubulin immunofluorescence microscopy. *Cell Motility*, **3**: 213–226.
- 29 Bestor, T. H. and Schatten, G. (1981) Antitubulin immunofluorescence microscopy of microtubules present during the pronuclear movements of sea urchin fertilization. *Dev. Biol.*, **88**: 80–91.
- 30 Harris, P., Osborn, M. and Weber, K. (1980) Distribution of tubulin-containing structures in the egg of the sea urchin, *Strongylocentrotus purpuratus*. *J. Cell Biol.*, **84**: 668–679.
- 31 Kuriyama, R., Borisy, G. G. and Masui, Y. (1986) Microtubule cycles in oocytes of the surf clam, *Spisula solidissima*: An immunofluorescence study. *Dev. Biol.*, **114**: 151–160.
- 32 Schatten, G., Simerly, C. and Schatten, H. (1985) Microtubule configurations during fertilization, mitosis, and early development in the mouse and the requirement for egg microtubule-mediated motility during mammalian fertilization. *Proc. Natl. Acad. Sci. USA.*, **82**: 4152–4156.
- 33 Bajer, A. S. and Mole-Bajer, J. (1986) Reorganization of microtubules in endosperm cells and cell fragments of the higher plant *Haemanthus* in vivo. *J. Cell Biol.*, **102**: 263–281.
- 34 Schmit, A.-C. and Lambert, A.-M. (1987) Characterization and dynamics of cytoplasmic F-actin in higher plant endosperm cells during interphase, mitosis and cytokinesis. *J. Cell Biol.*, **105**: 2157–2166.
- 35 Mazia, D., Schatten, H., Coffe, G., Szöke, E., Howard, C. and Schatten, G. (1987) Aggregation of the mitotic centrosomes into a single spherical centrosome by cold treatment in sea urchin eggs. *J. Cell Biol.*, **105**: 206a.
- 36 Rieder, C. L., Miller, F. J., Davison, E., Bowser, S. S., Lewis, K. and Sluder, G. (1987) *Proc. Electron. Microsc. Soc. Am.*, **45**: 578–581.
- 37 Szöllösi, D., Calarco, P. and Donahue, R. P. (1972) Absence of centrioles in the first and second meiotic spindles of mouse oocytes. *J. Cell Sci.*, **11**: 521–541.
- 38 Wooley, D. M. and Fawcett, D. W. (1973) The degeneration and disappearance of the centrioles during the development of rat spermatozoon. *Anat. Rec.*, **177**: 289–302.
- 39 Magnuson, T. and Epstein, C. I. (1984) Oligosyndactyly – a lethal mutation in the mouse that results in mitotic arrest very early in development. *Cell*, **38**: 823–833.
- 40 Olmsted, J. B. (1986) Microtubule-associated proteins. *Ann. Rev. Cell Biol.*, **2**: 421–457.
- 41 L'Hernault, S. W. and Rosenbaum, J. L. (1985) Reversal of the posttranslational modification on *Chlamydomonas* flagellar α -tubulin occurs during flagellar resorption. *J. Cell Biol.*, **100**: 457–462.
- 42 L'Hernault, S. W. and Rosenbaum, J. L. (1983) *Chlamydomonas* α -tubulin is posttranslationally modified in flagella during flagellar assembly. *J. Cell Biol.*, **97**: 258–263.
- 43 Piperno, G., LeDizet, M. and Chang, X. (1987) Microtubules containing acetylated α -tubulin in mammalian cells in culture. *J. Cell Biol.*, **104**: 289–302.
- 44 Piperno, G. and Fuller, M.T. (1985) Monoclonal antibodies specific for an acetylated form of α -tubulin recognize the antigen in cilia and flagella from a variety of organisms. *J. Cell Biol.*, **101**: 2085–2094.
- 45 Gundersen, G. G., and Bulinski, J. C. (1986) Distribution of tyrosinylated and nontyrosinylated α -tubulin during mitosis. *J. Cell Biol.*, **102**: 1118–1126.
- 46 Gundersen, G. G., Kalnoski, M. H. and Bulinski, J. C. (1984) Distinct populations of microtubules: Tyrosinylated and nontyrosinylated α -tubulin are distributed differently in vivo. *Cell*, **38**: 779–789.
- 47 Vacquier, V. D. (1981) Dynamic changes of the egg cortex. *Dev. Biol.*, **84**: 1–26.
- 48 Geuens, G., Gundersen, G. G., Nuydens, R., Cornelissen, F., Bulinski, J. C. and DeBrabander, M. (1986) Ultrastructural colocalization of tyrosinylated and detyrosinylated α -tubulin in interphase and mitotic cells. *J. Cell Biol.*, **103**: 1883–1893.
- 49 Eichenlaub-Ritter, U., Chandley, A. C., and Gosden, R. G. (1986) Alterations to the microtubular cytoskeleton and increased disorder of chromosome alignment in spontaneously ovulated mouse oocytes aged in vivo: An immunofluorescence study. *Chromosoma*, **94**: 337–345.
- 50 Kirschner, M. and Mitchison, T. (1986) Beyond self-assembly: From microtubules to morphogene-

- sis. *Cell*, **45**: 329–342.
- 51 Loeb, J. (1913) *Artificial Parthenogenesis and Fertilization*. Columbia Univ. Press, New York.
- 52 Epel, D. (1980) Ionic triggers in the fertilization of sea urchin eggs. *Ann. N.Y. Acad. Sci.*, **339**: 74–85.
- 53 Surani, M. A. H. and Barton, S. C. (1983) Development of gynogenetic eggs in the mouse: Implications for parthenogenetic embryos. *Science*, **222**: 1034–1036.
- 54 Kola, I. and Trounson, A. (1987) Trippronuclear human oocytes: Altered cleavage patterns and subsequent karyotypic analysis of embryos. *Biol Reprod.*, **37**: 395–401.
- 55 Schatten, H., Walter, M., Mazia, D., Biessmann, H., Paweletz, N., Coffe, G. and Schatten, G. (1987) Centrosome detection in sea urchin eggs with a monoclonal antibody against *Drosophila* intermediate filament proteins: Characterization of stages of the division cycle of centrosomes. *Proc. Natl. Acad. Sci., USA.*, **84**: 8488–8492.

Spontaneous Aster Formation in Cytoplasmic Extracts from Eggs of the Surf Clam

ROBERT E. PALAZZO, JENNIFER B. BRAWLEY
and LIONEL I. REBHUN

*Department of Biology, University of Virginia,
Charlottesville, VA 22901, U.S.A.*

ABSTRACT—Asters form spontaneously in cytoplasmic extracts prepared from eggs obtained from the surf clam *Spisula solidissima*. Astral birefringence is augmented and asters are stabilized by the addition of hexylene glycol. Asters form spindle-like structures, contain particles associated with their periphery, and aggregate to form multi-astral complexes. Studies with video microscopy and electron microscopy indicate that asters formed *in vitro* are composed of microtubules radiating from a central zone which contains a centriole. Asters were isolated and their associated proteins analyzed. In addition, astral microtubules and microtubule associated proteins were isolated by temperature dependent polymerization-depolymerization. Numerous proteins coassemble with astral tubulin through cycles of assembly-disassembly. We suggest that this will be a useful system for the isolation and characterization of centrosomal components which direct microtubule organization in cells.

INTRODUCTION

Microtubules are generally not randomly arranged in cells but are organized around discrete regions of the cytoplasm [1-3]. These foci of radiating microtubules, known as microtubule organizing centers (MTOCs) [4], are sites of initiation of microtubule assembly [1, 2] and may serve to capture preexisting microtubules [5]. Microtubule organizing centers play a significant role in cell division [5-7], organization of cellular morphology [2], and possibly in directing cellular migrations [8, 9]. In spite of the obvious significance of MTOCs to cell functions, remarkably little is known of their chemical composition or their regulation [1]. This is largely due to the inability to isolate and purify MTOCs on a sufficient scale for preparative and analytical biochemical approaches.

We describe here a system which allows the isolation of MTOCs from the surf clam *Spisula solidissima*. *Spisula* is available during the summer months off the north east coast of the United States at the Marine Biological Laboratory at

Woods Hole, Massachusetts. During the summer when the animals are gravid as much as 30 ml of eggs can be obtained from the gonad of a single female.

The eggs are obtained at diakinesis of the first meiotic division [10]. They contain a large germinal vesicle which houses a prominent nucleolus and condensed chromosomes. Eggs can be fertilized with sperm or activated parthenogenetically by the addition of KCl to an egg sea water suspension [11]. Usually within 8 min after the addition of KCl at room temperature the nucleolus disappears and the germinal vesicle envelope breaks down (GVBD). By 12 min a prominent meiotic spindle is formed within the egg center. The spindle subsequently migrates to the egg cortex where it performs oscillatory movements, a process reported in meiotic stages by Rebhun [10] and studied extensively in embryos undergoing cleavage by Dan and Inoue [12]. Finally, the egg undergoes two sequential meiotic divisions resulting in the formation of two polar bodies.

In recent years cytoplasmic extracts prepared by centrifugal crushing of cells in very low dilution conditions have been used to study nuclear envelope breakdown and assembly [13-18], chroma-

tin condensation and decondensation [14, 15], and DNA synthesis [19]. Using similar cytosolic extracts prepared from *Spisula* we found that asters formed spontaneously when the extract was warmed to room temperature. We report our initial studies using video and electron microscopy, which indicate that asters contain centrioles confirming the observation of Weisenberg and Rosenfeld [20]. Further, we have isolated these asters in sufficient quantity for biochemical analysis and described both astral protein composition and the astral microtubule associated proteins.

MATERIALS AND METHODS

Egg preparation and activation

Eggs were prepared by dissection of the gonads from *Spisula solidissima* females. The eggs were released into sea water by snipping the ovary with scissors and gently agitating the resulting pieces. The egg-sea water suspension was poured through cheese cloth to remove unwanted debris and gonadal tissue. The eggs were then washed at least three times by successive resuspension and settling with a minimum of $1,000 \times$'s volume of sea water per wash. Eggs were activated by the addition of 0.5 M KCl to a final ratio of 86:14 sea water to 0.5 M KCl according to Allen [11].

Preparation of cytosolic extract

Cytosolic extracts were prepared from *Spisula* eggs whose vitelline membranes were removed by washing twice using successive cycles of $1,000 \times g \times 30$ second centrifugations and resuspension with 10 mM NaPO_4 , 1 M glycerol at pH 8.0–8.2, followed by one wash with 1 M glycerol. Eggs were then resuspended in ice cold 20 mM PIPES buffer containing 100 mM KCl, and 5 mM MgSO_4 , pH 7.2 and quickly centrifuged at $1,000 \times g$ for 30 sec. The supernatant was removed and the pellet was loosened and eggs broken by resuspension with a pipette. The suspension was centrifuged at approximately $10,000 \times g$ for 10 min at 4°C which resulted in separation into three layers; an upper lipid layer, a lower yolk layer and a middle cytoplasmic layer similar to the preparations reported by others in amphibian eggs [14, 15]. The cyto-

plasmic extract was removed and centrifuged again at $10,000 \times g$ for 10 min at 4°C and the middle cytoplasmic layer collected and kept on ice until use.

Light and video microscopy

Twenty microliter drops of the extract were placed onto a glass slide and sealed with a coverslip lined with silicon grease. Aster formation was observed with a Zeiss photomicroscope-I equipped with strain free polarization lenses and micrographs were taken with Kodak Tri-X 400 film developed with Diafine. Video microscopy was carried out with a Zeiss Axiophot microscope equipped with a Hamamatsu C-2400 Newvicon camera linked to a Sony 5800H video recorder. Photographs of video images were taken from a Javelin video monitor using Kodak T-Max 400 film developed with T-Max developer.

Electron microscopy

After resuspension in MEMG (see below) and centrifugation, aster pellets were fixed with 1% glutaraldehyde in MEMG followed by postfixation with 1% osmium tetroxide, dehydrated through an ethanol series, and embedded in epon. Thin sections were prepared, stained with lead citrate and uranyl acetate and micrographs taken using a Hitachi HU-11E1 at 75 kv.

Aster isolation

Cytosolic extract, with or without added hexylene glycol to 3%, was incubated at room temperature for 5 min. Aster formation was monitored as described above with polarization microscopy. The cytosolic extract was then diluted with 10 volumes of MEMG (20 mM MES, 1 mM EGTA, 1 mM MgSO_4 , 10% glycerol, pH 6.5) and centrifuged at $1,000 \times g$ for 10 min. The pellets from multiple samples were pooled and washed by resuspension in MEMG (minimum of 100 volumes) and centrifuged again at $1,000 \times g$. The washed pellet was resuspended in a $100 \times$ volume of microtubule reassembly buffer (100 mM PIPES, 1 mM EGTA, 1 mM MgSO_4 , pH 6.9) and centrifuged at $1,000 \times g$. The supernatant was aspirated and GTP added to the pellet from a $100 \times$ stock to a final concentration of 1 mM. The aster suspen-

sion was then incubated on ice for 1 hr to depolymerize microtubules as monitored by polarization microscopy. The solution was centrifuged at $39,000\times g$ for 30 min at 4°C and the supernatant and pellet collected. The supernatant was warmed to 30°C for 30 min to repolymerize microtubules which were then centrifuged out of solution at $39,000\times g$ for 30 min at 30°C . The microtubule pellet and supernatant were collected. Samples at various stages of the preparation were taken for electrophoretic analysis as described below.

Electrophoresis

Proteins from the various stages of the astral protein preparation steps described above were analyzed by SDS gel electrophoresis according to Laemmli [21] using a running gel composed of 7.5% acrylamide and 4 M urea. Gels were stained with either Coomassie blue or silver [22] to visualize proteins.

RESULTS

Aster formation and migration

Eggs were activated with KCl (as described above) for 4 min, washed, and cytosolic extract prepared as described in Materials and Methods. Within 2 min after warming the extract to room temperature numerous asters were visible with polarization microscopy throughout the slide (Fig. 1a). The number of asters formed varied between preparations but was generally between 20–30 per $10\times$ field as visualized with a Zeiss photomicroscope-I with an optovar setting of 1.25. Aster formation occurred in almost all preparations with few exceptions.

Addition of hexylene glycol to the cytosolic extract to a final concentration of 3% before warming to room temperature resulted in the

stabilization and augmentation of the birefringence of asters (HG-asters) (Figs. 1b, 3 and 4). In addition, diasters and multiple aster complexes were observed (Figs. 2, 3 and 4b). After 10 min of warming the extract (with hexylene glycol) numer-

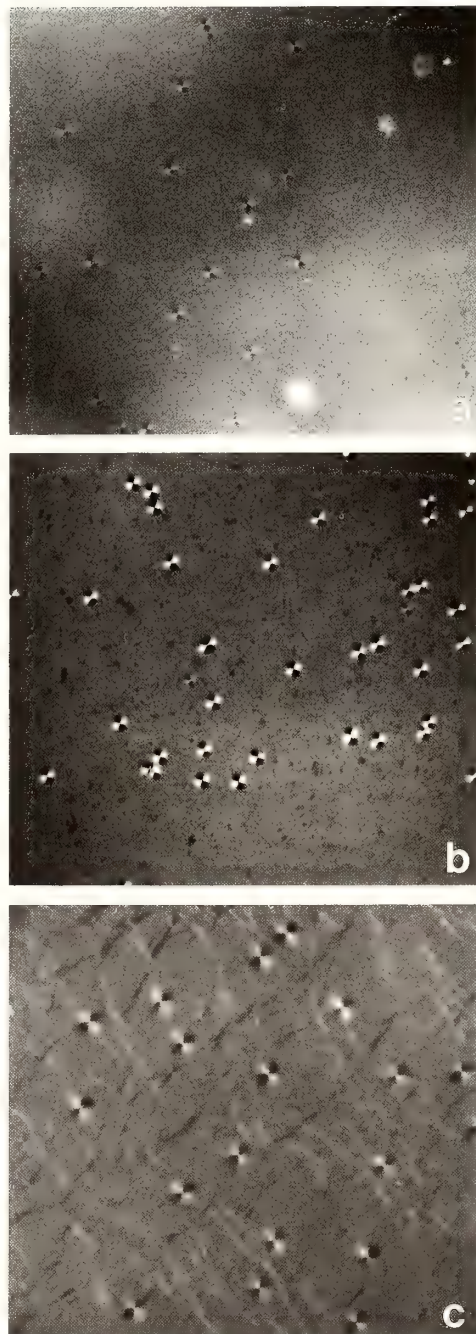


FIG. 1. Aster formation in cytoplasmic extracts. With polarization microscopy asters were observed within two minutes of warming extracts to room temperature (a). Addition of hexylene glycol to the extract resulted in augmentation of astral birefringence (b). In the presence of hexylene glycol birefringent fibers formed in the background approximately 10 min after warming to room temperature (c). (Magnification: $108\times$).

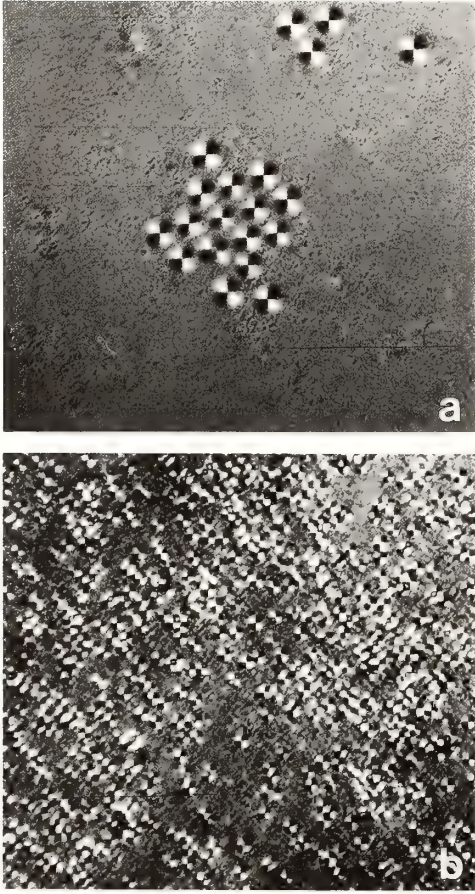


FIG. 2. Aggregation of asters. Aggregates of asters (a) and eventually astral complexes (b) formed in extracts. By 60 min after warming the extract to room temperature in the presence of hexylene glycol these complexes formed tight masses of asters which could be removed from the extract with forceps (b). (Magnification: $108\times$).

ous fibers were observed in the background (Fig. 1c). With time (10–20 min) asters congressed and ultimately formed multi-asteral complexes (Fig. 2). Indeed, if the reactions were allowed to occur in a test tube, the asters and secondary fibers eventually formed a complex which separated from the rest of the solution and could be removed with forceps (Fig. 2b). Preliminary evidence suggests that this movement and aggregation was independent of actin polymer formation since these migrations occur if cytochalasin-B is added to the extract before inducing aster formation (data not shown).

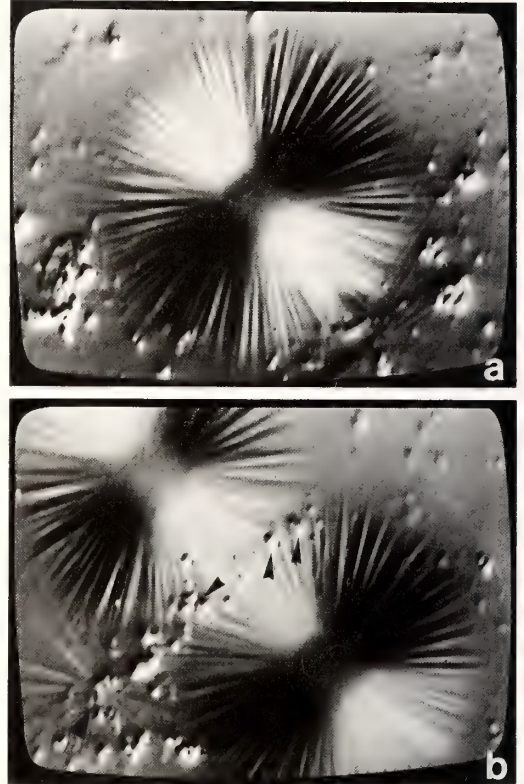


FIG. 3. Nomarski video-microscopy of an aster and a spindle-like structure. Asters were composed of fibers radiating from a central zone (a). Some asters formed spindle-like structures (b) which contained particles (small arrowheads) within their mid-zone. Fibers were also found radiating from particles not associated with astral centers (large arrowhead in b). (Magnification: $1,242\times$).

Video-microscopy and electron microscopy

HG-asters were studied using Nomarski optics and visualized using video imaging. The asters were composed of fibers radiating from a central zone (Figs. 3 and 4). Asters contained so many radial fibers that they appeared birefringent even with Nomarski optics. Within the central zone of the asters a small dense structure was observed (Fig. 4). All asters contained at least one such structure, although occasionally asters which contained two were found (data not shown). Analysis by electron microscopy confirmed the video-microscopy observation that asters were composed of radiating microtubules (Fig. 4c). Single centrioles were found at the center of the asters (Fig.

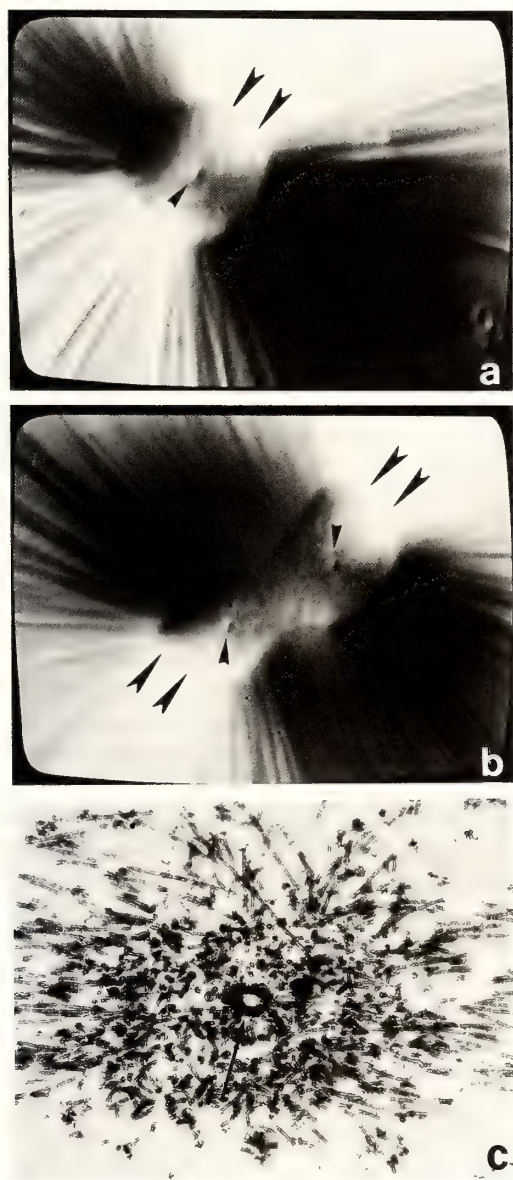


FIG. 4. Asters contain centrioles. High magnification Nomarski-video microscopy (a and b) revealed that astral centers were composed of a zone (large arrowheads in a and b) from which fibers radiated. These zones from two or more asters were occasionally found to overlap as if fused (b). Within these zones small refractile bodies were found (small arrowheads in a and b). Electron micrographs indicated that centrioles were present at the center of asters (c). (Magnification: $3,105\times$ (a and b) and $13,230\times$ (c)).

4c), although on one occasion two centrioles were observed.

Asters tended to form multiple aster complexes composed of two or more asters (Fig. 4b). These multi-astral complexes contained multiple centers with overlapping central zones which tended to distort and fuse rather than maintain discrete independent astral centers (Fig. 4b). Thus, the pericentriolar zone of asters is capable of fusion and interaction with the same zone of other asters. Nevertheless, we were always able to find a density corresponding to a centriole at the center of each zone (Fig. 4).

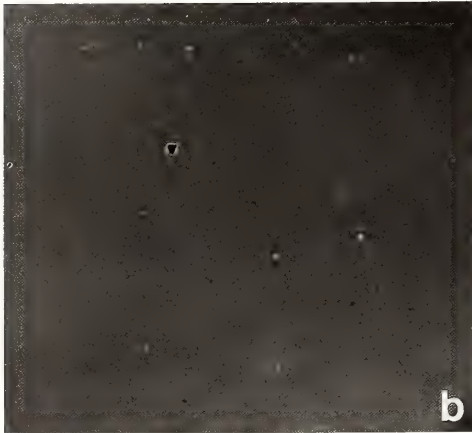
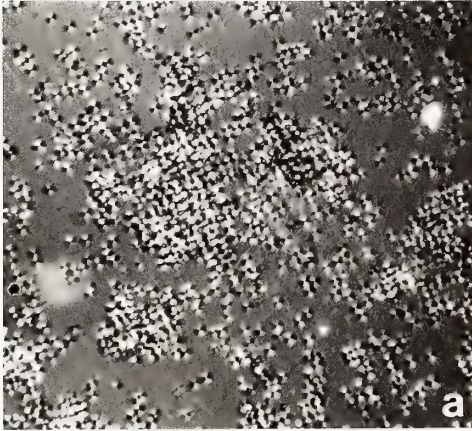
Biochemical analysis of astral components

Asters formed in the presence or absence of added hexylene glycol were isolated and analyzed by SDS-electrophoresis. As expected, one of the major components was tubulin. Few qualitative differences were observed when aster and HG-aster proteins were compared (Fig. 6). In addition, quantitative differences, particularly with respect to tubulin and high molecular weight proteins were found (Fig. 6). Thus hexylene glycol increased the tubulin content of asters but did not induce significant qualitative changes in astral composition.

Astral rays were depolymerized by cold treatment in a microtubule reassembly buffer (Fig. 5). The cold-labile components were separated from cold-stable material by centrifugation. In addition to tubulin, a number of other proteins became soluble upon treatment with cold temperatures and GTP (Fig. 6). When the cold-labile fraction was separated from the cold-stable components and warmed to 30°C , tubulin polymerized (Figs. 5c and 6) and a number of other proteins (presumably MAPs) coassembled (Fig. 6). Interestingly, some astral proteins which were cold labile and presumably solubilized as astral microtubules depolymerized, did not reassemble (coassemble) with the tubulin upon warming. Finally, while microtubules form, no asters were observed in the polymerized supernatant when assayed by polarized light microscopy (Fig. 5c), suggesting that the MTOCs were stable to treatment of cold temperature and GTP, and consequently pelleted during the $39,000\times g$ centrifugation.

DISCUSSION

Previous studies have suggested that cytoplasmic extracts can be useful in the study of cell cycle dependent events *in vitro*. For example, cytoplas-



mic preparations from sea urchin eggs can induce sperm chromatin to decondense [23]. In addition, extracts from *Xenopus laevis* oocytes induce a wide variety of processes *in vitro* such as DNA synthesis [19], formation of pronuclei [15], nuclear envelope assembly [13, 15, 16], chromatin decondensation [15, 23], chromosome condensation [14, 17], nuclear envelope breakdown [14, 17, 18] and spindle formation [14] *in vitro*. Finally, Weisenberg *et al.* reported that asters formed spontaneously in homogenates prepared from *Spisula* oocytes [20] and sea urchin eggs [24].

We have adapted the methods of Masui [25], Benbow and Ford [19] and Lohka and Maller [14, 15] to prepare similar cytoplasmic extracts from eggs obtained from *Spisula*. With these extracts we have consistently observed the spontaneous formation of asters *in vitro*. Birefringent asters formed within two minutes upon warming the extracts to room temperature and were augmented and stabilized by the addition of hexylene glycol, a known microtubule stabilizing agent [26]. Numerous astral complexes were observed including monasters, diasters or spindle-like structures, and multiastral complexes of three or more asters. In addition, aster formation was followed by the formation of non-astral background fibers which were also birefringent and which varied in amount from preparation to preparation. Preliminary evidence suggests that these background fibers contained tubulin and associated proteins in the form of free microtubules. Once formed, asters and background fibers aggregated together to form multi-astral aggregates. The significance of astral aggregation is not clear, but one possibility is that this *in vitro* process is related to spindle migrations in living *Spisula* eggs [10, 12].

We have studied asters with video-microscopy and electron microscopy and confirmed the pre-

FIG. 5. Isolation of asters and cycling of astral tubulin. Asters formed in the presence of hexylene glycol were isolated and washed in microtubule stabilizing buffer (a). Astral rays were depolymerized by treatment with cold temperatures and GTP (b). Cold stable material was separated by centrifugation and microtubules were isolated by temperature dependent polymerization-depolymerization cycles (c). (Magnification: 108 \times).

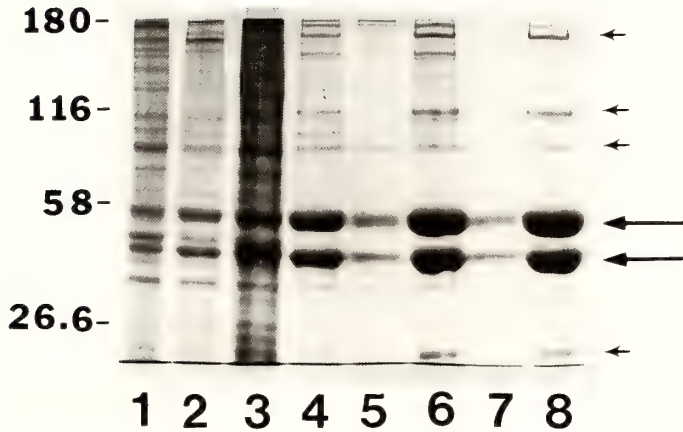


FIG. 6. Protein composition of asters and microtubule associated proteins analyzed by SDS electrophoresis. Lanes: 1) spontaneous asters, 2) hexylene glycol asters, 3) cold insoluble and 4) cold soluble astral proteins, 5) and 7) supernatants and 6) and 8) pellets of first and second cycle polymerizations respectively. Quantitative but no qualitative differences in proteins were found when hexylene glycol was used to augment aster birefringence (compare lanes 1 and 2). Several proteins (small arrows) in addition to tubulin (large arrows) coassembled during temperature dependent polymerization-depolymerization of microtubules. Numbers on left indicate approximate molecular weight in kilodaltons.

vious reports by Weisenberg [20, 24] that a) asters are composed of microtubules radiating from a central zone which contains a centriole, and b) asters form spindle-like structures and collect particles at their periphery. Using video-microscopy we have shown that each aster contained a single dense body which when investigated with electron microscopy was found to be a single centriole except in a one case where we found an aster containing two centrioles. We have presented evidence which suggests that the zone surrounding the centriole is dynamic and capable of interaction with the pericentriolar region of other asters so that when two or more asters were found in proximity, their central zones tended to fuse.

We have extended these studies by developing methods for the isolation of asters formed in cytoplasmic extracts and have begun to characterize their constitutive proteins. The protein composition of asters formed spontaneously was compared to that of asters augmented with hexylene glycol. Although some minor differences in protein composition were observed, the major effect of hexylene glycol was to increase the astral tubulin content. Electrophoretic analysis of cycled

astral tubulin revealed that a number of proteins, presumably MAPs, coassembled with microtubules. In addition, investigation of the cycled tubulin fractions with the polarization microscope revealed that although birefringent fibers were observed, no asters were present. This result suggests that the component(s) responsible for MTOC activity was separated from the fraction during the $39,000\times g$ centrifugation step which followed the initial cold depolymerization of astral microtubules.

With the use of video-microscopy we observed that particles present in the crude cytoplasmic extract much smaller than astral centers could also serve as sites from which fibers extended although such fibers were much fewer in number than those surrounding astral centers. These particles may be related to the granules from sea urchin spindles identified by Endo [27, 28] and isolated by Sakai and colleagues [29, 30] which are capable of organizing microtubules (MTOGs). These investigators have identified a granule associated 51 Kd protein which retains MTOC activity *in vitro*. In addition, antibodies raised against this protein localize to astral centers [30]. These results suggest that individual proteins may be responsible for

MTOC activity. Whether or not similar proteins exist in *Spisula* asters formed *in vitro* is not clear at this time, but since we can now isolate asters in sufficient quantities for preparative and analytical biochemistry we can begin to address such questions.

ACKNOWLEDGMENTS

This work was done with funds supplied by National Institutes of Health Grant No. GM 36550 to L. I. Rebhun. Dr. Palazzo was supported by Fellowships From National Institute of Health Grant Nos. 5T32HD07192 and 5-532-GM11502-02.

REFERENCES

- Brinkley, B. R. (1985) Microtubule organizing centers. *Ann. Rev. Cell Biol.*, **1**: 145-172.
- McIntosh, J. R. (1983) The centrosome as an organizer of the cytoskeleton. *Mod. Cell Biol.*, **2**: 115-142.
- Tucker, J. B. (1979) Spatial organization of microtubule organizing centers and microtubules. *J. Cell Biol.*, **99**: 55s-62s.
- Pickett-Heaps, J. D. (1969) The evolution of the mitotic apparatus: an attempt at comparative ultrastructural cytology in dividing plant cells. *Cytobios*, **1**: 257-280.
- Pickett-Heaps, J. D., Tippit, D. H. and Porter, K. R. (1982) Rethinking mitosis. *Cell*, **29**: 729-744.
- Inoue, S. (1981) Cell division and the mitotic spindle. *J. Cell Biol.*, **91**: 131s-147s.
- Mazia, D. (1984) Centrosomes and mitotic poles. *Exp. Cell Res.*, **153**: 1-15.
- Gotlieb, A. I., May, L. M., Subramanyan, L. and Kalnins, V. I. (1981) Distribution of microtubule organizing centers in migrating sheets of endothelial cells. *J. Cell Biol.*, **91**: 589-594.
- Koonce, M. P., Cloney, R. A. and Berns, M. W. (1984) Laser irradiation of centrosomes in newt eosinophils: Evidence for centriole role in motility. *J. Cell Biol.*, **98**: 2222-2229.
- Rebhun, L. I. (1958) Studies of early cleavage in the surf clam *Spisula solidissima*, using methylene blue and toluidine blue as vital stains. *Biol. Bull.*, **117**: 518-545.
- Allen, R. D. (1953) Fertilization and artificial activation in the egg of the surf clam *Spisula solidissima*. *Biol. Bull.*, **105**: 213-239.
- Dan, K. and Inoue, S. (1987) Studies of unequal cleavage in Molluscs II. Asymmetric nature of the two asters. *Int. J. Invertebr. Reprod. Dev.*, **11**: 335-354.
- Burke, B. and Gerace, L. (1986) A cell free system to study reassembly of the nuclear envelope at the end of mitosis. *Cell*, **44**: 639-652.
- Lohka, M. J. and Maller, J. L. (1985) Induction of nuclear envelope breakdown, chromosome condensation, and spindle formation in cell-free extracts. *J. Cell Biol.*, **101**: 518-523.
- Lohka, M. J. and Maller, J. L. (1987) Regulation of nuclear formation and breakdown in cell-free extracts of amphibian eggs. In "Molecular Regulation of Nuclear Events in Mitosis and Meiosis". Ed. by R. A. Schlegel, M. S. Halleck and P. N. Rao, Academic Press, Inc., New York, pp. 67-109.
- Newport, J. (1987) Nuclear reconstitution *in vitro*: stages of assembly around protein-free DNA. *Cell*, **48**: 205-217.
- Newport, J. and Spann, T. (1987) Disassembly of the nucleus in mitotic extracts: membrane vesicularization, lamin disassembly, and chromosome condensation are independent processes. *Cell*, **48**: 219-230.
- Suprynowicz, F. A. and Gerace, L. (1986) A fractionated cell-free system for analysis of prophase nuclear disassembly. *J. Cell Biol.*, **103**: 2073-2081.
- Benbow, R. M. and Ford, C. C. (1975) Cytoplasmic control of nuclear DNA synthesis during early development of *Xenopus laevis*: a cell-free assay. *Proc. Natl. Acad. Sci. U.S.A.*, **41**: 639-652.
- Weisenberg, R. C. and Rosenfeld, A. C. (1975) *In vitro* polymerization of microtubules into asters and spindles in homogenates of surf clam eggs. *J. Cell Biol.*, **64**: 146-158.
- Laemmli, U. K. (1970) Cleavage of structural proteins during the assembly of the head of bacteriophage T4. *Nature*, **227**: 680-685.
- Wray, W., Boulikas, T., Wray, V. P. and Hancock, R. (1981) Silver staining of proteins in polyacrylamide gels. *Anal. Biochem.*, **118**: 197-203.
- Kunkle, M., Magun, B. and Longo, F. J. (1978) Analysis of isolated sea urchin nuclei incubated in egg cytosol. *J. Exp. Zool.*, **203**: 381-390.
- Weisenberg, R. C. (1987) Assembly of sea urchin egg asters. In "Cell Reproduction". Ed. by E. R. Dirksen, D. M. Prescott and C. F. Fox., Academic Press, New York, pp. 366.
- Masui, Y. (1982) Oscillating activity of maturation promoting factor (MPF) in extracts of *Rana pipiens* eggs. *J. Exp. Zool.*, **224**: 389-399.
- Rebhun, L. I., Jemiolo, D. K., Ivy, N., Mellon, M. and Nath, J. (1975) Regulation of the *in vivo* mitotic apparatus by glycols and metabolic inhibitors. *Ann. N. Y. Acad. Sci.*, **253**: 362-377.
- Endo, S. (1979) The clusters of granular material around the centriole during mitosis. *Cell Struct. Funct.*, **4**: 71-74.
- Endo, S. (1980) Further observations of the clusters

- of granular material around the centriole in the sea urchin egg: Changes in distribution during mitosis. *Dev. Growth Differ.*, **25**: 307-314.
- 29 Toriyama, M., Endo, S. and Sakai, H. (1984) Aster formation in vitro is nucleated by granules isolated from the mitotic apparatus. *Cell Struct. Funct.*, **9**: 213-224.
- 30 Toriyama, M., Ohta, K., Endo, S. and Sakai, H. (1988) 51 Kd protein, a component of microtubule-organizing granules in the mitotic apparatus involved in aster formation in vitro. *Cell Motil. Cytosk.*, **9**: 117-128.

Mitotic Apparatus-Associated 51-kD Protein in Mitosis of Sea Urchin Eggs

KUNIHIRO OHTA, MASARU TORIYAMA, SACHIKO ENDO
and HIKOICHI SAKAI

*Department of Biophysics and Biochemistry, Faculty of Science,
University of Tokyo, Tokyo 113, Japan*

ABSTRACT—The centrosome of the sea urchin egg at metaphase consists of the centrioles and clusters of granular material with an average diameter of 90 nm which we call microtubule-organizing granules (MTOGs). MTOGs isolated from the isolated mitotic apparatus initiated astral microtubules in the presence of exogenous tubulin with the plus end distal to the center. Phosphocellulose column chromatography enabled the fractionation of a protein fraction from solubilized MTOGs which was capable of self-assembling into granules and initiating astral microtubules with plus end also distal to the center. A 51-kD protein with an isoelectric point of 9.8 was a major component of the granules. Lysine was the most prominent amino acid residue of the 51-kD protein. Polyclonal antibodies against the 51-kD protein stained the center of asters reconstructed *in vitro*. The antibody almost totally inhibited the aster forming ability of MTOGs. The antibody stained centrosomal regions, the proximal end of astral microtubules and half spindles. Immunofluorescence patterns of the mitotic apparatus stained with monoclonal antibody against the 51-kD protein were almost the same as those stained with polyclonal antibody. Microinjection of the monoclonal antibody into sea urchin eggs revealed that the antibody totally inhibited the formation of the mitotic apparatus when injected before prometaphase. We suggest that the 51-kD protein is a major component of the centrosome and plays a role in the initiation of astral and spindle microtubules at mitosis of the sea urchin egg.

INTRODUCTION

Tubulin self-assembles into microtubules with the aid of microtubule-associated proteins under physiological medium conditions *in vitro*. Nucleation of assembly and elongation of polymers are well known processes in microtubule reconstitution. However, the *in vitro* properties of microtubule assembly do not necessarily apply to microtubule dynamics in live cells, in which most of the microtubules are thought to be site-initiated from the so-called microtubule-organizing center (MTOC) [1], a ubiquitous structure that spatially organizes microtubules in cells [2, 3].

In mitotic cells, the centrosome that consists of pericentriolar materials and a pair of centrioles initiates astral and spindle microtubules. Formation of aster- and spindle-like structures in a homogenate of surf clam egg was described by

Weisenberg and Rosenfeld [4] who suggested that the granular material surrounding the centriole in the aster may be an MTOC. Furthermore, isolated centrosomes or mitotic centers radially nucleated microtubules [5-7]. The structures responsible for the initiation of astral microtubules are not the centrioles but the pericentriolar material, and the concept that pericentriolar material is of primary importance to this structural organization was brought forth by Gould and Borisy [8] who demonstrated that microtubule assembly is nucleated from isolated pericentriolar material. This nucleating ability was shown to be cell cycle- or mitotic cycle-dependent [9, 10]. Actual involvement of the pericentriolar material, not the centrioles, for spindle organization in live cells was then shown by Berns *et al.* [11, 12] in irradiation experiments of the centrosome with a laser microbeam.

The pericentriolar material in cultured cells was called the pericentriolar cloud as an amorphous assembly [13]. In contrast, the pericentriolar

material in sea urchin eggs was shown to consist of clusters of granular material [14] that surrounded the centrioles, which later came to be called microtubule-organizing granules (MTOGs) [15]. Extensive observations using electron microscopy showed that the clusters of granular material play a role in nucleating and organizing microtubules with marked changes in shape during mitosis [16–18]. This brief review describes recent studies on the 51-kD protein that is responsible for the aster-forming activity of MTOGs in the sea urchin egg.

ASSEMBLY OF MICROTUBULE-ORGANIZING GRANULES AT THE POLES

Prophase of the first division cycle of the sea urchin egg is characterized by the beginning of assembly of electron dense granules on the both sides of the nucleus [16]. The average diameter of the granules is estimated to be 90 nm. The gran-

ules gradually form clusters surrounding the centrioles. Microtubules seem to be nucleated by the granules to form asters, because they are focused on the clusters of such granules (Fig. 1a, arrow). At the very beginning of the aster formation at prophase, microtubules are observed to be connected to small clusters of granules. MTOGs accumulate around the poles from prometaphase through metaphase and accompany the growth of astral microtubules. Shortly after the breakdown of the nuclear envelope, no microtubules are observed in the nuclear region. However, the clusters of MTOGs which face the nucleus rapidly initiate spindle microtubules. The spindle microtubules are not curved but straight at the beginning of the formation of the spindle, therefore crossing each other around the equator (Fig. 1b). This is followed by a bending of the microtubules to the form of the spindle, probably due to the formation of crossbridges among the microtubules.

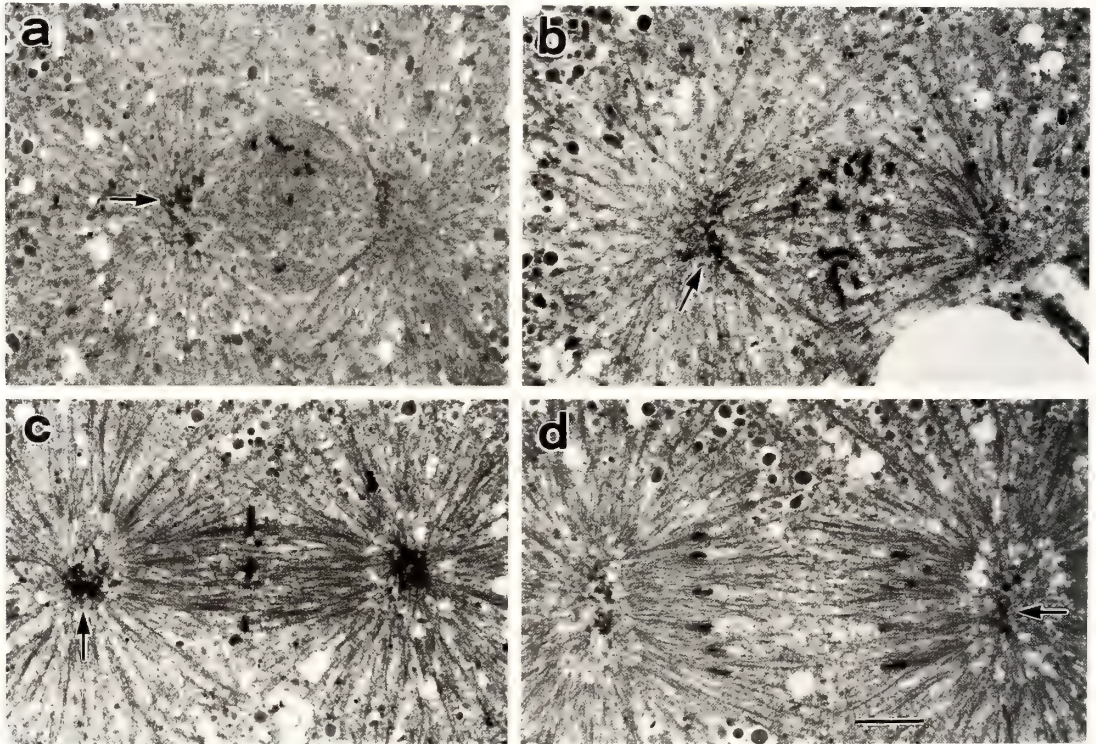


FIG. 1. Electron microscopic image of mitotic *Hemicentrotus* eggs [16]. Eggs at mitosis were fixed with glutaraldehyde and processed for sections of $0.3 \mu\text{m}$ in thickness. a: Beginning of prometaphase, b: Prometaphase, c: Metaphase, d: Anaphase. Arrows show clusters of granular material (MTOGs). Bar: $5 \mu\text{m}$. (By permission of Dev. Growth Differ.)

Metaphase is characterized by a maximum accumulation of MTOGs at both poles in the form of a spherical mass surrounding the centrioles (Fig. 1c). When the astral microtubules grow further at anaphase, the shape of the clusters of MTOGs changes from a sphere to a disc perpendicular to the axis of the spindle, forming flat centrosomes (Fig. 1d). Furthermore, the cluster adheres to the daughter nuclei at the end of mitosis [17].

That the clusters of MTOG initiate microtubules was confirmed by experiments in which MTOGs are dispersed by the action of hexyleneglycol [19]. When sea urchin eggs at prometaphase are treated with sea water containing 5% hexyleneglycol, assembled clusters of MTOGs at the pole disperse to form a centrosphere-like region. MTOGs are redistributed at the periphery of the 'pseudo-centrosphere' and each of the dispersed granules initiates microtubules so that an unusually large number of microtubules are formed, each focusing on the dispersed granules. Similar dispersion of

MTOGs and growth of unusually large numbers of microtubules are observed when hexyleneglycol treatment is carried out at metaphase [19].

INITIATION OF MICROTUBULES BY FRAGMENTS OF THE CENTROSOME *IN VITRO*

The first step in the investigation of the mechanism of microtubule initiation *in vivo* is the isolation of the centrosome and analysis of the ability to initiate microtubules. Isolated mitotic apparatuses favor a large supply of functional centrosomes. When the mitotic apparatuses isolated by the DMSO-glycerol method are chilled and gently homogenized, the isolated centrospheres initiate microtubules to form asters [20]. Further homogenization of the isolated mitotic apparatuses causes fragmentation of the centrosomes, resulting in the formation of numerous small asters when combined with tubulin. An indirect immunofluorescence image of the aster is shown in

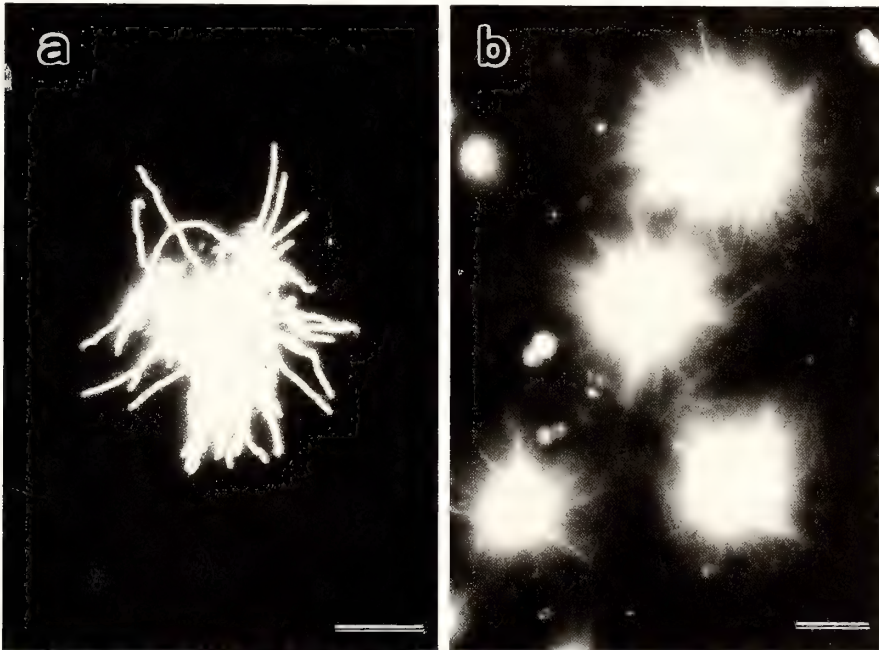


FIG. 2. Asters reconstructed from MTOGs and tubulin. a: Immunofluorescence image. MTOGs from isolated mitotic apparatuses were incubated with tubulin for 10 min and fixed with formaldehyde, followed by processing for immunofluorescence staining using anti-tubulin antibody and fluorescein-labeled goat anti-rabbit IgG. Bar: 5 μm . b: Dark-field microscopic image. Solubilized mitotic apparatuses were column chromatographed on phosphocellulose to obtain a 0.5 M KCl eluate, which was dialyzed against a solution of low ionic strength. Granules formed were incubated with tubulin for 10 min. Bar: 10 μm .

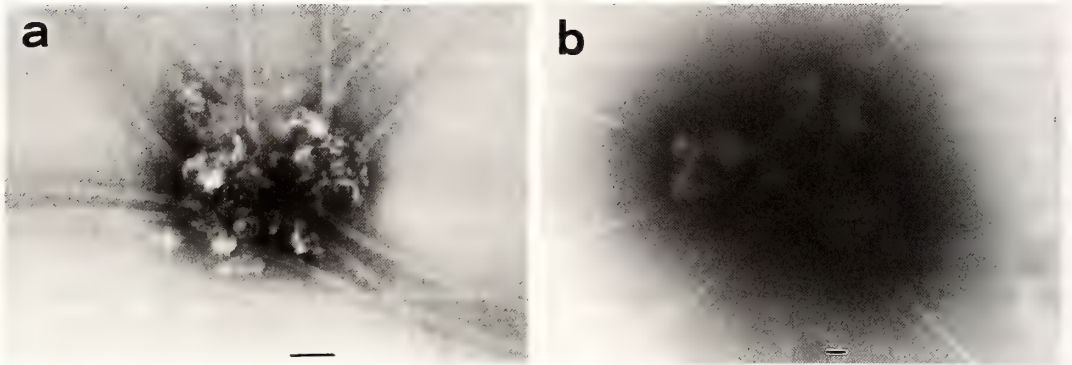


FIG. 3. Electron microscopic image of astral centers [21]. a: MTOGs from isolated mitotic apparatuses. b: MTOGs reconstructed from 0.5 M KCl eluate on a phosphocellulose column, to which a KCl extract of whole metaphase eggs were applied. Bar: 100 nm. (By permission of Alan R. Liss, Inc., New York)

Figure 2a where the microtubules form an astral configuration. Measurement of the growth rate of the microtubules reveals that the plus end is distal to the center [21]. Electron microscopy discloses that the center of these asters consists of small clusters of 10 to 20 granules with diameters ranging from 40 to 140 nm (Fig. 3a), and usually initiating ~100 microtubules. Therefore, it is conceivable that these asters are formed from fragmented centrosomes. We also noted that these granular aggregates appear to be derived only from centrosomes as judged by electron microscopy of the isolated mitotic apparatuses.

When a homogenized suspension of the isolated mitotic apparatuses is treated with trypsin, asters are no longer formed [20]. In contrast, treatment with RNase A does not destroy aster forming activity, but it is susceptible to heat treatment, i.e., incubation at 60°C for 2 min almost totally destroys it.

SOLUBILIZATION OF PROTEINS AND RECONSTITUTION OF MTOGs

Aster forming activity in the isolated mitotic apparatuses can be solubilized in a solution of higher ionic strength in the presence of glycerol. Dialysis of a 0.5 M KCl extract of mitotic apparatuses causes formation of granular aggregates from which small asters are formed when incubated with tubulin [20]. Phosphocellulose column chromatography of the solubilized MTOG fraction

enabled separation of a protein component that is capable of being reconstituted into granules by dialysis against a solution of low ionic strength and capable of initiating astral microtubules when incubated with tubulin. Starting from a KCl extract of whole fertilized eggs, a protein fraction is obtained by phosphocellulose column chromatography, and forms granules by dialysis that are capable of nucleating astral microtubules. Polarity of the astral microtubules is always such that the plus end is distal to the astral center. The same holds true with astral microtubules initiated from MTOGs freshly prepared from isolated MAs [21]. Furthermore, when microtubules are first initiated from MTOGs in a short time and then biotin-labeled tubulin is added (Fig. 4), one can measure the growth rate of microtubules more easily with the plus end distal to the center.

Electron microscopy shows that such granular aggregates resemble MTOGs with average diameters ranging from 100 to 300 nm (Fig. 3b). Small clusters that consist of 10 to 20 unit granules usually initiate more than 50 microtubules. Because quick dilution of a 0.5 M KCl extract of mitotic apparatuses leaves most of the proteins solubilized in solution, it is conceivable that the granules reconstitute in such a way that the constituent proteins self-assemble in an order dependent upon a gradual decrease in ionic strength.

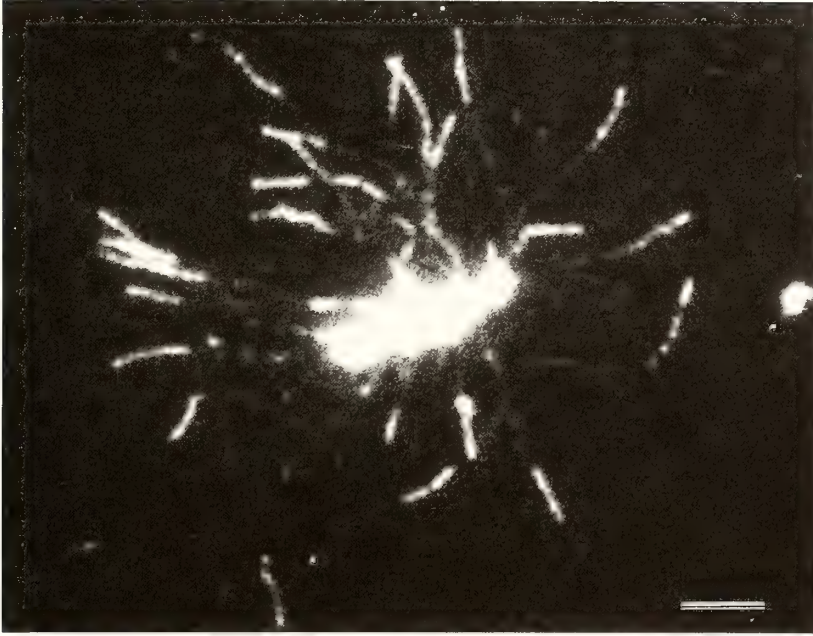


FIG. 4. Growth of astral microtubule from MTOGs. Isolated mitotic apparatuses were dispersed in the cold to fragment the centrosome. The granular suspension was briefly incubated with porcine brain tubulin, followed by further incubation with biotin-labeled tubulin. Microtubules reconstituted from labeled tubulin were visualized by rhodamine-labeled avidin. Bar: 5 μ m.

THE 51-kD PROTEIN, A MAJOR PROTEIN COMPONENT OF MTOGS

Starting from solubilized mitotic apparatuses, a fraction eluted by 0.5 M KCl from the phosphocellulose column contained a 51-kD protein as a major component and several minor components. The 51-kD protein is a basic protein with a pI of 9.8. Amino acid analysis of the 51-kD protein showed that the most prominent amino acid residue is lysine [21].

Polyclonal antibodies raised in rabbits against the 51-kD protein and affinity purified, stained only the center of asters reconstructed from tubulin and MTOGs prepared from the isolated mitotic apparatuses [21]. They also stained MTOGs reconstructed from the 0.5 M KCl eluate, from which astral microtubules were initiated. These results indicate that the 51-kD protein is a major component of MTOGs in the mitotic apparatus.

Antibody blocking experiments are necessary in order to further assess the role of the 51-kD protein in the initiation of astral microtubules from

MTOGs. The MTOG fraction freshly prepared from the isolated mitotic apparatuses was preincubated with polyclonal antibody in the presence of 50% glycerol which stabilizes aster forming activity, followed by the addition of tubulin. Compared with the control, in which incubation was carried out in the absence of the antibody, the formation of asters was substantially suppressed (up to 60%) by the antibody [20]. However, inhibition did not reach 100% in the presence of glycerol. Glycerol at a concentration of 50% exhibited an inhibitory effect of antibody binding to antigens [22]. When MTOG fraction prepared from freshly isolated MAs was first incubated with the antibody in the absence of glycerol followed by tubulin addition, aster formation was almost totally suppressed (up to 95%). Therefore, it seems safe to conclude that the 51-kD protein is involved in the initiation of microtubules from the MTOGs *in vitro*.

INHIBITION BY Ca^{2+} OF ASTER FORMING ABILITY OF MTOGS

The effect of Ca^{2+} on aster forming ability was examined using MTOGs prepared from isolated mitotic apparatus. The MTOGs were preincubated in a solution containing various concentrations of Ca^{2+} , followed by the addition of a tubulin solution containing EGTA to measure microtubule initiation. Figure 5 shows that concentrations of Ca^{2+} as low as $1 \mu\text{M}$ begin to block the aster forming ability of MTOGs. The time course of inhibition showed that a preincubation of ~ 5 min with $20 \mu\text{M}$ Ca^{2+} was critical to the MTOGs loss of ability. An incubation of the Ca^{2+} -treated MTOGs with an excess amount of EGTA prior to the addition of tubulin caused the MTOGs to restore the ability to initiate microtubules.

Ca^{2+} has been believed to play a role in mitosis since microtubules of sea urchin eggs have been shown to be highly susceptible to a micromolar level of free Ca ions [23]. Localization of calmodulin in the mitotic spindle [24, 25] and sensitivity of

number of asters

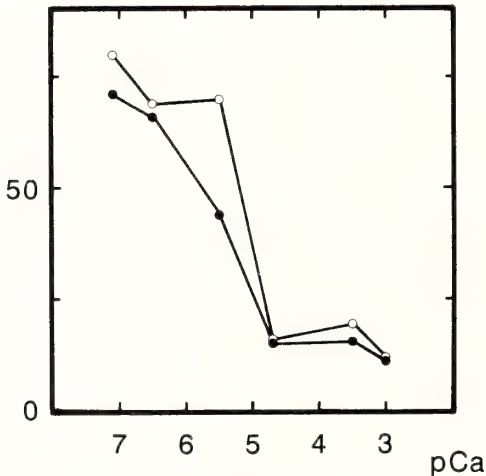


FIG. 5. Inhibition of the aster forming ability of MTOGs by Ca. MTOGs from isolated mitotic apparatuses were first incubated with various concentrations of Ca ions using Ca buffer for 20 min at 0°C . A tubulin solution containing excess EGTA was then mixed with the MTOG suspension and incubated for another 30 min at 35°C , followed by a count of the number of asters. Two series of independent experiments are shown.

tubulin to Ca^{2+} /calmodulin [26, 27] suggest that Ca^{2+} /calmodulin may be involved in depolymerization of the spindle microtubules after anaphase, provided that free Ca ions are released from the Ca^{2+} -sequestering vesicles [28] in the spindle. Although Ca ions seem to be necessary after anaphase [29], they must be sequestered at the beginning of the formation of the mitotic apparatus to support the microtubule nucleating function of the centrosome.

INTRACELLULAR LOCALIZATION OF THE 51-kD PROTEIN DURING MITOSIS DETECTED BY IMMUNOCYTOCHEMISTRY USING MONOCLONAL AND POLYCLONAL ANTIBODIES AGAINST THE 51-kD PROTEIN

Monoclonal antibodies against the 0.5 M KCl eluate on a phosphocellulose column were categorized into 4 groups [30]. Of these, HP1 and HP2 clones secreted IgG which cross-reacts with a protein of M. W. 51,000 in the eggs of the sea urchins, *Hemicentrotus pulcherrimus* and *Pseudocentrotus depressus*. On the other hand, the eggs of *Clypeaster japonicus*, *Anthocardia crassispina* and *Temnoplurus hardwicki* were shown to contain a protein of a slightly higher molecular weight (52,000) that specifically reacts with both of the antibodies.

Indirect immunofluorescence stainings of sectioned sea urchin eggs using monoclonal and polyclonal antibodies produced the same results [22, 30]. The 51-kD protein is localized in the centrosomal regions of the MAs from prophase through anaphase. At prometaphase, the astral microtubules are mostly attached to the centrosome so that the centrosphere cannot be observed at this stage. When the egg reaches metaphase, the proximal ends of the astral microtubules appear to detach from the centrosome, thereby forming the centrosphere region. The detached microtubules appear to be capped by granules at their proximal ends. It is possible that these granules are stained by the antibody. Figure 6a shows the staining of a metaphase egg with anti-tubulin antibody and Figure 6b, that of an early anaphase egg with anti-51-kD protein antibody showing immunofluorescence in the centrosomal

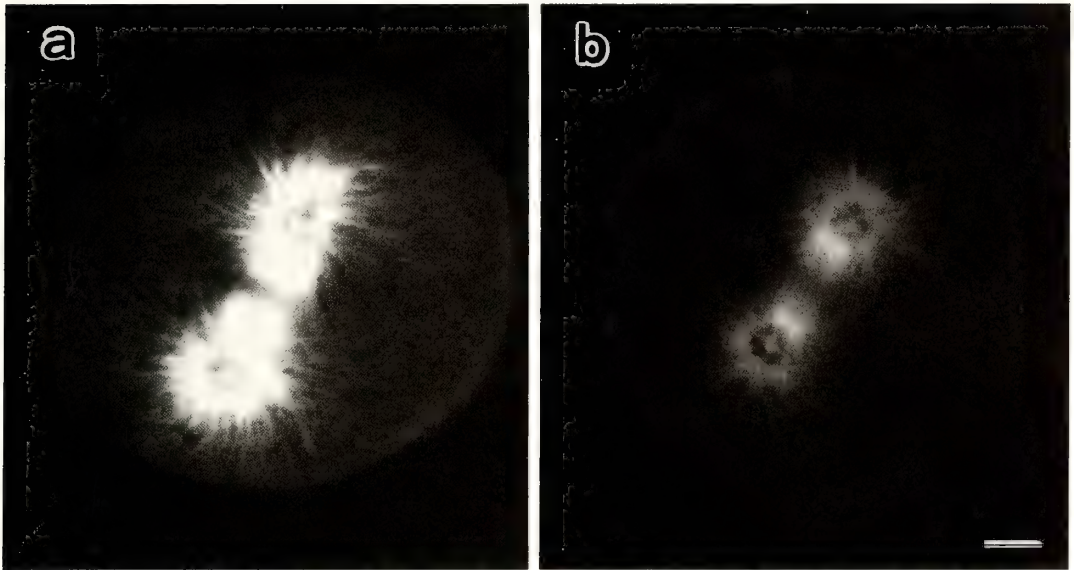


FIG. 6. Localization of the 51-kD protein in the mitotic apparatus. Paraffin-embedded sections were incubated with anti-tubulin antibody (a) and anti-51-kD protein antibody (b), followed by staining with fluorescein-labeled secondary antibody. a: Metaphase, b: Early anaphase. Bar: 10 μ m.

region, the proximal region of the astral microtubules and the half spindles. The spindle is always stained with antibody. Although the function of the 51-kD protein in the spindle is unknown at present, it may have a role in stabilizing spindle microtubules which lie through the spindle matrix. A preliminary experiment showed that the 51-kD protein causes microtubules to line up side by side (unpublished data). It is necessary to determine the sites where the 51-kD protein is situated in the spindle with a spatial reference to spindle microtubules.

If the 51-kD protein is actually involved in the initiation of microtubules *in vivo*, we can test another experimental design in such a way that unfertilized sea urchin eggs are artificially activated to determine whether the centers of the cytasters can be stained with antibody against the 51-kD protein. This was the case for *Hemicentrotus* eggs parthenogenetically activated by taxol [30].

MICROINJECTION OF MONOCLONAL ANTIBODY TO THE 51-KD PROTEIN INTO MITOTIC EGGS

The polyclonal antibody was highly monospecific to the 51-kD protein [21]. However, the antibody concentration was not high enough for some other purposes, i.e., experiments such as microinjection for analyses of the effect of antibodies need higher concentrations of IgG. Although one of the monoclonal antibodies, HP1 antibody, does not inhibit the aster forming activity of the MTOGs prepared from the isolated MAs, it suppressed the formation of the MA when injected before prophase [22]. Therefore, cleavage did not occur (Fig. 7). Differential interference microscopy enables us to observe the astral rays in the *Clypeaster* egg. When the antibody was injected into the egg at prometaphase, however, growth of the astral microtubules was not inhibited, but the formation of the spindle was suppressed. The spindle formed is extremely short and in the form of a sphere (Fig. 8). This inhibition of spindle formation brings about total suppression of the karyokinesis. Sometimes, an incomplete fur-

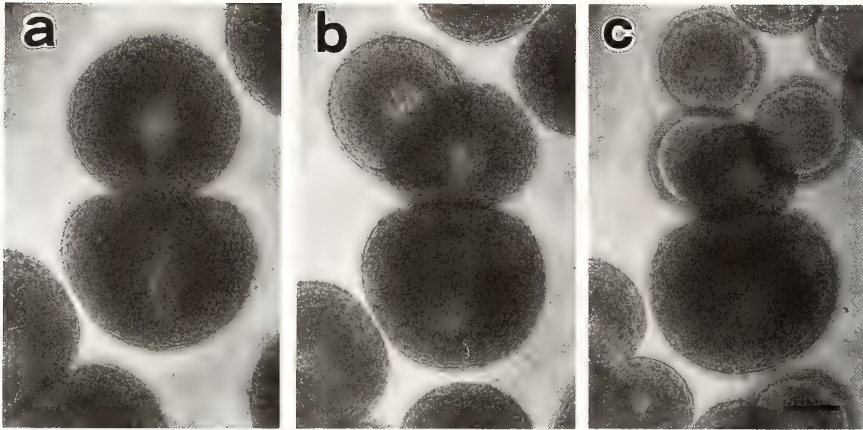


FIG. 7. Phase-contrast micrographs of a *Pseudocentrotus* egg injected with anti-51-kD protein antibody into one of the blastomeres after the first cleavage. Monoclonal antibody (6.1 pl) was injected into the lower blastomere. Note that the upper blastomere continued to divide. a: 120 min after fertilization, b: 148 min, c: 195 min. Bar: 50 μ m.

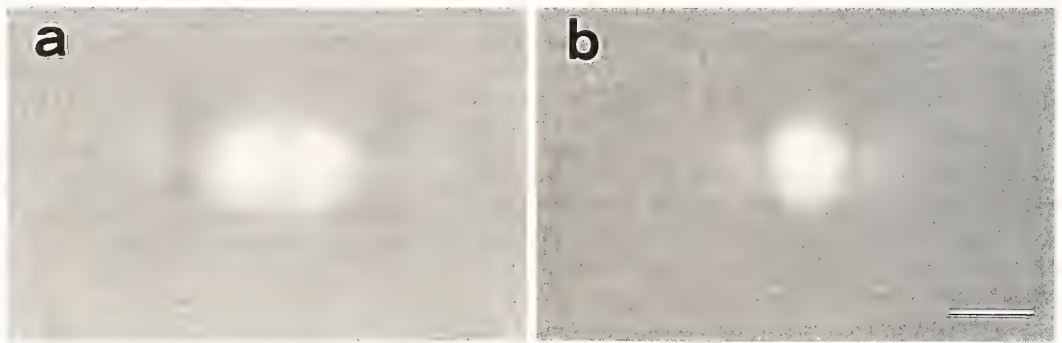


FIG. 8. Polarized-light micrographs of a *Clypeaster* egg injected with anti-51-kD protein antibody at prometaphase [22]. a: Control, b: Injected. After injection, the growth of asters did not appear disturbed, but the spindle formation did. Bar: 10 μ m. (By permission of Springer-Verlag New York Inc.)

row will be formed, but the furrow does not proceed further, and eventually regresses.

The apparent contradiction which arises because the antibody that does not inhibit aster formation *in vitro* totally suppresses the formation of the MA can be elucidated if we assume that the antibody blocks the assembly of MTOGs into the centrosome. It is important to make further observations of the changes in the distribution of the MTOGs by injection of the antibody using the techniques of immunocytochemistry.

In conclusion, the 51-kD protein was shown to be a component of MTOGs in the centrosome. This protein seems to be responsible for the initiation of microtubules in the formation of asters and

the spindle when it is incorporated into MTOGs possibly associated with other constituents as yet unidentified.

This series of work using the isolated mitotic apparatuses [19–22] is possible today, thanks to Professors Daniel Mazia and Katsuma Dan and their pioneering work on mitotic apparatus 36 years ago [31]. This paper is dedicated to Professor Emeritus Katsuma Dan.

ACKNOWLEDGMENT

This work is supported by a Grant-in-Aid for scientific research from the Ministry of Education, Science and Culture of Japan (60065005).

REFERENCES

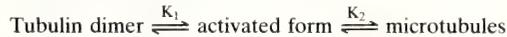
- 1 Pickett-Heaps, J. D. (1969) *Cytobios*, **1**: 257-280.
- 2 Pickett-Heaps, J. D. and Tippit, D. H. (1978) *Cell*, **14**: 455-467.
- 3 Brinkley, B. R. (1985) *Ann. Rev. Cell Biol.*, **1**: 145-172.
- 4 Weisenberg, R. C. and Rosenfeld, A. C. (1975) *J. Cell Biol.*, **64**: 146-158.
- 5 McGill, M. and Brinkley, B. R. (1975) *J. Cell Biol.*, **67**: 189-199.
- 6 Snyder, J. A. and McIntosh, J. R. (1975) *J. Cell Biol.*, **67**: 744-760.
- 7 Pepper, D. A. and Brinkley, B. R. (1979) *J. Cell Biol.*, **82**: 585-591.
- 8 Gould, R. R. and Borisy, G. G. (1977) *J. Cell Biol.*, **73**: 601-615.
- 9 Telzer, B. R. and Rosenbaum, J. L. (1979) *J. Cell Biol.*, **81**: 484-497.
- 10 Kuriyama, R. and Borisy, G. G. (1981) *J. Cell Biol.*, **91**: 822-826.
- 11 Berns, M. W., Rattner, J. B., Brenner, S. and Meredith, S. (1977) *J. Cell Biol.*, **72**: 351-367.
- 12 Berns, M. W. and Richardson, S. M. (1977) *J. Cell Biol.*, **75**: 977-982.
- 13 Robbins, E., Jentsch, G. and Micali, A. (1968) *J. Cell Biol.*, **36**: 329-339.
- 14 Endo, S. (1979) *Cell Struct. Funct.*, **4**: 71-74.
- 15 Endo, S., Toriyama, M. and Sakai, H. (1985) In "Cell Motility: Mechanism and Regulation". Ed. by H. Ishikawa, S. Hatano and H. Sato, Univ. Tokyo Press, Tokyo, pp. 403-414.
- 16 Endo, S. (1980) *Dev. Growth Differ.*, **22**: 509-516.
- 17 Paweletz, N., Mazia, D. and Finze, E.M. (1984) *Exp. Cell Res.*, **152**: 47-65.
- 18 Mazia, D. (1984) *Exp. Cell Res.*, **153**: 1-15.
- 19 Endo, S., Toriyama, M. and Sakai, H. (1983) *Dev. Growth Differ.*, **25**: 307-314.
- 20 Toriyama, M., Endo, S. and Sakai, H. (1984) *Cell Struct. Funct.*, **9**: 213-224.
- 21 Toriyama, M., Ohta, K., Endo, S. and Sakai, H. (1988) *Cell Motil. Cytoskel.*, **9**: 117-128.
- 22 Ohta, K., Toriyama, M., Hamaguchi, Y., Maekawa, S., Endo, S. and Sakai, H. (1988) *Protoplasma*, in press.
- 23 Nishida, E. and Kumagai, H. (1980) *J. Biochem. (Tokyo)*, **87**: 143-151.
- 24 Hamaguchi, Y. and Iwasa, F. (1980) *Biomed. Res.*, **1**: 502-509.
- 25 Zavortink, M., Welsh, M. J. and McIntosh, J. R. (1983) *Exp. Cell Res.*, **149**: 375-385.
- 26 Nishida, E., Kumagai, H., Ohtsuki, I. and Sakai, H. (1979) *J. Biochem. (Tokyo)*, **85**: 1257-1266.
- 27 Kumagai, H. and Nishida, E. (1980) *Biomed. Res.*, **1**: 223-229.
- 28 Silver, R. B., Cole, R. D. and Cande, W. Z. (1980) *Cell*, **19**: 505-516.
- 29 Hepler, P. K. and Callahan, D. A. (1987) *J. Cell Biol.*, **105**: 2137-2143.
- 30 Ohta, K., Toriyama, M., Endo, S. and Sakai, H. (1988) *Cell Motil. Cytoskel.*, in press.
- 31 Mazia, D. and Dan, K. (1952) *Proc. Natl. Acad. Sci. USA*, **38**: 826-838.

The Thermodynamics of Molecular Association in the Mitotic Spindle with or without Heavy Water (D₂O)¹

HIDEMI SATO and JOSEPH BRYAN²

Sugashima Marine Biological Laboratory, Nagoya University, Sugashima, Toba, Mie 517, Japan, and ²Department of Cell Biology, Baylor College of Medicine, One Baylor Plaza, Houston, Texas 77030, U.S.A.

ABSTRACT—Addition of heavy water (D₂O) or temperature shift to optimum range enhances spindle birefringence (BR) and volume in living, dividing cells. Knowing the form BR of spindle reflects the amount of oriented microtubules, we analyzed the association-dissociation reaction of the spindle with thermodynamic approach. Meiotic metaphase spindle of the mature oocyte of *Pisaster ochraceus* was chosen as experimental material. From BR of equilibrated metaphase spindle of living oocyte, and of spindles isolated in 12% hexylene glycol, pH 6.3, at various temperatures, we calculated thermodynamic parameters for the association reaction: In H₂O (19 parts of 0.53 M NaCl plus 1 part of 0.53 M KCl), $\Delta H=58.9$ kcal/mole, $\Delta S=205.9$ eu, and $\Delta F=-1.1$ kcal/mole. In 45% D₂O, $\Delta H=29.55$ kcal/mole, $\Delta S=106.3$ eu, and $\Delta F=-0.9$ kcal/mole. This reaction is observed between 3 and 13°C, at which temperature the spindle BR is maximum in both H₂O and D₂O. Kinetic data are obtained by BR measurements of rapidly isolated spindles after a varying interval following a temperature shift or the addition of D₂O. Both association and dissociation processes appear to follow first-order kinetics. Activation energy (E_{act}) for association reaction in H₂O is 41 kcal/mole; for D₂O, 39 kcal/mole; and for dissociation reaction on removing D₂O, 15 kcal/mole. For each condition these data are consistent with the hypothesis that the spindle BR measures the reversible polymerization of tubulin molecules into linearly aggregated polymers (microtubules) in a first-order reaction, even though associated or regulatory proteins are required *in vitro* tubulin polymerization. However, the difference of both ΔH and ΔS in H₂O and D₂O, and high but similar E_{act} in the association reaction suggest the spindle reaction in fact to be a two step reaction such as:



where, K_1 is primarily governed by D₂O and K_2 by temperature. The low E_{act} in the back reaction of the D₂O case suggests that the microtubules *in vivo* may first break down into random oligomers and then dissociate into tubulin dimers.

INTRODUCTION

Heavy water (D₂O) and temperature could independently enhance the form birefringence (BR) and the volume of the living mitotic spindle [1, 2]. Response of the mitotic spindle to these two physical parameters was completely reversible and could be repeated several times within certain limits [1-3]. Thermodynamics of the deuterated and non-deuterated spindle *in vivo* [4, 5] indicated that significant differences existed between the

calculated thermodynamic parameters of the deuterated and non-deuterated system [2-9]. However, few attempts were made to analyze the kinetics of the increase in volume and BR effected by temperature and D₂O. It partly could be due to the technical difficulties associated with measuring small retardation changes in the rapidly evolving system, even though some successful reports finally appeared to be real [2, 10, 11]. Another reason was based on the doubt of form BR yielded by mitotic spindle and reservation was expressed as spindle BR was not due to the oriented molecules or microtubules but yielded by the complex of gelled micells. However, Sato *et al.* [12] clearly demonstrated the applicability of Wiener's equa-

Accepted April 9, 1988

¹ This paper is dedicated to Emeritus Professor Katsuma Dan.

tion to the spindle form BR, and proved that the spindle BR reflected exactly oriented amount of microtubules within spindle using the isolated mitotic spindle from mature oocyte of starfish, *Pisaster ochraceus*. This could be an ideal material to circumvent the problem of temperature or D₂O effect on mitotic spindle and to obtain information of comparative value on another system [4, 5, 7].

The mature oocytes of *Pisaster ochraceus*, whose spindle persisted in meiosis I for one hour at 13°C, provided a plentiful source of material, thus were used as experimental material. These mitotic spindles in meiosis I have a strong BR, physically stable, and exhibited relatively slow response to a variety of physical parameters or chemical reagents [2, 12, 13].

Using this material, we attempted to further refine the comparison between the deuterated and the non-deuterated systems and to begin a kinetic analysis of the molecular association of the mitotic spindle.

We shall report our results obtained as followings.

MATERIAL AND METHODS

Mature oocytes of the starfish, *Pisaster ochraceus*, which were naturally arrested in meiosis I, were used in the present study due to the physical stability of the mitotic spindle. The methods of obtaining and preparing oocytes for spindle isolation and the procedures used for isolation have been described previously [12, 13].

The BR measurements used for the thermodynamic analysis were made on spindles isolated from oocytes which were washed twice in isotonic 0.53 M NaCl–27 mM KCl (“19:1” solution) and allowed to equilibrate in this solution at the given temperature for at least 5–10 min. The kinetic studies indicated that this was sufficient time to reach a new equilibrium. The kinetic measurements of BR were done by rapidly transferring oocytes into the “19:1” solution to the desired experimental condition (transfer time should be less than 10 sec), then subsequently transferring one volume of oocytes to 10 volumes of isolation medium at various time intervals. The isolation medium consisted of 12% hexylene glycol and 10

mM potassium phosphate, pH 6.3 at 20°C [14]. Oocytes were spun in a hand centrifuge, the pellet collected and resuspended in 5 volumes of ice cold 12% hexylene glycol, pH 6.3 solution. The oocyte suspension was vortexed to lyse the oocytes and to free the spindles from the oocytes. Spindles were concentrated by centrifugation at 1,000×g for 5 min. These concentrated preparations were stored on ice and retardation (BR) measurements were carried out within 6 hr. In particular case, corrections were made following the decay curve of BR of stored spindles [13]. This procedure served well to quickly stabilize the spindle at any given point in the reaction and preserve it for subsequent retardation measurement.

Optical methods

A modified Leitz Ortholux-polarizing microscope was used as the basic optical stand. A Zeiss Brace-Koehler type, rotating mica compensator with a retardance of 22.3 nm was used as the measuring device. Rectified strain free optics [15] were used to permit precise retardation measurements of spindles with great accuracy. A Leitz illuminator with HBO 200 WL 2 (Osram, the Netherlands) combined with Baird Atomic interference filter and heat absorbing filters to provide an intense mercury green light (546 nm) was used as routine illumination. Polaroid HN-22 non-laminated polarizing sheet film mounted on a light tight plastic support was used as the polarizer. A built-in Leitz polarizing film was used as the analyzer mounted behind the objectives. Extinction factor ($I_{\text{parallel}}/I_{\text{cross}}$) was maintained in an order of 10⁴. All photographic records were made on either Agfa KB-17 or Kodak Plus-X films exposed with the Leitz Orthomat automatic camera. Koehler illumination was maintained throughout all retardation measurements.

Calculation of BR

Since the retardation to be measured was much less than the wave length of illuminating light used for the measurements, the following formula was used (see, [1, 12]).

$$\frac{\sin \Delta X_{\text{spec}}}{2} \cdot \sin 2\theta = -\frac{\sin \Delta X_{\text{comp}}}{2} \cdot \sin 2\theta'$$

where, θ = azimuth angle between the vibrating plane of the incident polarized light,

θ' = measured compensation angle of the specimen by Brace-Koehler compensator,

Δx_{spec} = retardation of specimen (or BR),

Δx_{comp} = known retardance of compensator (22.3 nm in our case).

The standard deviations were calculated from the average triplicate measurements of 10 to 15 randomly sampled spindles at each point using the formula,

$$S = \left[\frac{\sum (X - \bar{X})^2}{N} \right]^{1/2}$$

where x = one value in a series of measurements,

\bar{x} = arithmetic mean of the series,

N = number of values in the series.

Electron microscopy

Metaphase spindles isolated were immediately cooled to 4°C, washed twice, centrifuged at 1,250 $\times g$ for 5 min, then fixed for 30 min in 3% glutaraldehyde–12% hexylene glycol at pH 6.3. The preparations were washed twice with cold isolation medium, and postfixed for 30 min in 1% OsO₄–hexylene glycol solution at pH 6.3, then again washed twice with isolation medium. Dehydration started with 30% ethanol–12% hexylene glycol, then 50% ethanol–12% HG. Hexylene glycol was omitted from the graded concentrations of ethanol above 70%. After dehydration, spindles were placed in propylene oxide, followed with a mixture of equal proportion of propylene oxide and Epon 812 (Shell Chem. Corp., CA). Embedding was accomplished in hard Epon rather than Araldite to provide good preservation of fine structure without shrinkage or compression upon sectioning. Sections were made with a Porter-Blum Ultramicrotome MK-II and examined with Phillips model 200 electron microscope.

RESULTS

Effect of D₂O

The effect of D₂O on the spindle BR and volume was shown in Figure 1. Spindle BR and

volume apparently increased as seen in b1 and b2 of Figure 1. As shown in Figure 2, isolated spindle from the mature oocyte was mainly occupied by oriented microtubules and little else. Thus, D₂O effect was studied by transferring mature oocytes in "19:1"–H₂O solution to various concentration of "19:1"–D₂O solution. All concentrations studied were done at 13°C, and equilibrium times were from 5 to 10 min. Examples of these experiments are shown in Figure 3, and from the retardation measurements, we noticed the spindle retardation became maximum at 45% D₂O–"19:1" solution, and similar results were obtained in 45% D₂O–artificial sea water. If the oocytes in D₂O were transferred to "19:1"–H₂O, spindles returned to normal size and BR. This effect was reversible and can be repeated several times.

The spindles isolated at various concentrations showed a pronounced volume increase, which can be roughly estimated by considering the spindle to be a rotating ellipsoid whose long axis was equal to the pole-to-pole distance and whose short axis was equal to the width at the mid point between the poles, the equator. Using this model, we compared spindles with and without D₂O and confirmed an average 8 fold increase in volume in 45% D₂O spindle. This indicated definite increase of spindle microtubules and number altered from 4,200 microtubules in control spindle (Fig. 2) to 10,000 microtubules in 45% D₂O spindles within 5 min. Pole-to-pole distance also increased suggesting elongation of each microtubules also occurred within D₂O, not disturbing the initial distribution pattern of microtubules within the spindle. Figure 4 showed a cross section of D₂O spindle with a same magnification with Figure 2b. Although not commonly noted, rapid alteration of pH from 6.3 to 6.8 during spindle isolation produced microtubule dissociation and lateral split of microtubules. Likewise, in the early stages of dehydration, change in pH or osmolarity could easily induce "C-tubules" within isolated spindles even during or after glutaraldehyde or OsO₄ fixation [2, 12].

Thermodynamic analysis

The retardation of spindles isolated from oocytes which have been fully equilibrated in "19:1"–H₂O or –D₂O, at various temperature

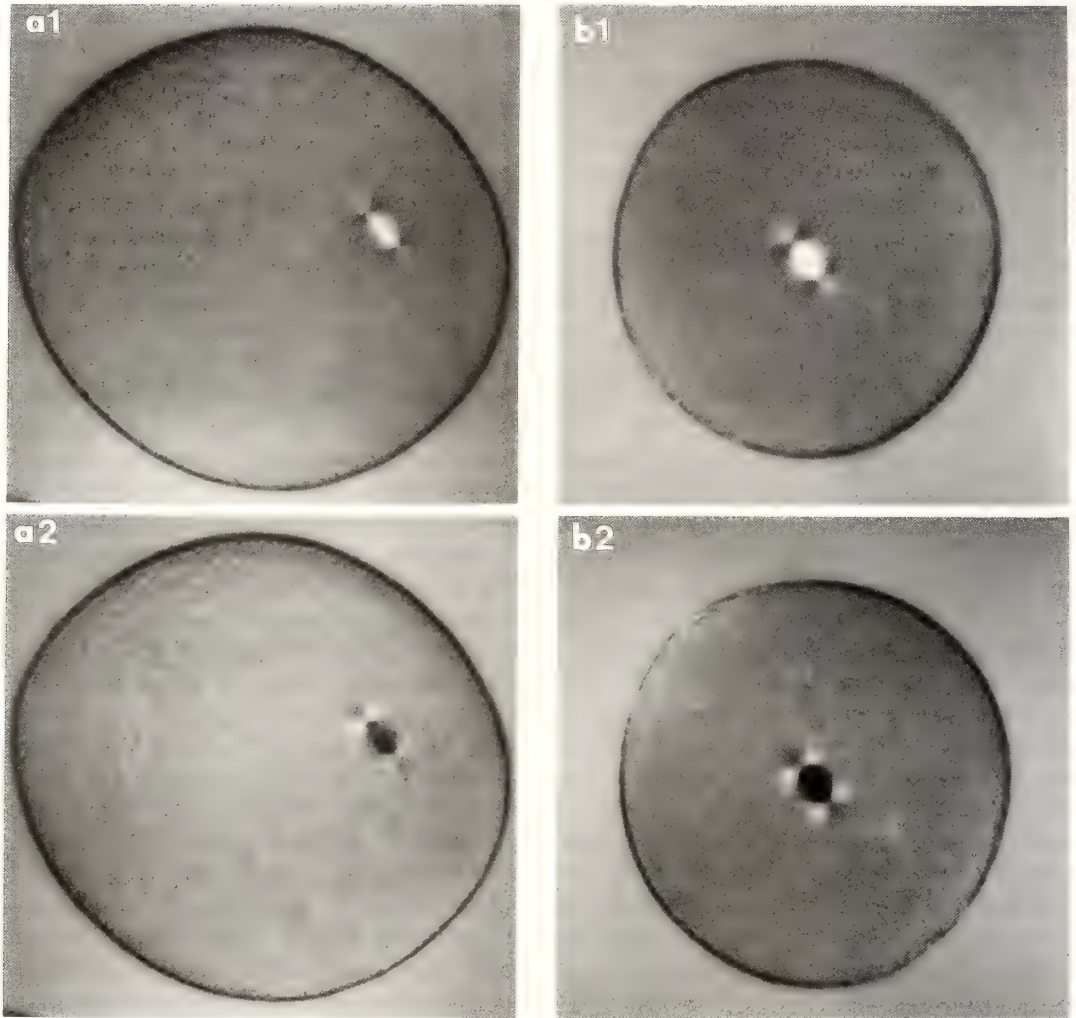
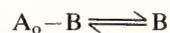


FIG. 1. Meiosis I spindles in mature oocytes of *Pisaster ochraceus*. a1 and a2; A control spindle with different contrast. b1 and b2; A spindle treated with 45% D₂O is shown in different contrast. Polarization microscopy. Scale; 1 div. = 10 μ m.

has been studied. Concentration of D₂O was 45% because it was the best concentration in term of BR, spindle volume and reversibility (Fig. 3). Plots of retardation as absolute temperature ($^{\circ}$ K) for both series were given in Figure 5. As expected, the "19:1"-45% D₂O values were always greater than those in "19:1"-H₂O. Both plots have a maximum at 13 $^{\circ}$ C, a temperature very close to the normal water temperature in which the mature organism was found. Further analysis of the association reactions was carried out using the

equilibrium model of Morales and Inoué [16]. This model assumed that the spindle could be described by an equilibrium between oriented, birefringent material (B) and a pool of unoriented material ($A_0 - B$), where A_0 was the value of retardation measured with the polarization microscope. The equilibrium was then written as:



and a generalized equilibrium constant calculated from:

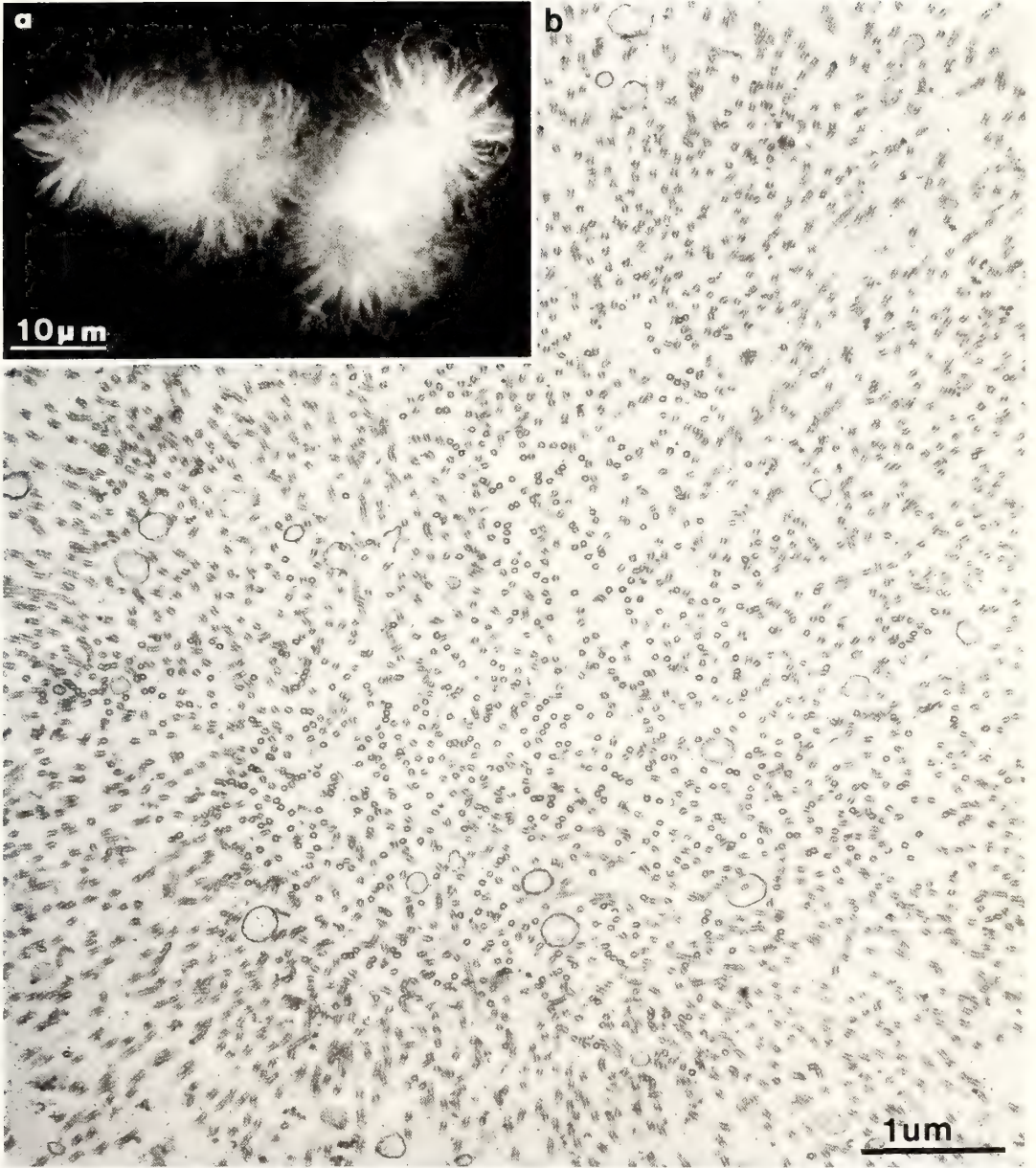


FIG. 2. a; Tubulin immunofluorescence of isolated spindles from mature oocytes of *P. ochraceus*. b; Cross section of an isolated meiosis I spindle is mainly occupied by microtubules and little else. Some of the vesicles in the photograph are degenerated mitochondria resulting from the isolation procedure (cited from Sato *et al.* [8], pp. 556 as a control electron micrograph).

$$K = B/A_0 - B$$

Using this approach, thermodynamic parameters were calculated. Morales and Inoué [16] suggested

A_0 was taken as the maximum value of retardation which B approached to asymptote as the temperature increased [4, 5]. In the present work, A_0 has been used as the selected parameter to give the

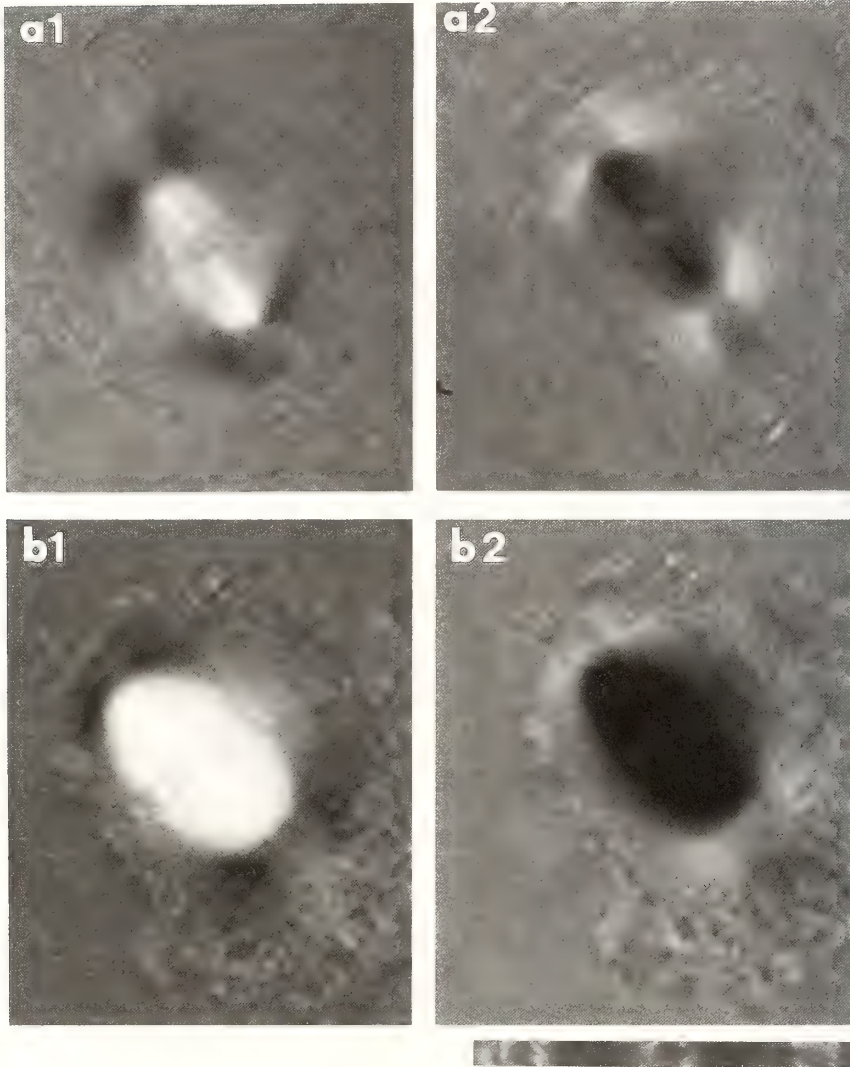


FIG. 3. a1 and a2; An equilibrated spindle at 18°C. b1 and b2; A spindle treated with 45% D₂O and equilibrated at 13°C. Polarization microscopy. Scale; 1 div. = 10 μ m.

best fit to van't Hoff's plot, using the assumption that ΔH was independent of temperature in a very limited temperature range. Two methods of estimating A_0 gave similar results.

With this approach, the Arrhenius plots [$\log B/(A_0 - B)$ versus $1/\text{temperature}$, where B was spindle retardation and A_0 , the asymptote B approaches] were made and the results were given in Figure 6. Two different A_0 values, 4.4 for H₂O-spindle and 6.3 for D₂O-spindle, were given to establish the van't Hoff's relationship. The

results obtained by Carolan *et al.* [4, 5] for *Pectinaria* and those of Inoué [17] for *Chaetopterus* are also shown for comparison. The calculated parameters for both H₂O- and D₂O-spindles indicated that the association reactions of spindles were endothermal with a large positive ΔH and have a large positive entropy change. The calculated parameters were consistently lower for D₂O equilibrated spindles than for the H₂O equilibrated spindles. In addition, the parameter A_0 for the D₂O samples was significantly larger, suggesting

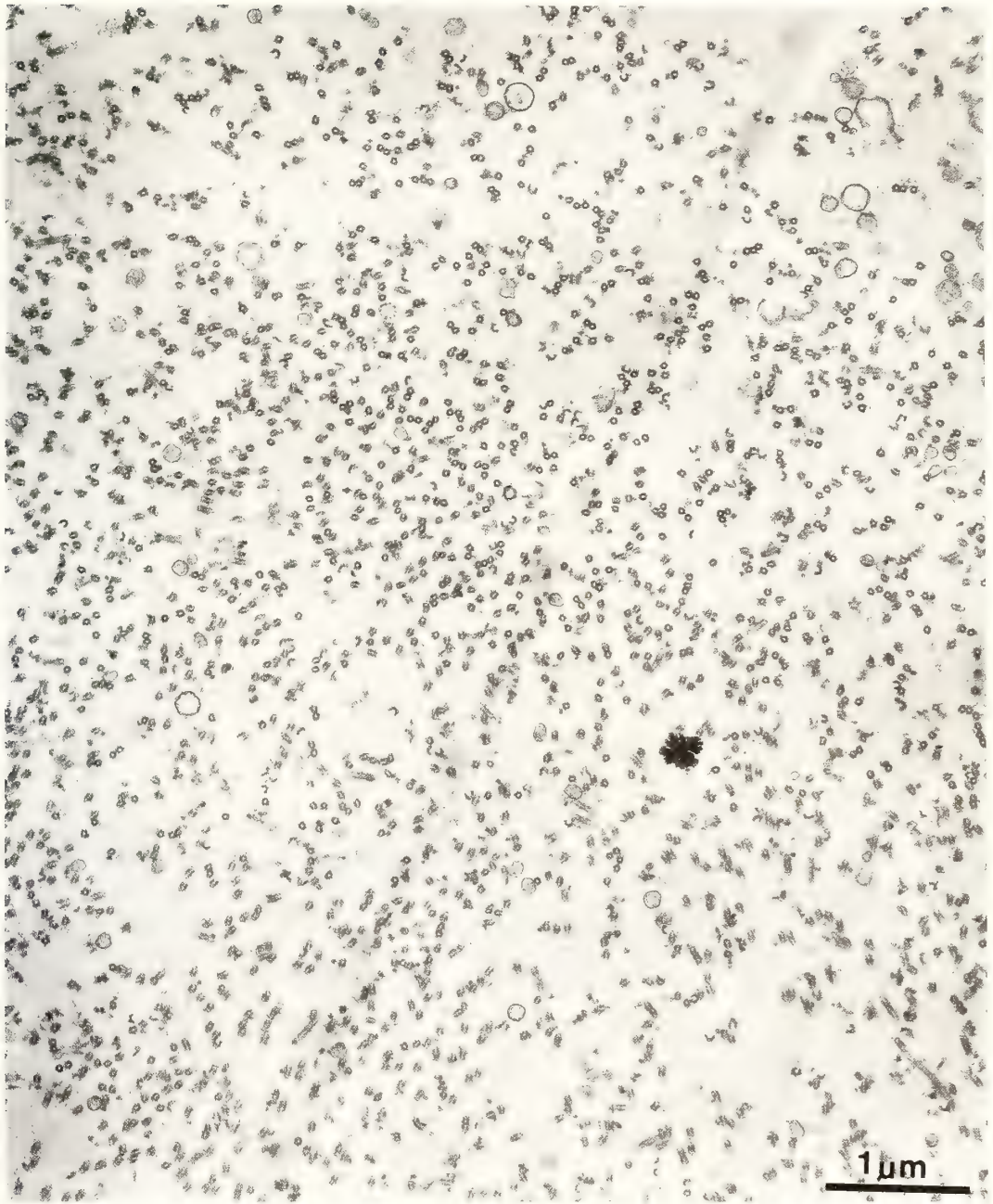


FIG. 4. Electron micrograph of a cross section of an isolated spindle treated with 45% D_2O . Spindle width is increased but the density of microtubules per μm^2 remains constant. Note the significant increase of C-tubules which are caused by the rapid association reaction.

an increase in pool size. A similar analysis for the spindle association reaction has hardly been applicable for temperature above $13^\circ C$ (see, Fig. 3),

and we believe this discrepancy could be caused by adding new parameters made spindle association reaction more complicate way and disturb the

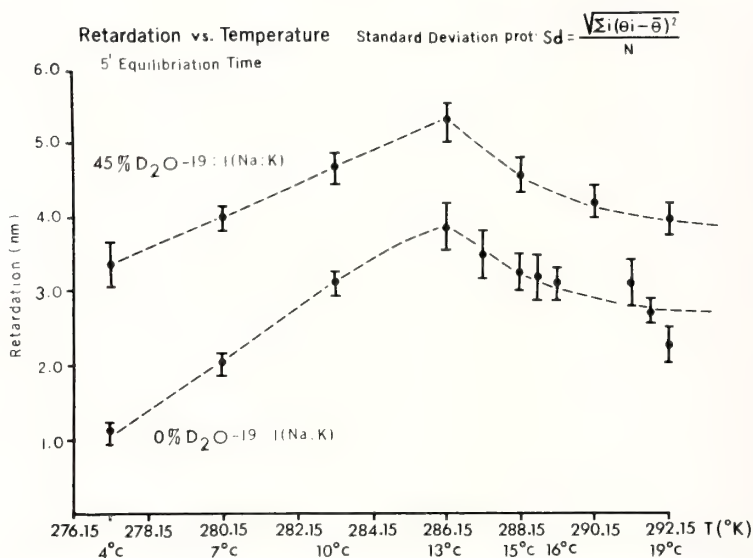


FIG. 5. Retardation measurements of isolated spindles equilibrated at various temperatures with or without D₂O.

Spindle Association Reaction

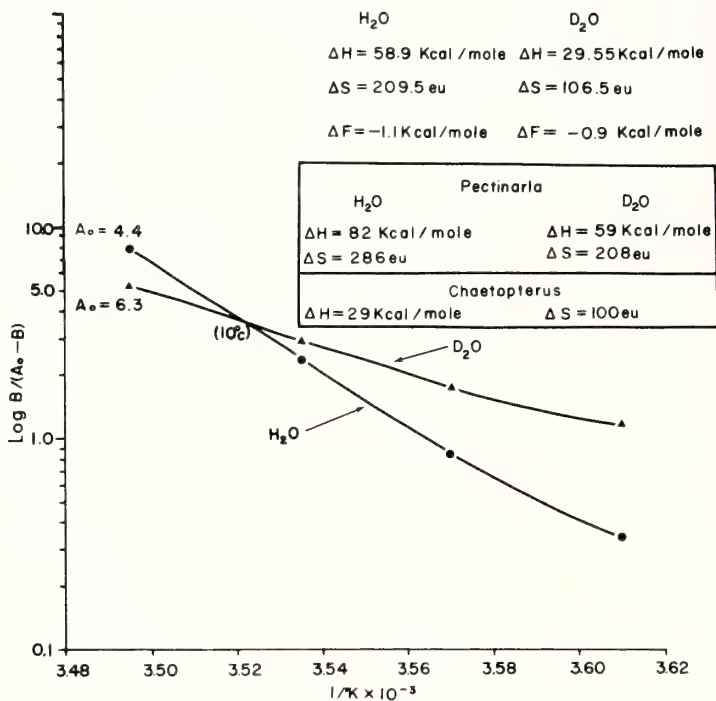


FIG. 6. van't Hoff plot of spindle association reaction.

thermodynamic analysis.

However, same tendencies were confirmed on the D₂O depending spindle association in dividing sea urchin eggs [7, 9, 18], and even *in vitro* tubulin polymerization with D₂O [6].

Kinetic measurements

A. Association reactions

The time course of the association of tubulin molecules into the spindle microtubules was carried out in order to investigate the kinetics of these reactions. Temperature shift was used as the parameter, where oocytes were equilibrated for 10 min in "19:1"-H₂O at 4°C, then transferred to the desired higher temperature.

For D₂O measurements, oocytes were equilibrated for 10 min at a given temperature in "19:1"-H₂O, then transferred to "19:1"-45% D₂O at the same temperature. Spindles were isolated at various times using the method outlined previously.

Figure 7 showed photographic illustrations of isolated spindles of both methods in one sequence. Oocytes were equilibrated at 4°C in "19:1"-H₂O and transferred to "19:1"-H₂O at 13°C, then after 5 min finally transferred to "19:1"-D₂O (45%) at

13°C. The increase in BR and spindle volume was quite apparent. The retardation values ranged from 1.2 nm at 4°C to 5.3 to 5.5 nm at 13°C in "19:1"-45% D₂O. Using ellipsoidal assumption described before, the volume change for the same condition was calculated as 70 to 80 fold.

The time course of the association reactions in "19:1"-H₂O using the temperature shift method was illustrated in Figure 8. These data have been analyzed in terms of the equilibrium model in the following manner. Even for complicated reactions, the return to equilibrium after a small perturbation usually followed first order kinetics, therefore it was assumed that the rate of growth of spindle (microtubule polymerization) was proportional to the amount of unpolymerized molecules, the tubulin molecules.

$$d/dt (\text{polymer}) \sim (\text{monomer})$$

In the symbols previously defined, this can be written as:

$$\frac{dB}{dt} = k \cdot (A_0 - B)$$

which could be integrated and rearranged to give:

$$\log_{10} (A_0 - B) = -k't + \text{constant}$$

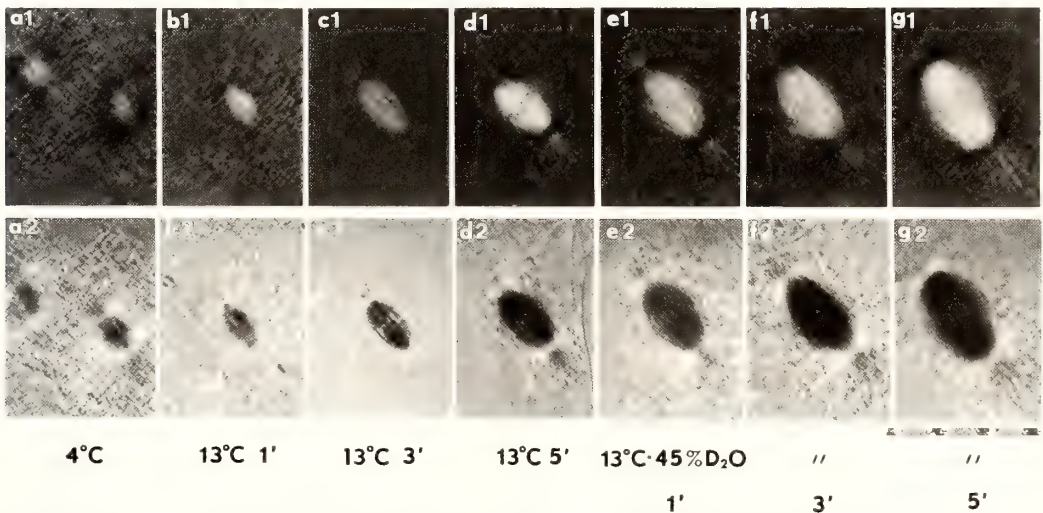


FIG. 7. Isolated spindles at various steps in temperature depending or D₂O depending reactions. a1 and a2; An equilibrated spindle at 4°C. When oocytes are transferred to 13°C, spindle volume and BR rapidly increased (b1, b2; c1, c2) and reached to maximum in 5 min (d1, d2). When equilibrated spindles at 13°C are transferred to 45% D₂O at 13°C, again spindle volume and BR go up and reach maximum values in 5 min. Polarization microscopy. Scale; 1 div. = 10 μm

Association Reaction of the Mitotic Spindle
Parameter ξ Temperature

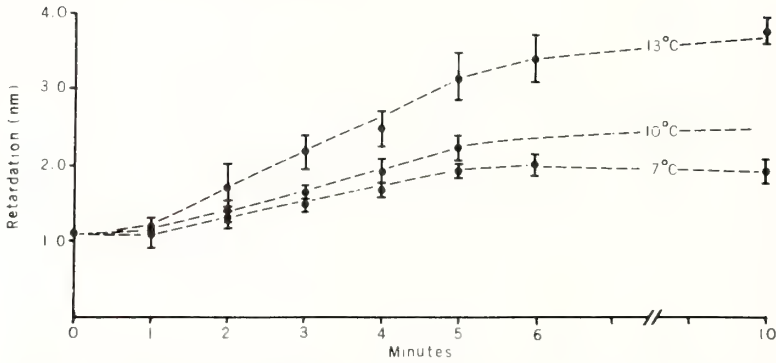


FIG. 8. Temperature depending association reaction of spindle in "19:1"-H₂O.

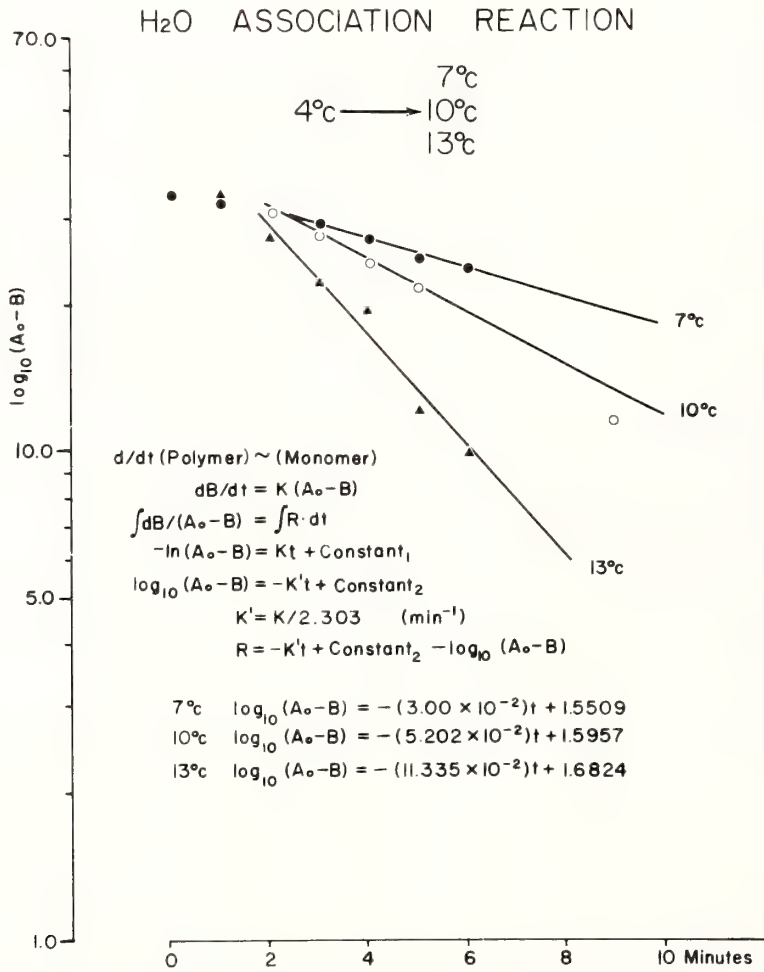


FIG. 9. Rate of reactions of temperature depending association of mitotic spindles.

$$k' = k/2.303$$

The data were fitted to this equation using a least squares procedure; measurements from 2 to 6 min were used for this procedure. The results of this procedure was shown in Figure 9. The rate constants (k) from these measurements were:

$$7^{\circ}\text{C}\cdot k = 11.5 \times 10^{-4} \cdot \text{sec}^{-1}$$

$$10^{\circ}\text{C}\cdot k = 20.0 \times 10^{-4} \cdot \text{sec}^{-1}$$

$$13^{\circ}\text{C}\cdot k = 43.5 \times 10^{-4} \cdot \text{sec}^{-1}$$

Using these constants, the apparent activation energy or temperature characteristic for the H₂O association was determined from the Arrhenius plot, as shown in Figure 10. The calculated values from the relation:

$$E_{\text{act}} = -R \frac{d \log k}{d(1/T)}$$

then, $E_{\text{act}} = 41.3 \text{ kcal/mole}$.

A similar analysis has been carried out for the D₂O transfer method. The time course of these reactions is shown in Figure 11. The first order rate constants obtained from these data were:

$$7^{\circ}\text{C}\cdot k = 11.3 \times 10^{-4} \cdot \text{sec}^{-1}$$

$$10^{\circ}\text{C}\cdot k = 23.8 \times 10^{-4} \cdot \text{sec}^{-1}$$

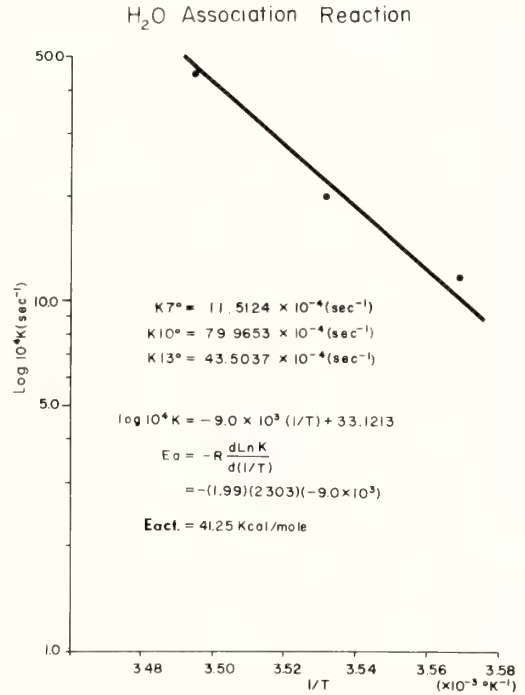


FIG. 10. Arrhenius plot and the kinetic data obtained from the temperature depending association reactions.

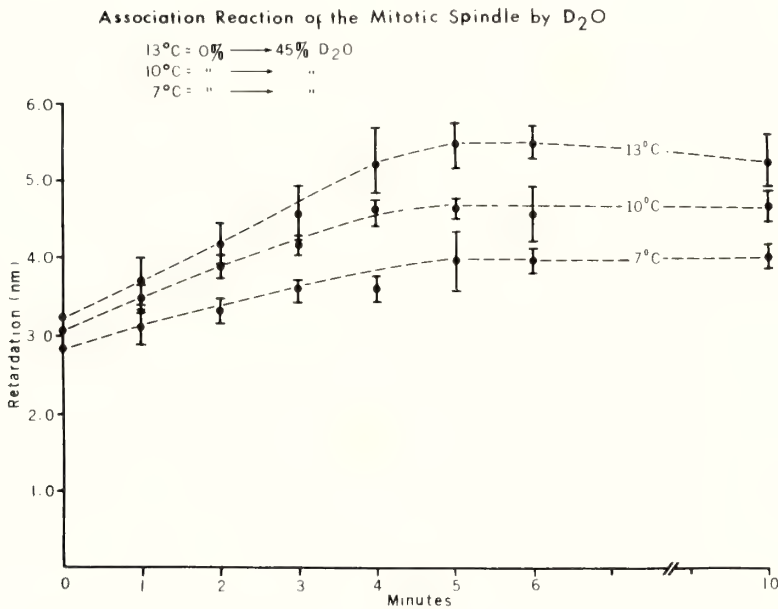


Fig. 11. Association reactions depending on "19:1"-45% D₂O of mitotic spindles at given temperatures.

$$13^{\circ}\text{C}\cdot k = 48.3 \times 10^{-4} \cdot \text{sec}^{-1}$$

An Arrhenius plot from these values showed in Figure 12 gives an apparent activation energy of 39.3 kcal/mole.

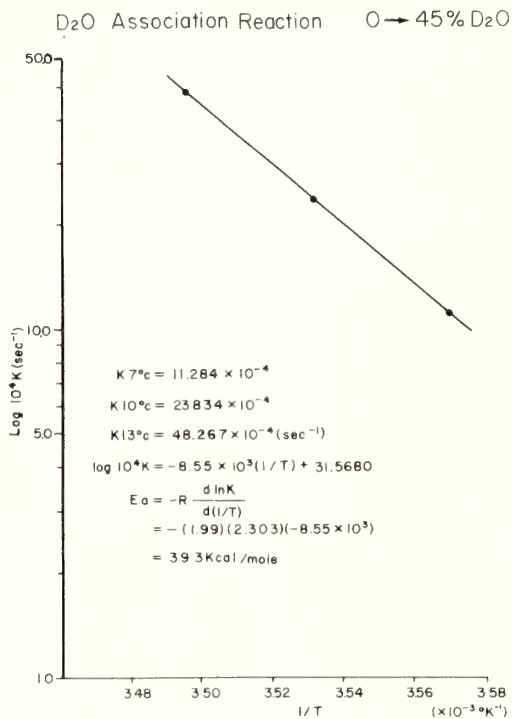


FIG. 12. Arrhenius plot and the kinetic data obtained from the D₂O depending association reaction.

B. Dissociation reaction

The time course of the dissociation reaction of the spindle has been studied using the reverse of the procedures described for initiating association. Oocytes in "19:1"-45% D₂O at a given temperature were transferred to "19:1-H₂O" at the same temperature. The results for this type of experiment were shown in Figure 13.

These data were treated as follows; it was assumed that the initial rate of dissociation was proportional to the initial amount of oriented material (B), then:

$$-\frac{dB}{dt} \sim B$$

or,

$$-\frac{dB}{dt} = k'_{-1} [B]$$

which can be integrated to give:

$$\log_{10} B = -k'_{-1} t + \text{constant}$$

and,

$$k'_{-1} = \frac{K_{-1}}{2.303}$$

The calculated first order rate constants from this procedure at each temperature were:

$$13^{\circ}\text{C}\cdot k = 24.2 \times 10^{-4} \cdot \text{sec}^{-1}$$

$$10^{\circ}\text{C}\cdot k = 18.3 \times 10^{-4} \cdot \text{sec}^{-1}$$

$$7^{\circ}\text{C}\cdot k = 13.9 \times 10^{-4} \cdot \text{sec}^{-1}$$

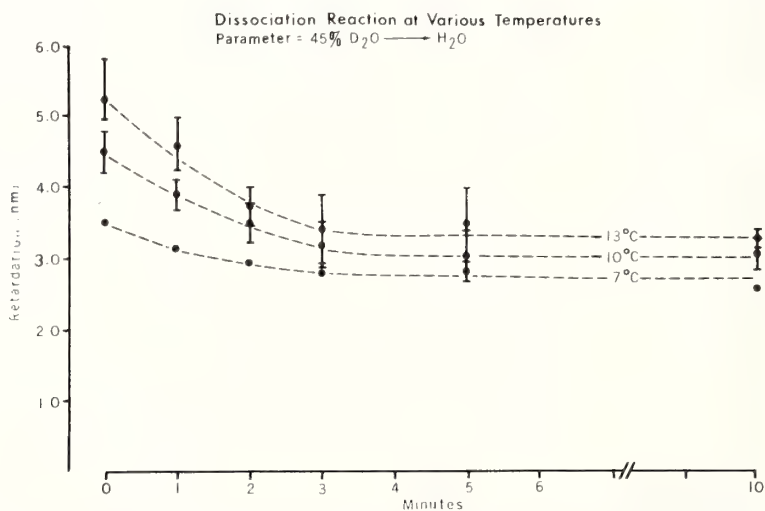


FIG. 13. Dissociation reaction of mitotic spindle subtracting 45% D₂O at given temperatures.

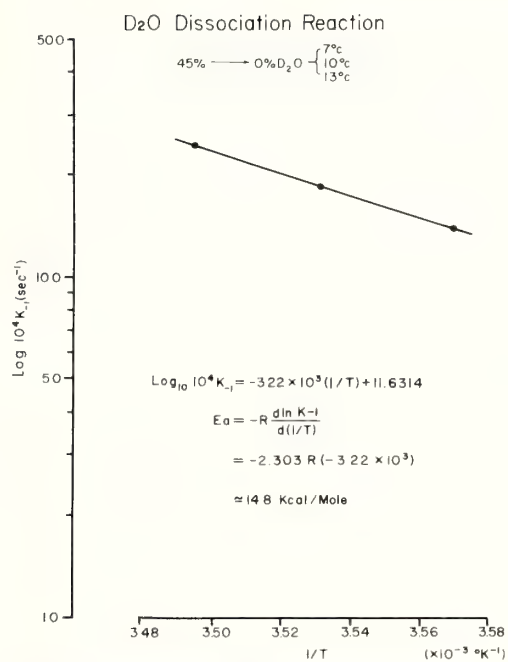


Fig. 14. Arrhenius plot and kinetic data obtained from D₂O depending dissociation reactions.

These values gave the Arrhenius plot illustrated in Figure 14. The apparent energy of activation calculated from this plot was $E_{\text{act}} = 14.8$ kcal/mole.

When temperature jump method was used from higher to lower temperatures, somewhat aberrant results were observed. The spindles lost oriented material much more rapidly at the lower temperatures. The first order decay constants for this process were:

$$\begin{aligned} 4^\circ\text{C} \cdot k &= 68 \times 10^{-4} \cdot \text{sec}^{-1} \\ 7^\circ\text{C} \cdot k &= 30.6 \times 10^{-4} \cdot \text{sec}^{-1} \\ 10^\circ\text{C} \cdot k &= 23.1 \times 10^{-4} \cdot \text{sec}^{-1} \end{aligned}$$

The use of an Arrhenius plot and these data led to an apparent negative activation energy.

DISCUSSION

Isotope effect of heavy water, especially D₂O, was one of the attractive subjects and many reports were published concerning the biochemistry and the physiology of living and dividing cells [19–23]. However, heavy water depending enhancement of spindle BR and volume was founded by Inoué and

Sato [1] using the metaphase arrested meiosis I spindle of mature oocyte of *Pectinaria gouldi* and spindle in dividing egg of sea urchin, *Lytechinus variegatus*. The increase of volume and BR of spindle depended on the concentration of D₂O, but the maximum increases were obtained by applying 45% D₂O during the metaphase or onset of anaphase. This maximum concentration to achieve the maximum effect of D₂O was common for metaphase spindles in eukaryotes even in tissue culture cells [3, 8]. The D₂O depending association reaction was rapid, and a new state of equilibrium being reached within 90 sec in developing Japanese sea urchin eggs [9, 18], about 2 min in *Pectinaria* oocyte [4, 5], and required 5 min in mature oocytes of present material. The D₂O effect is completely reversible and can be repeated many times on the same spindle.

H₂O¹⁸ has no effect whereas HDO and HDO¹⁸ have a half effect of D₂O. pD, which can be expressed as p²H and;

$$p^2H = pH_{\text{reading}} + \delta pH$$

where, $\delta pH = 0.3314 \cdot n + 0.0776 \cdot n^2$ and n is the mole fraction of D₂O, has also no significant effect for the spindle association reaction. In many respects, D₂O effect is quite similar to the elevating temperature within the physiological range. However, the spindle became overstabilized or freezed when higher concentration of D₂O was applied.

From the electron micrographs shown in Figures 2 and 4, we confirmed the coefficient of BR, $(n_e - n_o)$, was 5×10^{-4} , and the average measured density of microtubules in both types of spindle was constant and $108/\mu\text{m}^2$. However, microtubule number increased from normal 4,200 to 10,000 in D₂O, and also microtubules were elongated [8].

When observed in the living and dividing sea urchin eggs under the polarized light, the spindle displayed its dynamic nature and appeared as a very labile structure. To explain this dynamic state, Inoué [15, 17, 24] and Inoué and Sato [1] postulated a "dynamic equilibrium model" for the molecular nature of spindle. In this model, the birefringent spindle fibers were composed of oriented microtubules which were in equilibrium with a pool of polymerizable tubulin dimer. To

translate this model into terms which could be quantitated, we presumed that there were only two states of the spindle molecules (tubulin), polymerized and unpolymerized. Oriented materials, microtubules, could be measured directly as retardation (B). The maximum retardation was taken as a measure of the total molecules available for spindle assembly (A_o). The amount of un-oriented material at any given temperature was the difference between the two. This type of model gives a linear relationship on a van't Hoff plot of; $\log B/(A_o - B)$ vs $1/T$. From this, it was deduced that the orientation (tubulin polymerization) was an endothermal process with a large positive heat of activation (ΔH) and a very large increase in entropy (ΔS). It was subsequently proposed that the high heat and entropy increase could be explained on the basis of hydrophobic or apolar interactions. Higher temperatures were believed to dissociate bound water from the protein subunit and therefore permitted them to interact more strongly.

Several problems arose in the actual application of the two state model to interpret present results. These primarily concerned with the measurement of the total unpolymerized material [25-27], the interpretation of microtubules, and interpretation of the effect of D_2O substitution on the calculated thermodynamic parameters. Previous attempts appeared to underestimate the total amount of material which was potentially available for incorporation into the spindle [4, 5, 17]. First, the addition of D_2O invariably produced retardation which was larger than the original estimates of available material [7, 18, 22, 27, 28]. Observations on spontaneously occurring tri- or tetra-polar spindles or the tubulin paracrystals induced by vinblastine and Colcemid [2, 18] apparently indicated the pool size might be a great deal larger than any of the previous estimates. In fact, a ten fold increase in the amount of organized material was not uncommon in the tetrapolar configuration in the presence of D_2O . It appeared that a given orienting centers could interact with or assemble only a limited amount of the total available material [26]. The addition of more orienting centers resulted in the assembly of more monomeric or polymerizable material. The substitution of D_2O , on the other

hand, appeared to strengthen the interactions of a given orienting center [10,28].

Despite these obvious difficulties which arose in attempting a molecular interpretation, the two state model seems to be the best first approximation available and its use was justified until sufficient contradictory evidences were available.

As was pointed out previously, the technical difficulties involved in making very rapid retardation measurements prohibited studies on the time course of spindle assembly. This problem has been overcome through the use of rapid stabilization of spindles and the choice of a more slowly responding organism. The results demonstrated that when the spindle equilibria were shifted only a small fraction, the kinetics governing the response could be adequately described by simple first order differential equations. This did not imply that the reactions themselves were necessarily first order. Rather than to follow the usual procedure of calculating relaxation times, the data have been expressed in terms of Arrhenius plots and the corresponding apparent energies of activation (E_{act}). This allowed a comparison of the present data with a number of other processes. The calculated E_{act} for the assembly process were rather large, approximately 40 kcal/mole. These values are greater than those usually recorded for specific enzymatic reactions but approach the values measured for the denaturation of several proteins. This suggested that the polymerizable tubulin underwent a conformational change upon assembly. Similar energies of activation have been reported.

The energies of activation for the D_2O and H_2O reactions were very similar; 39.3 vs 41.3 kcal/mole. This fact and the numerical similarity of the rate constants at each temperature strongly supported the idea that there was no difference between the mechanism of assembly in D_2O and H_2O .

The partial disassembly of the spindle after transfer from D_2O to H_2O was well behaved in the sense that it followed an Arrhenius type relationship with a positive E_{act} . The E_{act} , 14.5 kcal/mole, was approximately one-third that for the assembly step, suggesting there was less of an energy barrier to dissociation.

The dissociation reaction of the spindle studied

using temperature shifts from higher to lower T produced somewhat anomalous results which suggested that the mechanism of temperature depending dissociation might be more complex. Here, the rate of retardation decrease became greater at lower temperatures. This led to the calculation of negative E_{act} . It seems more reasonable to believe that perhaps spindle microtubules which presumably assembled by end or ends [28], treadmilling [29], dynamic instability [10] or break and mend [10, 30, 31], we feel it dissociated in a more complex manner by breaking into smaller pieces or by shortening and splitting.

In order to adequately describe the present results, we believe two state equilibrium model [17] must be modified to some extent. One modification was to assume that it was not possible to adequately measure the pool size which should be very large compared to the amount of oriented material. This modification led to the conclusion that ΔH was no longer independent of temperature. This type of modification should be considered in the future.

An alternative modification was the introduction of second reaction, primarily introduced by Takahashi and Sato [18]. We suggest Figure 15 as a possible model. Two reactions were involved: one of which was primarily influenced by temperature, the other being mainly influenced by D_2O . The breaking to smaller fragments is shown to illustrate the possible complexity of the dissociation by temperature.

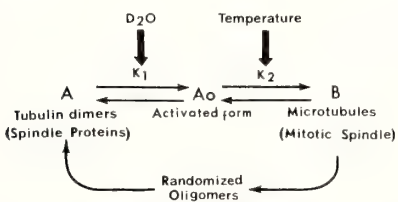


Fig. 15. A model postulated to interpret the temperature or D_2O depending spindle association and dissociation reaction.

The temperature sensitive reaction was the rate limiting step for which the energies of activation have been measured. This reaction was tacitly assumed to be the assembly reaction although other interpretations were possible. The effect of

D_2O on the temperature sensitive step was reflected in the difference in ΔH and ΔS for the normal and D_2O substituted systems. As described before, the decrease in ΔH and ΔS upon D_2O substitution suggested strongly that hydrophobic or apolar interactions were not involved.

We believe we are still far from real mechanism of the assembly and disassembly of tubulin or microtubule dynamics *in vivo*. Further study must be carried on physico-chemical bases.

ACKNOWLEDGMENTS

This work was supported by Grant-in-Aid for Scientific Research provided from the Ministry of Education, Science and Culture of Japan, numbered as 60480020, and Grant-in-Aid for Co-operative Researches numbered as 613040008, 62300004 and 62304062, and also Grant-in-Aid for Developmental Scientific Research numbered as 62890004.

We wish to extend our sincere thanks to all faculty and staff members in the Sugashima Marine Biological Laboratory, Nagoya University, for their kind cooperation and assistance during the course of present work.

We also extend our sincere appreciation to Dr. R. Fernald[†], who had been devoted for the Friday Harbour Laboratories as the director, and the staff of that laboratories where we made most of spindle isolations and retardation measurements during the summers of 1967 to 1969. Assistance for electron microscopy appreciated to Mrs. Bush[†].

REFERENCES

- Inoué, S. and Sato, H. (1967) Cell motility by labile association of molecules - The nature of mitotic spindle fibers and their role in chromosome movement. *J. Gen. Physiol.*, **50**: 259-292.
- Sato, H. (1975) The mitotic spindle. In "Aging Gametes". Ed. by R. Blandau, S. Kager A. G., Basel, pp. 19-49.
- Sato, H., Kato, T., Takahashi, T. C. and Itoh, T. J. (1982) Analysis of D_2O effect on *in vivo* and *in vitro* tubulin polymerization and depolymerization. In "Biological Functions of Microtubules and Related Structures". Ed. by H. Sakai, H. Mohri and G. G. Borisy, Academic Press, Tokyo, pp. 211-226.
- Carolan, R. M., Sato, H. and Inoué, S. (1965) A thermodynamic analysis of the effect of D_2O and H_2O on the mitotic spindle. *Biol. Bull.*, **129**: 402. (Abstract)
- Carolan, R. M., Sato, H. and Inoué, S. (1966) Further observations on the thermodynamics of the

- living mitotic spindles. *Biol. Bull.*, **131**: 385. (Abstract)
- 6 Ito, J. T. and Sato, H. (1984) The effect of deuterium oxide ($^2\text{H}_2\text{O}$) on the polymerization of tubulin in vitro. *Biochim. Biophys. Acta.* **800**: 21–27.
 - 7 Salmon, E. D. (1975) Spindle microtubules: Thermodynamics of in vivo assembly and role in chromosome movement. *Ann. New York Acad. Sci.*, **253**: 383–406.
 - 8 Sato, H., Ohnuki, Y. and Sato, Y. (1979) Assembly and disassembly of the mitotic spindle. In "Cell Motility: Molecules and Organization". Ed. by S. Hatano, H. Ishikawa and H. Sato, Univ. Tokyo Press, Tokyo, pp. 551–568.
 - 9 Takahashi, T. C. and Sato, H. (1982) Thermodynamic analysis of the effect of D_2O on mitotic spindle in developing sea urchin eggs. *Cell Struct. Funct.*, **7**: 349–357.
 - 10 Mitchison, T. J. and Kirschner, M. W. (1984) Dynamic instability of microtubule growth. *Nature (Lond.)*, **312**: 237–242.
 - 11 Salmon, E. D., Leslie, R. J., Saxton, W. M., Karow, M. L. and McIntosh, J. R. (1984) Spindle microtubule dynamics in sea urchin embryos: Analysis using a fluorescein-labeled tubulin and measurements of fluorescence redistribution after laser photobleaching. *J. Cell Biol.*, **99**: 2165–2174.
 - 12 Sato, H., Ellis, G. W. and Inoué, S. (1975) Microtubular origin of mitotic spindle form birefringence: Demonstration of the applicability of Wiener's equation. *J. Cell Biol.*, **67**: 501–517.
 - 13 Bryan, J. and Sato, H. (1970) The isolation of the meiosis I spindle from the mature oocyte of *Pisaster ochraceus*. *Exp. Cell Res.*, **59**: 371–378.
 - 14 Kane, R. E. (1965) The mitotic apparatus: Physical-chemical factors controlling stability. *J. Cell Biol.*, **25**: 137–144.
 - 15 Inoué, S. (1981) Cell division and the mitotic spindle. *J. Cell Biol.*, **91**: 131–147.
 - 16 Morales, M. and Inoué, S. (see, 17)
 - 17 Inoué, S. (1959) Motility of cilia and the mechanism of mitosis. *Rev. Mod. Physics*, **31**: 402–408.
 - 18 Takahashi, T. C. and Sato, H. (1984) Yields of tubulin paracrystals, vinblastine-crystals, induced in unfertilized and fertilized sea urchin eggs in the presence of D_2O . *Cell Struct. Funct.*, **9**: 45–52.
 - 19 Gross, P. R. and Spindel, W. (1960) The inhibition of mitosis by deuterium. *Ann. New York Acad. Sci.*, **84**: 745–754.
 - 20 Gross, P. R. and Spindel, W. (1960) Heavy water inhibition of cell division: An approach to mechanism. *Ann. New York Acad. Sci.*, **90**: 500–522.
 - 21 Kritchevsky, D. (1960) Deuterium isotope effects in chemistry and biology. *Ann. New York Acad. Sci.*, **84**: 573–781.
 - 22 Marsland, D. and Zimmermann, A. M. (1965) Structural stabilization of the mitotic apparatus by heavy water in the cleaving eggs of *Arbacia punctulata*. *Exp. Cell Res.*, **38**: 306–313.
 - 23 Thomson, J. F. (1963) Biological Effects of Deuterium. A Pergamon Press Book, Macmillan Co., New York.
 - 24 Inoué, S., Fuseler, J., Salmon, E. D. and Ellis, G. (1975) Functional organization of mitotic microtubules. Physical chemistry of the in vivo equilibrium system. *Biophys. J.*, **15**: 725–744.
 - 25 De Brabander, M., Geuens, G., Nuydens, R., Willebrods, R. and DeMey, J. (1981) Microtubule assembly in living cells after release from nocodazole block. *Cell Biol. Int. Rep.*, **5**: 913–920.
 - 26 Harris, P., Osborn, M. and Weber, K. (1980) Distribution of tubulin containing structures of the sea urchin *Strongylocentrotus purpuratus* from fertilization through first cleavage. *J. Cell Biol.*, **84**: 668–679.
 - 27 Sluder, G. (1976) Experimental manipulation of the amount on tubulin available for assembly into the spindle of dividing sea urchin eggs. *J. Cell Biol.*, **70**: 75–85.
 - 28 McIntosh, J. R. (1979) Cell division. In "Microtubules". Ed. by K. Roberts, and J. S. Hymes, Academic Press, New York, pp. 428–441.
 - 29 Margolis, R. L. and Wilson, L. (1981) Microtubule treadmills—possible molecular machinery. *Nature (Lond.)*, **293**: 705–711.
 - 30 Salmon, E. D., Saxton, W. M., Leslie, R. J., Karow, M. L. and McIntosh, J. R. (1984) Diffusion coefficient of fluorescein-labeled tubulin in the cytoplasm of embryonic cells of sea urchin *Lytechinus variegatus*: Measurement by video image analysis of fluorescence redistribution after photobleaching. *J. Cell Biol.*, **99**: 2157–2164.
 - 31 Saxton, W. D., Stemple, D. L., Leslie, R. J., Salmon, E. D., Zavortink, M. and McIntosh, J. R. (1984) Tubulin dynamics in cultured mammalian cells. *J. Cell Biol.*, **99**: 2175–2186.

Metaphase to Anaphase Transition of Sea Urchin Eggs Examined in Caffeine-Induced Monasters¹

PATRICIA J. HARRIS

*Department of Biology, University of Oregon,
Eugene, Oregon 97403, U.S.A.*

ABSTRACT—Monasters were produced by treating mitotic sea urchin eggs for 15 min with 10 mM caffeine. Microtubules of the mitotic apparatus disappeared and the centrosomes moved to the chromosomes. Eggs that had not yet passed the metaphase/anaphase transition regressed to early prophase, while the anaphase eggs continued on to form interphase nuclei. On recovery in normal sea water, all eggs formed a large monaster, but some were just entering mitosis, while the others were entering interphase, a half cycle out of phase. New microtubules growing from the centrosomes of the anaphase eggs were resistant to the caffeine treatment. The difference in stability between the old and the new microtubules may reflect some changes occurring in the centrosome itself at the transition to anaphase. The large size of the caffeine-induced monasters makes them an excellent experimental system for studying mitosis.

INTRODUCTION

The transition from metaphase to anaphase is marked by the abrupt onset of a number of processes, the most conspicuous being the separation of the chromatids and the beginning of their movement toward opposite poles. There are other processes associated with mitosis, however, that begin long before this transition point and extend long after it. For example, a poleward force is exerted on the chromosomes probably as soon as they become attached to kinetochore microtubules (MTs) in prometaphase [1], and in the astral mitosis of sea urchin zygotes, asters and their centrospheres enlarge continuously from the time of their origin in early prophase until late anaphase and telophase [2].

A useful tool for studying these processes is the mitotic monaster, frequently found naturally in newt lung cell cultures, where they have been used for the analysis of prometaphase chromosome movements [3], and artificially produced in sea urchin eggs treated with mercaptoethanol, where they have been used for studies of centrosome

duplication [4]. The structural characteristics of monasters produced by artificial activating agents in unfertilized eggs have been explored by Pawletz and Mazia [5]. Monasters can also be produced by treatment of prometaphase sea urchin eggs with 10 mM caffeine for 10–15 min [6]. This causes the breakdown of aster MTs and shrinkage of the spindle until the two centrosomes are brought together at the metaphase plate. On recovery a large monaster, twice the size of the normal mitotic aster, grows and proceeds through all the stages of mitosis. The size of this aster makes it especially useful for experimentation. Recently Mazia *et al.* [7] have reported that incubation of prometaphase eggs at 0°C for 18 hr shrinks the spindle and causes the two centrosomes to fuse at the metaphase plate in a manner very similar to that after 15 min in caffeine.

Described in this paper are the results of one of a number of experiments using a 15 min pulse of 10 mM caffeine to produce monasters. The inherent asynchrony in different batches of eggs, and the difficulty in determining the exact stage at which caffeine is added often results in samples containing intact prophase nuclei or eggs that have advanced into anaphase, and confuses the interpretation of results. In this case approximately half the

Accepted March 17, 1988

¹ This paper is dedicated to Professor Katsuma Dan.

eggs were either in prometaphase or early anaphase with no polyspermy, making the stages easy to distinguish. The recovery patterns of each of these populations of eggs is compared and the significance of their differences with regard to the transition from one MT system to another is discussed.

MATERIALS AND METHODS

Gametes of the sea urchin *Strongylocentrotus purpuratus* were obtained by injection of 0.5 M KCl. Eggs were fertilized and the fertilization membranes removed by addition of mercaptoethylgluconamide (Vega Biochemicals, Tucson, Arizona) at a concentration of 0.1 g/100 ml of egg suspension. After 15 min the softened membranes were stripped by passing through Nitex mesh. The eggs were washed by settling and decanting, and then incubated in normal filtered sea water at 12°C with constant stirring.

At prometaphase, eggs were collected and resuspended in 10 mM caffeine in sea water for 15 min, then washed and allowed to recover in normal sea water. Samples were taken at 10 min intervals through 60 min, at the time of the control second division. Eggs were fixed in 1% paraformaldehyde in 0.4 M Na acetate pH 6.5 for 20–30 min, dehydrated in ethanol series, and embedded in 20% methyl/80% butyl methacrylate in gelatine capsules, as described by Harris and Rubin [8]. For brightfield light microscopy, 1.0 μ m thick sections were stained with 1% azure 2, 1% methylene blue in 1% Na borate and mounted under cover-

slips with immersion oil.

RESULTS

Examination of sectioned control eggs fixed at the time of beginning caffeine treatment showed that there were approximately equal numbers of prometaphase (Fig. 1a) and anaphase (Fig. 1b) stages. Actually, Figure 1a is probably closer to late metaphase than prometaphase, but represents the latest stage before anaphase onset. After 15 min in 10 mM caffeine the asters of the prometaphase eggs had disappeared and the spindle had shrunk, moving the centrosomes (i.e. centrioles and peri-centriolar material) to the metaphase plate, where they often fused to form a single spherical body surrounded by the chromosomes (Fig. 2a).

In the anaphase eggs (Fig. 2b) the asters and kinetochore MTs were also depolymerized, and the centrosomes were apparently moved to the chromosomes, even though the chromosomes were no longer held together at the metaphase plate. Unlike in the prometaphase eggs, a number of MTs radiated from the centrosomes and also appeared to traverse the interzonal region between the separated sets of chromosomes.

When caffeine treated eggs were returned to normal sea water to recover for 10 min, prometaphase eggs formed a monaster, with MTs growing out from the centrosome and apparently pushing the condensed chromosomes outward as they grew (Fig. 3a). The resulting structure might be considered a monaster prometaphase. In the

FIGS. 1–5. Comparison of prometaphase (vertical column a) and anaphase (vertical column b) at different stages of monaster formation.

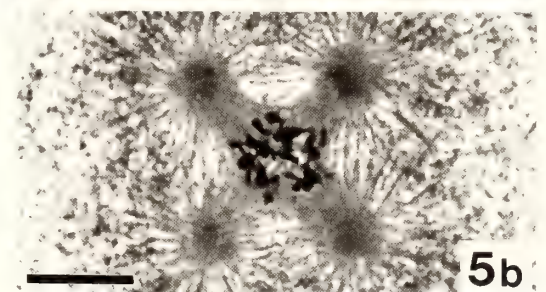
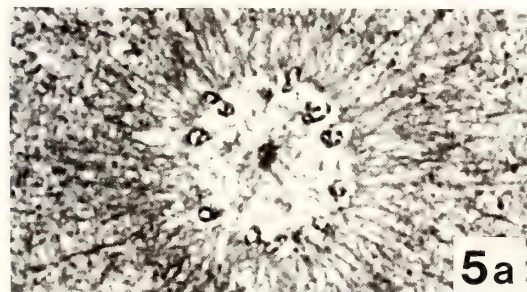
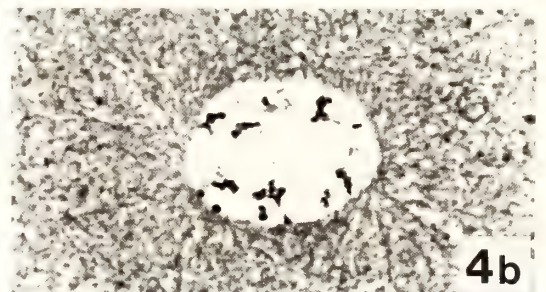
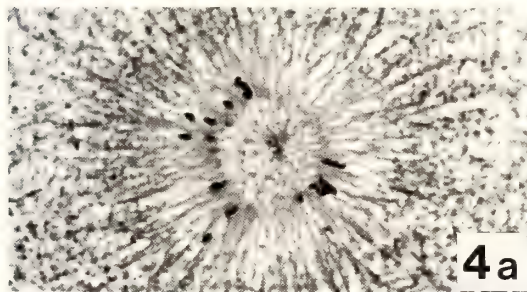
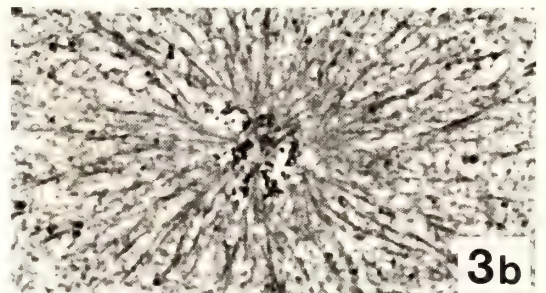
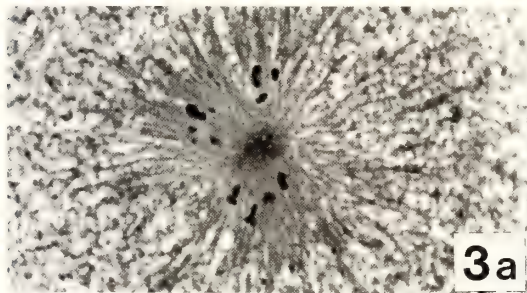
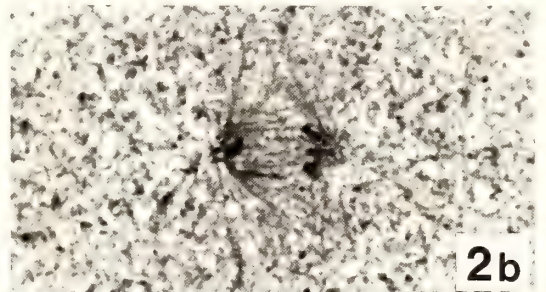
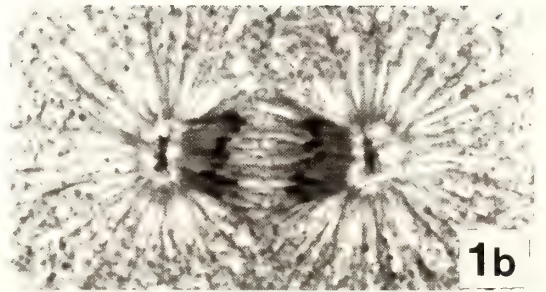
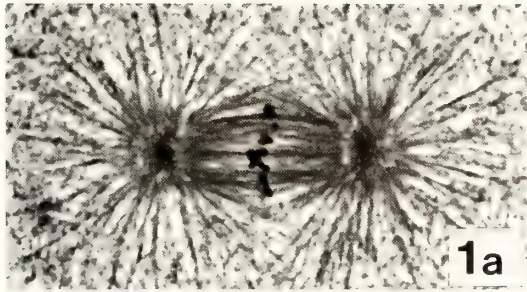
FIG. 1a, b. Mitotic stage at time of caffeine treatment. The metaphase figure in 1a is the latest stage in this population. The mid-anaphase stage in 1b is midway between very early anaphase and early telophase found in this population.

FIG. 2a, b. After 15 min in 10 mM caffeine-sea water. The centrosomes move to the chromosomes in both cases. Within this time period no MTs are present in metaphase eggs, but are seen originating from the centrosomes at the poleward sides of the two sets of anaphase chromosomes.

FIG. 3a, b. After 10 min recovery in normal sea water. All eggs have monasters, but the prometaphase eggs form a mitotic figure, while the anaphase eggs produce an interphase MT system. The two populations are now a half-cycle out of phase.

FIG. 4a, b. After 40 min recovery. Prometaphase eggs remain in the mitotic state, but increase the size of the centrosphere. The anaphase eggs are entering prophase of the next division.

FIG. 5a, b. After 60 min recovery. Prometaphase eggs begin to decondense their chromosomes and enter interphase. Anaphase eggs are now entering the next division, which is directly from one to four cells.



anaphase eggs (Fig. 3b), the chromosomes decondensed and began to fuse to form a centered interphase nucleus, while aster MTs continued to grow to form a large monaster. Thus, while all eggs in the 10 min recovery sample had large monasters, they actually represented two separate populations that were a half division cycle out of phase.

After 40 min recovery, the most conspicuous change in the prometaphase eggs was the great enlargement of the aster center, or centrosphere (Fig. 4a). The chromosomes remained condensed at the periphery of this region and aligned radially with respect to its center. Aster MTs inserted at the periphery, but did not penetrate the centrosphere. In some sections, aggregates of material in the center of this region contained one and sometimes two densely staining dots, possibly the centrioles. The reconstitution of the nucleus in the anaphase eggs was accompanied by a flattening of the nucleus and formation of a clear disk similar to the classical streak of the normal division cycle. During this time the centers or centrosomes, retaining their MTs, became separated and associated with the surface of the nucleus. Figure 4b shows a nucleus following the streak formation, with MTs somewhat reduced in number just before the beginning formation of mitotic asters.

The centrosphere region of the original prometaphase eggs continued to grow, until at 60 min recovery it reached a diameter at least five times that of the 10 min recovery sample. At this time the chromosomes began to decondense and coalesce to form interphase nuclei. There was some asynchrony, but most eggs were in the stage pictured in Figure 5a. Enlarging chromosomal vesicles moved toward the center of the aster, and new MTs originating from the aggregated material in the aster center rapidly grew to form a new monaster similar to the 10 min recovery sample of the original anaphase population. Further development of the prometaphase population apparently followed the same course as the anaphase population, but with approximately 60 min delay. While the nuclei were reforming in the prometaphase eggs, the anaphase eggs had entered mitosis, with most at metaphase or anaphase of a one-to-four division (Fig. 5b). A description of the

later division cycles of these populations will be reported elsewhere.

DISCUSSION

The actual mechanism by which caffeine affects the mitotic apparatus is not known, but indirect evidence suggests that it may bring about a release of intracellular calcium by affecting the calcium sequestering system [9, 10]. Whatever the mechanism is, the rapid depolymerization of MTs and the equally rapid recovery of the ability to reassemble them makes caffeine a useful tool for studying mitotic events.

In the studies reported here, two populations of eggs within the same experimental sample, those just before and those just after the metaphase to anaphase transition, and thus only a few seconds apart in developmental time, were separated by half a cell cycle by treatment with caffeine. Those eggs that had not passed the transition point regressed to the start of mitotic apparatus formation, while those that had passed that point continued their development.

The role of calcium in the metaphase to anaphase transition is suggested by calcium-dependent changes in chlorotetracycline fluorescence at anaphase onset [11], anaphase acceleration or delay with injection of EGTA-calcium buffers in mammalian cells [12], and a calcium transient at the onset of anaphase in sea urchin eggs [13] as well as in mammalian cells [14], detected with the fluorescent probe Fura-2. The exact function of the calcium release is not known, but it may be a signal for the dephosphorylation of the cyclically phosphorylated mitotic proteins, which occurs at the onset of anaphase [15]. At least some of these phosphorylated proteins are associated with the centrosome [16].

One of the consequences of the metaphase to anaphase signal appears to be some change in the ability of the centrosome to nucleate MTs. After 15 min in the 10 mM caffeine sea water, the prometaphase centrosome showed no evidence of MT nucleation, while in the anaphase eggs MT growth from the centrosomes indicated either new nucleation or continued growth onto already nucleated MTs. These MTs may represent the new growth

that begins at late anaphase and telophase in untreated eggs [8].

In both the prometaphase and the anaphase eggs, the old mitotic apparatus disappeared completely, demonstrating a difference in stability between the old and the newly forming MTs. One explanation for this difference may be that the centrosome loses its association with the old MTs before it begins to support new MT growth in anaphase. Endo [17] has described changes in the clusters of granular material around the centrioles of sea urchin eggs during mitosis, and noted that at metaphase there is a sharp separation of the granular clusters from the surrounding radial MT zone. Endo suggested that by metaphase the main function of these clusters has been accomplished, although she notes their association with MTs again at later stages. These later MTs may be those we see at anaphase, which are stabilized by their attachment to the centrosome.

The growth of the centrosphere in the recovering prometaphase eggs is quite spectacular. Unfortunately we have not yet found a good antibody to centrosomes that will react with our sectioned material, and so we can say little about the expansion and other shape changes of the centrosome as described by Mazia [18] and Schatten *et al.* [19]. In the paraformaldehyde fixed eggs described here, centrioles stain as very small dense dots, while the pericentriolar material that makes up the bulk of the centrosome is very lightly stained and difficult to identify. Therefore it is impossible to say from this work how much of the centrosomal material remains attached to the proximal ends of the aster MTs in these enlarged centrospheres, how much remains in the aster center, and how much may be distributed back into the cytoplasm.

The brief paraformaldehyde fixation and methacrylate embedding permit immunofluorescence localization of tubulin and fluorescent staining of the chromosomes. We hope to develop further probes to study the distribution of mitotic proteins. Certainly the caffeine-induced monasters provide an excellent experimental system for these studies.

ACKNOWLEDGMENTS

This work was supported by grant PCM 8409573 from the National Science Foundation (U.S.A.).

REFERENCES

- 1 Bajer, A. S. and Molé-Bajer, J. (1972) Spindle dynamics and chromosome movement. *Int. Rev. Cytol. (suppl.)*, **3**: 1-271.
- 2 Wilson, E. B. (1928) *The Cell in Development and Heredity*, The Macmillan Co., New York, 3rd ed.
- 3 Bajer, A. S. (1982) Functional autonomy of monopolar spindle and evidence for oscillatory movement in mitosis. *J. Cell Biol.*, **93**: 33-48.
- 4 Sluder, G. (1978) The reproduction of mitotic centers: new information on an old experiment. In "Cell Reproduction: in Honor of Daniel Mazia". Ed. by E. R. Dirksen, C. M. Prescott and C. F. Fox, Academic Press, New York, pp. 563-569.
- 5 Paweletz, N. and Mazia, D. (1979) Fine structure of the mitotic cycle of sea urchin eggs activated by ammoniacal sea water. *Eur. J. Cell Biol.*, **20**: 37-44.
- 6 Harris, P. J. (1983) Caffeine-induced monaster cycling in fertilized eggs of the sea urchin *Strongylocentrotus purpuratus*. *Dev. Biol.*, **96**: 277-284.
- 7 Mazia, D., Schatten, H., Coffe, G. Szöke, Howard, C. and Schatten, G. (1987) Aggregation of the mitotic centrosomes into a single spherical centrosome by cold treatment in sea urchin eggs. *J. Cell Biol.*, **105** (4, pt. 2): 206a.
- 8 Harris, P. J. and Rubin, B. P. (1987) Transition from mitosis to interphase in sea urchin first division: immunofluorescence studies of tubulin distribution in methacrylate sections. *J. Histochem. Cytochem.*, **35**: 343-349.
- 9 Weber, A. (1968) The mechanism of the action of caffeine on sarcoplasmic reticulum. *J. Gen. Physiol.*, **52**: 760-772.
- 10 Kiehart, D. P. (1981) Studies on the in vivo sensitivity of spindle microtubules to calcium ions and evidence for a vesicular calcium sequestering system. *J. Cell Biol.*, **88**: 604-617.
- 11 Wolniak, S. M., Hepler, P. K. and Jackson, W. T. (1983) Ionic changes in the mitotic apparatus during the metaphase/anaphase transition. *J. Cell Biol.*, **96**: 598-605.
- 12 Izant, J. G. (1983) The role of calcium ions during mitosis. Calcium participates in the anaphase trigger. *Chromosoma (Berl.)*, **88**: 1-10.
- 13 Poenie, M., Alderton, J., Tsien, R. Y. and Steinhardt, R. (1985) Changes of free calcium levels with stages of the cell division cycle. *Nature (Lond.)*, **315**: 147-149.
- 14 Poenie, M., Alderton, J., Steinhardt, R. and Tsien,

- R. (1986) Calcium rises abruptly and briefly throughout the cell at the onset of anaphase. *Science*, **233**: 886-889.
- 15 Karsenti, E., Bravo, R. and Kirschner, M. (1987) Phosphorylation changes associated with the early cell cycle in *Xenopus* eggs. *Dev. Biol.*, **119**: 442-453.
- 16 Kuriyama, R. (1987) Rapid turnover of phosphate in a centrosomal component of dividing sea urchin eggs. *J. Cell Biol.*, **105** (4, pt. 2): 284a.
- 17 Endo, S. (1980) Further observations on the clusters of granular material around the centriole on the sea urchin egg: changes in distribution during mitosis. *Dev. Growth Differ.*, **22**: 509-516.
- 18 Mazia, D. (1984) Centrosomes and mitotic poles. *Exp. Cell Res.*, **153**: 1-15.
- 19 Schatten, H., Schatten, G., Mazia, D., Balczon, R. and Simerly, C. (1986) Behavior of centrosomes during fertilization and cell division in mouse oocytes and in sea urchin eggs. *Proc. Natl. Acad. Sci. U.S.A.*, **83**: 105-109.

Marked Elongation of the Anaphase Spindle by Treatments with Local Anesthetics in Sea Urchin Eggs

MANABU K. KOJIMA

Department of Biology, Faculty of Science, Toyama University, 3190 Gofuku, Toyama-shi/ken 930, and Sugashima Marine Biological Laboratory, Nagoya University, Sugashima-cho, Toba-shi, Mie-ken 517, Japan

ABSTRACT—When fertilized sea urchin eggs are immersed in 1/32–1/16 M urethane (ethyl carbamate) sea water, cytoplasmic division is suppressed but the nuclear division continues as normal. In these eggs, aster formation is considerably disturbed but spindle can be formed and, moreover, can elongate markedly during the late anaphase-telophase. Such a spindle elongation occurs when eggs are put into a urethane solution at any time between 5 min after fertilization and the first metaphase. This elongation is inhibited if eggs, pretreated with 1/32 M urethane, are exposed to 0.1 mM colcemid, or 1/8 M urethane sea water in which nuclear division does not occur. Elongation of the anaphase spindle is also induced by treatments with isopropyl N-phenyl carbamate (IPC), procaine and tetracaine. However, caffeine treatments are not effective. The mechanism of spindle elongation is discussed from the standpoint of microtubule dynamics.

INTRODUCTION

It has been stated before that when fertilized sea urchin eggs are treated with Monogen or urethane sea water in appropriate concentrations, the cytoplasmic division is suppressed while the nuclear division goes on as normal and thus forming multinucleated eggs [1]. Recently, it has become clear that Monogen suppresses the cytoplasmic division by mostly impairing the egg cortex, without affecting the aster formation. Urethane, however, inhibits the division by mainly disturbing the formation of mitotic apparatus [2]. Furthermore, it was also found that urethane in appropriate concentrations can induce marked elongation of the anaphase spindle [2, 3]. Therefore the purpose of this paper is to report on this induced elongation of the anaphase spindle. It seems very worthwhile studying the induction mechanism of spindle elongation using local anesthetics, not only for elucidation of the mechanism of mitosis itself, but also for the analysis of microtubule dynamics. This paper is the first in a series of such studies.

MATERIALS AND METHODS

Materials

Eggs of the following four species of Japanese sea urchins were used as materials: *Anthocidaris crassispina*, *Temnopleurus toreumaticus*, *Pseudocentrotus depressus* and *Hemicentrotus pulcherrimus*. Since all of these species essentially gave the same results, experimental data of only the last species will be presented in this paper.

Chemicals

Stock solutions were as follows; 1 M solution of ethyl urethane (Katayama) in distilled water, 10 mM solution of procaine hydrochloride (Sigma) in sea water, 5 mM solution of tetracaine hydrochloride (Sigma) in sea water, a saturated solution of isopropyl N-phenyl carbamate (Sigma) in sea water, 50 mM solution of caffeine (Katayama) in sea water, 2×10^{-4} M solution of colcemid (Sigma) in

Abbreviations used: PIPES, 1,4 piperazine diethanesulfonic acid; DTT, dithiothreitol; TAME, p-tosyl-L-arginine methyl ester hydrochloride.

sea water and 1% solution of Monogen (Dai-ichi Kogyo Seiyaku) in sea water. These stock solutions were diluted to various concentrations by adding sea water before use.

Measurements of the spindle length

Eggs were photographed using an ordinary light microscope at regular intervals after fertilization. Measurements of the spindle length were made both from projected negatives and from printed photographic papers, which were enlarged to the definite magnification, using 20 eggs at different mitotic stages. In some experiments, photographs were taken with Nomarski (Olympus) and polarizing (Leitz) optics so as to be able to observe the features of spindle elongation in eggs treated with the above mentioned chemicals.

Isolation of mitotic apparatus

Thirty seconds after fertilization, the eggs were immersed in 1 M urea solution and gently blown and sucked with a pipette to remove the fertilization membrane. Two minutes later, they were returned to normal sea water and washed three

times by exchanging the sea water. Such denuded eggs were put into sea water containing various concentrations of local anesthetics at definite intervals after fertilization and allowed to develop there. At the desired stage, the eggs were transferred to Isolation Medium A (10 mM PIPES, pH 6.9; 5 mM EGTA; 0.5 mM MgSO₄; 1 M glycerol; 2 mM DTT; 1 mM TAME). They were then retransferred to Isolation Medium B (Isolation Medium A + 1% Emulgen 810 or Nonidet P-40). In this medium, all eggs swelled within a few minutes. One drop of such an egg suspension was placed on a slide glass and gently pushed under a cover slip. In this way, the mitotic apparatus were easily isolated. These mitotic apparatus were observed and photographed with phase contrast (Olympus) or Nomarski (Olympus) optics.

RESULTS

In the first series of experiments, eggs were immersed in urethane solution of various concentrations 5 min after fertilization and the features of

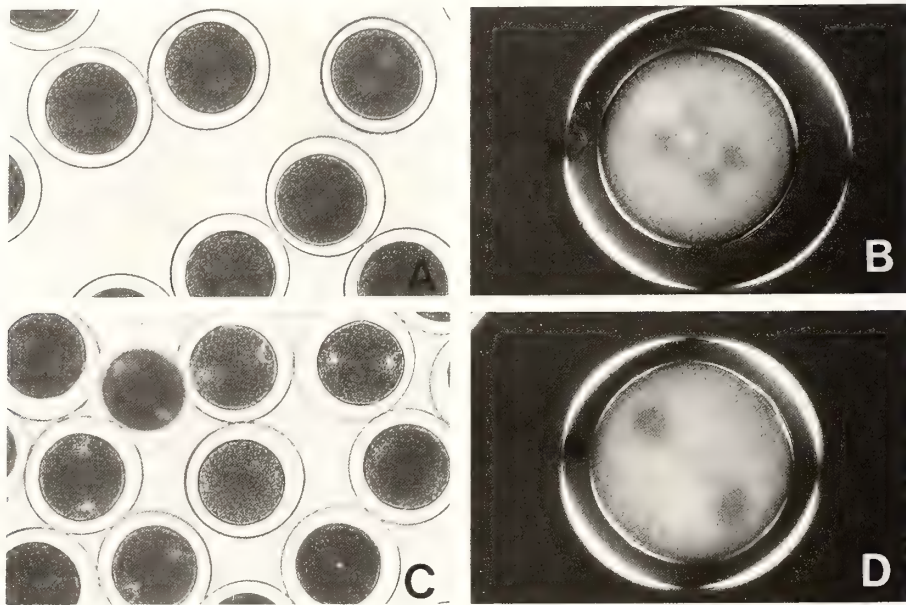


FIG. 1. Spindle elongation in urethane-treated eggs (19°C). *Hemicentrotus* eggs were exposed to 1/32 M urethane sea water solution at 5 min after fertilization and their mitotic figures were photographed with ordinary light microscope (A and C) and polarizing microscope (B and D). A and B: Control eggs (75 min after fertilization). C and D: 1/32 M urethane-treated eggs (95 min after fertilization).

the mitotic apparatus in the first cleavage cycle were determined. At the same time, another group of eggs were exposed to Monogen sea water in graded concentrations in order to compare the effects of this reagent with that of urethane. Some differences were noted in sensitivity to both chemicals in the different batches of eggs. However, generally speaking, when eggs are treated with 1/32–1/16 M urethane solutions which correspond to the minimum concentrations for inhibition of cytoplasmic division, the spindle can be formed although formation of the asters is considerably suppressed. In this case, the length of the anaphase spindle, i.e. the pole-to-pole distance, be-

comes much longer than that in the control eggs. It is very interesting to note that this elongation occurs even when the eggs themselves do not elongate and continue to remain spherical (Figs. 1 and 2). On the contrary, in Monogen-treated eggs, their mitotic apparatus are very similar in dimension and morphology to those of the control ones but they are unable to divide (Fig. 2). In eggs treated with urethane, a fibrous structure connecting the two mitotic centers or nuclei can be easily detected (Figs. 1 and 2). Therefore, isolation of such an elongated anaphase spindle from urethane-treated eggs was tried and it became clear, as shown in Figure 3, that two daughter

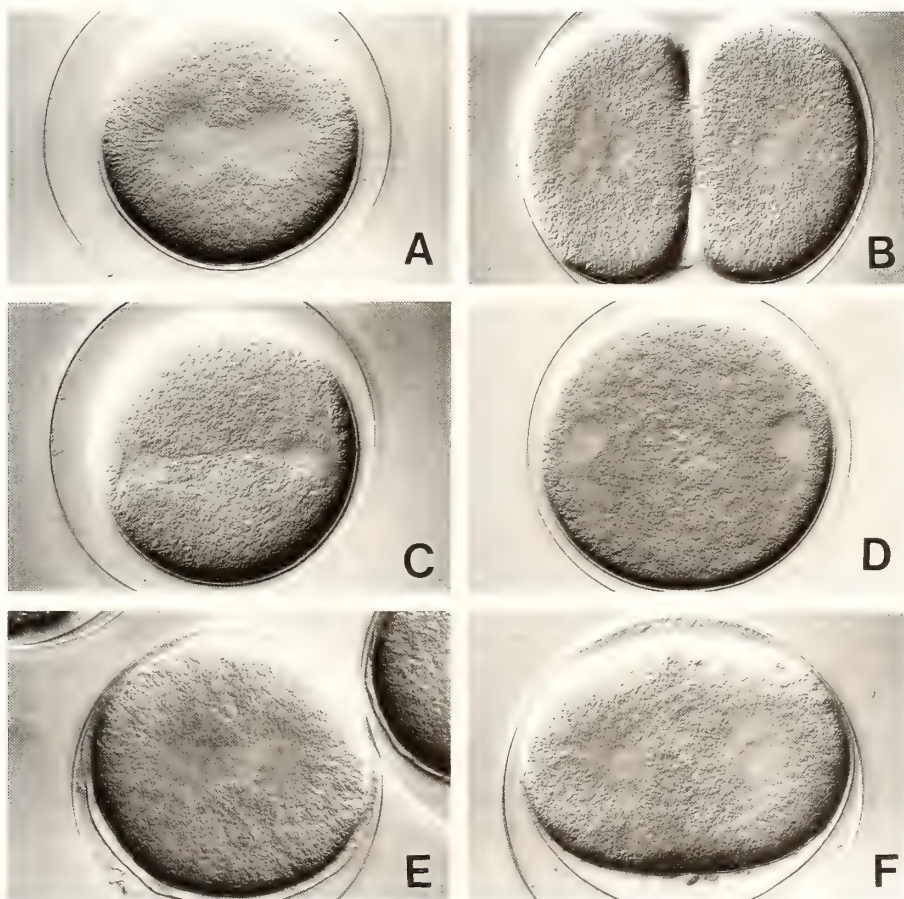


FIG. 2. Comparison of mitotic figures between Monogen- and urethane-treated eggs (19°C). *Hemicentrotus* eggs were transferred to 1/32 M urethane and 1/64% Monogen solutions at 5 min after fertilization and their mitotic figures in slightly depressed eggs were photographed with Nomarski optics. A and B: Control eggs (75 and 85 min after fertilization). C and D: 1/32 M urethane-treated eggs (90 and 110 min after fertilization). E and F: 1/64% Monogen-treated eggs (75 and 110 min after fertilization). In Monogen-treated eggs, furrowing sometimes occurred, but such cleavage furrow, once formed, regressed afterwards (F).

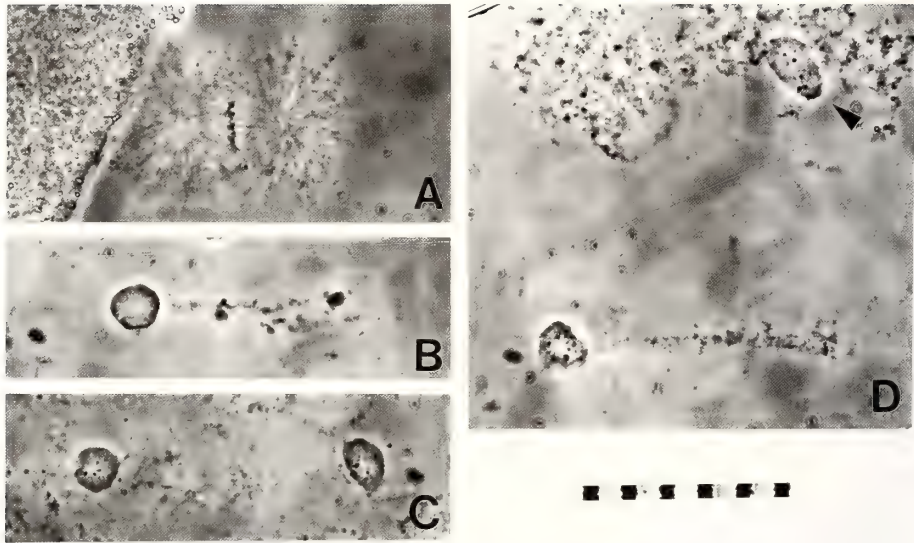


FIG. 3. Isolation of elongated mitotic spindle from urethane-treated eggs (18.5°C). *Hemicentrotus* eggs were deprived of fertilization membranes immediately after fertilization and, 15 min later, immersed in $1/32$ M urethane solution. These denuded eggs were then transferred to the isolation medium at 90 min after fertilization and their mitotic spindles were isolated according to the procedure described in "Materials and Methods". A: A metaphase spindle isolated from control eggs (75 min after fertilization). B–D: Elongated mitotic spindle which isolated from $1/32$ M urethane-treated eggs (90 min after fertilization). Arrow head in D indicates the daughter nucleus detached from the spindle fiber. One div. = $10\ \mu\text{m}$.

nuclei are connected by a fibrous structure, the so-called "continuous fiber". This fact suggests to us that two nuclei may be pushed away from each other by stretching this fiber.

In the second series of experiments, maximum pole-to-pole distances were measured in the control, Monogen- and urethane-treated eggs. One of the results of such measurements is given in Table 1. From this table it will be seen that the pole-to-pole distances in urethane-treated eggs reach nearly twice those in both the control and the Monogen-treated ones even when eggs still remain spherical before cleavage, and these interpolar distances are greater than the maximum values obtained just after the cleavage in the control ones. In addition, it should be noted that if the egg diameter is assumed as being 100, the maximum spindle length in undivided, control and Monogen-treated eggs is estimated at approximately 35. This coincides with the value, 35.47, calculated from Figure 6 in the paper by Dan [4].

In the third series of experiments, effects of colcemid on spindle elongation induced by urethane-treatments were examined. Eggs were

pretreated with $1/32$ M urethane solution from 5 min after fertilization. Seventy minutes later, half of them were put into $1/32$ – $1/8$ M urethane solutions and the rest were transferred to 5 – $100\ \mu\text{M}$ colcemid solutions. One example of such experiments is represented in Table 2. As will be seen from this table, urethane-pretreated eggs are put into $1/32$ – $1/16$ M urethane solutions at 75 min after fertilization, their anaphase spindles can elongate to the same degree as those in eggs continuously exposed to $1/32$ M urethane from 5 min after fertilization. When the pretreated eggs are transferred to $1/8$ M urethane in which nuclear division is disturbed, no marked spindle elongation occurs afterwards. On the other hand, it was also revealed when eggs are placed in $100\ \mu\text{M}$ colcemid solution after exposure to $1/32$ M urethane for 70 min, their spindles do not elongate further, but if a lower concentration of this drug is applied, some elongation of the spindle takes place. These facts suggest that, as concerns spindle elongation, urethane may affect some cytoplasmic changes during the late anaphase-telophase but not the changes which have occurred before the anaphase.

TABLE 1. Pole-to-pole distances in urethane- and Monogen-treated eggs (19.5°C)

Egg diameter (μm)	Pole-to-pole distances (μm)			
	Control		1/32 M urethane	1/64 % Monogen
	just before furrowing	just after furrowing		
95.7 \pm 0.4	33.1 \pm 1.7	52.8 \pm 2.2	64.5 \pm 3.6	33.4 \pm 1.3
	(100) ^a	(159.8) ^a	(195.0) ^a	(101.1) ^a
(100) ^b	(34.6) ^b	(55.2) ^b	(65.3) ^b	(34.9) ^b

Hemicentrotus eggs were put into 1/32 M urethane and 1/64 % Monogen solutions at 5 min after fertilization and were then photographed at 10 min intervals for 90 min. The pole-to-pole distances were measured from photomicrographic records using 20 eggs at each of the mitotic stages. Values in this table represent maximum interpolar distances in undivided, urethane- and Monogen-treated eggs. Each value is the mean (μm) \pm S.E. In addition, values of the spindle length just before furrowing (80 min after fertilization) and just after its completion (87 min after fertilization) in untreated eggs were given as the control. a: The numbers in parentheses express the percentage of each pole-to-pole distance when the value of the distance in eggs just before furrowing is assumed to be 100. b: The numbers in parentheses indicate the percentage of each pole-to-pole distance when the value of the egg diameter before cleavage is postulated as being 100.

TABLE 2. Effects of colcemid on spindle elongation in urethane-treated eggs (18.5°C)

75 min after fert.	125 min after fert.						
	urethane			colcemid			
1/32 M	1/32 M	1/16 M	1/8 M	5 μM	10 μM	20 μM	100 μM
24.9 \pm 1.1	54.4 \pm 4.3	57.1 \pm 4.0	32.6 \pm 3.3	38.7 \pm 4.5	37.9 \pm 2.2	35.8 \pm 1.1	25.9 \pm 2.6
(100)	(219.0)	(229.7)	(131.3)	(155.8)	(152.3)	(144.3)	(104.2)

Hemicentrotus eggs were exposed to 1/32 M urethane sea water at 5 min after fertilization and 70 min later, they were transferred to solutions containing urethane or colcemid in various concentrations, respectively. The length of the mitotic spindle was measured from photomicrographs taken at 75 and 125 min after fertilization (for more details, see "Materials and Methods"). Each value is the mean (μm) \pm S.E. The numbers in parentheses express the percentage of each pole-to-pole distance when the value of the spindle length in 1/32 M urethane-treated eggs at 75 min after fertilization is assumed to be 100.

In the last series of experiments, it was determined whether marked elongation of the anaphase spindle is induced not only by the treatment with ethyl urethane but also by treatments with other agents known to inhibit cytokinesis by disruption of the mitotic apparatus [5-8]. In the present experiments, effects of procaine, tetracaine and caffeine, and isopropyl N-phenyl carbamate (IPC) were tested. Eggs were exposed to sea water solutions of the above-described chemicals in various concentrations at 10 min intervals from 5 min after fertilization up to the beginning of the first cleavage and the features of spindle formation were examined. Generally speaking, ethyl

urethane (1/32-1/16 M) and IPC, a derivative of phenyl urethane, (40-50% dilution of the stock solution) are most effective in inducing spindle elongation and two amine compounds, procaine (10-15 mM) and tetracaine (0.2-0.5 mM), follow the former two in effectiveness. Such spindle elongation occurs when eggs are put into sea water solutions of each of these four above-mentioned agents in appropriate concentrations at any time from 5 min after fertilization up to the first metaphase (75 min after fertilization). Caffeine has no effect on spindle elongation under experimental conditions as used in the present study.

DISCUSSION

In the present study, it becomes clear that 1) when sea urchin eggs are put into 1/32–1/16 M urethane sea water at any time between 5 min after fertilization and the first metaphase, aster formation is considerably suppressed so that cytokinesis does not take place, but nuclear division goes on and, moreover, spindles elongate markedly during the late anaphase-telophase; 2) this spindle elongation is inhibited when 1/8 M urethane or 0.1 mM colcemid, in which nuclear division does not occur, is applied to eggs pretreated with 1/32 M urethane; 3) such an elongation of the anaphase spindle can be induced by treatments with procaine, tetracaine and IPC, but not by caffeine treatment.

It has been known that ethyl urethane and other anesthetics block cleavage in sea urchin eggs [9–12]. In 1984, for instance, Rappaport [12] reported that ethyl urethane (0.06 M) reduces the size of the mitotic apparatus and blocks cleavage in sand dollar eggs. However, he did not refer to a spindle elongation, though the concentration of urethane used in his experiments was almost the same as that employed in the present study. Such a discrepancy between the two papers may depend upon a difference in experimental methods and materials used.

Now, some questions arise: firstly, why can the spindle elongate as it does in urethane-treated eggs which have very poor asters? No definite answer can be made as yet concerning this question. However, it can be explained as follows. In normal cleavage, from metaphase to mid-anaphase, the astral rays are straight and comparatively short. At the late anaphase, when the asters develop fully, the tips of the rays extend and reach the egg cortex. Soon afterwards elongation of the spindle takes place and the rays are no longer straight but bent, exhibiting a "fountain figure" [4, 13, 14]. This means that as the spindle elongates the polar asters are pushed against the cell membrane so that the spindle is compelled to elongate against the resistant force of the asters in the opposite direction. As shown already in the present paper, the size of the asters in urethane-treated eggs is much smaller than that in the control eggs. Therefore, such resistant force of the

asters is assumed to be considerably weaker in urethane-treated eggs. If so, it seems reasonable that spindle can elongate much easier so that their length becomes longer than that in the control ones. In fact, a fibrous structure connecting the two asters or nuclei is actually isolated from such urethane-treated eggs and, as indicated in Table 1, maximum values of the spindle length in undivided, urethane-treated eggs reach nearly twice as long as those in the control eggs just before furrowing and, furthermore, these values are still greater than those in the control eggs just after cleavage.

Then the next question arises: How is the motive force for such a spindle elongation produced during the late anaphase-telophase? To this question, we again cannot completely answer yet, but at least the following may be said. In the present paper, it was revealed that the spindle in eggs treated with urethane in appropriate concentrations can elongate to nearly twice the length of those in the control eggs, while colcemid and urethane in higher concentrations inhibit spindle elongation. These facts strongly suggest to us the possibility that, in the mechanism of spindle elongation, not only the mutual sliding of the interpolar microtubules is involved but also elongation of those microtubules themselves is very important. At any rate, investigation of this possibility must be continued.

In addition, Saxton and McIntosh [15] very recently proposed a model for anaphase B in Ptk₁ cells in which plus end elongation of interdigitated microtubules and antiparallel sliding both contribute to chromosome separation.

ACKNOWLEDGMENTS

This work was done at the Sugashima Marine Biological Laboratory, Nagoya University. The author wishes to express his sincerest gratitude to Prof. Hidemi Sato, Director of the Laboratory. Thanks are due to Dr. T. Ôhara for her helpful assistance in the course of this work and to Prof. W. P. Hardwick, Sugiyama-jogakuen University, for reading the manuscript.

REFERENCES

- 1 Kuno, M. (1954) Comparative studies on ex-

- perimental formation of multinucleated eggs of sea urchins by means of various agents. *Embryologia*, **2**: 43-49.
- 2 Kojima, M. K. (1978) On the cleavage in Monogen- or urethane-treated eggs of the sea urchins. *Zool. Mag. (Tokyo)*, **87**: 314. (in Japanese)
 - 3 Kojima, M. K. and Ôhara, T. (1982) Effects of local anesthetics and a herbicide on the mitosis. *Dev. Growth Differ.*, **24**: 410.
 - 4 Dan, K. (1943) Behavior of the cell surface during cleavage. VI. *J. Fac. Sci., Tokyo Imp. Univ., Sec. IV*, **6**: 323-368.
 - 5 Cheney, R. H. (1948) Caffeine effects in fertilization and development in *Arbacia punctulata*. *Biol. Bull.*, **94**: 16-24.
 - 6 Kiehart, D. P. (1981) Studies on the in vitro sensitivity of spindle microtubules to calcium ions and evidence for a vesicular calcium-sequestering system. *J. Cell Biol.*, **88**: 604-617.
 - 7 Harris, P. (1983) Caffeine-induced monaster cycling in fertilized eggs of the sea urchin *Strongylocentrotus purpuratus*. *Dev. Biol.*, **96**: 277-284.
 - 8 Jackson, W. T. (1969) Regulation of mitosis. II. Interaction of isopropyl N-phenyl carbamate and melatonin. *J. Cell Sci.*, **5**: 745-755.
 - 9 Wilson, E. B. (1901) Experimental studies in cytology. II. Some phenomena of fertilization and cell division in etherized eggs. *Arch. Entwicklungsmech.*, **13**: 353-373.
 - 10 Kobayashi, N. (1962) Cleavage of the sea urchin egg recovering from the cleavage-blocking effect of demecolcine. *Embryologia*, **7**: 68-80.
 - 11 Rappaport, R. (1971) Reversal of chemical cleavage inhibition in echinoderm eggs. *J. Exp. Zool.*, **176**: 249-255.
 - 12 Rappaport, R. and Rappaport, B. N. (1984) Division of constricted and urethane-treated sand dollar eggs: A test of the polar stimulation hypothesis. *J. Exp. Zool.*, **231**: 81-92.
 - 13 Yatsu, N. (1909) Observations on ookinesis in *Cerebratulus lateus* Verrill. *J. Morphol.*, **20**: 353-402.
 - 14 Balczon, R. and Schatten, G. (1983) Microtubule-containing detergent-extracted cytoskeletons in sea urchin eggs from fertilization through cell division: Antitubulin immuno-fluorescence microscopy. *Cell Motility*, **3**: 213-226.
 - 15 Saxton, W. M. and McIntosh, J. R. (1987) Interzonal microtubule behavior in late anaphase and telophase spindle. *J. Cell Biol.*, **105**: 875-886.

Control Mechanisms of Mitosis: The Role of Spindle Microtubules in the Timing of Mitotic Events

GREENFIELD SLUDER

*Worcester Foundation for Experimental Biology, 222 Maple Avenue,
Shrewsbury, Massachusetts 01545, U.S.A.*

Cell division in higher eukaryotes consists of a series of nuclear and cytoplasmic events that have a highly conserved sequence and a predictable timing. It is of utmost importance for the cell to exert control at both the spatial and temporal levels. The chromosomes and the cytoplasmic components of the mitotic apparatus must be precisely arranged to insure equal partitioning of the daughter chromosomes into separate, equal nuclei. In addition, the cell has to tightly control when mitotic events occur. For example, anaphase chromosome movement must not start before the chromosomes are properly oriented and aligned on the metaphase plate. The cell must not cleave until the chromosomes have adequately separated. Also, the cell should not reform nuclear envelopes and start the next cell cycle before anaphase is complete. Mistakes in either spatial arrangements or in timing lead to an abnormal division and the loss of viability for the daughter cells.

In this article we review our studies which have sought to develop a better understanding of how the cell controls the timing of events during the mitosis portion of the cell cycle. Since we do not have the space to fully develop the data, the reader is directed to the original works for a rigorous demonstration of the points we will make.

For our work, we used fertilized eggs from the sea urchins *Lytechinus variegatus* and *Lytechinus pictus*. Their large size, optical clarity, and the rapidity of their cell cycle make these eggs an exceptionally favorable experimental system. Importantly, the lessons learned from the sea urchin egg are directly applicable to other types of cells. The sequence of mitotic events for these eggs is

shown in Figure 1. Figure 2 shows the average normal timing of the events we used as temporal markers.

Our studies were derived from work dating back to the 1930's which showed that the cell cycle in a variety of cell types can be stopped or prolonged in 'metaphase' by blocking spindle assembly with colchicine [1-4]. In the 1960's, other studies showed that colchicine, at moderate doses, prevents microtubule assembly by specifically binding to the tubulin dimer [5-7]. We reasoned that if the rate at which the cell traverses mitosis can be altered by preventing microtubule assembly, spindle microtubules might be an important part of the mechanisms that control the mitosis portion of the cell cycle. This possibility was especially attractive given our knowledge that microtubules are required for establishing the spatial arrangement of organelles at mitosis and for the execution of most mitotic events [8, 9]. As we will discuss below, spindle microtubules, in fact, do have a dual role during mitosis; they are not only necessary for the accomplishment of mitotic events, but also influence when the cell will 'decide' to execute these events.

In starting our work [10], we wanted to compare the cell cycle timing of normal fertilized eggs to eggs in which microtubule assembly had been experimentally reduced or blocked. For this we used Colcemid, a derivative of colchicine, which binds the tubulin dimer more tightly and is effective at lower external concentrations than colchicine [11]. We had to be certain that Colcemid, as we used it, blocked microtubule assembly without toxic side-effects that could non-specifically alter a cell cycle timing. Thus, we developed a new and simple way to apply Colcemid [12]. Since con-

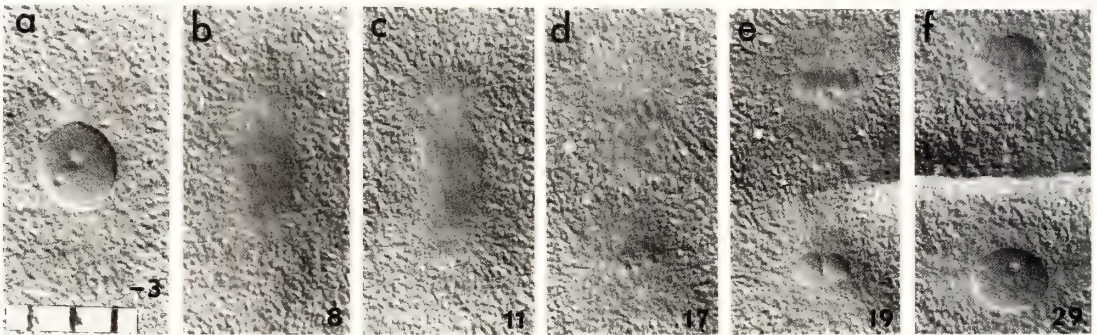
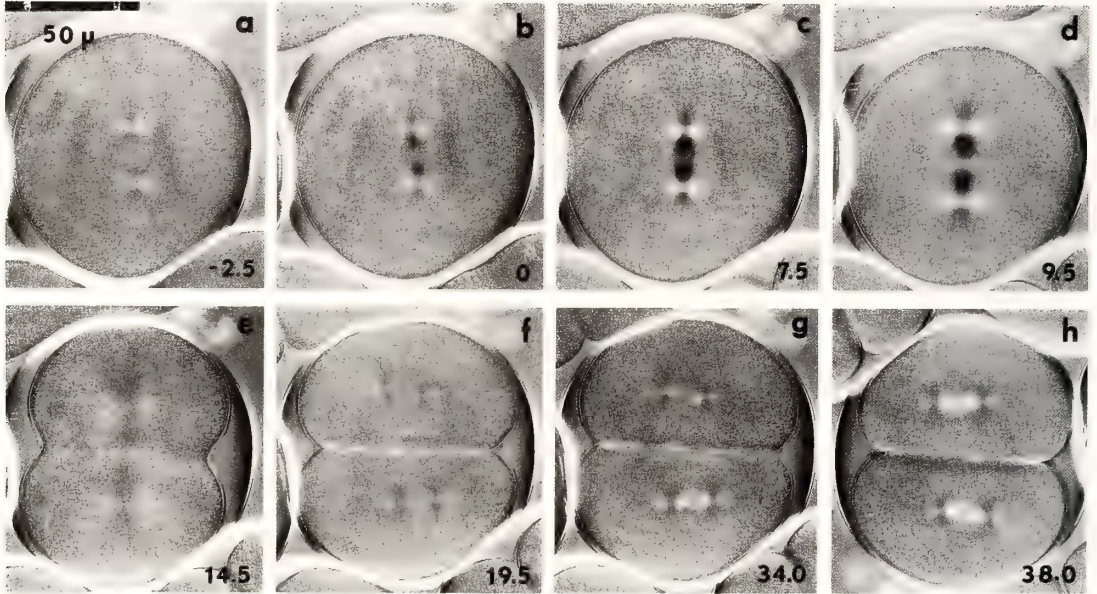


FIG. 1. Upper: First and second mitoses in a *L. variegatus* egg; Polarization microscopy. (a) before first nuclear envelope breakdown: (b) nuclear envelope breakdown: (c) metaphase: (d) early anaphase: (e) telophase and cleavage: (f) prophase of second mitosis: (g) second nuclear envelope breakdown: (h) prometaphase of second mitosis. Minutes before and after first nuclear envelope breakdown are shown in the lower corner of each frame. 50 μm per scale division.

Lower: First mitosis in a *L. variegatus* egg; differential interference contrast microscopy. Only the nuclear region is shown. (a) before nuclear envelope breakdown: (b) late prometaphase: (c) mid-anaphase: (d) telophase reformation of karyomeres: (e) telophase fusion of karyomeres: (f) daughter nuclei separated by cleavage furrow. Minutes before and after nuclear envelope breakdown shown in lower corner of each frame. 10 μm per scale division.

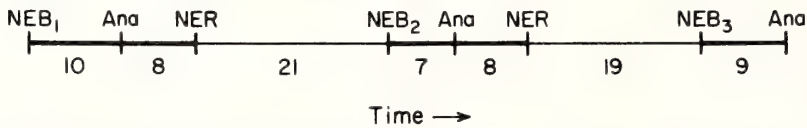


FIG. 2. Normal timing of mitotic events (at 22°C) used as temporal markers. Two cell cycles are displayed on a time axis. 'NEB₁, NEB₂, NEB₃' refers to nuclear envelope breakdown. 'Ana' is anaphase onset as detected with the polarization microscope. 'NER' indicates nuclear envelope reformation. The numerical values are average times, in minutes, for the intervals between the events indicated.

tinuous immersion of eggs in colchicine can lead to continued binding of the drug beyond that necessary to block microtubule assembly [5, 6], we treated the eggs in early prophase for a short time (4 min) with a moderate concentration (5×10^{-6} M) of Colcemid. By varying the duration of the pulse, we could precisely control the portion of the tubulin pool that was inactivated before mitosis [12]. In sea urchin eggs, Colcemid binds the tubulin dimer tightly; a single pulse administered in early prophase can completely prevent microtubule assembly for at least several cell cycles. Since the eggs are washed free of residual Colcemid, there is no continued binding of the drug beyond that necessary to block microtubule assembly. By being careful to use only the minimally effective dose of drug and conducting a series of control experiments with photo-chemically inactivated Colcemid, we showed that the changes in cell cycle timing we observed in our studies were due solely to the loss of spindle microtubules, not toxic side-effects of the drug.

First, we sought to determine if the prophase assembly of astral microtubules effects the time of first nuclear envelope breakdown, as had been previously suggested [13]. We compared the time-course of first nuclear envelope breakdown in untreated eggs and eggs treated with Colcemid to prevent microtubule assembly (Fig. 3). The fact that we found no significant difference in the time course of nuclear envelope breakdown between the control and treated populations indicated that the assembly of astral microtubules does not influence the timing of interphase events leading to mitosis.

We next investigated how far the cell cycle of sea urchin eggs will progress when microtubule assembly is prevented. Do the eggs arrest in mitosis or do they continue cycling? We always found that the cell cycle continues when microtubule assembly is prevented; Colcemid treated eggs show a repeated cycle of nuclear envelope breakdown and nuclear envelope reformation (Fig. 4). Also, the chromosomes repeatedly double in a normal

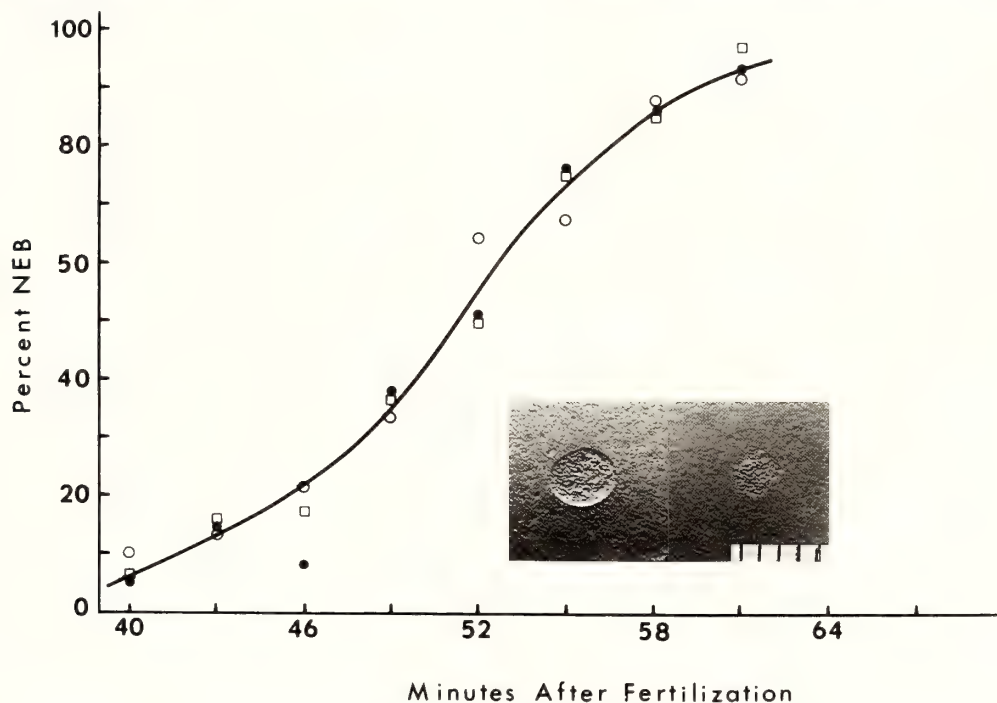


FIG. 3. Percent nuclear envelope breakdown (NEB) as a function of time after fertilization. Filled circles: untreated control eggs. Open circles: eggs treated for 3.5 min with 5×10^{-6} M Colcemid. Open squares: eggs treated for 7 min with 5×10^{-6} M Colcemid. 100–180 eggs were scored for each data point. Inset: before and after nuclear envelope breakdown (fixed eggs). Differential interference contrast micrographs. 10 μ m per scale division.

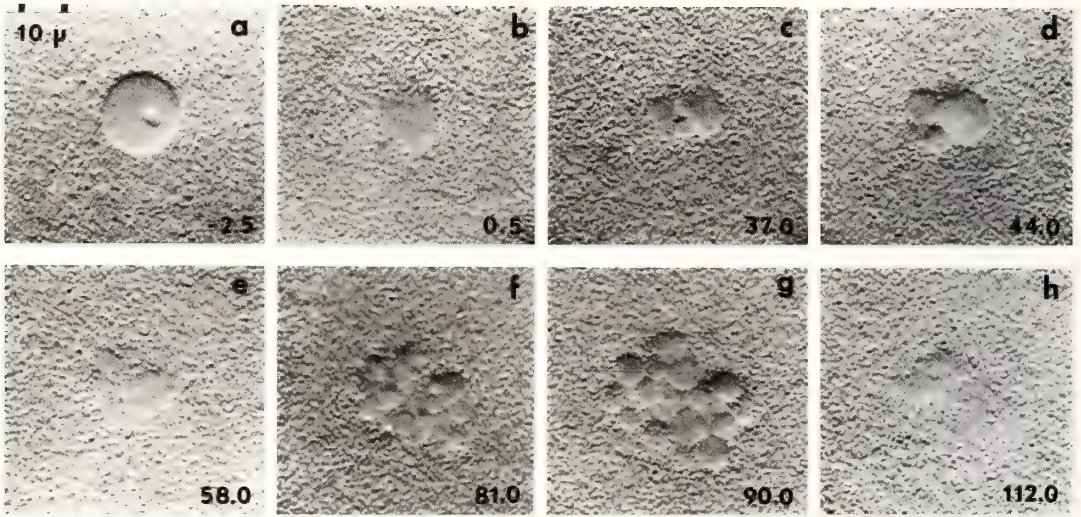


FIG. 4. Disappearance-reappearance cycling of nuclear envelopes in an egg treated for 4 min with 5×10^{-6} M Colcemid. (a) before first nuclear envelope breakdown; (b) after nuclear envelope breakdown; (c) karyomeres forming; (d) karyomeres swell; (e) karyomeres synchronously break down; (f) karyomeres form for the second time; (g) these swell; (h) they break down. Minutes before and after first nuclear envelope breakdown are shown in the lower corner of each frame. Differential interference contrast micrographs of the same living egg. $10 \mu\text{m}$ per scale division.

fashion as seen by the incorporation of ^3H Thymidine into DNA [14] and increases in chromosome number (Fig. 5).

We noted that Colcemid treated eggs always spend more time between nuclear envelope breakdown and nuclear envelope reformation than the controls. Therefore, we quantitated the timing of these events for both control and Colcemid treated cultures. Instead of working with populations of cells, we followed a number of individual eggs *in vivo*. This allowed us to circumvent a significant portion of the asynchrony found in any population of eggs. Much of the population asynchrony comes from variability in the period between fertilization and first nuclear envelope breakdown; thereafter, the timing of cell cycle events is reasonably constant from egg to egg. Thus, we normalized the time of nuclear envelope breakdown to zero for each control or treated egg we followed, because microtubule assembly does not influence when the cell undergoes first nuclear envelope breakdown (Fig. 3). We found that Colcemid treated eggs, on an average, spend twice as much time between nuclear envelope breakdown and nuclear envelope reformation than control eggs for both first and

second mitoses (Fig. 6). Interphase, the period from nuclear envelope reformation to the following nuclear envelope breakdown, is the same in both populations. Parenthetically, this last observation provides additional evidence that the Colcemid treatment we used does not produce detectable non-specific side effects.

We next wanted to know if the Colcemid treated eggs show 'C-anaphase' (splitting apart of the chromatids as in anaphase onset but without chromosome movement) and if so, determine when this event occurs relative to nuclear envelope breakdown. Does it happen at the normal time for anaphase onset or is it delayed? The chromosomes become hyper-condensed during the prolonged mitosis and all split synchronously in each cell before nuclear envelope reformation (Fig. 5). Without spindle microtubules the chromatids do not move apart. By fixing aliquots of control and Colcemid treated eggs at three minute intervals, we found that this 'C-anaphase' splitting of the chromosomes in Colcemid treated cultures occurs 25 min or more after nuclear envelope breakdown. Anaphase onset in normal eggs occurs 10 min after nuclear envelope breakdown. Thus, in Colcemid

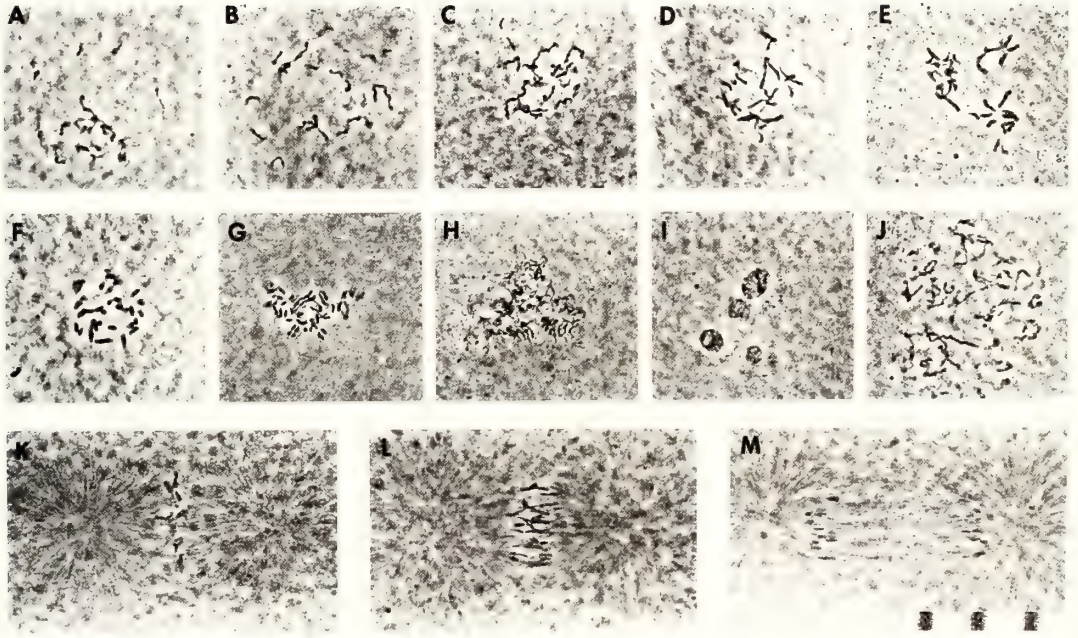


FIG. 5. (a-j) Chromosome morphology in Colcemid treated eggs which do not assemble any spindle microtubules. (a) Before nuclear envelope breakdown. (b-f) Progressive condensation of chromosomes at increasing times after nuclear envelope breakdown. (g) 'C-anaphase' splitting of the chromosomes. (h) Telophase decondensation of chromatin. (i) Karyomeres. (j) Increased number of chromosomes at second nuclear envelope breakdown. (k-m) Metaphase, anaphase onset, and late anaphase in untreated eggs. Eggs were fixed in acid-alcohol and stained with orcein. Phase contrast micrographs. 10 μ m per scale division.

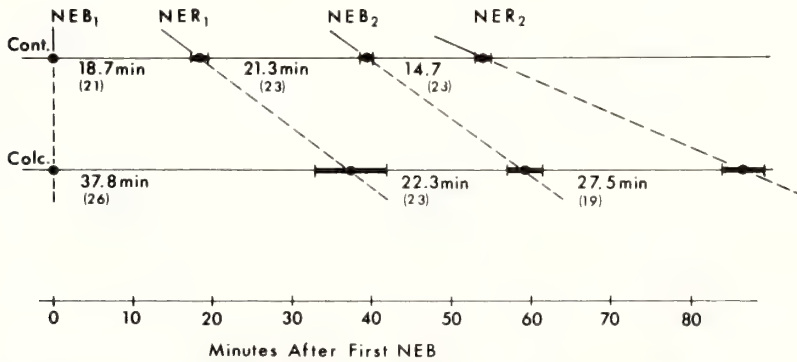


FIG. 6. Timing of nuclear envelope breakdown (NEB) and nuclear envelope reformation (NER) in untreated (upper line) and treated eggs (lower line). Eggs were treated for 4 min with 5×10^{-6} M Colcemid ~20 min before first nuclear envelope breakdown. The horizontal lines represent time axes. First nuclear envelope breakdown is normalized to 0 min for all individual eggs. The mean times of nuclear envelope reformation and breakdown are shown by filled circles on the time axes. The heavy horizontal bars delimit the 95% confidence limits of the means. The larger numbers under each time axis show the mean duration of the various intervals. The small numbers in parentheses give the sample sizes.

treated eggs, the period between nuclear envelope breakdown and anaphase onset is prolonged. In Colcemid treated eggs, nuclear envelope reformation

follows the 'C-anaphase' splitting of the chromosomes at approximately the normal interval of 8 min. Thus, microtubule assembly in-

fluences only the time from nuclear envelope breakdown to anaphase onset: the prometaphase/metaphase portion of mitosis.

Recently, the general applicability of these results to other species of echinoderms was brought into question by a study using high concentrations of colchicine on eggs of *Strongylocentrotus purpuratus* and *Dendraster excentricus* [15]. This study showed that 1–2 mM colchicine, applied continuously, blocked spindle assembly and altered cell cycle timing in qualitatively different fashions that those we had earlier reported for *Lytechinus*. Eggs of *S. purpuratus* were completely arrested in mitosis. For *D. excentricus* mitosis was of normal duration while interphase was prolonged. We were concerned that the relatively high dosages of colchicine used had toxic side effects (reviewed in [14]) which could cause these surprising patterns of timing. Therefore, we reinvestigated the role of spindle microtubules in the timing of the cell cycle of these two species of echinoderms using short treatments of Colcemid to block microtubule assembly [14]. The timing patterns we observed were entirely consistent with those we obtained from our studies on *Lytechinus*. In addition, we performed a series of control experiments using lumi-colchicine, a photo-isomer of colchicine which does not bind to tubulin [16] but shows the same toxic side effects as the native compound [17, 18]. One mM lumi-colchicine alone partially inhibits microtubule assembly and prolongs both mitosis and interphase. Thus, we feel that the timing patterns observed in the colchicine study are most easily explained by a combination of the specific and non-specific effects of continuously applied 1–2 mM native colchicine.

To further explore the relationship between spindle microtubule assembly and the timing of mitotic events, we delayed the onset of microtubule assembly for increasing periods of time after nuclear envelope breakdown and determined the extent to which this perturbation influenced the times of anaphase onset and entry into the next cell cycle. We blocked microtubule assembly and then followed individual eggs as they entered first mitosis. At various times after nuclear envelope breakdown, we irradiated individual eggs on the microscope with 366 nm light to photochemically inacti-

vate the Colcemid thereby allowing the eggs to assemble spindle microtubules. We wanted to know if anaphase onset and telophase events occurred at the normal times after nuclear envelope breakdown or alternatively, if the time of irradiation determined when the eggs would initiate anaphase and finish mitosis. This would tell us whether or not these events are controlled by a microtubule independent clock mechanism. Control irradiations of untreated eggs showed that the short (15 sec) irradiations used in this experiment do not alter the timing of mitotic events. When Colcemid treated eggs are irradiated at nuclear envelope breakdown, they assemble a functional spindle and divide in a normal fashion. The time from nuclear envelope breakdown to anaphase onset is the normal 10 min. Telophase events and second mitosis are also normal.

We then delayed the irradiation for increasing amounts of time after nuclear envelope breakdown. The eggs always assemble functional spindles over the normal time course and initiate anaphase, on average, 10 min after the irradiation. This is even true for eggs irradiated as long as 14 min after nuclear envelope breakdown, a time when the egg would normally have been in late anaphase (Fig. 7). These results show that the time of anaphase onset is not solely controlled by a microtubule independent clock mechanism but rather, is determined by the assembly of spindle microtubules. After anaphase onset, the sequence of telophase events proceeds with normal timing regardless of the duration of prometaphase. Second nuclear envelope breakdown follows first anaphase onset by a constant interval which is the same as that in the irradiated control eggs. Similar experiments on second division eggs showed that our results were not peculiar to the first division cycle.

These results also show that Colcemid (or colchicine) does not arrest cells at 'metaphase' as is often said. From the standpoint of the cell cycle's progress through mitosis, Colcemid arrests sea urchin eggs at the start of prometaphase for a significant amount of time. Had the eggs truly been arrested at metaphase, the time from irradiation to anaphase onset would not have been the 10 minutes we consistently observed; the irradiation

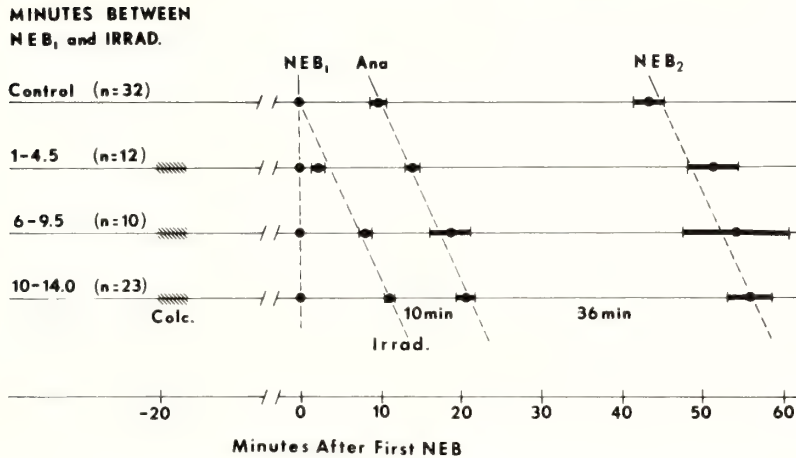


FIG. 7. Results of Colcemid reversal experiments. Fertilized eggs were treated for 3.5 min with 5×10^{-6} M Colcemid in early prophase of the first division (cross hatching). They were irradiated for 15 sec with 366 nm light at times ranging from 0.5 to 14 min after first nuclear envelope breakdown (NEB). The untreated control eggs (top line) were irradiated shortly after first nuclear envelope breakdown. Timing data from the Colcemid-treated eggs are collected into three classes based upon the number of minutes between nuclear envelope breakdown and irradiation. The light horizontal lines are the time axes. The time of first nuclear envelope breakdown is normalized to 0 min for all individual eggs. The mean times of irradiation, anaphase onset, and second nuclear envelope breakdown are shown as filled circles on the time axes. The heavy horizontal bars delimit the 95% confidence limits of the means. The parallel dotted lines are drawn through the irradiation, anaphase, and second nuclear envelope breakdown means to emphasize the constancy of the interval between irradiation and anaphase, as well as the interval between anaphase and second nuclear envelope breakdown. The numbers in parentheses give the sample sizes.

to anaphase onset interval would have depended on how long we delayed the irradiation.

When we irradiated Colcemid treated eggs more than 14 min after nuclear envelope breakdown, we observed incomplete and abortive spindle assembly which indicated that the eggs had spontaneously begun to finish mitosis and were entering the next cell cycle. This was understandable given our demonstration that the cell cycle does eventually continue when no spindle microtubules are assembled.

We next wanted to determine if the extent of spindle microtubule assembly influences the duration of prometaphase. Do eggs with small spindles traverse mitosis at the same rate as eggs with normal sized spindles? We allowed eggs to divide once and treated them late in first telophase with a short (1–3 min) pulse of Colcemid. At second nuclear envelope breakdown, the blastomeres assembled barrel-shaped spindles of reduced length and birefringence. Just after second nuclear envelope breakdown we irradiated one daughter

blastomere with 366 nm light which led to the immediate growth of that cell's spindle to a normal size. This provided us with a control cell against which to compare the timing of the blastomere with a diminished spindle. The cell with the normal sized spindle always enters anaphase and finishes mitosis earlier than the cell with the short spindle (Fig. 8). Here, prometaphase in the blastomere with the diminished spindle is approximately 50% longer than prometaphase in the irradiated control cell. By varying the duration of the Colcemid treatment we could vary the size of the spindles assembled at second mitosis. We found that the smaller the spindle, the later the cell initiates anaphase. After anaphase onset, telophase events proceed with normal kinetics regardless of the size of the spindle.

Collectively, these experiments show that spindle microtubules are necessary not only for the accomplishment of mitotic events, but also play an important role in the mechanisms that determine when the cell will 'decide' to initiate anaphase and

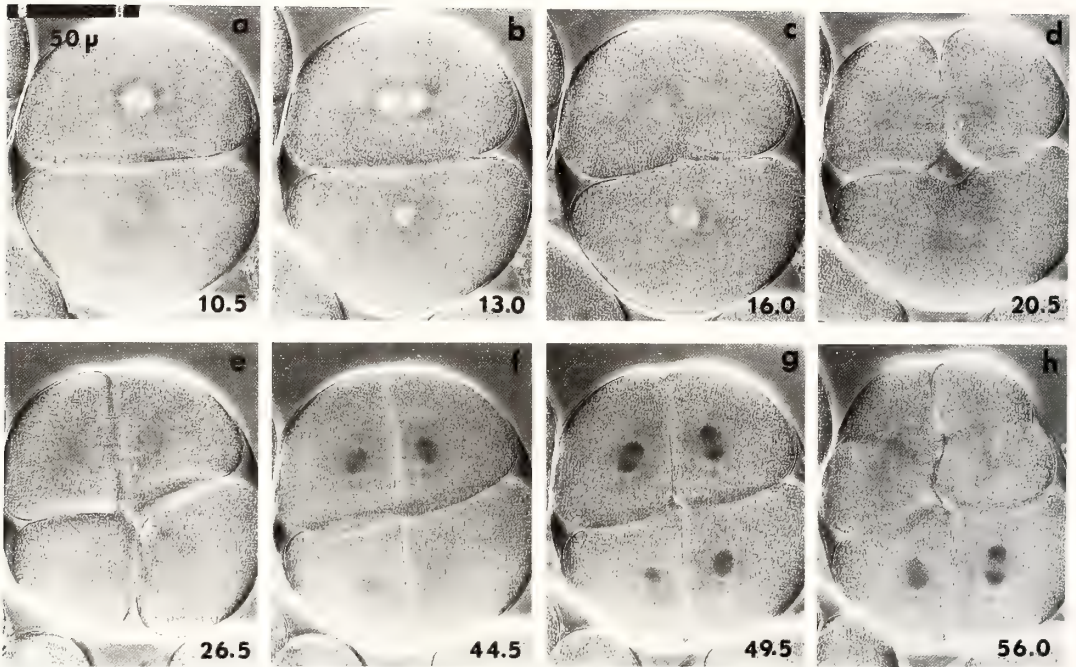


FIG. 8. Mitosis of daughter cells with different-sized spindles. This zygote was treated for 2.5 min with 5×10^{-6} M Colcemid at first cleavage. Second nuclear envelope breakdown occurred synchronously in both daughter cells. Shortly thereafter, the upper blastomere was irradiated for 15 sec with 366 nm light. The lower blastomere was irradiated for 15 sec when it was in telophase to equalize the doses of 366 nm light. (a) prometaphase in irradiated and unirradiated blastomeres; (b) anaphase in the irradiated blastomere while lower blastomere is in metaphase; (c) telophase and cleavage in irradiated cell while the unirradiated cell is in anaphase. The large spindle initiated anaphase 3 min earlier than the smaller one; (d) telophase and cleavage in lower blastomere; (e) nuclear envelope fully reformed in upper two cells but not in lower two; (f) prometaphase in upper cells while lower two are still in interphase; (g) anaphase in upper cells and prometaphase in lower cells; (h) cleavage in upper cells and anaphase in lower cells. Minutes after second nuclear envelope breakdown are shown in the lower corner of each frame. Polarization micrographs; 50 μ m per scale division.

finish mitosis. The cell appears to have a fundamental rhythm that allows more time for mitosis than is actually needed under normal circumstances. This fundamental rhythm is revealed when microtubule assembly is completely blocked. Starting with nuclear envelope breakdown, there is a waiting period that provides the cell with wide temporal tolerances to assemble the labile spindle structure in preparation for division. Within this period, spindle microtubules are part of the mechanism that leads to a necessary physiological change that triggers the cell to initiate anaphase, finish mitosis, and start the next cell cycle. Once triggered, the events that finish one mitosis and lead to the next mitosis, proceed at a normal pace independent of microtubule assembly. At the next

nuclear envelope breakdown, the timing of the cell cycle again becomes sensitive to the assembly of spindle microtubules. Thus, the cell cycle can be thought of as a stopwatch. Once the hand comes into the mitosis portion of the cycle, the watch can be reset to the start of the next cycle by mechanisms involving spindle microtubules. If these microtubules are not assembled, the watch will continue to cycle but does so at a fundamental rate. The observation that once the cell cycle is prolonged, subsequent cycle(s) are not shorter than normal, rules out the possibility that the cell cycle timing is governed solely by a continuous oscillator such as the ones proposed for *Physarum* and *Xenopus* eggs [19, 20].

Furthermore, our studies indicate the existence

of a physiological change that is an important transition point in the cell cycle. This change commits the cell to initiate anaphase, finish mitosis, and start the next cell cycle. In a normal cell, the splitting of the kinetochores at anaphase onset is the first visible manifestation that this change has occurred. However, from the standpoint of cell cycle timing, it does not matter if the chromosomes actually move apart or not. Once this transition point has passed, cleavage, reformation of nuclei, centrosome duplication, and the start of the next cell cycle follow as a temporal linkage group whose timing is insensitive to the extent of microtubule assembly. Such a transition point was first suggested by Mazia and termed 'a point of no return' [21]. Although we cannot yet identify this event in molecular or ionic terms, we can detect it by a change in the functional properties of the cell cycle. Before this point, the progress of the cell cycle through mitosis is influenced by microtubule assembly. After this point, the cell cycle proceeds at a normal rate, irrespective of the state of its microtubules. This is not surprising since late anaphase and telophase are the times when the cell normally disassembles spindle microtubules anyway.

Although we do not think that the anaphase splitting of the chromosomes *per se* is the causal event that commits the cell to finish mitosis, we must consider the possibility that the time of anaphase onset is determined by the assembly of a threshold quantity of microtubules sufficient to physically pull the chromosomes apart. This is not likely given observations which indicate that force production by the spindle does not trigger anaphase onset. First, chromatids will synchronously pop apart without microtubules pulling on them [3, 10, 22, 23]. Second, unattached chromosomes or acentric fragments that lie outside the spindle split and separate slightly when the chromosomes in the spindle start their normal anaphase movements [24, 25]. Thus, a change in cytoplasmic conditions, not force production by the spindle, determines when chromosomes can move apart in anaphase. Third, relatively few microtubules are required to produce or transmit the force necessary for chromosome movement [26].

Our work to this point left us with a seemingly

simple question: How could spindle microtubules participate in the mechanisms that control the duration of the prometaphase/metaphase portion of the cell cycle? Possibly, the cell monitors what fraction of the tubulin pool is used in spindle assembly. Alternatively, the effect of microtubules on cell cycle timing may be indirect, as for example, through the activity of some microtubule-associated enzymatic process that is active only on the assembled microtubules. A third possibility is that the organization of microtubules in a mitotic apparatus determines the distribution of organelles or cytoplasmic factors, which in turn influence the timing mechanisms. In other words, microtubules may act as a structural scaffolding that has the proper geometry for some important process to proceed.

To test between these alternatives, we investigated the relationship between the spatial arrangement of spindle microtubules and the duration of the mitosis [27]. To alter the organization of the spindle without significantly reducing the total tubulin polymer in the egg, we used a microneedle to cut spindle at the metaphase plate and separate the two half spindles. Would a cell with a cut spindle traverse mitosis at the same rate as a cell with an intact spindle? We performed the operation on second division eggs so that we could use one daughter blastomere as a control cell.

At the onset, we needed to know if the manipulation produced any non-specific, irreversible damage that would slow the cell cycle. Obviously, unhealthy eggs could not be expected to show normal timing. Therefore, we conducted a series of control experiments in which we stirred the cytoplasm with a microneedle and even moved the spindle without cutting it. In all cases, the manipulated blastomeres divide in complete synchrony with their controls. In addition, we cut spindles and then pushed the two half-spindles back together again. The half-spindles always reassociate to form a functional spindle of normal appearance. Even though mitosis is slightly prolonged in these cases, subsequent mitoses are normal. Thus, we were assured that the manipulations did not reduce the viability of the eggs.

Blastomeres with cut spindles always spend significantly more time in mitosis than their same

embryo controls (Fig. 9). Here, the experimental cell is just finishing second mitosis when the control is well into third mitosis. Since we could not observe anaphase chromosome splitting *in vivo*, we used the rapid telophase fading of astral birefringence as a measure of when the cell finishes mitosis. We found that blastomeres with cut spindles take, on average, 48 min to proceed from nuclear envelope breakdown to telophase as opposed to 15 min for the control cells. Once the manipulated cell enters telophase, the time to the start of the next mitosis is approximately normal. Thus, rearranging the spindle prolongs only the prometaphase/metaphase portion of the cell cycle. Importantly, the cell cycle of the manipulated cell never resynchronizes with that of the control blastomere. These results show that the timing mechanisms for mitosis do not monitor the utilization of the tubulin pool and are not dependent on some enzymatic process that is based strictly on the total amount of tubulin polymer in the cell.

As a second way to produce spindles of altered geometry, we indirectly induced the formation of monopolar spindles using methods described elsewhere [28, 29]. The timing of blastomeres with monopolar spindles was compared to same-embryo blastomeres in which a cleavage furrow had failed thereby allowing two monopoles to

come together to form a functional bipolar spindle of normal appearance. By using such cells as controls we were certain that all cells had been exposed to the same experimental regime. Cells with monopolar spindles always spend significantly more time in mitosis (49 min on average) than the same-embryo cells with bipolar spindles (15 min on average). These times are remarkably similar to those observed in the micromanipulation experiments. Presently, we cannot completely explain why eggs with spindles of altered geometry spend more time in mitosis than eggs that assemble no spindle microtubules (Fig. 6). In part, the answer lies in the fact that the eggs used in the cut spindle and monopolar spindle experiments (*L. pictus*) were run at a slightly lower temperature than those used in the Colcemid experiments (*L. variegatus*). However, other factors may be involved, and this issue deserves further study.

At this point, we were aware that our micromanipulation and monopolar spindle results might be explained by the fact that half-spindles or monopolar spindles have less total tubulin polymer than normal spindles. Cells with diminished spindles always spend more time in mitosis than cells with normal sized spindles (Fig. 8). For the micromanipulation experiments, the total number of microtubules is approximately normal on a total cell basis,

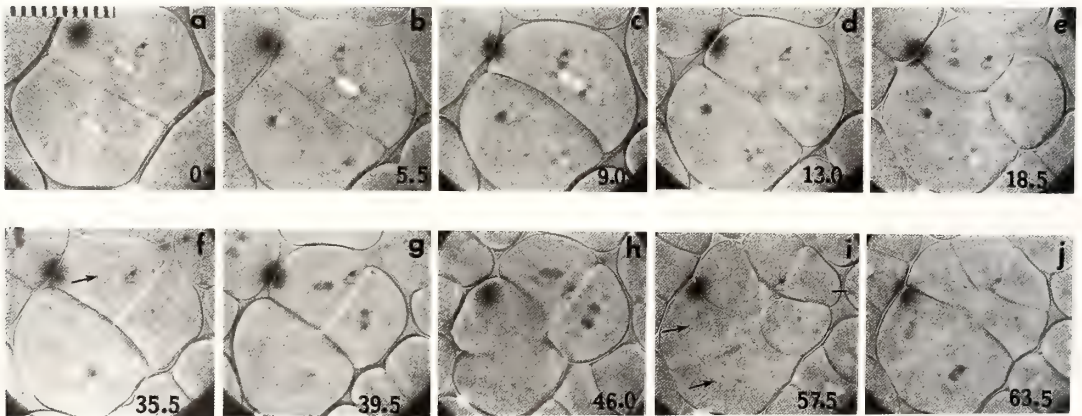


FIG. 9. Development of a cell with a cut spindle; (a) before manipulation, both daughter cells are in early prometaphase of second mitosis; (b) spindle in lower blastomere cut with microneedle; (c-e) manipulated cell stays in mitosis while control completes mitosis; (f-h) manipulated cell enters telophase and cleaves while control enters third mitosis; (i) manipulated cell reforms nuclei (arrows) while control cleaves; (j) manipulated cell enters third mitosis while control cells are preparing for fourth division. Minutes after second nuclear envelope breakdown are given in the lower corner of each frame. Polarization micrographs; 10 μm per scale division.

but the half-spindles are sufficiently separated that they might reside in physiologically distinct regions. Conceivably the timing of mitotic events is more sensitive to the quantity of microtubules in a given volume of cytoplasm than the total amount of tubulin polymer in the cell. To explore these issues, we compared the timing of second division eggs containing Colcemid-diminished bipolar spindles to those containing monopolar spindles or cut spindles. The following observations indicate that monopolar spindles should have at least as much total polymerized tubulin as diminished bipolar spindles. We compared typical monopolar, normal bipolar, and Colcemid diminished bipolar spindles (Fig. 10). The half-spindle length and birefringence are approximately the same in monopolar and normal bipolar spindles. Also, the extent of astral development is the same. Diminished spindles, on the other hand, are less than half as long as a normal spindle, have very small asters, and have half the normal half-spindle birefringence.

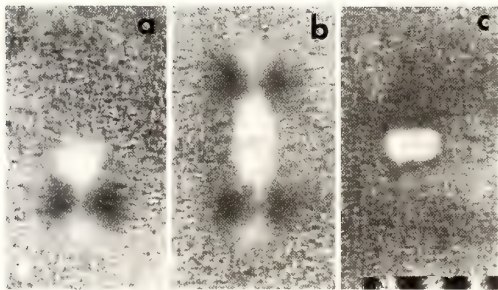


FIG. 10. Size comparison for (a) monopolar spindle, (b) normal bipolar spindle, (c) Colcemid-diminished spindle. All photographs are printed at the same magnification. The birefringence of the region between the chromosomes and the pole is the same in the monopolar and bipolar spindles. The measured birefringence of the diminished spindle is about half that of the other two, but is not evident in this photographic reproduction. Polarization micrographs; 10 μm per scale division.

We found that cells with monopolar or cut bipolar spindles spend, on average, more than twice as much time between nuclear envelope breakdown and telophase as cells with diminished bipolar spindles (48 vs 22 min). A bipolar spindle, even though much smaller than normal, enables a

cell to traverse mitosis faster than a spindle of altered geometry. These results clearly show that the timing mechanisms are more sensitive to the spatial arrangement of spindle microtubules than the total quantity of microtubules assembled. This observation is important because it rules out simple models for the involvement of spindle microtubules in the timing mechanisms. For example, if astral microtubules are helping to move substances and organelles, such as Ca^{++} sequestering vesicles, within the cell, a monopolar spindle with its significantly longer, more plentiful astral microtubules should be more effective than the two almost imperceptible asters of the diminished bipolar spindle.

How then could spindle microtubules participate in the mechanisms that control the timing of mitotic events? Although we do not have an answer to this question, we have noted correlations that suggest directions for future research. We noted that the spindle perturbations which influence when the cell will 'decide' to initiate anaphase and finish mitosis, also influence the extent to which an egg forms a cleavage furrow: 1. When spindle microtubule assembly is prevented, mitosis is significantly prolonged and a cleavage furrow is not formed. 2. When microtubule assembly is diminished, anaphase onset is delayed and only weak cleavage furrows, if any, form. There is a correlation between the size of the spindle, the delay in anaphase onset, and the strength of the cleavage furrows formed. 3. Cells with monopolar spindles traverse mitosis slowly and usually do not show any surface activity that could be regarded as a cleavage equivalent. 4. If a spindle is cut and the half spindles moved apart, mitosis is significantly prolonged and only weak furrows, if any, are formed. In addition, studies by Rappaport have shown that astral spacing influences furrow formation. If asters are too far apart, furrows do not form [30].

These correlations, in concert with studies showing that the cleavage furrow is triggered (but not yet visible) at the time of anaphase onset [30], suggest that we should look to aster-cortex interactions for more insight into how spindle microtubules participate in the timing of the mitosis portion of the cell cycle. Perhaps an aster-cortex

interaction leads to a local physiological change which is the key transition point that commits the cell to initiate anaphase and to finish mitosis. This aster-cortex interaction is also important in organizing the cleavage apparatus, as Rappaport has shown [30]. In saying this, we do not want to imply that the assembly of the contractile ring of actin filaments or the physical constriction of the cell plays a causal role in committing a cell to finish mitosis and start the next cell cycle. The first visible manifestation of the furrow occurs well after the cell has passed the transition point that commits it to finish mitosis. We simply want to draw attention to aster-cortex interactions as a possibly key factor in the triggering of the transition point as well as the formation of the cleavage furrow.

In conclusion, our work has shown that the assembly of spindle microtubules in a spatially correct fashion is an important facet of the mechanisms that control the timing of mitotic events. Of what relevance could this be to the dividing cell? Perhaps an answer to this question is that an important aspect of mitosis is the establishment and maintenance of a number of specific spatial relationships within the dividing cell. Before the cell commits itself to anaphase, the poles must separate to establish a division axis; the chromosomes must be aligned on the metaphase plate; and daughter chromatids must be oriented to opposite poles. Failure to maintain these spatial relationships results in abnormal division and the eventual loss of viability for the daughter cells. To minimize the chances of mistakes, the control mechanism for the timing of mitotic events has two important features. First, it provides more than enough time for the assembly of the labile spindle structure. Second, both the quantity and the spatial arrangement of spindle microtubules help determine when the cell will execute the critical transition point that commits it to finish mitosis and start the next cell cycle. In this way the cell can insure that it is ready to divide correctly before it actually commits itself to completing the process.

ACKNOWLEDGMENTS

These studies were conducted in the laboratories of

Drs. Shinya Inoue, Hidemi Sato, and Daniel Mazia. We thank them for their help and the use of their facilities. We also thank Dr. George Witman for a critical reading of this manuscript. Ms. Sandy Johnson and Ms. Carol Savage were of invaluable assistance in the typing of this manuscript. We also express our appreciation of Mr. Rick Miller's important efforts in reprinting the figures. Lastly, we thank the Rockefeller University Press for copyright permission to reproduce figures from *The Journal of Cell Biology*, **80**: 674-691, 1979 and **97**: 877-886, 1983.

REFERENCES

- 1 Biesele, J. J. (1958) *Mitotic Poisons and the Cancer Problem*. Elsevier Scientific Publ. Co., Amsterdam.
- 2 Deysson, G. (1968) Antimitotic substances. *Int. Rev. Cytol.*, **24**: 99-148.
- 3 Eigsti, O. J. and Dustin, P. (1955) *Colchicine- in Agriculture, Medicine, Biology and Chemistry*. Iowa State College Press, Ames, Iowa.
- 4 Kihlman, B. A. (1966) *Actions of Chemicals on Dividing Cells*. Prentice-Hall, Inc., Englewood Cliffs, N. J.
- 5 Taylor, E. W. (1965) The mechanism of colchicine inhibition of mitosis. I. Kinetics of inhibition and the binding of ^3H -colchicine. *J. Cell Biol.*, **25**: 145-160.
- 6 Borisy, G. G. and Taylor, E. (1967) The mechanism of action of colchicine; binding of colchicine- ^3H to cellular protein. *J. Cell Biol.*, **34**: 525-533.
- 7 Borisy, G. F., Olmsted, J. B., Marcum, J. M. and Allen, C. (1974) Microtubule assembly in vitro. *Fed. Proc.*, **33**: 167-174.
- 8 Nicklas, R. B. (1971) Mitosis. In "Advances in Cell Biology, Vol 2". Ed. by M. Prescott, L. Goldstein and E. McConkey, Appleton-Century-Crofts, New York, pp. 225-297.
- 9 Tilney, L. G. (1975) Origin and continuity of microtubules. In "Origin and Continuity of Cell Organelles". Ed. by J. Rinert and H. Ursprung, Springer-Verlag, Berlin, pp. 222-260.
- 10 Sluder, G. (1979) Role of spindle microtubules in the control of cell cycle timing. *J. Cell Biol.*, **80**: 674-691.
- 11 Ray, K., Bhattacharyya, B. and Biswas, B. B. (1980) Colcemid and colchicine binding to tubulin: Similarity and dissimilarity. *Eur. J. Cell Biol.*, **2**: 288.
- 12 Sluder, G. (1976) Experimental manipulation of the amount of tubulin available for assembly into the spindle of dividing sea urchin eggs. *J. Cell Biol.*, **70**: 75-85.
- 13 Bajer, A. and Mole-Bajer, J. (1969) Formation of spindle fibers, kinetochore orientation, and behavior of the nuclear envelope during mitosis in

- endosperm, fine structural and *in vitro* studies. *Chromosoma, Berl.*, **27**: 448–484.
- 14 Sluder, G., Miller, F. J. and Spanjian, K. (1986) The role of spindle microtubules in the timing of the cell cycle in echinoderm eggs. *J. Exp. Zool.*, **238**: 325–336.
 - 15 Yoneda, M. and Schroeder, T. E. (1984) Cell cycle timing in colchicine-treated sea urchin eggs: Persistent coordination between the nuclear cycles and the rhythm of cortical stiffness. *J. Exp. Zool.*, **231**: 367–378.
 - 16 Borisy, G. G. (1971) Mechanism of U. V. reversal of colchicine inhibition of microtubule aggregation *in vitro*. Proc. 11th Ann. Meeting of Am. Soc. for Cell Biol., **27**: 35a.
 - 17 Mizel, S. B. and Wilson, L. (1972) Nucleoside transport in mammalian cells. Inhibition by colchicine. *Biochem.*, **11**: 2573–2578.
 - 18 Stadler, J. and Franke, W. W. (1974) Characterization of the colchicine binding of membrane fractions from rat and mouse liver. *J. Cell Biol.*, **60**: 297–303.
 - 19 Tyson, J. and Kauffman, S. (1975) Control of mitosis by a continuous biochemical oscillation: synchronization; spatially inhomogeneous oscillations. *J. Math. Biol.*, **1**: 289–310.
 - 20 Hara, K., Tydeman, P. and Kirschner, M. (1980) A cytoplasmic clock with the same period as the division cycle in *Xenopus-laevis* eggs. Proc. Natl. Acad. Sci. USA., **77**: 462–466.
 - 21 Mazia, D. (1961) Mitosis and the physiology of cell division. In "The Cell, Biochemistry, Physiology, Morphology, Vol. 3". Ed. by J. Brachet and A. Mirsky, Academic Press, Inc., NY, pp. 77–412.
 - 22 Levan, A. (1954) Colchicine-induced c-mitosis in two mouse ascites tumors. *Hereditas*, **40**: 1–64.
 - 23 Mole-Bajer, J. (1958) Cine-micrographic analysis of c-mitosis in endosperm. *Chromosoma, Berl.*, **9**: 332–358.
 - 24 Zirkle, R. E. (1956) Cellular Aspects of Basic Mechanisms in Radiobiology. Nuclear Science Series Report, No. 8. Research Council, Washington, DC., Publication No. 450, p. 1.
 - 25 Bajer, A. (1958) Cine-micrographic studies on chromosome movements in β -irradiated cells. *Chromosoma, Berl.*, **9**: 319–331.
 - 26 Nicklas, R. B. (1985) Mitosis in Eukaryotic Cells: An Overview of Chromosome Distribution. Aneuploidy. Ed. by V.L. Dellarco, P.E. Voytek and A. Hollaender, Plenum Publishing Corp.
 - 27 Sluder, G. and Begg, D. (1983) Control mechanisms of the cell cycle: Role of the spatial arrangement of spindle components in the timing of mitotic events. *J. Cell Biol.*, **97**: 877–886.
 - 28 Mazia, D., Harris, P. J. and Bibring, T. (1960) The multiplicity of mitotic centers and the time-course of their duplication and separation. *J. Biophys. Biochem. Cytol.*, **7**: 1–10.
 - 29 Sluder, G. and Begg, D. A. (1985) Experimental analysis of the reproduction of spindle poles. *J. Cell Sci.*, **76**: 35–51.
 - 30 Rappaport, R. (1971) Cytokinesis in animal cells. *Int. Rev. Cytol.*, **31**: 169–213.

The Mechanism of Ooplasmic Segregation in the Ascidian Egg

TOMOO SAWADA

*Department of Anatomy, Yamaguchi University School of Medicine,
Ube City, Yamaguchi 755, Japan*

INTRODUCTION

Ooplasmic segregation, the accumulation, replacement or separation of certain components in egg cytoplasm is seen in many kinds of animals [1]. The mechanism of ooplasmic segregation, as gathered from investigations performed on several types of animals, seems to be associated with the contractile activity of the egg cortex and microtubular structures such as the sperm aster. Cortical contraction probably depends on the actin filaments at the egg cortex, and microtubules also play an important role in cell division and pro-nuclear movement at the same time [2, 3]. In ascidian eggs, the actin filaments and microtubules actually provide a motile system for ooplasmic segregation at the same time they exhibit successive changes in pursuit of meiosis or mitosis. Thus, the mechanism of ooplasmic segregation can not be separated from the mechanism of the cell division, especially in very early stage of development, i.e., from fertilization through the first cleavage when several kinds of movements are occurring together in a short time.

OOPLASMIC SEGREGATION IN ASCIDIANS

Ooplasmic segregation in ascidian early development was observed in detail by Conklin in 1905 [4]. His report laid the foundation for all subsequent investigations and is still the basis of work performed today. He was the first to distinguish three different cytoplasmic components in the egg of ascidian *Styela partita* according to pigmentation and was able to trace their movement and segregation.

He designated three cytoplasmic components (endo-, meso- and ectoplasm) and then five cytoplasmic components (ecto-, endo-, myo-, chymo- and chorda-neuroplasm) according to the fates of the blastomeres which included each cytoplasm [4, 5].

Conklin and subsequent workers theorized that some component of those cytoplasmic components may control the differentiation of the cells which are each provided with different cytoplasmic components by cleavage. Ascidian early development is thus basically "mosaic" [5-8], i.e., an embryo can not form a certain organ if it does not have the corresponding cytoplasmic component or the certain component in the corresponding cytoplasm. Recent biochemical and molecular studies have established that certain components essential for cell differentiation, namely the determinants, are segregated into the specific cell lines in ascidian early development [9-14].

Myoplasm, the cytoplasmic component which is segregated into the cell line to form embryonic muscle cells [4], is the most well-investigated among the cytoplasmic components defined by Conklin. Myoplasm includes numerous mitochondria [7, 8, 15, 16] in every species as well as specifically pigmented granules or other characteristic granules in some species [4, 7, 16]. According to recent studies [10, 11], myoplasm probably includes the determinant for muscular development. Myoplasm is distributed just beneath the egg cortex in unfertilized eggs as a layer which is thick near the vegetal pole and absent around the animal pole (Figs. 2A and 4A). The inner part of the egg is occupied by many yolk granules [4, 7, 16]. Within 2-3 min after fertilization, the myoplasm moves down and gathers near the vegetal pole (Figs. 2B and 4B, C, D). At the same time, inner yolk granules automatically fill

part of animal side of the myoplasm [4, 16, 17]. This movement is the first phase of ooplasmic segregation [7]. Myoplasm moves up again to the equatorial region after the second meiosis is completed (Fig. 4G, H, I). This is the second phase [7] of ooplasmic segregation and the myoplasmic crescent, the so-called yellow crescent according to Conklin's study in *Styela partita*, is formed by this movement. The side on which the myoplasmic crescent is formed corresponds to the posterior side of the embryo [4, 7, 8].

The movement of myoplasm described above is very clear and easy to trace even in species whose eggs do not have a special pigmentation in the myoplasm, by staining for mitochondria using Janus green [18], rhodamine 123 [19] or ethidium bromide [20]. Therefore, the movement of myoplasm has been observed mainly in ooplasmic segregation and the mechanism of its movement has been investigated well.

STUDIES ON THE MECHANISM OF OOPLASMIC SEGREGATION

There have been only few investigations regarding the mechanism of ascidian ooplasmic segregation in contrast to the many studies on the role of ooplasmic segregation in development. Costello [21] tried to explain ooplasmic movement of ascidian eggs by the 'diffusion effect' [22], although he was not successful.

As already mentioned, until first mitosis, ascidian ooplasmic segregation can be divided into two phases. They differ in the manner of cytoplasmic movement and in the motile mechanism for it. The first phase movement of ooplasmic segregation takes place within a short time (Fig. 4A, B, C, D). It starts within 30 sec after fertilization and occurs in 2–3 min in *Ciona savignyi** [16]. It is known that the egg cortex contracts and the test cells and particles on the egg surface are carried to the vegetal pole at the same time the myoplasm moves down to the vegetal pole [16, 24]. Recent evidence strongly supports the speculation that this contraction provides the motive force of the first phase

movement. The *Ciona savignyi* [16] egg was used to make detailed observations of the cortical contraction because shape modification upon cortical contraction is dramatic and an exceptionally clear constriction, not apparent in other species, in the course of this contraction (Fig. 1). The results suggested that the constriction is formed by the contraction of the cortex as a whole of the vegetal side, as clearly indicated by the accumulation of microvilli on the vegetal side surface which are equally distributed before fertilization. The disappearance of microvilli on the animal side indicates that the animal surface is expanded. Upon further contraction of the vegetal side cortex, the constriction shifts (Fig. 1) toward the vegetal pole [16]. It is as if the original cortex of the unfertilized egg, together with the subcortical myoplasm underlying the cortex, peels off and accumulates at the vegetal pole. This contraction is independent of the inner cytoplasm and is probably caused by the contractile structure specified at the cortex [25, 26]. This contractile structure is believed to be actin filaments because cytochalasin B [16, 27, 28]

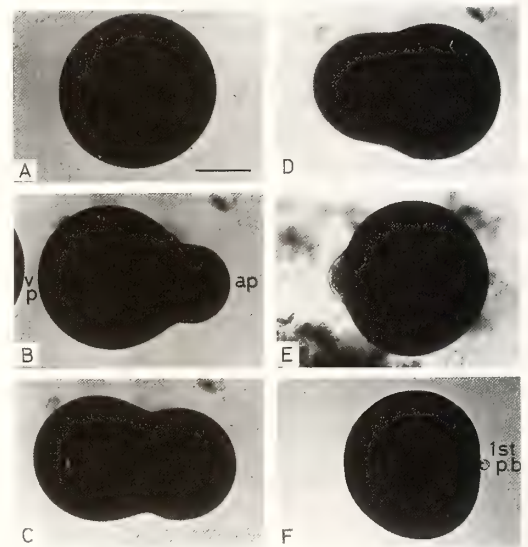


FIG. 1. Modification of egg shape in the first phase of ooplasmic segregation of *Ciona savignyi*. A. Unfertilized egg, the bar indicates 50 μ m. B–E. Successive shape modification of fertilized eggs from 1 to 3 min after insemination. The 'cap' is formed at the vegetal pole in E. F. After the formation of the first polar body (pb). ap, animal pole. vp, vegetal pole. (From Sawada and Osanai 1981 with permission).

* Previously known as *Ciona intestinalis* in Japan; re-defined as *Ciona savignyi* [23].

inhibits contraction and cytoplasmic movement. The existence of actin filaments in the contracting cortex was revealed [29, 30] and its distribution corresponds to the manner of cortical contraction [30]. This cortical contraction seems to be triggered by an increase in cytoplasmic Ca^{++} -ion. For calcium ionophore A23187 or direct injection of Ca^{++} -ion [31] is able to induce the contraction. An increase in Ca^{++} -ion during normal fertilization has also been detected [32]. The control mechanism which induces polarized contraction of such a wide area of egg cortex is not clear. More on this matter is discussed later.

In spite of the progress made in the investigations of the first phase movement, there have been only a few studies on the second phase movement. The second phase has sometimes lacked in investigations and arguments about the mechanism of ascidian ooplasmic segregation, it is an important step because this movement actually completes the myoplasmic crescent. As mentioned before, this phase is clearly independent and different from the first phase. Early investigators reported coincidences in the localization of sperm aster and myoplasm and their movement, expecting a role of the sperm aster as motile mechanism in this phase [4, 7, 8]. Inhibition of myoplasmic movement by colcemid and nocodazole in the second phase (Sawada and Schatten, unpublished data) supports the speculation that microtubular components, such as the sperm aster, are involved in the second phase movement of myoplasm. Detailed observations of the microtubular distribution in opaque ascidian eggs became possible using immunofluorescence [20]. By this method, serial changes in the microtubules of ascidian eggs during fertilization and ooplasmic segregation were revealed (Fig. 4) and experimental studies on the microtubular structures became possible.

SCHEMATIC MODEL OF THE MECHANISM OF OOPASMIC SEGREGATION

First phase movement After recent studies on the mechanism of the first phase movement, Jeffery [29, 33, 34] and I [16, 25, 35] proposed schematic models for the cortical contraction and cytoplasmic movement. Both of us mention that

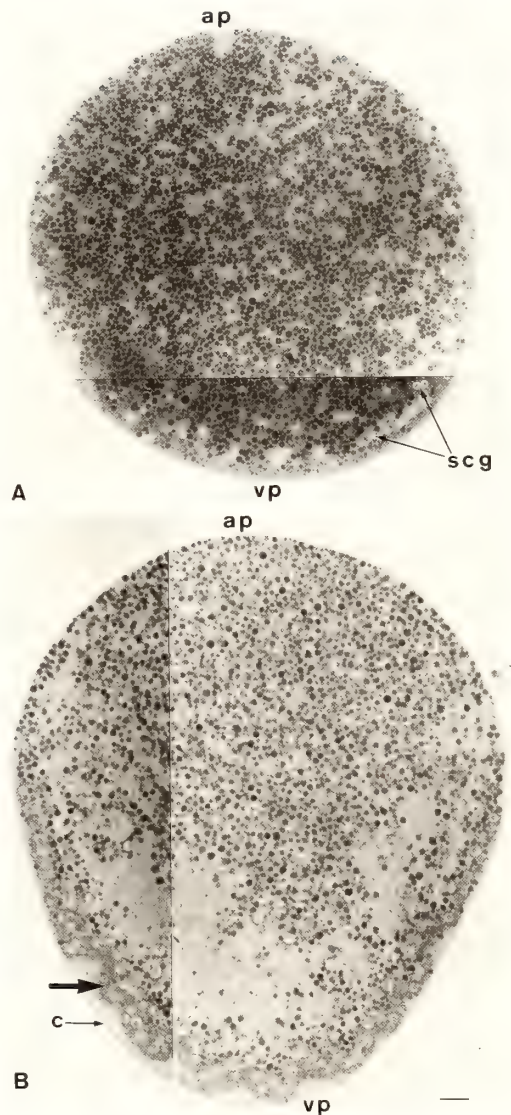


FIG. 2. Light micrographs of an unfertilized egg (A) and fertilized egg at the late stage of cytoplasmic movement (B) in *Ciona savignyi*. Subcortical granules (scg), specifically distributed in myoplasm and used as marker for the distribution of myoplasm, exist in the subcortical layer except for around the animal pole in the unfertilized egg (A). Myoplasmic layer (relatively dark area indicated by thick arrow in B) makes a fold and a gap is formed between the myoplasmic layer and the densely-stained cortex (c in B) of the vegetal area. ap, animal pole. vp, vegetal pole. Bar is 10 μ m. (B, from Sawada 1983 with permission).

the bipolar cytoplasmic segregation in the first phase is caused by the polarized contraction of the network of actin filaments underlying the egg surface and that this contraction is probably triggered by an increase in Ca^{++} -ion which widely occurs in animal eggs. However, there is a differ-

ence between the two models with regard to the distribution of the cortical actin network in the unfertilized egg. In Jeffery's model (1983, Fig. 3), the network covers all of the egg. In my model (Fig. 4A, B, C, D), an unequal distribution of actin filaments exists prior to fertilization and the

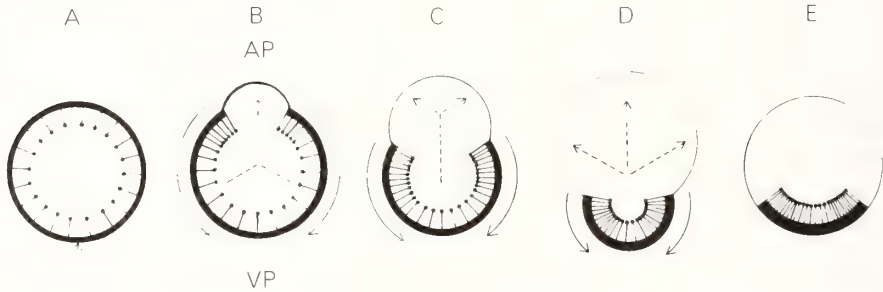


FIG. 3. The Jeffery and Meier model (1983) for the first phase of ooplasmic segregation. (A) An unfertilized egg. The vertical arrow indicates the future focal point for segregation. (B-D) Fertilized eggs in the process of ooplasmic segregation. The arrows show the directions of ooplasmic movement; solid line arrows represent myoplasm and broken line arrows represent the endoplasm. (E) Zygote which has completed the first phase of ooplasmic segregation. In each diagram, the thick egg boundaries represent the parts of the plasma membrane with PML (plasma membrane lamina, actin filament-network) underneath, and the thin egg boundaries represent the parts of the plasma membrane without PML. The structures attached to the inside of the thick egg boundary represent the deep filamentous lattice (DFL, probably consisting of intermediate filaments) and its associated components, pigment granules and localized mRNA molecules of myoplasmic cytoskeletal domain. Ap, animal pole; VP, vegetal pole. (From Jeffery and Meier 1983 with permission).

FIG. 4. My model for the first movement (A-D) and schematic representation of the serial changes of myoplasmic localization and sperm or mitotic aster in subsequent stages (E-L). Thick lines (in A-D) represent the cortical actin filament-network. The distribution of the cortical actin filament is ignored in E-L because it is not clearly known at those stages yet. Shape changes in E-L are also ignored for the same reason. Approximate time after insemination is indicated at the lower right side of the figures.

The cortical actin filaments are absent or very sparse near the meiotic spindle (ms) at the animal pole in the unfertilized egg (A). After the activation of the egg, the actin filament-network begins to contract so as to form a contracting 'basket' with its mouth near the animal pole. This contraction creates a constriction at the mouth of the 'basket' (B), causes the drifting of the constriction toward the vegetal pole (C) and finally results in the formation of a small cap at the vegetal pole (D). The myoplasm (dotted area) is dragged by this contraction, and infolding at a late stage of its movement (C), is gathered near the vegetal pole (D). The inner yolk is pushed out of the constricted part (the mouth of the 'basket') toward the animal pole (B-D, arrows indicate the direction of movement of the inner yolk).

The meiotic spindle rotates during this movement and becomes vertical to the egg-surface (E). A spermatozoon could then bind and fuse in the animal hemisphere and in that case, is carried to the vegetal pole (B-D). (The spermatozoon is supposed to be able to bind and fuse anywhere on the egg surface.) The sperm aster first appears near the vegetal pole at a late stage of first meiosis and the male nucleus (mn) swells (E). The sperm aster, keeping its center just beneath the cortex, grows slowly during first (E, F) and second (G) meiosis and rapidly becomes large after second meiosis is completed (H).

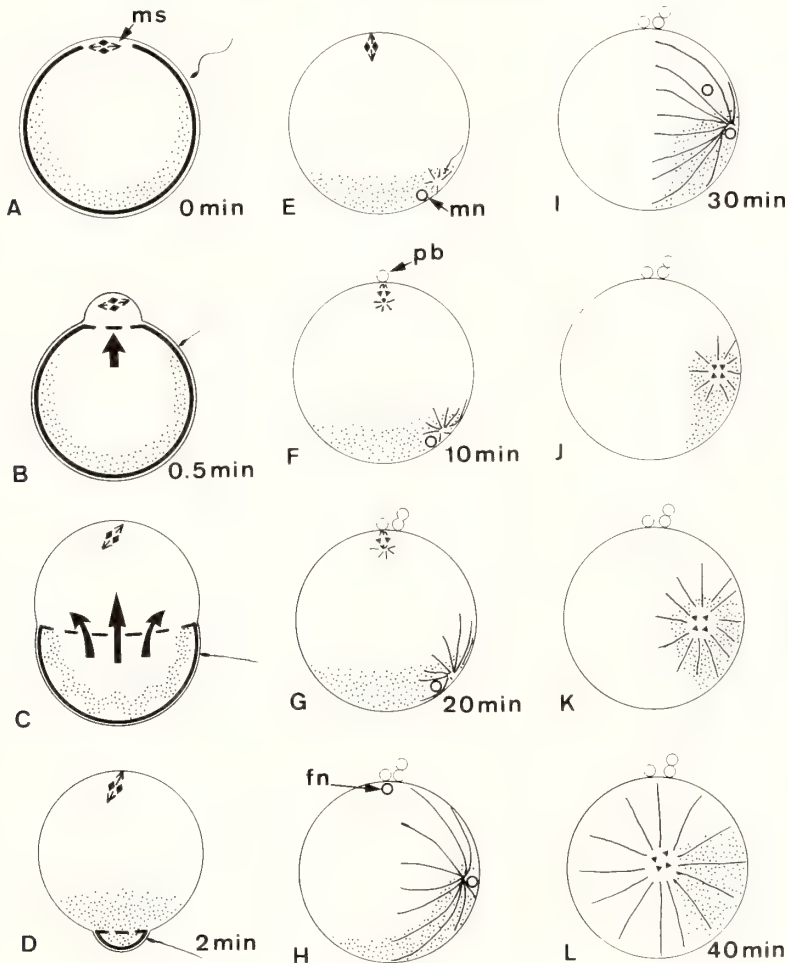
As the sperm aster grows into a large and unusually asymmetric aster, its center relocates to the equatorial region on the posterior side (H). The myoplasm undergoes the second phase movement (G-I), associated with the behavior of the sperm aster, from the vegetal pole up to the posterior-equatorial region and forms the myoplasmic crescent (I). The female pronucleus (fn) migrates toward the male pronucleus (I).

Then, the large sperm aster reduces into two small mitotic asters and chromosomes are formed. As the mitotic asters grow, they migrate into the center of the egg (J-L, mitotic spindle and another aster on the opposite side can not be seen from this direction). pb: polar body.

actin network does not cover or becomes sparse at the animal pole. Once the contraction starts, the whole cortex (Jeffery's model, 1983) or the whole cortex except for the animal pole (my model) contracts gathering into a small region near the vegetal pole. This contraction is not the one in which the cortex contracts only along the animal-vegetal direction but the one in which the cortex contracts in all directions [35], as to reduce the area of the original cortex, as in my model. Naturally, it also reduces the volume of the sphere covered by the original cortex (Figs. 3 and 4B, C, D). It is clear that a constriction, seen in *Ciona savignyi*, is formed at the border between the contracting area and the expanding area [16]. The appearance of the constriction means that contractile force also exists along the border. In eggs

which do not form a clear constriction during normal development such as the eggs of *Molgula occidentalis* [20] or *Halocynthia roretzi*, an apparent constriction can be produced when the eggs are put into a detergent solution, probably as a result of reducing internal pressure by breaking the membrane barrier (unpublished data), indicating the presence of a constricting force.

Cortical contraction causes movement of the egg surface and cytoplasm beneath it. As described before, myoplasm (or subcortical cytoplasm [16] according to its distribution) is located underneath the cortex (Figs. 2-4). This cytoplasm has a certain rigidity so as to allow a folding (Figs. 2B and 4C) of the myoplasmic layer during its movement [35]. Intermediate filaments were observed in the myoplasm of *Styela plicata* [29] as cytoskeletal



structures and they may possibly provide a structural connection between the cortex and myoplasmic layer (Fig. 3). Regardless, the contraction of the cortex would force the myoplasm to move toward the vegetal pole (Figs. 3 and 4). The connection between the myoplasm and the cortical actin network may be not so tight in the sense that the dislocation between the surface constriction and the border of myoplasm distribution occurs during movement (Fig. 4D), as observed in *Ciona savignyi*. In spite of this movement of myoplasm toward the vegetal pole, the inner yolk moves toward the animal pole, pushed by the contraction of the cortex out of the constricted part (Fig. 3: broken line arrows, Fig. 4: thick arrows). There may not be a clear boundary between the part which moves toward the animal pole and the part moving toward the vegetal pole. At least in *Halocynthia roretzi* eggs [35], the myoplasm all seems to all move toward the vegetal pole along with the outer part of the inner yolk mass.

Thus, the contraction of most of the egg cortex into the small region around the vegetal pole is the most important component of the mechanism of first phase movement. How the polarity of this contraction is generated is not absolutely clear, however. Jeffery proposed that the sperm entrance at the vegetal pole makes it the focal point of the cortical contraction in *Styela plicata* [29, 33]. On the other hand, in a previous paper, I proposed that the polarity of the cortical contraction is caused by the unequal distribution of the cortical actin filaments [35], and supposedly pre-exists in the unfertilized egg (actin filaments would be very sparse or would not exist at the animal pole).

Jeffery and Meier [29] (Fig. 3) speculated that the entrance or the first effective binding of a spermatozoon leads to the increase of cytoplasmic Ca^{++} -ion and the increase propagates the egg surface and originates the polarity of the contraction [35]. However, the current model by Jeffery and Bates [34] excludes the specificity of the sperm entrance at the vegetal pole. A wave-propagation of increased Ca^{++} -levels is observed in the eggs of some kinds of animals [36, 37] including the ascidian *Phallusia mammilata* [32]. In addition, Conklin [4] and Reverberi [8] reported that the incorporated spermatozoon is first found near the

vegetal pole. However, the first binding site of the spermatozoon in an ascidian egg has not been defined because the cortical contraction can carry the spermatozoon within 30–60 sec after fertilization, when it is on the surface or even beneath the cortex. In *Ciona savignyi*, spermatozoa first attach themselves all over the egg surface, but it was not possible to identify which spermatozoon bound effectively and then moved to the vegetal pole after cortical contraction [16]. Recently, Sardet *et al.* [38] reported that a membrane-fused spermatozoon is found more frequently in the animal hemisphere than the vegetal and it becomes restricted near the vegetal pole in the fertilization of *Phallusia mammilata*. In addition, when the cortical contraction is inhibited by cytochalasin E, the sperm aster can even be found near the animal pole with astral rays extending over the meiotic spindle [39].

The application of a concentration-gradient of calcium ionophore A23187 induces a crescent formation on the side of high concentration [40]. These observations might suggest that differences in the cytoplasmic Ca^{++} -ion concentration cause the polarized contraction of the egg cortex. It should be also noted, though, that activation by calcium ionophore A23187 is not same as that by a spermatozoon in propagation. Point-activation by calcium ionophore sometimes does not propagate all over the egg in sea urchin [41].

I speculated (Fig. 4A, B, C, D) that the local weakening of the cortex at the animal pole of the unfertilized egg (Fig. 4A) resulting from a sparse or absent cortical actin filament-network leads to the polarized contraction of the cortex. In *Ciona savignyi*, fluorescent staining with NBD-phalloidin revealed that there is a quantitatively unequal distribution of cortical actin filaments in the unfertilized egg [42]. Recently, Jeffery and Bates observed a defect in the cortical cytoplasm at the animal pole in *Styela plicata* (personal communication). They also think that the cortical actin-filament network does not exist at the animal pole in their current model [34], but the unequal distribution of actin filaments has not been confirmed in other species.

Second phase movement There have been very few studies concerning the second phase move-

ment, except for the observation of myoplasmic movement and the sperm aster by early workers [7, 8]. Coincidence in the location of myoplasm and sperm aster should be noted. Recent observations revealed that the sperm aster grew very large during this movement (Fig. 4K), extending its rays through the myoplasm to occupy half the volume of the egg and finally forming a very asymmetric aster with its center just beneath the cortex in the posterior-equatorial region (Fig. 4H). Along with its own growth after meiosis, the sperm aster moves from the vegetal pole to the posterior side. Sardet *et al.* observed that the myoplasm exhibited pulsatory movement, as if it were being pulled by the sperm aster, and then rapidly moved into the posterior region [38]. Myoplasmic movement up to the posterior region is inhibited by colcemid. More importantly, the mitochondria (the major component of myoplasm) as well as the asteral area became concentrated into a microtubule cluster when polar body-elimination was inhibited by cytochalasin E. The microtubule cluster is formed near the animal pole around the chromosomes descended from excess female pronuclei [39]. Thus, the observations suggest that the sperm aster plays a major role in second phase movement, at least in the myoplasmic movement. In many types of cells, there is a connection between cytoplasmic components and microtubules or a transportation of cytoplasmic granules along microtubules [43, 44]. Therefore, it could be considered that myoplasmic components such as mitochondria and pigmented granules are associated with microtubules and are carried in a centripetal direction, sometimes along with the microtubules of the sperm aster. This relationship may create the condition whereby the myoplasm is held by the sperm aster. Finally this relation between sperm aster and myoplasm leads to a corresponding spatial distribution and movement of myoplasm (Fig. 4G, H, I). However, a detailed investigation of the second phase movement is only beginning and so, much about the mechanism of the second phase movement remains as yet unknown.

ASCIDIAN OOPLASMIC SEGREGATION IN COMPARISON WITH OTHER CELL MOTILITIES

As already mentioned, the two major systems of cellular motility, microtubules and actin filaments, are apparently involved in the mechanism of ascidian ooplasmic segregation. The type of cortical contraction in the ascidian egg, i.e., where the cortex contracts in a wide area so as to reduce that area, may not be unique to the ascidians. Cortical contraction induced by ionophore A23187 in the frog egg is considered to be the same type of contraction, resulting in a 'cap' formation and accumulation of pigmented cytoplasm [45]. These types of cortical contractions or movements of cytoplasmic components associated with cortical contractions are observed in mollusks [46–49], annelids [50, 51], fish [52] and amphibians [53]. In mouse oocytes, the contractile activity which forms a furrow near the first meiotic apparatus is observed during the rotation of meiotic spindle [54]. There seems to be a similarity between such furrowing in mouse oocytes and the constriction-forming contraction of the ascidian *C. savignyi* egg at activation. The rotation of the meiotic spindle also occurs in ascidian eggs during this contraction [20].

Intra-cellular movements associated with microtubules are also seen widely in animal cells. Pronuclear migration is associated with microtubules in the sea urchin [2, 3].

The major components of the motile system in ascidian ooplasmic segregation are also the important components of motility in fertilization, karyokinesis and cytokinesis. Cortical actin filaments cause serial shape-modification through meiosis and mitosis, including constriction during polar body-formation and cleavage. The sperm aster may provide the motive force for pronuclear migration and would subsequently participate in the organization of mitotic asters. The structures are not unique to ascidian eggs, but very common in animal eggs. It is interesting and important that the structures in common are the main components in the mechanism of ooplasmic segregation unique to ascidian eggs. The movement in ooplasmic segregation of ascidian eggs might be an

extension of the cytoplasmic movements more or less common in animal eggs, i.e., having structures in common. The common components are uniquely constructed to produce a characteristic ascidian ooplasmic segregation.

ACKNOWLEDGMENT

The author is grateful to Dr. K. Osanai and all staffs in Asamushi Marine Biological Station of Tohoku University for many advices and technical supports. The Jean and Katsuma Dan Foundation is thanked for financial support. Particular thanks are due to Drs. G. and H. Schatten (University of Wisconsin, Madison) for their appropriate advices and discussions in the research on microtubules of the ascidian egg and to Dr. W. R. Jeffery (University of Texas, Austin) for permission to use his scheme in Figure 3.

REFERENCES

- Davidson, E. H. (1986) Cytoplasmic localization. In "Gene Activity in Early Development. Third Edition". Ed. by E. H. Davidson, Academic Press, Orlando, pp. 411-513.
- Schatten, G. (1983) Motility during fertilization. *Endeavour*, New Series, **7**: 173-182.
- Schatten, G. and Schatten, H. (1981) Effects of motility inhibitors during sea urchin fertilization. *Exp. Cell Res.*, **135**: 311-330.
- Conklin, E. G. (1905) The organization and cell-lineage of the ascidian egg. *J. Acad. Natl. Sci. Phila.*, **13**: 1-119.
- Conklin, E. G. (1905) Mosaic development in ascidian eggs. *J. Exp. Zool.*, **2**: 145-223.
- Minganti, A. (1960) Recent investigations on the development of ascidians. In "Symposium on the Germ Cells and Earliest Stages of Development". Ed. by S. Ranzi, Institut Intern. d'Embryologie and Fondazione A. Beselli, Milan, pp. 255-276.
- Reverberi, G. (1961) The embryology of ascidians. *Adv. Morphogenesis*, **1**: 55-101.
- Reverberi, G. (1971) Ascidians. In "Experimental Embryology of Marine and Fresh-Water Invertebrates". Ed. by G. Reverberi, North-Holland Publ. Co., Amsterdam, pp. 507-550.
- Whittaker, J. R. (1973) Segregation during ascidian embryogenesis of egg cytoplasmic information for tissue specific enzyme development. *Proc. Natl. Acad. Sci. USA*, **70**: 2096-2100.
- Whittaker, J. R. (1979) Cytoplasmic determinants of tissue differentiation in the ascidian egg. In "Determinants of Spetial Organization". Ed. by S. Subtelny and J. R. Konigsberg, Academic Press, New York, pp. 29-51.
- Deno, T. and Satoh, N. (1984) Studies on the cytoplasmic determinant for muscle cell differentiation in ascidian embryos: An attempt at transplantation of the myoplasm. *Dev. Growth Differ.*, **26**: 43-48.
- Nishida, H. and Satoh, N. (1985) Cell lineage analysis in ascidian embryos by intracellular injection of a tracer enzyme. II. The 16- and 32-cell stages. *Dev. Biol.*, **110**: 440-454.
- Meedel, T. H., Crowther, R. J. and Whittaker, J. R. (1987) Determinative properties of muscle lineages in ascidian embryos. *Development*, **100**: 245-260.
- Jeffery, W. R. (1985) Specification of cell fate by cytoplasmic determinants in ascidian embryos. *Cell*, **41**: 11-12.
- Mancuso, V. (1963) Distribution of the components of normal unfertilized eggs of *Ciona intestinalis* examined at the electron microscope. *Acta Embryol. Morphol. Exp.*, **6**: 260-274.
- Sawada, T. and Osanai, K. (1981) The cortical contraction related to the ooplasmic segregation in *Ciona intestinalis* egg. *Roux's Arch. Dev. Biol.*, **190**: 208-214.
- Mancuso, V. (1964) The distribution of the ooplasmic components in the unfertilized, fertilized and 16-cell stage egg of *Ciona intestinalis*. *Acta Embryol. Morphol. Exp.*, **7**: 71-82.
- Reverberi, G. (1956) The mitochondrial pattern in the development of the ascidian egg. *Experientia*, **12**: 55-60.
- Zalokar, M. and Sardet, C. (1984) Tracing of cell lineage in embryonic development of *Phallusia mammillata* (Ascidia) by vital staining of mitochondria. *Dev. Biol.*, **102**: 195-205.
- Sawada, T. and Schatten, G. (1985) Relation between the microtubule system and cytoplasmic movement in ascidian egg. *Zool. Sci.*, **2**: 948.
- Costello, D. P. (1948) Ooplasmic segregation in relation to differentiation. *Ann. New York Acad. Sci.*, **69**: 663-683.
- Teorell, T. (1937) Studies of the diffusion effect upon ionic distribution. II. Experiments on ionic accumulation. *J. Gen. Physiol.*, **21**: 107-122.
- Hoshino, Z. and Nishikawa, T. (1985) Taxonomic studies of *Ciona intestinalis* (L.) and its allies. *Publ. Seto Mar. Biol. Lab.*, **30**: 61-79.
- Ortolani, G. (1955) I movimenti corticali dell'uovo di ascidie alla fecondazione. *Riv. Biol.*, **46**: 169-177.
- Sawada, T. and Osanai, K. (1984) Cortical contraction and ooplasmic movement in centrifuged or artificially constricted eggs of *Ciona intestinalis*. *Roux's Arch. Dev. Biol.*, **193**: 127-132.
- Jeffery, W. R. and Meier, S. (1984) Ooplasmic segregation of the myoplasmic actin network in strat-

- ified ascidian eggs. Roux's Arch. Dev. Biol., **193**: 257-262.
- 27 Zalokar, M. (1974) Effect of colchicine and cytochalasin B on ascidian egg. Wilhelm Roux's Arch., **175**: 243-248.
- 28 Reverberi, G. (1975) On some effect of cytochalasin B on the eggs and tadpoles of the ascidians. Acta Embryol. Exp., **2**: 137-158.
- 29 Jeffery, W. R. and Meier, S. (1983) A yellow crescent cytoskeletal domain in ascidian eggs and its role in early development. Dev. Biol., **96**: 125-143.
- 30 Sawada, T. and Osanai, K. (1985) Distribution of actin filaments in fertilized egg of the ascidian *Ciona intestinalis*. Dev. Biol., **111**: 260-265.
- 31 Sensui, S. (1987) Reinitiation of meiosis in ascidian egg by the injection of calcium ion. Zool. Sci., **4**: 1041.
- 32 Speksnijder, J. E., Corson, D. W., Jaffe, L. F. and Sardet, C. (1986) Calcium pulses and waves through ascidian eggs. Biol. Bull., **171**: 488.
- 33 Jeffery, W. R. (1984) Pattern formation by ooplasmic segregation in ascidian eggs. Biol. Bull., **166**: 277-298.
- 34 Jeffery, W. R. and Bates, W. R. (1988) Ooplasmic segregation in the ascidian *Styela*. In "Molecular Biology of Fertilization". Ed. by H. Schatten and G. Schatten, Academic Press, N. Y., In press.
- 35 Sawada, T. (1983) How ooplasm segregates bipolarly in ascidian eggs. Bull. Mar. Biol. Stn. Asamushi, Tohoku Univ., **17**: 123-140.
- 36 Gilkey, J. C., Jaffe, L. F., Ridgway, E. B. and Reynolds, G. T. (1987) A free calcium wave traverses the activating egg of Medaka, *Oryzias latipes*. J. Cell Biol., **76**: 448-466.
- 37 Kubota, H. Y., Yoshimoto, Y., Yoneda, M. and Hiramoto, Y. (1987) Free calcium wave upon activation in *Xenopus* eggs. Dev. Biol., **119**: 129-136.
- 38 Sardet, C., Inoue, S., Jaffe, L. F. and Speksnijder, J. E. (1986) Surface and internal movements in fertilized *Phallusia* eggs. Biol. Bull., **171**: 488.
- 39 Sawada, T. and Schatten, G. (1988) Microtubules in ascidian egg during meiosis, fertilization and mitosis. Cell Motil. Cytoskel., **9**: 219-230.
- 40 Jeffery, W. R. (1982) Calcium ionophore polarizes ooplasmic segregation in ascidian eggs. Science, **216**: 545-547.
- 41 Chambers, E. L. and Hinkley, R. E. (1979) Non-propagated cortical reactions induced by the divalent ionophore A23187 in eggs of sea urchin, *Lytechinus variegatus*. Exp. Cell Res., **124**: 441-446.
- 42 Sawada, T. (1986) Cortical actin filaments in unfertilized eggs of *Ciona savignyi*. Zool. Sci., **3**: 1038.
- 43 Allen, R. D., Weiss, D. G., Hayden, J. H., Brown, D. T., Fujiwake, H. and Simpson, M. (1985) Gliding movement of bidirectional transport along single native microtubules from squid axoplasm: Evidence for and active role of microtubules in cytoplasmic transport. J. Cell Biol., **100**: 1736-1752.
- 44 Heggeness, M. H., Simon, M. and Singer, S. J. (1978) Association of mitochondria with microtubules in cultured cells. Proc. Natl. Acad. Sci. USA, **75**: 3863-3866.
- 45 Schroeder, T. E. and Strickland, D. L. (1974) Ionophore A23187, calcium and contractility in frog egg. Exp. Cell Res., **83**: 139-142.
- 46 Conrad, G. W. (1973) Control of polar lobe formation in fertilized egg of *Ilyanassa obsoleta* Stimpson. Am. Zool., **13**: 961-980.
- 47 Schmidt, B. A., Kelly, P. T., May, M. C., Davis, S. E. and Conrat, G. W. (1980) Characterization of actin from fertilized eggs of *Ilyanassa obsoleta* during polar lobe formation and cytokinesis. Dev. Biol., **76**: 126-140.
- 48 Dohmen, M. R. and Van der Mey, J. C. A. (1977) Local surface differentiations at the vegetal pole of the egg of *Nassarius reticulatus*, *Buccinum undatum* and *Grepidula fornicata* (Gastropoda, Prosobranchia). Dev. Biol., **61**: 104-113.
- 49 Speksnijder, J. E., Mulder, M. M., Dohmen, M. R., Hage, W. J. and Bluemink, J. G. (1985) Animal-vegetal polarity in the plasma membrane of a molluscan egg: A quantitative freeze-fracture study. Dev. Biol., **108**: 38-48.
- 50 Shimizu, T. (1984) Dynamics of the actin microfilament system in the *Tubifex* egg during ooplasmic segregation. Dev. Biol., **106**: 414-426.
- 51 Shimizu, T. (1986) Bipolar segregation of mitochondria, actin network, and surface in the *Tubifex* egg: Role of cortical polarity. Dev. Biol., **116**: 241-251.
- 52 Iwamatsu, T. (1973) On the mechanism of ooplasmic segregation upon fertilization in *Oryzias latipes*. Jpn. J. Ichthyol., **20**: 73-78.
- 53 Palecek, J., Ubbels, G. A. and Rzehak, K. (1978) Change of the external and internal pigment pattern upon fertilization in the egg of *Xenopus laevis*. J. Embryol. Exp. Morphol., **45**: 203-214.
- 54 Maro, B. (1985) Fertilization and the cytoskeleton in the mouse. BioEssays, **3**: 18-21.

The Contraction Wave in the Cortex of Dividing Neuroblasts of the Grasshopper

KEN-YA KAWAMURA

Laboratory of Biology, Rakuno Gakuen University,
Ebetsu, Hokkaido 069, Japan

ABSTRACT—Grasshopper neuroblasts divide unequally to produce a large daughter neuroblast to the ventral side of the embryo, and a small daughter ganglion cell (GC) to the dorsal side. Since the unequal division maintains a fixed polarity for many cell generations, a column of GCs is formed on one side of the neuroblast. In the present study, cortical movements throughout the mitotic cycle were analyzed by means of photokymography in both normal and Cytochalasin B (CB)-treated neuroblasts. In normal cells, a contraction wave (CW), which appeared at the cap cell (CC) pole at middle anaphase (opposite to the GC-side pole of the neuroblast), traveled toward the GC-side pole and disappeared upon reaching the GC pole at late anaphase. Only one transition of the CW was observed in normal neuroblasts, whereas repeated appearances of CWs at regular intervals occurred in CB-treated cells. The close correlation between CWs and mitotic stages suggests that the CW plays an important role in the unequal division of the neuroblast.

INTRODUCTION

Since 1937, Carlson [1] and his collaborators [2] have used living neuroblasts of the grasshopper in hanging-drop preparations for various experimental studies. The neuroblast exhibits a definite polarity from cell generation to cell generation. This is manifested in the piling up of ganglion cells (GC) on one side of the neuroblast. Each neuroblast of *Chortophaga* has one or more cap cells (CC) on the ventral side of the embryo and a column of GCs extending dorsally from it. During prometaphase and metaphase, the spindle is located on the CC-side. As the spindle body shifts to the GC pole of the neuroblast during anaphase, the cell divides unequally to form a large daughter neuroblast and a small daughter GC.

Using a microdissection technique on neuroblasts, Carlson [3] and Kawamura [4, 5] obtained information which indicates that the cell cortex plays a significant role in the orientation and shifting of the spindle body.

The aim of the present study is to analyze the

cortical movements of grasshopper neuroblasts during unequal division by using the time-lapse cinematography and photokymography.

MATERIALS AND METHODS

Embryos of the grasshopper, *Chortophaga viridifasciata* (De Geer), 15–16 days old at 26°C were used. Cover glasses, instruments and culture medium were sterilized with UV light before use in experiments.

For microscopic observation, an embryo was placed on a cover glass with a small amount of culture medium which did or did not contain 0.1 µg/ml Cytochalasin B (CB). The cover glass was inverted over a slide glass on which a few peices of short fiberglass and FC-47 oil were set beforehand.

Neuroblasts were observed with a Nomarski differential interference microscope (Olympus) at 40× objective. The mitotic process at 26°C was recorded by using a time-lapse cine camera (Bolex H 16) at the rate of 10 frames per minute.

The movements on the cell surface during cell division were analyzed by the following method (Fig. 1). The image of the film was projected at a

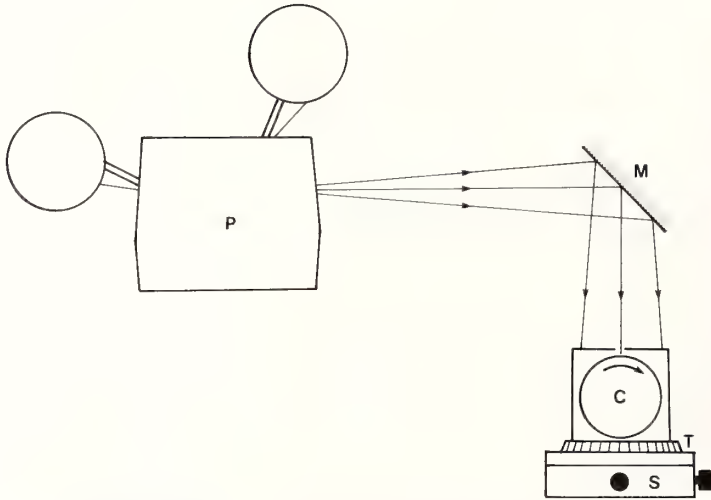


FIG. 1. The setup for photographic analysis of cortical movement during cell division. The image of a dividing neuroblast recorded on 16 mm cine film is projected with a projector (P) through a narrow slit on moving photographic paper in a paper camera (C) fixed on a turntable (T) and a mechanical stage (S). M: mirror.

constant frame rate on a sheet of photographic paper loaded in a paper camera (C) through a narrow slit. In order to set the axis of a spindle body in the image perpendicular to the slit, the position of the paper camera was adjusted using the mechanical stage (S) and turntable (T). The photographic paper under the slit was moved at a constant speed, so that the continuous movement of the cell surface could be recorded on a sheet of photographic paper. At first, the position of the slit was fixed at the pole of the cap cell (CC)-side of the neuroblast throughout one mitotic cycle. Then the position was moved 4 mm toward the ganglion cell (GC)-side and fixed during repeated projection of the same cell division. The same procedure was repeated until the position of the slit reached the GC-side pole of the cell. Since the whole cell was magnified 1600 times on the photographic paper, 4 mm corresponds to $2.5 \mu\text{m}$ of the cell. Fifteen sheets of photographic paper were thus needed for the largest neuroblast (56 mm image) in one mitotic cycle, and eleven sheets for the smallest (40 mm image).

From these photokymographs, we can analyze at what mitotic stage as well as where on the cell surface the contraction wave (CW) passes through during cell division.

The mitotic stages in the present study are

classified according to Carlson [6].

RESULTS

As reported in a previous paper [7], the neuroblast of *Chortophage* is a relatively large cell containing a peculiarly shaped nucleus. The nucleus is roughly hemispherical with a central cytoplasmic core that coincides with the spindle axis or the division axis. Each neuroblast has one or more cap cells (CC) on the ventral side of the embryo and a column of ganglion cells (GC) extending dorsally from it. At very late prophase, a tiny spindle with well-developed astral rays appears in the nuclear core cytoplasm. When the nuclear membrane becomes indistinct along the contour of the core, a gradual fusion of the nuclear substance into the cytoplasmic spindle takes place. During prometaphase and metaphase, the spindle is closer to the CC than GC. The spindle size and volume increase remarkably during anaphase and at the same time, the spindle body shifts to the GC-side. When the cell enters late anaphase (A5), a cleavage furrow is initiated across the middle part of the spindle body. After the furrow region of the cell surface attaches to the spindle body, further furrowing is accompanied by a remarkable reduction of the spindle volume. As the spindle at this stage

is closer to the GC-side pole, the neuroblast divides unequally to form a large daughter neuroblast and a small daughter GC. Finally, a nuclear membrane is formed in both daughter cells. The daughter cells are quite different in cell size, nu-

clear size and shape, and in mitotic activity. Unequal cell division in the living neuroblast is shown in Figure 2.

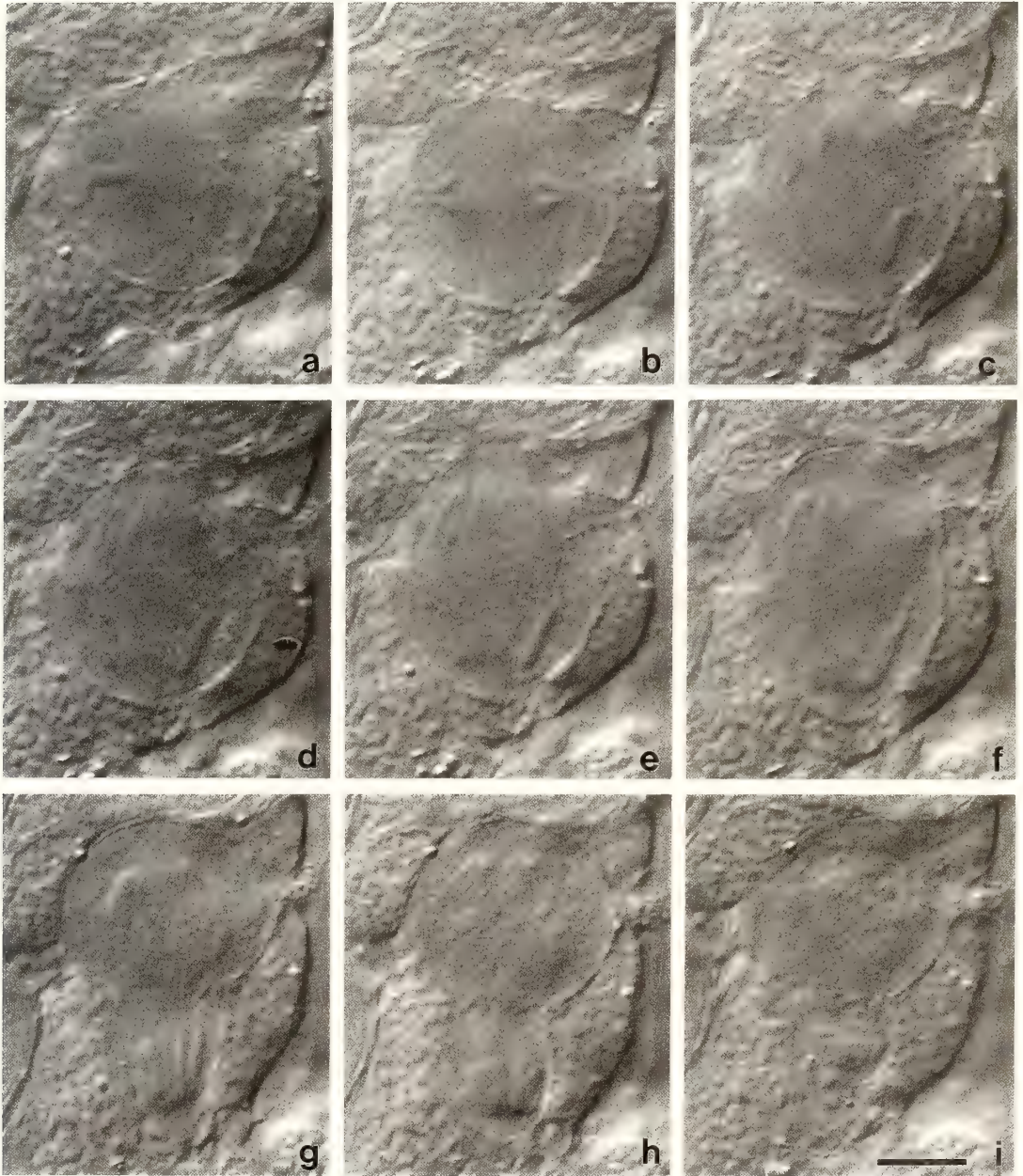


FIG. 2. Successive series depicting normal cytokinesis in a living neuroblast of the grasshopper. (a) metaphase, (b)–(c) early anaphase, (d)–(e) middle anaphase, (f)–(g) late anaphase, (h)–(i) early telophase. Bar: 10 μ m.

Contraction wave in normal neuroblasts

Figure 3 shows one of the photokymographs in a normal dividing neuroblast. The white line on the photograph of the cell reveals the position of the paper camera slit which was fixed at 5 μm from the CC-side pole of the cell. A contraction wave (CW) was recorded at middle anaphase (A3–A5). Thus, the figure indicates that the CW which had started

on the CC-side pole of the cell appeared on the surface 5 μm from the CC-side pole at middle anaphase.

In Figure 4, the position of the CW in the neuroblast is plotted in relation to the mitotic stages. The CW appeared at the CC pole shortly after the beginning of middle anaphase (A3), when the daughter chromosome tips separate. It traveled at a constant speed towards the GC-side,

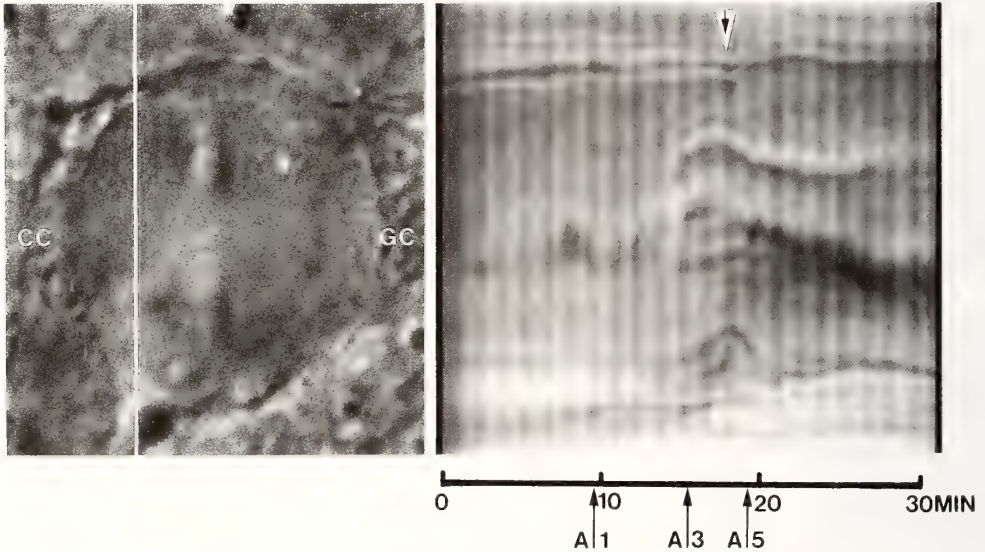


FIG. 3. A photokymographic record representing the cortical movements of a normal neuroblast. The arrow shows a contraction wave. The white line in the photograph shows the position of the slit. A1: beginning of early anaphase, A3: beginning of middle anaphase, A5: beginning of late anaphase (initiation of cleavage furrow).

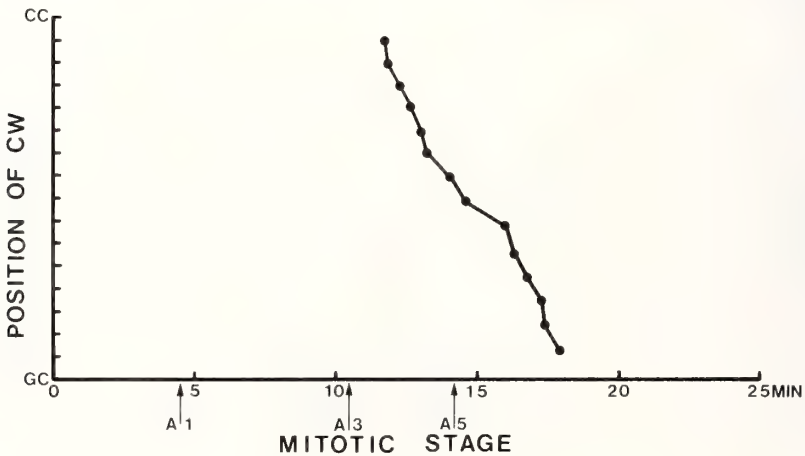


FIG. 4. Transition of a contraction wave (CW) in a normal neuroblast. CC: cap cell-side, GC: ganglion cell-side, A1: beginning of early anaphase, A3: beginning of middle anaphase, A5: beginning of late anaphase.

and reached the GC pole at late anaphase. The rate of CW transition on the cell surface was 3.5–6.5 μm per min (5.1 $\mu\text{m}/\text{min}$ on average), while the time necessary to pass from the CC pole to the GC pole ranged between 5.7 min and 10.6 min (7.8 min on average). The cleavage furrow was initiated (A5) when the CW was midway to the CG pole. Only one CW transition occurred during normal cell division.

Contraction wave in CB-treated neuroblasts

Cytochalasin B (CB) is known as a reagent that prevents cytokinesis. The minimum concentration effective for inhibiting cleavage furrow formation

is 0.1 $\mu\text{g}/\text{ml}$ CB, the level used in the present experiment. Figure 5 shows a photokymograph from CB-treated neuroblasts. The slit was fixed at 5 μm from the CC pole of the cell (white line). As shown by the arrows, CWs repeatedly passed through the region at equal intervals of time, contrary to the situation during normal division. Furthermore, these CWs revealed quite active movements during the period from prometaphase to middle anaphase, thereafter, becoming suddenly indistinct. No CWs were observed again until the neuroblast reached prometaphase of the succeeding mitosis.

In Figure 6, the position of the CWs from one

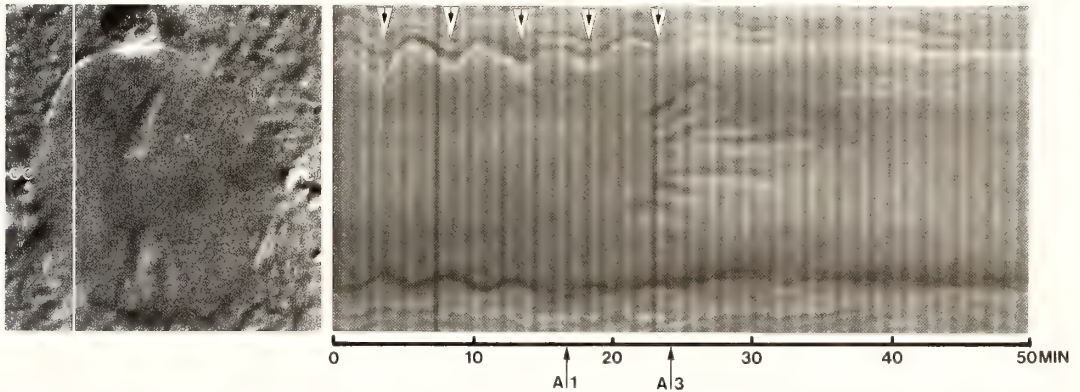


FIG. 5. A photokymographic record representing the cortical movements of a CB-treated neuroblast. The white line in the photograph shows the position of the slit. Arrows show contraction waves. A1: beginning of early anaphase, A3: beginning of middle anaphase.

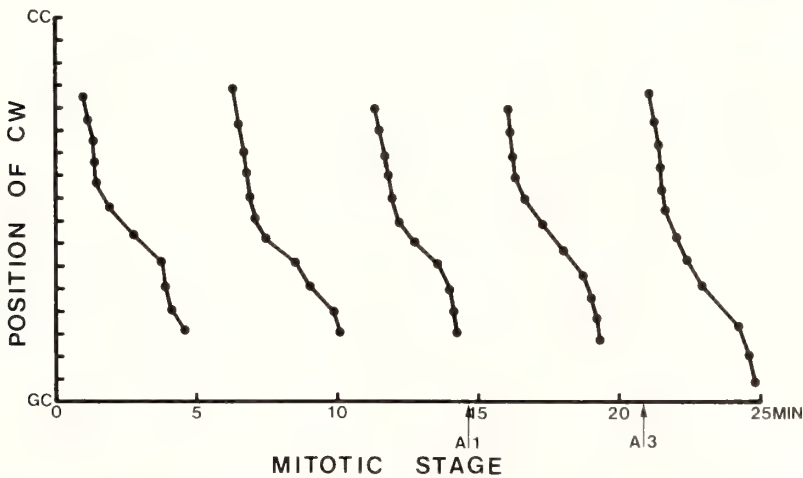


FIG. 6. Transition of contraction waves (CW) in a CB-treated neuroblast. A1: beginning of early anaphase, A3: beginning of middle anaphase.

set of 19 CB-treated neuroblasts was plotted in relation to the mitotic stages. As evidenced in the figure, these five CWs always started from the CC pole of the cell, propagating toward the GC pole. The pattern, the transition rate, and the intervals were almost definite in each neuroblast. The rate of transition of CWs ranged from $4.1 \mu\text{m}$ to $23.3 \mu\text{m}/\text{min}$ ($8.3 \mu\text{m}/\text{min}$ on average), while the intervals between two CWs ranged from 3.9 min to 13.6 min (7.6 min on average). It is noteworthy that the succeeding CW started from the CC pole only after the preceding CW reached the GC pole and disappeared. Two or more CWs were never found on the cell surface of a mitotic neuroblast. In most cells, the commencement of chromosome separation (A1) occurred in the short period between two CWs (in Fig. 6, between the third and the fourth CWs), while the time of daughter chromosome tip separation (A3) coincided with the initiation of the

last CW. A3 is the stage when the CW in normal cells was initiated at the CC-side pole.

In three sets of 19 CB-treated neuroblasts, the cells failed to enter anaphase, remaining in the metaphase state for a long period. As shown in Figure 7, distinct CWs continued to appear in these long-lasting metaphase cells.

The CW transition from the CC pole to the GC pole always occurred during the period between prometaphase and middle anaphase in CB-treated neuroblasts. However, weak CWs observed during late prophase showed different patterns. Figure 8 is an example of one case where eight CWs were recorded during late prophase. The pattern of CWs was not the same in each transition. Some of the CWs were initiated from the GC pole to the CC pole, while the others started in the middle region between the CC and the GC poles, propagating toward both poles. The region of the CW

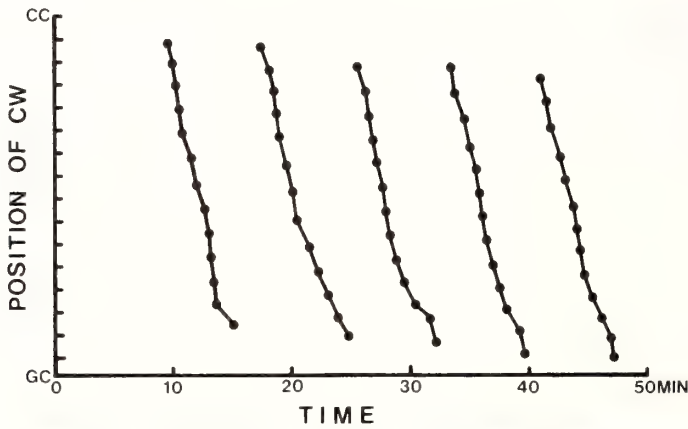


FIG. 7. Transition of contraction waves (CW) in a long-lasting metaphase neuroblast.

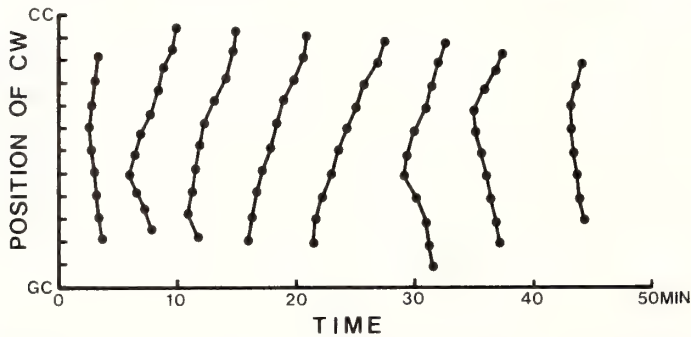


FIG. 8. Transition of contraction waves (CW) during late prophase in a CB-treated neuroblast.

initiation seemed to alternate between poles; in the first, second, third and fourth CWs in Figure 8 the regions moved to GC-side, while in the sixth, seventh and eighth CWs, they moved to the CC-side.

No significant correlations were recognized between the rate of CW transition and the interval, between the rate and the cell volume, or between the interval and the cell volume in CB-treated neuroblasts.

DISCUSSION

The grasshopper neuroblasts possess very distinctive characteristics in cell division as they produce a small ganglion cell in a definite direction with strict regularity. In the previous studies, Kawamura [4, 5] reported that the unequal division of neuroblasts is caused by the position of the spindle body which had shifted during middle anaphase to the cell pole where a ganglion cell is to be produced. The unique behavior of the spindle body in the neuroblast is invariably repeated in every unequal division. Applying a microdissection technique, Carlson [3] and Kawamura [4] rotated the spindle body at various mitotic stages. When the spindle body at metaphase was rotated 90° and a microneedle removed, the spindle body rotated back or forward, autonomously to the original axis (CC-GC axis). Any 180°-rotation experiments on the spindle body carried out up to middle anaphase could not prevent the spindle from shifting toward the GC-side, unless it was forcedly fixed by a needle. These results suggested that the cell cortex played a leading role in the orientation and shifting of the mitotic apparatus (MA) within the neuroblast during mitosis.

In the present study, a contraction wave (CW) closely related to the mitotic stages was observed on the surface of dividing neuroblasts. The CW started at the CC pole of the cell and traveled toward the GC pole. In normal neuroblasts, the CW appeared only once during cell division, while in CB-treated neuroblasts, which failed cytokinesis, a repeated appearance of CWs at regular intervals was noted from prometaphase to middle anaphase. The difference in normal and CB-treated neuroblasts may suggest that rhythmic

cortical movements, which are originally latent and appear only once in the normal state, are expressed by CB treatment. It is generally accepted that CB affects actin fibers which are constituents of the cytoskeleton in the cell cortex. When CB inhibits polymerization of actin fibers, or causes fragmentation, network formation with the fibers (gelation) is prevented. The treatment of neuroblasts with low-concentration CB probably induces changes in the rigidity of the cell cortex, and, as a result, repeated CWs which are latent in the normal condition are visualized.

Roberts [8] observed cell division of grasshopper neuroblasts isolated from embryos by trypsin and hyaluronidase, with time-lapse cinematography. He reported that the first polar expansion occurred in the cell cortex of the CC-side, followed by a second polar expansion on the GC-side cortex about 1.5–8 min after the first. Since the rate of transit and the stage of appearance of the CW in the present study seems to coincide well with the polar expansions observed by Roberts, he probably observed the first and last parts of CW transition at both poles of a neuroblast.

A phenomenon analogous to the CW of neuroblasts was observed in frog eggs by Hara *et al.* [9]. In the period from fertilization to first cleavage, two kinds of surface waves with dorso-ventral polarity, the activation wave and post-fertilization wave, were visualized by time-lapse cinematography. They assumed that the activation wave, spreading from the sperm entrance point, induces the extrusion of the cortical granules, as well as internal cytoplasmic movements.

Takeichi and Kubota [10], in *Xenopus* eggs, found that the activation wave is accompanied by contraction and relaxation of the egg surface.

In the present experiment, a weak CW propagating in reverse, i.e., from the GC pole to the CC pole, was observed during the period from late prophase to very late prophase. After prometaphase, when the nuclear membrane disappears and the spindle body grows, a CW with a large magnitude appeared at the CC pole and moved toward the GC pole, while, after middle anaphase on, no such CW was recorded. In three cases of CB-treated neuroblasts, the cells did not enter anaphase. These long-lasting metaphase cells showed

active and periodic CWs for a long period. These results strongly suggest a close relationship between CWs and the MA in their appearance and disappearance. It should be noted that the CW travels from the GC pole to the CC pole while the nuclear membrane is present, and upon the disappearance of the membrane, the direction of CW propagation is reversed. At that very stage, the shape of the neuroblasts, which had been concavo-convex up to late prophase, became round. What causes the change in the direction of CWs or what generates the CWs is not clear at the present time. However, observation of the ultrastructures of the neuroblast showed that an electron-dense layer appeared in a limited area of the CC-side cell cortex at the stage when the active CW was initiated [11]. Further studies are necessary in order to clarify the relationship between the structure of the cell cortex and the CW.

Observing the process of micromere formation in sea urchin eggs, Dan [12] and Dan *et al.* [13] concluded that the unequal division of four vegetal blastomeres during the fourth cleavage is caused by the eccentric position of the MAs. The resting nuclei of the four vegetal cells migrate to the narrow gaps in the vesicular row near the vegetal pole, and upon forming spindles, the spindle pole anchors the cell surface. Their observation showed that cortical differentiation for unequal division occurred in the four vegetal blastomeres of the 8-cell stage.

The stage of appearance of the CW at the CC pole coincides well with the stage of initiation of spindle body migration towards the GC pole. Anchoring of the spindle pole to the GC pole cortex and decision of the furrow position occur while the CW is still traveling on the cell surface between the poles. From these facts we can assume that the CW plays an important role in the unequal division of grasshopper neuroblasts. Using a squeezing action, the CW which appears at the CC pole pushes the cell contents including the spindle body toward the GC-side during the first half of its propagation. After the pole of the spindle body anchors to the GC pole cortex, the cell contents on the GC-side are squeezed toward the CC-side by the action of the CW now traveling the cell surface of the later half, leaving the spindle

body on the GC-side. Since the cleavage furrow is always induced in the cell cortex nearest the middle part of the spindle body, a small daughter ganglion cell and a daughter neuroblast with a large amount of cell contents are produced as a result.

REFERENCES

- 1 Carlson, J. G. (1937) Studies of the somatic mitotic cycle in the grasshopper. *J. Alabama Acad. Sci.*, **9**: 25–26.
- 2 Carlson, J. G. and Gaulden, M. E. (1964) Grasshopper neuroblast technique. In "Methods in Cell Physiology, Vol. 1". Ed. by D. M. Prescott, Academic Press, New York and London, pp. 229–276.
- 3 Carlson, J. G. (1952) Microdissection studies of the dividing neuroblast of the grasshopper, *Chortophaga viridifasciata* (De Geer). *Chromosoma*, **5**: 199–220.
- 4 Kawamura, K. (1960) Studies of cytokinesis in neuroblasts of the grasshopper, *Chortophaga viridifasciata* (De Geer). II. The role of mitotic apparatus in cytokinesis. *Exp. Cell Res.*, **21**: 9–18.
- 5 Kawamura, K. (1977) Microdissection studies on the dividing neuroblast of the grasshopper, with special reference to the mechanism of unequal cytokinesis. *Exp. Cell Res.*, **106**: 127–137.
- 6 Carlson, J. G. (1946) Protoplasmic viscosity changes in different regions of the grasshopper neuroblast during mitosis. *Biol. Bull.*, **90**: 109–121.
- 7 Kawamura, K. (1960) Studies on cytokinesis in neuroblasts of the grasshopper, *Chortophaga viridifasciata* (De Geer). I. Formation and behavior of the mitotic apparatus. *Exp. Cell Res.*, **21**: 1–9.
- 8 Roberts, S. H. (1955) The mechanism of cytokinesis in neuroblasts of *Chortophaga viridifasciata* (De Geer). *J. Exp. Zool.*, **130**: 83–106.
- 9 Hara, K., Tydeman, P. and Kirschner, M. (1980) A cytoplasmic clock with the same period as the division cycle in *Xenopus* egg. *Proc. Natl. Acad. Sci., U.S.A.*, **77**: 462–466.
- 10 Takeichi, T. and Kubota, H. Y. (1984) Structural basis of the activation wave in the egg of *Xenopus laevis*. *J. Embryol. Exp. Morphol.*, **81**: 1–16.
- 11 Kawamura, K. and Itani, G. (1983) Ultrastructural changes in grasshopper neuroblast during mitosis. *Dev. Growth Differ.*, **26**: 382.
- 12 Dan, K. (1979) Studies on unequal cleavage in sea urchins. I. Migration of the nuclei to the vegetal pole. *Dev. Growth Differ.*, **21**: 527–535.
- 13 Dan, K., Endo, S. and Uemura, I. (1983) Studies on unequal cleavage in sea urchins. II. Surface differentiation and direction of nuclear migration. *Dev. Growth Differ.*, **25**: 227–237.

Participation of the Subcortical and Interior Cytoplasm in Cleavage Division of Newt Eggs¹

TSUYOSHI SAWAI

*Department of Biology, Faculty of General Education,
Yamagata University, Yamagata 990, Japan*

ABSTRACT—In cleaving eggs of the newt, *Cynops pyrrhogaster*, a large amount of cytoplasm was removed from under the cortex along the cleavage plane or from the interior region, and replaced by cytoplasm from another egg. Replacement of the cytoplasm in the cleavage plane caused partial inhibition of cleavage at the site of replacement in many cases. Replacement of the interior region frequently resulted in regression of an established furrow after some deepening of the furrow.

In eggs in which a pale surface had extended on both walls of the cleavage furrow in the middle stage of the first cleavage, the cortex of the pale area was excised, and replaced by a piece of the pigmented cortex from the animal hemisphere of another egg. After this operation, the furrow of the host egg was formed on the graft.

INTRODUCTION

Previous studies on the mechanism of cytokinesis have demonstrated that the cortex of the cleavage plane receives some kind of stimulus necessary for furrow formation through the mitotic apparatus (MA) [cf. reviews; 1-3]. In echinoderm eggs, the cleavage was not prevented by removal [4] or destruction [5] of the MA after late metaphase of nuclear division, but was prevented by these procedures before early metaphase. Furthermore, when a large quantity of endoplasm was replaced by paraffin oil, sucrose solution or sea water shortly before the onset of the first cleavage, the egg containing the large drop of injected fluid divided completely into two parts [6]. These results indicate that the MA determines the cleavage plane in about anaphase of nuclear division and that only the cortical region takes part in visible events of the division process.

In amphibian eggs, the cleavage plane is also determined in about anaphase [7-9], and the furrow can be formed on the egg surface without the MA [7, 10, 11]. In amphibians, however, it is

unknown whether the entire process of cleavage can proceed without a large amount of the endoplasm, as in echinoderm eggs.

Reports from this laboratory have shown that in cleavage of amphibian eggs the subcortical cytoplasm along the cleavage plane contains some factor with activity to induce the furrow in the overlying cortex [12-15]. In our previous studies on the cytoplasmic factor, particular attention was paid to the subcortical region of cleaving eggs, not to the more interior region. Furthermore, our interest was chiefly directed to the early phase of furrow formation, not the late phase. In the present study the role of the cytoplasm of the deep interior region in the late phase of cleavage division of newt eggs was examined.

MATERIALS AND METHODS

Fertilized eggs of the newt, *Cynops pyrrhogaster*, were used. Spawning of the eggs was stimulated by injecting about 80 I. U. of chorionic gonadotropin (Gonatropin, Teikoku-zoki, Tokyo) every other day into the abdomen of females which had taken up spermatophores. The jelly coat of eggs was removed by treatment with about 1.5% sodium thioglycollate (pH 10) and the vitelline membrane was stripped off with two pairs of

Accepted March 17, 1988

¹ This paper is dedicated to Professor Katsuma Dan on the occasion of his 83rd birthday.

watchmaker's forceps. The naked eggs were put into a shallow depression in agar-gel-coated dishes containing Holtfreter's saline, where operations were carried out by hand under a dissecting microscope at a room temperature (20–25°C).

Cytoplasm was excised and introduced with a glass tube, one end of which was drawn out into a capillary of 50–70 μm diameter, and the other end of which was connected to rubber tubing for applying a negative or positive pressure by mouth [12].

The cortex was transplanted with a fine glass needle [16]. A piece of the cortex of the recipient egg was excised with the needle, and the wound was then covered by a piece of cortex from the animal hemisphere of another egg. The graft was fused to the recipient egg by pressing it along the edge of the wound with the needle.

RESULTS

Removal or replacement of the cytoplasm along the cleavage plane

Previously I reported that in newt eggs "furrow-

inducing cytoplasm" (FIC) is present in the subcortical layer along the cleavage furrow and also extends along the future furrow plane ahead of the furrow tips [12]. In the present experiment, the cytoplasm including the FIC was removed from the cleavage plane, or replaced by cytoplasm from another egg.

With eggs in the early stage of first cleavage when a large amount of cytoplasm (ca. 0.2–0.4 μl) was sucked out from under the cortex along the future furrow plane ahead of the furrow tip, furrow formation on this site was not disturbed appreciably. However, when tissue was removed in larger quantity (ca. 0.4–0.6 μl) and to deeper region, a furrow did not form on the region of operation, but appeared on the surface of the cleavage plane beyond the site of operation in many cases (Fig. 1). This partial deficiency of furrow formation was seen frequently when a large amount of cytoplasm of the future furrow plane was replaced by cytoplasm from another egg. This deficient furrow formation was seen in 7 of 9 cases. In 3 of these 7 cases a furrow eventually formed over the site of operation after more than 40 min, but in the other 4 cases it never formed.

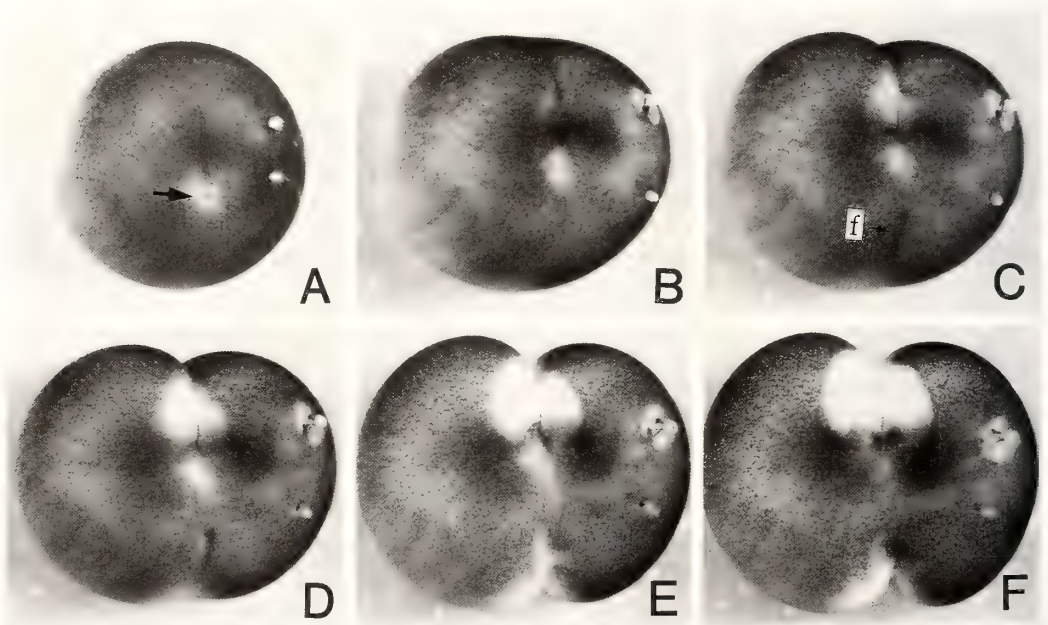


Fig. 1. Partial cleavage-arrest after replacement of cytoplasm in the future furrow region. The pale region (arrow) in A is the position of cytoplasm replacement. A furrow (f in C) appeared in the surface beyond this site. Time: A, just after cytoplasm replacement; B, C, D, E and F, 20, 30, 40, 60 and 80 min after A, respectively.

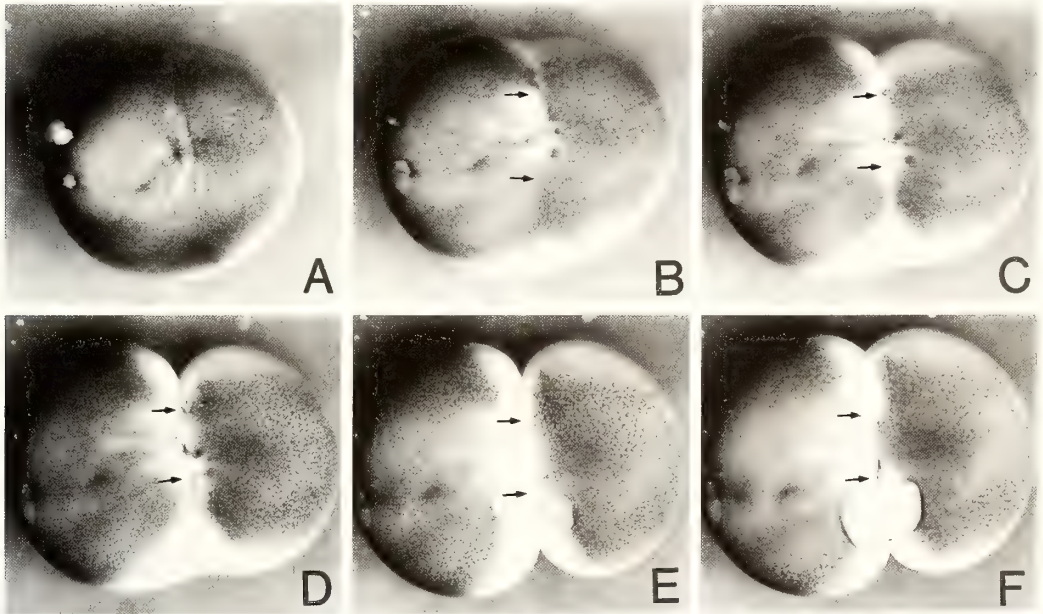


FIG. 2. Partial cleavage-arrest by replacement of cytoplasm under the furrow. The furrow regression occurred in the region between the two arrows. Time: A, just after the replacement; B, C, D, E and F, 20, 40, 60, 100 and 130 min after A, respectively.

Next, cytoplasm under an established furrow was removed or replaced. Removal of the cytoplasm along the furrow bottom resulted in a temporary regression of the furrow on the surface over the site of removal but after a few minutes cleavage was resumed. When cytoplasm was removed in larger quantity and not only from the subcortical, but also deeper regions, however, formation of the furrow was not resumed for a long time, if at all, in many cases. This partial arrest of cleavage occurred more frequently when the excised cytoplasm was replaced by that of another egg (Fig. 2). The latter result was obtained in 13 of 19 cases: cleavage of these 13 was arrested temporarily and resumed after about 40 min in 6 of these 13 cases, but was arrested permanently in the other 7 cases.

Replacement of cytoplasm in the interior region

A large amount of cytoplasm (ca. $0.8\text{--}1.0\ \mu\text{l}$) was removed from the interior part of eggs in the early to middle stages of first cleavage, and replaced by 1 M sucrose solution, 10% Ficoll solution or cytoplasm of another egg. In these eggs, roughly speaking, the cytoplasm was left in a layer of about $200\ \mu\text{m}$ depth in the animal pole region

and in a deeper layer in another region. After introduction of either of two chemical solutions, eggs showed morbid features as cleavage progressed, and the furrow regressed with abnormal expansion of the pale surface (Fig. 3). Replacement of the interior cytoplasm by cytoplasm of another egg resulted in cleavage-arrest after slight deepening of the furrow in 10 of 14 cases (Fig. 4). In these defective cases the furrow gradually degenerated.

Cortical grafting

In eggs in which the pale surface was expanding to both walls of the furrow, cortical grafting was made on the pale area, to investigate the furrow-inducing activity of the cytoplasm along the bottom of the deepening furrow. The pale cortex including the furrow bottom of the recipient egg was stripped of. The stripped cortex was an almost transparent thin layer. The removal site was grafted by a piece of pigmented cortex from the animal half of another egg (Fig. 5B). A furrow was formed on the graft 15–25 min after the grafting (Fig. 5C, D). The graft divided completely in 30 cases and partially in 13 cases, but did not divide in 10 cases. These results indicate that the FIC is

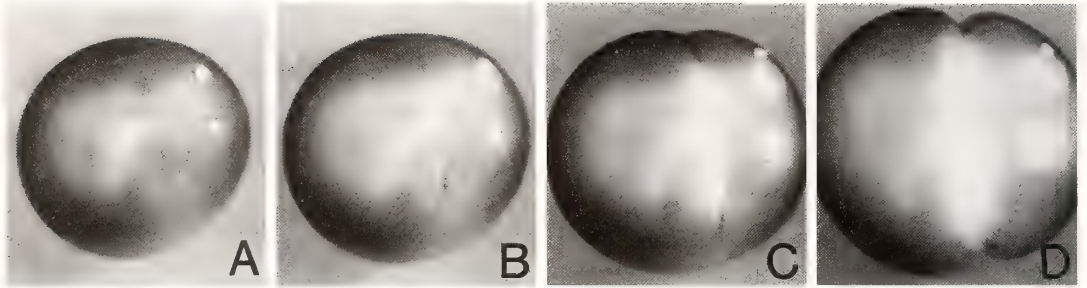


FIG. 3. Abnormal cleavage of an egg in which the interior cytoplasm was replaced by sucrose solution. Time: A, just after the replacement; B, C and D, 5, 15 and 25 min after A, respectively.

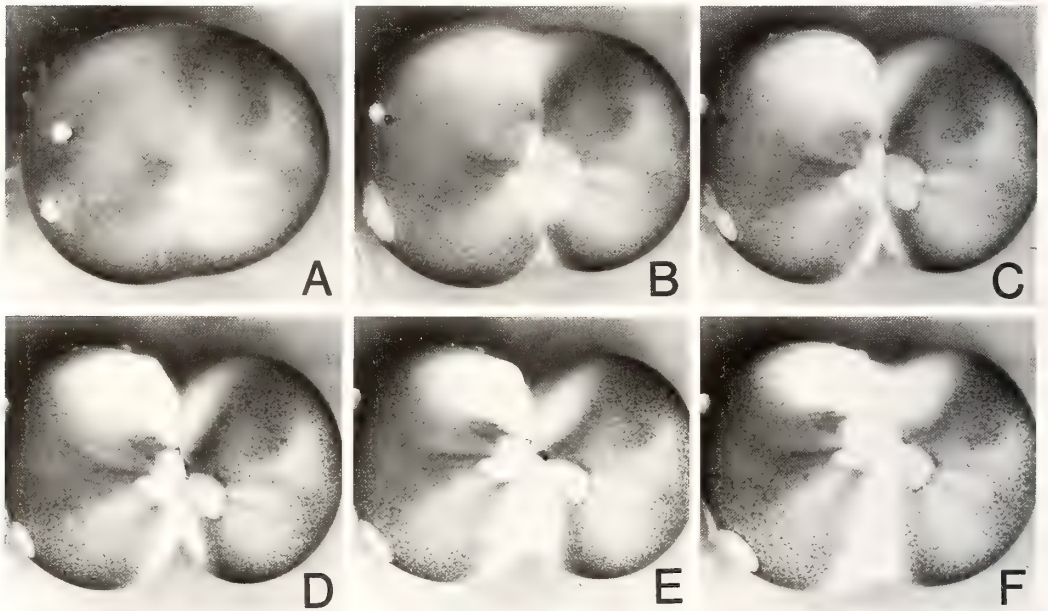


FIG. 4. Furrow regression in the eggs of which the interior cytoplasm was replaced by that of another egg. The furrow progressed half-way (A-C), but finally regressed (D-F). Time: A, just after the replacement; B, C, D, E and F, 25, 55, 75, 95 and 115 min after A, respectively.

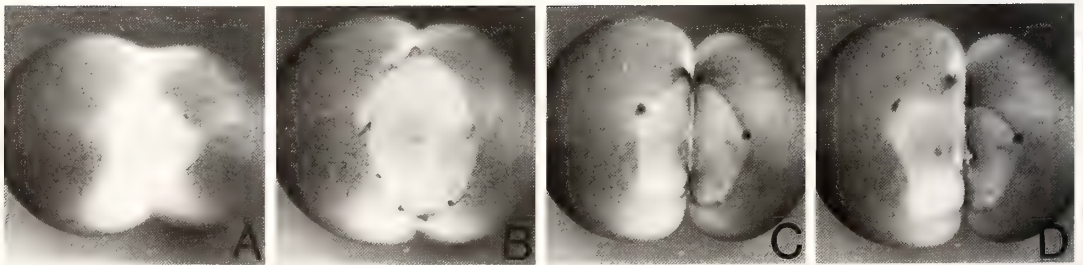


FIG. 5. Furrow formation on the graft transplanted into the deepening furrow region. A, just before the transplantation. B, just after the transplantation. C, 15 min after B. D, 25 min after B.

present under the cortex along the bottom of the deepening furrow.

Furrow formation on the graft was characterized by the simultaneous appearance of the furrow over the whole graft along the cleavage plane of the recipient, and quick expansion of the pale surface on both sides of the furrow. The former phenomenon was also observed in previous experiments on cortical grafting in the early stage of first cleavage [16], but the latter phenomenon has not been observed previously.

DISCUSSION

The present studies on *Cynops* eggs showed that the cytoplasm present along the cleavage plane is important for cleavage division during the period from the initial stage of furrow formation to the later stage of furrow deepening.

Studies on the mechanism of cleavage in echinoderm eggs have indicated that the cortex is important in furrow formation, since division was completed even after replacement of a large quantity of endoplasm by another substance [6]. Studies on cleavage of amphibian eggs have also suggested the importance of the cortical region in the furrow formation: namely they have demonstrated division of small egg fragments [10], division of eggs after removal of a large portion of the endoplasm [17], and division of eggs after separation of the cortical layer from the deep interior part of the egg [10, 17]. In these studies interest was mainly directed to the cortical region or the deep interior part, rather than the subcortical layer.

Kubota [18] first demonstrated the importance of the subcortical layer in studies on cleavage of amphibian eggs by the finding that the cleavage plane was directly determined by the cytoplasm in this layer. This cytoplasm was arbitrarily termed "furrow-inducing cytoplasm" (FIC), since it has the ability to induce a furrow in the overlying cortex [12].

In the present work, the localization of the FIC beneath the cortex along the cleavage plane was confirmed by different techniques from those used previously. In addition, results showed for the first time that the FIC is also present in a region deeper

than directly under the cortex of the cleavage plane.

Previous studies were chiefly concerned with the process of furrow formation in the initial stage of the cleavage, rather than the process of furrow deepening in the later stage. The present results indicated that the FIC or another cytoplasmic factor is also indispensable for the later stage, i.e., the maintenance of an established furrow and deepening of this furrow.

Ultrastructural studies have demonstrated that in amphibian cells, as in other animal cells, cytokinesis is brought about by contractile force of filamentous bundles mainly composed of actin fibers [19–24]. From these ultrastructural findings and results obtained by microsurgical techniques, the role of FIC seems to be as follows. In about anaphase of nuclear division, the FIC is distributed along the equatorial zone of the spindle between two asters. The FIC first comes in contact with the cortex at the animal pole, where it induces arrangement of microfilaments present in the cortical layer into a bundle structure in a definite direction along the cleavage plane, forming a contractile arc. This event occurs continuously ahead of the two tips of the arc, and so the contractile arc gradually extends toward the vegetal pole. The cleavage furrow is also deepened by the continuous contractile force of the established bundle, and addition of new membrane at the bottom of the furrow [25–30]. Judging from the present results, the bundle structure may not be in a steady state, but in a dynamic state of turnover, probably due to the activity of the FIC or another cytoplasmic factor.

REFERENCES

- 1 Conrad, G. W. and Rappaport, R. (1981) Mechanism of cytokinesis in animal cells. In "Mitosis/Cytokinesis". Ed. by A. M. Zimmerman, and A. Forer, Academic Press, pp. 365–396.
- 2 Rappaport, R. (1986) Establishment of the mechanism of cytokinesis in animal cells. *Int. Rev. Cytol.*, **105**: 245–281.
- 3 Mabuchi, I. (1986) Biochemical aspect of cytokinesis. *Int. Rev. Cytol.*, **101**: 175–213.
- 4 Hiramoto, Y. (1956) Cell division without mitotic apparatus in sea urchin eggs. *Exp. Cell Res.*, **11**: 630–636.

- 5 Hamaguchi, Y. (1975) Microinjection of colchicine into sea urchin eggs. *Dev. Growth Differ.*, **17**: 111-117.
- 6 Hiramoto, Y. (1965) Further studies on cell division without mitotic apparatus in sea urchin eggs. *J. Cell Biol.*, **25**: 161-166.
- 7 Kubota, T. (1966) Studies of the cleavage in the frog egg. I. On the temporal relation between furrow determination and nuclear division. *J. Exp. Biol.*, **44**: 545-552.
- 8 Selman, G. G. (1982) Determination of the first two cleavage furrows in developing eggs of *Triturus alpestris* compared with other forms. *Dev. Growth Differ.*, **24**: 1-6.
- 9 Zotin, A. I. (1964) The mechanism of cleavage in amphibian and sturgeon eggs. *J. Embryol. Exp. Morphol.*, **12**: 247-262.
- 10 Dan, K. and Kojima, M. K. (1963) A study on the mechanism of cleavage in the amphibian egg. *J. Exp. Biol.*, **40**: 7-14.
- 11 Sawai, T. (1980) On propagation of cortical factor and cytoplasmic factor participating in cleavage furrow formation of the newt's egg. *Dev. Growth Differ.*, **22**: 437-444.
- 12 Sawai, T. (1972) Roles of cortical and subcortical components in cleavage furrow formation in amphibia. *J. Cell Sci.*, **11**: 543-556.
- 13 Sawai, T. (1983) Cytoplasmic and cortical factors participating in cleavage furrow formation in eggs of three amphibian genera: *Ambystoma*, *Xenopus* and *Cynops*. *J. Embryol. Exp. Morphol.*, **77**: 243-254.
- 14 Sawai, T., Kubota, T. and Kojima, M. K. (1969) Cortical and subcortical changes preceding furrow formation in the cleavage of newt eggs. *Dev. Growth Differ.*, **11**: 246-254.
- 15 Kojima, M. K. (1972) Insertion of strips of cellophane or porous filters in the future course of the advancing cleavage furrow of the newt egg. *Dev. Growth Differ.*, **14**: 307-310.
- 16 Sawai, T. (1974) Furrow formation on a piece of cortex transplanted to the cleavage plane of the newt egg. *J. Cell Sci.*, **15**: 259-267.
- 17 Waddington, C. H. (1952) Preliminary observations on the mechanism of cleavage in the amphibian egg. *J. Exp. Biol.*, **29**: 484-489.
- 18 Kubota, T. (1969) Studies of the cleavage in the frog egg. II. On determination of the position of the furrow. *J. Embryol. Exp. Morphol.*, **21**: 119-129.
- 19 Bluemink, J. G. (1970) The first cleavage of the amphibian egg. An electron microscope study of the onset of cytokinesis in the egg of *Ambystoma mexicanum*. *J. Ultrastruct. Res.*, **32**: 142-166.
- 20 Bluemink, J. G. (1971) Cytokinesis and cytochalasin-induced furrow regression in the first cleavage zygote of *Xenopus laevis*. *Z. Zellforsch. Mikrosk. Anat.*, **121**: 102-126.
- 21 Selman, G. G. and Perry, M. M. (1970) Ultrastructural changes in the surface layers of the newt's egg in relation to the mechanism of its cleavage. *J. Cell Sci.*, **6**: 207-227.
- 22 Kalt, M. R. (1971) The relationship between cleavage and blastocoel formation in *Xenopus laevis*. II. Electron microscopic observation. *J. Embryol. Exp. Morphol.*, **26**: 51-61.
- 23 Kubota, T. (1976) Mechanism of cleavage of newt eggs. *J. Cell Sci.*, **37**: 39-45.
- 24 Perry, M. M., John, H. A. and Thomas, N. S. T. (1971) Actin-like filaments in the cleavage furrow of newt egg. *Exp. Cell Res.*, **65**: 249-253.
- 25 Byers, T. J. and Armstrong, P. B. (1986) Membrane protein redistribution during *Xenopus* first cleavage. *J. Cell Biol.*, **102**: 2176-2184.
- 26 Bluemink, J. G. and De Laat, S. M. (1973) New membrane formation during cytokinesis in normal and cytochalasin B-treated eggs of *Xenopus laevis*. I. Electron microscope observations. *J. Cell Biol.*, **59**: 89-108.
- 27 De Laat, S. W. and Bluemink, J. G. (1974) New membrane formation during cytokinesis in normal and cytochalasin B-treated eggs of *Xenopus laevis*. II. Electrophysiological observations. *J. Cell Biol.*, **60**: 529-540.
- 28 Singal, P. K. and Sanders, E. J. (1974) An ultrastructural study of the first cleavage of *Xenopus* embryos. *J. Ultrastruct. Res.*, **47**: 433-451.
- 29 Sanders, E. J. and Singal, P. K. (1975) Furrow formation in *Xenopus* embryos. Involvement of the Golgi body as revealed by ultrastructural localization of thiamine pyrophosphatase activity. *Exp. Cell Res.*, **93**: 219-224.
- 30 Sawai, T. (1987) Surface movement in the region of the cleavage furrow of amphibian eggs. *Zool. Sci.*, **4**: 825-832.

Partial Purification and Characterization of a Factor which Dissociates 45K Protein-Actin Complex from Sea Urchin Egg¹

MASAAKI OHNUMA and ISSEI MABUCHI

*Department of Biology, College of Arts and Sciences, University of Tokyo,
Komaba, Meguro-ku, Tokyo 153, Japan*

INTRODUCTION

During embryogenesis in animals, a dynamic rearrangement of the actin cytoskeleton is observed [1]. In particular, formations of the cortical actin cytoskeleton during and after fertilization and of the contractile ring at cytokinesis are marked events in the early development of the sea urchin egg. These events are thought to be regulated by actin-modulating proteins. In order to investigate the mechanism of regulation of the actin filaments, many actin-modulating proteins from the sea urchin egg have been isolated and characterized [2-9]. One of the major actin-modulating proteins is 45K protein, which severs the actin filament in the presence of micromolar Ca^{2+} and forms a 1:1 complex with actin (45K-A) [5, 6, 10, 11]. 45K-A is not able to sever F-actin, but it caps the barbed end of the actin filament in a Ca^{2+} independent manner [6]. This complex is very stable and it has not been possible to dissociate it under physiological conditions even by prolonged treatment with EGTA [6]. These properties of the 45K protein are similar to gelsolin from mammalian blood cells, although the latter binds two actin molecules [12]. It is not yet clear whether the 45K protein forms an irreversible complex with actin when Ca^{2+} levels increase in the cell at fertilization, for example, or if the complex dissociates reversibly and the 45K protein is used again.

In a previous paper, we reported that the dissociation of 45K-A occurred in the absence of Ca^{2+} when it was in a crude fraction [10]. This suggested that a factor which is able to dissociate 45K-A existed in such a fraction. This factor may be able to regulate actin filament elongation by removing the 45K protein which was capping the barbed end of the actin filament in the egg. It is also possible that the released 45K protein is used again as the actin severing factor. We planned to investigate the 45K-A dissociating factor in order to clarify the role of the 45K protein in the regulation of the actin cytoskeleton in the egg. In the present paper, we report partial purification and characterization of this factor. The dissociation factor lost its dissociating activity by heat treatment or protease digestion, but not by RNase treatment. These results suggested that the factor is a protein. Stokes radius of the factor was 4.1 nm as estimated by gel filtration.

MATERIALS AND METHODS

Protein purification

Sea urchin egg crude extract was prepared according to a procedure as described previously [3]. Free 45K protein was purified from the crude extract according to Wang and Spudich [5] with modifications [10]. The extract was dialyzed against DEAE-buffer (10 mM Tris-HCl, 0.5 mM ethyleneglycol-bis (β -aminoethyl ether) N, N, N', N'-tetraacetic acid (EGTA), 0.2 mM ATP, 0.2 mM dithiothreitol (DTT), 1 $\mu\text{g}/\text{ml}$ leupeptin, and 0.5 mM phenylmethylsulfonylfluoride (PMSF), pH 8.0) and applied to a DEAE-cellulose (DE-

Accepted May 17, 1988

¹ This paper is dedicated to Dr. Katsuma Dan for his great contributions to developmental biology and his continuous activity at the Misaki Marine Biological Station.

52, Whatman) column which was preequilibrated with DEAE-buffer. Adsorbed proteins were eluted by application of a 0–0.3 M linear NaCl gradient. 45K protein was eluted at 0.18–0.2 M NaCl. Ammonium sulfate was added to the 45K protein fraction up to 60% saturation. The fraction was then centrifuged at $20,000 \times g$ for 15 min. After the supernatant was collected, ammonium sulfate was added up to 85% saturation, the sample was centrifuged again and 45K protein was recovered in the pellet. The pellet was then dissolved and dialyzed against 10 mM potassium phosphate, 0.5 mM EGTA and 0.2 mM DTT (pH 7.0), and was applied to a hydroxylapatite (HTP, Bio-Rad Labs.) column. Adsorbed proteins were eluted with a 10–300 mM linear phosphate gradient. 45K protein was eluted at 130–150 mM phosphate, concentrated using Centriflo (Amicon Corp.) and further purified by gel filtration using a Sephadex G–100 (Pharmacia) column.

Rabbit skeletal muscle actin was prepared according to Spudich and Watt [13] and purified by gel filtration using a Sephadex G–100 column.

DACM-labeling of actin

Gel-filtered actin was dialyzed against G-buffer (1 mM N-Tris [Hydroxymethyl] methyl-2-aminoethanesulfonic acid (TES)-NaOH, pH 8.0, 50 μ M ATP and 50 μ M $MgCl_2$) overnight. Equimolar amounts of N-(7-Dimethylamino-4-methylcoumarinyl)-maleimide (DACM) was added to the actin and the sample was incubated for 5 min on ice. The reaction was stopped by addition of excess 2-mercaptoethanol and unreacted DACM was removed by dialysis.

Electrophoresis

Sodium dodecyl sulfate polyacrylamide gel electrophoresis (SDS-PAGE) was carried out according to Laemmli [14] using 10% acrylamide slab gels. The gels were stained with 0.025% Coomassie Brilliant Blue R–250, 25% (v/v) isopropanol and 10% (v/v) acetic acid. The following marker proteins were used for molecular weight estimation: bovine serum albumin (BSA, molecular weight, 68,000), ovalbumin (45,000), bovine erythrocyte carbonic anhydrase (30,000), soybean trypsin inhibitor (21,000), and horse heart

cytochrome C (13,000).

Protein determination

Protein concentration was determined according to Lowry *et al.* [15] using BSA as a standard.

Stokes radius

Stokes radius was estimated according to Laurent and Killander [16]. Standard marker proteins used for estimation were γ -globulin (5.2 nm), BSA (3.5 nm), and ovalbumin (3.0 nm).

RESULTS

We were able to devise a system to quantify the dissociation of 45K-A (Fig. 1). To each well of 96-well microtiter plate, we added 150 μ l of purified 45K protein (0.1 mg/ml) dissolved in

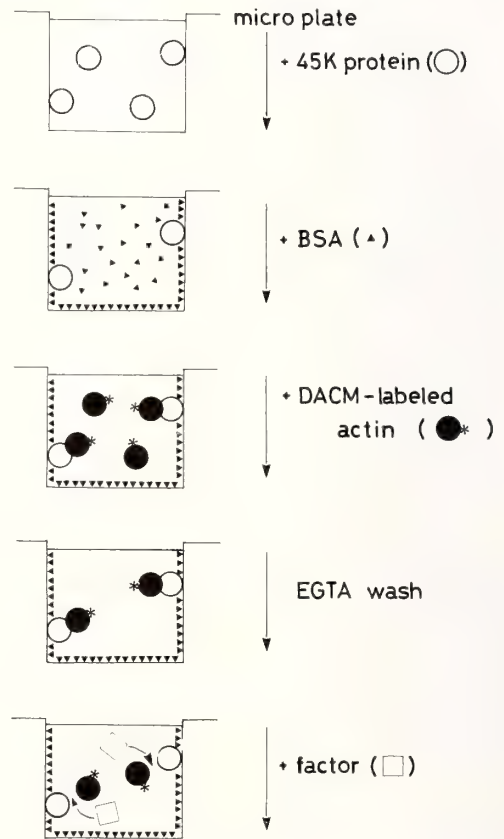


Fig. 1. Schematic diagram of a system for quantification of the dissociation of 45K-A.

DEAE-buffer and incubated the plate for 1 hr at 4°C. After removal of unadsorbed 45K protein, 150 μ l of BSA (1 mg/ml) dissolved in DEAE-buffer was added to each well and the plate was incubated again for 1 hr at 4°C to eliminate non-specific adsorption of actin in the later step. Excess BSA was removed and the wells were washed several times with G-buffer containing 2 mM CaCl₂. DACM-labeled G-actin in G-buffer plus 2 mM CaCl₂ was added to each well to form a complex with the adsorbed 45K protein. After 30 min incubation at 4°C, free DACM-labeled actin was removed and the wells were washed several times with DEAE-buffer. A 150 μ l aliquot of the

sample fraction containing 45K-A dissociating factor(s) was added to each well and incubated at 4°C. After certain periods, the increase in fluorescence of the sample fraction was monitored by a Shimadzu RF-540 spectrofluorophotometer at the excitation wave length of 395 nm and emission wave length of 460 nm.

Neither of the fluorescence spectrum nor intensity of DACM bound to actin was affected in the presence of either Ca²⁺ or EGTA (data not shown). The amount of adsorbed DACM-labeled 45K-A was estimated to be 0.5 μ g/well by dissolving adsorbed proteins with 1 N NaOH followed by fluorophotometry. DACM fluorescence was not

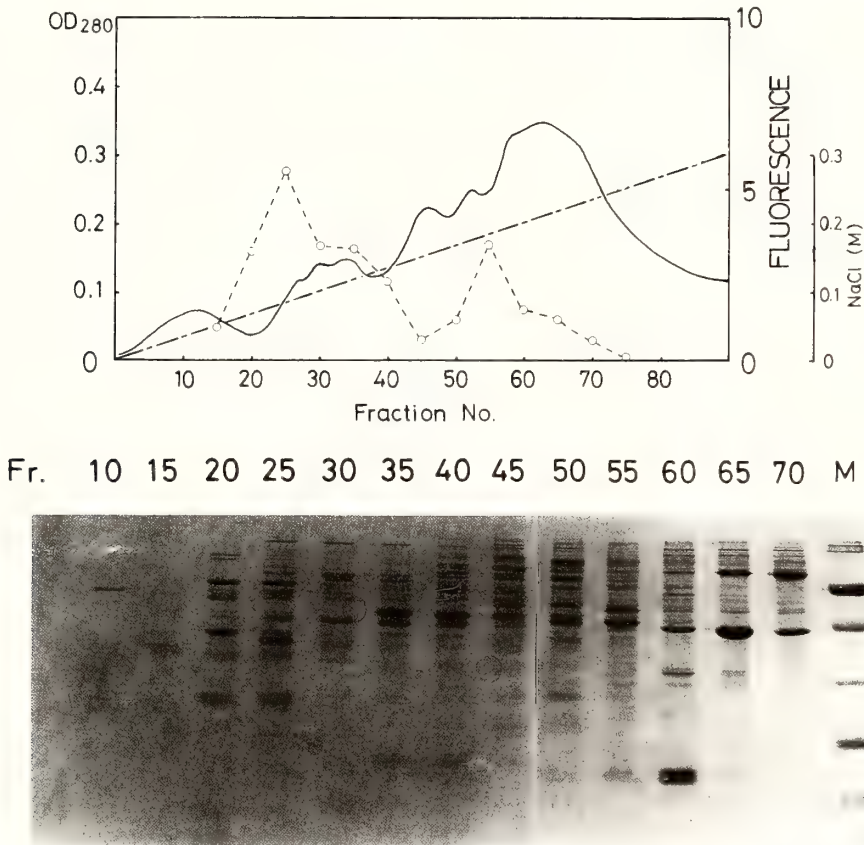


FIG. 2. DEAE-cellulose column chromatography. Sea urchin egg crude extract (240 mg protein) was dialyzed against DEAE-buffer and loaded onto a DEAE-cellulose column (3.2 \times 15 cm). The column was washed with DEAE-buffer and eluted with a 0–0.3 M linear NaCl gradient. Top: An elution pattern of the protein which was monitored by absorbance at 280 nm (solid line). 45K-A dissociating activity was monitored by fluorescence of DACM (broken line). Bottom: SDS-PAGE pattern of the eluted proteins. Numbers at the top indicate fraction numbers. Marker proteins (M) are BSA (MW, 68,000), ovalbumin (45,000), carbonic anhydrase (30,000), Soybean trypsin inhibitor (20,000), cytochrome C (13,000).

released at all by incubation up to 24 hr with DEAE-buffer which contained EGTA. This suggested that DACM-labeled actin was not adsorbed non-specifically but formed a complex with 45K protein that was not dissociated in the presence of EGTA.

Egg extract was dialyzed against DEAE-buffer overnight and applied to a DEAE-cellulose column which was preequilibrated with DEAE-buffer. Proteins were eluted with a 0–0.3 M linear

NaCl gradient. The dissociating activities of 45K-A were eluted as two peaks (Fig. 2). The fractions eluted between 0.09–0.11 M NaCl (DEAE fraction), that is the major peak, were pooled and used in the following experiments.

The DEAE fraction was diluted to various protein concentrations and assayed for 45K-A dissociating activity (Fig. 3). The rate of 45K-A dissociation was dependent upon the protein concentration of the DEAE fraction. The amount of

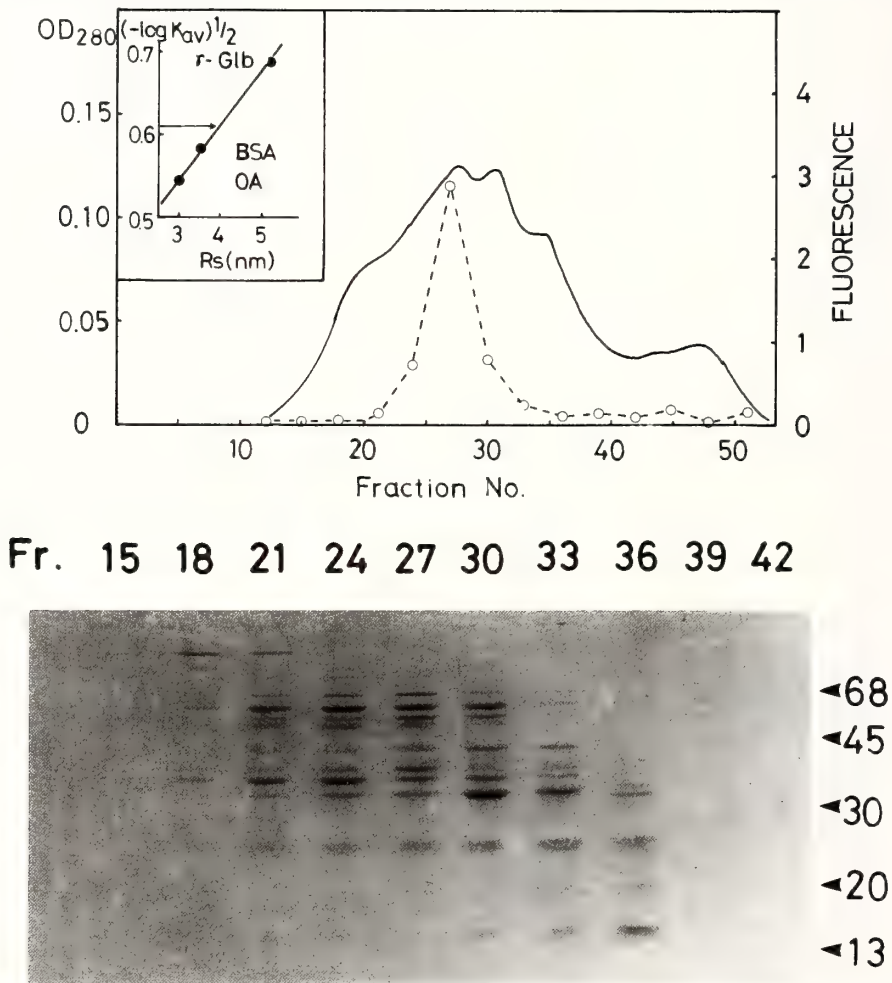


FIG. 3. Sephacryl S-300 column chromatography. DEAE fractions 25–30 were pooled, concentrated by Centriflo C-25, applied to a Sephacryl S-300 column (1.2×60 cm) which was preequilibrated and eluted with F-buffer. Top: Solid line represents an elution pattern of the protein which was monitored by absorbance at 280 nm. The 45K-A dissociating activity was monitored by fluorescence of DACM (broken line). Stokes radius of the 45K-A dissociation factor (s) was estimated from the elution volume of standard marker proteins (inset). Standard marker proteins used for estimation were γ -globulin (γ -Glb), BSA and ovalbumin (OA). Bottom: SDS-PAGE pattern of the active fractions. Numbers at the top indicate fraction numbers. Those at the right indicate MW×10⁻³.

fluorescence dissociated reached a plateau level within 18 hours. The final amount of the fluorescence dissociated was proportional to the protein concentration of the DEAE fraction. This suggested that the dissociation was not due to proteolysis or other enzymatic reactions.

In order to investigate the nature of the dissociating factor, the DEAE fraction was treated with heat, trypsin, or RNase (Table 1). Heat treatment at 100°C for 3 min reduced the dissociating activity to 2% of the original activity, while trypsin digestion reduced it to 24%. In contrast, RNase treatment did not affect the dissociating activity, suggesting that the dissociating factor(s) in the DEAE fraction is protein.

Since the factors could be other actin-modulating proteins, the effects of actin-depolymerizing proteins on the dissociation of 45K-A were investigated by incubating 45K-A with profilin or depactin. However, the dissociation of 45K-A was not observed (Table 2).

The DEAE fraction was concentrated with Centrifo C-25, applied to a Sephacryl S-300 (Pharmacia) column, and eluted with F-buffer (10 mM 3-[N-Morpholino] propanesulfonic acid (MOPS), 0.1 M KCl, 0.2 mM ATP, 0.2 mM DTT, 0.5 mM EGTA, 1 µg/ml leupeptin, and 5 mM NaN₃, pH 7.2) (Fig. 4). The dissociating activity was eluted as a symmetric peak at fractions 25-30. The top

fraction corresponded to the Stokes radius of 4.1 nm. The elution pattern of proteins was investigated by SDS-PAGE and was compared with that of the activity. It was found that three polypeptides, the molecular weight of which were 40,000, 60,000, and 70,000, coeluted with the activity.

DISCUSSION

Fluorescence energy transfer is often used to detect association or dissociation of proteins [17]. At first, we attempted to study the dissociation of 45K-A by this method. N-iodoacetyl-N'-(5-sulfo-1-naphthyl) ethylenediamine (IAEDANS) and fluorescein isothiocyanate (FITC) were chosen to be energy donor and acceptor, respectively. However, in this experiment, the addition of EGTA was required to remove Ca²⁺ and this step had an effect on the fluorescence of FITC. Although the presence of either EGTA or Ca²⁺ alone did not interfere with FITC fluorescence, FITC fluorescence was quenched in the presence of a micromolar order of EGTA-Ca²⁺ complex (data not shown). This made it impossible to quantify the amount of dissociated 45K-A by fluorescence energy transfer.

Therefore, we had to devise a new system. To quantify the amount of dissociated 45K-A, 45K

TABLE 1. Effect of heat, trypsin or RNase treatment on the 45K-A dissociating activity.

Sample	Relative amount of dissociated 45K-A
Untreated DEAE fraction (122 µg/ml)	100
Heat-treated DEAE fraction (100°C, 3 min)	2
Trypsin-digested DEAE fraction (1 µg/ml, 5 min)	24
RNase-treated DEAE fraction (10 µg/ml, 5 min)	100

TABLE 2. Effect of low molecular weight actin-modulating proteins on the dissociation of 45K-A.

Sample	Relative amount of dissociated 45K-A
DEAE fraction (122 µg/ml)	100
Sea urchin egg profilin (13 µg/ml)	3
Starfish oocyte depactin (20 µg/ml)	7

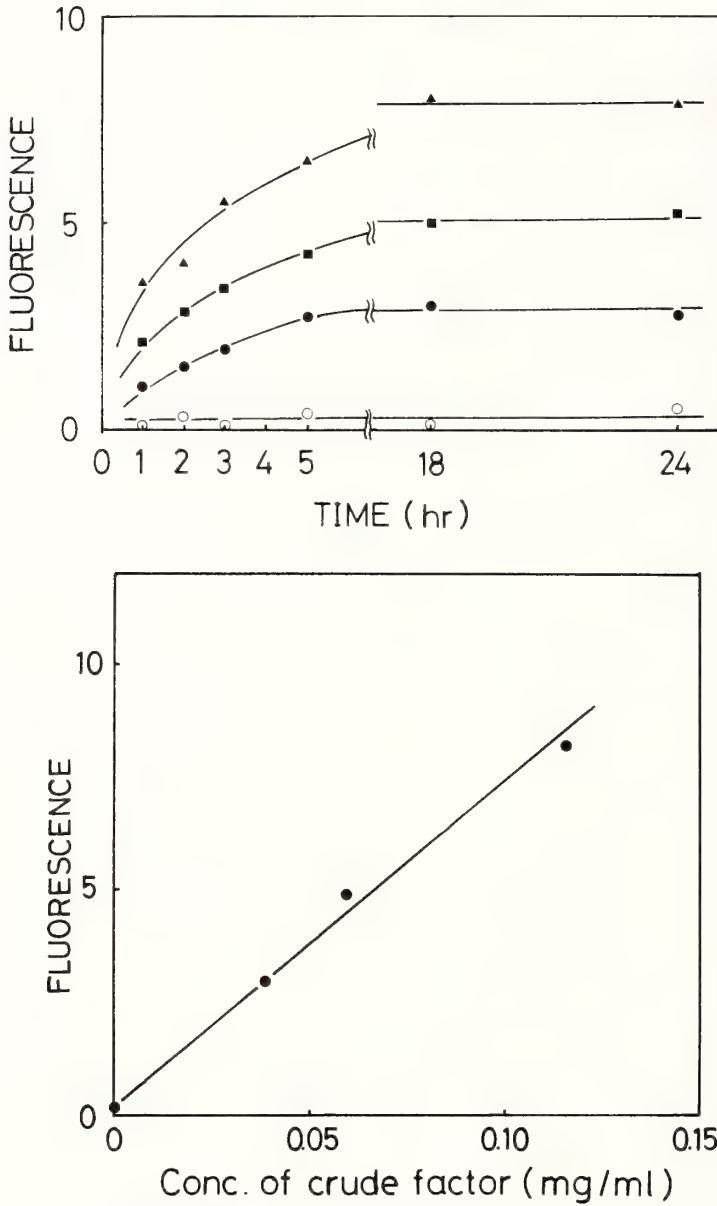


FIG. 4. Time course of the dissociation of 45K-A in the presence of the DEAE fraction. Top: The DEAE fraction having dissociating activity was diluted to various protein concentrations and 45K-A was dissociated by the addition of the diluted fractions. The amount of the dissociated 45K-A was monitored by the fluorescence of the DACM. ●: 41 $\mu\text{g/ml}$. ■: 61 $\mu\text{g/ml}$. ▲: 122 $\mu\text{g/ml}$. When DEAE-buffer was added instead of the DEAE fraction, no fluorescence was observed (○). Bottom: The amount of released fluorescence at 24 hr after addition of the DEAE fraction (ordinate) was plotted against the protein concentration of the added fraction (abscissa).

protein was adsorbed to the microtiter plate and DACM-labeled actin was added in the presence of Ca^{2+} to form 45K-A. By use of this system, we found that 45K-A was dissociated by incubation

with sea urchin egg extract, and that 45K-A dissociating activity was due to protein factors. The Stokes radius of the factors was estimated to be 4.1 nm.

The time course study (Fig. 3) showed that the dissociation of 45K-A was proportional to the protein concentration of DEAE fraction added. This suggested that the dissociation was not due to digestion of proteins by proteases or to other enzymatic reaction. The dissociation took 6–18 hours to reach a maximum level. We know of no reason why 45K-A dissociated so slowly, but it is likely that the conditions we used for dissociation were not optimal.

The dissociating activity decreased during the course of purification and we have not yet purified the factor(s). The reason for this decrease in the activity is not known.

We know that 45K protein from sea urchin egg severs the actin filament in the presence of micromolar Ca^{2+} [5]. Gelsolin and fragmin possess a similar activity [18–20]. These proteins also form complexes with actin in the presence of Ca^{2+} [17, 21], and once complex is formed, it is not dissociated readily by removal of Ca^{2+} with EGTA [22]. These EGTA-stable complexes do not have an actin-severing activity, but cap the barbed end of the actin filament and thus cause the depolymerization of actin. Therefore, the complex that is formed upon the fragmentation of actin caps the newly appearing barbed end of the actin filament. The 45K-A dissociating factor(s) may remove the 45K protein from the capping end of the actin filament to allow further elongation of the filament from this end at the rearrangement of the actin cytoskeleton during the development of the egg. This might result in the recirculation of the 45K protein. It is necessary to purify the dissociating factor and to clarify the mode of dissociation of 45K-A.

ACKNOWLEDGMENTS

This work was supported by Grants-in-aid for Scientific Research from the Ministry of Education, Science and Culture, Japan.

REFERENCES

- Mabuchi, I. (1986) Biochemical aspects of cytokinesis. *Int. Rev. Cytol.*, **101**: 175–213.
- Otto, J. J., Kane, R. E. and Bryan, J. (1979) Formation of filopodia in coelomocytes: Localization of fascin, a 58,000 dalton actin crosslinking protein. *Cell*, **17**: 285–293.
- Mabuchi, I. and Hosoya, H. (1982) Actin-modulating proteins in the sea urchin egg. II. Sea urchin egg profilin. *Biomed. Res.*, **3**: 465–476.
- Hosoya, H., Mabuchi, I. and Sakai, H. (1982) Actin modulating proteins in the sea urchin egg. I. Analysis of G-actin-binding proteins by DNase I-affinity chromatography and purification of a 17,000 molecular weight component. *J. Biochem.*, **92**: 1853–1862.
- Wang, L.-L. and Spudich, J. A. (1984) A 45,000-mol-wt protein from unfertilized sea urchin egg severs actin filaments in a calcium-dependent manner and increases the steady-state concentration of nonfilamentous actin. *J. Cell Biol.*, **99**: 844–851.
- Hosoya, H. and Mabuchi, I. (1984) A 45,000-mol-wt protein-actin complex from unfertilized sea urchin egg affects assembly properties of actin. *J. Cell Biol.*, **99**: 994–1001.
- Mabuchi, I., Hamaguchi, Y., Kobayashi, T., Hosoya, H., Tsukita, Sa. and Tsukita, Sh. (1985) Alpha-actinin from sea urchin eggs: biochemical properties, interaction with actin, and distribution in the cell during fertilization and cleavage. *J. Cell Biol.*, **100**: 375–383.
- Hosoya, H., Mabuchi, I. and Sakai, H. (1986) An 100-kDa Ca^{2+} -sensitive actin-fragmenting protein from unfertilized sea urchin egg. *Eur. J. Biochem.*, **154**: 233–239.
- Mabuchi, I. and Kane, R. E. (1987) A 250K-molecular-weight actin-binding protein from actin-based gels formed in sea urchin egg cytoplasmic extract. *J. Biochem.*, **102**: 947–956.
- Ohnuma, M. and Mabuchi, I. (1986) The 45K molecular weight actin-modulating protein from sea urchin egg forms a complex with actin in the presence of calcium ions. *J. Biochem.*, **100**: 817–820.
- Coluccio, L. M., Sedlar, P. A. and Bryan, J. (1986) The effects of a 45,000 molecular weight protein from unfertilized sea urchin eggs and its 1:1 actin complex on actin filaments. *J. Muscle Res. Cell Motility*, **7**: 133–141.
- Kurth, M. C. and Bryan, J. (1984) Platelet activation induces the formation of a stable gelsolin-actin complex from monomeric actin. *J. Biol. Chem.*, **259**: 7473–7479.
- Spudich, J. A. and Watt, S. (1971) The regulation of rabbit skeletal muscle contraction. I. Biochemical studies of the interaction of the tropomyosin-troponin complex with actin and the proteolytic fragments of myosin. *J. Biol. Chem.*, **245**: 4866–4871.
- Laemmli, U. K. (1970) Cleavage of structural proteins during the assembly of the head of bacteriophage T4. *Nature (London)*, **227**: 680–685.

- 15 Lowry, O. H., Rosebrough, N. J., Farr, A. L. and Randall, R. J. (1951) Protein measurement with the folin phenol reagent. *J. Biol. Chem.*, **193**: 265-275.
- 16 Laurent, T. C. and Killander, J. (1964) A theory of gel filtration and its experimental verification. *J. Chromatogr.*, **14**: 317-330.
- 17 Giffard, R. G., Weeds, A. G. and Spudich, J. A. (1984) Ca^{2+} -dependent binding of severin to actin: A one-to-one complex is formed. *J. Cell Biol.*, **98**: 1796-1803.
- 18 Yin, H. L. and Stossel, T. P. (1980) Purification and structural properties of gelsolin, a Ca^{2+} -activated regulatory protein of macrophages. *J. Biol. Chem.*, **255**: 9490-9493.
- 19 Hasegawa, T., Takahashi, S., Hayashi, H. and Hatano, S. (1980) Fragmin: a calcium ion sensitive regulatory factor on the formation of actin filaments. *Biochemistry*, **19**: 2677-2683.
- 20 Yamamoto, K., Pardee, J. D., Reidler, J., Stryer, L. and Spudich, J. A. (1982) Mechanism of interaction of *Dictyostelium* severin with actin filaments. *J. Cell Biol.*, **95**: 711-719.
- 21 Bryan, J. and Kurth, M. C. (1984) Actin-gelsolin interactions: evidence for two actin-binding sites. *J. Biol. Chem.*, **259**: 7480-7487.
- 22 Kurth, M. C., Wang, L.-L., Dingus, J. and Bryan, J. (1983) Purification and characterization of a gelsolin-actin complex from human platelets. *J. Biol. Chem.*, **258**: 10895-10903.

Actin in Cytokinesis: Formation of the Contractile Apparatus

EDWARD M. BONDER¹, DOUGLAS J. FISHKIND, JOHN H. HENSON,
NINA M. COTRAN and DAVID A. BEGG

*Department of Biological Sciences, Rutgers University, Newark, NJ 07102 and
Department of Anatomy and Cellular Biology, Harvard Medical
School, LHRB, Boston, MA 02115, U.S.A.*

ABSTRACT—The phenomenon of cytokinesis in animal cells is driven by the actin and myosin based contractile apparatus located within the cell's cleavage furrow. In this report, we have examined the organizational dynamics of the sea urchin egg's cortical actin cytoskeleton during the process of cytokinesis. Whole mounts, frozen sections and isolated cortices of fertilized and cleaving eggs were probed with either fluorescent-phalloidin or actin antibodies. Ultrastructural analysis of cortical actin filament organization was obtained by examining quick-frozen, deep-etched and rotary shadowed replicas of isolated zygote cortices. These experimental procedures demonstrated the change in spatial and temporal distribution of actin filaments within the dividing egg, leading to the extensive network organization of filaments within the contractile band apparatus. To address the mechanism of molecular regulation of the actin filament network, the structural properties of egg spectrin were analysed with regard to its relatedness to other spectrins, its relatedness to *T. gratilla* 220K actin binding protein and its presence in the fertilized egg cortex. Finally, the 'collapsing baby-gate' model for cytokinesis is presented, describing the genesis of the actin filament component of the contractile apparatus and its potential regulation by actin filament crosslinking proteins.

INTRODUCTION

The history of research examining the mechanism of cell division contains a wealth of exciting and ingenious experimentation (see [1-3] for excellent reviews). In many of these studies, eggs of marine organisms have often served as a primary experimental system. For example, Dan, his colleagues and others have used marine eggs and embryos to probe for cell membrane dynamics [4-6], cortical cytoplasm dynamics [4-6], spindle-membrane interactions [7, 8], microfilaments and myosin interactions [9, 10], and cytoplasmic rheological changes [11-13] associated with cytokinesis. In simplest terms, cytokinesis results from the action of an actin-myosin based contractile system, the contractile ring [1, 2, 9, 10, 14], whose temporal and spatial manifestation is in part deter-

mined by the mitotic spindle [1, 3, 7, 8]. The molecular signals and structural changes modulating the egg's actin cytoskeleton during cell division still remain largely unresolved.

Recently, using fluorescent cytochemistry of whole mounts, frozen sections and isolated cortices, in concert with rapid-freeze and deep-etch analysis of cortices, our labs have been able to define actin's molecular and structural disposition within the unfertilized egg cortex [15, 16]. In this report, the aforementioned methods were applied to fertilized and dividing sea urchin eggs in an effort to investigate the organizational changes in the actin cytoskeleton during cytokinesis. To begin dissecting the molecular basis of the egg's actin microfilament-membrane association, Fishkind *et al.* ([17], also see [18]) have isolated and identified sea urchin egg spectrin. Interestingly, the egg spectrin isoform is Ca⁺⁺-sensitive in its binding interaction with actin filaments [17]. Here, we present data demonstrating egg spectrin's presence in the isolated cortex of fertilized eggs and spectrin's relatedness to another egg actin filament

Accepted March 17, 1988

¹ Reprint requests to: Dr. E. M. Bonder, Department of Biological Sciences, Rutgers University, 101 Warren Street, Newark, NJ 07102, U.S.A.

crosslinking protein, *T. gratilla* 220K [19].

Based on our results using light and electron microscopy of fertilized eggs and isolated cortices, as well as the observations of many other investigators (for reviews see [1–3]), a model is presented describing the structural dynamics of the cortical actin cytoskeleton, leading to the formation of the 'contractile apparatus'. Finally, we discuss how Ca^{++} -sensitive actin filament crosslinking molecules may participate in modulating the physical characteristics of the actin cytoskeleton during the events of cell division.

MATERIALS AND METHODS

S. purpuratus (from Marinus, Inc., Westchester, CA), *A. punctulata* (from Marine Biological Laboratory, Woods Hole, MA) and *L. variegatus* (from Susan Decker, Hollywood, CA) eggs were obtained and prepared according to Begg and Rebhun [20] and used within two hours of collection. Eggs were fertilized by addition of dilute sperm solutions. Fertilization envelopes were removed by mechanical stripping and the eggs were subsequently washed and reared in gently circulating Ca^{++} -free sea water [21].

Light microscopy Developing zygotes were collected by gentle centrifugation in a hand operated centrifuge. The concentrated cells were fixed by rapid addition of a 20-fold volume excess of Ca^{++} -free sea water fortified with 50 mM EGTA containing 1–3.7% formaldehyde solution. The stock 37% formaldehyde solution contained 11% methanol or less and these methanol concentrations were of utmost importance for preserving visible surface microvilli and rhodamine (rh)-phalloidin (Molecular Probes, Junction City, OR) staining of actin filaments. Higher concentrations of methanol in the formaldehyde solutions resulted in a diminution of phalloidin staining in eggs (personal observation) and tissue culture cells (Dr. M. Rutten, personal communication). The zygotes were fixed for 1 hr on ice before further processing.

Fixed cells were washed out of fix by washing in 0.1% Triton X-100 in phosphate buffered saline (TX-PBS) and then incubated in TX-PBS contain-

ing 50 nM rh-phalloidin for 1 hr. After incubation, the cells were incubated in TX-PBS to remove excess label, mounted on slides [22] and examined by epifluorescence or Nomarski light microscopy.

Frozen sections were prepared according to the methods of Tokuyasu [23] as detailed by Bonder *et al.* [15]. Briefly, the fixed cells were embedded in gelatin, equilibrated in graded sucrose series and frozen by immersion into liquid nitrogen cooled Freon-22. Semi-thin sections were cut on a Reichert Ultracut E Ultramicrotome equipped with a cryo-stage. The sections were probed either with rh-phalloidin or with an affinity purified anti-actin antibody (generously donated by Drs. K. Fujiwara and S. Hagen). For indirect immunofluorescence a commercially available (Hyclone, Ogden City, Utah, USA) rhodamine labeled goat anti-rabbit antibody was used at a 1:200 dilution [15].

Electron microscopy Egg cortices were prepared according to the shearing method of Vacquier [24]. Isolated cortices were quick-frozen, deep-etched and rotary-shadowed using the Heuser and Kirschner technique [25]. Complete details of cortex preparation, fixation, myosin S-1 decoration and light microscopic rh-phalloidin staining are described in Henson and Begg [16]. Replicas of the cortices were examined on a JEOL-100CX at an accelerating voltage of 80 kV.

Egg spectrin preparation and analysis Egg spectrin was prepared according to Fishkind *et al.* [17]. Chicken erythrocyte spectrin was a gift from Dr. T. Coleman and human brain spectrin was a gift from Dr. A. Harris. Following extensive dialysis against 75 mM KCl, 1 mM MgCl_2 , 0.2 mM CaCl_2 and 10 mM Imidazole pH 7.2, the various spectrin preparations were rotary shadowed according to Tyler and Branton [26] and examined by electron microscopy.

Purified spectrins and egg preparations were analysed by immunoblotting [27] using monoclonal (a gift from Dr. J. Bryan) and polyclonal (a gift from Dr. J. Otto) antibodies raised against *T. gratilla* 220K actin binding protein [19]. Proteins were run on SDS-PAGE, transferred to Zeta-Probe (Bio-Rad, Richmond, CA) and reacted with

anti-220K anti-serum (1:250 dilution) followed by immunodetection using a 1:1000 dilution of alkaline phosphatase conjugated secondary antibody (Hyclone, Ogden City, Utah) according to Dubreuil *et al.* [28].

Analysis of spectrin-like proteins in fertilized egg cortices was carried out on cortices isolated according to Begg and Rebhun [20]. Following isolation, the cortices were incubated in Solution A (75 mM KCl, 5 mM MgCl₂, 5 mM EGTA, 0.5 mM DTT and 20 mM Hepes pH 7.5) or Solution A containing 250 mM KCl or Solution A containing 0.2 mM CaCl₂ for 30 min on ice. The cortices were then sedimented in a microfuge for 10 min and the resultant supernates and pellets stoichiometrically analysed on SDS-PAGE.

Other methods Myosin subfragment-1 was prepared according to Margossian and Lowey [29]. SDS-PAGE was carried out according to Laemmli [30] and gels were stained with Coomassie Blue [31]. Light microscopic observations were performed using a Zeiss ICM-405 and images were recorded on Kodak Tri-X 35 mm film.

RESULTS

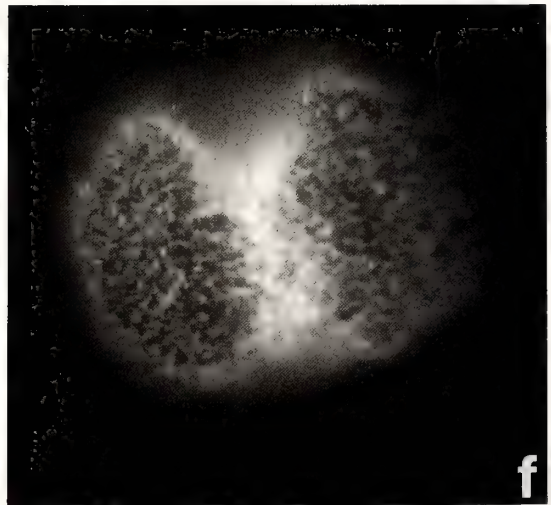
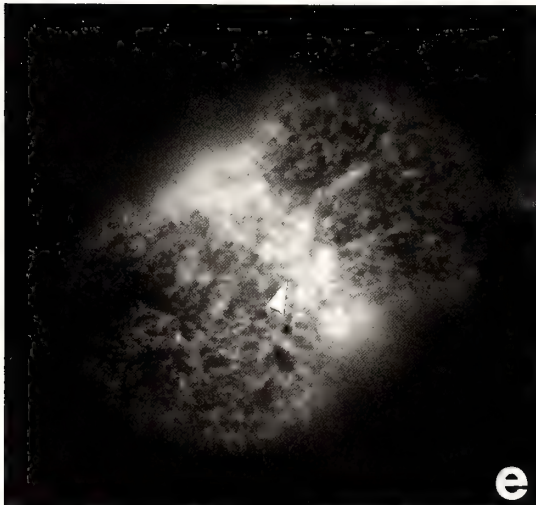
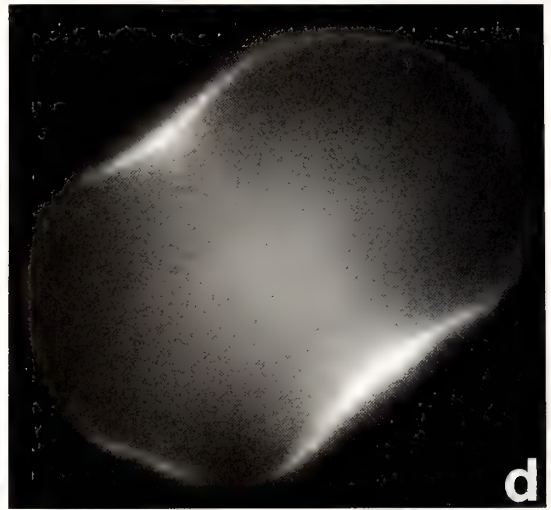
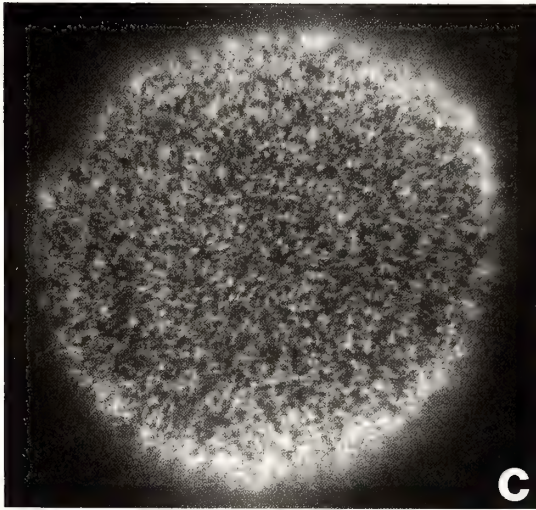
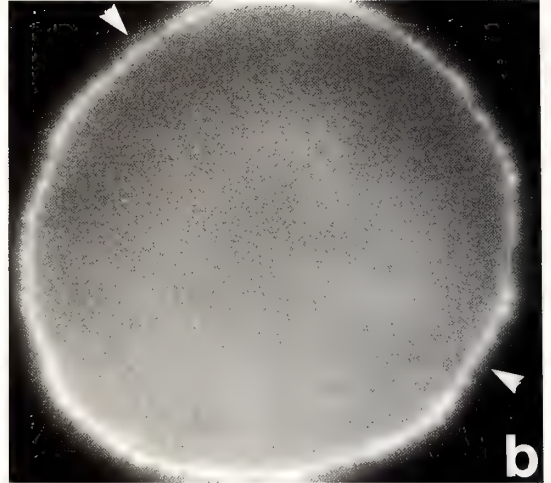
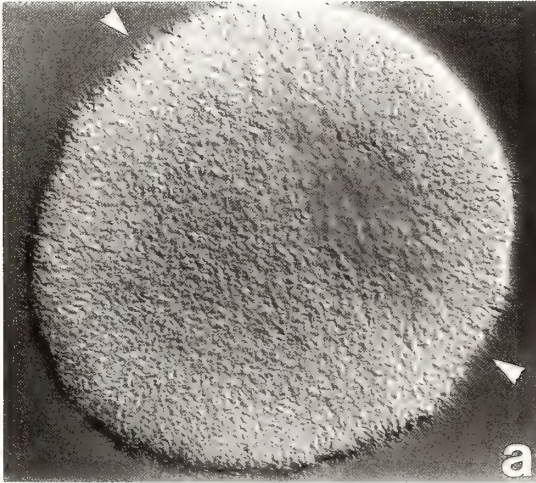
Rhodamine-phalloidin staining of fertilized and dividing sea urchin eggs

Staining of cells and tissues with rhodamine (rh)-phalloidin has become a primary method for identifying and localizing F-actin [32]. To investigate global changes in cortical (microvillar and sub-membraneous) actin distribution during cytokinesis, fertilized and dividing eggs were gently fixed, permeabilized and reacted with rh-phalloidin. As judged by light microscopic (Nomarski optics) comparisons of fixed and unfixed cells, there were no detectable structural alterations following fixation (Fig. 1a). Cytochemical staining of fertilized eggs with rh-phalloidin resulted in bright cortical fluorescence (Fig. 1b) with readily observable labeling of individual microvilli that are uniformly spread across the surface of the egg (Fig. 1b). Examination of the eggs *en face* further demonstrated the uniform distribution of microvillar staining across the egg surface (Fig.

1c). In these whole mount preparations it was difficult to definitively identify a sub-membraneous staining component (Fig. 1b).

Cleaving eggs displayed a dramatic increase in the staining intensity at the cleavage furrow (Fig. 1d). The increased fluorescence resulted both from an increase in fluorescence of the microvillar layer as well as from the appearance of a sub-membraneous band approximately 30 μ m wide (Fig. 1d). This sub-membraneous staining represents the nascent stages of contractile apparatus formation within the cleavage furrow region. Additionally, the microvillar staining density is greater within the cleavage furrow than out at the poles (Fig. 1d). This corresponds to the apparent increase in microvillar density within the cleavage furrow that is observed by light microscopy of live and fixed samples of dividing eggs (personal observations, reviewed in [1]). When the same dividing cell (as in Fig. 1d) is observed in surface views, the bright cleavage furrow band is composed of an extensive anastomosing network of fluorescence (Fig. 1e). Occasionally, small 'randomly' oriented filamentous bundles or fascicles are seen within this contractile band (Fig. 1e, see arrow). Figure 1f depicts a cell that is 50% cleaved and the furrowing region continues to be composed of an extensive meshwork of filaments and filament bundles. In all of our observations on whole dividing cells, an organized circumferential alignment of filaments was never observed with rh-phalloidin staining.

To further examine the redistribution of cortical actin during cell division, fertilized and cleaving eggs were processed for frozen sectioning [15]. Examination of semi-thin frozen sections of fertilized eggs revealed discrete staining of the individual microvilli, and a less intense staining of the sub-membraneous actin domain (Fig. 2a, b). Cleaving eggs exhibited an increase in cleavage furrow staining both within the microvillar and sub-membraneous components (Fig. 2c). The differential distribution of microvillar and sub-membraneous actin within dividing eggs is further substantiated by indirect immunofluorescent staining of frozen sections with an anti-actin antibody (Fig. 2d), which was monospecific for *S. purpuratus* egg actin [15].



Rapid freeze, deep-etch and rotary-shadow observations of isolated cortices from fertilized and cleaving eggs

To investigate the ultrastructural organization of the actin filaments within the contractile band, isolated cortices were examined using rapid freeze according to Heuser and Kirschner ([25], see [16] for details). Fertilized cortices isolated 15 min post fertilization demonstrated the presence of elongate microvilli containing actin core bundles (Fig. 3a, b). The cytoplasmic plasma membrane surface is covered with numerous invaginating clathrin coated vesicles (Fig. 3a, b) and a sparse network of actin-like filaments (Fig. 3a, b). Cortices isolated from cleaving eggs resulted in the isolation of 'butterfly' shaped cortices having the contractile band located in the constricted region between the two wings (Fig. 3f). Recently, Yonemura and Kinoshita [33] and Maekawa *et al.* [34] have reported the isolation of similar cortices using dividing eggs. Myosin S-1 decorated and rapid-frozen cortices from cleaving eggs demonstrate the presence of an extensive three dimensional network of sub-membraneous actin filaments (Fig. 3d, e). The sub-membraneous network in cleaving eggs is clearly more extensive than that found at early times after fertilization (compare Fig. 3a and d). The image depicted in Figure 3d appears to correspond to the cleavage furrow because this cortex has a central constriction and long surface microvilli characteristic of the furrow region. Noteworthy is a striking absence of any detectable circumferential alignment of filaments within the cleavage furrow (Fig. 3d). This organization was indeed

surprising since rh-phalloidin staining of the isolated cortex suggests the presence of circumferentially aligned filament structures (Fig. 3f).

Certainly, a more extensive characterization of the ultrastructure in the isolated cortices is needed to thoroughly substantiate these exciting preliminary observations.

Structural and immunological characterization of egg spectrin

The structural conservation of three functionally diverse spectrin molecules — chicken erythrocyte, human brain and sea urchin egg — was examined by rotary shadowing according to Tyler and Branton [26]. Under the experimental conditions employed, all three spectrin isoforms are tetramers composed of two intertwined heterodimers forming an elongate (2–4 by 200–210 nm) molecule (Fig. 4, also see [17, 33]). Interestingly, in the presence of Ca^{++} , the sea urchin spectrin molecule, at times, exhibits a disruption of the alpha/beta interaction at the actin binding domain (Fig. 4c, also Fishkind, unpublished observations). The observed disruption at the actin binding domain may, in part, be responsible for the observed Ca^{++} effects on egg spectrin binding to actin filaments [17].

Previously, Bryan and Kane [19] isolated a 220K egg protein, from gelled egg extracts, that demonstrated the same elution profile on size exclusion columns and the same inability to bind actin in the presence of 100 mM KCl as has been observed for egg spectrin [17]. To test the immunological relatedness of these two molecules, monoclonal and polyclonal antibodies raised

Fig. 1. Rhodamine phalloidin staining of fertilized and cleaving *A. punctulata* eggs.

Panel a. Nomarski light micrograph of a fertilized egg probed with rh-phalloidin at the onset of spindle formation. Note the numerous microvilli covering the egg surface. Panel b. Fluorescence light micrograph of an equatorial view of the egg shown in panel a. There is clearly a one-to-one correlation between microvilli and rh-phalloidin fluorescence (compare arrowheads in panels a and b). Panel c. *En face* image of the egg in panels a and b. Notice the uniform distribution of fluorescence without any observable pattern. Panel d. Equatorial image of an rh-phalloidin stained egg that has started to undergo cytokinesis. There is now an increase in fluorescence intensity in the cleavage furrow as compared to the poles. The increased fluorescence is associated with the microvillae and submembraneous layers. Panel e. *En face* image of the cleaving egg in panel d. As expected there is an increase in staining intensity within the cleavage furrow which is composed of a filamentous network lacking any readily definable continuous circumferential alignment of filaments. Occasionally, short fluorescent actin fascicles (see arrowhead) are observed within the contractile band. Panel f. Rh-phalloidin egg that is 50% cleaved. Again, observe the continued presence of a network-type organization lacking any identifiable circumferential actin bundle even at this late stage of cytokinesis. Magnification: $\times 600$.

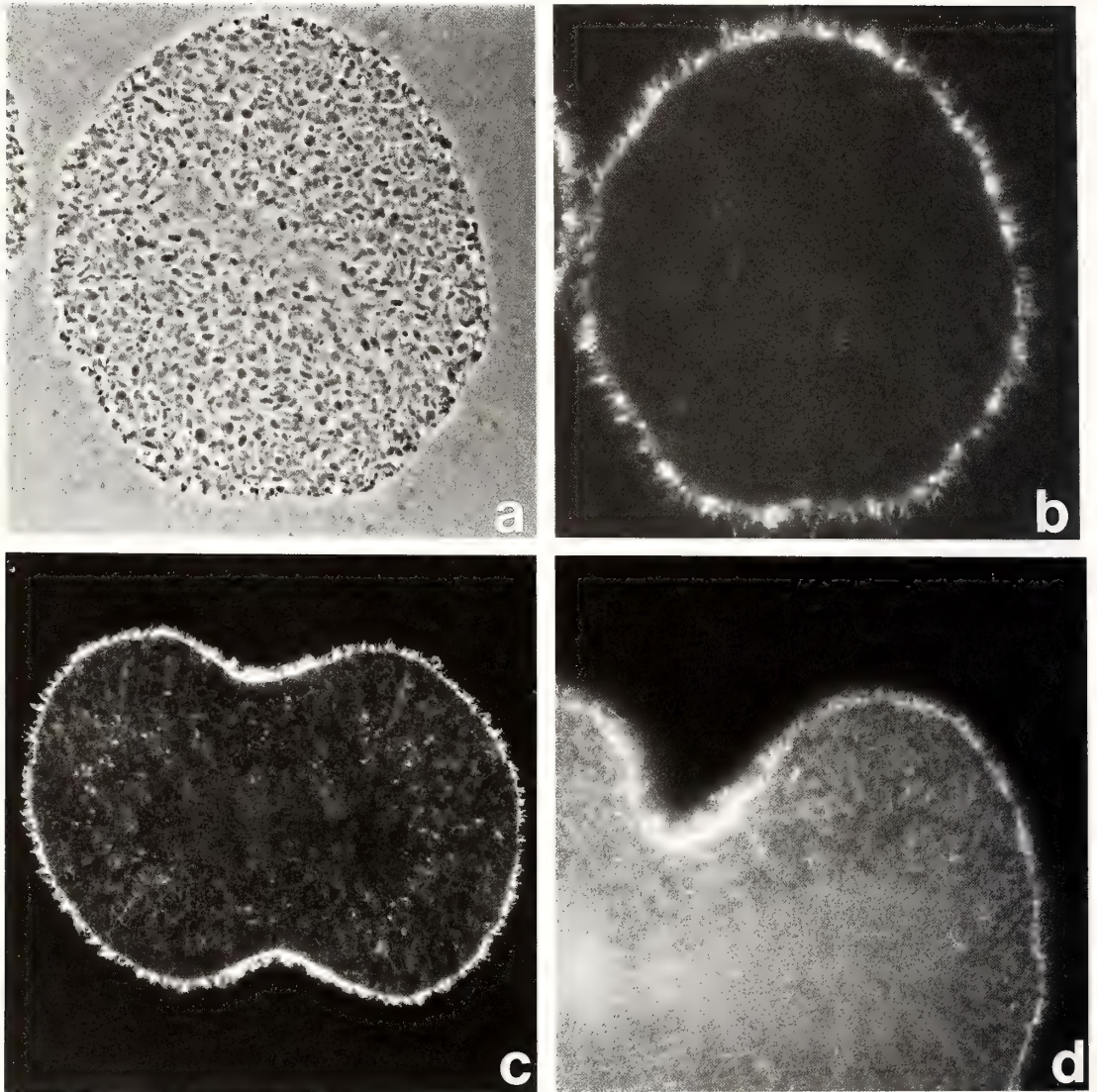


FIG. 2. Rh-phalloidin and actin immunofluorescence staining of frozen sections of fertilized and cleaving eggs.

Egg preparations equivalent to those used in Fig. 1 were prepared for semi-thin ($1-2\ \mu\text{m}$) frozen sections. Panel a. Phase contrast micrograph of a frozen section of fertilized *Arbacia* eggs probed with rh-phalloidin. In such preparations the elongate microvilli are readily observable. Panel b. Fluorescence micrograph of the egg shown in panel a. The microvilli are highly fluorescent with some indication of a submembraneous actin component. Panel c. Rh-phalloidin stained cleaving egg at approximately the same stage as shown in Fig. 1d. Notice the apparent increase in microvillar staining density at the cleavage furrow as compared to the poles. Additionally, there is the readily identifiable increase in fluorescence associated with the contractile band. Fluorescent staining of the mitotic spindle is never observed. Panel d. Indirect immunofluorescence of a *S. purpuratus* cleaving egg using monospecific actin antibodies. The actin immunofluorescence staining also demonstrates the increase in microvillar staining density compared to the poles and the increased concentration of actin within the contractile band of the cleavage furrow. Magnifications: a and b. $\times 700$; c. $\times 600$; d. $\times 1200$.

against the *T. gratilla* 220K protein were used for immunoblotting analysis. The monoclonal antibody cross-reacted with purified egg spectrin and a band that co-migrated with egg spectrin in *T. gratilla* gelled extract (Fig. 5). The polyclonal antiserum cross-reacted with purified egg spectrin as well as with both subunits of erythrocyte and brain spectrins (Fig. 5). Furthermore, the polyclonal antiserum is immunoreactive with a closely spaced doublet at 240 kDa in *T. gratilla* extracts similar to the closely spaced doublet composition of egg spectrin [17]. Recently, Mabuchi and Kane [35] have reported similar observations further demonstrating that *T. gratilla* 220K actin binding protein is actually a spectrin-related protein.

Unfortunately, we have not been successful at using the antibodies for immunocytochemical studies because the monoclonal does not appear to work on frozen sections and the polyclonal is highly immunoreactive, not only with spectrin, but also with a 250K polypeptide in eggs and isolated cortices (Fig. 5). Preliminary data (Fishkind, unpublished observations) suggests that the 250K cross-reactive polypeptide is a filamin-like protein and may be related to the 250K proteins isolated by two other groups [34, 35].

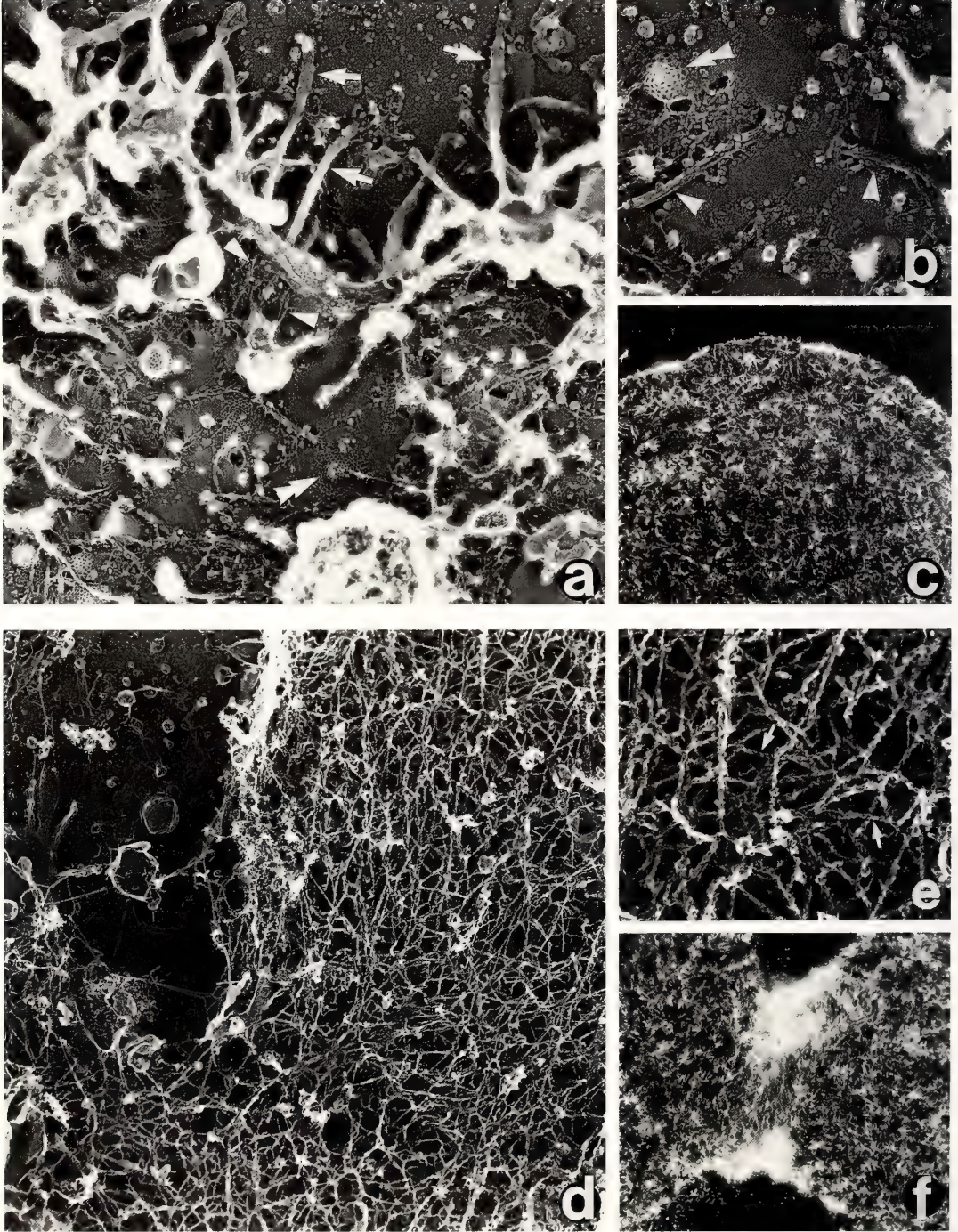
Immunoblotting fertilized egg cortices with the spectrin antibody (220K polyclonal) demonstrated the association of spectrin with the fertilized cortex. The salt and Ca^{++} sensitive extractability of the cortex associated spectrin was examined by incubating the isolated cortices in either Solution A or Solution A containing either 0.2 mM Ca^{++} or 250 mM KCl and 1 mM EGTA (see Materials and Methods). These experiments demonstrated the presence of a high molecular weight doublet in the isolated egg cortex that co-migrates with egg spectrin. The spectrin molecule is only slightly extracted by Ca^{++} even though greater than 50% of the actin is solubilized (Fig. 6). High salt was much more effective at liberating the egg spectrin from the cortex. Interestingly, the spectrin remained associated with the cortex in the presence of Ca^{++} even though the majority of the actin was solubilized (Fig. 6). This cortical association could be indicative of membrane anchorage by other red cell analogs present in the egg, such as ankyrin (see [36] for excellent review). Recent preliminary

results (Fishkind, unpublished observations) have shown a high affinity binding interaction ($K_d \sim 4 \times 10^{-7}$) between human red cell ankyrin and sea urchin egg spectrin.

DISCUSSION

The reorganization of cortical actin filaments during cytokinesis was investigated by examining whole mounts, frozen sections and rapid-freeze deep-etch preparations of fertilized and cleaving eggs. To follow the distribution of actin within the cortex, rh-phalloidin and indirect immunofluorescence were used for light microscopic observations. Three dimensional ultrastructural organization of the filaments was determined using rapid freeze techniques [16, 25]. The findings reported indicate that a global change in the distribution of cortical actin (microvillar core and submembraneous) occurs prior to or concomitant with the formation of the cleavage furrow. Redistribution brings about an increase in microvillar and submembraneous actin within the equatorial region as compared to the poles. This initial positional shift in actin probably establishes the actin component of the future actin-myosin contractile machinery [2, 9, 10, 14]. Careful inspection of the submembraneous actin indicates it is arranged as an extensive three-dimensional network of filaments and short bundles. This basic network organization is maintained throughout cytokinesis, and there are no detectable circumferentially aligned filaments. The visualization of circumferential contractile ring filaments [1, 14] by conventional thin section electron microscopy may in fact result from sectioning through the small filament fascicles observed by rh-phalloidin staining.

The temporal changes in the distribution of actin leading up to and during cytokinesis can be correlated to other changes within the cortex and membrane of the egg. Dan and colleagues, as well as others, have demonstrated that with the onset of cleavage there occurs: a. a 'stretching' or 'relaxation' of the membrane at the poles [4, 37]; b. a movement of cortically associated echinochrome granules away from the poles and toward the equator ([1, 4, 38, 39], and Begg, unpublished observations); c. a decrease in tension at the poles



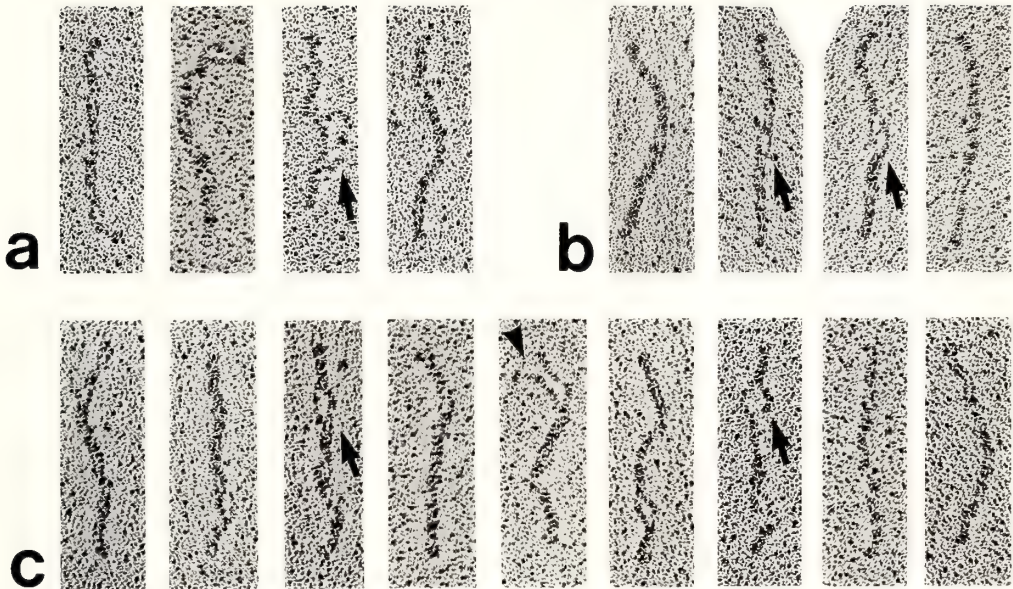


FIG. 4. Rotary shadowed images of three functionally diverse spectrin molecules.

Panel a. Chicken erythrocyte spectrin. Panel b. Human brain spectrin (fodrin). Panel c. Sea urchin egg spectrin. Each spectrin species shares an elongate (200–210 nm), interwoven morphology composed of two heterodimer units assembled into functional actin filament crosslinking tetramer. The ends of the tetramers often display an enlarged, globular domain while the interior portions show obvious regions of strand separation (see arrows). Note the disrupted subunit interaction within the egg spectrin molecule demonstrated in the panel c (center molecule, see arrowhead).

in association with the onset of cytokinesis [11–13, 40]. We believe the occurrence of these events is a direct consequence of the underlying cellular relocation of the actin filaments toward the plane of cleavage and away from the poles. For example, how does the actin cytoskeleton modulate cortical tension? Originally, increases and decreases in tension were attributed to an active contraction based on an actin-myosin interaction [40]. Recent-

ly, Schroeder [41] has demonstrated that myosin is not localized to the cortex of dividing blastomeres until the cleavage furrow starts to form, suggesting that cortical tension could be generated by an alternate mechanism. Rather than actin-myosin contraction, the cell could be regulating cortical tension by modulating the filament concentration in the cortex ([33, 42] and see Figs. 1–3) in coordination with changes in the degree of crosslinking

FIG. 3. Quick-freeze, deep-etch ultrastructural analysis of isolated *L. variegatus* fertilized and cleaving egg cortices.

Panel a. Replica of fertilized cortex isolated 15 min post-insemination depicting elongate microvilli at the edge of the cortex (see arrows). Microvillar core actin filament bundles (see arrowheads) can be seen emerging from the bases of the microvillar opening on the inner surface of the plasma membrane. Numerous invaginating clathrin coated vesicles (double arrowheads) are associated with the plasma membrane surface. Note, the relative absence of an actin filament network in association with the isolated cortex. Panel b. Higher magnification image of the microvillar actin filament bundles (arrowheads) observed in panel a. Panel c. Rh-phalloidin stained cortex of an equivalent preparation to panel a. Panel d. Quick-freeze replica of an isolated cortex from a dividing cell in the region of the cleavage furrow after decoration with myosin S-1. Note the presence of an extensive anastomosing network of decorated actin filaments and the apparent absence of a circumferentially aligned filament bundle. Panel e. Higher magnification of panel d illustrating the 'twisted rope' appearance (see arrows) of the isotropic network of decorated actin filaments. Panel f. Rh-phalloidin stained cortex from a preparation equivalent to panel d. Note the characteristic 'butterfly' shape of the cleaving egg cortex with the intense staining of the furrow region. Magnifications: a. $\times 20,000$; b and e. $\times 70,000$; c and f. $\times 520$; d. $\times 17,000$.

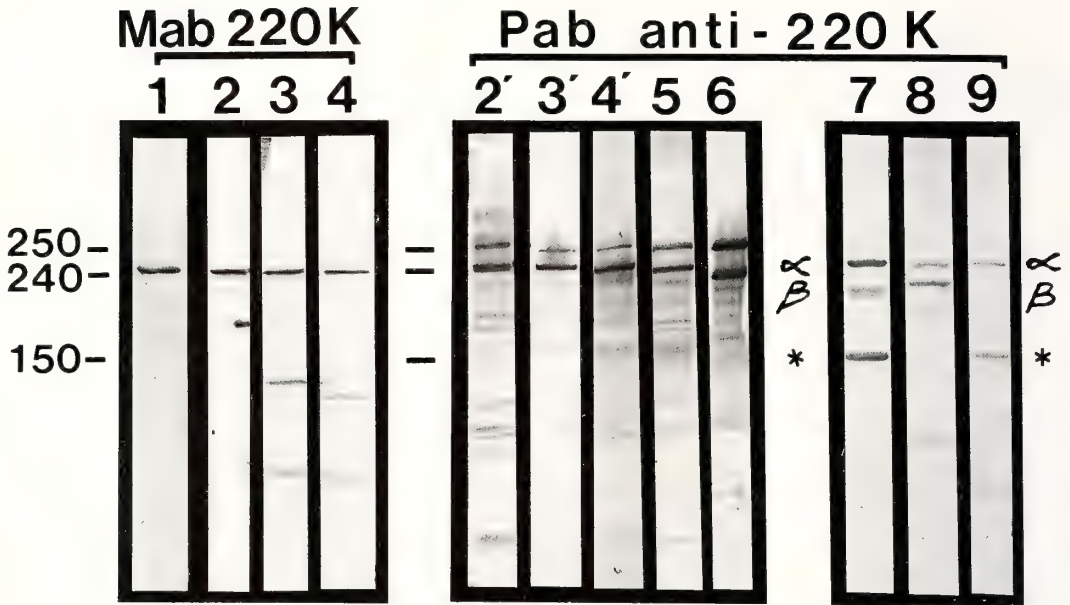


FIG. 5. Immunoblot analysis demonstrating the immunological relatedness of egg, red cell, and brain spectrins to *T. gratilla* 220K actin binding protein.

A monoclonal antibody (IgG1) raised against *T. gratilla* 220K protein (Mab 220K) crossreacts with purified *S. purpuratus* egg spectrin (lane 1), and a 240 kDa polypeptide present in *T. gratilla* egg extracts (lane 2), *A. punctulata* eggs (lane 3) and *S. purpuratus* eggs (lane 4). Additionally, a polyclonal antibody serum made against *T. gratilla* 220K (Pab 220K) crossreacts with both egg spectrin and a 250 kDa polypeptide in samples of *T. gratilla* extracts (lane 2'), *A. punctulata* eggs (lane 3') and *S. purpuratus* eggs (lane 4'). Pab 220K also recognizes spectrin and a 250 kDa in preparations of isolated *S. purpuratus* cortices (lane 5), 230 kDa and 250 kDa polypeptides in *S. purpuratus* coelomocytes (lane 6) chicken erythrocyte spectrin (lane 7), goat erythrocyte spectrin (lane 8) and human brain spectrin (lane 9). Note, the presence of an immunoreactive doublet at 240 kDa in *T. gratilla* egg extracts (lane 2'). Interestingly, the coelomocyte sample does not contain a 240 kDa polypeptide immunoreactive with Pab 220K. The asterisk marks the position of the 150 kDa proteolytic fragment of vertebrate spectrins.

of filaments to each other and to the membrane. A viable candidate for this crosslinking role is egg spectrin because it crosslinks filaments [17] and is associated with the fertilized egg cortex ([43], and see Fig. 6). For a more detailed discussion of egg spectrin's role in regulating the rheological properties of the egg cortex, see Fishkind *et al.* [17].

Coalescence of the cortical actin structure toward the future cleavage furrow may result from localized changes in the degree of regional crosslinking. Diminished crosslinking density between the poles and the equator would manifest itself as a gradual 'migration' of the cortical actin cytoskeleton away from the poles and toward the equator. This lower crosslinking at the poles is physically measured as a decrease in cortical tension [11-13, 40]. Additionally, the equatorial

translocation of actin would either passively or actively redistribute the echinochrome granules associated with the submembraneous actin network [1, 4, 38, 39].

Following the establishment of the actin component of the contractile band apparatus, myosin is finally positioned in the nascent cleavage furrow to provide the force needed for cell division [9, 10, 41, 44]. The force generation is isotropic, leading to a 'collapse' of the contractile band apparatus. Thus as modeled by White and Borisy [45], cell division proceeds by the tightening of an isotropic network of filaments rather than by the use of circumferentially aligned filaments. This revised version for the mechanism of constructing the contractile apparatus for cytokinesis is referred to, by our labs, as the 'Collapsing Baby-Gate' hypoth-

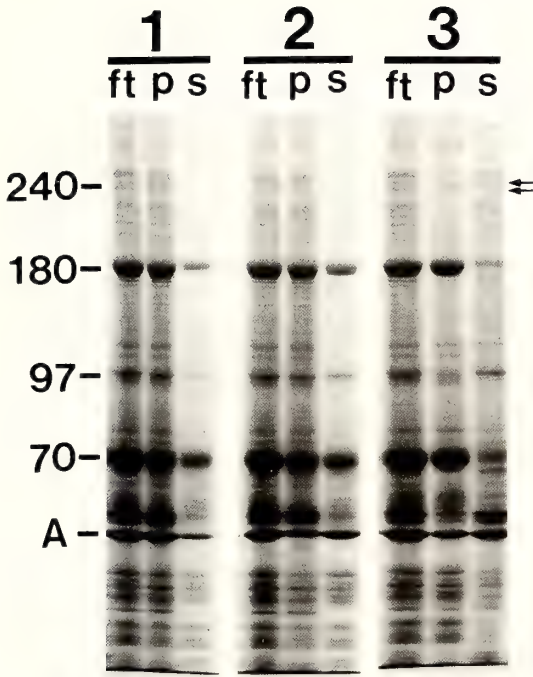


FIG. 6. Solubilization of proteins from isolated fertilized egg cortices.

Panel 1: Cortices prepared in Solution A (75 mM KCl, 5 mM MgCl₂, 5 mM EGTA and 20 mM Hepes, pH 7.5). Panel 2: Cortices in Solution A containing 0.2 mM CaCl₂ final concentration. Panel 3: Cortices in Solution A containing 250 mM KCl and 1 mM EGTA. Note, in the presence of Ca⁺⁺ (Panel 2) a small amount of spectrin (240K doublet, see arrows) is released into the supernatant (s). At higher ionic strength (Panel 3) this effect is greatly enhanced. Ft: sample of cortex prior to extraction. P: sample of pellet after extraction. S: sample of supernate after extraction.

esis.

Hypothetical model for the mechanism of cytokinesis

Over the years there have been many models proposed to describe the mechanism of cytokinesis [1-3, 11, 37, 40, 45, 46]. The model presented below incorporates our findings on actin dynamics within the egg and the finding and ideas of many previous investigators in an attempt to provide a testable hypothesis for the mechanism of cytokinesis.

1. Prior to the onset of cleavage there is a net

increase in filament number ([33, 42], also see Figs. 1-3) as well as a net increase in filament-filament and filament-membrane crosslinking within the egg cortex. This change in actin content and crosslinking is physically observed as an increase in surface tension [11-13, 40]. Actin binding proteins that may be involved in cortical actin filament crosslinking include spectrin [17, 18], alpha-actinin [47] and filamin ([34, 35], and Fishkind, unpublished observations).

2. There is a global migration of cortical actin (microvillar and sub-membraneous) away from the poles and toward the equator prior to or concomitant with the formation of the contractile apparatus (Figs. 1 and 2). The movement of actin away from the poles is detected as polar relaxation [11-13, 40] and the accumulation of actin at the equator establishes the actin component of the contractile apparatus. The stimulus for relaxation could be elevated Ca⁺⁺ [48-50], which would decrease the crosslinking capabilities of spectrin [17] and/or alpha-actinin [47]. Alternatively, effective crosslinking could be decreased by increasing filament number due to the activation of actin severing proteins [51-53].

3. Once the actin component is positioned in the plane of future cleavage furrow, myosin is recruited into the region [41, 44] and provides the force generating component of the contractile band apparatus [9, 10]. As division progresses, the interaction of actin and myosin is generally isotropic, leading to the collapse of the extensive actin network (collapsing baby-gate). For an excellent computer simulation of reorganizing networks see White and Borisy [45]. Within this isotropic collapse there is the occasional formation of small filament fascicles (Fig. 1) that by electron microscopy may be interpreted as the circumferential alignment of contractile ring filaments [14].

4. Active contraction continues until division is completed and the actin cytoskeleton returns to its resting state.

Undoubtedly this is an oversimplified model for cell division that will need future adjustments in its fine details as new experimental information is accumulated. However, the model is testable and our labs are currently investigating many of the ideas being presented to gain a more complete

understanding of how actin is organized and regulated during cell division. In conclusion, we extend our hearty thanks to Professor Dan whose experiments and insight have stimulated our thinking and understanding of cytokinesis and the process of cell division.

ACKNOWLEDGMENTS

The authors wish to gratefully acknowledge Drs. K. Fujiwara and S. Hagen (actin), J. Otto (220K polyclonal) and J. Bryan (220K monoclonal) for their generosity with the various antibody preparations used in this study. We also warmly thank Dr. M. Neutra for use of the Reichert microtome, Dr. T. Coleman for erythrocyte spectrin, Dr. A. Harris for human brain fodrin, Dr. T. Phillips and Mrs. T. Phillips for their help in starting-up the frozen sectioning, Ms. Carol Bonder for help in manuscript preparation and finally the children in our families whose presence provided the inspiration for the 'collapsing baby-gate' hypothesis.

This research was supported by National Institutes of Health grants GM 09788 (EB), GM 28307 (DB), GM 07226 and GM 07258 (DF) and HD 07130 (JH). EB was further supported by a Henry Rutgers Research Fellowship.

REFERENCES

- Schroeder, T. E. (1981) Interrelations between the cell surface and the cytoskeleton in cleaving sea urchin eggs. In "Cytoskeletal Elements and Plasma Membrane Organization". Ed. by G. Poste and G. L. Nicolson. Elsevier, North-Holland Biomedical Press, pp. 169-216.
- Mabuchi, I. (1986) Biochemical aspects of cytokinesis. *Int. Rev. Cytol.*, **101**: 175-213.
- Rappaport, R. (1986) Establishment of the mechanism of cytokinesis in animal cells. *Int. Rev. Cytol.*, **105**: 245-281.
- Scott, A. (1960) Surface changes during cell division. *Biol. Bull.*, **119**: 260-272.
- Dan, K. (1954) The cortical movement in *Arbacia punctulata* eggs through cleavage cycles. *Embryologia*, **2**: 115-122.
- Dan, K. and Ono, T. (1954) A method of computation of the surface and area of the cell. *Embryologia*, **2**: 87-98.
- Hiramoto, Y. (1971) Analysis of cleavage stimulus by means of micromanipulation of sea urchin eggs. *Exp. Cell Res.*, **68**: 291-298.
- Rappaport, R. and Rappaport, B. N. (1985) Surface contractile activity associated with isolated asters in cylindrical sand dollar eggs. *J. Exp. Zool.*, **235**: 217-226.
- Mabuchi, I. and Okuno, M. (1977) The effect of myosin antibody on the division of starfish blastomeres. *J. Cell Biol.*, **74**: 251-263.
- Kiehart, D. P., Mabuchi, I. and Inoue, S. (1982) Evidence that myosin does not contribute to force production in chromosome movement. *J. Cell Biol.*, **94**: 165-174.
- Wolpert, L. (1966) The mechanical properties of the membrane of the sea urchin egg during cleavage. *Exp. Cell Res.*, **41**: 385-396.
- Hiramoto, Y. (1970) Rheological properties of sea urchin eggs. *Biorheology*, **6**: 201-234.
- Yoneda, M. and Dan, K. (1972) Tension at the surface of the dividing sea urchin egg. *J. Exp. Biol.*, **57**: 575-587.
- Schroeder, T. E. (1972) The contractile ring II. Determining its brief existence, volumetric changes and vital role in cleaving *Arbacia* eggs. *J. Cell Biol.*, **53**: 419-438.
- Bonder, E. M., Cotran, N. M., Fishkind, D. J. and Begg, D. A. (1988) Identification and localization of filamentous actin, non-filamentous actin and spectrin domains. *J. Cell Biol.*, (in press).
- Henson, J. H. and Begg, D. A. (1988) Filamentous actin organization in the unfertilized sea urchin egg cortex. *Dev. Biol.*, (in press).
- Fishkind, D. J., Bonder, E. M. and Begg, D. A. (1987) Isolation and characterization of sea urchin egg spectrin: calcium modulation of the spectrin-actin interaction. *Cell Motil. Cytoskel.*, **7**: 304-314.
- Kuramochi, K., Mabuchi, I. and Owaribe, K. (1986) Spectrin from sea urchin eggs. *Biomed. Res.*, **7**: 65-68.
- Bryan, J. and Kane, R. E. (1978) Separation and interaction of the major components of sea urchin actin gel. *J. Mol. Biol.*, **125**: 207-224.
- Begg, D. A. and Rebhun, L. I. (1979) pH regulates the polymerization of actin in the sea urchin egg cortex. *J. Cell Biol.*, **83**: 241-248.
- Burgess, D. R. and Schroeder, T. E. (1977) Polarized bundles of actin filaments within the microvilli of fertilized sea urchin egg. *J. Cell Biol.*, **74**: 1032-1037.
- Platt, J. L. and Michael, A. F. (1988) Retardation of fading and enhancement of intensity of immunofluorescence by p-phenylenediamine. *J. Histochem. Cytochem.*, **31**: 840-842.
- Tokuyasu, K. T. (1980) Immunocytochemistry on ultrathin frozen sections. *Histochem. J.*, **12**: 381-403.
- Vacquier, V. D. (1975) The isolation of intact cortical granules from sea urchin eggs: calcium ions trigger granular discharge. *Dev. Biol.*, **43**: 62-74.
- Heuser, J. E. and Kirschner, M. W. (1980) Filament organization revealed in platinum replicas of

- freeze-dried cytoskeletons. *J. Cell Biol.*, **86**: 212–234.
- 26 Tyler, J. and Branton, D. (1980) Rotary shadowing of extended molecules dried from glycerol. *J. Ultrastruct. Res.*, **71**: 95–102.
- 27 Towbin, H., Staehelin, H. and Gordon, J. (1979) Electrophoretic transfer of protein from polyacrylamide gels to nitrocellulose sheets: procedure and some application. *Proc. Natl. Acad. Sci. USA*, **76**: 4350–4354.
- 28 Dubreuil, R., Byers, T. J., Branton, D., Goldstein, L. S. B. and Kiehart, D. P. (1987) *Drosophila spectrin*. I. Characterization of the purified protein. *J. Cell Biol.*, **105**: 2095–2102.
- 29 Margossian, S. S. and Lowey, S. (1973) Substructure of the myosin molecule. III. Preparation of single-headed derivatives of myosin. *J. Mol. Biol.*, **74**: 301–311.
- 30 Laemmli, U. K. (1970) Cleavage of structural proteins during the assembly of the head of bacteriophage T4. *Nature*, **227**: 680–685.
- 31 Fairbanks, G., Steck, T. L. and Wallach, D. F. H. (1971) Electrophoretic analysis of the major polypeptides of the human erythrocyte membrane. *Biochemistry*, **10**: 2606–2617.
- 32 Wulf, E., Deboben, A., Bautz, F. A., Faulstich, H. and Wieland, T. (1979) Fluorescent phalloxin, a tool for the visualization of cellular actin. *Proc. Natl. Acad. Sci. USA*, **76**: 4498–4502.
- 33 Yonemura, S. and Kinoshita, S. (1986) Actin filament organization in the sand dollar egg cortex. *Dev. Biol.*, **115**: 171–183.
- 34 Maekawa, S., Endo, S. and Sakai, H. (1987) A high molecular weight actin binding protein: Its localization in the cortex of the sea urchin egg. *Exp. Cell Res.*, **172**: 340–353.
- 35 Mabuchi, I. and Kane, R. E. (1987) A 250K molecular-weight actin-binding protein from the actin-based gels formed in sea urchin egg cytoplasmic extract. *J. Biochem.*, **102**: 947–956.
- 36 Marchesi, V. T. (1985) Stabilizing infrastructure of cell membranes. *Ann. Rev. Cell Biol.*, **1**: 531–561.
- 37 Swann, M. M. and Mitchison, J. M. (1958) The mechanism of cleavage in animal cells. *Biol. Res.*, **33**: 103–135.
- 38 Dan, K. (1954) Further study on the formation of the "new membrane" in the eggs of the sea urchin, *Hemicentrotus pulcherrimus*. *Embryologia*, **2**: 99–114.
- 39 Rappaport, R. and Rappaport, B. N. (1976) Prefurrow behavior of the equatorial surface in *Arbacia* eggs. *Dev. Growth Differ.*, **18**: 189–193.
- 40 Schroeder, T. E. (1981) The origin of the cleavage forces in dividing eggs: A mechanism in two steps. *Exp. Cell Res.*, **134**: 231–240.
- 41 Schroeder, T. E. (1987) Fourth cleavage of the sea urchin blastomeres: Microtubule patterns and myosin localization in equal and unequal cell divisions. *Dev. Biol.*, **124**: 9–22.
- 42 Usui, N. and Yoneda, M. (1982) Ultrastructural basis of the tension increase in sea urchin eggs prior to cytokinesis. *Dev. Growth Differ.*, **24**: 453–465.
- 43 Shatten, H., Cheney, R., Balczon, R., Willard, M., Cline, C., Simerly, C. and Shatten, G. (1986) Localization of fodrin during fertilization and early development of the sea urchins and mice. *Dev. Biol.*, **118**: 457–466.
- 44 Yumura, S. and Fukui, Y. (1985) Reversible cyclic AMP-dependent change in distribution of myosin thick filaments in *Dictyostelium*. *Nature*, **314**: 194–196.
- 45 White, J. G. and Borisy, G. G. (1983) On the mechanism of cytokinesis in animal cells. *J. Theor. Biol.*, **101**: 289–316.
- 46 Marsland, D. (1956) Protoplasmic contractility in relation to gel structure: Temperature-pressure experiments on cytokinesis and amoeboid movement. *Int. Rev. Cytol.*, **5**: 199–227.
- 47 Mabuchi, I., Hamaguchi, Y., Kobayashi, T., Hosoya, H., Tsukita, S. and Tsukita, S. (1985) Alpha-actinin from sea urchin eggs: Biochemical properties, interactions with actin, and distribution in the cell during fertilization and cleavage. *J. Cell Biol.*, **100**: 375–383.
- 48 Yoshimoto, Y., Iwamatsu, T. and Hiramoto, Y. (1985) Cyclic changes in intracellular free calcium associated with cleavage cycles in echinoderm and Medaka eggs. *Biomed. Res.*, **6**: 387–394.
- 49 Poenie, M. J., Alderton, J., Tsien, R. A. and Steinhardt, R. A. (1985) Changes of free calcium levels with stages of the cell division cycle. *Nature*, **315**: 147–149.
- 50 Yoshimoto, Y. and Hiramoto, Y. (1985) Cleavage in a saponin model of the sea urchin egg. *Cell Struct. Function*, **10**: 29–36.
- 51 Wang, L.-L. and Spudich, J. A. (1984) A 45,000-mol-wt protein from unfertilized sea urchin eggs severs actin filaments in a calcium-dependent manner and increases the steady-state concentration of nonfilamentous actin. *J. Cell Biol.*, **99**: 844–851.
- 53 Hosoya, H. and Mabuchi, I. (1984) A 45,000-mol-wt protein-actin complex from unfertilized sea urchin egg affects assembly properties of actin. *J. Cell Biol.*, **99**: 994–1001.
- 53 Hosoya, H., Mabuchi, I. and Sakai, H. (1986) A 100-kDa Ca^{++} -sensitive actin-fragmenting protein from unfertilized sea urchin eggs. *Eur. J. Biochem.*, **154**: 233–239.

Immunofluorescent Analysis of Actin and Myosin in Isolated Contractile Rings of Sea Urchin Eggs

THOMAS E. SCHROEDER and JOANN J. OTTO¹

Friday Harbor Laboratories, University of Washington, 620 University Road, Friday Harbor, WA 98250, and ¹Department of Biological Sciences, Purdue University, West Lafayette, IN 47907, U.S.A.

ABSTRACT—Contractile rings attached to coverslips were “isolated” from sea urchin eggs at the time of first cleavage. Actin and myosin were localized by immunofluorescence after various treatments designed to dissolve, dissociate or dislodge these contractile proteins in order to determine how they are associated and which component is attached to the plasma membrane independently of the other. Experiments using high salt (600 mM KCl), ATP or pyrophosphate did not detectably alter the presence or distribution of either contractile ring actin or myosin. Treatment with gelsolin, a protein that severs actin polymers under the conditions used, rapidly reduced actin in the contractile ring to an undetectable level; since myosin was unaffected by gelsolin, these results suggested that contractile ring myosin is attached to the plasma membrane independently of actin. Additional preparations traced the build-up of actin and myosin in the cortex from fertilization onward, as a means of gaining insight into the formation of the contractile ring. The contractile ring appears by local augmentation of actin and myosin in the furrow, rather than at the obvious expense of actin and myosin from other parts of the cortex; hence, we tentatively conclude that the contractile ring does not form by lateral recruitment of polymers already fixed in the cortex but by accretion of other subunits, perhaps from the deeper cytoplasm.

INTRODUCTION

The contractile ring is an array of microfilaments closely associated with the plasma membrane at the base of the cleavage furrow of dividing cells. It has been shown to be composed of contractile proteins, including actin and myosin, and to operate in a manner somewhat akin to contracting muscle in generating the constriction force of cleavage [1-3]. The intimate structural and functional details of actin and myosin molecules in the contractile ring, however, are poorly understood. For example, it is not known how they interact during contraction, what role is played by assembly-disassembly kinetics, where the actin and myosin subunits come from as cleavage is initiated, or which component is attached to the plasma membrane. Such topics have been nearly inac-

cessible to experimentation because the contractile ring is so short-lived and so small relative to the whole cell and because its actin and myosin represent such minor fractions of the cytoplasmic pools of these abundant cytoskeletal proteins.

Yonemura and Kinoshita [4] recently isolated cortices from sea urchin eggs that included contractile rings and used fluorescently-labeled phallotoxin to confirm that the contractile rings contain polymeric actin. We were inspired by their success to investigate the relative distributions of actin and myosin by double-label immunofluorescence. Accordingly, in the present study we trace the association of both actin and myosin with the cortical cytoskeleton from fertilization to the formation of the contractile ring and report our initial explorations of the associations between these contractile proteins themselves and with the plasma membrane. Our strategy for determining whether actin or myosin is attached to the plasma membrane independently is to identify which contractile protein remains associated with the iso-

Accepted March 17, 1988

Dedication: The authors dedicate this paper to Professor Katsuma Dan in recognition of his outstanding career in cell division research.

lated cortex after the other has been removed, for example by dissociating the actin-myosin complexes or by selectively disassembling or dissolving one of the components.

MATERIALS AND METHODS

Spawning of the sea urchin *Strongylocentrotus purpuratus* was induced by KCl injection. Procedures for fertilization, denuding in urea, and culturing as monolayers in artificial calcium-free seawater (CaFSW) at 12.0–14.0°C have been described elsewhere [5]. Egg cortices were obtained by attaching eggs to 22 × 22 mm coverslips pretreated with 1% polylysine and shearing them in a stream of buffer whose composition is described elsewhere [6], except that the detergent Triton X-100 was omitted. Cortices from unfertilized eggs were prepared from mechanically dejellied eggs with intact vitelline envelopes; eggs of all other stages were denuded. Cortices from unfertilized and post-fertilization stages, except for cleavage stages which are described below, were obtained from eggs that were allowed to attach to coverslips for 1 min before shearing. These preparations were fixed immediately after shearing.

Initial efforts to "isolate" contractile rings revealed that the optimum time for attaching cleavage stage eggs was difficult to predict, at least for the purpose of obtaining several coverslips-full of contractile rings from each culture, and also demonstrated that eggs attached for more than 10 min divided abnormally or not at all. Therefore, we developed a special procedure to avoid prolonged attachment while guaranteeing that each coverslip would contain at least some contractile rings. For each culture, several polylysine-covered coverslips were submerged in CaFSW in a Petri dish at the experimental temperature. When the onset of first cleavage was observed in the culture (about 120 min after fertilization), a pipetful of eggs was gently distributed among all of the coverslips; at 2-min intervals, until cleavage was obvious throughout the donor culture, additional pipetfuls were added to the same coverslips. By this procedure every coverslip included enough cortices isolated from cells at cleavage, although the stages were necessarily somewhat randomized.

After dividing cells were sheared, the coverslips bearing the cortices were either fixed immediately or were immersed in buffered experimental or control solutions of defined ionic, nucleotide or other contents at room temperature. ATP, GTP or sodium pyrophosphate was added to 50 mM KCl, 50 mM MgCl₂, 2 mM EGTA and 20 mM Hepes buffer at pH 7.4, to which 20 mM glycerol was sometimes added. Additional KCl was added to the above buffer solution to obtain high-salt concentrations. Solutions of the actin-severing protein gelsolin (5 μM) contained 50 mM KCl, 0.3 mM CaCl₂, 0.2 mM EGTA, 1 mM MgCl₂ and 20 mM Hepes buffer at pH 7.4. Human plasma gelsolin, prepared according to Cooper *et al.* [7], was generously supplied by Dr. Joseph Bryan (Baylor College of Medicine, Houston, TX).

For indirect immunofluorescence microscopy, cortical preparations were fixed with 1% formaldehyde in phosphate-buffered saline (PBS) for 5 min at room temperature and then with methanol for 10 min at -15°C. They were washed in PBS and rinsed in 1% bovine serum albumin in PBS. They were then double-labeled for actin and myosin by separate 45-min treatments at room temperature with antiactin and antimyosin followed by a mixture of secondary antibodies for 45 min. The specific primary antibodies were: 0.1 mg/ml of mouse monoclonal antiactin, provided by Dr. James L. Lessard (Children's Hospital Research Foundation, Cincinnati, OH), that reacts with all known vertebrate isoactins [8]; and 0.5 mg/ml of rabbit polyclonal antimyosin IgG. This antimyosin antiserum was prepared by one of us (JJO) in collaboration with Dr. Joseph Bryan (Baylor College of Medicine, Houston, TX) against sea urchin (*Tripneustes gratilla*) egg myosin purified as described by Kane [9]. It reacts with a ~200 kDa protein in eggs of the sea urchin *S. purpuratus* and oocytes of the starfish *Pisaster ochraceus* in immunoblots (Fig. 1). A ~180 kDa protein is also recognized in sea urchin egg samples and is probably a proteolytic fragment of myosin. This antimyosin antiserum was previously used to stain myosin in isolated cortices from starfish oocytes [6] and the contractile ring of intact sea urchin cells [5]. In the present experiments affinity-purified antimyosin gave similar staining pat-

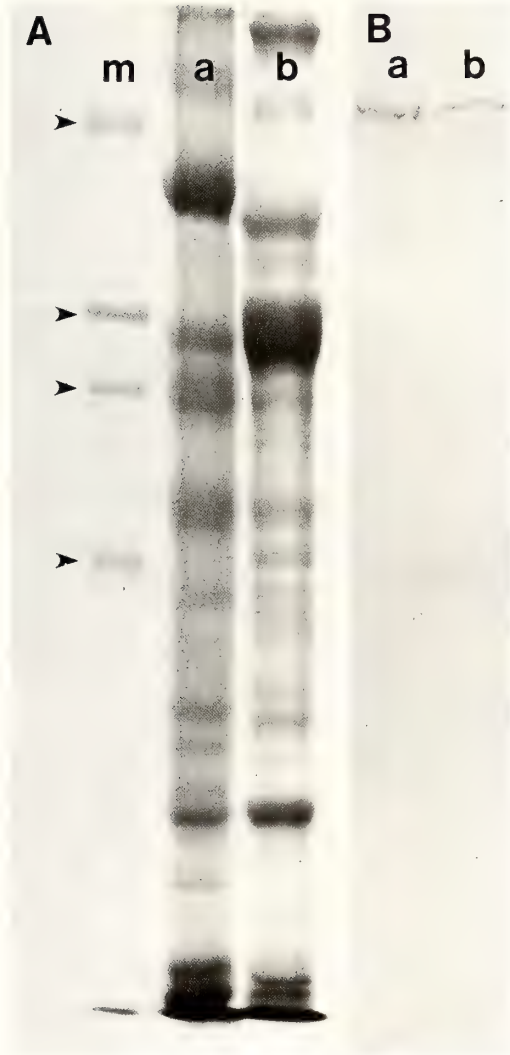


FIG. 1. Characterization of antibody against sea urchin egg myosin by immunoblotting. A. Coomassie blue-stained electrophoresis gel. B. Immunoblot of similar gel stained with antimyosin IgG. Lanes: a, *S. purpuratus* eggs; b, *Pisaster ochraceus* oocytes; m, molecular weight markers (arrowheads): rabbit muscle myosin (200 kDa), β -galactosidase (116 kDa), phosphorylase b (92.5 kDa), and bovine serum albumin (66 kDa). The antibody to sea urchin egg myosin primarily recognizes a \sim 200 kDa protein in both sea urchin eggs and starfish oocytes which is interpreted to be myosin. Occasionally lower molecular weight bands are also recognized and are thought to be proteolytic fragments of myosin.

terns as the unfractionated IgG (not shown).

The secondary antibodies were rhodamine-labeled goat antimouse (E-Y Laboratories, Inc.) and fluorescein-labeled goat antirabbit IgG (Miles-Yeda, Ltd.), mixed together so that each was diluted 1:10. Control preparations lacking all antibodies or treated only with the secondary antibodies resulted in cortices with extremely low fluorescence (not shown).

Stained cortices were observed by epifluorescence microscopy using a 50 W mercury or 100 M tungsten-halogen lamp and filter sets appropriate for rhodamine or fluorescein, respectively, and photographed with Kodak Tri-X Pan film, routinely using a 63x objective lens and exposure times of 5 or 15 sec. Figures 3c and d were photographed using a 40x objective.

For immunoblotting (Fig. 1), samples separated by SDS-polyacrylamide gel electrophoresis [10] were blotted onto nitrocellulose as described by Burnette [11]. After blocking nonspecific binding sites with 0.25% gelatin and 4% bovine serum albumin in 0.9% NaCl, 15 mM Tris-HCl (blocking buffer), the blots were stained with 75 μ g/ml antimyosin IgG followed by 2.5 μ g/ml Protein A (Kierkegaard and Perry, Gaithersburg, MD), each diluted in blocking buffer. The substrates for the peroxidase were H_2O_2 and chloronaphthol.

RESULTS

Cortices isolated from sea urchin eggs were 1–2 μ m in thickness and were attached to the coverslip by way of their outermost layer, which was the plasma membrane in all cases except for unfertilized eggs in which the vitelline coat was outermost. Since detergents were not used in the present method of isolation, we assume that the plasma membrane was relatively intact; thus, the persistence of any cortical material after isolation implies its attachment to the plasma membrane, either directly or indirectly. Before describing the staining patterns of isolated cortices by antiactin and antimyosin antibodies in detail, we must point out that: a) the polymerization states of actin and myosin cannot be definitively determined by these methods, since the antibodies presumably stain all forms, including monomers, oligomers and poly-

mers; b) the staining methods are qualitative, not quantitative; and c) actin-filled microvilli trapped between the isolated cortex and the coverslip inevitably contribute to the overall pattern of actin staining, confusing the pattern that may be due to actin in the cortex proper.

Cortical actin and myosin after fertilization

In cortices from unfertilized eggs, the staining pattern for actin was a faint uniform stippling (Figs. 2a and a'). The tiny dot-like structures appear evenly spaced 0.5–0.75 μm apart and probably indicate the presence of small quantities of actin in the papillae that later develop into microvilli after fertilization [12, 13]. Myosin staining in the same cortices was generally fainter and less regular than the actin staining (Figs. 2b and b'). Sparse myosin-positive spots, somewhat larger than the actin dots, were scattered randomly throughout the cortex against a nearly blank background. Before fertilization no coincidence between actin and myosin in the cortex could be detected and there were no fibrillar configurations.

Both the amount and organizational complexity of actin and myosin in isolated cortices from sea urchin eggs increased abruptly after fertilization (Fig. 2), and these changes eventually stabilized before the onset of cleavage. By 22 min after fertilization (Fig. 2c) the actin pattern was still essentially punctate but, in addition, some of the dots were more brightly stained and clustered. Myosin staining at 22 min (Fig. 2d) was also somewhat brighter; the pattern was still coarsely punctate, with early signs of a slightly fibrillar organization. Co-localization of actin and myosin was not yet evident.

During subsequent development prior to first division (Figs. 2e–h) the punctate patterns of actin and myosin staining gave way to more reticular patterns and the degree of co-localization in-

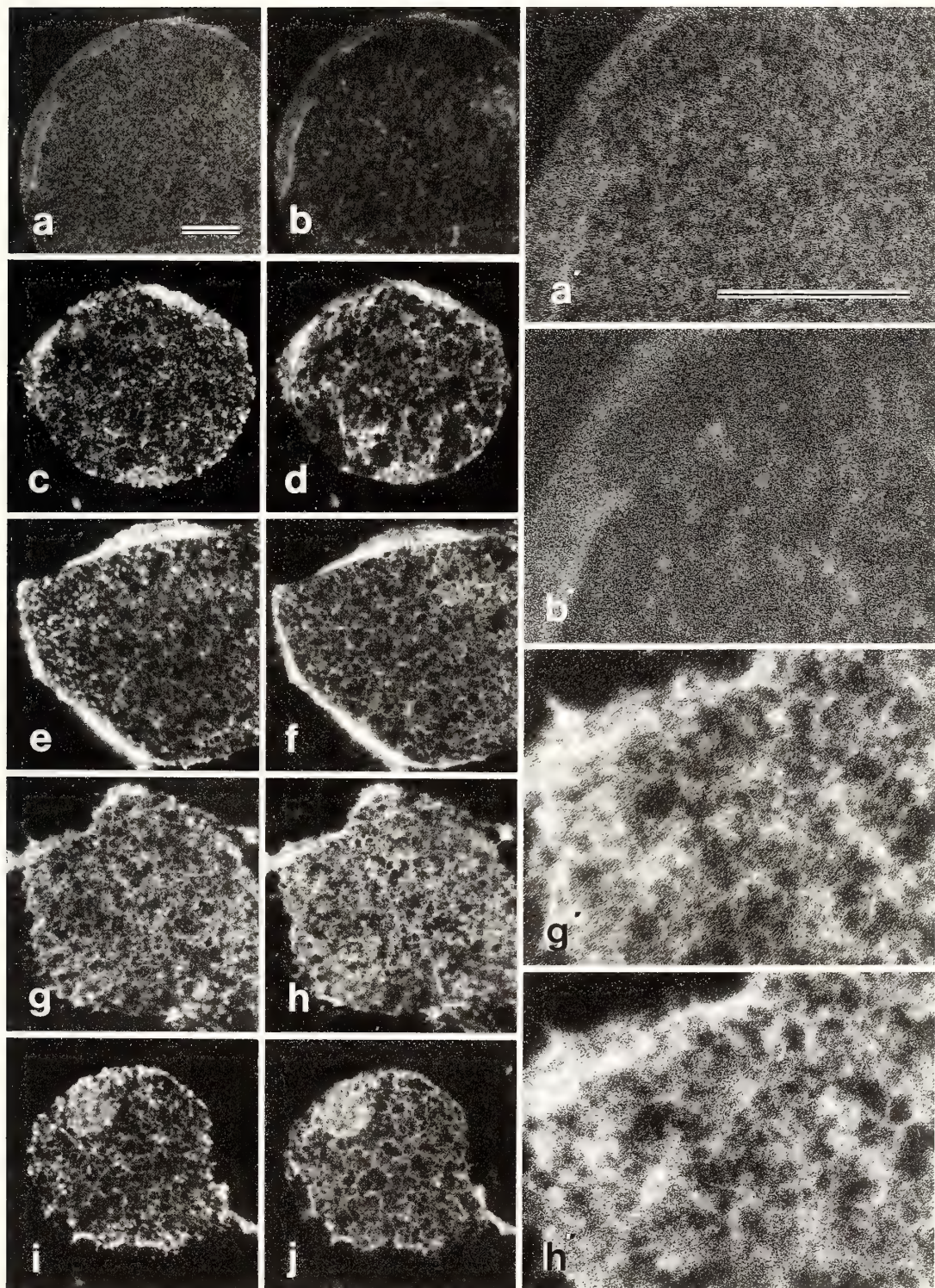
creased. By 61 min (Figs. 2e and f) this conversion was nearly complete. By 100 min (Figs. 2g and h), corresponding to the time of nuclear envelope breakdown of the first division, the patterns of actin and myosin staining were finely meshlike or reticular and there was considerable coincidence between them (Figs. 2g' and h').

Meshlike patterns of cortical actin and myosin persisted through mitosis with little change up to the onset of cleavage when the contractile ring appears, as described below. Furthermore, once first division was complete, cortices isolated from 2-cell blastomeres at interphase continued to present finely reticular patterns of actin and myosin that were largely coincident (Figs. 2i and j).

The cortex and contractile ring during cell division

Cortices isolated from unfertilized and early post-fertilization eggs were usually circular in outline; cortices isolated from cleaving eggs were often dumbbell-shaped, with the site of constriction (containing the contractile ring) sometimes imaging at a plane of focus different from the rest, presumably because the cleavage furrow was not intimately adhered to the coverslip at the time of shearing. Cortices were occasionally isolated as elongate strips, apparently as a result of eggs rolling along the adhesive coverslip surface during the shearing procedure (Fig. 3). Early in cleavage, the actin and myosin patterns were uniform throughout some of these long strips of cortical material, but in other cortical strips the contractile ring was evident as one or two transverse bands in which the intensities of actin and myosin staining were augmented (Figs. 3a–d). When two such transverse bands per strip were observed, they were about 100 μm apart (Figs. 3c and d), as would be expected if an 80- μm *S. purpuratus* egg rolled along during cortex isolation, peeling off two "sides" of the same contractile ring.

FIG. 2. Pairs of immunofluorescence micrographs of isolated cortices double-stained for actin (a, c, e, g, and i) and myosin (b, d, f, h, and j). Before fertilization, actin staining (a) is confined to an even field of low-intensity dots (a', higher magnification), probably representing the papillary precursors of microvilli; myosin staining (b) is represented by occasional dots, (b', higher magnification). More extensive staining for actin and myosin is present at 22 and 61 min after fertilization (c and d, and e and f). By 100 min after fertilization (g and h) the patterns of actin and myosin staining are reticular; the two patterns do not entirely correspond (g' and h', higher magnifications). Similar reticular patterns exist at 160 min (i and j), which is in the interphase between first and second cleavage. Scale bars: 10 μm .



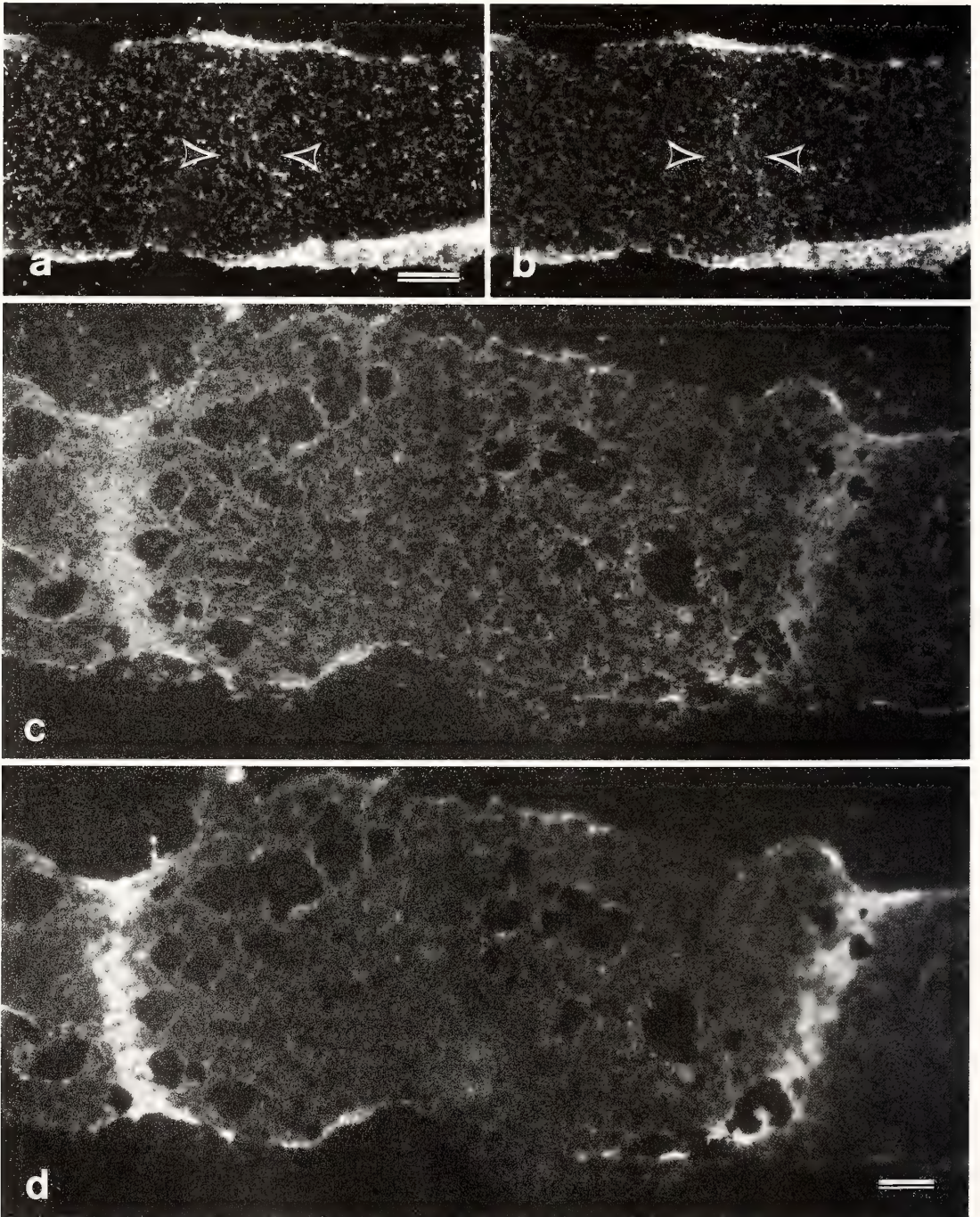


FIG. 3. Isolated cortices at the time of cleavage. In its earliest form, a contractile ring may appear as a faint transverse band (a and b, between arrowheads) across a strip of isolated cortex in which both actin (a) and myosin (b) are slightly enhanced. Occasionally, a cortical strip from a cleaving cell contains two bright transverse bands (c and d), representing two parts of the same contractile ring isolated as the cell rolled along the coverslip during the shearing process; staining for actin (c) and myosin (d) are considerably enhanced in these bands over the surrounding cortex. The strip of cortex between the bands represents cortex material from the cell poles and is neither enriched or diminished in actin or myosin relative to other parts of the cortex. Scale bars: 10 μm .

Sometimes, a visible transverse band in such a cortical strip was barely detectable (Figs. 3a and b), perhaps because it represented a contractile ring at an early stage of formation. In such images, the concentrations of actin and myosin were only slightly greater in the band than in the adjacent cortex and no distinctive substructure was evident. Of the two components in the band in Figures 3a and b, myosin seems slightly more prominent than actin.

As shown in Figures 3–6, fully-formed contractile rings routinely straddled the constrictions in isolated cortices. They were consistently 5–10 μm in width, were very thin and closely applied to the plasma membrane, and were markedly enriched for both actin and myosin relative to other parts of the cortex. The contrast between the contractile ring and adjacent cortex was consistently greater with myosin staining than with actin staining. At the poleward edges of the contractile ring, actin and myosin appeared to terminate quite abruptly rather than to merge gradually with the cytoskeletal reticulum of the general cortex. In some instances, regardless of experimental conditions, the contractile ring was sometimes disrupted, as if by the mechanical trauma of isolation (e.g. Fig. 5).

The actin and myosin patterns in portions of the cortex outside of the contractile ring at the time of cleavage roughly resembled the patterns before the onset of mitosis (Figs. 2g and h) or in the interphase after first cleavage (Figs. 2i and j), except possibly that the level of myosin staining was slightly reduced during cleavage. Furthermore, the cortex farthest from a contractile ring (the polar cortex) stained indistinguishably from the cortex right next to it. This was particularly evident in cortical strips where a complete transpolar transect was represented in the cortex between the two portions of the contractile ring (Figs. 3c and d); the cortex immediately adjacent to the contractile ring seemed equivalent to the cortex at the extreme pole in terms of the reticular organization of both actin and myosin.

Contractile rings typically exhibited a fibrillar substructure with linear elements aligned along the cell constriction, i.e. circumferentially with respect to the cleaving egg. The character of staining varied somewhat between specimens; in some

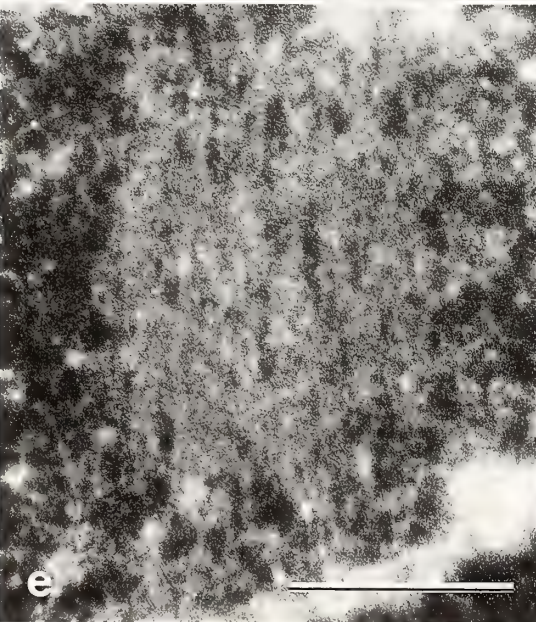
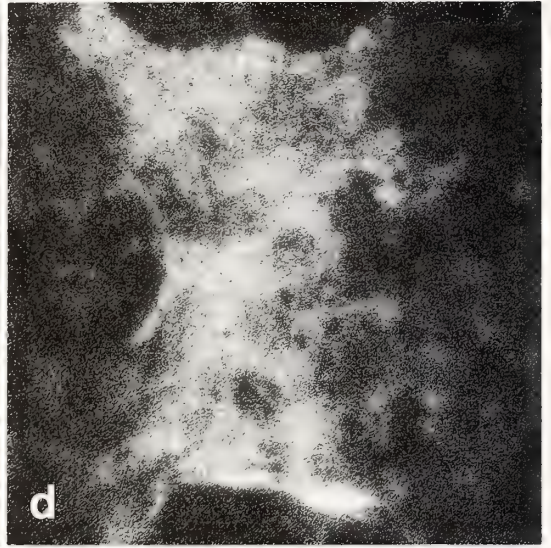
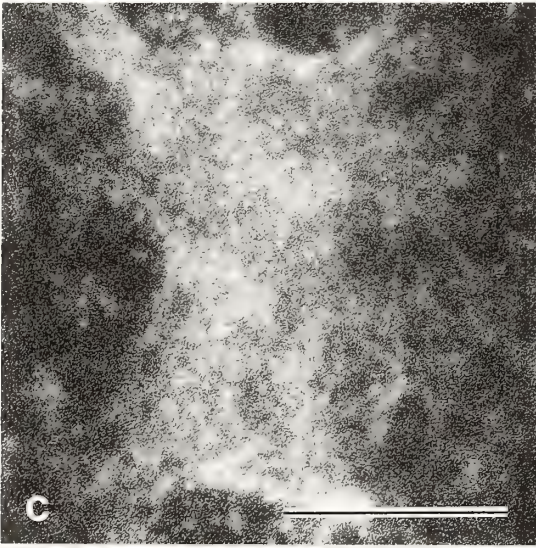
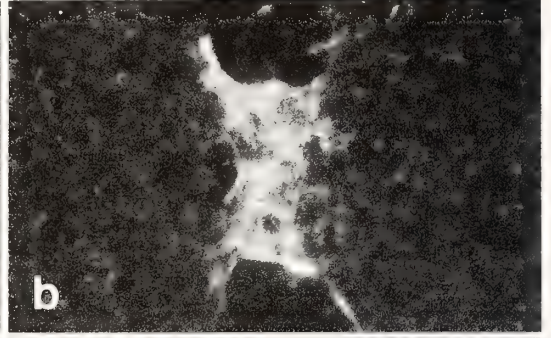
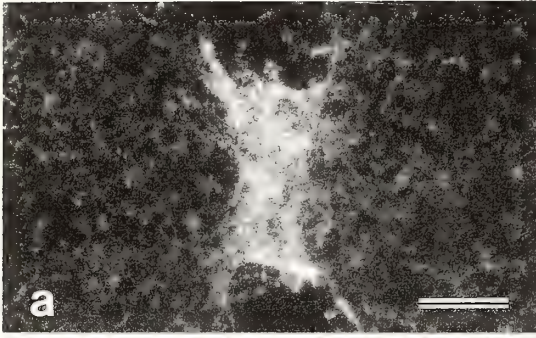
cases the myosin component appeared more fibrillar than the actin component (Figs. 4c and d), sometimes the actin appeared more fibrillar (Figs. 4e and f), and sometimes neither was particularly fibrillar. Fibrils stained by antiactin tended to be long and parallel, whereas fibrils stained with antimyosin tended to resemble a mesh composed of interlinked short elements. In most instances there was a fairly close correspondence between the staining patterns of actin and myosin in the contractile ring, but that correspondence was never perfect in all details and must be pursued at higher resolution.

Experimental attempts to extract the contractile ring

The following experiments were predicated on the assumption that actin and myosin in the contractile ring are structurally and functionally complexed together and that one of them, but probably not both, is attached to the plasma membrane. Accordingly, if actin-myosin complexes could be dissociated we would expect that the unattached component would be removed and that the attached component would persist.

Assuming that salt concentration of 600 mM would dissociate actin-myosin complexes by solubilizing myosin, coverslips containing isolated cortices were immersed into buffered solutions of 50, 150, 300 or 600 mM KCl, to which 20 mM glycerol was sometimes added, for 5 min immediately after shearing and before fixation. In terms of actin and myosin patterns, however, and contrary to expectations, contractile rings after all of these treatments (not shown) were consistently indistinguishable from controls (Figs. 2 and 3) which had been fixed immediately after shearing.

Likewise, when isolated cortices were transferred to 1, 2.5 or 5 mM ATP or inorganic pyrophosphate in buffered 50 mM KCl for 5 min, treatments also expected to dissociate actin-myosin complexes, the contractile rings again remained fundamentally intact (Fig. 5). After these treatments the adjacent cortical cytoskeleton frequently appeared slightly disorganized, but 5 mM GTP caused a similar disordering, so the effect was interpreted as being a non-specific relative to actin-myosin dissociation.



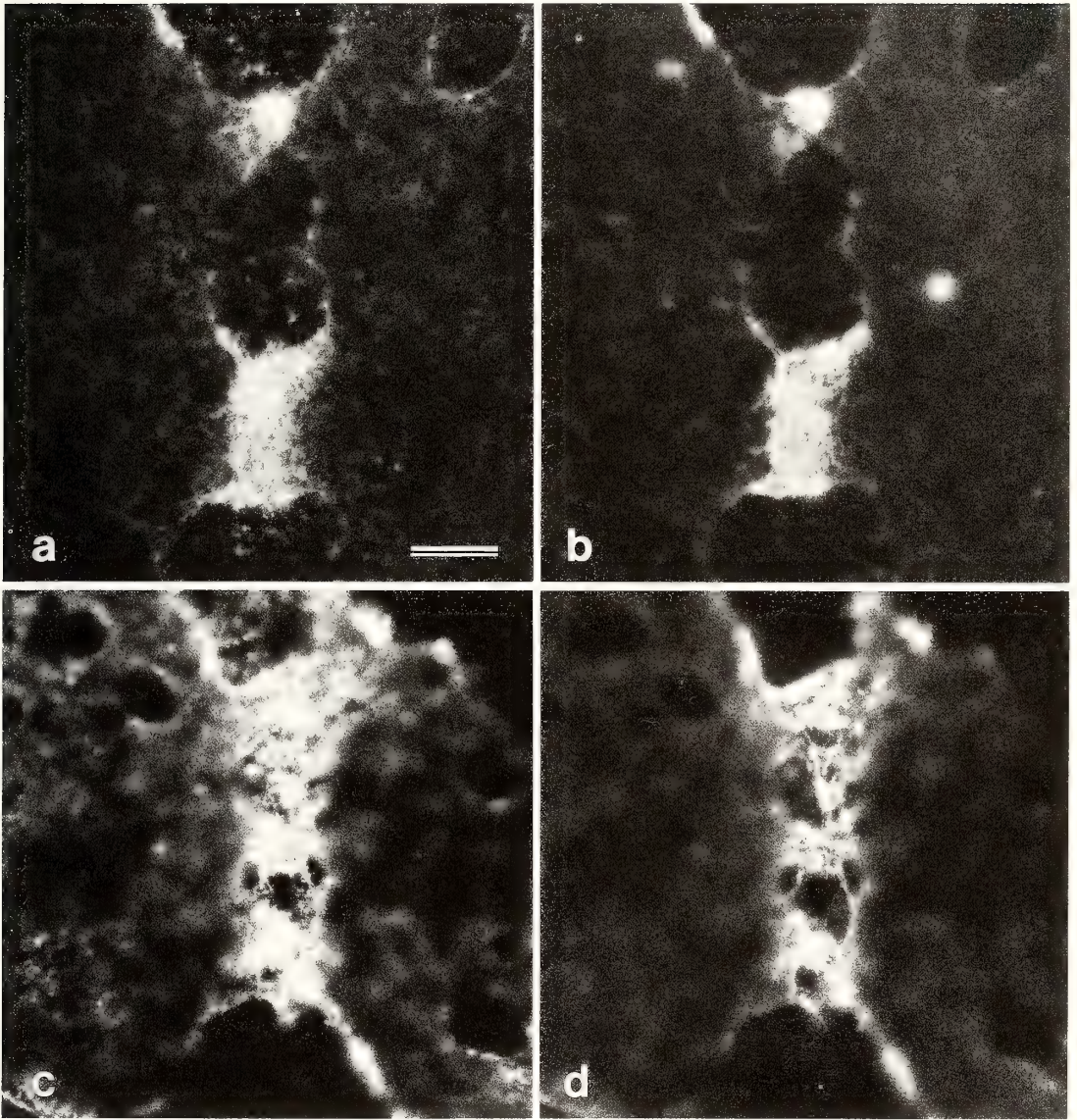


FIG. 5. Lack of effect of ATP on staining of contractile rings for actin (a and c) and myosin (b and d) after 5 min in 0 mM ATP (a and b) and 5 mM ATP (c and d). Gross fragmentation of the contractile ring, as seen here, was occasionally seen in all preparations. Scale bar: 10 μ m.

FIG. 4. Details of fully-formed contractile rings stained for actin (a, c, and e) and myosin (b, d, and f). The contractile ring is consistently less sharply distinguished from the nearby cortex after actin staining than after myosin staining, perhaps because of actin in the microvilli. In some instances the myosin component of the contractile ring seems to be slightly more fibrillar in organization (c and d) than the actin component, and sometimes the actin is more prominently fibrillar (e and f). Scale bars: 10 μ m.

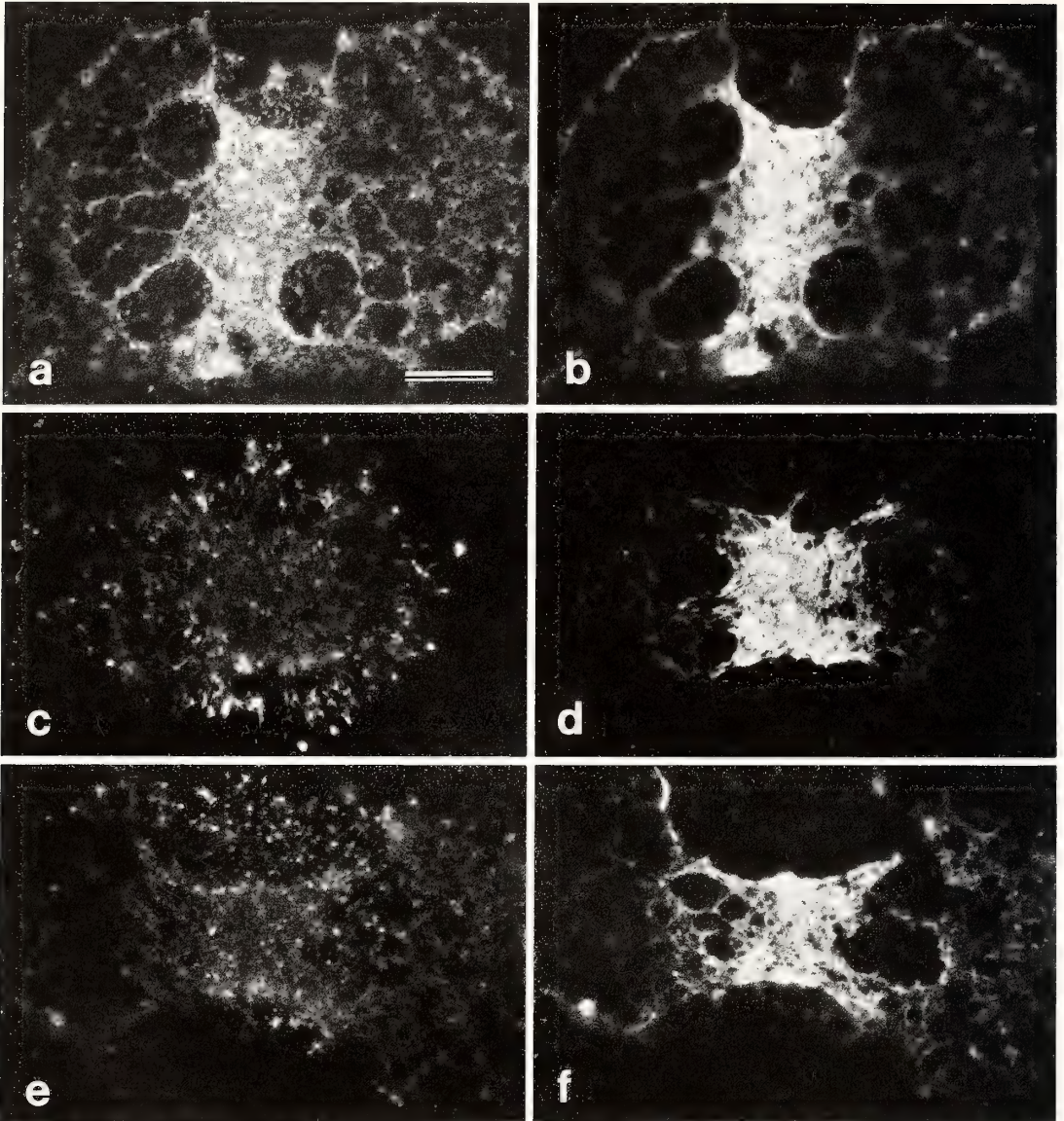


FIG. 6. Reduction of actin staining by treatment with the actin-severing protein gelsolin. Contractile rings were stained for actin (a, c, and e) and myosin (b, d, and f) after 15 min in control buffer lacking gelsolin (a and b), for 5 min in 5 μM gelsolin (c and d), and 15 min in 5 μM gelsolin (e and f). Myosin staining is unaltered despite the dissolution of actin. Scale bar: 10 μm .

Dissolution of actin by gelsolin treatment

The actin-severing protein gelsolin [14] was applied to isolated cortices at 1, 2.5 μM for 5–15 min. At the lowest concentration no effect was noticed, and the patterns of actin and myosin were indistinguishable from controls in buffer lacking gelsolin (Figs. 6a and b). Actin staining of the contrac-

tile ring was somewhat reduced after 2.5 μM gelsolin and was significantly reduced after 5 μM gelsolin (Figs. 6c and e); significantly, however, myosin staining was not altered by gelsolin (Figs. 6d and f). Even though actin in the contractile ring apparently disappeared completely after 5 min in 5 μM gelsolin (Fig. 6c), small amorphous aggregates

of antiactin-staining material still demarcated the cortical fragment even after 15 min (Fig. 6e).

DISCUSSION

Development of the cortical cytoskeleton
We infer that the membrane-associated cortical cytoskeletons shown here are reasonable representations of the cortices of normal living cells. On the other hand, these studies are still preliminary and therefore certain details may be altered by further study using additional protocols and other species.

Our results on the development of the cortical cytoskeleton through the first cell cycle compare favorably with evidence obtained in other ways. Prior to fertilization cortex-associated actin seems to be confined to the short papillary precursors of microvilli, and cortex-associated myosin is even sparser. Comparing our results with phalloxin-labeled cortices of unfertilized eggs [15] and other related findings [16, 17], the cortical actin at this stage is either largely or entirely in the polymeric form and very limited in amount. Cortical actin before fertilization is believed to be associated with the plasma membrane rather than cortical granules since it persists even after the latter have been selectively removed [18].

Based on the present immunofluorescence studies, the cortical content of actin and myosin increases during the first 60 min after fertilization, which coincides with biochemical quantifications during the same period [19] that show an 8-fold increase of cortical actin and a coordinate increase of a 200 kDa protein that was interpreted as myosin. After this time, as the cell undergoes mitosis and prepares to divide, no additional change in cortical actin or myosin was detected by either kind of investigation.

Origin and organization of the contractile ring
The source of contractile ring actin and myosin remains one of the important unsolved mysteries of cell division. Previous biochemical analyses of cortices from sea urchin eggs [3, 19] failed to show any increase in actin or myosin that correlated with the appearance of the contractile ring, thereby encouraging ideas that this structure

forms from cytoskeletal elements already present in the cortex. One postulate in this category is that the cortical cytoskeleton builds up during a global contraction in mitosis and that this material is accumulated laterally from subequatorial or polar regions of the cortex to form the contractile ring [20].

Contrary to ultrastructural findings supporting this idea [21], however, the amount or organization of actin and myosin by immunofluorescent staining does not seem to increase between 60 and 120 min when the global contraction occurs, and there is no obvious gradient of depleted cytoskeletal material from the polar to the subfurrow cortex, as might be expected. In terms of suggested scenarios for the formation of the contractile ring [2, 3], it thus seems improbable that the contractile ring is produced by mere rearrangement or lateral recruitment of pre-existing formed elements of the cortical cytoskeleton.

The present evidence seems to be more consistent with the proposition that the contractile ring forms as a result of actin and myosin being locally added to the furrow cortex by recruitment of mobile subunits, either from cortical actin and myosin not yet fixed into the cortical cytoskeleton or from the deeper cytoplasm. A similar conclusion was reached in recent studies of the appearance of myosin in the contractile rings of intact sea urchin cells by immunofluorescence [5] and in cultured cells by microinjection of fluorescent myosin light chain [22], although none of this evidence can as yet be considered conclusive.

As expected, actin and myosin appear to be intimately associated within the microfilamentous substructure of the contractile rings of sea urchin eggs, as in other cells. Important details of the association, however, remain unclear and require further study. Some features of the contractile rings shown here conflict with similar data obtained from other cell types; for example, contractile ring myosin in *Dictyostelium* has been shown to exist as discrete rods about 0.6 μm in length [23], and striations of about this same dimension have been observed in the contractile rings of myosin-stained cultured cells [24] and in sea urchin egg myosin aggregated *in vitro* [25]. In contractile rings of sea urchin cells, neither dis-

crete myosin rods nor striations have yet been clearly observed.

Is contractile ring myosin attached to the plasma membrane independently of actin? In this preliminary study, we unexpectedly failed to extract myosin from the contractile ring by disassembling its putative polymers in 600 mM KCl; this treatment was previously shown to be effective in extracting myosin from egg cortices prepared by a different procedure [19, 26], although the fate of contractile ring myosin was not specifically determined. Similarly, we observed no evidence that actin-myosin complexes in the contractile ring were dissociated in 5 mM ATP or 5 mM pyrophosphate, even though these procedures have been shown to be effective in muscle [27]. In these experiments, immunofluorescent staining of actin or myosin in the contractile ring was not noticeably reduced relative to controls; it remains to be determined if these results are due to some peculiarity caused by the preparative technique or if they reflect intrinsic properties of the contractile ring.

In our experiments with exogenous gelsolin to dissect the contractile ring, most or all contractile ring actin was removed, since none was detected by immunofluorescence, yet neither the quantity or distribution of myosin was affected. This result opposes the idea that myosin is anchored to the contractile ring solely by its interaction with actin filaments, so we tentatively conclude that myosin is associated with the cortex (and therefore the plasma membrane, if only indirectly) independently of actin. On the other hand, because of the nature of gelsolin's severing action on actin filaments, we cannot yet rule out the possibility that the myosin is attached to undetected residual actin dimers or oligomers persisting in the cortex.

In conclusion, isolated cortices from dividing sea urchin eggs present an unusual opportunity to dissect the molecular organization of the contractile ring, and we intend to extend the preliminary results reported here. For example, it will be interesting to explore the roles of the accessory proteins known to influence the polymerization states and association of actin and myosin in sea urchin cells [25, 28–33] and of other endogenous factors such as phosphorylation levels that may

modulate the fully-formed contractile ring. These and other approaches should help to resolve how myosin and actin are associated with each other and how they are attached to the cell cortex and the plasma membrane.

ACKNOWLEDGMENTS

The authors are grateful for research support from the U. S. National Institutes of Health (grant HD/GM 20306) to T. E. S. and from the American Cancer Society (grant CD-108) to J. J. O. We also thank Dr. Joseph Bryan for generously supplying gelsolin and Dr. Issei Mabuchi for suggestions concerning the manuscript.

REFERENCES

- Schroeder, T. E. (1975) Dynamics of the contractile ring. In "Molecules and Cell Movement". Ed. by S. Inoue and R. E. Stephens, Raven Press, New York, pp. 305–334.
- Schroeder, T. E. (1987) The origin and action of the contractile ring. In "Biomechanics of Cell Division". Ed. by N. Akkas, Plenum, New York. pp. 209–230.
- Mabuchi, I. (1986) Biochemical aspects of cytokinesis. *Int. Rev. Cytol.*, **101**: 175–213.
- Yonemura, S. and Kinoshita, S. (1986) Actin filament organization in the sand dollar egg cortex. *Dev. Biol.*, **115**: 171–183.
- Schroeder, T. E. (1987) Fourth cleavage in sea urchin blastomeres: microtubule patterns and myosin localization in equal and unequal cell divisions. *Dev. Biol.*, **124**: 9–22.
- Otto, J. J. and Schroeder, T. E. (1984) Assembly-disassembly of actin bundles in starfish oocytes: an analysis of actin-associated proteins in the isolated cortex. *Dev. Biol.*, **101**: 262–273.
- Cooper, J. A., Bryan, J., Schwab, B., Frieden, C., Loftus, D. J. and Elson, E. L. (1987) Microinjection of gelsolin into living cells. *J. Cell Biol.*, **104**: 419–501.
- Lessard, J. L., Scheffter, S., Engel, L. and Tepperman, K. (1983) Immunofluorescent localization of actins in differentiating chick myoblasts. *J. Cell Biol.*, **97**: 74a.
- Kane, R. E. (1980) Induction of either contractile or structural actin-based gels in sea urchin egg cytoplasmic extract. *J. Cell Biol.*, **86**: 803–809.
- Laemmli, U. K. (1970) Cleavage of structural proteins during assembly of the head of bacteriophage T4. *Nature*, **227**: 680–685.
- Burnette, W. N. (1981) "Western blotting": electrophoretic transfer of proteins from sodium dodecylsulfate-polyacrylamide gels to unmodified

- nitrocellulose and radiographic detection with antibody and radioiodinated Protein A. *Anal. Biochem.*, **112**: 195–203.
- 12 Vacquier, V. D. (1981) Dynamic changes of the cell cortex. *Dev. Biol.*, **84**: 1–26.
 - 13 Schroeder, T. E. (1986) The egg cortex in early development of sea urchins and starfish. In "Developmental Biology", vol. 2. Ed. by L. D. Browder, Plenum, pp. 59–100.
 - 14 Stossel, T. P., Chaponnier, C., Ezzell, R. M., Hartwig, J. H., Janmey, P. A., Kwiatkowski, D. J., Lind, S. E., Smith, D. B., Southwick, F. S., Yin, H. L. and Zaner, K. S. (1985) Nonmuscle actin-binding proteins. *Ann. Rev. Cell Biol.*, **1**: 353–402.
 - 15 Yonemura, S. and Mabuchi, I. (1987) Wave of actin polymerization in the sea urchin egg. *Cell Motil. Cytoskel.*, **7**: 46–53.
 - 16 Spudich, A. and Spudich, J. A. (1979) Actin in Triton-treated cortical preparations of fertilized and unfertilized sea urchin eggs. *J. Cell Biol.*, **82**: 212–226.
 - 17 Cline, C. A., Schatten, H., Balczon, R. and Schatten, G. (1983) Actin-mediated surface motility during sea urchin fertilization. *Cell Motil.*, **3**: 513–524.
 - 18 Kopf, G. S., Moy, G. W. and Vacquier, V. D. (1982) Isolation and characterization of sea urchin egg cortical granules. *J. Cell Biol.*, **95**: 924–932.
 - 19 Mabuchi, I., Hosoya, H. and Sakai, H. (1980) Actin in the cortical layer of the sea urchin egg. Changes in its content during and after fertilization. *Biomed. Res.*, **1**: 417–426.
 - 20 Schroeder, T. E. (1981) The origin of cleavage forces in dividing eggs: a mechanism in two steps. *Exp. Cell Res.*, **134**: 231–240.
 - 21 Usui, N. and Yoneda, M. (1982) Ultrastructural basis of the tension increase in sea-urchin eggs prior to cytokinesis. *Dev. Growth Differ.*, **24**: 453–465.
 - 22 Mittal, B., Sanger, J. M. and Sanger, J. W. (1987) Visualization of myosin in living cells. *J. Cell Biol.*, **105**: 1753–1760.
 - 23 Yumura, S. and Fukui, Y. (1985) Reversible cyclic AMP-dependent change in distribution of myosin thick filaments in *Dictyostelium*. *Nature*, **314**: 194–196.
 - 24 Sanger, J. M. and Sanger, J. W. (1980) Banding and polarity of actin filaments in interphase and cleaving cells. *J. Cell Biol.*, **86**: 568–575.
 - 25 Yabkowitz, R. and Burgess, D. R. (1987) Low ionic strength solubility of myosin in sea urchin egg extracts is mediated by a myosin-binding protein. *J. Cell Biol.*, **105**: 927–936.
 - 26 Mabuchi, I. (1973) A myosin-like protein in the cortical layer of the sea urchin egg. *J. Cell Biol.*, **59**: 542–547.
 - 27 Harrington, W. F. and Rodgers, M. E. (1984) Myosin. *Ann. Rev. Biochem.*, **53**: 35–73.
 - 28 Wang, L.-L. and Spudich, J. (1984) A 45,000-mol-wt protein from unfertilized sea urchin eggs severs actin filaments in a calcium-dependent manner and increases the steady-state concentration of non-filamentous actin. *J. Cell Biol.*, **99**: 844–851.
 - 29 Hosoya, H. and Mabuchi, I. (1984) A 45,000-mol-wt protein-actin complex from unfertilized sea urchin egg affects assembly properties of actin. *J. Cell Biol.*, **99**: 994–1001.
 - 30 Mabuchi, I., Hamaguchi, Y., Kobayashi, T., Hosoya, H., Tsukita, S. and Tsukita, S. (1985) Alpha-actinin from sea urchin eggs: biochemical properties, interaction with actin, and distribution in the cell during fertilization and cleavage. *J. Cell Biol.*, **100**: 375–383.
 - 31 Hosoya, H., Mabuchi, I. and Sakai, H. (1986) An 100-kDa Ca^{2+} -sensitive actin-fragmenting protein from unfertilized sea urchin egg. *Eur. J. Biochem.*, **154**: 233–239.
 - 32 Maekawa, S., Endo, S. and Sakai, H. (1987) A high molecular weight actin binding protein: its localization in the cortex of the sea urchin egg. *Exp. Cell Res.*, **172**: 340–353.
 - 33 Mabuchi, I. and Kane, R. E. (1987) A 250 K-molecular-weight actin-binding protein from actin-based gels formed in sea urchin egg cytoplasmic extract. *J. Biochem.*, **102**: 947–956.

Development

Growth & Differentiation

Published by

the Japanese Society of Developmental Biologists

Papers in Vol. 30, No. 3. (June 1988)

20. **REVIEW:** S. -I. ABE: Cell culture of spermatogenic cells from amphibians.
21. R. E. Hinkley, Jr. and A. N. NEWMAN: Changes in the distribution of calcium-sequestering membranes during the first cell cycle of the sea urchin, *Lytechinus variegatus*.
22. H. L. Hosick, Y. Inaguma, M. Kusakabe and T. SAKAKURA: Morphogenesis of mouse mammary epithelium in vivo in response to biomatrix prepared from a stimulatory fetal mesenchyme.
23. K. Takiguchi, S. Yasugi and T. MIZUNO: Popsinogen induction in chick stomach epithelia by reaggregated proventricular mesenchymal cells in vitro.
24. S. Kobayashi, Mizuno and M. OKADA: Accumulation and spatial distribution of poly(A)+ RNA in oocytes and early embryos of *Drosophila melanogaster*.
25. S. Tone, S. Tanaka and Y. KATO: The cell cycle and cell population kintion in the programmed cell death in the limb-buds of normal and 5-bromodeoxyuridine-treated chick embryos.
26. S. Noda and T. MITSUI: Distributions of actin, vinculin and fibronectin in the duodenum of developing chick embryos: Immunohistochemical studies at the light microscope level.
27. A. W. Gibson and R. D. BURKE: Localization and characterization of an intergral membrane protein antingen expressed by pigment cells in embryos of the sea urchin *Strongylocentrotus purpuratus*.
28. S. Ohta, Y. Suzuki, W. Hara, S. Tokiya and T. SUZUKI: Fibroin gene transcription in the embryonic stages of the silkworm, *Bombyx mori*.
29. O. Taguchi, R. M. Bigsby and G. R. CUNHA: Estrogen responsiveness and the estrogen receptor during development of the murine reproductive tract.
29. M. L. Wright, S. T. Jorey, Y. M. Meyrs, M. L. Fieldstad, C. M. Paquette and M. B. CLARK: Influence of photoperiod, daylength, and feeding schedule on tadpole growth and development.

Development, Growth and Differentiation (ISSN 0012-1592) is published bimonthly by The Japanese Society of Developmental Biologists, Department of Biology, School of Education, Waseda University, Tokyo 160, Japan. 1988: Volume 30. Annual subscription U. S. \$ 110.00 including air speed delivery except Japan. Application to mail at second class postage rate is pending at Jamaica, NY 11431, U. S. A.

Outside Japan: Send subscription orders and notices of change of address to Academic Press, Inc., Journal Subscription Fulfillment Department, 6277 Sea Harbor Drive, Orlando, FL 32887, U. S. A. Send notices of change of address at least 6-8 weeks in advance. Please include both old and new addresses. U. S. A. POSTMASTER: Send changes of address to *Development, Growth and Differentiation*, Academic Press, Inc., Journal Subscription Fulfillment Department, 6277 Sea Harbor Drive, Orlando, FL 32887, U. S. A.

In Japan: Send nonmember subscription orders and notices of change of address to Business Center for Academic Societies Japan, 16-3, Hongo 6-chome, Bunkyo-ku, Tokyo 113, Japan. Send inquiries about membership to Business Center for Academic Societies Japan, 4-16, Yayoi 2-chome, Bunkyo-ku, Tokyo 113, Japan.

Air freight and mailing in the U. S. A. by Publications Expediting, Inc., 200 Meacham Avenue, Elmont, NY 11003, U. S. A.

THE BOTANICAL MAGAZINE TOKYO

An international journal for plant sciences published quarterly by the Botanical Society of Japan. For a century, the journal has continuously published outstanding papers by Japanese as well as foreign botanical scientists. Contributors to the journal are not limited to the members of the Society and their papers are accepted by paying the page charge.

Papers in a Recent Issue :

- YOKOTA, M., S. HIGA, H. YOSHIOKA AND K. SHIMABUKU: *Viola stoloniflora* (Violaceae), a New Species from the Ryukyus
- RAJU, M.V.S., A. WALTHER AND W.A. QUICK: Growth and Development of Embryo Parts during the Germination of Caryopses of the Wild Oat (*Avena fatua* L.)
- FUKUDA, Y.: Phyllotaxis in Two Species of *Rubia*, *R. akane* and *R. sikkimensis*
- SOH, W.Y., S.S. HONG AND D.Y. CHO: The Ontogeny of the Vascular Cambium in *Ginkgo biloba* Roots
- AGUINAGALDE, I.: Flavonoids in *Brassica nigra* (L.) Koch, *B. oleracea* L., *B. campestris* L. and Their Natural Amphidiploids
- YAMAMOTO, S.: Seedling Recruitment of *Chamaecyparis obtusa* and *Sciadopitys verticillata* in Different Microenvironments in an Old-Growth *Sciadopitys verticillata* Forest
- MARIKO, S.: Maintenance and Constructive Respiration in Various Organs of *Helianthus annuus* L. and *Zinnia elegans* L.
- MOHR, H.: Control of Plant Development: Signals from Without — Signals from Within

Order form

Send to

THE BOTANICAL SOCIETY OF JAPAN

Toshin Building
Hongo 2-27-2, Bunkyo-ku,
Tokyo 113, Japan

THE BOTANICAL MAGAZINE, TOKYO

Individuals: ¥ 7,000 p.a.

Institutions: ¥ 17,500 p.a.

Name (Please print): _____

Address: _____

Date: _____ Signature: _____

NARISHIGE

THE ULTIMATE NAME IN MICROMANIPULATION

OUR NEW MODELS MO-102 and MO-103
MAKE PRECISION MICROMANIPULATION SO EASY!

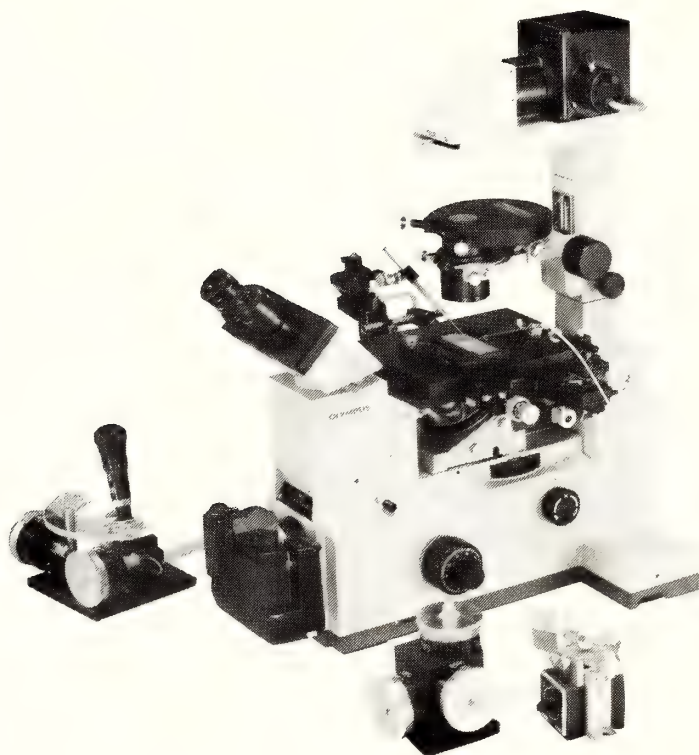


(Photo: by courtesy of Olympus Optical CO., LTD.)

SOME FEATURES of MO-102 and MO-103:

- * The manipulator head is so small that it can be mounted directly on the microscope stage. There is no need for a bulky stand.
- * Hydraulic remote control ensures totally vibration-free operation.
- * 3-D movements achieved with a single joystick.

Micromanipulators Microelectrode pullers Stereotaxic instruments



**NARISHIGE SCIENTIFIC INSTRUMENT
LABORATORY CO., LTD.**

4-9-28, Kasuya, Setagaya-ku, Tokyo 157 JAPAN
Telephone: 03-308-8233 Telex: NARISHG J27781

ZOOLOGICAL SCIENCE

VOLUME 5 NUMBER 3

JUNE 1988

CONTENTS OF SPECIAL ISSUE ON Advances in Cell Division Research

- Sakai, H.: General introduction to the special issue on Advances in Cell Division Research 505
- Dan, K.: Mechanism of equal cleavage of sea urchin egg: transposition from astral mechanism to constricting mechanism ... 507
- Mazia, D.: Mitotic poles in artificial parthenogenesis: a letter to Katsuma Dan 519
- Inoué, S.: The living spindle 529
- Nakano, Y. and Y. Hiramoto: Measurement of spindle birefringence by the optical integration method 539
- Hamaguchi, Y.: *In vivo* cytochemistry in cell division 545
- Yoneda, M.: Computed profiles of compressed sea-urchin eggs with elastic membranes .. 553
- Yamao, W. and T. Miki-Noumura: Effect of hexyleneglycol on meiotic division of starfish oocytes 563
- Longo, F., W. H. Clark, Jr. and G. W. Hirsch: Gamete interactions and sperm incorporation in the nemertean, *Cerebratulus lacteus* 573
- Schatten, H., C. Howard, G. Coffe, C. Simerly and G. Schatten: Centrosomes, centrioles and post-translationally modified microtubules during fertilization 585
- Palazzo, R. E., J. B. Brawley and L. I. Rebhun: Spontaneous aster formation in cytoplasmic extracts from eggs of the surf clam 603
- Ohta, K., M. Toriyama, S. Endo and H. Sakai: Mitotic apparatus-associated 51-kD protein in mitosis 613
- Sato, H. and J. Bryan: The thermodynamics of molecular association in the mitotic spindle with or without heavy water (D₂O) .. 623
- Harris, P. J.: Metaphase to anaphase transition of sea urchin eggs examined in caffeine-induced monasters 639
- Kojima, M. K.: Marked elongation of the anaphase spindle by treatments with local anesthetics in sea urchin eggs 645
- Sluder, G.: Control mechanisms of mitosis: The role of spindle microtubules in the timing of mitotic events 653
- Sawada, T.: The mechanism of ooplasmic segregation in the ascidian egg 667
- Kawamura, K.: The contraction wave in the cortex of dividing neuroblasts of the grasshopper 677
- Sawai, T.: Participation of the subcortical and interior cytoplasm in cleavage division of newt eggs 685
- Ohnuma, M. and I. Mabuchi: Partial purification and characterization of a factor which dissociates 45K protein-actin complex from sea urchin egg 691
- Bonder, E. M., D. J. Fishkind, J. H. Henson, N. M. Cotran and D. A. Begg: Actin in cytokinesis: Formation of the contractile apparatus 699
- Schroeder, T. E. and J. J. Otto: Immunofluorescent analysis of actin and myosin in isolated contractile rings of sea urchin eggs 713

INDEXED IN:

Current Contents/LS and AB & ES,
Science Citation Index,
ISI Online Database,
CABS Database

Issued on June 15
Printed by Daigaku Printing Co., Ltd.,
Hiroshima, Japan

3







SMITHSONIAN INSTITUTION LIBRARIES



3 9088 01261 2693

BHL